# TNT2007
## Trends in Nanotechnology

San Sebastian (Spain) September, 2007

http://www.tnt2007.org

TNT2007 "Trends in Nanotechnology" San sebastian (Spain) September 03-07, 2007

**TNT2007**
*Trends in NanoTechnology*
San Sebastian (Spain)
September 03-07, 2007

PHANTOMS foundation

CIC nanoGUNE
nanoscience cooperative research center

UAM
UNIVERSIDAD AUTONOMA
DE MADRID

Universidad de Oviedo
La universidad de Asturias

DONOSTIA INTERNATIONAL
PHYSICS CENTER
D.I.P.C.

NIMS
Nanomaterials Laboratory

Georgia Institute
of Technology

cea

leti

CSIC

# PHOTONIC CRYSTAL DENSE WAVELENGTH MULTIPLEXERS BASED ON NONLINEAR EFFECT

F. AbdelMalek[1] , W. Aroua[1] and S. Haxha[2]

Photonics Group, UK

[1]National Institute of Applied Sciences and Technology, BP-676, Cedex 1080, Tunis, Tunisia

Email: Fathi_Abdelmalek@yahoo.com

[2]Photonics Group, Department of Electronics, University of Kent, Canterbury CT2 7NT, UK

Tel: +44 (0) 1227 827257 fax: +44 (0) 1227 456084

Email: S.Haxha@kent.ac.uk

Low-power consumption in either optoelectronic or photonic circuits is crucial for future nanotechnology. In the last decade much of researcher's concerns have been focusing on this issue to find reliable system fitting their demands. In order to meet these challenging demands, novel optical nanostructures that strongly confine optical fields are essential. In order to minimise losses and their dependence on the proposed photonic crystal circuit (PIC), we present an active defect based optical circuit. Nonlinear optical materials use the non linear dependence of the refraction index on the electric field to produce different frequencies. The nonlinear effect can be used to design different kinds of photonic components such as dense multiplexers/demultiplixers and transmitters/receivers. Using a two-dimensional 2D Finite-difference time-domain (FDTD) method, we present an extensive study of a new type of the wavelength multiplexer system. In this study self focusing and defocusing are considered. Coupling efficiency between various components integrated in a single chip is investigated. It is worth mentioning that Ultra-Dense Wavelength Division Multiplexing system (UDWDM) is of high increasing demand since it provides a large broad spectrum that satisfies huge number of users world-wide. The UDWDM plays a central role in optical interconnection between various chips required for high-dense integrated system [1-3]. Such systems can be used in the high-capacity optical fibre communication systems.

In this study, the proposed approach is based on using an ultra-narrow optical filter together novel modulation formats for 10 Gb/s UDWDM transmission systems. The photonic crystal used here used as the background medium consists of air cylinders etched on silicon with refractive index 3.4. The air cylinders are squarely packed with a lattice constant $a$. The refractive index of the background is 3.4. Figure 1 shows the schematic of the ultra dense waveguide photonic crystal composed of two photonic crystal waveguides (PCWs) which are evanescently coupled. The lower waveguide contains a line of defects with nonlinear medium. The band structure is calculated and illustrated in figure 2. It can be seen that a transverse magnetic (TM) band gap is between $0.31a/\lambda$ to $0.44\ a/\lambda$. Transmission spectrum through the PCWs is illustrated ig Figs. 3 and 4. One can see that high transmission about 100% corresponds to the PCW incorporating nonlinear material. However, transmission which is about 80% corresponds to the PCW when the nonlinear material is not incorporated. It can be observed that both spectra minimum has been achieved at normalised frequency equal to 0.35 $a/\lambda$. The TM mode contour plot, when the upper PCW is excited, has been illustrated in figure 5. It can be anticipated that the optical mode is evanescently coupled into the lower waveguide.

## References

[1] W. J. Broad, "U.S. Redesigning Atomic Weapons," *The New York Times*, Feb. 7, 2005.

[2] B. Zhu, et. al. "High Spectral Density Long-Haul 40-Gb/s Transmission Using CSRZ-DPSK Format," *IEEE J. Lightwave Tech.*, vol. 22, pp. 208-214, 2004.
[3] C. Jin-Xing et. al., "Long-Haul 40 Gb/s DWDM Transmission with Aggregate Capacities Exceeding 1 Tb/s," *IEEE J. Lightwave Tech.*, vol. 20, pp. 2247-2258, 2002. 8). M. Salib, et. al. "Silicon Nanophotonics," *Intel Technology Journal*, vol. 8, pp. 143-160, May, 2004.

**Figure captions:**
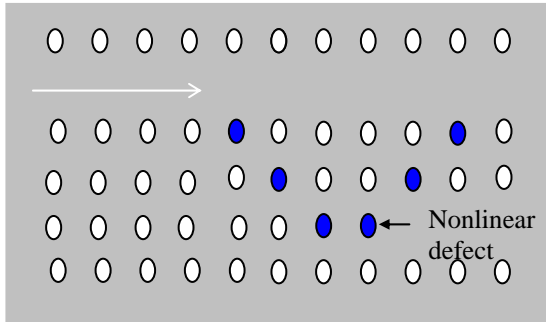
Figure 1
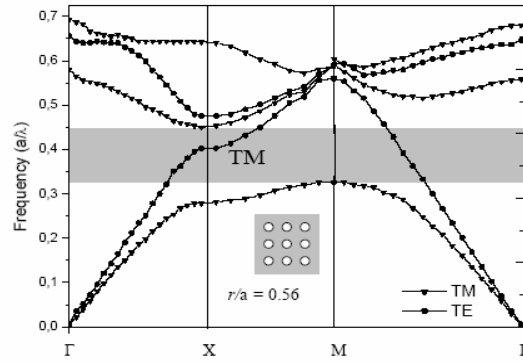
Figure 2
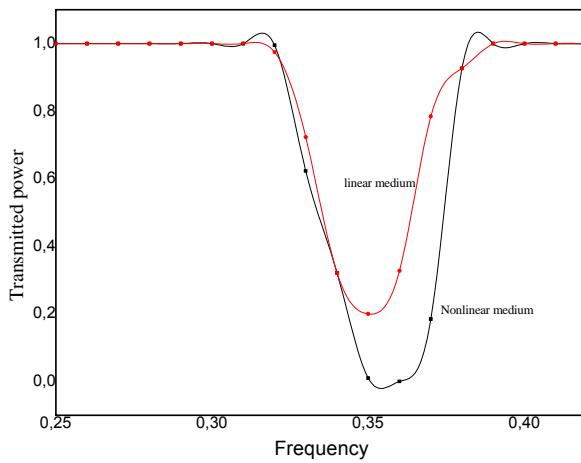
Figure 3
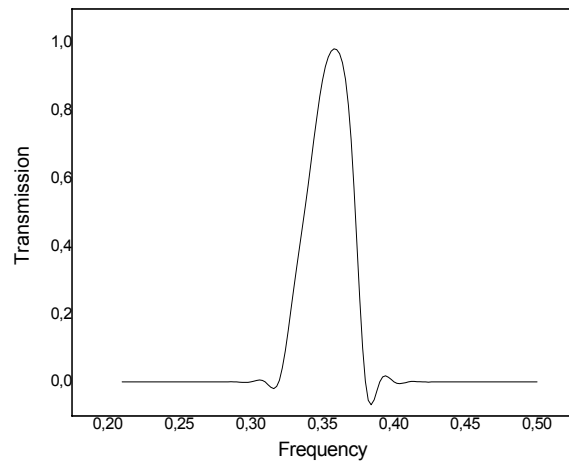
Figure 4

Figure 5

# STRONG ELECTROLUMINESCENCE FROM CARBON NANOTUBE FIELD-EFFECT TRANSISTORS

<u>É. Adam</u>[a], C.M. Aguirre[a], F. Meunier, B. C. St-Antoine, P. Desjardins[a], D. Ménard[a], R. Martel[b]

*a Département de Génie Physique, École Polytechnique de Montréal, Montréal, Canada*
*b Département de Chimie, Université de Montréal, Montréal, Canada*

The discovery of electroluminescence (EL) from ambipolar Carbon Nanotube Field-Effect Transistors (CNFET) [1] demonstrated the potential use of Single-Wall Carbon Nanotubes (SWNT) for promising optoelectronic devices. The mechanism proposed involved the radiative recombination of excitons produced by electrons and holes injected simultaneously from each ends of the SWNT. More recently, EL from unipolar CNFET has also been reported [2, 3] and the impact excitation by hot carriers was discussed as an important mechanism to explain the excitonic emission. In this contribution, we present an update of our EL measurements on unipolar CNFET. The devices are made from three different SWNT sources: HIPCO, CVD (CoMoCat) and laser ablation.

The spectrometer used to obtain spectra and images is the Spectrometer Infrared of MONtreal (SIMON), an infrared spectrometer designed to usually fit on the Mont-Mégantic astronomical telescope. The SIMON detector is a 1024 x 1024 HgCdTe array with a spatial resolution 30μm/pixel. The spectral detection range of this detector is 0.50 to 1.55 eV.

We obtain very bright EL emission from SWNT network devices and this is true for any of the sources tested so far (see figure). Strong light emission from these networks (compared to single tube devices) brings new opportunities for efficient CN-based optoelectronic devices. The EL is however specific to the diameter distribution of the nanotube source, which is deduced from the absorption spectra taken on the bulk samples. A significant energy redshift is observed between the main emission peak compared to the main absorption peak for the large diameter distribution source (CoMoCAT) suggesting that only large diameter tubes emit light. Resonant energy transfert mechanism is proposed to explain this observation. In fact, this work demonstrates that EL spectra from CNFET-networks can be tuned in wavelength by varying the diameter distribution of the SWNT.

Secondly, light emission mechanism is discussed according to observation of the light emitting light spot as a function of the voltage applied. Light emission is located in the region around the minority carrier injector electrode. These results suggest that light emission in our unipolar transistors involved radiative recombination of excitons

produced by electrons and holes injected simultaneously from each ends of the SWNT instead of impact excitation.
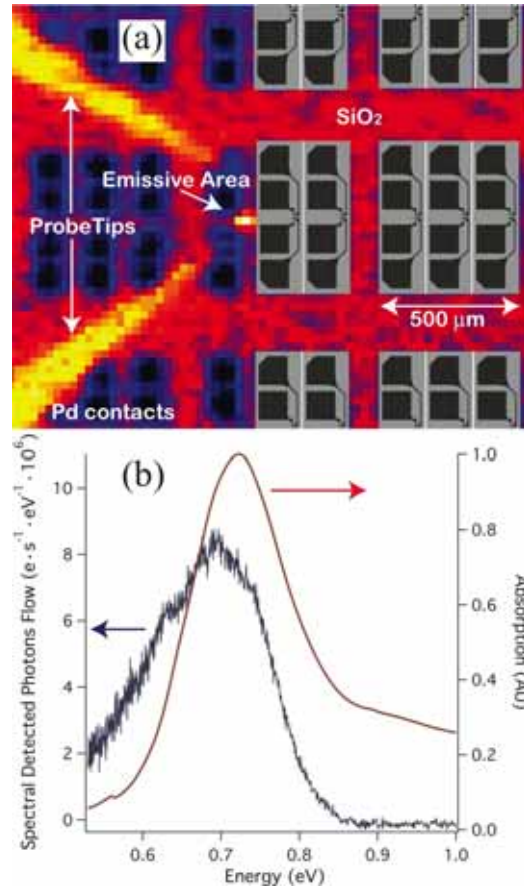


(a) A typical near-infrared image obtained with SIMON using the H filter (0.70 to 0.83 eV) with an exposition time of 30 s. The EL light emission area of the connected transistor is visible on the center of that image. The right part of that image is superimpose with an optical microscope image of the same zone but with a higher resolution. (b) Typical near-infrared electroluminescence spectra for a CNNFET made with laser ablation tubes with the following experimental conditions: Vd=-110V, Vg=-20V, texp=2 min. The absorption curve of laser ablation source is also shows for comparaison.

## References

(1)     J.A. Misewich, R. Martel, Ph. Avouris, J.C. Tsang, S. Heinze, J. Tersoff *Science* **2003**, *300*, 783
(2)     L. Marty, É. Adam, L. Albert, R. Doyon, D. Ménard, R. Martel *Phys Rev Lett* **2006**, *96*, 136803
(3)     J. Chen, V. Perebeinos, M. Freitag, J. Tsang, Q. Fu, J. Liu, P. Avouris, *Science* **2005**, *18*, 1171

# Influence of Vacuum Environment in Conductive AFM measurements on advanced MOS Gate dielectrics

*L. Aguilera[1], W.Polspoel[2], M.Porti[1], W. Vandervorst[2], M.Nafria[1] and X.Aymerich[1].*
*[1]Dept.Eng. Elect., Universidad Autónoma de Barcelona, 08193 Bellaterra, Spain.*
*[2]IMEC,Kapeldreef 75, B-3001 Leuven, Belgium.*

*Lidia.Aguilera@uab.es*

In the recent years, the Conductive Atomic Force Microscopy (C-AFM) has become a very useful technique in the study of the electrical properties of CMOS gate dielectrics at the nanoscale [1-3].  When scanning with the C-AFM technique, the tip gets covered by contaminants (water and hydrocarbons) and loses its conductivity and resolution. This effect is even worse with high-k devices [4,5]. To avoid problems involving anodic oxidation and tip contamination, one possibility is to measure in a controlled ambient. In this work, a setup has been built and tested to study the effect of the environment ambient in the conductive AFM measurements on gate dielectrics.

The vacuum system consists of a commercial C-AFM mounted on a chamber which can reach a pressure of $3 \cdot 10^{-5}$ mbar. The set-up can measure a maximum current of 10pA. In this condition, bipolarity measurements with $SiO_2$ and high-k samples have been performed and evaluated. The samples consist on $SiO_2$ (2nm ISSG on top of n-type Si) and high-k stacks (HfSiO 80%Hf with 700˚C and 1000˚C of annealing) provided to test the system. Measurements with the same C-AFM but in air ambient have been also performed to compare the effect of the environment.  Figure 1 shows the IV mean characteristics measured in a $SiO_2$ sample with the two environments. A shift in the onset gate voltage (voltage needed to measure current just above the noise level) is observed between the two IVs (5V in air and 4V in vacuum). In order to explore this behaviour, current maps have been done by scanning the sample's surface at a constant tip-substrate voltage. The first scans of each sample (fresh dielectric) can be compared to check the initial local conductivity. Here, the amount of current spots (spots of locally higher current), the average and total spot area, and the current magnitude provide insight about the initial local conductivity of the layers. As can be observed from figure 2 , for the same sample but a lower voltage, the amount of leaky spots is bigger in the current map measured in vacuum (figure 2a) than in air (figure 2b) , in agreement with the results presented in figure 1.A possible explanation of this behaviour is a reduction in the layer (water or contaminant) which forms on the tip during the scan. The same kind of experiments has been performed in high-k films to study the loss of conductivity that usually occurs when scanning the surface. To do that, consecutive current map scans on the same area have been done to study the electrical degradation of the layer due to electrical stress. The changes in the amount, area and current magnitude of the spots can be linked to charging and degradation of the layer. Figure 3 shows the consecutive current images obtained during 5V scans measured in vacuum on a high-k sample with 1000°C annealing. The number of leaky spots observed in the current map increases with every new scan and the conductivity in not lost as in figure 2. The same experiment has been performed in air and the conductivity of the tip has been lost after the first scan, so that leaky spots cannot be distinguished anymore. A loss of resolution can also be observed during the scan in air.

As a conclusion, the results show that vacuum environment for CAFM measurements allow for longer tip lifetime and lower onset voltage. This new set up can be used to study different parameters of the high-k materials with more accurate results.

**References:**

[1] Porti M., Aguilera L., Blasco X., Nafria M. and Aymerich X., Microelectron. Eng., **84** (2007) 501-505.

[2] Polspoel W. and Vandervorst W., Microelectron. Eng. **84** (2007), 495-500.

[3] Frammelsberger W., Benstetter G., Kiely J. and Richard S., APPL. SURF. SCI. **253(7)** (2007), 3615-3626.

[4] Petry, J.,Vandervorst, W., Pantisano, L. and Degraeve, R., Microelectron. Reliab., **45 (5)** , (2005),815-818.

[5] Landau S.A., Junghans N., Weiss P.A., Kolbesen B.O., Olbrich A., Schindler G., Hartner W., Hintermaier F., Dehm C., Mazure C . APPL. SURF. SCI.,**157 (4)** (2000) 387-392.

**Figures:**
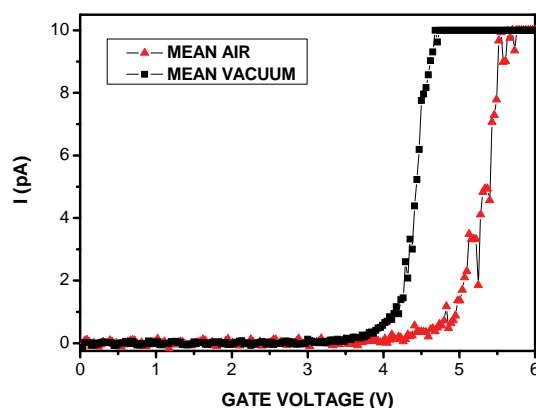


*Figure 1.Average of several IV characteristics of a 2nm SiO2 sample measured in vacuum and air ambient.*
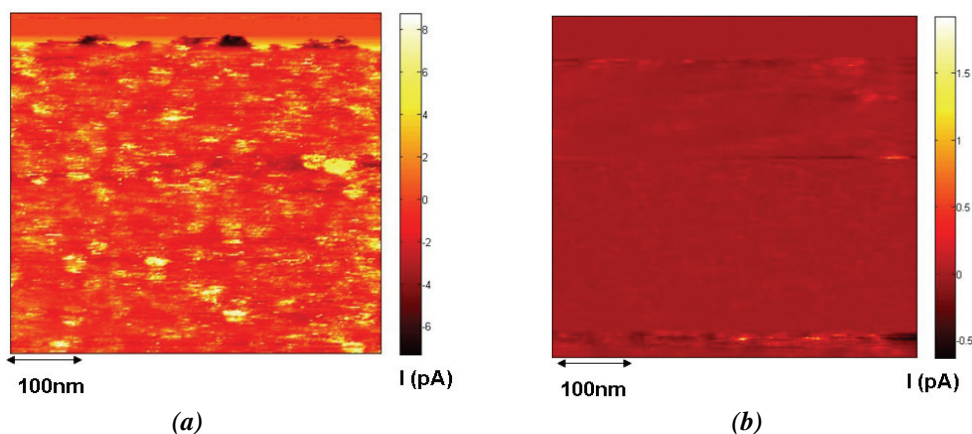


*Figure 2. Current maps measured at constant gate voltage of 4.5V in vacuum (a) and 5.8V in air (b) ambient in SiO$_2$ samples. Measurements in vacuum show better results.*
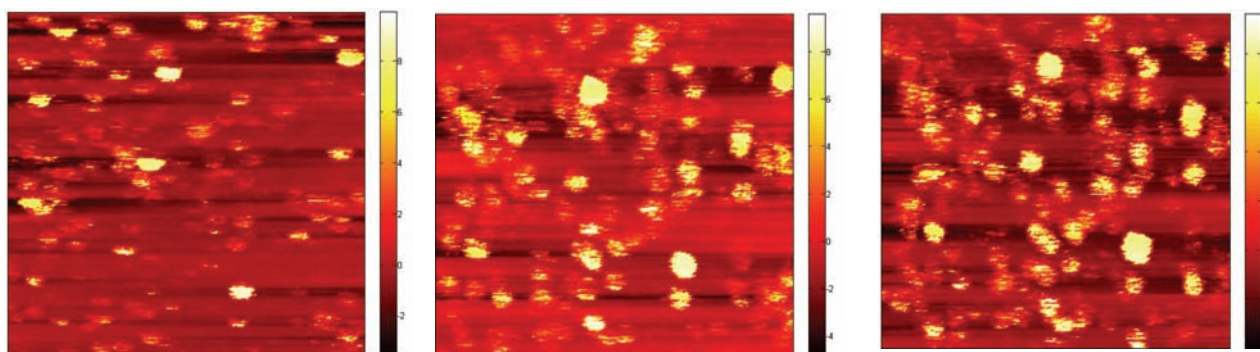


*Figure 3. Consecutive current maps at 5V on the same area of a high- k sample. The measurements were performed in vacuum. The same experiments can not be reproduced in air without loss of tip conductivity.*

# Synthesis and Study of Erbium Doped Zinc Sulfide Nanoparticles by Chemical Capping Method

*Mahshid Ahmadi, Sirus Javadpour, Ali R. Gharavi, Ali A. Khosravi*

*Department of Material Science and Engineering,*
*Eng. Building, Zand St.,*
Shiraz University, Shiraz, Iran.

*ahmadi.mahshid@gmail.com*

In recent years, preparation and study of nanostructured materials has become a growing field of research. II-VI Semiconductor nanoparticles, as an instance, play a significant role in several new technologies. The interest in using semiconductor nanoparticles arises from the fact that these materials are highly applicable in the fields of lighting, displays, laser, sensors, etc. Also doped semiconductors nanoparticles have been widely investigated [1].Doping is very important not only to control the transport properties of the semiconductors but also to modify their optical properties [2].

In the current research, zinc sulfide nanoparticles doped with erbium (ZnS:Er) has been produced at room temperature by aqueous chemical capping method. The study of ultra-violet visible absorption spectrum shows that there is a blue shifting toward a lower wavelength in colloidal nanoparticles compared to the spectrum of bulk samples. As expected the study of ultra-violet visible absorption spectrum Fig .1 shows that there is a red shifting towards a higher wavelength (under 10 nm) in colloidal doped nanoparticles compared to the spectrum of undoped samples.

Debye Scherer equation from XRD pattern was used to calculate the size range of particles which were between 1-3 nano meters. Scanning tunneling microscope confirmed our calculation. It can also be seen clearly that the cubic phase with (111), (220), and (311) planes exists indicating the crystalline nature of the clusters.

In general ,the luminescence process of rare earth in host is represented in terms of energy band level scheme [3].The $Er^{3+}$ ion has $4f^{11}$ electron configuration and the spectra are observed on the excitation spectra 4F  transition of these ions.

Photoluminescence spectroscopy of ZnS:Er, showed transition which belongs to visible emission of  $Er^{+3}$ in Fig 2.  In the present study the peak 520nm and 550nm of luminescence was monitored during pumped by 237nm.  The wavelength is related to the transition of Er ions from ($^2H_{11/2}$) to ($^4I_{15/2}$) and ($^4S_{3/2}$) to ($^4I_{15/2}$) at room temperature.

**References:**

[1] A.A. Koshravi, M. Kundu, B.A. Karuvilla, G.S. Shekhawat, R.P. Gupta, A.K. Sharma, P.D. Vyas, S.K. Kulkarni, Applied. Physics Letters, **67** (1995) 2506.
[2] H.Hu, W. Zhang, Optical Materials, **28** (2006) 536-550.
[3] A.A. Bol, R.V. Beek, A. Meijerink, Chemical Materials, **14** (2002) 1121.

**Figures:**
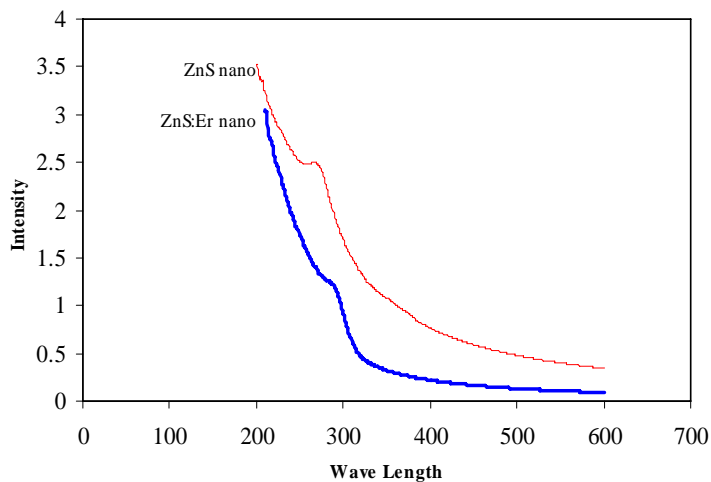
**Fig.1** Absorption spectra for doped and undoped ZnS
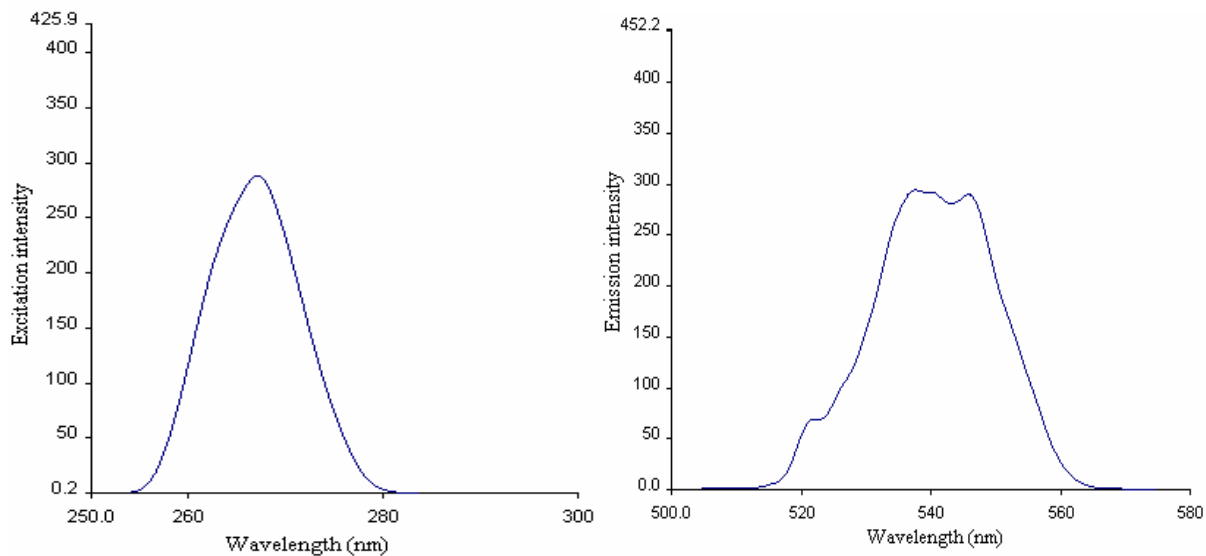
**Fig.2** Excitation and emission spectra of ZnS:Er

# DESIGN AND FABRICATION OF A DCPECVD SYSTEM IN ORDER TO GROWTH OF VERTICALLY ALIGNED CARBON NANOTUBES AND EFFECT OF $C_2H_2$ CONCENTRATON AND PLASMA CURRENT ON THE GROWTH BEHAVIOR OF CNTS

Ahmadzadeh,Fateme [1,2] ; Mojtahedzade larijani, Majid [*1] ; Zolanvari, Abdolali[2]

P1PThe School of Materials, Nuclear Science and Technology Research Institute, P.O.Box:31485-498, Karaj

[2]Physics Department, Arak university, Arak, Iran

[*] : mmojtahedzadeh@nrcam.org

*Abstract- In order to obtain the vertically well-aligned carbon nanotubes (CNTs) at a relatively low temperature with high purity and high yield ,a direct current plasma enhanced chemical vapor deposition (DCPECVD) apparatus has been designed and fabricated. Moreover the effect of $C_2H_2$ concentration and plasma current on growth of CNTs has been investigated .The synthesis of DCPECVD CNTs has been carried out in the presence of plasma in two steps: i) reduction step with $H_2$ and $NH_3$ gases for formation of catalyst nano particles, ii)subsequent CNTs growth step with $H_2$ and $C_2H_2$ gases. High-resolution transmission electron microscopy images clearly demonstrated the nanotubes to be multiwalled, and the graphitized structures were confirmed from the Raman spectra. Besides the results of scanning electron microscopy (SEM) clearly highlights the link between the plasma, $C_2H_2$ amount and CNTs structure. With increase or decrease amount of acetylene from a certain flow rate, cause to destruction results. A comparison between the micrographs of CNTs grown with and without plasma, illustrates that plasma play an important role on the formation of vertical and aligned CNTs.*

*Keywords: CNTs, Carbon nanotubes, PECVD, SEM*

.

# NEW TRENDS AND ACHIEVEMENTS IN PRODUCTION OF NANOFIBERS-BASED FILTER MEDIA

*M. Akbari, H. Ghanadzadeh, M. Hasanzadeh, A. K. Haghi*[*]
*The university of Guilan, P. O.Box 3756, Rasht, Iran*
*\*Corresponding author e-mail: Haghi@Guilan.ac.ir*

**Abstract:**

The use of fine fiber has become an important design tool for filter media. Nanofibers based filter media have some advantages as lower energy consumption, longer filter life, high filtration capacity, easier maintenance, low weight rather than other filter medias [1-3].The nanofibers based filter media made up of fibers of diameter ranging from 100 to 1000 nm can be conveniently produce by electrospinning technique (Figure 1)[4,5]. Common filter media have been prepared with a layer of fine fiber on typically formed the upstream or intake side of the media structure. The fine fiber increases the efficiency of filtration by trapping small particles which increases the overall particulate filtration efficiency of the structure. Improved fine fiber structures have been developed in this study in which a controlled amount of fine fiber is placed on both sides of the media to result in an improvement in filter efficiency and a substantial improvement in lifetime.

In this research, regenerated silk fibroin obtained from industrial silk wastes were used to produce filter media. Figure 2 shows a typical cross section of SEM for nanomatt based silk fibroin nanofiber produced.

Characteristics such as fibers diameter and its distribution, representative pore size, porosity and matt thickness of nanofiber filters which obtained in lab was examined by scanning electron microscopy (SEM).The air permeability of  this new nanofilter was investigated using  air flow meter instruments.

**References:**

 [1] R. Gopal, S. Kaur, Z. Ma, C. Chan, S. Ramakrishna, T. Matsuura, Journal of Membrane Science, **281** (2006) 581–586.
[2] Y.C. Ahn, S.K. Park, G.T. Kim, Y.J. Hwang, C.G. Lee, H.S. Shin, J.K. Lee, Current Applied Physics, **6** (2006) 1030–1035.
[3] R.S. Barhate, C. K. Loong, S. Ramakrishna, Journal of Membrane Science, **283** (2006) 209–218.
[4] A.K.Haghi  and  M. Akbari, *Physica Status Solidi*, DOI  , 2007.
[5] A.K.Haghi , M. Akbari and V. Mottaghitalab, *"Electrospinning of natural fibers"* , Book Chapter: in "Natural Fiber Reinforced Polymer Composites" Edited by S. Thomas and L.A. Pothan, Old City Publishing, USA,( 2007).
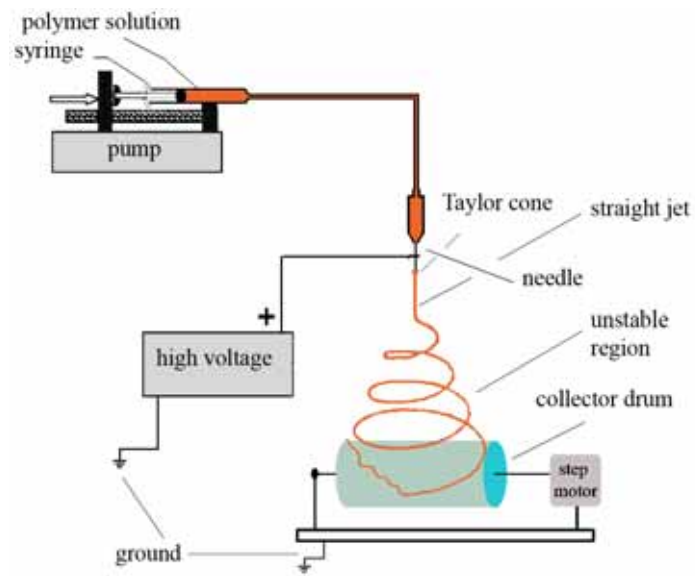
Figure1. Schematic of electrospinning set up for producing nanofilter.
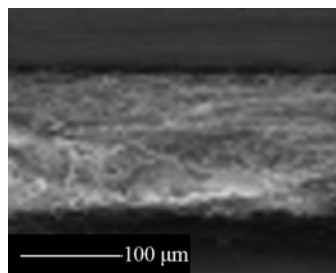


Figure2. Scanning electron microscopy of cross sectional silk fibroin nanofiber matt.

# CALCIUM UPTAKE BY NANOHYDROXYAPATITE CRYSTALS, IN COMPOSITE MATERIALS WILL CHANGE CELL CULTURE MEDIUM PROPERTIES.

*Jose Iñaki Alava, Beatriz Olalde, Maria Jesus Jurado, Nerea Garagorri.*
Health Unit, INASMET-Tecnalia, Paseo de Mikeletegi nº2, San Sebastian, 20009, Spain
ialava@inasmet.es

**Introduction.**
During the development of composite materials for cell proliferation and grow, selection of nano or micro fillers is a key question. Many authors have reported anomalous response of cells in culture when used nanohydroxyapatite (1,2,3). This work shows the effect of hydroxyapatite crystal size on cell culture medium properties when the composite scaffold is exposed.

**Material and Methods.**
Scaffold Production. In this process, the nanoparticles: single walled carbon nanotube (SWNT) and nanohydroxyapatite (nHAp) or microhydroxyapatite (mHAp) are dispersed through out the solvent, made of Dioxane (Dx) and water (87/13), in an ultrasound bath and over 30 minutes. Then, the poly(L-lactic acid) (PLLA) is added and the suspension is sonicated at 65ºC until the polymer is completely dissolved (3 hours). Finally, the temperature of the solution is quickly decreased to induce phase separation, that is, to form 2 separated phases: One having a higher polymer concentration (polymer-rich phase) and a second phase that is lower in polymer concentration (polymer-lean phase). After the solvent has been removed by sublimation, the polymer rich phase solidifies into the skeleton of the scaffold, and the spaces occupied by the solvent in the polymer-lean phase become the pores of the polymer foam. Scaffolds with these fixed characteristic were manufactured: Quenching temperature (Tq: -16ºC); Solvent ratio (Dx/H2O: 87/13); And the process variables were: the percentage of HAp and the grain size of HAp particles .Cells and culture medium. Osteoblast (ATCC, CRL-11372) cells have been used. A unique culture medium was used for the osteoblast (ATCC, CRL-11372). Each 200 ml of culture medium contained: 20 ml foetal bovine serum (FBS), 2ml Penicillin (1% h/v), 1080 µl Gentamicine (0.5% h/v), 2ml Glutamine (1% h/v), 174.92 ml MEM-F12 de ATCC. All the scaffolds were sterilized by Ethylene Oxide. Assay methodology After the sterilization process, all scaffolds were immersed in the culture medium at 37ºC for 1 week. The material-culture medium ratio was, approx., 20mg of scaffold per 1ml of medium. The same culture medium was used through out the week (it wan not replaced) in order to maximize the reactivity. Finally, after periods of 24h, 48h, and 6 days, the samples were removed from the culture medium and both the scaffold and the medium were characterized. Culture medium analysis. Determination of pH changes, samples were kept in culture medium at 37ºC. After 24, 48 hours and 6 days, the scaffolds were removed from the culture medium and the pH of the medium was tested electrochemically at 37ºC with partial pressure of CO2 compensation. (4). Evaluation of ions content was done, in the culture medium (calcium, phosphate, phosphorus, magnesium) by Inductively coupled plasma-atomic emission spectrometry (ICP-AES ) (4). Cytotoxcity after a cell-medium contact of 24h, cells were collected to put in contact with the extract of the sample during several hours. After that, the quantitative evaluation (staining collected cells with 7-Amino-Actinomycin D and quantifying the number of cells by a flow cytometry method (TruCOUNT Tubes, Beckton & Dickinson) of cell cultures were made.

**Results**
Fig (1). Firstly, when the percentage of hydroxyapatite increases from 1% to 10%, the effect on the pH is bigger, it decreased more. For example, the scaffold behaviour made of 10% of nanoHAp when kept in contact with the culture medium, induced a pH decrease of 7.40, but when 1% of the same CaP was used, this value was 7.43.And also, the effect of micro size HAp (mHAp) on the pH values is lower than the effect of the nano sized one (nHAp), due to the bigger grain size. For example, over 6 days, the pH of ref.10% nHAp was 7.40, while the

pH of the ref.10%mHAp was 7.42. Secondly, the nanoparticles dispersion into the foam could affect to the pH of the culture medium. Focusing on the samples 10% nHAp, where the scaffold composition was the same and the principal difference was the nanoparticles mixing method, the samples 10% nHAp shown a bigger decrease from the first stages. And all of this happens despite the fact that the change in the pH over the 6 day-period was similar. This behavior should be due to the poor dispersion of the nHAp into the foam. In general, Ca and P concentrations decreased in all culture medium that have been in contact with the scaffold. The scaffolds made of low percentage of nano and microHAp, 1%, show a slight decreased of these ions contents in the culture medium. However, the sample with 10% of nHAp or mHAp present a higher decreased. The culture medium that has been in contact with the scaffold made of 10% of nHAp the Ca and P concentration decreased down to 44 and 26 mg/l, and when the scaffold has 10% of mHAp, these values are 58 and 31 mg/l, respectively Fig. (2). On the other hand, the lowest obtained values for the percentage of the growth of cells are 70% (in the case of the 1% mHAp sample after 24 hours of lixiviation) and 77% (in the case of the 10% nHAp sample after 24 hours of lixiviation). In anyway, these percentages are not low enough to consider cytotoxic extracts for the bone cells, but one small inhibition of cell grow will be observed.

**Conclusion.**

This confirms that the presence of high nanocrystalline HA percentage, depletes the calcium and phosphorous and the effect of micro size HAp is lower due to the bigger grain size. This effect is attenuated when the percentage of HAp is lower. It can be concluded that the tested extracts of the samples are non-cytotoxic and there is no enough difference between the cytotoxicity of them. This work has been supported by EC inside Nanobiocom Project –NMP3-CT-2005-516943.

**References:**

(1) Xiaoming Li, Qingling Feng, Fuzhai Cui. Materials Science and Engineering **C 26** (2006) 716 – 720.

(2) Sang-Soo Kim, Min Sun Park, So-Jung Gwak, Cha Yong Choi, and Byung-Soo Kim. Tissue Engineering, **12**, Number 10, 2006.

(3) Sánchez-Salcedo S, Izquierdo-Barba I, Arcosand D, Vallet-Regí. M. Tissue Engineering **12**, 279-290 (2006)

(4) Standard Methods for the Examination of Water and Wastewater 20th edition

**Figures**
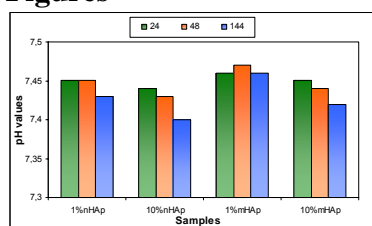


Fig.1: Evolution of pH of culture medium as a function of time in contact with different scaffolds
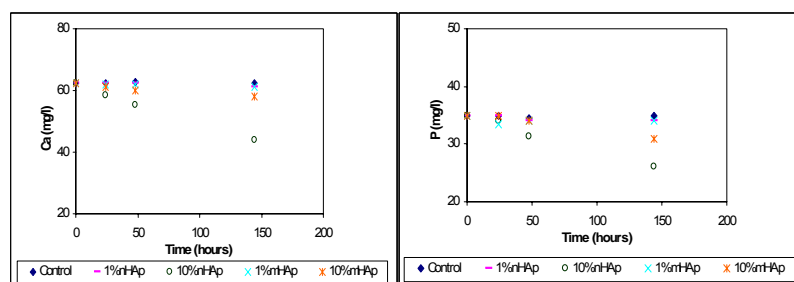


Fig.2: Evolution of Ca and P content of Medium in depended of the scaffold kind
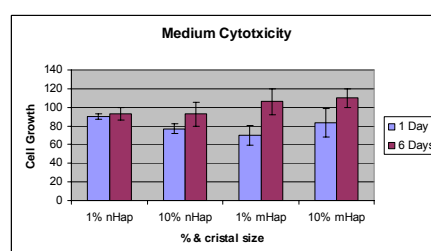


Fig 3: Induced cytotoxicity in the medium

# Pt and PtRu nanoparticles supported on ordered mesoporous carbons as electrocatalysts for Direct Methanol Fuel Cell anodes

*F. Alcaide[a], G. Álvarez[a], O. Miguel[a], L. Calvillo[b], M. J. Lázaro[b], J.J. Quintana[c], J.R.C. Salgado[c], E. Pastor[c], I. Esparbé[d], P. L. Cabot[d]*

*[a]Dpto. de Energía, CIDETEC, Pº Miramón, 196, 20009 Donostia/San Sebastián. [b]Instituto de Carboquímica, CSIC, Miguel Luesma Castán 4, 50018 Zaragoza. [c]Dpto. Química Física, Universidad de La Laguna, Avda. Astrofísico Francisco Sánchez s/n, 38071 La Laguna, Santa Cruz de Tenerife. [d]Dpto. Química Física, Universitat de Barcelona, Martí i Franquès, 1-11, 08028 Barcelona*

*falcaide@cidetec.es*

Direct Methanol Fuel Cells (DMFCs), which use liquid and renewable methanol fuel, are attracting much attention for portable applications, because liquid methanol has got a high energy density, and it can be easily stored and transported. In addition, it avoids the use of a reforming unit in the fuel cell system and simplifies the balance of plant.

On the other hand, the success of these fuel cells systems requires a further development of new DMFC anode catalysts with high performance and low cost. The most effective way to approach this task is to explore new catalyst materials (noble and non-noble metals) and supports (carbon nanomaterials, metal oxides,…), because supported electrocatalysts can lower the noble metal loading in fuel cell electrodes [1].

Methanol electrooxidation takes place over the surface of the metal nanoparticles located in the active layer of the DMFC anode, which is also responsible for the transport of reactants a and reaction products. Conventional carbon blacks usually used as a catalyst support lead to a low degree of catalyst utilization due to the relative abundance of micropores (< 2 nm), so that the catalyst particles deposited inside them remain inaccesible to the fuel. In this sense, the use of mesoporous ordered carbons (OMC) with controlled pore size in the range of 2-50 nm, can enhance the utilization and dispersion of metal catalyst.

In this presentation we report the electrocatalytic activity of Pt and PtRu nanoparticles supported on ordered mesoporous carbons towards methanol electrooxidation in a DMFC environment. OMC used as catalyst support were synthetized via mesoporous silica SBA-15 as templating material and had a specific area of 570 $m^2$ $g^{-1}$. Their hexagonally ordered structure was maintained after oxidation treatments in liquid phase using nitric acid as oxidizing agent [2]. OMC were used as platinum and platinum/ruthenium catalyst support using the method of reduction with $NaBH_4$ or HCOOH acid [3].

The results reported in this poster illustrate that DMFC anodes made with Pt nanoparticles supported on ordered mesoporous carbons show a good performance towards methanol electrooxidation. This behavior is enhanced using PtRu nanoparticles as anode catalyst.

## Acknowledgments

**References:**

[1] M.J. Lázaro, L. Calvillo, E.G. Bordejé, R. Moliner, R. Juan, C.R. Ruiz, Microporous Mesoporous Mat., **103** (2007) 158.

[2] L. Calvillo, M.J. Lázaro, E.García-Bordejé, R. Moliner, P.L. Cabot, I. Esparbé, E. Pastor, J.J. Quintana, J. Power Sources, **169** (2007) 59.

[3] H. Liu, C. Song, L. Zhang, J. Zhang, H. Wang, D.P. Wilkinson, J. Power Sources, **155** (2006) 95.

**Figures:**
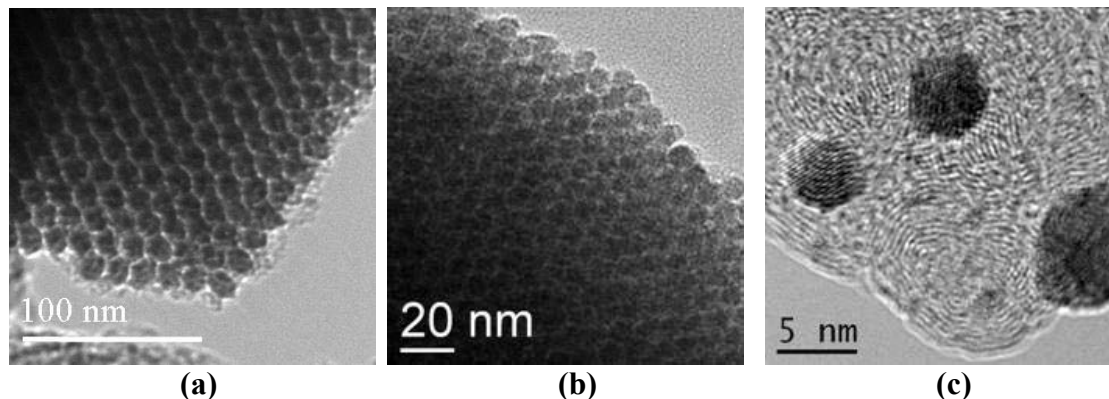


Fig. 1. TEM micrographs: (a) CMK-3 carbon, (b) CMK-3 carbon treated with $HNO_3$ (from ref. 1 and ref. 2, respectively), and (c) PtRu supported nanoparticles.
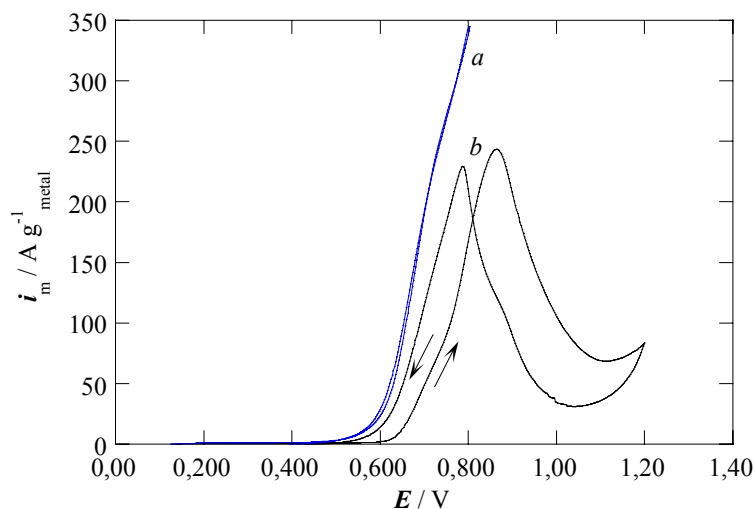


Fig. 2. Cyclic voltammograms of methanol oxidation on DMFC anodes catalyzed by: (a) PtRu/CMK3-Nc0.5 and (b) Pt/CMK3-Nd0.5, in 2.0 M $CH_3OH$ + 0.50 M $H_2SO_4$. T = 60°C. $v_b$ = 20 mV s$^{-1}$.
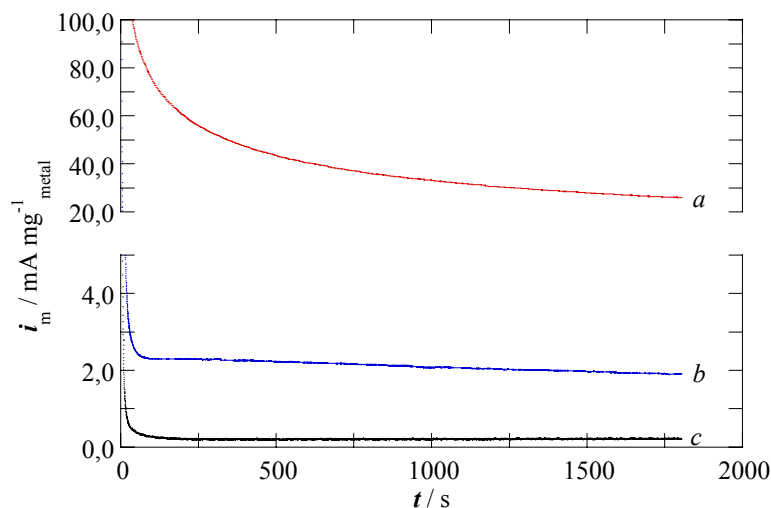


Fig. 3. Chronoamperometric curves of methanol oxidation on DMFC anodes catalyzed by: (a) PtRu/CMK3-Nc0.5, (b) Pt/CMK3-Nd0.5, and (c) Pt/CMK3-Nc2h in 2.0 M $CH_3OH$ + 0.50 M $H_2SO_4$. T = 60°C. $v_b$ = 20 mV s$^{-1}$.

# NANOPARTICLE ORGANIZATION AND ADVANCES IN STRUCTURAL DNA NANOTECHNOLOGY

*Faisal A. Aldaye* and *Hanadi F. Sleiman*[*]
*McGill University, 801 Sherbrooke St. W., Montreal QC H3A 2K6, Canada*
*hanadi.sleiman@mcgill.ca*

One of the central challenges of nanoscience is the organization of functional components according to a deliberately designed pattern, and the ability to modify this pattern at will. Because of its molecular recognition specificity and structural features, DNA presents a unique opportunity to address the above goal. Our research group has been examining the creation of branched DNA molecules containing organic vertices, and the study of their self-assembly into discrete, as well as extended DNA nanostructures.

(a) We discuss a method in which six gold nanoparticles are assembled into a well-defined discrete hexagonal arrangement. The approach involves labeling the individual nanoparticles with DNA containing building blocks that dictate their final location within the constructs.[1]

(b) We also report a straightforward method to selectively organize gold nanoparticles into libraries of discrete and well-defined structures, using a small number of single-stranded, dynamic DNA templates.[2] This approach not only provides the ability to finely control the geometry of the assembly, and the precise position of each nanoparticle, but it also allows for the modification and tuning of these structural features post- assembly. As such, the resulting nanoparticle groupings can undergo structural switching and write/erase functions in response to specific external agents. Access to libraries of precisely positioned particle groupings will allow for the systematic examination of their optical, electronic and catalytic properties as a function of their structure, and will also lead to advances in the use of these particles as components of nanoelectronic and nanophotonic circuitry, plasmonic tools, and surface-enhanced Raman scattering substrates.

(c) As the structural size and complexity of such artificial DNA architectures increases, so will the number of coding DNA sequences that will need to be designed. This inevitably results in overlapping, degenerate sequences that may assemble into undesirable products. We report the first example of guest mediated access to a *single DNA nanostructure*, from building blocks containing identical DNA strands that otherwise generate a complex library of multiple DNA assemblies. This guest template also re-equilibrates every other member of this self-assembled mixture into the same single nanostructure. The addition of a small DNA-binding molecule to alter and refine product outcome in DNA self-assembly not only allows for the incorporation of symmetry to construct more complex systems, but also presents the immediate advantage of auto-correcting errors that may form during the initial self-assembly process. We further applied this approach to predictably construct well-defined one-dimensional DNA fibers extending over tens of microns using two trifunctional DNA building blocks that otherwise generate ill-defined oligomeric networks.[3] Considering the wealth of DNA-binding molecules which can be employed to tune, modify and correct the assembly of DNA structures, this finding promises to lead to significant advances in the field of DNA nanotechnology.

**References:**

[1] Faisal A. Aldaye and Hanadi F. Slieman, *Angew. Chem. Int. Ed.*, **45** (2006) 2204-2209.
This contribution was also selected by the editors as a 'hot paper' and received its own cover page.

[2] Faisal A. Aldaye and Hanaid F. Sleiman, *J. Am. Chem. Soc.*, **129** (2007) 4130-4131.
This contribution was highlighted by *Nature Nanotechnology*, **2** (2007) 264.

[3] Faisal A. Aldaye and Hanadi F. Sleiman, *J. Am Chem. Soc.* (2007) *accepted*.

**Figures:**

(a)           (b)           (c)
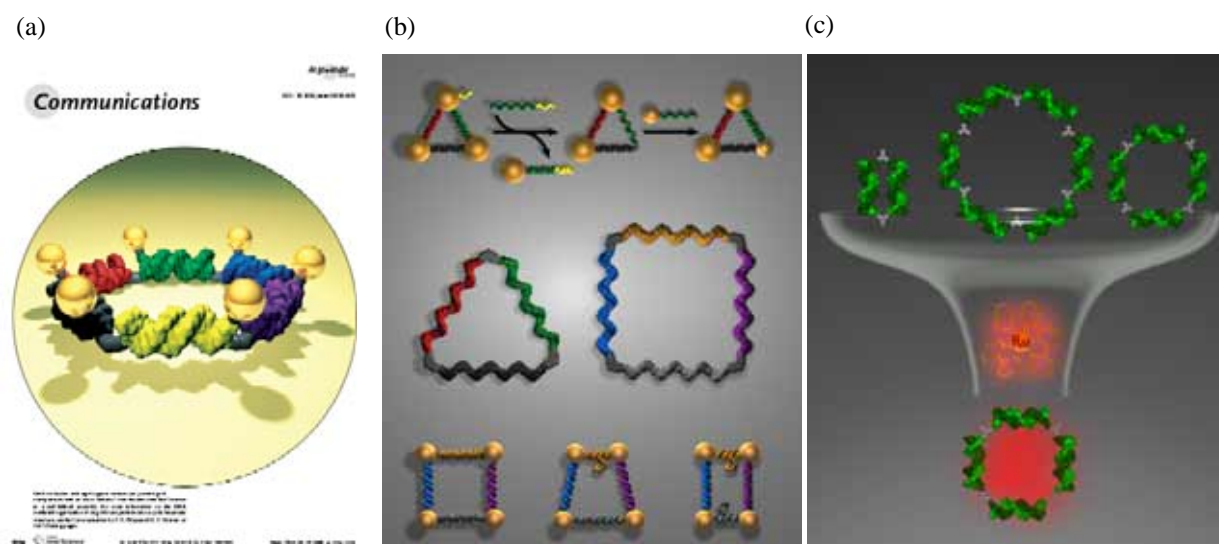
# Diffusion simulation of Cr-Fe bcc systems at atomic level using a random walk algorithm

*I. San Sebastian[1], J. Aldazabal[1], C. Capdevila[2], C. Garcia-Mateo[2]*

[1] *CEIT and Tecnun (University of Navarra), Paseo Manuel de Lardizábal 15, 20018 San Sebastián, Spain*
[2] *MATERALIA Research Group. Department of Physical Metallurgy, Centro Nacional de Investigaciones Metalúrgicas (CENIM-CSIC), Avda. Gregorio del Amo 8, E-28040 Madrid, Spain*

*jaldazabal@ceit.es*

From a "macroscopic" point of view, material composition is assumed to vary smoothly along its microstructure. A closer look reveals that, at the atomic level, the material composition does not change so smoothly. Single atoms jump randomly along the crystal lattice due to their thermal energy. These random jumps create sporadic zones of the crystal with higher concentration of certain elements, and they are responsible for many phenomena, such as spinodal decomposition, segregation, precipitation, Ostwald ripening… This work simulates the diffusion of Cr and Fe in a Fe-Cr system at atomic level. Simulated temperatures are in the range of 650-750 K, where the atomic structure of both isolated compounds are bcc.

The full 3D model developed takes into account for the random jumps of substitutional Cr through the Fe-bcc lattice sites, neglecting the system vacancies at this temperature [1]. The model was applied to simulate the evolution of a flat composition front in a prismatic domain. This domain was divided into small prisms to run simulation in a cluster of computers in parallel. The cluster used consist of 24 Pentium IV processors at 2.6 GHz and requiring about 13 GB of physical memory [2].

A set of simulations was run to study the relationship between the atomic jump rate and the macroscopic-continuum diffusion coefficient. This study was performed using continuum calculations using Dictra™ software [3]. Figure 1 shows concentration profiles obtained by the proposed model after 3761 jumps of each Cr atom and Dictra results for a diffusion time of 3072 hours at 748 K.

Different set of simulations was run to study the relationship between jump rate and temperature. Results of this part are represented in figure 2. These results were fitted to an Arrhenius type equation, allowing for the determination of the Cr atomic jump activation energy at 306 kJ/mol, which is in good agreement to the empirical value of Cr diffusion in Fe-bcc, 250 kJ/mol [4].

The results obtained by means of the model will be useful to study at atomic scale phenomena, such as the Cr segregation in Fe based alloys, or the spinodal decomposition that takes place in these materials at low temperatures.

**References:**

[1] J. Aldazabal, C. Garcia-Mateo, *Materials Science Forum*, **500-501** (2005) 719-726.
[2] M. Creel, http://idea.uab.es/mcreel/ParallelKnoppix (Online March 2007).
[3] Dictra User's guide (Dept. Of Materials Science and Engineering) Royal Institute of Technology, Sweden (1998) 63-71.
[4] A.W. Bowen, G.M. Leak, *Metallurgical Transactions*, **1** (1970) 1695-1700

**Figures:**
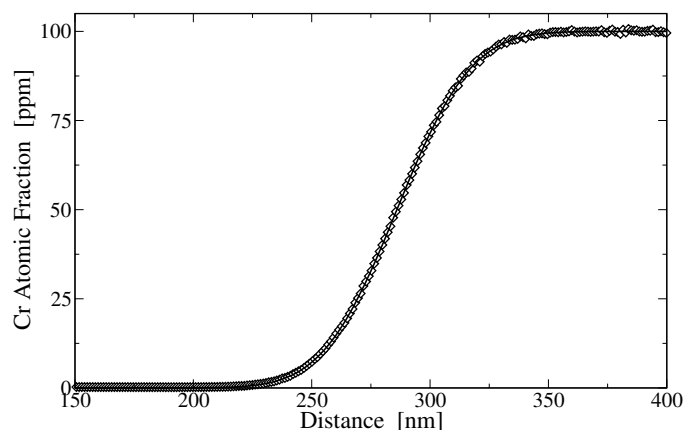


**Figure 1:** Comparison of concentration profiles obtained using proposed model after 3761 jumps of each Cr atom and continuum Dictra calculation for 3072 hours@748 K.
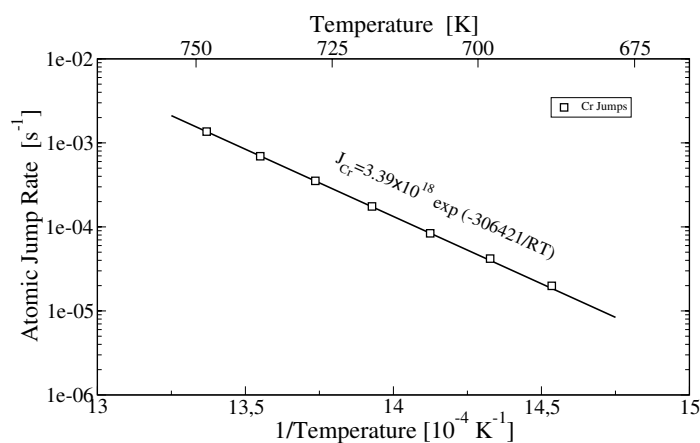


**Figure 2:** Simulated atomic jump rate of Cr in a pure bcc Fe matrix at different temperatures and its Arrhenius fitting.

# Simulation of effective atomic movements of substitutional impurities in cs, fcc and bcc lattices using a random walk algorithm

*J. Aldazabal*[1], *I. Aldazabal*[2]

[1] *CEIT and Tecnun (University of Navarra),*
*Paseo Manuel de Lardizabal 15, 20018 San Sebastián, Spain*

[2] *Departamento de Física de Materiales, Facultad de Químicas UPV/EHU,*
*Apartado 1072, 20080 San Sebastián, Spain*

*jaldazabal@ceit.es*

From a "macroscopic" point of view, material composition is assumed to vary smoothly along its microstructure. A closer look reveals that, at the atomic level, the material composition does not change so smoothly. Single atoms jump randomly along the crystal lattice due to their thermal energy. These random jumps create sporadic zones of the crystal with higher concentration of certain elements, and they are responsible for many phenomena, such as spinodal decomposition, segregation, precipitation, Ostwald ripening… This work obtains some useful relations between atomic jumping rate and macroscopic diffusivity, for substitutional impurities in simple cubic, face-centred cubic and body-centred cubic atomic lattices.

To simulate the diffusion of these impurities a random walk based parallel code was developed. This code handles two main elements, individual lattice cells and individual atoms. From the point of view of cells, the program knows the position of all system cells and their amount of impurities. From the point of view of atoms the code knows the position of each atom, via the cell that it belongs to. To simulate the diffusion, the program moves sequentially all impurities present in the system. On each diffusion step, each impurity is swapped with one of its nearest neighbours. The neighbour used for each swap is randomly chosen for each diffusion step and for each impurity [1].

Due to the fluctuations of the composition at atomic scale results obtained with the model are very noisy. In order to obtain statistically significant results we simulate systems with a huge number of atomic cells, to average the random nature of the model. Results shown in this work were obtained simulating a 1000×1000×1000 cells microstructure. To avoid border effects, periodical boundary conditions were applied to these microstructures [2].

A set of simulations was performed to obtain the relation between the macroscopic diffusivity and the atomic jumping frequency. The simulated microstructure consists on a prism initially divided in two halves, one of them without any impurity and the other one with an initial concentration of impurities of 100 ppm. These impurities are randomly placed within the second half of the prism. Once the initial microstructure is generated, atoms are allowed to jump. The evolution of the simulated concentration profile is compared, after each diffusion step, with the profile obtained analytically for a known diffusivity and for a fixed time [3]. From the diffusion steps needed to match the analytical profile it is possible to determine the atomic jumping frequency that corresponding to that diffusivity. Figure 1 shows the results for the atomic jumping frequency obtained for 3 different atomic lattices; simple cubic, body-centred cubic and face-centred cubic, with a lattice parameter of 1 nm.

From analytical-continuum results, and assuming that jumping frequency, $\Gamma$, is proportional to the diffusivity, $D$, it is possible to obtain the relation between the jumping frequency and the crystallographic cell size, $a$. Relations shown in equation 1 were obtained by matching simulations with these analytical calculations.

$$\Gamma_{cs} = 5.91 \, D / a^2$$
$$\Gamma_{bcc} = 3.93 \, D / a^2 \qquad (1)$$
$$\Gamma_{fcc} = 6.17 \, D / a^2$$

Only the simple cubic case agrees with the Einstein's Formula [4]. For the other two cases, the number of nearest neighbours, 8 and 12 for bcc and fcc cases respectively, and the distance between atoms, $\lambda_{bcc} = \sqrt{3}/2$ and $\lambda_{fcc} = \sqrt{2}/2$, do not make possible this agreement.

From the results obtained in this work it is possible to obtain, from the macroscopic diffusivity, the atomic jumping frequency needed to simulate the diffusion of substitutional impurities in cs, bcc and fcc lattices.

**References:**

[1] P.G. Shewmon: "Diffusion in solids", *Ed. McGraw-Hill*, (1963), pp. 47-54.
[2] D. Raabe: "Computational materials science: simulation of materials, microstructures and properties", *Ed. Wiley-VCH*, (1998), pp. 102-104.
[3] J. Crank, "The Mathematics of Diffusion", *Ed. Oxford University Press*, Uxbridge (1956), pp. 137-159.
[4] M.E. Glicksman, "Diffusion in Solids", *Ed. Wiley-Interscience*, (2000), pp. 207-209.

**Figures:**
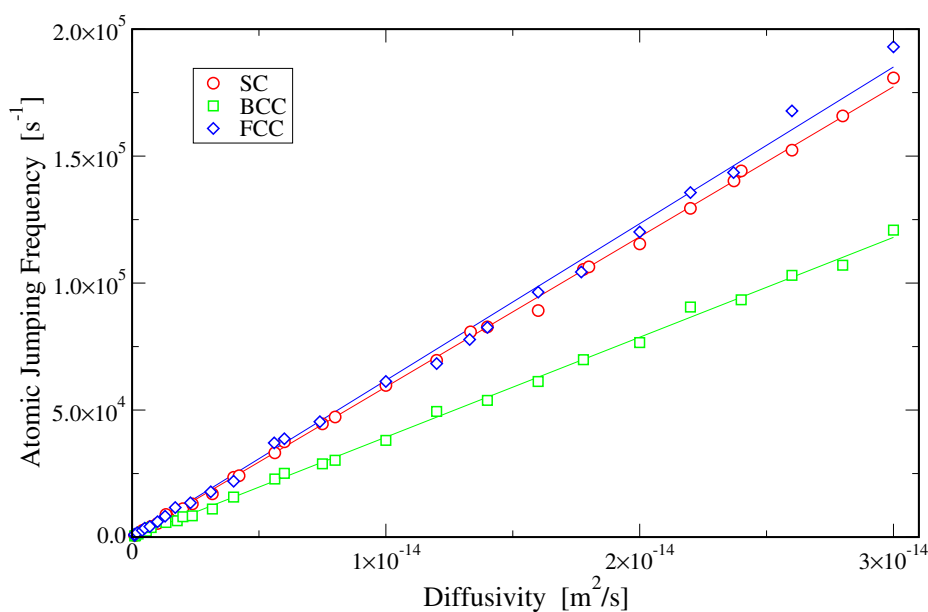


**Figure 1**: Atomic jumping frequencies needed to simulate different diffusivities for SC, BCC and FCC lattices, for a cell size of 1 nm.

# What rules the reactivity of thermal $N_2$ molecules on W surfaces?

<u>M. Alducin</u>,[1] G. A. Bocan,[1] H. F. Busnengo,[2] R. Díez Muiño,[1,3] J. I. Juaristi,[4] and A. Salin[1]

[1]*Donostia International Physics Center DIPC, San Sebastián, Spain*
[2]*Universidad Nacional de Rosario, Rosario, Argentina*
[3]*Centro de Física de Materiales CSIC-UPV/EHU, San Sebastián, Spain*
[4]*Departamento de Física de Materiales UPV/EHU, San Sebastián, Spain*
wapalocm@sq.ehu.es

The knowledge at atomic scale of the electronic properties and dynamical processes that rule gas–surface reactivity is crucial to understand and control key processes as oxidation, corrosion, hydrogen storage and heterogenous catalysis, among others. In the past, the theoretical analysis of surface reactivity was limited by the difficulty to provide a reliable description of all the variables involved in this kind of processes. The recent development of theoretical methods, based on ab initio calculations of the multidimensional potential energy surface, allows now a quite accurate description of the molecule–surface interaction. This achievement has contributed to get new insight into the field: assumptions that were conventionally accepted are currently questioned in view of the results obtained with more refined calculations. Our recent study on the dissociation of $N_2$ molecules on the W(110) surface is a good example of it [1, 2].

Early studies based on work function measurements and flash desorption spectroscopy showed that $N_2$ on W has the largest crystallographic anisotropies as regards adsorption yields and sticking coefficients [3, 4]. Later measurements of the initial sticking coefficient $S_0$ as a function of the $N_2$ initial kinetic energy $E_i$ showed that, while dissociation is considerable for vanishingly small beam energy on the W(100) surface [5], it is roughly two orders of magnitude smaller at T=800K on the W(110) face [6]. This remarkable difference in reactivity has been conventionally attributed to the non-activated and activated characters of the two processes respectively. It has been shown [7] that the high reactivity on the (100) surface is indeed associated with the fact that the $N_2$/W(100) system is non activated, i.e., there exist paths leading to dissociation without any energy barrier. On the (110) surface of W, however, the dissociation probability is of the order of a few $10^{-3}$ for beam energies below 300 meV, it increases rather quickly towards 0.2 until 1 eV, and goes on rising more smoothly until a value of 0.3 for an energy of 2.5 eV [6]. This behavior is usually considered as typical of that of an activated system, i.e., no path leads to dissociation without overcoming a barrier.

Using density functional theory to calculate the six dimensional potential energy surface and classical dynamics, we show that the large difference in reactive behavior between the (100) and (110) faces at low energies is entirely determined by the shape of the potential energy surface far from the surface (above 3 Å) [1, 2]. The explanation therefore lies neither on the geometry and energy of the final state (2 N atoms on the surface) nor on the presence or absence of an intermediate well in which the molecule could be temporarily trapped. Such a well exists for both the (110) and (100) faces. The crucial point is that only for the latter the well is accessible to low-energy molecules. We also show that there are non-activated paths to dissociation in the interaction of $N_2$ with W(110) surfaces. Nevertheless, the value of the sticking coefficient $S_0$ at low impact energies $E_i$ is very small. This result contradicts the standard along which dissociation probabilities that increase with the incident kinetic energy are the result of a direct activated process. Furthermore, it contravenes the common assumption that intermediate states (such as

dynamic trapping in our case) and non-activated paths always result in large values of the sticking coefficient at very low energies.

Finally, we will also investigate a new open question under discussion, the validity of the adiabatic approximation in the description of thermal molecules interacting with surfaces. Most of the theoretical studies that analyze gas–surface reactivity are based on such an approximation, that neglects energy dissipation effects. Here, we present a model to include the contribution of electron–hole excitations to the molecular dynamics and analyze under which conditions this energy dissipation channel can be relevant.

––––––––––

[1] M. Alducin, R. Díez Muiño, H. F. Busnengo, and A. Salin, Phys. Rev. Lett. **97**, 056102 (2006).
[2] M. Alducin, R. Díez Muiño, H. F. Busnengo, and A. Salin, J. of Chem. Phys. **125**, 144705 (2006).
[3] P.W. Tamm and L.D. Smith, Surf. Sci. **26**, 286 (1971).
[4] S. W. Singh-Boparai, M. Bowker, and D. A. King, Surf. Sci. **53**, 55 (1973).
[5] C. T. Rettner, E.K. Schweizer, H. Stein, and D.J. Auerbach, Phys. Rev. Lett. **61**, 986 (1988); C. T. Rettner, H. Stein, and E. K. Schweizer, J. Chem. Phys. **89**, 3337 (1988).
[6] H. E. Pfnür, C. T. Rettner, J. Lee, R. J. Madix, and D. J. Auerbach, J. Chem. Phys. **85**, 7452 (1986).
[7] G. Volpilhac and A. Salin, Surf. Sci. **556**, 129 (2004).

# EFFECT OF CONFINEMENT IN SEGREGATED BLOCK COPOLYMER ON THE POLYMER COMPONENTS MOLECULAR MOTIONS

*Angel Alegria#; Reidar Lund*; Juan Colmenero*#, Lutz Willner+ and Dieter Richter+*
*# UPV/EHU: Departamento de Física de Materiales /Centro de Física de Materiales (Centro Mixto CSIC-UPV/EHU), Universtity of the Basque Country, Donostia/San Sebastián, Spain.*
*\* Donostia International Physics Center, Donostia/San Sebastián, Spain.*
*+ Insititute of Solid State Research, Forschungszentrum Jülich, 52425 Jülich, Germany.*
*angel.alegria@ehu.es*

Block copolymers spontaneously self-assemble into well defined structures with variable geometry (spherical, cylindrical, lamellar etc) depending on the chemical details (molecular structure, composition etc) and external conditions such as temperature and pressure. This structure formation, typically in the range of some tenths to hundreds of nanometer, is useful to investigate how finite size effects influence the polymer chain dynamics.

For this purpose, poly(isoprene)-poly(dimethyl siloxane) block copolymer melts (PI-PDMS) are ideal as a model system as the both polymers exhibit a low glass transition temperature and a strong mutual repulsion ($\chi \sim 0.07$). Consequently PI-PDMS spontaneously self-assemble to well defined equilibrium structures. Most importantly in the context of dynamics, cis-PI exhibits a dipole both parallel and perpendicular to its backbone allowing a simultaneous observation of both the global normal mode relaxation (associated to the fluctuation of ten ed-end distance) as well as the local alpha relaxation (related to the glass transition) using dielectric relaxation spectroscopy. By comparing the dynamics of the corresponding pure PI homopolymers, the effect of confinement on the dynamics can be directly deduced.

In this communication we will present first results of a study of various PI-PDMS block copolymer melts where the PI part varies between 5 000 to 10 000 g/mole. Using small angle x-ray scattering (SAXS), we deduce the detailed structure and the ordering behaviour (crystal structure) of the system (see Figure 1). Dielectric spectroscopic measurements show that the confinement induces a faster and broadened normal as well as local relaxation process broadened having an extra fast relaxing component in the high frequency side of the dielectric loss peak (see Figure 2). Several scenarios to explain these findings, ranging from local density effects, and incomplete segregation to coupling of the PI chain dynamics to the interfacial PDMS motion will be presented.

# TRANSITION FROM THIN GOLD LAYERS TO NANO-ISLANDS ON ITO. INFLUENCE OF THE ANNEALING TEMPERATURE AND THE INITIAL THICKNESS

*P.-J. Alet[1,2], Serge Palacin[1], Pere Roca i Cabarrocas[2]*
*[1]CEA, DSM/DRECAM/SPCSI/LCSI, Centre de Saclay, 91191 Gif-sur-Yvette, France*
*[2]LPICM, École Polytechnique - CNRS, 91128 Palaiseau, France*
*pierre-jean.alet@polytechnique.edu*

Many processes in nanotechnology make use of organized arrays of metallic nanoparticles. In particular, growth of silicon nanowires [1, 2, 3] and carbon nanotubes [4] by the vapour-liquid-solid process is driven by metal droplets, which size and distribution partially control the diameter and density of the wires. Different methods have been investigated to obtain organized nanoparticles on a substrate, like photolithography, self-organization from colloids, patterning by diblock copolymers, etc. Annealing an evaporated thin film is one of the simplest, as long as the requirements on the organization and the size dispersion are not too high.

In this paper, we study the influence of the initial thickness of the metal layer and of the temperature and duration of annealing on the final size and shape of the nano-islands. As the clusters are meant to catalyze the growth of silicon nanowires to be used in hybrid solar cells [5], the substrate is here ITO-coated glass. Gold layers of thicknesses between 1 nm and 4 nm have been evaporated by electron beam and they have been annealed under vacuum at temperatures ranging between 70 °C and 650 °C. SEM pictures clearly show the formation of clusters at the surface, which size and shape heavily depends on the initial thickness of the layers (fig. 1).

Digital image analysis has been used to derive quantitative information and statistics about the number density of the clusters, their size and their geometry. Surprisingly, both the average value and the distribution of the final size of the islands are independent of the temperature for 15-minute long annealing.

From a fundamental point of view, the common explanation of the formation of the islands by the mismatch between the thermal expansion coefficient of the substrate and of the metal layer [6] is thus insufficient if not wrong. Moreover, the evolution is a very fast phenomenon. Two mechanisms remain possible: Ostwald ripening, where large aggregates grow by mass transfer from small ones, and coalescence, where mobile aggregates collide. They differ by their dynamics and by the statistical distribution they induce, which are compared to the experimental results.

From a more applied point of view, the possibility to obtain arrays of metallic nano-clusters with a weak dependence on the temperature opens the way to low-temperature growth of nanowires or nanotubes.

**References:**

[1]    J. Albuschies, M. Baus, O. Winkler, B. Hadam, B. Spangenberg, and H. Kurz, Microelectronic Engineering, **83** (2006) 1530–1533.

[2]    Yewu Wang, Volker Schmidt, Stephan Senz, and Ulrich Gosele, Nature Nanotechnology, **1** (2006) 186–189.

[3]    Hong Jin Fan, Peter Werner, and Margit Zacharias, Small, **2** (2006) 700–717.

[4]    Ch. Taschner, F. Pacal, A. Leonhardt, P. Spatenka, K. Bartsch, A. Graff, and R. Kaltofen, Surface and Coatings Technology, **174-175** (2003) 81–87.

[5]    P.-J. Alet, S. Palacin, P. Roca i Cabarrocas, B. Kalache, M. Firon, and R. de Bettignies, European Physical Journal-Applied Physics **36** (2006) 231-234.

[6]    V. I. Merkulov, D. H. Lowndes, Y.Y. Wei, G. Eres, and E. Voelkl, Applied Physics Letters **76** (2000) 3555-3557.

**Figures:**
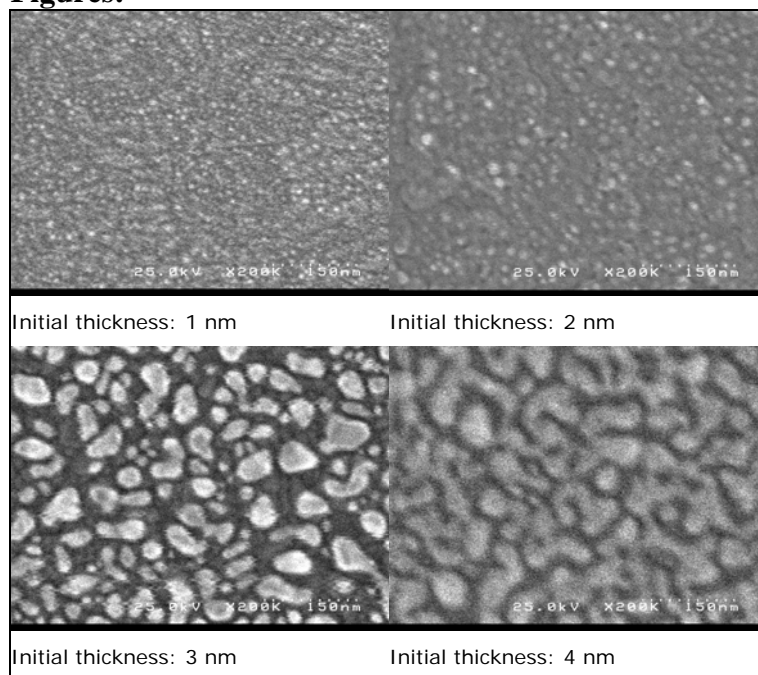


Fig. 1: SEM pictures of gold layers on ITO after annealing at 600 °C

# Donor-bound electrons in quantum rings under magnetic fields

M. Amado , R. P. A. Lima, C. González-Santander and F. Domínguez-Adame.

GISC-QNS, Departamento de Física de Materiales, Universidad Complutense, E-28040 Madrid, Spain.

Recent advances in nanofabrication of quantum devices enables to study electronic properties of quantum rings (QRs) in a very controllable way [1–3]. QRs are small semiconductor ring-shape structures in which electrons are confined in all spatial dimensions so as a consequence, QRs are very promising systems due to their physical properties as well as their potential application in electronic devices.

Donor or acceptor binding energies are also modified due to presence of a QR as compared to bulk semiconductors. Therefore, binding energy carries information about the confinement properties of electrons and holes in QRs. Consequently, spectroscopy studies of radiative recombinations of donor-bound electrons or acceptor-bound holes provide a unique tool to characterize the electronic properties of QRs.

In this work, we consider on-center and off-center donors in a two-dimensional (2D) QR within the effective-mass approximation. The QR is assumed to be of finite width, and a strong magnetic field is applied perpendicular to the plane of the QR. The binding energy of a single electron bound to an on-center donor is obtained by exact diagonalization of the radial Hamiltonian. In the case of off-center impurities, the standard perturbation approach allows us to calculate the binding energy as a function of the impurity position and magnetic field. As a major result, we find a strong dependence of the confining properties of the QR upon the magnetic field. In particular, an abrupt transition of the localization properties of the electronic envelope-function is observed at a critical magnetic field.

We will focus on electron states close to the bottom of the conduction-band and neglect nonparabolicity effects hereafter. Then, a one-band effective-mass Hamiltonian suffices to obtain accurate results. For simplicity, we assume the same effective-mass $m^*$ at the $\Gamma$ valley in both semiconductors, namely inside and outside the QR.

The radial function $R(\rho)$ satisfies the following effective-mass equation

$$\left[-\frac{\hbar^2}{2m^*}\frac{1}{\rho}\frac{d}{d\rho}\left(\rho\frac{d}{d\rho}\right) + \frac{\hbar^2}{2m^*}\frac{\ell^2}{\rho^2} + \frac{m}{8}\omega_c^2\rho^2 + V(\rho)\right]R(\rho) = \left(E - \frac{\ell}{2}\hbar\omega_c\right)R(\rho) ,\tag{1}$$

where the cyclotron frequency is $\omega_c = eB/m^*c$. The conduction band-edge profile along the radial direction of the QR is given by

$$V(\rho) = \begin{cases} 0 , & \rho_1 < \rho < \rho_2 , \\ V_0 , & \text{otherwise} , \end{cases}\tag{2}$$

with $V_0 > 0$. Here $\rho_1$ and $\rho_2$ are the inner and outer radii of the QR, respectively. Solution of Eq. (1) is given in Ref. [4].

Let us now introduce a single ionized donor at the center of the QR

$$V_C(\rho) = -\frac{e^2}{\epsilon_r\rho} ,\tag{3}$$

$\epsilon_r$ being the relative dielectric constant of the semiconductors. In this case, the axial symmetry is not broken and we obtain an equation similar to Eq. (1), with an addional Coulomb term. We solved it numerically using dimensionless coordinates and a standard finite-difference approach.

As we can see in the following figures an electronic tunneling-transition between the well and the donor-bound states occur at critical magnetic fields values regarding to the electronic state of the electron. In the Fig 1 the $|10>$ (where the first quantum number is $n$ and the second one is $|l| = 0...n-1$ the angular momentum) delocalization occurs at $B \sim 20T$ while in the Fig 2, the electronic state is $|20>$ and the delocalization occurs at lower magnetic fields. This behaviour is related to alignment between the energy levels of the QR and the imputity since the variation of a bulk level (impurity) is slower than the well-one Fig 3. In those figure two anicrossing points could be observed at the delocalization magnetic fields of the $|10>$ and $|20>$ states.

We have also consider the case of one off-center donor located at a distance $d = |\boldsymbol{\rho}_i|$ of the center, $\boldsymbol{\rho}_i$ being its position in the plane of the QR. Clearly the axial symmetry is broken and an equation similar to Eq. (1) does not
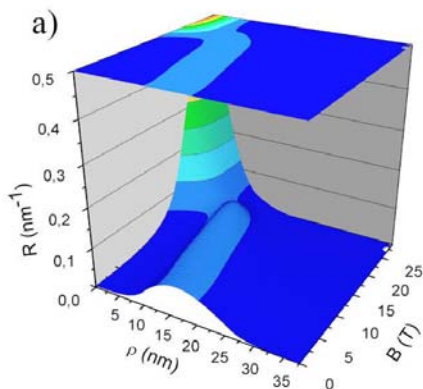
FIG. 1: Envelope function for $|10>$ versus applied magnetic field for a QR with an on-center impurity
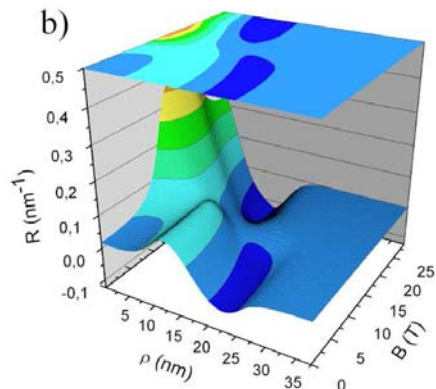
FIG. 2: Envelope function for $|20>$ versus applied magnetic field for a QR with an on-center impurity.
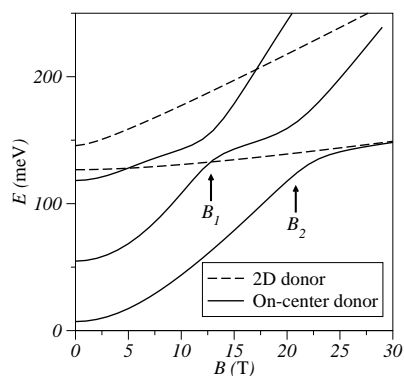


FIG. 3: Energy variation versus perpendicular applied magnetic field for the donor and the QR electron levels. Two anticrossing points between QR levels can be observed

hold. We are then faced to a 2D effective-mass equation for the complete $\chi(\boldsymbol{\rho})$ envelope-function that have been solved analitically in function of the distance to QR origin using the following equations

$$\langle \ell \,|\, V_C(\boldsymbol{\rho}) \,|\, \ell' \rangle = -\frac{e^2}{2\pi\epsilon_r} \sum_{m=0}^{\infty} A_m(\Delta\ell) \int_0^{\infty} d\rho\, \rho f_m(\rho) R_\ell(\rho) R_{\ell'}(\rho) \ , \tag{4a}$$

where $R_\ell(\rho)$ is the solution of Eq. (1), $\Delta\ell = \ell' - \ell$ and

$$A_m(\Delta\ell) = \int_0^{2\pi} d\phi\, e^{i\Delta\ell\phi} P_m(\cos\phi) \ . \tag{4b}$$

[1] A. Lorke, R. J. Luyken, J. M. García, and P. M. Petroff, Jpn. J. Appl. Phys. **40**, 1857 (2001).
[2] R. Blossey and A. Lorke, Phys. Rev. E **65**, 021603 (2002).
[3] D. Granados and J. M. García, Appl. Phys. Lett. **82**, 2401 (2003).
[4] T. V. Bandos, A. Cantarero, and A. García-Cristóbal, Eur. Phys. J. B **53**, 99 (2006).
[5] S. Flügge, *Practical Quantum Mechanics* (Springer Verlag, Berlin 1999).

# On Global Communications for Nano-Architectures: Brain versus Rent's Rule

*Hoda Amer[12], Valeriu Beiu[12], Martin McGinnity[1], Peter Kelly[1]*
*[1] School of Intelligent Systems, University of Ulster, Magee, UK*
*[2] College of Information Technology, UAEU, Al Ain, UAE*
hamer@uaeu.ac.ae; vbeiu@uaeu.ac.ae; TM.McGinnity@ulster.ac.uk; pm.kelly@ulster.ac.uk

At the architectural level, the communication challenge has not received as much attention as power and reliability. How should the interconnect topology, the communication protocol, and the encoding look like for Tera-scale integration (i.e., $10^{12}$ Nano-devices) needs significantly more consideration. The communication challenge is clearly bridging the power and the reliability challenges. The focus of this paper will be to investigate and compare possible interconnect (network) topologies.

By looking at nature, one finds that the mammalian brain is a quite efficient network of processing elements. At the highest level, the brain is segregated into white and gray matter. White matter ($W$) contains mostly long axons implementing all the global communications, while gray matter ($G$) contains cell bodies, dendrites, and axons for local communication and for information processing. Such a view of the brain has led to it being modeled as a layered network where global and local connections can be segregated [1].

For various mammalian species, as brain size increases, the volume of the $W$ beneath the cortex tends to increase faster than the volume of the cortical $G$ according to a power law [2]. This power law can adequately describe the relationship between the volume of $G$ (mostly processing elements), and the volume of $W$ (mostly connections) in 59 mammalian species.

$$\log_{10} W = (1.23 \pm 0.01)\log_{10} G - (1.47 \pm 0.04) \tag{1}$$

In the digital world, an equivalent rule establishes the relationship between the number of processing elements and the number of interconnects as well. Rent's rule is a power law for estimating the average number of terminals required to connect a sub-region of a circuit as a function of the number of gates in that region [3], [4] as:

$$T_{IO} = k \cdot N_{gates}^{p} \tag{2}$$

Rent's rule has been used in a variety of applications to estimate the wire length of electronic designs[5], [6], [7]. It has been recently revisited and a new interpretation was formulated. When referring back to the original memoranda written by Rent in 1960 [3], Lanzerotti et al. [8] were able to derive a historically-equivalent interpretation of Rent's rule, which was adapted for today's computer components. This new interpretation describes a power law that relates the number of gates (processing elements) to the number of connections used in a design.

$$N_{conn} = k_R \cdot N_{gates}^{p_R} \tag{3}$$

Many topological characteristics of networks have been examined in [9], [10]. Characteristics such as degree, diameter, number of links, and cost have been compared for network topologies such as Binary Hypercube (BHC), Torus, Generalized Hypercube (GHC), Spanning Bus Hypercube (SBH), Hierarchical Cubic Network (HCN), Cube Connected Cycle (CCC), Hyper-deBruijn (HdB), Folded Peterson (FPT), Hypermesh (HM), Optical Multi-Mesh Hypercube (OMMH), and Spanning Multichannel Linked Hypercube (SMLH).

The relationship between the number of processing elements (network size) and the number of connections (links), in such network topologies are plotted on a log-log graph, and compared to both the historically-equivalent interpretation of Rent's rule and to the curve

obtained from plotting the power law that describes the relationship between *G* and *W* in different mammalian neocortex.

Our findings indicate that for large number of processing elements (over $10^2$ and up to $10^6$), almost all these topologies have roughly the same slope as the new interpretation of Rent's rule, while the brain exhibiting the most efficient one of all!

## References:

[1] Q. Wen, and D.B. Chklovskii, "Segregation of the Brain into Gray and White Matter: A Design Minimizing Conduction Delays," *PLoS Comp Bio,* vol. 1, no. 7, pp. 617–630, Dec. 2005.
[2] K. Zhang, and T.J. Sejnowski, "A Universal Scaling Law between Gray Matter and White Matter of Cerebral Cortex," *Nat Acad Sci of the USA*, vol. 97, no. 10 , pp. 5621–5626, May 2000.
[3] E.F. Rent, "Microminiature Packaging—Logic Block to Pin Ratio," Memoranda, Nov. 28, 1960, and Dec. 12, 1960.
[4] D. Stroobandt, "Analytical Methods for a Priori Wire Length Estimates in Computer Systems," Ph.D. dissertation, Univ of Ghent., Faculty of Appl Sci, Ghent, Belgium, Nov. 29, 1998.
[5] J. Dambre, D. Stroobandt, and J.V. Campenhout, "Toward the Accurate Prediction of Placement Wire Length Distributions in VLSI Circuits," *IEEE Trans. VLSI Sys*, vol. 12, no. 4, pp. 339–348, Apr. 2004.
[6] S. Das, A.P. Chandrakasan, and R. Reif, "Calibration of Rent's Rule Models for Three-Dimensional Integrated Circuits," *IEEE Trans. VLSI Sys*, vol. 12, no. 4, pp. 359–366, Apr. 2004.
[7] A. Kumar, and S. Tiwari, "Testing and Defect Tolerance: A Rent's Rule Based Analysis and Implications on Nanoelectronics," *Proc. IEEE Int. Symp. Defect & Fault Tolerance VLSI Sys. DFT,04* Ithaca, NY, USA, pp. 280–288, Oct. 2004.
[8] M.Y. Lanzerotti, G. Fiorenza, and R.A. Rand, "Interpretation of Rent's Rule for Ultralarge-Scale Integrated Circuit Designs, with an Application to Wirelength Distribution Models," *IEEE Trans. VLSI Sys*, vol. 12, no. 12, pp. 1330–1347, Dec. 2004.
[9] A. Louri, and C. Neocleous, "A Spanning Bus Connected Hypercube: A New Scalable Optical Interconnection Network for Multiprocessors and Massively Parallel Systems," *J Lightwave Tech,* vol. 15, no. 7, pp. 1241–1252, Jul. 1997.
[10] A. Louri, B. Weech, and C. Neocleous, "A Spanning Multichannel Linked Hypercube: A Gradually Scalable Optical Interconnection Network for Massively Parallel Computing," *IEEE Trans. Parallel & Distrib Sys,* vol. 9, no. 5, pp. 497–512, May 1998.

## Figures:
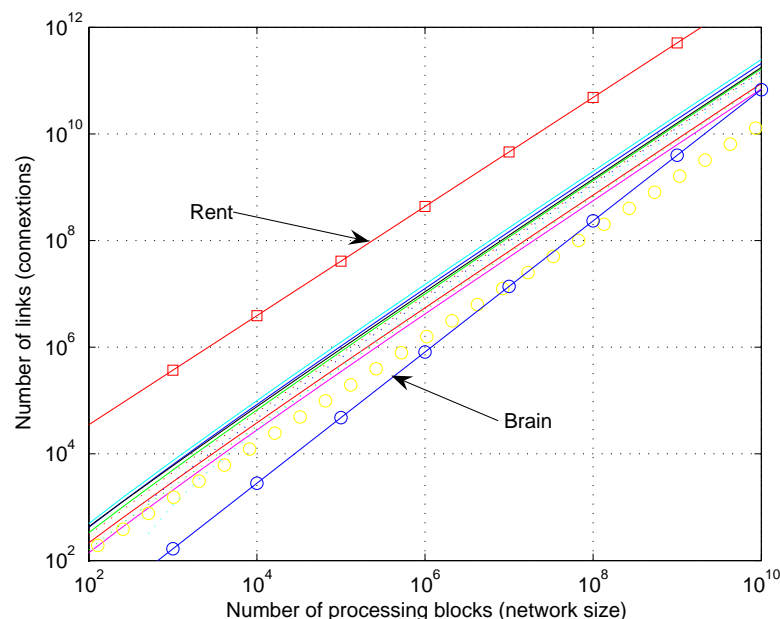


**Figure 1. The number of processing blocks (network size) versus the number of connections (links).**

# REFRACTIVE INDICES ANOMALY OF  SPUTTERED AMORPHOUS SIC THIN FILMS.

*Manoj Arora[a], Chillar.M and Swati Arora[b]*
*[a]Eritrea Institute of Technology, Mainefhi, Asmara, Eritrea, North-East Africa.*
*[b]Z.H.C. University of Delhi. Delhi-110002. India.*

The effects of laser annealing on the refractive indices of SiC thin films were studied in light of electrical and optical properties.  SiC films of thickness about 1μm were deposited by rf sputtering at a base pressure of $10^{-5}$ mbar in the presence of Ar gas on the glass and quartz substrate. The films were annealed using He-Ne laser (3-8mW) using different time. XRD and SEM studies revealed that transition from amorphous to polycrystalline structure and the value of the extraordinary and ordinary refractive indices initially decrease with annealing time and later increased before becoming constant with further annealing The variation in refractive indices was explained on the basis of lattice contraction and packing density.

[a]Present Position : Director-Research & Development, EITTE, Asmara. Eritrea.
[a]Permanent Position : Reader, RJC. University of Delhi, Delhi-110007. India.
E-Mail Id- drmanojarora@yahoo.com

# SUPERPRISM EFFECT ON 2D-PHOTONIC CRYSTALS

W. Aroua[1,3], F. AbdelMalek[1,3], S. Haxha[2], H. Bouchriha[3]

[1]National Institute of Applied Sciences and Technology, BP-676, Cedex 1080, Tunis, Tunisia

[2]Photonics Group, Department of Electronics, University of Kent, Canterbury CT2 7NT, UK

Tel: +44 (0) 1227 827257 fax: +44 (0) 1227 456084

[3]Laboratoire de Physique Quantique, Faculté des Sciences de Tunis, Tunisia

Email: waroua@yahoo.com

abdelmalek.f@mailcity.com

We report a noveltype of dispersive structure for wavelength multiplexer/demultiplxer, based on a 2D photonic crystal (PC) prism. Simulation is carried out to determine the angular dispersion as a function of period. The design has been optimized to improve the performance of a system with moderate refractive index contrast. We also confirmed that the light propagation simulated using the FDTD [1-3] method agreed with the results obtained by the dispersion surface analysis. It is shown that by varying the incident angle in a wavelength range from 1.3µm to 1.5µm, a superprism effect is observed. The performance of the devices is investigated, in term of sensitivity and resolution, witch help for future fabrication of a superprism integrated in photonic circuits.

Over this decade, the dispersive properties of PCs has been under extensive study. Owing to these properties the wavelength selective devices has emerged as novel class of superprism based on PCs. The fundamental effect of superprism consists of splitting light into different wavelengths due to the natural dispersion[4,5]. However, in a PC superprism a microstructured material leads to a huge increased dispersion (see Figure 1). This means that the Gaussian incident beam is decomposed in different wavelengths where each one is emitted at a different angle. The PC based superprism under study is composed of air holes arranged in triangular lattice with a lattice constant $a$ and an air-hole radius of $0.48a$. The background material is of a refractive index is n =3.4. A Gaussian pulse with a TE polarised source, was launched at the entrance of the PC. Figure 2 shows the deviation angle η of the prism versus the incident one for two wavelengths, which are $\lambda_1$= 1.55µm and $\lambda_2$ =1.3µm, respectively. It can be observed that for an incident angle of 5°, the deviation angles are 37° for $\lambda_1$ and is about 32° for $\lambda_2$, also, the deviation angle decreases when the incident angle is increasing.

The angular dispersion $\dfrac{d\eta}{d\lambda}$ is calculated as a function of the incident angle for TE and TM polarisations, the result is shown in Fig.3. This figure shows that the variation of the angular dispersion for TE and TM polarisations reaches a minimum when the incident angle is of 5°. Figure 4 shows the variation of the angular dispersion for 1.55µm and 1.3µm respectively, it can be observed that the angular dispersion for 1.55µm is about -73 and is equal to -68 for 1.33µm. The variation of the deviation angle for versus operating wavelengths is reported in figure 5, which clearly demonstrates that the deviation angle decreases when the wavelength increases. By keeping the incident angle at 18°, the deviation angle reaches 38° when the wavelength ranges from 1.2µm to 1.7µm. Finally, a superprism has been proposed using super dispersion of a 2D photonic crystal. The superprism combined with two lenses makes a new class of multiplexer. All simulated results are carried out by using the FDTD method.

**References**

[1] K. S. Yee, IEEE Trans. Antennas and propagation, vol. 14, no.3, 1966.

[2] A. Taflove and K. R. Umashankar, Journal. Electrmagnetic waves and applications, vol. 1, no.3, 1987.

[3] T. Matsumoto and T. Baba, IEICE TRANS. Electron, Vol. E87-C, No. 3, March, 2004

[4] S. Kawakami, J. Ligthwave technol, 17 (11), pp 2032-2038, 1999.

[5] W. Lijum, M. Mazilu, TF. Krauss, Journal of ligthwave Technology, 21 (2), pp. 561-566, 2003
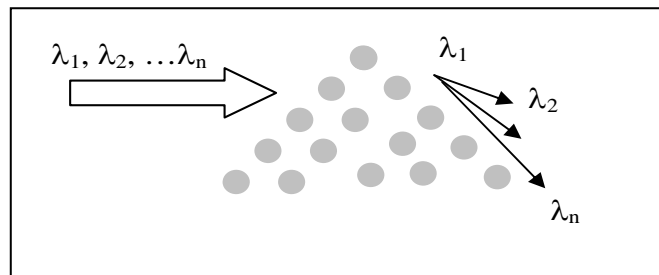

Fig. 1 Schematic diagram of the PBG superprism
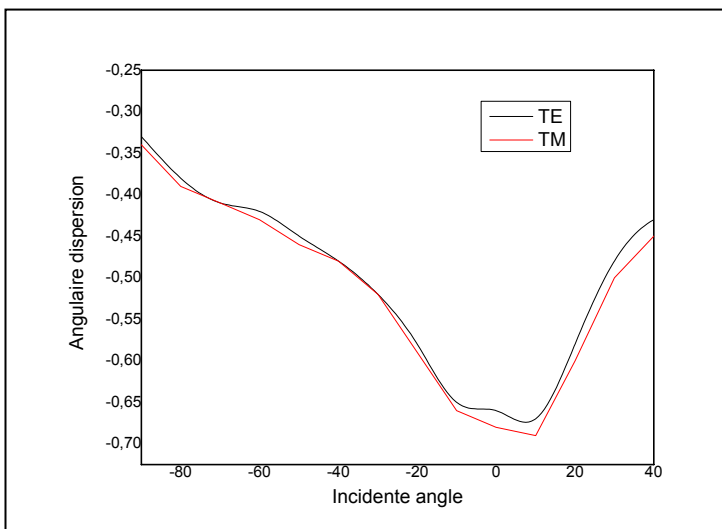

Fig. 2 Variation of the deviation angle for various incident angles
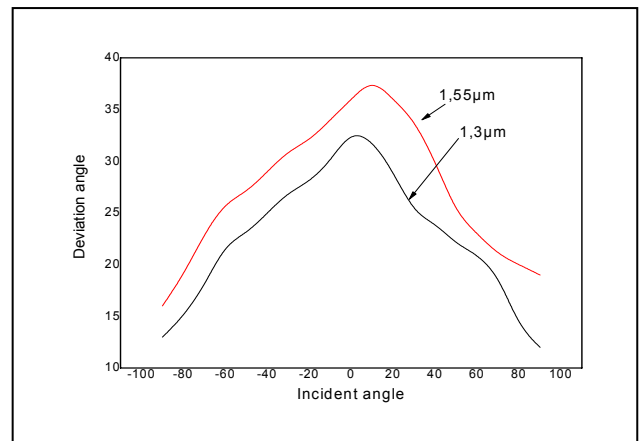

Fig. 3 Angular dispersion angles for various incident angles for TE and TM polarisation
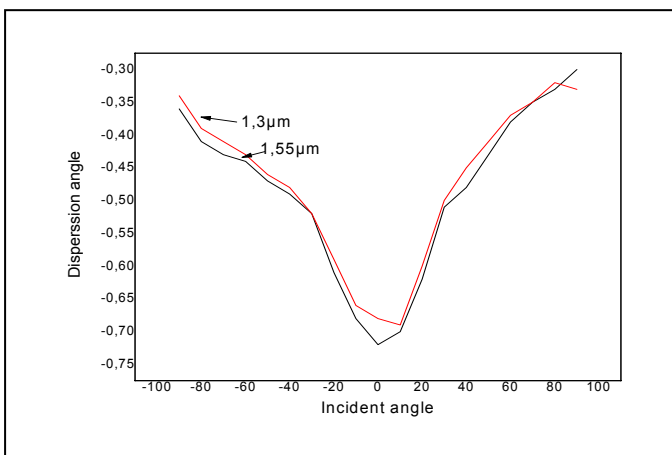

Fig. 4 Variation of the dispersion angle for various incident angles
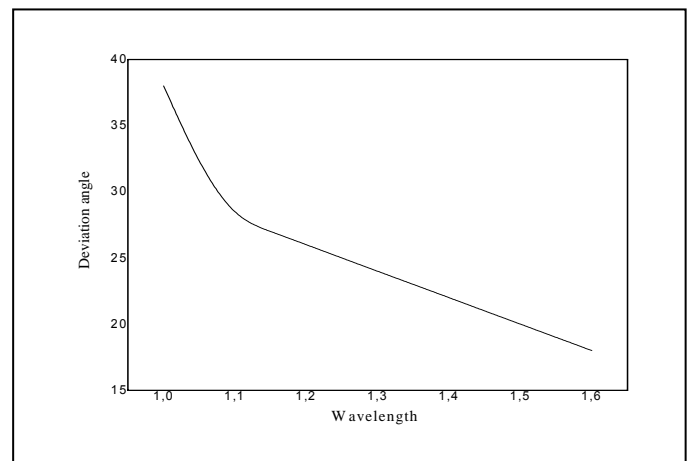

Fig. 5 Deviation angle for various operating wavelength

# NANOSTRUCTURES FORMATION FROM PALADIUM-COBALT PRECURSOR ON HIGHLY ORDERED PYROLYTIC GRAPHITE SURFACES

*Lisandra Arroyo-Ramírez, Raphael G. Raptis and Carlos R. Cabrera*
*Department of Chemistry and Center for Nanoscale Materials,*
*University of Puerto Rico-Río Piedras, PO Box 23346, San Juan, PR 00931-3346*
*lisyarroyo@gmail.com*

Nano-sized metal particles continue to attract interest for different researcher areas due to their different physical and chemical properties when compared to bulk material. Nanomaterials synthesis can be done with different techniques and methods. The common methods use many processes to obtain the nanomaterials. Metal nanostructures and nanoparticles can be prepared by chemical methods allowing the control of size and composition distribution of the particles. In this methods molecular or ionic precursors are usually used as the starting material.[1,2] Additionally, the demand for tailored catalytic nanoparticles has encouraged the used of heterobimetallic precursors. For example, palladium-cobalt alloy has resulted in an extremely active catalyst for the oxygen reduction reaction.[3,4] This reaction is of most importance for developing high efficiency, stability, and durability $H_2$-$O_2$ fuel cell systems.

Our group has been working in the nanostructures and nanoparticles formation from precursors on highly ordered pyrolytic graphite (HOPG) surfaces.[5,6,7] This research focuses on the development of palladium-cobalt nanostructures with defined size and composition distribution which can be controlled by support chemical structure conditions and the atmosphere used in the deposition process. In this work, we describe the study of deposition and reductive decomposition of the heterobimetallic precursor $CoPd_2(Me_2Ipz)_4Cl_4 \cdot 2NH_4$ ($CoPd_2$) on the HOPG surfaces. We propose an easy and economic methodology for the nanostructures formation. The nanostructures formation were characterized by surface analysis techniques, such as: atomic force microscopy (AFM), scanning electron microscopy (SEM) and X-ray photoelectron spectroscopy (XPS).

The HOPG surfaces was imaged by AFM and SEM to study their morphology change in the modification process. AFM image of modified HOPG with $CoPd_2(Me_2Ipz)_4Cl_4 \cdot 2NH_4$ ionic precursors showed the formation of organized circular nanostructures with different sizes (Figure 1). These circles (tubes) have a diameter between 0.46 to 2.15 µm and height between 71 and 390 nm. Figure 2 shows the SEM images for modified HOPG with control of the atmosphere in the deposition process. The $CoPd_2$ precursor was thermally reduced under hydrogen atmosphere, a procedure which removes the organic ligads, forming bimetallic nanoparticles. We observed in the AFM images a particles formation tendency after reduction process of $CoPd_2$ precursor on HOPG surface. Also, the nanostructures persisted after the reduction process.

The composition of the modified surface described was characterized by XPS analysis. Typical elements peaks for modified HOPG surface are present in the XPS spectrum (Figure 3). After the reduction, the characteristic peaks of the ligands disappear and the Pd and Co peaks shift their binding energy. This is due to the adsorption of $CoPd_2$ complex on the surface and the change in oxidation state.

In summary, the deposition with atmosphere control offers an alternative methodology for the nanostructures formation to large-scale production. These results suggest that the Pd-Co structures might be promising new nanomaterials for different applications such as: electronics, sensors, storage and fuel cell. In future work we are going to obtain optimal

conditions for the nanostructures formation. Additionally, to study electrocatalytic activity of metallic palladium-cobalt nanoparticles for oxygen reduction reaction.

**References:**

[1] Nashner, M. S.; Frenkel, A. I.; Somerville, D.; Hills, C. W.; Shapley, J. R.; Nuzzo, R G. *J. Am. Chem. Soc*. **120** (1998) 8093.

[2] Hills, C. W.; Nashner, M. S.; Frenkel, A. I.; Shapley, J. R.; Nuzzo, R G. *Langmuir* **15** (1999) 690.

[3] Savadogo, O.; Lee, K.; Oishi, K; Mitsushima, S.; Kamiya, N.; Ota, K. I. *Electrochem. Comm.* **6** (2004) 105.

[4] Mostain, W. E.; Kepler, K.; Prakash, J. *Electrochimica Acta* **52** (2007) 2102.

[5] Díaz-Ayala, R.; Arroyo, L.; Raptis, R.; Cabrera, C. R. *Langmuir* **20** (2004) 8329.

[6] Díaz-Ayala, R.; Raptis, R.; Cabrera, C. R. *Rev. Adv. Mater. Sci.* **10** (2005), 375.

[7] Díaz-Ayala, R.; Fachini, E. R.; Raptis, R.; Cabrera, C. R. *Langmuir* **22** (2006) 10185.

**Figures:**
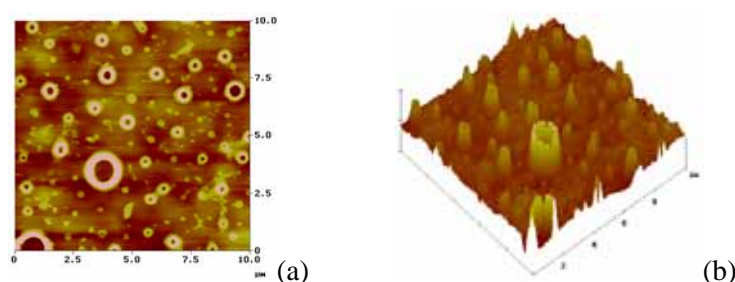


**Figure 1.** AFM images (a) top and (b) 3D view (z = 380 nm) for deposition of $CoPd_2(Me_2Ipz)_4 \cdot 2NH_4$ on HOPG surface.
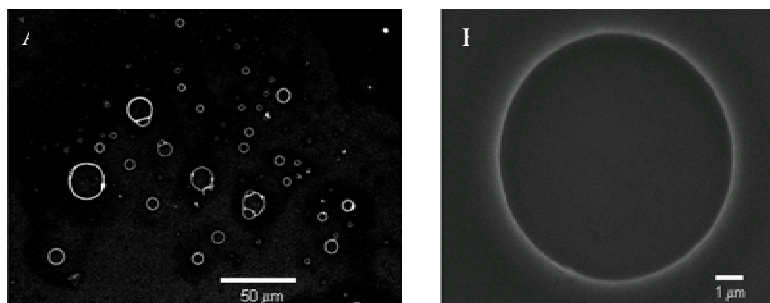


**Figure 2.** SEM images (A) x500, and (B) x10,000 for deposition of $CoPd_2(Me_2Ipz)_4Cl_4$ on HOPG at 21°C and $77 \pm 1$ %RH.
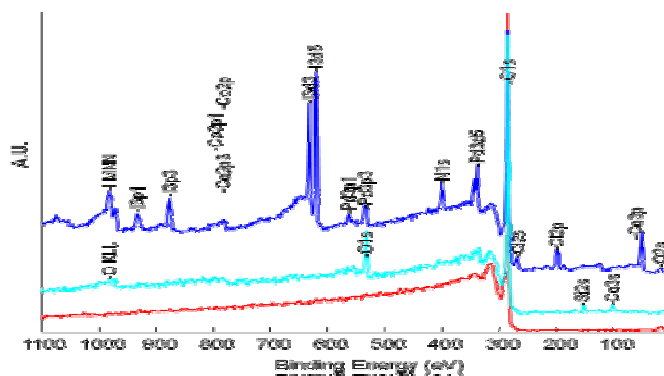


**Figure 3.** XPS spectrum of the surface of HOPG (red), the $CoPd_2(Me_2Ipz)_4Cl_4 \cdot 2NH_4$ before (blue), and after (clear blue) reduction process on HOPG.

# BIOMEDICAL APPLICATIONS OF NANOPOROUS SILICA PARTICLES AND SILICA-BASED COATINGS

*Manuel Arruebo, Clara Yagüe, Sara Puertas, Luís Manuel Pérez, Valeria Grazu, Ricardo Ibarra, Jesús Santamaría*
*Aragon Nanoscience Institute, Pedro Cerbuna 12, Zaragoza University, 50009 Zaragoza, Spain*
*arruebom@unizar.es*

Several attractive features, such as large specific surface areas, narrow pore-size distributions, chemical and mechanical stability, biocompatibility, non-toxicity, and easy surface functionalization of silica-based materials have made them ideal for drug delivery and biosensing applications [1], for transfection [2], as well as for acting as functionalizable coatings on medical devices [3] and on nanoparticles (i.e., contrast agents) [4].

Mesoporous silica shows regular pore openings and can also have different pore arrangements: hexagonal (MCM-41), cubic (MCM-48) and lamellar (MCM-50) with average pore diameters that can be selected between 15 and 100 Å, by adjusting the synthesis conditions and/or by employing surfactants with different chain lengths in their preparation.

For drug-delivery applications a volume-based rather than surface-based approach to drug delivery is also possible. Thus, unlike MCM particles, where the drug is loaded by adsorption on the surface area of the material, with hollow spheres or particles the drug could also be stored in the empty inner volume, thus leading to higher loads per unit mass of drug delivery vector. A variety of preparation methods is now available to produce silica-based hollow spheres, consisting of mesoporous silica and with or without functionalized interiors (e.g., Schult-Eklo et al. [5], Caruso et al. [6], Dong et al. [7], Valtchev and Mintova [8]). These could in principle be used in drug delivery applications given their characteristics of biocompatibility and comparatively high drug loading capability.

For magnetic targeting in drug delivery, a drug or therapeutic radionuclide is bound to a magnetic compound (which can be grafted in a silica based matrix), introduced in the body, and then concentrated in the target area by means of a magnetic field (using an internally implanted permanent magnet or an externally applied field). Depending on the application, the particles then release the drug or give rise to a local effect (irradiation from radioactive microspheres or hyperthermia with magnetic nanoparticles). Drug release can proceed by simple diffusion or take place through mechanisms requiring enzymatic activity or changes in physiological conditions such as pH, osmolality, or temperature; drug release can also be magnetically triggered from the drug-conjugated magnetic nanoparticles.

For diagnosis applications, we have developed different types of silica-coated magnetic nanoparticles as contrast agents for magnetic resonance imaging (MRI). The silica shell provides a hydrophilic surface that helps to retard the process of nanoparticle clearance by the macrophages of the reticuloendothelial system (RES). The silanol groups on the silica coating offer many possibilities for surface functionalization as we mentioned before. The silica shell helps to avoid magnetic and electrostatic agglomeration, since the isoelectrical point of silica is reached at pH 2-3 and therefore silica-coated nanoparticles would display a significant negative surface charge at the pH of the blood.
We have developed silica-coated magnetic nanoparticles functionalized with an antibody as a contrast agent with potential active targeting properties. Superparamagnetism implies that there is not coercivity, and the magnetization is close to zero in the absence of an external

field. To this end, we have: i) synthesized superparamagnetic nanoparticles that can be used as the core of targeted contrast systems; ii) developed a silica shell, on account of the above described advantages of silica, with a size of the core-shell ensemble under 100 nm; iii) attached covalently bio-active entities (an antibody in this case) to the silica coating to develop antibody-conjugated magnetic nanoparticles. The antibody anti-hCG was chosen as a test compound because it is widely studied due to its common use in pregnancy testing kits. Different nanoparticles synthesized are shown below (Figure 1).

**References:**
[1] I. I. Slowing, B.G. Trewyn, S. Giri, V.S.Y. Lin, Advanced Functional Materials, (Early view, 2007).
[2] C. Kneuer, M. Sameti, U. Bakowsky, T. Schiestel, H. Schirra, H. Schmidt, C.M. Lehr, Bioconjugate Chemistry, 11 (2000) 926.
[3] L.M. Pérez, M. Arruebo, S. Irusta, L. Gracia-Villa, J Santamaría, J.A. Puértolas, Microporous and Mesoporous Materials, 98 (2007) 292.
[4] M. Arruebo, R. Fernández-Pacheco, B. Velasco, C. Marquina, J. Arbiol, S. Irusta, M. Ricardo Ibarra, J. Santamaría, Advanced Functional Materials, (Early View 2007).
[5] G. Schult-Eklo, J. Rathousk, A. Zukal, International Journal of Inorganic Materials, 1 (1999) 97.
[6] F. Caruso, H. Möhwald, Science, 282 (1998) 1111.
[7] A. Dong, Y. Wang, D. Wang, W. Yang, Y. Zhang, N. Ren, Z. Gao, Y. Tang, Y, Microporous and Mesoporous Materials, 64(2003) 69.
[8] V. Valtchev, S. Mintova, Microporous and Mesoporous Materials 43 (2000) 41.

**Figures:**
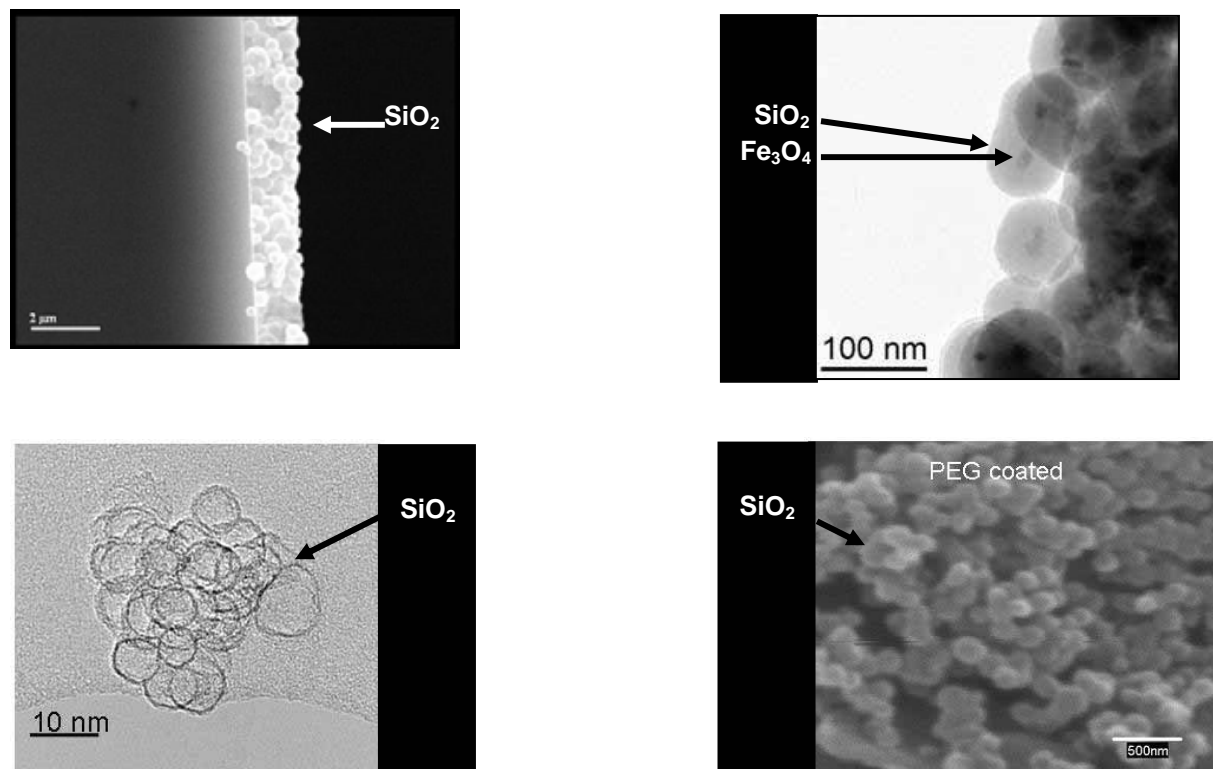


**Figure 1.** Silica-based nanoparticles synthesized by the Aragon Nanoscience Institute.

# Optimized Geometry of the Cluster $Gd_2O_3$ and Proposed Antiferromagnetic Alignment of f-electron Magnetic Moment

A. Ayuela[1,2,*], N.H. March[2,3,4], and D. J. Klein[5]

[1] *Centro Mixto CSIC/UPV. Unidad de Física de Materiales. 20018 San Sebastian*

[2] *Donostia International Physics Centre (DIPC),*

*P.O.Box 1072, 20018 San Sebastian/Donostia. Spain*

[3] *Oxford University, Oxford, UK.*

[4] *Department of Physics, University of Antwerp, Antwerp, Belgium*

[5] *Dept. of Marine Science, Texas A&M University of Galveston, Galveston, Texas, USA and*

[*] *Corresponding author. E-mail: swxayfea@sw.ehu.es.*

## Abstract

There is currently experimental interest in assemblies of $Gd_2O_3$ clusters. This has motivated the present study in which a single such cluster in free space is examined quantitatively by spin-density functional theory, with appropriate relativistic correction incorporated for Gd. First the nuclear geometry of the cluster is optimized and found to be such that the two Gd atoms lie in a symmetry axis perpendicular to the isosceles triangle formed by the O atoms. Then, a careful study is made of the magnetic arrangement of the localized f-electron moments on the two Gd atoms. The prediction of the present treatment is that the localized spins are aligned antiferromagnetically. An alternative picture using superexchange ideas leads to the same conclusion.

PACS numbers:

# COMPARATIVE STUDY OF THE STRUCTURE AND ELECTRONIC PROPERTIES OF BILAYER CdSe-CdS AND CdTe-CdS QUANTUM DOTS AND QUANTUM WELLS BY AB INITIO CLUSTER AND FIRST-PRINCIPLES SLAB CALCULATIONS

*R.F. Minibaev, E.A. Rykova, A.A. Knizhnik, and <u>A.A. Bagatur'yants</u>*

*Photochemistry Center, Russian Academy of Science, Moscow, 119421 Russia*

*Kintech Lab, Moscow, Russia*
*sasha@photonics.ru*

Semiconductor nanoparticles and nanofilms find increasing use as efficient converters of electric energy to light (light-emitting devices) and light to electric energy (solar cells), as quantum dots in self-assembled quantum-dot arrays, as quantum wells in heterojunctions, and in many other electronic, photonic, and spintronic applications. In this work, CdS, CdSe and CdTe single-component nanostructures and CdSe-CdS and CdTe-CdS bilayer (core/shell) systems with the wider bandgap semiconductor as the shell and the narrower bandgap semiconductor as the core are studied theoretically using ab initio cluster and first-principles slab calculations. The structure and most important electronic properties (work function, band structure, etc.) are calculated and analyzed. The spectral properties of these nanostructures are analyzed.

# DIELECTROPHORESIS OF SINGLE-WALLED CARBON NANOTUBES: SURFACE CONDUCTANCE CONTROL

*Seunghyun Baik [1,2], Seunghyun Hong[1], Dokyung Yoon[1], Jaeboong Choi [2], Youngjin Kim [1, 2]*

[1] *SKKU Advanced Institute of Nanotechnology (SAINT), Sungkyunkwan University, Suwon, KyungGi-Do, 440-746, Korea*

[2] *School of Mechanical Engineering, Sungkyunkwan University, Suwon, KyungGi-Do, 440-746, Korea*

*sbaik@me.skku.ac.kr*

Single-walled carbon nanotubes (SWNTs) have attracted considerable attention as promising building blocks for future nanoscale electronic applications. For the realization of nanotube-based electronics, it is necessarily needed to develop reliable approachs to disperse the bundles of nanotubes individually and sort by electronic type. Recently we have demonstrated a protocol to quantitatively evaluate the degree of dispersion. [1] Also, various approachs to separate nanotubes according to their eletronic stuructures have been demonstrated such as chemically selective functionalization, ion exchange chromatography and density-gradient ultracentrifugation. Among them, alternating current dielectrophoreis has attracted much interest for separation SWNTs. Dielectrophoresis has been demonstrated to separate metallic from semiconducting tubes by their opposite movement in a solvent when interacting with an external alternating electric field. [2, 3] The effect is based on the different electric-field-induced polarizabilities.

Here, we present electrical transport characteristics of the surface charge controlled, dielectrophoretically deposited nanotubes arrays. The modulation in surface conductance of nanotubes effects the polarizability of especially semiconducting nanotubes, resulting in more effective separation between metallic and semiconducting species. The surface conductance was controlled by cationic/anionic surfactant mixtures since the surface conductance is directly proportional to the surface charge. [4] A theoretical analysis about the influence of electrical double layer on nanotube electrokinetics is shown in Figure 1.[5] The Clausius-Mossotti factor ($f_{CM}$) represents the effective polarizability of the nanotubes. Nanotubes move toward the regions of high electric field strength (positive DEP) if the polarisability of the tube is greater than the suspending medium ($Re[f_{CM}]>0$) whereas nanotubes move in the opposite direction (negative DEP) when the polarisability of the tube is less than the suspending medium ($Re[f_{CM}]<0$). [5]

Experimental observation based on electrical transport measurement showed consistency with theoretical analysis, displaying different electrokinetic behaviors of semiconducting nanotubes depending on surface conductance, as shown in Figure 2. [5] The matted sheet of nanotubes deposited via dielectrophoresis usually did not show modulation under variable high field, indicating metallic dominent pathway. The current through metallic pathways should be greater than that through semiconducting species. In order to check out this possibility, preferential electrical breakdown of metallic species was performed by applying $V_G = 30$ V and $V_{SD} = 12$ V. The preferential electrical breakdown showed different resulting transport behaviors depending on surface conductance. Resulting transport behaviors demonstrated surface conductace modulation induced more effective separation. We will also present a more detailed theoretical study, using zeta potential measurement, and dielectrophoresis results carried out using sub-micron gap electrodes.

**References:**

[1] Yoon, D.K., Kang, S. J., Choi, J. B., Kim, Y. J., Baik, S., *Accepted to J. Nanosci. Nanotech.*

[2] Krupke, R.; Hennrich, F.; Lohneysen, H.; Kappes, M., *Science* **2003**, 301, 344

[3] Baik, S.; Usrey, M.; Rotkina, L.; Strano, M. S. *J. Phys. Chem. B* **2004**, 108, 15560

[4] Tomašić, V.; Štefanić, I.; Filipović-Vinceković, N. *Colloid Polym. Sci.* **1999**, 277, 153

[5] Hong, S., Jung, S. H., Choi, J. B., Kim, Y. J., Baik, S. *Langmuir* 23(2007) 4749

**Figures:**
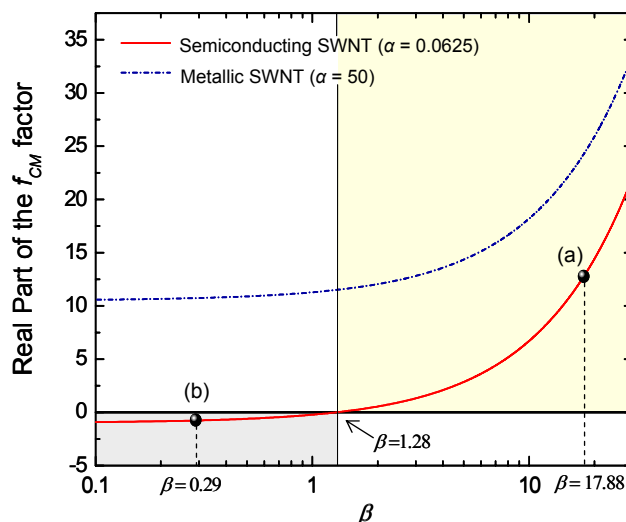


Figure 1 Theoretical plot showing the variation in the real part of the Clausius-Mossotti ($f_{CM}$) factor as a function of two parameters, $\alpha = \varepsilon_p/\varepsilon_m$ and $\beta = K_p/K_m$. The real part of $f_{CM}$ was zero at $\beta = 1.28$ (a) $\beta = 17.88$ was calculated for the SDS suspended SWNT ($\zeta = 50$ mV). (b) $\beta = 0.29$ was calculated for the CTADS suspended SWNT ($\zeta = 5$ mV). [5]
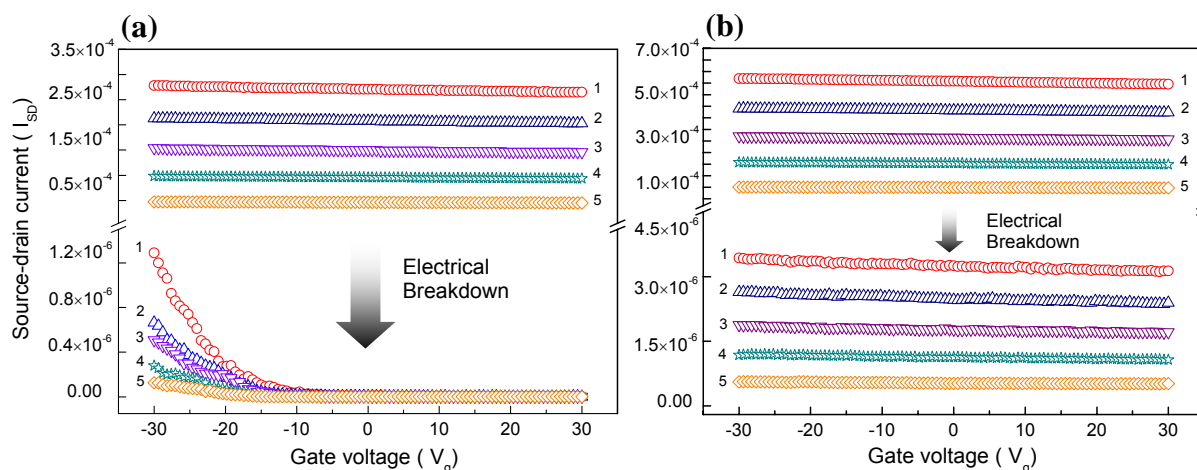


Figure 2 The electrical transport data before and after the preferential electrical breakdown procedure. The source-drain current was measured at 5 different source-drain biases (1: 2V, 2:1.6V, 3:1.2V, 4:0.8V, 5:0.4V) as a function of the back gate voltage. (a) dielectrophoretically deposited nanotubes from the SDS-SWNT suspension (b) dielectrophoretically deposited nanotubes from the SDS-CTAB-SWNT suspension. [5]

# FORMATION OF AgCl NANOPARTICLES FROM SILVER SCRAPS

**Dr. Kh.Sadrnejhad and L.Bakhish**
**Sharif university of technology**

Kinetics of dissolution of silver and cupper present in scraps in HNO3 were studied in temperature range of 0~80°C. Effects of acid concentration and temperature on the rate of dissolving were evaluated. Dissolution rate increases with temperature and acid concentration. Shrinking core model with mixed controlled equation could be used to explain the mechanism of the reaction. From the temperature dependence of the rate constant the activation energies have been calculated. Subsequent of dissolution AgCl nanoparticles were prepared in the presence of polyvinylpyrrolidone(PVP) by using NaCl. The effect of PVP, NaCl and silver concentration in acid solution, time and temperature of reaction on the precipitation and size of AgCl nanoparticles were evaluated. Optimum of those parameters were discussed. Scanning electron microscopy and energy dispersive spectroscopy were applied to characterize the morphology and the composition of AgCl nanoparticles. Results were tangible for applications in the recycling of material from electronic silver-bearing scraps, dental alloys, jewelry, silverware and anodic slime precious metal recovery and then formation of AgCl nanoparticles for photocatalyst and semiconductors application.

# ROLE OF THE MAGNETIC ANISOTROPY IN THE MAGNETOCALORIC EFFECT FOR A SUPERPARAMAGNETIC NANOPARTICLE SYSTEM: A MONTE CARLO STUDY.

*D. Baldomir,[1,2] D. Serantes,[1,2] M. Pereiro,[1,2] J. Rivas,[2]*
*C. Vázquez-Vázquez,[3] M. C. Buján-Núñez,[3] J. E. Arias[1]*

[1] *Instituto de Investigacións Tecnolóxicas, Universidade de Santiago de Compostela; 15782 Santiago de Compostela, Galicia (Spain)*

[2] *Facultade de Física, Departamento de Física Aplicada, Universidade de Santiago de Compostela; 15782 Santiago de Compostela, Galicia (Spain)*

[3] *Facultade de Química, Departamento de Química Física, Universidade de Santiago de Compostela; 15782 Santiago de Compostela , Galicia (Spain)*
*fadbal@usc.es*

The magnetocaloric properties of a fine magnetic particle system are studied by means of a Monte Carlo technique, focusing on the role played by the magnetic anisotropy. Fixing the size and magnetization of the particles, it is possible to fit a particular value of the anisotropy that leads to a larger entropy change. It is also observed that the blocking temperature increases with increasing values of the anisotropy, as it is expected.

# Theoretical Study of Charge Mobility in Organic Materials using a Mesoscopic Model

*Hélder M C Barbosa, Marta M D Ramos*

*Department of Physics, University of Minho, Campus de Gualtar, 4710 – 057 Braga, Portugal*

*helder@fisica.uminho.ptl*

Since the late 1980s, researchers have been reporting the success in making electronic and optoelectronic devices from *undoped* conjugate polymers, such as thin-film field-effect transistors (FETs) [1, 2], electroluminescent diodes (LEDs) [3, 4] and solar cells [5, 6] , with the perspective to obtain cheap devices due to the low cost fabrication and easy processing. Although conjugated polymers exhibit many advantages, devices performance made with these materials are far from the ones obtained with inorganic semiconductors.

One of the key parameters for the low efficiency of devices based on semiconducting polymers is their low charge mobility that has its origin in the molecular properties of the polymer chains and the nanostructure of polymer bulk. Conjugated polymers do not have a well-ordered structural configuration, where the polymer backbone is disrupted by chemical or structural defects, such as chain kinks or twists, which leads to charge localization along a conjugated segment. In order to move the charge along the polymer layer due to an apply electric field, charge carriers must hop between conjugate segments. This hopping process was first suggested by Conwell [7] and Mott [8] for inorganic semiconductors. Due to the several factors that influence charge transport in conjugated polymers, like energetic and spatial disorder, doping, inter/intra-chain interactions, morphology, interfaces, among others, theoretical studies based on first principles are inefficient to give a whole picture of the underlying semiconductor physics in these materials, and even the concept of band conduction for free charges does not apply.

It is well establish that the energetic and spatial disorder leads to a density of states inside of the polymer with a Gaussian distribution of energy (Gaussian density of states - DOS), that was first proposed by Bassler [9] and is based on the observation of Gaussian shaped absorption spectra in polymer materials. In 1993, Bassler proposed the Gaussian disorder model (GDM) [9] for charge transport in organic disordered materials. In his model, he assumes that electron-phonon coupling is sufficiently weak so the polaronic effects can be neglected and the hopping rates can be described by the Miller-Abrahams formalism[10]. Alternative models are based in Marcus formalism [11] for hopping rates between the DOS that considers strong charge-phonon interaction. Both models are valid in a short range of temperature and applied electric field but none of them considers the molecular properties of the conjugated polymer used (i.e. the ionization potential and electron affinity) or the mechanism of charge mobility along a polymer strand (intra-molecular mobility).

Here we present our first results obtained with our mesoscopic model for charge transport in organic materials. The main innovation of our model is taking into account: intra-molecular mobility along polymer chains and the zero-field energy barrier heights for inter-molecular charge mobility, both obtained from atomistic simulations [12-16]. Like other models, we use a dynamical Monte Carlo method to simulate charge transport, where the algorithm is based on the first reaction method (FRM) [17]. In our model we consider two processes for charge transport: intra-molecular charge transport along a polymer chain, where we assume that the coupling between the electronic and atomic motion in the polymer chain creates a quasi-particle known as polaron [18], that can move along the strand due the local electric field; inter-molecular charge transport between polymer chains, where charge transport occurs by a process thermally activated (hopping). In our simulations, the organic material is made of cylinders with different sizes and orientations that represent the different lengths of the conjugated polymer segments and the anisotropy of the material. In this way we incorporate the spatial disorder effect in charge transport. The effect of the energetic disorder

in charge transport is taken into account by the different zero-field energy barrier heights for the inter-molecular charge transport that depends on the type of polymer used and the length of the conjugated segment. Although at this moment we do not use any molecular dynamic process to generating morphologies of the polymer layer, the way that the cylinders distribute in the bulk is representative of the known morphology for the polymer films.

The hopping rate for an electron or hole is given by [16]:

$$w_{ij} = w_{0,hop} f(\vec{E}) g(r_{ij}) j(E_{ij})$$

where $j(E_{ij})$ is the energy barrier height dependence factor for charge hopping and accounts for the temperature dependence, $g(r_{ij})$ is the distance dependence factor for charge tunnelling between two sites, $f(\vec{E})$ is a factor that depends on the angle between the local electric field direction and the jump direction and $w_{0,hop}$ is the maximum hopping frequency for a charge which depends on its sign.

Our first results show that charge mobility depends on the orientation on the polymer strands and the chemical structure of the polymer used. Since in our model we use the molecular properties of the materials used in several organic optoelectronic devices and our results are strongly affected by the nanostructure of the organic bulk (e.g. polymer chain orientation that creates crystalline and amorphous regions, dimension of the aggregation zones for one kind of material, the presence of defects and impurities), we hope this new model can give some insight about charge mobility in organic semiconductors and give some guidelines for improving organic-based devices efficiency.

**References:**
[1] A. Assadi, C. Svensson, M. Willander, O. Inganas, Applied Physics Letters, **3** (1988) 195.
[2] S. Forrest, P. Burrows, M. Thompson, Ieee Spectrum, **8** (2000) 29.
[3] R.H. Friend, R.W. Gymer, A.B. Holmes, J.H. Burroughes, R.N. Marks, C. Taliani, D.D.C. Bradley, D.A. Dos Santos, J.L. Bredas, M. Logdlund, W.R. Salaneck, Nature, **6715** (1999) 121.
[4] A. Moliton, R.C. Hiorns, Polymer International, **10** (2004) 1397.
[5] H. Hoppe, N.S. Sariciftci, Journal of Materials Research, **7** (2004) 1924.
[6] N.S. Sariciftci, L. Smilowitz, A.J. Heeger, F. Wudl, Science, **5087** (1992) 1474.
[7] E.M. Conwell, Physical Review, **1** (1956) 51.
[8] N.F. Mott, Canadian Journal of Physics, **12** (1956) 1356.
[9] H. Bassler, Physica Status Solidi B-Basic Research, **1** (1993) 15.
[10] A. Miller, E. Abrahams, Physical Review, **3** (1960) 745.
[11] R.A. Marcus, Reviews of Modern Physics, **3** (1993) 599.
[12] A.M. Almeida, M.M.D. Ramos, A.M. Cadilhe, Computational Materials Science, **1-2** (2002) 54.
[13] A.M. Almeida, M.M.D. Ramos, H.G. Correia, Computational Materials Science, **1-2** (2003) 128.
[14] A.M. Almeida, M.M.D. Ramos, R.M. Ribeiro, Macromolecular Symposia, (2002) 479.
[15] M.M.D. Ramos, A.M. Almeida, H.M.G. Correia, R.M. Ribeiro, A.M. Stoneham, Applied Surface Science, **1-4** (2004) 438.
[16] M.M.D. Ramos, H.M.G. Correia, Thin Solid Films, **1-2** (2006) 394.
[17] J.J. Lukkien, J.P.L. Segers, P.A.J. Hilbers, R.J. Gelten, A.P.J. Jansen, Physical Review E, **2** (1998) 2598.
[18] M.M.D. Ramos, A.M. Almeida, Vacuum, **2** (2001) 99.

# CHIRALITY EFFECT ON THE MECHANICAL MOTION BETWEEN MWNT SHELLS

*Amelia Barreiro[1,2], Joel Moser[1], Thomas Pichler[2], Laszlo Forro[3], Adrian Bachtold[1]*
*[1] Institut Català de Nanotecnologia and Centro Nacional Microelectrónica, Campus Universitat Autónoma de Barcelona, E-08193 Bellaterra, Spain*
*[2] Leibniz Institut für Festkörper und Werkstoffforschung, Helmholtzstrasse 20, P.O. Box 270116, 01171 Dresden, Germany*
*[3] EPFL, CH-1015 Lausanne, Switzerland*

*Amelia.barreiro.icn@uab.es*

We have fabricated nano-electromechanical devices consisting of a suspended multiwall carbon nanotube (MWNT). The device allows the outermost shell to move and/or rotate along and/or around the MWNT axis (inset of Fig. 1). To make this motion possible, the MWNT has been engineered using the electrical-breakdown method [1, 2, 3]. A gold pellet has been added on the moveable shell in order to observe the motion. It is possible to make the gold pellet slide in a controlled manner along the suspended MWNT using an AFM tip (Fig. 1). The motion of the moveable shell can also be actuated by passing a current through the MWNT. Depending on the device, the moveable shell either moves and/or rotates along and/or around the MWNT axis. The longitudinal, rotational or spiral motion is attributed to the potential barrier of the relative barrier between two shells, which depends on the chirality of the shells [4]. To our knowledge this is the first experimental evidence of the chirality effect on the mechanical motion. The motion of the moveable shell always occurs when a large current flows through the MWNT. At these currents, the gold pellet is often observed to melt, thereby suggesting that the movement is thermally induced.

**References:**

[1] P.G. Collins, M. S. Arnold, Ph. Avouris, Science **292** (2001) 706.
[2] P.G. Collins, M. Hersam, M. Arnold, R. Martel, Ph. Avouris, Phys. Rev. Lett. **86** (2001) 3128.
[3] B. Bourlon, D.C. Glattli, B. Placais,  J.M. Berroir, C. Miko, L. Forro, A. Bachtold, Phys. Rev. Lett. **92** (2004) 26804.
[4] R. Saito, R. Matsuo, T. Kimura, G. Dresselhaus, M.S. Dresselhaus, Chem. Phys. Lett. **348** (2001) 187.

**Figures:**
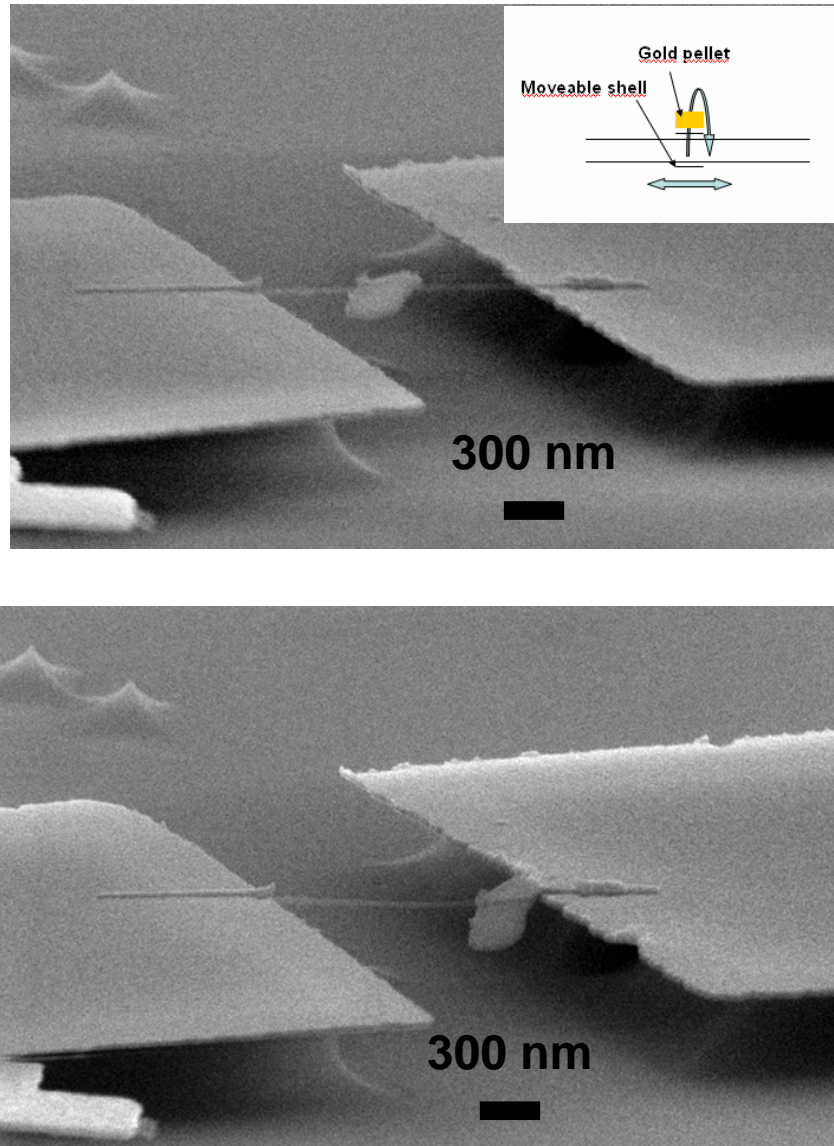




Fig. 1. SEM images of one device with the gold pellet that has been moved using an AFM tip. The inset illustrates the degrees of freedom of the moveable shell structure.

# FABRICATION OF A MEA FROM METAL-POLYMER NANOCOMPOSITE MEMBRANES FOR FUEL CELLS APPLICATIONS

Parrondo J., Barrio A., Muraviev D. N.[*], Lombraña J.I. and Mijangos F.[(1)]

Departamento de Ingeniería Química, Universidad del País Vasco, Apdo. 644, 48080, Bilbao, Spain.

[*]Unitat de Química Analítica, Departament de Química, Universitat Autònoma de Barcelona, 08193, Bellaterra, Spain.

[(1)]federico.mijangos@ehu.es

The synthesis and characterization of Metal NanoParticles (MNP) has attracted great interest of scientists and technologists within the last years due their unique physical and chemical properties [1]. These properties can be advantageous in various practical applications including catalysis- and electrocatalysis-based processes, which occur in, for example, fuel cells or sensing devices. In this sense, nanoparticles composed of, for example, gold, cobalt, palladium, copper, and cadmium selenide are of great interest due to their potential use in various nanotechnology applications [2].

At the same time, the main drawback of MNP, which still limits their wide application, is insufficient stability dealing with a high trend for aggregation. The coalescence of nanoparticles leads to the loose of their nanometric size and, as the result, of their unique properties. In order to overcome this drawback, stabilization of MNPs in polymeric matrices of different types has been proven to be one of the most promising strategies to prevent their aggregation and to stabilize their properties [3]. As a result, Polymer-Stabilized MNPs (PSMNPs) and Metal-Polymer Nanocomposites (MPNCs) on their base start to find different applications in various fields of science and technology [4].

The polymer used in this work was SPEEK that has been traditionally used for the development of Proton Exchange Membranes (PEM) and their application in both fuel cells and electrolysers. PEM fuel cells are regarded as a possible alternative power source for stationary and mobile applications [5]. Due to the catalyst costs, many

researchers have been studying the membrane and the electrode assembly (MEA) manufacturing processes that can reduce the content of Pt in the electrocatalyst layer while maintaining the performance. The MEA is the heart of the PEM fuel cells and catalyst plays an important role into the fuel cell operation.

In this paper the catalyst layer for a PEMFC-electrode was prepared from metal nanoparticles synthesized and stabilized on SPEEK (PSMNPs). These polymer composites were dissolved with dimethyl formamide to prepare inks that were dispersed with an aerograph on the gas diffusion layer (GDL). Finally, activated GDLs were glued to the membrane by hot pressing. The optimal conditions for this process were established in a previous work [6].

Once the MEA was assembled using MNP, it was mainly characterized by means of polarization curves (current density vs. voltage) obtained from a single hydrogen fuel cell of 5 cm$^2$. The activation drop and ohmic resistance that could be established through these curves are discussed along the whole paper comparing activity of PSMNP against standard PEMFC electrodes.

**References**

[1] G. Schmid, Nanoparticles: From Theory to Application, Wiley-VCH, Weinheim (2004)

[2] A. P. Alivisatos, J. Phys. Chem., **100**, (1996), 13226

[3] A. D. Pomogailo, G. I. Dzhardimalieva, A. S. Rozenberg, D. N. Muraviev, J. Nanoparticles Res., **5**, (2003), 497

[4] J. A. Schwarz, C. I. Contestu, K. Putyera, Encyclopedia of Nanoscience and Nanotechnology, Marcel Dekker, NY, (2004)

[5] S. Litster, G. McLean, Journal of Power Sources, **130,** (2004), 61-76

[6] J. Parrondo, M. Uresandi, A. Barrio, International Journal of Hydrogen Energy, (under review)

# Nanostructured Fiber Optics as Highly Sensitive Mechanical Sensors

*R.-M. Beiu, C-tin.D. Stanescu, V. Beiu*

*University "Politehnica" of Bucharest, Spl. Independenţei 313, 060042, Bucharest, Romania*
*College of Information Technology, UAE University, PO Box 17555, Al Ain, UAE*
[rbeiu@yahoo.com](rbeiu@yahoo.com), [vbeiu@uaeu.ac.ae](vbeiu@uaeu.ac.ae)

The enduring trend towards miniaturization has lead to many new theoretical advancements—which have enabled countless applications—in electronics, optics, and fine mechanics. Riding on the nanotechnology boost, these fields are now coming together allowing us to envisage the development of new nanoscale sensors, as well as novel ways of processing (and communicating) information.

Currently, fibre optic (FO) based systems are playing a major role in communications, but the particular qualities they posses makes them a very attractive candidate for both sensing and processing information [1], [2], [3]. Another recent development was that of photonic crystals (PCs). These are regular (dielectric modulated) structures, with a periodicity comparable to that of the input wavelength. They exhibit very strong interaction with light [4]-[8], and present peculiar characteristics (as light interacts with PCs in ways completely different from what is knows from classical optics), including inhibition of light transmission (inside the PC), and photonic band gap formation. Such phenomena can be used in modern information transmission and processing systems, as well as in sensory devices [8]-[11].

In this paper we will show that embedding PC structures into standard monomode FOs allows for highly sensitive detection of mechanical deformations. The paper starts by briefly reviewing the basic characteristics of FOs and PCs. Afterwards we present the new FO sensor (Fig. 1 (a)). Simulations were done using EMExplorer. They reveal both the transversal electric (TE) and magnetic (TM) components of the electromagnetic field ($E_x$, $E_y$, $E_z$, $H_x$, $H_y$, $H_z$), showing their amplitude (Fig. 2(a)) and phase (Fig. 2(b)). These simulations have been performed at loading (elongating) forces $F$ ranging from 0N to 10N. When a force $F$ is applied to the system, an elongation $\Delta L$ will appear (see Fig. 1(b)), while all the elementary dimensions of the PC ($a$, $b$, $\phi_1$, $\phi_2$ in Fig. 1(c)) will also be affected. These, in turn, will change the PCs' optical characteristics. Fig. 2(b) shows very sharp phase variations of TM ($H_x$ and $H_z$). These transitions of $H_x$ and $H_z$ can be used to detect very small mechanical deformations (see also Fig. 3). For example, for a variation of 1N (i.e., for $F$ varying from 2N to 3N) the phase on $H_x$ varies from –3.134 to 3.075 radians (Fig. 2(b), and Fig. 3). This means that the PC embedded sensor will exhibit a phase variation (on $H_x$) of 3.075 – (–3.134) = 6.25 radians = 358° for a mechanical deformation of $\Delta L$=4.48 nm (corresponding to 1N). This means that the sensor has a sensitivity of 4.48 nm/358° = 0.0125 nm/°. The main conclusion is that *the sensitivity of the PC embedded sensor described in this paper is in the tens of pico-meter range*. Improvements (e.g., hexagonal array PCs [7]) and future directions of research (e.g., faster simulations [12] and variation analysis [13]) are ending the paper.

**References:**
[1]  B. Lee, Optical Fiber Tech., **9** (2003), pp. 57–79.
[2]  K.S.C. Kuang, S.T. Quek, and M. Maalej, J. Meas. Sci. Tech., **15** (2004), pp. 2133–2141.
[3]  C. Gorecki, J. Optics, **26** (1995), pp. 29–34.
[4]  E. Yablonovitch, Sci. Amer., **285** (2001), pp. 47–55.
[5]  S. John, O. Toader, and K. Busch, Encyclopedia of Physical Sci. & Tech., **12** (2002), Acad. Press, pp. 133–145.
[6]  A.S. Jugessur, P. Pottier, and R.M. De La Rue, Optics Expr., **12** (2004), pp. 1304–1312.
[7]  A.S. Jugessur, P. Pottier, and R.M. De La Rue, Phot. & Nanostr. – Fundam. & Appls., **3** (2005), pp. 25–29.

[8] R.M. Beiu, C.D. Stanescu, and A. Cârstoiu, UPB Sci. Bull., under review (2007/8).
[9] R.M. Beiu, C.D. Stanescu, and V. Beiu, Proc. IEEE-NANO'07, Hong Kong, in press.
[10] R.M. Beiu, C.D. Stanescu, and V. Beiu, Proc. IEEE-MWSCAS'07, Montreal, in press.
[10] Z. Xu, L. Cao, C. Gu, Q. He, and G. Jin, Optics Expr., **14** (2006), pp. 298–305.
[11] Y. Jiao, S. Fan, and D.A.B. Miller, IEEE J. Quant. Electr., **42** (2006), pp. 266–279.
[12] D.A.B. Miller, Proc. IEEE, 88, 2000, pp. 728–749.

**Figures:**
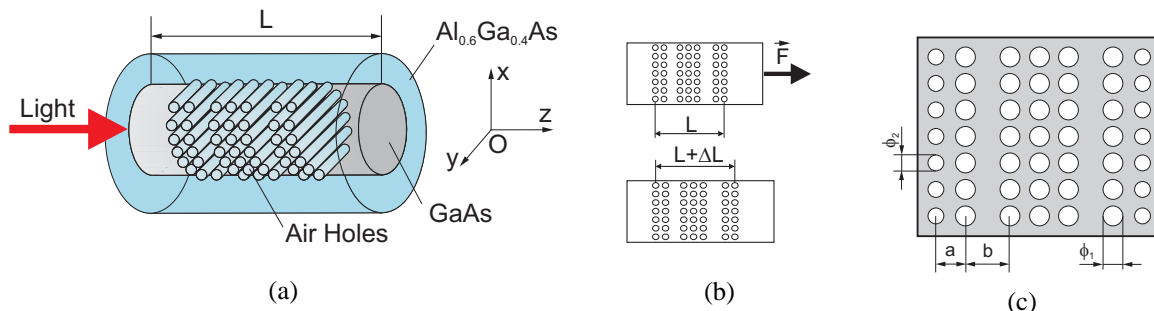


Fig. 1. (a) Schematic view of the PC sensor embedded in a FO; (b) Deformation of the sensor of length *L,* under a loading force *F*; and (c) A section through the PC (air holes) showing the elementary geometrical dimensions *a*, *b*, $\phi_1$, $\phi_2$.
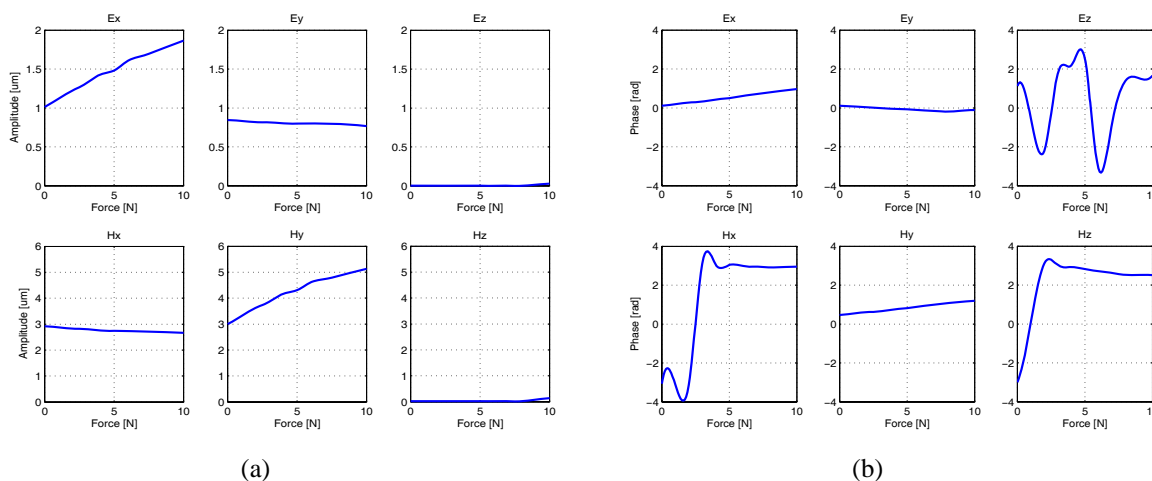


Fig. 2. (a) Amplitude ($\vec{E}$ and $\vec{H}$) versus elongating (loading) force *F*; (b) Phase ($\vec{E}$ and $\vec{H}$) versus elongating (loading) force *F*.
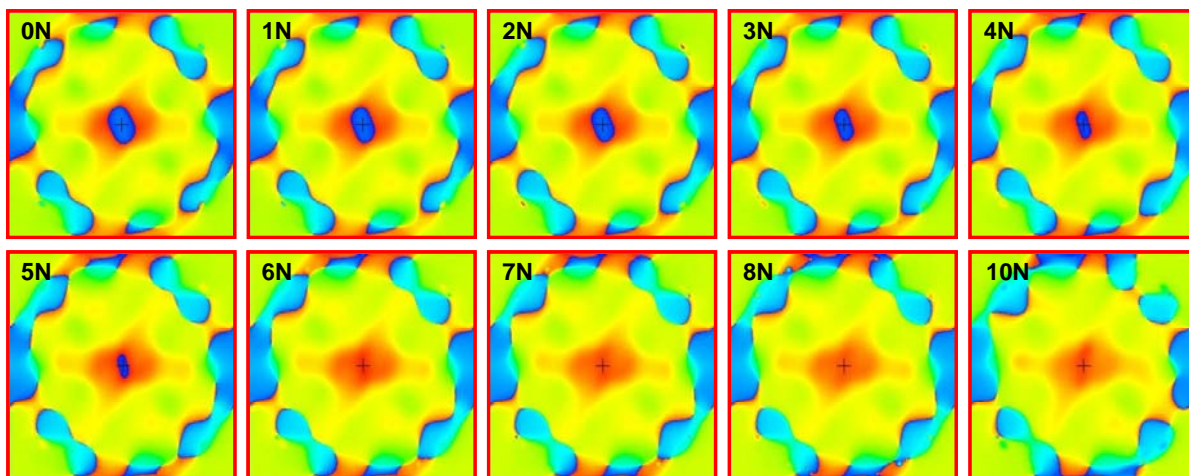


Fig. 3. The $H_x$ phase component ($O_z$ section at the end of the FO) for elongating (loading) forces *F* in the range 0N to 10N. A "blue opening" is clearly visible in the center at 0N (surrounded in red), but it is quickly fading (see top row), while completely vanishing (disappearing) at 6N.

# POLARISATION AND FOCUSING SYSTEM IN PHOTONIC CRYSTALS

W. Belhadj[1], F. AbdelMalek[1,2], S. Haxha[3], H. Bouchriha[1]

[1]Department of Physics, Quantum Physics, Faculty of Sciences of Tunis

[2]National Institute of Applied Sciences and Technology, BP 676 Cedex 1080 of Tunis, Tunisia

[3]Photonics Group, Department of Electronics, Kent University, UK

During the past few years, there have been growing interests in studying a novel class of media that have simultaneous negative dielectric permittivity and magnetic permeability. These materials are also known as left-handed materials (LHMs)[1], where $\vec{k}$, $\vec{E}, \vec{H}$ form a left-handed (LH) set of vectors. The wavevector is untiparallel to the Poynting vector (i.e., $\vec{S}.\vec{k} \, \pi \, 0$, where $\vec{S}$ is the Poynting vector). Pendry [2] has studied a slab of LHMs that have permittivity $\varepsilon$ =-1 and permeability $\mu$=-1 and showed that this material can refocus propagating waves emitted by a point source placed closely to one side of the surface of the slab into a perfect point image on the other side of the slab. The superlens possesses many advantages compared to conventional lenses. This type of lens can overcome the limitation on lens performance by focusing light onto a subwavelength area. Images based on the LHM superlens have been observed both numerically and experimentally [3]. The superlensing phenomenon can be explained by using rays in traditional optics, however, the propagation of evanescent waves is achieved due to the amplification of transmission through the negative index. The transmission considered here differs fundamentally from its conventional of energy transport, evanescent waves need not carry energy in their decaying directions. It seams that the transmission of evanescent waves is large and can exceed unity without any violation of energy conservation. Recently, Pendry [2] used Veslago's analysis and has suggested that evanescent waves could be amplified inside the LHM slab, this character has been used to accurately reconstruct the point source in the image plane.

We focus on the design of a polarisation independent focusing system of waves in a two dimensional (2D) photonic crystal (PC). The design is conducted by using the finite difference time domain (FDTD) method. The variation of the air hole radius and the refractive index of the high index material leads to a complete all-angle negative refraction can be obtained for both TE and TM polarisations. The PC simulated is composed of dielectric cylinders in air of dielectric permittivity 12 arranged in a square lattice. A Gaussian source is located at a distance $a$ from the left-side of the surface of the slab, where $a$ is the lattice constant.

The band structure is performed by utilising the plane wave, the result appears in fig.1, which shows that in this configuration the photonic crystal exhibits a partial photonic band gap for the transverse electric (TE) polarisation. While, this structure does not show a photonic band gap for the transverse magnetic (TM) polarisation. Fig. 2 shows the snapshot of the electric field for a continuous wave point source placed at a from the left-hand surface. Fig.2 shows that a point image has created located on the right-hand side of the slab. The frequency of the image is $f$ = 0.192 $a/\lambda$. In order to improve the image, the radius of the dielectric cylinder is increased from 0.35 $a$ to 0.45 $a$, by keeping the permitivity equal to 12. The band structure is calculated and presented in Fig. 3. This figure shows that TE band gap is destroyed, whereas, a TM photonic band gap has appeared. In fig.4, we report the image of the source shown on the right-hand side of the photonic crystal slab, it is clearly shown that the image has much better resolution than its counterpart presented in Fig. 2. This is mainly due to the strong amplification of the evanescent components through the slab. It was shown that the amplification of evanescent components can be performed for regions with an effective positive index of refraction. This is due to the resonant coupling of evanescent waves with

bound photon modes, which is known as all-angle negative refraction (AANR) [4]. The amplified evanescent components are the key in the formation of the focused image. The image frequency is obtained at 0.2$a/\lambda$.

**References**

[1] V.G. Veselago, *Soviet Physics* USPEKI 10, 509 (1968).

[2] J. B. Pendry, *Phys. Rev. Lett*. 85, 3966 (2000).

[3] Pendry, J. B., Holden, A. J., Robbins, D. J., and Steward, W. J., *IEEE trans. MTT*, 47, 2075 (1999).

[4] R.A. Shelby, D. R. Smith, and S. Schultz, *Science* 292, 77 (2001).
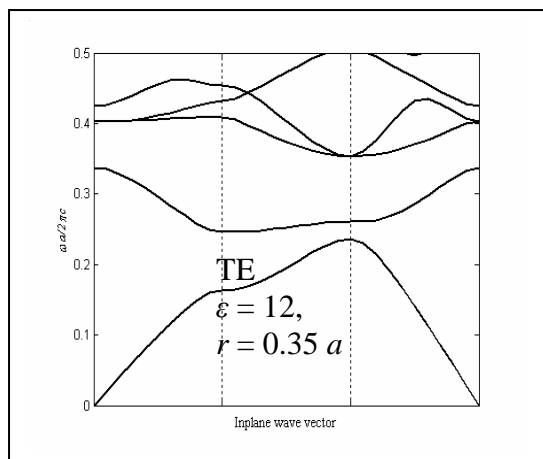
Fig.1 Band structure, TE
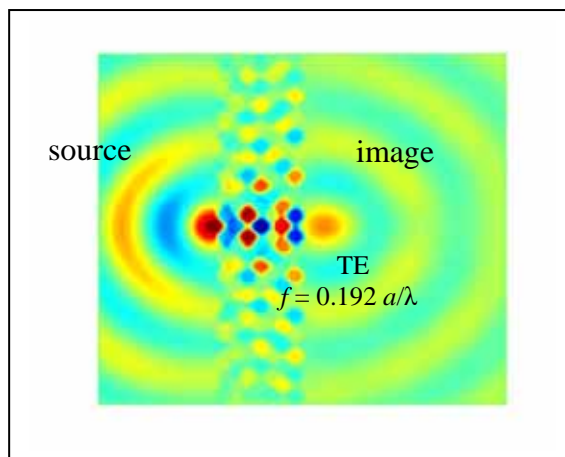


Fig.2 Snapshot of the (TE) $H_z$
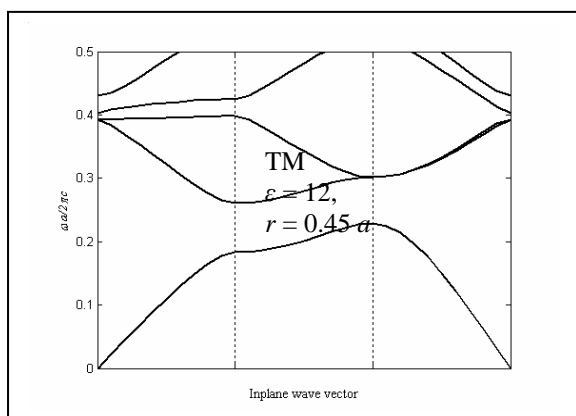


Fig.3 Band structure, TM
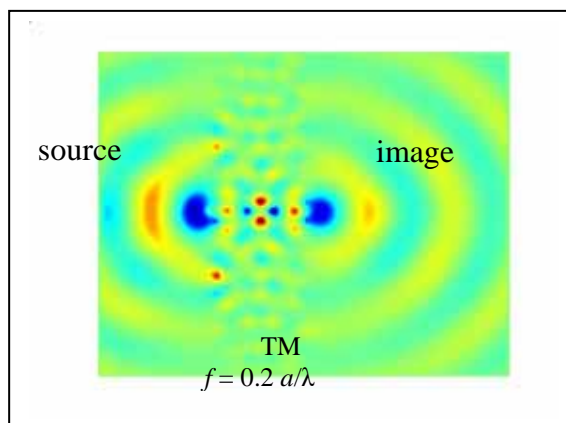


Fig.4 Snapshot of the (TM) $E_z$

**The growth and characterisation of zinc oxide nanomaterials for optoelectronic devices.**

*J.S. Bendall. M.E. Welland*
*Nanoscience Centre, University of Cambridge, United Kingdom*
*jsb53@cam.ac.uk*

Zinc oxide is an extremely versatile material and research into it has recently undergone a renaissance as people explore its potential use in optoelectronics, gas sensor technology or electronic circuits, to name but a few. Coupled with this is the fact that it is an extremely easy material to manufacture, with several high temperature and low temperature routes available, and the reaction conditions and parameters chosen have been shown to influence the fundamental structure and properties of the final product. Any potential application of ZnO will be dependent on the final morphology of the product e.g. surface area, stochiometry, particle size, etc.

Our research is concerned with the synthesis and characterisation of zinc oxide nanomaterials, with a view to incorporating the structures into optoelectronic devices. Due to temperature restrictions from the substrate, these structures have been shown to grow at temperatures lower than 100°C from a solution based method. This renders the synthesis cheap and easily reproducible. Furthermore, by altering reaction conditions one can gain full control of the size and shape of nanoparticles obtained. We have demonstrated that, by utilising and adapting the reagent chemicals and conditions, we can get full control of the size and shape of nanostructure formed in the secondary growth regime. This can be explained in terms of the polarity and activity of the wurtzite crystal faces. Furthermore, we can utilise many of our synthesis techniques in the production of novel optoelectronic devices.
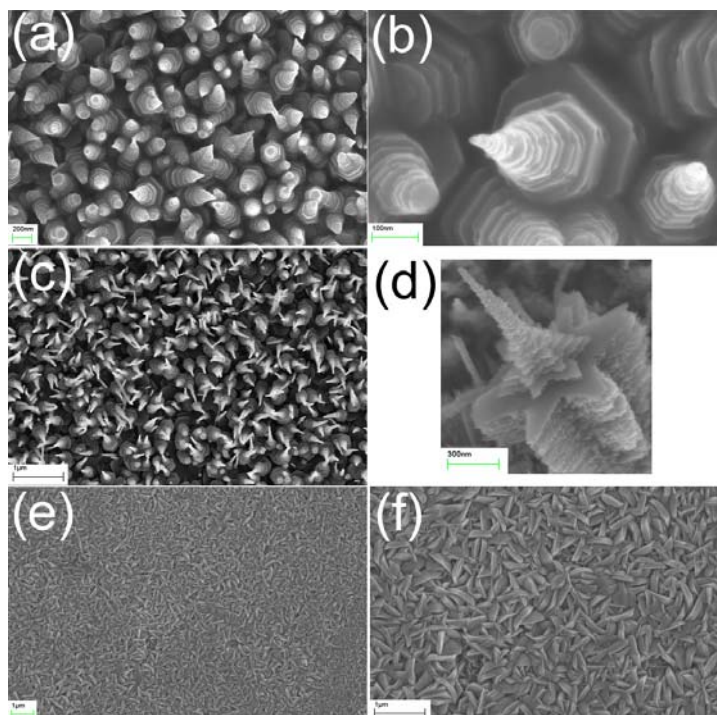


ZnO nanostructures from solution growth methods.

# FIRST-PRINCIPLES ANALYSIS OF STM IMAGE HEIGHTS ON SI(100)

*Kirk Bevan*
*Purdue University*
*United States*
*kbevan@purdue.edu*

We report on theoretical investigations of STM image heights on Si(100). Calculations are performed using density functional theory (DFT) within the Keldysh non-equilibrium Green's function (NEGF) formalism. The non-equilibrium potential drop between Si(100) and a scanning tunneling microscope (STM) tip is determined self-consistently. This potential drop is found to play an important role in the calculated image height characteristics of adsorbed hydrocarbons, by lowering the vacuum barrier and shifting molecular levels.

Numerical data collected for image heights of styrene against a hydrogen passivated Si(100) background are found to agree quantitatively with the corresponding experimental results. We also present a comparison between results obtained by the NEGF-DFT formalism and the Tersoff-Hamann approximation, showing that non-equilibrium analysis can be important in the study of STM image heights of molecules.

# Semiconductor quantum dots containing a magnetic impurity: Exciton spectrum and spin precession

A. K. Bhattacharjee

Laboratoire de Physique des Solides, UMR du CNRS, Université Paris-Sud,
91405 Orsay, France
*bhattacharjee@lps.u-psud.fr*

Diluted magnetic semiconductor (DMS) quantum dots (QDs) have been studied for more than a decade, mostly focusing on the confinement-enhanced $sp-d$ exchange interaction effects such as exciton magnetic polaron. The extreme dilution limit with one transition-metal impurity, i. e., one localized spin per QD seems particularly promising for spintronics and quantum information processing. The optical and magneto-optical properties of such Mn-doped ZnS [1], CdS [2] and ZnSe [3] nanocrystals (NCs) have been investigated, the last system revealing an order-of-magnitude enhancement of the giant Zeeman effect with respect to the corresponding bulk DMS. More recently, a zero-field splitting of the exciton line into six components was reported [4] in Mn-doped CdTe/ZnTe self-assembled quantum dots (SAQDs), providing a more direct evidence of the confinement-induced enhancement of $sp-d$ exchange.

We shall discuss a theoretical study of the optical properties of QDs containing a single magnetic impurity based on a multiband envelope function formalism. It provides a unified treatment of Mn-doped semiconductor QDs of different symmetries: Spherical/ellipsoidal NCs and epitaxial SAQDs, focusing on their respective potentialities for the optical detection and manipulation of the Mn spin state. The zero-field splitting pattern of the exciton arising from the confinement-enhanced $sp-d$ and electron-hole exchange interactions is deduced. The optical absorption spectrum shows a strong dependence on the Mn spin orientation with respect to the polarization of light, promising for optical detection. The theoretical results, which are analytical in the high-symmetry cases, show a good agreement with the measured optical and magneto-optical properties of Mn-doped ZnSe NCs and CdTe/ZnTe SAQDs. Predictions for ellipsoidal wurtzite-structure CdSe NCs are also presented. Typically, NCs are smaller in size than SAQDs and show a correspondingly larger spin coupling and overall splitting. But the splitting pattern is simpler in SAQDs, with fewer components, making for easier spin detection. The coherent precession of the Mn spin induced by a resonant circularly polarized laser pulse is also studied. A zero-field precession of substantial amplitude is obtained in nearly spherical NCs with strongly allowed hole-Mn spin flips. The amplitude is negligibly small in typical SAQDs, but the application of a transverse magnetic field (Voigt configuration) makes it measurable. Interestingly, in SAQDs containing a resident hole such as neutral GaAs:Mn or positively charged II-VI:Mn QDs, a significant zero-field spin precession of single frequency is predicted.

[1] R. N. Bhargava *et al.*, Phys. Rev. Lett. **72**, 416 (1994).
[2] D. M. Hoffman *et al.*, Solid State Commun. **114**, 547 (2000).
[3] D. J. Norris *et al.*, Nano Letters **1**, 3 (2001).
[4] L. Besombes *et al.*, Phys. Rev. Lett. **93**, 207403 (2004).

# CHARACTERIZATION OF NANOSTRUCTURED ELECTRODES FOR NEURAL IMPLANT

*O. Bibari, F. Sauter-Starace, P. Mailley, J. Dijon, E. Rouvière,*
*G. Charvet, S. Boisseau, C. Arnoult, P. Caillat and A.L. Benabid*
*CEA Grenoble, 17 Rue des Martyrs 38054 Grenoble,France*
*olivier.bibari@cea.fr*

In recent years, researchers have been working on a way to interface living cells, such as neurons, to an electronic chain of acquisition to create a brain computer interface (BCI) system. Significant success has been reported using multi-electrode arrays implanted in motor cortex of paraplegic patient [1] to control a computer mouse or in a monkey's cortex [2] to move a mechanical arm. But all these devises have a limited efficiency for chronicle application due to the development of a fibrous shell around the implant, which degraded its electrical performances.

Carbon nanotubes structured surface seems to be a good candidate to make future biocompatible and biostable electrodes [3]. Indeed, numerous nanomaterials exhibit great affinity with biological samples [4], which could be link to the mimetism between the topology of nanomaterials and biological tissues. Furthermore, carbon nanotubes electrodes (CNT-Es) hold remarkable electrical properties coupled with a great surface area, which tends to a reduction of the electrode output impedance and an increase of its capacitance. Consequently, CNT-Es improve the stimulation capability and increases signal/noise ratio by limiting the thermal noise proportional to the interfacial impedance.

In this paper we expose our results on the integration of such system based on original nanotubes functionalization, electrochemical characterization related to electrical model, in-vitro biocompatibility testing and stimulation-sensing performance evaluation using a specific electronic system of measurement developed through the NEUROCOM project [5].

- Electrode fabrication

To produce CNT-Es, we first fabricate silicon based TiN microelectrodes of different diameter (50μm, 100μm, 150μm) on which we deposited by a lift-off process 5 nm of NiFe (80:20) catalyst layer. Finally, carbon nanotubes were synthesized on chip by CVD process at 570°C under acetylene atmosphere [6].

- Surface treatment and characterization

Carbon nanotubes surface treatment is a fundamental issue to overcome their hydrophobic property. Indeed, neurons growth requires hydrophilic surfaces and electrolyte has to go through pores to take advantage of the maximum surface area. Different treatments have been characterized such as, oxygen plasma, liquid phase oxidation in acidic or basic solution using XPS, surface energy measurement and impedance spectroscopy. Electrodes treated by AC-bias between -0.2V and +1.2 V in Brown solution (NaOH 1M in DI water: Ethanol; 1:1) show best results. We were able to measure by cyclic voltamperometry a capacitance of 1.3 mF/cm², which is 100 times the one of untreated electrodes. We also used impedance spectroscopy technique to characterized interfacial impedance between CNT-Es and a phosphate buffer solution (PBS) and develop an electrical model of the interface based on ladder representation and correlated with electrode porosity checked by BET.

- In vitro biocompatibility

We assessed the biocompatible properties of CNT-Es on NG108 neuron-like cells. For this study, we also investigated the influence of adhesion promoting layers such as poly-L-lysine coating. To visualize the NG108 cells we revealed by fluorescence with Tuj1 fluorescent dye

and observed that cell tend to grow preferentially on CNT-Es. This result has been constantly observed independently to the use of a cell poly-L-Lysine coating.

- Electrical characterization and spike measurement

We first evaluated electrical noise of CNT-Es immerged in PBS and connected to NEUROCOM bench. 50µm diameter CNT-Es treated with brown solution were tested and show noise amplitude of 13µV pic to pic, which is remarkable considering that the electrical noise of NEUROCOM system by itself is 10µV.

Conclusion and Outlook

These first results are very promising. Indeed our carbon nanotubes have been shown to promote cell growth. Moreover, they improve our chip design by increasing signal to noise ratio which makes them compatible with applications of spike recording. To complete this study and confirm our results, CNT-Es are now being tested on their ability to record and stimulate the electrophysiological activity of cortical neural cells from embryonic mice. and these outcomes will be presented in future communication.

**References:**

[1]  P. R. Kennedy, R. A. E. Bakay, M. M. Moore, K. Adams, and J. Goldwaithe, IEEE Transactions on rehabilitation engineering, vol. 8, June 2000, pp.198-202.
[2]  M.A. Nicolelis et al. (2003), Proc. Natl. Acad. Sci. U. S. A. 100, pp. 11041–11046.
[3]  K. Smart, A.I. Cassady, G.Q. Lu, D.J. Martin, Carbon, vol. 44, 2006, pp. 1034–1047.
[4]  K.A. Moxon, N.M. Kalkhoran, M.Markert, M.A. Sambito, J. L. McKenzie and J. Thomas Webster, IEEE Transactions of biomedical engineering, vol. 51, June 2004, pp. 881-889.
[5]  G. Charvet et al., SFN Neuroscience 2006.
[6]  T. Goislard De Monsabert, J. Dijon, P. Gadelle , Carbon, vol. 43, 2005, pp. 2441–2452.

**Figures :**
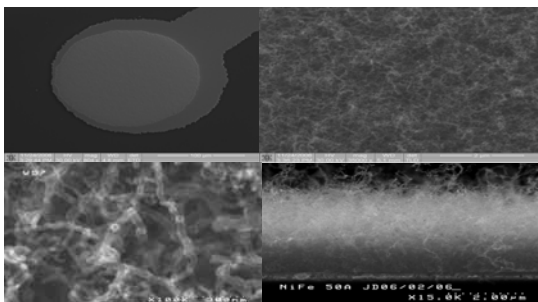


*Figure 1: SEM of carbon nanotubes electrode on TiN, 150µm*
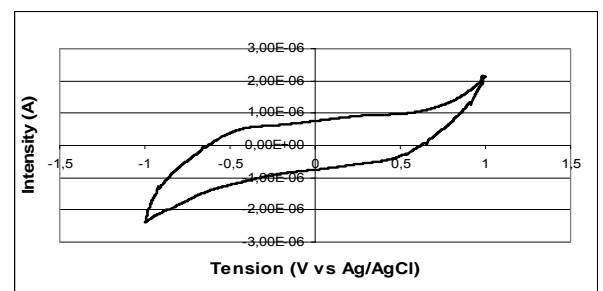


*Figure 2: Voltamogram in PBS of TiN electrode, 150µm, v=100 mV/s*
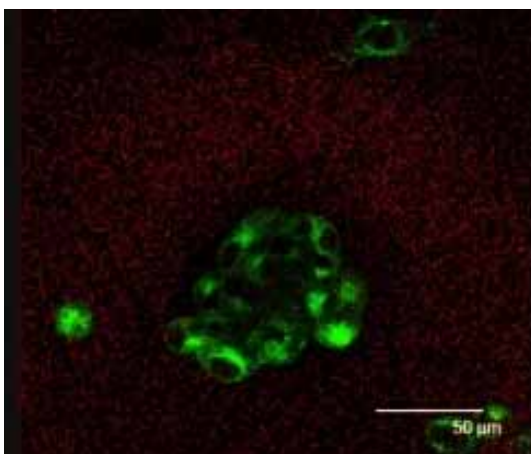


*Figure 3: NG108 culture on CNT-E, 50µm, treated with Brown solution. UV picture of NG108 cells under fluorescence excitation.*

# COLOUR REVEALS STACKING ORDER IN ULTRA THIN SELF-ASSEMBLED PHOTONIC CRYSTALS

*X. Checoury,[1] S. Enoch,[2] C. López,  and A. Blanco[3]*
*1)Institut d'Electronique Fondamentale, Univ Paris-Sud, UMR8622, Orsay, F-91405 and CNRS, Orsay, F-91405*
*2)Institut Fresnel, UMR CNRS 6133,Faculté des Sciences et Techniques, case 161, 13397 Marseille cedex 20, France*
*3)Instituto de Ciencia de Materiales de Madrid (CSIC) and Unidad Asociada CSIC-UVigo, C/ Sor Juana Inés de la Cruz 3, 28049 Madrid, Spain.*

## Abstract

In this work we present both experimental and numerical studies of the optical properties of artificial opals. The staking of up to four layers of spheres may arise according to three different arrangements: face-centered cubic, hexagonal close-packed or double hexagonal close-packed. Our study shows that the transmission spectra features are characteristic of the type of stacking and thus, each color region observed under the optical microscope can be unambiguously associated with one of the staking type. These features can be very faithfully modelled by the calculation even with no adjustable parameters. Inclusion of spectral dispersion and geometric detail allows nearly perfect fits the spectra. This result may have important repercussions for the control of the quality of the opals.
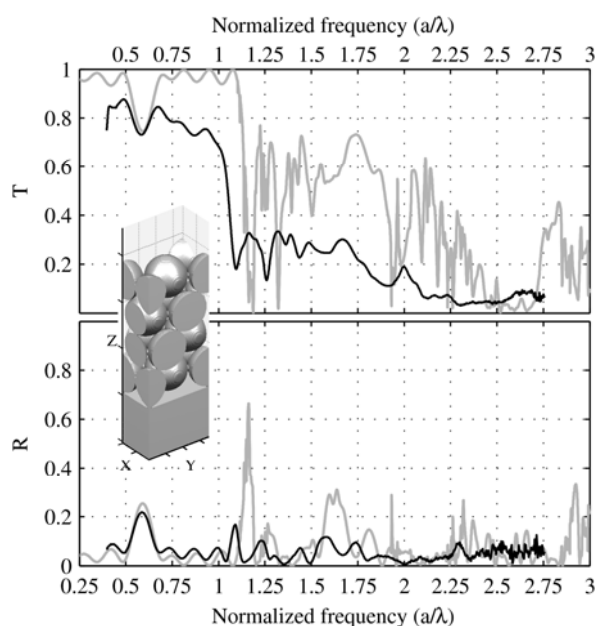
Transmission (top) and reflection (bottom) spectra of a four-layer opal arranged in a face centered cubic structure (i.e. with a stacking of the form ABCA). The black and gray curves represent experimental and simulated results respectively. In both case, the incident light is perpendicular to the stacking direction (i.e. the Z direction).

## References

X. Checoury, S. Enoch, C. López, and A. Blanco, *Appl. Phys. Lett*. 90, 161131 (2007)

# FORMATION OF NEW PHASES DURING THERMAL RE-ARRANGEMENT ON THE Cu(110)-(2X1):O SURFACE.

K. Bobrov and L. Guillemot

*Laboratoire des Collisions Atomiques et Moléculaires (Unité Mixte de Recherche CNRS-Université Paris-Sud  N° 8625) Bât. 351, Université de Paris-Sud, Orsay, France*

## Abstract

It is well known that oxygen adsorption on a Cu(110) surface is characterized by mass-transport of surface copper atoms from step edges and formation of a (2x1) oxygen strip phase [1-4].

Here we report on a discovery of new phases produced during thermal re-arrangement of the oxygen adsorbed Cu(110) surface. The oxygen-adsorbed surface was prepared by in-situ 3.7 L molecular oxygen adsorption at room temperature. The (2x1):O domains, randomly distributed on flat terraces having a characteristic zig-zag structure of etched step edges, were found to exist on the surface. Thermal annealing of the oxygen adsorbed surface resulted in: (i) structural re-arrangement of the step edges (ii) ordering of the (2x1):O strips into a superstructure and (ii) formation of new phases.

These minor phases, coexisting with the dominating (2x1):O superstructure, were found on specific surface locations only and were always confined by terrace steps. The symmetry, morphology and electronic structure of these new phases were characterized by STM. The origin of the new phases is discussed in terms of a step-confined copper atoms re-arrangement in vicinity of the surface steps.

**References**

[1] K. Kern, H. Niehus, A. Schatz, P. Zeppenfeld, J. Goerge, and G. Comsa. Phys. Rev. Let.. **67** (1991) 855.

[2] Y. Kuk, F. M. Chua, P. J. Silverman, and J. A. Meyer. Phys. Rev. B. **41**(18) (1990) 12393.

[3] R. Feidenhans, F. Grey, R. L. Johnson, S. G. J. Mochrie, J. Bohr, and M. Nielsen. Phys. Rev. B. **41** (1990) 5420.

[4] H. Dürr, R. Schneider, and T. Fauster. Phys. Rev. B. **43** (1991) 1802.

# A CHEMICAL REACTION AS A TRIGGER FOR NANOSTRUCTURE FORMATION ON A SILVER SURFACE.

K. Bobrov and L. Guillemot

*Laboratoire des Collisions Atomiques et Moléculaires (Unité Mixte de Recherche CNRS-Université Paris-Sud N° 8625), bât.351, Université de Paris-Sud, Orsay, France*

Oxygen adsorption on the (110) face of silver has been one of the most studied system, particularly interesting for two reasons: i) it is very reactive and an excellent oxygen provider for the oxidation of many molecules, ii) the O(nx1)-Ag(110) reconstructed surface provides a nice nano-structured template for the formation of layers of reacting molecules. Its reaction with water has attracted much attention in the past [1-5] as formation of stable and long range ordered hydroxyl layers has been evidenced and more recently some further insights has been gained by STM measurements [6, 7].

We will present results of our STM investigation of water interaction with an oxygen covered Ag(110) on the example of the O(4x1) reconstructed surface and show how they point to a more complex reaction dynamics than previously described. Indeed the new feature revealed by this local probe study, is the formation of quasi-rectangular islands evenly distributed across the terraces for temperatures below 230K. These features are attributed to silver islands of mono-atomic height, formed by clustering of silver ad-atoms released during reaction of the O atoms with the water molecules.

We also performed real time STM measurements during the water dosing, at two temperatures (200K and 240K), to monitor the modifications induced at the surface. We will present and discuss the drastic differences evidenced in the reaction dynamics at these two temperatures.

**References**

[1] M. Canepa, P. Cantini, L. Mattera, E. Narducci, M. Salvietti, and S. Terreni. Surf. Sci. **322** (1995) 271.
[2] M. Canepa, P. Cantini, E. Narducci, M. Salvietti, S. Terreni, and L. Mattera. Surf. Sci. **343** (1995) 176.
[3] M. Borbach, W. Stenzel, H. Conrad, and A. M. Bradshaw. Surf. Sci. **377-379** (1997) 796.
[4] K. Bange, T. E. Madey, and J. K. Sass. Surf. Sci. **152**(1) (1985) 550.
[5] M. A. Barteau and M. R. J.. Surf. Sci. **140**(1) (1984) 108.
[6] L. Guillemot and K. Bobrov. Surf. Sci. **601** (2007) 871.
[7] L. Savio, M. Smerieri, L. Vattuone, A. Gussoni, C. Tassistro, and M. Rocca. Phys. Rev. B. **74** (2006) 235412.

# Synthesis and magnetic properties of Co nanoparticles embedded in a zeolite matrix

*P. M. Botta[1], P. G. Bercoff[2], H. R. Bertorello[2], C. Saux[3], L. B. Pierella[3], J. Rivas[1]*

*[1]Departamento de Física Aplicada, Universidad de Santiago de Compostela,*
*Facultad de Física, Campus Sur, 15782 Santiago de Compostela, Spain*
*[2]Facultad de Matemática, Astronomía y Física, Universidad Nacional de Córdoba, Córdoba,*
*and CONICET, Argentina*
*[3]Grupo de Fisicoquímica de los Nuevos Materiales, CITeQ,*
*Facultad Regional Córdoba, Universidad Tecnológica Nacional, Argentina*
*pbotta@usc.es*

In the last decades nanoscale magnetism has drawn great scientific interest due to its potential applications [1]. When the size of magnetic particles is reduced to a few nanometers, they often exhibit a number of outstanding physical properties such as giant magnetoresistance, superparamagnetism, large coercivity, as compared to the corresponding bulk values. Due to these unique physical properties upon size reduction, magnetic nanoparticles contribute to revolutionary changes in a variety of applications from biomedicine to spintronics [2,3].

The structure of zeolites with pores or channels of well defined size are particularly suitable for the study of magnetic properties of magnetic cations introduced into the structure.6,14 In the case of zeolites of the type ZSM-5 (structure MFI: mirror framework inversion; Mobil five) the diameter of the channels is 0:51 – 0:56 nm [4].

Co-HZSM-5 zeolites were prepared by wet impregnation of $NH_4$-MFI with aqueous solution of cobalt salt to yield the desired wt % of the cation (2.8 Co wt% and 4.9 Co wt%,). The samples were dried at 110ºC and calcined at 500ºC under $N_2$ flow (10 ml/min) and then under an oxidizing atmosphere for 12 h. Finally, these powders were reduced from room temperature to 500ºC at 5ºC/min and holding at 500ºC for 5 h, in $H_2$ flow (5 ml/min). These samples were called reduced zeolites (CoxIR, x = 2.8, 4.9). The Co content was accurately determined by atomic absorption. Crystal structure was studied by means of X-ray diffraction in a powder diffractometer using CuKα radiation. Scanning electron micrographs (SEM) and energy dispersive spectra (EDS) were used to characterize the microstructure and elemental composition of the samples. Magnetic measurements were performed in a commercial SQUID, varying the temperature from 5 to 300 K, with applied fields ranging from 25 to 200 Oe, and at several constant temperatures with applied fields up to 5 T.

XRD patterns of the reduced samples reveal the presence of metallic Co in a cubic phase, as well as traces of hexagonal Co. However, the oxides were not completely reduced, as some peaks corresponding to CoO and $Co_3O_4$ are still present. EDS microanalyses show for both reduced samples bright spots on the surface of the zeolite matrix which would be Co metal, as there is not enough oxygen to account for any Co oxide on these spots. Moreover, the spectra on the matrix show some traces of Co. As this element is not part of the zeolitic framework, this indicates that some Co is below the surface, inside the channels of the zeolite (Fig. 1).

Curves of magnetization as a function of temperature are shown in Figure 2 for sample Co2.8IR. ZFC and FC curves diverge before 300 K. In the ZFC curve there is a sharp maximum at T = 7 K and two wider peaks around 160 and 285 K of much lower intensity (approximately 9% of the 7 K peak). The abrupt decrease of the first peak can not be fitted either with Brillouin nor Langevin functions but an exponential of the type $\exp(-T/T_1)$, with a decay constant $T_1$= 3.5 K. The most important contribution is a high background (ferromagnetic, and also observed at room temperature) to which the contribution of two different kinds of clusters is superimposed, with blocking temperatures of 160 and 285 K, corresponding to the broad maxima observed at these temperatures. For sample Co4.9IR, the

same behavior is observed, but with higher magnetization values, as expected for higher Co content.

Measurements of the low-temperature peak in the ZFC curves were performed in both reduced samples with different applied fields in order to study the blocking temperature dependence with the field. A decrease of the blocking temperature with increasing applied field is observed.

The M(T)-ZFC curves (see inset of Fig. 2) show a prominent feature —the appearance of a well-defined magnetization peak at low temperature followed by an exponential decay. We consider that two processes take place at low temperature, which give rise to this peak over the background produced by other contributions to the magnetization. For temperatures lower than a certain $T_{crit}$ a tendency towards the equilibrium state with magnetization $M_{eq}(T,H)$ given by the Curie law. It is this process that produces a blocking temperature $T_B$. For temperatures above $T_{crit}$ a fast evolution towards an equilibrium state with $M_{eq} = 0$, that produces an exponential variation of magnetization with temperature. This is consistent with a spins reorientation mechanism and the fact that the relaxation rate is constant allows us to propose that we are in presence of a mesoscopic quantum tunneling process.

**References:**

[1] B. Barbara, Solid State Sci. 7, 668(2005).
[2] R. Hergt, S. Dutz, R. M¨uller, M. Zeisberger, J. Phys.: Condens. Matter 18, S2919 (2006).
[3] S. Parkin, X. Jiang, C. Kaiser, A. Panchula, K. Roche, M. Samant, Proc. IEEE 91, 661 (2003).
[4] W.M. Meier, D.H. Olson. Atlas of Zeolite Structure Types. (Butterworth-Heinemann, USA 1992).

**Figures:**
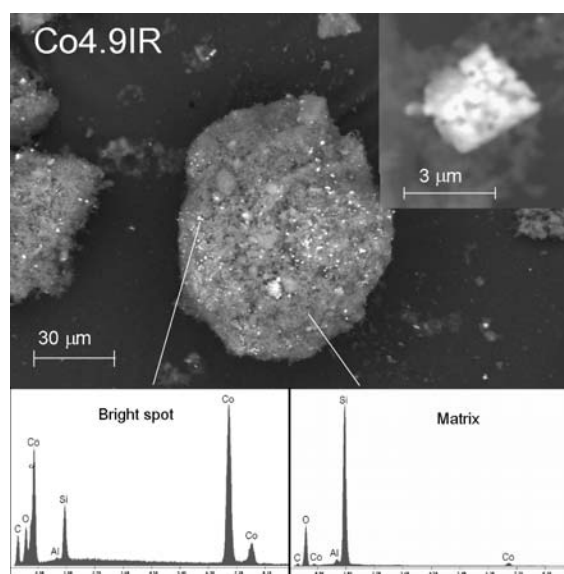


**Figure 1.** SEM micrograph of Co4.9IR (top) and EDS spectra taken to a bright spot on the particle (left bottom) and to the matrix (right bottom).
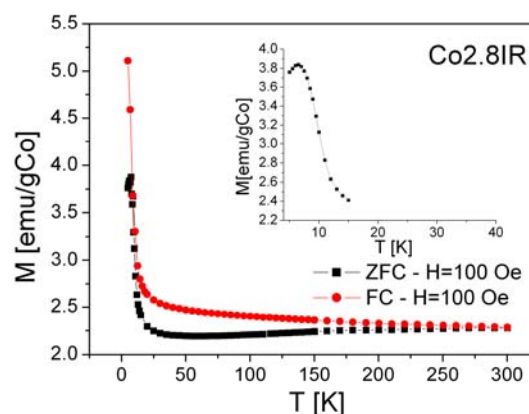


**Figure 2.** ZFC-FC magnetization curves for sample Co2.8IR. The inset shows in detail the low temperature peak.

# SIZE-MANIPULABLE SYNTHESIS AND STRUCTURAL CHARACTERIZATION OF TiO$_2$ NANOPARTICULES

K. Boulahya, A. Varela, M. Parras, J. M. González Calbet

[1]*Departamento de Química Inorgánica, Facultad de Químicas, Universidad Complutense,*

*E28040-Madrid,*

In the last decade, a great deal of effort has been devoted to develop materials with high photocatalytic activities for their wide environmental applications such as air purification, water disinfection,… Among the various oxides with photocatalytic activity, titanium dioxide has been proved to be one of the best photocatalysts due to its biological and chemical inertness, strong oxidizing power and long-term stability against photocorrosion and chemical corrosion for widespread environmental applications. However, the photocatalytic activity of titania must be further enhanced from the point of view of practical use. To achieve this purpose, the prepared rutile TiO$_2$ powders with good crystallization, small crystallite size and high specific surface area are prerequisite to enhance good photocatalytic activity. There are many methods available for the synthesis of nano-sized TiO$_2$ powder photocatalyst, such as, ultrasonic irradiation, UV light assistance, solvent evaporation-induced crystallization, sol-gel, hydrothermal etc… We have used for the synthesis of TiO$_2$ nanoparticules, the mechanical milling method, this technique provides a direct, simple, economical and free of solvents route to eventually obtain a ceramic of interest, with homogeneous particule size and highly pure product.

In this paper, we show the results obtained by mechanical milling method in the synthesis of TiO$_2$ nanoparticules with different size, the obtained materials were studied by high resolution electron microscopy and associated techniques.

The evolution of X-ray diffraction patterns for samples prepared using a rotating disc speed of 500 rpm, taken after 0, 24, 48, 72 and 96 hours of milling are shown in figure 1; a loss of crystallinity as a function of milling times can be observed. Figure 2corresponds to the HREM image obtained for the sample prepared for 96 hours. As it can be seen, the powder consists of agglomerates of homogeneous, crystalline particles with an average size clearly below 20 nm. Moreover, nanoparticules of 5 nm size were obtained as revealed by HREM (see the inset of figure 2). Reduction experiments are in progress is order to compare photocatalytic activity of both TiO$_2$ and oxygen deficient nanoparticles.
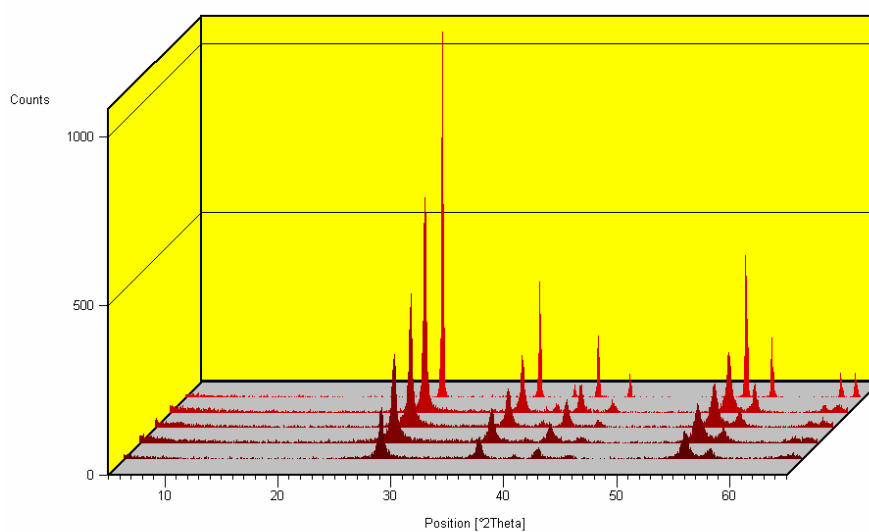
Figure **1.** Powder X-ray diffraction patterns evolution of TiO₂. Samples were taken after 0, 24, 48, 72 and 96 hours of milling.
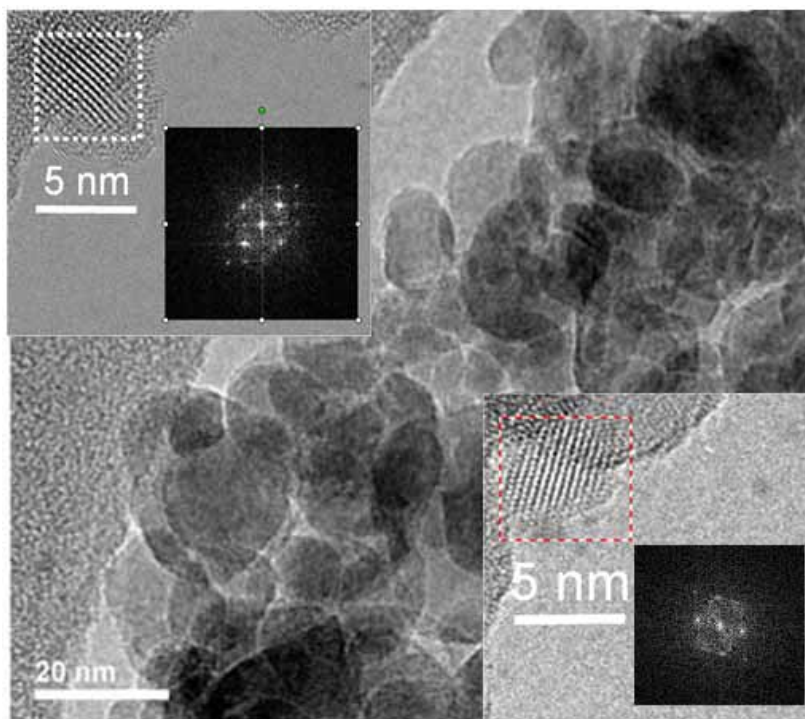


Figure **2**. HREM of a sample obtained after milling for 96 hours.

References:

1) *Wolfrum, E. J. - Huang, J. - Blake, D. M. - Maness, P.-C. - Huang, Z. - Fiest, J. - Jacoby, W. A.*,  Environmental Science & Technology 36 (15): 3412-3419 (2002)

# SINGLE CARBON NANOTUBE ELECTRICAL CONNEXION BY ELECTRON BEAM AND ION BEAM PLATINUM DEPOSITION

D. Brunel, M. Zdrojek, T. Mélin, D. Troadec

*Institut d'Electronique de Microélectronique et de Nanotechnologie, CNRS UMR 8520,
Avenue Poincaré BP60069 Villeneuve d'Ascq Cedex, France*

✍ *E-mail : david.brunel@isen.iemn.univ-lille1.fr*

In this poster, we will discuss the issue of the nanopatterning of electrical connexions to carbon nanotubes using *focused Ion Beam* or *focused Electron Beam* Platinum deposition [1]. These solutions apply for a quick characterization of Carbon Nanotube Field Effect Transistors [2].

The electrical properties of the e-beam or i-beam deposited platinum electrical contacts will be presented. Both beams are seen to lead to halos surrounding the platinum deposition patterns, as seen for instance from SEM images. The leakage conduction through these halos is investigated, and imaged using from Kelvin force microscopy [3] experiments on biased nanotubes (fig. 1).

It is shown that on the one hand the ion-beam deposition creates highly conductive electrical connections, however associated with fairly conductive µm-size halos. This limits the CNT electrode separation by a few microns. On the other hand, electron beam induced platinum deposition creates poorly conducting halos, but also generate higher resistivity platinum patterns. Four-probe measurements are then required to characterize the nanotubes electrically.

Using EFM, we demonstrated the possibility to quantify the presence of charges on nanotubes. This allows the possibility to demonstrate and quantify stored charges inside a MWCNT (fig.2).

**References:**
[1] Vidyut Gopal, Eric A. Stach and Vladimir R Radmilovic, *Applied Physics Letters*, **85**, 1 (2004)
[2] Ebessen T.W, Lezec H.J, Hiur, H., Bennett J.W., Ghaemi H.F, Thio T., *Nature*, **382**, 6586 (1996)
 [3] B. N. Nonnenmacher, M.P. O'Boyle, and H. K. Wickramsinghe, *Applied Physics Letters*, **58**, 2921 (1991)

**Figures:**
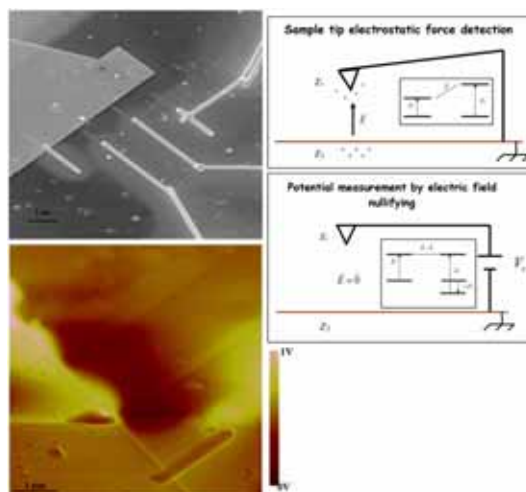


**Figure 1** Top : SEM image of a MWCNT contacted by ion beam induced platinum deposition. Two separated groups of halos can be identified. The inset shows the principle of KFM imaging. Bottom: Kelvin force Microscopy image of the biased MWCNT (here through the outer electrodes), showing surface potential distribution along the nanotubes. Each group of halos is seen to be equipotential.
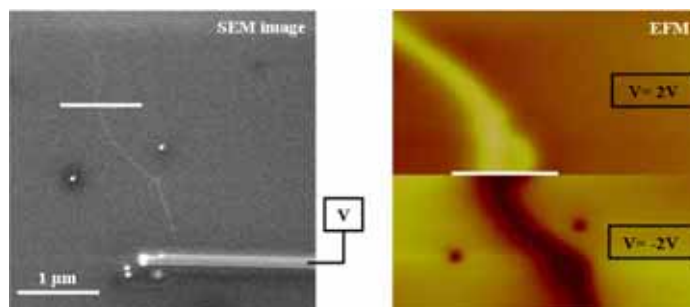


. **Figure 2**. Left: SEM Image of a MWCNT contacted by electron beam induced platinum deposition. Right: Electrostatic force microscopy (EFM) image of the MWCNT biased from the contact electrode. The white line shows the correspondence between the EFM and the SEM image. The electrode polarization is reversed ad mid-scan, corresponding to the contrast inversion in the EFM image.

# NANOWELDING AND NANOTOOL FABRICATION USING ELECTRON-BEAM-INDUCED DEPOSITION

*Daniel Burbridge[1], A. Moskalenko[1], G. Viau[2], S. Gordeev[1]*
*1. Department of Physics, University of Bath, Claverton down, Bath, BA2 7AY, United Kingdom*
*2. INSA Toulouse - Département Génie Physique, LNMO; 135 avenue de Rangueil 31077, Toulouse Cedex 4, France*
*D.J.Burbridge@bath.ac.uk*

Electron-Beam-Induced-Deposition (EBID) is a versatile, single-step fabrication technique that promises to find many interesting applications in nanotechnology [1]. We demonstrate that EBID can be used for welding of 3D nanoscale objects from beneath to the substrate and for fabrication of a large variety of nanotools. These tools can be used for manipulation of nanoobjects using an Atomic Force Microscope (AFM) and for different biological applications. EBID occurs when a sample is exposed to the electron beam in an electron microscope (EM). The electron beam decomposes hydrocarbon molecules that are always present in small quantities in the vacuum chamber of the EM and forms a layer of carbonaceous deposit on the sample surface. This deposit is mechanically very strong and can be grown in different shapes. Fig. 1 shows modifications to AFM probes that were grown by the EBID method. They include a high-aspect-ratio needle of 20 nm in diameter for imaging of biological objects (a), hooks and tweezers of different shapes (b and d) for manipulation with biological molecules and a nanoscalpel (c). The nanoscalpel was used to cut a narrow (20 nm) gap in a thin gold film (Fig. 2). This formed nanoelectrodes for measurements of electron conductance through a nanoparticle that was manipulated into the gap. The tools shown in Fig 1 were grown by slow scanning of the electron beam out from the AFM tip surface into vacuum. The shape of the deposited free standing structures was controlled by varying deposition parameters and scan direction using a lithography package.

It is known that EBID is mainly caused by the secondary electrons backscattered by atoms of both the sample and substrate [2]. We discovered that, because the secondary electrons are spread beyond the exposed area, this deposit can be grown in areas of geometric shadow. Fig 3 shows a pseudo-3D image obtained with an AFM of the area around and beneath a 300 nm Fe-Ni-Co nanoparticle that was first exposed to an electron beam in an EM and then removed using an AFM tip. The larger circle corresponds to the diameter of the nanoparticle. A 5 nm layer of deposit can be seen in the area of the geometrical shadow. This layer forms a very strong weld. The strength of EBID welding is investigated by welding 100 nm polycrystalline Fe-Ni-Co nanoparticles to a $SiO_2$ substrate and attempting to remove them by AFM manipulation. This generally resulted in breaking the particle or AFM probe unless the probe was first strengthened by deposition of a layer of EBID. We suggested using a short time exposure to the electron beam for welding complex 3D objects from beneath to the substrate [3].

We have obtained a number of complex 3D shapes by rotating the sample and thus changing the deposition angle. In particular, we found that when a blade-shape structure like that shown in Fig. 4 is rotated at 90º and then exposed to the electron beam, the deposit starts to grow simultaneously on both sides of the blade. To get insight into the mechanism of EBID we performed Dynamic Monte Carlo simulations.

**References:**

[1] H W P Koops, J Kretz, m Rudolph M Weber J. Vac. Sci. Technol. B. **11(6)** (1993) 2386
[2] N. Silvis-Cividjian, C.W. Hagen, L.H.A. Leunissen, P. Kruit, Microelectronic Engineering **61–62** (2002) 693–699.
[3] A V Moskelenko, D J Burbridge, G Viau, S N Gordeev, Nanotechnology, **18** (2007) 025304

**Figures:**
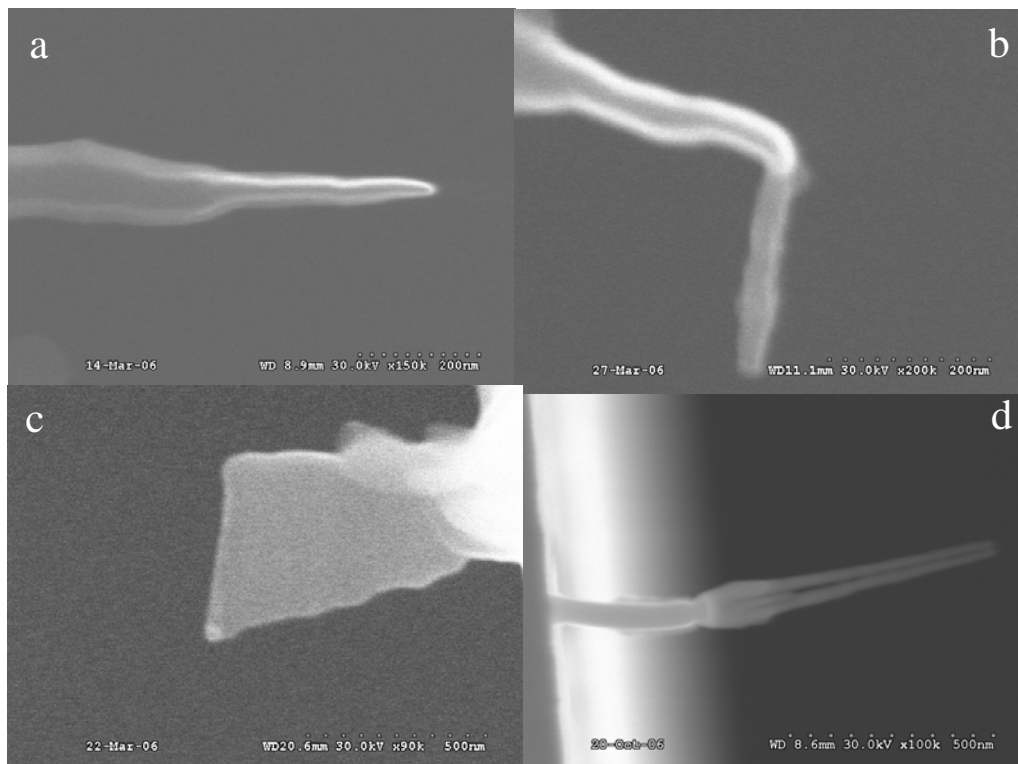


**Figure 1. EBID tools deposited on AFM probes. (a) High aspect ratio probe (b) Scalpel for side incisions. (c) nanoscalpel viewed side on. (d) nanotweezers.**
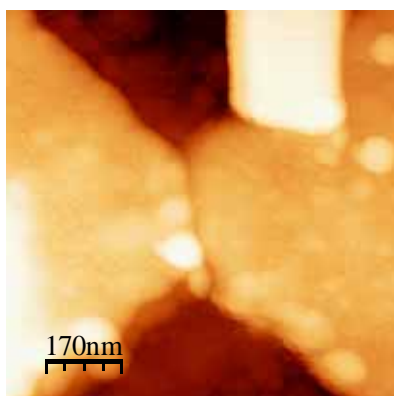


**Figure 2. 20nm electrode gap formed by scratching gold with an EBID acalpel.**
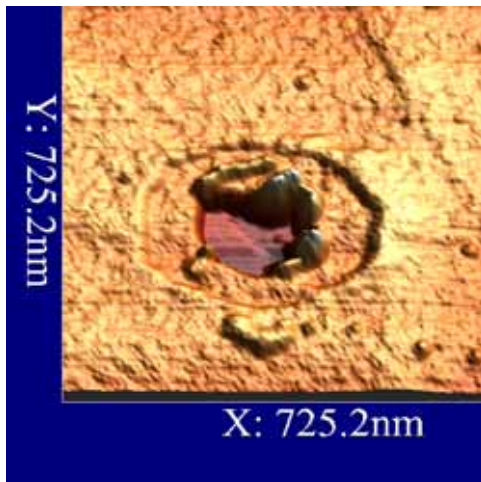
**Figure 3. 3D representation of an AFM image showing deposit formed in the area of geometric shadow beneath a 300nm particle, the particle has been removed.**
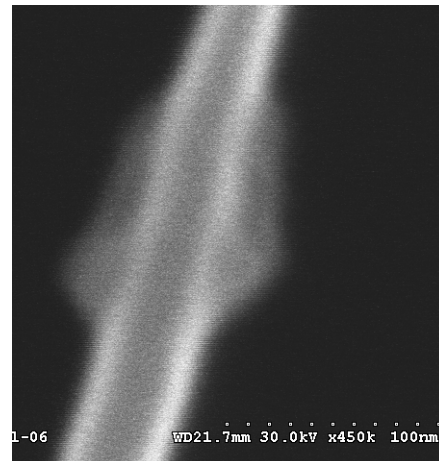
**Figure 4. Growth through a deposited blade.**

# UNCOVERING MOLECULAR MORPHOLOGIES OF $C_{60}$ AND PTCDA ON INSULATORS: DEWETTING IN TWO PROTOTYPICAL ORGANIC SEMICONDUCTORS

*Sarah Burke, Jeffrey Mativetsky, Shawn Fostner, Peter Grütter*
*Department of Physics, McGill University, 3600 rue University, Montreal, Canada*
*burkes@physics.mcgill.ca*

There has been considerable interest in recent years in the use of organic molecules as active electronic and optoelectronic materials for devices. As such, research into the properties and structures of molecular films, crystallites and isolated molecules on surfaces has become an active field, both for the promise of single molecule devices and the prospect of thin film organic electronics. However, despite the importance of insulating materials in typical device structures, there has been minimal study of molecular deposits on insulating surfaces due to difficulties with the use of many traditional surface science tools on such systems. Over the past decade, non-contact atomic force microscopy (nc-AFM) has proven to be a powerful surface science tool on insulators as well as other surfaces, and more recently on heterogeneous samples. Here, we have used UHV nc-AFM as a high resolution tool to study the growth and morphology of two commonly used prototypical molecular semiconductors: $C_{60}$ and PTCDA, on alkali halides. The alkali halides used, KBr and NaCl, cleave well *in situ* with large atomically flat terraces (up to 1 micron) making them ideal for growth studies.

$C_{60}$ deposited on KBr and NaCl forms islands with an unusual branched morphology [1,2]. The mechanism for the formation of branches appears to be related to a dewetting process occurring immediately after growth. The final stages of this process were observed directly in a series of nc-AFM images showing single layer film edges receding to form the types of structures observed at a later time. A transition from compact islands to branched islands was investigated quantitatively, and it is believed that an instability in the dewetting at the length scale where this transition occurs is responsible for for initiating branch formation. Stability of the structures was tested by annealing and growth at elevated substrate temperature. Although compact islands were determined to be the equilibrium morphology from the high temperature growth, the branched islands grown at room temperature are stable under heating. The epitaxy, though different at steps and on open terraces, does not appear to play any significant role in the island morphology, indicating that the substrate plays a minor role in the formation of the island shapes. Disconnected regions of seemingly connected islands have the same orientational relation to the substrate, while such "communication" seems unlikely, in a dewetting scenario these disconnected regions would have originated as one single layer island and only have become separated during dewetting.

PTCDA on NaCl also undergoes a dewetting process, though in a rather different manner. At low coverages, single layer islands are observed in a highly strained epitaxial structure. In areas where there are several substrate steps close together, tall islands with the familiar herringbone arrangement for PTCDA are observed with a depletion in the surrounding single layer islands corresponding to the volume of molecular material in the crystallite. At a coverage of 0.8ML single layer strained islands and tall herringbone crystallites coexist, indicating a coverage induced dewetting transition [3]. To confirm this hypothesis of dewetting, the single layer islands observed at a coverage near the transition were annealed and found to form very large crystalline islands of PTCDA, with no evidence of a monolayer on the substrate.

Dewetting has recently been reported in other molecular systems and found to be a significant factor in growth and morphology [4,5]. These two example systems may indicate that dewetting is also an important consideration in molecule-on-insulator systems as well.

**References:**

[1] S.A. Burke, J.M. Mativetsky, R. Hoffmann, P. Grütter, PRL, **94**(2005) 096102.
[2] S.A. Burke, J.M. Mativetsky, S. Fostner, P. Grütter, *submitted to PRB*.
[3] F. Silly and M. Castell, PRL, **96**(2006), 086104.
[4] G. Witte and Ch. Woll, Appl. Phys. A, **82**(2006), 447-455.
[5] D.Käfer, L. Ruppel, G. Witte, PRB, **75**(2007), 085309.

**Figures:**
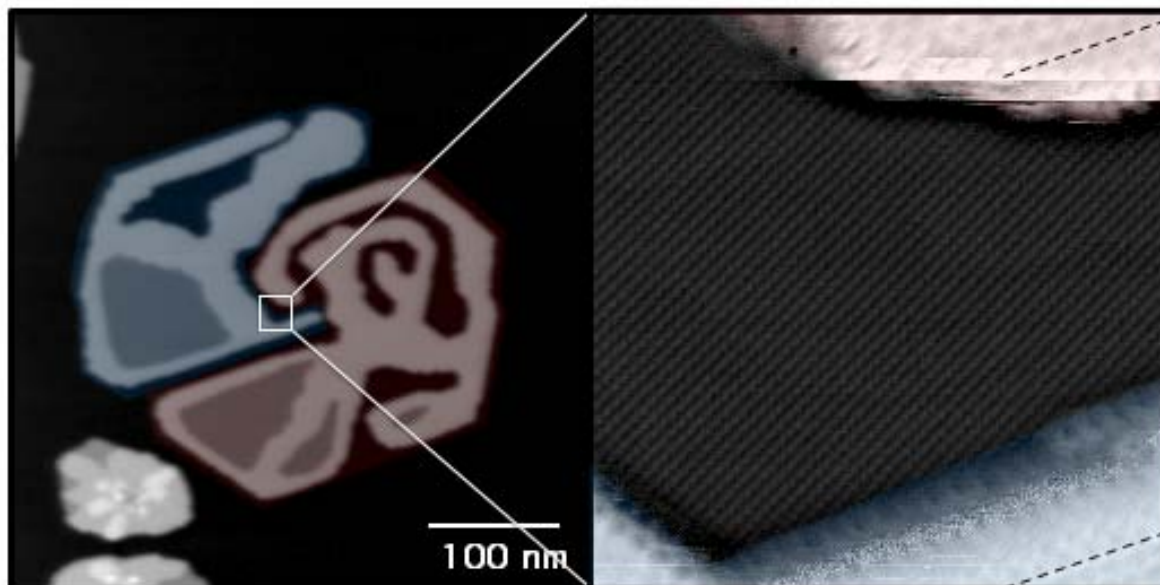


**Fig. 1:** 2 disconnected regions of a C60 island on KBr separated by dewetting (left), showing the same orientational relation in high resolution (right).
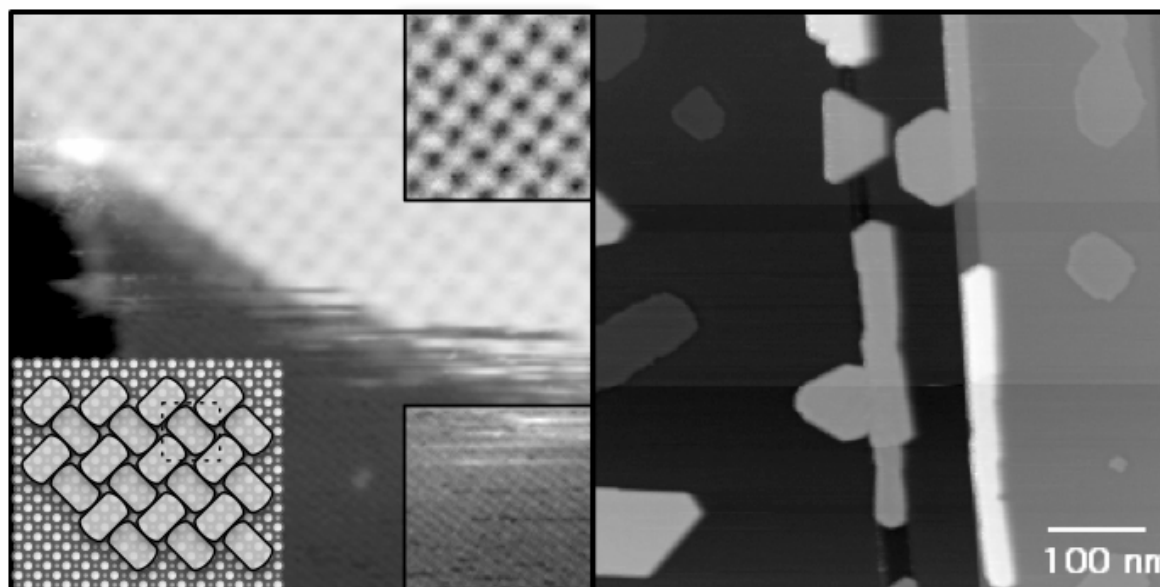


**Fig. 2:** High resolution nc-AFM on PTCDA overlayer on NaCl with insets adjusted for better contrast (left) used to determine the strained c3x3 epitaxy (lower left inset). Overview image of co-existing monolayer and multilayer islands at 0.8ML coverage (right)

# FIRST-PRINCIPLES INVESTIGATION OF ELECTRON-INDUCED CROSS-LINKING OF AROMATIC SELF-ASSEMBLED MONOLAYERS ON Au(111)

Pepa Cabrera-Sanfelix[1], Daniel Sánchez-Portal[2] and Andrés Arnau[2,3]

[1] Donostia International Physics Center (DIPC), Manuel de Lardizabal 4, San Sebastian, Spain.

[2] Unidad de Física de Materiales, Centro Mixto CSIC-UPV, Manuel de Lardizabal 4, San Sebastian 20018, Spain.

[3] Departamento de Física de Materiales UPV/EHU, Facultad de Química, Apartado 1072, San Sebastián 20080, Spain.

swbcasam@sc.ehu.es

Experimental techniques, such as X-ray photoelectron, infrared and near edge X-ray absorption fine structure spectroscopy show that self-assembled monolayers (SAMs) of 1,1´-biphenyl-4-thiol (BPT) adsorbed on Au(111) arrange well ordered. Upon electron irradiation these films undergo strong structural modifications that have been investigated recently. After irradiation with 50 eV electrons, important changes appear in the corresponding X-ray photoemission (XP) and infrared (IR) spectra.[1,2] These changes are believed to be mainly due to the dehydrogenation of BPTs and the cross-link between neighbouring phenyl groups. Through chemical treatments, cross-linked regions can be removed from the substrate and form free-standing sheets of ~15Å thickness. We present here a first theoretical approach to this complex problem. We use Density Functional Theory (DFT) calculation to study the adsorption of one layer of BPT molecules on Au(111) surface, as well as several plausible cross-linked structures that dehydrogenated BPT and biphenyl (Bph) molecules can adopt depending on different input conditions. The possible role of the gold substrate is examined in detail.

(1)     Eck, W.; Stadler, V.; Geyer, W.; Zharnikov, M.; Golzhauser, A.; Grunze, M. *Advanced Materials* **2000**, *12*, 805-808.

(2)     Geyer, W.; Stadler, V.; Eck, W.; Zharnikov, M.; Golzhauser, A.; Grunze, M. *Applied Physics Letters* **1999**, *75*, 2401-2403.

# MICROWAVE CHARACTERIZATION OF A CNT BUCKY PAPER TRANSMISSION LINE

*S. Capdevila, J. Pérez, M. Jofre, N. Ferrer-Anglada, A. Aguasca, S. Blanch, J. Romeu, L. Jofre*

*Universitat Politècnica de Catalunya, Jordi Girona 1-3, Barcelona, Spain*
*scapdevila@tsc.upc.edu*

The technological advances in integrated circuit and nano manufacturing are leading to the inception of a new range of electronic devices that operate in the GHz frequency range. It is the aim of this paper to study the electromagnetic properties that a carbon nanotubes bucky paper sheet may present in the GHz range, and how this could be used in the construction of miniaturized antenna systems.

The miniaturization of antenna devices in general, and of resonant antennas in particular, becomes harder as the targeted size becomes much smaller than the wavelength, as they usually require a dimension on the order of the wavelength. Several techniques exist that allow miniaturising antenna systems, but they also present some side effect on the performance of the antenna. One of this technique relies on the use of dielectrics with high permitivitties in order to reduce the effective wavelength and so the dimensions of the antenna, but these materials may present some limitation when the size of the device becomes too small (like for example a extreme reduction of its bandwidth), therefore it becomes necessary the study of new materials that could present some advantage in terms of resonant size that would fit the requirements of constructing miniaturised antennas.

Possible structures that could be used in the development of such systems are nanotubes. Carbon nanotubes could be defined as a cylinder made from a graphene sheet, presenting metallic or semiconductor behaviour, [1], depending on the direction of folding the graphene sheet, and may present a slow wave velocity, allowing significant reduction of the wavelength and hence resonant antenna dimensions, [2]. The theoretical behaviour has been studied in several papers, [2], [3], as well as some studies towards its applications, [4]. But in these studies the nanotubes where considered isolated.

In this work the approach will not consider an isolated carbon nanotube, but we will characterize the *macroscopic* properties of a material formed by single-walled carbon nanotubes, what it is known as 'bucky paper'. There has been some similar study on the behaviour of carbon nanotube composite, [5], but they did not focus on its usage as a conductive sheet. The study will be done by measuring the S-Parameters of a transmission line in a broad range of frequencies up to 50GHz using the setup of Figure 1. Once the measurements are done, it is possible to extract some electrical parameters of the bucky paper strip that may be of interest, as it may be the case of the conductivity that presents the strip.

Figure 2 shows the preliminary results for the conductivity measured from the attenuation of the S-parameters of the microstrip line made with bucky paper. It can be observed that the conductivity of a sheet of bucky paper may be in the order of $10^4$ and $10^5$ S/m, although further measurements will be made in order to assess the dependence of the strip conductivity with respect to the excitation power or the existence of a polarization voltage.

References:

[1]. R. Saito, G. Dresselhaus, and M. Dresselhaus, **Physical properties of Carbon Nanotubes**, 1st ed. Imperial College Press, 1998.

[2]. G. Hanson, "Current on an infinitely-long carbon nanotube antenna excited by a gap generator," **Antennas and Propagation, IEEE Transactions on**, vol. 54, no. 1, pp. 76–81, Jan. 2006.

[3]. J. Hao and G. W. Hanson, "Infrared and optical properties of carbon nanotube dipole antennas**," Nanotechnology, IEEE Transactions on**, vol. 5, no. 6, pp. 766–775, Nov. 2006.

[4]. V. Sazonova, Y. Yaish, H. Ustunel, D. Roundy, T. A. Arias, and P. L. McEuen, "A tunable carbon nanotube electromechanical oscillator," **Nature**, vol. 431, no. 7006, pp. 284–287, Sep. 2004. [Online]. Available: http://dx.doi.org/10.1038/nature02905

[5]. J. Li and J. Lumpp, "Electrical and mechanical characterization of carbon nanotube filled conductive adhesive**," 2006 IEEE Aerospace Conference**,4-11 March 2006, p. 6pp.

**Figures:**
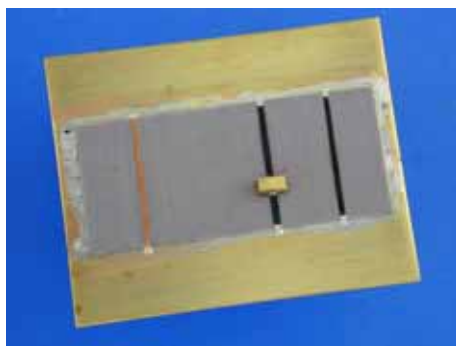


**Figure 1. Measurement setup, to the left a metallic (copper) microstrip line that is taken as a reference in the measurements, to the right two different microstrip lines: the first one present a shortcircuit in the middle, in order to get a reflection coefficient with different lengths, and most to the right a pass-through line, for measuring in a transmission fashion.**
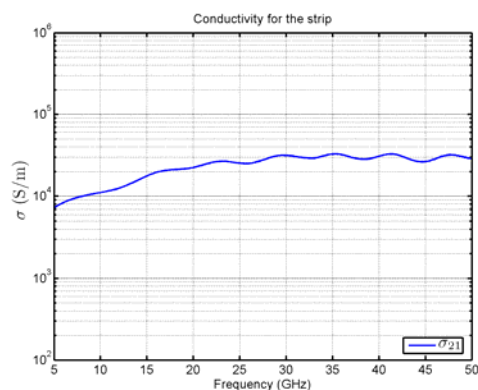


**Figure 2. Preliminary results on the conductivity of a CNT bucky paper strip measured in a microstrip transmission line. It can be observed how the value of the conductivity is in the order of $10^4$ S/m**

# EFFECT OF SURFACE NANO-PATTERNIG ON BOUNDARY LUBRICATION

Rosario Capozza [1], Annalisa Fasolino [2], Andrea Vanossi [1], and Mauro Ferrario [1]

[1] *CNR-INFM-S3 e Dipartimento di Fisica, Università di Modena e Reggio Emilia,*
*Via Campi 213/A, 41100 Modena , Italy*
[2] *Solid State Theory, Institute for Molecules and Materials, Radboud University of Nijmegen,*
*Toernooiveld 1, 6525 ED Nijmegen, The Netherland*

*rcapozza@unimore.it*

Introduction of specific micro-textures onto a sliding surface, involving flat and smooth regions interrupted by local depressions, is a well-known approach to improve its tribological properties [1-2]. The effects of scaling down the texturing dimensions to the nanoscale have not yet been investigated to a comparable extent.

We implement a computational MD model, capable of describing how the sliding frictional properties of a thin lubricant film are significantly affected by the presence of nanoscale superficial patterning of the moving confining walls [3]. Our 2-dimensional system consists of a rigid, patterned, substrate (to simulate the texturing of experimental surfaces) a rigid layer (mimicking the driven top wall) and a confined Lennard-Jones lubricant in between (Fig.1). In particular we investigate the friction and the tribological response when the top layer is pulled through a spring connected to a stage moving at constant velocity. In presence of flat walls, for suitable applied load, temperature and due to the effect of confinement, the lubricant film solidify even at temperatures significantly higher than its bulk melting temperature [4-7]. In this situation (and for not too high external driving), the system is in the so called high dissipative stick-slip regime.

On the contrary in the presence of surface patterning and under the same operative conditions, our numerical simulations show a drastic reduction of sliding friction (Fig.2). This decrease is ascribed to a local melting of the film nearby the surface grooves (reduced effect of the confinement) and to a 'pattern-increased' interlayer diffusion in the lubricant film. We believe these findings to be relevant for nanotechnology applications.

**References:**

|1| U. Pettersson et al. , Tribol. Lett. **17**, 553 (2004)
|2| A. Blatter et al. , Tribol. Lett. **4**, 237 (1998)
|3| C. Cottin-Bizonne et al. , Nature Materials **2**, 237 (2003)
|4| J. Klein et al., J. Chem. Phys., **108,** 16, 6996 (1998)
|5| A. Weinstein et al., Europhys. Lett. **42**, 61 (1998)
|6| O.M. Braun et al. , Phys. Rev. E **63**, 046110 (2001)

|7| O.M. Braun et al. , Phys. Rev. E **68**, 011506 (2003)

**Figures:**
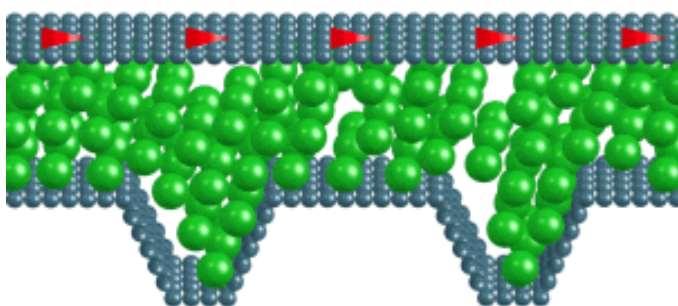


**Figure. 1**

*Illustrative sketch of a boundary lubricated system confined between a driven top plate and a fixed patterned substrate.*
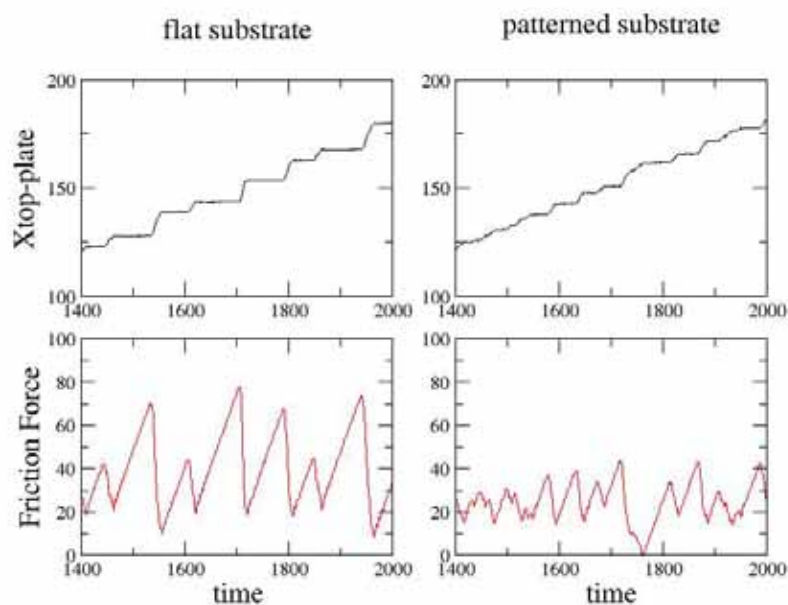


**Figure. 2**

*Comparison between the stick-slip behavior in the case of flat substrate (left panels) and patterned substrate (right panels).*

# REVERSIBLY UV-LIGHT-INDUCED HYDROPHOBIC/OLEOFILIC TO AMPHIPHILIC SURFACE TRANSITION IN THIN FILMS OF ORGANIC-CAPPED TIO$_2$ NANORODS

*Gianvito Caputo,[1*] Athanassia Athanassiou,[1] Concetta Nobile,[1] Tobias Kipp,[2] Roman Krahne,[1]*

*Elvio Carlino,[2] Liberato Manna,[1] Roberto Cingolani,[1] and P. Davide Cozzoli[1]*

[1] National Nanotechnology Laboratory of CNR-INFM, Unità di Ricerca IIT, Distretto Tecnologico ISUFI, via per Arnesano km 5, I-73100 Lecce, Italy.
[2] Institut für Angewandte Physik und Zentrum für Mikrostrukturforschung, Universität Hamburg, Jungiusstrasse 11, 20355 Hamburg
[2] TASC-INFM-CNR National Laboratory, Area Science Park - Basovizza, Bld MM, SS 14, Km 163.5, I-34012 Trieste, Italy

* To whom all correspondence should be addressed: Phone:+39-0832-298271. Fax: +39-0832-298238. E-mail: gianvito.caputo@unile.it

Nanocrystalline TiO$_2$ is among the most studied semiconductor oxides, owing to its low-cost widespread applications in light-assisted environmental clean-up, in solar energy conversion, in sensing, and in the photodynamic deactivation of micro-organisms and of malignant cells. More recently, it has been discovered that UV-irradiation of TiO$_2$ surfaces rapidly converts them from an initially hydrophobic state to a highly amphiphilic one, followed by a slow back-recovery of the starting properties under ambient conditions.[1-4] These findings have stimulated the fabrication and the study of inorganic coatings which exhibit simultaneous self-cleaning and antifogging behaviour.[5, 6] However, the understanding the mechanism leading to light-induced wettability modification on TiO$_2$ surfaces remains elusive yet and the ability to control them has to be developed further.

In this contribution we will present a novel approach to engineer TiO$_2$ surfaces with UV-switchable wettability, which relies on the use of organic-capped TiO$_2$ nanorods (NRs)[7] for the fabrication of thin films made of close-packed laterally aligned arrays of TiO$_2$ crystalline domains exposing well-defined light-active crystal facets. As opposed to conventional polycrystalline or single-crystal TiO$_2$ surfaces, such NR-based films exhibit a reversible surface transition from a highly hydrophobic/oleofilic state (water and octadecene contact angles of 110° and 8°, respectively) to a highly amphiphilic state (water and octadecene contact angles of 20° and 3°, respectively) under remarkably milder UV-irradiation conditions (energy density as low as 1-2 mJ/cm$^2$). By using a combination of techniques (XRD, HRTEM, SEM, UV-vis, FTIR and Raman spectroscopy, and contact angle measurements), we will demonstrate that the observed light-driven wettability changes are accomplished by progressive hydroxylation of the TiO$_2$ surface irrespective of the presence of the native shell of surfactant molecules, which simultaneously undergo conformational changes without suffering for significant photocatalytic degradation.

### References

1.    R. Wang, K. Hashimoto, A. Fujishima, M. Chikuni, E. Kojima, A. Kitamura, M. Shimohigoshi, T. Watanabe *Nature* **1997,** 388, 431-432.
2.    R. Wang, K. Hashimoto, A. Fujishima, M. Chikuni, E. Kojima, A. Kitamura, M. Shimohigoshi, T. Watanabe *Adv. Mater.* **1998,** 10, (2), 135-138.
3.    N.Sakai, A. Fujishima, T. Watanabe, K. Hashimoto *J. Phys. Chem. B* **2003,** 107, (4), 1028-1035.
4.    X. Feng, J. Zhai, L. Jiang *Angew. Chem. In. Ed* **2005,** 44, (32), 5115-5118.
5.    K. Qi, W. A. Daoud, J. H. Xin, C. L. Mak, W. Tang, W. P. Cheung *J. Mater. Chem.* **2006,** 16, (47), 4567-4574.
6.    E. Allain, S. Besson, C. Durand, M. Moreau, T. Gacoin, J.-P. Boilot *Adv. Func. Mater.* **2007,** 17, (4), 549-554.
7.    P. D. Cozzoli, A.Kornowski, H. Weller *J. Am. Chem. Soc.* **2003,** 125, (47), 14539-14548.

# SELF-ASSEMBLED GROWTH AND ELECTRICAL CHARACTERISTICS OF GERMANIUM NANOSTRUCTURES FORMED USING ELECTRON BEAM ANNEALING

Damian Carder[1], Andreas Markwitz[1,2] and H. Baumann[1]

[1] National Isotope Centre, GNS Science, Lower Hutt, New Zealand
[2] The MacDiarmid Institute for Advanced Materials and Nanotechnology, New Zealand

d.carder@gns.cri.nz

The growth and characterisation of nanoscale-islands of SiGe and Ge quantum dots has been of considerable interest in recent years [1]. Possible applications for such structures include mid-infrared photodetectors or as a model system to study fundamental quantum mechanical effects [2]. Conventionally these structures are synthesised during epitaxial growth of SiGe or Ge layers on Si – utilising the inherent strain in the material system for self-assembly of nanostructures.

Presented here is a study into the self-assembly of Ge nanostructures using thin film deposition followed by a rapid and uncomplicated post-growth annealing method. The aim of the work is to produce controlled and predictable assembly of the surface features, central to the development of any application.

Our group has recently demonstrated the nanostructuring of untreated silicon substrates using an electron beam annealing (EBA) technique [3], with the so-called nanowhisker surface structure showing immediate promise in field-emission and vacuum electronics applications [4]. This study extends the use of the technique in an attempt to produce germanium nanostructures from layers of germanium grown on a silicon substrate.

Ion-beam sputtered layers of germanium, ~100-300 nm thick, were deposited near room temperature on a Si substrate. The thin films were then annealed at temperatures ranging from 400$^{o}$C up to 800$^{o}$C using the EBA technique. Atomic force microscope images of the Ge surface following annealing reveal dramatic surface roughening on the nanoscale (figure 1).

The electrical characteristics of the annealed germanium thin films have been measured in a field-emitting diode configuration. Figure 2 shows the current-voltage curve for a germanium nanostructure sample, with a clear non-linear relationship at positive voltages and significantly reduced current flow at negative voltages. A study has been undertaken to uncover the conduction mechanism leading to current flow between the germanium nanostructured cathode and aluminium anode.

## References

[1] J-M Baribeau, X Wu, N L Rowell and D J Lockwood, J. Phys.: Condens. Matter, 18, R139 (2006)
[2] K. Brunner, Rep. Prog. Phys., 65, 27 (2002)
[3] S. Johnson, A. Markwitz, M. Rudolphi, and H. Baumann, J. Appl. Phys. 96, 605 (2004)
[4] S. Johnson, A. Markwitz, M. Rudolphi, H. Baumann, S. P. Oei, K. B. K. Teo and W. I. Milne, Appl. Phys. Lett. 85, 3277 (2004)

**Figures:**

Figure 1: Atomic force microscope images of a sputtered germanium film (a) before and (b) after electron beam annealing.
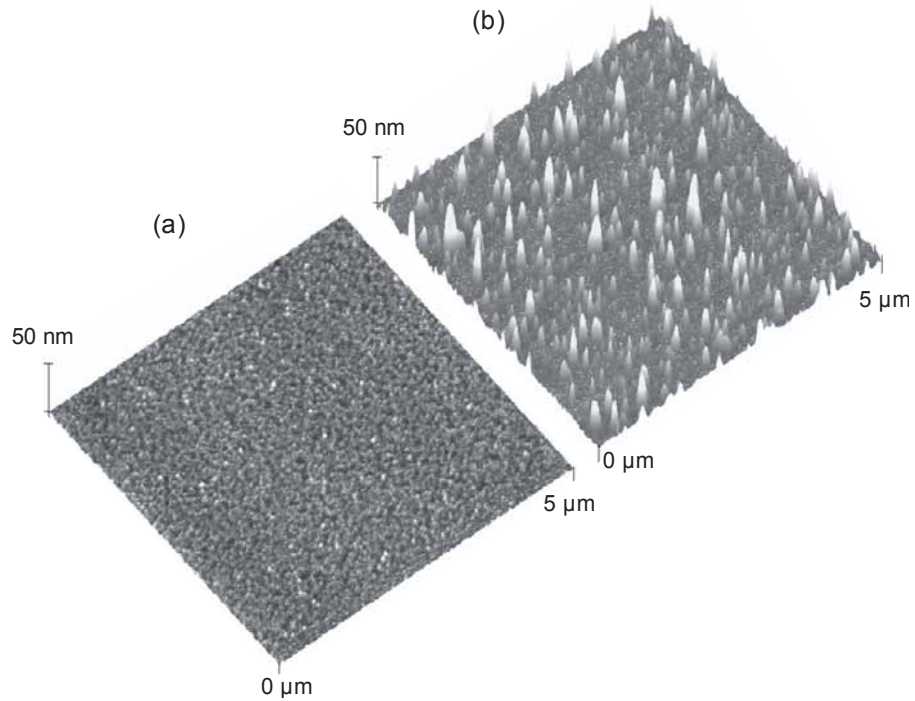


Figure 2: Current-voltage characteristic of a nanostructured germanium layer in a field-emitting diode configuration. Shown in the inset is a schematic of the system configuration.
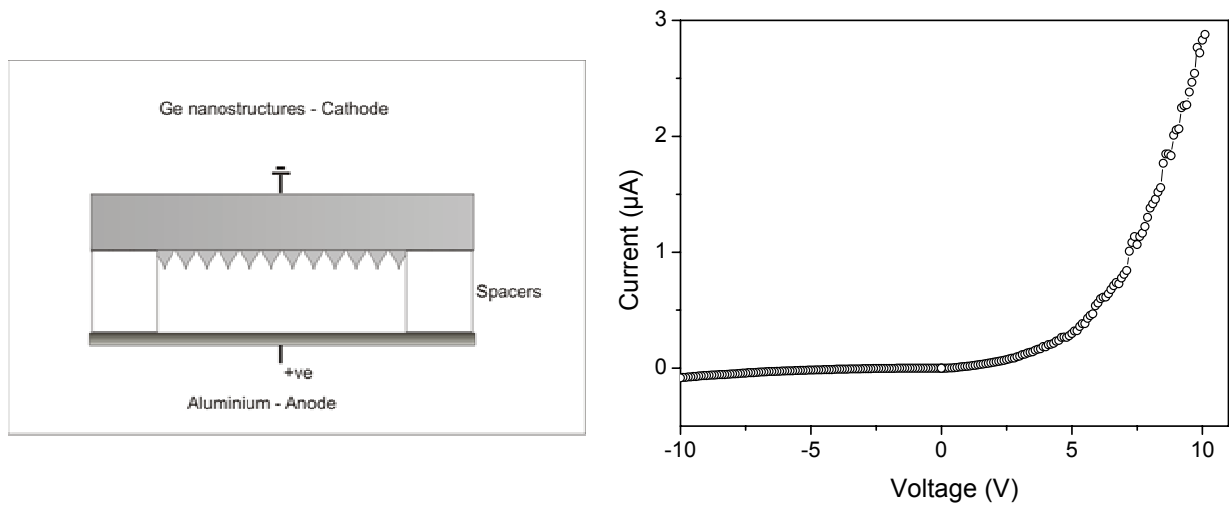
# CARBON NANOTUBE NETWORKS: EXCEPTIONAL ELECTRICAL PROPERTIES

B. Cardin St-Antoine, C. M. Aguirre, C. Ternon, D. Ménard and R. Martel.

Carbon nanotubes network open a promising route for the integration of nanotubes in electronics for that they circumvent major issues related to their fabrication. [1] Another advantage of networks over individual carbon nanotube transistors is their reduced device-to-device discrepancies because their electrical and optical properties derive from an ensemble of different nanotube species.

In our laboratory, we developed different fabrication schemes to obtain networks with either metallic or semi-conducting behaviour. Most interestingly, both kinds of networks were made with a blend of metallic and semi-conducting nanotubes from the same source (laser ablation). Metallic networks are produced by a filtration based technique while semi-conducting are made by spin-coating nanotube solution on a functionalised surface. We believe that the different electrical properties of those networks originate from the thickness variations of our films. In semi-conducting networks, the coverage is precisely controlled in order to allow the percolation of semi-conducting nanotubes, while remaining below the metallic percolation threshold.
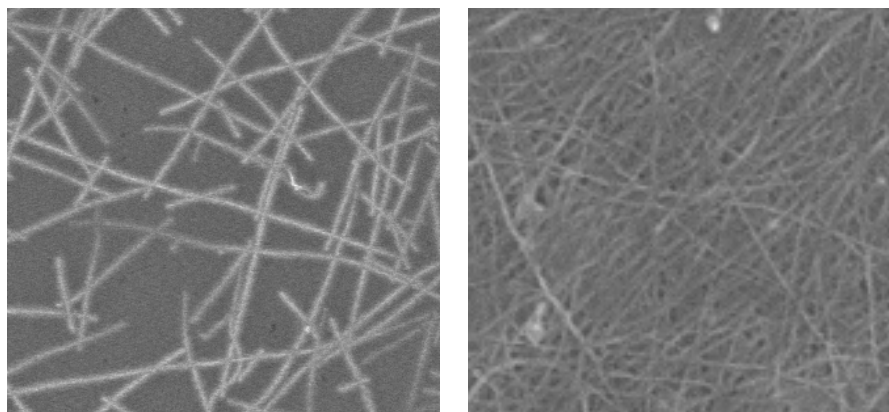


Figure 1. SEM images. On the left, a very sparse network which exhibits semi-conductive behaviour. On the right, a much more dense film with metallic properties.

The performances of those semiconducting network are very exciting. The transistors are stable in air and present a $I_{on}/I_{off}$ ration of over 6 orders of magnitude. Semi-conductive carbon nanotube networks are generally p-type transistor but we achieve ambipolarity by encapsulating our devices with an organic layer. We measure mobility superior to 1 cm$^2$ s$^{-1}$ V$^{-1}$, for the p type regime. Such mobility is outstanding when compared to other organic transistors. Combined with the mechanical flexibility of carbon nanotube films, it forecasts a bright future for carbon nanotube network transistors.

Filtration allows much thicker films, so that metallic nanotubes are above the percolation threshold. It is possible to fabricate thinner but still continuous films with this technique and monitor the transition from metallic to semi-conducting networks. Those networks were also optimised to improve their conductivity while keeping a good optical transparency, for OLED application.

Finally, we achieve to suspend metallic carbon nanotube networks in air. Free standing films are known to exhibit an enhanced photoresponse, because of the absence of interaction with the substrate.[2] Their study will lead to a better understanding of the transport mechanisms involved in networks and could open up interesting applications like infrared detector.
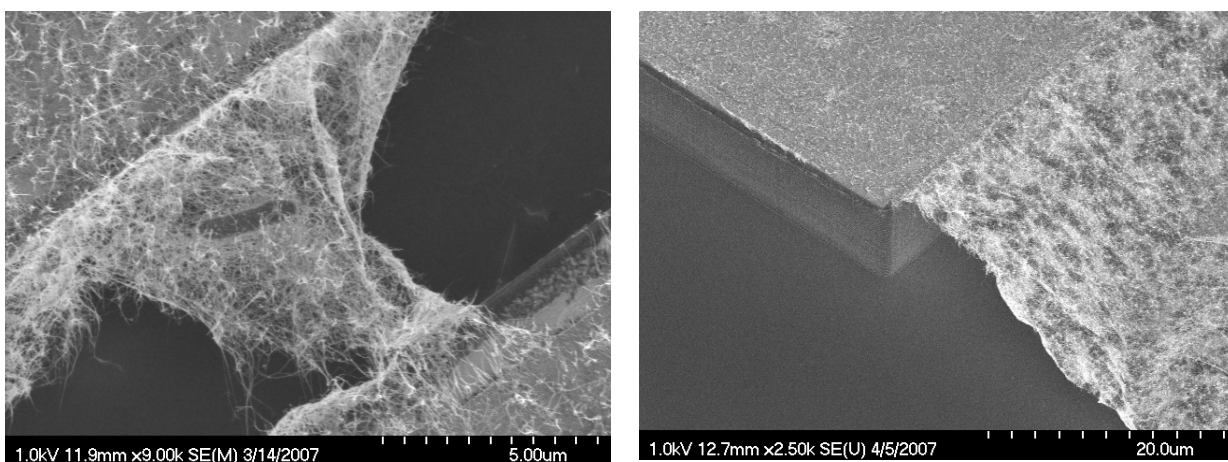


Figure 2. SEM images of suspended carbon nanotube networks. On the left, the network is bridging a 8 microns width trench. On the right, the network is connecting a pillar to the substrate.

(1) E.S. Snow, P.M. Campbell, M.G. Ancona, *Appl. Phys. Lett.*, **2005**, 86, 033105.

(2) M.E. Itkis et al. Science **2006**, 312, 403.

# SIMULTANEOUS SIZING OF NANOPARTICLES BY INDIVIDUALLY VISUALIZING AND SEPARATELY TRACKING THEIR BROWNIAN MOTION WITHIN A SUSPENSION.

*Bob Carr, Andrew Malloy and Patrick Hole*

*NanoSight Ltd, 2 Centre One, Old Sarum Park, Salisbury SP4 6BU, Wilts, UK*
*bob.carr@nanosight.co.uk*

## Introduction

The analysis of nanoparticle size is a ubiquitous requirement in a wide range of applications areas (and increasingly in the drug delivery sector) and is usually carried out by either electron microscopy or dynamic light scattering. Both techniques suffer from disadvantages; the former requiring significant cost and sample preparation, the latter generating only a population average which itself can be heavily weighted towards larger particles within the population. A new method of microscopically visualizing individual nanoparticles in a suspension allows their Brownian motion to be simultaneously analysed and from which the particle size distribution profile (and changes therein in time) can be obtained on a particle-by-particle basis.

## Experimental Methods

A small (250µl) sample of liquid containing particles at a concentration in the range 106-10/ml is introduced into the scattering cell through which a finely focused laser beam (approx. 20mW at $\lambda$=635nm) is passed. Particles within the path of the beam are observed via a microscope-based system (NanoSight LM10) or dedicated non-microscope optical instrument (NanoSight LM20) onto which is fitted a CCD camera. The motion of the particles in the field of view (approx 100x100µm) is recorded (at 30fps) and the subsequent video analysed. Each and every particle visible in the image is individually but simultaneously tracked from frame to frame and the average mean square displacement determined by the analytical program and from which can be obtained the particle's diffusion coefficient. Results are displayed as a sphere-equivalent, hydrodynamic diameter particle distribution profile (Fig 1). The only information required to be input is the temperature of the liquid under analysis and the viscosity (at that temperature) of the solvent in which the nanoparticles are suspended. Otherwise the technique is one of the few analytical techniques which is absolute and therefore requires no calibration. Results can be obtained in typically 30-60 seconds and displayed in a variety of familiar formats (diameter, surface area or volume on either linear or log scale). The instrument can be programmed to carry out repeat measurements of dynamically changing samples to analyse dissolution, aggregation and particle-particle interactions. Notably, because the instrument visualizes particles on an individual basis, particle number concentration is recoverable. Once analysed, the sample is simply withdrawn from the unit for re-use, if required.

## Results and Discussion

A number of results on calibration microspheres and mixtures thereof, colloidal gold and liposomes are shown below which indicate the advantages of the technique. The minimum particle size detectable depends on the particle refractive index but for highly efficient scatterers, such as colloidal silver, 10nm particles can be detected and analysed. For weakly scattering (e.g. biological) particles, the minimum detectable size may only be >50nm. The upper size limit to this technique is defined by the point at which a particle becomes so large (>1000nm) that Brownian motion becomes too limited to be able to track accurately. This will vary with particle type and solvent viscosity but in normal (e.g. aqueous) applications is approximately 800-1000nm. (Fig 2). All particle types can be measured and in any solvent

type providing that the particles scatter sufficient light to be visible (i.e. are not too small or indexed matched).

The results shown in Fig 3 obtained from an analysis of a mixture of 200 and 300nm latex beads (overlaid with the normal particle size distribution plot) show that the two populations can be well resolved from each other. Furthermore, because the technique analyses particles on an individual basis and can collect information on their relative brightness as well as their size (measured dynamically) these two data can be combined to give an intensity v size plot (Fig 3c). This capability shares many features in common with conventional flow cytometry but is unique to method in this deeply sub-micron size range. Finally, the technique has been successfully applied to the analysis of a wide range of viruses and liposomes, vesicles and nano-emulsions. See [1] for more information and examples of playable videos of a variety of samples.

**Conclusion**

The technique is robust and low cost representing an attractive alternative or complement to higher cost and more complex methods of nanoparticle analysis such as photon correlation spectroscopy (PCS) or electron microscopy that are currently employed in a wide range of technical and scientific sectors. Finally, the technique uniquely allows the user a simple and direct qualitative view of the sample under analysis (perhaps to validate data obtained from other techniques such as PCS) and from which an independent quantitative estimation of sample size, size distribution and concentration can be immediately obtained.

REFERENCES:
[1] www.nanosight.co.uk
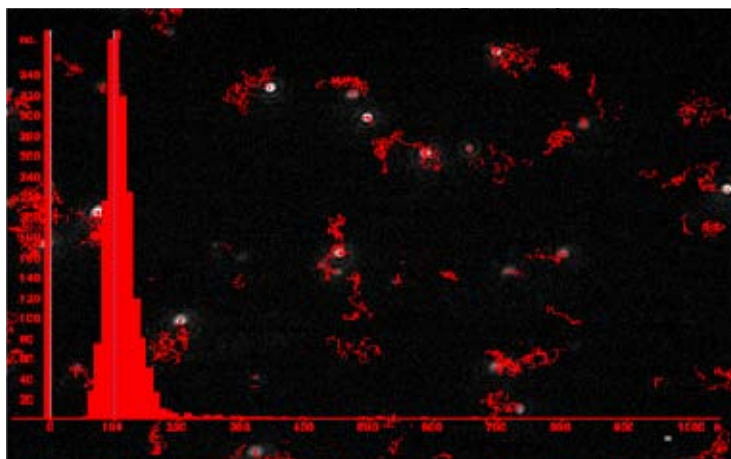


**Fig 1. A still from a video of 100nm polystyrene calibration particles showing *some* (for clarity) of the Brownian motion trajectories analysed and which is overlaid with the corresponding size plot.**
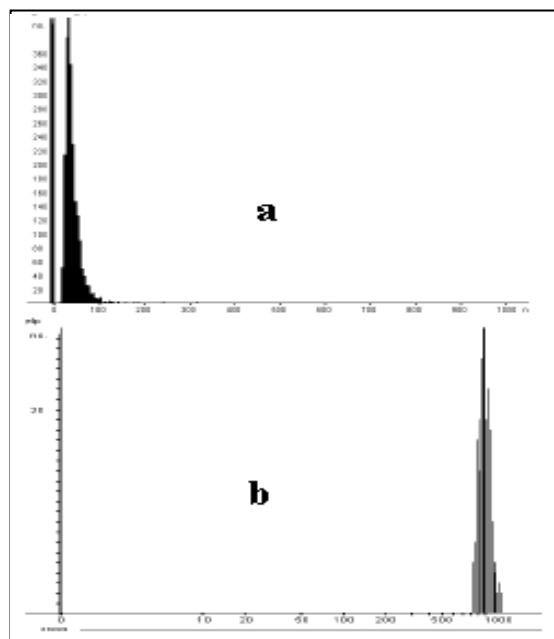
**Fig. 2 Size distribution plots of a) 30nm gold colloid (linear scale) and b) 900nm polymeric (log scale) particles.**
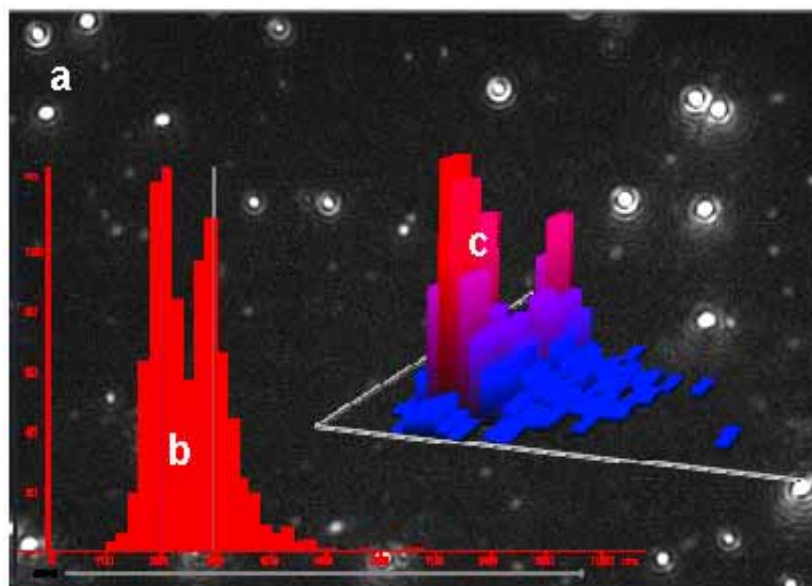


**Fig. 3 A mixture of 200nm and 300nm particles; a) still image, overlaid with b) analysis plot and c) 3D number v. relative intensity v. diameter plot.**

# RESOLVING SINGLE KINESIN MOTORS IN MOTION BY ATOMIC FORCE MICROSCOPY

*Carolina Carrasco[1], Iwan A. T. Schaap[2], Pedro J. de Pablo[1], Christoph f. Schmidt[3]*
*[1] Departamento de Física de la Materia Condensada C-III,*
*Universidad Autónoma de Madrid, 28049 Madrid, Spain*
*[2] National Institute for Medical Research,*
*The Ridgeway, Mill Hill, London, NW7 1AA, United Kingdom*
*[3] Physikalisches Institut, Fakultät für Physik, Georg-August-Universität,*
*Friedrich-Hund-Platz 1, 37077 Göttingen, Germany*

*carolina.carrasco@uam.es*

Kinesins are dimeric motor proteins involved in intracellular transport along microtubules in eukaryotic cells. Kinesin-1s are composed of two identical subunits, each consisting of a globular head of 4nm diameter and an extended α-helical stalk [1]. Single motor proteins of the Kinesin-1 family move along microtubules (MTs) in steps of 8 nm powered by the hydrolysis of ATP and can travel hundreds of nanometres before releasing from their track [2]. MTs are the largest and most rigid of the filaments that make up the cytoskeleton, the mechanical framework of the cell. The MT outer diameter is ~25 nm, while their length can reach many micrometers. MTs *in vivo* are composed of 13 protofilaments. The protofilaments run parallel to the MT axis and consist of head-to-tail joined dimers of α and β tubulin. Kinesin binds to β tubulin [3]. Recent experiments have demonstrated that kinesin moves along a line parallel to a protofilament in an asymmetric hand-over-hand mechanism, where the two heads exchange the leading position by taking non-identical alternating steps [4, 5, 6].

How exactly a single motor proceeds and how dense traffic is accommodated and regulated on the 13 narrow protofilaments of a microtubule remains unknown because the required resolution lies beyond the reach of light microscopy. A technique with which one can perform molecular dynamic imaging is atomic force microscopy (AFM). Here we have combined several recent advances in AFM methodology to visualize individual kinesin motors on MTs. We have recently succeeded to follow single Kinesin-1 dimers in their motion along microtubules with nanometre resolution by AFM in buffer. We found that both heads of one Kinesin-1 dimer are bound for the major part of the chemical cycle time to the microtubule. Furthermore, we could resolve that both heads bind to the same protofilament (fig.1), instead of straddling two, and remain on this track during processive movement.

## References:

[1] Kozielski F, Sack S, Marx A, Thormahlen M, Schonbrunn E, Biou V, Thompson A, Mandelkow EM, Mandelkow E. The crystal structure of dimeric kinesin and implications for microtubule-dependent motility. *Cell* **91**(1997)**:** 985-994

[2] Svoboda K, Schmidt CF, Schnapp BJ, Block SM. Direct observation of kinesin stepping by optical trapping interferometry. *Nature* **365**(1993)**:** 721-727

[3] Song YH, Mandelkow E. Recombinant kinesin motor domain binds to beta-tubulin and decorates microtubules with a B surface lattice. *Proc Natl Acad Sci USA* **90**(1993)**:** 1671-1675

[4] Asbury CL, Fehr AN, Block SM. Kinesin moves by an asymmetric hand-over-hand mechanism. *Science* **302**(2003)**:** 2130-2134

[5] Hua W, Chung J, Gelles J. Distinguishing inchworm and hand-over-hand processive kinesin movement by neck rotation measurements. *Science* **295**(2002)**:** 844-848

[6] Kaseda K, Higuchi H, Hirose K. Alternate fast and slow stepping of a heterodimeric kinesin molecule. *Nat Cell Biol* **5**(2003)**:** 1079-1082

## Figures:

**a)**　　　　　　　　　　　　　　　　**b)**
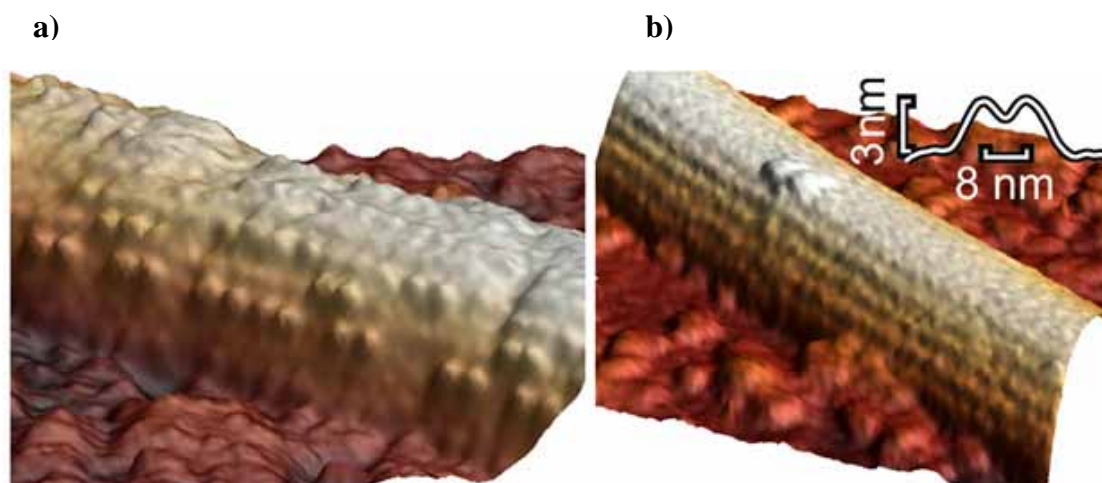


**Figure 1. AFM imaging of kinesin on MTs.  a)** 3D-rendered image, individual motors could be clearly distinguished, heads always appeared in pairs aligned along protofilaments. **b)** 3D-rendered image, isolated motors could be seen, both heads bound on the same protofilament. Upper inset: averaged axial profile of 17 kinesin molecules, interhead spacing: 8 nm, height: 3.5 nm.

# Pyridine- and $C_{10}H_{10}BN$-based nanotubes: A route to always semiconducting NTs

X. Cartoixà* and R. Rurali

*Departament d'Enginyeria Electrònica; Universitat Autònoma
de Barcelona; 08193 Bellaterra, Barcelona; Catalonia, Spain.*

The synthesis of carbon nanotubes (CNTs) doped with different impurities is a way to tailor their electronic properties. Several groups have achieved high nitrogen concentration with CVD techniques [1, 2]. Recently Chen *et al.* [3] have demonstrated the Vapor-Liquid-Solid (VLS) fabrication of nanotubes with an ultra-high N concentration and control over the N arrangements, based on a pyridine [see Fig. 1.a)] precursor gas and an Fe–Co catalyst.

We have performed first-principles calculations with the SIESTA [4] program showing that the metallic or semiconducting character of pyridine-based nanotubes will depend on the specific arrangement of the N atoms within and the chirality of the NT.

On the other hand, changing to a different precursor where the extra nitrogen atoms are compensated by boron atoms, such as a borabenzene-pyridine adduct [5, 6] [Fig. 1.b)], we show that a gap will open for pristine metallic CNTs (Fig. 2), while for pristine semiconducting CNTs the gap will be reduced by some amount (Fig. 3), but maintaining the semiconducting character.

Therefore, a $C_{10}BN$ nanotube (CBNNT) would always be semiconductor, easing the fabrication of CNT-based circuitry.

---

[1] M. Natha, B. C. Satishkumara, A. Govindaraja, C. P. Vinoda, and C. N. R. Rao, Chem. Phys. Lett. **322**, 333 (2000).

[2] J. Liu, S. Webster, and D. L. Carroll, J. Phys. Chem. B **109**, 15769 (2005).

[3] H. Chen, Y. Yang, Z. Hu, K. Huo, Y. Ma, Y. Chen, X. Wang, and Y. Lu, J. Phys. Chem. B **110**, 16422 (2006).

[4] J. M. Soler, E. Artacho, J. D. Gale, A. García, J. Junquera, P. Ordejón, and D. Sánchez-Portal, J. Phys.: Condens. Matter **14**, 2745 (2002).

[5] R. Böse, N. Finke, J. Henkelmann, G. Maier, P. Pätzold, H. P. Reisenauer, and G. Schmid, Chem. Ber. **118**, 1644 (1985).

[6] S. G. Semenov and Y. F. Sigolaev, Zh. Obshch. Khim. **76**, 2014 (2006), [Russ. J. Gen. Chem. **76**(12), 1925 (2006)].

---

*Electronic address: Xavier.Cartoixa@uab.es
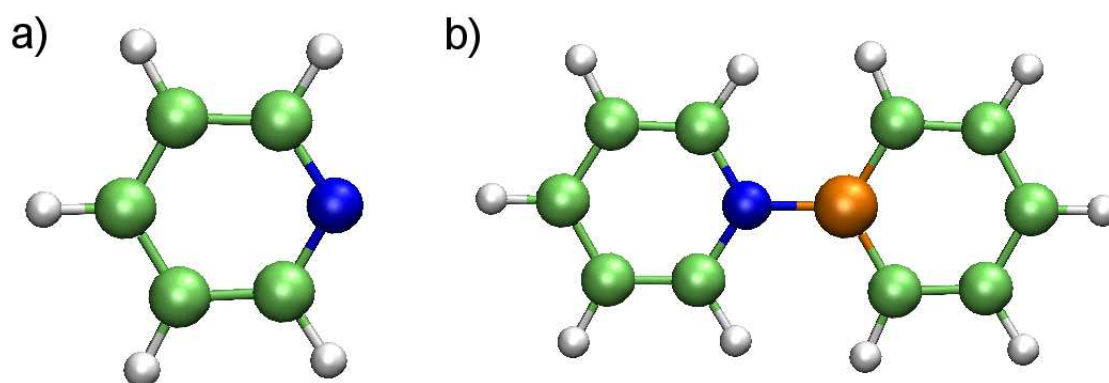
FIG. 1: a) Pyridine ($C_5H_5N$) molecule. b) Pyridine-borabenzene adduct ($C_{10}H_{10}BN$) molecule. The blue (dark) atom corresponds to nitrogen.
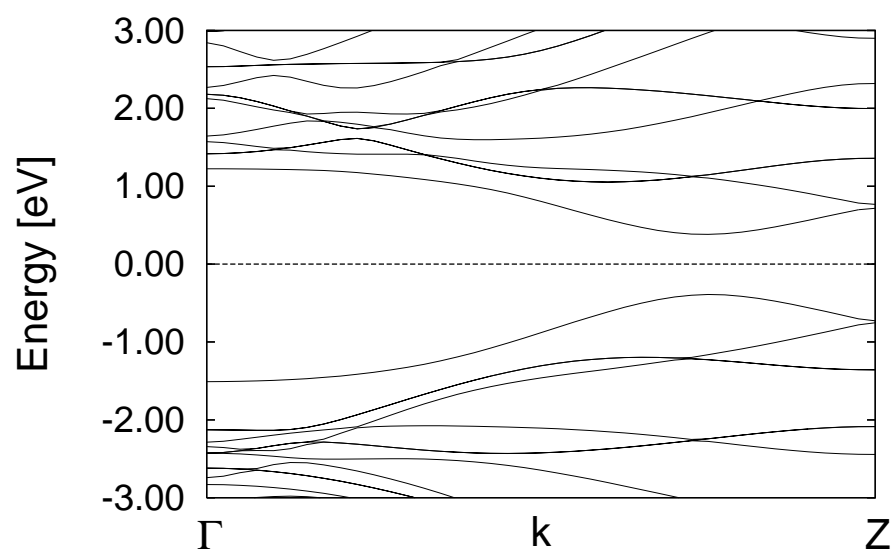


FIG. 2: Band structure of a (6,6) CBNNT showing the opening of a gap, where the CNT analog would be metallic. The dashed line corresponds to the Fermi level.
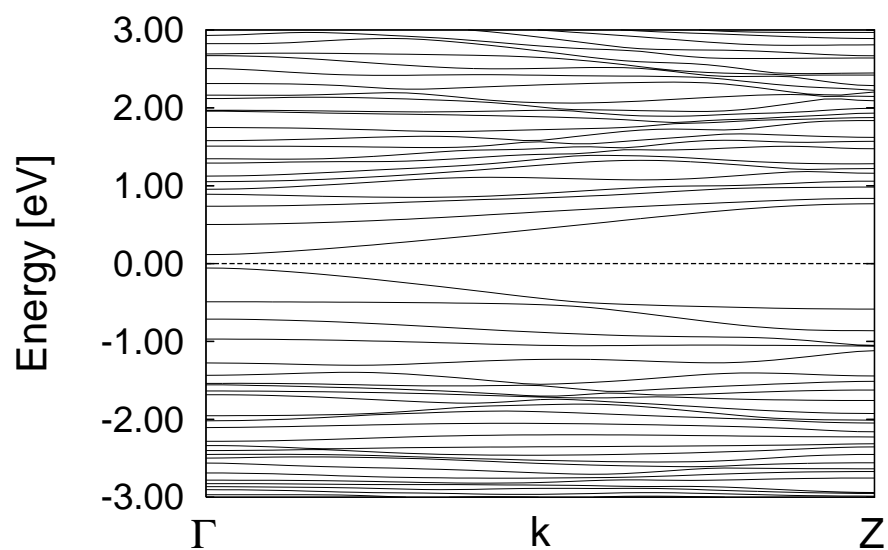


FIG. 3: Band structure of a (10,0) CBNNT showing the existence of a gap, which is reduced in numerical value with respect to its pristine CNT analogue.

# Clustering and growth of intermetallic alloy nanodroplets

*E. Sarantopoulou[1], S.Kobe[2], M. Janeva[3], G. Dražić[2], Z. Kollia[1], A. C. Cefalas[1]*
*[1]National Hellenic Research Foundation, TPCI, Athens 11635 Greece.*
*[2]Jožef Stefan Institute, Nanostructured Materials, Jamova 39, Ljubljana, Slovenia*
*[3]National Institute of Chemistry, Hajdrihova 19, 1000 Ljubljana, Slovenia*

*ccefalas@eie.gr*

The magnetic response of rare earth-iron intermetallic alloy thin films depends on the crystal structure, size and stochiometry of the film's nanocomposites [1].

However, films with nanodroplet-like morphologies, grown with pulse laser deposition exhibit ferromagnetic response even without annealing and nitriding [2]. The magnetism has its origin on the growth of 5-10 nm crystals included inside ~ 50 nm amorphous spherical nanodroplets, which are created in the plume at superheated (non-equilibrium) conditions. The size of the nano-crystalline islands and nanodroplets depends on the target composition the background pressure, the energy and the fluence of the laser and on the distance between the substrate and the target. $Sm_2Fe_{17-x}Ta_xN_{3-\sigma}$ nano-droplets were fabricated in situ in nitrogen background pressure from $Sm_{13.8}Fe_{82.2}Ta_{4.0}$ target by pulse laser deposition using a molecular fluorine laser at 157 nm. The bi/phase nanocrystaline phase was formed during the fast cooling of the nanodroplet on the Ta substrate and in the plume. In this communication the morphology, the stochiometry and the structure of the nanodroplets are analyzed with high-resolution transmission electron microscopy. For a distance of 0.5 cm between the target and the substrate, more than one nano islands were crystallized and agglomerated inside only one nanodroplet, Fig. 1. Furthermore clustering of individual nanodroplets was formed on the Ta substrate, Fig. 2. At longer separation distance nanodroplets of larger size and different stochiometry were formed on the substrate. The thermodynamics of the system for the optimum conditions of nanodroplet formation is discussed.

**References:**

[1] K. Žužek, P. J. McGuiness, S. Kobe, Magnetic monitoring of the nitriding process in Sm-Fe-Ta-based alloys. *IEEE Trans. Magn.* 39, 2983-2985, 2003.

[2] S. Kobe, E. Sarantopoulou, G. Dražič, J. Kovač, M. Janeva, Z. Kollia, A.C. Cefalas. To be published in *Appl. Surf. Science* in 2007.

**Figures:**
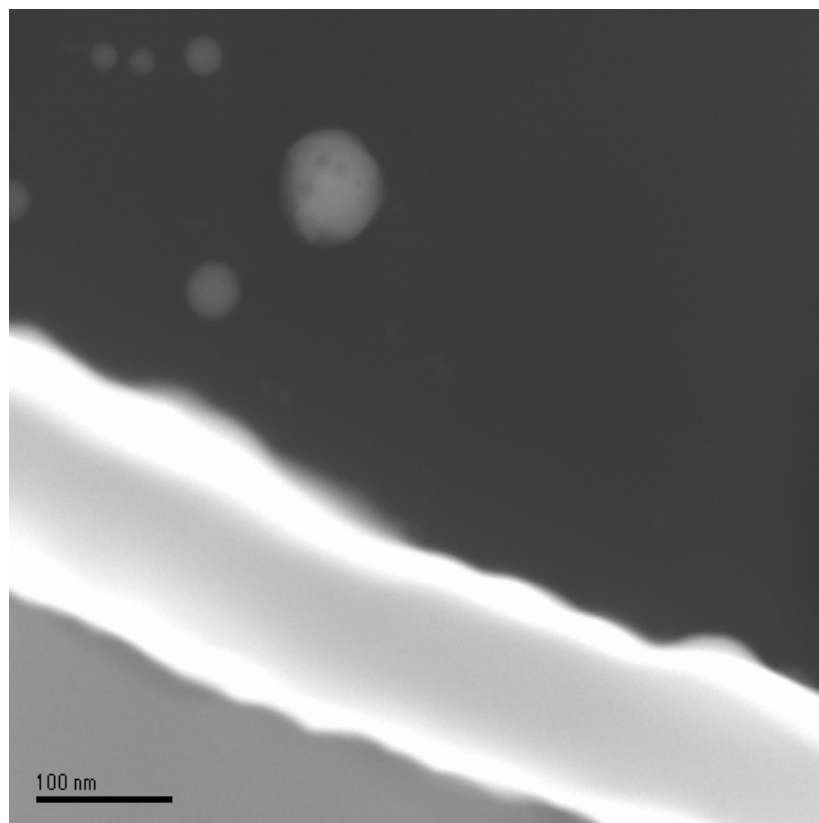


**Figure. 1** A TEM image of a single ~ 62 nm wide $Sm_2Fe_{17-x}Ta_xN_{3-\sigma}$ nanodroplet on a Si substrate sputtered with Ta. Four 15 nm nano-crystal islands were grown on the top of the Ta substrate surrounded by the amorphous material.
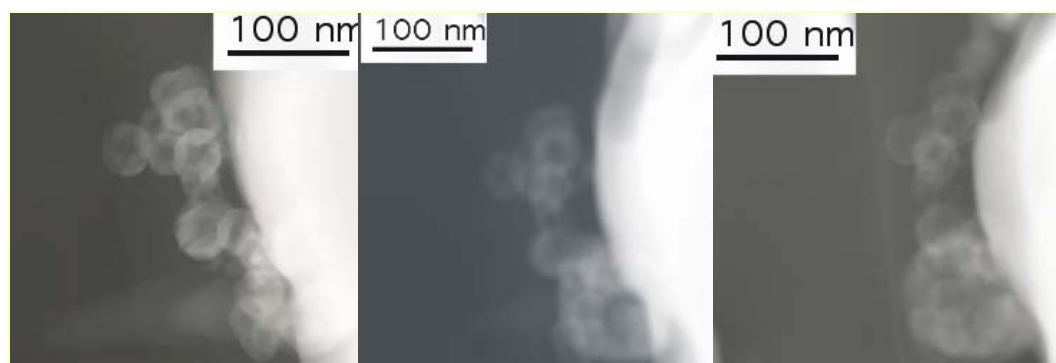


**Figure 2.** TEM image of clusters of $Sm_2Fe_{17-x}Ta_xN_{3-\sigma}$ nanodroplets on a Si substrate coated with Ta.

# PREPARATION OF COLOURED DLC NANOLAYERS AND THEIR NANOINDENTATION TESTING

*F. Cerny, R. Stefec, J. Gurovic, V. Jech and S. Konvickova*
*Faculty of Mechanical Engineering of Czech Technical University, Technicka 4. Prague,*
*Czech Republic, 16607*
*Frantisek.Cerny@fs.cvut.cz*

We prepared coloured DLC (Diamond-Like Carbon) nanolayers as decorative coatings of stainless steel sheets. These coatings must be adherent and hard for good wear resistance.

All films were prepared on grade Cr13 SS sheet substrate (10 x 10) cm. For the deposition of adherent DLC films on stainless steel substrate we applied deposition of very thin interlayer of Si-O-C. Deposition by PACVD (Plasma Assisted Chemical Vapour Depositin) of DLC films and of Si-O-C interlayer was performed using dc plasma without additional heating and with the HMDSO (hexamethyldisiloxane) and methane as precursors.

Microhardness was determined by nanoindentation using a Berkovich type diamond indentor in type NanoTest NT600 apparatus; the measurements were averages of at least 6 indentations at identical loads of 0.25 mN; loading and unloading (relief) time was 20 s, delay (creep at maximum load) was 10 s. The microhardness data were thickness-dependent, influenced by substrate. The highest measured value was 23 GPa.

Effect of film thickness on colour is following: The reference specimen (bare SS) has a bright metallic sheen. In the order of increasing thickness, the DLC films produced by PACVD have colours as follows: dark violet at ~50 nm; medium blue at ~100 nm; golden light at ~150 nm; deep rose pink at ~240 nm; golden brown at ~320 nm; and soot black at >500 nm.

# FIRST PRINCIPLES STUDIES OF INTERACTION BETWEEN DNA AND CARBON NANOTUBES FOR THE POTENTIAL DNA SENSOR APPLICATIONS

Hyunju Chang, Ki-jeong Kong, Gyoung-Ho Buh, and Jeong-O Lee

Korea Research Institute of Chemical Technology, Daejeon, 305-600, KOREA

*hjchang@krict.re.kr*

Recently biosensor applications of carbon nanotube (CNT) devices have been intensively investigated. Since the ultra-sensitivity of CNT field effect transistor (FET) sensor is expected, CNT FET sensor is suggested as a DNA sensor to detect even single nucleotide polymorphism

Here we report the first principles studies to understand the interaction between DNA and CNTs for the DNA sensor applications. Firstly, we have carried out first principles electronic structure calculations on the interaction of individual DNA nucleobases (especially guanine and cytosine) with single walled carbon nanotubes (SWNTs). The binding energies of various configurations including π-stacking and direct bonding ones are compared. Secondly, we have calculated the interaction of the thiolated nucleotides with gold nanoparticles to simulate the DNA sensor applications. From the calculated results of above two systems, we tried to propose the mechanism of binding of single-stranded DNA (ss-DNA) on the SWNTs and the hybridization of complementary DNA on the pre-bound ss-DNA.

# SIMULATION OF THE GATE LEAKAGE CURRENT IN SURROUNDING GATE (SG) MOSFETS BASED ON AN ANALYTIC POTENTIAL MODEL

Ferney Chaves*, David Jiménez, Jordi Suñé

Departament d'Enginyeria Electrònica, Escola Tècnica Superior d'Enginyeria, Universitat Autònoma de Barcelona, 08193-Bellaterra, Barcelona, Spain.

*Edifici Q-Campus de la UAB – 08193 Bellaterra, Barcelona, Spain.
ferneyalveiro.chaves@uab.es

Over the past three decades, the exponential growth of the microelectronics industry has been enabled primarily by continuous scaling of dimension reduction of metal-oxide-semiconductor field-effect transistor (MOSFET). The inherent benefits of MOSFET scaling are the speed improvement and energy reduction associated with a binary-logic transition. Various device structures such as double gate fully depleted SOI, triple-gate and gate-all-around structures hence, have been extensively studied to restrict short-channel effects (SCEs) within a limit while achieving the primary advantages of scaling, i.e. higher performance, lower power, and ever increasing integration density [1,2]. Among these devices SG-MOSFET, illustrated in Figure 1, have recently drawn wide research interest due to their excellent SCEs immunity compared to other contemporary device structures [3]. Several physical limiting factors associated with the ultrathin gate oxides have been identified, including direct tunneling currents [4]-[5], polysilicon depletion effects [6], and oxide reliability [7]. Among them, the direct tunneling is the most sensitive one to the oxide thickness and it plays a significant role in a SG-MOSFET because is a source of parasitic current and contribute to the stand-by power consumption of integrated circuits. Many papers on modelling the tunneling current in the MOS system consider the tunnel current under equilibrium ($V_{ds} = 0$). However, if the equilibrium is broken ($V_{ds} \neq 0$) the distribution of the potential energy and the quasi Fermi level changes along the channel and calculation of the gate tunnel current requires taking into account this effect. In this study we use analytic physics based expressions for the potential energy and Fermi level of the SG MOSFET [8], which depends on the position through the channel. To account for the quantum effects we solve the Schrödinger equation for correcting the classical surface potential [9]. The direct tunneling current is calculated by means of three fundamentals parameters: i) the transmission probability, calculated with a modified WKB approximation and taking into account the reflections from all boundaries within of the oxide, ii) the frequency $f$ at which the electrons tunnel through the gate oxide, iii) the inversion charge density, which depends on 1-D density of states and Fermi-Dirac statistic [10]. The main result is the comparison between classical and quantum models for direct tunneling current and the leakage current dependence on the source-drain voltage, gate-source voltage and thickness of the silicon. Besides we show the differences between gate tunneling current results obtained with the commercial DESSIS^TM simulator and our model.

**References:**
[1] M. T. Borh, IEEE Trans. Nanotechnol. **1** (2002) 56.
[2] J. P. Collinge, Solid State Electron. **48** (2004) 897.
[3] J. Wang, E. Polizzi, and M. Lundstrom. IEDM Tech. Dig., Washingtong DC. 695 (Dec 2003)
[4] F. Rana, S. Tiwari, and D. A. Buchanan, Appl. Phys. Lett. **69** (1996) 1104.
[5] S. H. Lo, D. A. Buchanan and Y. Taur, IBM J. RES. Develop. **43** (1999) 327.
[6] Y. Taur, and T. H. Ning, Fundamental of Modern VLSI Devices. Cambridge, U. K.: Cambridge Univ. Press. (1998).
[7] J. H. Stathis, and D. J. Dimaria, IEDM Tech. Dig. (1998) 167.
[8] D. Jimenéz, B. Iñiguez, J. Suñe, L. F. Marsal, J. Pallarès, J. Roig, and D. Flores. IEEE Electron Device Lett. **25** (2004) 571
[9] V. P. Trivedi and J. G. Fossum, IEEE Electron Device Lett. **26** (2005) 579.
[10] D. Jimenéz, J. J. Sáenz, B. Iñiguez, J. Suñe, L. F. Marsal and J. Pallarès. J. Appl. Phys. **94** (2003)1061.

**Figures:**
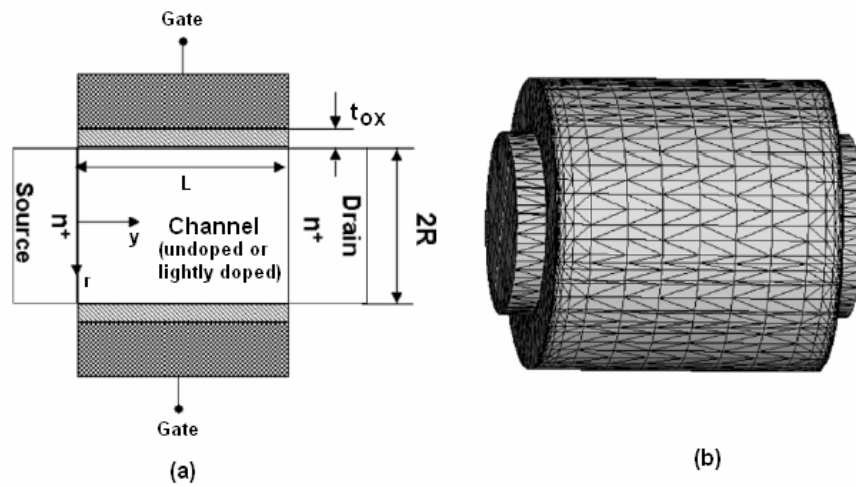


**Fig. 1**. (a) Cross section of the SG-MOSFET. (b) Simulated geometry of the SG-MOSFET using ISE-TCAD[TM].

# Comparison of Modified Biopolymers on Non-Specific Protein Adsorption for a Novel Microsphere Immunoassay

**Annie Chen,** Darby Kozak, Bronwyn Battersby and Matt Trau

*Centre for Nanotechnology and Biomaterials,*

*Australian Institute of Bioengineering and Nanotechnology*

*University of Queensland, Brisbane, Australia 4072*

Telephone: +61 7 334 64161

Fax: +61 7 334 63973

*s4029182@student.uq.edu.au*

Proteomic assays provide rapid and highly sensitive early disease diagnosis [1] which has the potential to decrease the fatality rate of diseases [2]. The features of early disease detection and identification are able to greatly reduce the spread of many rapidly expanding global health issues, such as HIV, West Nile virus, and Dengue virus. However, current diagnostic proteomic assays are hindered by their lack of clear and reproducible results which arise from a poor signal to background noise. This can be substantially improved by creating an effective antifouling layer between the assay surface and biological solution and/or increasing the target loading on the assay surface. Polyethylene glycol (PEG) has been shown to provide an effective boundary in preventing biomolecular non-specific adsorption [3]. However, target loading and grafting structure of unmodified PEG is limited due to its linear structure. In contrast, the polysaccharide-based biopolymer Dextran has multiple potential reactive alcohol sites along the polymer chain for target loading while also exhibiting good antifouling properties [4]. Therefore, dextran potentially provides a greater ability to increase signal to background noise ratio.

In this research, organosilica microspheres were used as an assay platform for polymer grafting and subsequent protein adsorption experiments. Five $M_W$ PEGs (2k, 3.4k, 6k, 10k and 20k) and three $M_W$ dextrans (10 kDa, 66.9 kDa, and 445 kDa) were modified and grafted with increasing concentrations (0.01 ~ 30 % w/v) to the surfaces of the particles. The amount of grafted polymers was characterised by XPS. A diverse polymer thickness (2 Å ~ 15 Å) and density (2 ~ 35 x $10^{-3}$) was grafted onto the particle surfaces. Similar amounts of polymer could be grafted onto the surfaces using both 2k and 20k $M_W$ PEG regardless the difference between their hydrodynamic volume and chain length in a hydrated condition.

The protein antifouling ability of these polymer grafted surfaces were examined by the exposure to fluorescently labelled protein G (6.5 kDa), BSA (68 kDa), and IgG (150 kDa).

Amounts of proteins adsorbed onto the modified surfaces were analysed using flow cytometry. This technique provides a sensitive and high through-put screening of particles while using small sample quantities. A definite correlation between the quantities of polymers grafted onto the particle surfaces to their antifouling properties was determined. It was found that surfaces grafted with similar amounts of polymer although using different polymer chain lengths exhibited similar protein antifouling performances. A transition region of polymer thickness (5 – 7 Å) on particle surfaces was found to have great impact on the amount of non-specific protein adsorption.

- 1. Aebersold, R., et al., *Perspective: A Program to Improve Protein Biomarker Discovery for Cancer.* J. Proteome Res., 2005. **4**(4): p. 1104-1109.
- 2. Hartwell, L., et al., *Cancer biomarkers: a systems approach.* 2006. **24**(8): p. 905-908.
- 3. D. J. Irvine, A.M.M., S. K. Satija, J. G. Barker, S. J. Sofia-Allgor, L. G. Griffith,, *Comparison of tethered star and linear poly(ethylene oxide) for control of biomaterials surface properties.* Journal of Biomedical Materials Research, 1998. **40**(3): p. 498-509.
- 4. Stephen P. Massia, J.S., *Immobilized RGD peptides on surface-grafted dextran promote biospecific cell attachment.* Journal of Biomedical Materials Research, 2001. **56**(3): p. 390-399.
-

# Thermal Analysis of PT Ceramics Obtained by Sol-Gel Processing

*Irinela Chilibon[a], José Marat-Mendes[b]*
*[a] National Institute of Research and Development for Optoelectronics,*
*INOE-2000, 77125, PO Box MG-5, Bucharest, Romania*
[qilib@yahoo.com](qilib@yahoo.com)
*[b] Faculty of Science and Technology, New University of L isbon,*
*2829-516 Caparica, Portugal,*
[jnm@fct.unl.pt](jnm@fct.unl.pt)

$PbTiO_3$ (PT) ceramics are prepared by sol-gel method, utilising as precursors Titanium (IV) isopropoxide $Ti[OCH(CH_3)_2]_4$, 99.99% purity and Lead (II) acetate trihydrate $Pb(CH_3COO)_2 \cdot 3H_2O$, 99% purity, and 2-methoxyethanol $CH_3OCH_2CH_2OH$ as solvent. Thermal analysis was performed in the temperature range 400ºC up to 500ºC, with 5ºC/min rate. Crystallised ceramics present high transition temperatures, high Curie points and thermal hysteresis, closed to 490 $^0$C. Crystallisation and morphology properties are investigated by SEM, and DSC analysis. SEM micrographs analysis proves crystallisation structure for the PT powders.

## 1. Introduction

Lead titanate $PbTiO_3$ (PT), which exhibits a perovskite structure and a Curie temperature of 490 $^0$C, belongs to the most important ferroelectric and piezoelectric families. The sol-gel method advantages of Lead titanate $PbTiO_3$ processing are the mixing of reactants on a molecular level, a better control of stoichiometry, higher purity raw materials, and the easy formation of ultrafine and crystallized powders [1]. The starting materials used in the preparation of the "sol" are usually inorganic metal salts or metal organic compounds such as metal alkoxides [2]. The sol-gel method applies to porous materials, dense materials like glasses and ceramics, organic-inorganic hybrids and nanocomposites [3]. It was found that a possible improvement of the crystallization process is to use power ultrasound [4].

## 2. Experimental sol-gel method for $PbTiO_3$ ceramics

$PbTiO_3$ (PT) ceramics are prepared by sol-gel method, utilising as precursors Titanium (IV) isopropoxide $Ti[OCH(CH_3)_2]_4$, 99.99% purity and Lead(II) acetate trihydrate $Pb(CH_3COO)_2 \cdot 3H_2O$, 99% purity, and 2-metoxietanol $CH_3OCH_2CH_2OH$ as solvent. The gel is prepared by addition of equal volumes of precursor solution (sol) and a solution, containing water (Rw = 2.5) and 2-metoxietanol as solvent. In the preliminary gel drying process, the gel is heated at 200 $^0$C for 12 hours. After that, the amorphous powder is heated at 300 $^0$C for 24 hours. Secondarily, the drying process is made at 500 $^0$C for 2 hours. The amorphous powder is crystallised at 800 $^0$C for 2 hours, and cooled in air.

Two $PbTiO_3$ samples are obtained, namely A and C (ultrasound gel). Before the drying process the gel was ultrasound irradiated. Ultrasonic vibrations propagated through the gel and induced cavitation effects. To obtain C sample, after gel ultrasound irradiation the preliminary drying of gel was performed at 200 $^0$C, during one hour, instead of 12 hours that in the case of A sample. The crystallisation and morphology properties of ceramic powders are investigated by DSC analysis. The thermal properties were obtained in the temperature range 400ºC up to 500ºC, with a rate of 5ºC/min. Figure 1 presents the heat flux function of temperature curves, for A and C samples. Figure 2 presents the heat flux curves function of time for A and C samples, at 5ºC/min temperature rate. The SEM micrograph presented in

Figure 4 shows the grater size grains for C sample, comparatively with the grains of A sample (Figure 3).

## 3. Conclusions and discussions

Crystallization preparation by a thermal process of dense crystalline ceramics depends on the process duration. Also, the temperature conditions have influence in the size increasing of the crystal grains. The study of the crystallization upon heating was performed using the technique differential scanning calorimetry (DSC). Thermal curves were determined in the temperature range 400ºC up to 500ºC, with a rate of 5ºC/min. The two $PbTiO_3$ powders have also been comparatively studied in thermal analysis and particle morphology. It has been observed that the crystalline structure of PT powder type C has been modified by ultrasound irradiation. Ultrasound irradiation implies a better nucleation, and has influence on the growth rate and the crystals size distribution. Both PT crystallised ceramics present high transition temperatures, high Curie points closed to 490 $^0$C and thermal hysteresis.

**References:**

[1] S. Kazaoui, J. Ravez, J Mater. Sci, **28**, 1211-1219 (1993).
[2] C.J. Brinker, G.W. Scherer, Sol-Gel Science, The Physics and Chemistry of Sol-Gel Processing, New York: Academic Press, Inc., (1990).
[3] S. Sakka, Hanbook of Sol-Gel Science and Technology, Kluwer Academic Publishers, Vol. I, Sol-Gel Processing, (2005).
[4] N. Amara, B. Ratsimba, A. Wilhelm, H. Delmas, Ultrason Sonochem, **11**, 17-21 (2004).

**Figures:**
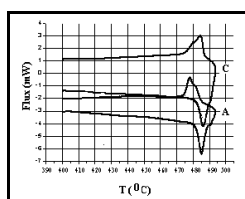


*Fig. 1 Heat flux curves function of temperature for A and C samples, at 5ºC/min temperature rate*
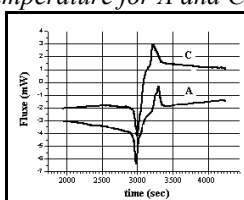


*Fig. 2 Heat flux curves function of time for A and C samples, at 5ºC/min temperature rate*
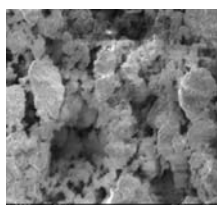


*Fig.3 SEM microstructure of PT sol-gel powder (A sample)*
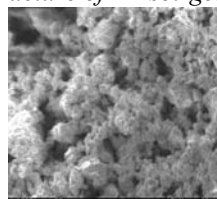


Fig.4 SEM microstructure of PT sol-gel powder (C sample)

# DIRECT SYNTHESIS OF SIC NANORODS BY ANNEALING CARBON NANOCAPSULES AND SiO₂ SPHERES

*Sheng-Cheng Chiu, Chih-Che Hsieh and Yuan-Yao Li\**
*Department of Chemical Engineering, National Chung Cheng University, Chia-Yi 62102,*
*Taiwan, R.O.C*
*Presenting author: hpop@ms38.hinet.net*
*\*Corrosponding author: chmyyl@ccu.edu.tw*

Silicon carbide nanorods (SiC NRs) exhibit excellent properties for unique mechanical and optical properties in the applications of cold cathode field emission display (FED), nanodevices and sensors [1-2]. Various carbon precursors, such as activated carbon fibers [3], platelet carbon nanofibers (PCNF) [4] and  graphite powders [5], have been fabricated SiC NWs successfully. In this study, a new carbon precursor to prepare SiC NRs is reported.

A mixture of carbon nanocapsules and $SiO_2$ sphere powders in a weight ratio of 1:1 was mixed for 60 min at room temperature (Fig. 1a and 1b) [6]. The mixture powders were loaded an alumina boat with cap and placed in the middle of a horizontal tube furnace. SiC NRs were synthesized through mixture powders under an argon atmosphere at 1300 $^{o}$C for 8 hours. The observation of the as-synthesized SiC NRs using field-emission scanning electron showed that the diameter of the nanowires was about 20-90 nm and the length was up to several micrometers (Fig 2). The surface of SiC NRs revealed zigzag structure. In the conventional transmission electron microscopy image and selected area electron diffraction (SAED) shown in Fig. 3, the SiC NR is single-crystalline structure with lattice fringes perpendicular to the nanorod axis and possesses a high density of stacking fault. The SAED pattern (inset of Fig. 3) demonstrates that SiC NRs has a single and continuous crystalline phase. The lattice spacing of 0.25 nm corresponded to the d-spacing of <111> crystal plane of the β-SiC.

**References:**

[1]   [1] Mo Y.H., Shajahan M.D., Lee Y.S., Hahn Y.B., Nahm K.S., Synth. Met., **140** (2004) 309.
[2]   Lo H.C., Das D., Hwang J.S., Chen K.H., Hsn C.H., Chen C.F., Chen L.C., Appl. Phys. Lett., **83** (2003) 1420.
[3]   Zhou W.M., Yang B., Yang Z.X., Zhu F., Yan L.J., Zhang Y.F., Applied surface science, **252** (2006) 5143-5148.
[4]   Qiao W.M., Lim S.Y., Yoon S.H., Mochida I., Ling L.C., Yang J.H., Applied Surface Science, **253** (2007) 4467-4471.
[5]   Ryu Y.H, Tak Y.G., Yong K.J., Nanotechnology, **16** (2005) S370-S374.
[6]   Liu T.C., Li Y.Y., Carbon, **44** (2006) 2045-2050.

**Figures:**
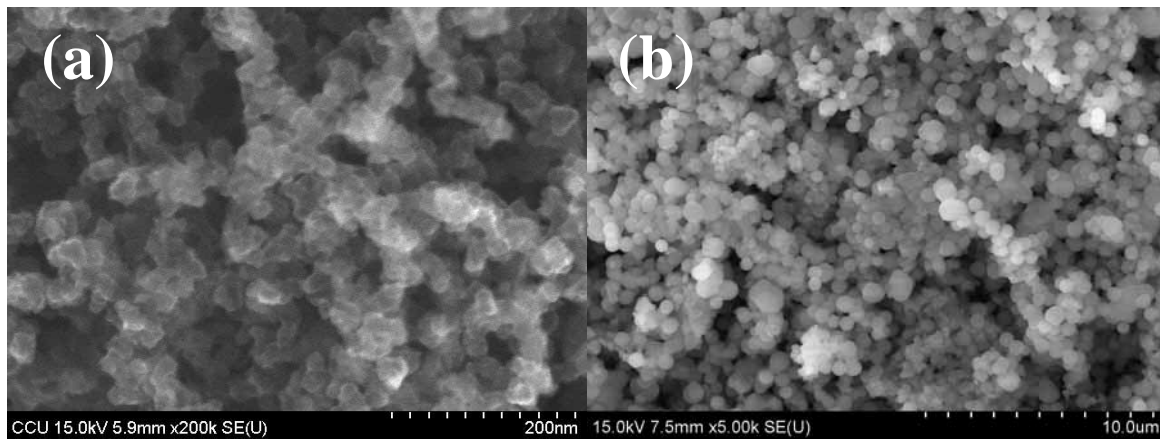


Figrue1. SEM of as-synthesized (a) carbon nanocapusles and (b) SiO₂ spheres
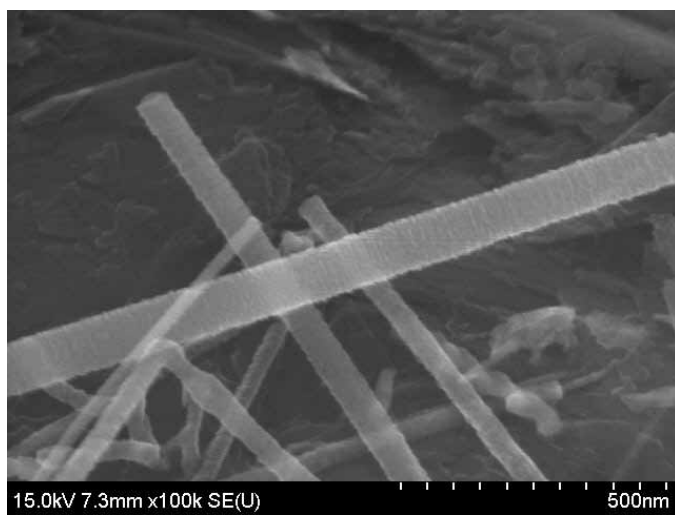


Figrue2. High magnification SEM of SiC nanorods
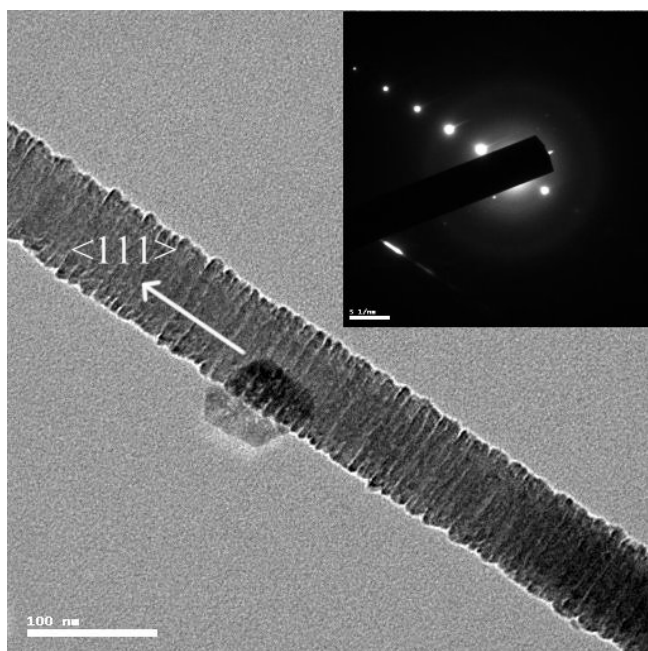


Figrue3. TEM image of SiC nanorod. Inset shows a SAED pattern of SiC nanorod.

# Synthesis of Nanoparticles Targeting Liver Cancer

*Wan-Seob Cho, Sheenhee Kim, Seongjun Kim, Seung Hee Kim, Hyoung Ook Kim, Min Jung Cho, Mina Choi, Beom Seok Han, Jayoung Jeong*
*National Institute of Toxicological Research, Seoul, Korea*
*chows77@kfda.go.kr*

The purpose of this study was (1) synthesis of fluorescence magnetic nanoparticle, (2) conjugation of GST-p antibody that is considered as a biomarker of preneoplastic lesions of liver cancer on rats, and (3) *in vitro* and *in vivo* targeting.

The structures of fluorescence magnetic nanoparticles were composed of 10 nm size cobalt ferrite core nanoparticle and water soluble silica was coated on the cobalt ferrite core. Then, nanoparticles were incorporated with rhodamine B isothiocyanate (RITC) and the GST-p antibody was conjugated with the nanoparticles.

GST-p expression in cell and tissue was confirmed with fluorescence immunohistochemistry and western blot analysis in H-4-II-E cell and paraffin embedded rat liver tissue which is treated with DEN. The strong positive signal in cytoplasm and nucleus was detected in H-4-II-E cell and in hyperplastic nodule and surrounding liver tissue.

The GST-p conjugated fluorescence magnetic nanoparticles were incubated with H-4-II-E cell and paraffin embedded rat liver tissue. The strong positive signal was detected mainly in cytoplasm and little in nucleus of H-4-II-E cell. Furthermore, there were positive signals in hepatocyte of paraffin embedded rat liver tissue.

## References

(1)Brigger I, Dubernet C, Couvreur P. Adv Drug Deliv Rev. 2002, 54, 631-651.

(2) Niu ZS, Wang M. World J Gastroenterol. 2005, 28, 4404-4408.

(3) Yezhelyev MV, Gao X, Xing Y, Al-Hajj A, Nie S, O'Regan RM. The Lancet 2006, 7, 657-667.

**Figures**
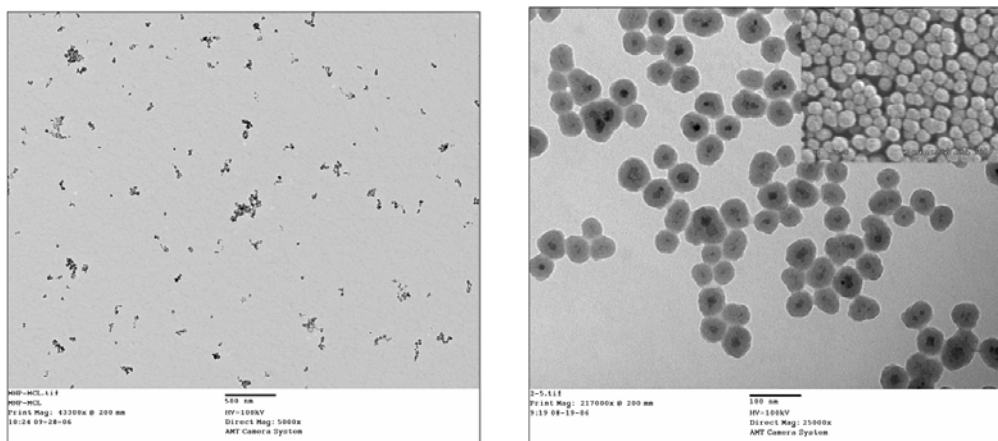


Figure 1. TEM images of synthesized cobalt ferrite nanoparticles (left) and silica coated nanoparticles (right)
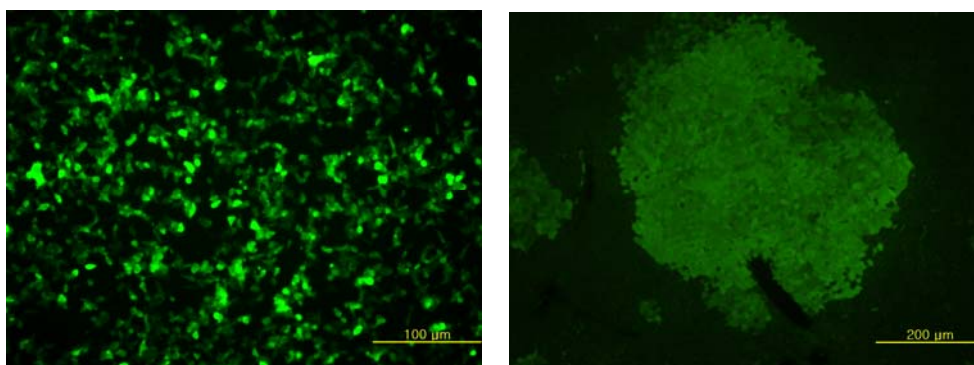


Figure 2. GST-p immunofluorescence images of H-4-II-E cell (left) and rat hyperplastic nodule (right)
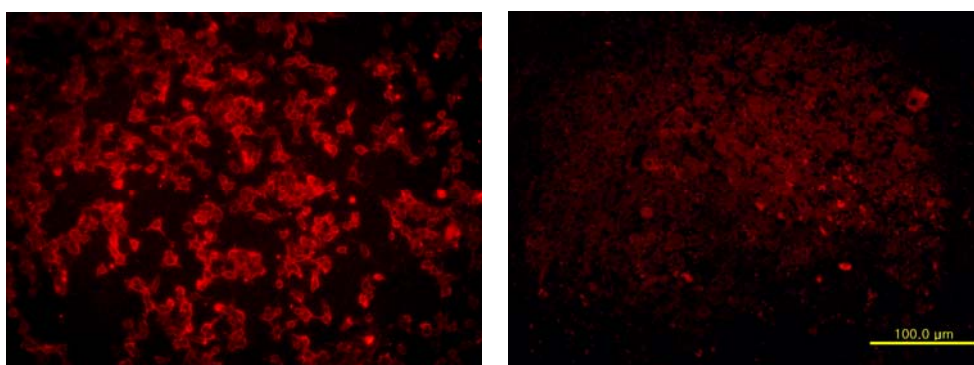


Figure 3. Immunofluorescence staining of MNP-GST-p nanoparticles with H-4-II-E cell (left) and rat hyperplastic nodule (right)

# CARBON NANOTUBE BASED ION SELECTIVE FIELD EFFECT TRANSISTORS

Cristina C. Cid, Jordi Riu, Alicia Maroto and F. Xavier Rius
Department of Analytical Chemistry and Organic Chemistry
Rovira i Virgili University
C/ Marcel·lí Domingo s/n. 43007-Tarragona. Spain
cristina.cid@urv.cat

In this communication we report a novel type of ion selective field effect transistors (ISFETs).They incorporate a network of carbon nanotubes as transduction layer, and do not need an external reference electrode.

ISFETs were first reported in 1970.[1] They are potentiometric sensors, of the family of chemically modified field effect transistors (CHEMFETs), and have several similarities to the well known ion selective electrodes (ISEs). ISFETs are based on an ion selective membrane that replaces the gate electrode in metal oxide field effect transistors (MOSFET). The membrane is able to selectively detect ions in solution. Nowadays, the future of ISFETs is compromised by the difficulty of miniaturizing the necessary external reference electrode. Another technical problem is the instability associated to the interface between the membrane and the transducer electronics due to the conversion of the ionic current to an electronic one.

Dekker et al[2] successfully integrated a carbon nanotube (CNT) as the semiconductor element into a field effect transistor in 1998. As CNTs are very sensitive to minimal variations in their chemical environment their usefulness in sensing devices is enormous. One of their drawbacks, however, is that they have to be effectively isolated from interferences to be selective enough and even specific to the target analyte. In the last years, sensors based on carbon nanotube field effect transistors (CNTFETs) have appeared.[3-5] All of these sensors link the sensory layer to the CNT transducer by means of either weak forces or covalent bonds. In this way, different kinds of analytes can be detected, but they are all medium-large. The selectivity is achieved by covering CNTs, covalently or noncovalently, with molecules that have a specific molecular recognition receptor and introducing blocking reagents to prevent non specific binding.

In the present communication we report the development of a CNT based ISFET selective to potassium. We cover the carbon nanotubes with a membrane containing valinomycin in a matrix of polyvinylchloride (PVC). This membrane has already been demonstrated to be effective in the ISFET technology.[6] With this device we are able to selectively detect concentrations of $10^{-7}$M of potassium in the presence of interferences that do not influence on the instrumental response.

The advantages of this CNTFET device are clear. On the one hand, we take advantage of the nanotubes so that the reference electrode does not have to be used, and the sensitivity of the system is good. This is an effective way of miniaturizing the ISFET technology. On the other hand, the ion selective membrane covering the CNTs operates as an isolation layer, which effectively shields the CNTs from the presence of the small charged ions or polar molecules in solution.

**References:**

[1] Bergveld, P., IEEE Trans. Biomed. Eng, **BME-19** (1970) 70.
[2] Tans, S.J., A.R. Verschueren, and C. Dekker, Nature, **393** (1998) 49.
[3] Besteman, K., J. Lee, F.G.M. Wiertz, H.A. Heering, and C. Dekker, Nano Lett., **3** (2003) 727.
[4] Li, J., Y. Lu, Q. Ye, M. Cinke, J. Han, and M. Meyyappan, Nano Lett., **3** (2003) 929.
[5] Kojima, A., C.K. Huon, T. Kamimura, M. Maeda, and K. Matsumoto, Jpn. J. Appl. Phys., **44** (2005) 1596–1598.
[6] Moss, S.D., J. Janata, and C.C. Johnson, Anal. Chem., **47** (1975) 2238.

# SUB-NANOMETER AU MPCs SYNTHESIZED BY MULTIPODAND CALIXARENE PROTECTION

*Flavio Ciesa, Arturo Arduini, Andrea Pochini, and Andrea Secchi*
*Dipartimento di Chimica Organica e Industriale, Università degli Studi, V. le G.P. Usberti 17/a, 43100 Parma, Italy.*
*flavio.ciesa@hotmail.it*

Monolayer-protected Au clusters[1] (MPCs) have aroused significant scientific interest because these structures are known to be useful in many fields such as optoelectronics, catalysis and molecular sensing.[2] MPCs of subnanometer core dimension are particularly enticing owing to their quantum size effects.[3] Indeed, it is known that as the core size decreases under the nanometer limit, the particles attain discrete electronic states and thus can show semiconductor-like electronic properties. The preparation of these compounds through direct methods has been, however, restricted to nanoparticles in which the gold passivation has been obtained with specific ligands such as tripeptides (glutathione), mercaptosuccinic acid and thiphenylphosphine derivatives.

Despite the large amount of data present in the literature on the synthesis of MPCs prepared with several thiol-based ligands, using the two phase method developed by Brust,[4] the role played by the ligand "sulphur denticity" on the gold clusters size has not been yet systematically studied.

In this context we have recently explored the possibility to use multidentate calix[n]arene derivatives **1** and **2** (see Figure 1), characterized by the presence of two and three convergent undecanthiol chains onto their lower rim, respectively, for the preparation of Au MPCs. The particular multidentate structure of the calixarene derivatives allows the preparation of rather monodispersed clusters as shown by TEM measurements (see Figure 2) and powder XRD analysis. In particular, when the calixarene is used in excess with respect the aurate salt $AuCl_4^-$, clusters having a core of subnanometer size were obtained. These results open new possibilities for the synthesis of MPCs with controlled and reduced size to be employed in the emerging field of the nanotechnology.

**References:**

[1] Love, J. C.; Estroff, L. A.; Kriebel, J. K.; Nuzzo, R. G.; Whiteside, G. M. *Chem. Rev*. **2005**, *105*, 1103-1169.

[2] *Nanoparticles: From Theory to Application*; Schmid, G. Ed.; Wiley-VCH:Weinheim, **2004**.

[3] Volokitin, Y.; Sinzig, J.; de Jongh, L. J.; Schmid, G.; Vargaftik, M. N.; Moiseev, I. I. *Nature* **1996**, *384*, 621-622.

[4] Brust, M.; Fink, J.; Bethell, D.; Schiffrin, D. J.; Kiely, C. *J. Chem. Soc., Chem. Commun*. **1995**, 1665-1656.

**Figures:**
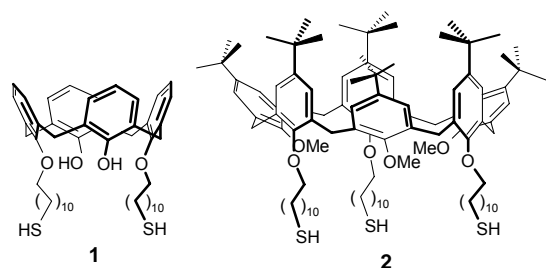


Figure 1. Polyalkylthiols lower rim functionalized calixarene derivatives for the preparation of Au MPCs.
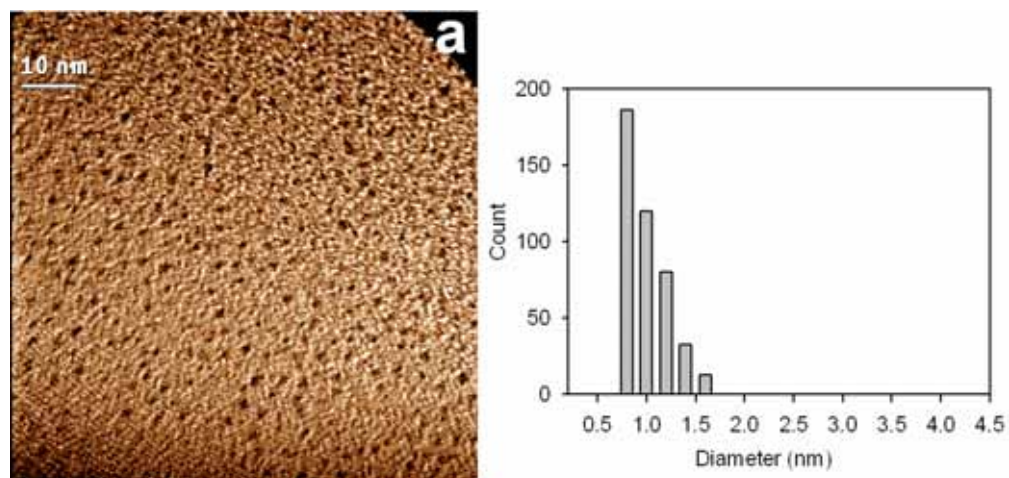


Figure 2. TEM image and core size distribution diagram of MPCs coated with calix[4]arene **1**.

# OPTICAL AND BIOLOGICAL CHARACTERIZATION OF SURFACE MODIFIED QUANTUM DOTS

*Samuel J Clarke* and Jay L Nadeau

*Department of Biomedical Engineering, McGill University, 3775 University Street, Montreal, Canada*

*samuel.clarke@mail.mcgill.ca*

Quantum dots (QDs) are gaining in popularity as fluorescent probes in the life sciences. Their popularity can be attributed to the unique optical properties of these colloidal nanoparticles (NPs). In most biological applications, the surface of QDs are modified with a small molecule, protein or antibody in order to lend specificity towards a biological target. The chemical, optical and biological properties of QDs can be drastically influenced by modification of their surface properties. In fact, this apparent drawback has been recently exploited for use in a broad range of sensing applications [1]. In our own work, we have shown that modification to the QDs with the small molecule dopamine (DA) can serve as an intracellular redox indicator [2].

In order to understand the effects of chemically modifying the surface of QDs. We have chosen the QD-DA construct as a model to investigate the optical and biological properties of QDs that have various levels of DA loading on the surface of the particles. To this end, we have developed and assay that can be used to asses the amount of dopamine that binds to the surface of the particles during the coupling reaction [3].

When DA is bound to the surface of CdSe/ZnS QDs, it quenches the fluorescent emission of the particles in a predictable manner. Figure 1 shows the quenching of the QD emission over a range of DA loading from zero to near saturation. Quenching is linear in this range and this is consistent with the notion that the quenching is due to a single molecular species. We have shown that the quenching of QD emission can be exploited for sensing applications. In the case of QD-DA, the probe is sensitive to oxidation by chemical and photo-related processes. The effect of oxidation is unquenching (restoration) of the QD emission. Our results also show that the kinetics of the QD unquenching by photo-oxidation are dependant on the level of DA loading [4].

The biological activity of QDs as a function of DA loading were investigated. The preliminary experiments suggest that the interactions of these bioprobes with cell lines expressing the D2 DA receptors are quite complicated in nature. First of all, there is a minimum level of DA loading that is required for visible association of QD-DA to cells. This requirement suggests that the bulk of the QD in comparison to DA may contribute to some steric hinderance and therefore restrict the activity of DA at its receptor on the cell surface. Another possibility is that with high DA loading, closely spaced DA ligands may be participating in multivalent interactions with the surface receptors. Qualitative information is hard to extract from fluorescence microscopy data as these results are skewed by various degrees of quenching and unquenching. We have designed a series of experiments that will reveal quantitative information on these interactions in a hope to elucidate the nature of the binding interactions of these probes with the surface receptors.

In summary, we have investigated the properties of QDs modified with a small molecule. The level of loading on the surface of the particles is an important parameter that modulates the optical and biological properties of the probes. These results are generalizable and valid for most NP based bioprobes.

**References:**

1.      Medintz, I.L., et al., *Quantum dot bioconjugates for imaging, labelling and sensing.* Nat Mater, 2005. **4**(6): p. 435-46.

2.      Clarke, S.J., et al., *Photophysics of dopamine-modified quantumdots and effects on biological systems.* Nature Materials, 2006. **5**(5): p. 409-417.

3.      Clarke, S.J., et al., *Effect of ligand density on the spectral and affinity characteristics of quantum dot conjugates.* Submitted, 2007.

4.      Khatchadourian, R., et al., *Fluorescence intensity and intermittency as tools for tracking bioconjugate processing in living cells.* Submitted, 2007.

**Figures:**
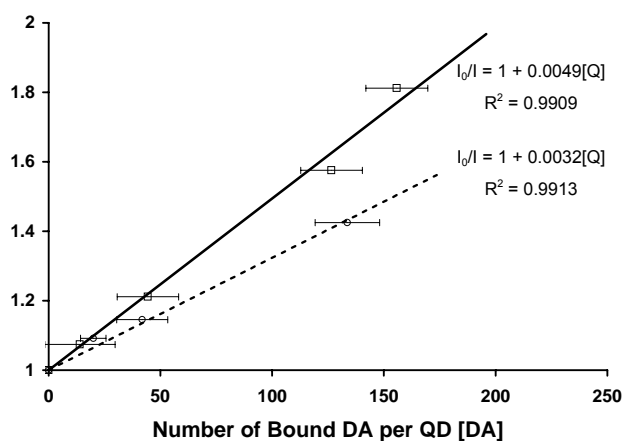


**Figure 1 - Relationship between the number of DA particles bound to the surface of the QD and the resulting emission quenching.  For both green QDs (dashed line, cross marker) and red QDs (black line, square marker) the relationship can be fitted to the linear equations depicted on the graph.**
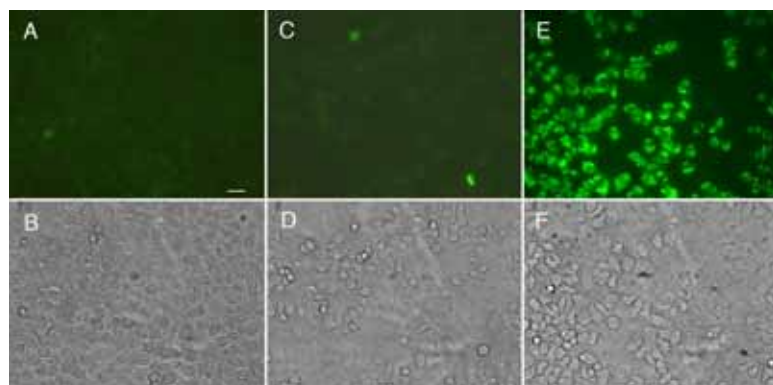


**Figure 2 - Incubation of green QD-DA with PC12 cells confirmed to have the D2 DA receptor.  Cells were incubated with 2nM QD-DA for 30 minutes and washed extensively in PBS. Scale bar = 20 μm and applies to all panels. (A,B).  QDs without DA do not associate with cells.  (C,D)  QD-DA with ca. 50 DA ligands has little specificity for cells. (E,F)  With ca. 100 DA ligands, QD-DA had a high specificity for the surface D2 DA receptors.**

# CARBON NANOTUBE BASED INTERCONNECTS

*Jean-Christophe Coiffic[1], H. Le Poche[2], M. Fayolle[1], S. Maîtrejean[1], G.Passemard[1]*
*[1]CEA LETI D2NT/LBE 17, av. des Martyrs 38054 GRENOBLE Cedex9 France*
*[2]CEA LITEN  DTNM/LCH 17, avenue des Martyrs 38054 GRENOBLE Cedex9 France*
*+33438785311*
*jean-christophe.coiffic@cea.fr*

Achieving always faster and smaller devices implies new challenges. The whole wiring scheme (fig.a) used to interconnect different transistors in chips is highly sensitive to scale reduction and, in the following decade years, the microelectronic industries will be faced with insurmountable issues [1]. Indeed interconnect RC delay, crosstalk and power consumption increase. Moreover current densities and heat dissipation are becoming critical points which largely affect interconnections reliability. A solution could be the use of carbon nanotube (CNT) [2-3] instead of traditional copper vertical interconnects called vias. Our work is focused on integrating CNT as metallic wires for ULSI on 200mm diameter wafers with standard microelectronic industry requirements. Main issues are thermal budget limitation and selective CNT growth in the bottom of high aspect ratio vias holes on copper line.

For this study, a new highly conductive diffusion barrier between copper and catalyst has been developed. After catalyst localization, a low thermal CVD (520°C) method is then employed to grow multiwall nanotubes. The process has been engineered to grow nanotubes on 300 cm2 substrates in a single run, showing the industrial scalability of such parallel method. Via holes down to 140nm wide have been realized. CNTs grown are multiwalls and a high density of $5.10^{10}$ CNT/cm2 per via is obtained (fig.c). After depositing and patterning AuPd contacts, electrical measurements are performed. First measurements (fig.d) on 300nm wide CNTs vias show ohmic behaviour at low voltage (<2V) with low resistance of 80Ω. By increasing voltage, current follows a power law. Interestingly, resistance decreases as voltage increases. This behaviour could be the result of inner shell transport enhancement.

**References:**

[1] International technology roadmap for semiconductors http://public.itrs.net/
[2] F. Kreupl, IEDM Tech. Dig., pp. 683 - 686, December 2004
[3] M. Nihei, M. Horibe, Japan, IITC 2006

**Figures:**
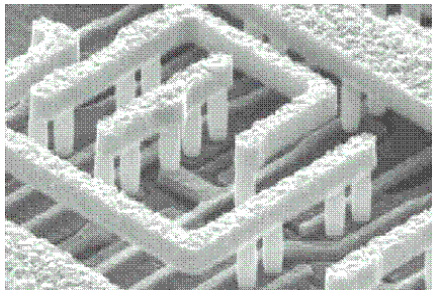


Fig.a:  Copper interconnections (lines [horizontal] and vias [vertical]) in a chip after removing the dielectric filling.
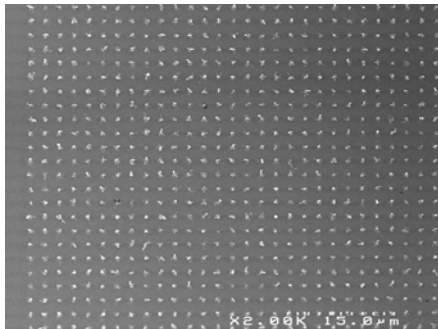


Fig.b: SEM view of an array of CNTs filled vias (top view)
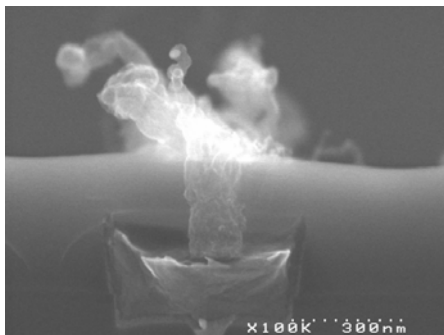


Fig.c: SEM cross section of a 140nm wide via on a copper line. Surrounding dielectric is silicon dioxide. Nanotube density is $5.10^{10}$ CNT/cm$^2$ per via.
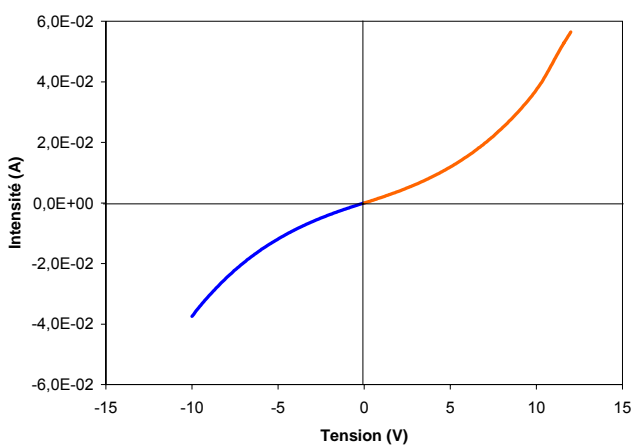


Fig.d: Electrical characteristic of a 300nm wide via. Low voltage show ohmic behaviour and for a higher voltage current follows a power law.

# MECHANICAL PROPERTIES OF ORDERED SINGLE WALLED CARBON NANOTUBE NETWORKS

*Vitor R. Coluci[1], N.M. Pugno[2], S.O. Dantas[3], D.S. Galvão[1], and A. Jorio[4]*
*[1]Universidade Estadual de Campinas,13083-970 Campinas-SP, Brazil*
*[2]Department of Structural Engineering, Politecnico di Torino, 10129 Torino, Italy*
*[3]Universidade Federal de Juiz de Fora, 36036-330 Juiz de for a-MG, Brazil*
*[4]Universidade Federal de Minas Gerais, 30123-970 Belo Horizonte-MG, Brazil*
*coluci@ifi.unicamp.br*

Many attempts have been made in order to develop procedures to controllably assemble large number of single walled carbon nanotubes (SWCNTs) in terms of position and orientation [1-4]. The achievement of such procedures would allow the fabrication of ordered SWCNT networks representing a breakthrough in the "bottom-up" manufacturing approach. These ordered networks would open possibilities to design new materials with desirable electronic and mechanical properties.

We present here results of classical molecular dynamics simulations of the mechanical response of carbon nanotube networks (CNNs) under different types of mechanical tests. The interactions between carbon atoms were described by the adaptive intermolecular reactive empirical bond-order potential [5]. The CNNs were constructed connecting SWCNTs through Y- or X-like junctions yielding to hexagonal and crossbar networks, respectively. Figure 1(a) shows an example of a crossbar CNN. Our results showed that CNNs exhibit very high flexibility dependent on the network architectures, showing elasticity modulus ~10-100 GPa and bulk modulus ~10 GPa. Due to the network topology involving SWCNTs and junctions, different response mechanisms under normal deformation for suspended networks are expected. They are associated with the carbon nanotube stretching and nanotube-junction-nanotube angle bending which differently contribute depending on the degree of deformation of the network. The symmetry presented by the junctions that constitute the network and the network disorder are important aspects on the resulting mechanical properties [6].

Using the same heuristic method for generating SWCNTs from a graphene layer, CNNs can be rolled up to form CNNs with a tubular geometry. The resulting structures, the so-called 'super' carbon nanotubes (STs) [7], which are carbon nanotubes made of SWCNTs. Similarly to a $(n,m)$ SWCNT, $[N,M]$ ST with different chiralities can be constructed. The STs are represented as $[N,M]@(n,m)$ and characterized by: the $(n,m)$ SWCNT used to form them; the necessary junctions to weld consecutive SWCNTs; and the distance between these junctions. Figure 1(b) shows an example of a ST.

From tensile tests of impact loads, we have found that STs are more flexible than the SWCNT used to form them but in some cases they show comparable tensile strengths (Figure 1(c)). The ST Young's modulus have been predicted to have an inverse dependence on the ST radius. During tensile deformations the shape and aperture of pores in ST sidewalls can be modified providing a way to vary the accessible channels to the inner parts of STs through the application of mechanical loads. The ST rupture occurs basically at regions near the SWCNT junctions and it is influenced by the ST chirality. Based on the predicted geometrical and mechanical properties, STs may represent hypothetical candidates for novel porous, flexible, and high-strength materials.

**References:**

[1] Diehl M R, Yaliraki S N, Beckman R A, Barahoma M, Heath J R, **114** Angew. Chem. (2002) 363.

[2] Derycke V, Martel R, Radosavljevic M, Ross F M, Avouris P, **2** Nano Lett.(2002) 1043.

[3] Ago H, Nakamura K, Ikeda K, Uehara N, Ishigami N, Tsuji M, **408** Chem. Phys. Lett. (2005) 433.

[4] Ismach A, Joselevich E, **6** Nano Lett. (2006) 1706.

[5]Stuart S J, Tutein A B, Harrison J A, **112** J. Chem. Phys. (2000) 6472.

[6]Coluci V R,Dantas S O, Jorio A, Galvão D S, **75** Phys. Rev. B (2007) 075417.

[7]Coluci V R, Galvão D S, Jorio A, **17** Nanotechnology (2006) 617.

**Figures:**
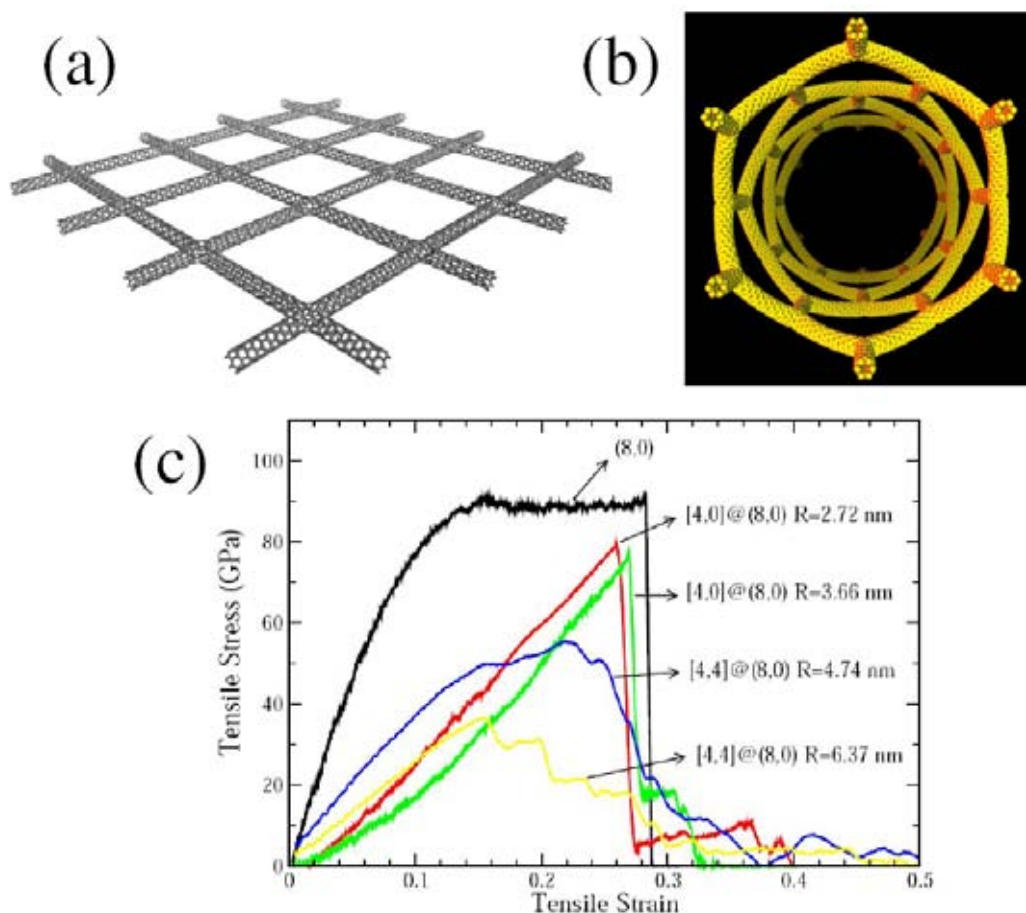


**Figure 1: (a) Crossbar ordered single walled carbon nanotube network. (b) Configuration of a [6,0]@(6,0) super carbon nanotube. (c) Tensile failure behavior for super carbon nanotubes with different chiralities and radii (R) and for the (8,0) SWCNT at 300 K.**

# ENGINEERING ELECTRON BANDS IN DISLOCATION NETWORKS

*J. CORDÓN [1], F. SCHILLER [1], M. CORSO [2], and J. E. ORTEGA [1,2,3]*
*[1]Dpto. Física Aplicada, Universidad del País Vasco, Plaza Oñate 2, San Sebastián, Spain*
*[2]DlPC, Manuel Lardizaba14, E-20018 San Sebastián, Spain*
*[3]Unidad Física de Materiales, CSIC, Manuel Lardizaba13, E-20018 San Sebastián, Spain*

*cordon@ehu.esl*

Dislocation networks are frequently observed during the heteroepitaxy of materials with different lattice constant. They appear as a way of relaxing close-packed surface layers around energetically-unfavourable on-top positions. Surface dislocation networks become attractive as self-assembled lateral nanostructures with a periodic modulation of the surface potential in the nanometre scale. In particular, in noble metal surfaces and overlayers, which possess free-electron-like surface states that may scatter at the network potential. In fact, electron scattering and superlattice bands have been already probed in herring-bone like patterns in stepped Au(111) [l] and Ag monolayers on Cu(111) [2]. Noble metals are also attractive since Fermi wavelengths ($\lambda_F$) and network periodicities (p) have the same dimensions, and hence electronic/structural instabilities may arise around "nesting" ($\lambda_F = 2 \times p$). In order to study this issue, we explore the ability of further tuning surface bands at noble metal dislocation networks. This can be done by forcing electron bands, e.g. by external doping, or by smoothly varying the lattice constant.

Angular Photoemission experiments have been performed at beam line 7 at the SLS synchrotron in Berkeley and at PGM beam line at the SRC synchrotron in Stoughton (Wisconsin). Both are equipped with high energy and angular resolution, display-type Scienta analyzers. In Ag/Cu(111) we track the surface band transformation from the Moiré pattern at low temperature to the triangular dislocation network at 300 K. The same Ag/Cu(111) system has been also doped with K, leading to a rigid band structure shift. The Au/Ni(111) system offers the possibility of smoothly tuning the superlattice constant by varying the Au coverage. In such case we find the surface state band rather complex, namely it appears split in Au-like and Ni-like features that evolve with the amount of deposited Au

**References:**

[l] C. Didiot, Y. Fagot-Revurat, S. Pons, B. Kierren, C. Chatelain, and D. Malterre, Phys. Rev. B **74**, 081404 (2006).

[2] F. Schiller, 1. Cordón, D. Vyalikh, A. Rubio, and 1. E. Ortega, Phys. Rev. Lett. **94**, 016103 (2005).

# QUANTUM-SIZE AND FINITE-SIZE EFFECTS IN THE ELECTRICAL TRANSPORT PROPERTIES OF SINGLE BISMUTH NANOWIRES

*T.W. Cornelius[1], M.E. Toimil-Molares[1], S. Karim[2], O. Picht[1], R. Neumann[1]*
*[1]Gesellschaft für Schwerionenforschung, Planckstr. 1, 64291 Darmstadt, Germany*
*[2]Fachbereich Chemie, Marburg University, Hans-Meerwein-Str., 35032 Marburg, Germany*
*th.cornelius@gsi.de*

In recent years, bismuth nanowires were intensively studied both because of their unique electronic properties and possible future application in thermoelectric devices. When the size of an object becomes comparable to the electron mean free path $l_e$ and Fermi wavelength $\lambda_F$, finite-size and quantum-size effects are expected, respectively [1]. Since these parameters are large in bismuth ($l_e \sim 100$ nm and $\lambda_F \sim 40$ nm at room temperature), such effects are anticipated for wires of comparatively large diameter, making bismuth an ideal material for studies on the nanoscale. Finite-size effects include additional electron scattering from inner grain boundaries and from the wire surface for which Mayadas et. al [2] and Dingle [3] developed a model, respectively. Quantum-size effects lead to a subband splitting which involves a diameter dependent oscillation of both charge carrier density and mobility. Consequently, the transport properties are modulated as a function of the wire diameter [4].

Single bismuth nanowires with diameters ranging from 70 nm to 1 µm were grown electrochemically in ion track-etched polycarbonate membranes [5]. The crystallinity was controlled by the fabrication conditions, in particular the choice of overpotential and temperature. The depositions were continued until caps were formed on top of the wires. In order to contact the wires electrically, while they were left embedded in the template, the cap was coated by an additional gold layer.

The specific electrical resistivity was found to be strongly influenced by the mean grain size $D$ and increases with decreasing $D$ which is attributed to additional electron scattering from grain boundaries. For wires with diameters $d < 150$ nm the resistivity rises with diminishing $d$ being assigned to additional scattering from the surface (Fig. 1). Further, a non-monotonic resistance versus temperature behaviour was found. While the carrier mobility for bulk Bi increases by three to four orders of magnitude when cooling down from room temperature to 4 K, it saturates at a few ten Kelvin for nanowires because of finite-size effects [6] (Fig. 2). The saturation value diminishes with decreasing $D$. For the first time, the specific electrical conductivity shows evidence for oscillations as a function of $d$ which can be attributed to quantum size effects.

**References:**

[1] V.B. Sandormirskii, Sov. Phys. JETP **25** (1967) 101.

[2] A.F. Mayadas, M. Shatzkes, Phys. Rev. B **1** (1970) 1382

[3] R.B. Dingle, Proc. R. Soc. London A **201** (1950) 545

[4] S. Farhangfar, Phys. Rev. B **74** (2006) 205318.

[5] T.W. Cornelius, J. Brötz, N. Chtanko, D. Dobrev, G. Miehe, R. Neumann, M.E. Toimil-Molares, Nanotechnology **16** (2005) S246.

[6] T.W. Cornelius, M.E. Toimil-Molares, R. Neumann, S. Karim, J. Appl. Phys. **100** (2006) 114307.

**Figures:**
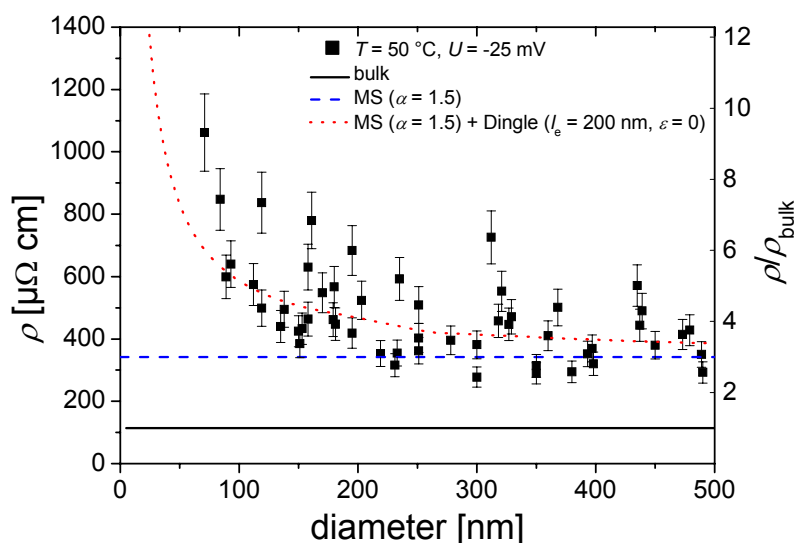


Fig. 1: Specific electrical resistivity of single bismuth nanowires. The solid line represents the specific electrical resistivity of bulk Bi. The dashed line considers electron scattering from grain boundaries, while the dotted curve takes into account also completely diffuse scattering from the wire surface.
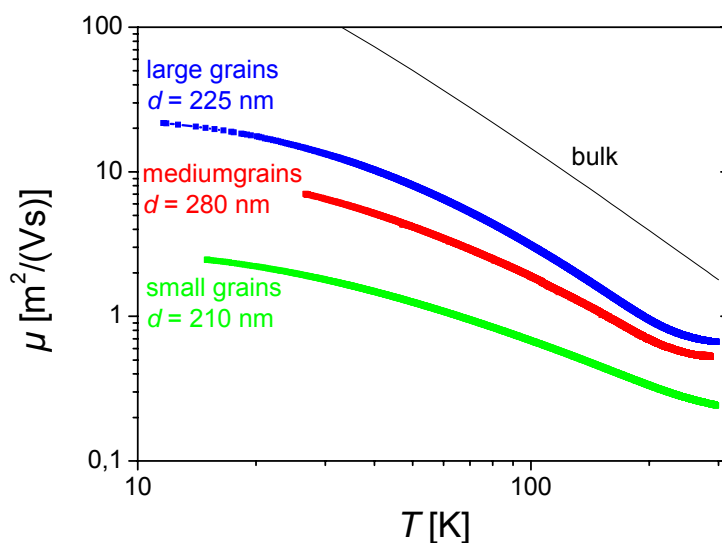


Fig. 2: Mobility of charge carriers for single bismuth nanowires as a function of temperature and mean grain size.

# MODIFICATION OF THE Ag/Cu(111) DISLOCATION NETWORK BY DOPING

<u>Martina Corso</u>[1], Frederik Schiller[2], Javier Cordon[3], and Enrique Ortega[1,2,3]
*[1]DIPC, Manuel Lardizabal 4, E-20018 San Sebastián, Spain*
*[2]Unidad de Física de Materiales, CSIC, Manuel Lardizabal 3, E-20018 San Sebastián, Spain*
*[3]Dpto. de Física Aplicada, Universidad del País Vasco, Plaza Oñate 2, E-20018 San Sebastián, Spain*

martina_corso@ehu.es

At low temperatures a single Ag layer on a Cu(111) surface forms an unstrained hexagonal Moirè structure where several Ag atoms occupy energetically unfavourable on-top positions [1]. At room temperature the Ag overlayer relaxes by the formation of misfit dislocation loops on the Cu substrate leading to a well ordered network of triangles at the surface. When the system is doped with submonolayer amount of K a rigid band structure shift is observed by angle resolved photoemission (ARPES). If Au is used instead, STM images reveal that the periodicity of the triangular array varies: it gets larger with the increase of the Au coverage.

Different aspects of the K- or Au-modified Ag/Cu(111) misfit dislocation network are investigated with STM and ARPES.

**References**
1.  F. Besenbacher, L. Pleth Nielsen, and P. T. Sprunger, in *Chemical Physics of Solid Surfaces and Heterogeneous Catalysis*, edited by D.A. King and D. P. Woodruff (Elsevier Science, Amsterdam, 1997), Vol. 8, Chap. 10.

# Spatial correlations of self-assembled nanostructures using a squared lattice InP/InGaP template

*J.R.R.Bortoleto [1,a], J.G.Zelcovit[1], H.R.Gutiérrez[3], J.Bettini[2] and <u>M.A.Cotta</u>[1]*
*[1]Instituto de Física Gleb Wataghin, UNICAMP, 13083-970, Campinas, SP, Brazil*
*[2]Laboratório Nacional de Luz Sincrotron,13084-971, Campinas, SP, Brazil*
*[3]Penn State University, Department of Physics, University Park, PA 16802, USA*
<u>monica@ifi.unicamp.br</u>T

Semiconductor nanostructures have shown properties that can be tailored during fabrication, making possible the engineering of quantum effects in finite low-dimensional systems. Such nanostructures can be synthesized by different techniques; one of the most common relies on strained heteroepitaxial growth. In this process, coherently strained islands are formed on the surface, presenting a continuous variation of the lattice parameter (from bottom to top) and making them energetically stable against the formation of a uniform (flat) strained film. Strain distribution is thus one of the significant factors that determine the shape, size and facet formation in these self-assembled semiconductor nanostructures.

We present here results on material systems where different structural characteristics were obtained by changing the InGaP buffer layer properties and creating a stress field to drive the nucleation of a first InP dot layer. Once buried, this two-dimensional array of InP dots was used as a template for the lateral ordering of both InAs and GaP dots in InAs/GaAs and GaP/GaAs bilayers, respectively. In both cases, a two-dimensional array very similar to the InP template buried underneath the bilayer was observed. Also, an increase in the dot dimensions – as compared to those grown on unstressed surfaces - occurred due to the buried strain field lateral period.  For the InAs in particular, clustering of small dots is observable, probably due to a finite size effect of the InP dots.

The correlation between the ordering of the top dot layer and the buried InP template was investigated by cross-section High Resolution Transmission Electron Microscopy (HRTEM) measurements. Our results show that the InAs dots are vertically correlated to the InP template, while the GaP dots are vertically anti-correlated, nucleating in the position between two InP dots. In this latter case, grazing incidence X-ray diffraction measurements have shown that the strain relaxation rate is not significantly altered with regard to the GaP dots grown on unstressed GaAs, although the strain at the base of the dots is lowered when the template is used. These results validate this approach as a new path to produce high quality III-V self-assembled pseudocrystals.

[a]Present address: Unidade Diferenciada Sorocaba/Iperó, GPM, UNESP, 18087-180 Sorocaba-SP, Brazil

**Figures:**
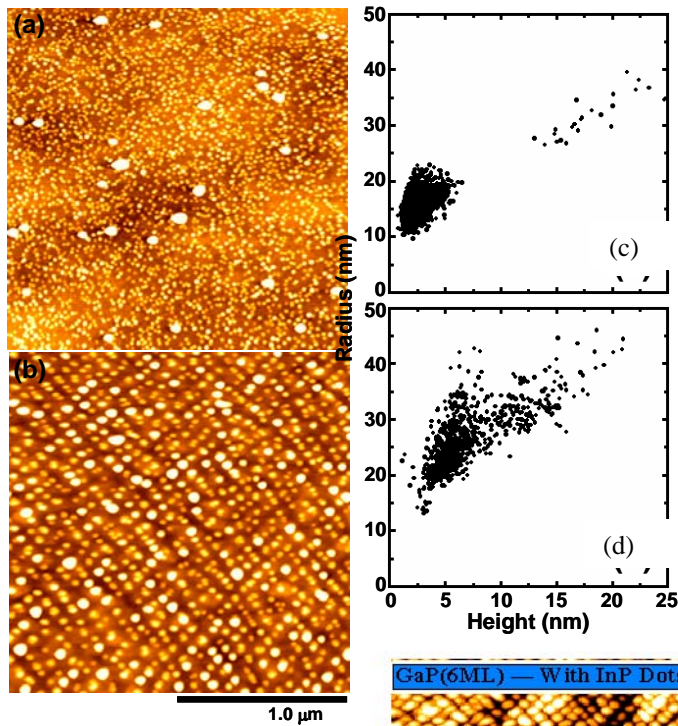


Fig.1 – AFM images and dot size distribution for InAs dots grown on (a,c) GaAs and (b,d) the InP template (GaAs/InP/InGaP/GaAs); (bottom) HRTEM image showing the vertical correlation between InAs and InP dots.
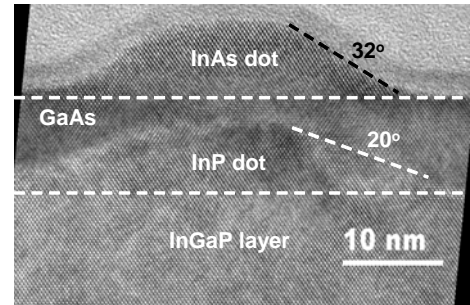
Fig.2 – (left) AFM image of the laterally ordered GaP dots, the inset shows the Fast Fouried Transform of the image; (right) HRTEM image showing the vertical anti-correlation of GaP and InP dots.
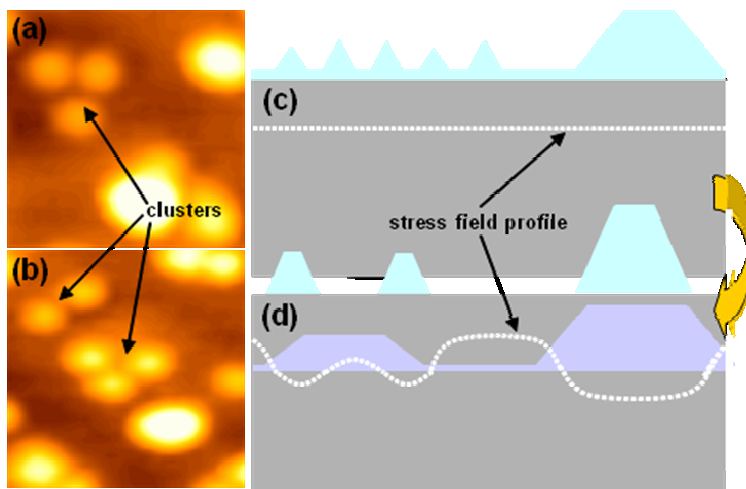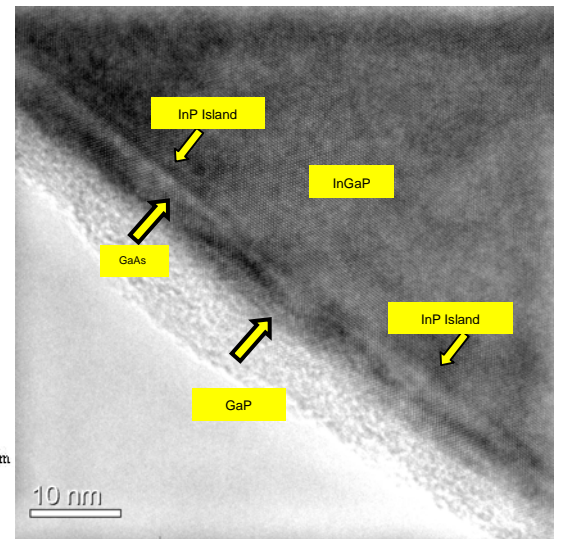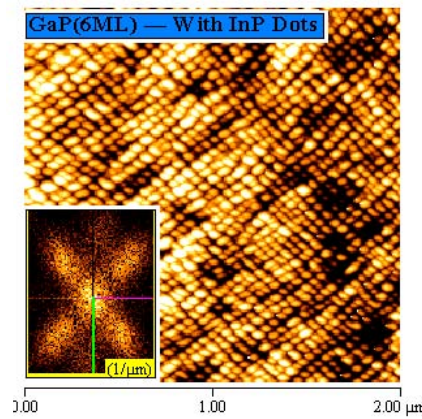


Figure 3- (a) and (b) typical clusters of 2 or 3 small InAs islands formed on top of one buried InP/InGaP dot; (c) schematic distribution of InAs when deposited on GaAs buffer without InP/InGaP template. Two ensembles of islands randomly distributed on top of the wetting layer are formed; (d) schematic distribution of InAs when deposited on GaAs with InP/InGaP template. The stress field on top GaAs due to InP/InGaP template induces the InAs island nucleation on top of buried InP dot in two different ways due to the height distribution of the buried InP dots. The wetting layer may be absent due to non-uniform strain field created by InP/InGaP template.

# BIREFRINGENT THIN FILMS OF NANOCRYSTALLINE CELLULOSE

*Emily D. Cranston, Derek G. Gray*
*McGill University, Montreal, Canada*
*emily.cranston@mail.mcgill.ca*

Electrostatic layer-by-layer self-assembled films of nanocrystalline cellulose and poly(allyl)amine hydrochloride (PAH) were prepared by spin-coating and conventional solution dipping. The nanocrystalline cellulose was obtained by acid hydrolysis of cellulose fibres resulting in a stable colloidal suspension of rod-shaped crystals (100-200 nm long by 5-10 nm wide)[1]. Surface characterization was performed by AFM, SEM, XPS and optical reflectometry. Complete surface coverage was achieved leading to smooth films that displayed high film stability under various conditions due to ionic crosslinking. Samples assembled by spin-coating were substantially thicker, leading to iridescent films after only a few deposition steps.[2] As a novel route to prepare ordered films, nanocrystalline cellulose and PAH were adsorbed from solution in a magnetic field.[3] Optical properties for the various film types were compared and birefringence was measured to determine the orientation of nanocrystalline cellulose in multilayered thin films. Surface order was quantified from AFM data with magnetically aligned films displaying the most order followed by radial order in spin-coated films. Surface forces near the films in water and salt solutions were measured by colloid-probe AFM as a function of film thickness, surface charge and cellulose nanocrystal orientation. These aqueous methods for film preparation present an alternative to iridescent coatings made by chemical vapour deposition, and the anisotropic nature of the system imparts a way to tailor optical properties in thin organic films.

## References:

1. Revol, J.F., et al., *Helicoidal self-ordering of cellulose microfibrils in aqueous suspension.* International Journal of Biological Macromolecules. **14**(1992): p. 170.

2. Cranston, E.D. and D.G. Gray, *Morphological and optical characterization of polyelectrolyte multilayers incorporating nanocrystalline cellulose.* Biomacromolecules. **7**(2006): p. 2522.

3. Cranston, E.D. and D.G. Gray, *Formation of cellulose-based electrostatic layer-by-layer films in a magnetic field.* Science and Technology of Advanced Materials. **7**(2006): p. 319.

## Figures:
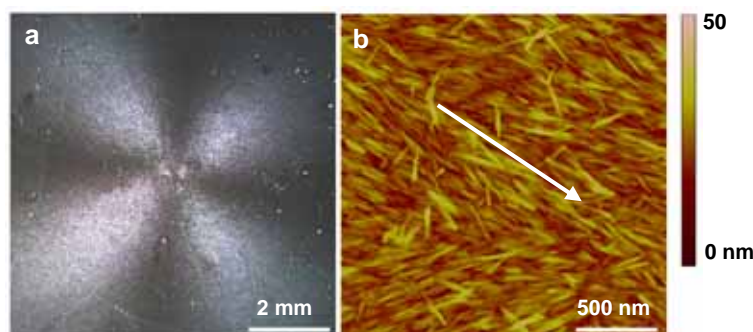


The orientation of cellulose nanocrystals can be seen on many length scales. a) Polarized-light microscopy image of LbL films of (PAH/cellulose)$_{10}$ b) tapping mode AFM height image of the same film.

# THE SELF-ASSEMBLY OF CADMIUM TELLURIDE NANOWIRES FROM NANOPARTICLES

Kevin Critchley, Stephen D. Evans, Nicholas .A. Kotov

1 Department of Chemical Engineering, University of Michigan, Ann Arbor, Michigan 48109. USA.
2 School of Physics and Astronomy, University of Leeds, Leeds LS2 9JT. United Kingdom.

We consider the use of nanoparticles and nanowires as potential building blocks for the fabrication of novel nanoscale devices and components. We focus our attention on semiconducting materials due to their current use in electronic and optoelectronic devices, such as solar cells, light emitting diodes, and lasers.[1] Cadmium Telluride is a direct band-gap II-IV compound semiconductor that has recently received a rise in interest within the scientific community. Direct band-gap semiconducting nanowires are particularly interesting because they can be used for the generation, wave-guiding, and detection of light on the nanoscale.

In this study, a wet chemical synthesis is used to produce highly luminescent thiol stabilized CdTe quantum dots. The band-gap of the quantum dots can be controlled during the synthesis to select the emission of the quantum dots to be between green and red. The fact that the emission falls in the visible range makes them desirable for optoelectronic devices. Interestingly, if the amount of stabilizer and the pH of the nanoparticle solution are controlled, the CdTe nanoparticles can self-assemble into 1D structures up to several microns in length.[2,3] By varying the conditions during the synthesis one can also produce CdTe nanoribbons. The aim of this study is to electronically characterize single nanowires using a multiprobe scanning tunneling microscope.

1. Agarwal R., Lieber C.M., Applied Physics A **2006**, 85, 209
2. Tang Z., Kotov N.A., Giersig M. *Science* **2002**, 297, 237
3. Wang Y., Tang Z., Tan S., Kotov N.A. *Nano Letters* **2005**, 5, 243

# High performance organic light emitting transistor based on hexylstyryl tetracene

A.Dadvand,[a,b] F.Cicoira,[a] C.Santato,[b] C.Harnagea,[a] A.Pignolet,[a] H.Meng,[c] F.Rosei,[a] D.F.Perepichka,[b]

[a] INRS-EMT, University of Quebec,
[b] Department of Chemistry, McGill University
[c] DuPont Experimental Station

Up-growing interest in organic semiconducting materials results from their successful application in optoelectronic devices such as Organic Field Effect Transistors (OFET), Organic Light Emitting Diodes (OLED), and Photovoltaic (PV) cells. The unlimited choice of organic materials provides unique possibilities to develop integrated circuit technologies based on OFETs for various large areas, low-cost applications. A large variety of organic semiconductors and modification of their molecular and morphological structure make it possible to build transistors for different type of applications. We fabricated high performance transistors employing well-known organic semiconductors (OSCs) such as pentacene as well as newly synthesized OSCs.

Organic light emitting transistors (OLETs) are a new type of devices leading towards nano-scale light sources and highly integrated optoelectronic devices. This structure is ideal to improve the electroluminescence quantum efficiency and lifetime of OSCs due to the different driving conditions comparing to OLEDs. We used a new synthesized tetracene derivative, [2-(4-hexylstyryl) tetracene] (HST), as an active layer to fabricate OLETs. HST is a conjugated trans-phenylvinylene substitutes linked to tetracene core. For HST vacuum sublimated films, we carried out optoelectronic characterizations in field effect transistor configuration and also AFM measurements of films grown at different deposition fluxes and with variable thickness. The HST film grows in circular shape and almost covers the whole substrate with relatively large grains comparing to pentacene. Continuous films with large grains are formed at low nominal thickness, which is important for OFET applications since charge transport occurs within the first monolayer.

References:
[1] C. T. Kuo, S. Z. Weng, Adv. Tech., 13, 753–758 (2002)

[2] Hepp, A. et al. Phys. Rev. Lett., 91, 157406 (2003)

[3] Rost, C. et al. Appl. Phys. Lett., 85, 1613–1615 (2004)

[4] Bader, M. A. et al. J. Opt. Soc. Am. B 19, 2250–2262 (2002)

[5] E. J. Meije et al. Nature Materials, 2, 678–682 (2003)

[6] Michele Muccini, Nature Materials, 5, 605-613 (2006)

[7] A. Hepp et al. Phys. Rev. Lett., 91, 157406 (2003)
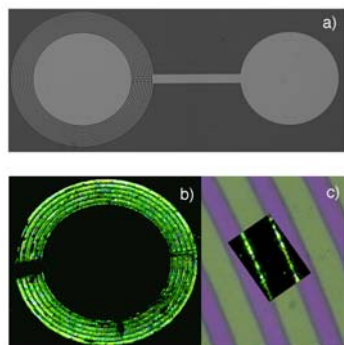
Optical images of: a) Interdigitated bottom-contact device b) Green electroluminescence of HST-LEFT c) magnified contacts and localized light emission



AFM images and corresponding height histograms of HST films vacuum sublimed at 0.2 A°/s.



Electroluminescence spectrum (blue) of a HST-LET biased at Vds = Vg = - 60 V and photoluminescence spectrum (red) of the same film
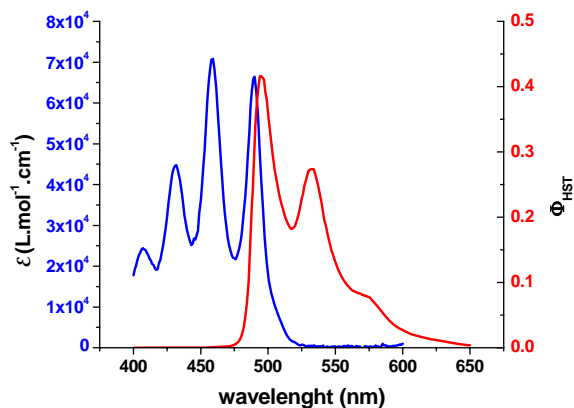


The extinction coefficient and normalized fluorescence spectrum versus wavelength of HST molecule dissolved in 98% dichlorobenzene.



**Optoelectronic characteristics of HST-OLET**

$V_G$= 0 V
$V_G$=-15 V
$V_G$=-30 V
$V_G$=-45 V
$V_G$=-60 V



$V_{DS}$= - 60 V
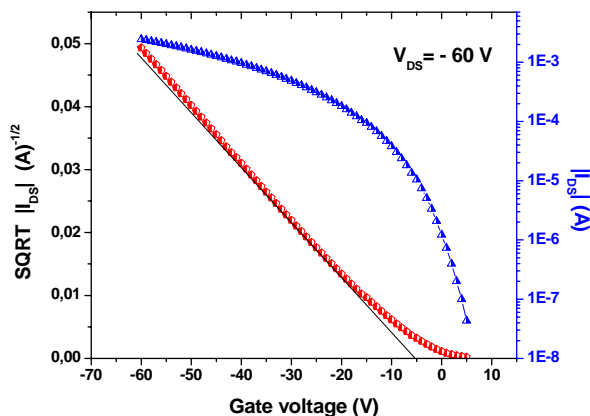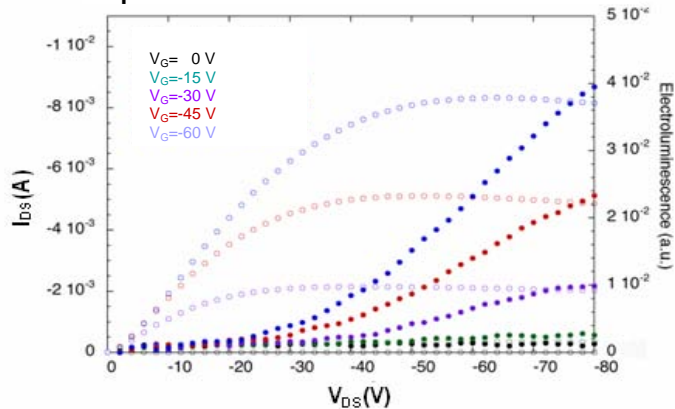
Transfer characteristics of a HST-OFET (deposition rate = 0.2 A°/s, nominal thickness = 18 nm, W/L=18800/40 µm/µm)

# Study of structures deposited by focused ion beam induced deposition on membrane

*Hervé Dallaporta*[1]*, Alan Reguer*[1]*, Frédéric Bedu*[1]*, D. Tonneau*[1]  *and A .Houël,  P. Sudraud*[2]

[1]CRMC-N-CNRS 163 Avenue de Luminy case 901 13288 Marseille Cedex 9 France,

[2]Orsay Physics, 95 Avenue des Monts Auréliens - ZA Saint-Charles - F - 13710 Fuveau

*dallaporta@crmcn.univ-mrs.fr*

## 1 – Introduction

We will show that using the local decomposition of molecules induced by focused ion beam (FIBID), it is possible to constructed nanostructures on very thin membranes. The interest of using very thin membranes is that it allows the study by transmission electronic microscopy. We have tried different membranes on which we are able to deposit an electrical circuit and follow the modification of deposited FIBID wire when a high current density flows through it. The behavior of FIBID nanowires in tungsten and platinum will be compared. We will show that on such membranes new phenomena can take place: for tungsten nanowire connected to gold pad the high current density can induced migration of gold around the nanowire.

## 2 – Experimental setup:

II.1. Nanofabrication station

The experimental setup is a cross-beam system coupling a JSM 5910 Scanning Electron Microscope (SEM, JEOL) and a Canion 31+ Focused Ion Beam (FIB, Orsay Physics), equipped with a gas injection system (GIS, Orsay Physics). The two beams are focused on the same point of the sample. This allows real time simultaneous FIB machining and non-destructive non-contaminating SEM imaging. The FIB column operates at an accelerating voltage of Ga+ ions ranging from 10 to 30 kV with a minimal Gaussian beam diameter around 7 nm. The beam current can be varied from 1 pA for the lowest current to few nA. The precursor vapor is delivered via a Gas Injection System composed of 5 heated reservoirs coupled to the injection lines driven by a 3-axis microstage. The system is equipped with an in situ electrical measurement allowing the deposition between pads

II.2. Supports

We have designed two type of supports for this study. The first one is composed of a thin aluminium foil (width:10μm) stuck on a ceramic disc. The foil is cut by laser ablation creating two macroscopic electrodes separated by a 10 μm wide groove. A FIBID carbon membrane is deposited between the two aluminium electrodes. Then a FIBID nanowire can bridge the electrodes. The other support consists of a silicon nitride membrane window specifically designed for TEM. This support consists of a 2.65 mm x 2.65 mm, 200 μm thick silicon frame which contains a single 0.5 mm x 0.5 mm silicon nitride membrane (thickness 50nm). Thermally evaporated Au was deposited, through a mask, onto the surface as electrodes. We obtained four electrical contacts separated by 30 μm. Like for the former support we can bridge the electrodes by a FIBID nanowire.

## 3 – Results

Both tungsten and platinum nanowires has been treated by applying a slow ramp voltage to the electrodes from 0 to 2,5V. The resistance of the tungsten nanowire drops by a factor 25 after this electrical treatment while for platinum the resistance increases. SEM image of treated nanowire shows that for W the gallium incorporated during the deposition process is rejected outside the wire forming one gallium droplet, for platinum we observed the formation of droplets along the wire. From the transmission electron microscopy studies the as deposited FIBID nanowires are always amorphous while on treated nanowires we obtained diffraction pattern and resolved high resolution images. The treated W nanowire is mostly a bcc crystalline structure of tungsten mixed with tungsten carbide structure. The treated Pt nanowire is formed by platinum crystalline clusters with droplets of $PtGa_2$.

# The First Willgerodt-Kindler Reaction on Functionalized Single-Walled Carbon Nanotubes

*Hossein Reza Darabi,* Shabnam Mohandessi, Farshid Mohsenzadeh, Kioumars Aghapoor

Nano & Organic synthesis Lab, Chemistry & Chemical Engineering Research Center of Iran (CCERCI), Tehran, 14335-186, Iran
*darabi@ccerci.ac.ir*

Because of the exceptional electronic and mechanical properties, single-walled carbon nanotubes (SWNTs) have attracted the interest of academic and industrial researches worldwide. However, several technical challenges need to be overcome before the extraordinary properties of these unique materials can be fully utilized. One of the approaches that have opened a large number of research opportunities and potential applications is chemical functionalization. The chemical functionalization has involved the formation of both covalent bonds and noncovalant interactions.

The three-component *Willgerodt-Kindler* (*WK*) reaction is well known as an important method for the synthesis of thioamides. In the original reaction, an aryl alkyl ketone or aryl aldehyde can be reacted with sulfur and a primary or secondary amine, and the product is the terminal thioamide. The importance of thioamides and their widespread applications as versatile intermediates in medicine and organic synthesis have enlarged the synthesis utility of the *WK* reaction.

In embracing the reaction principles and considering the important role of thioamide in medicine and in continuation of our investigation on this reaction, we report a generally new approach to the preparation of thioamide functionalization of CNTs.
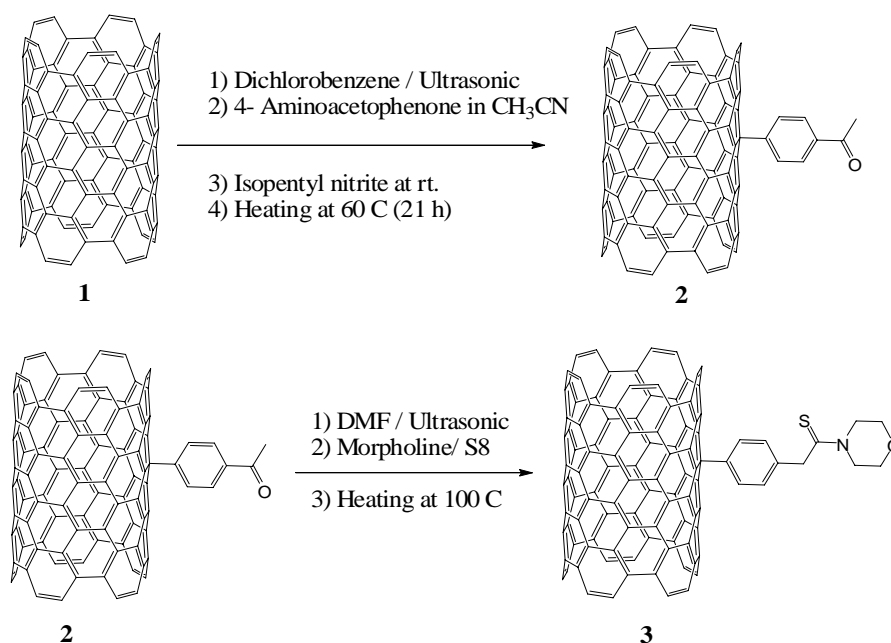


**Scheme 1.** Two steps reaction for the preparation of thioamide functionalized nanotube **3**.

In this contribution, we report a novel functionalization that follows the approach of the diazonium salts, employed 4-acethylaniline as the reagent to prepare **2** (see Scheme 1). The purpose of using 4-acethylaniline is to leave the functionalized nanotube with a carbonyl

group accessible for the WK reaction to obtain the thioamide functionalized nanotube **3**. The interesting finding in that the work-up of functionalized nanotube **3** is very simple, when compared to classical WK reaction.[1] It is due to lower solubility of functionalized nanotube than those of reactants and reagents.

The functionalized SWNTs were then characterized using spectroscopic and microscopic methods along with thermogravimetric analysis (TGA). A UV/vis/NIR absorption spectrum of the starting material displays the characteristic van Hove singularities.

A UV/vis/NIR absorption spectrum of the functionalized SWNTs shows the lack of the van Hove transitions, consistent with covalent functionalization of the SWNTs. TGA of the material (Ar, 10 °C/min to 800 °C) showed comparable weight loss.

Although it was not possible to judge by TEM if the functional groups were covalently attached to the tubes, the solubility of the material in organic solvents, the spectroscopic data and TGA, and the different form of the bundles are decisive arguments in support of the organic functionalization of the tubes.
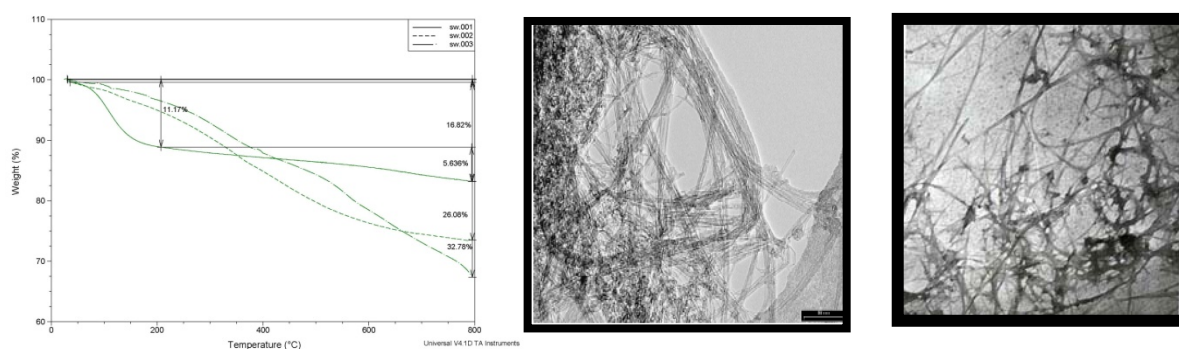


**Figure 1**. (left) TGA of **1 (___)**, **2(…)** and **3 (-.-)**, (middle) TEM image of **1**, (right) TEM image of **3**.

In conclusion, we have described a new, versatile, and powerful methodology for functionalization of carbon nanotubes, using WK reaction. The modified nanotubes are soluble in most organic solvents and even in ethanol. Given in novelty in the modified nanotubes, this result opens the way to a high number of opportunities, including the preparation of biosensors and drug delivery.

**References:**

[1] Nooshabadi M, Aghapoor K, Darabi HR, Mojtahedi, MM. *Tetrahedron Lett*. **1999**, *40*, 7549; Darabi HR, Aghapoor K, Tajbakhsh M *Tetrahedron Lett* **2004**, *45*, 4167; Darabi, HR, Aghapoor K, Nakhshab L. *Z. Naturforsch*. **2004**, *59b*, 601; Aghapoor K, Mohsenzadeh F, Khanalizadeh G, Darabi HR, *Monatschefte Chemie*, **2007**, 138, 61.

# CONTROL OF ENERGY BAND STRUCTURES OF SI QUANTUM DOT WITH AN INTRODUCTION OF GE CORE AS DETECTED BY AFM/KELVIN PROBE TECHNIQUE

*Yudi Darma[1], Seichi Miyazaki[2]*

[1]*Dept of Physics, Institut Teknologi Bandung, Ganesha 10 Bandung, Indonesia 40132*
[2]*Dept of Semiconductor Electronic and Integration Sciences, Hiroshima Univ., Kagamiyama 1-3-1, Higashi-Hiroshima Japan 739-8530.*
*yudi@fi.itb.ac.id*

Silicon (Si) quantum dot is a promising candidate for novel functional devices such as floating gate memory devices [1] and single electron transistor [2]. Recently, to modify the energy band structure in the dots, we have proposed the Si dots with Germanium(Ge) core [3] that enables us to take advantage of a narrow band gap of Ge rather than that of Si. Here we experimentally show the role of Ge core through the surface potential changes induced by electron charging and discharging at each of isolated Si quantum dot with and without Ge core using AFM/Kelvin probe force microscopy (KFM).

Si dot with and without Ge core have been prepared by controlling the early stages of low-pressure chemical vapor deposition (LPCVD) on 4.1nm-thick $SiO_2$ with p-type Si(100) as the substrates. After the Si dots formation, the dots surface were covered with ~2nm-thick $SiO_2$ grown by 900°C oxidation. Cross-sectional HR-TEM images of Si dot with and without Ge core are shown in Fig.1. To investigate the charging and discharging experiments, electron and hole injection to each Si dot with or without Ge core was performed at room temperature in clean room air by scanning an electrically-biased AFM probe with a tapping mode using an Rh-coated Si cantilever. The probe biases with respect to the Si(100) substrate were -3V for electron injection and +1 to +3V for electron extraction. Before and after electron charging or discharging, the topographic and corresponding surface potential images were simultaneously measured with non-contact Kelvin-probe mode.

Topographic and the corresponding surface potential images of a single Si dot with Ge core measured with the Kelvin probe mode are shown in Fig. 2. Before the voltage application to the sample surface, a uniform surface potential is detected (Fig. 2(b)). After electron injection to the dot by applying -3V in the tapping mode, the potential image taken in the Kelvin probe mode shows the surface potential change of ~120mV on the dot (Fig.2 (c)), but no surface potential change elsewhere. Obviously, the stored electron can be extracted by applying the tip bias of +1V to the charged dot on tapping mode (Fig. 2(d)). It is important to note that, the surface potential change near the peripheral region of the charged dot with Ge core is much higher than that of the center of the dot after electron injection. The electron extraction from the neutral dot and the neutralization of the positively charged dot are also verified from the surface potential change of ~84mV by applying +3 and -1V to the dot in the tapping mode as indicated in Fig. 3. For the electron extraction from the neutral dot, the maximum potential change appears in the center of the dot. These results indicate that the injected electrons are located in the Si clad rather than the Ge core due to the coulomb repulsion between each electron. On the other hand, electron can be extracted from the valence band of Si clad and remaining hole move and then stably retained in the Ge core as indication of a deep potential well for hole providing by Ge core.

From the calculation results using a simple equivalent circuit, we estimated that the potential changes observed in Figs. 2(c) and 3(c) are equal to the theoretically predicted values for charging the dot by 3 electrons and 2~3 holes, respectively.

**References:**

[1] S. Tiwari et al , *Appl. Phys. Lett.* **68** (1996)1377-1379
[2] A. Fujiwara & Y. Takahashi, *Nature,* **410** (2001)560-562
[3] Y. Darma., et al., *Jpn. J. Appl. Phys.*, Part 1 **42** (2003) 4129-4133.

**Figures:**
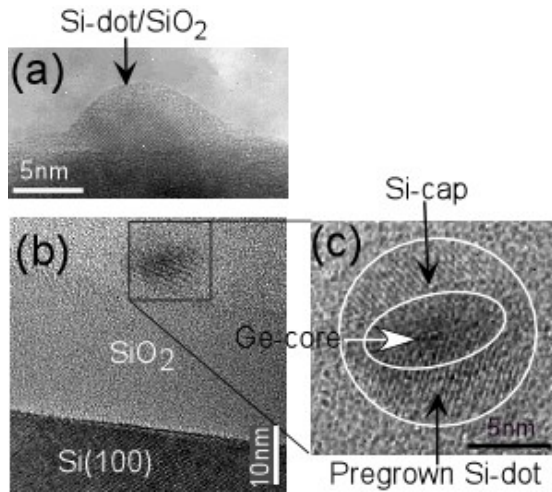


**Fig.1** Cross-sectional HR-TEM images of hemispherical Si dot pregrown on $SiO_2$ (a) and Si dots with Ge core (b) accompanied with a magnified image of an isolated dot (c).
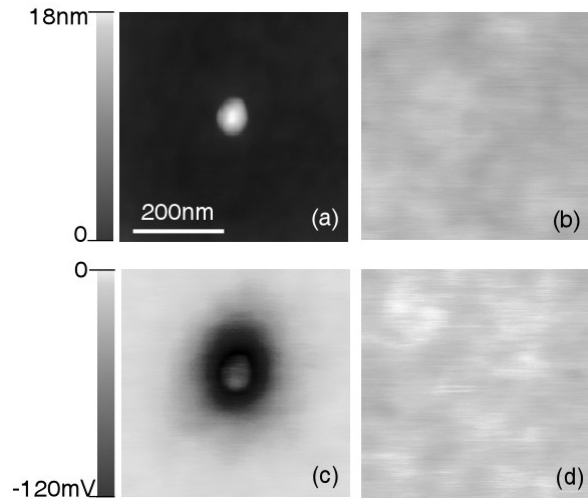


**Fig.2** Topographic image (a) and corresponding surface potential images of an isolated Si dot with a Ge core measured by AFM/Kelvin probe mode before (b) and after electron injection (c) at –3V, and after electron emission at +1V from the charged Si dot in the tapping mode (d).
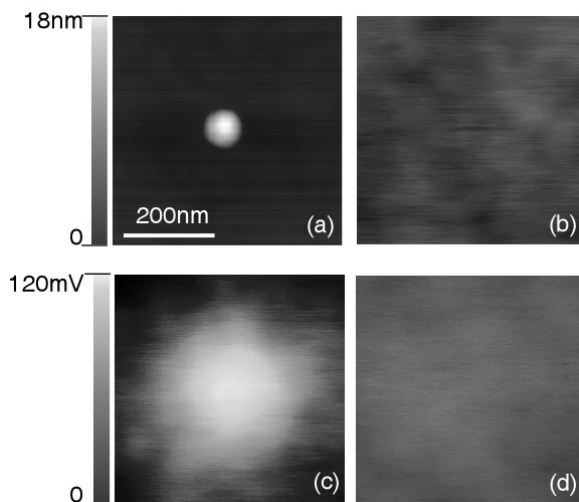


**Fig.3** Topographic image (a) and corresponding surface potential images of an isolated Si dot with a Ge core with a total dot height of ~18nm measured by AFM/Kelvin probe mode before (b) and after injected (c) at +3V, and after electron emission at -1V from the charged Si dot in the tapping mode (d).

# ELECTROCATALYTICAL BIOSENSING BASED ON GOLD NANOPARTICLES

Alfredo de la Escosura Muñiz[1], Marisa Maltez da Costa[1,2], M. Teresa Castañeda Briones [1,3],

Salvador Alegret[3], Arben Merkoçi[1,3]

[1]*Nanobioelectronics & Biosensors Group, Institut Català de Nanotecnologia, Barcelona,Spain*
[2]*Department of Chemistry, University of Aveiro, Aveiro, Portugal*
[3]*Group of Sensors & Biosensors, Autonomous University of Barcelona, Barcelona, Spain*
*Tel.: +34 935 81 49 18. Fax: +34 985 81 47 47*
*e-mail: alfredo.escosura.icn@uab.es*

Gold nanoparticles (AuNPs) have been used for analytical and biomedical purposes for many years. Rapid and simple chemical synthesis, optical and electrochemical properties, a narrow size distribution and efficient coating by thiols or other bioligands has enabled AuNPs to be used as labels for several biorecognition binding applications.

In this work, electrocatalytical methods are developed in order to improve the sensitivity of model biosensors (immuno- and genosensors) based on a labelling method using AuNPs. Microparamagnetic beads (MB) are used as primary biological molecules immobilisation platforms and AuNPs modified with secondary biological molecules as high sensitive electrochemical labels. The carbon electrodes, used as transducer, incorporate a magnet that allows the collection / immobilization on its surface of the biological sandwich attached to the MB.

Briefly, the sandwich type assay consists in the incubation of streptavidin-coupled-MB with an anti-human IgG or a single stranded DNA (ss-DNA) probe biotin conjugate, and then, the biological reaction with the human IgG antigen or the ss-DNA target takes place. After that, a gold labelled anti-human IgG (immunosensor case) or ss-DNA probe (genosensor case) reacts with the corresponding antigen or the target . The final detection is based on the catalytic effect of AuNPs on the electroreduction of either silver ions or protons. The main parameters that affect the different steps of the developed assays are optimised so as to reach high sensitive electrochemical detections of the corresponding biological molecules.

The low levels of AuNPs detected with these methods allow the obtaining of biosensors with low protein and ss-DNA target detection limits, with special interest for further applications in clinical analysis, food quality and safety as well as other industrial applications.

# Hybrid polyelectrolyte/bacterial protein (nano)biomimetic surfaces: a model to study bacterial surface layer recovery and bacterial affinity

*Mihaela Delcea[1], Dietmar Pum[2], Rumen Krastev[3], Uwe B. Sleytr[2]*
*and José Luis Toca-Herrera[1]*

[1]Biosurfaces Unit, CICbiomaGUNE, Paseo Miramón 182, Parque Tecnológico de San Sebastián, 20009 San Sebastián (Gipuzkoa), Spain
[2]Center for Nanobiotechnology, BOKU, Gregor-Mendel Str. 33, 1180 Vienna, Austria
[3]Max-Planck Institute for Colloids and Interfaces, Am Muehlenberg 1, 14420 Potsdam, Germany
*mdelcea@cicbiomagune.es; jltocaherrera@cicbiomagune.es*

Robust (nano)biomimetic surfaces that mimic the behaviour of cell membranes can be built by combining polyelectrolyte multilayer (PEM) deposition and bacterial surface layer technology [1]. This symbiosis can provide a variety of model systems and applications such as, artificial cells and biosensor development.

Polyelectrolytes are used as a cushion for crystalline bacterial cell surface layers (S-layers), replacing the secondary cell wall polymer from bacteria. S-layers are one of the most common cell envelope components of prokaryotic organisms, composed of a single (glyco)protein, representing the simplest biological membrane developed during evolution [2]. Isolated S-layer subunits have the ability to self-assemble into 2-D crystalline structures at the air-water interface [3], on lipid films [4], on liposomes [5], on solid support [6], on solid supports coated with polyelectrolytes and on hollow polyelectrolyte microcapsules [1]. The study of the stability of S-layers is relevant in microbiology and nanotechnology since they play among others, a protective role and can serve as a (nano)matrix for bio-immobilization.

Our studies show that recrystallized S-layers (from *Bacillus sphaericus*) preserve their crystalline structure for three ethanol/water mixtures (20%, 40% and 60% ethanol). After exposing the S-layer surface to an ethanol/water mixture 80:20 (v/v), the 2-D crystalline structure was lost. Treatment with recrystallization buffer led to a recovering of the crystalline structure, showing that the S-layer surface can be denatured and renaturated in a switched on-off process (see Figure 1). This fact could not be observed when the S-layer was exposed at different pH solutions and thermally treated. It was found that the 2-D crystalline structure was lost at pH 3 and at 55ºC.

After studying the chemical and thermal stability of recrystallized S-layers on PEM, a novel hybrid sandwich-like supramolecular structure (polyelectrolyte/S-layer/polyelectrolyte/S-layer) was built. The supramolecular construct permitted to elucidate the bacterial affinity for different polyelectrolytes (Figure 2). It was found that only positive polyelectrolytes could adsorb on the exposed S-layer surface [7]. These results open a possibility to build functional hybrid supramolecular structures with potential applications in nanobiotechnology, and give insight about bacterial adhesion.

**References:**

[1] J. L. Toca-Herrera, R. Krastev, V. Bosio, S. Küpcü, D. Pum, A. Fery, M. Sara, U. B. Sleytr, *Small*, **1** (2005) 339.
[2] U. B. Sleytr, M. Sara, D. Pum, B. Schuster, *Progress in Surface Science*, **68** (2001) 231.
[3] D. Pum and U. B. Sleytr, *Landesr Academic Press*, Austin, TX, (1996) 175.
[4] B. Schuster and U. B. Sleytr, *Reviews in Molecular Biotechnology*, **74** (2000) 233.
[5] S. Küpcü, M. Sara, U. B. Sleytr, *Biochim. Biophys. Acta*, **1235** (1995) 263.
[6] D. Pum and U. B. Sleytr, *Thin Solid Films*, **244** (1994) 882.
[7] M. Delcea, R. Krastev, Th. Gutlebert, D. Pum, U. B. Sleytr, J. L. Toca-Herrera, *J. Nanosci. Nanotechnol. In press.*

**Figures:**
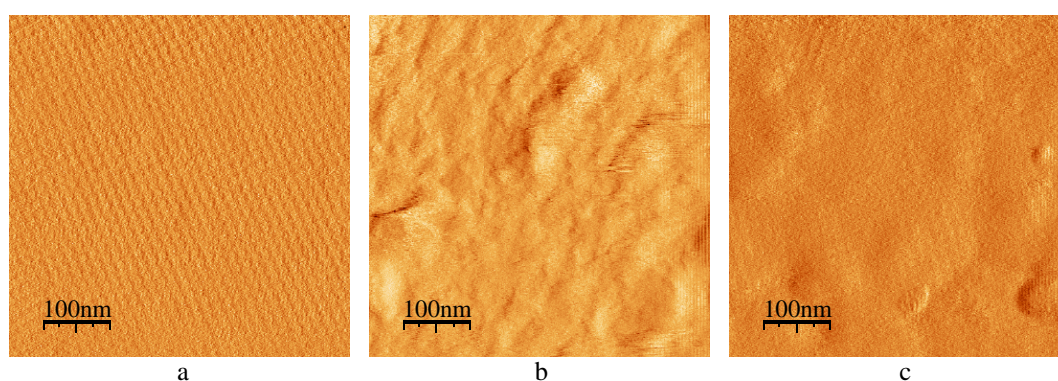


Figure 1. Atomic force microscopy deflection images of S-layers recrystallized on PEM. a) S-layer just as it was formed; b) S-layer treated with EtOH/H2O 80/20 (v/v); c) Recovered S-layer after treatment with recrystallization buffer (S-layer protein renaturation).
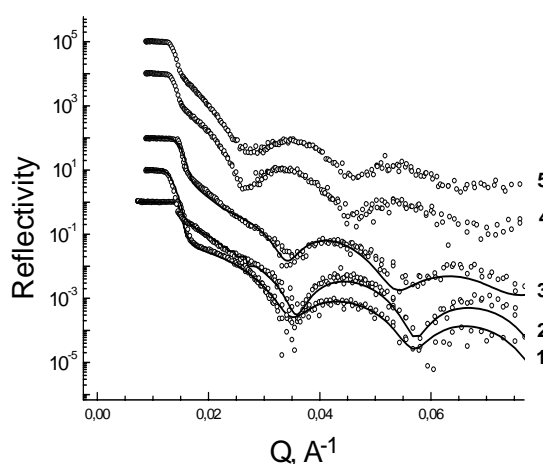


Figure 2. Neutron reflectivity as a function of Q for the following macromolecular structures: 1- Si/PE/PSS-terminated, 2- Si/PE/PSS/S-layer, 3- Si/PE/PSS/S-layer/PAH, 4- Si/PE/PSS/S-layer/(PAH/PSS)$_2$ and 5-Si/PE/PSS/S-layer/(PAH/PSS)$_2$/S-layer. Curves 2 and 3 show respectively the formation of the S-layer on PSS and the affinity of PAH to the S-layer. Note that curves 4 and 5 are similar, meaning that no homogenous S-layer was formed. PE=polyelectrolyte; PSS= Poly(sodium 4-styrenesulfonate); PAH= Poly(allylamine hydrochloride).

# MACROPOROUS 3D ARCHITECTURES OF SELF-ASSEMBLED MWCNTS SURFACE DECORATED WITH PT NANOPARTICLES AS ANODES FOR A DIRECT METHANOL FUEL CELL

**Authors:** María C. Gutiérrez, María J. Hortigüela, J. Manuel Amarilla, Ricardo Jiménez,  María L. Ferrer, Francisco del Monte

**Abstract:**

Microchannelled 3D architectures composed of multiwall carbon nanotubes (MWCNTs) surface decorated with Pt nanoparticles and chitosan (CHI) are prepared by ice segregation induce self assembly (ISISA) process. The microchannelled structures are highly porous (specific gravity $\sim 10^{-2}$), and exhibit excellent electron conductivity thanks to both the high content of MWCNTs (up to 89 wt.%) and their interconnection. The Pt/MWCNTs/CHI 3D architectures provide remarkable performance as anodes for a direct methanol fuel cell (DMFC).

# $C_{60}$/SI AND $C_{60}$/SiO$_2$ COMPOSITE THIN FILMS: A PHOTOELECTRON SPECTROSCOPY STUDY OF THEIR MATRIX-DEPENDENT THERMAL STABILITY

*Teresa de los Arcos[*], Peter Oelhafen [*], Concepción Domingo[♣]*
[*]*Department of Physics, University of Basel, Klingelbergstr 82, CH-4056 Basel Switzerland,*
[♣]*Instituto de Estructura de la Materia, CSIC, c/Serrano 123, 28006 Madrid, Spain*
*t.arcos@unibas.ch*

Cluster-based materials are highly versatile systems with a wide range of applications in nanotechnology.

In the case of fullerene-composite films, most studies to date concentrate on the fundamental aspects of the composite film growth, the electronic properties of the interface between cluster and fullerene, and the electronic properties. However, there are relatively few studies where the incorporation of fullerenes in a semi-conducting matrix has been attempted, and to the extent of our knowledge nothing has been done on dielectric matrixes.

In this work we present measurements done in a co-deposition experiment of fullerenes and Si or SiO$_2$ matrix. In-situ analysis of the deposited films was done with photoelectron spectroscopy in the X-ray range (XPS) and UV-range (UPS). This has allowed us to follow the compositional changes and the modifications in the electronic structure of the valence band with increasing temperature. The films where further analyzed ex-situ by micro-Raman spectroscopy.

We have investigated the stability of the films, and the tendency of the fullerenes to form chemical binding with the surrounding matrix, as function of temperature. The deposition method is a combination of evaporation technique (for the fullerenes) and non-reactive sputtering (for the Si or SiO$_2$ matrix). We have observed marked differences in temperature-dependent stability of the films as a function of the surrounding matrix.

When $C_{60}$ is co-deposited with pure Si, there is a small fraction of C which binds to the Si, forming carbide, even at room temperature. Progressive annealing of the film results in massive formation of more SiC for temperatures above 700°C, which consumes all the available Si.

By contrast, co-deposition of $C_{60}$ with SiO$_2$ (by sputtering of a quartz target) results in a very stable film. Similar to the previous case, there is a small fraction of the original $C_{60}$ that has been oxidized already during the deposition at room temperature. However, unlike the Si case, the SiO$_2$ matrix provides a great thermal stability to the fullerenes, which do not undergo any chemical transformation, (neither carbidization nor oxidation) during annealing up to temperatures close to the decomposition temperature of the $C_{60}$.

# Absence of extended states in a ladder model of DNA

E. Díaz[1] and F. Domínguez-Adame[1]

[1]*GISC, Departamento de Física de Materiales, Universidad Complutense, E-28040 Madrid, Spain*

According to standard theories of disordered systems, [1] all states in low-dimensional systems with uncorrelated disorder are spatially localized. Therefore, in a pure quantum-mechanical regime, disordered models of DNA might lead to insulator behaviour unless the localization length reaches anomalously large values. To explain long range charge transport found experimentally, [2] several authors considered spatial correlations of the nucleobasis along the DNA molecule. [3–8] Those models are based in the fact that random sequences, having a power-law spectral density $S(k) \sim 1/k^\alpha$ with $\alpha > 0$, result in a phase of extended states at the band center, provided $\alpha$ is larger than a critical value $\alpha_c$. [9–12] As a consequence, long range charge transport might be feasible even at very low temperature, provided the chemical potential lies within the band of extended states.

Recently, Caetano and Schulz claimed that intrinsic DNA-correlations, due to the base pairing (A–T and C–G) between the two strands, lead to electron delocalization even if the sequence of bases along one of the strands is uncorrelated. [13] Furthermore, they pointed out that there is a localization-delocalization transition (LDT) for certain parameters range. If these results were correct, then *transverse* correlations arising intrinsically in DNA could explain long range electronic transport. However, we have claimed that this is not the case and all states remain localized, thus excluding a LDT. [14]

In this work we provides further analytical and numerical support to our above mentioned claim, aiming to understand the role of intrinsic DNA-correlations in electronic transport. To this end, we address signatures of the spatial extend of the electronic states by means of the analysis of the Landauer and Lyapunov coefficients. Thus we introduce the ladder model of DNA [13] and diagnostic tools we use to elucidate the spatial extend of electronic states in the static lattice. Afterwards we discuss the analytical calculation of the Landauer and show that this exponent never vanishes in the thermodinamics limit for any value of the system parameters. From this result we conclude that extended states never arises in the model.
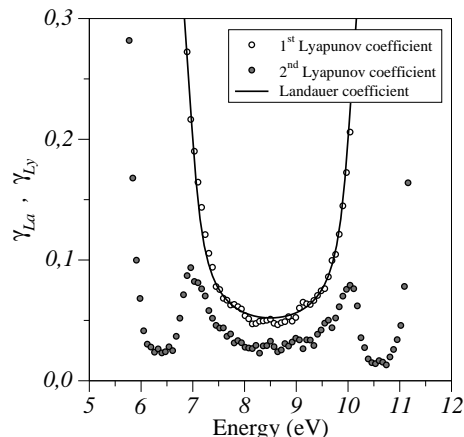


FIG. 1: 2/3 of Landauer exponent $\gamma_{\mathrm{La}}$ (solid line) and the largest Lyapunov exponent $\gamma_{\mathrm{Ly}}$ (white circles), as a function of energy, for $t_\perp = 0.5\,\mathrm{eV}$ and $t_\parallel = 1.0\,\mathrm{eV}$. The second, smaller Lyapunov exponent (grey circles) is also shown.

We then proceed to calculate the Lyapunov and the Landauer exponent for finite samples for the paramaters used by Caetano and Schulz [13], althoug these values of the interstrand and intrastrand hoppings are larger than those usually considered in the literature, [15, 16]. In Fig.1 it becomes clear that neither the largest Lyapunov exponents nor the Landauer one vanish over the whole energy spectrum. Most important, its minimum value is size independent within the numerical accuracy, suggesting the occurrence of truly localized states. Notice that the minimum value of these exponents is always much larger than the inverse of the number of base pairs ($1/N = 0,00025$), indicating that DNA-pairing can hardly explain long range charge transport at low temperature. From the inverse of the minimum value of the second Lyapunov coefficient we can estimate that the localization length is of the order of 80 base pairs (i.e. roughly eight turns of the double helix), therefore being smaller than typical sizes used in experiments. [2]

To elucidate the effects of the base pairing on the localization length, we have also considered the artificial case of
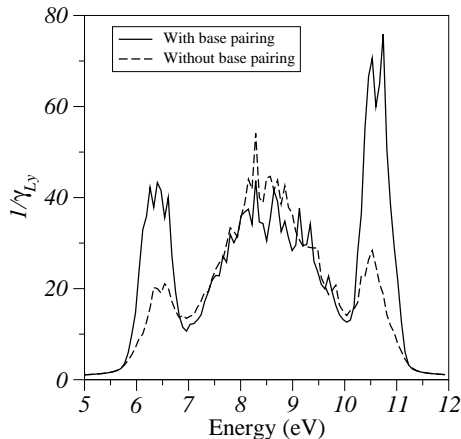
FIG. 2: Inverse of the second Lyapunov coefficient for $N = 4000$ $t_\perp = 0.5\,\text{eV}$ and $t_\parallel = 1.0\,\text{eV}$, when the base pairing is present (solid line) and absent (dashed line)
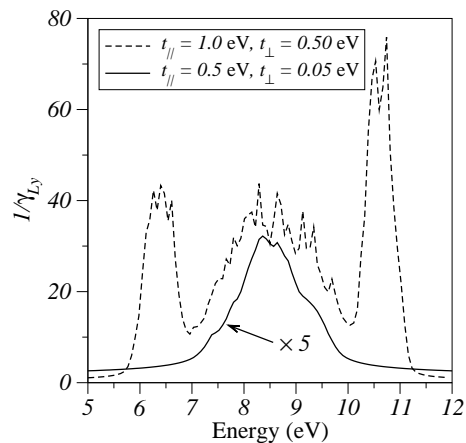
FIG. 3: Inverse of the second Lyapunov coefficient for $N = 4000$ and two sets of hopping parameters, indicated on the legend box. Notice the scaling factor indicated on the lower curve.

ladder models without pairing. Therefore, the system becomes much more disordered and one could naively expect a dramatic decrease of the localization length, as compared to the system with base pairing. Fig.2 indicates that this is not the case. The inverse of the second Lyapunov exponent remains almost unchanged over a large region of the energy spectrum, except close to the two resonances at about $6.4\,\text{eV}$ and $10.6\,\text{eV}$. At resonances the localization length is reduced by a factor 2.5 at most when the pairing constraint is relaxed. In any event, resonances still appear so they cannot be associated to base pairing.

Higher hoppings lead to a *less-effective* disorder and higher localization lengths are to be expected. We have calculated the inverse of the second Lyapunov exponent for more realistic values of the hopping parameter and checked that this claim is indeed correct. For instance, for $t_\perp = 0.05\,\text{eV}$ and $t_\parallel = 0.5\,\text{eV}$ (see Ref. 16) the localization length at the center of the band is reduced by a factor 5 as compared to the case shown in Fig.2, while an even larger decrease is noticed at resonances. Therefore, we come to the conclusion that hopping is a more important mechanism for delocalization than base-pairing in this ladder model.

After discussing in detail these exponents' dependence on the model parameters, especially inter- and intrastrand hoppings, we conclude that the localization length is only of the order of very few turns of the double helix for realistic values of the model parameters. Therefore, this shows that intrinsic DNA-correlations alone cannot explain long range electronic transport. found in long DNA molecules. [2]

[1] E. Abrahams, P. W. Anderson, D. C. Licciardello, and T. V. Ramakrishnan, Phys. Rev. Lett. **42**, 673 (1979).
[2] D. Porath, A. Bezryadin, S. de Vries, and C. Dekker, Nature **403**, 635 (2000).
[3] P. Carpena, P. Bernaola-Galván, P. Ch. Ivanov, and H. E. Stanley, Nature **418**, 955 (2002); *ibid* **421**, 764 (2003).
[4] S. Roche, Phys. Rev. Lett. **91**, 108101 (2003).
[5] S. Roche, D. Bicout, E. Maciá, and E. Kats, Phys. Rev. Lett. **91**, 228101 (2003).
[6] M. Unge and S. Stafstrom, Nanolett. **3**, 1417 (2003).
[7] S. Roche and E. Maciá, Mod. Phys. Lett. **18**, 847 (2004).
[8] H. Yamada, Phys. Lett. A **332**, 65 (2004); Int. J. Mod. Phys. B **18**, 1697 (2004); Phys. Rev. B **69**, 014205 (2004).
[9] F. A. B. F. de Moura and M. L. Lyra, Phys. Rev. Lett. **81**, 3735 (1998); Physica A, **266**, 465 (1999).
[10] F. M. Izrailev and A. A. Krokhin, Phys. Rev. Lett. **82**, 4062 (1999).
[11] H. Shima, T. Nomura, and T. Nakayama, Phys. Rev. B **70**, 075116 (2004).
[12] E. Díaz, A. Rodríguez, F. Domínguez-Adame, and V. A. Malyshev, Europhys. Lett. **72**, 1018 (2005).
[13] R. A. Caetano and P. A. Schulz, Phys. Rev. Lett. **95**, 126601 (2005); *ibid.* **96**, 059704 (2006).
[14] A. Sedrakyan and F. Domínguez-Adame, Phys. Rev. Lett. **96**, 059703 (2006).
[15] Y. J. Yan and H. Zhang, J. Theor. Comp. Chem. **1**, 225 (2002).
[16] D. Klotsa, R. A. Römer, and M. S. Turner, Biophys. J. **89**, 2187 (2005).

# HOW TO IMPROVE THE DISSOCIATIVE REACTIVITY OF $O_2$ ON CLEAN AG(100) SURFACES

R. Díez Muiño[1], M. Alducin [1], H.F. Busnengo[2], A. Salin[3]

[1]*Centro de Física de Materiales, CSIC-UPV/EHU,San Sebastián ( Spain)*
[2] *Universidad Nacional de Rosario, Rosario (Argentina)*
[3] *Donostia International Physics Center, San Sebastián (Spain)*

*...*
E-mail: wapalocm@sq.ehu.es

The interaction of oxygen with silver surfaces has been extensively studied during last years using different experimental techniques. All these studies point to the Ag(100) surface as one of the less reactive faces regarding $O_2$ dissociation. At low surface temperatures T<150K, molecular beam experiments performed with $O_2$ incidence energies below 1 eV show that only molecular adsorption can occur on clean Ag(100) [1]. Dissociation was partially observed on defected Ag(100) surfaces [2], or induced on $O_2$-precovered surfaces by atom impact techniques [3]. In this theoretical study we propose an alternative mechanism to improve the low dissociative reactivity of the clean Ag(100) surface, the use of molecular beams in which the $O_2$ molecules are initially excited at the singlet state.

The interaction of singlet $O_2$ molecules with the Ag(100) surface is represented by constructing the six dimensional potential energy surface (6D PES) from the interpolation of spin-unpolarized ab initio data. Interpolation is performed using the reduced corrugation procedure. Furthermore, we also calculate the adiabatic 6D PES in which the $O_2$ molecular beam is initially in the triplet ground state. In both cases density functional theory with the generalized gradient approximation (non-spin density dependent for the singlet PES and spin-density dependent for the adiabatic PES) is used. Classical trajectory calculations performed with both PESs show that for the singlet $O_2$, dissociation occurs even at the lowest incidence energies. On the contrary, $O_2$ molecules initially in the triplet state only dissociate for incidence energies above 1.1 eV.

**References**
1. L. Vattuone, U. Burghaus, U. Valbusa, M. Rocca, Surf. Sci. **408**, L698 (1998).
2. F. Buatier de Mongeot, A. Cupolillo, U. Valbusa, M. Rocca, Chem. Phys. Lett. **270,** 345 (1997)
3. L. Vattuone *et al.* J. Chem. Phys. **109**, 2490 (1998)

# DETERMINATION OF THE NANO SCALE ENERGY LANDSCAPE OF H-BN/Rh(111) NANOMESH BY PHOTOEMISSION FROM ADSORBED XENON

*Hugo Dil[1,2], Jorge Lobo-Checa[1,2], Jürg Osterwalder[1], and Thomas Greber[1]*

[1]*Physik-Institut, Universität Zürich, Winterthurerstrasse 190, CH-8057 Zürich, Switzerland*
[2]*Swiss Light Source, Paul Scherrer Institute, CH-5232 Villigen, Switzerland*
*jan-hugo.dil@psi.ch*

At 1000 K the adsorption of borazine $(HBNH)_3$ on Rh(111) leads to the formation of hexagonal boron nitride layers with a 3.2 nm superstructure, called nanomesh [1]. From recent low temperature scanning tunnelling microscopy (STM) studies [2] and from theoretical considerations [3] it follows that the surface consists of a corrugated single monolayer h-BN film on top of the rhodium substrate. The corrugation pattern looks like a mesh where 'holes' with a diameter of about 2 nm are separated by 'wires' of 0.5 Å height.

Because of its structure and thermal stability this surface is a good candidate for functionalisation by means of adsorption of molecules or metal clusters. In order to understand and eventually predict the bonding mechanism of such adsorbates, the detailed energy landscape on the nanometer scale has to be accurately determined. One of the goals of the present work is to provide complementary information which is not easily accessible by other techniques, on a nano structured surface which has recently received a lot of attention especially in the STM community.

In this work we show results obtained by Photoemission-spectroscopy of Adsorbed Xe (PAX) on the nanomesh formed on Rh(111). We find a difference in the Xe 5p binding energy between the holes and the wires of 450 meV, which is close to theoretical predictions for an idealised mesh. Furthermore from photoemission spectra recorded during temperature programmed Xe desorption it is possible to determine the Xe bond energy difference between adsorption in the holes and on the wires. Using this technique we also succeeded in mapping the Xe/nanomesh bond energy landscape inside the holes, where the observations suggest that Xe is most strongly bound to the rims of the holes. These results suggest that the nanomesh can be used as a template for a wide variety of adsorbates.

**References:**

[1] M. Corso et al. Science, **303** (2004) 5655.

[2] S. Berner et al. Angewandte Chemie (2007) in press.

[3] R. Laskowski, P. Blaha, Th. Gallauner, K. Schwarz, Phys. Rev. Lett, **98** (2007) 106802.

# NANOCRISTALLITES OBTAINED THROUGH THE PYROSOL METHOD

*ELENA DINU[1], Elisabeth SIEBERT[2], Ecaterina ANDRONESCU[1], Elisabeth DJURADO[2], Laurent DESSEMOND[2], Cristina Daniela GHITULICA[1]*
*[1] University Politehnica of Bucharest - Faculty of Applied Chemistry and Materials Science, 1 – 7, Gh. Polizu Street, sect. 1, PO BOX 12-134, Bucharest, Romania*
*[2] Polytechnic National Institute of Grenoble - LEPMI / ENSEEG, Dom. Universitaire, 1130, Street Rue de la Piscine, B.P. 75, 38 402 - Saint Martin d'Hères Cedex – Grenoble, France*
*Email: elena.dinu@yahoo.com*

The decrease of particles size from micrometric to the nanometric scale is allowing the development of new materials, with dramatically improved properties.

The pyrolysis of solutions is a very interesting method of production for reactive nanopowders. A great range of composition, size and morphology can be obtained through modifying the characteristics of precursors, the properties of solutions used and the experimental parameters of the selected [1]. The pyrosol process is based on the pyrolysis of an aerosol, produced by ultrasonic pulverization. The vibrations generated on the surface of a solution by a beam of ultrasounds, directed towards the interface gas/liquid, are used for generating the aerosol. The ultrasounds beam is generated by a piezoelectric ceramic. The wavelength of the vibrations depends mainly on the frequency "f" of the ultrasounds and the characteristics of the irradiated solution [2]. The average diameter of drops is inversely proportional to $f^{2/3}$. The aerosol thus formed is pulled by a carrier gas, whose flow is fixed, in a furnace at high temperature, in which the drops undergo a sequence of physicochemical transformations, described into details by Messing and coll. [1, 3, 4, 5, 6]. The high temperature causes evaporation of solvent and also determines the precipitation of soluble species in the volume of a dense and spherical particle. At the exit from the furnace, an electrostatic filter allows the recovery of powders. The schema of a typical pyrolisis installation is presented in Figure 1.

In this study, the influence of the various synthesis parameters on the crystallinity and the composition of calcium phosphate powders were investigated. Firstly, the influence of the chemical nature of precursory calcium salt was studied, by using two types of water soluble calcium salts: $CaCl_2 \cdot 2H_2O$ and $Ca(NO_3)_2$. The precursor used for $P_2O_5$ is $(NH_4)H_2PO_4$. In the second time, it was studied the effect of the pyrolisis temperature, in the interval 600˚C-1000˚C.

The obtained powders were investigated through thermal analysis: thermo gravimetric-TGA and thermal differential analyses-DTA, X-ray diffraction and electronic scanning microscopy. Whatever the temperature of pyrolysis of the aerosol, the apatite structure is recognizable - JCPDS 09-0432), if the precursor used for the calcium oxide is calcium chloride. If the powders are elaborated starting from calcium nitrate, the only phase identified is β-calcium phosphate.

For the powders synthesized from calcium chloride the microscopic observations highlight a majority of approximately spherical particles, of hundreds of nanometers size. Can also be noticed larger particles, of around 4μm, which we suppose that are containing inside smaller particles (Figure 2a). The general aspect of powders is kept for those obtained starting from calcium nitrate. The smaller spherical particles are however more deformed and the larger ones are highly porous, presenting a rough surface (Figure 2b).

The average size of grains was calculated using the Scherrer formula, from diffraction data. It was found that the lowest crystallite sizes are obtained for the lowest pyrolysis temperature. The size of crystallites for the powder obtained starting from calcium chloride is of 30nm, for a pyrolisis temperature of 600˚C and it is increasing to 50nm at 900˚C and to 66nm for a temperature of 1000˚C.

In all cases, the synthesis by pyrosol makes it possible to obtain powders with various compositions, made up of spherical particles, with sizes in the nanometric range, that can have many applications.

**References:**

[1] G. L. Messing, S.-C. Zhang, G. V. Jaganthi, J. Am. Soc. Ceram. Soc., 76 (1993) 2707.
[2] E. Djurado, E. Meunier, J. Solid State Chem., 141 (1998) 191.
[3] K. Ytatani, O. Takahashi, A. Kishioka, Gypsam & Lime, 213 (1988) 19.
[4] M. Aizawa, K. Ytatani, F. S. Howell, A. Kishioka, J. Ceram. Soc. Jpn., 104 (1996) 126.
[5] P. Luo, T. G. Nieh, Mat. Sci. Eng., C3 (1995) 75.
[6] M.Aizawa, T.Hanazawa, K.Ytatani, F.S.Howell, A.Kishioka, J.Mat. Sci., 34 (1999) 2685.
[7] B.E. Warren in X-ray Diffraction, New York: Dover Publications, Inc., 251.

**Figures:**
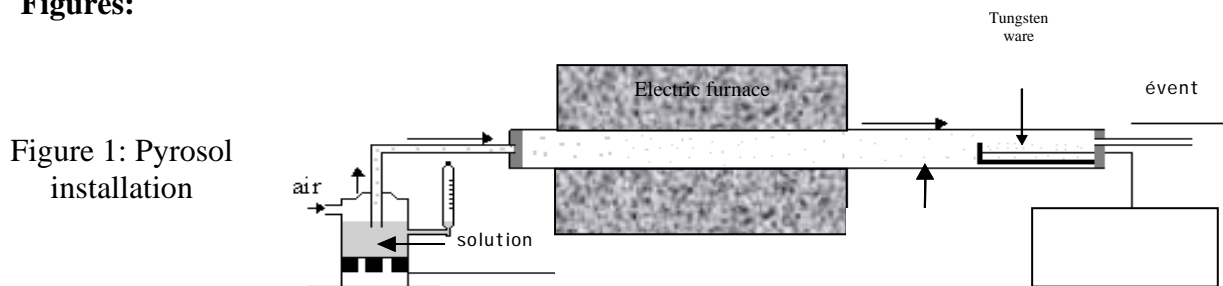
Figure 1: Pyrosol installation



Figure 2: SEM images of the powders obtained from chloride (a) and nitrate (b)
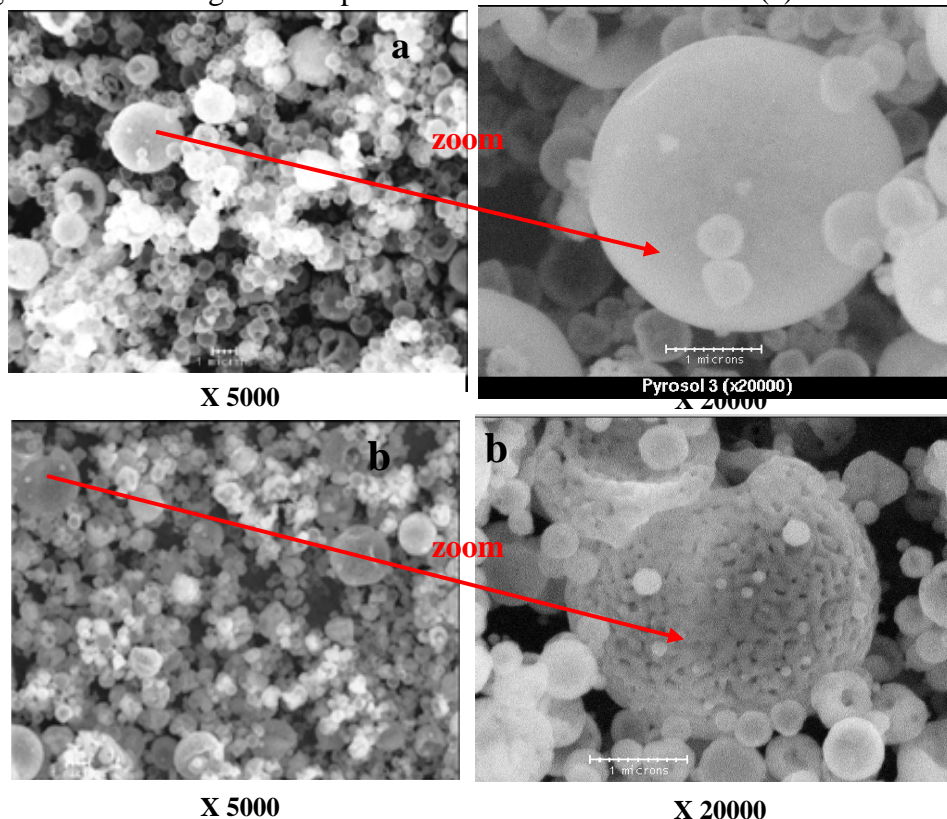
# Investigation of nanostructured films of antibodies and polymers.

E.A. Dontsova

*Department of Chemistry, M.V. Lomonosov Moscow State University*
*119992 Leninskie Gory 1/3, Moscow, Russia*
*ekaterina.dontsova@gmail.com*

Enzyme-linked immunosorbent assay (ELISA) is widely used for a great number of analytical problems in the medical diagnostics and the quality control of foods and environment. Now ELISA technique continues to develop for constructing more sensitive, miniaturized, reliable, and less time consuming immunoassay devices and also for creating more simple and cheap automatic technologies for their manufacture.

Antibodies immobilization is an essential part of any ELISA construction. In the present study the method of antibodies immobilization via formation of nanostructured films with polymers was developed and the properties of these films were investigated. This method is much more simple, cheap and less time consuming than the covalent modification method and suitable for a wide range of surfaces. To form nanostructured films we used monoclonal mouse antibodies which were adsorbed from a solution onto the investigated surface modified with polymer nanofilms. The polymer nanofilms were obtained in the same way – via adsorbing from the solution.

The properties of nanostructured polymer and antibodies films obtained on the surface of highly oriented pirolytic graphite (HOPG) were studied. With the help of ELISA method we also investigated correlation between antibodies activity and the polymer used for film formation. Structure and stability of the films were studied using Scanning Force Microscopy (SFM).

Our investigations show that the activity of antibodies depends on the kind of polymer used in the nanostructured film. The highest activity was obtained for two polymers: poly(2-acrylamido-2-ethylpropansulfonic acid) (PAMPS) and poly(diethylaminophosphozen) (PPh) [1]. The films with other polymers were less active or gave the high level of background non-specific signal.

SFM images showed that initially we obtained regular films which thickness is about several nanometers (see fig.). The most stable films were obtained with PPh, while using of the other polymers leads to easy deformation of the films. Obtained structure of the films explains low activity of the antibodies for some polymers - when deformation of antibodies occurs. In the case of high background nonspecific signal we could see the rearrangement in the film structure on SFM image [2].

It was also shown that the method developed allows antibodies immobilization on different surfaces but the influence of the surface should be studied individually for every used material.

**References:**

[1] V.S. Papkov , M.N. Il'ina, etc, Macromolec., Volume 25, No 7 (1992), pp. 2033-2040.
[2] E.G. Evtushenko, I.N. Kurochkin, E.A. Dontsova, etc, J. Rus. Nanotechnology, Volume 2, No 1-2 (February 2007), pp. 145-153.

**Figures:**
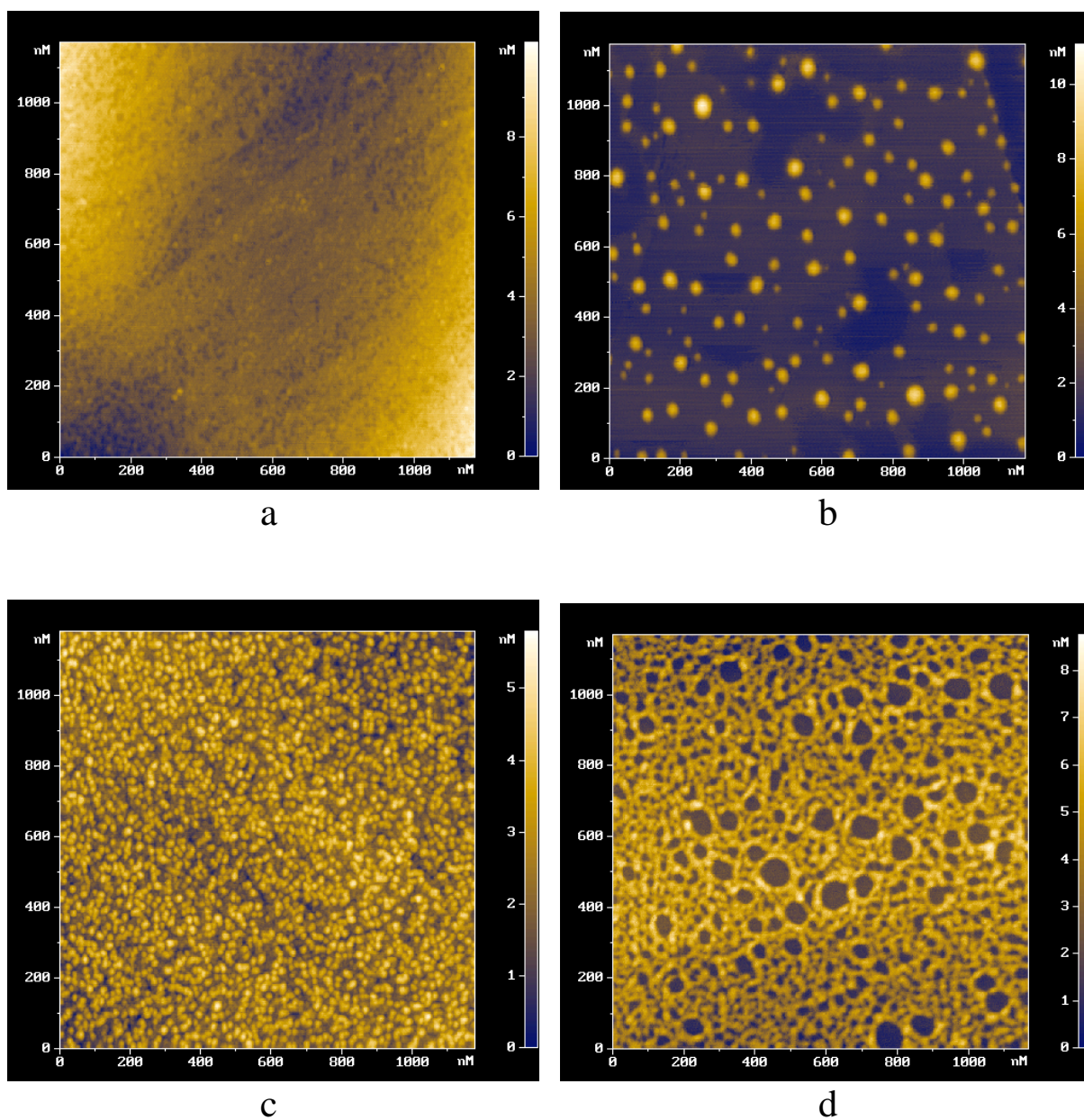


SFM images of nanofilms: a) PPh on HOPG surface; b) poly((dimethyldiallylammonium) chloride) (PDDA) on HOPG surface; c) antibodies on PPh film (HOPG); d) antibodies on PDDA film (HOPG).

# BIOFILM GROWTH FORM WASTE WATER ON MWNTs AND CARBON AEROGELS

*Anca Dumitru[1], Adina Morozan[1], M. Ghiurea[1], K.Scott[2] and I. Stamatin[1]*

[1]3Nano-SAE Research Centre, University of Bucharest, P.O. Box MG-38, 077125, Magurele, Romania
[2] School of Chemical Engineering and Advanced Materials, University of Newcastle upon Tyne, Newcastle upon Tyne NE1 7RU, United Kingdom
*anka.dumitru@gmail.com; ancad@3nanosae.unibuc.ro*

The improving carbon nanostructure bioactivity related to a specific microorganism community is an important research goal of bionanotechnology [1]. The desired carbon nanotube properties are usually obtained after chemical modification. In this way, the functionalized CNTs are used to improve the bioaffinity of working electrode in biofuel cells and waste water treatment. Beside CNTs, carbon aerogel is another carbon nanomaterials with high surface area, high open porosity and controllable morpho-structural characteristics.

In the present work we investigate the biofilm growth in waste water on functionalized CNT and carbon aerogels. The biofilm growth on the MWNTs (Fig.1a) and carbon aerogel (Fig.1b) was monitored by optical and scanning electron microscopy. The influence of the bacterial growth phase on the voltammetry measurements was assessed by obtaining a cyclic voltammogram of the bacterial consortium growth on carbon electrode in waste water and 0,5 M phosphate buffer.

**References:**
[1] B.E.Logan and J.M.Regan, *Environ. Sci. Technol*. 40(17) (2006):5172-5180.
[2] C.G. Hu, W.L. Wang, K.J. Liao, G.B. Liu, Y.T. Wang, *Journal of Physics and Chemistry of Solids* 65 (2004) 1731–1736
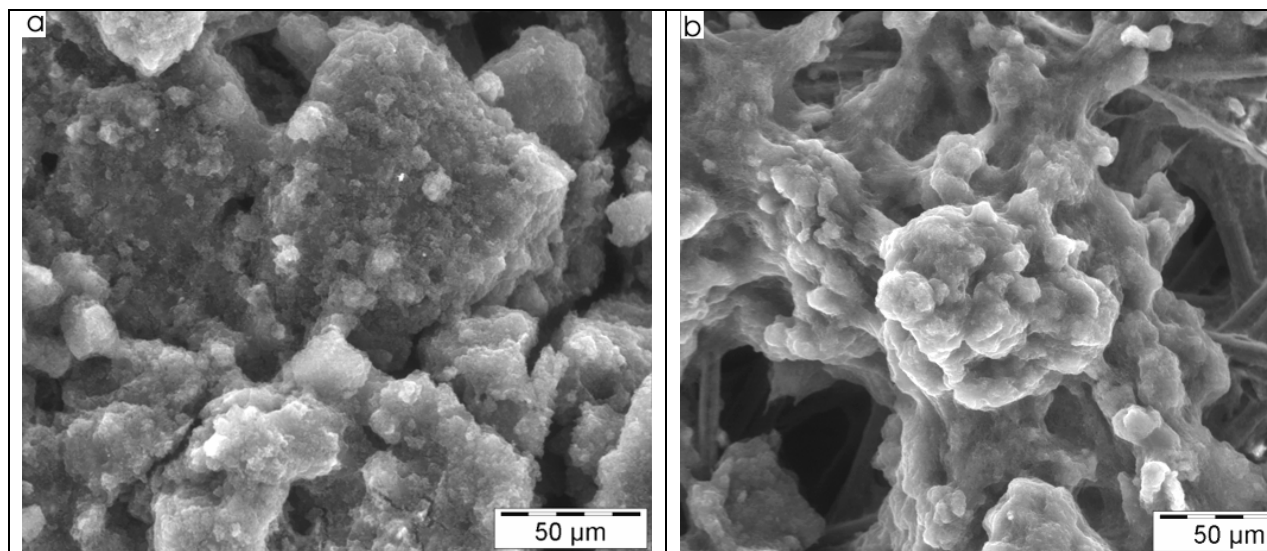


**Figure1.** Scanning electron microcopy images of biofilm growth on: a) carbon aerogel and b) MWNT

# Nanocrystals of Mn-doped CdTe: A theoretical approach on magnetic properties

*C. Echeverría-Arrondo[1], A. Ayuela[2], J. Pérez-Conde[1], A.K. Bhattacharjee[3]*

*[1]Dpto. de Física, Universidad Pública de Navarra, campus Arrosadía, s/n., Pamplona, Spain*
*[2]Donostia International Physics Center, Paseo Manuel de Lardizábal, 4, San Sebastián, Spain*
*[3]Laboratoire de Physique des Solides, UMR du CNRS, Université Paris-Sud, Orsay, France*

*carlos.echeverria@unavarra.es*

Progress in materials chemical synthesis, computational capabilities and scanning-probe techniques has permitted a detailed understanding of semiconductor nanocrystals, also referred to as quantum dots (QD's). Their properties are unusual at the macroscale, strongly dependent on size [1,2], doping [3-6] and shape [7]. In particular, Mn-doped II-VI nanocrystals, succesfully synthesized and characterized during the last fifteen years [3-6,8-13], show remarkable magneto-optical effects. Their interesting physical properties arise from strong *sp-d* exchange interactions between manganese impurities and band-edge states.

In this work we investigate the magnetic properties of Mn-doped CdTe nanocrystals in the frame of the density-functional theory, by means of the projector augmented-wave method. Mn impurities replace Cd atoms in the zinc blende lattice. When a single manganese atom is embedded, the calculated total magnetic moment associated with the quantum dot is $\mu_{QD} = 5\ \mu_B$, but the local moment on the manganese site is found to be smaller: $\mu_{Mn} = 4.65\ \mu_B$. This effect is attributed to the *sp-d* hybridization, which is also responsible for the appearance of small local moments on the manganese nearest neighbor tellurium atoms, which also contribute to the total moment $\mu_{QD}$. When two impurities are included, we study two magnetic configurations, which correspond to the Mn moments initially parallel ($\mu_{QD} = 10\ \mu_B$) and antiparallel ($\mu_{QD} = 0\ \mu_B$). We find that the latter is the ground state. For the same reason than before, the calculated Mn local moments are found to be smaller in modulus than $5\ \mu_B$. We also analyze the excited states $\mu*_{QD} = 10, 0, 2, -2, 8$ and $12\ \mu_B$ (a star stands for "excited"). In the excited ground state the Mn local moments are parallel with a total magnetic moment $10\ \mu_B$. The differences in the magnetic behavior between the non-excited (antiparallel Mn moments) and the excited ground states can be attributed to a hole-mediated exchange interaction between the Mn magnetic moments. The derived *sp*-band-Mn-*d* and Mn-Mn exchange constants present smaller values than in bulk diluted magnetic semiconductors [14]. Nanocrystals with an extra electron, i.e. charged quantum dots, are also considered.

**References:**

[1] Y. Wang and N. Herron, J. Phys. Chem. **95** (1991) 525
[2] J. Pérez-Conde and A.K. Bhattacharjee, Solid State Communications, **110** (1999) 259
[3] Y. Wang *et al.*, Solid State Communications, **77** (1991) 33
[4] R.N. Bhargava *et al.*, Physical Review Letters, **72** (1994) 416
[5] V. Albe *et al.*, Physical Review B, **57** (1998) 8778
[6] S.C. Erwin *et al.*, Nature, **436** (2005) 91
[7] G. Schmid *et al.*, *Nanoparticles: From Theory to Application,* WILEY, Weinheim, 2004
[8] D.M. Hoffman *et al.*, Solid State Communications, **114** (2000) 547
[9] D.J. Norris *et al.*, Nano Letters, **1** (2001) 3
[10] A.K. Bhattacharjee and J. Pérez-Conde, Physica Status Solidi B, **241** (2004) 672
[11] L. Besombes *et al.*, Physical Review Letters, **93** (2004) 207403
[12] T. Gurung *et al.*, Journal of Applied Physics, **96** (2004) 7407
[13] X. Huang *et al.*, Physical Review Letters, **94** (2005) 236801
[14] B.E. Larson *et al.*, Physical Review B, **37** (1988) 4137

# Recrystallization of bacterial surface layers: how fast S-proteins self assemble to build 2-D nanobiostructures

*Aitziber Eleta[1], Susana Moreno-Flores[1], Mihaela Delcea[1], Dietmar Pum[2], Uwe B. Sleytr[2] and José Luis Toca-Herrera[1]*

[1]Biosurfaces Unit, CICbiomaGUNE, Paseo Miramón 182, Parque Tecnológico de San Sebastián, 20009 San Sebastián (Gipuzkoa), Spain
[2]Center for Nanobiotechnology, BOKU, Gregor-Mendel Str. 33, 1180 Vienna, Austria

*eleta@cicbiomagune.es ; jltocaherrera@cicbiomagune.es*

Crystalline monomolecular cell surface layers, S-layers, are one of the most common outermost cell envelope components of the prokaryotic organisms (bacteria and archaea). They are composed of a single protein or glycoprotein and exhibit oblique, square or hexagonal (nano)lattice symmetry. Due to this fact, in the last fifteen years much effort has been focused on two directions in nanobiotechnology [1-2]: i) the recrystallization of (truncated) S- proteins on different substrates [3-8] and ii) genetic modification of S-protein with biomolecules (such as streptavidin or green fluorescence molecule) [9-10]. Both research lines are intimacy interconnected, since good recrystallization conditions assure the necessary know-how to build biosensors composed of a biological matrix made up of S-layers that hosts spatially well oriented molecules.

In this work we are presenting the first results on the kinetics of the recrystallization of the S-protein SbpA on different supports: silicon oxide, silane, polyelectrolyte, and thiol substrates. We will show that adsorption kinetics does not only depend on the protein concentration but also on the substrate chemistry.

Atomic force microscopy (AFM) was used to investigate the 2-D structure of the protein layer. Quartz microbalance (QCM) and surface plasmon resonance (SPR) were used to investigate the adsorption kinetics of the S-proteins.

These results are the first results up to date that monitore the building of robust biomimetic surfaces, either a native bacterial surface or a more advanced nanostructured functional surface that mimics the behaviour of biomolecules at the nanoscale.

**References:**
[1] U. B. Sleytr, E. M Egelseer, N. Ilk, D. Pum, and B. Schuster, *FEBS* J 274 (2007) 323
[2] U. B. Sleytr, M. Sara, D. Pum, B. Schuster, *Progress in Surface Science*, **68** (2001) 231
[3] U. B. Sleytr, P. Messner, D. Pum, M. Sára, *Angew. Chem. Intern. Ed.* 38 (1999) 1034
[4] E. *G*yörvary, O. Stein, D. Pum, U. B. Sleytr, *J. Microscopy* 202 (2003) 300
[5] J. L. Toca-Herrera, S. Moreno-Flores, J. Friedmann, D. Pum and U. B. Sleytr
*Microsc. Res. Techn.* 65 (2004) 226
[6] J. L. Toca-Herrera, R. Krastev, V. Bosio, S. Küpcu, D. Pum, A. Fery, M Sara and U. B. Sleytr , *Small* 1 (2005) 339
[7] A. Martin-Molina, S. Moreno-Flores, E. Perez, D. Pum, U. B. Sleytr, and J. L. Toca-Herrera, *Biophysical J.* 90 (2006) 1821
[8] V. Saravia, S. Küpcü, M. Nolte, C. Huber, D. Pum, A. Fery, U.B. Sleytr, and J. L. Toca-Herrera, *Journal of Biotechnology* in press
[9] Dieter Moll, Carina Huber, Birgit Schlegel, Dietmar Pum, Uwe B. Sleytr, and Margit Sára, *PNAS* 99 (2002)14646
[10] Völlenkle, C., S. Weigert, N. Ilk, E. M. Egelseer, V. Weber, F. Loth, D. Falkenhagen, U. B. Sleytr, M. Sára, *Appl. Environ. Microbiol. 70*, (2004) 1514
[11] J. L. Toca-Herrera, S. Küpcü, V. Diederichs, G.moncayo, D. Pum, and U. B. Sleytr
Biomacromolecules 12 (2006) 3298

# GPAW: REAL-SPACE IMPLEMENTATION OF PROJECTOR AUGMENTED WAVE METHOD

*Jussi Enkovaara[1], J. J. Mortensen[2], K. W. Jacobsen[2]*
*[1]CSC – Scientific Computing, P.O. Box 405, FI-02101 , Espoo, Finland*
*[2]Department of Physics, Technical University of Denmark, DK-2800 Kgs Lyngby, Denmark*
*jussi.enkovaarat@csc.fi*

Electronic structure calculations have become valuable tool for materials specific simulations of nanostructures. One of the most succesful frameworks for electronic structure calculations is the density functional theory. We have developed a program package GPAW [1] for density functional calculations using real-space grids together with the projector augmented wave method [2]. The wave functions, densities and potentials are represented on three dimensional uniform real-space grids and a finite difference discretization is used for the Laplacian. Real-space description allows flexible boundary conditions, efficient multigrid algorithms, and efficient parallelization with domain decomposition. However, the wave functions vary rapidly near the nuclei which makes their description on a uniform grid difficult. This problem is solved in projector augmented wave method where accurate all-electron calculations can be performed with smooth wave functions.

We demonstrate the accuracy of the method by calculating atomization energies and bond lengths of small molecules as well as by calculating lattice constants and bulk moduli of some bulk systems. We present also examples about the performance and the parallel scaling of the program. We discuss some future prospects of the method, especially the currently on-going implementation of time-dependent density functional theory

## References

[1] J. J. Mortensen, L. B. Hansen, and K. W. Jacobsen, Phys. Rev. B 71, 035109 (2005)

[2] P. Blöchl, Phys. Rev. B 50, 17953 (1994)

# SIMULATION OF NANOTUBE-BASED NEMS CONTROLLED BY NONUNIFORM ELECTRIC FIELD

*O.V. Ershova*[±], *A.M. Popov*[\*], *Yu.E. Lozovik*[\*], *O.N. Bubeĺ*[^], *E.F. Kislyakov*[^], *N.A. Poklonskí*[^],
*A.A. Knizhnik*[#], *I.V. Lebedeva*[+]

[+]*Moscow Institute of Physics and Technology, 141700, 9, Institutskii per., Dolgoprudny, Moscow Region, Russia*
[\*]*Institute of Spectroscopy, 142190, Troitsk, Moscow Region, Russia*
[^]*Belorusian State University, 220030, 4, Nezavisimosti Ave., Minsk, Belarus*
[#]*Kurchatov Institute, 123098, 1, Kurchatova Square, Moscow, Russia*
*cantik_jelita@mail.ru*

The set of nanoelectromechanical systems (NEMS) based on relative motion of the walls of nanotubes has been suggested recently [1-3]. Thus elaboration of methods to control the motion of nanotube walls is an actual problem of nanomechanics.

We propose new method to control the motion of nanotube-based NEMS. It is based on the chemical adsorption of atoms and molecules on the open edges of the single-walled carbon nanotube, which results in the appearance of electric dipole moment. In this case the functionalized nanotube can be actuated by non-uniform electric field. Semi-empirical method of molecular orbitals with PM3 parameterization of Hamiltonian [4] has been used to calculate the electric dipole moments of functionalized (5,5) nanotubes [5].

Potential of the proposed method of controlling the motion of nanotube-based NEMS is demonstrated by the example of the gigahertz oscillator based on relative sliding of carbon nanotube walls. The scheme, operational principles and theory of such oscillator were considered recently [2]. The molecular dynamics simulations show that the Q-factor of the gigahertz oscillator is about $Q = 100–1000$ and the frequency of its free vibrations increases with time [3]. Therefore to keep constant frequency of oscillator it is necessary to compensate the energy dissipation by an external force. Here we consider the possibility to compensate the energy dissipation by application to the movable wall of the control force $F(t) = F_0 \cos \omega t$, where $\omega$ is the desirable oscillation frequency. The analysis of the energy balance shows that the critical amplitude $F_0^{cr}$ of control force which is necessary for the exact loss compensation is the smallest in the case of the oscillator with the walls of the same length and equals to $F_0^{cr} = \pi F_W/32Q$, where $F_W$ is the force retracting the inner wall into the outer one. If the amplitude $F_0$ greater than $F_0^{cr}$, the stationary mode of operation with constant frequency is possible. For the functionalized (5,5) nanotubes [5] the amplitude $F_0^{cr}$ is estimated to be 0.1–1 pN. The voltage 2–10 V is sufficient to apply such force to the wall in a cylindrical or spherical capacitor. The parameters of the system and control forces enabling to obtain the stationary operation are determined by the analysis of the equation of motion. We have found that oscillation amplitude is varied with time since the switching on of the control force and the stationary mode of operation is achieved in tens nanoseconds (see Fig.1). The dependencies of the parameters which characterize the establishment of the stationary mode on the amplitude $F_0$ and Q-factor are obtained. At the stationary mode the phase shift $\Delta\varphi$ between control force $F(t) = F_0 \cos \omega t$ and oscillation amplitude $A(t) = A_0 \cos(\omega t - \Delta\varphi)$ has been established so that the oscillation energy dissipation is exactly compensated by the work of the control force (see Fig.2). The condition $F_0 \geq F_0^{cr}$ of the possibility of the stationary mode is obtained for the case where the phase shift $\Delta\varphi = 0$ and the frequency $\omega$ of the control force coincides with the initial oscillation frequency $\omega_0$ at the moment of control force switching on. The start conditions where the stationary mode is possible are shown on Fig. 3.

We perform the molecular dynamics simulations of (5,5)@(10,10) nanotube-based oscillator and have found the considerable Q-factor fluctuations. The influence of the Q-factor

fluctuations on the parameters of the system and control forces enabling to obtain the stationary operation is studied.

**References:**

[1] Yu.E. Lozovik, A.G. Nikolaev, and A.M. Popov, JETP, **103** (2006) 447.
[2] Q. Zheng and Q. Jiang, Phys. Rev. Lett., **88** (2002) 045503.
[3] Y. Zhao, C.-C. Ma, G. Chen and Q. Jiang, Phys. Rev. Lett., **91** (2003) 175504.
[4] J.J.P. Stewart, J. Comp. Chem., **10** (1989) 209.
[5] A.M. Popov, Y.E. Lozovik, O.V. Ershova, O.N. Bubel', E.F. Kislyakov, N.A. Poklonski, Physics, Chemistry and Application of Nanostructures: Reviews and Short Notes to Nanomeeting-2007, Minsk, 22–25 May 2007 / Ed. by V.E. Borisenko, S.V. Gaponenko, V.S. Gurin (Singapore: World Scientific, 2007) P. 581.

**Figures:**
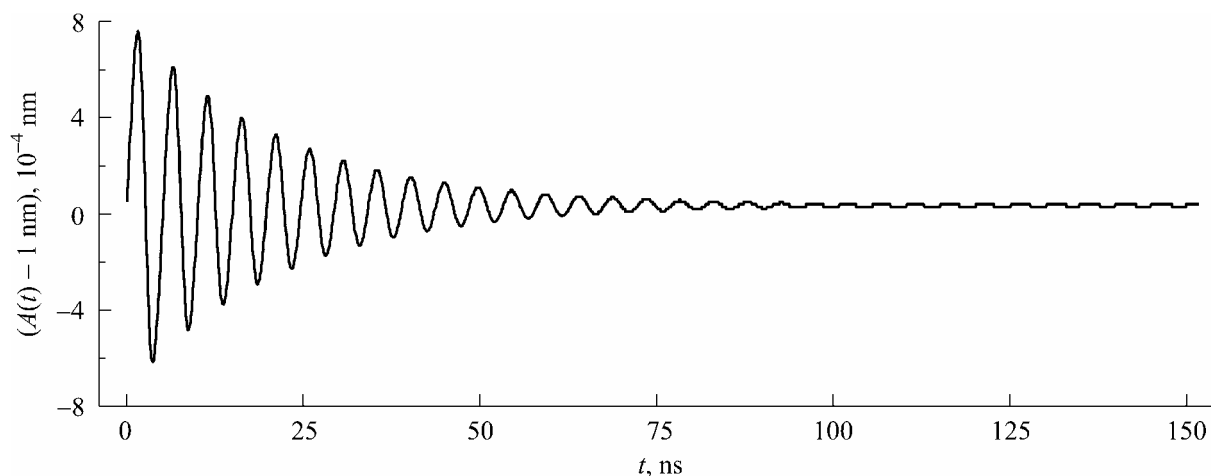


Fig. 1. Dependence of the oscillation amplitude on the time since the switching on of the control force with the amplitude $F_0 = 1.01 F_0^{cr}$ for the system with $Q = 1000$
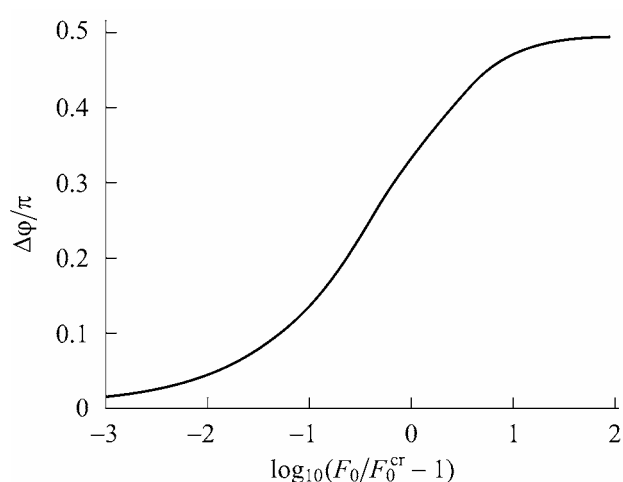




Fig. 2. Phase shift at the stationary mode between the control force and the oscillation amplitude as a function of $\log_{10}(F_0/F_0^{cr} - 1)$
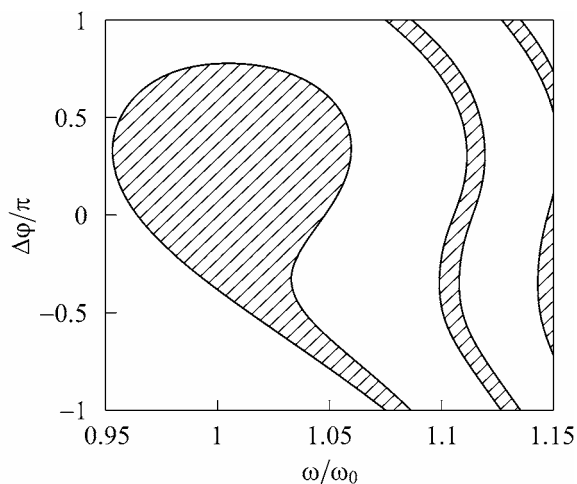
Fig. 3. Start phase shift $\Delta\varphi$ and the frequency ratio $\omega/\omega_0$ where the stationary mode is possible in the case of system with $Q = 100$ and control force amplitude $F_0 = 2F_0^{cr}$ are hatched

# SELF-SUSTAINED CURRENT OSCILLATIONS IN A MULTIQUANTUM WELL SPIN POLARIZED STRUCTURE WITH NORMAL CONTACTS

*R. Escobedo*[1], *M. Carretero*[2], *L. L. Bonilla*[2], *G. Platero*[3]

[1]*Dpto. Matemática Aplicada, Universidad de Cantabria, 39005 Santander – Spain*
[2]*Modeling, Simulation and Industrial Mathematics Group,*
*Universidad Carlos III de Madrid, 28911 Leganés, Madrid – Spain,*
*and Unidad asociada al  Instituto de Ciencias de Materiales, CSIC, Spain*
[3]*Instituto de Ciencia de Materiales de Madrid, CSIC, 28049 Cantoblanco, Madrid –  Spain*

*escobedo@unican.es*

We analyze nonlinear electron spin dynamics of a n-doped dc voltage biased semiconductor I-VI multi-quantum well structure (MQWS) having one or more of its wells doped with Mn.

Even if normal contacts have been attached to this nanostructure, spin polarized current can be obtained provided one well is doped with magnetic impurities.

We have studied the conditions for the system to exhibit static electric field domains and stationary current or moving domains and time-dependent oscillatory current.

There are self-sustained current oscillations (SSCO) for nanostructures with four or more QWs. Moreover, SSCO may appear or not depending on the spin splitting induced by both, the exchange interaction and the external magnetic field. We calculate the minimal doping density needed to have SSCO, which is crucial to design a device behaving as a spin polarized current oscillator.

**References:**

L. L. Bonilla, J. Phys.: Cond. Matter **14** (2002) 341.
D. Sánchez, A. H. MacDonald, G. Platero, Phys. Rev. B **65** (2001) 035301.
M. Béjar, D. Sánchez, G. Platero, A. H. MacDonald, Phys. Rev. B **67** (2003) 045324.
H. Kroemer, Proc. IEEE **52** (1964) 1736
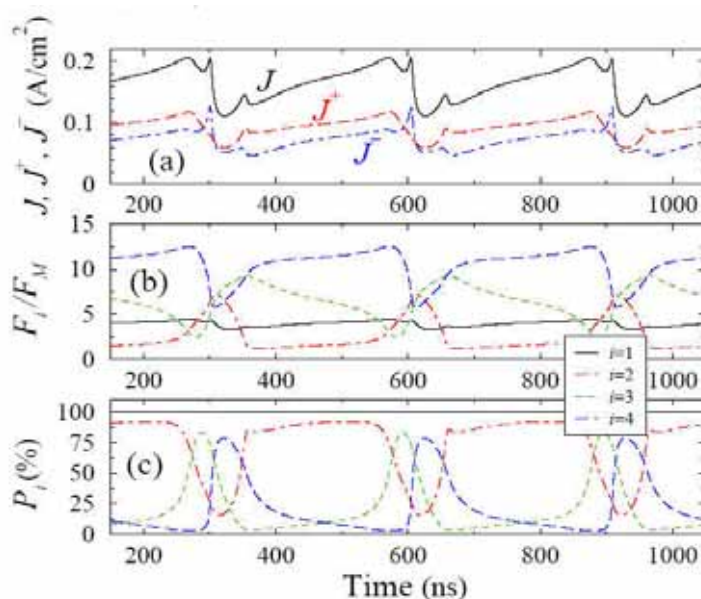
(a) Tunneling current (b) electric field and (c) polarization in a MQWS with 4 wells

# Magnetic Surface Microscopy and Pattern Formation in Ferromagnetic Films

*A. Zolanvari, <u>A. Fathi</u>*
*Department of Physics, University of Arak,  P.O. Box: 38156-879, Arak, IRAN*

Magnetic materials display a complex variety of patterns and singular structures on many different length scales. The way such patterns form and evolve in time is vitally important for many key technologies related to sensors, memories and recording devices where particularly magnetic thin films offer them in practice. Very recently strong interest in magnetic films stems from their combination with semiconductor elements in view of hybrid devices for future spin electronics, a rapidly developing new technology. A widely accepted theoretical framework for ferromagnetism is based on a continuum model due to Landau and Lifshitz. Within their theory, a universal energy functional, the micromagnetic energy, that captures in principle magnetic phenomena on every relevant length scale, including the coarse domain structures as well as fine substructures of domain walls and their mutual interaction. Mathematically, the formation of these patterns and structures is driven by the interplay of non-convexity and non-locality due to the coupling with Maxwell's equations. In practice, however, the general model is by far to complex in order to extract interesting predictions or to effectively perform suitable computations in high resolution. Hence there is a need for suitable reduced or effective models that capture specific features in parameter regimes of specific interest. The morphology of films grown by molecular beam epitaxy varies widely depending on how effectively the roughness induced by the random nature of the impinging atom flux is counterbalanced by a smoothing process resulting from the mobility of the atoms diffusing on the surface. We investigated multilayer homoepitaxial growth of ferromagnetic film surface at room temperature and measured the homoepitaxial growth at room temperature using STM. An efficient dynamic description of magnetic patterns, however, requires in the first place the derivation of the effective dynamics of micromagnetic singularities like sharp domain walls and vortices. It remains a challenge in the context of reduced models for magnetic thin films: If, for a soft material, the dimensions of the specimen are much larger than the single-domain wall, closed-flux magnetizations with vanishing stray-field, somewhat comparable with velocity fields in hydro-dynamics, are favored. We will investigate the gradient flow associated to a divergence constrained model from the gradient theory of phase transitions.

**References:**

[1] C. Melcher, Physica D 192 (2004).

[2] C. Melcher, Commun. Part. Diff. Eqn., 30 (5) (2005).

[3] R. Engel-Herbert and J. Mohanty and A. Ney and T. Hesjedal and L. Däweritz and K. H. Ploog, Appl. Phys. Lett., 84 (7) (2004).

# GROWTH OF TTF-TCNQ ON METAL SURFACES

I. Fernández-Torrente[1], S. Monturet[2], K.J. Franke[1], N. Henningsen[1], J. Fraxedas[3] , N. Lorente[2] and J.I. Pascual[1]

[1]Freie Universität Berlin, Arnimallee 14, D-14195 Berlin, Germany.
[2] Université Paul Sabatier, Toulouse, France.
[3] ICMAB CSIC, CampusUAB, Bellaterra, Spain.

Molecular charge transfer (CT) complexes are defined as the association of electron donor and electron acceptor molecules. The self-assembling properties of molecules open the possibility of building different donor-acceptor stacking structures which rule the electronic funcionality of the compound. Tetrathiafulvalene 7,7,8,8-tetracyanoquinodimethane (TTF-TCNQ) is a well-known example of a CT complex which shows a metal conducting behaviour at Room Temperature. The stacking of TTF and TCNQ forms in bulk one-dimensional partially occupied energy bands that gives rise to the metallicity. By means of Low Temperature Scanning Tunneling Microscopy/Spectroscopy we have characterised for the first time the mixed growth of TTF and TCNQ on a metallic surface in submonolayer and monolayer regimes. The self-assembled growth is governed by donor-acceptor recognition. In particular a one dimensional phase with alternating lines of TTF and TCNQ is formed and can be considered as the precursor stage for the bulk structure. A new phase, not existing in solid state has been additionally found having a 2:1 stoichiometry. This new phase tuned out to dominate in the regime of higher coverage frustrating that a linear phase can be grown beyond the first monolayer. By Scanning Tunneling Spectroscopy we associate electronic resonances with the Highest Occupied Molecular Orbital (HOMO) and the Lowest Unoccupied Molecular Orbital (LUMO) of TTF and TCNQ and the self-assembled TTF-TCNQ. In the mixed phase the electronic configuration of TCNQ is strongly modified by the presence of TTF.

# UNSTRAINED MAGNETOSTRICTIVE FE$_{80}$B$_{20}$ FILMS FOR MEMS/NEMS ACTUATORS.

*I. Fernández-Martínez* and *F. Briones*

*Instituto de Microelectrónica de Madrid, IMM-CNM-CSIC, Isaac Newton 8 PTM, 28760 Tres Cantos, Madrid, Spain*

*ivan@imm.cnm.csic.es*

Magnetic thin films with large magnetostriction constant and low intrinsic stress are demanded for magnetically actuated MEMS and NEMS [1,2]. Amorphous Fe$_{80}$B$_{20}$ thin films are adequate candidates for MEMS operating in liquids, due to their low anisotropy and high magnetostriction, together with their excellent adhesion, stability and corrosion resistance properties. However, residual deposition stress for sputtered amorphous thin films tends to be large and causes undesirable bending or distortion of cantilevers and actuators. On the other hand, strain effects modify strongly magnetic anisotropy and consequent magnetic field dependent properties.

Therefore, a study on the sputtering conditions dependence of deposition induced strain for Fe$_{80}$B$_{20}$ amorphous has been carried out using an in-situ, real time, highly sensitive optical method monitoring substrate curvature. Results allow us to optimize mechanical and magnetic properties by controlling deposition parameters. In this way, nearly unstrained Fe$_{80}$B$_{20}$ amorphous alloy films have been grown by DC triode sputtering on glass substrates.

Our triode sputtering operates under a wide range of Ar sputtering pressures ($1 \times 10^{-3}$– $2.5 \times 10^{-2}$ mbar) and cathode voltages in the 0.5-2kV range, thus allowing to determine the influence of impinging atoms energy on thin film stress evolution during deposition. Main intrinsic stresses were compressive and related to local distortion induced by energetic particles striking the film (ion peening mechanism). A significant stress generated at the film-substrate interface during the early stages of growth (initial 2.5nm) we also observe. Finally, it is shown how the total residual film strain can be controlled by varying Fe80B20 target potential or by energetic particles thermalization by gas-phase collisions under enough gas pressures (Fig 1), and consequently totally unstrained films have been achieved.

To demonstrate the feasibility of using magnetostrictive in micrometer-scale and on fast time acting actuators scales, a path-stabilized Michelson interferometer was used to detect displacements of a GaAs microcantilever coated with amorphous Fe$_{80}$B$_{20}$ when an alternating magnetic field was applied (Fig 2). Results are discussed in view of the optimized magnetic properties which allow magnetic operation at high frequencies.

## References:

[1] A. Ludwig and E. Quandt, J. Appl. Phys. **87**, 4691 (2000).
[2] K.L.Ekinci , Small **1**, 786 (2005).

*Figure 1: Total accumulated stress in function of cathode voltage. Optimal conditions for near-zero stress is achieved below 1kV cathode voltage, at a sputtering pressure of $8*10^{-3}$ mbar.*
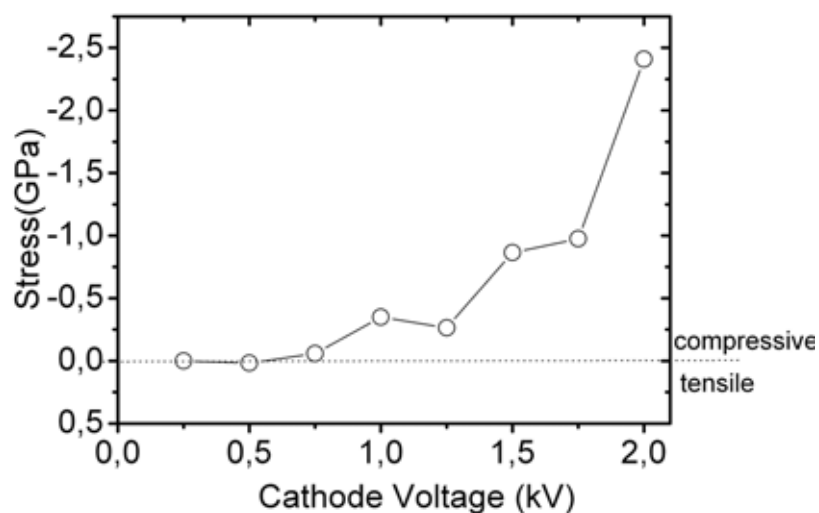




*Figure 2: Left: SEM picture of GaAs microcantilever sputter coated with amorphous $Fe_{80}B_{20}$ film. Right: Fundamentalmagnetically actuated flexural resonance of a 20 $\mu$m long and 200nm thick beam measured in air by optical interferometric displacement detection .*
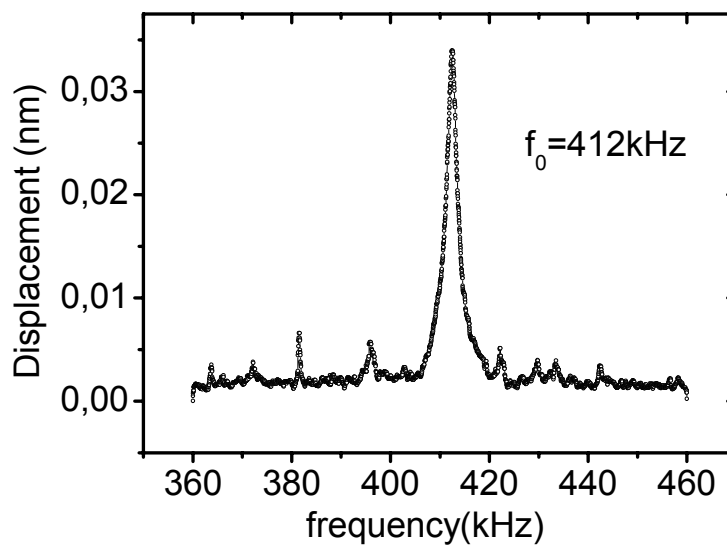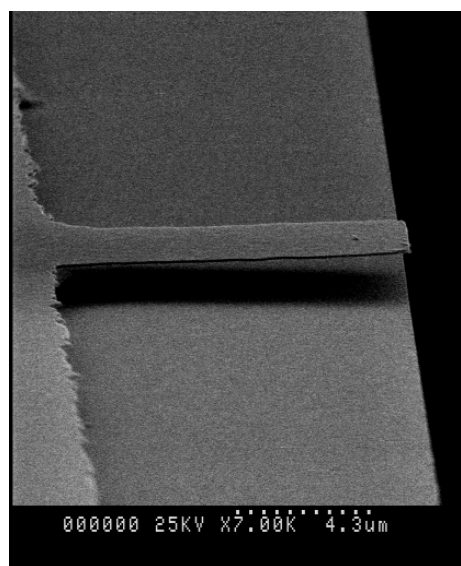
# SELF-ASSEMBLY OF SILICIDE QUANTUM DOTS ON STEPPED SILICON SURFACES BY REACTIVE EPITAXY

Laura Fernández[1], Mathias Löffler[2], Javier Cordón[2] , Enrique Ortega[1,2,3].

[1]Departamento de Física Aplicada I, Universidad del País Vasco. Plaza de Oñate 2, E-20018 San Sebastián, Spain.
[2]Lehrstuhl für Festkörperphysik, Staudtstrasse 7, D-91058 Erlangen, Germany
[3]DIPC, P.Manuel de Lardizabal 4, E-20018 San Sebastián, Spain.
[4]Unidad de Física de Materiales, Centro Mixto CSIC-UPV/EHU, P.Manuel de Lardizabal 3, E-20018 San Sebastián, Spain.

**Abstract:**

Reactive epitaxy of Co on vicinal Si(111) surfaces is found to be a flexible and convenient method for the preparation of a dense array of Co silicide quantum dots. The motivation of this study is the technological interest in transition metals silicide that can be used as low-resistivity interconnects and future nanoscale contacts. In the present work, submonolayer amounts of Co were deposited on diverse vicinal and flat Si surfaces, analysing the resulting silicide structure by scanning tunnelling microscopy. The use of vicinal Si(111) surfaces with a narrow terrace width of around 40 Å is found to be the key for the formation of self-assembled silicide quatum dots with a regular size and distribution function. This situation contrasts with the growth of Co found on flat Si(111), where nanocluster structures are notably scarce and multiple phases are found.

# SIZE-CONTROLLED BIMAGNETIC FEPT/IRON OXIDE HYBRID NANOCRYSTALS: ONE-POT SYNTHESIS, STRUCTURAL-MAGNETIC CHARACTERIZATION AND POTENTIAL APPLICATIONS IN BIOMEDICINE

*Albert Figuerola,[a] Cinzia Giannini,[b] Andrea Falqui,[c] Maurizio Corti,[d]*
*Roberto Cingolani,[a] Teresa Pellegrino,[a] Davide Cozzoli,[a] Liberato Manna [a]*
*[a]National Nanotechnology Laboratory of CNR Distretto Tecnologico ISUFI Via per Arnesano Km.5 73100 Lecce (Italy), [b] CNR-Istituto di Cristallografia (IC) Via Amendola 122/D 70126 Bari (Italy), [c]Institut National de Sciences Appliqueés – INSA Departement de Genie Physique 135 Avenue de Rangueil 31077 Toulouse Cedex 4 (France), [d]Dip. di Fisica "A. Volta" Via Bassi 6 27100 Pavia (Italy)*
*albert.figuerola@qi.ub.es*

Developments in wet-chemical approaches to inorganic nanostructures have opened access to finely size and shape controlled nanocrystals (NCs) of a variety of semiconductor, metal and magnetic materials. Considerable advances in the preparation of structurally complex NCs in liquid media have been recently devised with the synthesis of first prototypes of colloidal hybrid nanocrystals (HNCs), in which multiple material domains are assembled together in a unique particle via epitaxial interfaces [1]. The ability to control the topological distribution of the chemical composition in colloidal nanoheterostructures is among the most challenging goals of current nanochemistry research. HNCs hold promise as novel generations of revolutionary nanoscale building blocks, to which the coexistence of different chemical-physical properties (e.g., luminescence, magnetism, and catalytic activity) naturally attributes multifunctionality and unprecedented chemical-physical behavior, as compared to that exhibited by the individual components alone [2-5].

In this contribution, we present a step further in this field, demonstrating a facile one-pot approach of a novel type of noncentrosymmetric bimagnetic HNCs with tailorable geometric parameters. We show seedless, surfactant-assisted synthesis to prepare dimer-like HNCs, individually comprising one "hard" FePt and one "soft" iron oxide magnetic section, both of which are size-tunable in the 3-20 nm range. Our strategy allows one to control the nucleation and growth stages for each material domain separately by temperature-programmed heating of a suitable mixture containing all the necessary molecular precursors and organic stabilizers. The influence of various reaction parameters on the structural-compositional features of the final FePt-iron oxide heterodimers, such as the relative reactant to ligand molar ratio, their absolute concentrations, and the temperature modulation, has been examined in detail by a combination of powder XRD Diffraction measurements, ICP and EDS elemental analyses, and HRTEM investigations.

The size-related magnetic properties of the HNCs and the involved magnetic exchange coupling have been disclosed by temperature and field-dependent measurements with a SQUID magnetometer. The control over the absolute and relative sizes of the two materials in the heterostructure allows the synthesis of several nanosystems with a wide rage of magnetic properties.

Superparamagnetic nanoparticles suspensions, also known as *ferrofluids*, have been shown to be useful as multifunctional tools in biomedical applications.[6] Both diagnosis and therapeutic functions can be achieved due to the magnetic response of the ferrofluid during its exposure to an external magnetic field. Their main advantatges are the absence of residual magnetization in the fluid after the removal of the field, avoiding possible undesired tissue damages or nanoparticles aggregation, and the potential magnetic addresing of the ferrofluid

to a specific tissue that would allow injection of minor doses of either inorganic material and/or chemotherapeutic drugs and would simultaneously decrease further collateral effects in healthy tissues. Relaxivity ($T_1$ and $T_2$) measurements have been also complemented to verify the potential of these FePt/iron oxide bimagnetic HNCs as magnetic resonance contrast agents.

**References:**

[1] P. Davide Cozzoli, Teresa Pellegrino, Liberato Manna, *Chem. Soc. Rev.*, **35** (2006) 1195.

[2] Hyungrak Kim, Marc Achermann, Laurent P. Balet, Jennifer A. Hollingsworth, Victor I. Klimov, *J. Am. Chem. Soc.*, **127** (2005) 544.

[3] a) Raffaella Buonsanti, Vicenzo Grillo, Elvio Carlino, Cinzia Giannini, Maria Lucia Curri, Claudia Innocenti, Claudio Sangregorio, Klaus Achterhold, Fritz Günter Parak, Angela Agostiano, P. Davide Cozzoli, *J. Am. Chem. Soc.*, **128** (2006) 16953. b) Marianna Casavola, Vicenzo Grillo, Elvio Carlino, Cinzia Giannini, Fabia Gozzo, Enrique Fernandez Pinel, Miguel Angel Garcia, Liberato Manna, Roberto Cingolani, P. Davide Cozzoli, *Nano Lett.*, **7** (2007) 1386.

[4] a) Dmitri V. Talapin, Robert Koeppe, Stephan Götzinger, Andreas Kornowski, John M. Lupton, Andrey L. Rogach, Oliver Benson, Jochen Feldmann, Horst Weller, *Nano Lett.*, **3** (2003) 1677. b) Hao Zeng, Jing Li, Z. L. Wang, J. P. Liu, Shouheng Sun, *Nano Lett.*, **4** (2004) 187.

[5] Teresa Pellegrino, Angela Fiore, Elvio Carlino, Cinzia Giannini, P. Davide Cozzoli, Giuseppe Ciccarella, Marc Respaud, Luca Palmirotta, Roberto Cingolani, Liberato Manna, *J. Am. Chem. Soc.*, **128** (2006) 6690.

[6] Venkatasubramaniam S. Kalambur, Bumsoo Han, Bruce E. Hammer, Thomas W. Shield, John C. Bischof, *Nanotech.*, **16** (2005) 1221.

**Figures:**
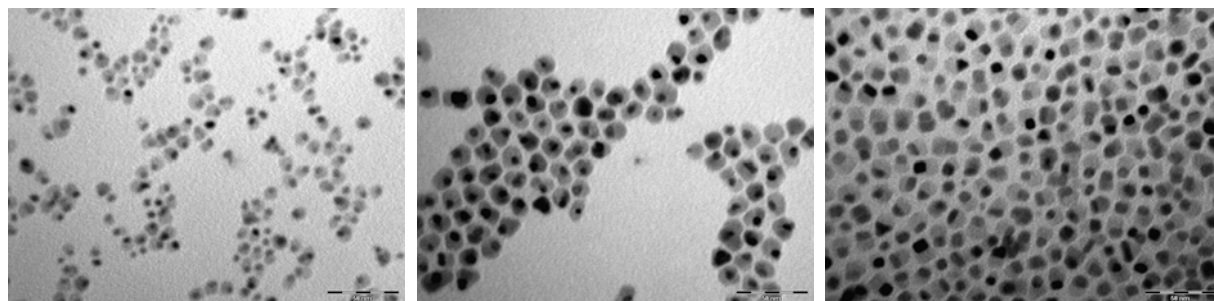
**Bioinspired nano-architectures based on chemically functionalized carbon nanotubes**

*I. Firkowska, S. Giannona, JA. Rojas-Chapana and M. Giersig*
Research Center CAESAR, Ludwig-Erhard-Allee 2, 53175 Germany
*firkowska@caesar.de*

Bio-nanotechnology is a branch of nanoscience that uses cellular basic building blocks or molecular design principles together with man-made nanomaterials for creating composites with life-science applications. The fact that the dimensions of man-made nanomaterials are analogous to those of natural biological materials greatly facilitates their development and the path to product application. Thus, the convergence between materials science and biomedicine enables the design of new devices that could play a central role in drug delivery or tissue engineering.

In the field of tissue engineering, carbon nanotubes (CNTs) are among the technologically most interesting nanoscale materials currently under investigation for medical application. CNTs are mechanically tough, chemically inert, and highly conductive and they are pure carbon. It is particularly noteworthy, that their diameters of molecular dimensions, and their potential for bio-interfacial engineering make them highly attractive tools for cell scaffold design.

Our research is mainly focused to reproduce at least partially, both the exceptional nanotopography and nanochemistry presented on the extracellular matrix (ECM) of bone utilizing for this purpose NSL technique combined with the layer-by-layer (LBL) assembly process. The complete network architecture consists of successive layers of cross-linked carbon nanotubes that self-assemble into orderly structures (Fig.1). The method enables controlled shaping and considerable chemical and mechanical stability of the self-assembled monolayers, allowing for high reproducibility in manufacturing. The films as free-standing substrates are characterized by controlled geometry, surface topography, and chemical composition (1).

To address the role of nano-sized features in complex nanostructured substrates, both texture and surface roughness of free-standing films were tested for their ability to promote cell growth. For these experiments, osteoblast-like cell were seeded onto nanostructured films to evaluate cell viability and proliferation (Fig. 2). The osteoblast cells were found to be viable in all nanostructured films. Remarkably, cells showed enhanced proliferate response to the interconnected nanotubes and nano-sized cavities.

We have further studied the biocompatibility of LBL film made up of CNTs modified by acids and polymer wrapping with Poly(allylamine hydrochloride)(PAH). Figure 3 shows fluorescent microscopy images of cells on the CNT-based nanostructures with carboxylate (Fig. 3A) and ammonium groups (Fig. 3B) after 7 days incubation and further labelled with luminescence probe. This clearly demonstrates the striking difference between the cell's adhesion and proliferation on differently functionalized carbon nanotubes. This observation indicates that the polymer-modified nanotube-based films support growth and proliferation of osteoblast cells. Solely for polyelectrolyte multilayer film made from PAH a very small number of cells were observed (not shown). The latter experiment reveals that CNTs significantly contribute to the biocompatible nature of the film, which can probably be attributed to the mechanical and structural properties of carbon nanotubes.

**References:**

[1] Firkowska I. et.al. ,Langmuir (2006), 5427- 34.

**Figures:**
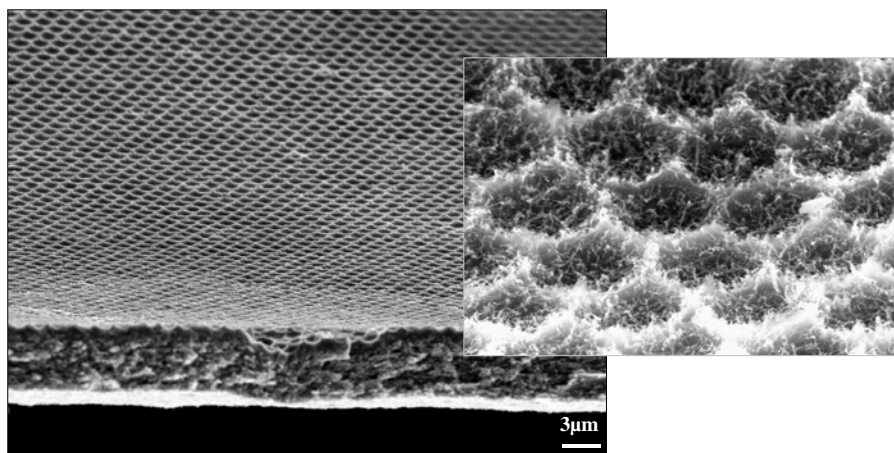


Fig. 1. SEM image showing a bioinspired free-standing substrate made up of carbon nanotubes arranged in a regular network of micro-cavities.
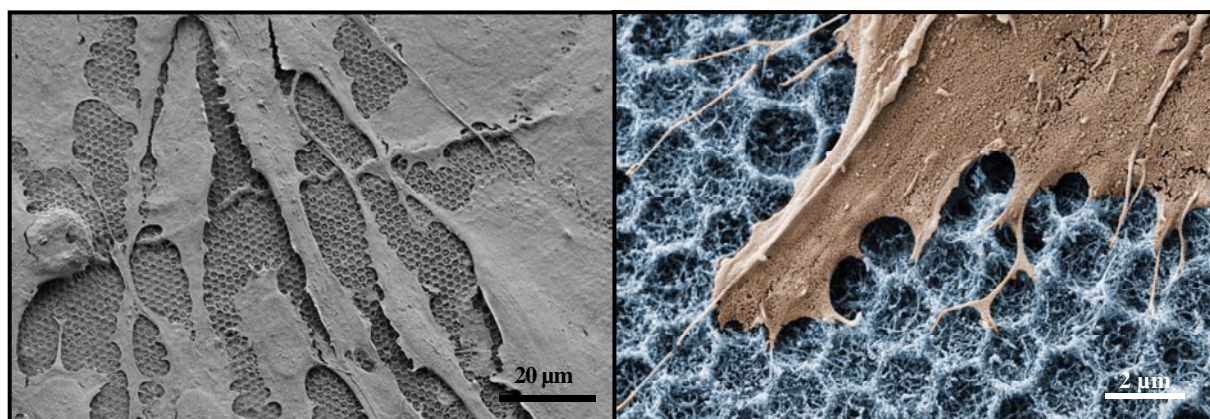


Fig. 2. SEM image depicting cell growth of osteoblast- like cells on bioinspired CNT-based substrates.
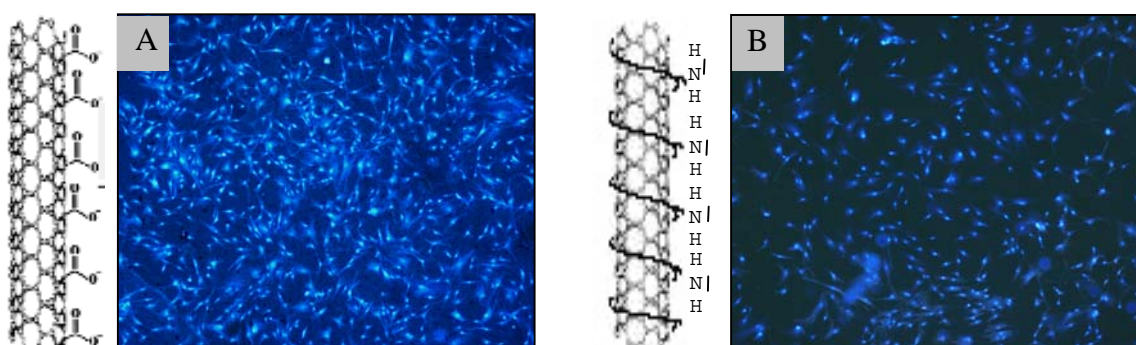


Fig. 3. Digital camera images showing the difference in the number of osteoblast-like cells growing onto nanostructured substrate made up of CNTs functionalized with carboxylate (A) and ammonium groups (B).

# INELASTIC TRANSPORT THEORY FOR NANOSCALE SYSTEMS: LOCAL HEATING IN A Cu–C$_{60}$–Cu JUNCTION

*Thomas Frederiksen,[1,2] Mads Brandbyge[1]*
*[1] Department of Micro and Nanotechnology, NanoDTU, Technical University of Denmark*
*[2] DIPC – Donostia International Physics Center, Donostia – San Sebastián, Spain*
*email: thomas_frederiksen@ehu.es / thf@mic.dtu.dk*

When an electric current is passed through a nanoscale device – such as a single molecule or an atomic-size contact – the junction will heat up due to excitation of nuclear vibrations. In this presentation we describe results using a first-principles computational scheme for calculating conductance properties of nanoscale systems, taking into account inelastic scattering and energy dissipation [1]. The methods are based on a combination of density functional theory (DFT) and nonequilibrium Green's functions (NEGF) [1,2]. It involves quantitative calculations of electronic structure, vibrational modes and frequencies, electron-phonon (e-ph) couplings, and inelastic current-voltage characteristics in the weak e-ph coupling limit.

Specifically we consider the transport through individual C$_{60}$ molecules on a Cu(100) surface contacted with the tip of a scanning tunneling microscope (STM) [3]. As a model for the system we work with the supercell structure shown in Fig. 1. Depending on the tip-molecule distance we find that the conductance varies several orders of magnitude. In the tunneling regime the conductance varies exponentially with distance. In the contact regime, when the tip comes sufficiently close – and a bond is formed between the tip apex and the C$_{60}$ molecule – the conductance levels off to reach a plateau. In the transition region between these different regimes our calculations show how the conductance is affected by current-induced fluctuations that modulate the tip-molecule distance. From an analysis of the vibrational excitations we quantify the local heating and extract the bias-dependent effective temperature of the junction.

**References:**

[1] T. Frederiksen, M. Paulsson, M. Brandbyge, and A.-P. Jauho, Phys. Rev. B **75**, 205413 (2007).

[2] M. Brandbyge, J. L. Mozos, P. Ordejón, J. Taylor, and K. Stokbro, Phys. Rev. B **65**, 165401 (2002).

[3] N. Néel, J. Kröger, L. Limot, T. Frederiksen, M. Brandbyge, and R. Berndt, Phys. Rev. Lett. **98**, 065502 (2007).

**Figures:**
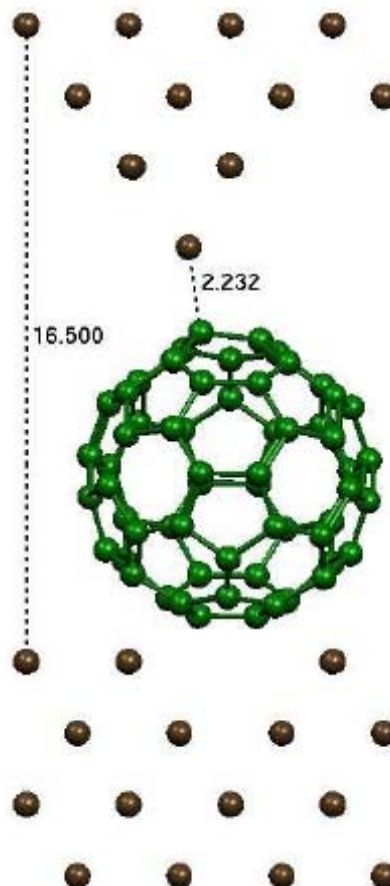


**Fig. 1:** Side view of the $C_{60}$-Cu(100) supercell used in the transport calculations.

# ELECTRICAL FIELD-INDUCED NANOLITHOGRAPHY OF THIN TA-C FILMS UNDER AMBIENT CONDITIONS

*<u>V.D. Frolov</u> [1], E.V. Zavedeev [1], V.A. Gerasimenko [1], S.M. Pimenov [1], H.-J. Scheibe [2]*

*[1] A.M. Prokhorov General Physics Institute, Vavilov str 38, Moscow 119991, Russia*
*[2] Fraunhofer Institute for Material and Beam Technology, Dresden, Germany*
*Contact e-mail: frolov@ran.gpi.ru*

We report on nanostructuring of tetragonal-bonded amorphous carbon (ta-C) films using a Scanning Probe Microscope (SPM)-based nanolithography technique. The original ta-C films were deposited on Si substrates by special pulsed vacuum arc techniques (Laser-Arco® process) as described elsewhere [1]. These amorphous, hydrogen-free carbon films, called as Diamor® films, are characterized by a high content of tetrahedral $sp^3$ bonds and high hardness that, along with their high smoothness and low adhesion activity to other materials, result in superior behavior concerning wear resistance and friction.

The Diamor® films of 85 nm thickness were further examined for the purpose of nanoscale modifications under the action of local electric field. The experiments were carried out in an air-operated SPM setup Solver P47 (NT-MDT Co., Russia) using conducting cantilevers coated with DLC layers as the probes for SPM actions in contact mode, and also for testing the samples in tapping mode before and after the actions. To induce the electric field underneath the probe, rectangular voltage pulses with the magnitude up to U=10 V and duration T= 10 ms – 5 s were applied between the sample and the grounded probe at given points of the scanned area. In the course of experiments, the ambient relative humidity (RH) was controllably changed in the range from 5% to 50%.

The obtained results can be summarized as follows. It is established that, above a threshold of U~5 V, the point actions lead to the formation of hill-like nanoprotrusions on the film surface. The nanoprotrusion is found to permanently grow in height with increasing voltage but tends to saturation in diameter (the diameter is 50-150 nm depending on the pulse duration). Experimental data on the nanoprotrusion height H fit in the formula $H=H_0 \cdot \log(T/T_0)$, where $H_0$ is a function of U, $T_0$ is the characteristic exposure (at $T=T_0$ $H=0$). It is particularly remarkable that $T_0$ is reversely proportional to RH; i.e. $H \rightarrow 0$ when RH$\rightarrow 0$. It means that the presence of absorbed water vapors on the ta-C film surface is the necessary condition of the nanolithography processing. The formed nanoprotrusions show a lower electrical conductivity as compared to the conductivity of the as-grown ta-C film.
The developed SPM-based process is highly reproducible that allowed us to draw images with the surface density of ~ $5 \times 10^{10}$ elements/cm$^2$ (Fig. 1). Possible mechanisms of SPM-based nanostructuring of the ta-C films will be discussed.

## References

[1] H. Schulz, H.-J. Scheibe, P. Siemroth, B. Schultrich, Appl. Phys. A, **78** (2004) 675–679.

**Figures:**
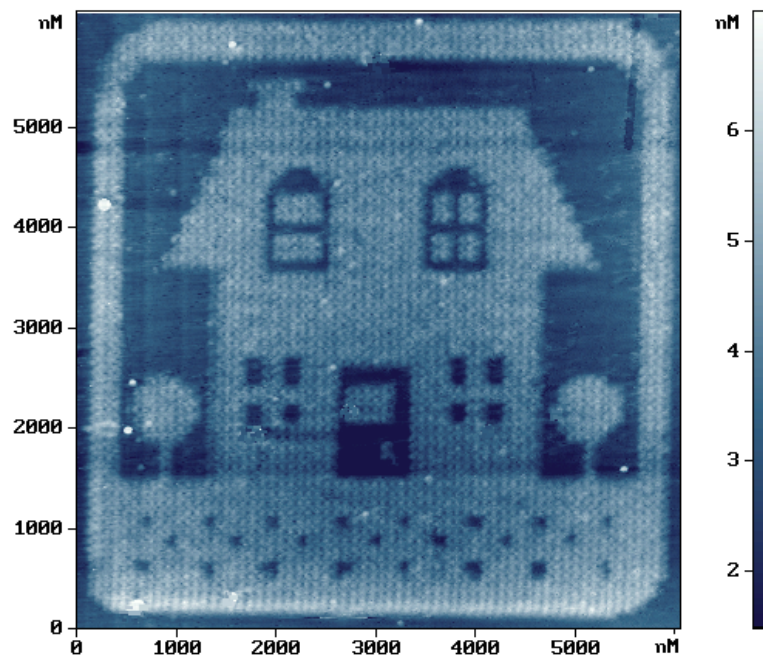


Fig. 1. The SPM nanolithography image (128×128 pixels) on the ta-C film surface.

# Inorganic Sol-Gel derived glass-like Zr-Ge-O nano-system:
## Optically-active centers formation

*Elena V. Frolova, Yulia V. Bokshits, Elena A.. Tyavlovskaya, Valerii S. Gurin, Sergei K. Rakhmanov*
*Research Institute for Physical Chemical Problems of BSU,*
*Leningradskaya str., 14, 220030 Minsk, Belarus*

*evfrolova@yahoo.com*

Alternative ways to high temperature solid-state reactions for producing of mixed oxides afford the sol-gel and related soft chemistry methods [1]. The advantages and uniqueness of the Inorganic modification of the Sol-Gel method have already been described [2].

Ge- and $GeO_2$-contained films and glasses with efficient photoluminescence (PL) have been investigated for a long time because of their applications in optoelectronics [3]. In those systems there are two main possible mechanisms for its light emission: quantum confinement of Ge nanocrystals and Ge-related structural defects [4]. It was shown that the photosensitivity in $GeO_2$-doped silica glass and thin films is related to the oxygen deficiency (oxigen vacancies or $V_o$) associated with Ge(II) ions [5, 6]. So many researches have been done and all of them display the many types of defect formation under different treatment like laser X-ray or γ-radiation, hydrogen or other reduction and *etc,* but no reports on the structural defects formation under low temperature (<1000 $^o$C) thermal treatment **in air** were done for the best of our knowledge.

In the present report we provide the evidences of an unexpected reducing of germanium energetic state (Ge(IV) to Ge(II), according to XPS data) as well as on the oxigen-related defects formation under thermal treatment **in air**.

Herein we report on successful preparation of the glass-like $ZrGeO_4/GeO_x$ nano-system via organic-free modification of the sol-gel technique, and characterization of their structural peculiarities and optical properties. AEA, TEM, XRD, DTA, TG, FTIR, EPR, XPS, DRS, UV-Vis and PL methods were used to investigate the Zr-Ge-O samples with variable zirconium content (25-50 mol.%).

Calcined at 800°C Zr-Ge-O xerogels (i.e. air dried sols before heating) are present differently colored transparent glassy pallets. It must be noticed that the depth of samples color depends on zirconium content (50 at. % – colorless, 32 – pale-yellow, 24 – deep brown). Calcinations of samples at 900°C, as it was seen in optical microscope, resulted in clear appearance of platelet-like inclusions within the glasses that is dominating in the sample with high germanium content (>60 mol. %). According to the further determinations this sample can be considered as composite oxygen deficient germania glasses with crystalline inclusions of $ZrGeO_4$ [7] or $ZrGeO_4/GeO_x$.

The UV-visible spectra of the Zr<<Ge samples show an-resolvable additional absorption in visible region (>400nm) compared with individual zirconia and germania that could explain the color of the samples (Fig. 1 *a*). EPR data shown that depending on the Zr content the systems undergos the transitions from local to the delocalised charge compensation by means of non-bridging oxygens (NBOs) or $O^-$ interaction (Fig. 1 *b*). The idea of NBO interaction was somewhat supported by IR-spectroscopy.

The most incredible results we received by XPS studying of the calcined at 900 $^o$C in air Zr-Ge-O glassy samples (Fig. 1 *c*). The position of the 3d core level peak evidences that germanium exists in non-pure $Ge^{4+}$ state. Also we supose that formation of Ge-Ge bonds rather than only Ge-O-Ge that would leave it as $Ge^{4+}$ is possible in this sistem. This proposition is well consistent with features of the samples in optical absorption that provides pale-yellow and brown colors of the samples with >50% germanium content.

According to PL data the Zr<<Ge samples possess strong luminescence signal under excitation 350 nm with maximum at 440 nm (Fig. 1 *d*).

The possible mechanism of defects formation and organization that caused the unusual optical properties of the materials received will be proposed.

**References:**

[1] S.P. Mukherjee, J. of Non Cryst. Solids. **63** (1984) 35.

[2] C.J. Brinker, G.W. Scherer, Sol-Gel Science. The Physics & Chemistry of Sol-Gel Processing, Academic Press, Inc. USA, 1990.

[3] J. Qui, N. Wada, F. Ogura et al., J. of Phys.: Condens. Matter., **14** (2002) 2561.

[4] M. Takahashi, H. Shigemura, Y. Kawamoto et al., J.of Non-Cryst. Solids, **259** (1999) 149.

[5] L. Skuja, J. of Non-Cryst. Solids, **149** (1992) 77.

[6] J. Qui, A.L. Gaeta, K. Hirao, Chem. Phys. Lett. **33** (2001) 236.

[7] E.V. Frolova, Mater. Sci. & Engin. C, **23** (2003) 1093.

**Figures:**
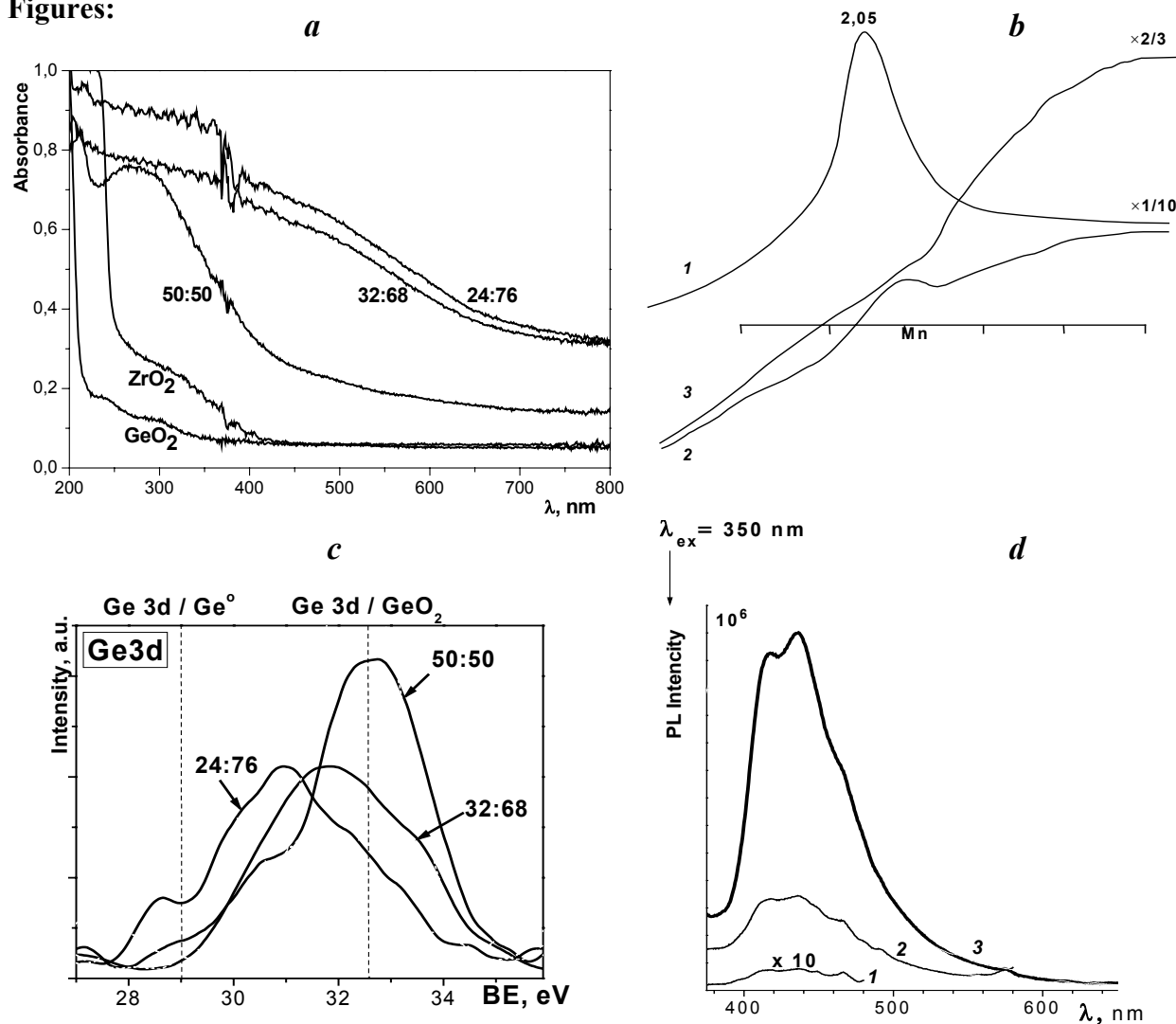


**Fig. 1.** (*a*) UV-visible diffuse reflectance spectra (DRS) of Zr-Ge-O glassy samples calcined at 900°C in air, with different molar ratio of Zr:Ge (indicated) in comparison with individual zirconia and germania, prepared by the method of this work.

    (*b*) Single scans first-derivative EPR spectra of Zr-Ge-O glassy samples calcined at 900°C in air, with different molar ratio of Zr:Ge: *1* – 50:50; *2* – 32:68; *3* – 24:76.

    (*c*) XPS-spectra of Ge 3d core levels of Zr-Ge-O glassy samples calcined at 900°C in air, with different molar ratio of Zr:Ge (indicated).

    (*d*) PL emission spectra (300 K) of Zr-Ge-O glassy samples calcined at 900°C in air, with different molar ratio of Zr:Ge: *1* – 50:50; *2* – 32:68; *3* – 24:76.

# Controlling Single Molecule Fluorescence Lifetime Through Slabs of Metallic and Negative Index Materials

**L. S. Froufe-Pérez**[*] **and R. Carminati**

*Laboratoire d'Energétique Moléculaire et Macroscopique, Combustion; Ecole Centrale Paris, Centre National de la Recherche Scientifique, 92295 Châtenay-Malabry Cedex, France.*

*[*]Author e-mail address : luis.froufe@em2c.ecp.fr*

**Abstract** :  The fluorescence dynamics of a single emitter can be controlled at large distances through slabs of metallic and negative-index materials. This is achieved by positioning a metallic nanoparticle in the vicinity of the emitter image.

## 1. Introduction

The advent of near-field optics techniques has made possible the detection and spectroscopy of single molecules in complex environments, with a lateral resolution below 100 nm. Near-field optics also stimulated the use of sharp metallic tips or nanoparticles to modify the lifetime and to enhance (or quench) the fluorescence of single molecules. The role of such nanoantennas is twofold: an enhancement of the exciting local intensity, and a modification of the radiative emission rate, both in amplitude (Purcell effect [1]) and angular dependence. A drawback when using metallic objects is the presence of absorption, which creates additional non-radiative channels. In the case of small nanoparticles, we have studied recently the trade-off between radiative and non-radiative processes using a dipole-dipole model [2]. This study has shown that the non-radiative decay rate follows a $R^{-6}$ dependence at short range, where R is the distance between the emitter and the center of the nanoparticle, whereas the distance dependence of the radiative decay rate is more subtle. It is chiefly dominated by a $R^{-3}$ dependence, a $R^{-6}$ dependence being visible at plasmon resonance. This distance dependence might be used to control fluorescence lifetimes and fluorescence signals emitted by single molecules.  Nevertheless, substantial influence of the nanoparticle on the emitter dynamics is obtained at distances on the order of a few nanometers. This can be a severe limitation, e.g., when the molecule is embedded in a substrate or in a biological medium.

On the other hand, is has been shown [3] that spontaneous emission lifetime of a single emitter is also greatly modified in the presence of a slabs made of different materials. Again, substantial changes occur when the emitter is placed at distances of a few ten nanometers from the surface of the slabs, and hence, practical limitations are of the same kind as in the case of  using a nanoparticle to modify fluorescent emission.

In this work, we study theoretically and numerically the possibility of controlling the spontaneous decay rate and the fluorescence signal of a single molecule at large distance (in the micron range), through a film made of either a metallic or a negative-index material working in the so-called perfect-lens regime [4]. It has been shown recently that images with sub-wavelength resolution can be produced through such films [5]. We extend this idea to the control of spontaneous emission by placing the emitter on one-side of the slab, and a metallic nanoparticle on the other side. When the particle is brought close to the focus of the image of the single molecule, both systems are coupled and substantial modification of the emitter spontaneous emission is observed. Although the nanoparticle is placed in vacuum above a flat interface, with the molecule at large distance, in the superlens regime the effect on the molecule is similar to that obtained with a nanoparticle placed at a few nanometers.

## 2. Model and results

We consider a slab of material of width w (see inset in Fig. 1) with electric permittivity $\varepsilon(\omega)$ and magnetic permeability $\mu(\omega)$ at the transition frequency $\omega$. The emitter is modelled through its transition dipole **p**. This emitter is placed at a distance $Z_s$ from the closest face of the slab. Analogously, a nanoparticle of radius a is placed on the other side of the slab at a distance $Z_p$ from the surface. The radial positions of both emitter and nanoparticle can be chosen arbitrarily.

The normalized spontaneous emission rate $\Gamma/\Gamma_0$ is given by $\Gamma/\Gamma_0 = 1 + (6\pi/k)\text{Im}\{\mathbf{u}.\mathbf{S}(Z_s,Z_s,\omega).\mathbf{u}\}$, where $\Gamma_0$ is the decay rate of the emitter and k is the wavenumber in the medium where the particle is placed. $\mathbf{S}(z_s,z_s,\omega)$ stands for the modification of the free space Green tensor  due to the presence of the slab and the nanoparticle,  and **u** is the direction of the transition dipole.

In the case where the particle is small enough so that it can be treated in the electric dipole approximation (see e.g. [2]), the Green tensor of the full system can be computed exactly, accounting for multiple scattering between slab interfaces and the nanoparticle.  This is done by using  an angular spectral decomposition and appropriate Fresnel coefficients for the transmitted and reflected fields at the slab interfaces.
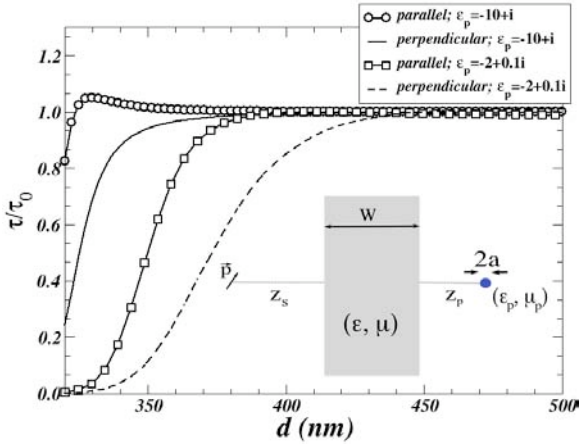
Fig. 1: lifetimes (normalized to its value in vacuum) for transition dipoles, parallel or perpendicular to a perfect left-handed material slab with ε=-1 and μ=-1, as a function of the distance between emitter and particle. In all cases a=10nm, Zs=100nm and w=100nm, the transition wavelength is λ=500nm. The two sets of curves (see legends) correspond to a metallic particle out of resonance (circles and continuous line) with $\varepsilon_p$=-10+i, and a particle at resonance, with $\varepsilon_p$=-2+0.1i (in both cases $\mu_p$=1, sub-index p stands for particle's properties). Both emitter and nanoparticle lie in the same line perpendicular to the slab. Inset: Scheme of the system under consideration.
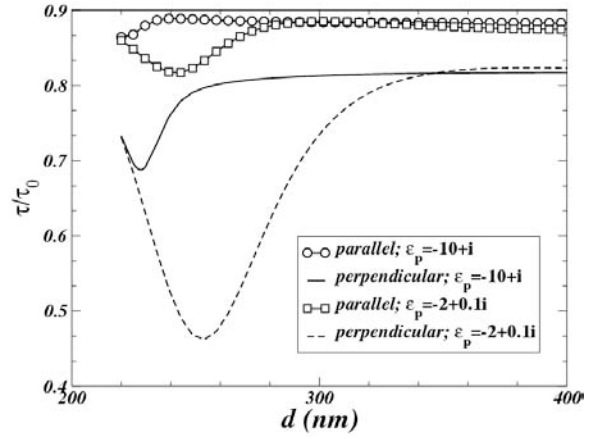
Fig. 2: lifetimes (normalized to its value in vacuum) for transition dipoles, parallel or perpendicular to a left-handed material slab with some absorption, ε=-1+0.01i and μ=-1+0.01i; as a function of the distance between emitter an particle (placed on the other side of the slab). The remaining parameters are the same as in figure 1.

In figure 1, we plot the spontaneous emission lifetimes of an emitter 100 nm above a slab (100 nm in width) made of perfect left-handed material, with ε=-1 and μ=-1. In this case strong focusing effects are expected to happen in the other side of the slab. Hence, a small particle placed near the focus of the perfect lens, will change the lifetime to a large extent. Furthermore, if the small particle exhibits a resonance (e.g. plasmon resonance), the effect will be larger. As can be seen in Fig.1, for a particle out of resonance (circles and continuous lines), the lifetime for both parallel and perpendicular orientations of the transition dipole, decreases rapidly at distances of the order of 350 nm from the source. For a particle at resonance (Re($\varepsilon_p$)=-2 for spherical particles) the effect is even more pronounced, starting the lifetime to fall at distances of the order of 400 nm. With this example, we demonstrate that fluorescence decay rates can be enlarged by an important amount using this geometry and suitable materials, even at distances of the order of the wavelength.

Obviously there are strong practical limitations to implement this set-up experimentally, mainly due to the lack of suitable metamaterials at optical frequencies. But it seems reasonable to obtain a left-handed material with some losses, or index mismatches in general, at optical frequencies. In this case, perfect lensing is known to be destroyed, at least partially, due to absorption. In our work we demonstrate that, even in this case, lifetime can still be notably modified, although the effect is weaker than in the lossless case, and the distance between source and particle should be slightly smaller. As can be seen in figure 2, this is the case for a system like the one considered above, but with some degree of absorption in the left-handed material slab, modelled through a small positive imaginary part in both the permeability and permittivity.

In the case of metallic slabs (relative permeability μ=1), easier to realize in actual experiments, we have also observed changes in the lifetime when the material is chosen such that the transition wavelength coincides with a surface plasmon excitation on the slab surfaces. This situation is very close to the one considered in reference [5].

### 3. Conclusions

We provide numerical examples illustrating the result, which to our knowledge has never been discussed so far, that the lifetime of fluorescent emission can be dramatically changed at distances even comparable to the wavelength. This hold for the case of perfect lenses, although the effect is achieved even in the presence of index mismatches or even using metallic slabs. We investigate the potential of this novel scheme for the control of fluorescent emitters embedded in dense media without direct physical access (e.g. nanophotonics devices or biological samples).

### 4. References

[1] E.M. Purcell, "Spontaneous emission probabilities at radio frequencies", *Phys. Rev.* **69**, 681 (1946).
[2] R. Carminati, J. J. Greffet, C. Henkel, and J. M. Vigoureux, "Radiative and non-radiative decay of a single molecule close to a metallic nanoparticle", *Opt. Comm.* **261**, 368 (2006).
[3] Raphael Ruppin and Olivier J. F. Martin, "Lifetime of an emitting dipole near various types of interfaces including magnetic and negative refractive materials". *J. Chem. Phys.* **121**, 11358 (2004).
[4] J. B. Pendry, "Negative refraction makes a perfect lens", *Phys. Rev. Lett.* **85**, 3966 (2000)
[5] T. Taubner, D. Korobkin, Y. Urzhumov, G. Shvets and R. Hillenbrand, "Near-field microscopy through a SiC superlens", *Science* **313**, 1595 (2006).

# TEMPERATURE-DEPENDENT CHIROPTICAL RESPONSES OF CHIRAL MONOLAYER-PROTECTED GOLD NANOCLUSTERS

*<u>Toshiyuki Fukui</u>, Hiroshi Yao, Keisaku Kimura*
*Graduate School of Material Science, University of Hyogo, 3-2-1 Koto, Kamigori-cho, Ako-gun, Hyogo, 678-1297, Japan*
*skmasterhelm@yahoo.co.jp*

Recently, we have reported the synthesis and chiroptical properties of optically active gold nanoclusters protected by a pair of enantiomers of penicillamine [1]. On the basis of kinetic and structural considerations, we have attributed the observed optical activity to a dissymmetric field induced by the chiral penicillamine shell. A recent theoretical study supports the dissymmetric field model [2]; symmetric metal cores can be optically active when perturbed by a dissymmetric field originating from the surface adsorbates. On the other hand, the origin of optical activity of glutathione-protected gold nanoclusters has been discussed in the context of an inherently chiral core model [3,4]. Thus the arguments on the origin of optical activity are still fragmentary due to few examples of well-defined optically active nanoclusters. In the present study, to further determine the factors that govern the optical activity of such gold nanoclusters, we have investigated circular dichroism (CD) of the chiral penicillamine-protected gold nanoclusters in aqueous solution as a function of temperature. On the basis of the temperature-dependent chiroptical behaviors, the origins of their optical activity are discussed.

Each of two kinds of penicillamines (D- or L-form) was used as a monolayer protecting agent. Briefly, a freshly prepared aqueous $NaBH_4$ solution was added into mixture of $HAuCl_4$ and penicillamine (D-pen or L-pen) in methanol under vigorous stirring, followed by the addition of ethanol into the stored solution yielding a dark-brown crude precipitate. After completely washing the precipitate, the sample power was obtained by a freeze-drying procedure. The gold nanocluster sample prepared by using D-pen or L-pen is termed as Au-D-pen or Au-L-pen, respectively. To separate or purify the gold nanoclusters that differ in size, charge or conformation, we applied polyacrylamide gel electrophoresis (PAGE) using a slab gel unit that employs a gel of 2-mm thickness. On the basis of electrophoretic mobility of the gold nanocluster compounds, the separated compounds are referred to as **1,2**, … (consecutive numbers), with the order of mobility **1** > **2** > …. When distinguishing these compounds in regard to the stereochemistry of the surface ligands, a suffix L or D is added at the end the compound number; for example, **1**$_D$, **2**$_D$, … for the Au-D-pen nanocluster sample.

A CD signal of the gold nanocluster compound should be correlated with its overall structure involving the core geometry and surface ligand conformations or fluctuations, so that perturbation by the temperature change may vary the CD response. CD spectra of the fractioned compounds **1**$_D$ and **1**$_L$ measured at 20 and 40 are shown in Figure 1a. The core diameter of compound **1** has been determined to be 0.6 nm by using small-angle X-ray scattering analysis [1]. The compounds **1**$_D$/**1**$_L$ showed considerably complicated CD behaviors having a clear mirror-image relationship between the D- and L-form species. In addition, the spectra exhibited a temperature dependence. Figure 1b shows the difference between the spectra measured at 40 and 20 . In the figure, the CD differences observed in the wavelength region shorter than 270 nm are essentially attributed to those by chiral penicillamine itself. Note that we have confirmed the spectral reversibility in the CD response.

We can know the striking feature showing obvious spectral changes in the metal-based transition region of the CD signal (500-700 nm). For example, the difference spectrum exhibits CD signals with a positive (negative) band at around 600 nm and a negative (positive) band around 265 nm. More importantly, the difference spectra exhibited an

unequivocal mirror-image relationship between the compounds $1_D$ and $1_L$, suggesting occurrence of similar stereochemical changes between the cluster enantiomers. We have confirmed that the ordinary absorption spectra of these compounds measured at 40 were almost identical with those at 20 , respectively. Therefore, the CD differences for compounds $1_D/1_L$ perturbed by the temperature change are exclusively correlated with the surface stereostructure of the gold nanoclusters. Further considerations based on the temperature-dependent chiroptical behaviors of the nanoclusters give us indication for the origins of their optical activity, and thus, we will give explanations in terms of a dissymmetric field model at the meeting

**References:**

[1] Yao, H.; Miki, K. Nishida, N.; Sasaki, A.; Kimura, K. *J. Am Chem. Soc.*, **127** (2005) 15536.
[2] Goldsmith, M.-R.; George, C. B.; Zuber, G.; Naaman, R.; Waldeck, D. H.; Wipf, P.; Beratan, D. N. *Phys. Chem. Chem. Phys.*, **8** (2006) 63.
[3] Garzón, I. L.; Reyes-Nava, J. A.; Rodríguez-Hernández, J. I.; Sigal, I.; Beltrán, M. R.; Michaelian, K. *Phys. Rev. B*, **66** (2002) 073403.
[4] Schaaff, T. G.; Whetten, R. L. *J.Phys. Chem. B*, **104** (2000) 2630.
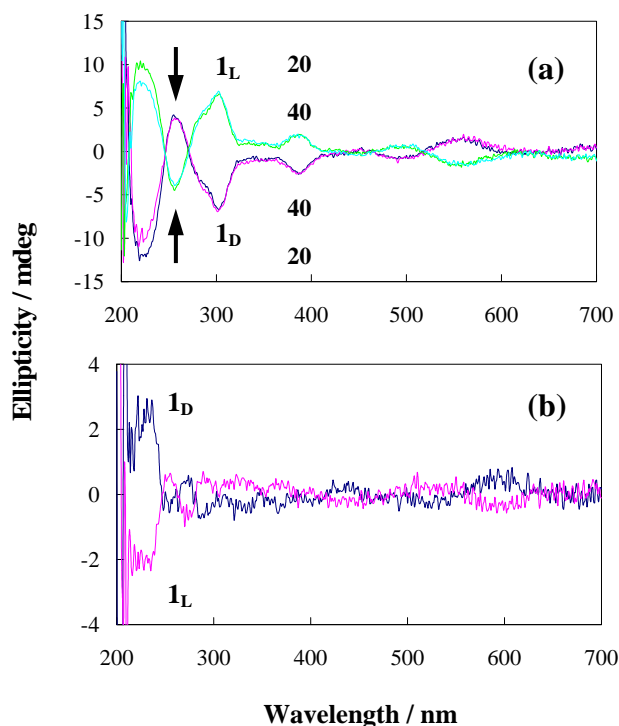
**Figures:**



**Figure 1.** (a) Temperature-dependent CD spectra of $1_D/1_L$ in aqueous solution. (b) CD signal differences between the spectra at 40 and 20 .

# CHARACTERIZATION OF SUPRAMOLECULAR ASSEMBLIES OF MALTOSE NEOGLYCOCONJUGATES AND GLYCONANOPARTICLES BY NON-CONTACT AFM

M. Fuss, M. Luna, D. Alcántara, J.M. de la Fuente, F. Briones and S. Penadés

## Introduction

Since the field of Glyconanotechnology was introduced by our group in 2001, different kinds of nanostructures have been reported ranging from gold nanoparticles to self-assembled monolayers. These innovative nanostructured biomaterials have demonstrated very interesting biological and biomedical applications. As an example, we previously reported the preparation of water soluble Au-Fe$_x$O$_y$ nanoparticles functionalized with a maltose neoglycoconjugate. In this work, we have been able to obtain information about the organic coverage of these gold nanoparticles by means of non-contact dynamic AFM. This method, based on long-range attrctive interactions between tip and sample, is particularly indicated for compliant materials since there is no damage to the sample due to the impact or friction.

## Methods

For AFM analysis, 10µl of a solution of maltose-protected AuFe nanoparticles or neoglycoconjugate (70µg/ml) was deposited on freshly cleaved graphite. These samples were then left to dry at about 6ºC during 24 hours, allowing a slow evaporation of the water. AFM imaging took place at normal ambient conditions (~30% RH), except for the study at varying RH.

Images shown were obtained using a commercial AFM operated in non-contact amplitude modulation mode. The cantilevers had a nominal force constant of 0.7-2 N/m and a resonance frequency of about 71 kHz. Small peak-to-peak oscillation amplitudes (~5 nm) were used during imaging.

## Results and Discussion

In a previous paper, our group reported the synthesis of Au-FexOy nanoparticles functionalized with biologically relevant carbohydrates covalently linked to the inorganic cluster. The so prepared glyconanoparticles have less than 2 nm diameter core and formed stable dispersions over several months. TEM micrographs show very small Au-FexOy nanoparticles perfectly aligned and encapsulated in what seems organic material (fig. 1). The existence of glyconanoparticle aggregates with an organic covering on a Au substrate was confirmed by non-contact AFM. Micelle formation in water is probably caused by the amphiphilic nature of the neoglycoconjugate, containing a hydrophilic head (sugar) and a lipophilic spacer (alkane chain).
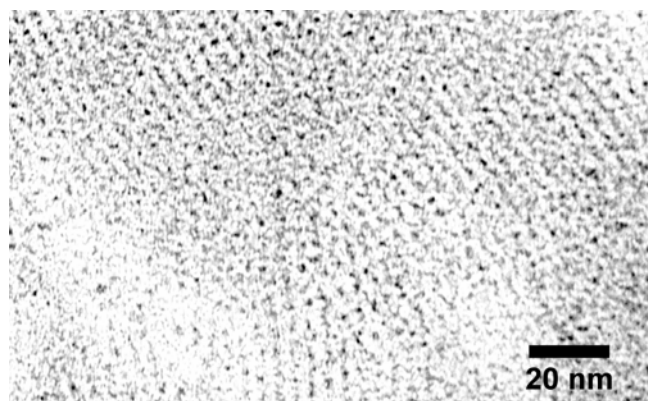


**Fig. 1:** TEM image showing maltose-protected gold nanoparticles perfectly aligned. The neoglycoconjugate forms micelles with a tubular shape and gold cores are found encapsulated in the organic material.

In the AFM characterization carried out on highly-oriented pyrolytic graphite, we found that maltose glyconanoparticle aggregates were no longer present. Instead, multilayers of organic material of reproducible height were observed. From profiles like the one shown in figure 2, a step height of 4.2nm was determined. Since the same structure and height was found in a control sample prepared with a solution of the neoglycoconjugate without metallic nanocores, the multilayers are believed to originate from excess maltoC$_{11}$SH molecules. In figure 3, a model of the multilayer formation is proposed.
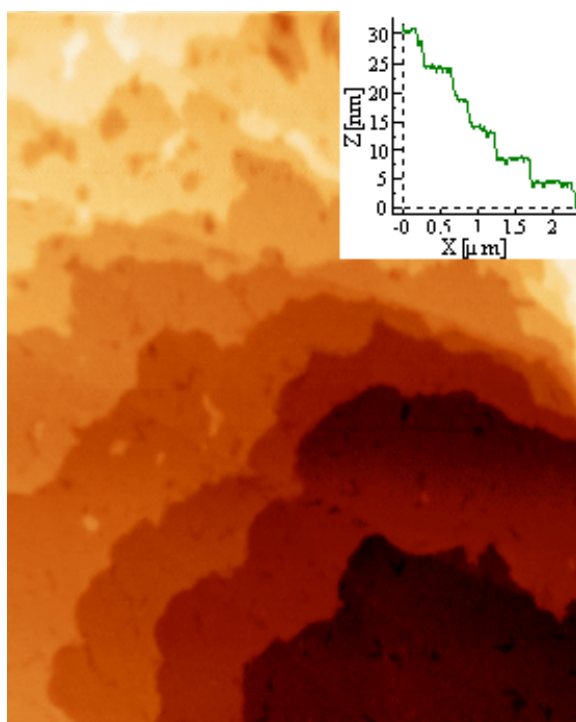
**Fig. 2:** In non-contact AFM mode, more than ten layers of (maltoC$_{11}$S-)$_2$ molecules were formed on graphite (2.4 x 3 µm$^2$ AFM image) from the solution containing the glyconanoparticles. The inset shows a profile through eight layers. The height of the graphite terrace visible was used for z-calibration.
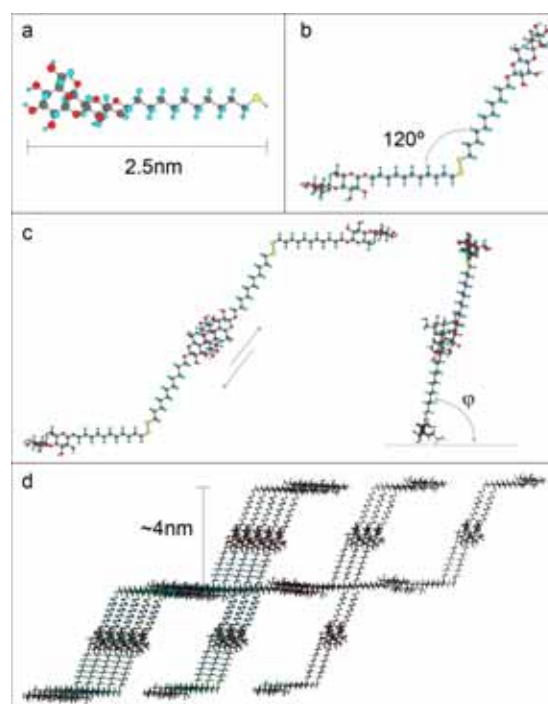


**Fig. 3:** Multilayer formation on graphite: (a) Excess maltoC$_{11}$SH molecule in aqueous solution. (b) Formation of disulfide bonds. (c) Pairs of maltose molecules form weak hydrogen bonds. The lower alkane chain adsorbs hydrophobically to the HOPG substrate. (d) Formation of organic multilayers driven by hydrophobic forces between alkane chains. The vertical step height is about 4 nm but depends on the location of hydrogen bonds (overlap of the two sugars) and the angle $\varphi$ as illustrated in (c).

Again, the amphiphilic nature of the organic molecule studied seems to play a major role. The hydrophobic interaction between alkane chains and graphite, helped by weak hydrogen bond formation between maltose molecules, can facilitate the self-assembly of the neoglycoconjugate.

Owing to the weak interaction forces holding the molecules together (hydrophobic and van der Waals forces and hydrogen bonds), the organic layers cannot be probed in contact mode under normal conditions. A further consequence is the high mobility of the (maltoC$_{11}$S-)$_2$ layers observed at high relative humidities (80-90%): a rearrangement takes place which joins small islands to form larger ones, covers holes, and finally smoothes all surface features.

**Conclusions**

In this work, we report the characterization of maltose glyconanoparticles by non-contact AFM. These maltose glyconanoparticles, due to the amphiphilic character of the maltose neoglycoconjugate, adopt different arrangements when adsorbed on hydrophilic (Au) or hydrophobic (graphite) surfaces. On HOPG the tubular arrangement of the maltose conjugate aggregates is decomposed to form multilayers of the maltose neoglycoconjugate by itself. We propose a model for the formation of these multilayers based on the hydrophobic interactions between the molecules and with the substrate surface.

# Supercurrent and Coulomb blockade in multiwall CNTs with Nb contacts

M. Gaaß, E. Pallecchi, and Ch. Strunk

*Institut für Experimentelle and Angewandte Physik,*

*Universität Regensburg, D-93025 Regensburg, Germany*

(Dated: May 14th, 2007)

It has been shown that, under proper conditions, there can be dissipationless current flowing across nanotubes coupled to superconducting leads [1]. We present here first measurements of the characteristics of multiwall carbon nanotubes contacted to electrodes made of Niobium. We were able to reach critical currents of up to 20nA which are, to our knowledge, the highest currents reached so far.

Our samples are fabricated by standard lithographic and metal deposition means after locating the nanotubes with a SEM on either a $SiO_2$ or an $Al_2O_3$ substrate. In addition to the layer of Niobium with a thickness of around 40nm we cared for good electrical coupling between the contacts and the tube with a roughly 5nm thick layer of Palladium. This process resulted in typical room temperature resistances of around $10k\Omega$. The approximate contact spacing that we defined was between 250nm and 400nm, Fig. 1(a). A special feature of our design is that we defined rather long resistive leads made of AuPd and large enough bonding pads, Fig. 1(b). By this on-chip resistance and capacitance we are damping thermally activated switching of the junction into the resistive state which is equal to increasing the switching current towards the intrinsic value of the critical current [2]. Another important ingredient of the measurement setup are well filtered lines. In addition to the usual $\pi$- and Copper powder filters we use a two stage RC-filter setup following [1].

The measurements performed so far on a sample with a $SiO_2$ backgate include the investigation of the differential resistance over a wide gate voltage range and were all done in our dilution refrigerator at T = 25mK. The results showed that with gate voltage we are tuning the sample from a relatively weak Coulomb blockade regime into deep Coulomb blockade upon which, for even lower gate voltages, we reach a region where the sample only occasionally jumps back from the superconducting state into the normal state Fig. 2.
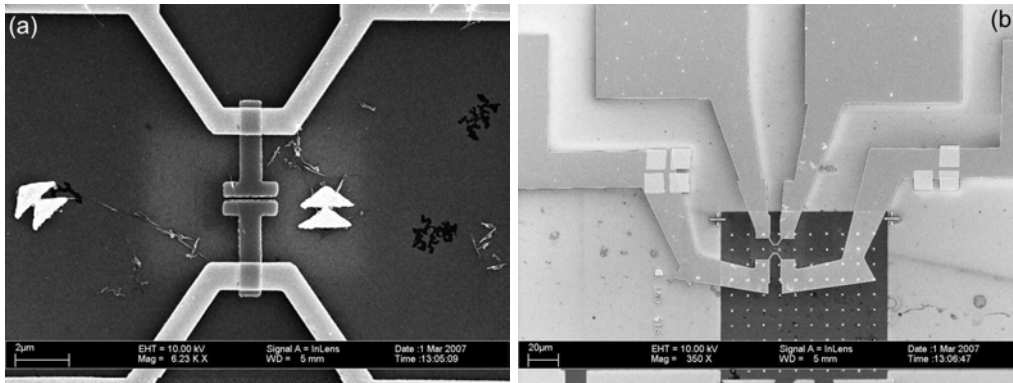
FIG. 1: (a) SEM image of a typical sample from this work. The superconducting contacts are clearly visible and are connected by a multiwall carbon nanotube which sits, barely visible, towards the left end of the contact electrodes. (b) The Nb contacts on top and bottom are connected to the resistive AuPd leads which help us achieving an appropriate on-chip resistance in order to damp together with the capacitance from the bonding pads the thermal activated switching of the junction into the resistive state.

Finally, for gate voltages below $V_G = -15V$ the sample remains completely superconducting. In the superconducting state we investigate the dependence of the critical current on gate voltage, temperature and magnetic field. While the first two show the expected behavior, the magnetic field dependence remains unclear. This we attribute to trapped flux in the superconducting electrodes. The next series of measurements will be done in
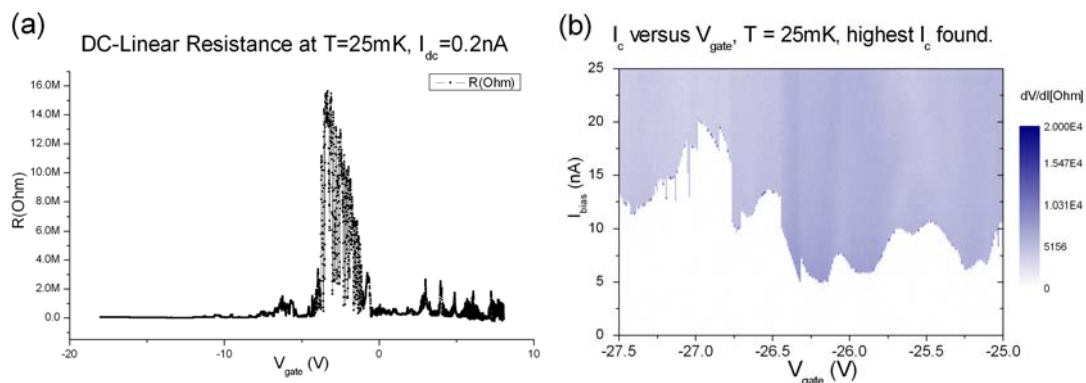


FIG. 2: (a) Differential resistance collected over a wide gate voltage range. The transport properties change from slight Coulomb blockade to clear Coulomb blockade before it switches into the superconducting state. (b) Dependence of the critical current on the gate voltage around $V_G = -27V$. A maximum value of $I_c = 20nA$ could be reached.
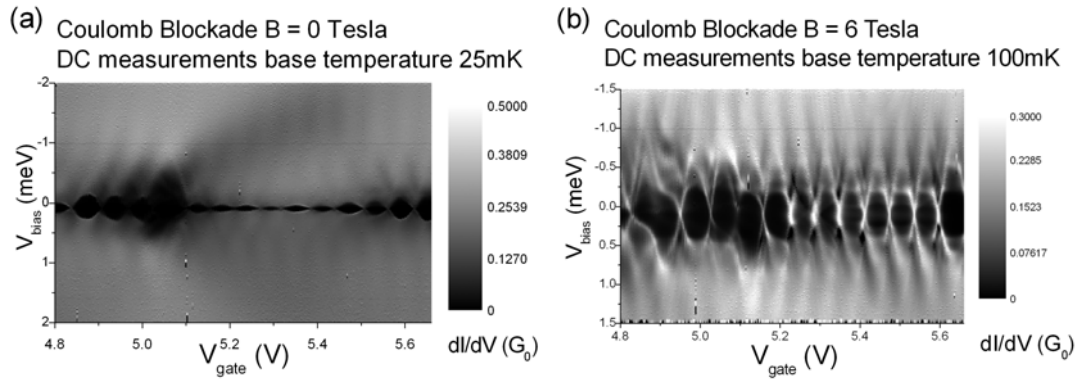
FIG. 3: (a) Differential conductance at zero magnetic field with superconducting electrodes. (b) Differential conductance for the same gate voltage region as in (a) but with a magnetic field of B = 6T in order to drive the electrodes into the normal state.

parallel field to minimize this effect.

One focus in the gate voltage regime of zero resistance was set on trying to correlate the size of the supercurrent and the normal state resistance which was measured at B = 6T. The results of this measurements still need further interpretation.

Furthermore we investigated the Coulomb blockade regime for any signature of the superconducting leads at low temperature for different magnetic fields. The results of these measurements are shown in Fig. 3.

[1] P. Jarillo-Herrero, J. A. van Dam, L. P. Kouwenhoven, Nature **439**, 953 (2006).

[2] M. F. Goffman, R. Cron, A. Levy Yeyati, P. Joyez, M.H. Devoret, D. Esteve, and C. Urbina, PRL **85**, 170 (2000).

# ON-SURFACE SYNTHESIS OF METALLO-PORPHYRIN NANO-TUBES BY VACUUM SUBLIMATION ONTO NOBLE METALS SUBSTRATES

*Marta Trelka [1], Christian Urban [1], David Écija [1], Paula de Mendoza [2], José María Gallego [3], Roberto Otero [1], Antonio M. Echavarren [2], Rodolfo Miranda [1]*

*[1] Dpto. de Física de la Materia Condensada, Universidad Autónoma de Madrid Cantoblanco, 28049 – Madrid, Spain*
*[2] Institut Català d'Investigació Química, 43007 – Tarragona, Spain*
*[3] Instituto de Ciencia de Materiales de Madrid - CSIC, Cantoblanco, 28049 – Madrid, Spain*

*josemaria.gallego@uam.es*

Molecular electronics is a promising alternative for the continuing miniaturization of electronic devices. The capability of synthesizing and depositing molecular wires on solid surfaces is a key step within this context. The majority of the most promising current candidates to molecular wires, such as carbon nanotubes, DNA strands or individual polymer molecules [1], are too large and fragile for depositing them on solid surfaces by in-vacuum sublimation. Other kinds of wet deposition methods, such as drop-casting, are not so well controlled, which, in turn, hinders the understanding and design of their conductivity.

Since the molecular mass of the chemical species well-suited for deposition on solid surfaces by in-vacuum sublimation is limited, one could envisage a mechanism to grow the polymeric molecular wires by depositing smaller subunits that would subsequently assemble into the polymer after they have been adsorbed on the surface. This approach has successfully been used to steer the assembly of organic molecules into 1D structures [2], although the electrical conductivity of such "supramolecular" wires is still to be addressed. The 1D molecular wires so created are mostly like "ribbons", due to the fact that the molecules tend to lie flat on the surface to maximize substrate-adsorbate interaction. The on-surface synthesis of molecular wires with more complex geometrical shapes, such as tubular or cylindrical, has only been described for the case of carbon nanotubes, and only on surfaces covered with catalytic nanoparticles [3] or on silicon carbide surfaces, where the constituent carbon for the nanotube growth arises from bulk segregation [4]. The aforementioned ideal situation in which molecular subunits assemble into 1D structures with cylindrical symmetry has not been described so far in the literature.

In this work we describe the growth of 1D tube or cylinder-looking structures obtained after deposition of the organic compound Zn *meso*-tetramesitylporphyrin (Zn-TMP, see Figure 1) on the noble-metal surfaces Au(111) and Cu(100) by vacuum sublimation (See Figure 2) with the substrate held at room temperature (RT). Our experiments indicate that the "nanotubes" are only a meta-stable structure, since they disassemble into flat-lying Zn-TMP monomers upon annealing to 500 K (see Figure 3). The disassembled Zn-TMP adsorbates are tightly bound to the surface, as evidenced by the fact that they can be easily imaged by Scanning Tunnelling Microscopy even at room temperature, and the difficulty to manipulate them even under the harsher tunnelling conditions. Two mechanisms for such a phenomenon will be discussed.

**References:**

[1] N. Robertson, C. A. McGowan, *Chem. Soc. Rev.*, **32** (2003) 96.

[2] J. Weckesser, A. De Vita, J.V. Barth, C. Cai, K. Kern, *Phys. Rev. Lett.*, **87** (2001) 096101; R. Otero, Y. Naitoh, F. Rosei, P. Jiang, P. Thostrup, A. Gourdon, E. Laegsgaard, I. Stensgaard, C. Joachim, F. Besenbacher, *Angew. Chem. Intl. Ed.* **43** (2004) 2091; T. Yokoyama, S. Yokoyama, T. Kamikado, Y. Okuno, S. Mashiko, *Nature* **413** (2001) 619.

[3] J. Liu, A. G. Rinzler, H. Dai, J. H. Hafner, R. K. Bradley, P. J. Boul, A. Lu, T. Iverson, K. Shelimov, C. B. Huffman, F. Rodriguez-Macias, Y.-S. Shon, T. R. Lee, D. T. Colbert, R. E. Smalley, *Science* **280** (1998) 1253.

[4] V. Derycke, R. Martel, M. Radosavljevic, F. M. Ross, Ph. Avouris, *Nano Lett.* **2** (2002) 1043

**Figures:**



**Figure 1**. Stick-and-ball model of the Zn porphyrin used in this study.
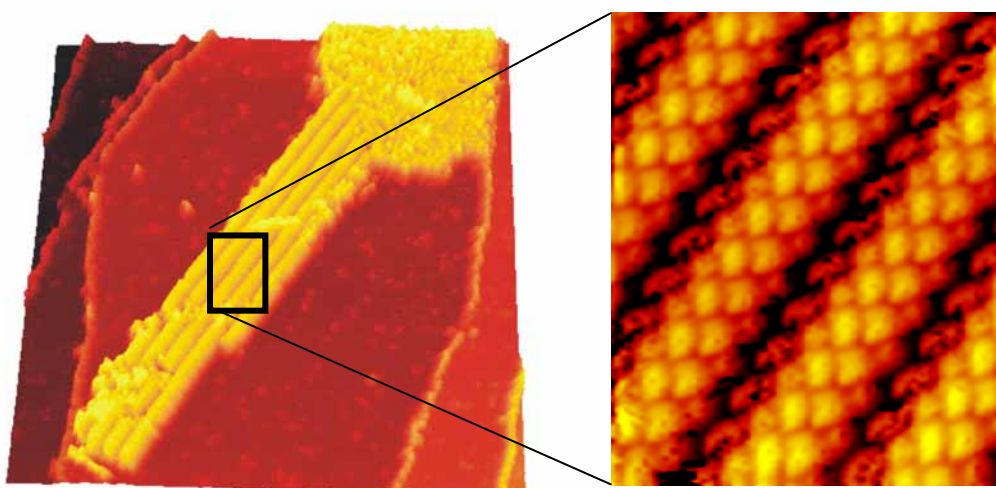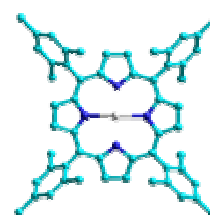


**Figure 2**. $98.4 \times 98.4$ nm$^2$ STM image of long tubes coexisting with disorder after depositing ZnTMP on Cu(100) and a zoom-in showing the spiral shape of the tubes

**Figure 3.** $21 \times 25$ nm$^2$ STM image showing individual flat lying ZnTMP molecules on Cu(100) after annealing the tubes to 500 K.
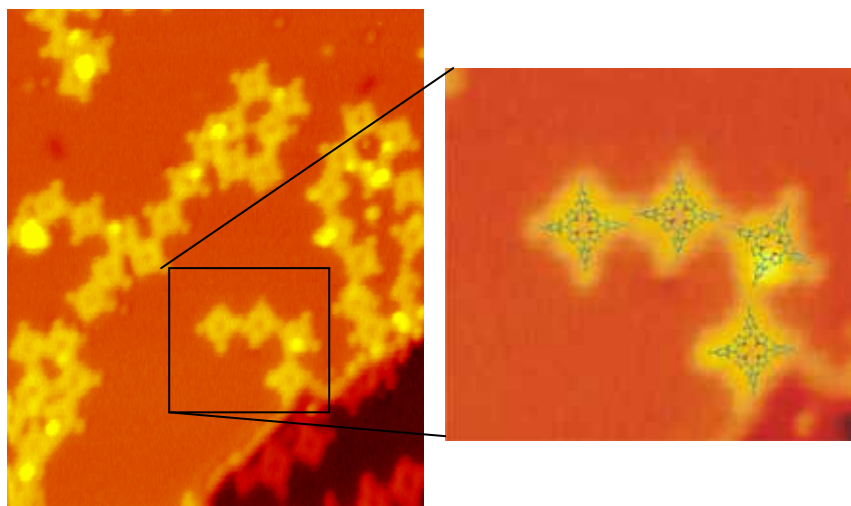
# A molecular dynamics investigation of ink diffusion on self-assembled monolayers as applied to nanopatterning

*Greg Gannon, Damien Thompson, J. Andreas Larsson and James C. Greer*
*Tyndall National Institute, Lee Maltings, Prospect Row, Cork, Ireland.*
*greg.gannon@tyndall.ie*

Self-assembled monolayers (SAMs) are widely used in areas as diverse as corrosion protection, nanodevices and biotechnology. Despite numerous experimental and theoretical studies of SAM structure and behaviour[1], there are still areas requiring further investigation. Alkanethiol molecular ink diffusion on alkanethiol SAMs is one such area, and one which is amenable to a computational study. Ink diffusion is an important consideration when one performs microcontact printing - "... the quality of the printed pattern strongly depends on the mobility of the ink compound ..."[2]. An understanding of ink diffusion is therefore crucial to the production of stable, high-resolution nanopatterns. We calculated alkanethiol self-diffusion coefficients in bulk liquid from molecular dynamics (MD) simulations and obtained good agreement with measured values[3], as shown in Table 1 below. The Einstein diffusion equation (Equation 1 below), was used to calculate the diffusion coefficients in all instances.

$$D \equiv \frac{1}{2d} \lim_{t \to \infty} \frac{\left\langle [\underline{r}(t_o + t) - \underline{r}(t_o)]^2 \right\rangle}{t}$$

Equation 1. **D** is the self-diffusion coefficient and **d** is the dimensionality of the system. The numerator is the mean square displacement; the angled brackets indicate an ensemble average has been taken.

Simulations of alkanethiol SAMs were performed and the temperature dependence of the SAM tilt angle was found to be in good agreement with literature values[4]. Having validated our method both for calculating diffusion and the SAM structural models, we calculated the diffusion of both a single alkanethiol molecule (Figure 1) and a 75-molecule "droplet" (Figure 2), on a range of perfect and defect SAMs thereby establishing a range for ink diffusion in different environments. The defects introduced to the system were based on the experimentally observed defects [5], and a typical defect is shown below in Figure 3. D values obtained indicate that alkanethiol molecules diffuse at different rates in the order: single molecule on SAM > drop on SAM > bulk self-diffusion.

Table 1. Comparison of experimental and theoretical diffusion coefficients.

| Alkane | Experimental[3] ($10^{-9}$ms$^{-1}$) | Theoretical (this work) ($10^{-9}$ms$^{-1}$) |
|---|---|---|
| Octane (C8) | 2.36 | 2.70 |
| Undecane (C11) | 1.11 | 0.87 |
| Dodecane (C12) | 0.87 | 0.65 |
| **Dodecanethiol (DDT)** | N/A | 0.33 |
| Hexadecane (C16) | 0.39 | 0.20 |
| Diffusion coefficients were calculated from 1 ns MD runs at 298 K. | | |

Figure 1. Side view of a dodecanethiol SAM with a free dodecanethiol molecule diffusing on top (hydrogens are omitted for clarity).
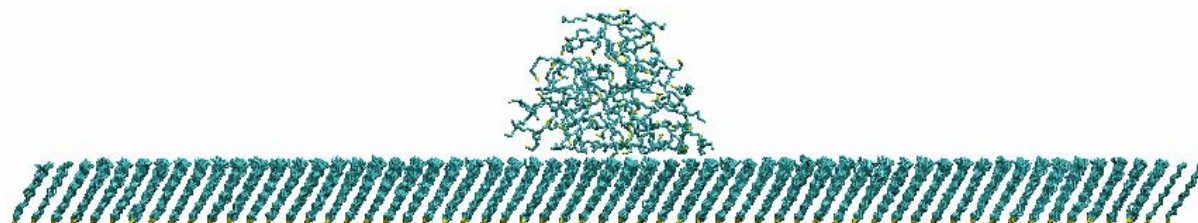


Figure 2. Side view of a dodecanethiol SAM with a 75-molecule dodecanethiol "droplet" diffusing on top (hydrogens are omitted for clarity).
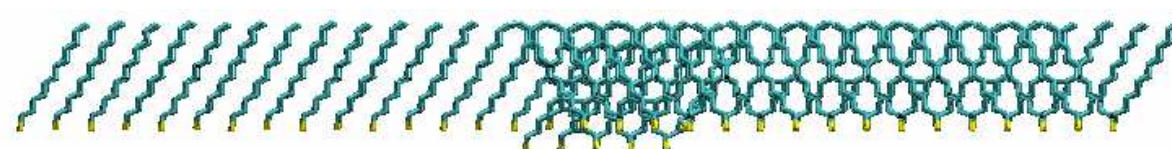


Figure 3: Side view of dodecanethiol SAM incorporating a domain boundary on the right hand side and a depression in the centre (hydrogens are omitted for clarity).

**References**

1. J.C. Love, L.A. Estroff, J.K. Kriebel, R.G. Nuzzo and G.M. Whitesides, *Chem. Rev.*, **2005**, *105*, 1103.

2. T.E. Balmer, H. Schmid, R. Stutz, E. Delamarche, B. Michel, N.D. Spencer and H. Wolf, *Langmuir*, **2005**, *21*, 622.

3. P.S. Tofts, D. Lloyd, C.A. Clark, G. J. Barker, G. J. M. Parker, P. McConville, C. Baldock and J.M. Pope, *Magn. Reson. Med.*, **2000**, *43*, 368.

4. S. Vemparala, B. B. Karki, R. K. Kalia, A. Nakano and P. Vashishta, *J. Chem. Phys.*, **2004**, *121*, 4323.

5. C. A. McDermott, M. T. McDermott. J. B. Green and M. D. Porter, *J.Phys.Chem*, **1995**, *99*, 13257.

# NANOSPEAR PLASMONS

*Aitzol Garcia Etxarri, and Javier Aizpurua*
*Donostia International Physics Center, and Centro Mixto CSIC-UPV/EHU,*
*Paseo Manuel Lardizabal 4, Donostia-San Sebastián E-20018, Spain*
*aitzol_garcia@ehu.es*

Design and engineering effective near-field scanning optical microscopy tips is a challenging topic of research to improve field-enhanced microscopy and spectroscopy. Current approaches focus on different resonant antenna effects to obtain maximum scattering signal and enhanced molecular fluorescence. Other research efforts are devoted to take advantage of certain structural resonances, such as those in cavity modes [1], or in sets of varying-size nanoparticles [2] where hot spots of field enhancement are created.

In this contribution, we propose a nanospear structure at the end of a scattering metallic tip as an effective geometry that generates largely increased field enhancement at the arms of the spear. The mechanism of the additional enhancement of the nanospear, compared to a standard conical or ellipsoidal tip, is based on the presence of the additional cavities that act as reservoirs of induced charge oscillation, allowing a larger enhancement to occur in the proximity of the tip arms, in what we describe as the nanospear plasmon.

With use of a boundary element method (BEM), we perform full electromagnetic calculations of the optical scattering by a metallic nanospear-shaped tip, and map the plasmon patterns induced in this geometry (Fig. 1). The field enhancement around the nanospear tip is 10 times larger than in a standard rounded tip of the same radius. These results corroborate the influence of the combined presence of concave and convex surfaces as the sources of the enhancement. We study plasmon patterns and surface charge density in different nanospears to obtain maximum efficiency. The maximum enhancement occurs at the edges of the nanospear arms with values around 500, that make this structure a robust candidate to be used in tip-enhanced spectroscopies.

**References:**

[1] I.Romero, J.Aizpurua, G.W.Bryant, F.J.García de Abajo, Optics Express **14**, 9988 (2006).

[2] L. Kuiru, M.I. Stockman, and D.J. Bergman, Phys. Rev. Lett. **91**, 227402 (2003).

**Figures:**
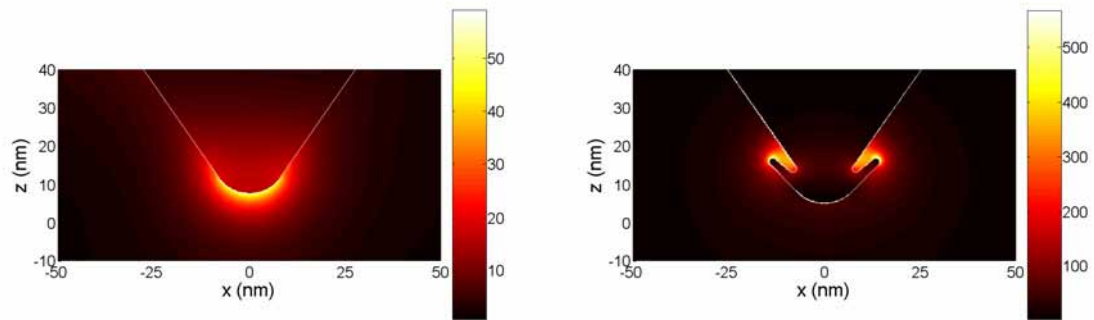


**Fig. 1:** (Left) Near-field distribution around a silver rounded tip with a radius of curvature R=10nm for a polarized planewave coming from the left hand side. (Right) Near-field distribution around a nanospear shaped tip, with the same overall radius of curvature. An amplitude field enhancement larger than 500 is observed around the arms of the nanospear

# SYNTHESIS OF DENDRIMER-CARBON NANOTUBE CONJUGATES

*García A.* [†#], *Herrero M.A.* [†], *Frein S.* [§], *Deschenaux R.* [§], *Muñoz R.* [#], *Bustero I.* [#], *Prato M.* [†]

[†]*Dipartamento di Scienze Farmaceutiche, Università di Trieste, Piazzale Europa 1, 34127 Trieste (Italy)*

[#]*Department of Biomaterials and Nanotechnologies, Inasmet Foundation, Mikeletegi Pasealekua 1, Teknologi Parkea, San Sebastián (Spain)*

[§]*Institut de Chimie, Université de Neuchâtel, Av. de Bellevaux 51, Case postale 158, 2009 Neuchâtel, Switzerland*

*ainara.garcia@inasmet.es*

Carbon Nanotubes (CNTs) have interesting physical and chemical properties that open attractive possibilities in many research areas. The main problem for further applications is the chemical inertness of the CNTs that makes difficult the attachment of molecules at the surface. The objective of our work is a high degree of functionalization on CNTs with a covalent attachment of the interesting molecules without provoking damage to the conjugated π-system. One approach is the attachment of dendrimers at the SWNTs with high density of functional groups that serve as anchor point for further reactions. For that, we have carried out a primary modification with 1,3 dipolar cycloaddition reaction [1] with different kinds of commercial CNTs. Once the terminal Boc groups were deprotected and the amount of functionalities was quantified in each sample, the most reactive CNTs were chosen. Finally, dendrimers attachments were performed by carbodiimide chemistry and in all cases the final products were fully characterized.
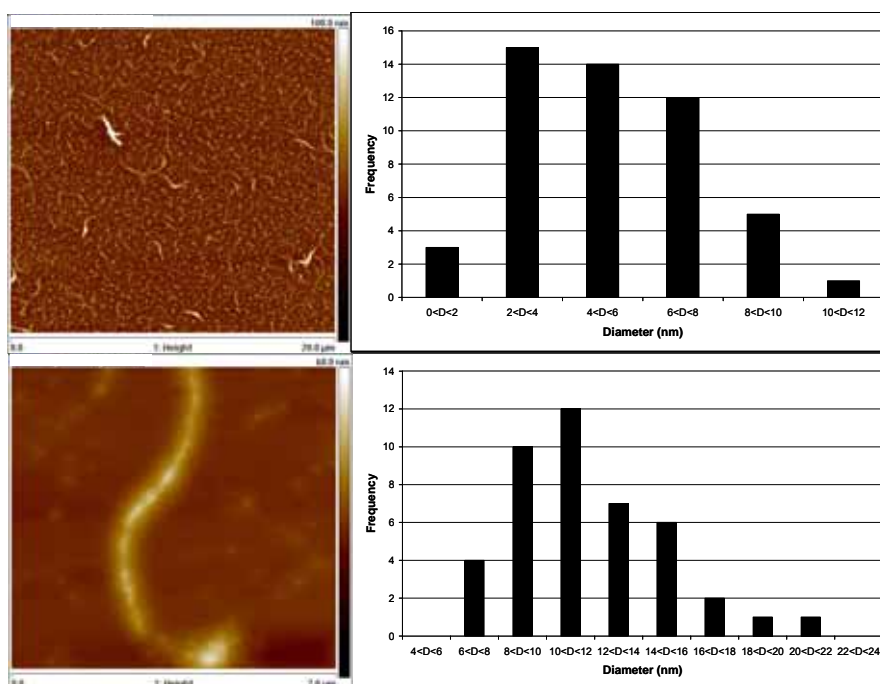


**Figure 1.** AFM image of SWNT modified with the cycloaddition reaction and diameter distribution of the sample (top) and that of the SWNT- dendrimer conjugated (down).

**References:**

[1] (a) Georgakilas, V., Kordatos, K., Prato, M., Guldi, D.M., Holzinger, M., Hirsch, A., *J. Am. Chem. Soc.*, **124** (2002) 760. (b) Georgakilas, V., Tagmatarchis, N., Pantarotto, D., Bianco, A., Briand, J.–P., Prato, M., *Chem. Commun,* **24** (2002), 3050

# ELASTIC QUANTUM TRANSPORT FOR MOLECULAR NANOSWITCHES USING PLANE WAVES

_A. Garcia-Lekue_[1], _I._ Silanes[1], _D._ Sanchez-Portal[1,3], _L.W._ Wang[4] and _A._ Arnau[2,3]

[1]*Donostia International Physics Center (DIPC), Donostia, Spain*
[2] *Materialen Fisika Saila, Euskal Herriko Unibertsitatea, Donostia, Spain*
[3] *Centro Mixo CSIC-UPV/EHU, Donostia, Spain*
[4] *Lawrence Berkeley National Laboratory (LBNL), Berkeley, United States*
*AGarcia-Lekue@lbl.gov*

Molecular electronics represents an interdisciplinary area that spans physics, chemistry and material science, and is based on the use of molecular building blocks for the fabrication of electronic components. In recent years, new advances have made possible a real technology based on molecular electronic devices, such as rectifiers, resonant tunnel junctions and molecular switches. The later refer to electronic switching devices that use molecules as active components, and have been extensively studied these years. Switching behaviour has been observed in different species and various schemes have been suggested to describe the physical origin of the molecular switching processes.

In this work, the switching behaviour of phenyl-based molecules attached to copper electrodes through thiol end groups is investigated, where the switching is driven by conformational changes involving the rotation of one of the phenyl groups. The elastic quantum transport of such nanodevices is calculated using a recently developed numerical method.[1,2] This method is based on a solution of scattering states using plane waves and auxiliary periodic boundary conditions, includes evanescent states exactly, and its computational time is close to that of a ground-state DFT calculation. To test the accuracy of this approach, a benching mark problem is first considered, which consists of a di-thiol benzene (DBT) molecule connected by two Cu wires.

Subsequently, di-thiol biphenyl and di-thiol biphenyl-acetylene molecular devices have been studied. For each molecular nanosystem two different configurations are considered, with phenyl rings either lying on the same plane or rotated 90 degrees with respect to each other. Compared to the result for the DBT molecule, the zero-bias conductance is not significantly affected by the inclusion of a second coplanar phenyl ring (ON state), whereas rotating one phenyl ring drops the conductance greatly (OFF state). As a result, large ON-OFF ratios are found by simple rotation of one of the benzene molecules.

The approach presented here provides a computationally inexpensive and accurate way to methodically describe switching behaviour of molecular nanodevices, and work is in progress for its implementation to non-zero applied bias voltages, which require a non-self consistent treatment of the out-of-equilibrium situation.

## References

[1] L.W. Wang, Phys. Rev. B. **72**, 045417 (2005).
[2] A. Garcia-Lekue and L.W. Wang, Phys. Rev. B. **74**, 245204 (2006).

# SURFACE PLASMON RESONANCE EFFECTS IN THE MAGNETO OPTICAL ACTIVITY OF NOBLE METAL-FERROMAGNET ULTRATHIN FILMS

*A. García-Martín, J. B. González-Díaz, G. Armelles, J.M. García-Martín, C. Clavero*
*Instituto de Microelectrónica de Madrid, CSIC, Isaac Newton 8, 28760 Tres Cantos, Spain*
*A. Cebollada*
*Instituto de Microelectrónica de Madrid, CSIC, Isaac Newton 8, 28760 Tres Cantos, Spain*
*and FOCUS Center, University of Michigan, Ann Arbor, USA*
*R. Clarke, D. Kumah*
*FOCUS Center, University of Michigan, Ann Arbor, USA*
*R.A. Lukaszew, J. Skuza*
*University of Toledo, Toledo, USA*

*antonio@imm.cnm.csic.es*

We present a combined experimental and theoretical study elucidating the role of surface plasmon resonances in the enhancement of magneto optical activity. Au/Co/Au trilayers were grown on glass substrates by ultra-high-vacuum deposition and the thickness of the ferromagnetic layer was systematically varied between 0.3 and 10 nm. A comprehensive structural, magnetic and magneto-optical characterization of the different layers is provided. Simulations of both Kerr spectra and reflectivity were carried out using a transfer matrix algorithm applied to the multilayers. [1]

For specific Co and Au layer thicknesses, the excitation of surface plasmon resonance at the Au/air interface in the Kreschmann configuration leads to an enhanced transverse Kerr effect. This is due to the optimized coupling of the incident light with the excited plasmon resonance and the subsequent enhancement of the electromagnetic field at the magneto-optically active layer. Theoretical calculations permit the separation of the individual contributions to the transverse Kerr signal ($\Delta R/R$) from the purely magnetic ($\Delta R$) and optical (R) parts. It is found that the enhancement in $\Delta R/R$ is not only due to a reduction in R [2] but also due to an enhancement in $\Delta R$ for specific layer thickness and incidence angles, correlated with the specific absorption coefficients of Co. This finding provides new insights in the understanding and interpretation of magneto-plasmonic phenomena.

**References:**

[1] J.B. González-Díaz, submitted to Phys. Rev. Lett., (2007).
[2] V.I.Safarov et al., Phys. Rev. Lett. **73** (1994) 3584; N. Richard et al., Phys. Rev. B **59**, 5936 (1999); C. Herman et al., Phys. Rev. B **64**, 235422 (2001).

**Figures:**
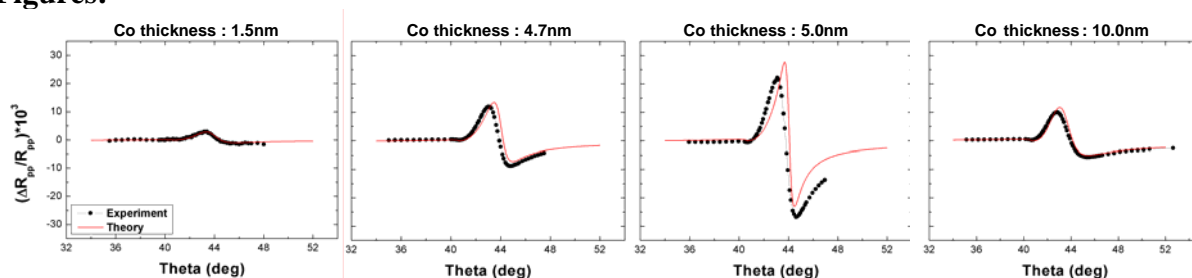


Figure: $\Delta R/R$ vs incidence angle for different Co thickness (6nm Au/Co/16nm Au/glass). $\Delta R/R$ does not continuously increase with Co thickness, but reaches a maximum value for 5 nm Co.

# TOWARDS CONTROLLED BOTTOM-UP ARCHITECTURES IN ORGANIC HETEROEPITAXY

*<u>Dimas G. de Oteyza</u>,(a) Esther Barrena,(a,b) Tobias Kraus,(a) Stefan Sellner,(a) Oriol Ossó,(c) Helmut Dosch (a,b)*
*(a) Max Planck Institute for Metals Research, Heisenbergstr. 3, Stuttgart, Germany*
*(b) Institut für Theoretische und Angewandte Physik, Universität Stuttgart, Stuttgart, Germany*
*(c) Institut de Ciència de Materials de Barcelona CSIC, Bellaterra, Spain*
*[dgoteyza@mf.mpg.de](mailto:dgoteyza@mf.mpg.de)*

The last decade has witnessed an increased interest on the development of devices based on semiconductor organic materials. Yet, the present day-knowledge that enables the controlled growth of organic architectures is in an early stage. Moreover when sequential deposition of two organic materials is involved (organic heterostructures), as required for multiplayers or p-n heterojunctions.

Here we report a study on the growth of organic heterostructures combining diindenoperylene (DIP), which shows preferential p-type conduction, with fluorinated copper-phthalocyanines ($F_{16}CuPc$), one of the few air-stable oligomers showing preferred n-type conduction. The heterostructures are grown in form of bilayers, by depositing films of one of the molecular species onto $Si/SiO_2$, and using it as substrate for subsequent deposition of the other molecular species. Both deposition sequences have been studied as function of the growth temperature by in-situ X-ray scattering and atomic force microscopy (AFM).

When DIP is deposited onto $F_{16}CuPc$ above a threshold substrate temperature of 90ºC, the formation of highly crystalline DIP islands takes place via Stranski-Krastanov growth. Their growth is intimately related to a novel type of reconstruction of the underlying organic film, which affects three monolayers adjacent to the organic interface.[1] Below 90ºC, the reconstruction of the underlying $F_{16}CuPc$ does not take place and DIP follows a close layer-by-layer growth. The temperature dependence of the growth behaviour can thus be exploited to control the resulting morphologies, ranging from well ordered layered heterostructures to the self-organization of highly crystalline DIP islands with tunable size and density (Figure 1).

Deposition in the opposite sequence, i.e. $F_{16}CuPc$ on DIP, differs from the previous case in the sense that well ordered layered heterostructures form independently of the growth temperature. However, while $F_{16}CuPc$ deposited at low temperature orders in the known β-structure,[2] at high temperature $F_{16}CuPc$ grows with the same structure as that of the reconstructed layers below DIP in the case of DIP on $F_{16}CuPc$ at high T.

In spite of the close resemblance with the formation of semiconductor nanostructures for inorganic heteroepitaxy, the present results conclusively demonstrate a distinctly different growth mechanism for organic heteroexpitaxy.

**References:**

[1] Esther Barrena, Dimas G. de Oteyza, Stefan Sellner, Helmut Dosch, J. Oriol Ossó, Bernd Struth, Phys. Rev. Lett., **97** (2006) 076102.

[2] Dimas G. de Oteyza, Esther Barrena, J. Oriol Ossó, Stefan Sellner, Helmut Dosch, J. Am. Chem. Soc., **128** (2006) 15052
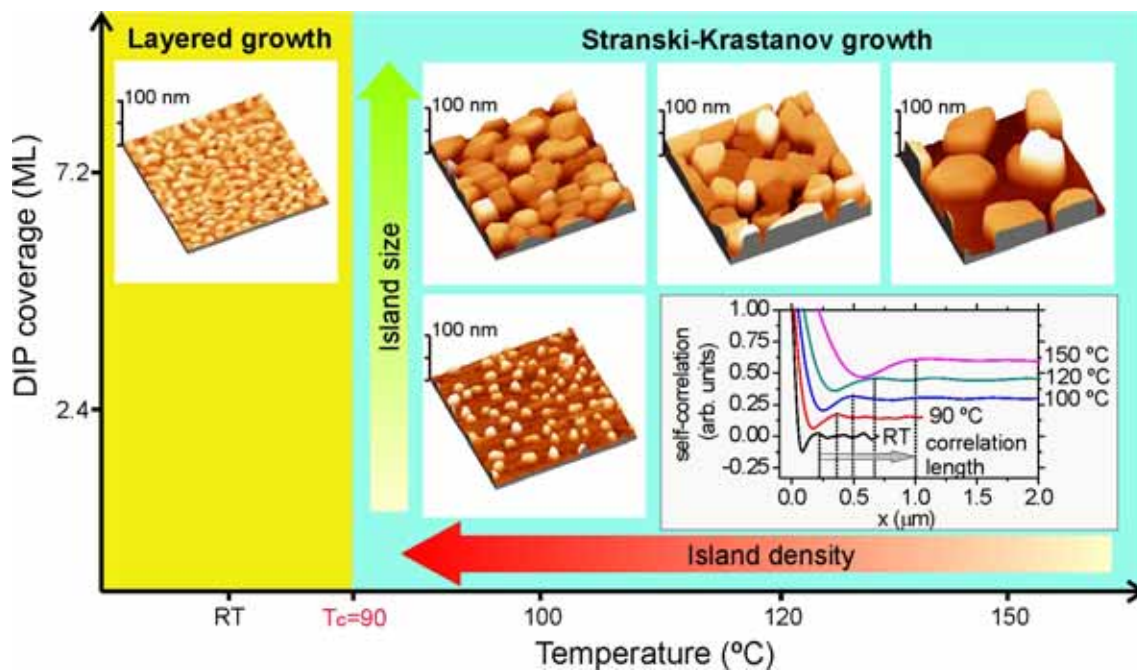
**Figures:**



**Figure 1.** Morphology of the heterostructures consisting in DIP on $F_{16}CuPc$, grown at different temperatures and with different DIP coverage. All images show areas of 2x2 $\mu m^2$ and are plotted according to the same z-scale bar, in order to allow a better comparison among samples. The colored arrows indicate the tunability of island size and density by the appropriate choice of growth temperature and DIP coverage. The self-correlation functions of the different samples give further evidence on the increasing correlation length with temperature.

# ELECTRICAL CHARACTERIZATION OF HYBRID METAL-POLYMER NANOWIRES

*L. Gence, S. Faniel, V. Callegari, S. Demoustier-Champagne, S. Melinte, V. Bayot*
CERMIN, Université catholique de Louvain, B-1348 Louvain-la-Neuve, Belgium
Loik.gence@uclouvain.be

In the recent years, many studies have been devoted to the characterization of low-dimensional structures. Organic and hybrid organic-inorganic nanomaterials are at the heart of the emerging field of nanotechnology. Among them, organic nanowires (NWs) and nanotubes are promising components for a wide variety of electronic applications. The fabrication, manipulation, and characterization of such systems are quite challenging.

Here, we investigate the electrical properties of hybrid metal(Au)-polypyrrole(PPy)-metal(Au) NWs from room-temperature down to very low temperature ($T \sim 0.5$ K). Furthermore, we highlight our strategy for the fabrication of a platform adapted to both electrical and thermopower measurements of NWs.

Segmented composite PPy NWs presenting diameters of 50 [M50], 70 [S70], and 90 nm [M90], with a nominal PPy length between 300 and 1500 nm, were prepared by an all-electrochemical template method described in detail in Ref. [1]. Variable temperature electrical measurements of multiple NWs embedded in the polycarbonate template (samples M50 and M90) are compared to those of the single NW sample S70.

In all samples, current-voltage ($I-V$) characteristics are symmetrical and show no rectification effect. They are linear from room temperature down to $T \sim 100$ K and nonlinear at lower temperatures. The current-voltage $I-V$ characteristics of sample S70 are given Fig. 1(a). We show that the Mott variable-range hopping (VRH) model provides a complete framework for the understanding of transport in our PPy NWs. In this model, the resistance follows the relation $R(T) \sim \exp(T_0/T)^{1/4}$, where $T_0 = 16a^3/k_B N(E_F)$, $k_B$ is the Boltzmann constant, $a$ is the localization length, and $N(E_F)$ is the density of states at the Fermi energy. The VRH plots are shown Fig. 1(b) and are used to extract $T_0$. To estimate the localization length in our samples, we performed low-$T$ magnetoresistance measurements. The plot of *ln[R(B)/R(0)]* with respect to the magnetic field ($B$) for sample M90 is given in Fig. 1(c). Data fits the wavefunction shrinkage model developed by Shklovskii and Efros [2]. From this model, we deduce a localization length of about 1.5 nm in our samples and, thus, calculate $N(E_F)$.

We reveal here our strategy for the fabrication of devices designed to perform both electrical and thermopower measurements of single NWs. These devices essentially consist of two platinum electrodes on top of two 80 nm thick silicon nitride ($Si_3N_4$) membranes. On each membrane, we pattern a platinum resistance serving as thermometer and heater, respectively. Membranes are supported by 1 µm wide and 240 µm long $Si_3N_4$ beams. A close-up view of the two membranes is given Fig. 1(d).

**References:**
[1] O. Reynes *et al.,* J. Electrochem. Soc. **152,** (2005) D130.
[2] B.I. Shklovskii and A.L. Efros, *Electronic Properties of Doped Semiconductors*, Springer, (1984).

**Figure:**
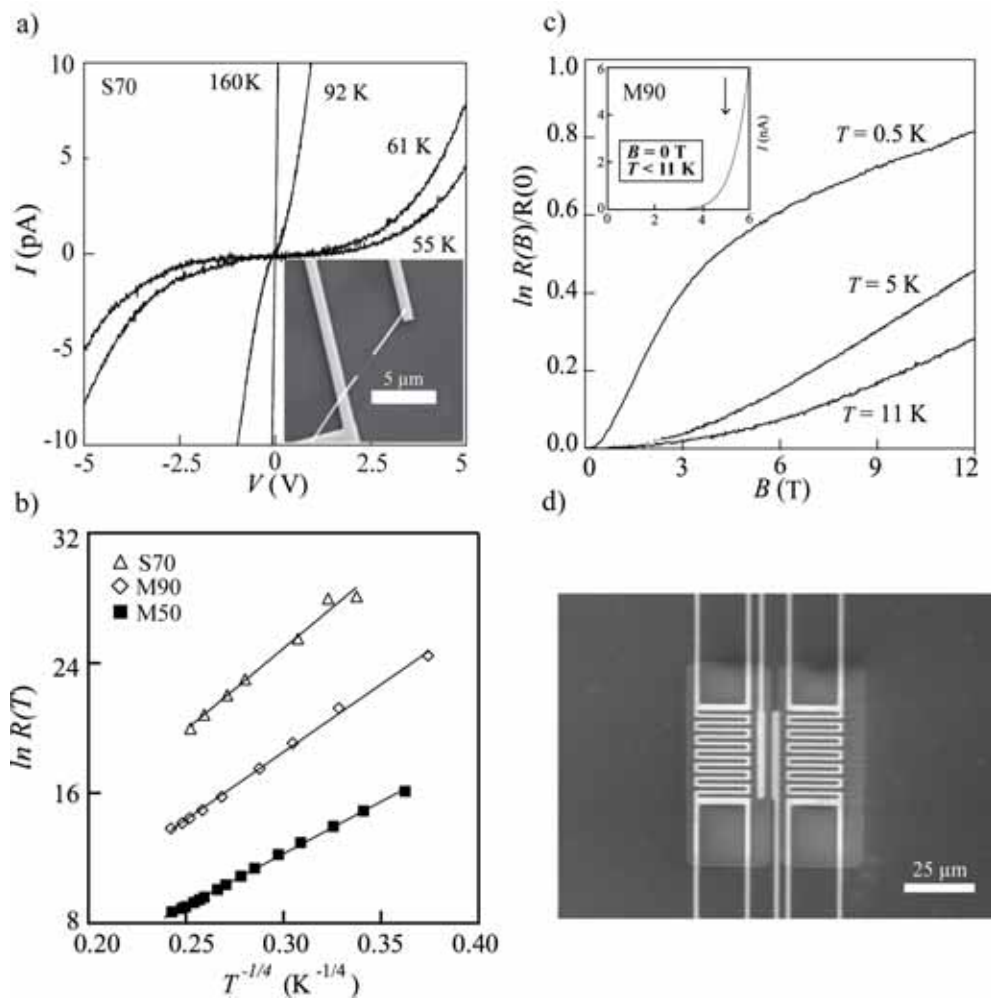


Fig.1 (a) *I−V* characteristics of sample S70. (b) VRH plots for samples S70, M90, and M50. The solid lines are fits to the data. c) Variation of *ln[R(B)/R(0)]* with *B* at indicated *T*'s for the sample M90. Inset: Below *T* = 11 K the *I−V* curves are indistinguishable. (d) SEM image of the device for thermopower measurements.

# DISSIPATIVE VAN DER WAALS INTERACTION BETWEEN A HYDROGEN ATOM AND A METAL SURFACE

*A. Zolanvari, R. Ghemmaghami*
*Department of Physics, University of Arak,  P.O. Box: 38156-879, Arak, IRAN*

We use a general theory of the fluctuating electromagnetic filed to calculate the firiction force acting on a Hydrogen atom, moving near a metal surface. We consider the dependence of the electromagnetic firiction on the temperature T,the separation d ,and discuss the role of screening, non-local and retardation effects.We find that for high resistivity materials,the dissipative van der waals interaction can be an important mechanism of vibrational energy relaxation of physisorbed molecules,and friction for microscopic solids.

Reference

M.S.Tomasson and A.Widom,Phys.Rev.B 56,4938,(1997).
B.N.J.Persson and Z. Zhang,Phys.Rev.B57,7327,(1998).
A.I.Volokitin and B.N.J.Persson, J.Phys.:Condens.Matter 14, 859 (2001).
B.Gostman, C.Seidel, B.Anczykowski, H.Fuchs, Phys. Rev. B 60, 11051 (1999).
B.C. Stipe, H.J. Mamin, T.D. Stowe, T.W. Kenny and D. Rugar, Phys. Rev. Lett. 87 096801 (2001).
E.T.Watts, J.Krim, A.Widom, Phys.Rev. B 41, 3466 (1990).

# SYNTHESIS AND CHARACTERIZATION OF HYDROXYAPATITE NANOPOWDERS WITH HIGH STABILITY

*Ecaterina Andronescu, Elena Dinu, Cristina Daniela Ghitulica, Oana Nicola, Mihaela Barsan*
*University POLITEHNICA from Bucharest*
*1-7, Gh. Polizu Street, 1-Bucharest, PO – BOX 12-134, Romania*
*Email: cghitulica@yahoo.com, elena_dinu@yahoo.com*

Hydroxyapatite (HAp: $Ca_{10}(PO_4)_6(OH)_2$) is chemically similar to the mineral component of bones and hard tissues, being one of the few synthetic materials that shows bioactivity [1-3]. However, its applications are limited, because of HAp instability when processed at elevate temperatures [1-4]. Preparation of dense HAp ceramics with superior stability is possible if the starting powders are very fine [1-5]. Synthesis methods that are imitating the physiological conditions seem also to lead to materials with improved properties [1-6].

The hydroxyapatite powders were obtained through chemical methods, from $Ca(NO_3)_2 \cdot 10H_2O$ and $(NH_4)_2HPO_4$, mixed in stoichiometric proportions. The reaction was performed in SBF (Simulated Body Fluid) solution, in the presence of urea. There were used two different ways for mixing the precursors: "initial" addition and "successive" addition [7-10]. For the "initial" addition method the solutions of precursors were mixed instantly, and for the "successive" addition, the solutions were mixed in droplets.

The powders were calcinated at $600^0C$ and characterized in what it concerns the mineralogical composition (using an X-ray difractometer *SCHIMADZU XRD 6000)* and the microstructure (using a scanning electronic microscope *EDAX - HITACHI S2600N*). The diffraction images showed the presence of hydroxyapatite (JCPDS 09-0432) as unique phase, for all experimental conditions, that proved to be stable even after sintering treatments at temperatures between 1000 and 1500°C, for 6 hours.

The scanning electron microscopy showed that the powder obtained by "initial" addition, thermally treated at 1000°C for 2h, is constituted of particles with elongated shape, needle-like, with dimensions between 0.5 and 1.0 µm. Intergranular porosity is present, with dimensions of approximately 0.5µm (figure 2A). If the temperature increases to 1500°C, the SEM images are demonstrating a higher densification of samples, with importantly reduced porosity (figure 2B).

The powder synthesized by the „successive" addition, thermally treated at 1000°C/2h, it has the same morphology, but this time the length of needles is bigger, reaching even 20 µm (figure 3A). Higher densification is achieved also for this powder at higher temperature.

We might conclude that all experimental conditions considered led to the formation of hydroxyapatite nanopowders, stable at high temperature thermal treatments. That will permit better densification of hydroxyapatite compacts, which could potentially develop better mechanical properties.

**References:**
[1] W. Suchanek and M. Yoshimura, J. Mater. Res. 13 (1998) 94.
[2] W. Suchanek, H. Suda, M. Yashima, M. Kakihana, and M. Yoshimura, J. Mater. Res. 10 (1995) 521.
[3] P. Shuk, W. L. Suchanek, T. Hao, E. Gulliver, R. E. Riman, M. Senna, K. S. Tenhuisen and V. F. Janas, J. Mater. Res. 16 (2001) 1231.
[4] M. F. Hsieh, T. S. Chin, L. H. Perng and H. G. Perng, J. Am. Ceram. Soc. 84 (2001) 2123.
[5] E. Tkalcec, M. Sauer, R. Nonninger and H. Schmidt, J. Mater. Sci. 36 (2001) 5253.
[6] S. Raynaud, E. Champion, D. Bernache-Assollant and J. P. Laval, J. Am. Ceram. Soc. 84 (2001) 359.

[7] K.C.B Yeong, J.Wang- Fabricating densified hydroxiapatite ceramics from a precipitated precursor, Materials Letters 38(1999) 208-213.

[8] Hassna Rehman Ramay, Miqin Zhang- Preparation of porous hydroxiapatite scaffolds by combination of the gel-casting and polymer sponge methods, Biomaterials 2003; 345-346.

[9] Ming-Fa Hsieh, Li-Hsiang Perng- Phase purity of sol-gel derived hydroxiapatite ceramic, Biomaterials 22(2001), 2601-2607.

[10] Kui Cheng, Ge Shen, Wejian Weng- Synthsis of hydroxiapatite/fluoroapatite solid solution by a sol-gel method, Biomaterials 51(2001), 37.

**Figures:**
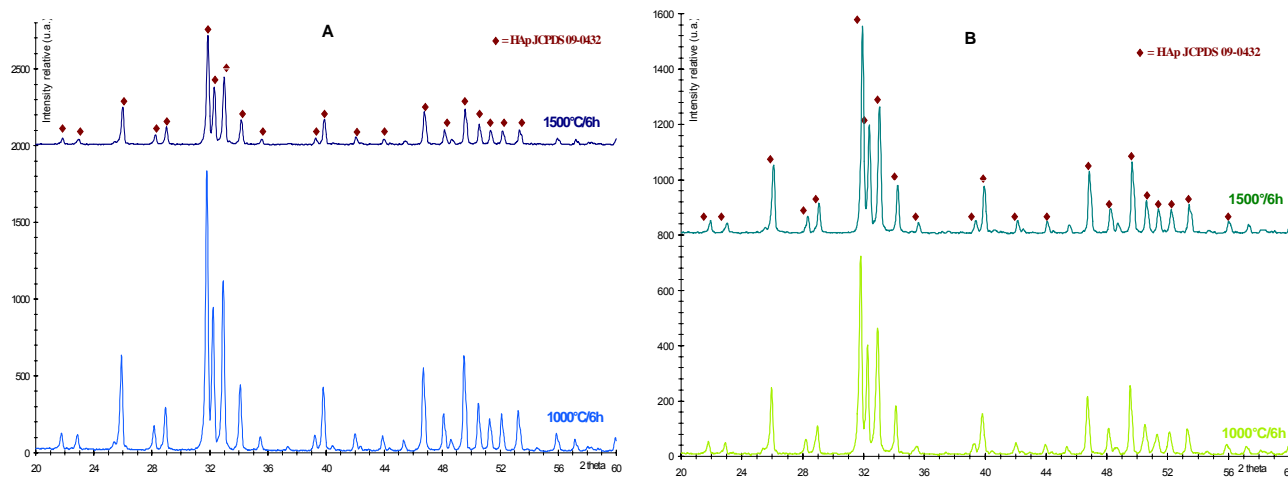


Figure 1. The X-ray diffraction spectrum for powders synthesized by "initial" addition (A) and "successive" addition (B), for temperatures of thermal treatment of 1000 and 1500$^{o}$C
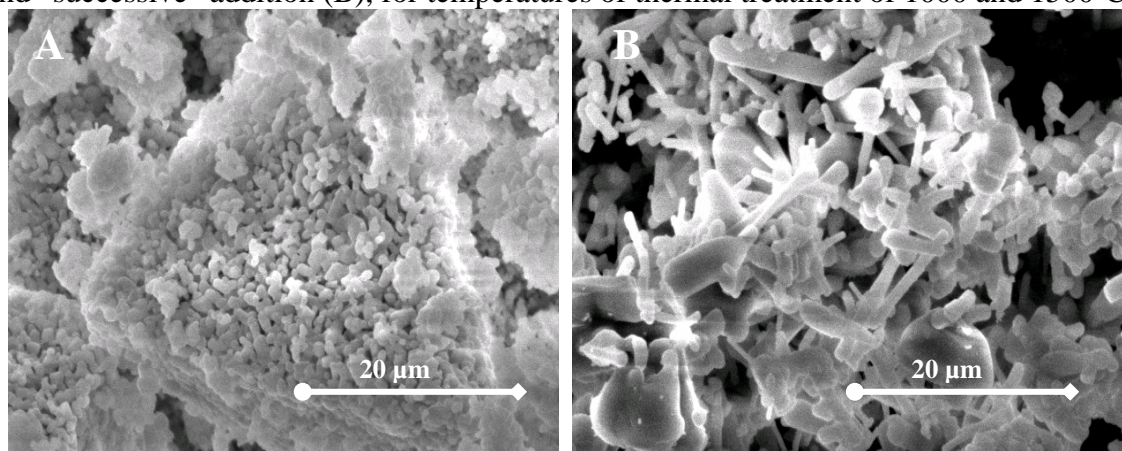


Figure 2: Scanning electron microscopy images of powder synthesized by "initial" addition (A) and "successive" addition (B) thermally treated at 1000°C/6h (X 2000)
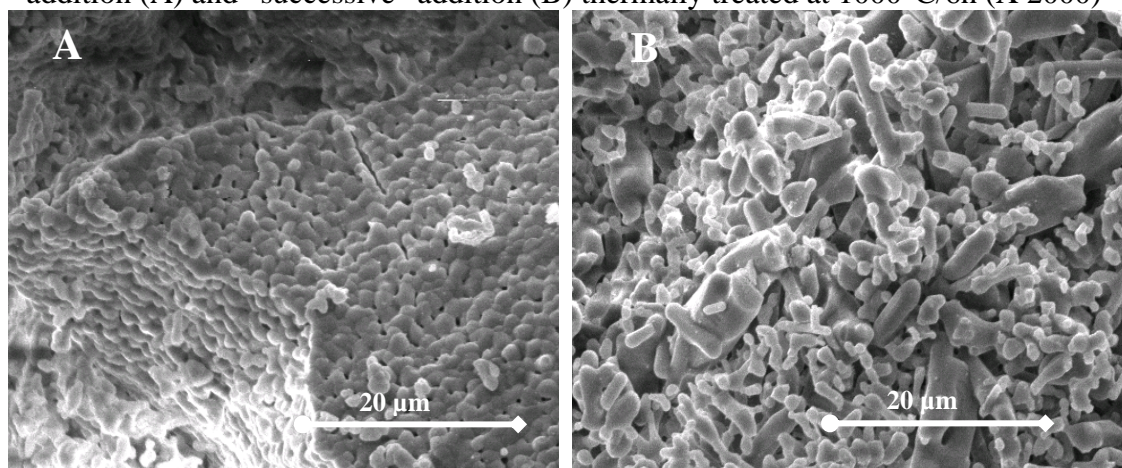


Figure 3: Scanning electron microscopy images of powder synthesized by "initial" addition (A) and "successive" addition (B) thermally treated at 1500°C/6h (X 2000)

# DEVELOPMENT OF NANOSTRUCTURED MAGNETIC MATERIALS FOR HIGH FREQUENCY APPLICATIONS THROUGH POWDER METALLURGY

*Sixto Giménez, Jon Echeberría, Francisco Castro*

*CEIT and TECNUN, Paseo Manuel de Lardizábal 15, 20018 San Sebastián, Spain*

*sgimenez@ceit.es*

Nanostructured magnetic materials possess excellent soft magnetic properties, high saturation magnetization and high temperature stability. This is due to the fact that the grains are exchange coupled and that the structural correlation length is smaller than the ferromagnetic exchange length. Consequently, the local anisotropies are randomly averaged out similarly to the case of amorphous metals [1]. Manufacturing of these materials normally involves obtaining an amorphous precursor, which is subsequently heat treated for nanostructuring. Processing through powder metallurgical processes adds compositional and geometrical flexibility to the design of final components [2]. During the last year, CEIT has targeted the processing, structural and magnetic characterisation of nanostructured magnetic powders for high frequency applications (nanodevices for automotive, communications and control systems).

The commercial amorphous powders were obtained by a spinning water atomisation process (KUALMET grade) and conventional water atomisation (AW2-08 grade). The powders were manufactured at EPSON ATMIX Co. (Hachinohe, Japan). The qualitative composition provided by the manufacturer is Fe-Si-Cr-B.These materials are developed for power electronics applications. Two different size fractions were supplied (<53 μm and <150 μm). The processing methodology involves nanostructuring of the amorphous powders by heat treatment and consolidation into final shapes by uniaxial pressing. The structural and magnetic properties of the material were monitored after each processing step. SEM, TEM, XRD, DSC and MFM were employed for structural characterisation focusing on the crystallisation behaviour of the materials and the interaction of the structural and magnetic domains microstructures. The magnetic characterisation was carried out by VSM.

The SEM microscructures of the two different materials can be observed in Figure 1. Basically, the powder morphology is practically equiaxial, the bigger the particle size, the less degree of symmetry is observed, evolving from spherical to ellipsoidal. Apart from the difference in size of the three powders reported, the powders are quite similar in terms of composition. The crystallization behaviour can be inferred from Figure 2a, where the DSC scans of the three materials is illustrated. The narrow peak occurring from 818 K on accounts for a sudden primary crystallization event. The peak width is 30 K. The amorphous structure of the as-received materials is confirmed by the XRD diffractograms shown in Figure 2b. The microstructural evolution of the materials with the heat treatment temperature has been quantitatively analysed in terms of crystallised fraction and crystallite size. Figure 3 shows the surface domain structure identified by MFM for the KUALMET grade. The surface magnetic contrast is the phase difference between the bright and dark regions, corresponding to upward and downward magnetization states, respectively. The width of the magnetic domains ranges 100-300 nm, accounting for the excellent soft magnetic properties of the material: $H_c = 0.4$ Oe at 800 K, $\mu_i = 90$-110 (up to 1 MHz), losses = 660 kW/m$^3$ (at 100 kHz, Bm = 0.1 T), $B_m = 10$ kG (at H=300 Oe) [3].
.

**References**
[1] M. E. McHenry, M. A. Willard and D. E. Laughlin, Progress in Materials Science, 44 (1999) 291-433.
[2] R.M. German. Powder Metallurgy Science, Ed. Metal Powder Industry (1994).
[3] I. Otsuka, A. Watanabe, H. Izaki, and M. Yagi. Proceedings of the European Conference on Powder Metallurgy, PM2006, October 21-25, Gent, Belgium, EPMA. ISBN 1-899072-34-9.

**Figures**



(a)       (b)       (c)
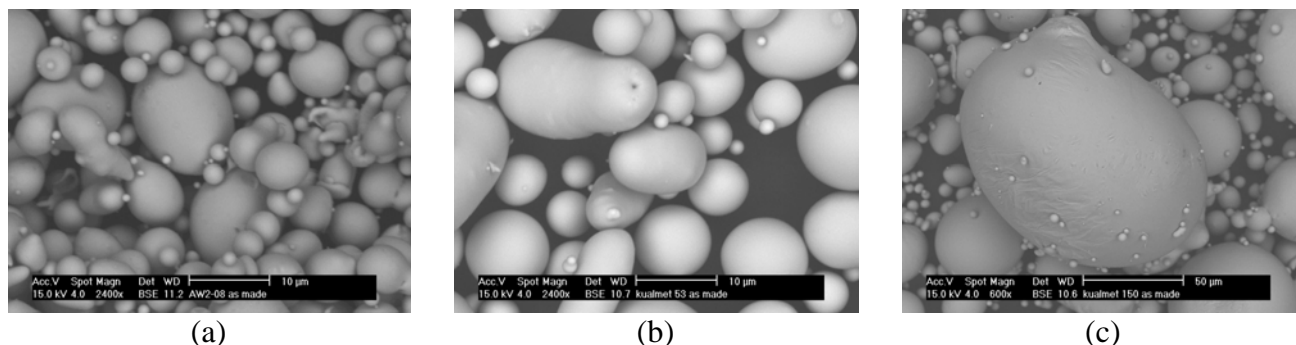
*Figure 1.- SEM microstructure of the as-received powders (a) AW2-08 and KUALMET (b) < 53 μm (c) < 150 μm.*



(a)       (b)
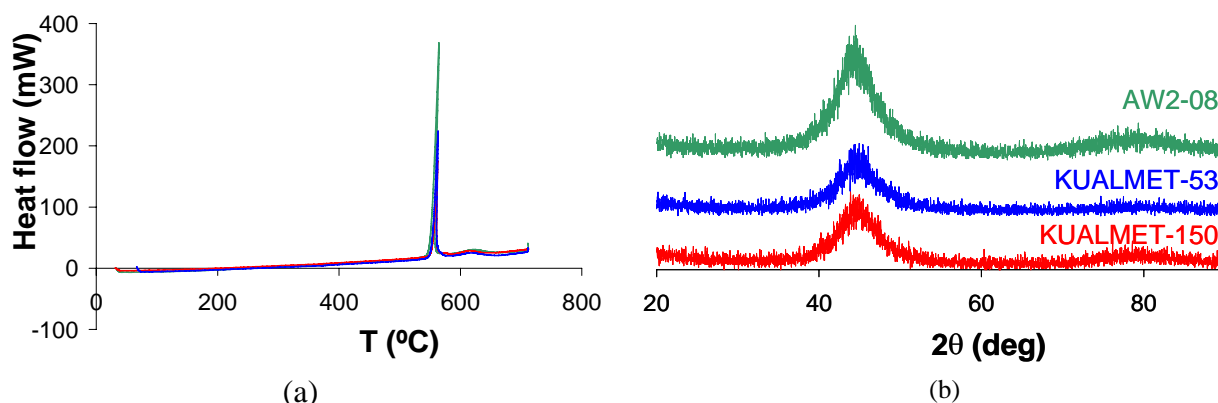
*Figure 2.- (a) DSC scans of the three different materials, (b) XRD diffractograms of the three different materials evidencing the amorphous structure of the as-received powders.*



(a)       (b)       (c)
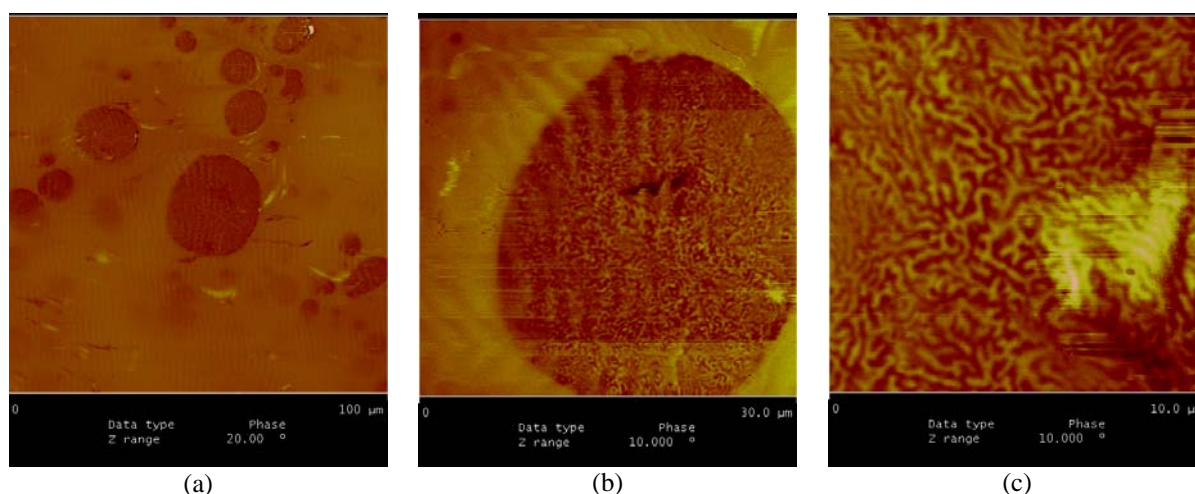
*Figure 3.- MFM imaging of the as-received KUALMET powders at different magnifications (a) 100 x 100 μm (b) 30 x 30 μm (c) 10 x 10 μm.*

# Numerical simulation of electron transport in nanoscaled silicon-on-insulator multigate devices

*A. Godoy, F. Gámiz, C. Sampedro, F.G. Ruiz, I.M. Tienda-Luna*
*Departamento de Electrónica, Universidad de Granada, Granada, 18071, Spain*
*agodoy@ugr.es*

The 45 and 32 nm technology nodes will require substantial changes in the traditional MOS architecture. Between all of them we can mention the introduction of silicon layers of nanometric thickness, strained substrates, and the use of multiple gate transistors which allow the control of the SCEs. Such reduced dimensions imply a significant increase in manufacturing costs. Moreover, new physical phenomena become involved in the device behavior which will produce an additional difficulty to forecast the circuit performance. For these reasons physically based semiconductor device simulation is a necessary tool providing insight of device operation and allowing a shortening of the development cycle for each new technology generation.

Depending on the carrier confinement, three different types of semiconductor structures can be considered: 1.- Quantum-wells; 2.- Quantum-wires (QWI) and 3.- Quantum-dots. In the first group, where electrons are confined in 1D and move freely in the other two, we can consider devices such as, single and double gate SOI. In the second group, where electrons are confined in two dimensions, other structures such as Trigate or Gate All Around (GAA) can be mentioned. In the third group, electrons are confined in the three dimensions.

It is possible to define a hierarchy of models to simulate the electron transport in those devices belonging to the first and second group. The most popular method for classical simulations is the drift-diffusion approximation. Its success comes from their computational efficiency and it has been widely used for circuit simulation. On the other hand, full quantum simulators based on numerical solutions of the Schrödinger equation or the Non-Equilibrium Green's Functions theory (NEGF) has also been developed. However, the introduction of scattering in the simulations implies a very high computational cost and only simplified models can be used in practical quantum simulations [1].

Between these approaches, Ensemble Monte Carlo (EMC) simulators have been widely used since they show a reduced computational cost compared with full quantum approaches and higher accuracy than the drift-diffusion approximation. There are different methods to include quantum corrections in the EMC scheme, however it is preferable express this correction in terms of the electrostatic potential which is a smoother magnitude. Following this idea, the Effective Conduction Band-Edge (ECBE) method was developed [2] where the different valley characteristics and arbitrary transport and confinement directions are considered. Different results obtained following this procedure are shown in the figures.

On the other hand, QWIs are characterized for extremely reduced lateral dimensions which make necessary the self-consistent solution of the 2D Schrödinger and Poisson equations in the channel cross-section. The simulation of long wires justifies the use of a semi-classical MC simulation with the inclusion of the quantum effects. However, the traditional MC algorithm used to calculate the electron transport properties in silicon inversion layers has to be modified to take into account the specific characteristics of the 1D density of states which presents a large number of peaks. It has been observed that the increase in phonon scattering produced when the lateral size was reduced to below 10nm causes a noticeable degradation of the transport properties.

**References:**
[1] U. Ravaioli and T. Van der Straaten, Simulation of Nanoscale Molecular Systems. Handbook of Theoretical and Computational Nanotechnology; American Scientific Publishers, 2006.
[2] C. Sampedro, F. Gámiz, A. Godoy, and F. García-Ruiz, IEEE Trans. Electron Dev. **53** (2006) 2703.
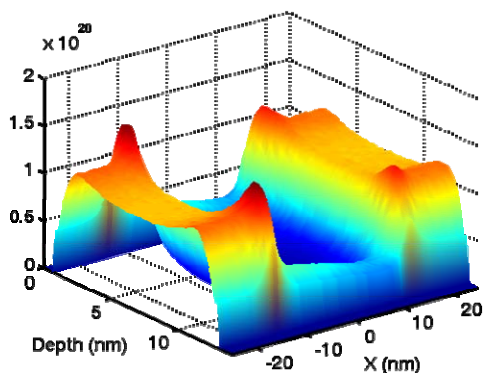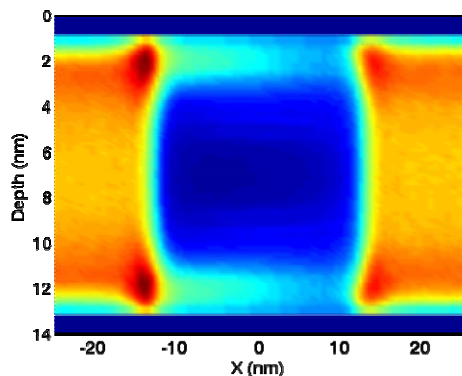
**Figure 1.-** Electron density distribution in a DGSOI transitor
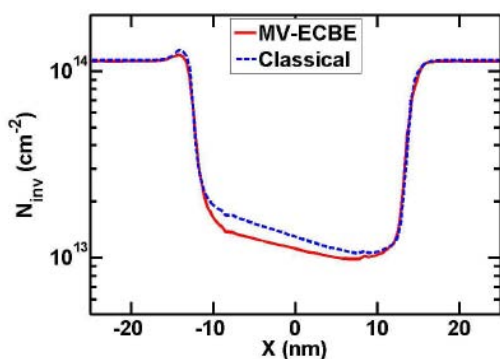


**Figure 2.-** Comparison of the inversion charge along the channel direction for classical (dashed) and MV-ECBE (solid) simulations. Quantum effects produce an increase in the threshold voltage
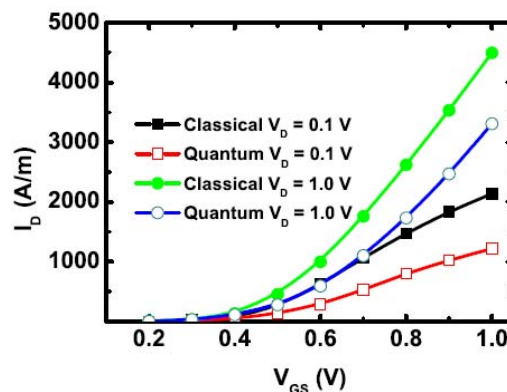


**Figure 3.-** $I_D$–$V_{GS}$ curves comparison calculated for $V_{DS}$=0.1V and 1V when classical and quantum description are used.
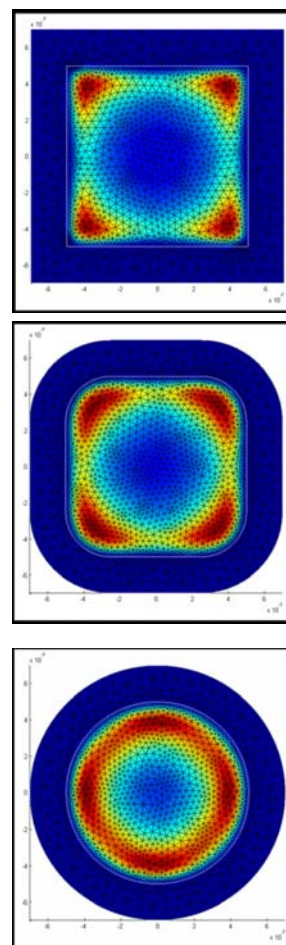


**Figure 4.-** Electron density in silicon QWIs with variable cross-section, from square to circular.

**Nanotube-Based Interconnects for Nanotechnology Circuits: An Introspection**

*Ashok K. Goel*

*Electrical & Computer Engineering, Michigan Tech University, Houghton, MI 49931, USA*
*goel@mtu.edu*

As progress along the ITRS road map continues, physical and electromagnetic limitations make scaling of silicon FETs increasingly difficult. One solution is to replace FETs by completely new structures such as nanoscale molecular, biological or quantum devices. Before considering this changeover, an interconnect technology must be developed that is suitable for these new device concepts. To connect ultra-small devices, interconnects must be less than 10 nanometers (nm) in diameter. However, they still must be easy to fabricate, have low resistance, high maximum current carrying capacity and be isolated by low-k dielectric materials for applications in ultra-high density nanotechnology circuits. As the sizes of the active devices approach the nanometer dimensions, the wires that connect them must also be scaled down. Today, several IC manufacturers are in the process of commercializing 100 nm CMOS-based IC technologies and the research & development work for the 70 and 50 nm devices is well underway. Successful IC development below these feature sizes faces the fundamental challenges imposed by the basic lays of quantum physics. The surface scattering from the boundaries of ultra-narrow conductors as well as the grain boundary scattering would inhibit electronic conduction in the wires to an unacceptable level.

Nanotechnology circuits with devices on the sub 100 nm scale will require interconnects with sizes from 50 nm down to molecular and atomic dimensions. If metallic conducting lines such as copper are used for the interconnects then the miniaturization process will result in rise in the copper resistivity because the dimensions of the conducting lines will be of the same order of magnitude as the mean free path of electrons which is 39.3 nm in copper at room temperature. This rise in resistivity may dramatically slow the circuit's functioning and as a result jeopardize the ability to improve the circuit speed expected from miniaturization. Electromigration which is the result of momentum transfer from the electrons moving under the applied electric field to the ions making up the lattice structure of the interconnect material imposes another serious problem. Continuing miniaturization of the thin-film metallic interconnects results in increasingly high current densities leading to the open- and/or short-circuit electrical failures of interconnects in a relatively short time. The higher the temperature of operation, higher the electromigration-induced failure of the metallic interconnects is. Clearly, interconnects will play a crucial role in the development of the nanoscale integrated circuits and that, in addition to the development of the various nano devices, interconnects that will be used to connect these devices deserve a very special attention. In this paper, the applicability of carbon nanotubes (CNTs) as interconnects for nanotechnology circuits will be investigated.

Nanotubes are tiny tubes about 10,000 times thinner than a human hair and consist of rolled up sheets of carbon hexagons. They have the potential for use as minuscule wires in ultra small electronic devices. The electrical properties of CNTs are fascinating because they can exhibit metallic or semiconducting behavior depending on their structure and dimensions. This has made

carbon nanotubes a unique candidate material for potential nanotechnology applications as nanoscale electronic devices and interconnections.

To a large extent, the unique electrical properties of CNTs such as their extremely low electric resistance are derived from their one dimensional character and the unique electronic structure of graphite. Resistance primarily occurs due to defects in crystal structure, impurity atoms or an atom vibrating about its position in the crystal. In the case of a CNT, the electrons are not so easily scattered. Due to the small diameter and the huge aspect ratio (length to width), nanotubes are essentially 1-D systems and therefore electrons have low chance of scattering giving rise to very low resistance. The electronic properties of perfect MWNTs are rather similar to those of perfect SWNTs because the coupling between the cylinders is weak in MWNTs.

Electrical transport in metallic SWNTs and MWNTs is ballistic, i.e., without scattering over long nanotube lengths enabling them to carry high currents with essentially no heating. In contrast, electrons in copper travel only 40-50 nm before they scatter. Phonons also propagate easily along the nanotube. Superconductivity has also been observed at low temperatures with transition temperatures of nearly 0.55 K for 1.4 nm diameter SWNTs and nearly 5 K for 0.5 nm SWNTs.

The low resistance ensures that the energy dissipated in carbon nanotubes is very small thereby solving the problem of dissipated power density that adversely affects silicon circuits. Current densities of more than $10^{10}$ A/cm$^2$ have been reported for the metallic configuration of CNTs. Since carbon nanotubes do not have any leftover bonds there is no need to grow a film on the surface in order to tie-up the free bonds and there is no need to restrict the gate insulator to silicon dioxide. This fact implies the use of other superior materials to insulate the gate terminal in a transistor which can result in a much faster device.

Carbon nanotubes have shown great promise for use as interconnections in nanotechnology circuit applications. This is particularly because they can conduct large currents of the order of a $10^6$ A/cm$^2$ without any deterioration thus avoiding the electromigration problems characteristic of metallic interconnections. The scattering-free transport of electrons possible in defect-free carbon nanotubes is a very attractive feature of CNTs for microelectronic applications. The reduction in the thickness of conventional metallic or polycrystalline interconnections leads to additional scattering at the surfaces and grain boundaries thereby deteriorating the interconnection resistance. CNTs provide undistributed quasi-crystalline wire-like structure where pulses can travel uninterrupted by length dependent ohmic scattering. The approximate estimation of signal delays with a simple model proves that nanotubes would surpass classical wires with respect to signal delays. Plenty of work on using carbon nanotubes for building integrated circuits is in progress. Researchers are also trying to develop complex gates and circuits by fabricating devices along the length of a single CNT.

―――――――――――――――――

# X-RAY MAGNETIC CIRCULAR DICHROISM STYUDY OF MAGNETIC DODECANETHIOL-CAPPED Au NANOPARTICLES.

*E. Goikolea[a], M. Suzuki[b], I. Gil de Muro[a], M. Insausti[a], J. S. Garitaonandia[a]*

[a]*Zientzia eta Teknologia Fakultatea, UPV/EHU, Apdo. 644, 48080, Bilbao, Spain*
[b]*Japan Synchrotron Radiation Research Institute (JASRI / Spring-8), 1-1-1 Kouto, Mikazuki, Sayou 679-5198,* Japan
*qibgonue@ehu.es*

From some years now, metallic nanoparticles are acquiring increased scientific importance in fields such as chemistry, physics, biology or medicine. Their useful potential applications, from carriers for cancer-treatment drugs to digital data storage, are rapidly increasing as the scientific studies progress.

Since the first publications about magnetic Au nanoparticles [1,2], various research groups from very different backgrounds have tried to explain this novel behavior. When a metal particle having bulk properties is reduced in size to a few atoms the electronic structure changes dramatically which affects noticeably to the physical properties, this is known as the size effect. This size reduction also increases the surface to volume relation, the surface effect. As a result of both effects, all atoms from a nanoparticle undergo electron redistribution.

In this work, we show a direct evidence of the intrinsic ferromagnetism of dodecanethiol capped Au nanoparticles of an average size of 1.8 nm (Fig 1) by means of element-specific magnetization (ESM) measurements based on the x-ray magnetic circular dichroism (XMCD) technique. XMCD allows the detection of the magnetic moments of a particular element through sensitivity to the difference between the up- and down- spin densities around the Fermi level. XMCD experiments were performed at the beamline BL39XU of the SPring8 Facility.[3] XMCD spectra were recorded in the transmission mode at Au $L_{2,3}$ edges using the helicity-modulation technique.[4]. The XMCD spectra were recorded at room temperature and under the action of an applied magnetic field of up to 10 T (Fig. 2). The spin-dependent absorption coefficient was obtained as the difference of the absorption coefficient $\mu_c = (\mu^- - \mu^+)$ for antiparallel, $\mu^-$, and parallel, $\mu^+$, orientation of the photon helicity and sample magnetization.

Considering the XMCD signal to be proportional to the magnetization, ESM is obtained by recording the peak amplitude of the XMCD spectra at the Au $L_3$-edge as a function of external magnetic field and temperature. Both the ESM measurement and that measured by means of SQUID magnetometer show similar magnetization process. In either ESM or SQUID curves there is a distinguishable hysteric behaviour and, the magnetization increases when increasing the magnetic field until the saturation is reached which is characteristic of a ferromagnetic material.

## References:

[1] P. Crespo, R. Litran, T. C. Rojas, M. Multigner, J. M. de la Fuente, J. C. Sánchez-López, M. A. García, A. Hernando, S. Penadés, and A. Fernández, Phys. Rev. Lett., **93** (2004) 087204-1.
[2] Y. Yamamoto, T. Miura, M. Suzuki, N. Kawamura, H. Miyagawa, T. Nakamura, K. Kobayashi, T. Teranishi, and H. Hori, Phys. Rev. Lett., 93 (2004) 116801-1.
[3] H. Maruyama, J. Synchrotron Radiat. **6**, (1999) 1133.
[4] M. Suzuki, N. Kawamura, M. Mizumaki, A. Urata, H. Maruyama, S. Goto, and T. Ishikawa, Jpn. J. Appl. Phys., Part 2 **37** (1998) L1488.

**Figures:**
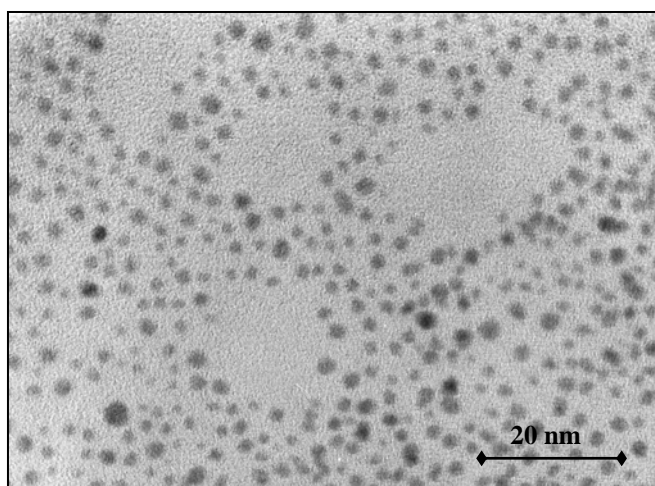


**Figure 1.** TEM micrograph od dodecanethiol-capped Au nanoparticles.
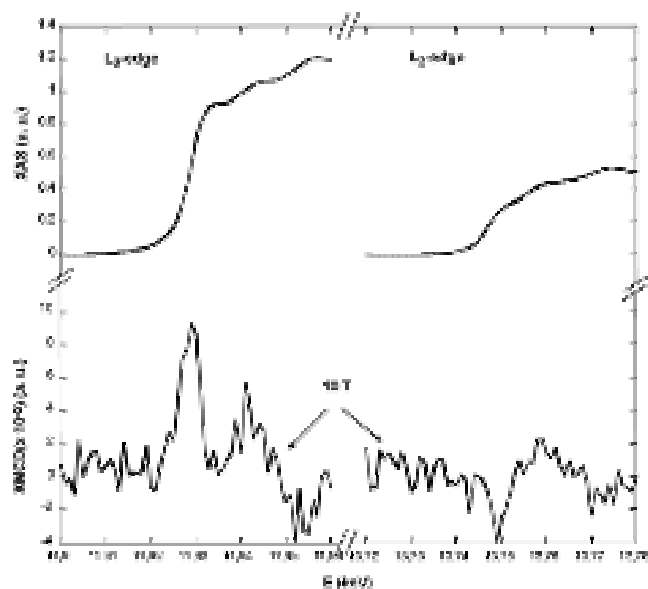


**Figure 2.** XMCD and XAS spectra at the Au $L_3$- and $L_2$-edge with an applied magnetic field of 10 T.

# Ab initio study of substitutionally Ni-doped
# single wall carbon nanotubes: structural and electronic properties

*E. J. G. Santos[1,2], A. Ayuela[1,2], S. B. Fagan[3], J. Mendes Filho[4],*
*D. L. Azevedo[5], A. G. Souza Filho[4] and D. Sánchez-Portal[1,2]*

[1]*Donostia International Physics Center – DIPC, San Sebastian, Spain.*

[2]*Centro de Física de Materiales, Centro Mixto CSIC/UPV/EHU, San Sebastian, Spain.*

[3]*Area de Ciencias Naturais e Tecnologicas - UNIFRA, Rio Grande do Sul, Brazil.*

[4]*Universidade Federal do Ceara – UFC, Ceara, Brazil.*

[5]*Universidade Federal do Maranhao – UFMA, Maranhao, Brazil.*

*eltonjose_gomes@ehu.es*

We report the structural and electronic properties of substitutionally Ni-doped in armchair and zigzag single-wall carbon nanotube (SWNT) [1] by using spin-polarized total-energy ab initio calculations. We find two stable geometries for these systems with Ni atom in an outward or inward local distortion relative to the tube surface (Figure 1). These structures agree with the previous experimental results by Ushiro et al. using extended x-ray absorption fine structure (EXAFS) and x-ray absorption near edge structure (XANES) techniques [2]. The outward configurations are always more stable that the inward ones. We explore the change on the electronic properties after Ni doping SWNT's. A strong dependence between the Ni concentration and the electronic features have been observed. Varying the Ni concentration the, initially metallic, (5,5) SWNT can become either semiconducting, with an energy gap of 0.33 eV for the outward geometry (Figure 1) and 0.14 eV for the inward one, without magnetic behaviour, or remain metallic, but with a total magnetization mean of 0.61 (μ). For the (8,0) SWNT a reduction of the gap is observed from 0.80 eV to 0.39 eV for the outward geometry and 0.37 eV for the inward one. We study in detail the changes in the electronic band structure after the doping. Due to the symmetry reduction most of the expected degeneracies for the tubes are removed. Several bands with strong Ni 3d character appear near the Fermi level. The character and symmetry of these d-bands and its dependence on the bonding configuration and curvature are also studied (Figure 1) [3].
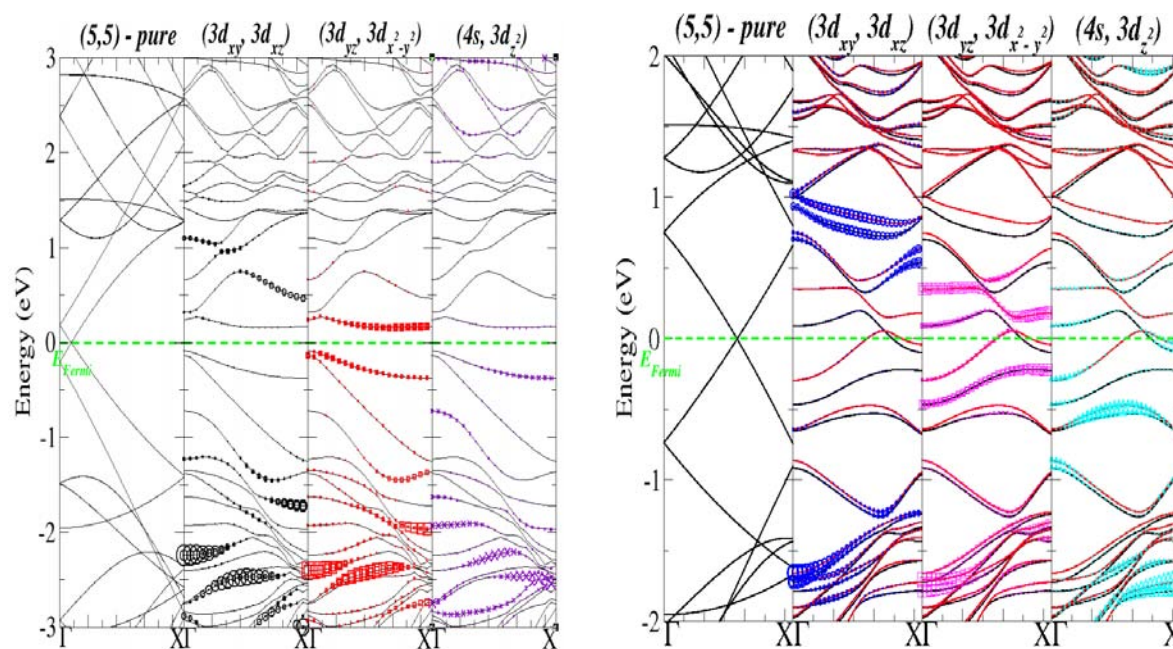
**Figure 1.** The representation of the electronic band structures for the Ni-doped (5,5) in the outward configuration for a Ni concentration of 1.69 % (right panel) and 1.27 % (left panel). The bands mainly associated with the Ni orbitals has been highlighted using solid symbols. The Ni-orbitals are grouped following the remaining symmetries after the Ni dopping. The strong spin split is one of the principal features of the right panel, where the states around the $E_{Fermi}$ have a major contribution from the d-levels. The states in approximatelly -1.70 eV have also a large hibridization with the sp-carbon states, but the contribution of the $3d_{xy}$, $3d_{xz}$, $3d_{yz}$, $3d_{x2-y2}$ orbitals near to the $\Gamma$ point is important to stress.

**References:**

[1] M. S. Dresselhaus and G. Dresselhaus and P. C. Eklund *Science of Fulerenes and Carbon Nanotubes* edited by ed., Academic Press New York (1996).

[2] M. Ushiro and K. Uno and T. Fujikawa and Y. Sato and K. Tohki and F. Watari and W. J. Chun and Y. Koike and K. Asakura , Phys. Rev. B **73** (2006) 144103.

[3] E. J. G. Santos, A. Ayuela, Solange B. Fagan, J. Mendes Filho, D. L. Azevedo, A. G. Souza Filho and D. Sánchez-Portal , Submitted (2007).

# MULTIWALLED CARBON NANOTUBES-GRAPHITE SHEETS CONTACT RESISTANCE

*Miriam Moreno-Moreno, Andrés Castellano-Gómez, Nicolás Agraït,*
*and  Julio Gómez-Herrero*
*Dpto. Física de la Materia Condensada,*
*Facultad de Ciencias. Universidad Autónoma de Madrid*
*Madrid 28049, Spain*

*julio.gomez@uam.es*

In this work we study the electrical contact resistance between multiwalled carbon nanotubes MWNT and graphite sheets composed of a few graphene layers that partially cover the nanotubes. The contact resistance is compared with the one obtained with the gold electrodes for both the graphite sheets and the MWNT. The studies are performed using a conductance atomic force microscope [1] from Nanotec Electrónica. The tips are covered with gold-palladium and used as a second mobile electrode. The experiments show very low contact resistance with the graphite sheets (~4 kΩ). For the case of the MWNT the contact resistance with the gold and graphite sheets depends on the particular type of nanotube. Remarkably, the contact resistance of nanotubes and graphite sheets does not depend on the SWNT length in contact with the graphite thin layers.
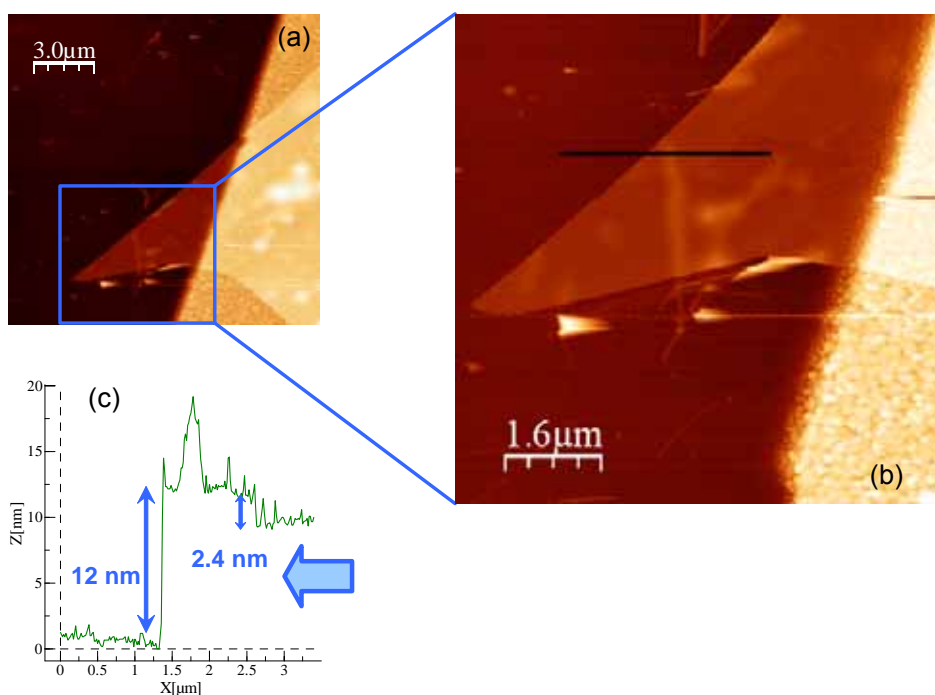


Figure (a) Long range area showing the oxide silicon substrate, the graphite sheets, MWNT and the gold edge. (b) Zoom in the graphite-gold border region in figure (a). Profile taken along the thick black line in figure (b)

[1] I. Horcas, R. Fernández, J. M. Gómez-Rodríguez, J. Colchero, J. Gómez-Herrero, and A. M. Baró, Rev. Sci. Instrum. **78**, 013705 (2007).

# MAGNETOCALORIC EFFECT IN NANOGRANULAR GLASS COATED MICROWIRES

*M. I. Ilyn [1], V. Zhukova[2], J.D. Santos[3], M.L. Sánchez[3], V.M. Prida[3], B. Hernando[3], V. Larin[4], J. González[2], A. M. Tishin[1] and A. Zhukov[2]*

[1]Department of Physics, M. V. Lomonosov Moscow State University, 119992
Leninskye Gory, Moscow, Russia
[2]Department Materials Physics, Faculty of Chemistry, UPV/EHU, Paseo Manuel de Lardizabal 3, 20018
San Sebastián, Spain
[3]Department of Physics, Faculty of Physics, 33007 Oviedo, Spain
[4]TAMAG Iberica, Parque Tecnológico de Miramón, Paseo Mikeletegi 56, 20009 San Sebastián, Spain

The magnetocaloric effect (MCE) in magnetic materials has been widely used for attaining very low temperatures by applying a magnetic field isothermally and removing it adiabatically. As it is well known, in general an isothermal application of a magnetic field decreases the configurational entropy of the spin structure. A subsequent adiabatic demagnetization allows the spins to become disordered again, by means of the thermal energy provided by the phonon bath of the isolated sample. This causes cooling. To note that this effect has been, recently, exploited for room-temperature refrigeration by using giant MCE materials.

Magnetic room-temperature refrigerators are considered as an innovative, energy saving and environmentally friendly technology. The working body of the system is a solid magnetic substance. It leads to higher amount of heat absorption/extraction per volume than in the conventional gas based systems. However it takes a large heat transfer area to provide high heat exchange efficiency. Number of working prototypes utilized gadolinium in the form of small spheres to resolve this technical issue. Meanwhile extension of the surface promotes chemical reactions of solid refrigerant with liquid coolant used to transfer heat inside the system.

On the other hand, ferromagnetic glass-coated microwires have a number of attractive features that make them strong candidates for use as a sensing element in high performance magnetic field or stress sensors, magnetic labels, and micro machines. Although the research on magnetic microwires is well established, it was only very recently proposed to utilise them within artificially structured materials. As a new example we propose in this work the use of magnetic glass-coated microwires as magnetocaloric material to engineer magnetic functionality of advanced materials, for example, for exhibiting significant magnetic entropy changes around the Curie temperature ($T_C$) associated to MCE due to magnetic wire actuating performance. Therefore, a type of a smart material is proposed exhibiting MCE and coated with chemically inactive layer.

Glass-coated microwires of nominal composition $Fe_3P$ have been investigated. Adiabatic temperature change, related with the MCE have been measured directly on special set-up created in Department of Physics of MSU using thermo-couple at room temperature in applied field of 10 kOe. The temporal change of the dT showed maximum value of about 0.02 K at room temperature. In according to our knowledge, this effect is firstly observed by us in these glass-coated microwires.

# MAGNETIC CHARACTERIZATION OF MANGANESE OXIDE NANOFIBRES

*N. Iturriza[1], J.J. del Val[1], J. González[1*], C. Gómez-Polo [2], D. Frías[3], P. Navarro[3], M.I.Domínguez[4], J.J. Delgado[5], J.A. Odriozola[4], M. Montes[3]*

[1] Dep. Materials Physics. University of the Basque Country, P. M de Lardizabal, 3 , 20080 San Sebastián, Spain

[1] Dep. Física. Universidad Pública de Navarra, Campus de Arrosadía, 31006 Pamplona, Spain

[13] Dep. de Ingeniería Química. Universidad del País Vasco, P. M de Lardizabal, 3 , 20080 San Sebastián, Spsin

[24] Instituto de Ciencia de Materiales de Sevilla (Centro Mixto US-CSIC), Avda. Américo Vespucio s/n, 41092 Sevilla, Spain

[35] Grupo de Química de Sólidos y Catálisis, Departamento de Ciencia de los Materiales e Ingeniería Metalúrgica y Química, Inorgánica de la Universidad de Cádiz. C/. República Saharaui s/n. Aptdo. 40, Puerto Real. Cádiz. Spain.

Advanced magnetic materials displaying fascinating magnetic properties together with extremely low dimensions are of great interest for technological applications. Consequently, different kinds of magnetic materials have been developed and thoroughly investigated in the last recent years. In this context, manganese oxide compounds that additionally exhibit magnetic behaviour can be considered as very promising candidates to be used in several applications (such as those related with catalysis, ion storage and separation battery electrodes, chemical sensors, and patterning) and, consequently, significant efforts have been expended in a continuous attempt to optimize and improve this kind of materials. Therefore, several characterization techniques have been proposed (microscopy techniques, XRD diffraction and more recently that involve magnetic behaviour).

In this work we deal on the microstructural and magnetic characterization in manganese oxide nanofibres of the OMS (Octahedral Molecular Sieve) family. These materials usually called Cryptomelane were prepared from $Mn^{7+}$ and $Mn^{2+}$ by two methods: reflux and ball milling.

Microstructural characterization was carried out by DRX, $N_2$ adsorption, HRTEM, XPS and DRITS. $KMn_8O_{16}$ phase is confirmed by XRD in the form of d(110) oriented fibres with diameters from 7 to 15nm and aspect ratio 10-50 presenting high surface area. Mn average oxidation state measured by different techniques varies between 3.66 and 3.94. 2x2 channels of the OMS structure are not accessible because they filled with K and water stabilizing the structure.

Magnetic susceptibility measurements in manganese oxide compounds (Cryptomelane and reference materials, $MnO_2$ and $Mn_2O_3$) were performed by means of a SQUID magnetometer. From such measurements, the antiferromagnetic behaviour of the samples was evidenced with Nèel temperature, $T_N$, below 50 K, while for $T>T_N$, the thermal dependence of the magnetic susceptibility was, satisfactorily, fitted according to

the Curie-Weiss law. The Curie-Weiss law allows estimating the effective magnetic moment, $_{eff}$, of the magnetic Mn atoms and, finally, the atomic fraction of $Mn^{3+}$ and $Mn^{4+}$ in the compound.

The excellent catalytic activity in the total oxidation of acetyl acetate is explained by the non-stoichiometry character (balance between $Mn^{3+}$ and $Mn^{4+}$) confirmed by different techniques and the textural properties resulting from its nanofibre character.

*) Author responsible

# EFFECTS OF THE PROCESSING SEQUENCE AND CRITICAL INTERPARTICLE DISTANCE IN PA6-CLAY/MSEBS NANOCOMPOSITES

*Imanol González, José Ignacio Eguiazábal, Jon Nazabal*
*"POLYMAT"-UPV/EHU, Pº Manuel Lardizabal 3, San Sebastián/Donostia, Spain.*
igonzalez@ikasle.ehu.es

Polymer/clay nanocomposites are an active research subject. Within this field, there is increasing interest in the possibility of linking nanocomposite production by clay addition, to blending with a second polymeric component [1-4]. As a consequence, polymeric nanocomposites with a matrix composed of a blend of two thermoplastics, and nanocomposites with a pure polymer matrix toughened by a rubber have been studied. The latter will offer the possibility to overcome the tendency to notch sensitivity and low-notched fracture toughness of nanocomposites by means of rubber modification. In this way, the technique of rubber toughening of brittle polymers (which deform by crazing), later extended to ductile polymers (mostly deformed by shear), could also be used for nanocomposites. This would mean that the only major mechanical property that is not enhanced upon organoclay addition, i.e. toughness, could increase with respect to that of the matrix, and that the decrease in stiffness observed upon rubber addition in toughened blends could be counteracted by the presence of the organoclay.

The aim of this work is to ameliorate the microstructure and performance of the polyamide 6 (PA6)/Clay/maleinized styrene-ethylene-butadiene-styrene triblock copolymer (mSEBS) nanocomposites (PN´s) through a modified processing, as well as to examine the parameters that make the brittle/ductile transition of nanocomposites change. The studied parameters were the rubber and the organoclay contents. The results showed that after the modified processing, the average dispersed particle size decreased with respect to that obtained with a standard processing, and an overall increase in the impact performance occurred (Figure 1). This is attributed to a more effective reaction between the maleic groups of the rubber and the amine end groups of the PA6 when there is no surfactant present in a first processing step. The analysis of the variation of the critical interparticle distance ($\tau_c$) indicates that it depends on the modulus of elasticity of the matrix (i.e. on the organoclay content) (Figure 2) and on the interfacial adhesion, higher modulus of elasticity and higher adhesion leading to smaller $\tau_c$ values.

**References:**

[1] Ahn, Y. C.; Paul, D. R., Polymer, **47** (2006) 2830-2838.

[2] Lee, H. S.; Fasulo, P. D.; Rodgers, W. R.; Paul, D. R., Polymer, **46** (2005) 11673-11689.

[3] Liu, B.; Zhang, Y.; Wan, C.; Zhang, Y.; Su, Y.; Ji, J., Journal of Macromolecular Science, Part B: Physics, **45** (2006) 1159-1169.

[4] Li, C. C.; Xiao, Y. N.; Guan, G. H.; Liu, X. Q.; Zhang, D., Journal of Applied Polymer Science, **101** (2006) 2512-2517.

**Figures:**
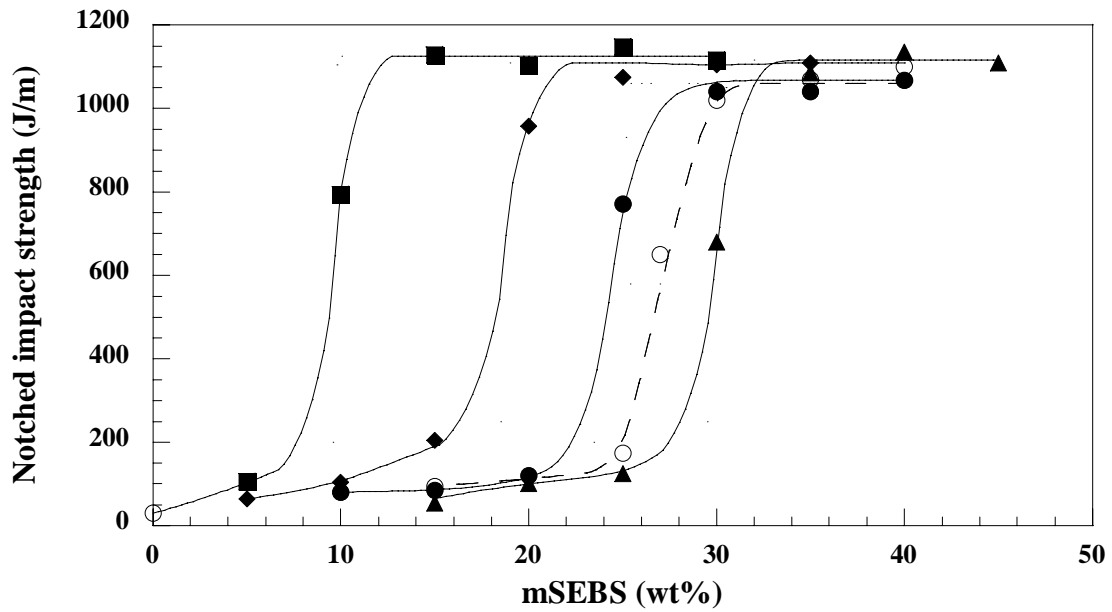


Figure 1. Notched Izod impact strength of the reference blends (■), PN1.5% (◆), PN3.0% (●) and PN4.5% (▲). The values of the PN3% (○) obtained through the standard processing method are also shown as reference.
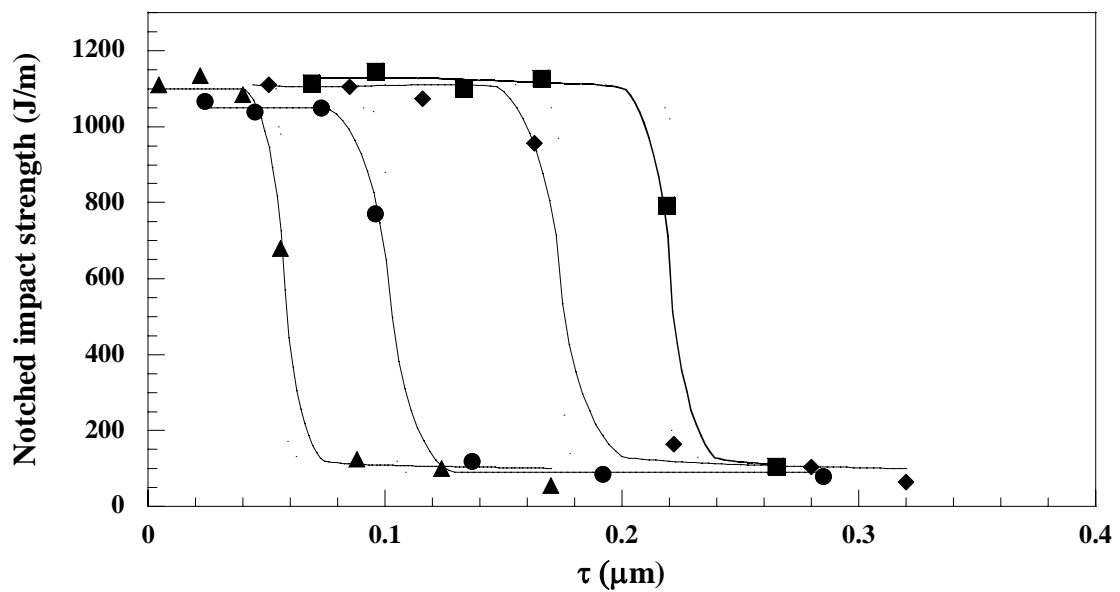


Figure 2. Corrected notched Izod impact strength of the PN´s against the interparticle distance. Reference blends (■), PN1.5% (◆), PN3.0% (●) and PN4.5% (▲).

# EFFECTS OF SPATIAL SYMMETRIES AND DIRECT PROCESSES ON QUANTUM ELECTRONIC TRANSPORT IN CHAOTIC QUANTUM DOTS

Victor Gopar

Instituto de Biocomputacion y Fisica de Sistemas Complejos

Corona de Aragon 42 – Zaragoza (Spain)

e-mail: gopar@unizar.es

The photoluminescence spectrum of the freshly photosynthesized porous silicon (PS) has been investigated, this measurement was repeated after three and six months for the same sample after storage under ambient condition (open air at room temperature). Photoluminescence (PL) measurements of the stored PS show different peak positions and intensity width as compared with the results of the fresh PS. A blue shift in PL peak positions with aging time was observed. PL relative intensity is strongly diminished after 6 months of aging. Dark I-V characteristics of Al/PS/n-Si/Al structure shows a behavior of PS/n-Si isotype heterojunction for fresh device and a MIS (metal-insulator-semiconductor) device due to contribution of Al/PS Schottky barrier after aging essentially after 6 months.

# ELECTRICAL CHARACTERIZATION OF TMV-BASED NANOSTRUCTURES

*Marcin Gorzny, Stephen Evans*
*School of Physics and Astronomy, University of Leeds, Leeds, UK*
*phymkg@leeds.ac.uk*

The wild-type Tobacco mosaic virus (TMV) is a 300nm long tube with 18nm outer and 4nm inner diameters. TMV virus is characterized by the extraordinary chemical and physical stability.

The internal and external surfaces of the virion protein consist of repeated patterns of charged amino acid residues, such as glutamate, aspartate, arginine, and lysine. These functionalities offer a wide variety of nucleation sites for surface-controlled inorganic deposition, which, in association with the high thermal and pH stability, can exploited in the synthesis of unusual materials such as high aspect ratio nanowires.

Using the TMV, nanostructures consisting of platinum, palladium, nickel, zinc, and gold have been prepared on surface and within the TMV channel using electroless deposition. Electrical properties of single nanowires has been investigated by four-probe electrical transport measurement.
Four independently controlled STM tips were used to contact the virus and high resolution scanning electron microscope (SEM) were used for real-time imagining. Multiple I-V measurements were taken at varying tip separations and the change in resistance with separation was observed to be in good agreement with predictions based on the nanowire geometry.

**Figures:**
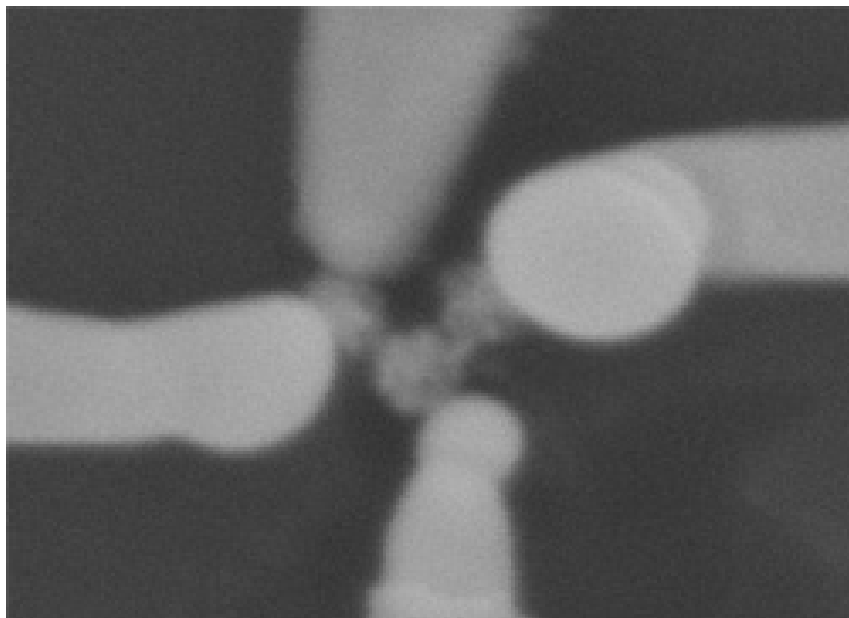


*An SEM image of a 4 probe measurement on a coated TMV virus*

# Formation of self-assembled metal/silicon nanocomposites

*P. Granitzer [a], K. Rumpf [a], P. Pölt [b], A. Reichmann [b], H. Krenn [a]*
*[a] Institue of Physics, Karl Franzens University Graz, Universitaetsplatz 5, A-8010 Graz, Austria*
*[b] Institute for Electron Microscopy, University of Technology Graz, Steyrergasse 17, A-8010 Graz, Austria*
*petra.granitzer@uni-graz.at*

The fabrication of nanoscopic silicon based membranes has been carried out by using a non-expensive electrochemical preparation technique. For these purposes an $n^+$-silicon wafer is anodized to create oriented pores with typical diameters around 50 nm. The length of the channels is up to 50 μm which yields to an aspect ratio of 1000. Pores with diameters in the micrometer range exhibit quite smooth pore walls [1] but get rougher and more dendritic with the reduction of the diameter. The generated mesopores offer a dendritic growth but the length of the side-pores could be sufficiently suppressed to obtain clearly separated channels with even a quite regular self-assembled pore-arrangement. The pores of such templates are filled with a metal, especially a ferromagnetic one to obtain an array of nanostructures. Metal-deposition within such high aspect ratio pores down to the pore-tips is a great challenge [2] but succeeded. The metal-loading consists of precipitated particles of different shapes from spheres to elongated particles up to wires. The extension of the deposited wires reaches a few micrometers (aspect ratio 100). This achieved nanocomposite can be varied in two ways. On the one hand by the modification of the nano-architecture of the silicon template, on the other hand by altering the metal deposition process. The porous silicon membrane can be modified within a certain regime in pore-diameter, pore-length as well as interpore-spacing which can be influenced by the current density and the electrolyte concentration, respectively. The spatial distribution of the deposited metal can be influenced by varying the applied current and the frequency of the current pulses. The nanoparticles can either be distributed over the whole template or accumulated in the lower third part of the porous layer or occur mainly in the surface region. Also the preferential shape (spheres, ellipsoids, wires) of the metallic nanostructures can be regulated. Furthermore a metal-layer covering the surface can be realized by longer pulse durations. A calamity of managing the structure of the described system is that some of the influencing parameters are not completely independent from each other. Characterization of the template as well as of the deposited metal-particles is performed by scanning electron microscopy (SEM), especially in recording the back scattered electrons and EDX-mapping respectively to get element sensitive information. The introduced silicon based nanocomposite offers the opportunity to change between different nano-architectures by accurate adjustment of the electrochemical fabrication parameters and promises applicability for magneto-optical, magnetic and spintronic devices suitable for silicon based technology.

**References:**

[1] V. Lehmann, U. Grüning, Thin Solid Films, **297** (1997) 13.
[2] C. Fang, E. Foca, S. Xu, J. Carstensen, H. Föll, J. Electrochem. Soc. **154** (2007) D45

**Figures:**
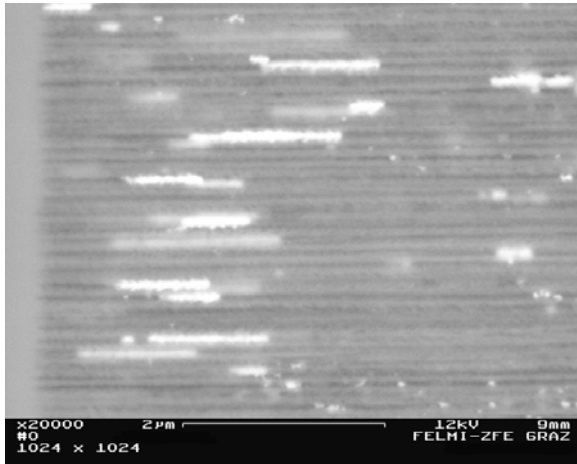


a)
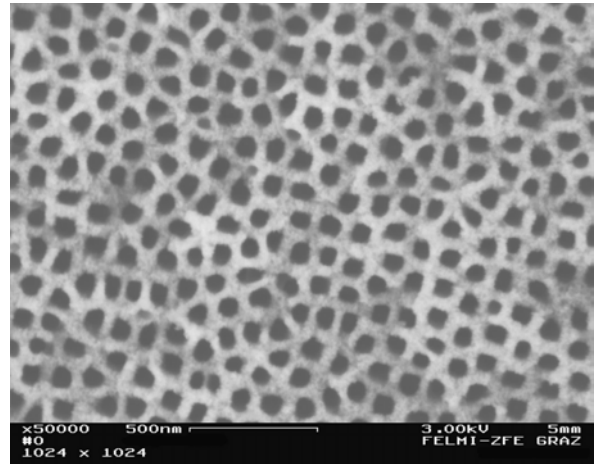


b)

a) Ni-wires (length 2 μm, diameter 50 nm) precipitated within the channels of a silicon matrix.
b) Scanning electron micrograph showing the top-view of the sample.

# Synthesis and purification of produced Carbon Nanotubes in NaCl solution

*Jahanshahi Mohsen [1], Raoof Jahan-bakhsh[2], Hajizadeh Solmaz [1], Jabari Razieh [1]*

*[1] Nanobiotechnology Research Lab., Faculty of Chemical Engineering, Noshirvani Mazandaran University of Technical, Babol, Iran.*
*[2] Electroanalytical Chemistry Research Laboratory, Department of Chemistry, Faculty of Basic Science, Mazandaran University, Babolsar, Iran*
*mmohse@yahoo.com*

Carbon nanotubes (CNTs) are fascinating structures with a wide range of applications due to their outstanding physical and electronic properties. These applications include field emission display devices, scanning probe microscope tips, nanoelectronic and optoelectronic devices, and composites. CNT can be made by chemical vapor deposition, carbon arc methods, or laser evaporation and can be divided into single-wall carbon-nanotubes (SWCNT) and multi-wall carbon- nanotubes (MWCNT). Several methods have been developed for the bulk synthesis of which the electric arc-discharge method is a popular technique for producing CNTs. Properties of carbon nanotubes obtained by arc-discharge are affected by various parameters such as voltage, current, kind and ratio of catalysts, plasma and so on. In this work we considered the effect of these factors separately on the carbon nanotube synthesis and purified them with new modified acid treatment. By using Ni/Fe as a Catalyst with specific ratio and NaCl 0.2N as a solution CNT's diameters were decreased and the amount of SWCNTs increased. The SEM and Raman spectroscopy were applied to prove this claim.

**References:**
[1] Iijima S. Nature 354, (1991) 56–58.
[2] Z. Xu, X. Chen, X. Qu, J. Jia, Sh. Dong, Biosensors and Bioelectronics **20**, (2004) 579–584.
[3] H.W. Zhu, X.S. Li, B. Jiang, C.L. Xu, Y.F. Zhu, D.H. Wu, X.H. Chen, Chemical Physics Letters **366**, (2002) 664–669.
[4] Sh. Wang, M. Chang, K. M. Lan, Ch. Wu, J. Cheng, H. Chang, Letters to the Editor / Carbon **43**, (2005)1778–1814.
[5] H. Lange, M. Sioda, A. Huczko, Y.Q. Zhu, H.W. Kroto, Carbon **41**, (2003)1617–1623.
[6] J. Ting, Ch. Chang, Sh. Chen, D. Lu, Ch. Kung, F. Huang, Thin Solid Films **496**, (2006) 299 – 305.
[7] H. Huang, H. Kajiura, A. Yamada, M. Ata, Chemical Physics Letters **356**, (2002) 567–572.
[8] R.B. Mathur, S. Seth, Ch. Lal, R. Rao, B.P. Singh, T.L. Dhami, A.M. Rao, carbon, in press.
[9] Y. Feng, G. Zhou, G. Wang, M. Qu, Z. Yu, Chemical Physics Letters, **375** (2003)645–648.
[10] N. Sano, H. Wang, M. Chhowalla, I. Alexandrou, G.A.J. Amaratunga, Nature (London) **414**, (2001) 506.

**Figures:**



FIGURE 1. The schematic setup arrangement,a) cathode graphite b) Anode graphite c) Arc Plasma d) DC Arc Supplier e) wires
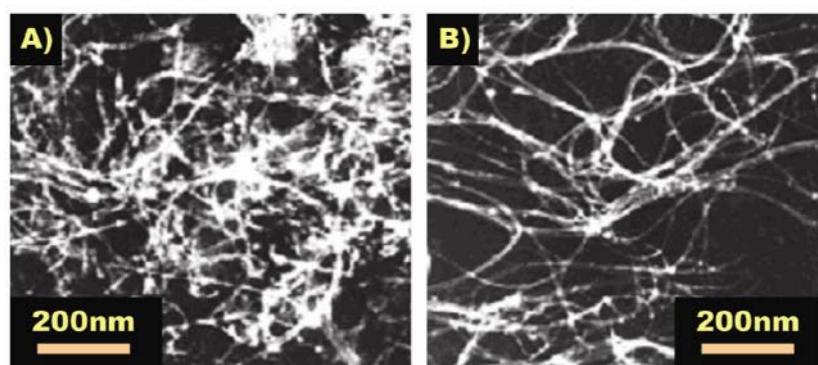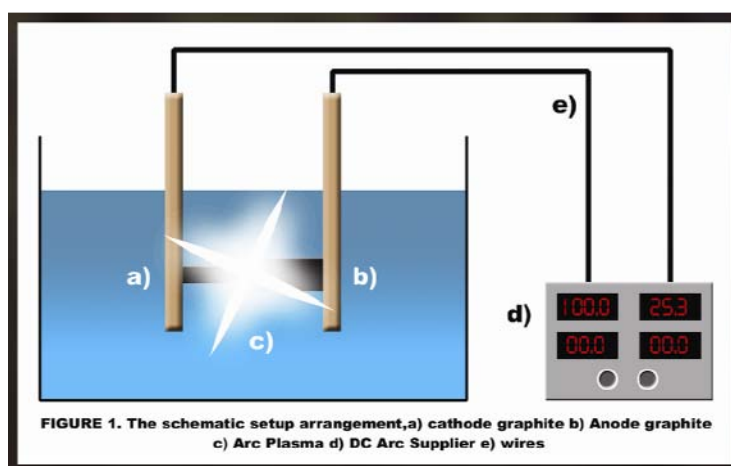


FIGURE 2. The SEM images of CNTs A) before B) after purification stage

# Gelatin nanoparticles fabrication and evaluation effectiveness parameters

*Mohsen Jahanshahi[*1], Mohammad Hossein Sanati[2], Solmaz Hajizadeh[1], Zahra Babaei[1]*

[1] *Nanobiotechnology Research Laboratory, Faculty of Chemical Engineering, Noshirvani Mazandaran University of Technical, Babol, Iran*
[2] *The National Research Center for Genetic Engineering and Biotechnology, Tehran, Iran*

*mmohse@yahoo.com*

The biotechnology industry has recently been demanding second generation of bioproducts such as viruses, plasmids, virus-like particles and drug delivery assemblies (20-300 nm). These products are mainly used as gene delivery systems in gene therapy protocols. Nanoparticles possess certain advantages over the other colloidal drug delivery systems such as greater stability during storage, stability in vivo, after administration and ease of scale up during manufacture. Nanoparticles as drugs-carrier were developed in the early 1980s but over the past few decades, there has been considerable interest in developing biodegradable nanoparticles (NPs) as effective drug delivery de-vices. Here nanoparticles of gelatin type A were prepared by a two-step desolvation method as a colloidal drug delivery system and the essential parameters in fabrication were optimized by Taguchi design method. Gelatin was dissolved in distilled water under room temperature range. Acetone was added as a desolvating agent to precipitate the high molecular weight (HMW) gelatin. The supernatant was discarded and the HMW gelatin re-dissolved by distilled water and stirring at 600 rpm. Acetone were added drop-wise to form nanoparticles. At the end of the process, glutaraldehyde solution was used as a cross-linking agent for preparing nanoparticles. The centrifuge was applied for purification stage. For characterizing the nanoparticle sample AFM, SEM, as well as FTIR was employed. By introducing 4 factors (temperature, gelatin concentration, agitation speed and the amount of acetone) in 4 levels to the software 16 experiments were done and the optimum condition was happened in 50º C, 50 mg/ml gelatin concentration, 75 ml the amount of acetone had the best result and the nanoparticle size was under 160 nm. The mechanistic of the optimum conditions for preparing protein nanoparticles as well as their characterization were discussed.

**References:**
[1] C. Coester, P. Nayyar, J. Samuel. Eu. J. of Pharmaceutic and Biopharmaceutics **62**, (2006) 306.
[2] A.Saxena, K.Sachin, H.B. Bohidar, Verma. Colloids and Surfaces B: Biointerfaces **45**, (2005) 42.
[3] Couvreur P., Gref R., Andrieux K., Malvy C, Progress in Solid State Chem. **34**, (2006)231.
[4] B L. Mua, P.H. Seowc, Colloids and Surfaces B: Biointerfaces **47**, (2006) 90.
[5] S. K. Soppimath, T. M. Aminabhavi, A. R. Kulkarni, J. of Controlled Release **70**, (2002) 1.
[6] M. Jahanshahi, H. Aghajani and TC Ling. Int. J. of Nanoscience and Nanotech. **1**( 1), (2005) 9.
[7] Sh. Azarmi, Y. Huang, H. Chend, Abramse, Millera, R. Löbenberga. J Pharm Pharmaceut Sci **9**(1), (2006)124.
[8] S. Balthasar, K. Michaelis, N. Dinauer, H.V. Briesen, K. Langer. Biomat. **26**, (2005)2723.
[9] CJ. Coester, K. Langer, H. Van Briesen, J. Kreuter J Microencapsul.**17**, (2000) 187.
[10] C. Weber, C. Coester, J. Kreuter, K. Langer. Int J Pharm **194**, (2000) 91.

**Figures:**
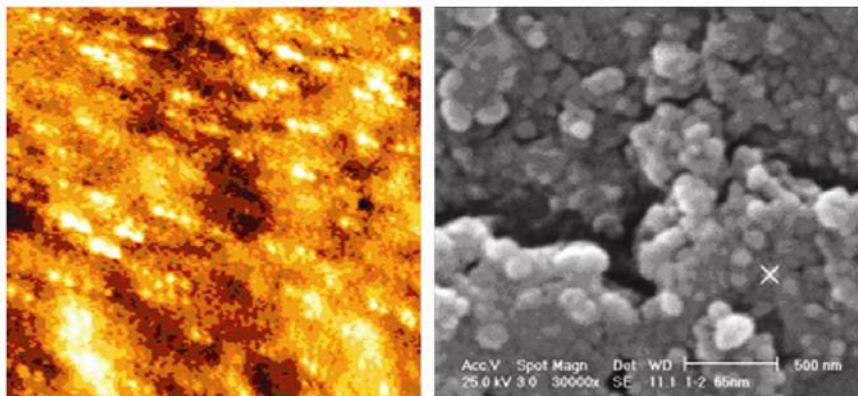


**FIGURE 1.** The AFM and SEM images of Gelatin nanoparticles at optimum condition

# HUGE NEGATIVE DIFFERENTIAL CONDUCTANCE IN MOLECULAR NANOJUNCTIONS DUE TO A TWO-LEVEL SYSTEM WITH ASYMMETRIC COUPLING

*A. Halbritter, P. Makk, Sz. Csonka, G. Mihály*
*Budapest University of Technology and Economics, Department of Physics, 1111 Budafoki street, Budapest, Hungary*
*halbritt@math.bme.hu*

The study of molecular nanojunctions built form simple molecules has attracted wide interest in the recent years [1]. The behaviour of some simple molecules bridging atomic-sized metallic junctions can already be understood in great detail mainly due to the detection of the vibrational modes with point-contact spectroscopy providing a fingerprint of the molecule. These studies are complemented by number of conductance channels analysis with conductance fluctuation and shot-noise measurements, and the quantitative predictive power of computer simulations. The above tools of mesoscopic physics were successfully used to describe platinum-hydrogen junctions [2-3], it was shown that a molecular hydrogen bridge with a single, perfectly transmitting channel is formed between the platinum electrodes.

For a wide variety of junctions with different electrode material and molecule however, the direct measurement of the vibrational modes fails due to the appearance of peak-like structures in the differential conductance curves [4]. We show that molecular nanojunctions can even show huge negative differential conductance as demonstrated in the figure. This phenomenon is found not to be a unique feature of a special atomic configuration, but it is frequently occurring in a wide conductance range and with almost all the studied molecules and contact materials implying the presence of a general physical phenomenon producing a similar feature under a wide range of experimental conditions. We present a detailed analysis of the observations in terms of two-level system models, demonstrating the failure of a simple TLS model [5] and the necessary ingredients for producing peak-like structures instead of simple conductance steps. A model based on an asymmetrically coupled two-level system is proposed, which can describe the observations. The comparison of the model with experimental data implies a huge asymmetry in the coupling strength, which can be explained with the physical picture of a molecule strongly bound to the junction being "kicked out" into a loosely bound but strongly degenerated state. The proposed model grabs a general feature that can lead to peak-like structures or even negative differential conductance in the dI/dV curves of molecular nanojunctions.

**References:**

[1] N. Agraït, A. Levy Yeyati and J.M. van Ruitenbeek, Physics Reports **377** (2003) 81-380.
[2] R. H. M. Smit et al., Nature 419, **906** (2002)
[3] D. Djukic and J.M. van Ruitenbeek, Nano Letters, **6** (2006) 789.
[4] W.H.A. Thijssen et al., Phys. Rev. Lett. **97** (2006) 226806.
[5] A. Halbritter, L. Borda and A. Zawadowski, Advances in Physics **53** (2004) 939-1010.

**Figures:**
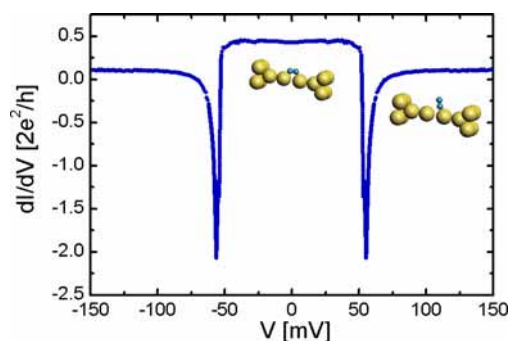
# INKJET PRINTING OF SINGLE WALLED CARBON NANOTUBES

Chang-Soo Han

Korea Institute of Machinery & Materials

Korea

e-mail: cshan@kimm.re.kr

Single walled carbon nanotubes (SWCNTs) were patterned by a simple inkjet printing method. Inkjet printing is a popular method in the conventional printing industry due to fine and arbitrary pattern generation, non-contact injection, solution saving effects, high repeatability, and scalability, all of which are advantageous to large area processes. In addition, inkjet printing of SWCNTs can readily control pattern thickness, line width, and uniformity for the printed pattern.

In our research, we investigated the deposition conditions of SWCNTs during inkjet dropping. The network formations of SWCNTs in dropped solution were significant to make a conductive pattern. Factors to affect the network formation were investigated. We made line patterns along with the number of overwrite and the increasing width. The electrical characterization for the fabricated patterns was performed by impedance analyzer and I-V curves.

The inkjet printing of SWCNTs has a high potential to be adopted in the various applications, such as sensors, field emission display, and interconnections.

# MONTE CARLO SIMULATION OF THE ADSORPTION OF A MIXTURE OF HYDROGEN AND NITROGEN ON SINGLE-WALLED CARBON NANOTUBES

S.M. Hashemianzadeh, Y. Ghadarghadr, S.M. Mousavi-khosdel

College of Chemistry-Iran University of Science and Technology

Tehran-Iran

Hashemianzadeh@iust.ac.ir

Hydrogen has been recognized as an ideal energy carrier but has not yet been used as such to any great extent .One of the major problems is the difficulty for achieving an efficient storage. In the recent years, carbon-based materials have attracted attention due to the discovery of novel carbon nanomaterials like fullerence, nano fibers and nanotubes.

Carbon nanotubes have many fascinating properties. Their well defined structures with hollow nanosize interiors suggest their potential use as adsorbents for gas adsorption and separation. The adsorption of a nitrogen and hydrogen mixture on two types of single-walled carbon nanotube bundles at different temperatures were studied using canonical Monte Carlo molecular simulation. The adsorption in SWNT will occur both

inside and outside isolated nanotubes as well as in adsorption sites due to aggregations of nanotubes.

In this research work, adsorptions of pure nitrogen, hydrogen and a nitrogen-hydrogen mixture is on (7,7) armchair carbon nanotubes were studied. We used Lennard-Jones potential for the gas-gas and gas-carbon nanotube interactions. Potential parameters for hydrogen-nitrogen, hydrogen-nanotube and nitrogen-nanotube interactions were obtained from the Lorentz-Berthelot combining rules.

We also wished to study the effect of another gas like nitrogen on hydrogen adsorption. As we used the Virial equation of state to calculate the number of gas molecules, this work was affected by pressure and temperature. The work was carried out at 300 K and $10^6$Pa in different mole fractions of gases. As shown in figures below we calculated the density of adsorption as a function of distance from the nanotube layer. We saw that by increasing the amount of nitrogen in the mixture, hydrogen adsorption increases and also we obtained the maximum adsorption peak near the center of the nanotube.

As shown in the figures, adsorption peaks for hydrogen increases when the amount of nitrogen increases and also as difference between the peaks are large enough the separation is possible.

The results show that $N_2$ pressure affects the amount of hydrogen adsorption

**References**

1. Jianwen Jiang* and Stanley I. Sandler, Langmuir 2004, 20, 10910-10918

2. Juan I. Paredes, Fabia´n Sua´rez-Garcı´a, Silvia Villar-Rodil, Amelia Martı´nez-Alonso, and Juan M. D. Tasco´n, Eduardo J. Bottani*J.Phys.Chem.B 2003,107, 8905-8916

**Figure:**
Comparing the hydrogen adsorption in presence of nitrogen and pure hydrogen in different mole fraction.

| Hydrogen density in presence of nitrogen molecules/nm$^3$ | Pure hydrogen density molecules/nm$^3$ |
|---|---|
| 2.91 | 2.67    ( Hydrogen percentage  0.3%  ) |
| 5.21 | 4.45       (Hydrogen percentage  0.5% ) |
| 6.91 | 6.23       (Hydrogen percentage  0.7% ) |
| 8.9 | (Hydrogen percentage 100%) |

# Guided Immobilization of Quantum Dots on Gold Nanogratings for Enhanced Surface Plasmon Resonance Biosensing

*<u>X.D. Hoa</u>[1], M. Martin[3], A. Jimenez[3], J. Beauvais[3], P. Charette[3], A. G. Kirk[2] and M. Tabrizian[1]*
*[1]McGill University, 3775 University St., Montreal, Canada, H3A 2B4*
*[2]McGill University, 3480 University St., Montreal, Canada, H3A 2A7*
*[3]Université de Sherbrooke, 2500 Boul. Université, Sherbrooke, Canada, J1K 2R1*
*xuyen.hoa@mcgill.ca*

## I. Introduction

The literature points to a vast array of plasmonic enhancement effects being studied for biosensing applications. Plasmonic biosensors utilise surface plasmon waves to sense the surface adsorption of analytes from a complex sample solution. In this report, we present a surface plasmon resonance (SPR) biosensor (based on the Kretchmann configuration) which incorporates surface nanogratings and guided quantum dot immobilization. The adsorption of fluorophores on plasmonic surfaces is interesting due to two known physical effects associated with the interaction between the fluorophore and the electromagnetic field. The propagating surface plasmon wave generates, along the nanograting structures, high electromagnetic (EM) field intensities that can excite the adsorbed fluorophores to produce a highly directional and polarized emission [1]. Moreover, the presence of fluorophores causes an important change in both the real and imaginary parts of refractive index near the plasmonic surface affecting the excitation and propagation of the plasmon wave [2]. Therefore, there is significant scope in exploring these EM interactions as amplification methods for enhanced SPR [3].

## II. Guided Quantum Dots Immobilization on Gold Nanogratings

The enhanced SPR biosensor features nanogratings with differentiated surface chemistry. It allows the binding of the analytes to receptor probes attached to the troughs or the mesas of the nanogratings where SP fields are strongest. The substrate is passivated against non-specific adsorption of proteins. Quantum dots conjugated to a secondary receptor are allowed to be adsorbed on the captured analytes (figure 1). The guided and periodic immobilization of analytes and quantum dots generates an additional optical contrast that perturbs the propagating surface plasmon.

## III. Fabrication and Characterization Methods

The electromagnetic field enhancements of surface gold nanogratings are initially studied via rigorous coupled wave analysis method (RCWA). Nanogratings with 250 and 400 nm periods are fabricated by E-beam lithography and metal lift-off (figure 2). The differentiated surface chemistry is applied in a two-step process. Prior of the metal lift-off, a first surface chemistry is applied using a self-assembled monolayer of 16-mercaptohexadecanoic acid activated for the attachment of biomolecular receptor probes. Metal lift-off in acetone/MEK is applied and then followed by the second surface modification by self-assembled poly-ethylene glycol (PEG) to passivate the surface. The surface is then incubated in successive solutions of the primary surface receptor probes (anti-TNF-α), analytes (TNF-α), and quantum dots (CdSe). The characterization of the nano-structured surface is performed by atomic force microscopy (Nanoscope III SPM). The patterned immobilization of the quantum dots and the fluorescence emission are imaged via custom-built near-field scanning optical microscope (NSOM).

## IV. Results

The numerical modelling suggests that the localized field enhancement and the concentration of the adsorbed analytes lead to SPR sensitivity enhancement (figure 3). Depending on the excitation wavelength, the field gradient can be tuned to be localised on the grating troughs or mesas. Preliminary characterisations show good surface topography (figure 4), and

differentiated surface chemistry [4]. The on-going work focuses on imaging the emission from surface immobilized quantum dots via NSOM and measuring their interactions with the surface plasmons via SPR imaging. In particular, we seek to evaluate the effect of this approach on the improvement of sensitivity for the detection of small biomolecular analytes.

## References:

[1] J.R.Lakowicz, J.Malicka, E.Matveeva, I.Gryczynski, Z.Gryczynski.  Plasmonic technology: novel approach to ultrasensitive immunoassays, Clin.Chem., 51, (2005) 1914-1922.

[2] H.Komatsu, M.Miyachi, E.Fujii, D.Citterio, K.Yamada, Y.Sato, K.Kurihara, H.Kawaguchi, K.Suzuki. SPR sensor signal amplification based on dye-doped polymer particles, Science and Technology of Advanced Materials, 7, (2006) 150-155.

[3] O.Stranik, H.M.Mcevoy, C.McDonagh, B.D.MacCraith.  Plasmonic enhancement of fluorescence for sensor applications, Sensors and Actuators B-Chemical, 107, (2005) 148-153.

[4] X.D.Hoa, A.G.Kirk, M.Tabrizian.  Modelling and Implementation of a Novel SPR Biointerface for Time-Effective Detection of Sepsis Biomarkers, Proc.IEEE Workshop on Computer Architecture for Perception and Sensing (CAMPS 2006), (2006).

## Figures:
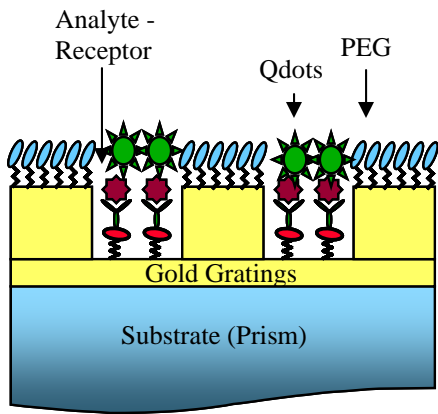


Figure 1:  Guided quantum dots immobilization on SPR gold nano-grating surface
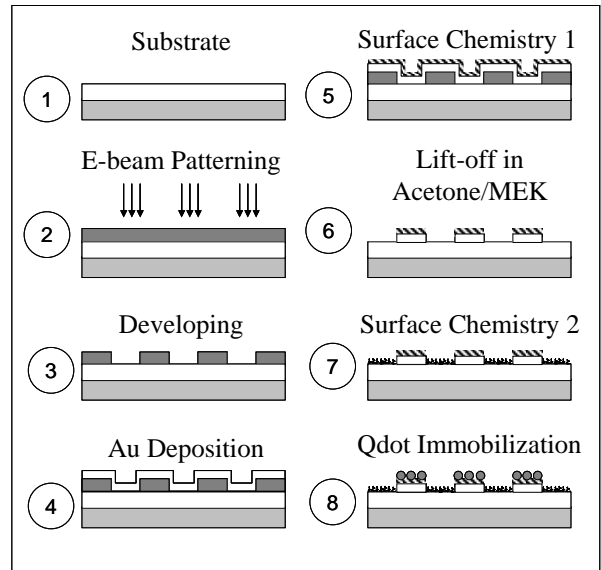


Figure 2:  Fabrication of patterned surface via electron-beam lithography and metal lift-off
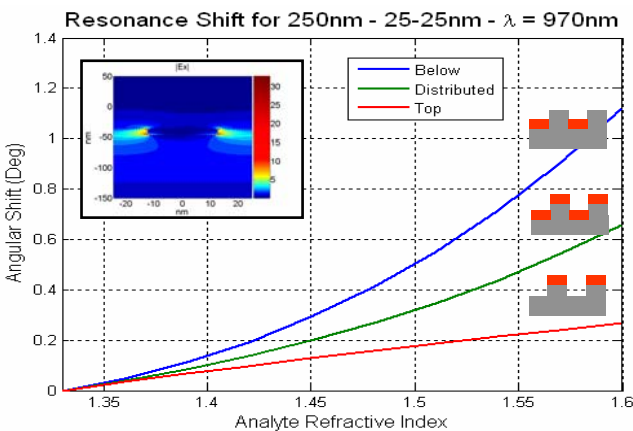


Figure 3:  RCWA simulation results for immobilization in the grating troughs (below), mesas (top) and uniformly distributed. (Insert) field distribution
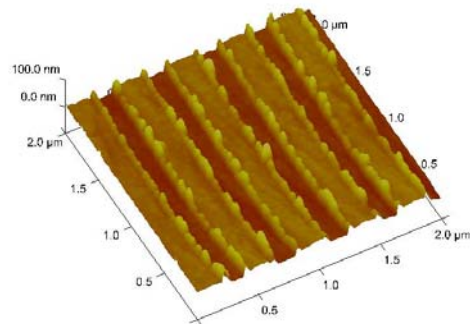


Figure 4:  AFM nanograting structures

# One-Pot Preparation of Gold-Elastomer Nanocomposites Using PDMS-*graft*-PEO copolymer Micelles as Nanoreactors

*C. E. Hoppe, [1] C. Rodríguez-Abreu,[2] M. Lazzari, [1] M. A. López-Quintela[1] and C. Solans [2]*
*[1]Laboratory of Magnetism and Nanotechnology, Institute of Technological Investigations and Dpt. of Physical Chemistry, University of Santiago de Compostela, 15782 Santiago de Compostela, Spain;*
*[2]Institut d`Investigacions Químiques i Ambientals de Barcelona (IIQAB/CSIC), Jordi Girona, 18-26, 08034 Barcelona, Spain.*
*e-mail:* hoppe@fi.mdp.edu.ar

One of the greatest challenges to face regarding the design and synthesis of advanced nanocomposites is to avoid the typical nonuniform particle aggregation process that takes place when polymers and nanoparticles (NPs) are mixed.[1] An attractive way to overcome this problem is to synthesize the nanofiller inside the matrix or matrix precursor in such a way that the nanocomposite can be prepared following an one-pot strategy, which is simpler and less time and cost consuming than multi-step procedures. Additional advantages would be envisaged if size and shape of the NPs could be modified by simple changes of the reaction conditions. Siloxane amphiphilic copolymers consist of a methylated siloxane hydrophobe grafted with one or more polar chains. These copolymers are able to form micellar aggregates in nonaqueous media, which make them very attractive as potential nanoreactors and structured templates for the organization of nanocrystals.[2] Based on this potentiality, here we present our first results obtained by using poly(dimethylsiloxane)-*graft*-poly(ethylene oxide) (PDMS-*g*-PEO) micellar aggregates dispersed in a siloxane elastomer precursor as nanoreactors for the synthesis of gold nanocomposites.

The copolymer PDMS-*g*-PEO, traded under the name BYK-UV3510, was kindly supplied by BYK Chemie (Wesel, Germany). Molecular and structural characterization was carried out by size exclusion chromatography and ^{1}H NMR, respectively. BYK-UV3510 has an average molecular weight of 12,900 g/mol and a polydispersity index of 1.5, whereas the molar ratio of grafted to ungrafted DMS units, $DMS_{g\text{-PEO}}/DMS$ is 3/97. In a first step, selected amounts of the copolymer and a hydroxyl-terminated poly(dimethylsiloxane) (Mn ≈ 550, Aldrich) were thoroughly mixed with a vortex. The resulting clear dispersion was loaded with an aqueous solution of $HAuCl_4.3H_2O$ and heated in an oven at a selected temperature between 50 and 80ºC. After this treatment, the dispersion developed a characteristic pink color associated to the plasmon resonance absorption of gold NPs. The absence of additional reducing agents in the system supports previous results that showed that ethylene oxide chains, facing the interior of micelles, could induce the reduction of metal salt to generate NPs. In a final step, an elastomeric siloxane network was formed by adding tetraethyl orthosilicate (TEOS) as a cross-linker and tin (II) 2-ethylhexanoate as a catalyst.

The evolution of the reaction was followed by monitoring the development of the plasmon band as a function of time by UV-Vis spectrophotometry (Figure 1). After an induction time of several minutes, the appearance of a characteristic single feature typical of spherical NPs was observed.[3] The reaction rate was very susceptible to the temperature in the 50-80ºC range (see inset in figure 1), although the position and shape of the band were hardly affected by this variable. It is worth noting that the optical characteristics of the samples (position and shape of the plasmon band) were not affected by the polymerization process.

Figure 2 shows photographs of monoliths and films of the modified elastomers obtained under different conditions. As can be observed, the copolymer/metal mass ratio (R) is a fundamental variable to be tuned in order to adjust the final colour and transparency of the nanocomposites. A decrease in R from 3060 to 2470 produced nanocomposites characterized by a wider and red-shifted band, probably due to an increase in size and degree of aggregation of the formed nanostructures. It seems possible that a decrease in R produced a drop in the

protection efficiency against growth and aggregation. On the other hand, a high R value was necessary but not sufficient to generate small, spherical nanoparticles with a narrow plasmon band. As an example, a sample prepared with a higher copolymer concentration and R = 3860 produced blue nanocomposites characterized by a wide absorption band in the visible region of the spectrum. The origin of this behaviour is still not clear, although it could be related with a shifting of the composition of the system to a different zone of the copolymer/PDMS-OH/HAuCl$_4$(aq) phase diagram.

In summary, in this work we demonstrated that elastomeric nanocomposites can be obtained in a one-pot process using micelles of a random graft amphiphilic copolymer as reducing nanoreactors. The possibility to produce anisotropic particles working in different regions of the copolymer/PDMS-OH/HAuCl$_4$(aq) phase diagram is currently under investigation.

**References:**

[1] A. C. Balazs, T. Emrick and T. P. Russell, Science, **314** (2006) 1107.
[2] C. Rodríguez-Abreu, M. Lazzari, D. Varade, M. Kaneko, K. Aramaki and M. A. López-Quintela, Colloid Polym. Sci., **285** (2007) 673.
[3] L. M. Liz-Marzán, Langmuir, **22** (2006) 32.

**Figures:**
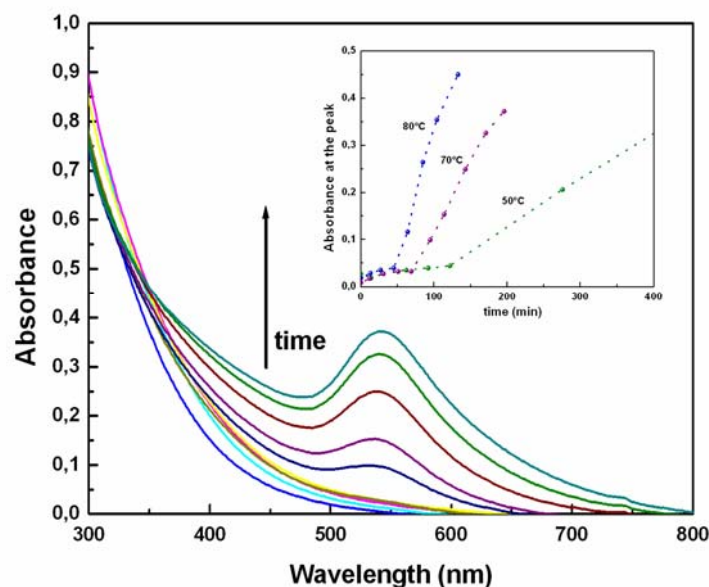


**Figure 1.** Evolution of the plasmon band of a sample prepared with 10wt% of BYK-UV3510 and R=3060 at 70ºC. Inset: Temporal evolution at different reaction temperatures.



**(a)**          **(b)**
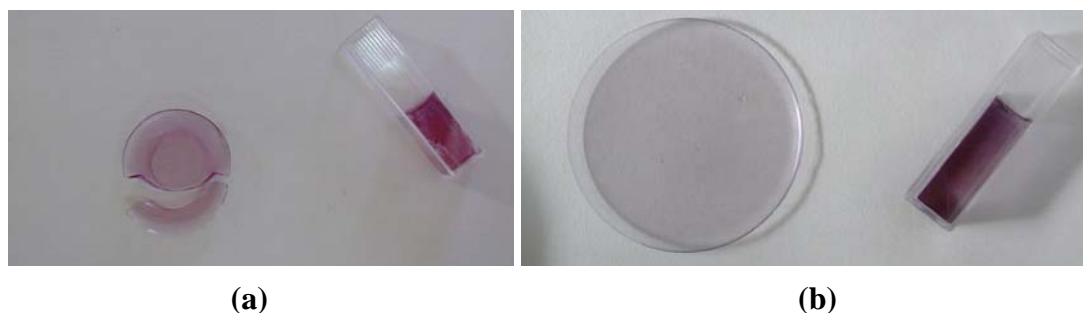
**Figure 2.** Photographs of nanocomposites prepared with (a) R=3060; (b) R=2470.

# Growth of the α-Fe$_2$O$_3$ nanowires by oxidation of iron films

*Li–Chieh Hsu and Yuan-Yao Li\**

*Department of Chemical Engineering, National Chung Cheng University, Chia-Yi 62102, Taiwan*

*preseneting author: g9144026@ccu.edu.tw*
*\*corresponding author: chmyyl@ccu.edu.tw*

α-Fe$_2$O$_3$ (hematite) is a semiconductor (Eg=2.1eV) and the most stable iron oxide under ambient environment.[1] The applications of α-Fe$_2$O$_3$ nanomaterial were extensively studied for water splitting,[2] photocatalysts/catalyst,[3] solar cell,[4] field emission devices[5] and field effect transistors (FET).[6]

In this study, we demonstrate a rapid and easy method to synthesis α-Fe$_2$O$_3$ nanowires. The density of the α-Fe$_2$O$_3$ nanowires were successfully control by different thickness of Fe thin film within 10 hours by thermal oxidation at 350 $^{o}$C in oven. The three iron films were of 50nm, 100nm and 150nm thickness. We found that more nanowires can be growth while the iron film was thicker. Observations using field-emission scanning electron microscopy revealed α-Fe$_2$O$_3$ nanowires with different density, and uniform diameters of 10-30 nm. (Fig. 1a, 1b and 1c)

**References:**

[1]     R. Dieckmann, Philos. Mag. A, **68** (1993) 725.

[2]     I. Cesar, A. Kay, J. A. G. Martinez, M. Gratzel, J. AM. CHEM. SOC., **128** (2006) 4582.

[3]     T. Ohmori, H. Takahashi, H. Mametsuka, E. Suzuki, Phys. Chem. Chem. Phys., **2** (2000) 3519.

[4]     N. Beermann, L. vayssieres, S.-E. Lindquist, A. Hagfeldt, J. Electrochem. Soc., **147** (2000) 2456.

[5]     T. Yu, Y. W. Zhu, X. J. Xu, K. S. Yeong, Z. X. Shen, P. Chen, C. T. Lim, J. T. L. Thong, C. H. Sow, Small, **2** (2006) 80.

[6]     Z. Y. Fan, X. G. Wen, S. H. Yang, J. G. Lu, Appl. Phys. Lett., **87** (2005) 013113.

**Figures:**
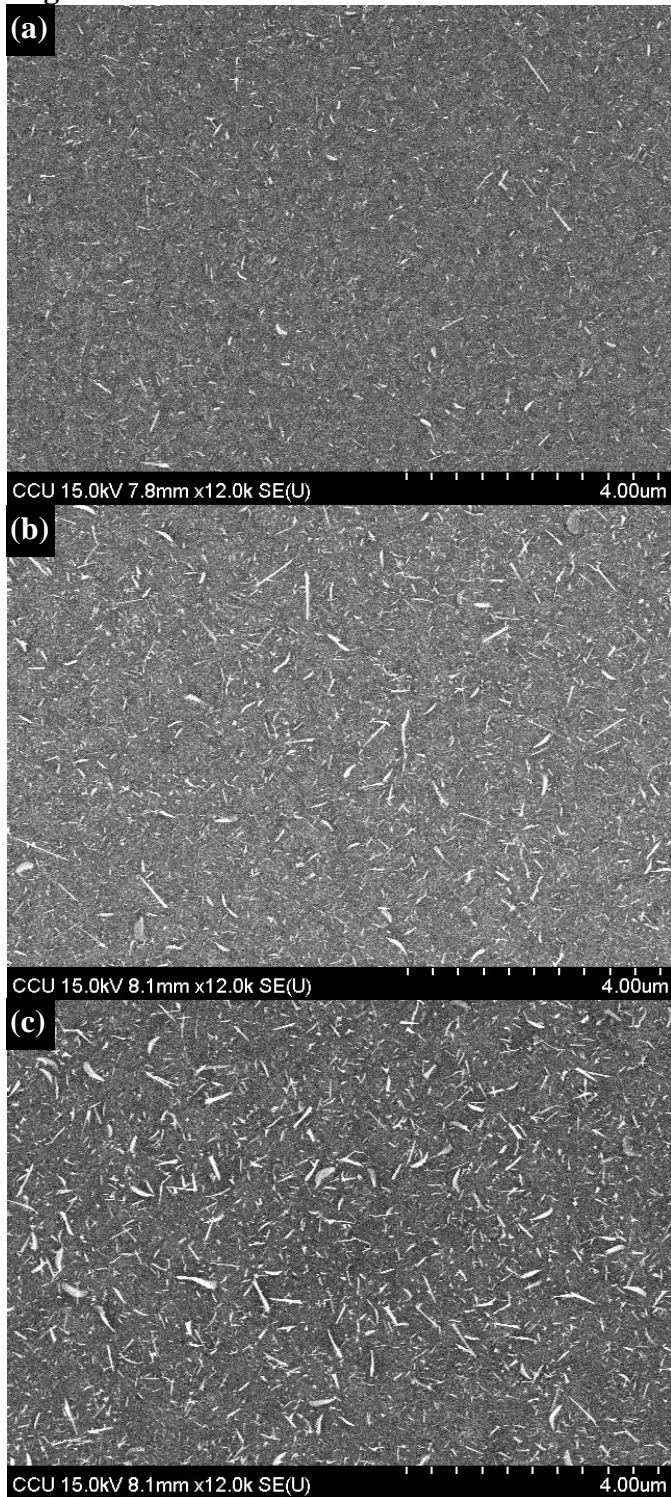


Fig. 1. FE-SEM of α-Fe$_2$O$_3$ nanowires growth on (a) 50nm, (b) 100nm and (c) 150nm of the iron films..

# THE EFFECTS OF SURFACE FUNCTIONALIZATION AND TEMPERATURE IN AFM LITHOGRAPHY ON SILICON

*Yu-Hui Huang, Ching-Ling Hsu*
*Department of Physics, Chung Yuan Christian University, Chung Li, Taiwan*
*chsu@phys.cycu.edu.tw*

The thickness of the water layer on the silicon surface is an important factor of AFM anodic oxidation lithography. After appropriate surface functionalization, the water layer thickness is expected to be changed due to the change of the hydrophilicity of the surface. Our experiments show that the AFM tip-induced oxide height and width are affected by such surface functionalization treatments with APS (3-aminopropyl triethoxysilane) and OTS (octadecyltrichlorosilane). As the surface is more hydrophilic, the oxide is higher and wider, as shown in Fig. 1. On the other hand, the oxidation mechanism is also influenced strongly by surface temperature. While the temperature may affect both the dissociated ion diffusion rate and the water layer thickness, the volume of the oxide is found to decrease with the increasing temperature, as shown in Fig. 2.

**Figures:**
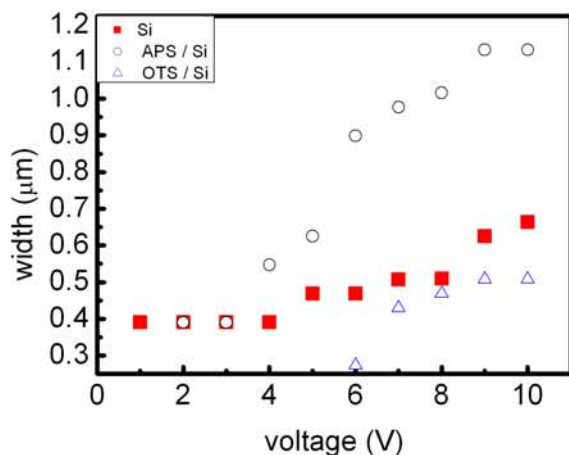


Figure 1: The width of the tip-induced oxidation vs. the applied voltage of the AFM tip under different surface functionalizations.
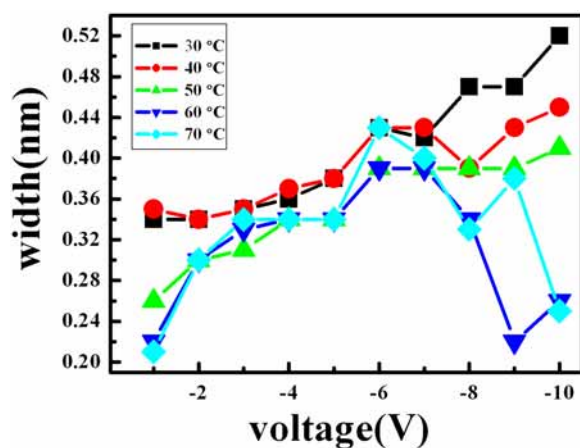


Figure 2: The width of the tip-induced oxidation vs. the applied voltage of the AFM tip under different surface temperatures.

# Study of Ti$_3$SiC$_2$ plastic deformation via high-resolution transmission electron microscopy

*Tsung-Yen Haung*[1] *and Chien-Chong Chen*[2]
*Chaoramics Laboratory, Department of Chemical Engineering, National Chung Cheng University, Chia-Yi 621, Taiwan.*
[1]*presenting author: d92425008@ccu.edu.tw*
[2]*corresponding author: chmccc@ccu.edu.tw*

Titanium silicon carbide (Ti$_3$SiC$_2$, TSC) is an interesting ceramics that can be readily machined to complex shapes [1, 2]. In this work, plastic deformation of TSC introduced by extremely small loading was studied. Thin TSC specimen was subjected to small loading by taping of the AFM tip. FESEM images revealed nano crack as well as bending were found at the sample edge. These deformations were subjected to detailed analysis using HRTEM. First, HRTEM images showed sample right next to nano crack was of β-TSC, the relatively unstable phase of TSC, but only a few unit cells of β-TSC were found. Beyond the β-TSC unit cells, there were normal α-TSC lattices. Next, in bending area (Fig. 1a), the TSC crystal was shown to have typical bending-induced tensile-compressive behavior like up-tensile and bottom-compressive features. Form the tensile area to the compressive area, number of missing atoms increased and three dislocation edges were found in every period along the c-axis of TSC (Fig. 1b). On the other hand, despite the Ti and Si atoms were highly disoriented in compressive area, the crystalline structure remained in tact and without any fracture. In addition, β-TSC was also found at locations near bending as shown in Fig. 1b. Due to the relatively weak bonding between Ti and Si lattices in TSC unit cell [3], this weak Ti-Si bonding is suggested to account for the emergence of β-TSC via the sliding of either Ti or Si lattice, resulting in the high capability of TSC deformation.

## References:

[1]     M.W. Barsoum, Prog. Solid State Chem. 28 (2000) 201.
[2]     M.W. Barsoum, T. El-Raghy, J. Am. Ceram. Soc. 79 (1996) 1953.
[3]    C.M. Fang, R. Ahuja, O. Eriksson, S. Li, U. Jansson, O. Wilhelmsson, and L. Hultman, Phys. Rev. B 74 (2006) 54106.

**Figure:**
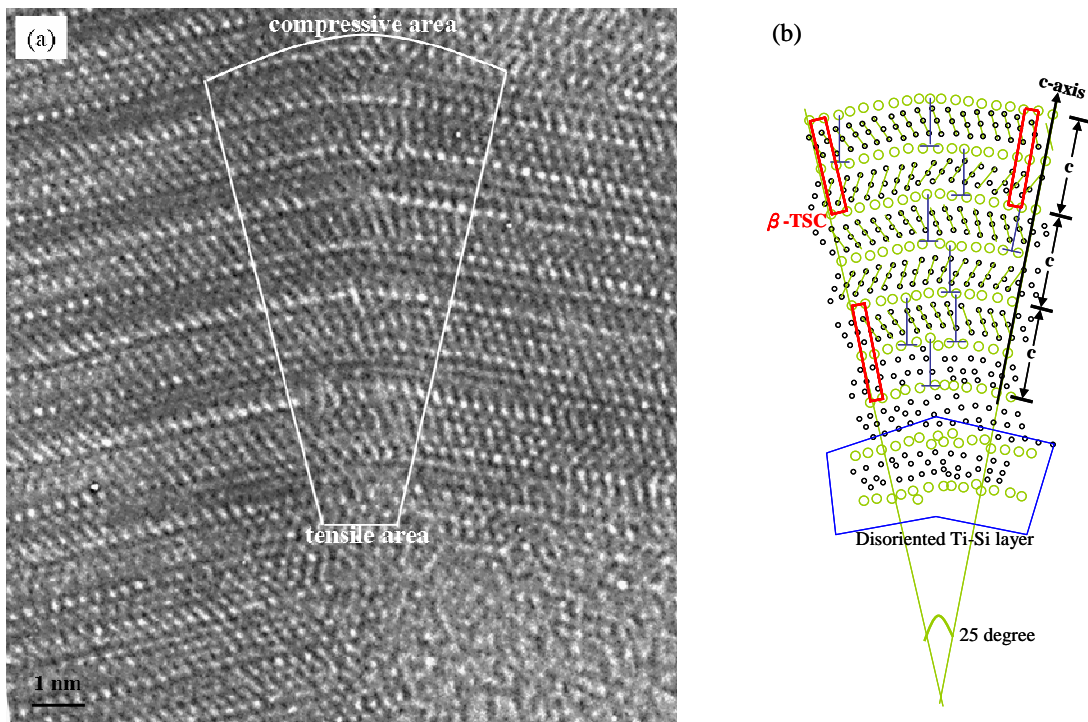


Figure 1. (a) HRTEM image of bending area. (b) Compared atomic position recorded from fan-shaped frame in (a). Green and black circle represents Si and Ti position, respectively.

# Synthesis of platelet graphite nanofibers from thermal decomposition of a mixture containing polyethylene glycol and catalyst

*Chao-Wei Huang[1], Bob Shen[2] and Yuan-Yao Li[1],\**

*[1]Department of Chemical Engineering, National Chung Cheng University, Chia-Yi 62102, Taiwan*

*[2]Advance Nanopower.INC., Nei-Hu Dist. Taipei 11491, Taiwan*

*[1]preseneting author: d92425004@ccu.edu.tw*

*\*corresponding author: chmyyl@ccu.edu.tw*

Platelet graphite nanofibers (PGNFs) exhibited a large portion of open edges, unique stacking, and well graphene layer arrangement to the fiber axis have been intensively studied. The extraordinary physical and chemical properties lead to a wide range of potential applications such as hydrogen storage [1], fuel cell [2], Li-ion secondary battery [3], and catalyst supports [4]. In this study, PGNFs were synthesized by thermal decomposition from a mixture containing polyethylene glycol (PEG) serving as the carbon source and nickel chloride ($NiCl_2$) serving as the catalytic precursor. The mixture was conducted by thermal treatment under a nitrogen atmosphere at 750 $^o$C and results found PGNFs with high purity and a uniform diameter distribution formed without hydrocarbon and reduced ($H_2$) gases in the process. Observations using field-emission scanning electron microscopy and high-resolution transmission electron microscopy revealed PGNFs with high degree of graphitization, well-ordered graphene layers, and uniform diameters of 10-20 nm (Fig. 1a and 1b).

**References:**

[1] A. Chambers, C. Park, R. T. K. Baker, N. M. Rodriguez, J. Phys. Chem. B, **102** (1998) 4253.

[2] C. A. Bessel, K. Laubernds, N. M. Rodriguez, R. T. K. Baker, J. Phys. Chem. B, **105** (2001) 1115.

[3] S. H. Yoon, C. W. Park, H. Yang, Y. Korai, I. Mochida, R. T. K. Baker, N. M. Rodriguez, Carbon, **42** (2004) 21.

[4] O. C. Carneiro, P. E. Anderson, N. M. Rodriguez, R. T. K. Baker, J. Phys. Chem. B, **108** (2004) 13307.

**Figures:**
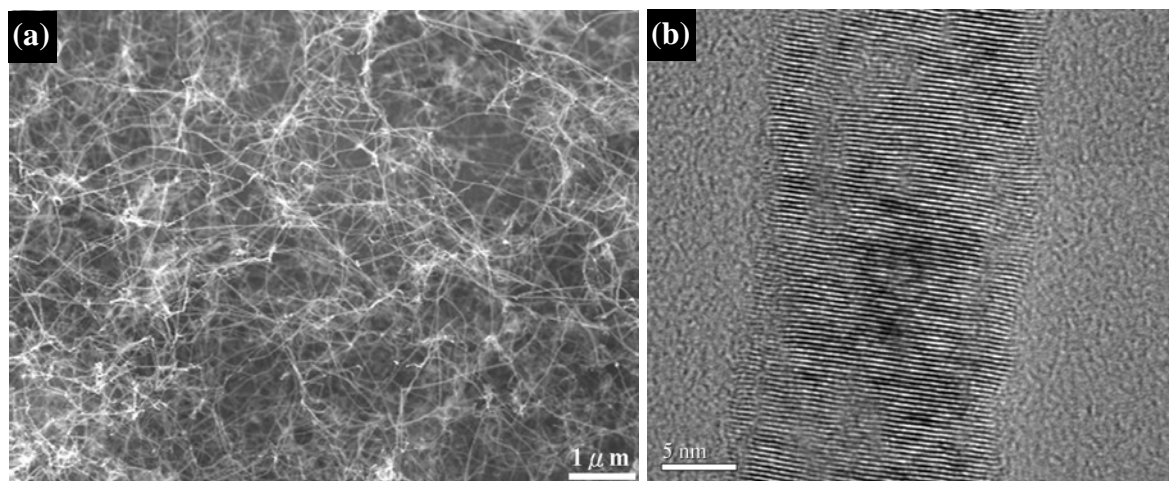


Fig. 1. (a) SEM and (b) HR-TEM image of PGNFs.

# Vertically Aligned Arrays of Metal Nanostructures Fabricated by Direct Galvanostatic Electrodeposition Using Anodic Alumina Templates

*Jaromír Hubálek, Kateřina Klosová*
*Department of Microelectronics, FEEC, Brno University of Technology*
*Údolní 53, 602 00 Brno, Czech Republic*

*email: hubalek@feec.vutbr.cz*

Metal nanostructures (nanowires and nanotubes) are created by electrodeposition of a metal on a conductive substrate which is covered by a nanoporous non-conductive structure. After that, the nanoporous non-conductive structure, which serves as the template, is removed and only the metal nanostructures remain. The whole procedure of nanostructure fabrication is illustrated in Fig. 1.

The nanoporous non-conductive structure is produced by anodization of a thin vapour deposited or sputtered aluminium film. Aluminium (as well as titanium) has a self-assembling ability which occurs during anodization under specific conditions. This ability enables to create the template which contains hexagonally arrayed nanopores. The anodization process can be either one-step or two-step. Two-step anodization, which consists of the first anodization (the first step), subsequent dissolving of the anodized layer, and another anodization (the second step), provides significantly more ordered nanopore array then just one-step anodization [1]. An example of the nanoporous alumina structure is in Fig. 2-a (anodization was carried out in 10% $H_2SO_4$ and at 24 V. The temperature of the electrolyte did not exceed 10°C).

It is possible to create both nanowires and nanotubes by the template-assisted method. In the case of nanotubes, two techniques for their fabrication exist. A double-templating approach (first reported by Sander et al [2]) consists in creation of nanowires using the $Al_2O_3$ template, subsequent electrodeposition of another metal and dissolution of the previously created metal nanowires. Therefore, this technique of nanotubes fabrication consists of two electrodeposition processes. The first one leads to creation of a metal template while the second one results in creation of the nanotubes. The other way to create nanotubes using $Al_2O_3$ template is a single-templating approach (which has been used by our research team). In this case, only one electrodeposition is required. Specific electrodeposition conditions, such as the pH, the concentration, etc., are adjusted in order to create the nanotubes. The nanotubes are probably formed by hydrogen bubbles evolved during electrodeposition. This method is less time-consuming then the double-templating approach because it consists of only one electrodeposition process. An example of nanowires is in Fig. 2-b and nanotubes (created by the single-templating approach) are in Fig. 2-c.

Fabrication of nanostructures can be advantageous in many technological applications, such as cooling systems, optoelectronics, microsensors, etc.

The nanostructures which had been formed by this template-assisted method, as well as the template itself, were examined by scanning electron microscopy (SEM). The SEM analyses were provided by **TESCAN s.r.o.**

**Acknowledgement:**

**References:**

[1] Yakovleva N. M., Yakovlev A. N., Chupakhina E. A. *Inorganic Materials*, Vol. 34, No.7, (1998), 711-713.

[2] Sander M. S., Gao H. *J. Am. Chem. Soc.,* Vol. 127, No. 35., (2005), 12158-12159

**Figures:**



**Fig. 1:** Template-assisted electrodeposition method



**Fig. 2:** Nanostructures

  a) *nanoporous alumina template*    b) *nanowires*    c) *nanotubes*

# MÖSSBAUER SPECTROSCOPY STUDIES OF IRON-FILLED CARBON NANOTUBES

## Steve Hudziak, Mark Baxendale

Department of Physics
Queen Mary, University of London,
Mile End Rd.,
London, E1 4NS, UK.
s.hudziak@qmul.ac.uk

Iron-filled single- and multi-walled carbon nanotubes were synthesized by high temperature heat treatment of $FeCl_3$-impregnated single walled nanotubes [1] and pyrolysis of a ferrocene:C-60 mixture [2] respectively. Mössbauer spectroscopy measurements are used to probe the quality of the iron encapsulated inside to better understand the properties for magnetic composites, MFM tips and other future device applications.

## References

1. Borowiak-Palen, E., et al., *Iron filled single-wall carbon nanotubes – A novel ferromagnetic medium.* Chem. Phys. Letts., 2006. **421**: p. 129-133.
2. Grobert, N., et al., *Enhanced magnetic coercivities in Fe nanowires.* App. Phys. Letts., 1999. **75**(21).

# Accurate Nano-Circuits Reliability Evaluations Based on Hybrid Monte Carlo—Numerical Simulations

*Walid Ibrahim, Valeriu Beiu, Sanja Lazarova-Molnar*
*College of Information Technology, UAE University, Al Ain, UAE*
*walidibr@uaeu.ac.ae*

The development of ever-smaller devices brings promise for further improvement in the performance of future integrated circuits (ICs), yet also leads to several new technical challenges, including *the need for architectures that reduce the uncertainty inherent to computations at very small scales* [1]-[4]. In particular, as feature sizes are aggressively scaled, the design and manufacturing of ICs becomes more complex and inevitably introduces more defects. The devices' small sizes, and consequently the tiny amounts of energy required in their switching, makes them susceptible to transient failures [5], [6]. Architectures built from emerging nanodevices, such as RTD, SET, CNT, silicon nanowires, molecular devices, etc., will be even more sensitive to parameter variations, fabrication noise, and transient failures induced by environmental/external causes [1], [7].

Trying to determine the reliability of a (larger) logic circuit through simulations would allow not only verifying the theoretical results [8], [9], but could also help in designing/ selecting better (nano)architectures. The methods used for simulating stochastic systems can be divided into *experimental* and *numerical*. In the case of *experimental methods*, the analysis is performed implicitly by observing the results obtained from many experiment runs. The most popular experimental method is Monte Carlo simulation (MC), which reproduces the behavior of the system. The biggest advantages of MC are its intuitiveness and its ability of simulating models for which deterministic solutions are intractable. However, MC is a very time consuming process which limits its application in the nanoera to the simulation at the device and gate levels. Using MC for simulation at the circuit/architectural level will be timely prohibited due to the massive size and complexity of future nanocircuits.

*Numerical methods* are designed for analyzing stochastic models without incorporating the random behavior. The simulation results that they deliver are the same for the same model parameters. These methods work by describing the flow of probabilities within the system— usually using differential equations and numerical methods for solving them. Markov chains can be used for describing and analyzing models that contain exclusively exponentially distributed state changes. Depending on the character of the time domain, there are discrete-time Markov chains (DTMCs) and continuous-time Markov chains (CTMCs). However, due to the usage of random number generator, numerical methods sometimes fail to capture the real behavior of the simulated process [10], [11].

In this paper we propose a new approach that combines the accuracy and intuitiveness of the MC simulations with the simplicity and high modelling capacity of the numerical methods. Our approach (Fig. 1) is based on using MC simulations to evaluate the probability of failure ($pf_{GATE}$) at the gate level. These *pf* functions are stored in a *reliability library* that represents the gates' genuine behaviour with respect to the parameter variations during the manufacturing process. Numerical simulations are then used (with polynomial functions from the reliability library as inputs) to calculate the *pf* at the circuit/architecture level.

Several proof of concept experiments have been conducted to verify our approach. In the first experiment the reliability of a minimum fan-in majority gate (MAJ-3) von-Neumann multiplexer [9] (vN-Mux) (see Fig. 2) is calculated using MC simulation. In the second experiment, MC simulation is used to calculate the *pf* at the gate level (MAJ-3) and the probability transfer matrix (PTM) [11] is used to calculate the *pf* at the circuit level (vN-Mux). The simulation results (see Fig. 3) show that the circuit level *pf* calculated in the two experiments are very comparable. This verifies the ability of the proposed approach to calculate realistic *pf* at the circuit level while consuming much less time and processing power. Other simulations results will be discussed in the full manuscript.

## References:

[1] Semiconductor Industry Association (SIA), Intl. Tech. Roadmap for Semicond. (ITRS), SEMATECH, Austin, TX, USA, 2005 Edition and 2006 Update, available at public.itrs.net

[2] D.J. Frank, R.H. Dennard, E. Nowak, P.M. Solomon, Y. Taur, and H.-S.P. Wong, "Device scaling limits of Si MOSFETs and their application dependencies," Proc. IEEE, vol. 89, Mar. 2001, pp. 259–288.

[3] J.D. Meindl, Q. Chen, and J.A. Davis, "Limits on silicon nanoelectronics for Terascale integration," Science, vol. 293, 14 Sep. 2001, pp. 2044–2049.

[4] V. Beiu, "A Novel Highly Reliable Low-Power Nano Architecture: When von Neumann Augments Kolmogorov," *Proc. Intl. Conf. App.-specific Sys., Arch. & Processors ASAP'04*, Galveston, TX, USA, Sep. 2004, 167–177.

[5] R. Compañó, L. Molenkamp, and D.J. Paul (Eds.), *Technology Roadmap for Nanoelectronics*, European Commission, IST Programme, Future and Emerging Technologies, Microelectronics Advanced Research Initiative (MEL-ARI NANO), 2000. Available: http://www.cordis.lu/esprit/src/melna-rm.htm

[6] C. Constantinescu, "Trends and challenges in VLSI circuit reliability," *IEEE Micro*, vol. 23, Jul.-Aug. 2003, pp. 14–19.

[7] P. Sivakumar, M. Kistler, S. W. Keckler, D. Burger, and L. Alvisi, "Modeling the effect of technology trends on soft error rate of combinatorial logic," *Proc. Intl. Conf. Dependable Sys. and Networks DSN'02*, Washington, DC, USA, Jun. 23-26, 2002, pp. 389–398.

[8] E. F. Moore, and C. E. Shannon, "Reliable circuits using less reliable relays," *J. Franklin Inst.*, vol. 262, 1956, pp. 191–208.

[9] J. von Neumann, "Probabilistic logics and the synthesis of reliable organisms from unreliable components," in C. E. Shannon, and J. McCarthy (Eds.), *Automata Studies*, Princeton, NJ: Princeton Univ. Press, 1956, pp. 43–98.

[10] M. Kwiatkowska, G. Norman, and D. Parker, "Verifying randomized distributed algorithms with PRISM," Proc. Workshop Adv. Verif. WAVe'00, Chicago, IL, USA, Jul. 2000.

[11] S. Krishnaswamy, G.F. Viamontes, I.L. Markov, and J.P. Hayes, "Accurate reliability evaluation and enhancements via probabilistic transfer matrices," Proc. Design Autom. & Test Europe DATE'05, Munich, Germany, Mar. 2005, pp. 282–287.

## Figures:
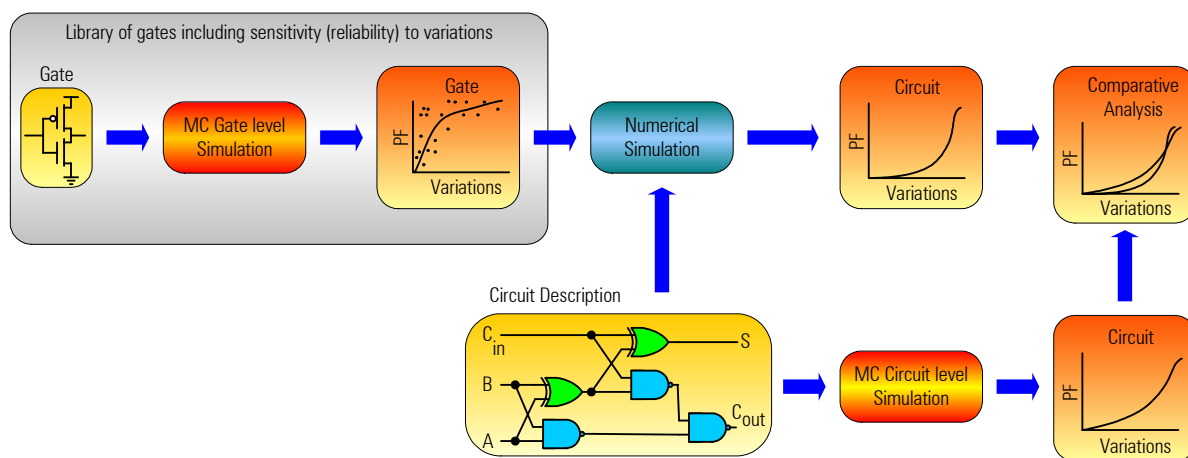


**Figure 1**. Hybrid MC-PTM Simulation Flowchart.
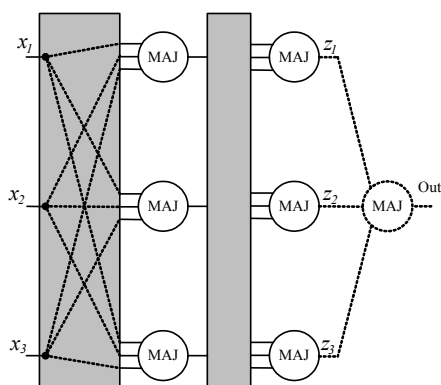


**Figure 2.** MAJ-3 vN-Mux.
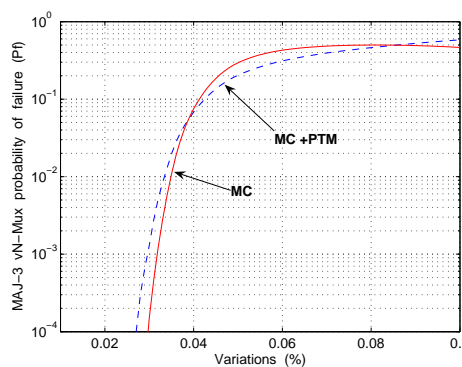


**Figure 3.** MAJ-3 vN-Mux Probability of Failure calculated using MC and hybrid MC-PTM simulations

# AN ANALYTICAL SPECTROSCOPY STUDY OF CHITOSAN NANOPARTICLES FOR DRUG DELIVERY APPLICATIONS

E. Ieva[a] *, A. Trapani[b], N. Cioffi[a], L. Sabbatini[a], A. Nacci[a]
*[a]Dip. Chimica, Università di Bari, Bari -Italy*
*[b]Dip. Farmaco-Chimico, Università di Bari*
* e.ieva@chimica.uniba.it

Chitosan (poly[β-(1-4)-2-amino-2-deoxy-D-glucan], CS) is obtained by the alkaline deacetylation of chitin, a polysaccharide that is found in the exoskeleton of crustaceans, the cuticle of insects and the cell walls of most fungi.

Typical properties of CS such as high biocompatibility, biodegradability, and low-toxicity have motivated an intense research in different fields among which agriculture, food, pharmaceutical and biomedical [1]. Several applications of CS include its activity as plantar antivirus [2], hypolipidic dietary material [2], film-forming agent in cosmetics [3].

In the last two decades, CS micro- and nano-particles were investigated as novel carriers for sustained drug release. Remarkably, chitosan-based nanoparticles have shown an increase in the drug payload and bioadhesive properties and the enhancement in the oral bioavailability and intestinal absorption of proteins were also observed [4, 5].

In the present work, chitosan nanoparticles (CS-NPs) were prepared in presence of cyclodextrin according to a modified ionic gelation technique [6] with the aim to study the potential of such nanomaterial as oral vector for a model peptide, glutathione (γ–glutamylcysteinylglycine, GSH). The role of cyclodextrin is both to protect the GSH and to modulate the drug release. To the best of our knowledge, there is no GSH oral dosage form available, this peptide being administered only parentally.

CS-NPs were characterized by zeta potential measurements and their GSH encapsulation efficiency values were found equal to 25%. Furthermore, X-ray Photoelectron Spectroscopy (XPS) was carried out to explore the NPs surface chemical composition (table 1) and ion-etching assisted XPS provided information on the elemental in-depth distribution. High resolution $S_{2p}$ XP spectra were recorded at different etch times and were used to calculate the depth-variation of the GSH concentration into the NPs. Typical spectra of the pristine and etched nanoparticles are reported in figure 1. The $S_{2p}$ region of the pristine material is composed by only one doublet ($BE_{S2p3/2}$=167.9± 0.1 eV), due to the sulphonate chemical environment of the sulfo-butyl-cyclodextrin.

Ion-etching exposes inner parts of the particle and, after a 160 s etching, a second doublet becomes evident in the $S_{2p}$ region. This feature, falling at low binding energy values ($BE_{S2p3/2}$=163.9± 0.1 eV), is attributed to S-H and/or S-S groups belonging to GSH and/or its dimeric species and can be easily used as a marker for the presence of the peptide [7].

Noteworthy, the relative abundance of the sulfo- and sulphide species changed during the in-depth analysis. In particular, the concentration of the latter functional group increased when inner layers were exposed. Curve-fitting data were used to calculate the GSH concentration anisotropy into the nanomaterial. GSH is more abundant in the inner layers of the nanoparticles, while the external NPs shell is formed by chitosan and sulfo-butyl-cyclodextrin, acting as a sort of protective coating for the pharmacologically active analyte.

**References:**

[1] Marguerite Rinaudo, Prog. Polym. Sci., **31** (2006) 603.

[2] Zhang, M.; Yang, H., Rui, C., J. Bioactive and compatible polymers, **18** (2003)391.

[3] Koide, S.S., Nutrition Research, **18** (1998) 1091.

[4] Dong-Gon Kim, Young-Il Jeong , Changyong Choi , Sung-Hee Roh, Seong-Koo Kang, Mi-Kyeong Jang , Jae-Woon Nah, International Journal of Pharmaceutics **319** (2006) 130.

[5] (a)V.R. Sinha A.K. Singla, S. Wadhawan, R. Kaushik, R. Kumria, K. Bansal, S. Dhawan, International Journal of Pharmaceutics **274** (2004) 1; (b) Hejazi, R., Amiji, M., J. Controlled Release **89** (2003) 151.

[6] P. Calvo, C. Remuñan-Lopez, J.L. Vila-J, M.J. Alonso, J. Appl. Polym. Sci. **63** (1997) 125.

[7] Cantrell, K.J.; Yabusaki, S.B.; Engelhard, M.H., Mitroshkov, A.V.; Thornton, E.C., Environ. Sci. Technol. **37** (2003) 2192.

| *Etch time /s* | *C%* | *O%* | *N%* | *S%* | *Cl%* |
|---|---|---|---|---|---|
| 0 | 65.2 | 29.2 | 3.3 | 2.0 | 0.3 |
| 160 | 66.3 | 27.3 | 3.5 | 2.6 | 0.3 |

Table 1. XPS elemental analysis recorded on chitosan nanoparticles as a function of the etching time. Error on the atomic percentages is ±0.3%.
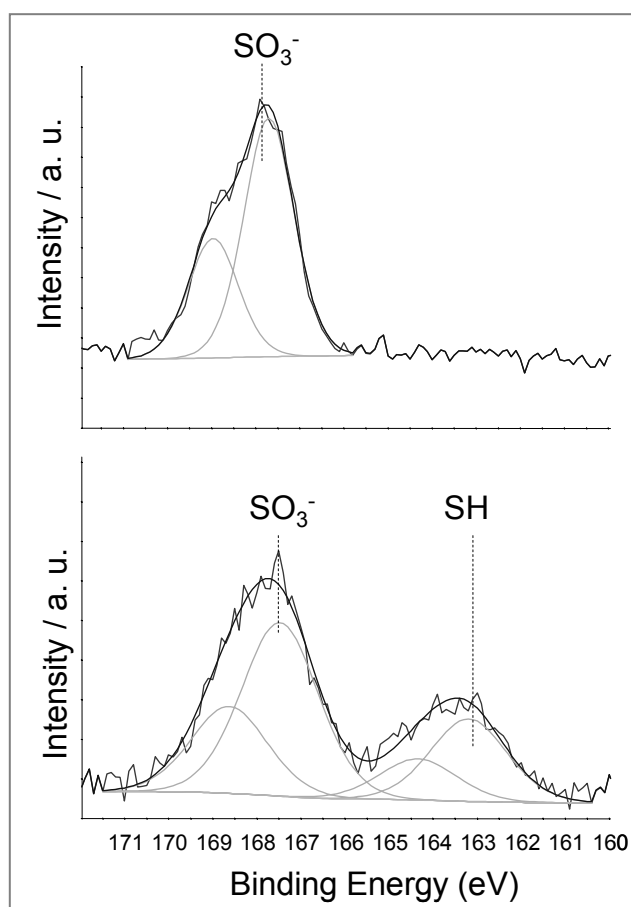


Figure 1. $S_{2p}$ XP spectra relevant to the pristine (*upper panel*) and etched (*lower panel,* etch time = 160 s) chitosan nanoparticles. Doublet attribution is reported as a label of the $S2p_{3/2}$ peak.

# OVERHAUSER FIELD-INDUCED ELECTRON TRANSPORT THROUGH WEAKLY COUPLED DOUBLE QUANTUM DOTS.

C. López Monis*1*, J. Inarrea*1,2*, G. Platero*1* and  Allan H. McDonald[3].

*1*Instituto de Ciencia de Materiales(CSIC), Cantoblanco, Madrid, Spain.

*2*Escuela Politecnica Superior,Universidad Carlos III,Leganes,Madrid,Spain.

[3]Department of Physics, University of Texas at Austin.Austin, Texas 78712

Recent transport experiments in double quantum dots show that Pauli
exclusion principle plays an important role [1-5] in current rectification. Thus these devices could behave as externally controllable spin-Coulomb rectifiers with potential application in spintronics as spin memories or transistors.
We analyze the electronic transport through a double quantum dot in the regime where spin blockade occurs as a function of a DC magnetic field. We have developed a model where the Overhauser interaction between both electronic and nuclear spins and their interplay with the external magnetic field are proposed to lift spin blockade regime. Our results indicate that the current leakage experimentally observed in the spin blockade region [1], occurs mainly due to the latter spin-flip processes, affecting the electrical response and properties of the potential current rectifying device.

Triplet states, in the double quantum dot, are responsible for spin blockade. This blockade is lifted by a electron spin flip to a singlet state generating a leakage current. In our model we consider both, interdot (1,1) and intradot(0,2) singlet states, which hybridize due to singlet-triplet exchange interaction. In this scenario, two opposite flip-flop processes can occur, one gives rise to a nuclear magnetic field which supports the external one, meanwhile the other counteracts the external magnetic field. Thus the leakage current obtained strongly depends on the external magnetic field and also on the Coulomb interaction, the interdot tunneling and the level detuning between the two dots. Transport experiments at the spin blockade region show strongly non linear behavior of the leakage current as a function of the applied magnetic field including instabilities and hysteretic behavior [2-5].
Our model consists on rate equations for the charge occupations and nuclei spin polarizations in the quantum dots in the presence of Hyperfine interaction assisted by phonons, which are selfconsistently solved. We analyze the current through a double quantum dot in a static magnetic field at different level detunings. The external field produces singlet-triplet crossings which increase abruptly the current due to electron-nucleus spin flip flop, giving rise to abrupt steps in the current, as experimentally observed [2,4]. The calculated current as a function of magnetic field, presents hysteresis which is explained in terms of the induced dynamical nuclear polarization by Hyperfine interaction.

References:
[1] K. Ono, et al., Science, **297**, 1313 (2002).
[2]K. Ono et al., Phys. Rev. Lett., **92**, 256803 (2004).
[3] F.H.L. Koppens et al., Science, **309**, 1346 (2005).
[4] S. Tarucha et al., Phys. Stat. Solid (b) **243**,14, 3673, (2006).
[5]A. Pfund et al., cond-mat 0701054.

# Magnetoresistivity response of microwave excited 2D electron systems under different regimes.

J. Iñarrea[1,2], G. Platero[2]

[1]*Escuela Politécnica Superior,Universidad Carlos III,Leganes,Madrid,Spain.*
[2]*Instituto de Ciencia de Materiales (CSIC), Cantoblanco, Madrid, Spain.*

In the field of Condensed Matter Physics, very few problems have produced such an intense activity, experimental and theoretical, like Microwave Induced Resistivity Oscillations (MIRO) and Zero Resistance States (ZRS) in two dimensional electron systems (2DES). From the experimental standpoint, new and remarkable contributions are being published in a continuous basis. All these new experimental evidences establish new and real challenges for the theoretical models presented to date. Considering that all these models are not able to achieve consensus about the true origin of these striking phenomena, the new experimental results can be regarded as crucial tests for theories, for the existing ones, and for the new ones to come.

Among these new experimental results we can highlight three of them: the first one shows up when a 2DES is subjected to bichromatic MW radiation coming from two monochromatic sources with different frequencies. The unexpected result consists in a magnetoresistivity response which is clearly modulated in the oscillations amplitude[1]. In the second one, the authors[2] report on the observation of new MIRO's at the subharmonics of the cyclotron frequency and some distortion in the shape of the main oscillations. Finally the observation that MIRO and ZRS are notably immune to the polarization of MW radiation[3] is one of the most surprising results. In this experiment different MW polarizations were used, circular in both senses (left and right) and also linear in x (current direction) and y directions.

Here we provide an explanation to each of the three experimental evidences from above using a theoretical model developed by the authors as a common basis. In this model it was demonstrated that the origin of MIRO's and ZRS of a 2DES subjected to a perpendicular and low magnetic field and MW radiation, can be explained by the dynamics of the Larmor orbit centers which oscillate classically back and forth with the same frequency as the MW field. Good agreement between experiment and theory is achieved for the three cases. The first experimental result is explained in terms of superposition of both oscillations giving rise to a oscillatory movement in the orbits center whose amplitude is modulated in the way of pulses[5]. The second experiment is explained as a non-linear effect which shows up when the MW frequency reaches a small enough value. Because of this, large amplitudes are obtained for the Larmor orbit oscillations which become anharmonic[6]. Finally the polarization immunity can be explained through a damping mechanism: along with the Larmor orbit oscillations, interactions occur between electrons and lattice ions, yielding acoustic phonons and producing a damping effect in the electronic motion. The lattice damping is able to quench the influence of different MW polarizations equalizing their effects on the MIRO's[7].

# References

[1] M.A. Zudov, R.R. Du, N. Pfeiffer, K.W. West, Phys. Rev. Lett. 96, 236804 (2006).

[2] S.I. Dorozhkin et al. cond-mat/0608633.

[3] J.H.Smet, et al, Phys. Rev. Lett. **95**, 116804 (2005).

[4] J. Iñarrea and G. Platero, Phys. Rev. Lett. **94** 016806, (2005)

[5] J. Iñarrea and G. Platero, Appl. Phys. Lett. **89**, 172114, (2006).

[6] J. Iñarrea, unpublished

[7] J. Iñarrea and G. Platero, cond-mat/0612429.

# SOFT MAGNETIC PROPERTIES OF NANOCRYSTALLINE
## $(Co_{77}Si_{13.5}B_{9.5})_{90}Fe_7Nb_3$ ALLOY

*N. Iturriza[1,2], A. Zhukov[1], J.J. del Val[1], N. Murillo[2] and J. González[1*]*

[1] Dep. Materials Physics. University of the Basque Country, P. M de Lardizabal, 3 , 20080 San Sebastián, Spain
[1] New Materials Department, CIDETEC, Pº Miramón 196, 20.009-San Sebastián. Spain

Nanocrystalline soft magnetic alloys with very fine microstructure, combine high-saturation magnetization with very small coercive force and very low effective saturation magnetostriction and are, therefore, especially interesting from the standpoint of their use as soft magnetic materials. These materials are characterized by a microstructure consisting basically of two phases, i.e., crystalline grains (with sizes of the order of the tens of nm and random orientation of their easy axes) embedded in a residual amorphous matrix. Such a microstructure is usually produced by partial crystallization of an amorphous precursor. Such as has been evidenced by different studies, the basic mechanism leading to the achievement of such a good soft magnetic behaviour is that the magneto-crystalline anisotropy of the randomly oriented nanocrystalline grains is averaged out by the exchange interactions.

In the present work we analyse the experimental results of magnetic properties deduced from the hysteresis loop (saturation magnetization and coercive field) of a current annealed (current density 56 A/mm$^2$ and duration 2 minutes) in the amorphous $(Co_{77}Si_{13.5}B_{9.5})_{90}Fe_7Nb_3$ alloy exhibiting two-phases (nanograins embedded in a residual amorphous matrix). Temperature dependence of the coercivity in this nanocrystalline alloy allows us to dilucidate on the intergranular exchange coupling leading to a deeper knowledge of the soft magnetic character of this nanocrystalline material. The explanation offered is in agreement with actual paradigm of the outstanding soft magnetic behaviour of suc kind of nanomaterial.

*) Author responsible

# ELECTRODEPOSITION OF PbSe NANOPARTICLES ONTO *N*- AND *P*-Si WAFERS AND INTO NANOPOROUS SiO₂/Si TEMPLATE

*Yu.A. Ivanova, D.K. Ivanou, E.A. Streltsov, A.K. Fedotov*

*Belarusian State University, Leningradskaya st. 14, 220050 Minsk, Belarus*
*kosarevay@mail.ru, Iv_Dm_Kon@tut.by*

Due to its properties ($E_g = 0.27$ V) PbSe is in a current use for IR electronic device manufacturing. Producing of PbSe/Si heterostructures is of great practical interest as Si is a basic material for modern electronics. PbSe deposition into nanopores in SiO₂ layer on Si wafer (SiO₂/Si system) is important since the structures based on nanoporous SiO₂ and silicon wafers could be transitive between traditional silicon-based electronic devices and nanoelectronic ones [1]. Many methods are used for PbSe/Si heterostructures formation: MBE, thermal evaporation in vacuum, liquid-phase epitaxy, pulsed laser deposition, etc. Today the electrochemical methods for chalcogenides deposition onto different substrates are being successfully developed [2]. The electrochemical approach does not require vacuum, high temperatures, expensive equipment and provides an accurate control of product composition and structure. Also, electrodeposition is an unique technique for template synthesis: deposition occurs only into the pores that have an electric contact with substrate [3].

We report on successful preparation of PbSe/Si heterostructures as well as PbSe nanoparticles in porous SiO₂/Si system by electrodeposition technique. PbSe particles with sizes from 70 to 150 nm were cathodically deposited at ambient conditions onto silicon wafers with different types of conductivity (*n*- and *p*-Si) and into nanoporous SiO₂/Si template from 0.1 M HNO₃ + 50 mM Pb(NO₃)₂ + 1 mM SeO₂ solution.

In the case of *n*-Si substrate PbSe deposition takes place at potentials less than flat band potential ($E_{fb}$) of silicon substrate. It was found out that monophase *C*-PbSe deposit with composition close to the stoichiometric could be obtained at rather narrow potential range (from -0.43 to -0.45 V *vs. Ag/AgCl/KCl$_{sat.}$*). These potentials are more negative than equilibrium potential of lead reduction ($E_{Pb^{2+}/Pb^0} = -0.38$ V). However bulk Pb deposition was not observed. It was shown that on the first stages of PbSe nucleation bulk Pb and Se simultaneously deposited onto Si and chemically interact resulting in PbSe nanoparticles formation. Provided PbSe is presented on *n*-Si surface the overvoltage of bulk Pb reduction increases. Further growth of PbSe deposit is realised due to Pb UPD and Se OPD onto *n*-Si/PbSe heterostructure. At potentials $E = -0.38 – -0.41$ V the deposit contains a large excess of amorphous Se while at $E \leq -0.47$ V bulk lead deposition occurs. The illumination does not significantly exert upon PbSe electrodeposition onto *n*-Si.

PbSe deposition onto *p*-Si takes place at potentials $E < +0.1$ V only under illumination due to photoelectrons generated in silicon substrate. The stages of PbSe deposition onto *p*-Si includes simultaneously Pb and Se deposition onto Si followed by their chemical interaction. The deposits obtained in the wide potential range (from -0.20 to -0.50 V) are characterized by the same element and phase composition and represent *C*-PbSe ($a = 0.612$ nm) with Pb:Se ratio ~0.9:1.

Being electrodeposited both onto *n*- and *p*-Si PbSe forms cubic-shaped particles uniformly distributed on the substrate. Typical SEM patterns of PbSe deposited onto Si are given on Fig 1a.

Photoelectrochemical properties of PbSe/*n*-Si and PbSe/*p*-Si were studied. Cathodic deposition of PbSe onto *n*-Si is irreversible – barrier is formed on *n*-Si/PbSe interface. Anodic oxidation of PbSe on *n*-Si is observed only under illumination when the photoholes are formed in silicon substrate. Being electrodeposited onto *p*-Si, PbSe undergoes anodic oxidation in the dark and under illumination as well. Both for PbSe/*n*-Si and PbSe/*p*-Si

heterostructures anodic stripping of PbSe does not proceed completely – a part of Se-rich phase is left on Si electrode and protects PbSe from oxidation.

Electrodeposition of PbSe into nanoporous $SiO_2/Si$ template was realized at $E$=-0.43 V for both types of Si substrates.

To produce nanoporous $SiO_2/Si$ template, $SiO_2$ layer was thermally grown on $n$-Si (100) and $p$-Si (111) substrates at $1100^oC$ during 10 h in oxygen atmosphere. The initial thickness of $SiO_2$ layer was found to be $0.9 \pm 0.1$ µm. Then the samples were irradiated by scanned beams of 350 MeV $^{197}Au^+$ ions with fluence of $5 \cdot 10^8$ $cm^{-2}$ to produce latent ion tracks in silicon oxide. Pores were formed under selective chemical etching of the irradiated $SiO_2$ layer in dilute HF. It caused the formation of pores randomly distributed over the surface and looked like truncated cones in shape. The pores diameter was controlled by etching time and varied from tens to hundreds nm.

Electrodeposition of PbSe into porous $SiO_2/p$-Si system was carried out under illumination. For both types of templates the deposition occurred only into the pores, deposition on insulating $SiO_2$ layer was excluded. The degree of pore filling depended on the duration of deposition. The techniques used in the work permitted obtain a $SiO_2/Si$ template with all the pores uniformly filled with PbSe nanoparticles (Fig 1b).

**References:**

[1] D. Fink, A.V. Petrov, K. Hoppe, W.R. Fahrner et al, Nucl. Instr. Meth. Phys. Res., **218** (2004) 355.
[2] E.A. Streltsov, N.P. Osipovich, D.K. Ivanou, in Focus on Surface Science Research / Ed. Charles P. Norris. – Nova Science Publishers (2005) 1.
[3] I.U. Schuchert, M.E. Toimil Molares, D. Dobrev, J. Vetter, R. Neumann, M. Martin, J. Electrochem. Soc., **150** (2003) C189.

**Figures:**
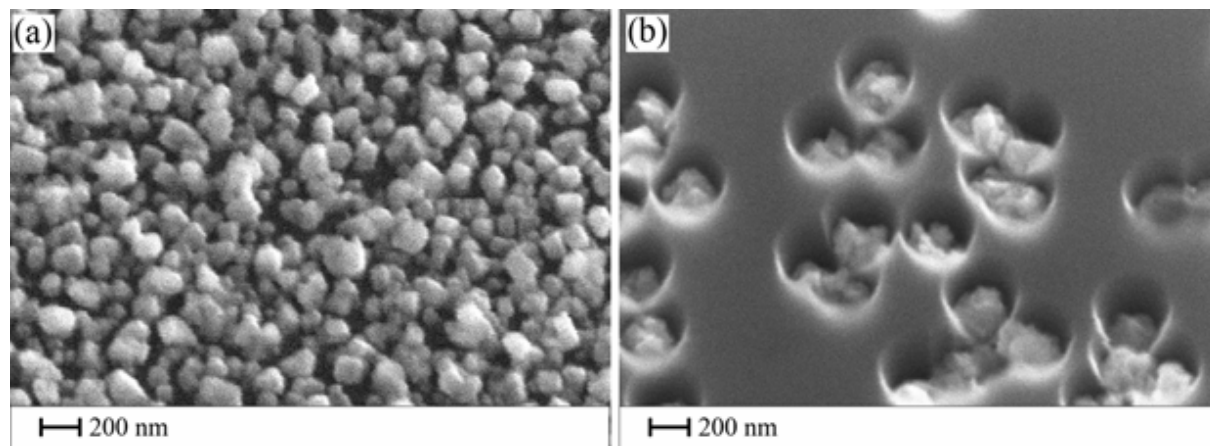


Figure 1. SEM patterns of PbSe electrodeposited at $E$ = -0.43 V from 0.1 M $HNO_3$ + 50 mM $Pb(NO_3)_2$ + 1 mM $SeO_2$ solution onto Si wafer (a) and into porous $SiO_2/Si$ template (b).

# VIBRATIONS OF TIMOSHENKO CARBON NANOTUBES

*Mohsen Jabbari, Amir Hossein Mohazzab*
*Islamic Azad University, South Tehran Branch, North Jamalzadeh St., Tehran, Iran*
*Mohsen.jabbari@gmail.com*

Carbon nanotubes are being found significant applications in many devices because of higher tensile strength and lower weight in comparison with metals and it is an interesting subject in analytical studies.

Fu et al [1] reported nonlinear free vibration of embedded multi-wall carbon nanotubes considering intertube radial displacement and the related internal degrees of freedom is investigated by using the incremental harmonic balanced method. Ritter et al [2] considered the influence of the radiation damage to multi-walled carbon nanotubes during the high-energy electron irradiation with different doses of absorbtion on their Raman vibrational spectra. The modification of both radial and tangential optical vibration is observed depending on radiation dose. Himanshu et al. [3] studied the stiffness and damping properties of carbon nanotube-epoxy composite for use in structural vibration applications. The influence of several parameters such as nanotube proportion (weight ratio), nanotube type and frequency dependence is analyzed. Free and forced vibration tests are conducted on these samples (in the form of cantilevered beams) to extract natural frequency and damping ratio from the acquired responses. Yoon et al. [4] studied the influence of internal moving fluid on free vibration and flow-induced structural instability of carbon nanotubes. Yoon et al. [5] reported resonant frequencies and the associated vibrational modes of an individual multiwall carbon nanotube embedded in an elastic medium. The analysis is based on multiple-elastic beam model, which considers intertube radial displacements and the related internal degrees of freedom. New intertube resonant frequencies an the associated non-coaxial vibrational modes are calculated. Yu et al [6] considered vibrations of single-wall carbon nanotubes: lattice models and low frequency dispersion. They find that the low-frequency dispersion of the TA modes is manifestly parabolic in agreement with the continuum analysis and with the earlier lattic study by popov but contrary to the conclusion of a linear dispersion reached in many other lattic calculations. Zhang et al [7] found out that Normal Raman scattering and surface-enhanced Raman scattering have been performed on single-walled and multi-walled carbon nanotubes to observe fine vibrational structures at the low- and intermediate-frequency regions. Following surface enhancement with silver particles, it is observed that the radial breathing mode, tangential mode, the overtone phonon peaks and coupling phonon peaks are suppressed. Cao et al. [8] by using molecular dynamics simulation, a systematic numerical investigation is carried out to explore the natural thermal vibration behaviors of single-walled carbon nanotubes and their quantitative contributions to the apparent thermal contraction behaviors. It is found that the thermo-mechanical behavior of single walled carbon nanotubes is exhibited through the competition between quasi-static thermal expansion and dynamic thermal vibration, while the vibration effect is more prominent and induces apparent contraction in both radial and axial directions. Branca et al. [9] presented a comparision between neutron scattering data and computational results, derived from a Hartree simulation, for fullerence. In order to apply the same computational approach for carbon nanotubes produced by catalysis, the structural properties of these samples have been investigated by means of transmission electron microscopy and Fourier transform infrared spectroscopy. Yoon et al. [10] studied the flow-induced flutter instability of cantilever carbon nanotubes.

This work presents vibrational analysis of nanotubes with Timoshenko assumption. In Timoshenko beam assumption further of bending, we have rotation, shear deformation and coupling between rotation and shear deformations. This paper compares the results between Euler-Bernuli and Timoshenko nanotubes. Also it illustrates the validity of two assumptions in different aspect ratios and finds out in which modes the Euler-Bernuli assumption reports the less error respect to Timoshenko analysis. Besides, in this work, Nanotubes are surrounded by the elastic medium and the effect of it over natural frequencies is discussed. Many of boundary conditions as fixed-fixed, fixed-free, hinged-free, free-free, hinged-hinged, fixed-hinged could apply in presented paper.

**REFERENCES**

[1] Y.M. Fu, J.W. Hong, X.Q. Wang, J. Sound and Vibration, vol. 296, **Analysis of nonlinear vibrations for embedded carbon nanotubes** (2006), pp. 746--756.

[2] U. Ritter. P. Scharff, C. Siegmund et al, Carbon, **Radiation damage to multi-walled carbon nanotubes and their Raman vibrational modes** (2006).

[3] Himanshu Rajoria, Nader Jalili, Composites Sience and Technology, vol. 65, **Passive vibration damping enhancement using carbon nanotube-epoxy reinforced composites** (2005), pp. 2079--2093.

[4] J. Yoon, C.Q. Ru, A. Mioduchowski, Composites Sience and Technology, vol. 65, **Vibration and instability of carbon nanotubes conveying fluid** (2005), pp. 1326--1336.

[5] J. Yoon, C.Q. Ru, A. Mioduchowski, Composites Sience and Technology, vol. 63, **Vibration of an embedded multiwall carbon nanotube** (2003), pp. 1533--1542.

[6] Yu.N. Gartstein, Physics Letters A, vol. 327, **Vibration of single-wall carbon nanotubes: lattice models and low-frequency dispersion** (2004), pp. 83--89.

[7] Xu Zhang, Weide Zhang, Lei Liu, Z.X. Shen, Chemical Physics Letters, vol. 372, Surface-enhanced Raman of Z-vibration mode in single-walled and multi-walled carbon nanotube (2003), pp. 497--502.

[8] Guoxin Cao, Xi Chen, Jeffrey W. Kysar, J. Mechanics and Physics of Solids. vol. 54, **Thermal vibration and apparent thermal contraction of single-walled carbon nanotubes** (2006), pp. 1206--1236.

[9] C. Branca, C. Corsaro, F. Frusteri et al, Diamond and Related Materials, vol. 13, **Structural and vibrational properties of carbon nanotubes by TEM and infrared spectroscopy** (2004)**,** pp. 1249--1253.

[10] J. Yoon, C.Q. Ru, A. Mioduchowski, Int. J. Solids and Structures, vol. 43, **Flow-induced flutter instability of cantilever carbon nanotubes** (2006) pp. 3337--3349.

# Ga-catalysed and self-catalysed growth of GaAs nanowires by molecular beam epitaxy.

*F. Jabeen[a], V. Grillo, M. Prasciolu, S. Rubini and F. Martelli*
*Laboratorio Nazionale TASC-INFM-CNR, Basovizza I-34012, Trieste, Italy*
*[a]also with Sincrotrone Trieste I-34012, Trieste, Italy*

*jabeen@tasc.infm.it*

Nnanowires (NWs) of elemental semiconductors, of III-V and II-VI binary compounds, together with a small number of ternary alloys, have been synthesised in the last years using a variety of growth techniques [1]. Typically the anisotropic growth of the wires is assisted by the presence of a metal particle, commonly called the catalyst.

Catalyst-assisted growth can be in principle exploited to obtain a precise location of the nanowires on the substrate by nano-patterning of the catalyst. However, the diffusion of the catalyst in the nanowire body during the growth may change the electronic characteristics of the semiconductor in an unpredicted way. We have recently demonstrated evidences of Au in ZnSe nanowires [2], as well as indication of diffusion of Mn in Mn-catalysed GaAs NWs [3]. Here we report on Ga catalysed, as well as on catalyst-free growth of GaAs NWs by molecular beam epitaxy.

A number of papers [4] recently reported the growth of III-V NWs obtained by using the group III material of the binary compound as the catalyst. However, our work represents the first success of a completely self-assembled technique for the growth of GaAs NWs without the use of outside catalysts.

The GaAs NWs have been grown on cleaved edges of Si(100) wafers. The wafers were cleaved in air a few minutes before being inserted in the ultra high vacuum (UHV) system. The substrates were then degassed at 300° C in UHV for 30' before being introduced in the MBE chamber. The wires have been grown using Ga and As molecular fluxes corresponding to a two-dimensional GaAs growth rate of 1 μm/h, with a V/III beam equivalent pressure ratio of 15.

For Ga catalysed growth, we have deposited on the substrate an amount of Ga corresponding to a nominal thickness between 2 and 5 Ga monolayer (ML, Ga atomic density on GaAs (100) surface: 1 ML=6.258 E14 atoms/cm$^2$). The deposition has been performed at the selected growth temperature in the 500-650°C range. It is well known that in the absence of group V overpressure Ga tends to form liquid droplets. A 30' long GaAs growth was started immediately after Ga deposition.

Both with and without Ga pre-deposition, one-dimensional nanostructures were obtained on the cleaved edges of Si(100) wafers. In Fig. 1 a scanning electron microscopy (SEM) image of NWs obtained growing GaAs at 600°C after depositing 5 ML of Ga is shown. The NWs are about 5 μm long and have a section diameter in the range of tens of nm. Energy dispersive X-ray spectroscopy (EDS) performed in the SEM demonstrates that the spherical particle found on the top of the NWs is composed of Ga, and confirms that the NW body is GaAs. Very analogous results are obtained by depositing GaAs at 600°C with no Ga pre-deposition. A representative image of the nanowires grown with this latter method is shown in Fig. 2. Also in this case, a spherical particle is observed at the NWs tip, and EDS confirms that it is a Ga particle, suggesting that a Ga induced self-catalysed growth occurred. The NWs density appears to be dependent on the crystallographic orientation of the facets that compose the cleaved edges of the Si-wafers.

As can be seen in Fig. 1 and 2, the growth also produces another type of NWs that generally display a smaller aspect ratio, and have no metallic tip on their top. In those cases EDS demonstrates that the whole nanostructure, including the top part, is composed of GaAs. Work is in progress to understand the growth process and in particular to understand if the

droplet-less NWs grow through a different process or the absence of a Ga droplet could be due to its lost during growth or sample manipulation.

**Figures:**
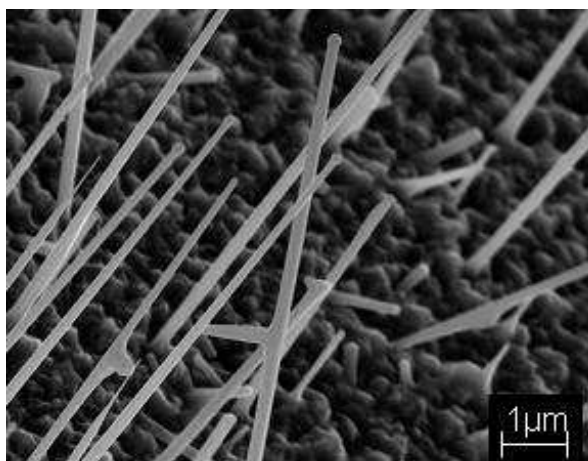


**Fig.(1).** SEM image of Ga-catalyzed GaAs NWs grown on cleaved edge of Si (100). Ga droplet is clearly visible at the top of NWs and nanorods in the back ground with no droplets at the top.
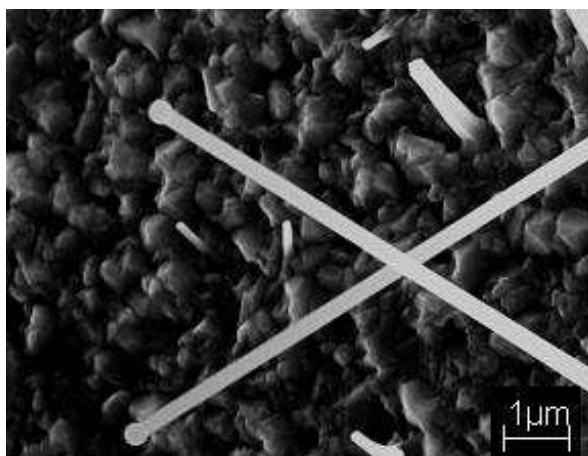


**Fig. (2).** SEM image of self-catalyzed GaAs grown on cleaved edge of Si (100). NWs have Ga droplet at the top demonstrating self-catalyzed growth and nanorods are also present with no droplet at the top.

**References:**

[1] see, e.g., W. Lu and C. M. Leiber, J. Phys. **D 39,** (2006) R387 and references therein
[2] E. Carlino et al., Phil. Mag. Lett. **86**, 261 (2006).
[3] Martelli at al., Nano Letters **6**, 2130 (2006).
[4] see, e.g,. Clint J. Novotny and Paul K. L. Yu, Appl. Phys. Lett. **87**, 203111 (2005), M. Mattila, et al., Appl. Phys. Lett. 89, 063119 (2006); Bernhard Mandl et al., Nano Letters 6 1817 (2006).

# NANOSTRUCTURES FORMING DURING THE SYNTHESIS OF PEROVSKITE CaTiO$_3$ UNDER HYDROTHERMAL CONDITIONS

Bostjan Jancar, Saso Sturm, Ines Bracko, Danilo Suvorov
Jozef Stefan Institute, Ljubljana, Slovenia

Perovskite materials exhibit a variety of properties that have made them interesting for applications in different electronic devices during the past few decades. In the bulk form they have been utilized as high-permittivity capacitor materials, piezoelectric sensors and actuators, dielectric resonators, electrode materials, phase shifters, etc. Lately, these properties have become attractive for the expanding field of nanotechnology, and much effort has been put into the synthesis of various nanostructures that will potentially serve as building blocks in future nano-electronic circuits. Particularly interesting are single-crystalline one-dimensional nanostructures, such as nanowires and nanotubes. One of the most promising routes for the synthesis of single-crystalline perovskite nanowires appears to be the hydrothermal method. Several successful syntheses of ferroelectric perovskite nanowires of BaTiO$_3$, PbTiO$_3$ and KNbO$_3$ under hydrothermal conditions have been reported in the literature. There is, however, a lack of insight into the formation mechanisms, which hinders the prediction of the conditions under which such nanostructures form. For this reason we systematically studied the formation of perovskite CaTiO$_3$ from an organometallic precursor, titanium isopropoxide, and a salt, calcium acetate, in a hydrothermal environment. By applying high-resolution transmission electron microscopy (HRTEM), electron energy-loss spectroscopy (EELS) and energy-dipersive X-ray spectroscopy (EDS) we found that prior to the formation of perovskite at least two distinct phases appear that differ in composition, morphology and crystal structure. The first of the phases is in the shape of poorly crystalline nanowires with a Ca:Ti ratio of roughly 1:3, whereas the second phase appears in the form of single-crystalline sheets with a Ca:Ti ratio of 0.45. Furthermore, the EEL spectrum reveals differences in the Ti L$_{2,3}$ fine structures, which is most likely connected to the differences in the distortion of the [TiO$_6$] octahedra between the phases. In combination with X-ray diffraction (XRD) and differential thermal analyses (DTA) we found that the latter phase is structurally closely related to either kassite CaTi$_2$O$_4$(OH)$_2$ or cafetite CaTi$_2$O$_5$(H$_2$O). We believe that by controlling the formation of these intermediate phases the morphology of perovskite CaTiO$_3$ nanostructures under hydrothermal conditions can be controlled.

# MBE GROWTH OF NANODOT ARRAYS USING ANODIC ALUMINUM OXIDE TEMPLATES

*Se Young Jeong[1,2], Fucheng Yu[1], Dojin Kim[1,*], Mun Cheol Paek[2], Kwang-Young Kang[2]*

*[1] Department of Materials Science and Engineering, Chungnam National University,
220 Gung-dong, Yuseong-gu, Daejeon, Korea*
*[2] Tera-electronics Device Team, Electronics and Telecommunications Research Institute,
138 Gajeongno, Yuseong-gu, Daejeon, Korea*

*Contact@E-mail : dojin@cnu.ac.rk*

Recently, there have been increasing studies on the fabrication of quantum dots of nano-sized fine structures because of their unique physical properties in electronics, optics, and magnetism. For the maximum quantum dot effect, highly ordered nanodots with uniform size, shape, and composition are required. It is well known that anodic aluminum oxide (AAO) is useful for the growth of nanodot arrays because of its well ordered arrays of nanoholes of the pore sizes from 30 to 80   diameter. Therefore, AAO can be taken as a template for the fabrication of highly ordered nanodot arrays.[1,2] In this work, we have studied the MBE growth of nanodot arrays by using AAO as a masking template. Generally, freestanding AAO templates fabricated by anodizing Al foils are used for the MBE growth of nanodot arrays by attaching it on the substrate. With this way, well arranged pores can be obtained. However, it's not easy to handle and make a large area template with the freestanding AAO. Thus, we have directly fabricated the AAO templates on silicon substrates and grown nanodot arrays of GaAs, GaN and GaMnAs by using MBE.

Al layers of 2   thickness were deposited by a sputtering method on a silicon wafer. And after post-annealing at 500   for 30minutes in nitrogen ambient, the Al layers were oxidized by two step anodization process proposed by Masuda et. al.[3] An aqueous solution of 0.3M oxalic acid was used for an electrolyte at 10   with the anodic potential of 45V to control the inter-pore distance. A pore-widening process was carried out in an aqueous solution of 0.1M phosphoric acid at 30   for 45minutes to determine the final pore diameter. We have fabricated an AAO template on a silicon substrate having pore diameter of 60 ~ 65   and pore length of 200  , of which the aspect ratio is a proper condition of MBE growth to avoid the shadow effect. SEM images of the AAO templates fabricated are shown in fig. 1.

GaAs, GaN, and GaMnAs nanodot arrays were grown on AAO template respectively by varying the growth conditions such as substrate temperature, source flux, and growing time. The GaAs and GaMnAs nanodot arrays were grown by using the solid source, and the GaN nanodot arrays was grown by using a single precursor $Et_2Ga(N_3) NH_2CH_3$. The growth rate of GaAs nanodots was highly dependent on the Ga flux and the substrate temperature. In the temperature range of our experiments, 280   to 650  , it showed that the lower the Ga flux or the substrate temperature, the higher the growth rate of the GaAs nano-dots. At 650  , it showed no growth of nanodots, and at 620   as shown in the fig. 2, the upper end of the nanochannel is clogged with the GaAs particles, indicating that the shadow effect activated. The growth rate of GaN nano-dots also showed the same results as the GaAs case at the temperature range 500   to 700  , where at the lower source flux or temperature, it showed higher growth rate.

It suggests that the re-evaporation rate of the deposited GaAs or GaN nano-dots is higher than the deposition rate at higher temperature. And with higher flux of the sources, shadow effect prevents the GaAs or GaN particles from depositing through the nano channels. In case of the GaMnAs, the growth rate of nanodots also depends on the Mn flux. When the

temperature of Mn source was 930 , a secondary phase was found on the surface of the template, which was identified to be MnAs by x-ray diffraction method. Fig. 2 reveals the SEM images of the nanodots of GaAs, GaN and GaMnAs, respectively with the AAO templates on silicon substate.

**Acknowledgments :**

**References:**

[1] H. Chik, and J. M. Xu, Materials Science and Engineering R 43 (2004) 103–138
[2] X. Mei, D. Kim, and H. E. Ruda, Appl. Phys. Lett. 81, (2002) 361
[3] H. Masuda, and K. Fukuda, Science, 268, (1995) 1466

**Figures:**
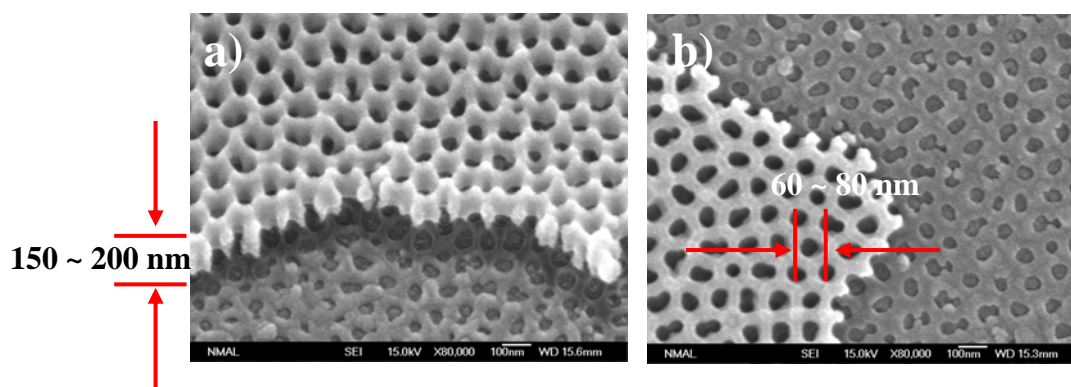


Fig. 1 SEM images of an AAO template(bright part) on a silicon sustrate ; a) oblique view, b) top view.
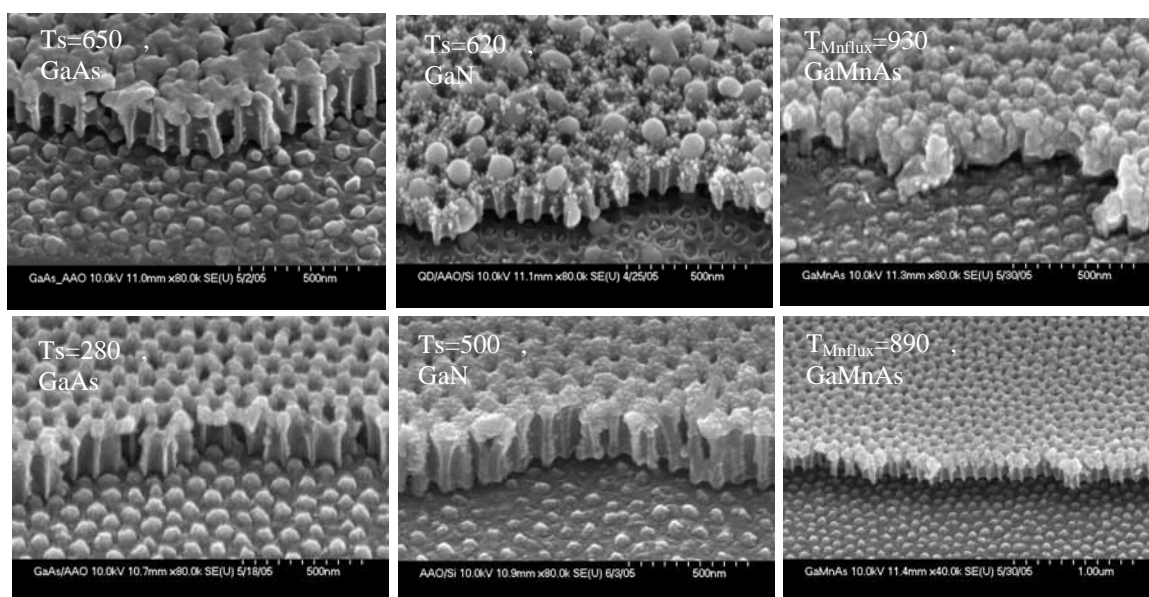


Fig. 2 SEM images of nanodot arrays of GaAs(left), b)GaN(center), and GaMnAs(right) with AAO templates.

# EPITAXY OF SOFTLY DEPOSITED SMALL Co NANOCLUSTERS ON Cu(001) SURFACES

*J.C. Jiménez-Sáez*[1]*, A.M.C. Pérez-Martín*[2] *and J.J. Jiménez-Rodríguez*[2]
[1]*Departamento de Física y Química Aplicadas a la Técnica Aeronáutica,*
*E.U.I.T.Aeronáutica, Universidad Politécnica de Madrid (UPM), E-28040 Madrid, Spain.*
[2]*Departamento de Electricidad y Electrónica, Facultad de Ciencias Físicas, Universidad Complutense, E-28040 Madrid, Spain.*
*jc.jimenez@upm.es*

Cobalt clusters are considered as possible building blocks for magnetic storage devices. For any technical applications, the clusters must be deposited on surfaces or embedded in matrices. The physical properties of these supported clusters are usually size- and shape-dependent and clearly differ from both the atom and bulk material.

The **deposition at low energies** (~ meV/atom) of **Co nanoclusters on a Cu(001) substrate** is studied by **constant-temperature molecular-dynamics simulations**. Initially clusters had icosahedral or Wulff shapes and their number of atoms ranged from 13 to 1289. The deposition energy and the temperature were, respectively, 17 meV/atom and 300 K. Nevertheless changes in cluster morphology with both magnitudes were also analyzed. Atomic interactions are mimicked by a many-body potential based on the second moment tight binding approximation (TB-SMA).

A **different epitaxial behaviour** of the clusters has been found as a function of the **number of atoms**. Below a hundred of atoms, Co clusters grow epitaxially with the substrate, that is, they mimic the orientation of this. Larger clusters do not achieve full epitaxy since stacking faults arise. In these cases, the influence of the substrate is small and in a lot of cases this is reduced to the zone nearest to the interface. Hexagonal close-packed (hcp) arrangement of atoms, characteristic of the bulk cobalt, is not stabilized practically in any system. By increasing **the temperature and the deposition energy** one can enlarge the parts of the cluster grown epitaxially even attaining a complete epitaxy.

# EXPLORING THE MAGNETICALLY INDUCED FIELD EFFECT IN CARBON NANOTUBE BASED DEVICES

*Georgy Fedorov[1], Alexander Tselev[2], David Jiménez[3*], Sylvain Latil[4], Nikolai G. Kalugin[5], Paola Barbara[2], Dmitry Smirnov[1] and Stephan Roche[6]*

[1]*National High Magnetic Field Laboratory, Tallahassee, FL 32310, USA*
[2]*Department of Physics, Georgetown University, Washington, DC 20057, USA*
[3]*Departament d'Enginyeria Electrònica, Escola Tècnica Superior d'Enginyeria, Universitat Autònoma de Barcelona, 08193-Bellaterra, Barcelona, Spain*
[4]*Department of Physics, Facultes Universitaires Notre-Dame de la Paix, 61 Rue de Bruxelles,B 5000 Namur, Belgium*
[5]*Department of Chemistry, New Mexico Tech, Socorro, New Mexico 87801, USA*
[6]*Commissariat à l'Energie Atomique, DSM/DRFMC/SPSMS/GT, 17 rue des Martyrs, 38054 Grenoble, France*
(*) *david.jimenez@uab.es*

Remarkable modifications of the electronic structure due to the Aharonov-Bohm (AB) effect have been predicted for carbon nanotubes (CNTs) subjected to a parallel magnetic field [1]. In particular, an increasing magnetic flux through the cross-section of a nanotube leads to an opening of the gap at the Fermi energy in metallic CNTs, thus tuning the band structure of a CNT from a metal into a semiconductor. Here we report on the high magnetic field study of transport properties of gated small diameter (quasi)-metallic SWNTs. We show that initially metallic CNT devices operate as CNT field effect transistors under strong magnetic fields [2]. This effect results from the AB phenomena at the origin of a band gap opening in metallic nanotubes. Strong exponential magnetoresistance observed up to room temperature is the ultimate consequence of the linear increase of the band gap with a magnetic field. Finally, we show that intrinsic characteristics of a quasimetallic CNT, such as the helical symmetry, as well as the parameters of the Schottky barriers formed at the contacts, can be deduced from temperature dependent magnetoconductance measurements.

[1] H. Ajiki and T. Ando, *J. Phys. Soc. Jpn*. **62**, 1255 (1993).
[2] G. Fedorov, A. Tselev, D. Jiménez, S. Latil, N. G. Kalugin, P. Barbara, D. Smirnov, and S. Roche, *Nano Letters* **7**, 960 (2007)
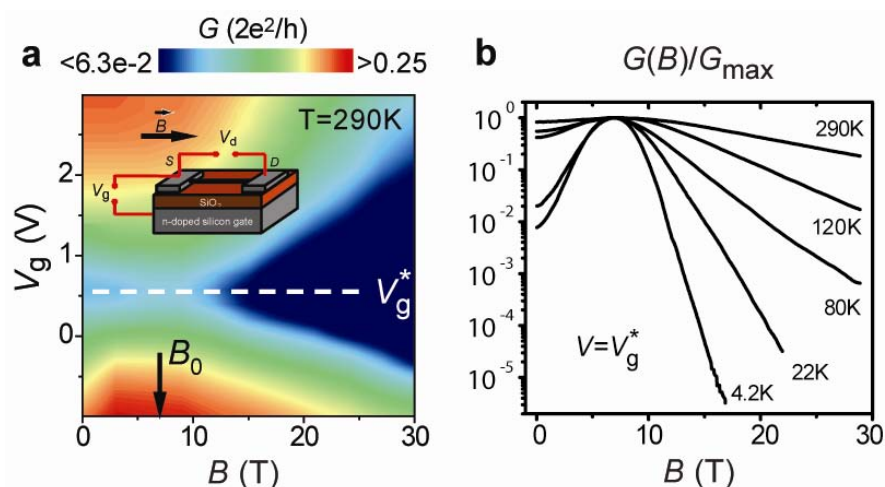


**Figure 1**. Magnetically induced field effect in carbon nanotube based devices. (a) Plot of the sample 1 conductance versus the gate voltage and the axial magnetic field. A dark arrow indicates the value of $B_0$, where the gap $\varepsilon_g(B)$ has a minimum. (b) Off-state magnetoconductance of sample 1. At $B>10$ T the $G(B)$ curves appear as straight lines in the log-vs-linear scale
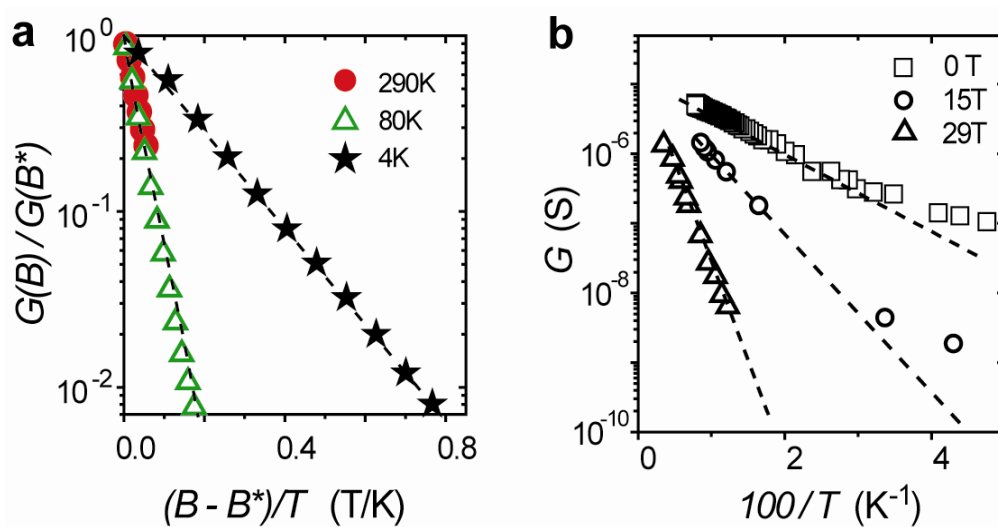
**Figure 2.** (a) Normalized off-state magnetoconductance $G(B)/G(B^*)$ of sample 1 as a function of the rescaled magnetic field $B' = (B - B^*)/T$, where $B^* = 12$ T. (b) Arrhenius plots of the conductance of sample 1.
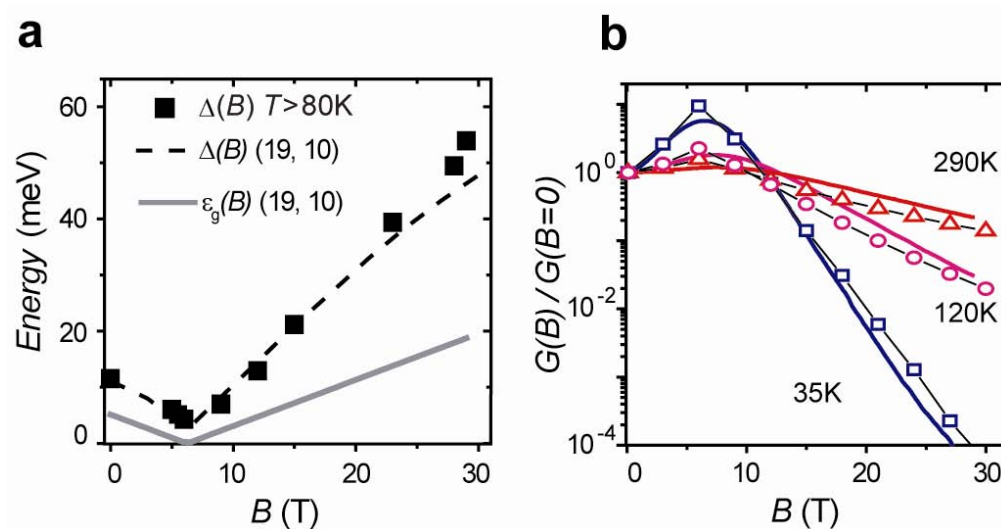


**Figure 3.** (a) Transport activation energies $\Delta(B)$ determined from the conductance Arrhenius plots (sample 1) and $\Delta(B)$ calculated for the (19,10) CNT. Gray line shows calculated $\varepsilon_g(B)$ dependence. (b) Solid lines show simulation results for the (19,10) CNT. (b) Normalized off-state magnetoconductance of sample 1 compared to simulations for the (19,10) CNT.

# Electron confinement in Cavities of Carbon Nanotubes.

Esther Jódar*[a], Antonio Pérez–Garrido[a] and Fernando Rojas[b].
[a] *Dpto. Física Aplicada, Antiguo Hospital de Marina, Campus Muralla del Mar, UPCT, Cartagena 30202 Murcia, Spain.*
[b]*Centro de Ciencias de la Materia Condensada-UNAM, Apartado Postal 2681, Ensenada, B.C. 22800, Mexico*

*esther.jferrandez@upct.es

We investigate the dynamical properties of electrons in cavities of nanotubes under the influence of an external electric field. The cavities of nanotubes are structures denoted as $(n_1, m_1)/N(n_2, m_2)/(n_3, m_3)$, where the diametre of the nanotubes used as contacts is smaller than the diametre of nanotubes used in the central part of the structure. There are many important properties associated to this kind of geometry as the generation of quasi-bound states inside the cavity for certain energies, or the behaviour as quantum-dot structures when the contacts are formed with semiconductor nanotubes [1, 2]. In this work we deal with cavities made of armchair nanotubes. We study the dynamical behaviour of waves when the structure is connected to two electrodes at different electric potential, that gives rise to a one-dimensional constant electric field along the structure.

According to the work of Bloch [3] and Zener [4], electrons in periodic linear chains of atoms under an electric field show Bloch oscillations. These oscillations take place due to Bragg reflections at the edges of the Brillouin regions. The behaviour of extended and localized waves under a constant electric field is quite different. The centre of the wavepacket oscillates in the case of extended waves but, on the other hand, for localized waves the electron changes its localization radius periodically with its center remaining at the same position In both cases, the period and the amplitude of these Bloch oscillations are given, respectively, by:

$$T_B = \frac{h}{eFd}, \qquad A_B = \frac{\Delta}{eF}, \qquad (1)$$

where $d$ is the period of the potential, $\Delta$ is the width of the energy band, and $F$ is the electric field applied. We already checked that Bloch oscillations arise in carbon nanotubes [5].

In this work we study the behaviour of electrons under electric fields in cavities of carbon nanotubes. We obtain the Hamiltonian and solve the Schrödinger equation for CNT obtaining the wavefunction as a function of time. This allows us to calculate the occupation probability for any time. Furthermore, we obtain the averaged quadratic displacement and the inverse participation radius. Through the calculation of the Fourier transform of this function we obtain the frecuency of the oscillation, which we compare with the eq. 1, obtaining a good fit to the theoretical results.

The occupation probability along the nanotube axis can be represented versus time assigning a different colour for different values of probability. The figures obtained clearly show the behaviour of the wavefunction with time. The electric field can be placed in different regions of the structure, i. e. the central part of the cavity, one of the contacts, or the whole structure. We observe, for example, that if we place the electric field along the whole nanotube, the wave keeps confined at its initial region, instead of spread along the whole structure.

# References

[1] E. Jódar, A. Pérez-Garrido and A. Díaz-Sánchez, Phys. Rev. B **73** (2006) 205403.

[2] E. Jódar and A. Pérez-Garrido, Physica Statud Solidi **204** (2007) 1892.

[3] F. Bloch, Z Phys. **52** (1928) 555.

[4] C. Zener, Proc. R. Soc. London Ser. A **145** (1934) 1523.

[5] E. Jódar, A. Pérez-Garrido and F. Rojas, (2007) (submitted).

# THE POSIBILITY OF SUPERPARAMAGNETIC CHARACTER IN NANOMAGNETIC STRUCTURE OF Fe$_X$Co$_{1-X}$

*F. Karami, A. Yazdani, Z. Shadrokh*
*Tarbiat Modares University, P.O.Box: 14115-175, Tehran, Iran*
*yazdania@modares.ac.ir*

Even though much intrest, and extensive researches [1, 2] about controlling the average size distribution, in the clinical magnetic nanoparticles have been directed to iron oxides, but;

1) its low saturation of magnetization and hence the low magnetic moment per unit volume of S.P.I.O. (Super Paramagnetizatic Iron-Oxide) nanoparticle is a problem in spite of its super paramagnetic character[3].

2) some times negative contrusts extends beyond their immediate surroundings and other related phenomena in MRI contrast agents [4].

In spite of the limited value of supperparamagnetic effect and chemical stability, biological compatibility of Fe$_3$O$_4$ and γ-Fe$_2$O$_3$ with the pure transition metals (Fe , Co) or metallic alloys or compounds of FeCo, the metal nanoparticles of which tend to have a large magnetic moment as well as high saturation magnetization effect, are suggested. But the availability of a feasible lifetime and relaxation time of these materials[5], could be still a challenge in order to consider the limit of field-induced magnetization reversal of Fe-Co alloys, which exist in the α or bcc-based phase and have soft ferromagnetic character with large saturation inductions (about 15 percent greater than Fe) [4]. The following investigations should be considered in order to reach to the goal of the biocompatible nano structure, while a key issue of fundamental research in nanostructure materials is to understand the base of formation of nanoparticles for which the defect, structure disorder and the grain growth (that are thermodynamically unstable parameters) are the basic affects;

i) The stability of chemical and crystal structure of Fe-Co at some values of x on Fe$_x$Co$_{1-x}$ during the formation of alloys or intermetallic phases, whose magnetic structure are different, as a rule changes the structure, bond type and bond strength as well as the coordination. The investigation is carried out by SEM and x-ray spectroscopy.

ii) The effect of annealing process is considered in each case where, the structural defect due to the large deviations of atomic positions as well as the grain boundaries are the main parameters of the nanoparticle size effects.

iii) The size-effect and size distribution of Fe$_x$Co$_{1-x}$ are also studied. The competition of both the crystal field effect and exchange interaction which are the main controlling factors for the magnetic moment saturation were determined and hence,

iv) The hysteresis loop of the selected samples is considered by VSM.

As the atomic-electronic structure can be the main cause of the above suggested characters, specially the stability of crystal structure hence the systematic variation of pressure, compressibility of the pure 3d-elements, the functional of internal energy and the chemical pressure of K$_f$ are studied (Fig.1 a, b, Fig. 2 a, b). The manifested deviation in figs 1 and 2 can be due to the range of fluctuation of "s-d" electron or even "s-d" hybridization, where the reconstructive crystal structure can be formed. The cause is manifested by the density of d-electrons at the Fermi surface (Table 1) on which the density of state of degenerated symmetry T$_{2g}$ and e$_g$ plays an important role in transition metals. However in the case of equi-atomic Fe$_x$Co$_{1-x}$, inter atomic exchange interactions are also calculated to investigate the effects of "H$_c$" and "M$_r$" functions on increasing of the Co concentration (Fig. 3a, b). The hysteresis loops of two selected samples are still far away from the biocompatible-interest.

**Refrences:**

[1] P.Tartaj,M.Morales,S.Verdaguer,T.Carreno J.Phys.D36R(2003)182
[2] Wanquan Jiang,H.C.Yang, et.al J.M.M.M 283(2004) 210
[3] Paula Gould nanotoday Vol .1 No4 (2006) 34
[4] S.I.Deniso,T.V.Lyutyy,Haggi,Physical Review Letter 97 (2006) 227202-1
[5] J.M.Maclaran,T.C.Schulthess, et.al J.Applied Physics Vol.85,No8, 4833-4835

**Table and Figures:**

| element | Ti | V | Cr | Mn | Fe | Co | Ni |
|---------|-------|-------|------|-------|-------|-------|-------|
| $n_d$(au) | 21.63 | 20.95 | 9.25 | 21.23 | 41.63 | 27.35 | 55.24 |

Table 1: The density of d-electron at the Fermi surface
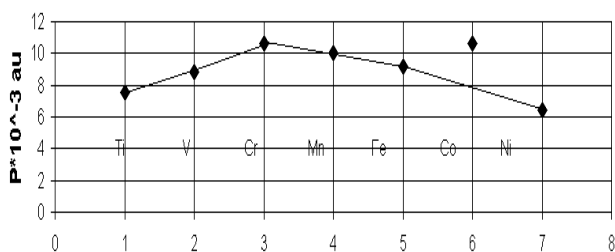


Fig.1 (a) The variation of chemical pressure of 3-d element
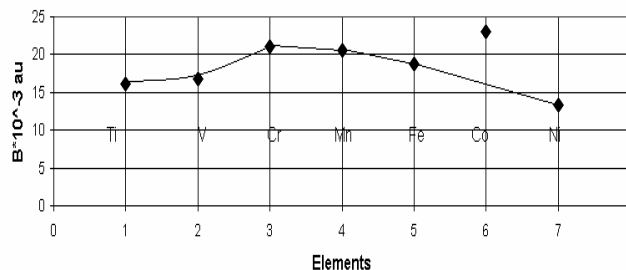


Fig.1 (b) The variation of compressibility whit3-d element
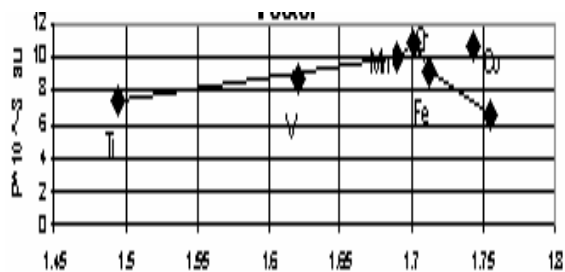


Fig.2 (a) The variation of presuer vs $K_f$
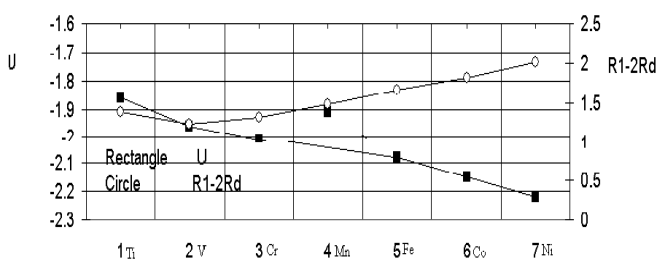


Fig.2 (b) The variation of internal energy and the free accessible space vs 3-d element
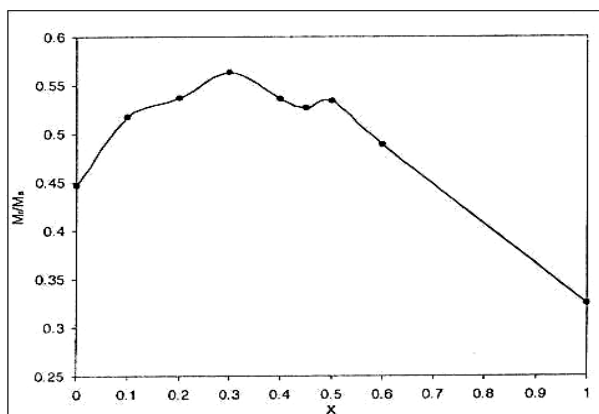


Fig.4 (a) Variation of Mr/Ms vs of Co% for the $Fe_xCo_{1-x}$
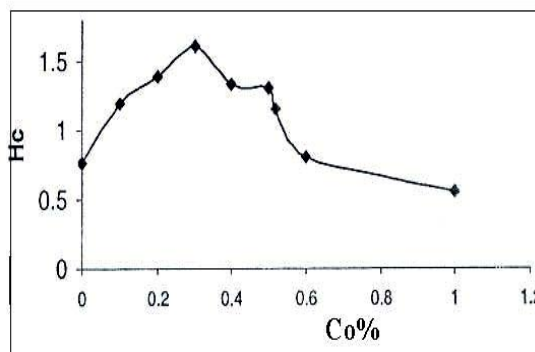


Fig.4 (b) Variation of coersivity whit Co%

# ELECTRICAL TRANSPORT PROPERTIES AND THERMAL INSTABILITY OF GOLD NANOWIRES

S. Karim[1], M.E. Toimil-Molares[2], A.G. Balogh[3], W. Ensinger[1,3], T.W. Cornelius[2], and R. Neumann[2]

[1]*University of Marburg, Department of Chemistry and Materials Science Center, Hans-Meerwein-Str., D-35032, Marburg, Germany*
[2]*Gesellschaft für Schwerionenforschung (GSI), Planckstr. 1, D-64291, Darmstadt, Germany*
[3]*Darmstadt University of Technology, Institute of Materials Science, Petersenstr. 23, D-64287, Darmstadt, Germany*

In polycarbonate templates, prepared by heavy-ion irradiation and subsequent chemical etching, Au wires with well-controlled characteristics were electrochemically synthesized [1, 2]. The structural firmness of wires was studied in detail. The Au wires became morphologically fragile due to the Rayleigh instability when annealed at high temperatures. During this process the wires broke up into chains of nanospheres at temperatures far below the bulk melting point [3]. Investigations on the decay of wires of different crystallinity revealed that the single-crystalline $\langle 110 \rangle$ textured wires were more resistant against the Rayleigh decay. This preferential stability can be explained by the presence of highly stable $\{111\}$ facets on the surface of $\langle 110 \rangle$ oriented needles.

The electrical resistance of single gold nanowires embedded in the template has been investigated. The wire resistivity was higher than the bulk value over a wide range of diameters. This is attributed to the additional electron scattering from the wire surface and inner grain boundaries. Measurements of resistivity as a function of temperature demonstrated that in this respect the wires behavior do not differ significantly from bulk metal. The resistivity decreased linearly with temperature up to ~ 50 K and finally approached a residual value.

[1]    Karim S, Toimil-Molares M E, Maurer F, Miehe G, Ensinger W, Liu J, Cornelius T W, Neumann R 2006 *Appl. Phys.* A **84** 403

[2]    Liu J, Duan J L, Toimil-Molares M E, Karim S, Cornelius T W, Dobrev D, Yao H J, Sun Y M, Hou M D, Mo D, Wang Z G, Neumann R 2006 *Nanotechnology* **17** 1922

[3]    Karim S, Toimil-Molares M E, Balogh A G, Ensinger W, Cornelius T W, Khan E U, Neumann R 2006 *Nanotechnology* **17** 5954

# SUPERCONDUCTIVITY IN LONG AND SHORT MOLECULES

*Kasumov A.Yu.*

*Laboratoire de Physique des Solides,Universite Paris-Sud, Bat. 510, 91405 Orsay, France*
*kasumov@lps.u-psud.fr*

We present the results of experimental study of superconductivity in individual molecules of carbon nanotubes, DNAs and metallofullerenes. Critical currents of supeconductor-molecule-superconductor junctions were extensively studied as a function of temperature and magnetic field. The mechanism of current induced superconductor-normal state transition for a long molecule (carbon nanotubes and DNAs) is the creation of phase slip centers and for a short molecule (metallofullerens) – multiple Andreev reflections. We observe an influence of spin state of encapsulated atom on the induced superconductvity in a metallofullerene molecule. We also discuss the mechanism of intrinsic superconductivity in carbon nanotubes and influence of defects ("bubbles") on transport in DNAs.

# Nano-Circuits composed of Resonant Nano-Particles Spheres

H. Khalili, A. Zolanvar and H. Sadeghi

Department of physics, University of Arak, Arak, P.O.Box 38156-879, Iran.

Keywords: nano-structure, nano-circuit, permittivity .

Optical electronics would make it possible to create faster computer processors, construct nano-scale antennas or build more information-dense data- storage devices. Optical electronics could also have exotic applications that simply are not possible with conventional electronics, such as the ability to couple an electronic signal to an individual molecule or the creation of biological circuits. The wavelength of light can be measured in hundreds of nanometers and the technology is now available to create structures that would operate on the same or smaller scale as the wavelength of light, N. Engheta,et. al demonstrated that nano-sized sphere made up of a nonmetallic material such as glass with permittivity greater than zero would act like a miniaturized capacitor[1]. A nano-sized sphere made up of a metallic material such as gold or silver with a permittivity less than zero would act like a miniaturized inductor. Either material could also function like a miniaturized resistor, depending on how the optical energy is lost in it.

The purpose of the present paper is to study an improved mixing rule for the effective permittivity of a composite material consisting of two sets of N plasmonic and N non-plasmonic spheres in a homogeneous background of nano-particles as nano-circuit elements.

The effective permittivity and permeability can be calculated using effective medium models if the wavelength outside spheres is large compared to sphere diameters and the polarizability of spheres is known. An illustration of the homogenization problem is shown in Fig.1.
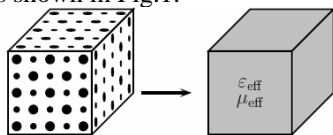


**Fig. 1** A composite construct with two sets of dielectric spheres. If the wavelength is much larger than the radii of the spheres and the distance between them.

The effective permittivity for a material with two types of inclusions having two different electric polarizabilities can be calculated from Claussius-Mossotti relation. The effective permittivity for a material with two types of inclusions having two

different electric polarizabilities can be calculated from the generalized Claussius-Mossotti relation [2]:

$$\frac{\epsilon_{\text{eff}} - \epsilon_b}{\epsilon_{\text{eff}} + 2\epsilon_b} = \frac{n_e \alpha_e}{3\epsilon_b} + \frac{n_m \alpha_m}{3\epsilon_b}$$

where $n_m$ and $n_e$ are the number of spheres per unit volume in the magnetic resonance and in the electric resonance, respectively, $\alpha_m$ and $\alpha_e$ are the electric polarizabilities of spheres in the magnetic resonance and in the electric resonance mode. When a set of spheres is manufactured, the sphere dimensions are statistically distributed because of production inaccuracies. The effect of a continuous statistical size distribution on the real part of the effective permittivity and the losses will be estimated next. The Clausius-Mossotti equation for K spheres in electric resonance and N spheres in magnetic resonance reads:

$$\frac{\epsilon_{\text{eff}} - \epsilon_b}{\epsilon_{\text{eff}} + 2\epsilon_b} = \frac{1}{3\epsilon_b} \left( \sum_{k=1}^{K} n_{ek} \alpha_{ek} + \sum_{n=1}^{N} n_{mn} \alpha_{mn} \right)$$

By substituting the electric polarizabilites

$$\alpha = 4\pi r^3 \epsilon_b \frac{\epsilon_b - \epsilon_i F(\Theta)}{2\epsilon_b + \epsilon_i F(\Theta)} = \frac{3f\epsilon_b}{n} \frac{\epsilon_b - \epsilon_i F(\Theta)}{2\epsilon_b + \epsilon_i F(\Theta)} \; ; \; \Theta = k_0 r \sqrt{\epsilon_i \mu_i}$$

$$F(\Theta) = \frac{2(\sin\Theta - \Theta\cos\Theta)}{(\Theta^2 - 1)\sin\Theta + \Theta\cos\Theta}, \quad G(\Theta_i) = \frac{\epsilon_b - \epsilon_i F(\Theta_i)}{2\epsilon_b + \epsilon_i F(\Theta_i)}$$

into equation, with $r=r_e$ for the spheres in the electric resonance and $r=r_m$ for the spheres in the magnetic resonance, we get:

$$\frac{\epsilon_{\text{eff}} - \epsilon_b}{\epsilon_{\text{eff}} + 2\epsilon_b} = \sum_{k=1}^{K} \frac{f_{ek}}{G(\Theta_{ek})} + \sum_{n=1}^{N} \frac{f_{mn}}{G(\Theta_{mn})}$$

This is a solution for the effective permittivity with two sets of spheres. One set of spheres is in the magnetic resonance and the other set is in the electric resonance. The effective permeability can be calculated in a similar way. We have not analyzed how the nonidealises in the lattice structure will affect the scattering losses or how scattering losses will increase because of the size distribution of spheres.

Possible applications would include direct processing of optical signals with nano-antennas, nano-circuit-filters, nano-resonators, and even nano-scaled negative-index optical structures.

## References

1. N. Engheta, A. Salandrino, A. Alu, Physical Review Letter, 95, 095504 (2005).
2. A. Sihvola, lectromagnetic mixing formulas and applications, The Institution of Electrical Engineers, (1999).

# STUDY OF THE ELECTRICAL TRANSPORT PROPERTIES IN CARBON NANOTUBES

*Jesús Rangel Cárdenas, Oxana Vasilievna Kharissova*
*Facultad de Ciencias Físico-Matemáticas, Universidad Autónoma de Nuevo León. E-mail okhariss@mail.uanl.mx.*

In the present work the carbon nanotubes synthesis by the thermal chemical Carbon Vapor Deposition method (CVD) is carried out as well a study of his electrical transport properties as temperature function. As precursor was used carbon disulfide and there were used three combinations of iron and silver as catalyst. In the case only iron was used as catalyst an anomaly is observed in the characteristic R (T) about zero degrees centigrade due to the absorption of water molecules in the carbon nanotube. Also we present studies of the material morphology using Atomic Force Microscopy (AFM).

# MORPHOLOGY CONTROL OF SELF-CATALYTIC INDIUM TIN OXIDE NANOWIRES BY OXYGEN

*Kim Soo-Ho*[1], *Roh Yong-Suk*[1]*, Phan Van Cuong*[1]*, Chang-Hwan Chang*[2]*, Kim Do-Hyung*[1]
[1]*Department of Physics, Kyungpook National University, Nano Applied Physics Laboratory (NAPL), Daegu 702-701, Republic of Korea*
[1]*Research Institute of Industrial Science & Technology (RIST), Pohang, 790-600, Republic of Korea*

*Kimdh@knu.ac.kr*

## Introduction

Control of nanostructures growth is of great importance for applications of future nanodevices based on bottom-up approach. Recently, a variety of oxide nanomaterials have been synthesized and studied for a number of their novel properties and applications [1,2]. Sn-doped $In_2O_3$, called indium-tin oxide (ITO), is one of most widely used transparent conducting oxides. There have been some reports on the synthesis and the structure characterization of ITO nanostructures [3,4]. The morphologies of ITO nanostructures can be influenced by multiple factors such as the growth temperature, the nature of substrate, growth time, growth ambient, and etc. However the effects of oxygen ambient on the control of morphologies of self-catalyzed ITO nanowires have not been discussed.

## Experimental

The ITO nanowires were synthesized by a vapor transport and condensation method including a carbothermal reduction and a self-catalytic growth were used. First, Equal amounts of commercial ITO powder (10 wt% $SnO_2$ and 90 wt% $In_2O_3$, 99.99% purity) and graphite powder (99.99%) were mechanically pulverized together and transferred to an alumina boat. The alumina boat was placed in the center of the quartz tube furnace. Bare silicon substrates were inserted the tube positioned about 20 cm from the center of the boat under a constant flow of argon (Ar, 99.999%, 50 sccm) as the carrier. The oxygen ($O_2$, 99.999%, 2 sccm) was added as the reactive gas in order to for investigate the effect of oxygen gas on the nanowire growth. The pressure was maintained at 1.7 Torr. Then, the furnace heated to 900 $^o$C and the corresponding substrate temperature is about 600 $^o$C. The characterization of the ITO nanowires was analyzed using X-ray diffractometer (Philips, X PERT), scanning electron microscopy (SEM) (Hitachi, S-4300), and high-resolution transmission electron microscopy (HRTEM) (Philips, CM 200).

## Results and discussion

Fig. 1(a) and (b) shows the SEM images of the as-grown ITO nanowires synthesized with and without the oxygen. With the exception of the oxygen, the other growth conditions were identical. The long pin-like nanowires (p-NWs) with the catalysts nanoparticles on the tip were grown in the absence of the oxygen, as shown in Fig 1(b). Elemental mapping of the Sn, In, and O content of the nanowire reveals that the spherical catalysts on the tip is metal Sn. Meanwhile the cone-like ITO nanowires (c-NWs) without the nanosized catalyst on the tip were grown in the presence of oxygen, as shown in Fig 1(a). The energy dispersive spectrum (EDS) reveals that the c-NWs consist mainly of In, Sn, and O showing a different atomic % ratio at the tip, body, and bottom parts. The XRD measurements show the significant metal Sn peak for the p-NWs without oxygen which was originated from the catalyst nanoparticles on the tip. The Sn metal peak of p-NW disappears during the heating at 150 $^o$C. However, metal Sn in the XRD patterns of the c-NWs is not detectable, as shown in the inset of Fig 2. The Sn catalyst nanoparticles on the tip of the nanowire are effectively consumed to form the sharp nanowire during the growth in the presence of oxygen. However, the Sn nanoparticles can be remained on the tip in an oxygen deficient ambient without adding the oxygen. We will

suggest more detailed mechanism for the sharpening process and additional morphology control of the ITO nanostructures.

**References:**

[1] C.N.R. Rao et al., Pro. Sol. Sta. Chem., **31**, (2003) 5..
[2] Y. Li et al., Materials today, **9**. (2006) 18
[3] P. Nguyen et al., Nano Lett. **3**, (2003) 925.
[4] Q. Wang et al., Adv. Mat. **18**, (2006) 234.

**Figures:**
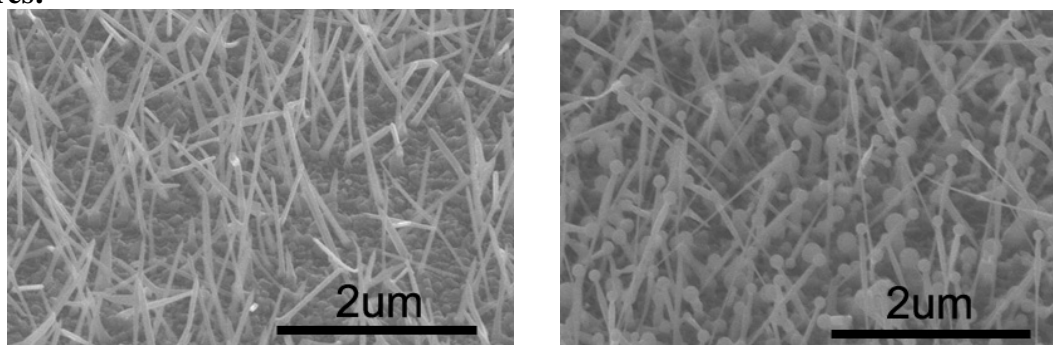


Figure 1. SEM images of ITO nanowires grown (a) with oxygen and (b) without oxygen.
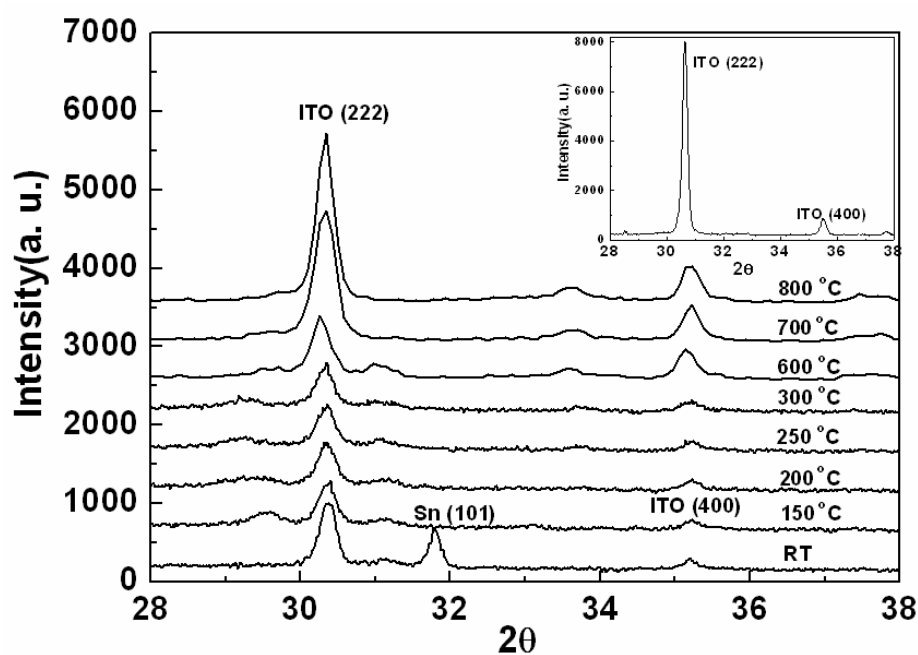


Figure 2. Temperature dependant XRD patterns of ITO nanowire grown without oxygen. (The inset shows XRD pattern measured at the room temperature for the nanowire grown without oxygen)

# ATOMIC ALIGNMENT OVER SUPERLATTICES OF WATER SOLUBLE AU NANOPARTICLES

*Keisaku Kimura, Seiichi Sato, Suhua Wang*
*Department of Material Science, Graduate School of Science, University of Hyogo, 3-2-1*
*Koto, Kamigori-cho, Ako-gun, Hyogo 678-1297, Japan*
*kimura@sci.u-hyogo.ac.jp*

A quality superlattice made of hydrophilic Au nanoparticles was grown at an air/water interface within several days or a week. A self-correcting process took place during this period. The superlattice revealed both narrow angle and wide angle electron diffraction, indicating that there were both translational and orientational ordering in a superlattice. A model structure of this superlattice was constructed based on a truncated octahedral shape at an atomic level. The ordering misfit angle was derived from the analysis of the crescent pattern in a wide-angle diffraction region.

Mercapto-succinic acid-coated gold nanoparticles in the average size of 3.7 nm was prepared by a procedure basically similar to that described in the former work. A superlattice formation was also followed by the published method. After 3-5 days under room temperature, the crystallization took place in a range of HCl concentration (0.3±0.2M) giving numerous faceted crystals with micrometer sizes. These gold nanoparticle crystals were transferred to silicon(XRD), glass(optical), amorphous carbon(TEM, SAED) and NaCl(FTIR) substrates for analysis.

Several morphologies are noticeable such as pyramidal, triangle and hexagonal plate in an optical micrograph of the Au quality superlattice of 10 μm in size. Figure 1a is the magnified TEM image of one thin plate, in which six fold symmetry is obvious as indicated by 60-degree arrows. Figure 1b is WAED from the sample of Figure 1a. There are central spots in NAED(c and d) as well as the six-fold crescent in WAED region, which is successfully indexed as fcc metallic gold. A magnified image (d) shows even 5-th Bragg diffraction spots. It should be noted that the diffraction spot in WAED region is not a point nor arc in Fig.1b but crescent shape and that both WAED and NAED have exact six fold symmetry. We should also note that the relative orientation direction of WAED to NAED spot. Figure 2 illustrates how atomic lattice alignment in a superlattice reflects to ED. Case a stands for the situation of both translational and orientational orderliness, spots in NAED are arising from translational alignment of particles, which are surrounded by peripheral spots from atomic scale regularity. Case b is the translational ordering with no atomic orientational alignment, which comprises peripheral rings from random orientation of atoms. Note that rings or spots in WAED region can classify these two cases. Thus based on the ED patterns, we constructed a structural model of Au nanoparticle superlattice. If we accept the truncated octahedron (TO) morphology as the shape of the Au cores, the component Au nanocrystals of average core diameter 3.65 nm consist of 1709 atoms, which are close to the observed size, 3.7nm. That is, there is a magic number even for a large size particle comprised of thousand of atoms.

The resultant three-dimensional structure is shown in Figure 3a. Inverse space projection of each atom is presented in Fig.3b, in which we notice a lack of six-fold symmetry. The two-dimensional projection of this model shows that the core dimension is 3.26 and 3.30 nm for different direction suggesting that it is possible to rotate 60 degree for randomly selected particles. After allowing this rotation, the estimated ED becomes hexagonal symmetry as shown in Fig.3c. We further analyzed the structure of crescent diffraction spot and found that there is 0.5 degree misfit among neighboring particles. Detailed analysis will be presented on the session.

**References:**
[1]Seiichi Sato, Suhua Wang, Keisaku Kimura, J.Phys.Chem.C(2007) in press.
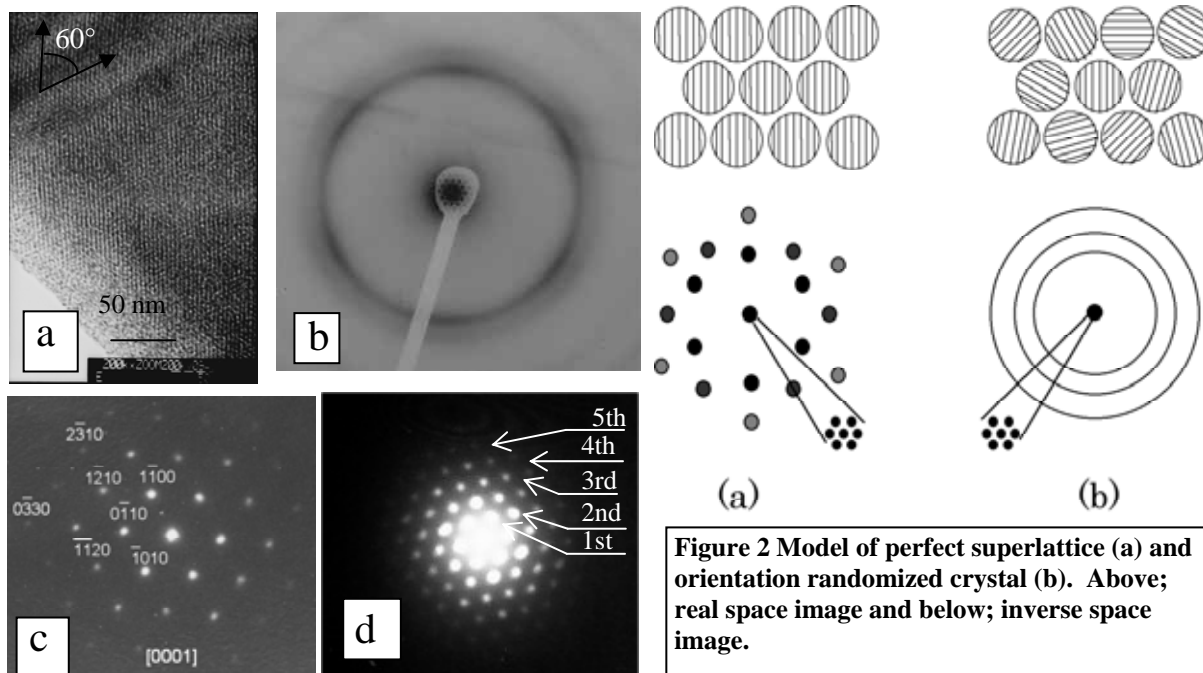


Figure 2 Model of perfect superlattice (a) and orientation randomized crystal (b). Above; real space image and below; inverse space image.

Figure 1 HRTEM(a), TED(b), NAED(c, d) of superlattice of MSA-Au.
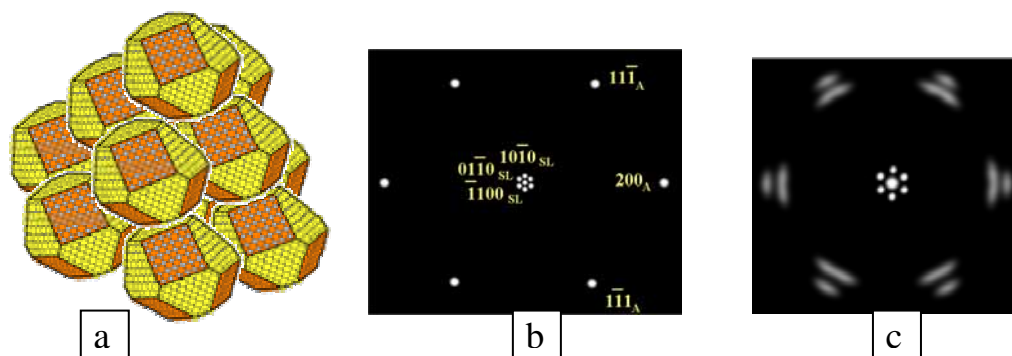


Figure 3 A model structure of MSA-Au superlattice (a), and it's TED(b). In order to fit the observed WAED(Fig.1b), the orientation of arbitrarily selected particle in a superlattice must rotate just 60 degree giving Fig.3c model ED.

# Advanced Electrodes with Nanostructured Surfaces for Electrochemical Microsensors

*<u>Kateřina Klosová</u>, Jaromír Hubálek*
*Department of Microelectronics, FEEC, Brno University of Technology*
*Údolní 53, 602 00 Brno, Czech Republic*

*email: xkloso00@stud.feec.vutbr.cz*

Nanostructures have recently attracted great interest because of their unique properties and potential use in a broad range of technological applications. In the case of microsensors, an array of nanostructures can be used to enlarge the surface area of sensing electrodes. It is assumed that microsensors will then have higher sensitivity due to the surface modification.

One of the simplest ways to modify an electrode surface by nanostructures is to deposit a metal into a thin nanoporous $Al_2O_3$ template which covers a gold electrode. Metal ions are attracted to the cathode (the gold electrode) during electrodeposition and fill the nanoporous template. After finishing the electrodeposition process, the template is dissolved and the metal nanostructures are obtained. The process of creating nanostructures is illustrated in *Fig. 1*.

The $Al_2O_3$ template is produced by anodic oxidation of a thin layer of very pure aluminium. The aluminium layer can be deposited either by sputtering or vapour deposition. However, vapour deposition is more suitable for template preparation because the deposited layer contains only small crystals of aluminium and is uniform [1].

Diameters and density of nanostructures are determined by the template. The length of the nanostructures depends on the amount of the metal which is deposited into the template. The weight of the metal is usually directly proportional to the current density and the duration of deposition. However, in the case of nanopores with high aspect ratios (length to diameter), mass transport is limited only to diffusion [2].

The electrolyte, used for the majority of the experiments on the nanostructure growth, was Watts Bath (containing 250 g/l of $NiSO_4$, 50 g/l of $NiCl_2$, and 34 g/l of $H_3BO_3$). The nanostructures were created under various electroplating conditions, such as the use of ultrasound waves, a wide range of current densities, various concentrations, various diameters of the nanopores, etc. In the case of the latest experiments, standard stirring of the solution has been replaced by a new local deposition method in which only a small volume of an electrolyte is employed.

Both nanowires (*Fig. 2*) and nanotubes (*Fig. 3*) of various wall-thicknesses can be created by this method. It has been found that the type of the structure depends on specific electroplating conditions (e.g. the pH and the concentration) and used template (i.e. the diameters of the nanopores). Therefore, it is possible to control the type of the nanostructure by adjusting these electroplating parameters and to create either nanotubes or nanowires purposely.

**Acknowledgement:**

This research has been supported by Grant Agency of the Academy of Sciencies of the Czech Republic under the contract GAAV 1QS201710508 Impedimetric chemical microsensors with nanostructured electrode surface, and by the Czech Ministry of Education within the framework of Research Plan MSM 0021630503 MIKROSYN New Trends in Microelectronic Systems and Nanotechnologies.

**References:**

[1]  Hrdý R., Hubálek J., *Acta Metallurgica Slovaca*, Vol. 13, No.2, (2007), 155-158.

[2]  Stulík K., Amatore Ch., Holub K., Mareček V., Kutner W. *Pure Appl. Chem., ©IUPAC.*, Vol. 72, No. 8., (2000), 1483-1492

**Figures:**



*nanoporous Al₂O₃ template*  *metal deposited into nanopores*  *metal nanostructures*

*metal layer (cathode)*  electrodeposition  dissolving of Al₂O₃

**A**  **B**  **C**
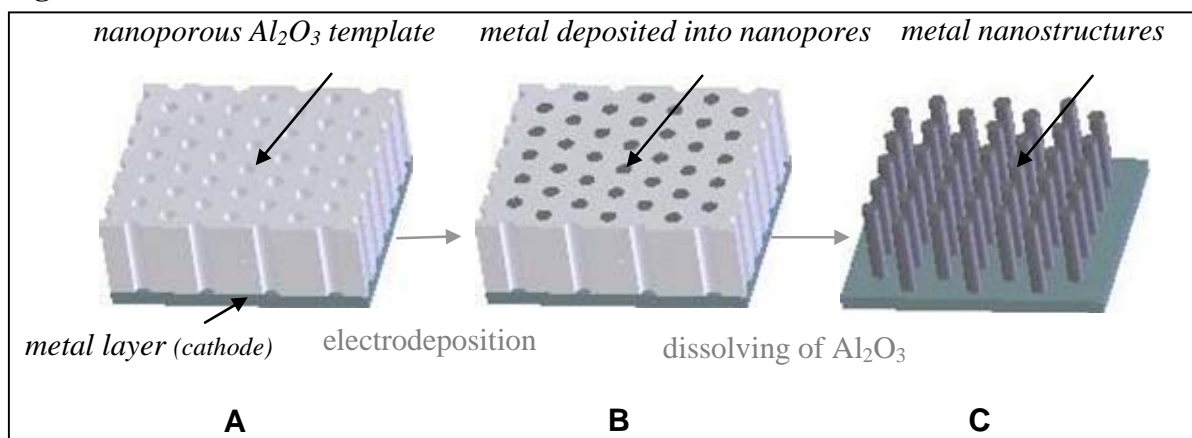
**Fig. 1:** Process of nanostructures creation
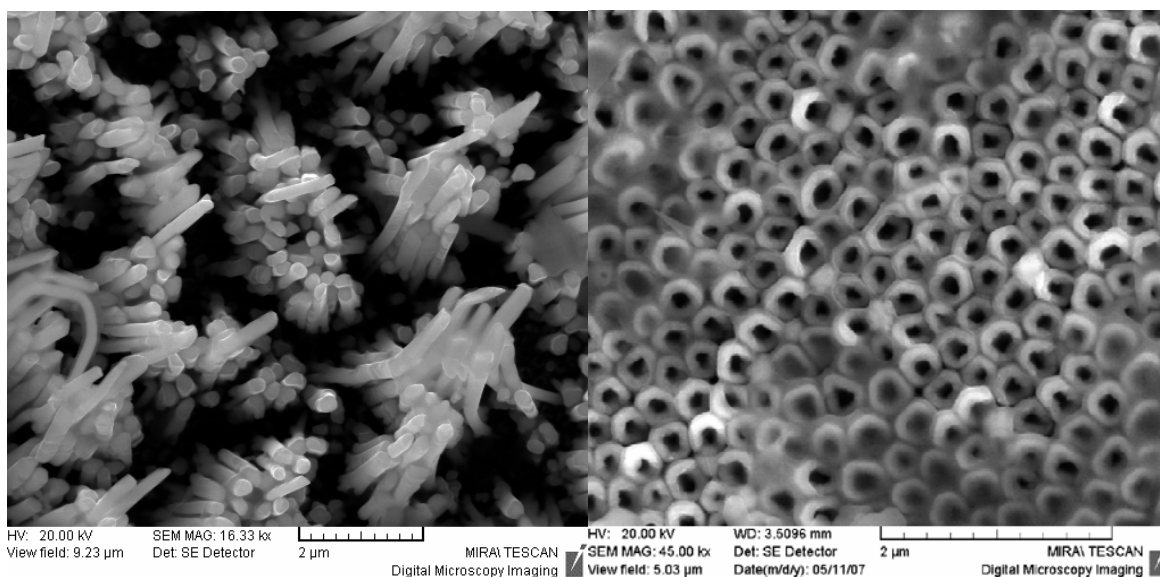


**Fig.2:** Nanowires     **Fig. 3:** Nanotubes

# Atomistic modeling of metal/high-k oxide interface properties as function of gas treatment

*A.A. Knizhnik[1], A.V. Gavrikov[1], I.M. Iskandarova[1], A.A. Bagatur'yants[1], B.V. Potapkin[1],*
*L.R.C. Fonseca[2], M.W. Stoker[3], and J. Schaeffer[3]*
*[1]Kinetic Technologies Ltd, Kurchatov Sq. 1, Moscow, Russia*
*[2]Wernher von Braun Center for Advanced Research, Av. Perimetral Norte 301, Campinas,*
*Sao Paulo, Brazil*
*[3]Freescale Semiconductor Inc., 3501 Ed Bluestein Blvd., Austin, USA*
*knizhnik@kintech.ru*

The depletion length in the current polysilicon gate technology increases the effective oxide thickness and thus reduces the advantages of using high-k dielectrics in the future generations of CMOS technology. Moreover, it was recognized that new high-k materials can react with the polySi gate causing undesirable changes in the electrical properties. All these problems can be solved by using a combination of a high-k ceramics with a suitable metal gate as a replacement for $SiO_2$ and polySi. In this work we considered dependence of metal / high-k oxide interface properties on the gas treatment conditions.

We present an atomistic investigation of the structure and properties of the interfaces between metal and high-k oxide materials, considering as an example metal/$HfO_2$ interface.

The dependence of Pt/$HfO_2$ interface structures and properties (the adhesion and the band offset at the interface) on the interfacial oxygen concentration is determined (see Fig. 1). Using calculated energies for series of structures with different interfacial oxygen concentration we predicted equilibrium interface structure dependence on partial pressure of oxygen and temperature. The predicted oxygen-pressure dependence of the interface composition provides a satisfactory explanation of the known dependence [1] of electrical properties on the gate deposition conditions (see Fig. 2).

It is also shown by calculated results that oxygen chemical potential strongly influences on the segregation trends at the oxide/metal alloy interface, in particular, for the Mo–Pt/$HfO_2$ interface large oxygen chemical potential leads to Mo segregation to the interface.

The possibility of tuning electrical properties by interface doping with impurity atoms such as N, F, or Cl is discussed. We found that N doping of the Pt/$HfO_2$ interface is unstable with respect to thermodynamics of desorption to gas phase, while doping with Cl is thermoneutral and doping with F atoms is exothermic. F atoms at the Pt/$HfO_2$ results in increasing of valence band offset at the interface with respect to oxygen-free Pt/$HfO_2$ interface. Doping of Mo/$HfO_2$ interface with nitrogen is stable with respect to nitrogen desorption to gas phase and results in increasing of effective work function of Mo.

**References:**

[1] J.K. Schaeffer, L.R.C Fonseca, S.B. Samavedam, Y. Liang, P.J. Tobin, and B.E. White, Appl. Phys. Lett., **85** (2004) 1826.

**Figures:**
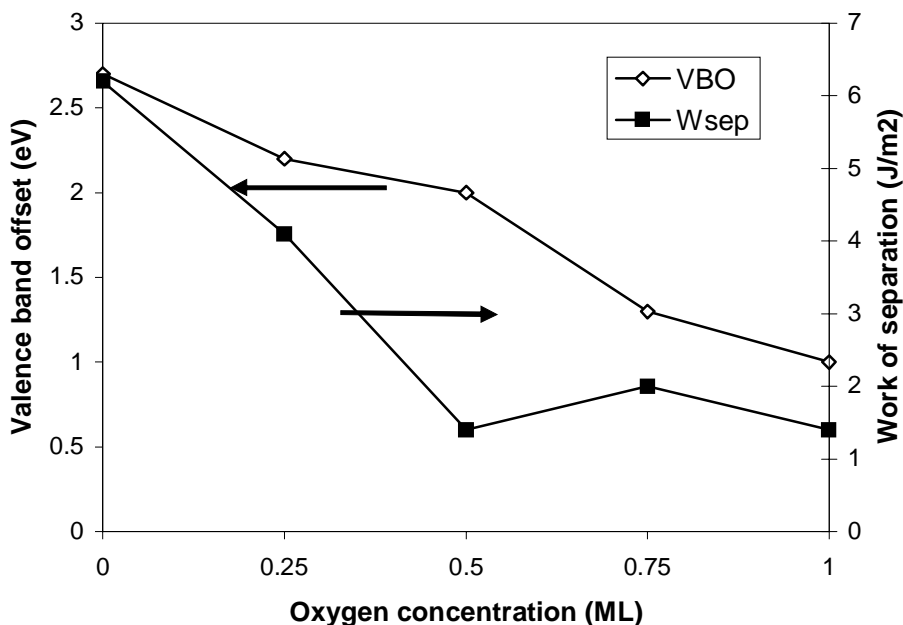


Fig. 1. Calculated valence band offset (VBO) and work of separation ($W_{sep}$) for the Pt/HfO$_2$ interface as a function of interfacial oxygen concentration.
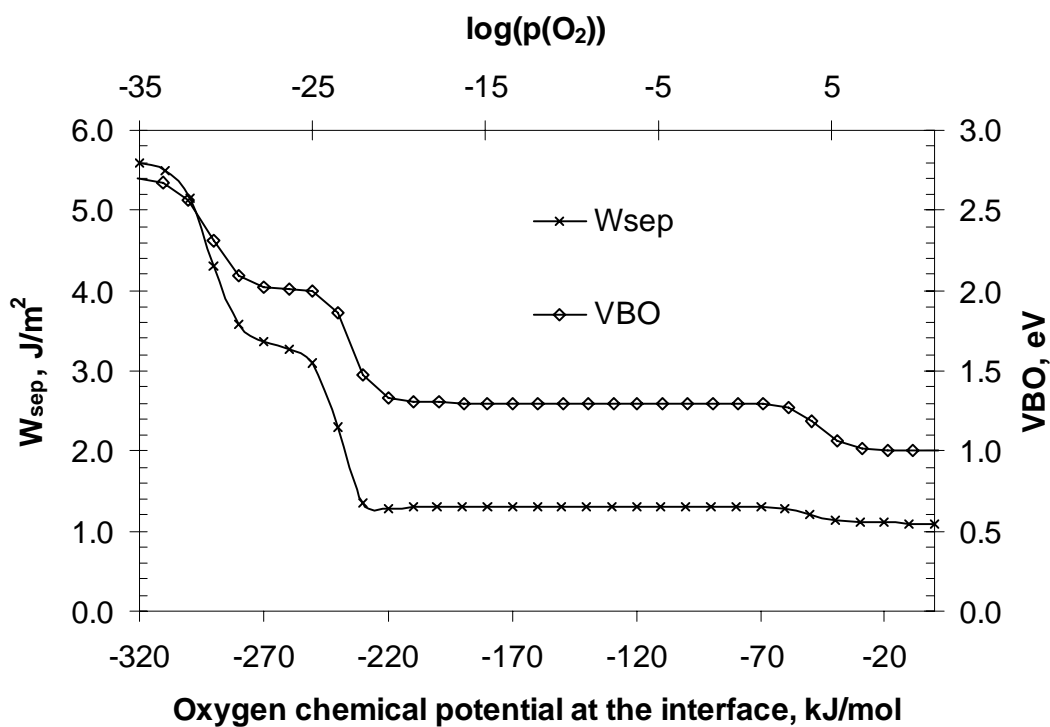


Fig. 2. Work of separation and valence band offset (VBO) for the Pt/HfO$_2$ interface as a function of the oxygen chemical potential at 500$^o$C.

# ENERGY DISSIPATION AT THE NANO-SCALE DUE TO CONTACT FORCES: A THEORETICAL AND EXPERIMENTAL STUDY BY MEANS OF DYNAMIC AFM

*<u>M. Koeber</u>[1], E. Sahagún[2], M. Fuss[1], M. Luna[1], F. Briones[1], and J. J. Sáenz[2]*

[1]*Instituto de Microelectrónica de Madrid (IMM-CSIC), C/ Isaac Newton 8, E-28760 Tres Cantos, Madrid, Spain*
[2]*Departamento de Física de la Materia Condensada, Universidad Autónoma de Madrid, E-28049 Madrid, Spain*

Understanding energy dissipation processes at the nanoscale is a key issue in many applied and fundamental aspects of micro- and nano-technologies. In this field, the atomic force microscope (AFM) has emerged as the most versatile tool for studying energy losses at nanometer and even atomic [1] scales. The acquisition of energy dissipation images [2] in dynamic modes is interesting for several reasons. In first place, this energy can be potentially translated into substrate physical properties. The problem is that this translation is not yet fully understood. Several theoretical studies have tried to relate the energy loss with its physical source [3, 4]. In second place, energy loss images present higher contrast than other well known imaging methods (amplitude or phase imaging).

There exist several sources of cantilever energy dissipation: loss of kinetic energy due to taps with the surface, formation of stable bonds between tip and sample, movement of charges on tip or substrate, capillary process, etc. Recent theoretical work [3] suggested that the dynamics of dissipation in Amplitude Modulation AFM is the result of a nontrivial interplay between the energy dissipated in each tip-sample interaction process and the bistable motion of the cantilever. Bistability gives rise to two mechanical regimes: low amplitude (or attractive) regime and high amplitude (or repulsive) regime. The results indicate that while in the attractive regime dissipation is sensitive to elastic properties of the system (in particular to the free amplitude), in the repulsive regime it is independent of these and the energy dissipated per oscillation depends only on the energy that is lost in each contact oscillation.

The objective of this work is to experimentally evaluate the validity of this theoretical model where the only source of dissipation is through contact and it is the same for all the amplitudes. If no tap occurs, the system remains conservative. In the experiments zero relative humidity was chosen in order to avoid dissipation due to capillary condensation. The cantilever constant is 3 N/m, the resonance frequency 85.3 kHz. The substrate is recently cleaved mica. The results of experimental and theoretical dissipated power vs. normalized amplitude curves are depicted in figures 1 and 2. In both cases, dissipated power is obtained as the distance between the sample and the fixed end of the cantilever is reduced, for different free oscillation amplitudes. Assuming that the cantilever looses 56 eV per tap, there is a striking agreement between theory and experiments.

Although the low controlled humidity rules out capillary condensation of liquid necks, it is not possible to ensure that there is a single dissipation source. However, it is remarkable that a single simple dissipation source, the contact between tip and surface, is needed to simulate the whole experiment. Work is in progress to explain the noise at the maximum of the dissipated power.

**References:**

[1] Y. Sugimoto, P. Pou, M. Abe, P. Jelinek, R. Pérez, S. Morita, and O. Custance, Nature **446**, 64 (2007).
[2] J. P. Cleveland, B. Anczykowski, A. E. Schmid and V. B. Elings, Appl. Phys. Lett **72**, 2613 (1998).
[3] E. Sahagún, P. García-Mochales, G. M. Sacha, and J. J. Sáenz, Phys. Rev. Lett. **98**, 176106 (2007).
[4] R. Garcia, C.J. Gómez, N.F. Martinez, S.Patil, C. Dietz, and R. Magerle, Phys. Rev. Lett. **97**, 016103 (2006).

**Figures:**
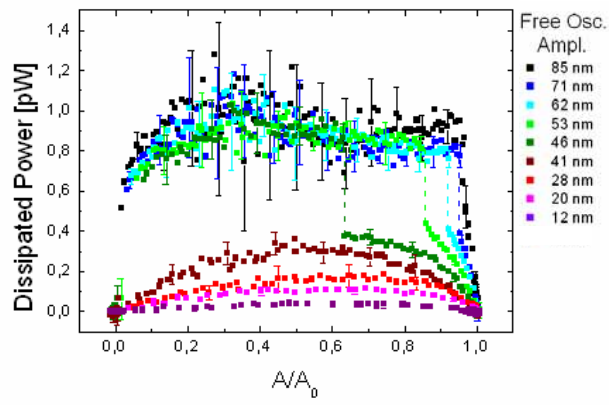


*Figure 1: Experimental results of dissipated power vs. normalized amplitude for various free oscillation amplitudes.*
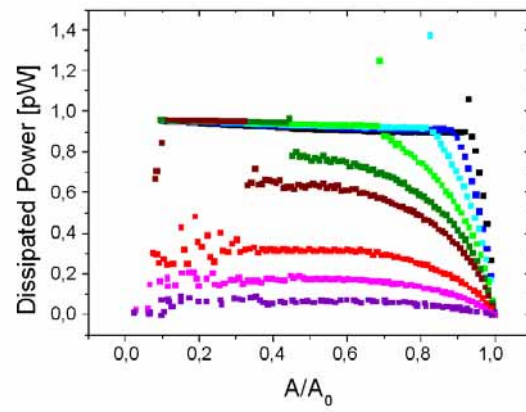
*Figure 2: Theoretical simulation of dissipated power vs. normalized amplitude curves, for the same free oscillation amplitudes as in figure 1.*

# LASER "MICROEXPLOSIONS" OF THE GOLD NANOPARTICLES TO INHIBIT TUMOR GROWTH

*Kogan Boris[1], Pankratov Alexander[2], Khlebtsov Boris[3], Khlebtsov Nikolai[3], Butenin Alexander[1], Zolotavkina Julia[2], Yakubovskaya Raisa[2], Vorozhtsov Georgy[1]*

*[1] FGUP GNC NIOPIK, ¼ B. Sadovaya street 123995, Moscow, Russia.*
*[2] P.A. Hertsen Moscow Research Oncology Institute, 3, 2th Botkinsky proesd 125284,*
*[3] IBPPM RAS, 13 Prospekt Entuziastov, Saratov 410049, Russia. Tel.: +7 8452 97-04-44*
*E-mail: bkogan@mail.mipt.ru*

## Introduction

Light-absorbing nanoparticles incorporated in a tissue can be heated by short-pulsed laser irradiation up to several thousand Kelvin degrees. Average tissue temperature may be kept normal if the concentration of these particles is low. Antitumor effect of such "microexplosions" of different carbon nanoparticles against animal tumors has been studied by us earlier [1]. Here we report results of study with use of gold nanoparticles.

## Materials and methods

Gold nanoshells (No1 and No2) and gold nanorods were used as nanoparticles. Nanoshells No1 have a 100 nm silica core diameter with 25 nm thick gold shells and a 17000 $nm^2$ cross-section of light absorption at a 694 nm wavelength. For nanoshells No2 these parameters are 150, 20 nm and 10500 $nm^2$ correspondingly. Nanorods have length of 50 nm, width of 15 nm and cross-section of 2100 $nm^2$.

S-37 sarcoma (hybrid $BDF_1$ male mice) was used as experimental tumor model. Aqueous suspensions of nanoparticles were injected in tail vein in a dose of 2.8, 3.6 and 1.25 (mg of gold on kg of weight, for nanoshells No1, No2 and nanorods correspondingly) on the 6th day after tumor transplantation when size of tumors was about 4-5 mm. Right after that tumors were irradiated by the Q-switched ruby laser (wavelength of 694 nm, pulse energy density of 0.6-0.8 $J/cm^2$, 100 pulses). Hair on the site of irradiation was removed several days before.

Tumor growth inhibition coefficient (TGI) is defined as TGI = $[(V_0 - V)/ V_0]$ 100%, where $V_0$ and V are tumor volumes of control and tested animals groups correspondingly.

Tumor growth kinetics in the treated animal groups was compared with control group. Animal death within 2 weeks after treatment was the test of toxicity of this method.

## Results and discussion

Tumor growth inhibition (TGI, %) in the treated animal groups is presented in Table.

| Nanoparticles | Dose, mg/kg | TGI on the days after treatment, % | | | | | |
|---|---|---|---|---|---|---|---|
| | | 7 | 10 | 12 | 14 | 17 | 19 |
| Nanoshells No1 | 2,8 | 67 | 70 | 57 | 59 | 48 | 50 |
| Nanoshells No2 | 3,6 | 49 | 32 | 13 | 16 | -13 | -26 |
| Nanorods | 1,25 | 46 | - | 17 | 10 | -15 | -21 |

Significant antitumor effect (TGI > 50%) was observed only in case of nanoshells No1 that can be heated up to higher temperature because of higher light absorption cross-section. Animal death was not observed.

Preparation of suspensions with higher nanoparticles concentration is needed for study effects of higher dosage.

## References

[1]. B.Ya. Kogan, R.I. Yakubovskaya, A.A. Pankratov, T.N. Andreeva, L.D. Kvacheva, A.A. Titov, V.A. Puchnova, R.A. Feysulova, G.N. Vorozhtsov, Technical Proc., NSTI Nanotech 2006, Boston, Vol. 2, Chapter 1 (2006) pp. 71-74.
[2]. Kogan B.Ya., Ostrovskaya L.A., Bluchterova N.V., Fomina M.M., Rykova V.A., Titov A.A., Vorozhtsov G.N., Book of Abstracts, ECHO 2005, Graz, Austria (2005) pp. 104-105.

# NONLINEAR PARAMETER ON ANALYZING POLYCATIONS POLYMER INTERACTING WITH RBCS.

*Ana M. Korol, P.G.Foresto, C.Grandfilds*
Depto. Matemática, Facultad de Ciencias Bioquímicas, UNR, Rosario, Argentina.
Centre Interfacultaire des Biomateriaux (CEIB) University of Liege, Belgium.
*korol@ifir.edu.ar*

Polycationic-polymer, already evaluated during the last decades have brought some interesting findings regarding the permeability enhancement through different epithelia. But their mode of interacting with the red blood cell membrane is not fully understood. However, till now, there are not clear relationships existing between the macromolecular properties of the polycations, and their bioreactivity. This lack of knowledge can be related to the fact that most of the polycations studied belong to the same families of polymers, which interactionwith blood proteins is often neglected. Taking that the majority of them are are negatively charged, it can be anticipated that when released in the bloodstream polycations should rapidly form plyelectrolitic complexes. Obviously the biological behaviour of these later ones will be quite different from the free polycations. One of the main objective of finding a nonlinear quantifier will be to better understand the molecular interactions between well-controlled synthetic polycations and the red blood cell membrane.

A numerical method formulated on the basis of fractal approximation for ordinary (OBM) and fractionary brownian motion (FBM), is proposed to evaluate sensitive dependence on initial conditions, based on the assumption that diffractometric data from samples of polycation polymers interacting with RBCs, involves both deterministic and stochastic components, so it could be modelled as a system of bounded correlated random walk. The Correlation Coefficient, a nonlinear parameter, proposed by R. May and G. Sugihara, is Calculated for samples belonging from healthy donors and polycation polymers interacting with RBCs.

The basic idea of our application of time series analysis is to extract a nonlinear parameter from the series that could reflect the different dynamical properties of the erythrocytes from healthy donors from those erythrocytes interacting with polymer polycations.
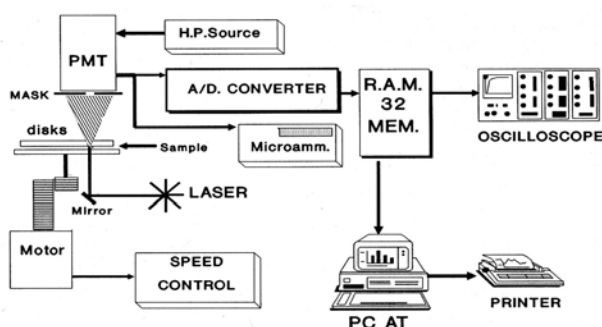


The experimental determination were carried out in a home made device called erythrodeformeter, which has been developed and constructed in our laboratory for rheological measurements on red blood cells subjected to definite fluid shear stress. A laser beam (He-Ne laser), transverses the layer of shear deformed erythrocytes producing an elliptical pattern, the diffracted intensity falls onto a photomultiplier tube (PMT), after passing through a thin straight slot in a mask placed exactly on the corresponding axis of the elliptical pattern. This photometric readings are stored in files and used to calculate the sensitive dependence on initial conditions, that is the Correlation Coefficient.

We hypothesize that the photometric readings could be modelled as a system of bounded correlated random walk. This approach is based on the assumption that diffractometric data involves both deterministic and stochastic components. A very convenient way, to reconstruct the dynamics of the process is to unfold the time series by successively higher shifts defined as integer multiples of a fixed lag $\tau$ ( $\tau = m.\Delta t$), and taking N (N = 256), equidistant points for creep and recovery process.

In order to calculate the correlation coefficient (sensitive dependence with initial conditions), we generated two three dimensional phase space, the first one with diffractometric data corresponding to the process while the erythrocytes become deformed, which will be the creep space, and the second one with diffractometric data while the erythrocytes become relaxed. The first ten steps were studied and very different behaviours appears for healthy donors and polycation polymers interacting with RBCs.

Here we report studies on 20 donors: 10 healthy donors and 10 samples of polycation polymers interacting with RBCs .

In order to compress information contained in the diffractometric data, in such a way that emphasizes the most significant characteristics, we must use not merely the observers judgement but objective methods of analysis. The most simplest one is the Fourier transform, but it does not distinguish between chaos involving a small number of degrees of freedom and white noise, so this limits its application and leads us to turn to other method, notably that of a studying phase space trajectories, which offers significant advantages. We shall argue that the red blood cells viscoelastic properties behave as a complex dynamical system, in which, under certain conditions, spatio-temporal patterns emerge spontaneously and techniques derived from non linear dynamics and chaos theory can be adapted to quantify their dynamical behaviour,

The *Correlation Coefficient* results suggests that in polycation polymers interacting with RBCs, it decreases while we increase the steps, in other words, the stress process gives us some special information of the relaxation one and the series exhibit a great sensitivity to initial conditions. On the other hand, on healthy donors, as well as on patients that received medical treatment, it seems to be independent of the steps and intrinsically unpredictable.

The evidence of the influence of the changes in the erythrocytes viscoelastic properties that could be detected by light diffraction patterns and by the nonlinear parameter, shows a good deal of promise and the possibility of a better understanding of the rheological erythrocytes aspects and also in clinical diagnosis.

**References**

1. Korol,A and Rasia,R . "Signatures of deterministic chaos in dyslipidemic erythrocytes under shear stress"
 *CHAOS, Interdisciplinary Journal of Nonlinear Science. American Institute of Physics*. Vol. **13**, N1, pp 87-93. March 03

2. Korol,A, Valverde,J and Rasia,R "Viscoelaticity: Fractal Parameters Studied on Mammalian Erythrocytes Under Shear Stress." *Experimental Mechanics*, IOS PRESS-USA, Vol. **42**, No.2, pp 101-108.June 2002

3. Korol,A,  Rasia,R and Rosso,O. "Alterations of thalassemic erythrocytes detected by wavelet entropy". *Physica A*,  pp. 80-87(2006).

# SELF-ASSEMBLED NANOCOMPOSITES BASED ON BLOCK COPOLYMERS CONTAINING MAGNETIC NANOPARTICLES

*G. Kortaberria, I. Garcia, A. Tercjak, J. Gutierrez, C. Ocando, I. Mondragon*
*"Materials + Technologies" Group, Escuela Universitaria Politécnica, UPV/EHU,Plaza*
*Europa 1, 20018, Donostia, Spain*
*galder.cortaberria@ehu.es*

During the last years nanocomposites containing nanoparticles have received increasing interest as potential candidates to replace traditional materials. One of the most important problems is the difficulty of controlling the dispersion of inorganic materials inside an organic medium as a homopolymer or block copolymer. To overcome this problem, it is often necessary to functionalise the nanoparticles, hence ensuring an effective control of dispersion. In this work, following previous attempts to functionalise magnetic nanoparticles with acrylic polymers[1,2], we have functionalised iron oxide nanoparticles ($Fe_3O_4$) with polystyrene (PS) brushes via atom transfer radical polymerisation (ATRP) 'grafting from' technique.

Block copolymers offer distinct intriguing possibilities to prepare novel nanostructured materials mainly due to their unique property to self-assemble. This ability is explored in this study with the but to obtain new nanostructured nanocomposites.

Magnetic nanoparticles (MN) modified with PS have been mixed with polystyrene-b-polybutadiene-b-polystyrene (SBS) block copolymer, to develop nanocomposites in which the nanoparticles are selectively segregated in one of the matrix self-assembled phases.

The nanoparticles used, magnetic iron oxide nanoparticles ($Fe_3O_4$), MN, were kindly supplied by Integran Technologies Inc. Polystyrene-b-polybutadiene-b-polystyrene block copolymer was purchased from Dynasol.

Techniques such as Fourier transform infrared (FTIR) spectroscopy, differential scanning calorimetry (DSC) and atomic force microscopy (AFM) were used to characterize the functionalised particles. SBS copolymer and its composites have been characterised by DSC, rheological and AFM measurements.

Magnetic nanoparticles (MN) were modified first with an initiator (2-(4-chlorosulfonylphenyl) ethyl trichlorosilane) (CTCS)[1,2] that allows the initiation of the polymerisation. The second step was the polymerisation of polystyrene by ATRP. The reaction of hydroxyl groups of MN and CTCS was confirmed by FTIR (Fig. 1). Two new peaks were observed in the magnetic nanoparticles spectrum modified with the initiator (MN-CTCS) with respect to neat CTCS spectrum (not shown here); one of them was attributed to the appearance of the formed Si-O-Si bond ($v$ Si-O-Si 1039 cm$^{-1}$) that indicates that trichlorosilane groups have self-condensed to form a polysiloxane film on the iron oxide surface. The other peak ($v$ Si-O 1129 cm$^{-1}$) was attributed to formed MN-O-Si bonds that were created between MN and CTCS. Other peaks were observed in both spectra, one of them was assigned to the symmetric stretching of S=O ($v$ S=O 1377 cm$^{-1}$) of CTCS, another peak was attributed to asymmetric stretching of S=O ($v$ S-O 1178 cm$^{-1}$) of CTCS. These results confirm that there was CTCS anchored on surface of MN.

The modification of MN-CTCS with PS[3,4] was confirmed by FTIR (Fig. 1), where three new peaks attributed to PS appeared at 1600 cm$^{-1}$, 1500 cm$^{-1}$, 1450 cm$^{-1}$. A relative shift of the S=O peak due to the influence of neighbour groups was also observed. The position for this group Ar-$SO_2$-Cl ($v$ S=O 1377 cm$^{-1}$) was different to the position of Ar-$SO_2$-R ($v$ S=O 1318 cm$^{-1}$). There was a new peak at 730 cm$^{-1}$, which can be attributed to stretching of the S-C bond ($v$ S-C 730 cm$^{-1}$). A high increase of the characteristic stretching bands of aryl and alkyl groups at 3200-2800 cm$^{-1}$ was observed in MN-PS.

MN modified with PS were mixed with SBS block copolymer. Preliminary results seem to indicate that the modified MN could be segregated[5,6] in one of the phases (PS), thus opening up the possibility of creating novel nanocomposites.

A corona of brushes of PS were grown onto surface of commercial magnetite MN powders using "graft from" technique by ATRP. Those MN were characterized using FTIR, confirming that brushes of PS were anchored onto surface of MN.

Novel nanocomposites can be created by mixing PS-modified MN with SBS block copolymer by selective functionalization of the magnetic particles.

**Acknowledgement**

**References:**

[1] Marutani, E.; Yamamoto, S.; Ninjbadgar, T.; Tsujii, Y.; Fukuda, T. and Takano. M. Polymer **2004**, 45, 2231.

[2] Garcia, I.; Zafeiropoulos N.E.; Janke, A.; Tercjak, A.; Eceiza, A.; Stamm, M. and Mondragon, I. Journal of Polymer Science. Part A: Polymer Chemistry **2007**, 45, 925-932.

[3] Ejaz, M.; Yamamoto, S.; Ohno, K.; Tsujii, Y. and Fukuda T. Macromolecules **1998**, 31, 5934-5936.

[4] Böttcher, H.; Hallenslebem, M.L.; NuB, S. and Wurm H. Polymer Bulletin **2000**, 44, 223-229.

[5] Lin, Y.; Böker, A.; He, J.; Sill, K.; Xiang, H.; Abetz, C.; Li, X.; Wang, J.; Emrick, T.; Long, S.; Wang, Q.; Balazs, A. and Russell, T.P. Nature **2005**, 434, 55-59.

[6] Breiner, U.; Krappe, U.; Jakob, T.; Abetz, V. and Standler. R. Macromolecular Chemistry and Physics **1997**, 198, 1051-1083.
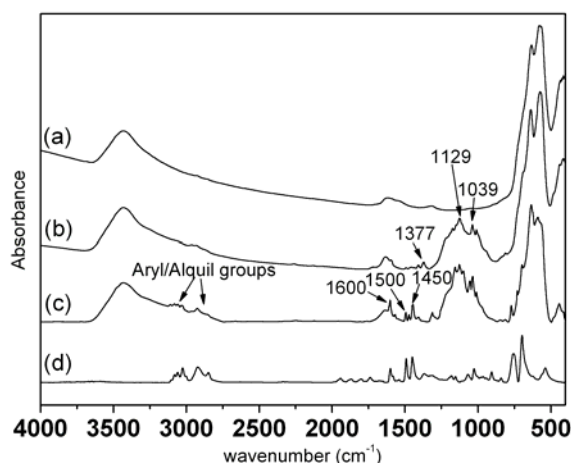


Fig.1. FTIR spectra for: (a) MN, (b) MN-CTCS and (c) MN-PS brushes, (d) PS homopolymer.

# STM AND STS EXPLORATIONS OF SELF-ASSEMBLED DODECAKIS(PHENYLTHIO)CORONENE FILMS ON HOPG

*P. Kowalzik[1], S. Karthäuser[1], J.-M. Raimundo[3], M. Gingras[3], R. Waser[1,2]*

[1]*Institute of Solid State Research and CNI-Center for Nanoelectronic Systems for Information Technology, Research Center Juelich GmbH, 52425 Juelich, Germany*
[2]*Institute of Materials for Electronic Engineering 2, RWTH Aachen, Sommerfeldstraße 24, 52074 Aachen, Germany*
[3]*Université de La Méditerranée Aix-Marseille II, Groupe de Chimie Organique et Matériaux Moléculaires (GCOM2) Département de Chimie, Case 901 13288 Marseille Cedex 09*

*p.kowalzik@fz-juelich.de*

Promising physical and chemical properties of novel organic compounds [1] and their use as active components in electronic devices is the motivation for an intense research activity in the field of highly ordered organic thin films [2]. In particular, large polycyclic aromatic molecules like hexa-peri-hexabenzocoronenes which have been shown to self-assemble to supramolecular structures seem to have advantageous electronic features such as the characteristics of a single-molecular rectifier in the junction of a STM [3] and the potential use as nanowires with high charge carrier mobilities [4].

Here we report on a scanning tunneling microscopy and spectroscopy study of the self-assembly and the electronic properties of dodecakis(phenylthio)coronenes. It has been shown that such derivatised coronenes may for instance present a potential class of electron accepting units in molecular devices [5,6].

Dry layers of the investigated molecules were grown on freshly cleaved highly oriented pyrolytic graphite (HOPG) from solution and then characterized by means of STM under UHV-conditions. The deposition method results in highly ordered two dimensional crystal structures where several phases of the assembled molecules could be found. Monolayers of dodecakis(phenylthio)coronenes exhibit a hexagonally close-packed structure of flat-lying molecules (see fig. 1) with defect-free domain sizes larger than $100 \times 100$ nm$^2$. Tunneling spectra were taken on these molecular layers to study the electronic states and transport properties of the adsorbed molecules.

In addition to layers of separated single molecules we observed hexagonal arrangements of clustered molecules. Several dodecakis(phenylthio)coronene aggregates assemble again in ordered films on the substrate. We will show that structures of these molecule clusters with different size and lattice constants can be self-assembled.

**References:**

[1] G. Maruccio, R. Cingolani, R. Rinaldi, J. Mater. Chem., **14** (2004) 542.
[2] S. De Feyter, F. C. De Schryver, Chem. Soc. Rev., **32** (2003) 139.
[3] A. Stabel, P. Herwig, K. Müllen, J. P. Rabe, Angew. Chem. Int. Ed., **34** (1995) 1609.
[4] A. van de Craats, J. M. Warman, K. Müllen, Y. Geerts, J. D. Brand, Adv. Mater., **10** (1998) 36.
[5] J. H. R. Tucker, M. Gingras, H. Brand, J.-M. Lehn, J. Chem. Soc. Perkin Trans., **2** (1997) 1303.
[6] M. Gingras, J.-M. Raimundo, Y. M. Chabre, Angew. Chem. Int. Ed., **45** (2006) 1686.

**Figures:**

a)



b)
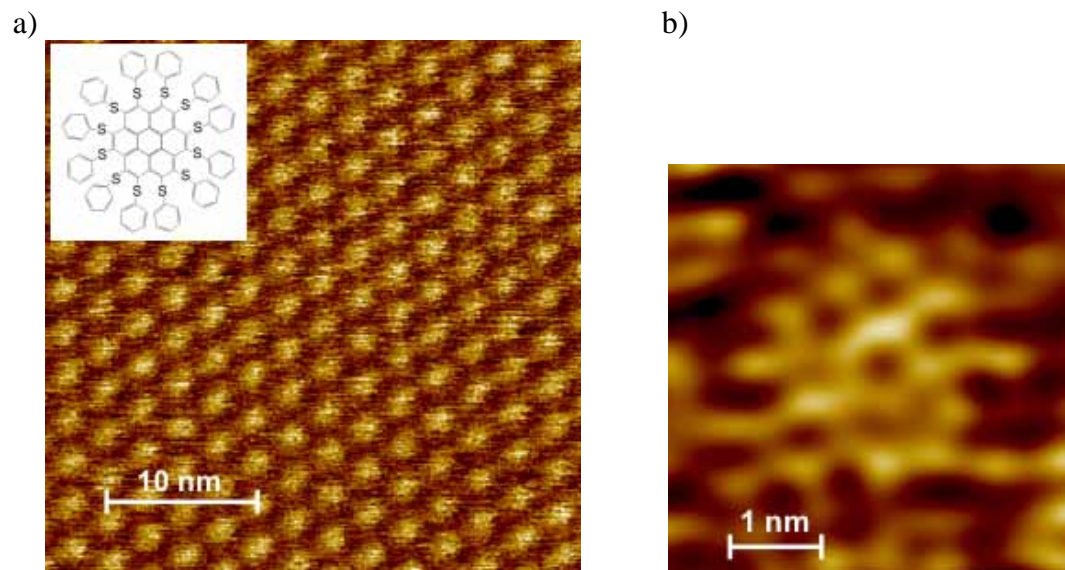


**Fig. 1** STM images showing a) the hexagonal structure of a self-assembled layer of dodecakis(phenylthio)coronene (inset: chemical sturcture of the molecule) and b) the molecule in submolecular resolution.

# PROFILING PROTEIN SURFACE INTERACTIONS OF MULTICOMPONENT SUSPENSIONS VIA FLOW CYTOMETRY

*Darby Kozak and Matt Trau*
*Centre for Nanotechnology and Biomaterials*
*Australian Institute for Bioengineering and Nanotechnology*
*The University of Queensland, Brisbane, Australia 4072*
*Telephone: +61 7 334 64173*
*Fax: +61 7 334 63973*
*d.kozak@uq.edu.au*

Protein adsorption is a complex process which has impact upon industrial and medical applications. These range form reducing fuel effecency of marine transport to the potential rejection of a medical implant or even the misdiagnosis of a patient by molecular diagnostics. Therefore, considerable focus has been given to the characterisation of protein surface interactions and preventative surface coatings. However, the vast number of different proteins, biological media and surfaces present in even the most basic industrial or medical application makes this a formidable task. Toward this goal, a high-throughput particle based screening method using flow cytometry was examined.

Flow cytometry offers the advantage of analysing multiple parameters on an individual particle basis. This enables flow cytometry to distinguish between individual adsorbent particles and adsorbate components within a suspension. The adsorption of three proteins: bovine serum albumin (BSA), bovine immunoglobulin gamma (IgG) and fibrinogen, onto five surface modified organosilica microsphere populations was used as a model multicomponent system for analysis. By uniquely labeling each protein and microsphere polulation with spectrally distinguishable fluorescent dyes, the adsorption process could be 'multiplexed' allowing the simultaneous screening of multiple adsorbent (particle surface) and adsorbate (protein) interactions Figure **1**. This in turn enables the characterisation of both competitve and cooperative protein adsorption along with determining the relative adsorption affinity between different modified surfaces.
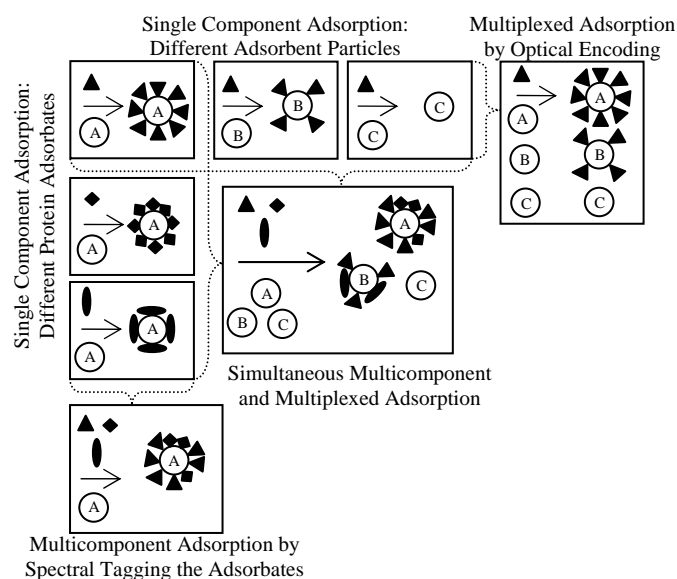


Figure **1**. Single component adsorbent (A), (B) and (C) particles and adsorbate (▲), (♦) and (ı) adsorption. Use of fluorescent tagging of the adsorbents and adsorbates and flow cytometry to characterise multicomponent and multiplexed adsorption simultaneously.

Protein adsorption experiments quantified by flow cytometry were comparable to single component adsorption studies using solution depletion. Quantitative distribution of the simultaneous competitive adsorption of BSA and IgG indicated both proteins adsorbed onto the surface at concentrations below surface saturation. However, at concentrations greater than surface saturation, BSA preferentially adsorbed. Multiplexed particle suspensions of optically encoded particles were modified to produce a positively and negatively charged surface, a grafted 3,400 Mw polyethylene glycol layer, or a physisorbed BSA or IgG layer. It was observed that adsorption was rapid and irreversible on all of the surfaces and pre-adsorbed protein layers were the most effective in preventing further protein adsorption. We believe that this high-throughput multicomponent and multiplexed analysis technique will offer convenient and rapid screening and characterisation of complex protein surface interactions. This holds promise for the rapid development and improvement of preventive surface coatings for future biological materials and biosensors.

# THE CRYSTALLOGRAPHY OF IRON CARBIDES FORMATION IN THE PROCESS OF CATALYTIC GROWTH OF CARBON NANOSTRUCTURES: HRTEM STUDIES.

B. A. Kulnitskiy, V. D. Blank, I.A.Perezhogin, Yu.L. Alshevskiy, N.V.Kazennov

*Technological Institute for Superhard and Novel Carbon Materials (TISNCM), 7a Centralnaya Street, 142190, Troitsk, Moscow region, Russia.*
*boris@ntcstm.troitsk.ru*

It is known that in the process of carbon nanostructures formation a catalyst particle is often transforms into one of iron carbides. The growth process is determined by the dissolution of carbon in the quasi-liquid catalyst particle, its diffusion through the particle and its segregation in the form of graphene layers in the case of supersaturation. Carbon nanofibers were grown in the present study by CVD process. TEM analysis has been carried out by JEM-2010 high resolution transmission electron microscope, equipped with EDS-detector.

Catalytic particles, found inside nanofibers, revealed the structure of $\alpha$-iron as well as structures of $Fe_3C$, $Fe_5C_2$ and $Fe_7C_3$ carbides. Crystallographic peculiarities: the orientation of the catalyst particle in the fiber, orientation relationships between lattices of $\alpha$-iron and carbides have been studied. Twins were identified in $Fe_5C_2$. It was found, that (100) is the twin plane in the monoclinic $Fe_5C_2$ lattice, which is corresponds to {112} twinning plane of $\alpha$-Fe[1]. The orientation of $Fe_5C_2$ catalyst coincides with [100]-direction, which is corresponds to [112] direction of $\alpha$-Fe bcc lattice. It is known that the catalyst with bcc lattice is oriented mainly along [100], not along [112] direction. This disagreement may be explained in the following way. It is assumed that $Fe_5C_2$ is formed from $\alpha$-Fe through $Fe_3C$-phase. It was shown, that the orientation of $Fe_3C$ – catalyst [$3\overline{9}\overline{1}$] with accuracy of 3° coincides with [100] $\alpha$-Fe. It can be shown, that [$39\overline{1}$] direction in $Fe_3C$–lattice with the same accuracy coincides with [$\overline{1}21$] of $\alpha$-Fe. The alteration of the crystallographic orientation occurs probably as the result of the twinning in $\epsilon$-Fe lattice. Further saturation of $Fe_3C$ lattice by carbon resulted in the formation of $Fe_5C_2$ lattice.

It was found that catalytic particles of $Fe_7C_3$ structures take the octahedron shape, whereas the $Fe_5C_2$ catalyst particles are characterized by flattened shape, coincident with the lens shape. Carbon nanofibers, containing $Fe_5C_2$ catalyst, have unordinary form. Fibers are consisted of graphene layers, which cover the lens surface. At the same time direct parallel lines crossing fiber from the catalyst surface up to fiber's boundary, can be distinctly seen. It was found by HRTEM analysis that these lines contain ruptures of graphene layers. The possible mechanism of such structure formation is explained by the deformation, arising in the nanofiber growth process.

[1]. V.D.Blank, Yu.L.Alshevskiy, A.I. Zaitsev, N.V.Kazennov, I.A.Perezhogin, B.A.Kulnitskiy, Structure and phase composition of a catalyst for carbon nanofiber formation, Scripta Materialia, 55, 2006, 1035-1038.

# SYNTHESIS OF VERTICALLY ALIGNED ARRAYS OF MIXED SINGLE-MULTI WALL CARBON NANOTUBES BY CVD METHOD WITH THE VOLATILE CATALIST.

Labunov V.A.[1], Filatov S.A.[2], Shulitski B.G.[1], Prudnikava A.L.[1], ShamanY.P.[1]

[1] Belarusian State University of Informatics and Radioelectronics, P.Brovki St. 6, Minsk 220027 Belarus

[2] Heat and Mass Transfer Institute of National Academy of Sciences, P.Brovka St. 15, ITMO, Minsk, 220072, Belarus

Email: labunov@its.bsuir.edu.by

More research - more unusual properties Carbon Nanotubes (CNTs) are demonstrating. Special curiosity are exiting a Single Wall Carbon Nanotubes (SWCNTs) because the specificity of their properties and huge variety of their applications. SWCNTs should be produced of high quality, in large quantity, with the accepted prize and the given geometry (diameter and length).

The main methods of the CNTs synthesis are: arc discharge, pulsed laser ablation and chemical vapor deposition (CVD) .

In most cases SWCNTs are obtained by the arc discharge and laser ablation. These methods do not satisfy the above requirements. By use of them the disordered bundles of SWCNTs of non standart length and diameters are obtained. Equipment and technology of their realization are very costly. The additional prize should be paid for the CNTs bundles cutting to the commonly used short specimens.

For the Multi Wall Carbon Nanotubes (MWCNT) synthesis CVD method is mostly used. This method ensures the synthesis of the arrays of vertically aligned MWCNTs and in general satisfies the above requirements.

The aim of the present investigation is to find the conditions of CVD method realization at which the arrays of vertically aligned SWCNTs would be synthesized at least in the combination with the MWCNTs.

The atmospheric pressure CVD method of CNTs synthesis was realized by the high temperature pyrolysis of fluid hydrocarbon (p-xylole [$C_8H_{10}$]) in the presence of volatile catalyst (ferrocene [$Fe(C_5H_5)_2$]) with the use of Ar as a gas-carrier. The aerosol of the solution: fluid hydrocarbon- volatile catalyst was delivering into the synthesis zone by the dosed injection. The advantage of the injection process is that it ensures the possibility to very in vide range the type of hydrocarbons, percentage content of the catalyst in the solution, do not require to preliminary form the nanostructured clusters-catalysts on the surface of the substrate. This process is characterized also by low energy consumption and non toxicity of the initial reagents.

The synthesis process was realized in the tubular type quartz reactor of the specially constructed equipment .$SiO_2$ substrate was used. Reactor was heated to the temperature of $850^oC$ in Ar atmosphere (Ar flow rate-1000$cm^3$/min). After the one minute of process duration reactor was cooled up to room temperature. A series of experiments were carried on with the variation of the ferrocene percentage in solution (1,0%-10%) injected into the Ar flow.

As SEM and TEM analysis showed in this regime of CNTs synthesis the arrays of tightly packed MWCNTs with the inclusion of the ordered bundles of SWCNTs were obtained. The structure of CNTs with1,0% (specimen 1) and10% (specimen 2) of ferrocene in solution was identical. The outer diameter of MWCNTs was in the range of 20-30 nm and

the diameter of SWCNTs – in the range of 1-3 nm. The height of the arrays (the length of CNTs) is some dozens of micrometers.

Raman spectra of the specimens 1,2 contain three picks. Pick in the range of 1580 $sm^{-1}$ (G-line) corresponding to the twice degenerated deformation oscillations of the hexamerous ring in $E_{2g}$ electronic configuration of $D^4_{6h}$ crystal symmetry. This testifies to the presence of carbon in the form of ordered hexagonal lattice. It might be grafen, SW or MW CNTs. Second pick in the range of 1360 $sm^{-1}$ (D-line) corresponds to vibration state of the ruinous hexagonal lattice near the crystals boundary and witnesses the presence of the not fully ordered transition forms of carbon (milled graphite, soot, another carbonized substances).

The ratio of the intensities $I_G/I_D$ characterizes qualitatively the structure of synthesized CNT arrays: higher this ratio - higher quality of CNTs. In the case of specimen 1 the ratio $I_G/I_D = 1,08$ (Fig. 1a), but in the case of specimen 2 the ratio $I_G/I_D = 0,70$. It means that in the case of 1,0% of ferrocene in solution CNT arrays contain less of ruinous forms of carbon than in the case of 10% i.e. the smaller concentration of catalyst in the array - the higher quality of CNTs.

The presence of pick in the low frequency spectrum range - Radial Breathing Mode (RBM) testifies to the presence of SWCNT in the arrays. More over it contains the characteristic information on SWCNTs structure according to the expression $\sqrt{}(cm^{-1}) = 6.5 + 223.75/d$, $9+235/d$ where $\sqrt{}$ is the frequency of the radial modes of the oscillations of the SWCNTs hexagonal lattice and $d$ is the SWCNT diameter in nanometers. Using this expression $d$ was calculated. In both cases of specimens 1and 2 the presence of SWCNT is observed. In the case of of specimen 1 $\sqrt{}=183,1\ cm^{-1}$ and calculated value of *d is equal to* 1,2 nm. In the case of specimen 2 $\sqrt{}=132,9\ cm^{-1}$ and calculated value of *d is equal to* 1,8 nm. So Raman spectroscopy showed qualitatively the presence of carbon in different forms in the CNT arrays and quantitatively gave the possibility to reveal SWCNTs and to calculate their diameter.

The results of thermogravimetric analysis (TGA) are presented by typical TG and differential TG of CNT arrays of specimen 1 and specimen 2.

TG indicates that in a case of specimen 1 it starts burning near 545 ℃ and ends burning near 615 ℃.

In a case of specimen 2 it starts burning near 594 ℃ and ends burning near 650 ℃.

The burning temperature of CNTs is related to the number of walls, quality of nanotubes, presence of catalyst and even bundle size in the case of SWCNTs. High burning temperature indicates high crystal quality. The increase in burning temperature was attributed to the formation of bundles and removal of catalyst.

It was estimated that unburned mass in boss cases less than 2% and may include ferrous particles This value is quite low, so CNT arrays synthesized by our method are pure enough to be used in different applications without purification process.

Differential TG curve revealed two picks (545 ℃ and 615 ℃) in the case of specimen 1 and (594 ℃ and 644 ℃) in the case of specimen 2. Different picks correspond to the different burning temperatures of CNTs. First pick is attributed to CNTs with the small number of walls up to single-wall. Second pick is conditioned by the majority of multi-wall nanotubes in our CNT arrays.

So thermographic measurements of the obtained CNT arrays showed that they consist of two major components - SW and MW CNTs.

By both methods – Raman spectroscopy and thermogravimetric analysis it was shown that in the case of SW/MW CNT arrays more that 70% are SWCNTs

# PHOSFOROUS AND ANTIMONIUM DOPED-ZnO THIN FILMS

*A.G. Rolo[1], T. Viseu[1], J. Ayres de Campos[1], T. de Lacerda-Arôso[1], M.F. Cerqueira[1] and E. Alves[2]*

*[1]Departamento de Física, Universidade do Minho, Campus de Gualtar 4710-057 Braga, Portugal*
*[2]Instituto Técnico Nuclear ITN, EN 10, 2686-953 Sacavém, Portugal*
*fcerqueira@fisica.uminho.pt*

Zinc oxide (ZnO) is a II–VI wide direct-gap semiconductor with a band gap of 3.37 eV at room temperature and a free exciton energy of $\approx$ 60 meV. Both characteristics make it interesting for optoelectronic applications in the near ultraviolet (UV) region. ZnO has intensively been studied for the past fifty years. A renewed interest in ZnO derived materials arouse in the mid nineties of the last century, due to its potential technological applications [1, 2]. Since then, ZnO thin films [3], quantum wells, nano-rods and quantum dots have been produced and studied hoping to apply them to optoelectronics and electronic devices as alternative to ITO. However the difficulty in obtaining a reproducible and stable p-doping ZnO is still an unsolved problem [4].

We present a study on optical and electrical properties of P and Sb doped-ZnO thin films. The films have been produced by r.f. magnetron sputtering method, using a metallic ZnO target in an oxygen atmosphere. Doping has been performed by ion implantation in two kinds of samples having different microstructure, namely, average crystal size and crystalline volume fraction. Implantation doses have been: $1\times10^{15}$; $5\times10^{15}$ and $10\times10^{15}$ ats/cm$^2$. We report on the effect of the as-grown structure, doping doses and thermal treatment on the electrical and optical properties of these films.

Raman spectroscopy and X-ray diffraction have been used to characterize the films microstructure. X-ray photoelectron spectroscopy (XPS) analysis has been performed as well. Optical parameters in the visible and near infrared range have been obtained from transmission spectra by the Minkov method. Electrical dark conductivity, $\sigma_d$, has been measured from 25 ºC to 95 ºC and activation energy has been obtained.

After implantation the films were annealed at different temperatures. X-ray diffraction and Raman scattering confirm that, after implantation and annealing treatment, they keep a polycrystalline nature with (002) preferred orientation (Figure 1). In non-doped samples as well as doped ones, annealing treatment releases the compressive stress within the films. Furthermore, on the 500 ºC annealed samples a slightly tensile stress was found as shown in Figure 1.

These films remain very transparent and the electrical conductivity increases at least 6 orders, reaching values of 10.9 ($\Omega$cm)$^{-1}$ in the P-doped and 0.56 ($\Omega$cm)$^{-1}$ in the Sb-doped samples.

From XPS analyses we were able to infer that dopant ions are effectively incorporated at zinc sites in ZnO lattice and also that a higher temperature treatment promotes their more uniform depth distribution.

**References:**

[1] Zhang Xiaodan, Fan Hongbing, Zhao Ying, Sun Jian, Wei Changchun, Zhang Cunshan, Appl. Surface Science **253** (2007) 3825.

[2] V. A. Coleman, H. H. Tan, C. Jagadish, S. O. Kucheyev, J. Zou, Appl. Phys. Lett. **87** (2005) 231912.

[3] A.G. Rolo, J. Ayres de Campos, T. Viseu, T. de Lacerda-Arôso, M.F. Cerqueira, Superlattices and Microstructure in print (2007).

[4] J. Lee, J. Metson, P.J. Evans, R. Kinsey, D. Bhattacharyya, Appl. Surface Science **253** (2007) 4317.

**Figure:**
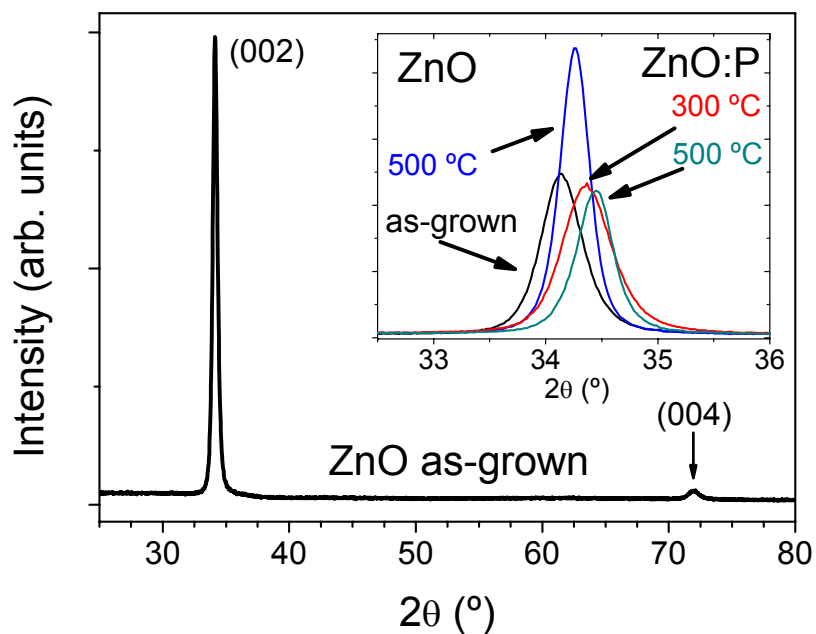


Fig.1. XRD difractogram of an as-grown ZnO thin film exhibiting (002) and (004) peaks. Inset shows the temperature annealing effect on the (002) peak position for ZnO and ZnO:P.

# SPM studies of SWCNTs decorated by Oligodeoxyribonucleotides

*<u>Roya R. Lahiji</u>[1,2], Bridget D. Dolash[2,3,4], Dmitry Zemlyanov[2], Donald E. Bergstrom[2,3,4] and Ronald Reifenberger[1,2]*
*[1]Department of Physics, Purdue University, West Lafayette, IN 47907*
*[2]Birck Nanotechnology Center, West Lafayette, IN 47907*
*[3]Department of Medicinal Chemistry and Molecular Pharmacology, Purdue University, West Lafayette, IN 47907*
*[4]The Walther Cancer Institute, Indianapolis, Indiana 46208*

*rlahiji@purdue.edu*

The dispersion of Single Walled Carbon Nanotubes (SWCNT) is an important step often required for different applications in engineering and biology.[1-4] For engineering applications, the dispersion of SWCNTs in solvents has been reported.[5-8] For biological applications, Zheng and *et al*[9, 10] have shown DNA facilitates the dispersion of SWCNTs in aqueous solution. Molecular modeling suggests the mechanism for association is a non-covalent "wrapping" of the Oligodeoxyribonucleotide (ODN) around the nanotubes[9]. Yet the chemistry and strength of this association has not been investigated.

A series of studies utilizing different characterization techniques have been conducted to characterize the ODN:SWCNT hybrids.[11] After dispersing the SWCNTs with T30 ODN, Transmission Electron Microscopy (TEM) has shown different morphologies of ODN:SWCNT hybrids. The morphologies vary depending on the sonication time. Atomic force microscopy (AFM) studies confirm the TEM data and provided more detailed images. At higher sonication times (>90min), isolated SWCNTs decorated with features that are attributed to ODN are observed (Figure 1). These features have an average height of 1-2nm above the SWCNT agreeing with the approximate height of single stranded ODN. X-ray Photoemission Spectroscopy (XPS) showed two distinct peaks for P and N, two key elements in T30 ODN, and confirm the decorative features are ODN (Figure 2). Chemically oxidizing SWCNTs increases the number of ODN features decorating the nanotubes (Figure 3), suggesting the association of ODN to defects.

Continued studies are underway to chemically characterize the association of ODN with SWCNTs and to determine if SWCNTs can be selectively linked by combining complimentary base pairs.

**References:**

[1]    P. Avouris, J. Appenzeller, R. Martel, S. J. Wind, T. J. Watson, *IBM Res. Div.* 2003, *91*, 1772.

[2]    A. Bianco, K. Kostarelos, C. D. Partidos, M. Prato, *Chem Commun* 2005, 571.

[3]    Y. H. Lin, W. Yantasee, J. Wang, *Frontiers in Bioscience* 2005, *10*, 492.

[4]    J. P. Lukaszewicz, *Sensor Letters* 2006, *4*, 53.

[5]    R. Bandyopadhyaya, E. Native-Roth, O. Regev, R. Yerushalim-Rozen, *Nano letters* 2002, *2*, 25.

[6]    M. J. O'Connell, S. M. Bachilo, C. B. Huffman, V. C. Moore, M. S. Strano, E. H. Haroz, K. L. Rialon, P. J. Boul, W. H. Noon, C. Kittrell, J. Ma, R. H. Hauge, R. B. Weisman, R. E. Smalley, *Science* 2002, *297*, 593.

[7]     C. Park, Z. Ounaies, K. A.Watson, R. E.Crooks, J. S. Jr., S. E.Lowther, J. W.Connell, E. J.Siochi, J. S.Harrison, T. L.St.Clair, *Chemical Physics Letters* 2002, *364*, 303.

[8]     H. Wang, W. Zhou, D. Ho, K. Winey, J. Fischer, C. Glinka, E. Hobbie, *Nano Letters* 2004, *4*, 1789.

[9]     M. Zheng, A. Jagota, E. D. Semke, B. A. Diner, R. S. Mclean, S. R. Lustig, R. E. Richardson, N. G. Tassi, *Nat Mater* 2003, *2*, 338.

[10]    M. Zheng, A. Jagota, M. S. Strano, A. P. Santos, P. Barone, S. G. Chou, B. A. Diner, M. S. Dresselhaus, R. S. McLean, G. B. Onoa, G. G. Samsonidze, E. D. Semke, M. Usrey, D. J. Walls, *Science* 2003, *302*, 1545.

[11]    R. R. Lahiji, B. D. Dolash, D.E. Bergstrom and R. Reifenberger (submitted).
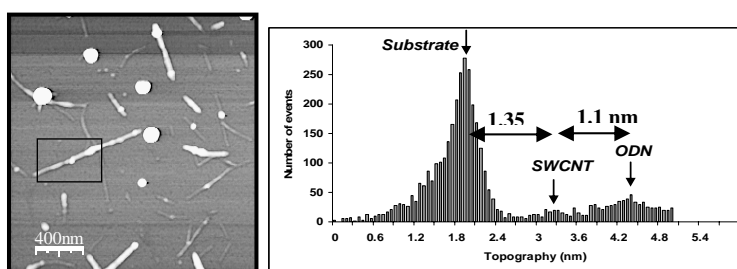


**Figure 1:** On left a non-contact SPM images of a mica substrate after depositing a T30:SWCNT solution that has been sonicated for 90 min. On right a topographic height histogram of the image inside the square shown in the image on left. The large peak at 1.95 nm is representative of the mica substrate and serves as a convenient baseline. A peak 1.35 nm above the substrate is a measure of the diameter (height) of the SWCNT. A second peak at 2.45 nm above the substrate measures the height of the T30 ODN feature.
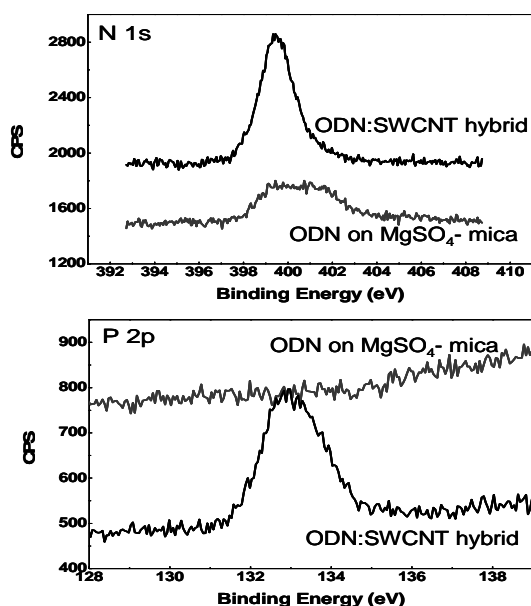




**Figure 2:** XPS data from ODN and ODN:SWCNT samples. On top the N1s XPS signal from ODN covered MgSO$_4$ treated mica is compared with the signal from SWCNT:ODN hybrid sample. The data indicate that the mica substrate contributes a small nitrogen signal. The nitrogen signal increases by factor of ~4 when ODN:SWCNTs are present. In bottom, the P2p XPS signal from ODN covered mica is compared with the signal from ODN:SWCNT hybrid sample. In this case, phosphorus is detected only when ODN:SWCNTs are present.
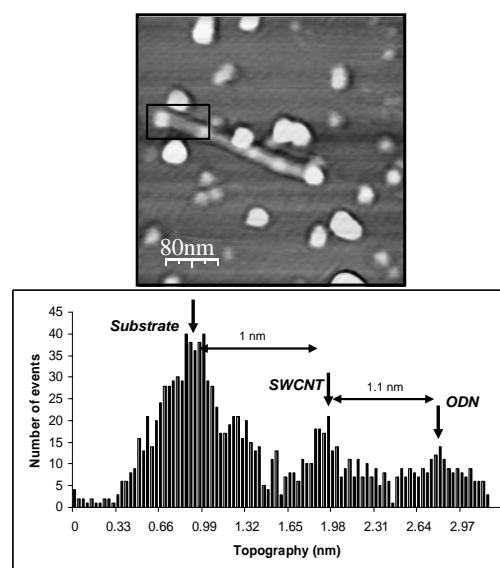
**Figure 3:** On top, a non-contact SPM image of MgSO$_4$ treated mica substrate after depositing SWCNTs that have been chemically oxidized before sonication with T30 ODN. In addition to the ~20 dot-like objects that are characteristic of all electric-arc samples, the image shows five localized features decorating the length of the SWCNT, which is ~250nm long. The separation between the features is ~50-70 nm. The bottom figure shows a topographic height histogram from a region of the image inside the box drawn in the top figure. The diameter of the SWCNT is ~1 nm. The feature attributed to ODN at the end of the SWCNT is ~1.1 nm above the SWCNT.

# EFFECT OF ZNS SHELL ON THE RAMAN SPECTRA FROM CDSE NANORODS

*Holger Lange*
*Institut für Festkörperphysik TU Berlin – Germany*
*holger.lange@physik.tu-berlin.de*

We investigated the influence of an epitaxially grown ZnS shell on the phonon spectra of CdSe nanorods of different sizes. The CdSe related Raman peaks shift with addition of a ZnS shell. This allows the determination of the lattice contraction introduced in the core: 0.4% for small nanorods, comparable to colloidal core/shell CdSe/ZnS quantum dots of equal size, while neglectable for larger nanorods. The low-energy shoulder shifts stronger with addition of a shell which can be explained within a model for surface optical phonons.

# ACOUSTIC PHONON ENGINEERING: CONTROLLING SOUND AND LIGHT AT THE NANOSCALE

_N. D. Lanzillotti-Kimura[1,2]_, A. Fainstein[1], B. Perrin[2], B. Jusserand[2], A. Huynh[2],
A. Miard[3] and A. Lemaître [3]

[1]*Instituto Balseiro and Centro Atómico Bariloche, C.N.E.A.,
8400 S.C. de Bariloche, Río Negro, Argentina*
[2]*Institut des NanoSciences de Paris, Universités Paris 6 et 7,
Campus Boucicaut, 140 Rue de Lourmel, 75015 Paris, France*
[3]*Laboratoire de Photonique et des Nanostructures,
C.N.R.S., Route de Nozay, 91460 Marcoussis, France*
*kimura@ib.cnea.gov.ar*

Acoustic phonon engineering is relevant for the manipulation of sound and heat and, through the electron-phonon interaction, to control charge and light at high frequencies and reduced dimensions. The development of mirrors, cavities, and devices to control sound at the nanoscale represents an active research field. In this work, we address the study of acoustic nanocavities. The considered devices are semiconductor multilayers in the nm scale and with atomically flat interfaces achievable by molecular beam epitaxy (MBE). They are constituted by two distributed Bragg reflectors (DBRs) enclosing a spacer of thickness equal to an integer number of half acoustic wavelengths [1]. They can confine and amplify GHz – THz acoustic phonons (with wavelengths of a few nm) both spatially and in the spectral domain [1-3]. In addition, they can constitute the feedback mechanism of an acoustic "laser".

A system constituted by an acoustic cavity embedded in an optical microcavity presents an enhancement of the Raman efficiency that can be as high as five orders of magnitude [2], and gives access to forward scattering features of the Raman spectra. This double resonator, which confines both acoustic nanowaves and photons, is a structure where electrical, acoustical and optical properties can be easily tailored. Taking into account the existing relations between the coherent phonon generation and detection mechanisms and the Raman scattering processes, we analyze the feasibility of using such systems in standard coherent phonon generation experiments (pump-probe), and what the limitations are associated with the physics of the experiment and materials involved such as maximum optical confinement, number of layers, contrast of the refraction indexes, electronic gaps, etc…

We study a structure consisting of a GaAs/AlAs acoustic nanocavity coupled to an optical distributed Bragg mirror made of AlAs/AlGaAs (see figure 1) [4]. The structure was grown by MBE with characteristic layer thicknesses of a few nanometers for the acoustic cavity and a few tens of nanometers for the optical mirror. We performed Raman scattering experiments in backscattering geometry changing the wavelength. We show how forward scattering features become observable as the excitation enters in the high optical reflectivity region of the DBR, in particular the presence of the phonon cavity mode. These experiments help us to identify the different peaks of the spectra. We report the results of femtosecond laser pump probe experiments [5]. We measure the time dependent optical reflectivity changes of the structure due to the presence of acoustic phonons. Performing a Fourier transform, it is possible to observe what the energy bands generated and detected are in the full structure.

We analyze the improvements in the efficiency of the acoustic cavity to generate and detect acoustic phonons due to the presence of the optical Bragg mirror as a function of the pump-

probe laser wavelength. Changing the laser wavelength allows us to go from a low optical reflectivity condition to an optical resonant condition. Two main amplification sources can be identified in this system: the first one corresponding to this optical resonant condition and the matching of the maximum of the electric field with the acoustic cavity position; and the second one, related to the electronic resonance with the quantum wells forming the acoustic mirrors. Using a photoelastic model for both the generation and detection mechanisms, we simulated the experiments. This puts in evidence how each of the factors takes part in the amplification of the signal.

Finally, we studied the actual acoustic phonon dynamics in the acoustic nanocavity analyzing both the temporal traces and the spectral domain signals of picosecond ultrasonics experiments [3]. The use of time windowed Fourier transforms, and wavelet transforms show not only that THz monochromatic acoustic waves are confined within acoustic nanocavities but also that these structures may act as monochromatic generators and detectors of coherent phonons.

**References:**

[1] M. Trigo, A. Bruchhausen, A. Fainstein, B. Jusserand, V. Thierry-Mieg, Phys. Rev. Lett. **89**, 227402 (2002)

[2] P. Lacharmoise, A. Fainstein, B. Jusserand, V. Thierry-Mieg. Appl. Phys. Lett. **84**, 3274 (2004).

[3] A. Huynh, N. D. Lanzillotti-Kimura, B. Jusserand, B. Perrin, A. Fainstein, and A. Lemaitre, Phys. Rev. Lett. **97**, 115502 (2006)

[4] N. D. Lanzillotti-Kimura, A. Fainstein, A. Huynh, B. Perrin, B. Jusserand, A. Miard, A. Lemaitre, submitted to ?? (2007)

[5] B. Perrin, B. Bonello et al., Physica (Amsterdam) 219B–220B, 681 (1996)

**Figures:**
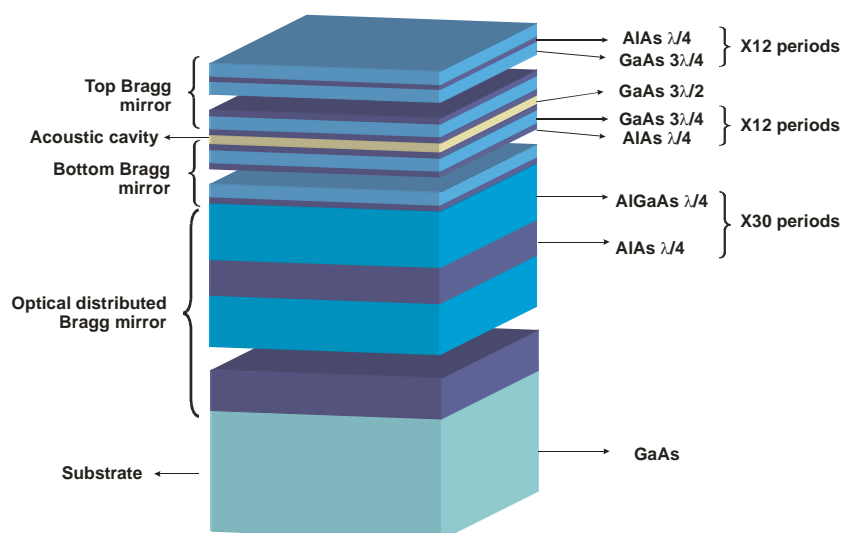


Figure 1: Scheme of the studied resonator for light and sound. The acoustic cavity acts as the spacer of the optical cavity.

# Proxels for Reliability Assessment of Future Nano-Circuits

*Sanja Lazarova-Molnar, Valeriu Beiu, Walid Ibrahim*
*United Arab Emirates University, P.O. Box 17555, Al Ain, UAE*
*sanja@uaeu.ac.ae*

As electronic devices are scaling towards nano-regime, the frequencies of failures that they exhibit will increase. This is a statement that has been made and confirmed on numerous occasions recently (see e.g. [1]). Thus, accurate evaluating of reliability should be considered, besides area, power, and speed, for the design of future nano circuits.

The available reliability analysis methods (and tools) can be divided in two categories: special-purpose ones, dedicated to reliability modelling of (nano-) circuits, and general ones. The special-purpose ones (such as RAMP [2] and NANO-PRISM [3]) are sometimes expensive in terms of computation time and memory, or tend to oversimplify the models. This leads to approximate results and inaccurate conclusions about systems' behaviour. Hence, an accurate special-purpose reliability assessment method, which can deal with complex models in reasonably short computation times, is needed. The method should allow for a wide class of models to be analysed.

The errors that occur in circuits can be either permanent or transient errors. Permanent errors occur either due to errors in the manufacturing process, or due to wear-out. Usually they are unrecoverable and in some cases can lead to replacements of chips. Transient errors, on the other hand, are of temporal character, and the system typically recovers from them. They are also referred to as soft errors. A possible effect of a soft error is an inversion of the value of a single bit. Our goal is to provide a method which would model both types of errors and accurately assess the reliability of systems with respect to both of them simultaneously. For this purpose we intend to utilize the recently introduced proxel-based simulation method [4][5].

The proxel-based method is a simulation approach based on the method of supplementary variables [6]. This is an alternative to the well-known discrete-event simulation. We will show how the proxel-based method can be applied to reliability assessment of future nano-circuits. As shown in [7], failures that appear in nano-circuits cannot typically be modelled using exponential distribution. In fact, in [2], it has been shown that the lognormal distribution is much more adequate for describing device failures; as opposed to the memoryless alternative, i.e. the exponential distribution which has been in use for some time. For that reason, Markovian methods are not sufficient for accurate reliability analysis of future nano-circuits. Discrete-event simulation is often also not an option, as it tends to be very time-consuming. The proxel-based method, on the other hand, is very flexible and it can easily analyse models with transient errors, as well as errors that appear due to wear-out (see [4]).

There are many different classes of circuit models with respect to complexity, topology and types of failures. Our research will focus on defining the classes of circuits to which the proxel-based method can be successfully applied for assessing reliability.

We will briefly describe the proxel-based method and modification to make it applicable to nano-circuit reliability evaluation. In addition, we will demonstrate our approach on a few models. The models will contain both transient and permanent failures to test our claims and demonstrate the strengths of our approach.

In Figure 1, we present two of the models which we will use to test our approach. The models are taken from Srinivasan's doctoral dissertation which describes RAMP and its algorithms [2]. Connected structures, A, B, C and D, have various failure rate functions. The first system is a series one, while the second one is a series-parallel. The same models are analysed in RAMP using discrete-event simulation and averaging out the solutions obtained using the MIN-MAX method. Our solutions obtained using the proxel-based method will be functions that describe the transient behaviour of the analyzed systems. We will perform experiments to compare our approach with the one based on discrete-event simulation.

We do believe that our approach can be systematized and integrated into a more complex EDA (Electronic Design Automation) tool. This will form a part of our future research and development plans.

**References:**

[1] International Technology Roadmap for Semiconductors, ITRS 2005 (http://public.itrs.net/)
[2] Srinivasan, J., PhD Thesis, (2006).
    http://www.cs.uiuc.edu/research/techreports.php?report=UIUCDCS-R-2006-2614&download=pdf
[3] Bhaduri, D. and Shukla, S., Proc. GLSVLSI'04 (2004) 109–112.
[4] Lazarova-Molnar, S., PhD Thesis, (2005).
    http://diglib.uni-magdeburg.de/Dissertationen/2005/sanlazarova.pdf
[5] Horton, G., Proc. ESS'02 (2002).
[6] Cox, D. R., Proc. Camb. Philos. Soc., 51(3) (1955) 433–441.
[7] Beiu, V., Ibrahim, W., Alkhawwar, Y. A., and Sulieman, M. H., Proc. DFT'06 (2006) 29–40.

**Figures:**
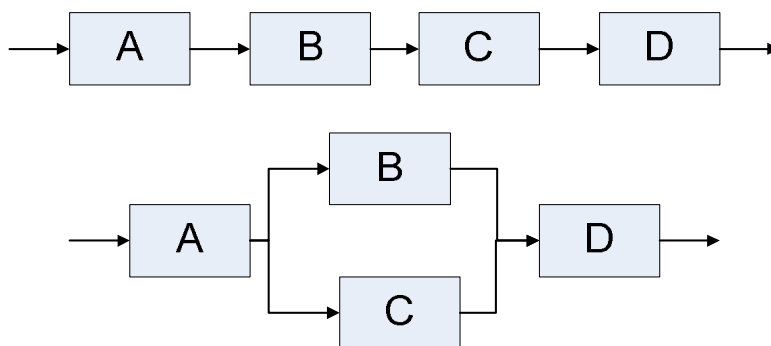


**Figure 1:** Two of the models that will be used to test the suitability of the proxel-based method and compare it against discrete-event simulation

# KINETICS OF 2D-3D TRANSFORMATIONS OF CARBON NANOSTRUCTURES

*I.V. Lebedeva*[1]*, A.A.Knizhnik*[2,3]*, A.A. Bagatur'yants*[3]*, B.V. Potapkin*[2,3]

[1]*Moscow Institute of Physics and Technology, 141700, 9, Institutskii per., Dolgoprudny, Moscow Region, Russia*
[2]*RRC "Kurchatov Institute", Kurchatov Sq. 1, Moscow, 123182, Russia*
[3]*Kinetic Technologies Ltd, Kurchatov Sq. 1, Moscow, 123182, Russia*
*liv_ira@list.ru*

In this work we consider the gas-phase formation of carbon nanostructures from graphite sheets under high-energy processing, such as arc discharge or laser evaporation [1]. Though there are quite a few of papers that examined fullerene and nanotube formation, the folding of a single plane sheet into a three-dimensional structure has not been investigated. Thus, here we discuss this process. Elementary processes resulting in both the folding and relaxation of the imperfect structure formed are also examined. A simple evaluation of the elastic energies of nanotubes indicates that the folding of a perfect graphite sheet requires overcoming a huge energy barrier (about 15 eV for square sheets) and, therefore, it can not be observed at an arc discharge temperature. In order to obtain kinetic characteristics of the process and to examine its mechanism we carried out molecular dynamics simulations [2].

Although the energy barrier is very high, our simulations showed that the folding of a graphite sheet proceeds in about 1 ns at 3500 K (Fig. 1). This is explained by the formation of numerous defects, which increase the system entropy and, hence, substantially reduce its free energy at high temperatures. Furthermore, the folding begins not simultaneously on both sides of the sheet but only at one corner having the highest density of defects. The defects are mostly localized at the edges and their density rapidly decreases towards the sheet interior. Consequently, defects should be mainly formed in surface reactions. The folding occurs when the density of defects at one of the corners reaches its critical value.

The graphite sheets of different size and shape were considered. The energy barrier of the process is 20–25 eV, being only slightly dependent on the sheet size. As the sheet size increases, the folding time and the energy change in the overall process rise. A hexagonal sheet takes somewhat more time for folding than a rectangular one, because it has more obtuse corners. In a long and thin sheet many atoms are close to the edges and the critical density of defects can be reached in any area of the sheet. All these facts correspond to the suggested mechanism.

During the simulation, the main reactions of defects were detected and then their kinetic characteristics were evaluated for a plane graphite sheet. The simulation showed that the most important reactions of defect transformation proceed with the breaking of only one bond and thus have a barrier of about 3 eV. The reactions that require two bonds to be broken, such as the modified Stone-Wales rearrangement [3], take a negligible part in the folding. The process of defect formation can be kinetically limited at low temperatures. Furthermore, the mechanism of defect penetration into the interior of the graphite sheet is most likely associated with the formation of small defects adjacent to a ten or more-membered ring. The curvature of the sheet only slightly affects the characteristics of the reactions if its radius is more than 10 Å.

Based on the elementary processes examined, we suggested a simple scheme of defect formation at sheet edges and used it for determining the equilibrium densities of defects. According to this scheme, the minimal temperature at which the folding of graphite sheets can be observed experimentally (proceeds in about 1 s) is 2500 K.

In addition to the processes that take place before the folding, the transformation of the formed structure to more perfect one containing a less number of defects was considered. After the folding process is completed the further relaxation of the structure proceeds via the Stone–Wales rearrangements [4] and the modified Stone–Wales rearrangements of defects [3]. Nevertheless, these reactions involve many steps rather than one (Fig. 2). First a big ring forms, then two small defects adjacent to it transform into two different rings and ultimately a bond forms inside the big one, dividing it into two smaller rings. Although the structures of

the transition states of the one-step reaction and the rate-limiting step of the multistep process are almost the same, their reaction coordinates are different. We suggest that in the latter case it corresponds to vibrational modes with higher frequencies and the multistep process proceeds faster.

We also examined the possibility that the number of defects in the imperfect structure can be reduced through the addition of carbon atoms and dimers [5]. The process of the addition was shown to proceed in two steps (Fig. 3). First, an atom or a dimer is attached to an atom of the fullerene to make it four-coordinated almost without an energy barrier. Then, this new atom or dimer is built into a neighboring bond. The barrier of this step is lower than the energy released in the first one. If the first step has proceeded, the overall process will definitely result in the product formation. Moreover, atoms and dimers are eventually built into a bond to form new defects. Therefore, the addition of carbon atoms and dimers to defects is not more favorable than their addition to hexagons and should not be considered as a way of reducing the number of defects.

**References:**

[1] R.B. Little, Journal of Cluster Science, **14** (2003) 135.
[2] M.P. Allen, D.J. Tildesley, Computer Simulation of Liquids. – Oxford: Clarendon Press (1987).
[3] B.-C. Wang, H.-W. Wang, J.-C. Chang, Journal of Molecular Structure, **540** (2001) 171.
[4] Y. Kumeda, D.J. Wales, Chem. Phys. Lett., **374** (2003) 125.
[5] J. Xiaodun, J.R. Chelikowsky, Phys. Rev.B, **46** (1992-II) 5028.

**Figures:**
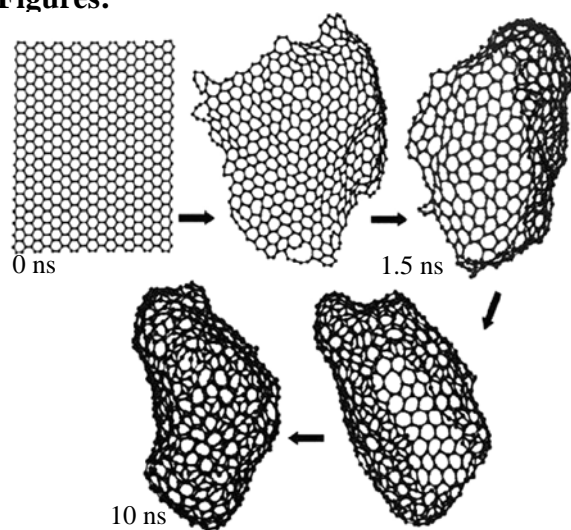


Fig.1. Evolution of a graphite sheet at 3500K.



Fig 2. The modified Stone-Wales rearrangement of defects [3]. The solid line corresponds to the one-step process. The dashed line corresponds to the multistep process.



Fig. 3. The addition of a carbon atom to a common bond of two adjacent pentagons.

# QUANTUM KNOTS OF VORTICES: A NEW FRONTIER IN NANOMAGNETISM

*Viktor O. Ledenyov, Dimitri O. Ledenyov[1] and Oleg P. Ledenyov*
*National Scientific Centre Kharkov Institute of Physics and Technology,*
*Academicheskaya 1, Kharkov 61108, Ukraine*
*[1]James Cook University, Townsville Queensland 4811, Australia*
*ledenyov@univer.kharkov.ua*

The new theoretical approach to the physical problem on current transport in magnetic nanostructures in Type II superconductors is proposed. In the case of the parallel alignment of both the current and the external magnetic field, directed along the long axis of superconducting cylindrical sample, the Abricosov vortices are generated. Vortices are nanoscopic objects with lateral dimensions of a few nm. It is assumed that vortex core has one localized state. Vortex carries a quantum of magnetic flux and has spiral like shape with the current transported along its longitudinal axis [1]. However, there is a particular discrepancy between the generally accepted model of vortex, and the obtained experimental results [2,3]. Authors propose a new theoretical model of a self-knotted magnetic vortex with the transport current flowing along the axis creating a magnetic vortex in vortical magnetic nanostructure [4-10]. The graphic results of researched physical parameters of a self-knotted magnetic vortex, their relations and orientation of their vectors in selected geometrical representation are shown [4]. The computer modeling and simulation, including the calculation of main physical parameters of quantum system, are performed in given theoretical approximation [5]. It is firstly proposed to consider that the knot of vortex is in an extreme quantum limit in vortical magnetic nanostructures. The recent neutron scattering research of the flux line lattice in crystalline Nb of longitudinal geometry $(J \| H)$ shows that the vortex system has the longitudinal correlation length, which decreases with the increase of current as $\sim 1/J$ [11]. Authors suppose that the knots may destroy the longitudinal order of vortices, and produce this kind of dependence.

**References:**

[1] A.M. Campbell and J.E. Evetts, Critical currents in superconductors, Taylor and Francis, Ltd., London, U.K. (1972)
[2] J.R. Clem, Phys. Lett., **54A**, (1975) 452
[3] H. Brandt, J. Low. Temp. Phys. **39**, (1980) 41
[4] O.P. Ledenyov, Some Old Tasks of Shubnikov Laboratory –the New Physics, Shubnikov Memorial International Conference on Low Temperature Physics, B.Verkin Institute for Low Temperature Physics & Engineering, Kharkov, Ukraine (2001)
[5] D.O. Ledenyov, Invited Talk on Quantum Knots, Marconi seminar organized by M.J. Lancaster, Birmingham University, Birmingham, U.K. (2000)
[6] V.O. Ledenyov, Invited Talk on Measurements of Magnetic Flux Qubit by dc-SQUID, Kamerlingh Onnes Laboratorium seminar organized by P. Kes, Leiden University, Leiden, The Netherlands (1998)
[7] D.O. Ledenyov, Thesis on Nonlinear Phenomena in Microwave Superconductivity supervised by J. Mazierska, James Cook University, Queensland, Australia (2000-2007)
[8] V.O. Ledenyov, D.O. Ledenyov and O.P. Ledenyov, Problems of Atomic Science and Technology, **n.1 (15)**, (2006) 76-82
[9] P. Kes, Private Communications, Kamerlingh Onnes Laboratory, Leiden University, Leiden, The Netherlands (1998 and 1999)
[10] O Fischer, Private Communications, International Advanced School "Leonardo da Vinci", Bologna, Italy (1998) and NCSS-4 & SIO-97 Alesund, Norway (1997)
[11] P.L. Gammel et. al., Phys. Rev. Lett. **80**, (1998) 833

**Figures:**
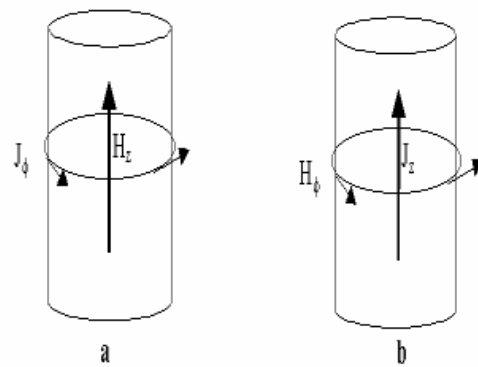


*Fig. 1. a) Vortex in superconductor without transport current*
*b) Vortex in superconductor with transport current flowing along vortex*
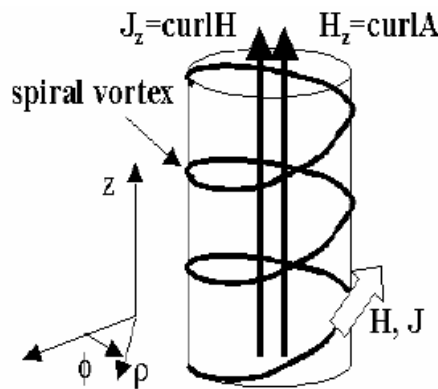


*Fig. 2. Model of a magnetic vortex in generally accepted geometrical*
*representation shown in cylindrical coordinate system (r, j, z)*
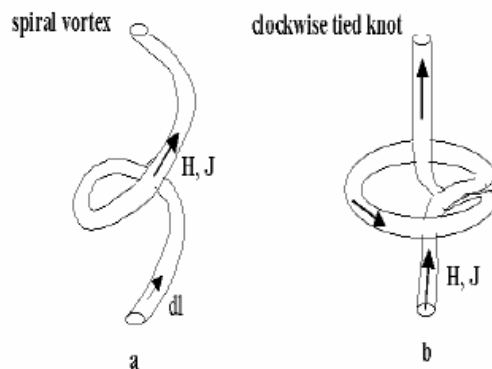


*Fig. 3. a) Spiral vortex in superconductor*
*b) Clockwise tied knot of vortex, which is in an extreme quantum limit in*
*vortical magnetic nanostructures in superconductor*

# FABRICATION AND OPTIMIZATION OF BENT FIBER PROBES

*J. LeDue, P. Grütter*
*McGill University Physics Department, 3600 rue University, Montreal, Canada*
*leduej@physics.mcgill.ca*

Scanning near-field optical microscopy (SNOM) is a scanning probe technique which allows nanometer optical resolution by scanning a sub-wavelength aperture in close proximity to a sample. Among other applications, SNOM is well suited to studies of single molecules and biological samples when used as a fluorescence source because the evanescent illumination provided by the SNOM tip makes it highly surface sensitive. The cell membrane is of particular interest as protein clustering can be revealed at high resolution by fluorophores, such as GFP. [1,2]

SNOM probes can be fabricated from bent fiber optic cable. [3,4] These probes can be operated using a normal force mode and optical beam deflection (OBD) for distance regulation. This makes them compatible with many commercial atomic force microscopes (AFM) unlike the usual straight fiber probes used in combination with quartz tuning forks in a shear force mode. Normal force imaging modes are well understood in terms of the forces applied to the sample. [5,6] Thus, using a bent fiber probe, quantitative force spectroscopy can be performed simultaneously with optical measurements.

Fabrication of the bent fiber probes proceeds with a number of steps. The fibers are bent with a high frequency electric arc. The angle is controlled to the desired precision by bending in multiple stages. As with all fiber based SNOM probes it is necessary to taper the fiber to connect the core-cladding index difference waveguide to the sub-wavelength aperture. Chemical etching is used to create the tapers, making use of the meniscus, tube, and selective techniques. In addition, by employing multiple techniques it is possible to create probes (so-called 'pencil probes') combining the high reproducibility of selective etching with the overall geometry of meniscus or tube etching. [7] A thin film of aluminum is deposited on the taper by thermal evaporation in order to confine the light. A high yield of smooth, pinhole free coatings is obtained. The bent, tapered and coated fibers are glued to microfabricated silicon v-groove chips. The chips have the same dimensions as a microfabricated AFM cantilever chip allowing easy mounting in commercial instruments while the v-groove aids in positioning of the fiber. Finally, the sub-wavelength aperture is created by FIB milling. The aperture size can be controlled in 25-30 nm increments by repetitive slicing perpendicular to the axis of the fiber.

The final product is a combined AFM/SNOM probe with typical resonance frequencies in the range of 10-20 kHz, spring constant of ~200 N/m, and Q-factors of 300-400. Submersion of only the fiber tip beyond the bend and special shaping of its end-face allows the resonance characteristics of the probe to remain virtually unchanged while in fluid. [8] The high Q-factor and well defined resonance enable the possibility of using a commercial AFM in non-contact mode in fluid which usually requires custom OBD hardware to accommodate the low Q-factor of a cantilever in water. [9] Optimal parameters for the bent fiber probe (spring constant, Q-factor, resonance frequency, diameter, length) will be presented.

**References:**

[1] Koopman et al., FEBS Letters, **573** (2004) 6.
[2] Ianoul et al., Nature Chemical Biology, **1** (2005) 196.
[3] Muramatsu et al., Ultramicroscopy, **57** (1995) 141.
[4] Taylor et al., Proc. SPIE, **3009** (1997) 119.
[5] Sader and Jarvis, APL, **84** (2004) 1801.
[6] Lee and Jhe, PRL, **97** (2006) 036104.
[7] Mononobe and Ohtsu, Journal of Lightwave Technology, **14** (1996) 2231.
[8] Lu et al., NFO9 Poster Presentation.
[9] Fukuma and Jarvis, RSI, **77** (2006) 043701.

**Figures:**
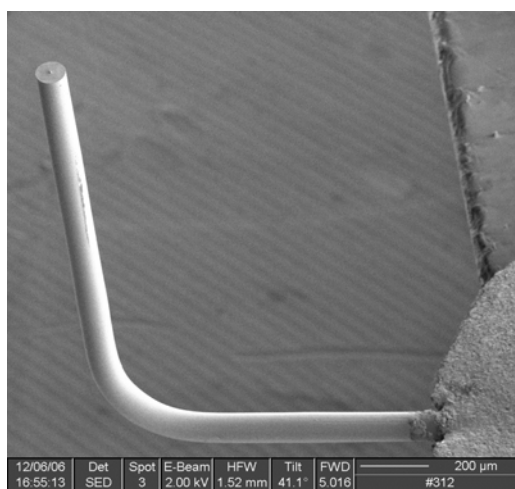


**Fig. 1:** An example of a probe fabricated by electric arc bending, selective etching, Al coating and FIB milling.  The conical taper created by selective etching is visible on the end of the tip.
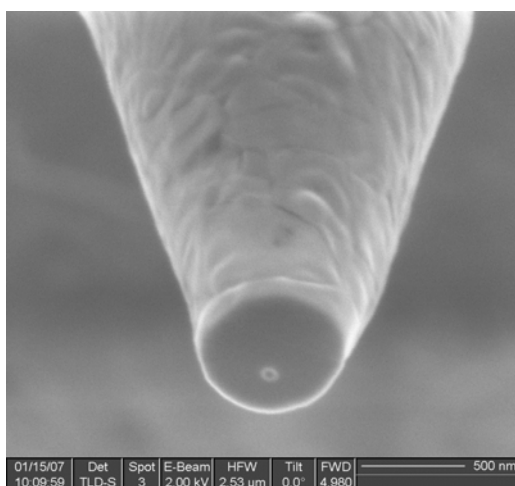


**Fig. 2:** An example of an aperture created at the end of the tapered fiber by FIB milling.  The diameter of the aperture is 70 nm.

# A NEW STRUCTURE OF BENZOIC ACID ON Cu(110) INCLUDING COPPER ADATOMS STM INVESTIGATIONS AND DFT CALCULATIONS

*C. Lennartz[1], L. Müller-Meskamp[1], S. Karthäuser[1], N. Atodiresei, R. Waser[1,2]*

[1]*Institute of Solid State Research and CNI-Center for Nanoelectronic Systems for Information Technology, Research Center Juelich GmbH, 52425 Juelich, Germany*
[2]*Intitute of Materials for Electronic Engineering 2, RWTH Aachen, Sommerfeldstraße 24, 52074 Aachen, Germany*
[m.c.lennartz@fz-juelich.de](mailto:m.c.lennartz@fz-juelich.de)

The feature sizes in semiconductor technology have been reduced very fast and continuously so that the feature size reduction seems to hit, physical and economical limits. Furthermore the tools to investigate nanoscale objects have improved tremendously, mainly driven by the invention of scanning probe methods. So it is a promising opportunity to replace the known systems by integrating molecules in electronic circuits [1].
It is necessary to develop reproducible contacting methods of molecules to some, usually metallic electrodes, and secondly to find suitable molecule/metal combinations that provide the desired functionality reliably.

In this report we will focus on the second point. The carboxylate/copper system is a promising alternative to the thiol/gold systems which are studied in many other projects, for instance in [2,3,4]. Today an advantageously employed metal for wires or interconnects in electronics industry is copper, due to its low resistance. Copper in combination with new dielectric materials is thought to have the prerequisites for developing integrated circuits with decreasing switching times, reduced heat dissipation and higher reliability. According to this strategy it is essential to get a fundamental understanding of the organic/copper interface, like the carboxylate/copper interface for example we are focusing on.
Carboxylic acids are chosen because both oxygen atoms of the carboxyl group link with the copper surface. The carboxylates create ordered monolayers. Because of this binding situation (angles) the carboxylate/copper system has less structure formation possibilities than the thiol/gold system for example. If a copper surface with [110]-direction is chosen, the specific surface structure (lines) leads additionally to a confinement of the spatial diffusion possibility of the molecules on the surface and further to a texturing with a preferred direction. With increasing coverage, several large area and large domain with well ordered structures occur containing species oriented both parallel and perpendicular to the surface with defined unit cells [5].
To get a statement about the basic geometries and electron transport properties, benzoic acid ($C_6H_5COOH$) is deposited from the gas phase on Cu(110) surfaces and the arising benzoate monolayers are characterized by UHV-STM.
By topographical analysis with the UHV-STM we found some of the structures described by Frederick and Barlow [5,6] e.g. the close-packed c(8x2)-structure (see fig. 1) of all upright standing molecules.
Beside the structures shown there, we found a new structure with a higher packing-density of the molecules in the monolayer (see fig. 1). This structure can be described as structure with a (1 1, -4 2) periodicity. All molecules in this structure are upright standing with a packing-density of one molecule per three outermost surface copper atoms. Compared to the packing-density of the common c(8x2)-structure with four copper surface atoms per molecule, this represents a strong increase in the molecular packing-density and the structure with the highest surface coverage, observed so far. Looking at the height-profiles of the close-packed phase, a slight elevation of around 0.25 nm is found for the central molecule row, leading to the suggestion of an adatom stabilized structure.

Matching the new structure to the copper lattice, results in energetically unfavourable adsorption sites for every second row of molecules, supporting the adatom suggestion.

By DFT calculations, the overall energies of the adatom structure and a structure without adatoms are computed. The calculations show, that the structure without adatoms is unstable and relaxes into an energetically even less favourable structure. Both structures, relaxed and unrelaxed, are energetically less favourable, than the adatom stabilized structure. The evolution of the adatom stabilized surface is also supported by the observation of benzoate-adatom complexes on the surface for lower coverages in literature [7].

A model of the surface structure built by benzoic acid on a Cu(110) surface including copper adatoms based on STM investigations with linescans and height-profiles will be presented. The stability of the new structure will be discussed based on DFT-calculations.

**References:**

[1] H. Kuhn, D. Möbius, Angewandte Chemie International Edition, **10** (1971) 460.
[2] F. Schreiber, Progress in Surface Science, **65** (2000) 151.
[3] B. Lüssem, L. Müller-Meskamp, S. Karthäuser, R. Waser, Langmuir, **21** (2005) 5256.
[4] L. Müller-Meskamp et al., Journal of Physics: Conference Series, **61** (2007) 852.
[5] B.G. Frederick et al., Surface Review and Letters, **3** (1996) 1523.
[6] S.M. Barlow, R. Raval, Surface Science Report, **50** (2003) 201.
[7] Q. Chen et al., Surface Science, **446** (2000) 63.

**Figures:**



**Fig. 1** STM-Topography of benzoic acid on a Cu(110) surface. The lower left circle assigned an area with a c(8x2)-structure of all upright standing molecules. The structure in the upper right area is a higher packed structure of upright standing molecules and is based on molecules situated on copper adatoms.
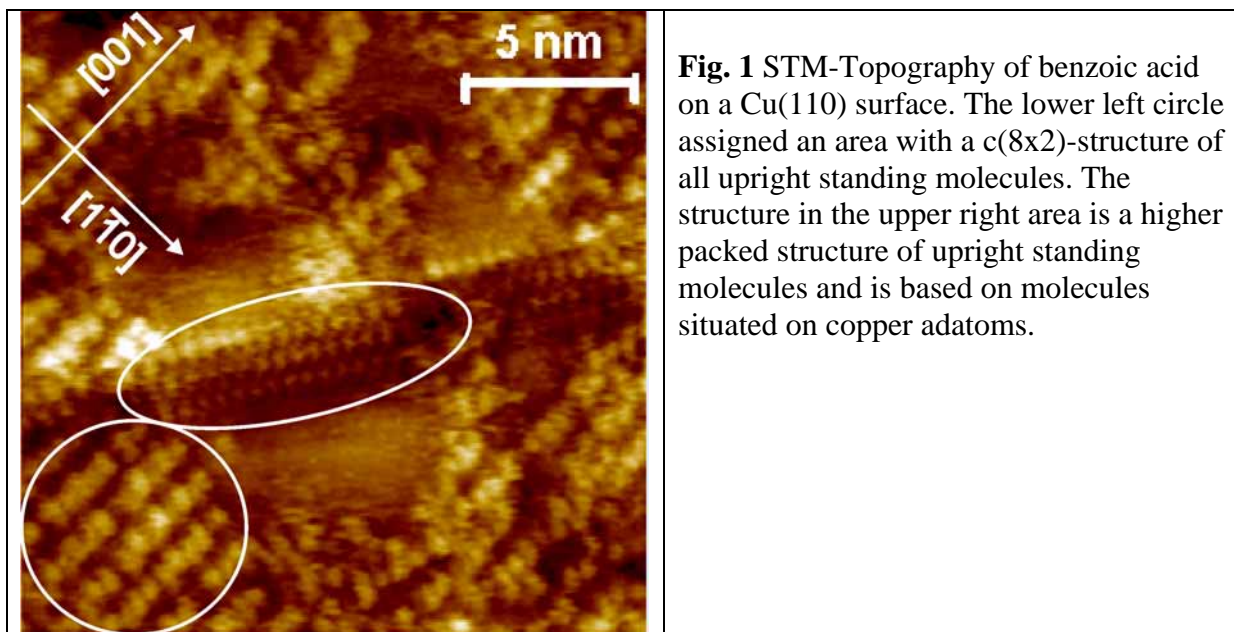
# CONFINEMENT EFFECT IN CdTe NANOCRYSTALS EMBEDDED IN SILICA THIN FILMS

*S. Levichev[1], A. G. Rolo[1], A. Chahboun[2], O. Conde[3], M. J. M. Gomes[1], A.I. Kovalev[4], and D.L. Wainstein[4]*

[1] *Physics Department, University of Minho, 4710 - 057 Braga, Portugal*
[2] *Physics Department, Dhar Mehraz Sciences Faculty, BP 1796, Fès, Morocco*
[3] *Physics Department, University of Lisbon, 1749 - 016 Lisbon, Portugal*
[4] *Surface Phenomena Researches Group LLC, 2nd Baumanskaya 9/23, 105005 Moscow, Russia*

*mjesus@fisica.uminho.pt*

Nanostructures based on II–VI materials have attracted much attention for their great fundamental, experimental and applied interests. Extensive investigations of the optical properties of films containing semiconductor nanocrystals (NCs) have demonstrated their potential applications in optoelectronics [1]. These NCs have the properties of narrow size distribution, good crystallinity, and high PL efficiency [2]. However, their widen application has been restricted due to their liquid form. Embedding these NCs in a rigid matrix is a solution to this as well photostability. As a rigid support, glass has several good properties such as transparency, robustness against atmospheric attack and UV irradiation. Semiconductor nanoparticles dispersed in optically transparent glass matrix have many applications in optical switching, optical filters, optical sensors, and wave guides. In this work $SiO_2$ matrix grown by the rf magnetron co- sputtering technique with subsequent annealing in vacuum. Absorption spectroscopy, Raman scattering, grazing incidence X-ray diffraction (GIXRD), X-ray photoemission spectra (XPS) and photoluminescence (PL) were used to study the grown samples.

GIXRD indicates that the as-grown samples have an amorphous nature, in agreement with earlier observations [3]. Fig. 1 shows the GIXRD spectra of the annealed CdTe doped silica films grown at different conditions. The comparison of these spectra with the JCPDS database (card 15- 770) allows us to conclude that CdTe NCs in the cubic phase were grown inside the silica matrix. We can estimate the NCs sizes from the GIXRD results using the well known Scherrer equation. Depending on the grown conditions, different NCs average size was obtained ranging from 3 to 10 nm. Raman spectroscopy applied to annealed samples show a slightly asymmetric and broad peak centred at 169 cm$^{-1}$, corresponding to LO phonons in the CdTe.

The post-grown annealed samples show shoulders on the absorption spectrum in the range of 650 – 700 nm, clearly shifted from the bulk CdTe energy band gap (825 nm). These shoulders could be attributed to NCs exciton line, clearly indicating the effect of quantum confinement. A typical PL spectrum (Fig. 2) obtained from these samples display two peaks. A narrow one centered at 709 nm that we attribute to carriers recombination in the ground states of CdTe NCs. The broader one centered at 478 nm could be attributed to radiative recombination at defects in the interface NC/matrix.

The chemical and phase composition was determined using XPS technique taking into account the coefficients of elemental sensitivity (photoelectrons output cross section). We observed the size-dependent shift of the CdTe nanocrystal component of the Cd3d and Te3d photoelectron lines that was described in [4]: when a crystal reduces its size down to a nanometer scale, its electronic structure is changed and the entire core-level features moves simultaneously toward to high binding energy. The theoretically predicted value of this shift is size-dependent. The binding energy of Cd and Te core levels increases on +0.7 eV in comparison with the bulk standard. This shift is connected to the nanocrystallinity of the

chemical compound. The Te $3d_{5/2}$ component at 576.6 eV binding energy is connected with oxidized Te atoms located on the nanocrystal/matrix interfaces. The relative number of these atoms is 23 at.%. Analyzing of this concentration, and assuming the spherical shape of the nanocrystals, we can calculate the diameter of CdTe nanoparticles. The size of CdTe NCs is 4.5 nm on base of XPS data. This value is in a good agreement with the one, evaluated from GIXRD data (5.2 nm).

**Acknowledgements:**

**References:**

[1] G.I. Stegeman, R.H. Stolen, J. Opt. Soc. Am. B **6** (1987) 652.

[2] M.Y. Gao, S. Kirstein, H. Mo.hwald, A.L. Rogach, A. Kornowski, A. Eychmu. ller, H. Weller, J. Phys. Chem. B **102** (1998) 8369.

[3] P. B. Dayal, B. R. Metha, Y. Aparna, and S. M. Shivaprasad, Appl. Phys. Lett. **81** (2002) 4254.

[4] Chang Q. Sun, B.K. Tay, Y.Q. Fu, S.Li, T.P. Chen, H.L. Bai, and E.Y. Jiang. *J. Phys. Chem. B*, **107** (2003) 411.

**Figures:**
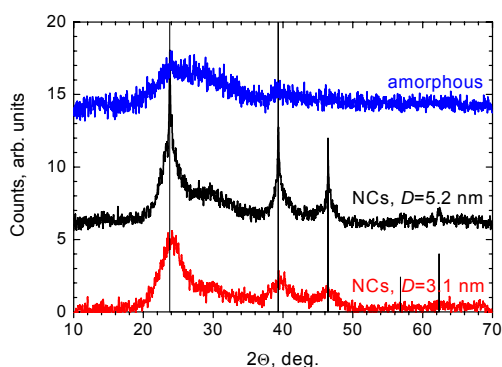


Fig. 1. GIXRD spectra of the CdTe NCs doped SiO$_2$ glass films. The peak position of cubic CdTe are shown as vertical lines (from JCPDS database 15-770).
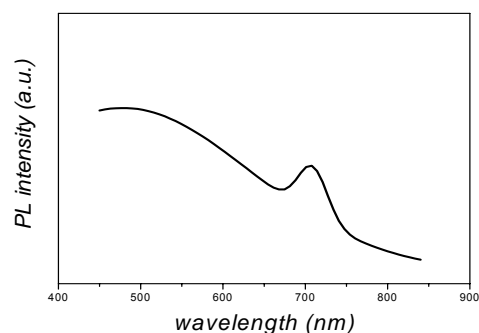


Fig. 2**.** PL spectrum of CdTe doped glass obtained at room temperature, with an excitation wavelength of 400nm.
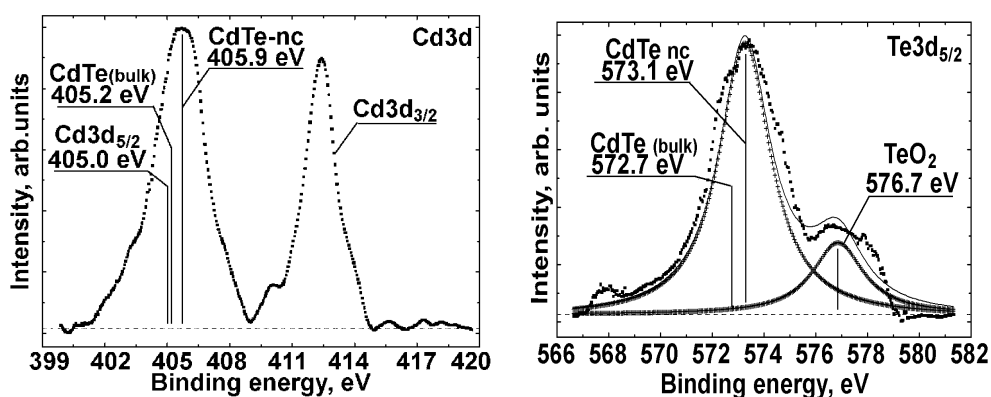


Fig. 2. Cd 3d and Te 3d photoelectron spectra of  S31.

# Synthesis of ZnO nanowires by thermal evaporation method and its photoluminescence property

*Chih-Cheng Lin, and Yuan-Yao Li\**
*Department of Chemical Engineering, National Chung Cheng University, Chia-Yi 62102,*
*Taiwan*
*preseneting author: g9044035@ccu.edu.tw*
*\*corresponding author: chmyyl@ccu.edu.tw*

One-dimensional (1D) nanostructures have attracted many research interests due to their unique properties and a wide range of applications. Zinc oxide is a direct wide band gap (3.37eV) semiconductor with a large excitation binding energy (60 meV) and excellent chemical stability. Therefore, many practical applications such as field emitters [1], dye-sensitized solar cells [2], photodetectors [3] and light emitting diodes [4] can be considered. In this study, zinc oxide nanowires were synthesized by low temperature evaporation method growth on a gold coated catalyst ITO glass substrate. The zinc powder was conducted by thermal evaporation under argon and air atmosphere at 400 $^o$C and the results found that ZnO nanowires with high purity and a uniform diameter distribution were formed in this process. The morphology and microstructure characterization of the ZnO nanowires were analysized using field-emission scanning electron microscopy and high-resolution transmission electron microscopy. It revealed high purity, good crystalline structure and uniform diameters about 40 nm (Fig. 1a and 1b). Photoluminescence (PL) spectra of the ZnO nanowires showed a higher UV emission ( 390nm) and a relatively weak blue emission (450nm) at room temperature (Fig. 2).

**References:**

[1]   C. J. Lee, T. J. Lee, S. C. Lyu, Y. Zhang, H. Ruh, H. J. Lee, Appl. Phys. Lett. **81** (2002) 3648.
[2]   M. Law, L. E. Greene, J. C. Johnson, R. Saykally, P. D. Yang, Nat. Mater. **4** (2005) 455.
[3]   C. Y. Lu, S. J. Chang, S. P. Chang, C. T. Lee, C. F. Kuo, H. M. Chang, Y. Z. Chiou, C. L. Hsu, I. C. Chen, Appl. Phys. Lett. **89** (2006) 153101.
[4]   N. Saito, H. Haneda, T. Sekiguchi, N. Ohashi, I. Sakaguchi, K. Koumoto, Adv. Mater. **14** (2002) 418.

**Figures:**
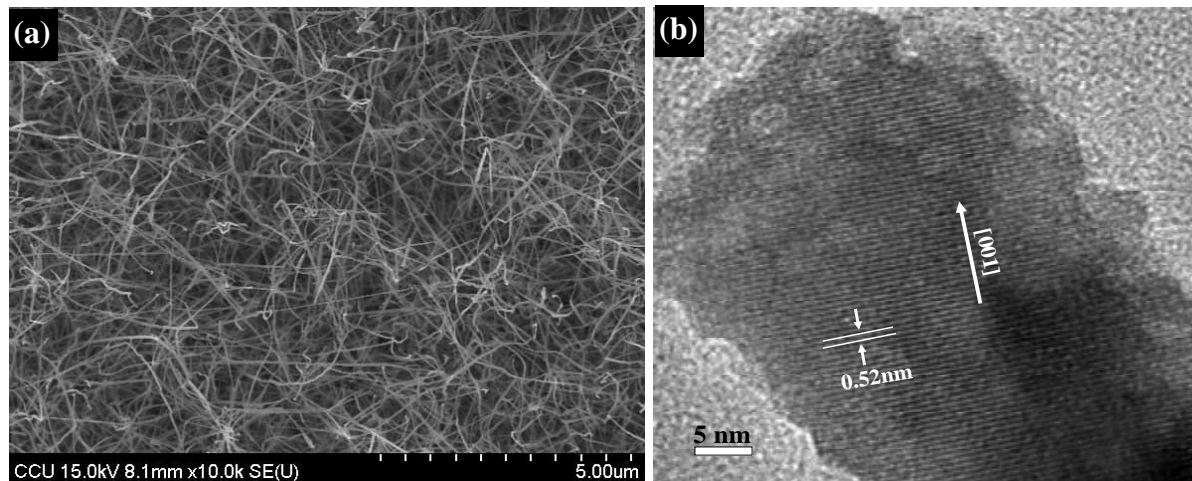


Fig. 1. (a) SEM and (b) HR-TEM image of ZnO nanowires.
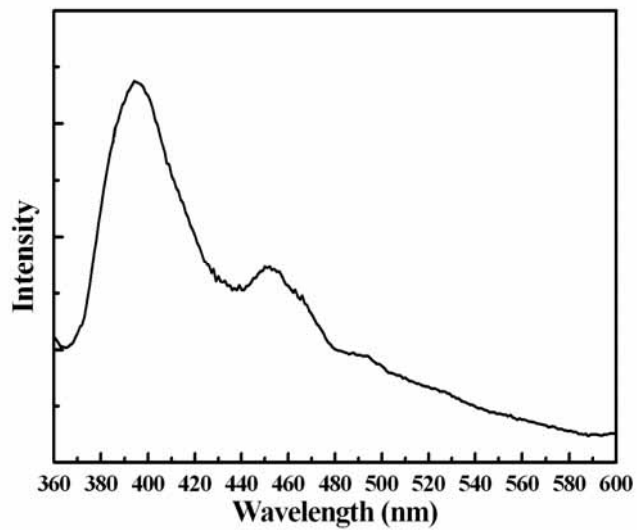


Fig. 2. PL spectra of ZnO nanowires synthesized in ITO glass substrate.

## Anisotropy of Fluorescence Dyes Intercalated into Nanostructured Interlayer Space of Clay Films.

*F. López Arbeloa, V. Martínez, S. Salleres, J. Bañuelos,T. Arbeloa and I. López Arbeloa*
*Physical Chemistry Department, University of the Basque Country, Bilbao, SPAIN*
*fernando.lopezarbeloa@ehu.es*

The intercalation of fluorescence dyes into nanostructured host materials is fundamental in the design of new optical devices with interesting technological applications. Fluorescent dyes are normally used in photonics as active media of tunable dye laser. They are also successfully applied as molecular probes to study multitude of microheterogeneous systems, including biological systems, such as proteins, membranes, biosensors, etc. The fluorescence properties are generally dependent on the environmental characteristics and fluorescence techniques can provide information on the physicochemical properties of surrounding ambiences. Since fluorescence is a very rapid phenomenon, in the pico- and nano-sesond time-domains, these techniques can be applied to study the dynamics of very fast processes occurring in the excited states.

The adsorption of fluorescence dyes with a preferential orientation into nanostructured solid host materials can induce a macroscopic arrangement of fluorescence molecules with special interest in non-lineal optics. In this contribution we shows the anisotropy behaviour of rhodamine 6G (R6G) dye intercalated into laponite clay films with respect to the plane of the linearly-polarized light. This anisotropic photoresponse is a consequence of the preferential orientation of R6G molecules with respect of the plane of the films. Indeed, the absorption and fluorescence spectra of R6G with linearly polarized light can be used to evaluate the twisted angle of the long-molecular axis of R6G with respect to the layer of Lap clay [1].

Clay minerals are aluminosillicates with a lamellar structure formed by the condensation of tetrahedral (T) $SiO_2$ and octahedral (O) $Al_2O_3$ (dioctahedral) or $MgO$ (trioctahedral) sheets. Part of the structural $Si^{4+}$, $Al^{3+}$ or $Mg^{2+}$ can be isomorphycally substituted by cations with lower valence providing to the clay lamellas a net negative charge. This negative charge is compensated by inorganic cations ($Na^+$, $K^+$, $Ca^{2+}$) which are adsorbed at the external surface of the layers. These hydrated cations are interchangeable and induces the stacking of clay layers in parallel planes given rise to the tactoidal structure of clays with a interlayer distance around 1-2 nm (Figure 1(A)). This interlayer space is expandable and can accommodate a great variety of inorganic and organic cations by simple cation exchange mechanisms.
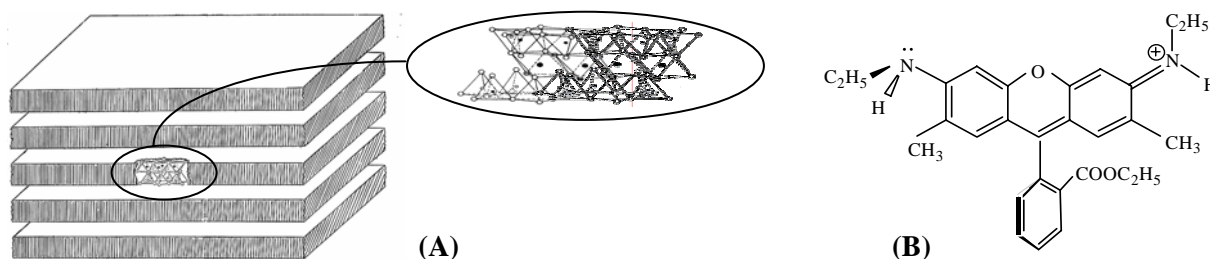


Figure 1. Tactoidal structure of clay minerals (A) and molecular structure of rhodamine 6G dye (B).

In this contribution we used the laponite (Lap) clay because it is characterized by its high chemical purity, its very low particle size (< 30 nm) and its very low iron content (iron is an efficient quencher for the fluorescence emission of many aromatic systems, including organic

dyes). Supported Lap films in glass substrate were obtained by the spin-coating technique. AFM images of these films reveal a correct topographic distribution of the Lap particles in the film. X-ray diffraction profiles suggest a parallel distribution of the Lap layers in the plane of the film. [2]

Rhodamine 6G (R6G, Figure 1 (B)) dye was chosen as fluorescence dye because probably this is the most-used laser dye. This fluorescent cation can be easily intercalated into the interlayer space of clays by simple cation exchange mechanism, for instance by immersion the Lap films into a dye solution. The loading of the dye can be controlled by the dye concentration in the immersion solution and the immersion time. The intercalation of R6G molecules into the interlayer space of Lap films was confirmed by XR diffraction technique.

The evolution of the absorption and fluorescence spectra of R6G in Lap films with the dye content suggest that R6G molecules can be adsorbed as different species such as monomeric (for low loadings) and as aggregates (moderated and high loadings). Both, non-fluorescent H-type and fluorescent J-type dimers and higher aggregates has been characterized in Lap films [3].
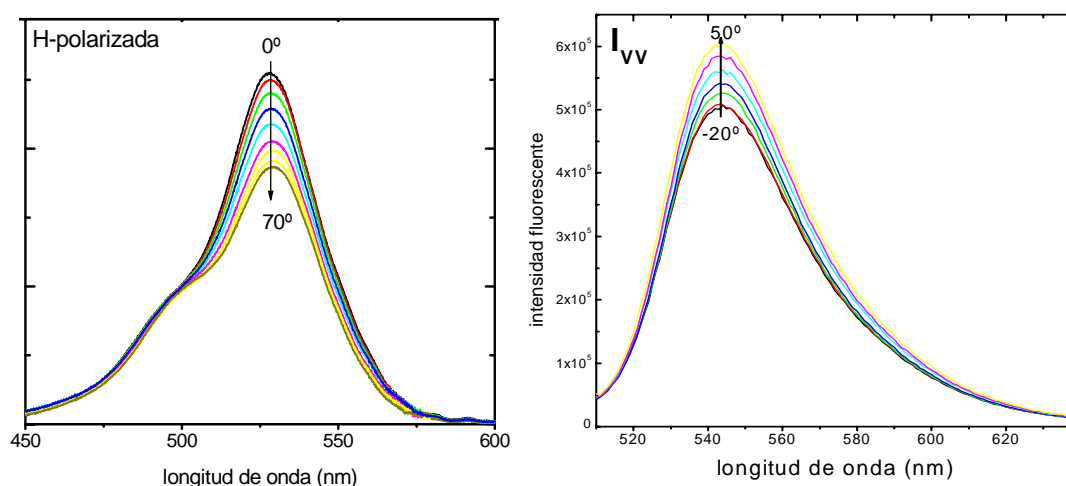


Figure 2: Evolution of the absorption (left) and fluorescence (right) spectra of a R6G/Lap film with the twisted angle for spectra recorded with linearly-polarized light

Figure 2 shows some representative evolution of the absorption and fluorescence spectra of R6G monomers adsorbed in Lap films with linearly-polarized light as a function of the twisted angle between the film and the incident beam. These anisotropic behaviours suggest a preferential orientation of R6G species adsorbed in the interlayer space of Lap films. From the lineal relationship between the corresponding dichroic ratio and the twisted angle, the preferential angle of R6G species adsorbed on Lap film can be evaluated. Experimental results suggest that the R6G monomers are J-type aggregates are disposed with an orientation angle around 70º with respect to the normal to the Lap layers. H-type aggregates are disposed more to the perpendicular as the dye loading is increased.

Present results confirm that the adsorption of fluorescent dye into ordered clay layers is a good strategy to design new optical devices with an anisotropy response to the plane of linearly polarized light based in the incorporation of fluorescent dye into organized clay films.

[1] F. Lopez Arbeloa et al. *Chem. Mat*.**17** (2005), 4734 and **18** (2006) 1407
[2] V. Martinez et al. *Langmuir* **20** (2004), 4715
[3] V. Martinez et al. *J. Chem. Phys. B* **108** (2004), 20030 and **109** (2005), 7443

# ADSORPTION OF NEUTRAL AND CHARGED NITROGEN DIOXIDE MOLECULES ON CARBON NANOTUBES: THE SELECTIVE REMOVAL OF THE METALLIC TUBES.

*María J. López, Iván Cabria, and Julio A. Alonso*
*Departamento de Física Teórica, Universidad de Valladolid, 47011 Valladolid, Spain*
*maria.lopez@fta.uva.es*

After more than 15 years of intense research on carbon nantotubes, CNTs, since its discovery, most of the production techniques yield bundles of CNTs of mixed radii and chiralities. However, samples of CNTs of well defined characteristics, specific radius and either metallic or semiconducting character, are required for many applications and also for basic research. Therefore, the selective production and the separation and sorting of CNTs become key issues for further scientific and technological developments based on CNTs.

Recently, a new experimental technique has been introduced which leads to the selective removal of the metallic, mCNTs, from the semiconducting, sCNTs, single wall carbon nanotubes in the presence of nitronium ions ($NO_2^+$) [1]. To investigate the mechanism through which the nitronium ions selectively attack the metallic CNTs, leaving intact the semiconducting ones, we have performed Density Functional (DFT) calculations of the adsorption of nitronium ions and neutral nitrogen dioxide ($NO_2$) molecules on both metallic and semiconducting nanotubes. The calculations show that the nitronium ions bind to both, metallic and semiconducting tubes through a charge transfer mechanism. One electron is transferred from the tube to the LUMO of the nitronium ion that becomes the HOMO of a neutral $NO_2$ molecule (see Fig. 1) adsorbed onto a charged nanotube. The bonding in the semiconducting tubes is due almost exclusively to the charge transfer and very little further electronic density redistribution takes place, as can be seen in Fig.2 (left panel). However, in the case of metallic tubes, there is a substantial redistribution of the electronic density after the electron has been  transferred to the nitronium ion (see Fig.2, right panel). This redistribution leads to a stronger adsorption of the nitronium ions in the mCNTs (2.1 eV) than in the sCNTs (1.4 eV). Moreover, the geometric structure of the sCNTs remains almost unaffected upon adsorption whereas the structure of the mCNTs  relaxes outwards the tube in the vicinity of the adsorbed molecule. The adsorption of more than one nitronium ions is also analyzed.

On the other hand, the binding mechanism of neutral nitrogen dioxide molecules, $NO_2$, to CNTs is completely different. $NO_2$ molecules bind to the tubes through weak Van der Waals forces. A small charge transfer of about 0.2 e from the tube to the molecule also contributes to the molecular adsorption. The structure of both metallic and semiconducting tubes remains unaffected upon adsorption of these neutral molecules. The changes in the electronic structure of the tubes and a possible sensor effect are discussed.

From our results it becomes apparent that although the neutral $NO_2$ molecules can be adsorbed on CNTs through weak interactions, these molecules are not able to modify or destroy the nanotube structure. However, the relatively strong adsorption of nitronium ions on mCNTs  (stronger than on sCNTs) together with the structural changes taking place in those tubes upon adsorption of the nitronium ions provide the basis to understand the selective removal of the metallic tubes found in the experiments.

**References:**

[1] K.H. An, et al., J. Am. Chem. Soc., **127** (2005) 5196.

**Figures:**
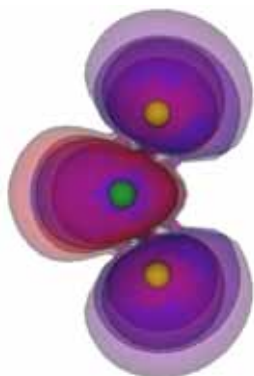


**Fig. 1.-** Highest occupied molecular orbital, HOMO, of the free neutral $NO_2$ molecule.

**(7,0)**          **(4,4)**
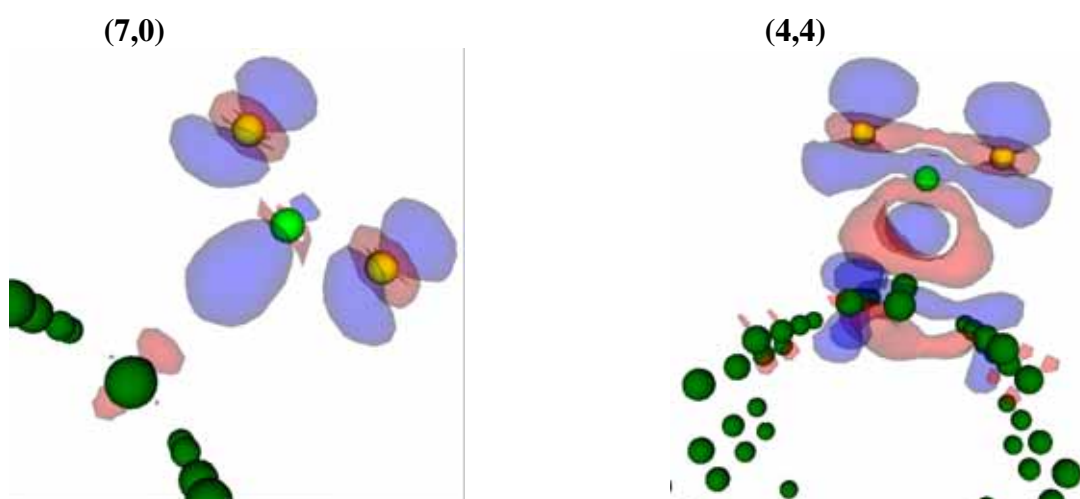


**Fig. 2.-**. Electronic density redistribution upon adsorption of a nitronium ion on a semiconducting (left) and a metallic (right) Carbon nanotube. Blue areas correspond to an increase of the electronic density and the red areas correspond to a reduction of the electronic density.

# STUDIES OF THE DEPENDENCE OF THE SWNTs LENGHT WITH THE GROWTH TEMPERATURE BY CVD

Vicente López[1], Lorena Welte[1], Miguel A. Fernández[1], Pedro J. De Pablo[2], Félix Zamora[1].

[1] Departamento de Química Inorgánica C-VIII, Universidad Autónoma de Madrid 28049 Madrid, Spain.
[2] Departamento de Física de la Materia Condensada C-III, Universidad Autónoma de Madrid 28049 Madrid, Spain.

vicente.lopez@uam.es

The goal of this work is to establish Chemical Vapour Deposition (CVD) conditions that affect the growth of SWNTs with the aim to generate as long as possible SWNTs to be useful for electronics, mechanical, and thermal transport applications.[1,2]

Casting solution of $Fe(NO_3)_3 \cdot 9H_2O$ concentration on a native silicon surface, produce an homogeneous distribution of particles of *ca.* 2 nm height. Adsorption of more concentrated $Fe(NO_3)_3 \cdot 9H_2O$ solutions give rise to inhomogeneous (height ranging from 5-20 nm) and less effective surfaces for the growth of SWNTs.

An interesting effect in the length and diameter of the SWNT has been observed in the CVD-growths.

Thus varying the CVD temperature from 800 to 950 ºC, the lengths of the SWNTs increase from $2.6 \pm 0.55$ μm to more than 30 μm (Figure 1). This effect, is reported herein for the first time, however similar observations have been done in MWNTs (with average diameters from 30 nm to 130 nm).[3] A feasible explanation to this phenomenon could be that the increase of growth rate with the temperature is due to the enhanced diffusion and reaction rates.

On the other hand, the diameters of the SWNT synthesized by CVD varying from $2.63 \pm 0.55$ µm (800 ºC) to >30 µm (950 ºC) (Figure 1). The migration rate of Fe particles on silicon surface increases with the temperature to facilitate iron aggregation and, therefore, inducing an increase on the SWNTs diameters.

Therefore, this work demonstrates that the temperature is an essential factor allowing the control on the length and diameter of the SWNT growth by CVD.

**Figures:**
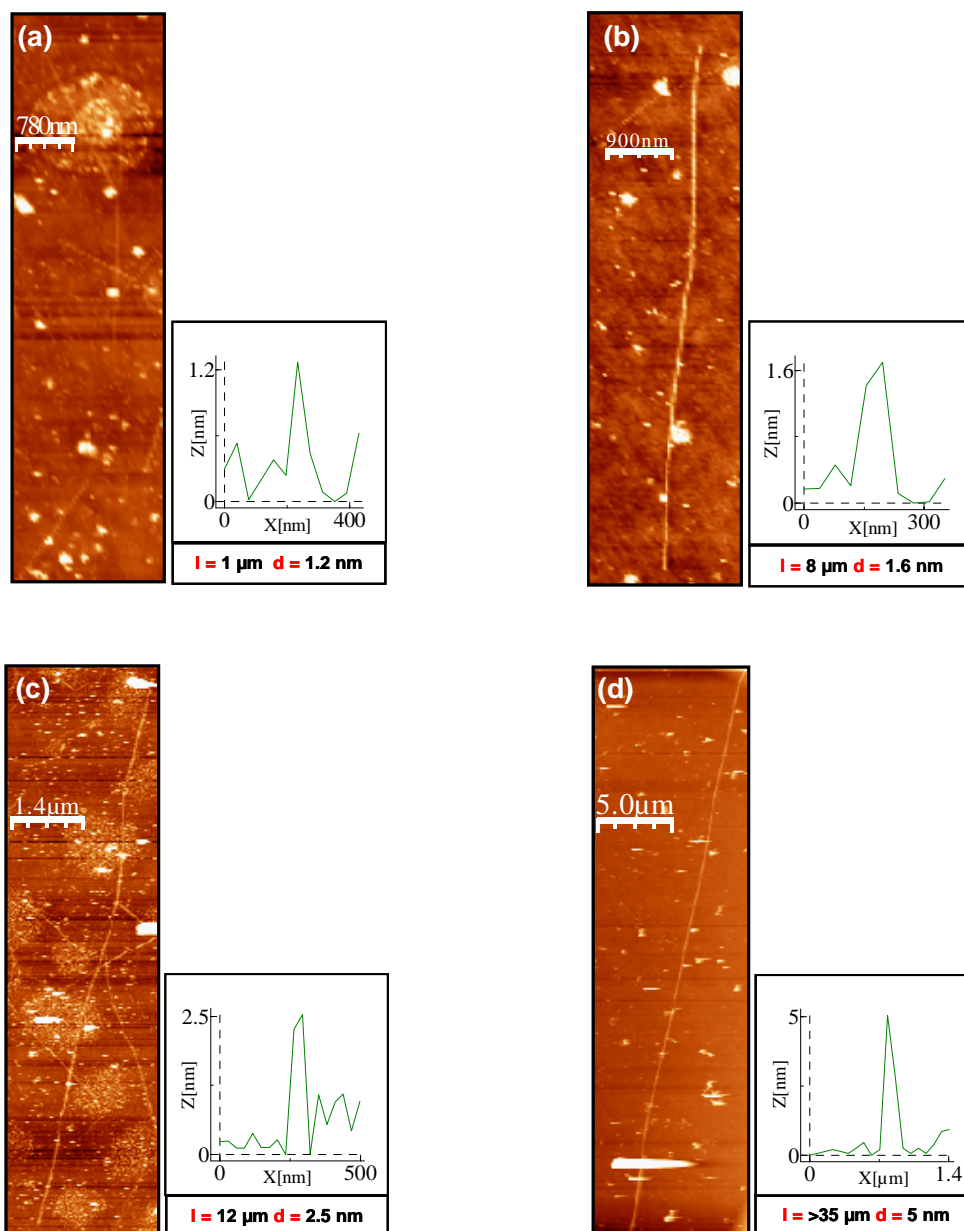


**Figure 1** AFM topography images of SWNT growth by CVD on silicon substrates:
(a) SWNTs growth at 800 ºC, length  2.63 ± 0.55 µm and diameter 1.7 ± 0.6 nm; (b) SWNTs growth at 850 ºC mean length  8.03 ± 1.73 µm and diameter 1.7 ± 0.7 nm; (c) SWNTs growth at 900 ºC length  10.87 ± 1.17 µm and diameter 2.1 ± 0.9 nm; and (d) CNTs growth at 950 ºC length  > 30 µm and diameter 10 nm.

**References:**

(1)    Wang, J. A.; Wang, J. S. *Appl Phys Lett* **2006**, *88*, -.
(2)    Tans, S. J.; Devoret, M. H.; Dai, H. J.; Thess, A.; Smalley, R. E.; Geerligs, L. J.; Dekker, C. *Nature* **1997**, *386*, 474-477.
(3)    Lee, C. J.; Park, J.; Huh, Y.; Lee, J. Y. *Chem Phys Lett* **2001**, *343*, 33-38.

# FORMATION OF IN SITU MN-DOPED ZnO STRUCTURES BY RAPID HEATING METHOD

*I. Lorite, F. Rubio-Marcos, J. F. Fernandez*
*Electroceramic Department, Instituto de Cerámica y Vidrio, CSIC,*
*Kelsen º5, 28049 Madrid, Spain*
ilorite@ivc.csic.es

In recent years, ZnO nanostructures have attracted much interest. ZnO with wurzite structures is an n-type semiconductor material with both good electrical and optical properties. To enhance the electrical/optical properties ZnO was usually doped with some dopants such as Al, Si, In [1]. Recently many investigations have paid attention to Mn-Doped ZnO and expect it to be one promising transparent diluted magnetic semiconductor to be used potentially in spintronic [2]. Several methods are used to fabricated structures, including aqueous solution growth methods, metal- organic chemical vapour deposition, thermal evaporation, hydrothermal method, and pulsed laser deposition, etc. In practicum it is no easy to control its shape and order its orientation of growth into three-dimensional arrays.

In this work Mn-doped ZnO multipods were produced from metallic Zn in air atmosphere. $MnO_2$ was used as substrate where metallic Zn wire was embedded by uniaxial double load pressing to obtain a disk shaped pellet. There is no other metal catalyst in the process. The $MnO_2$ disk containing the Zn wire was heated in an alumina crucible sealed with another alumina crucible. The oxidation process was attempted by a rapid temperature cycle at 1220º 6 minutes with heating and cooling rates >50ºC/min. After thermal cycling a yellowish structure was observed in the manganese disk. This structure had carpet type fibre morphology, figure 1. The fibres were supported directly on the manganese oxide sintered substrate. EDX microanalysis confirms the presence of nearby 2 wt % of manganese ions in the fibres.

If the experiment were performed with metallic Zn powder as reported previously [3] but under the same rapid thermal heating proposed in this work, two white and yellowish tetrapods type structures were obtained, figure 2. The white like cotton was collected outside of the alumina crucible and the yellowish one inside the alumina crucible.

To elucidate the influence of manganese in the fibres formation, XRD diffraction patterns were realized. The calculated lattice parameters of pure ZnO tetrapods were a=3.250 Å, c=5.207 Å that are similar than pure ZnO wurzite, meanwhile the lattice parameters of the carpet type fibres were a=3.251 Å, c=5.210Å that suggest an effective incorporation of Mn ions into ZnO structure.

Raman Spectroscopy shown a characteristic vibration spectra for ZnO tetrapopds but when carpet type fibres were analyzed a new vibration state at 521,5 cm$^{-1}$ can be observe characteristic of the Mn-doping in ZnO [3].

In summary it is possible to in situ synthesize Mn-doped ZnO structures having a carpet type fibre morphology by rapid heating method in air by using metal Zn and $MnO_2$ as substrate without additional catalyst system. Based on EDS microanalysis, XRD and Raman spectroscopy, the carpet type fibres were ZnO having Mn$^{2+}$ ions occupying the Zn sites.

**References:**

[1] J. Zhong, S Muthukumar, Y. Chen, Y. Lu, H.M.. NG, W. Jiang, E.L. Garfunel, Appl. Phys. Lett. 83 (2003) 3401
[2] P. Sharma et al., Nat Mat. 2(2003) 639
[3] L.W. Yang, X.L. Wu, G.S. Huang, T. Qiu, and Y.M. Yang, J. Appl. Phys. 87(2005)014308

**Figures:**
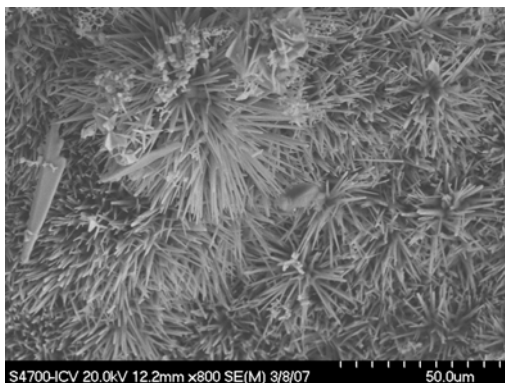


Fig 1: MEB micrograph of Mn-doped ZnO fibres.
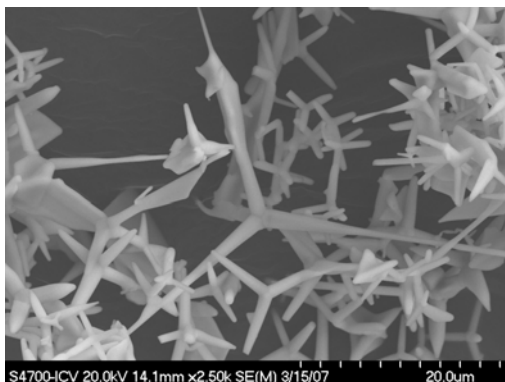


Fig 2: MEB micrograph of pure ZnO tetrapod
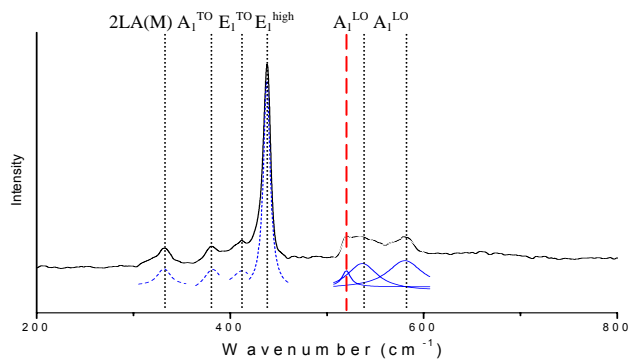


Fig3. Room temperature Raman spectra of Mn:ZnO carpet type fibres. The black line corresponds to the experimental spectra and the blue lines to the Lorentz fitting.

# Study of energy transfer in mixed system of two different sized quantum dots

*W. Lü,[1] I. Umezu,[1,2] and A. Sugimura,[1,2]*
*[1]Quantum Nanotechnology Laboratory, Konan University, Kobe 658-8501, Japan*
*[2]Department of Physics, Konan University, Kobe 658-8501, Japan*
*luwei@certer.konan-u.ac.jp*

It is important to investigate resonance energy transfer (RET) between quantum dots (QDs) because RET provides an approach for communication and coupling between QDs which is one of the central themes in numerous scientific efforts of present physical and technological interest [1, 2].

In this work, we characterized energy transfer process in mixed system of two different sized CdSe QDs by steady-state and time-resolved photoluminescence (PL) spectroscopy. Two kinds of CdSe QDs (2.6nm and 4nm in diameters) were used in this work. The concentration of small dots (donor) was 18.4nmol/ml and that of large dots (acceptor) was 10.4nmol/ml. The mixed sample was dispersed in toluene solvent (the concentration of small dots is 13.2nmol/ml and that of large dots is 3nmol/ml). The mixed solution was put in a quartz cell. The steady-state and time-resolved PL spectra were observed during evaporation of the solvent.

Figure.1 shows PL band variation of mixed sample with the increasing evaporation time. The PL emission band is composed of small QD emission (peak around 556nm) and large QD emission (peak around 586nm). It should be noticed that the both emission intensities of small and large dots drop monotonously with increasing evaporation time. This is called concentration quenching [3] originated from energy transfer between the same sized QDs. With increasing evaporation time, the PL intensity ratio of small to large QDs in PL band gradually decreases. The emission of small QDs is finally depressed by that of large QDs, which can be explained by RET process from small to large QDs [4, 5]. In order to confirm RET from small to large dots in mixed system, time-resolved PL spectra of small and large QDs are investigated in pure and mixed systems. The results show that the lifetimes of both small and large dots in mixed solution are the same as that of QDs in pure solution. However, compared with lifetimes of small and large QDs in pure solid films, in the mixed solid film the lifetime of the small QDs decreased while that of the large QDs increased, which can not be explained by concentration quenching. The observations strongly indicate that the transfer of excitation energy from small to large QDs is consistent with RET mechanism [4, 5]. We modeled our system using a proposed equation system. The RET rate from small to large dots and nonradiative recombination rate originated from concentration quenching are quantitatively estimated to be 0.13ns$^{-1}$ and 0.08ns$^{-1}$, respectively. The variation of integrated intensity ratio of small to large dots during the evaporation is shown in Fig.2. Three stages can be distinguished during the evaporation: initial stage (before 12.5min), transition stage (12.5-22.5min), and final stage (after 22.5min). In transition stage, since the ratio drastically decreases accompanied by the emission depression of small dots by that of large dots, we suggest that RET rate from small to large dots begins to increase in this stage. The effect of distance between small and large dots on RET in the three stages is evaluated.

**References:**

[1] S. A. Crooker, J. A. Hollingsworth, S. Tretiak, and V. I. Klimov, Phys. Rev. Lett. **89** (2002) 1868021.

[2] A. Imamoglu D. D. Awschalom, G. Burkard, D. P. DiVincenzo, D. Loss, M. Sherwin, and A. Small, Phys. Rev. Lett. **83** (1999) 4204.

[3] E. Snoeks, P.G. Kik, and A. Polman, Optical Materials. **5** 196 (1996).

[4] D. L. Dexter, J. Chem. Phys. **21** (1953) 836.

[5] Th. Förster, in *Comparative Effects of Radiation,* edited by M. Burton, J. S. Kirby-Smith, and J. L. Magee (Wiley, New York, 1960).

**Figures:**
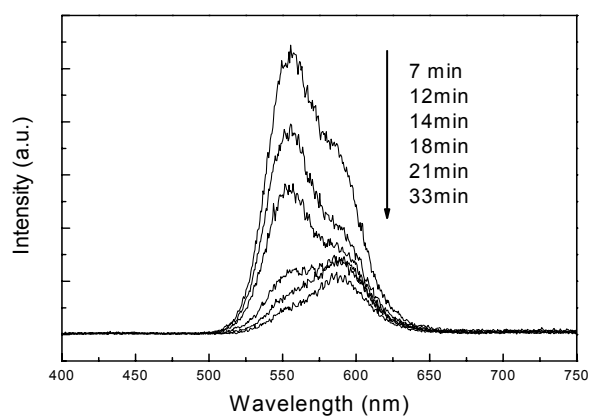


Fig.1: The PL band variation of mixed sample with the increasing evaporation time.
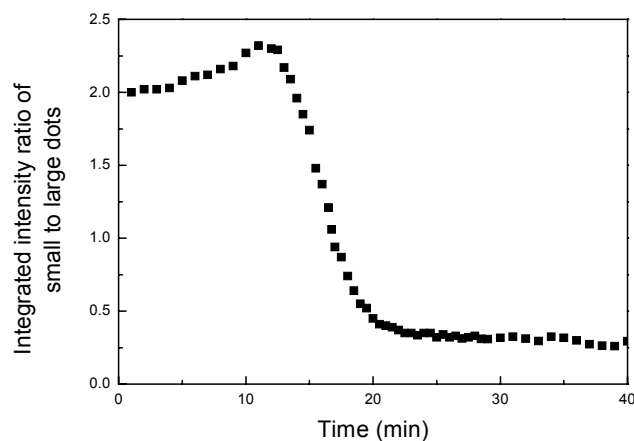


Fig.2: The variation of integrated intensity ratio of small to large dots with the increasing evaporation time.

# Multiwalled carbon nanocoils synthesized by the catalyst of uniformly composed Fe-Sn

*L. Pan[1], R. Kanada[1], S. Akita[1], K. Hirahara[2], N. Okazaki[3] and Y. Nakayama[1,2]*
*[1]Department of Physics and Electronics, Osaka Prefecture University, 1-1 Gakuen-cho,*
*Naka-ku, Sakai, Osaka 599-8531, Japan*
*[2]Department of Mechanical Engineering, Osaka University, Japan*
*[3]Osaka Science and Technology Center, Japan*
*pan@pe.osakafu-u.ac.jp*

Carbon nanocoil (CNC) is a kind of promising nanomaterial, that can be widely applied to electromagnetic wave absorber, parts for nano electromechanical systems, field-emission devices [1] etc. CNCs have been successfully synthesized by the catalysts of Fe/ITO [2] or Fe-In-Sn-O [3] so far. However, CNCs synthesized by these catalysts are lack of crystallinity, which may result in their relatively lower mechanical strength and electric conductivity compared with the normal multiwalled carbon nanotubes (CNTs). We have developed a new method to prepare the thin catalyst film, in which Fe and Sn clusters are uniformly composed. It is found that this method is valid in synthesizing CNCs that have much higher crystallinity than conventional CNCs.

Thin films consisting of Fe and Sn clusters were prepared by an arc plasma discharge method, where two sources of Fe and Sn can be evaporated alternatively or simutaniousely to fabricate the Fe-Sn thin films by co-deposition or by layer-by-layer deposition on $SiO_2$/Si substrates as shown in Fig. 1. The compositions of Fe and Sn in the films were controlled by the number of pulse discharge. The samples were then annealed at 150°C in air for 12 hours in order to oxidize the catalysts to prevent the Sn from vaporization during heating process. Carbon nanocoils were synthesized by the thermal CVD at 700°C for 15 min by introducing acetylene gas of 30 sccm in a He flow with a rate of 230 sccm.

Figure 2 shows the AFM images of the changes of the catalyst surfaces of co-deposited 4-nm-thick Fe-Sn (a) as deposited, (b) after annealing in air, (c) after heating to 700°C, and (d) after 1 s acetylene supply, respectively. It is found that the process of (a) to (c) is similar to that of a 4-nm-thick Fe film used for growth of multiwalled CNTs. The large difference appears in the process (d) where large particles with the diameters of larger than 40 nm are formed in the Fe-Sn catalyst, whereas only particles with diameters of 10 to 20 nm are formed in the case of thin Fe film. This is speculated to be resulted from the Sn, which has a lower melting point and a different surface energy from Fe. It is revealed by SEM observation that the CNCs are grown in a higher yield by the co-deposited Fe-Sn than by the multilayered catalyst, suggesting that the uniformly composed Fe-Sn catalyst is more valid in synthesizing CNCs. The coil diameters of grown CNCs are less than 100 nm, which are thinner than those of the conventional CNCs synthesized by the Fe/ITO catalysts [2]. The line diameters of these CNCs are around 20 nm, which is the same as the CNTs grown under the same CVD conditions by Fe catalyst. Figure 3 shows the TEM images of a grown CNC, composed of a coiled CNT with some strains in its body, which is called multiwalled CNC. It is also found that the multiwalled CNCs have a possible base growth mechanism, which is different from that of conventional CNCs with a tip growth mechanism [2]. The high potential of the thinner and high crystallized multiwalled CNCs indicates that they would have wide applications in new nanotechnology.

**References:**

[1] L. Pan, T. Hayashida, and Y. Nakayama Jpn. J. Appl. Phys. **40** (2001) L235.
[2] M. Zhang, Y. Nakayama, and L. Pan, Jpn. J. Appl. Phys. **39** (2000) L1242.
[3] T. Nosaka, O. Suekane, and Y. Nakayama: Abstr. Int. Conf. Science and Application of Nanotubes, 2003, p. 42.

**Figures:**
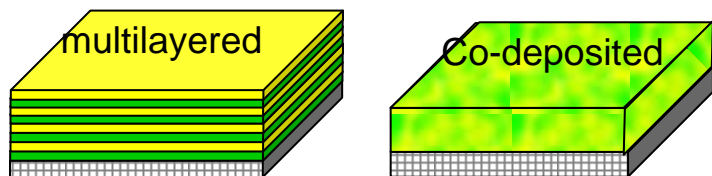


Fig. 1. Structures of two kinds of deposited Fe-Sn thin films
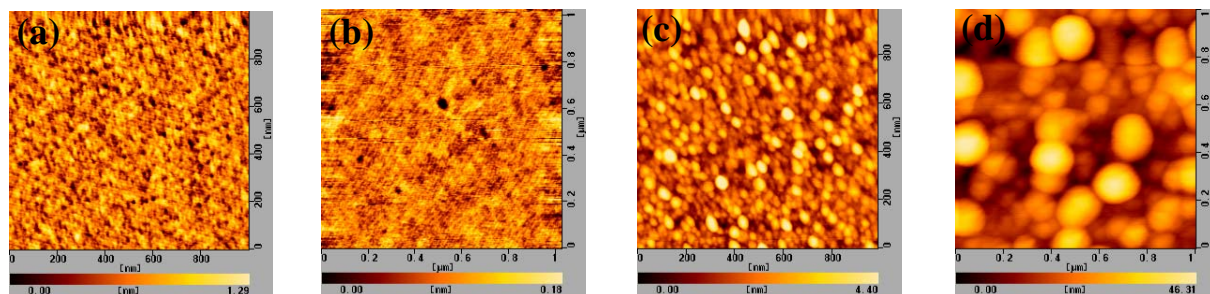


Fig. 2. AFM images of the surfaces of the co-deposited Fe-Sn catalyst (a) as deposited, (b) after annealing in air, (c) after heating to 700°C, and (d) after 1 s acetylene supply.
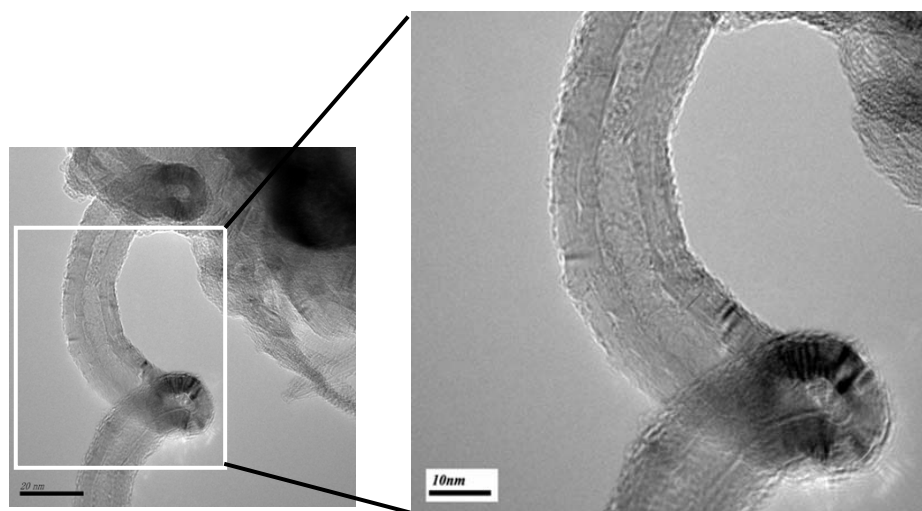


Fig. 3. TEM images of a synthesized CNC

# DEPHASING EFFECT IN A*B INITIO* MODELING OF QUANTUM TRANSPORT THROUGH MOLECULAR DEVICES

*Jesse Maassen*, *Hong Guo,* and *Yu Zhu*
*Center for the Physics of Materials and Department of Physics, McGill University, 3600
University, Montreal, Quebec, Canada H3A 2T8*
*maassenj@physics.mcgill.ca*

In recent years much attention has been directed towards the development of nanometer scale devices. This interest has been mainly fuelled by the advancements in experimental micro/nano-fabrication methods as well as the search for alternative electronic devices that bypass the upcoming miniaturization limits of CMOS technology [1] where certain undesirable quantum effects appear. It is clear that self-organised nanostructures, such as molecules and carbon nanotubes, are excellent candidates for sub-micron electronic systems and will potentially play a crucial role in future technologies. Electron transport in these systems is partially coherent, that is interference effects are present but attenuated due to interactions. Therefore theoretical tools allowing one to accurately design and predict the characteristics of nanodevices from an atomistic viewpoint are of growing importance.

In this work, we study the effect of decoherence on the current-voltage (*I-V*) characteristics of a benzene molecule connected to carbon nanotube leads (see fig. 1) using a self-consistent *ab initio* technique. For calculating nonequilibrium quantum transport (i.e. any external bias potential) properties of atomic/molecular electronic devices, we employ the first principles density functional theory (DFT) approach used in parallel with nonequilibrium Green`s functions (NEGF) [2,3]. DFT allows us to find the energy levels of the system and once this is known we can determine the nonequilibrium density matrix from NEGF. The self-consistent procedure is shown in fig. 2. This DFT-NEGF *ab initio* formalism permits us to study open quantum systems composed of a central region (i.e. the molecule) and the connecting semi-infinite leads, in which the particular atomic structure and effective electron potential are calculated. This powerful technique has been shown to be very useful and accurate, in comparison with experimental data, in many atomic/molecular scale systems [4-7].

A drawback of this method is that transport is entirely coherent. In real devices inelastic collisions result in partial and eventually complete loss of coherence. These processes must be included in the calculations in order to accurately simulate nanoscale devices. It is possible to include *ab initio* electron-phonon interactions, but this becomes impractical for systems larger than several atoms. Using the fictitious voltage probe model proposed by Büttiker [8] in the NEGF formalism, we have worked out a single-parameter analytical method of introducing dephasing in a quantum device of any size. This result is expressed simply as a modified transmission coefficient *T* given by the sum of a coherent and an incoherent contribution.

In Büttiker`s approach, typically employed in quantum dot or 1D atomic chain systems, the energy levels found in the central region of the device are connected to artificial electron reservoirs via fictitious voltage probes. A certain fraction of electrons, determined by the value of the adjustable parameter, travelling through the central region will scatter into a reservoir losing their phase memory before being reinjected into the device. The conservation of current is imposed by choosing the chemical potential in each reservoir so no net current flows through the fictitious probes. This condition is automatically satisfied in our expression of *T*. We show that our result is a generalization of Büttiker`s original result for a single scatterer. The effect of decoherence is included into the calculations, by matrix multiplication, once the DFT-NEGF procedure has achieved self-consistence (see fig. 2). The main advantages of this tool are it`s simplicity and the fact that is does not add any computational

time. Eventually, using this method, we hope to analyse complex nanocircuits in which the connecting partially coherent elements would be partitioned.

We shall present the total transmission coefficient *T* as a function of energy for different values of applied voltage and dephasing constant. We shall also show a plot of the current versus the applied voltage for different values of dephasing constant. Note : We expect to obtain all simulated results before long.

**References:**
[1] Y. Taur, IBM Jour. Res. Dev., **46** (2002) 213.
[2] J. Taylor, H. Guo, and J. Wang, Phys. Rev. B, **63** (2001) 245407; **63** (2001) 121104.
[3] Y. Xue, S. Datta, and M. A. Ratner, J. Chem. Phys., **115** (2001) 4292; Chem. Phys., **281** (2001) 151.
[4] D. Waldron, V. Timoshevskii, Y. Hu, K. Xia, and H. Guo, Phys. Rev. Lett., **97** (2006) 226802.
[5] T. Frederiksen, M. Brandbyge, N. Lorente, and A.-P. Jauho, Phys. Rev. Lett., **93** (2004) 256601.
[6] C. C. Kaun, B. Larade, and H. Guo, Phys. Rev. B., **67** (2003) 121411(R).
[7] C. C. Kaun and H. Guo, Nano Lett., **3** (2003) 1521.
[8] M. Büttiker, Phys. Rev. B., **33** (1986) 3020; IBM Jour. Res. Dev., **32** (1988) 63.

**Figures:**
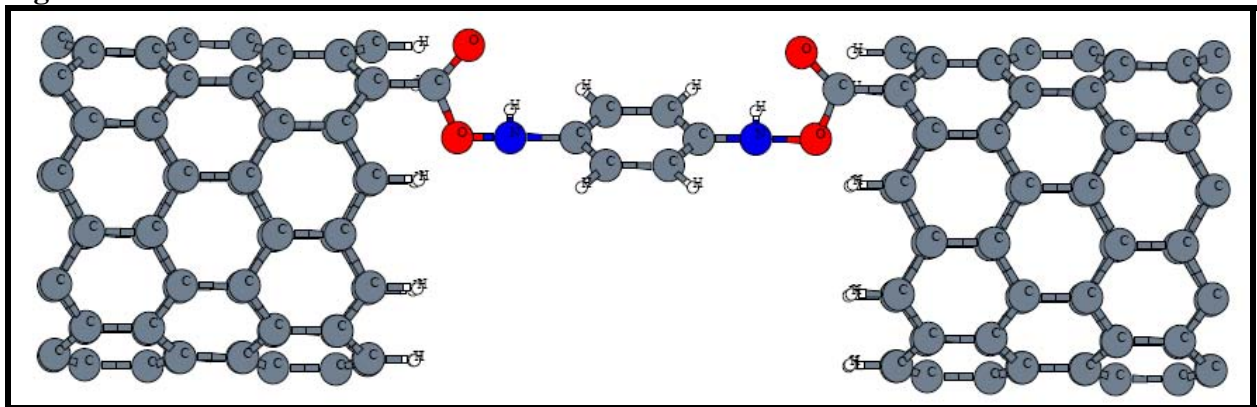


Figure 1 : Benzene molecule coupled to carbon nanotube leads.
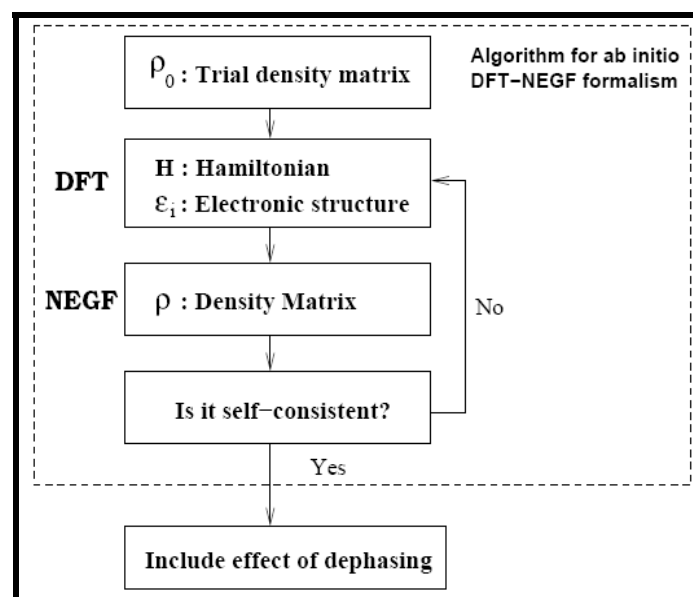


Figure 2 : Algorithm for DFT-NEGF formalism.

# USING STANDING WAVES FOR COMMUNICATIONS MIGHT WORK FOR CROSSBAR ARCHITECTURES

*Basheer A. M. Madappuram*[1,2], *V. Beiu* [1,2], *Peter M. Kelly*[1], *Martin McGinnity*[1]
[1]*School of Intelligent Systems, University of Ulster*
[2]*College of Information Technology, United Arab Emirates University, UAE.*
*basheera@uaeu.ac.ae; VBeiu@uaeu.ac.ae; tm.mcginnity@ulster.ac.uk,*
*pm.kelly@ulster.ac.uk*

Transmission line analysis is taking more significance as we are integrating billions of components in the smallest possible area [1]. More importantly, transmission lines consume power depending on their characteristics. The massive integration of components results in huge numbers of connecting wires. The total effect on power consumption of the connecting wires is already significant. Any attempt to minimise the power consumption dissipated on the connecting wires would result in significant reduction of the power consumed by the whole system [1, 2].

In this study, wires are precisely modelled in spice by including not only their resistive and capacitive but also inductive components. The behaviour of the circuit is simulated by applying an AC source and sweeping the frequency from 10Hz to 100GHz. Figure1 shows a simple RC circuit and its frequency response plot. As the frequency increases, the capacitive reactance decreases, which results in more power consumption. Figure 2 represents a precise model for a connecting wire. The behaviour is studied with RC load. Input current and load current are measured by sweeping the frequency over the entire range in steps of 100 points per decade. Current versus frequency plot in Figure 2 shows that, at the resonant frequency (1.4 KHz in simulated model) the current dissipated on the wires is significantly reduced. This raises questions with respect to alternative ways for low power communication relying on precise frequency sine modulation.

Therefore, if the transmitted signal is from a narrow region of around the resonant frequency, the loss from the connecting wires can be reduced considerably. In normal VLSI, the path length and path shape varies, each of these wires will have its own response characteristics making it impossible to exploit and implement any particular resonant frequency. A solution for this problem could be to consider implementing this idea on Crossbar Architecture[3, 4]. We can reasonably assume, equal length and shape of the connecting wires in Crossbar Architecture would lead to unique response characteristics for the entire Crossbar based circuit. At the resonant frequency of the Crossbar based circuit, the power dissipated on the connecting wires will be minimised. So we can think of using standing waves[5], which is at the resonant frequency of the Crossbar based circuit, for communication with significantly reduced power dissipation on the connecting wires. In distributed integrated systems multiple parallel signal paths and devices will be working in harmony to perform a desired task [6]. Standing waves will be the ideal choice in these types of systems because of its inherent Crossbar architecture

CONCLUSION
This paper precisely simulates a wire model by including not only their resistive and capacitive but also inductive components. Simulation shows significant reduction in power dissipation at the resonant frequency. By theoretical analysis, it is suggested that standing waves at the resonant frequency of the Crossbar based circuit can be used for the communication purposes. This might be an alternative way to realise low power communication.

**References:**

[1]     V. Beiu, "Limits. Challenges, and issues in nano-scale and bio-inspired computing," in *M.M. Eshaghian-Wilner (Ed.), Bio-inspired and Nano-scale Integrated Computing, John Wiley & Sons,* in progress, 2007/8

[2].    V. Beiu and W. Ibrahim, "On computing nano-architectures using unreliable nano-devices " in *S.E. Lyshevski(Ed.): Nano and Molecular Electronics Handbook, London,UK:Francis & Taylor,* in press, 2007.

[3]     A. Raychowdhury and K. Roy, "Performance estimation of molecular crossbar architecture considering capacitive and inductive coupling between interconnects," *IEEE Transaction on nanotechnology,* pp. 445 - 448, 2003.

[4]     M. M. Ziegler and M. R. Stan, "CMOS/Nano Co-Design for Crossbar-Based Molecular Electronic Systems," *IEEE Transaction on nanotechnology,* vol. 2, pp. 217 - 230, 2003.

[5]     F. O'Mahony, C. P. Yue, M. Horowitz, and S. S. Wong, "Design of a 10GHz Clock Distribution Using Coupled Standing-Wave Oscillators," in *IEEE International Conference on Solid-State Circuits*, pp. 428 - 504, 2003.

[6]     A. Hajimiri, "An Alternative Approach to High-Frequency Design," in *IEEE Communications Magazine,* February 2002.

**Figures:**
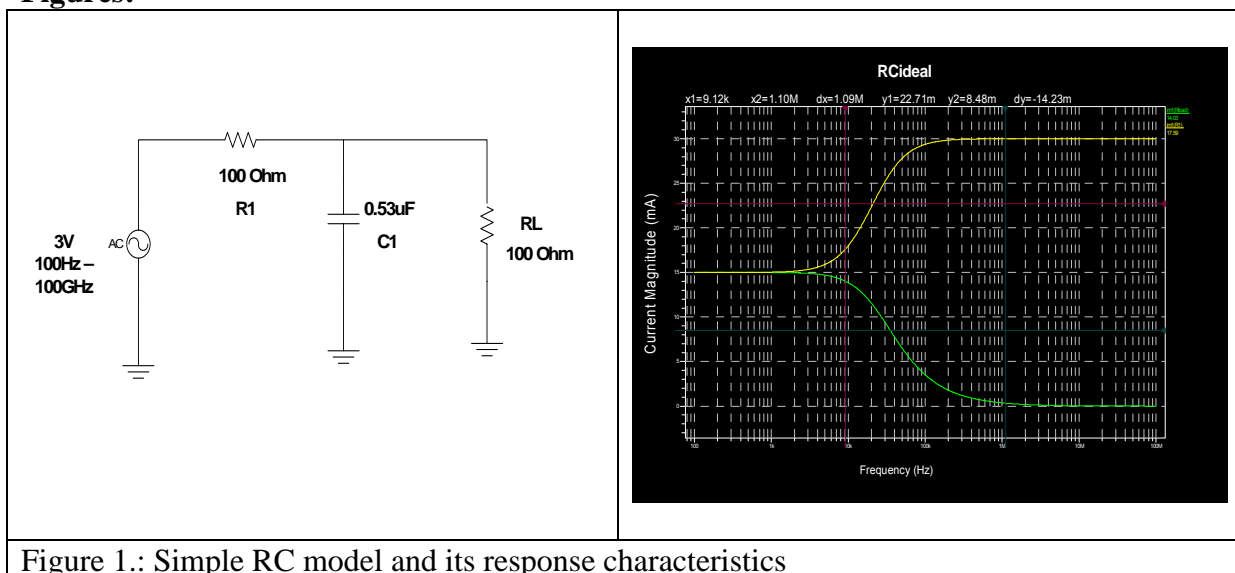


Figure 1.: Simple RC model and its response characteristics
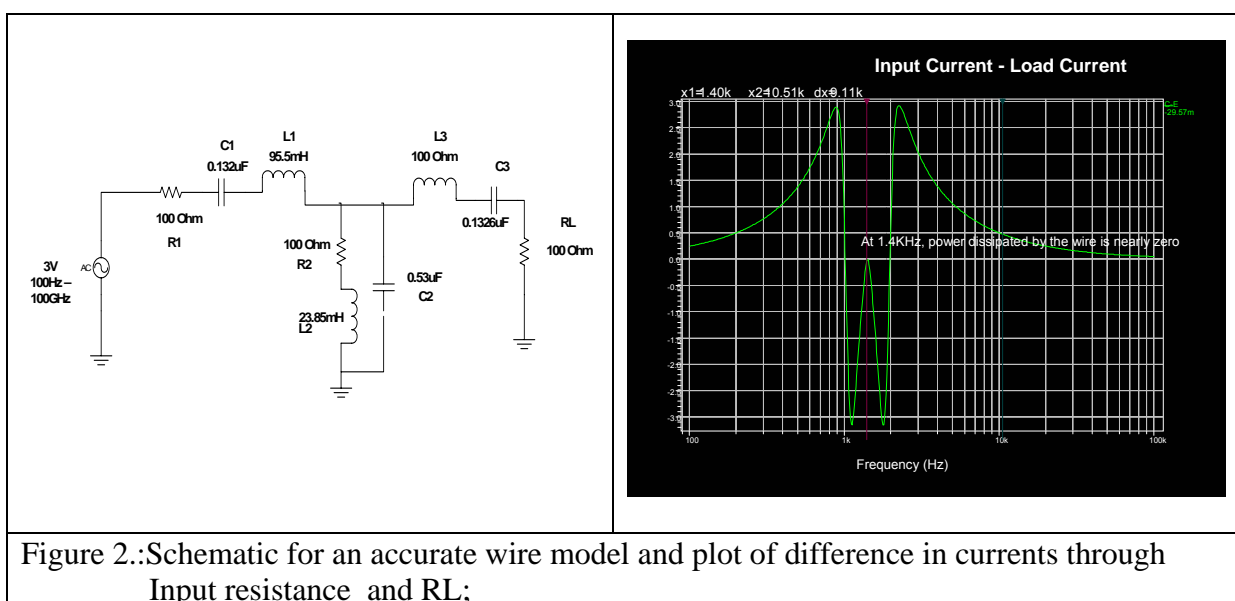


Figure 2.:Schematic for an accurate wire model and plot of difference in currents through Input resistance  and RL;

# SYNTHESIS AND FUNCTIONALIZATION OF SUPERPARAMAGNETIC IRON OXIDE NANOPARTICLES WITH GUM ARABIC (GA) AS A SUPPORT FOR ENZYME IMMOBILIZATION

**Mahmood, Iram**
Laboratory of Separation Sciences and Engineering,
Institute of Process Engineering, Chinese Academy of Sciences
Zhongguancun N 1, St 2, P.O.Box 353 Beijing 100080 PRChina
Ph: +861062555005    Fax: +861062554264
Email:  iram@home.ipe.ac.cn

Emerging applications

**Summary**
During synthesis, iron oxide nanoparticles tend to agglomerate. In order to obtain biocompatible and well-dispersed particles, $Fe_3O_4$ nano-particles were synthesized and modified with GA and well characterized by TEM, VSM, XRD, FTIR, TGA and Zeta Potential. Further, their potential use as a support for enzyme immobilization was also investigated.

**Background**
Magnetic nanoparticles of iron oxides have many important applications in the fields of magnetic resonance imaging (MRI) contrast agent, enzyme and protein separations, targeted drug delivery, magnetic Ferro fluids, and so forth. Most of these applications require the magnetic nanoparticles to be chemically stable, uniform in size, and well-dispersed in liquid media. Due to the anisotropic dipolar attraction, unmodified magnetic nanoparticles of iron oxides tend to aggregate into large clusters and thus lose the specific properties associated with single-domain Novel and easy methods have been developed for preparation of superparamagnetic particles stabilized by surface modification. It has been postulated that the glycoprotein in GA is capable of strong binding interactions due to the electrostatic attraction between a negatively charged group of a GA molecule and a positive site on the oxide surface (Leong YK, *et al*. 2001. Colloids and Surfaces A 182:263-68).

**Methodology**
Superparamagnetic $Fe_3O_4$ nanoparticles were synthesized by coprecipitation method and were fully characterized by TEM, VSM, FTIR, and XRD (Zhiya Ma *et al:* J Polym Sci A Polym Chem 43, 3433–3439, 2005). Particles were functionalized by coating their surfaces with GA to improve biocompatibility (Darryl N.*et al*. Journal of Nanoparticle Research (2006) 8: 749–753) as well as support for Lipase immobilization. For the immobilized lipase, hydrolysis of oleic acid, glycerol and olive oil was compared. Before immobilization, lipase was pretreated with these substrates to effectively block the enzymes active sites, to avoid nonspecific binding. Such activated particles were then used for immobilization

**Results and Conclusions**
TEM images were taken of magnetite particles and coated GA. In both cases, the average primary particle size between 5 and 10 nm was observed. The results from TEM indicated that the GA-treated nanoparticles formed smaller agglomerates as compared to the untreated samples. FTIR spectra confirmed the efficient functionalization of particles surface with GA. TGA analysis data showed that GA has a strong affinity toward the particle surface, contributing to steric

stabilization, which therefore, prevented the nanoparticles from further agglomeration. Zeta potential was also measured, as well as a highest magnetization of 21.5 emu/g was noted.

An adsorbed GA glycoprotein molecule contains both adsorbed and free carboxylate and amino groups. The free carboxylate groups attach to the particle surface when the negatively charged group of GA binds to a positive site on the surface of the iron oxide.. The natural polymer has a strong affinity for the oxide surface due to the binding of the carboxylate groups to sites along the oxide surfaces.

# The Study on Structural Properties of Simulated Nano Webs by Image Processing Method

*M.Maleki, M.Latifi, M.Amani-Tehran, A.Ghare-Aghaji*
*Department of Textile Engineering, Amirkabir University of Technology (Tehran Polytechnic), Tehran, Iran*
*m_maleki84@aut.ac.ir*

Nano webs have the potential of numerous applications such as medical, filtration, composite, army garments, protective clothing material, insulation, tissue engineering, intelligent textiles etc. It is very important to know structural characteristics of nano webs for determining and controlling their mechanical & physical properties. These characteristics are including, fiber diameter distribution, fiber orientation distribution, web density, pore size & shape, fiber bonding and uniformity of nano webs. . Thus, quality and quantity evaluation and measuring of these parameters can determine the compatibility of them to their end-uses. Furthermore, it's a useful tool for evaluation of nano webs produced in industry.

Image processing techniques are utilized for extracting fiber diameter distribution, fiber orientation distribution, pore size & shape, fiber bonding and uniformity of nano webs from their images. The orientation distribution function is a function of angle a. The mean orientation direction and its standard deviation are given by a new way of direct tracking method. Fiber diameter of nano webs are estimate by considering horizontal and vertical diameter and related equations. The pore structure of nano webs is quite complex and their shape can't be characterized by a single measure. Several indexes have been defined to specify shape characteristics. Fiber bonding is also determined since it has an important role in mechanical and physical properties of nano webs. In order to define uniformity of nano webs, web images are broken up into number of windows. For each window area density is recorded and uniformity index is measured.

In the present research, Structure and morphology of the simulated nano webs are studied. Therefore, with suitable simulated images and image processing method can propose an applied way for industry to determine and optimize products properties easily and shortly.

**Figures:**



Orientation distribution      Diameter distribution      Pore size
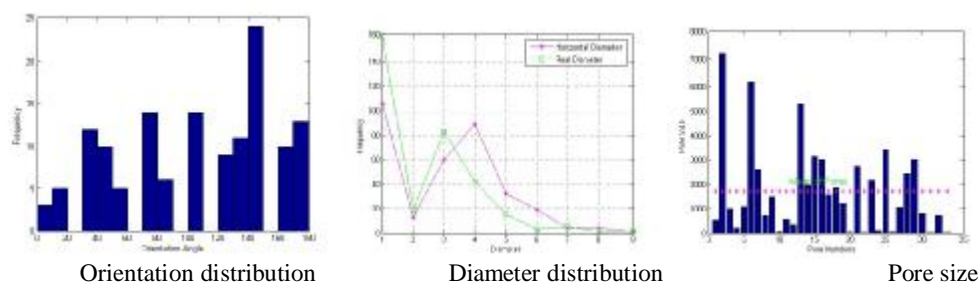
**References:**

[1]  Grafe, T., Graham, K., "Polymeric Nanofibers and Nanofiber Webs: A New Class of Nonwovens", *International Nonwovens Technical Conference*, INTC, pp.1-13, 2002.
[2]  Subbial, T.,et all, "Electrospinning of Nanofibers", *Wiley InterScience*, pp.1-13, 2004.

[3] Laurencin, C.T., Nair, L.S., "Polyphosphazene Nano Fibers for Biomedical Applications: Preliminary Studies", pp.281-300

[4] Velu, Y., Farer, R., Ghosh, T., Seyam, A., "Formation of Shaped/Molded Meltblowing Nonwoven Structures", *JTATM*, Vol.1, Issue.1, pp.4-13, 2000.

[5] Grafe, T., Graham, K., "Polymeric Nanofibers and Nanofiber Webs: A New Class of Nonwovens", *International Nonwovens Technical Conference*, INTC, pp.1-13, 2002.

[6] Pourdeyhimi, B., Ramanathan, R., Dent, R., "Measuring Fiber Orientation in Nonwovens, partI: Simulation", *Textile Research Journal*, Vol.66, No.11, pp.713-722, 1996.

[7] Pourdeyhimi, B., Dent, R., Davis, H.," Measuring Fiber Orientation in Nonwovens, partIII: Fourier Transform", *Textile Research Journal*, Vol.67, No.2, pp.143-151, 1997.

[8] Pourdeyhimi, B., Kim, H.S.," Measuring Fiber Orientation in Nonwovens: The Hough Transform", *Textile Research Journal*, Vol.72, No.9, pp.803-809, 2002.

[9] Pourdeyhimi, B., Dent, R.," Measuring Fiber Orientation in Nonwovens, partIV: Flow Field Analysis", *Textile Research Journal*, No.3, pp.181-187, 1997

[10] Pourdeyhimi, B., Ramanathan, R., Dent, R.," Measuring Fiber Orientation in Nonwovens, partII: Direct Tracking", *Textile Research Journal*, Vol.66, No.12, pp.747-753, 1996.

[11] Pourdeyhimi, B., Dent, R.," Measuring Fiber Diameter Distribution in Nonwovens", *Textile Research Journal*, Vol.69, No.4, pp.233-236, 1999.

[12] Aydilek, A.H., Oguz, S.H., Edil, T.B., "Digital Image Analysis to Determine Pore Opening Size Distribution of Nonwoven Geotextiles", *Journal of Computing in Civil engineering*, pp.280-290, Oct 2002.

[13] Image Processing Toolbox User's Guide, MATLAB 7.0

[14] Pourdeyhimi, B., "Image Processing Basics", 1994.

[15] Noesis S.A., "A Tutorial on Image Processing", Manchester Computing Center, University of Manchester, 1991.

[16] Chhabra, R.," Nonwoven Uniformity-Measurements Using Image Analysis", *INJ*, pp.43-50, 2003.

# STUDY OF AUGER CVV LINESHAPES FROM SINGLE WALLED CARBON NANOTUBES.

*A. Sindona, <u>S. Maletta</u>, M. Commisso, A. Bonanno, P. Barone, P. Riccardi, G. Falcone*
*Dipartimento di Fisica, Universita` della Calabria, Via P. Bucci 31C, 87036 Rende (CS),*
*INFN, Gruppo collegato di Cosenza, Italy*
*<u>Sindona@fis.unical.it</u>*

We present a model to describe Auger CVV lineshapes from bundles of clean and $Na^+$ irradiated single-walled carbon nanotubes, specifically examining shake up processes in both metallic and semiconducting bands, with energy gaps below 1 eV.

Auger electrons are ejected by a primary electron beam of 1.8 keV and acquired either with the clean sample or after $Na^+$ bombardment at different temperatures (see Fig.1).

Using the tight binding approach, we determine the effect of the suddenly created core hole, in the 1s-state of a carbon atom, on the many electron states of $\pi$ and $\pi*$ bands of the target material.

We compute the energy distributions of many body excitations, created at the expense of ejected electrons in (10, 10) and (16, 0) tubes, thus, obtaining the core hole propagator in tubes with different chirality, as function of the concentration Na+ atoms.

We find a good agreement between the theory and the experiments.

**References:**

References

[1] A. Sindona, R. A. Baragiola, G. Falcone, A. Oliva, and P. Riccardi, Phys. Rev. A 71, 052903 (2005)

[2] A. Sindona, S.A. Rudi, S. Maletta, R.A. Baragiola, G. Falcone and P. Riccardi, Surf. Sci. 601, 1205 (2007)

[3] A. Sindona, F. Plastina, A. Cupolillo, C. Giallombardo, G. Falcone and L. Papagno, Surf. Sci., in press (Available online 22 December 2006)

**Figure 1**
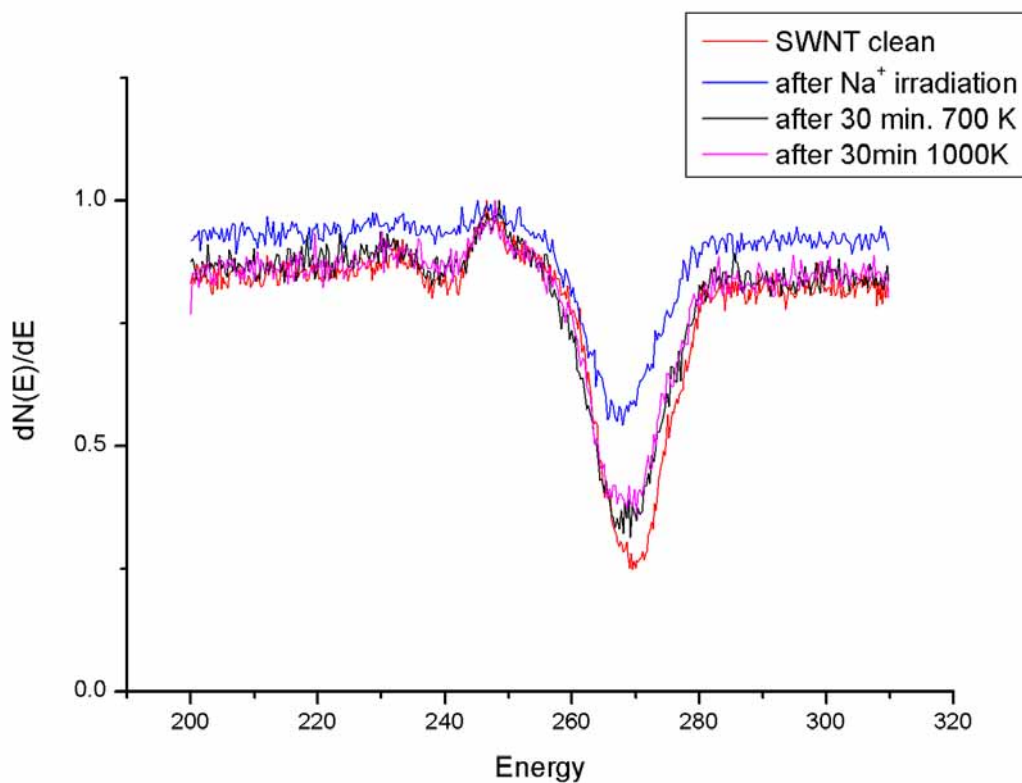
# ELECTRONIC PROPERTIES OF SINGLE WALL CARBON NANOTUBES BONDED TO Al$_{13}$H CLUSTER

*A. Mañanes[1], F. Duque[1], M. J. López[2] and J. A. Alonso[2]*
*[1]Departamento de Física Moderna, Universidad de Cantabria, 39005 Santander, Spain*
*[2]Departamento de Física Teórica, Atómica y Óptica, Universidad de Valladolid,*
*47011 Valladolid, Spain*
*angel.mananes@unican.es*

We analyze the equilibrium geometries and the changes in the electronic properties of single walled carbon nanotubes SWCNT when they interact with clusters of metallic elements. We have chosen the magic cluster Al$_{13}$H which, due to its high stability, could be synthesized and manipulated to modify the properties of electronic nanodevices based on carbon nanotubes.

It is well established that the presence of clusters of metallic elements on SWCNTs can produce novel electronic properties as it has been shown in detailed experimental analysis of the interaction between those clusters and SWCNTs [1]. Furthermore, recent detailed calculations [2] indicate that the aluminium cluster Al$_{13}$ adsorbed on the walls of SWCNTs can appreciably modify the electrical conductance of the system when a molecular spice is adsorbed on the active sites of the nanocluster, a modification which is ruled by the charge transfer upon the adsorption of the molecule.

Our calculations are performed within density functional theory using the ADF 2006.01 code. Both LDA and GGA approximations for the exchange correlation energy are considered. We have first analyzed the interaction of the cluster with a graphene sheet to fix the equilibrium distance, 5.38 Å, which we have used as approximate radius for the carbon nanotubes in order to optimize the interaction between the cluster and the nanotube when the cluster is inside the SWCNT. Two different nanotubes are considered: The metallic armchair (8,8) and the semiconducting zig-zag (14,0). They are simulated using finite pieces, C$_{176}$H$_{32}$ and C$_{168}$H$_{28}$ respectively, with the correct symmetry in which the H atoms saturate the dangling bonds of the carbon atoms at the borders. We have compared the electronic densities of states obtained in our calculations with those of a π-electron tight-binding model obtaining a reasonable agreement, in spite of the effects associated with the finite size of our nanotubes which show up as more important for the semiconducting nanotube .

In Fig. 1 we present the evolution of the binding energy of the cluster to the (8,8) metallic nanotube as a function of the distance between their centres. Two calculations are given: LDA and GGA using the revPBE functional: Only the LDA calculations produce a reasonable binding. In our equilibrium geometry, the edge of the nearly icosahedral structure of Al$_{13}$H which is closer to the wall of the nanotube is parallel to its axis and also parallel to a diagonal of the carbon hexagon closer to the cluster. This geometry is different to the on-top one found in previous calculations [2]; however the equilibrium distance and binding energies are comparable. We give in Fig. 2 the evolution of the frontier orbitals. The presence of the aggregate induces a large increment in the number of electronic states under the HOMO level; these new states are located at the cluster with a very small hybridization with the states of the nanotube. As is indicated in Fig. 2 there is a very small electronic gap in the global system and the LUMO state results distributed both in the cluster and in the nanotube. The charge transfer obtained, calculated as the Hirshfeld charge, is of 0.1 electrons from the SWCNT to the cluster, a result that is analogous to previous estimations [2]. Similar results are obtained when the cluster is located inside the nanotube.

For the semiconducting (14,0) tube both the equilibrium geometry and binding energy are analogous to those of the metallic case. However, the electronic properties have more influence of the finite size approximation considered for the carbon nanotube.

**References:**

**[1]** Q. Zhao, M. Buongiorno Nardelli, W. Lu, and J. Bernholc, Nano Lett., **5** (2005) 847.
T. W. Odom, J-L Huang, Ch. L. Cheung, and Ch. M. Lieber, Science **290** (2000) 1549-1552.
**[2]** B-K Kim, N. Park, P. S. Na, H-M So, J-J Kim, H. Kim, K-J Kong, H. Chang, B-H Ryu, Y. Choi, and J-O Lee, Nanotech., **17** (2006) 496.

**Figures:**
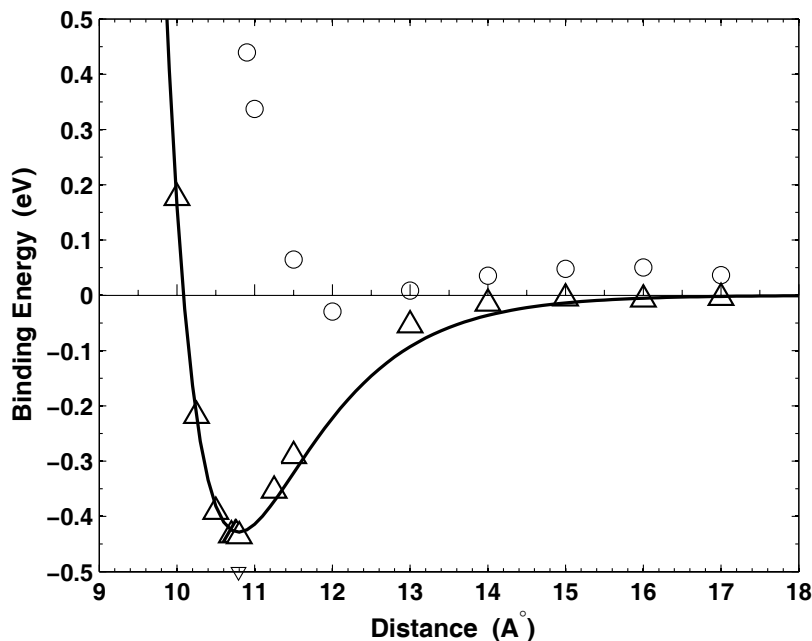


**Fig. 1.-** Binding energy between the metallic armchair (8,8) SWCNT and the cluster $Al_{13}H$ as a function of the distance between their centers. The triangles indicate the LDA results and the open circles the GGA values. The curve corresponds to the fitted Morse potential.
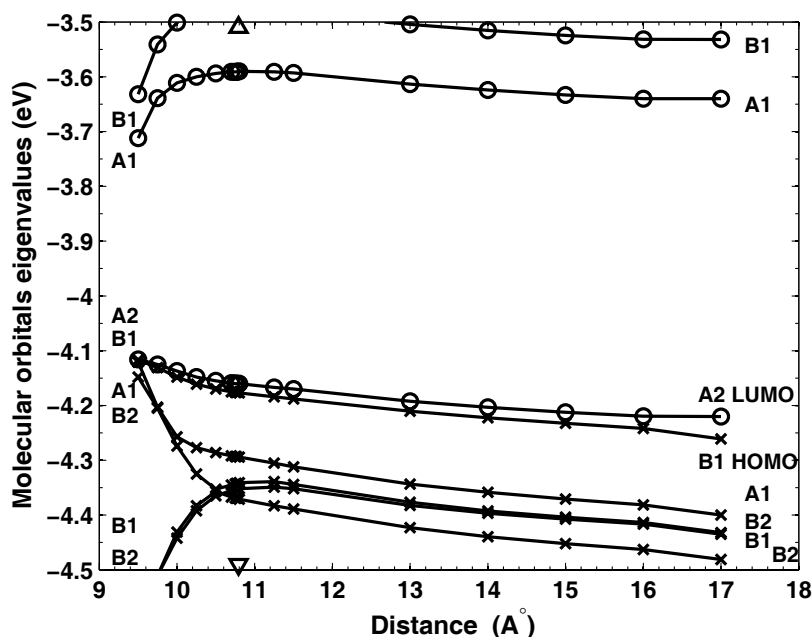


**Fig. 2.-** Evolution of the eigenvalues of the frontier molecular orbitals as a function of the distance for the LDA calculations of Fig.1. The labels of the orbitals correspond to the global $C_{2V}$ symmetry of the system. The small triangles indicate the equilibrium distance.

# THEORETICAL STUDY OF THE REACTIVITY OF ICOSAHEDRAL C@Al$_{12}$ CLUSTER WITH A GRAPHENE SHEET

*F. Duque[1], A. Mañanes[1], M. J. López[2] and J. A. Alonso[2]*
*[1]Departamento de Física Moderna, Universidad de Cantabria, 39005 Santander. Spain*
*[2]Departamento de Física Teórica, Atómica y Óptica, Universidad de Valladolid,*
*47011 Valladolid. Spain*
*fernando.duque@unican.es*

The interaction between the magic cluster CAl$_{12}$ and a graphene sheet is studied in the framework of Density Functional Theory, using both Local Density Approximation (LDA) and Generalized Gradient Approximation (GGA), for the exchange-correlation energy.

First, we have analyzed the stability of two isomers of the magic cluster CAl$_{12}$, the first one with the carbon atom in the center of Al$_{12}$ icosahedral cage and the second one with the carbon atom located at the surface of the cluster, since photoelectron spectroscopy (PES) experiments [1] indicate that the carbon atom is located at the surface of cluster in de anionic case. Our calculations show that the anionic cluster is more stable with the carbon atom at the cluster´s surface than with the C at the central position. However, the neutral cluster isomer is more stable with the C located at the central position of the Al$_{12}$ icosahedral cage. Our results are in agreement with previous calculations [2]. This is the reason why in order to study the interaction between the magic cluster CAl$_{12}$ and a sheet of graphene, we have used the cluster C@Al$_{12}$ (C located in center of the cage). As a previous step, we have performed a complete relaxation of C@Al$_{12}$ resulting a structure which can be considered as a slightly distorted icosahedron.

Second, we have simulated a graphene sheet, considering only a finite piece of 96 carbon and 24 hydrogen atoms with D$_{6h}$ symmetry. The H atoms are located at the border of the sheet in order to saturate the sp$^2$ carbon bonds, and trying to reproduce the electronic structure of the infinite graphene.

To study the interaction between C@Al$_{12}$ and C$_{96}$H$_{24}$ we have placed the cluster above the central hexagon of the graphene sheet, so that a binary axis of C@Al$_{12}$ matches the principal 6-fold axis of C$_{96}$H$_{24}$. Two possibilities are studied: first we consider the edge of C@Al$_{12}$ which is closer to the graphene as parallel to a diagonal of the carbon hexagon; in a second configuration, that edge is orthogonal to two parallel sides of the hexagon. In both cases the global symmetry is C$_{2v}$. The interaction energy between the cluster and the sheet is calculated as a function of the distance between the centers of the fragments.

The LDA calculations show that the C@Al$_{12}$ with the edge parallel to a diagonal of the carbon hexagon of the graphene sheet is slightly more stable than the other one. With GGA calculations we obtain a very slight binding and at a larger distance than in the LDA case, as can be seen in Fig.1. This is a well known drawback of the GGA approximation for the calculation of sparse systems.

To quantify the results obtained with LDA calculations, we have fitted the binding energy values as a function of distance cluster–sheet, with a Morse potential, obtaining 0.455 eV for the binding energy, and 5.26 Å for the equilibrium distance (Fig. 1). Also, we have analysed the partial contributions to the energy (Fig 1. lower panel), together with the HOMO–LUMO gap and the charge transfer between both fragments as a function of the distance. At the equilibrium distance, the HOMO–LUMO gap is about 0.8 eV. To estimate the charge transfer

we have used the Hirshfeld charges, obtaining a net charge transfer from the cluster C@Al$_{12}$ to the graphene sheet of about 0.1 electrons.

**References:**

[1] Xi Li and Lai-Sheng Wang, Phys. Rev. B, **65** (2002) 153404
[2] S. F. Li and X. G. Gong, Phys. Rev. B, **70** (2004) 75404

**Figures:**
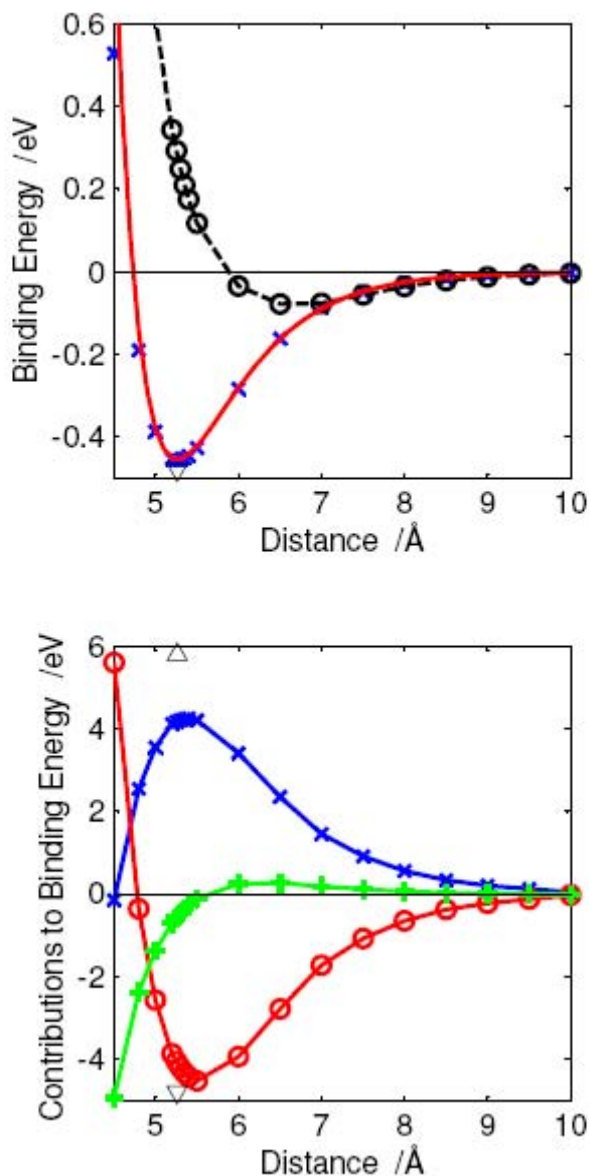




Fig. 1. The upper panel shows the calculated values of LDA binding energy indicated by crosses and the fitted Morse potential. The empty black circles correspond to the GGA values. The lower panel shows the partial contributions to total binding energy. The blue curve is the Coulombic electronic energy, the red one is the kinetic energy contribution and the green curve gives the exchange-correlation energy. The small triangles indicate the equilibrium distance (5.26 Å).

# Domain wall rectification in thin magnetic films with arrays of asymmetric holes

V. I. Marconi[1]* and A. Pérez-Junquera[2], A.B. Kolton[1], L.M. Alvarez-Prado[2], J.V. Anguita[3],
Y. Souche[4], A. Alija[2], M. Vélez[2], J.M. Alameda[2], J.M.R. Parrondo[1], J.I. Martín[2].

[1]*Dep. de Física Atómica, Molecular y Nuclear, Universidad Complutense de Madrid, 28040 Madrid, Spain.*
[2]*Dpto de Física, Universidad de Oviedo, 33007 Oviedo, Spain.*
[3]*Instituto de Microelectrónica de Madrid, CNM-CSIC, Tres Cantos 28760 Madrid, Spain.*
[4]*Laboratoire Louis Néel, CNRS, BP 166, 38042, Grenoble Cedex 9, France.*

Modern techniques in nanotechnology provide a very versatile tool to fabricate thin films with a well controlled pinning potential for magnetic domain walls. This system rises basic physical questions which are relevant for technological applications such as the dynamical magnetic response under an applied external field for different pinning geometries. We study both experimentally and theoretically, the magnetic wall dynamics on thin films patterned with an asymmetric array of holes under an external magnetic field applied along the easy direction. We observe for first time rectification effects of Néel walls in conventional continuous thin films with defects. Moreover a rectification reversal effect induced by the asymmetric wall kinks motion is obtained at low applied magnetic fields (see Fig.1).

A simple phenomenological $\phi^4$-model succesfully explain the observed phenomena, suggesting that the interplay among the driving force, elasticity and pinning of domain walls is at the root of the observed macroscopic phenomena.

* Electronic address: `veromarconi@fis.ucm.es`
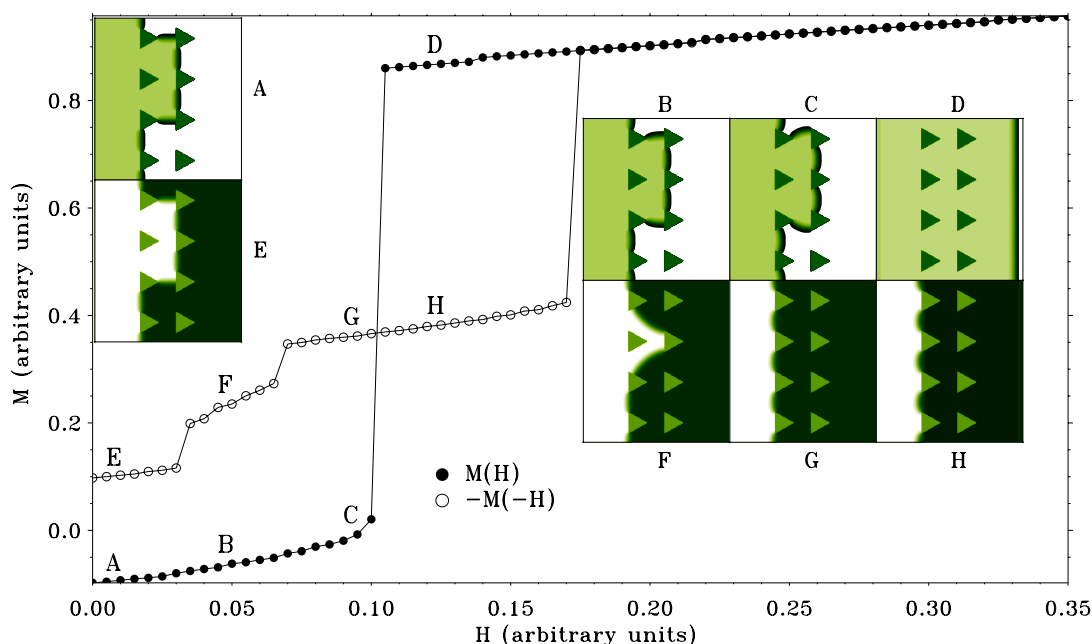
FIG. 1: Magnetization vs applied magnetic field. Results obtained using a $\phi^4$-model. The initial state at $H = 0$ is a wall with a kink-antikink pair (A,E) which evolves asymmetrically with respect to $H$ and $-H$. Insets are $\phi$ snapshots corresponding to the points, A,B,C,D,E,F,G and H marked in $M(H)$ and $M(-H)$ curves. The curves show clearly that is easier to move a straight wall to the right than to the left but on the contrary a wall with a kink-antikink pair is harder to move to the right than to the left.

# MAGNETIC DOMAINS OBSERVATIONS OF CUSTOM ASSEMBLED FECO NANOGRAINS MICROSTRUCTURES TAILORED BY MEANS OF COBALT PERCENTAGE AND ANNEALING MAGNETIC FIELD DIRECTION

*P. Marín, R. Schafer[1], M. López, A. Hernando*

*Instituto de Magnetismo Aplicado. Dpto. Física de Materiales (UCM-ADI). P.O. Box 155 28230 (Las Rozas) Madrid (SPAIN)*
*[1]IFW. Helmholtzstraße 20. 01069 Dresden (GERMANY)*

*pmarin@adif.es*

As reported in previous works [1,2] it is possible to tune the nanocrystalline microstructure of Co-rich samples by magnetic field annealing. Nanocrystalline grains can be directionally ordered by thermal annealing of amorphous ribbons in the presence of magnetic field. The intensity of the field allows controlling different degrees of order. The effect is observed when the annealing temperature corresponds to the first stages of nanocrystallization process associated with temperatures between 713 K and 753 K. The field effect can be described by a relative increase of the crystallized volume fraction and a linear alignment of the nucleated grains. The energy barrier for nucleation is directionally affected by the applied field. The influence of grains assembling on exchange coupling between grains has been analysed by means of magnetic domains observation and magnetic properties study.

**References:**

[1] P. Marín, M. López, A. Vlad, A. Hernando, M. L. Ruiz-González and J. M. González-Calbet, Applied Physics Letter, **Issue 89**,(2006) page 1
[2] G. Herzer, Nanocrystalline Soft Magnetic Alloys, Handbook of Magnetic Materials (Eds. Busckow K.H.J, Elsevier Science B.-V., The Neherlands), **Vol 10** (1997) page 415

**Figures:**



**Fig 2.-** Influence of custom assembly on Hysteris loop: FeCo sample annealed without magnetic field (-),and under 140 Oe (--) longitudinal field

**Fig1.-** HRTEM observation of magnetic grains and corresponding magnetic domains obtained by Kerr effect: FeCo sample annealed without field (a), under 50 Oe (b) and 140 (Oe)

# IRON-GOLD CORE-SHELL NANOPARTICLE FORMATION UTILIZING NONIONIC SURFACTANTS AND REVERSE MICELLES

*J.R. Marin[1], M. D. Shultz[2], J.M. Laza[1], E. E. Carpenter[2], J.L.Vilas[1], L.M. Leon[1]*
*[1]Basque Country University, Bº Sarriena s/n, Leioa, Spain*
*[2]Virginia Commonwealth University, Richmond, VA, USA*
*marin@gaiker.es*

In recent years, the nanoparticles which present onion-like structures are of great interest due to the combination of the metallic core properties with other properties of a metallic or oxide shell [1]. This can allow for deceleration of oxidation or protection in aqueous solutions, which enables use in many different applications [2]. Previous work in the literature has shown the use of CTAB as a surfactant to form a micro-emulsion for the synthesis of iron-gold core-shell nanoparticles [3]. In this research, a new kind of micellar system is used to produce a gold coated iron onion-like structure. This new system was performed by using nonylphenoxy poly(ethyleneoxy) ethanol (IGEPAL NP7 or NP4 depending on the number of ethyleneoxy groups) as a non-ionic surfactant in a water-in-oil reverse micelle system. Details of the IGEPAL system and some of the advantages over ionic systems have been presented in the literature [4]. This work reports on the iron-gold core-shell nanoparticles synthesized by this method and the affect of parameters such as metal concentrations, metal to metal ratios, and water to surfactant ratios were investigated to give insight into the mechanism of this synthetic procedure.

Powder X-ray diffraction (XRD) patterns for the nanoparticles showed no evidence of crystalline iron oxide in the diffraction pattern and only revealed peaks that reference to α-Fe and Au as seen in Figure 1. From previous work, the Fe in the core is most likely distorted through the incorporation of boron or existing in a disordered iron oxide structure [5,6], and thus XRD pattern only confirms crystalline Au. The diffraction data was collected a few weeks post synthesis and exposure to air, thus showing a resistance to oxidation by the absence of iron oxide peaks. Transmission electron microscopy (TEM) images indicate the presence of core-shell structures with a mean diameter of 15.7 nm with a shell thickness of 2.7 nm. Magnetic characterization via vibrating sample magnetometry (VSM) showed a saturation magnetization of 18 emu/g, which is comparable to iron-gold core-shells found in the literature [3,7,8], especially since the mass of the gold is also included in this value.

Mechanistic insight was gained for the core-shell formation from the results of varying the before mentioned parameters. When lowering the metal concentrations and maintaining the Au/Fe ratio, the mean diameter seen on TEM stayed constant while the size distribution increased. This increase in size distribution was also due to what appeared to be two different particle morphologies; one core-shell and one solid particle. Then, upon increasing the Au/Fe ratio, the size distribution decreased as well did the morphological distribution. There are two possible contributing factors for this observation. First, there may be a critical concentration gradient required to exchange enough material fast enough between micelles to induce core-shell formation. The second factor is that the Au is growing by an islanding mechanism around the Fe core. If there is not enough Au reaching the core particle fast enough to fill in the island forms on the surface, then the Au breaks off the core particle and grows to form separate particles. This approach to the core-shell formation explains the size and

morphology distributions, as well as the presence of darker zones in the shell that are more present when increasing the Au/Fe ratio. Smaller sizes were also reached when maintaining a "critical" concentration of metals, while decreasing the water/surfactant ratio in the reverse micelle system.

**References:**

[1] Morrison, S. A.; Carpenter, E. E.; Harris, V. G.; Cahill, C. A., Journal of Nanoscience and Nanotechnology, **9,** (2005), 1323-1344.
[2] Carpenter, E. E., Journal of Magnetism and Magnetic Materials, **1-2** (2001) 17-20.
[3] Carpenter, E. E.; Kumbhar, A.; Wiemann, J. A.; Srikanth, H.; Wiggins, J.; Zhou, W. L.; O'Connor, C. J., Materials Science and Engineering a-Structural Materials Properties Microstructure and Processing, **1,** (2000) 81-86.
[4] Michaels, M. A.; Sherwood, S.; Kidwell, M.; Allsbrook, M. J.; Morrison, S. A.; Rutan, S. C.; Carpenter, E. E., Journal of Colloid and Interface Science, **1**, (2007) 70-76.
[5] Calvin, S.; Carpenter, E. E.; Harris, V. G., Physical Review B, **3** (2003) 033411/1-033411/4.
[6] Shultz, M. D.; Calvin, S.; Fatouros, P. P.; Morrison, S. A.; Carpenter, E. E., Journal of Magnetism and Magnetic Materials, **311** (2007) 464-468.
[7] Wiggins, J.; Carpenter, E. E.; O'Connor, C. J., Journal of Applied Physics, **9** (2000) 5651-5653.
[8] Lin, J.; Zhou, W. L.; Kumbhar, A.; Wiemann, J.; Fang, J. Y.; Carpenter, E. E.; O'Connor, C. J., Journal of Solid State Chemistry, **1** (2001) 26-31.

Figures:
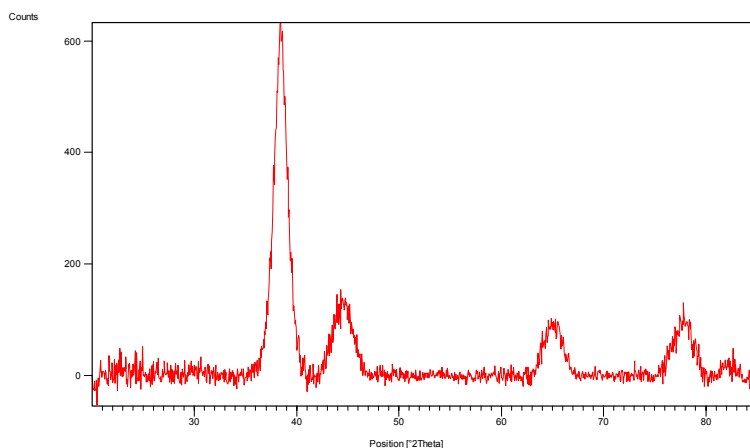


Figure 1. Powder X-ray diffraction pattern of iron-gold core-shell nanoparticles synthesized by the IGEPAL systems.

# Si-SiO$_2$ interface band-gap transition: effects on MOS inversion layer characteristics

S. Markov*[†], P. Sushko[‡], S. Roy*, C. Fiegna[†], E. Sangiorgi[†], A. Shluger[‡], and A. Asenov*

*EEE Dept., Univ. of Glasgow, Glasgow G12 8LT, United Kingdom
[†]ARCES-IUNET, Univ. of Bologna, v. Venezia 52, Cesena 47023, Italy
[‡]Dept. Physics and Astronomy, Univ. College London, WC1E 6BT, United Kingdom
e-mail: s.markov@elec.gla.ac.uk

## INTRODUCTION

The change of the atomic structure at the Si-SiO$_2$ interface leaves additional electronic states, energetically aligned closer to the Si conduction band, in the first $2-6$ Å of the SiO$_2$ away from the interface [1], [2], [3], [4]. This implies a gradual transition of the band-gap at the SiO$_2$ side, as shown on Fig. 1 from [2]. Recently, we studied the impact of this transition on the metal-oxide-semiconductor (MOS) inversion layer characteristics [5], simulating linear transition of the band-gap, similarly to earlier studies [6], [7]. For the first time here, MOS inversion layer quantisation, capacitance and tunnelling characteristics are analysed for a realistic band-gap transition, derived from first principles simulations of the Si-SiO$_2$ interface.

## SIMULATION APPROACH AND RESULTS

This study is based on a 1-D self-consistent solution of the Poisson and Schrödinger equations, using a modified version of Schred 2.0 solver [8], as in [9] and [5]. Further modifications allow us to incorporate the interface band-gap profile from Fig. 1. We have re-scaled the values extracted from Fig. 1, since this profile results from density-functional theory, which is known to underestimate the band-gap, compared to experimentally observed values [4]. Since non-linear features of the transition are preserved, we confront the results obtained from this transition profile, with simulations of a linearly graded band-gap transition in the range of $0.2-0.6$ nm. The simulated MOS structures has a SiO$_2$ dielectric of thickness in the range of $1.0-1.8$ nm, and a p-Si (100) substrate, uniformly doped to $2 \times 10^{18}$ cm$^{-3}$. Metal gate with a 4.1 V work function is assumed, to avoid poly-Si depletion.

Conduction band profile and electron density distribution are compared on Fig. 2, for three different interface band-gap transition profiles. Although the full band-gap for the realistic profile extracted from Fig. 1 develops in 0.5 nm, the electrostatic effects correspond to a linear transition of 0.6 nm. The effectively wider potential well corresponding to the realistic profile lowers the ground states for both 2-fold and 4-fold degenerate Si valleys, as shown on Fig. 3, and leads to more dramatic redistribution of carriers (lower graphs on Fig. 3). Figure 4 shows an increase of gate capacitance due to the band-gap transition. The enhancement is strongest for the realistic profile, due to the strongest penetration of the corresponding wave-functions (lower part of Fig. 2). Similarly, tunnelling is mostly increased for the realistic profile, due to the thinnest tunnelling barrier for the energy range of interest - Fig. 4. Figures 5 and 6 show the relative effect of band-gap transition on quantisation, tunnelling and gate capacitance. The isolated points show where the realistic profile stands with respect to the trend of increasing the transition width of a linear profile.

We conclude that not so much the total width, but the exact profile of the band-gap transition in the first few Å is deterministic for the impact of Si-SiO$_2$ transition on MOS inversion layer characteristics.

## REFERENCES

[1] D. A. Muller *et al*, Nature **399**, 758 (1999).
[2] C. Kaneta *et al*, Microelectr. Engineering, **48**, 117 (1999).
[3] T. Hattori *et al*, Appl. Surf. Sci. 212-213 (2003) 547.
[4] F. Giustino, A. Pasquarello, Surface Sci. **586**, 183 (2005).
[5] S. Markov *et al*, Proc.Int.Conf.SISPAD'07,to be published
[6] F. Stern, Solid State Commun. **21**, 163 (1977).
[7] H. Watanabe *et al*, IEEE Trans.Electr.Dev. **53**,1323,(2006)
[8] D. Vasileska, Z. Ren SCHRED 2.0 User Manual.
[9] N. Barin *et al*, Proc. ESSDERC, 169-172 (2004).
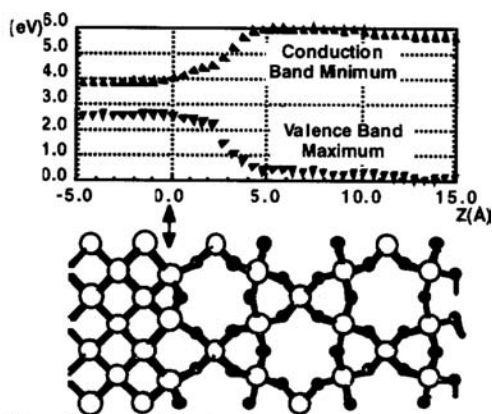
Fig. 1. Non-abrupt band-gap transition at the Si-SiO$_2$ interface (top), corresponding to the *ab-initio* simulated atomic structure of the interface (bottom), from Kaneta et al. [2].
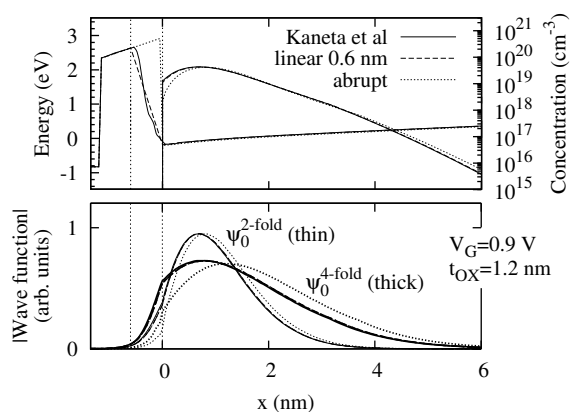


Fig. 2. Conduction band profile and electron density (upper) for three different band profiles at the interface - abrupt, linearly graded, and the band profile extracted from Fig. 1. Normalised wave functions (modulus) corresponding to the lowest sub-bands in the 2- and 4-fold valleys (lower).
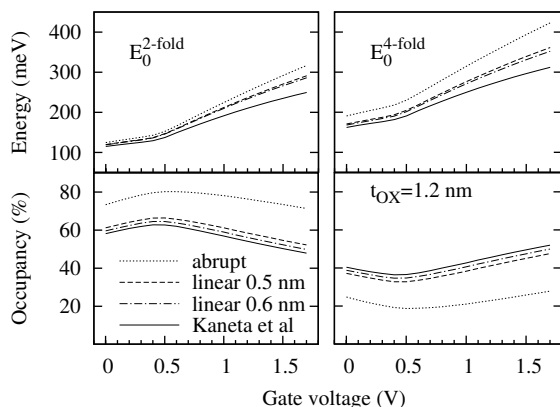


Fig. 3. Sub-band energy and sub-band occupancy (percentage of the total inversion charge density) dependence on gate voltage, for the three different interface band-gap transition profiles, as on Fig. 2, at a given oxide thickness $t_{OX}$.
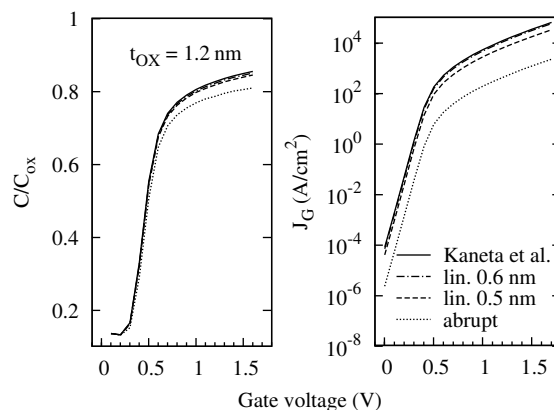


Fig. 4. $C - V$ (left) and $J_G - V$ (right) characteristics of the structure, for the three different band-gap transition profiles, as on Fig. 2, at a given oxide thickness $t_{OX}$.
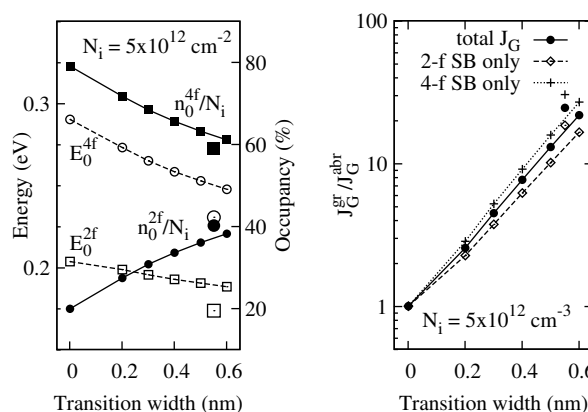


Fig. 5. Sub-band energy and occupancy (left), and direct tunnelling current (right) dependence on transition width for a constant inversion charge, $N_i$. The non-connected points correspond to the band-gap transition profile from Fig. 1. These resutls are independent of the simulated oxide thickness.
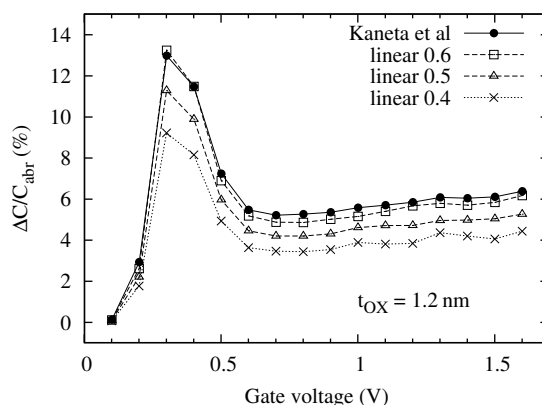


Fig. 6. Gate capacitance relative difference, with respect to abrupt interface, for various linear transition widths and for the profile from Fig. 1, at a given oxide thickness, $t_{OX}$.

# ALUMINA MEMBRANES AS ETCHING MASK

B. Marquardt, S. Xavier, G. Cho, L. Eude, M. Gowtham, C. Cojocaru and D. Pribat
*LPICM, Ecole Polytechnique, 91128 Palaiseau, France*
contact: bernd.marquardt@polytechnique.edu

Porous alumina membranes recently have attracted much attention as it is a very appropriate material to realize ordered nanostructure arrays [1], [2]. A lot of work has been done on the study of these membranes and it has been shown that the pore diameter, pore density and the thickness of the membranes can easily be controlled[3].

One promising way of using alumina membranes for the fabrication of devices would be to transfer the ordered pore structure to layers of different materials [4]. The most obvious way to realize such transfer is to use the alumina membranes as etching mask and to etch thereby the same porous structure inside an underlying layer. However, prior to this, the barrier layer at the bottom of the pores has to be removed. The alumina barrier layer is inevitable during the creation of the porous structure. Its thickness is close to the pore diameter and proportional to the voltage applied during anodic oxidation process.

In our work, we have demonstrated such transfer to different type of layers. We first perform a double anodic oxidation process of an Al layer at the top of a multilayer structure. Once the ordered porous structure is obtained we applied different methods to remove the barrier layer at the bottom of the pores and finally we performed the etching of the underlying layers.

The etching by high-energy ICP has been first studied in order to remove the barrier layer and to etch inside the subsequent Al layer. By using a gas mixture of $Cl_2$ and Ar and a high platen power, perfectly straight pores have been transferred into an Al layer showing exactly the same order like the alumina membranes (Fig.1).

Secondly, we have shown the transfer inside an n-poly-Si layer and subsequently inside a $SiO_2$ layer. For this, high energy etching is not appropriate as it destroys easily the n-poly-Si and $SiO_2$. Thus, we first removed the barrier layer by a highly controlled anodic oxidation process of the alumina (Fig.2). Then, RIE etching has been performed to etch the n-poly-Si and $SiO_2$ layers by using a low chamber pressure and high acceleration energy. This combination allows to realize an an-isotropic etching which leads to the same pore structures in the etched layers (Fig.3).
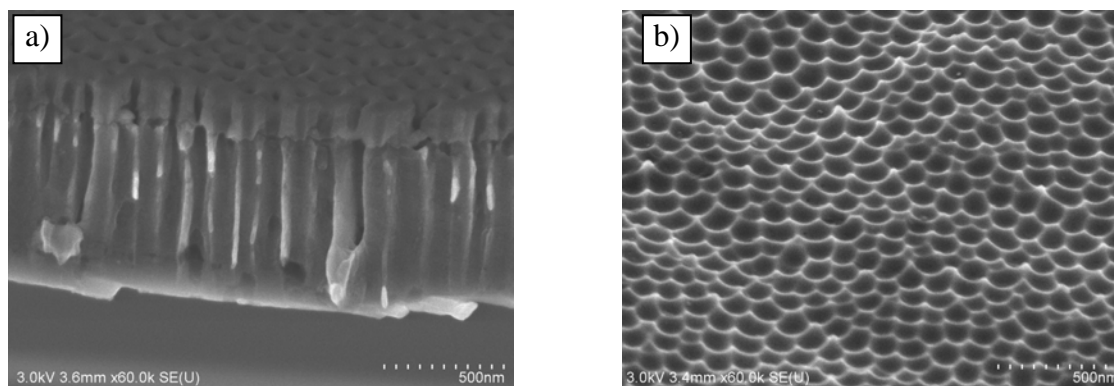


*Fig.1: Porous alumina as etching mask for Al, SEM images. a) side view of the etched pore structure in an Al layer with alumina membrane on top; b) top view of the pores inside the same Al layer after removing of the alumina membrane.*
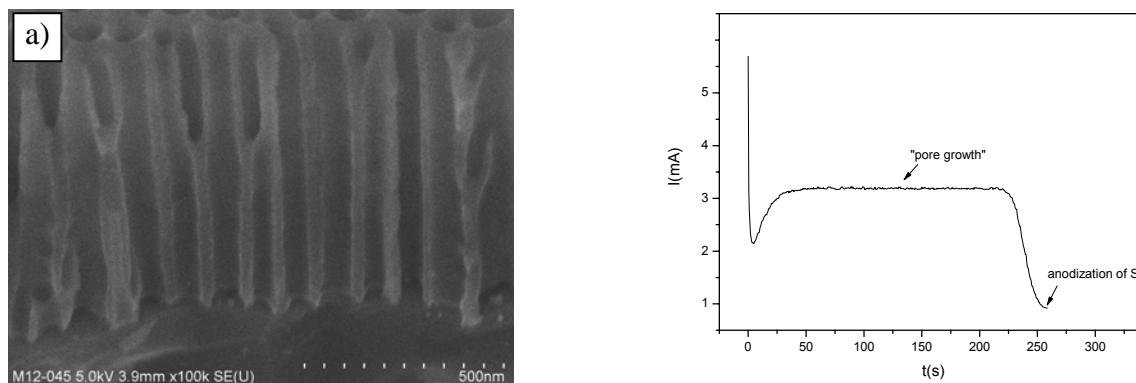
Fig.2: *Realization of opened bottom pores on top of a n-poly-Si layer by highly controlled anodization. a) SEM image of the alumina membranes with open pores on n-poly-Si layer; b) current characteristics during anodic oxidation.*
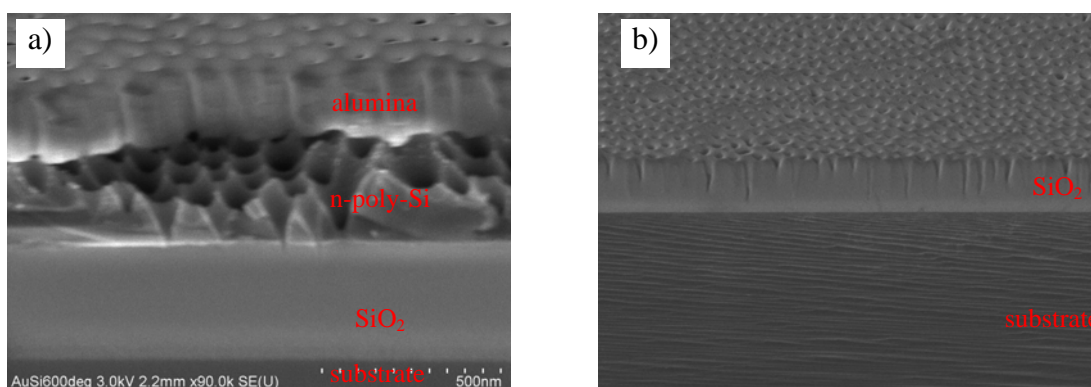


Fig.3: *Porous alumina as etching mask for the n-poly-Si and SiO$_2$ layers, SEM images. a) RIE etching at 30 W and 3 mTorr for 20 min; b) RIE etching at 50 W and 3 mTorr for 50 min followed by removal of the alumina membrane and n-poly-Si to show the transfer of the ordered structure (same sample as in a)).*

**References:**

[1] S.-H. Jeong, H.-Y. Hwang, S.-K. Hwang, K.-H. Lee, 'Carbon nanotubes based on anodic aluminum oxide nano-template', *Carbon* 2004, 42 (2073).
[2] J. Choi, G. Sauer, K. Nielsch, R. Wehrspohn, U. Gösele, 'Hexagonally Arranged Monodisperse Silver Nanowires with Adjustable Diameter and High Aspect Ratio', *Chem. Mat.* 2003, 15 (776).
[3] O. Jessensky, F. Müller, U. Gösele, 'Self-organized formation of hexagonal pore arrays in anodic alumina', *Appl. Phys. Let.* 1998, 72 (10).
[4] S. Ono, A. Oide, H. Asoh, 'Nanopatterning of silicon with use of self-organized porous alumina and colloidal crystals as mask, *Electrochimica* 2007, 52 (2898).

# MAGNETIC GLYCONANOPARTICLES AS CONTRAST AGENTS FOR BRAIN TUMOR TARGETING BY MRI

*Marco Marradi,[1] Jesús M de la Fuente,[1] David Alcántara,[1] María Luisa García,[2] Sebastián Cerdán[2] and Soledad Penadés[1]*
*[1]Laboratory of Glyconanotechnology, CICbiomaGUNE, Parque Tecnológico de San Sebastian, Pº de Miramon 182, 20009 San Sebastián, and Instituto de Investigaciones Químicas-CSIC, Americo Vespucio 49, 41092 Sevilla, Spain;*
*[2]Instituto de Investigaciones Biomédicas "Alberto Sols", Arturo Duperier 4E, 28029-Madrid, Spain*
mmarradi@cicbiomagune.es

Magnetic nanoparticles offer exciting new opportunities including improving the quality of magnetic resonance imaging (MRI), hyperthermic treatment for malignant cells and site-specific drug delivery. The development of functional magnetic nanoparticles is mainly based on proteins and nucleic acids. However, as far as we know, magnetic nanoparticles conjugated to biologically relevant oligosaccharides for specific cell targeting have not yet been prepared. Our laboratory has recently been successful in preparing gold nanoclusters and semiconductor nanocrystals functionalized with carbohydrate antigens (glyconanoparticles) [1]. These glyconanoparticles have been shown to be excellent platforms for basic studies of carbohydrate interactions and potential tools for biotechnological and biomedical applications.

We also explored the potential of these tools for cell labelling and imaging of carbohydrate-mediated biological processes. To this end, we propose the use of magnetic glyconanoparticles as potential MRI agents. Therefore, in this study, magnetic gold-iron nanoparticles (MGNPs) coated with different saccharides (glucose, maltose and lactose) [2] and hybrid DOTA-$Gd^{3+}$/saccharides (glucose and lactose) have been prepared using straightforward and economical methodologies. The influence of these nanoparticles on human dermal fibroblasts in vitro has been assessed in terms of cytotoxicity, light microscopy and scanning electron microscopy (SEM). From the results, we observed that, although maltose-MGNP presents an extremely high cytotoxicity, lactose and glucose are innocuous. We have also observed that lactose and maltose- MGNPs are able to internalize the cell membrane via endocytosis, but this effect was not detected for gluco-MGNPs.

To confirm their application as MRI contrast agents, the longitudinal and transversal relaxation times ($T_1$ and $T_2$) of our GNPs were measured. All the MGNPs showed similar relaxivities and they have an acceptable value, in spite of the low content in iron in all of them. However, DOTA-$Gd^{3+}$-GNPs showed very good relaxivities values, even better than commercial available contrast agents. In vivo experiments have also been carried out with gluco-GNPs and lacto-GNPs to demonstrate their utility as contrast agents for tumoral processes. Only gluco-GNPs could reach brain tumours and accumulate there, allowing their visualization by MRI and indicating a different role in the carbohydrate activity in the process.

**References:**

[1] de la Fuente, J.M.; Penades, S. BBA-Gen. Subjects, **4** (2006) 636.
[2] de la Fuente, J.M.; Alcántara, D.; Eaton, P.; Crespo, P.; Rojas, T.C.; Fernández, A.; Hernando, A.; Penadés, S. J. Phys. Chem. B, **26** (2006) 13021.

# ORDERED ARRAYS OF POLYMER MICROFIBERS OBTAINED USING MACROPOROUS SILICON AS TEMPLATE

*L. F. Marsal, P. Formentin, R. Palacios, T. Trifonov, J. Ferré-Borrull, A. Rodriguez, J. Pallarés, and R. Alcubilla.*

*NePhoS (Nano-electronic and Photonic Systems), Departament d'Enginyeria Electrònica, University Rovira i Virgili, Av. Països Catalans 26, 43007 Tarragona, Spain*
*Departament d'Enginyeria Electrònica, Universitat Polit`ecnica de Catalunya, Edifici C4, Campus Nord,c/ Jordi Girona 1-3, 08034 Barcelona, Spain*

*lluis.marsal@urv.cat*

In recent years, the fabrication of nanostructures and microstructures based on porous templates has caused much interest [1,2]. The deposition of specific materials into porous templates allows tailoring structures as inverse replicas of the porous. The use of ordered porous arranged in a regular lattice allows fabrication of ordered fiber arrays.

In this context, we have used a simple technique for the fabrication of polymer microfibers with a monodispersive size distribution and uniform orientation using ordered macroporous silicon templates.

We prepared the ordered porous silicon membranes by light-assisted electrochemical etching [3]. The starting material was n-type silicon with a resistivity of 2–6 $\Omega$cm. The front side of the wafers was patterned with inverted pyramid shaped pits by oxidation, photolithography, and subsequent tetramethyl ammonium hydroxide (TMAH) etching. These inverted pyramids act as nucleation sites for the ordered pore growth. The wafers were incorporated in an electrochemical etching cell containing a 2.5 wt% aqueous solution of HF acid. The quality and size of the pores was controlled by a computerized feedback mechanism to maintain a constant current. After pore growth, the back side of the wafer was etched until the holes opened. As shown in Figure 1, the pores of the silicon templates were very uniform in size and depth (~146 μm)

Ordered polymer microfibers were prepared immersing the template in a precursor solution, PMMA/Toluene to obtain rigid polymer or in silicone elastomer (PDMS) mixed with curing agent (10:1) to obtain elastic polymer, and then cured at 110°C for 3h. To removed the template, it was immersed into 40 wt% KOH(aq) at 40°C in the case of PMMA or it was mechanically peeled off the substrate in the case of the PDMS. Scanning electron microscopy (SEM) confirms that the photonic structure of the porous Si is retained in the polymer casting (Figures 2 and 3).

**References:**

[1] X. Chen, M. Steinhart, C. Hess and U. Gösele, Advanced Materials, **18** (2006) 2153
[2] M. Steinhart, J.H. Wendorff, A. Creiner, R.B. Wehrspohn, K. Nielsch, J. Schilling, J. Choi, U. Gösele, Science, **296** (20032) 1997
[3] T. Trifonov, L. F. Marsal, A. Rodríguez, J. Pallarès, R. Alcubilla, Physica Status Solidi (c), 2 (2005) 3104.

**Figures:**



a)

b)
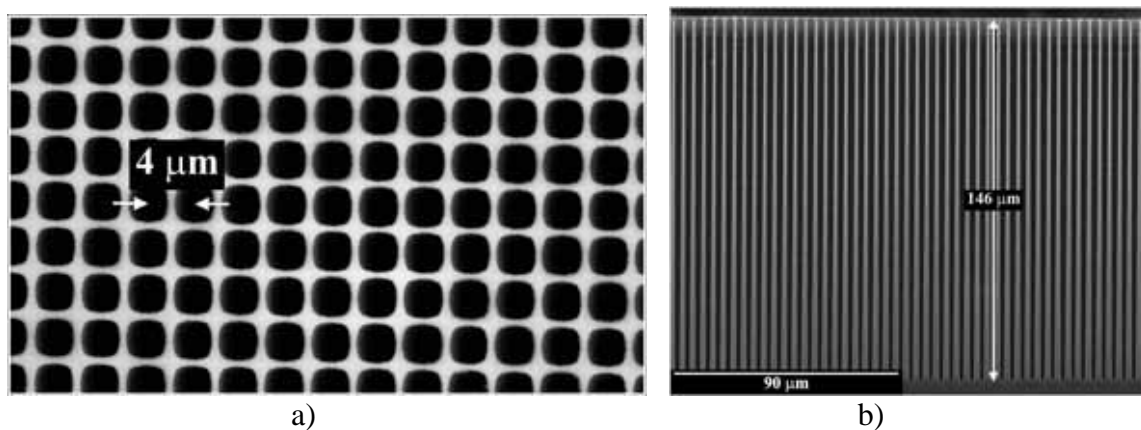
**Figure 1.** Scanning electron microscopy (SEM) images of top surface (a) and cross section (b) of an n-type ordered porous silicon template.



a)

b)
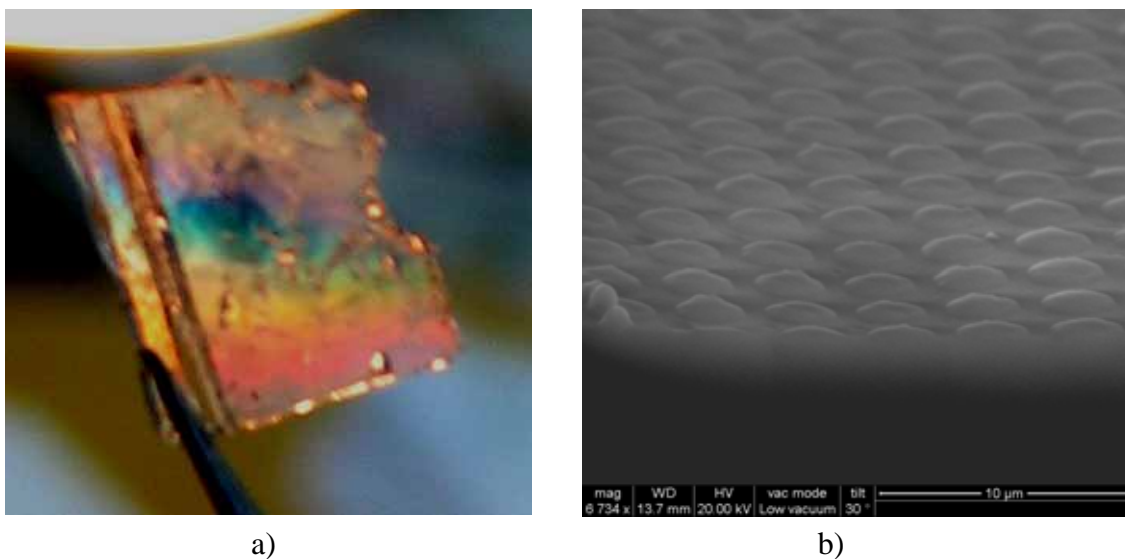
**Figure 2**. a) Iridescent color resulting from the scattering of visible light by the periodic structure of PDMS. b) SEM image of the PDMS surface after pull-off the silicon template.



a)

b)
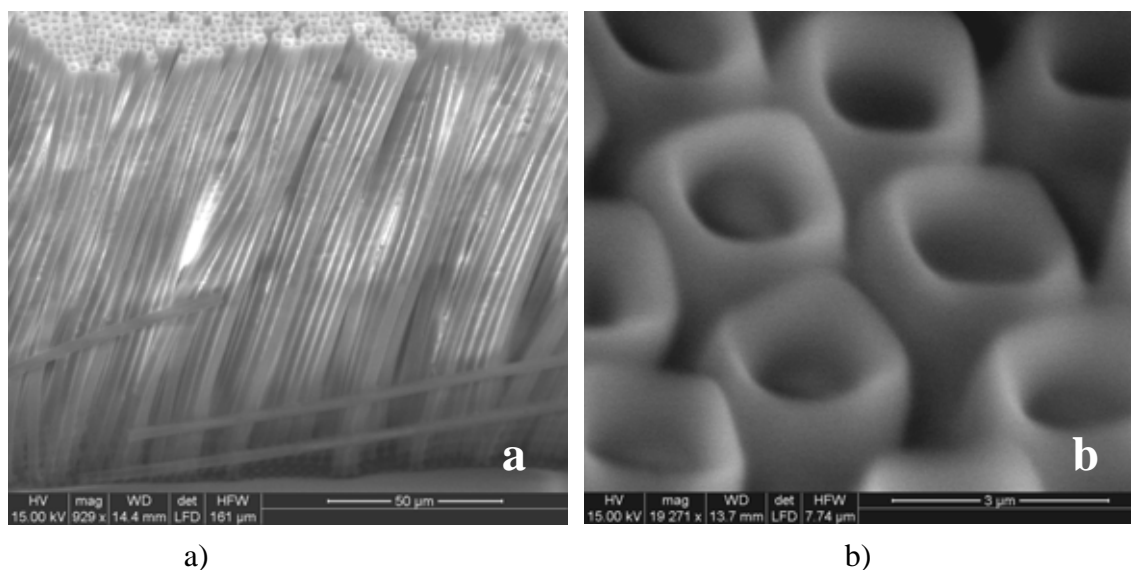
**Figure 3.** SEM images of PMMA microfibers after removed the silicon template. a) Cross-sectional view of some PMMA microfibers. b) Top view of the PMMA microfibers.

# Néel wall attractive and repulsive pinning in amorphous Co-Si films with diluted arrays of empty or filled antidots

A. Pérez-Junquera,[a] J. I. Martín,[a*] G. Rodríguez,[a] M. Vélez,[a] J. V. Anguita [b] y
J. M. Alameda,[a]

*[a]Dpto. Física, Universidad de Oviedo, c/ Calvo Sotelo s/n, 33007 Oviedo, SPAIN*

*[b]Instituto de Microelectrónica de Madrid, CNM-CSIC, Isaac Newton 8, PTM, Tres Cantos, 28760 Madrid, SPAIN*

*jmartin@condmat.uniovi.es*

Patterned magnetic nanostructures have received much interest in recent years as they provide the ability to control and design the magnetic behavior for specific applications, as well as to study fundamental magnetic properties [1]. Much attention has been devoted to the analysis of small magnetic particles surrounded by non magnetic material. However, the reverse structures, i.e. antidot arrays defined over continuous magnetic films, present potential advantages for magnetic data storage [2] and offer the possibility of tailoring the properties of the continuous film such as coercivity or magnetic anisotropy [3]. In this work, 50 nm thick amorphous $Co_xSi_{1-x}$ films, that present well-defined in-plane uniaxial anisotropy [4], have been patterned with square arrays of elliptical antidots by electron beam lithography and plasma etching [5].

Furthermore, it has been studied how the magnetic properties of a $Co_xSi_{1-x}$ nanostructured film are modified if the antidots are filled with Co or with a more complex material like an alloy of $Co_xGd_{1-x}$. In this case, it has been observed how the original coercivity values of the films can be modified by a factor of two.

Once the nanostructures have been made, the changes on the coercivity and anisotropy of the films induced by the antidots have been studied as a function of the the applied magnetic field direction. The combination of the histeresis loops that correspond with the parallel component of the magnetization with the ones of the perpendicular component have allowed to obtain the values of the switching field, and the angle between magnetization and applied field direction when the reversal process takes place. Consequently, the magnetization reversal processes have been studied, comparing the results with well known reversal models such as the coherent rotation, the 180º domain wall displacement or the incoherent reversal process of Curling. It has been found how the nanostructures modify the behaviour of the continuous film by pinning the Néel wall movement.

In particular, square lattice arrays (20 μm × 20 μm) of elliptical holes (5 μm long and 3.5 μm wide) with the long axis either parallel (Array I) or perpendicular (Array II) to the easy axis, with empty or filled antidots, have been prepared. They have been characterized by atomic force microscopy and SEM measurements (see Fig. 1), with center-to-center interhole distances much larger than hole dimensions, so that they are in the diluted regime where each antidot can be considered as an isolated inclusion in the homogeneous film.

The magnetic behavior of the arrays has been analyzed by magnetooptical transverse kerr effect (MOTKE) with a focused laser of 300 μm in diameter in an experimental setup that allows the determination of the sample magnetization vector. Some of the changes observed in the patterned structures respect to the continuous amorphous film are: (i) an increase in the coercive field respect to the continuous film of up to 100% in the case of antidots filled with $Co_xGd_{1-x}$ (Fig 2 and Fig. 3); (ii) a change in the anisotropy, either an increase or a decrease, that can be tuned depending on the material used to fill the antidots (Fig. 2 and Fig. 3).

---

\* Corresponding aut. Tel.: 00-34-985109611; fax: 34-985103686; e-mail: junquera@condmat.uniovi.es

**References:**
[1] For a review, see J. I. Martín, J. Nogués, K. Liu, J. L. Vicent and I. K. Schuller, J. Magn. Magn. Mater. 256 (2003) 449.
[2] R. P. Cowburn, A. O. Adeyeye, and J. A. C. Bland, Appl. Phys. Lett. 70 (1997) 2309.
[3] A. Pérez-Junquera et al., J. Appl. Phys. 99 (2006) 033902.
[4] M. Vélez *et al.* , IEEE Trans. Magn. 38 (2002) 3078.
[5] J.I. Martín *et al.*, IEEE Trans. Magn. 36 (2000) 3002.

**Figures:**
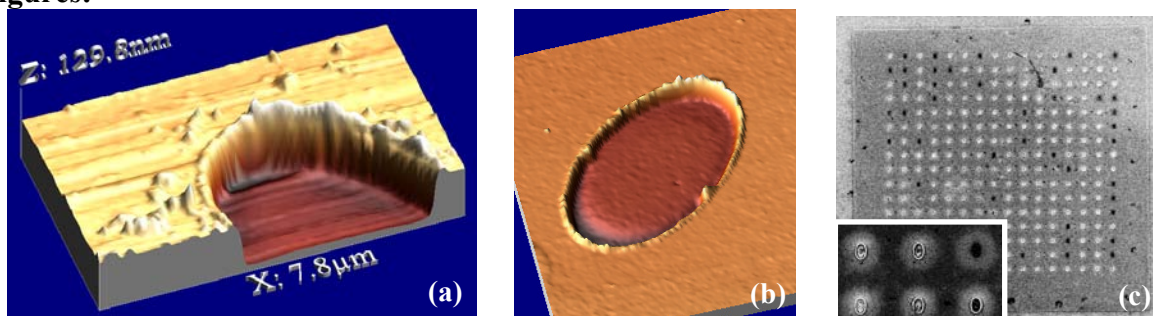


Fig. 1: (a) and (b) Atomic force microscopy images of an empty elliptical antidot and a filled one respectively both patterned on $Co_xSi_{1-x}$ thing film. (c) SEM image of a square array of elliptical fill antiodots. The inset shows that more than the 80 % of the antidots are filled.
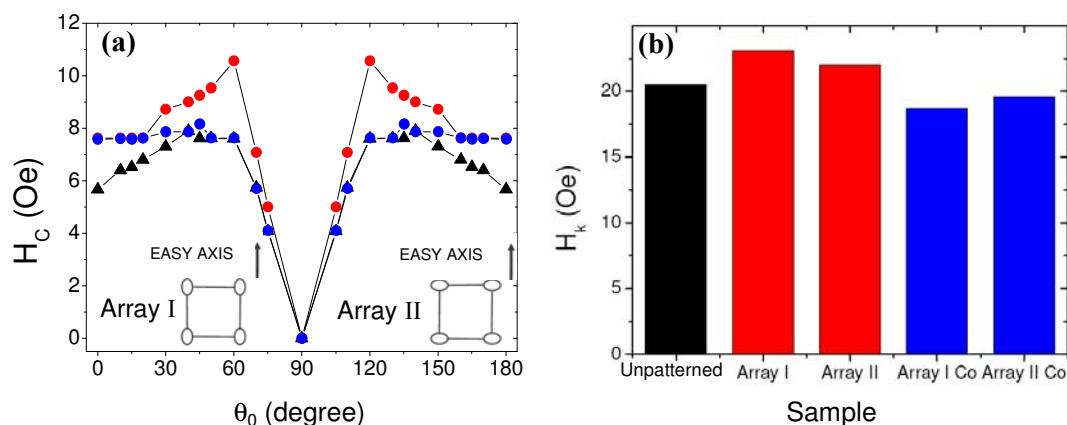


Fig. 2: (a) Angular dependence of the coercivity for magnetooptical transverse Kerr effect hysteresis loops. Black triangles, unpatterned film; red circles, Array I with empty holes; blue circles, Array I with Co filled holes. (b) Anisotropy field values for: unpatterned film (black); Array I and Array II with empty holes (red); Array I and Array II with Co filled holes (blue).
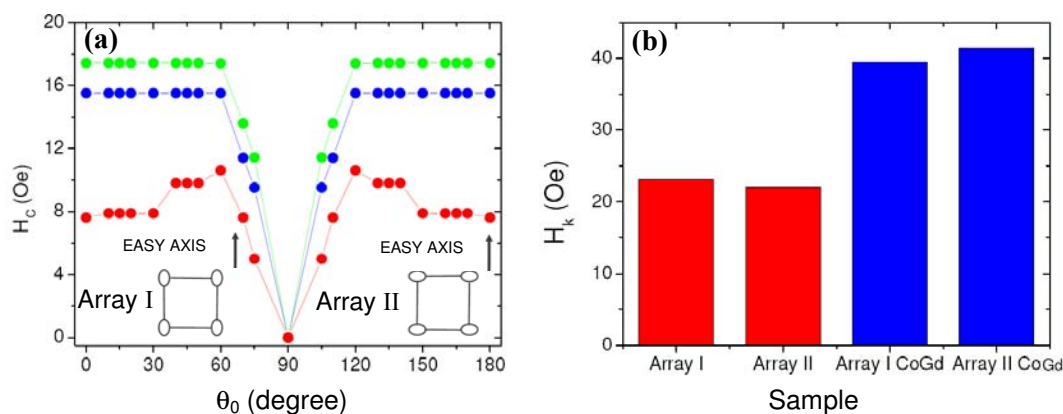


Fig. 3: (a) Angular dependence of the coercivity for magnetooptical transverse Kerr effect hysteresis loops. Red circles, Array I with empty holes; blue circles, Array I with $Co_xGd_{1-x}$ filled holes; green circles, Array II with $Co_xGd_{1-x}$ filled holes (b) Anisotropy field values for: Arrays I and II with empty holes (red); Arrays I and II with $Co_xGd_{1-x}$ filled holes (blue).

# GOLD MANNO-NANOPARTICLES AS POTENTIAL MICROBICIDES AGAINST HIV INFECTION

*O. Martinez-Ávila,[1] C. Clavel,[1] S. Penadés,[1] M. Stefanidou,[2] M. Hayes,[2] R. Shattock,[2] K. Hijazi[3] and C. Kelly[3]*

[1] *Laboratory of Glyconanotechnology, Biofunctional Nanomaterials, CIC biomaGUNE. San Sebastián, Spain.*
[2] *St George's, University of London, UK.*
[3] *King's College London, London, UK.*
omartinez@cicbiomagune.es

One of the mechanisms of vaginal infection by HIV is mediated by interactions between the virus envelope glycoprotein gp120 and DC-SIGN receptor of dendritic cells [1, 2]. The high mannose oligosaccharide $Man_9GlcNAc_2$ and the hybrid type oligosaccharide $GlcNAc_2Man_3$ seem to be involved in these interactions.

In order to inhibit the interaction between gp120 and DC-SIGN we have prepared gold nanoclusters capped with the mannose structural motives present in the gp120. These so-called Glyconanoparticles (GNPs) have been prepared by means of Glyconanotechnology, a technology developed in our laboratory to obtain multifunctional carbohydrate functionalised nanoclusters [3, 4]. GNPs are water soluble biofunctional gold nanoclusters, with globular shape, chemically well defined composition and an exceptional small core size which can be prepared in a simple way.

We have prepared and characterized a set of new water soluble mannose GNPs. The first step consists in synthesizing the neoglycoconjugates. Each of them are constituted of a mono- or oligomannoside head functionalized with different linkers. The linker were endowed of either a thiol group for attaching the neoglycoconjugate to the gold surface through a Au-S covalent bond. The neoglycoconjugates (mono-, di-, trisaccharides) are based on high mannose oligosaccharides and hybrid type structures present in the gp120 of the HIV virus. The resulting ligands have been incorporated with different densities (5 to 100%) at the surface of the gold nanocluster. Finally, mannose GNPs of different sizes (1 to 6 nm) have been synthesized to study if the GNP size can influence carbohydrate-protein interaction.

Fourteen gold *manno*-GNPs were first tested by surface plasmon resonance (SPR) as potential inhibitors of DC-SIGN binding to gp120 and in cell-based models to evaluate their effect inhibiting binding and dissemination of HIV-1 from cells bearing DC-SIGN to T cell populations. GNPs bearing Manα1-2Man showed 100% inhibition of DC-SIGN binding to gp120 at 50 nM concentrations by SPR and can directly inhibit HIV-1 binding to DC-SIGN^{+} cells and subsequent *trans*-infection of T-cells. For complementary studies by SPR and flow cytometry, fluorescein-labelled and biotin-containing GNPs bearing Manα1-2Man are being prepared.

[1] Calarese *et al*, Science, **300** (2003) 2065.
[2] H. Feiberg *et al*, Science, **294** (2001) 2163.
[3] J.M. de la Fuente *et al*, Angew. Chem. Int. Ed. Engl, **40** (2001) 2258.
[4] A. G. Barrientos *et al*. Chem.Eur. J., **9** (2003) 1909.

# SURFACE POTENTIAL DYNAMIC ON HIGHLY ORIENTED PYROLYTIC GRAPHITE

D. Martínez-Martín and J. Gómez-Herrero

Dpto. Física de la Materia Condensada,

Facultad de Ciencias. Universidad Autónoma de Madrid

Madrid 28049, Spain

Carbon allotropes: diamond, graphite, nanotubes and fullerens, exhibit highly interesting fundamental properties[1] and a variety of applications in material science. Specifically, graphite is an interlayer compound with good electrical conductance in-plane but a weak bounding between layers resulting in a low electrical conductivity along the surface perpendicular direction[2]. If this perpendicular conductivity is low enough, it may result in high electrical resistance between adjacent domains, giving rise to surface potential fluctuations (SPF) as reported by Yonghua Lu et al[3]. However a recent comment to this work[4] attributes the SPF to surface contamination. In this letter we provide a procedure to create SPF in any type of highly oriented (HOPG) graphite sample. By using an atomic force microscope (AFM) inserted on a high vacuum chamber we measure potential maps that show an SPF dynamic that depends on the system pressure. Our results suggest that SPF dynamic is strongly influenced by the mechanical stress introduced by the sample cleaving and do not support contamination as the main cause for the observed SPF.

---

[1] Wallace PR.The band theory of **graphite.** *Phys Rev* 71, 622(1947)

[2] Y. Kopelevich *et al.*, in *Advances in Solid State Physics*, edited by B. Kramer (Springer, Berlin, 2003) Vol. 43p. 207.

[3] Lu, Y. H. *et al*. Electrostatic force microscopy on oriented graphite surfaces. Coexistence of insulating and conducting behaviors. *Phys. Rev. Lett.* **97**, 076805 (2006).

[4] S. Sadewasser and Th. Glatzel. Comment on 'Electrostatic Force Microscopy onoriented Graphite Surfaces: Coexistence of Insulating and Conducting Behaviors. *Phys. Rev. Lett.* **98**, 269701 (2007)

# SCANNING TUNNELING MICROSCOPY STUDY OF PTCDA GROWTH ON Ge(111)-c(2x8) SURFACES

*A.J. Martínez-Galera, Zheng Wei[a], N. Nicoara, I. Brihuega[b] and J.M. Gómez-Rodríguez*
*Departamento de Física de la Materia Condensada, Universidad Autónoma de Madrid,*
*E-28049, Madrid, Spain*
[a] *Permanent address: Department of Modern Physics, University of Science and Technology of China, Hefei, 230026 China*
[b] *Present address: Max-Planck-Institut für Festkörperforschung, Heisenbergstrasse 1, D-70569 Stuttgart, Germany*
antonio.galera@uam.es

The epitaxial growth of organic molecules on metallic or semiconductors substrates is a highly interesting topic both from a fundamental point of view –in order to understand the physical properties of the interfaces of organic/inorganic materials- as well as by its applications in optoelectronics devices. The perylene and its derivatives have been proposed as appropriate materials for being used in these devices. Particularly, PTCDA (3,4,9,10 perylene tetracarboxylic dianhidride) has been proposed as a model system for the study of the epitaxial growth in metallic surfaces, since ultra thin well ordered films can be easily obtained [1,2]. However, in semiconductors substrates, due to the high reactivity of their surfaces, it is usually necessary to apply pasivation processes in order to induce molecular order [3]. In this work the initial stages of the growth of PTCDA at room temperature (RT) on the semiconductor surface Ge(111)-c(2x8) have been studied by means of scanning tunneling microscopy (STM). The results show that PTCDA molecules have a high mobility at RT on the well ordered areas of the substrate, since at submonolayer coverage nucleation is only observed in domain walls and defects of the substrate (Fig. 1). For higher coverages, it has been observed the formation of three-dimensional molecular islands, with crystalline structures close to those of the molecular bulk crystal, and grown on top of a first disordered molecular layer.

## References:

[1] S. R. Forrest, Chem. Rev., **97** (1997),1793.
[2] N. Nicoara, E. Román, J. M. Gómez-Rodríguez, J. A. Martín-Gago and J. Méndez, Org. Electron. **7** (2006), 287.
[3] N. Nicoara, O. Custance, D. Granados, J.M. García, J.M. Gómez-Rodríguez, A.M. Baró and J. Méndez, J. Phys.: Condens. Matter **15** (2003), S2619.

## Figures:
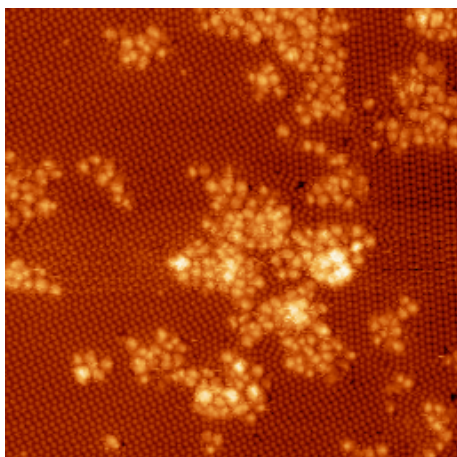


**Fig. 1**: STM image (50x50 nm$^2$) showing disordered molecular islands of PTCDA as well as clean substrate areas presenting the Ge(111)-c(2x8) reconstruction. Tunneling parameters: Vs = +1.5 V; I = 85 pA.

# TWO-DIMENSIONAL SURFACE EMITTING PHOTONIC CRYSTAL LASER WITH HYBRID TRIANGULAR-GRAPHITE STRUCTURE

L.J. Martínez[1], A.R. Alija[1], P.A. Postigo[1], Ch. Seassal[2] and P. Viktorovitch[2]

*1.- Instituto de Microelectrónica de Madrid,* Centro Nacional de Microelectrónica, Consejo Superior de Investigaciones Científicas, Isaac Newton 8, PTM Tres Cantos, 28760 Madrid, Spain
2.- Institut des Nanotechnologies de Lyon (INL), UMR 5270 CNRS-ECL-INSA-UCBL, Ecole Centrale de Lyon 36, Avenue Guy de Collongue, BP 163, F - 69134 Ecully Cedex, France

luisja@imm.cnm.csic.es

Laser emission of a compact surface-emitting microlaser, optical pumped and operating at 1.5 μm at room temperature is presented. The two-dimensional photonic crystal (PC) is conformed in a hybrid triangular-graphite lattice [1] designed for vertical emission. The structures have been fabricated on InP slabs including four InAsP quantum wells, a $SiO_2$ bonding layer, and a bottom high index contrast $Si/SiO_2$ Bragg mirror deposited on a Si wafer [2]. Standard techniques of electron-beam lithography and reactive ion-etching have been used for the patterning. The optical characterization was performed by microphotoluminescence spectroscopy. Laser emission (see Fig1: Right) has been achieved with high quality factors around Q~4000.

[1]  L. J. Martínez et al., Optics Express **12**, 23, pp 5684 (2004)
[2]  B. Ben Bakir et al., Applied Physics Letters **88**, 081113 (2006)
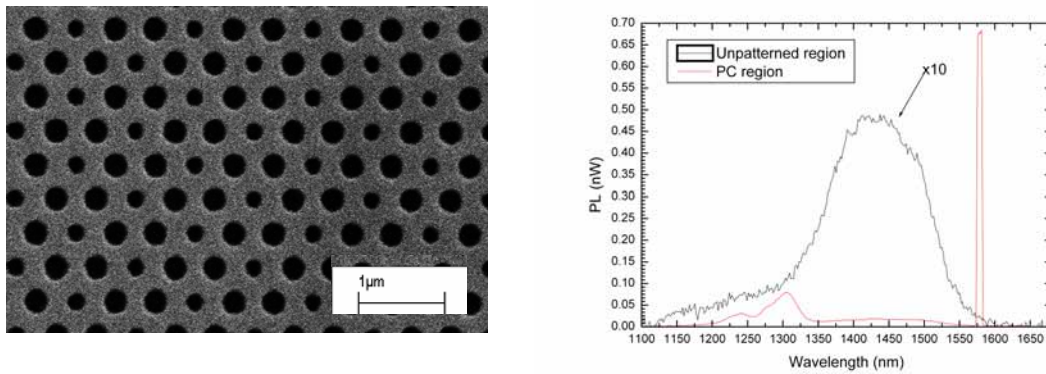
Fig.1. Left panel: SEM micrograph of the fabricated hybrid triangular-graphite structure. Right: Room-temperature photoluminescence spectra at of the PC structure (red line) and of the unpatterned sample (black line).

# NEGF Simulations of Scaled Double Gate MOSFETs using extracted masses from DFT calculations

A. Martinez[1], K. Kalna[1], P. Sushko[2], A. L. Shluger[2], J. R. Barker[1] and A. Asenov[1]

[1]*Device Modelling Group, Dept. of Electronics & Electric Engineering, University of Glasgow, Glasgow G12 8LT, United Kingdom*
[2]*Dept. of Physics & Astronomy, University College London, Gower Street, London WC1E 6BT, United Kingdom*
Email: *antonio@elec.gla.ac.uk*      Fax: *+44 (0)141 330 4907*    Tel: *+44 (0)141 330 4792*

According to the 2006 update of the ITRS [1] ultrathin-body multi-gate transistors are expected to replace the conventional MOSFETs at 22 nm technology generation and beyond. One of the favoured candidates is the double gate (DG) MOSFET architecture due to its superior transport and electrostatic integrity. The ultimate scaling of the UTB DG MOSFETs beyond the 10 nm channel length mark requires body thickness below 5 nm. At such body thicknesses, the silicon channel losses its translation symmetry in the confinement direction and the reciprocal lattice becomes 2D. Si 2D bandstructure confined in the $\langle 100 \rangle$ direction becomes direct and the longitudinal and transversal masses of $\Gamma$, L and X valleys will depend on the channel thickness. Therefore, the predictive modelling of next generation UTB device performance has to take the channel thickness dependence of the bandstructure into account.

In this work, we employ a hierarchical simulation approach to study the impact of the Si-channel thickness dependence on the ultimate scaling of DG MOSFETs to the sub-10 nm channel lengths. First principles Density Functional Theory (DFT) [2] simulations of the confined bandstructure have been carried out for Si slabs with different thicknesses passivated by hydrogen (Fig. 1). The B3LYP DFT crystal orbital method using a 88-31G* basis was used in CRYSTAL03 code [3] yielding a good agreement for the bulk transversal ($m_t$) and longitudinal ($m_l$) effective masses. The simulated bandstructures for three different Si channel thicknesses are illustrated in Fig. 2. The variations of electron transversal and longitudinal masses on the thickness (Fig. 3) have been extracted by fitting the $E(\mathbf{k})$ dependence of the LUMO state. The variation of confined masses are in good agreement with more scattered results from the DFT method published previously [4].

The extracted thickness dependent masses have been used to calculate the $I_D$-$V_G$ characteristics of DG MOSFETs with corresponding body thicknesses using a 2D Non-Equilibrium Green's Functions (NEGF) simulator [5,6] in a ballistic regime. In order to illustrate the impact of the thickness dependence of the effective masses, the results were compared with simulations assuming constant bulk effective mass values. The effect associated with the impact of the thickness dependence of the longitudinal and transversal masses on the device characteristic have been studied.

DG MOSFETs with 10, 6 and 4 nm gate lengths having body thicknesses of 6.1, 2.6 and 1.3 nm and oxide thicknesses of 0.6, 0.5 and 0.5 nm, respectively, follow the prescriptions of the ITRS [1]. The simulation domain for a device with the 10 nm gate length is shown in Fig. 4. All transistors have a S/D doping of $2\times10^{20}$ cm$^{-3}$ and an undoped channel. The corresponding 2D potential and electron density distributions in the mid channel plane are shown in Figs. 5 and 6. The simulated $I_D$-$V_G$ characteristics of the 10 nm DG MOSFET illustrated in Fig. 7 indicate that there is practically no change at $V_D$=0.8 V when the bulk transversal effective mass is replaced by its confined value but the threshold voltage slightly increases at $V_D$=0.05 V. Figs. 8 and 9 show $I_D$-$V_G$ characteristics of the 6 nm gate length transistor with a body thickness of 2.6 and 1.3 nm, respectively. There is a small change of 5 and 10 mV/dec in the subthreshold slope (SS) between the confined and corresponding bulk masses in the 2.6 and 1.3 nm body devices, respectively. The SS change from 88 to 65 mV/dec indicates a better electrostatic control in the thinner channel transistor when the device body narrows from 2.6 nm to 1.3 nm. Fig. 10 shows the $I_D$-$V_G$ characteristics for the 4 nm gate length device with a 1.3 nm body thickness. The characteristics obtained by using bulk mass have an order of magnitude higher leakage current compared to those obtained by using confined transversal mass. At such channel thickness, the transversal mass increases from its bulk value of 0.19 $m_0$ to 0.294 $m_0$ thus reducing the S/D tunnelling. The impact of the confined $m_t$ and $m_l$ in the subthreshold regime can be distinguished in Fig. 11. When only the bulk transversal mass is replaced by its confined value then the SS increases. When, in addition, the bulk longitudinal mass is replaced by its confined value the SS remains unchanged but the threshold voltage decreases. The behaviour of the $I_D$-$V_G$ characteristics is related to that of transmission coefficients in Fig. 12. Here, a contribution of the first valley only is shown because the second and third valleys are positioned energetically higher (by 0.5 eV) and do not contribute to the transport. At the onset, the transmission obtained using the bulk masses for both $m_t$ and $m_l$ is larger. As energy increases, the transmission obtained using the confined mass for $m_t$ becomes larger, eventually crossing the transmission obtained using the bulk masses only thus exactly mimicking the behaviour observed in the $I_D$-$V_G$ characteristics of Fig. 11.

In conclusion, the channel thickness dependence of the Si bandstructure starts to affect noticeably the DG MOSFET performance at channel lengths below 6 nm.

**References:**
[1] Int. Technol. Roadmap for Semiconductors, 2005 Edition [http://public.itrs.net] (SEMATECH, 2005).
[2] J. P. Perdew, K. Burke, and M. Ernzerhof, Phys. Rev. Lett. **77,** 3865-3868 (1996).
[3] V. R. Saunders et al., CRYSTAL2003 User's Manual, University of Torino, Torino (2003).
[4] Y. Teratani et al., Ext. Abst. SSDM, 270-271 (2005).
[5] A. Svizhenko et al., J. Appl. Phys. **91**, 2343-2354 (2002).
[6] A. Martinez et al., IEDM 2005 Tech. Dig., 627-630 (2005).
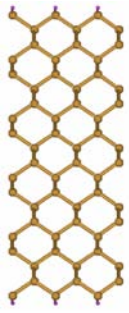
**Fig. 1:** Atomic structure of a confined Si used in the DFT calculations.
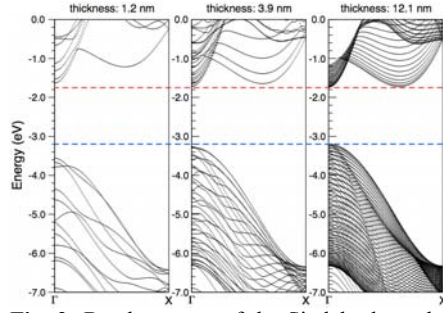


**Fig. 2:** Bandstructure of the Si slab along the Γ to X direction. The total density has been calculated by 4 **k**-points.
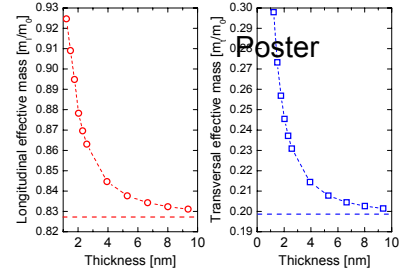


**Fig. 3**: Longitudinal [m(l)] and transversal [m(t)] electron effective masses versus the slab thickness extracted from calculated bandstructures. The values of extracted bulk masses are indicated by dash lines.
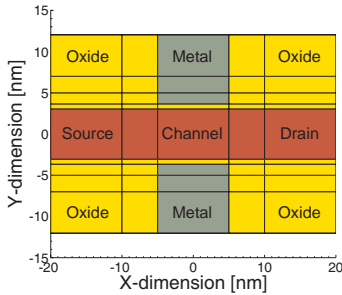


**Fig. 4:** 2D domain of DG MOSFETs as considered in the NEGF simulator. The source and drain contacts are assumed to be heavily doped to $2 \times 10^{20}$ cm$^{-3}$.
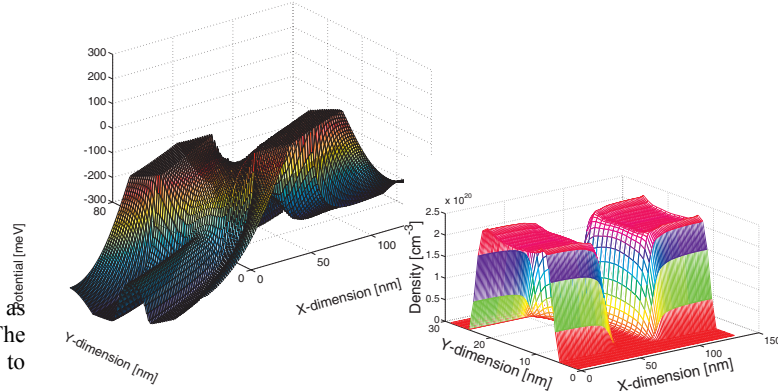


**Fig. 5:** Potential profile at $V_D$=0.05 V and $V_G$=0.2 V in the 10 nm gate length, 6.1 nm thick body DG MOSFET.



**Fig. 6**: Electron density at $V_D$=0.05 V and $V_G$=0.2 V in the 10 nm gate length, 6.1 nm thick body DG MOSFET.
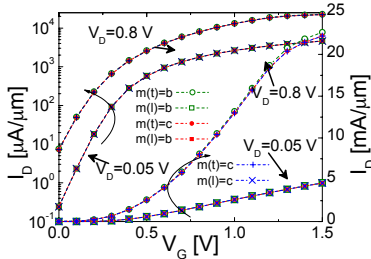


**Fig. 7:** $I_D$-$V_G$ characteristics for the 10 nm gate length DG MOSFET obtained from NEGF simulations. The impact of confined (c) masses in transversal [m(t)] and longitudinal [m(l)] transport directions is compared with that of bulk (b) masses.
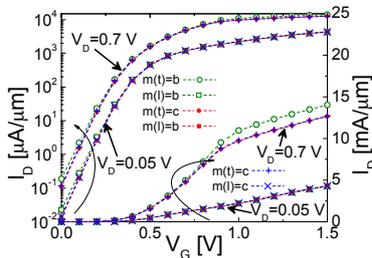


**Fig. 8:** $I_D$-$V_G$ characteristics for the 6 nm gate length, 2.6 nm thick body DG MOSFET comparing the effect of confined (c) and bulk (b) Si masses in transversal [m(t)] and longitudinal [m(l)] transport directions.
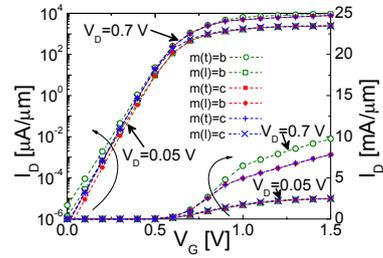


**Fig. 9:** $I_D$-$V_G$ characteristics for the 6 nm gate length, 1.3 nm thick body DG MOSFET comparing the effect of confined (c) and bulk (b) Si masses.
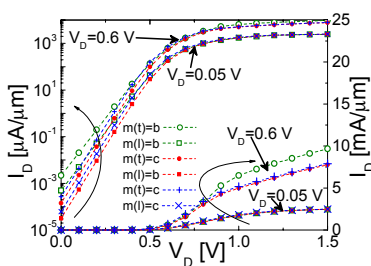


**Fig. 10:** $I_D$-$V_G$ characteristics for the 4 nm gate length, 1.3 nm thick body DG MOSFET comparing the effect of confined (c) and bulk (b) Si masses.
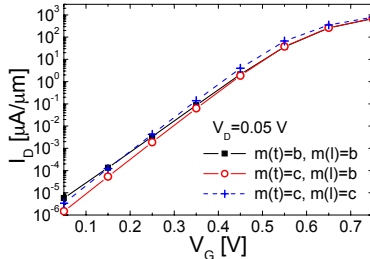


**Fig. 11:** The detail of $I_D$-$V_G$ characteristics for the 6 nm gate length, 1.3 nm body DG MOSFET. The effect of systematically replacing bulk values of m(t) and m(l) with their confined values is demonstrated.
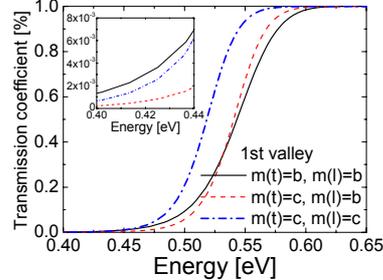


**Fig. 12:** Transmission coefficients as a function of energy at $V_G$=0.15 V and $V_D$=0.05 V in the 6 nm gate length, 1.3 nm thick body DG MOSFET. The inset shows the detailed onset of the transmission.

# A NEW 3-STATE CATECHOL-BASED FLUORESCENT SWITCH ON SURFACE

*A. Martínez[1], E. Evangelio[3], F. Busquets[2], J. Hernando[2], D. Ruiz-Molina[3*]*
*1) Instituto Catalan de Nanotecnología, Campus UAB, Bellaterra, Spain*
*2) Departament de Química, Universitat Autònoma de Barcelona, Bellaterra, Spain*
*3) Instituto de Ciencia de Materiales de Barcelona, Campus UAB, Bellaterra, Spain*

*dani@icmab.es*

The development of compounds that can be easily and reversibly interconverted between different forms, each one characterized by clearly detectable signals (i.e., molecular switches) is of great interest in fundamental and applied research. Different read-out for such switches can be envisioned although among them, luminescence is a very effective readout signal to monitor the state of the switch. On the other side, organic molecules appear to be potential candidates for the realization of future data-elaboration, -storage, and –communication devices[1]. Among them, catechol-based pH sensors are scarce in spite of their interest. Indeed, catechols have been already shown to have a crucial role in different biological processes, decontamination of soils as part of humic and fulvic acids or even in the field of molecular electronics as components of bistable valence tautomeric complexes.

To overcome this situation, a new catechol derivative exhibiting an acid/base induced switching of the fluorescence in solution was synthesized in our group. The 3-states of the molecule and their respective fluorescence spectra are shown in the Figure 1. However, for this switching behaviour in solution to become a real integrated device, the nanostructuration of the molecules on the surface and the study of their response after acid/base stimuli are highly required.
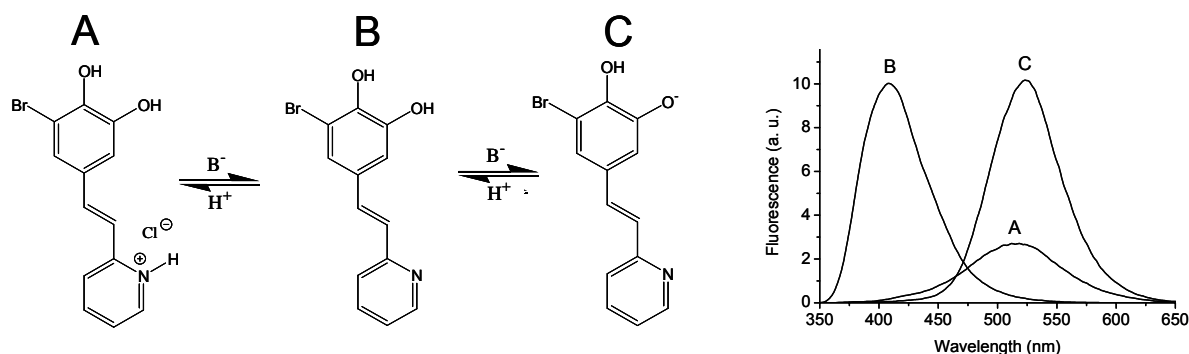


*Figure 1. Catechol-based switch, (left) states of the molecule, (right) fluorescent spectra.*

Prior to this work, advanced nanofabrication and self-assembly techniques have been used in fabrication of molecular-scale systems[2-3]. Among them, the Lithographically Controlled Wetting (LCW) technique, developed by Biscarini et al. [4], is a convergent approach based on the stamp-assisted deposition of molecules from a solution together with dewetting phenomena arising from competing interactions between the molecules and the substrate.

Herein we report for the first time the switching behaviour between the three states of the molecules deposited by the LCW technique on Highly Oriented Pyrolitic Graphite (HOPG) and glass. After controlled deposition of the molecule on the surface, the switching was successfully done and followed by confocal microscopy although accompanied by some degradation of the molecular stripes of molecules with repeating cycles of gas bubbling, fact that was confirmed by AFM studies.

Representative images of the switching of the fluorescence upon exposure to the acid/base flow is shown in Figure 2.
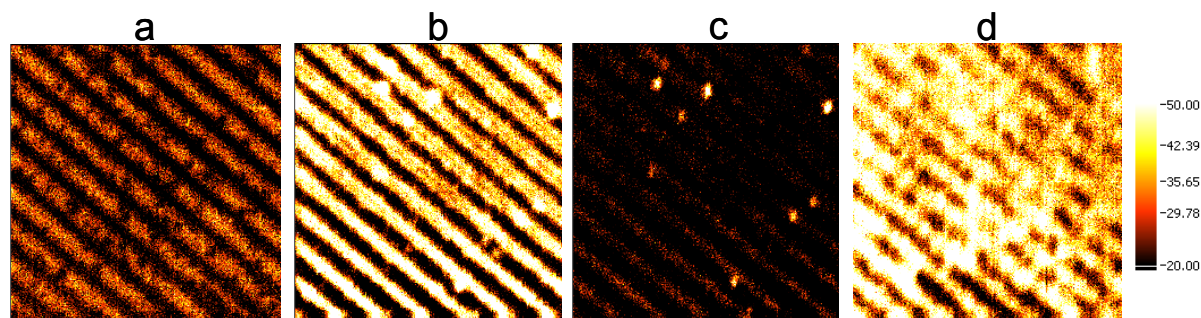


*Figure 2. Fluorescence images of 15x15 µm² areas of a glass substrate with stripes of catechol-based molecules on top after successive exposure of the sample to: (a) air; (b) Et₃N/N₂ flow; (c) HCl/N₂ flow; (d) HCl/N₂ flow for 5 min. All six images were recorded with the same instrument settings. The fluorescence intensity scale is also equal for all displayed images.*

*Experimental*. For this experiment a custom made scanning fluorescence confocal microscope was used. The detection window ($\lambda_{det}$>550 nm) was set in the way changes between the 3-states can be appreciated (see fluorescence spectra above). Then, flows of acid (HCl) and base (Et₃N) were used "in situ" by bubbling nitrogen over solutions of these acid and base while the fluorescence images were taken. No liquids were drop on the surface to prevent desorption of molecules.

**References:**

(1) Bard, A. J. Integrated Chemical Systems: a Chemical Approach to Nanotechnology; Wiley: New York, 1994.

(2) T. Hassenkam, K. Moth-Poulsen, N. Stuhr-Hansen, K. Nørgaard, M.S. Kabir, T. Bjørnholm, Nanoletter **4** (2004) 19.

(3) D.P. Long, C.H. Patterson, M.H. Moore, D.S. Seferos, G.C. Bazan, J.G. Kushmerick, Appl. Phys. Lett. **86** (2005) 153105.

(4) M. Cavallini, F. Biscarini Nano Lett. **3** (2003) 1269.

# BEHAVIOR OF THE UFM SIGNAL IN DIFFERENT KNOWN SAMPLES AND COMPARISON WITH COMPUTER SIMULATIONS.

J. J. Martínez and M. T. Cuberes
Laboratory of Nanothechnics, University of Castilla-La Mancha (Spain)
juanjillo_a@yahoo.com, teresa.cuberes@uclm.es

In ultrasonic force microscope (UFM) [1], we can map the mechanical properties of a sample material. The technique is based in the extra deflection that experiment the lever in an AFM experiment, when an ultrasonic vibration of an appropriate frequency, is transmitted throw the sample to the sharp tip in the extreme of the lever [2]. Due to the inertia of the lever, this can't follow the ultrasonic frequency and experiment an average of the non linear tip-sample interaction force designated "ultrasonic force". The extra deflection of the lever is more bigger for a threshold amplitude that depend of the sample, frequency, humidity,… and can disappear for some frequencies. The friction can reduce and disappear for a sufficient amplitudes and appropriate frequency. The signal obtained from the deflection of the lever (ultrasonic signal), have information about the mechanical properties of the sample how stiffness or adhesion.

In our experiments, we apply an amplitude modulation to the ultrasonic vibration in order to know the threshold amplitude of the UFM signal, the max amplitude of the UFM signal, the difference between the ultrasonic amplitude after and before of the threshold input amplitude, and other parameters. All this can give us quantitative information about the mechanical properties of the sample. We can get some examples of this in the literature [3][4][5].

We have observed noticeable differences between the UFM signals measured in different samples [Fig.1] with different mechanical properties. We are trying to describe the differences in the UFM signals for different samples, and trying to extract quantitative information of this. Too, at the same time, we are simulating the models in the literature and comparing this with the experimental signals, changing all the parameters possible, and determining the validity of the models for different samples. This simulations have help us to do a new explanation of the UFM hysteresis behavior [Fig.2] when the amplitude of the ultrasonic vibration is increased and decreased, that let us to have a better knowledge of the physic fenomenon.

**References:**

[1] Yamanaka et al., Appl. Phys. Lett. 64 (1994) 178; M.T.Cuberes, G.A.D.Briggs, O.Kolosov, *Nanotechnology* 12, 53-59 (2000) y referencias incluídas.
[2] O.Kolosov, K.Yamanaka, *Jpn.Appl.Phys*. 32, 1095-1098 (1993)
[3] F. Dinelli et al. Phys. Rev. 61 (2000) 13997
[4] K. Inagaki. App. Phys. Lett. 80 (2002) 13.
[5] R. Szoszkiewicz. App. Surf. Science. 210 (2003) 54-60.

**Figures:**

[Fig.1] Different UFM signals for each sample.
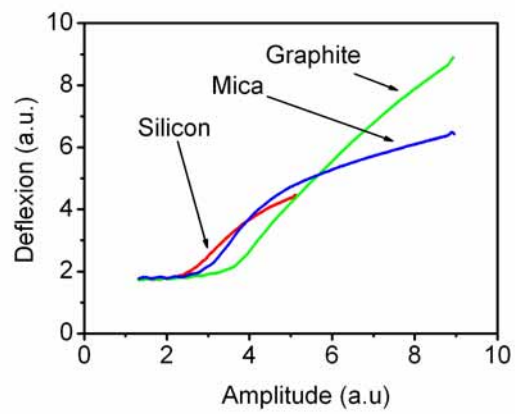


[Fig.2] Ultrasonic hysteresis.
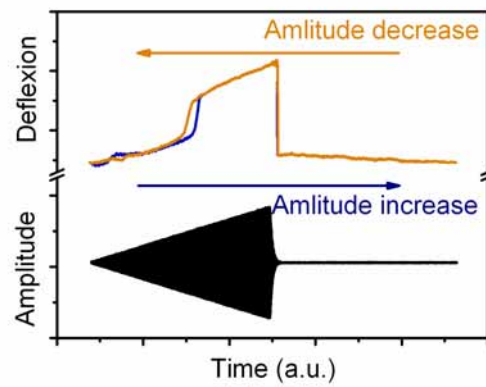
# FISRT STAGES OF THE GROWTH OF PT-CLUSTERS ON QUASI-METALLIC 1D ROWS OF TiO$_2$(110)-(1X2) SURFACES.

C. Sánchez-Sánchez, M. Blanco-Rey[*], J. Abad[+], J. Mendez,  M.F. López,  P.L. de Andrés, J.A. Martin-Gago

*Instituto de Ciencia de Materiales de Madrid (CSIC), Cantoblanco 28049 Madrid, Spain.*
*\* Department of Chemistry, Lensfield Rd, Cambridge CB2 1EW, UK*
*+Centro de Investigación en Optica y Nanofísica, Universidad de Murcia, Campus Espinardo, 30100 Murcia, Spain*

*Gago@icmm.csic.es*

The surface of metal oxide materials is of huge technological relevance in a wide variety of fields, ranging from catalysis to fundamental chemistry. Although the rutile TiO2(110) surface has been extensively studied, the intrinsic difficulties, associated to defects and *history* of the sample, has lead to a limited basic knowledge on these materials. This is particularly true for the non-stoichiometric (1x2) reconstruction formed after reducing the surface by annealing up to about 800ºC. This reconstruction, although widely studied, presents a large variety of defects, which rends the understanding of its basic properties, still nowadays, unclear.  Several models have been proposed to date, but they differ even in the stoichiometry [1,2]. Combining STM, quantitative LEED, Angle resolved ultraviolet photoemission spectroscopy (ARUPS) and density functional theory (DFT), we have determined the atomic surface structure and electronic properties of rutile TiO$_2$(110)-(1x2). STM images show monoatomic steps, wide terraces and no cross-link features. The most suitable model to explain them consists of added Ti$_2$O$_3$ rows along the [001] direction [2]. A more detailed LEED-IV analysis, using a large database of intensities, recorded both normal and off-normal incidences, yields the relaxed surface parameters with a Pendry R-factor Rp = 0.29. Atomic coordinates are in good agreement with the minimum energy structure provided by DFT. Discrepancies can be explained by the large thermal vibration amplitudes found for the Ti$_2$O$_3$ group[2].

Surprisingly, the electronic structure derived from DFT shows a metallic character along the [001] direction. This striking feature is evidenced by parabollic dispersion bands crossing the Fermi level along the [001] direction, whereas in the perpendicular direction bands are rather flat [1]. The long quasi-1D chains display metallic character, do not show any interaction between them, and cannot couple to bulk or surface states in the gap region, forming good one-dimensional atomic wires. These electronic bands cannot be found in ARUPS because they are very close to the Fermi edge and disperse upwards, towards the conduction band. STM images show the presence of defect-free atomic chains covering all

terraces from one monoatomic step to the next. STS current-voltage curves, which reflect the local DOS, show qualitative agreement with UPS spectra.

On this deeply atomic and electronically characterized surface, we have deposited Pt at submonolayer coverages. The idea behind is that the catalytic properties of the surface could be enhanced due to the larger $Ti_2O_3$ conductivity. We have followed the first stages of adsorption from the first arriving adatoms to the cluster formation at about 1 ML. The ridges between $Ti_2O_3$ rows appear by DFT as the most favorable adsorption sites, making easier the formation of 1D structures. The growth process has been followed by angle resolved UPS and STM, gathering a picture of the main growth mechanisms.

Summarizing, by a combination of different experimental techniques and theoretical methods we have characterized the atomic structure and the electronic properties of the 1x2 reconstructed $TiO_2(110)$ surface, which consist of quasi-1D metallic chains with a $Ti_2O_3$ stoichiometry. On these chains we have deposited and characterized, both atomic and electronically, submonolayers of Pt which evolves from low-dimensional features to metallic clusters

**References:**

[1] M. Blanco-Rey, J. Abad, C. Rogero, J. Mendez, M. F. Lopez, J. A. Martin- Gago, P. L. de Andres, Phys. Rev. Lett. **96** (2006) 055502.

[2].- M. Blanco-Rey, J. Abad, C. Rogero, J. Mendez, M. F. Lopez, E. Roman, J. A. Martin-Gago, P. L. de Andres,. Phys Rev.B, **75** (2007) 081402(R).

**Figures:**
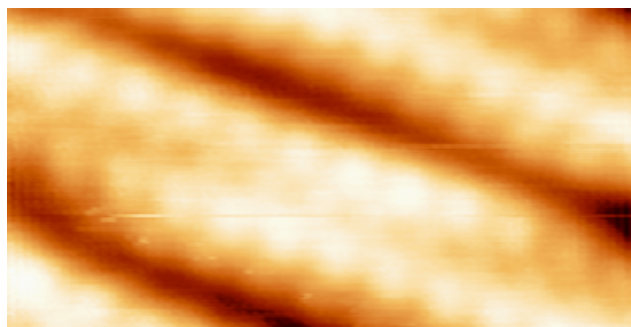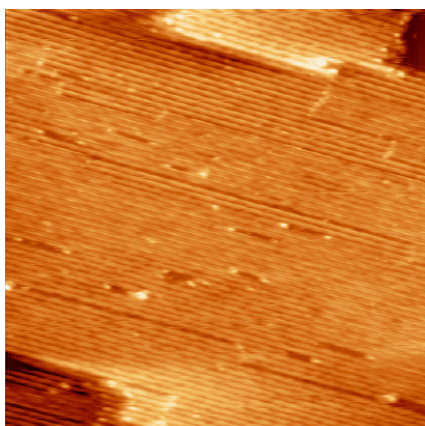


**Left:** Typical STM image of the $1 \times 2$ reconstruction of the TiO2(110), showing large chains running continuously along the [001] surface direction. The total width of the image is $100 \times 100$ nm$^2$ . **Right**: Typical atomic resolved STM image of the $1 \times 2$ reconstruction of the TiO2 (110). The total width of the image is $4 \times 2.7$ nm$^2$.

# Manipulation of covalently bound molecules with STM and AFM: a comparative theoretical study

*Natalia Martsinovich, Lev Kantorovich*
*Department of Physics, King's College London, Strand, London, UK*
*natalia.martsinovich@kcl.ac.uk*

Controlled manipulation of atoms and molecules is the route to the assembly of complex molecular and atomic patterns in nanotechnology. Scanning tunnelling microscopy (STM) has been widely used to manipulate atoms and molecules laterally across the surface; vertical manipulation of atoms and small molecules has been achieved as well. An important feature of STM is that a bias voltage is applied to the surface, which is likely to disrupt the adsorbate-surface bonding and assist manipulation, but may also damage large complex molecules. In contrast, atomic force microscopy (AFM) manipulation relies solely on interatomic interactions. Vertical manipulation of atoms has been achieved by AFM. Manipulation of molecules with AFM, however, has not been thoroughly studied either experimentally or theoretically.

In this paper, we present the results of our theoretical modelling of manipulation of a large molecule, the $C_{60}$ fullerene, covalently bound to the Si(001) surface. We first discuss its vertical manipulation and demonstrate using density-functional theory (DFT) calculations the possibility of lifting this molecule from the surface due to the tip-molecule chemical interaction only, without applying bias voltage. To achieve a vertical manipulation, the molecule needs to be brought to a precursor state where its bonding to the surface is minimised. This type of manipulation is possible in STM but not in AFM, where the cantilever oscillation period is much longer than atomic relaxation times, and the molecule would relax from the metastable precursor state to a stable site.

Thus, manipulation of molecules due to tip-molecule chemical bonding is not likely to operate in AFM. However, a different mechanism can be employed: the lowering of a manipulation barrier due to the tip-molecule interaction. We explore the values of the $C_{60}$ manipulation barrier for various tip positions. We perform kinetic Monte Carlo simulations to determine the probabilities of the molecule jumping to a new adsorption site as a result of its interaction with an oscillating AFM tip. The potential energy surface calculated using DFT is fed into the virtual AFM code to study the actual response of the dynamic mode AFM apparatus to the successful manipulation of the fullerene molecule.

# SPIN-DEPENDENT CURRENT STATES IN NONEQUILIBRIUM 2D NANOSYSTEMS – NEW PERSPECTIVES

*V. A. Mashkov*
*St.Petersburg State Polytechnic University*
*29 Polytechnicheskaya Street, St.Petersburg, Russia 195251*
*Mashkov@tuexph.stu.neva.ru*

A new type of spontaneously broken symmetry in two-dimensional nano-spintronics is discussed in detail. This broken symmetry is a 2D space inversion transformation that conserves the in-plane $x$ and $y$ spin components of a charge carrier and reverses the sign of its 2D quasi-momentum vector. The 2D space inversion symmetry breaking is specific to quasi 2D many free electron or hole systems located in space-charge layers experiencing strong inhomogeneous nano-scale strains near unrelaxed interfaces in quantum wells, quantum wires, and quantum dots.

Physical mechanisms that lead to the 2D band structure modifications characterized by the spontaneously broken 2D space inversion symmetry are investigated. The main mechanism is a well-known Rashba spin-orbit interaction coupled to 2D band structure. On the basis of eigenmode calculations for an inhomogeneously strained Rashba model it is shown that the 2D charge carriers are described by a natural basis of the spinor eigenfunctions corresponding to some circular spin-polarized states that should be distinguished from the so-called spinor helicity states. It is demonstrated that the ground state of a many particle 2D nanosystem is time-inversion invariant and 2D space inversion non-invariant. However, because of a complete mutual compensation of contributions from different circular spin-polarized states, the total microscopic spin polarization in the ground state of the system is zero that makes it difficult to observe this symmetry breaking directly. By making use of the Kubo formalism it is shown that a slightly nonequilibrium 2D many particle system in strained and biased space-charge nanolayers demonstrates nonequilibrium spin-dependent current states. Quantitative conditions for observability of such a quantum object as the spin-dependent current state are found and analyzed. First of all, these are the strength of the spin-orbit coupling in the inhomogeneously strained interface conditions and the averaged time of the carrier spin relaxation due to spin-phonon and/or spin flip-flop quantum transitions. The case of partially compensated electric fields due to strains of the variable sign, i.e. compression-dilatation, near the interface is also analyzed and the corresponding Rashba spin-orbit coupling constant is presented. The slightly nonequilibrium spin-dependent current states are further described in terms of the time- and 2D space-inversion properties of the system under consideration and the related energy splitting of the coupled spin-momentum states of a charge carrier. Keldysh-technique density matrix calculations have revealed the main quantum transition probabilities that govern the nonequilibrium dynamics of the resulting spin polarization coupled to the induced currents.

The presented and discussed signatures of the spontaneously broken symmetry relative to the 2D space inversion transformation in 2D strained and biased nanosystems are of doubtless interest regarding the contemporary trends in nanotechnology and applications of nano-spintronics to spin-transistors, effective spin-polarized emitters, spin-sensitive sensors, etc. It is nonequilibrium dynamic spin-dependent current states in nanosystems that determine their new spin-dependent transport and spin polarization properties.

# AN ATOMIC SCALE MODEL FOR THE SELF-ORGANIZATION OF S-CYSTEINE ON AU(111) SURFACES.

*Eva Mateo-Martí[(1)], Celia Rogero[(1)], Pedro De Andres [(2)], Jose-Angel Martín-Gago [(1,2)]*
*[(1)] Centro de Astrobiología. INTA-CSIC. Torrejón de Ardoz, 28850 Madrid. Spain.*
*[(2)] Instituto de Ciencia de Materiales de Madrid (CSIC), Cantoblanco 28049 Madrid, Spain.*
*mateome@inta.es*

Understanding the interaction of biomolecules on metal surfaces is issue of relevance due to the wide number of scientific and technological areas in which are involved. Among them, biosensors, biomaterials, biocatalysis and biocompatibility. Due to its simple structure, amino-acids can be used as a good model system to study biomolecule-surface interaction, which can indeed assist in the understanding of more complex systems. In addition, it has been found that a number of amino-acids self-organise to form well ordered-two-dimensional structures at metal surfaces [1]. The local adsorption geometry and the two-dimensional self-assembly of *S*-cysteine are of particular interest because it is the only amino-acid having a thiol side group. It is well known the affinity of thiol groups for noble metals, therefore, cysteine can be used as a bonding group for self-assembled monolayers formation. In addition, cysteine is located on the outer side of proteins, being a potential linker to anchor these proteins to inorganic or organic supports.

We present a characterization of cysteine adsorption on Au(111) at submonolayer coverage performed by a combination of experimental techniques (scanning tunnelling microscopy-STM, X-ray photoemission spectroscopy-XPS and ultraviolet photoemission spectroscopy-UPS) and theoretical *ab-initio* methods. XPS data show the adsorption of the zwitterionic form of S-cysteine molecule on the Au(111) surface (desprotonation of the carboxylic group and protonation of the amino group). Furthermore, the interaction of the amino-acid with the surface goes through the $COO^-$ and the thiol group (S-Au), which is the anchoring point of the molecule. This adsorption chemistry is similar to the depicted for the adsorption on Cu(110) surfaces by infrared spectroscopy [2]. The STM characterization performed under UHV conditions at room temperature reveals an structural evolution with time of the Cys/Au(111) system. Just after cysteine dosing at room temperature, the diffusion of molecules on the surface is very high. These diffusing molecules coexist with molecular islands lacking of internal order, which appear mainly anchored to the step edges, and with long ordered molecular rows. By means of video-STM we show that after a period of time, the long molecular rows evolves to develop an ordered molecular network of *S*-cysteine. The row separation is 12 Å, and the molecules interact with each other along the [112] surface direction, in good agreement with works from other authors [3]. An example of this growth is shown in figure 1. We show that the self-organized molecular island formation is related to the vanishing of the disordered areas due to surface diffusion. Thus, the interaction between molecules plays an important role, driving the formation of the self-organized structure.

This process can be fully explained by Density Functional Theory (DFT) calculations, which show that the on-top site is the most stable for the sulphur adsorption, being the carboxylate group also on-top. The diffusion barrier through the bridge site is small enough to lead diffusing molecules on the surface at room temperature. The optimized molecular geometry by DFT reproduces the main features described by XPS and infrared spectroscopy, i.e, interaction to the surface through the $COO^-$ and the thiol group. The cysteine molecule is deformed on the surface, adopting a flattened geometry and H-bridge bonding stabilizes the molecular rows imaged by STM.

Therefore, the above mentioned multi-technique approach let us to propose an atomic scale model for the interaction of the molecule with the surface, which accounts for the self-organization of the S-cysteine on Au(111).

**References:**

[1] E. Mateo-Marti, S.M. Barlow, S. Haq, R. Raval, Surface Science **501** (2002) 191-202.
[2] E. Mateo-Marti, Ch. Methivier, C.M.Pradier, Langmuir **20** (2004) 10223-10230.
[3] A. Kuhnle, T.R. Linderoth, M. Schunack, F. Besenbacher, Langmuir **22** (2006) 2156-2160.

**Figures:**
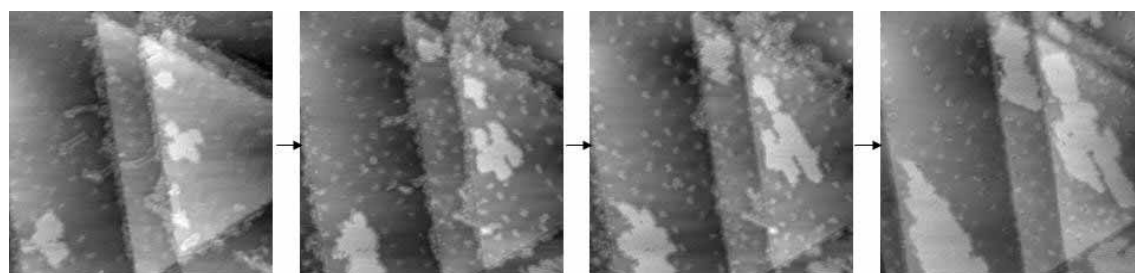


Figure 1: subsequent serie of STM images of *S*-cysteine adsorbed on Au(111) surface, where the growth of the islands is observed.

# Endohedral stannaspherenes: $Mn@Sn_{12}$ and its dimer. Ferromagnetic or antiferromagnetic?

Jon M. Matxain,[*] Elena Formoso, Jose M. Mercero, Mario Piris, and Jesus M. Ugalde

*Kimika Fakultatea, Euskal Herriko Unibertsitatea and Donostia International*
*Physics Center (DIPC), P.K. 1072, 20018 Donostia, Euskadi (Spain)*

The endohedral $Mn@Sn_{12}$ has been characterized, where a $Mn^{2+}$ cation is trapped inside an icosahedral $Sn_{12}^{2-}$, also called stannasphere, as can be seen in Figure 1. This endohedral structure is a sextuplet, with the 3d orbitals of $Mn^{2+}$ singly occupied. Thermodynamically, this encapsulation process is highly permitted, being the encapsulation free energy of around 24 kcal/mol. These monomers yields to a ferromagnetic or antiferromagnetic coupling in the case of the dimer. Three different dimers have been tried. The difference between dimers is the orientation of the monomers, where one atom of one monomer faces one atom, or two atoms another two, or finally three atoms face other three atoms. The most stable dimer is the one where three atoms face another three. In all cases the ferromagnetic and the antiferromagnetic dimers are near degenerate.

Figure 1: Structure of the ground state of the endohedral $Mn@Sn_{12}$ (left) and its radial electronic density distribution (right)
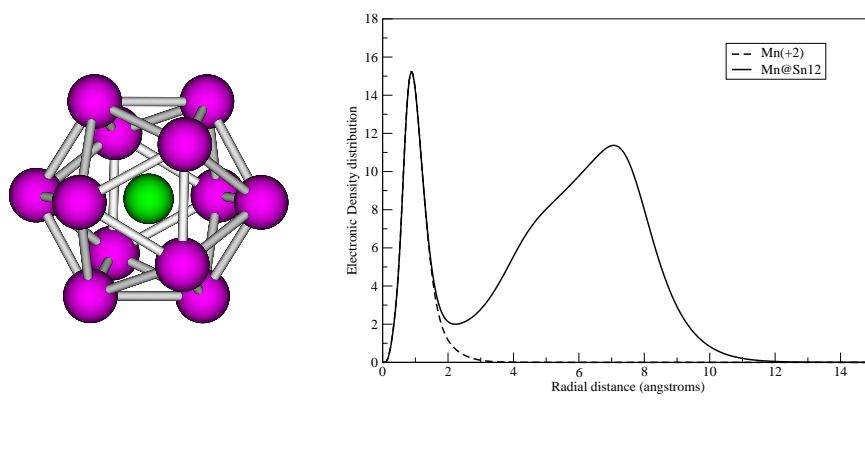
[*] Electronic address: jonmattin.matxain@ehu.es

## Selective growth of carbon nanotubes using preformed cobalt nanoparticle catalysts

*K. Subramanya Mayya, Seongho Moon, Youngmoon Choi, In-Seok Yeo, Sung-Tae Kim, Woosung Han*

*Advanced Process Development Team, Samsung Electronics Ltd., San#24 Nongseo-Dong, Giheung-gu, Yongin, South Korea*

*mayya@samsung.com*

Since their discovery in 1991, carbon nanotubes have been investigated in detail for their use for various applications including Field effect transistors, interconnects, sensors etc.[1,2] We at Samsung are interested in their ballistic transport properties that make them attractive candidates to replace electromigration prone copper interconnects.[3] Currently, multiwalled nanotubes are being investigated for this purpose firmly focusing on achieving lower resistance (including contact resistance), better process integration, etc. One of the important parameters to reduce the resistance is by providing multiple pathways for transport of electrons. This can be achieved by simultaneously decreasing the diameter of the nanotube and increasing their density. In general nanotube diameter sizes well with the diameter of the transistion metal catalyst used for their growth. While use of metals in the semiconductor fabrication lines is limited to few metals that catalyse growth of the nanotube, it is highly preferable if a would-be candidate catalyzes selective growth of CNT on metals. This selectivity would greatly assist in decreasing the complexity of the overall process. As reported recently, cobalt nanoparticles fit very well into this description.[4]

In this presentation we use preformed cobalt nanoparticles synthesized using wet-colloidal approach as catalysts for selective growth of carbon nanotubes on model metal in TiN. We observed that under CVD conditions, cobalt nanoparticles on TiN catalysed growth of nanotubes, while the same was not observed on silicon oxide (figure 1). CNT growth profiles on various patterned substrates including hole patterns will be reported. A plausible mechanism behind selectivity will be provided by characterizing the nanoparticles' composition on various substrates using x-ray photoelectron spectroscopy, TEM,etc.

**References:**

[1] Iijima, S.; *Nature*, **1991**, *354*, 56.

[2] (a) Tans, S. J.; Verschueren, A. R. M.; Dekker, C. *Nature*, **1998**, *393*, 49. (b) Martel, R.; Schmidt, T.; Shea, H. R.; Hertel, T.; Avouris, P. *Appl. Phys. Lett.* **1998**, *73*, 2447. (c) Zhou, C.; Kong, J.; Dai, H. *Appl. Phys. Lett.* **2000**, *76*, 1597. (d) Avouris, P.; Appenzeller, J. *The Industrial Physicist* **2004**, 18. (e) Postma, H. W. C.; Teepen, T.; Yao, Z.; Grifoni, C. Dekker, *Science*, **2001**, *293*, 76. (f) Tans, S. J.; Devoret, M. H.; Dai, H. J.; Thess, A.; Smalley, R.E.; Geerligs, L. J.; Dekker, C. *Nature*, **1997**, *386*, 474. (g) Bockrath, M.; Cobden, D.H.; McEuen, P.L. *Science*, **1997**, *275*, 1922.

[3] (a) Li, J.; Ye, Q.; Cassell, A.; Ng, H.T.; Stevens, R.; Han, J.; Meyyappan, M. *Appl. Phys. Lett.* **2003**, *82*, 2491. (b) Duesberg, G. S.; Graham, A.P.; Liebau, M.; Seidel, R.; Unger, E.; Kreupl, F.; Hoenlein, W. *Nano Letters*, **2003**, *3*, 257.

[4] Nihie, M et al, Proceeding of IEEE/IITC, **2004**, 251.
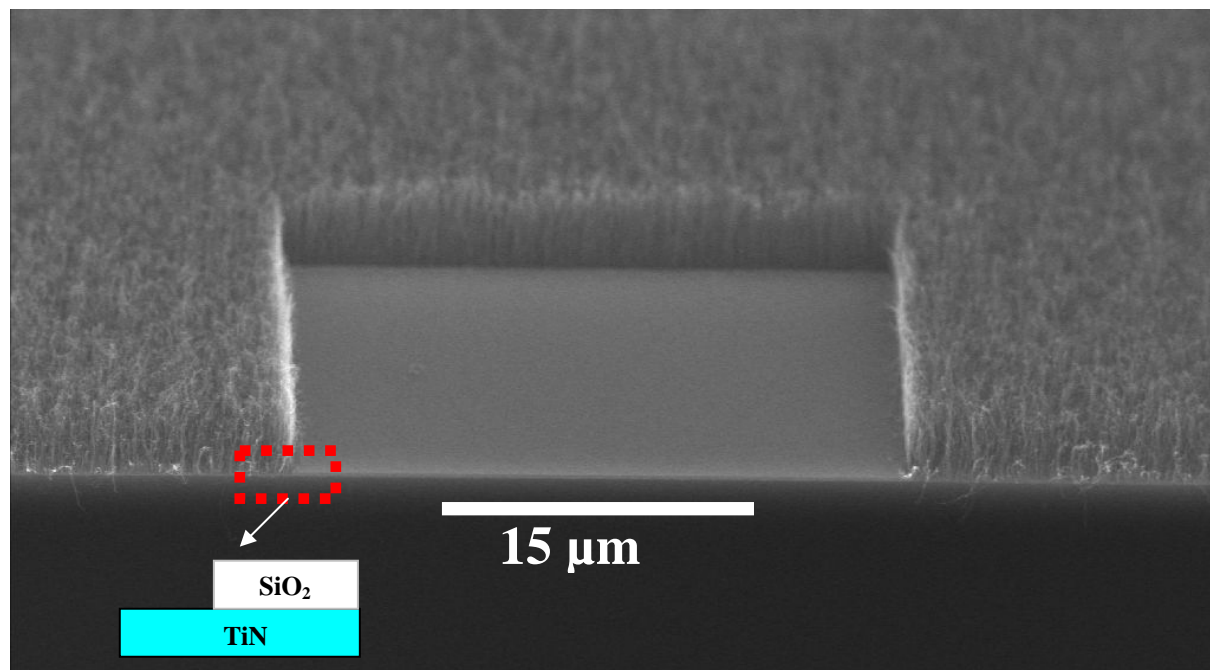
`Figure 1: SEM image of CNT grown using cobalt nanoparticles on patterned substrates.**

# MAGNETIC FIELD ENHANCED TIP FABRICATION FOR FOUR-PROBE STM STUDIES

*Jonathan McKendry, Stephen Evans*
*School of Physics and Astronomy, University of Leeds, Leeds, United Kingdom*
phy1jem@leeds.ac.uk

Here we demonstrate that the presence of a magnetic field produces a significant enhancement of tip length and a concomitant reduction in cone angle. We propose a model in which the Lorentz force acting on the ionic buffer prevents the adhesion of small bubbles at the anode which otherwise limit the tip quality [1]. An increase the magnetic field results in the formation of tips with a smaller cone angle and greater length, allowing the tips to be brought into close proximity. We demonstrate the use of such tips for four-probe conductivity measurements on metallic, template grown nanowires.

**References:**

[1] I. Ekvall, E. Wahlström, D. Claesson, H. Olin, and E. Olsson. Meas. Sci. Technol., **10** (1999) 11-18

**Figures:**
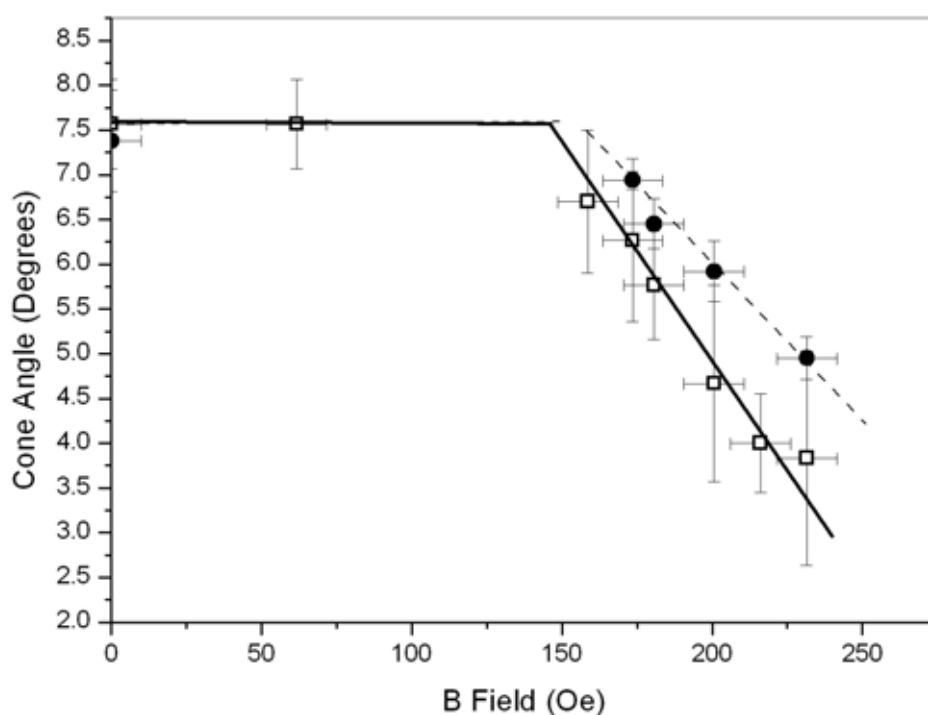


Figure 1. Graph showing the variation in cone angle as a function of the magnetic field. The solid circle points represent cone angles measured at 30000x magnification. The hollow square points represent cone angles measured at 900x magnification. The lines are guides to the eye.

# CONTROLLED FABRICATION OF NANOSTRUCTURES USING SP1 PROTEIN-NANOPARTICLE HYBRIDS

**Izhar Medalsy**,[1] Or Dgany,[2] Mukhles Sowwan,[1,3] Hezy Cohen,[1] Alevtyna Yukashevska,[4] Sharon G. Wolf,[5] Amnon Wolf,[6] Abraham Koster,[7] Orna Almog,[7] Ira Marton,[5] Yehonathan Pouny,[5] Arie Altman,[8] Oded Shoseyov[2]* and Danny Porath[1]*

*1-Physical Chemistry department, The Hebrew University, Jerusalem 91904, Israel. 2-The Institute of Plant Sciences, and Genetics in Agriculture, The Faculty of Agriculture, The Hebrew University, Rehovot 76100, Israel 3-Materials Engineering Department, Al Quds University, East Jerusalem 4-Utrecht University, 3584 CH Utrecht, the Netherlands. 5-Electron Microscopy Unit, Weizmann Institute of Science, Rehovot 76100 Israel, 6-Fulcrum SP Ltd P.O.Box 3206, Herzliya 46104, Israel , 7-Department Molecular Cell Biology, Leiden University Medical Center, Leiden 2300 RC, The Netherlands, 8-Department of Clinical Biochemistry, Health Sciences Faculty, Ben-Gurion University, Beer-Sheva 84105, Israel*

**Contact E-mail : Izhar@chem.ch.huji.ac.il**

The development of nanoelectronics is one of the essential goals of the electronic industry and the nanoscience community [1,2]. Biomolecular nanoelectronics has the potential to offer the ultimate solution for the problems of shrinking the size and increasing the complexity of conventional microelectronic circuits. Within the search for ideal candidates to realize self-assembling wires, devices, and circuits, proteins are believed to be valuable building blocks. The realization of nanoelectronics with novel self-assembling hybrid components bears a huge potential. On one hand, it has been demonstrated that natural protein functions can be exploited to develop device functions; on the other hand, proteins may be used to self-assemble functional inorganic objects.

In this work we implement nanoelectronic concepts based on protein-nanoparticle hybrids. SP1, an exceptionally stable protein circumvents the major problem in using proteins for nanotechnology: poor stability and low heat resistance [3-5]. We construct "lego-like" building blocks made of different recombinant SP1 proteins and inorganic nanoparticles. Once optimized, we expect that the designed structures will behave as efficient tunable electrical devices, with electrical response ranging from that of an ohmic wire to various non linear regimes, depending on the bio-inorganic sequence and on the geometrical setup. At the same time arrays of such protein-nanoparticles hybrids may serve as ultra high density memory arrays.

Long nanowires have been synthesized from protein-gold nanoparticle hybrids. Functionalized gold nanoparticles were attached to the central cavity of an extremely stable ring-like protein complex, termed SP1, with a diameter of 11 nanometers and height of 5 nm. The SP1-nanoparticle hybrids serve as building blocks in a "lego-like fashion". The size,

height, central cavity and binding groups of the building blocks and the distance between them can be tuned by genetic engineering and therefore their electrical properties may be manipulated. TEM, HAADF-STEM, AFM and EFM were used to demonstrate successful binding of gold nano-particles to the SP1 central cavity and the formation of wires with different inter-particle separations. We also demonstrate the formation of large ordered 2D crystalline arrays of SP1 rings induced by a phospholipid interface.

References:

1.  Lieber, C. M. The incredible shrinking circuit - Researchers have built nanotransistors and nanowires. Now they just need to find a way to put them all together. Scientific American 285, 58-64 (2001).
2.  R. Compano, L. M., D. J. Paul. Future and Emerging Technologies,Microelectronics Advanced Research Initiative. Technology Roadmap for Nanoelectronics, European Commission IST Programme http:// nanoworld.org/NanoLibrary/nanoroad.pdf.
3.  Dgany, O. et al. The structural basis of the thermostability of SP1, a novel plant (Populus tremula) boiling stable protein. Journal Of Biological Chemistry 279, 51516-51523 (2004).
4.  Wang, W. X. et al. Crystallization and preliminary X-ray crystallographic analysis of SP1, a novel chaperone-like protein. Acta Crystallographica Section D-Biological Crystallography 59, 512-514 (2003).
5.  Wang, W. X., Pelah, D., Alergand, T., Shoseyov, O. & Altman, A. Characterization of SP1, a stress-responsive, boiling-soluble, homo-oligomeric protein from aspen. Plant Physiology 130, 865-875 (2002).

Figures:
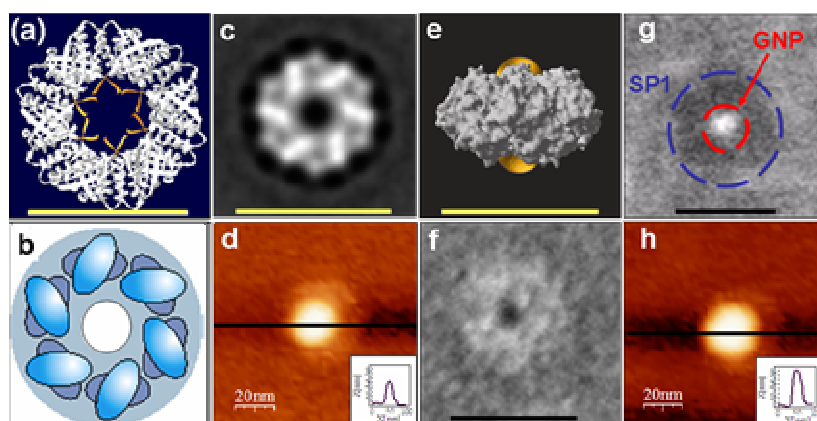


(a) X-ray structure of the SP1, showing the N-termini of the monomers in orange. (b) Scheme of the SP1 dodecamer. (c) Top-view TEM. (d) AFM image of a single dodecamer (inset-cross section). (e) Computer simulation of SP1-GNP in a side view. (f) Top view TEM of SP1-GNP. (g) Top view HAADF-STEM of SP1-GNP. (h) Top view AFM image of single SP1-GNP (inset-cross section). Scale bar 11nm.
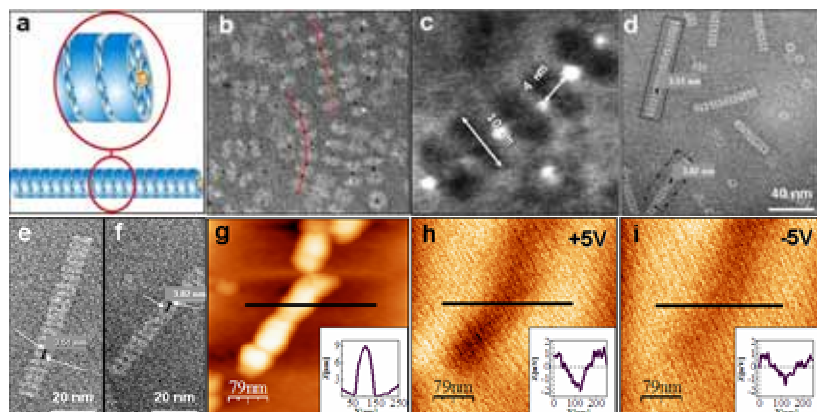


(a) A scheme representing the organization of nanowires composed of SP1-GNP.(b) TEM image of 6HSP1-GNP nanowires (marked by red lines). (c) HAADF-STEM image of 6HSP1-GNP nanowires with 4 nm GNP separation. (d) TEM image of 6HN-terminal truncated SP1-GNP nanowires with 3.5 and 3.8 nm GNP separation. (e,f) Enlargement of the bold, dashed line boxed nanowire from figure d respectively. (g) 6HSP1-GNP tube formation on mica. (h, i) EFM of 6HSP1-GNP tube formation on mica, a clear polarization effect of the embedded GNP is seen.

# MECHANICALLY RESPONDING NANOVALVES BASED ON POLYELECTROLYTE MULTILAYERS

D. Mertz[a], J. Hemmerlé[a], J.-C. Voegel[a], P. Schaaf[b], Ph. Lavalle[a]

[a]INSERM Unité 595 "Biomaterials", University Louis Pasteur, 11 rue Humann, 67085 Strasbourg, France
[b]Institut Charles Sadron, CNRS, 6 rue Boussingault, Strasbourg, France

The alternate deposition of polyanions and polycations on charged surfaces leads to the formation of nanostructured films called polyelectrolyte multilayers [1,2]. The layer-by-layer deposition constitutes a formidable tool to functionalize surfaces and its potential applications are optical coatings, filtration devices, self-supported membranes with highly enhanced Young's moduli, fuel cell membranes, drug release or biologically active coatings [3,4]. The layer by layer deposition process of polyelectrolytes is used to construct films equipped by compartments containing "free" polymers or biomolecules [5-8]. Each compartment corresponds to a stratum of an exponentially growing polyelectrolyte multilayer film and two consecutive compartments can be separated by a stratum composed of linearly growing multilayers that act as a barrier preventing polyelectrolyte diffusion from one compartment to another.

 Whereas a first generation of polyelectrolyte multilayers was designed to functionalize a surface in a stable way, such multicompartment films may constitute a new generation of functionalized coatings leading to *adaptative surfaces*. Most reported adaptative surfaces are aimed to respond, reversibly if possible, to external stimuli as for example pH, temperature or electrical stimuli and they are usually obtained by grafting polymers to solid substrates. The multilayer technology constitutes also an original way to develop these adaptative coatings and a second generation of multilayers responding to similar external stimuli is now emerging [9]. These films are usually designed to deliver active compounds consecutively to a change of pH [10] or temperature [11]. These stimuli, even if of great interest do not cover the whole possible stimuli range and others stimuli are envisioned for these surfaces. To our knowledge, only very few adaptative films responding to mechanical stimuli were reported up to now [12], despite the fact that mechanical stimuli can be of great convenient applications. One can, for example, anticipate their use in drug delivery patches, self repairing systems or nano-bio-sensor technology. We thus wish to make use of the great versatility of the multilayer technology to develop mechanically responding polyelectrolyte multilayers.

Such multicompartment films are now built up on an extensible silicon sheet to design stimuli responding films [13]. Nanometer-sized multilayer barriers deposited on or between multilayer compartments will act as nanovalves [14]. For the investigated system, the stretching induces the formation of pores in the barriers once a critical stretching degree is reached and consequently allows a diffusion process through the barrier of polyelectrolyte chains initially contained in the different compartments. This critical stretching degree depends upon the number of bilayers constituting the barrier.

Finally, the diffusion of polyelectrolytes through the barrier from one compartment to another can be switched on/off by tuning the mechanical stretching and thereby opening or closing nanopores in the barrier. This work represents a first step toward the design of chemically or biologically active films responding to mechanical stresses.
.

**References:**

**[1]** Decher, G., *Science,* 277**,** 1232 (1997).

**[2]** Picart, C., Mutterer, J., Richert, L., Luo, Y., Prestwich, G. D., Schaaf, P., Voegel, J.-C., Lavalle, Ph., *Proc. Natl. Acad. Sci. USA,* 99, 12531 (2002).

**[3]** Jessel, N., Lavalle, Ph., Meyer, F., Audouin, F., Frisch, B., Schaaf, P., Ogier, J., Decher, G., Voegel, J.-C., *Adv. Materials***,** 16, 1507 (2004).

**[4]** Jessel, N., Oulad-Abdelghani, M., Meyer, F., Lavalle, P., Haikel,Y., Schaaf, P., Voegel, J. C., *Proc. Natl. Acad. Sci. U.S.A,* 103, 8618 (2006).

**[5]** Garza, J. M., Schaaf, P., Muller, S., Ball, V., Stoltz, J.-F., Voegel, J.-C., Lavalle, Ph., *Langmuir*, 20, 7298 (2004).

**[6]** Garza, J. M., Jessel, N., Ladam, G., Dupray, V., Muller, S., Stoltz, J.-F., Schaaf, P., Voegel, J.-C., Lavalle, Ph., *Langmuir*, 21, 12372 (2005).

**[7]** Vodouhe, C., Le Guen, E., Garza J.M., Francius, G., Dejugnat, C., Ogier, J., Schaaf, P., Voegel, J.C., Lavalle, Ph., *Biomaterials*, 27, 4149 (2006).

**[8]** Jourdainne, L., Arntz, Y., Senger, B., Debry, C., Voegel, J.-C., Schaaf, P., Lavalle, Ph., *Macromolecules,* 40, 316 (2007).

**[9]** Sukhishvili, S. A., *Curr. Opinion Colloid Interf. Sci.***,** 10, 37-44 (2005).

**[10]** Izumrudov, V. A., Kharlampieva, E.; Sukhishvili, S. A., *Biomacromolecules***,** 6, 1782-1788 (2005).

**[11]** Quinn, J. F.; Caruso, F., *Macromolecules,* 38, 3414-3419 (2005).

**[12]** Russell, T. P., *Science* 297, 964-967 (2002).

**[13]** Hemmerlé, J., Roucoules, V., Fleith, G., Nardin, M., Ball, V., Lavalle, Ph., Marie, P., Voegel, J.-C., Schaaf P., *Langmuir*, 21, 10328 (2005).

**[14]** Mertz, D., *Hemmerlé*, J., Mutterer, J., Ollivier, S., Voegel, J.-C., Schaaf, P., Lavalle, Ph., *Nano Letters*, 7,657 (2007).

**Figure:**



*Unstretched state*          *Stretched state*
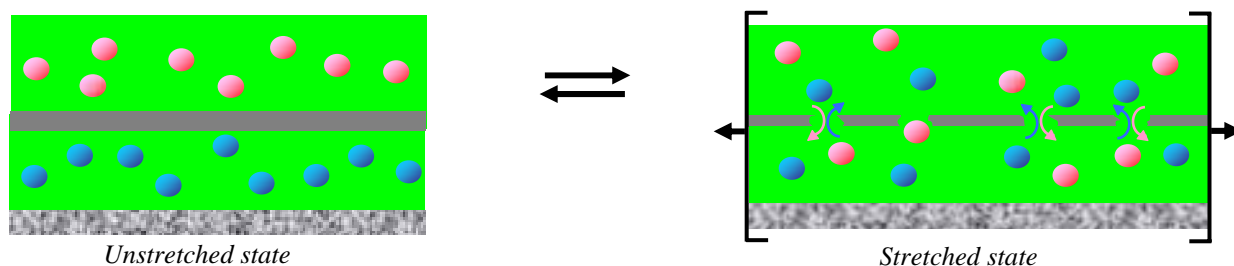
*Schematic representation of a multicompartment film before and during the stretching state. The gray line corresponds to the barrier that allows diffusion of molecules from one compartment to the other when the stretching is applied and nanopores are formed.*

# SYNTHESIS OF AlCuFe QUASICRYSTAL/POLYMER COMPOSITES

*C. Mihoc, R. Nicula, M. Stir, E. Otterstein, E. Burkel*
*Institute of Physiks, Rostock University,*
*August-Bebel-Strasse 55, D – 18055 Rostock, Germany*
*mihoc@physik1.uni-rostock.de*

Ultrahigh molecular weight polyethylene (UHMWPE) is used in orthopaedic implants due to outstanding wear properties. In spite of the low wear behaviour of UHMWPE compared to other polymers, wear remains a major problem in total joint replacements. Submicron wear particles cause foreign body response leading to bone resorption (osteolysis) and loosening of implant components. This further limits the life expectancy of hip prostheses [1-2]. Therefore, improving the wear resistance of UHMWPE can substantially extend the clinical life span of total hip prostheses. It was recently reported that quasicrystalline fillers may significantly improve wear resistance in polymer-based composites [3-4].

Since the discovery of icosahedral phases in rapidly-quenched Al-Mn alloys [5], quasicrystals (QCs) were observed in over 100 alloy systems. Among them, the ternary Al–Cu–Fe alloy is most interesting [6-9], thanks to excellent properties, such as the low electrical and thermal conductivity, high hardness, low friction and wear, and good oxidation resistance.

In this work polymer composites of Al-Cu-Fe quasicrystal and polyethylene were synthesized. The nanocrystalline Al-Cu-Fe powders were prepared by mechanical alloying (MA). Wet-milling in hexane was employed to counteract severe powder losses, to avoid contamination from grinding media and prevent oxidation effects.

The formation of the quasicrystalline phase during isothermal annealing of the prepared Al-Cu-Fe nanopowders at temperatures between 700-800°C was studied by differential scanning calorimetry (DSC). The annealed powders were characterized by X-ray diffraction analysis using a D8 GADDS diffractometer (Bruker AXS) using monochromatic Cu $K_\alpha$ radiation.

Mixtures of polyethylene and Al-Cu-Fe powders (were weighted, added together with a solvent and mixed. The resulting Al-Cu-Fe/UHMWPE mixture was dried at room temperature, then shaped into disk pellets by uniaxial pressing.

Our preliminary results show that quasicrystal/UHMWPE composites with a highly uniform dispersion of AlCuFe QC nanoparticles in the polyethylene matrix can readily be achieved by wet-mixing. The resulting composite powders may further be shaped into bulk solid bodies by pressing or extrusion. Research is underway to investigate properties of the composites, like biocompatibility, mechanical response, as well as the wear and oxidation resistance.

**References:**

[1] W. Harris, J. Biomed. Mater. Res. 31 (1996) 19-26.
[2] D.H. Sochart, Clin. Orthop. Relat. Res. 363 (1999) 135-150.
[3] P.D. Bloom, K.G. Baikerikar, J.U. Otaigbe, V.V. Sheares, Mater. Sci. Eng. 294-296 (2000) 156.
[4] B.C. Anderson, P.D. Bloom, K.G. Baikerikar, V.V. Sheares, S.K. Mallapragada, Biomaterials 23 (2002) 1761.
[5] D. Shechtmann, I. Blech, D. Gratias, J.W. Cahn, Phys. Rev. Lett. 53 (1984) 1951.
[6] H-R. Trebin (Ed.), Quasicrystals, Wiley-VCH, Weinheim, 2003.
[7] A.I. Salimon et al, Acta Mater. 49 (2001) 1821.
[8] R. Nicula et al., J. Alloys Compd. 434-435 (2007) 319-323.
[9] V. Srinivas, P. Barua, B.S. Murty, Mater. Sci. Eng. 294-296 (2000) 65-67

# ANOMALOUS PROXIMITY EFFECTS IN FERROMAGNET-SUPERCONDUCTOR SrRuO$_3$-YBa$_2$Cu$_3$O$_{7-\delta}$ BILAYERS

*Oded Millo, Ofer Yuli and Itay Asulin*

*Racah Institute of Physics, The Hebrew University, Jerusalem 91904, Israel.*

**milode@vms.huji.ac.il**

The study of superconductor-ferromagnet proximity systems allows a direct investigation of the interplay between the two competing orders of superconductivity and ferromagnetism, and is relevant also to the field of spintronics. We applied cryogenic Scanning Tunneling Spectroscopy on bilayers of YBa$_2$Cu$_3$O$_{7-\delta}$ (YBCO), a *d*-wave superconductor, and the itinerant ferromagnet SrRuO$_3$ (SRO). Our data revealed two novel phenomena. 1. When the YBCO film is (100) oriented, we find localized regions, consisting of narrow stripes (~ 8 nm wide) along which the superconductor order-parameter penetrates the SRO to a distance significantly larger than expected. This behaviour is attributed to the crossed Andreev reflection process, an effect observed for the first time in our work, taking place in the vicinity of magnetic domain walls in the SRO. Here, an electron impinging in one magnetic domain is retro-reflected as a hole with opposite spin in an adjacent domain, effectively transferring a Cooper pair from the YBCO to the SRO layer. 2. When the YBCO film is oriented along the nodal (110) direction, our spectroscopy measurements reveal a penetration of the Andreev bound states into the ferromagnetic layer. The penetration is manifested in the density of states of the SRO as a split zero bias conductance peak with an imbalance between peak heights. Our data indicates that the splitting occurs at the superconductor side as a consequence of induced magnetization, while the imbalance results from the spin polarization in the ferromagnet.

# A mesoscopic approach to the progressive breakdown dynamics in ultra-thin SiO₂ films

*Enrique Miranda*

*Dept. Enginyeria Electrónica, Universitat Autonoma de Barcelona, Barcelona, Spain*
*enrique.miranda@uab.es*

*Abstract:* The formation of electrically induced nanocontacts across ultra-thin (sub-2nm) SiO₂ layers in MOS structures is investigated within the framework of the physics of mesoscopic systems. We are able to establish a link between the leakage current increase associated with the progressive dielectric breakdown and the power dissipation dynamics within the breakdown spot. Using a simple equivalent electrical circuit model and the transmission properties of a quantum point contact, it is shown that there is a gradual transfer of dissipated power from the bottleneck of the constriction to the semiconductor electrodes.

In recent years, progressive breakdown (PBD) in MOS devices has attracted the attention of many research groups mainly because of its implication for oxide reliability assessment [1]. Several attempts have been made to model this evolution in terms of empirical equations [2-4] or circuital descriptions [5]. The role of power dissipation during the PBD transient has also been specifically addressed in Ref. [6], but those works were not aimed at providing a description of the PBD trajectory (*I-t*). For the experiments we used MOS capacitors with poly-Si gate, p-type Si substrate ($10^{15}$ cm$^{-3}$) and 2.1 nm-thick oxides. Fig. 1 shows a schematic representation of the proposed model. The total current through the device, $I_G$, is the sum of the tunneling current, $I_T$, and the post-BD current, $I_{BD}$, and can be expressed as:

$$I_G = I_T + I_{BD} = A \exp(B V_{OX}) + G_{BD} V_{OX} \qquad (1)$$

where $V_{OX}=V_G-I_G R_S$ is the potential drop across the oxide layer and $G_{BD}$ the post-BD conductance in the linear regime [7]. We have considered a very simple tunneling model with parameters $A=2.16\times10^{-9}$ A and $B=2.9$ V$^{-1}$ extracted from the fresh *I-V* characteristic as shown in Fig. 2. From this plot we obtain the series resistance $R_S=1.75$ KΩ, which is assumed to remain constant after breakdown. An experimental $I_G$-*t* curve is shown by the solid line in Fig. 3. From (1), we can find the relationship between $G_{BD}$ and $I_G$. Fig. 4 illustrates how the total dissipated power distributes among the different parts of the proposed circuit. Initially, the dissipated power is mostly associated with the tunneling mechanism and the dissipation takes place at the capacitor plates. On the other hand, after saturation, the dissipated power is mostly associated with the breakdown spot. In order to investigate where the power is being dissipated in this latter case, we can calculate an average transmission probability $\widetilde{T}$ using the Landauer formula for the conductance of a single-mode quantum point contact [8]:

$$\widetilde{T} = G_0^{-1} G_{BD} = \left(G_0 V_{OX}\right)^{-1} I_{BD} \qquad (2)$$

where $G_0=2e^2/h=(12.9$ KΩ$)^{-1}$ is the quantum conductance unit, *e* and *h* being the electron charge and the Planck's constant, respectively. The power dissipated at the narrowest part of the constriction, $P_C$, is given by:

$$P_C = I_{BD} V_C = \left(1 - \widetilde{T}\right) I_{BD} V_{OX} = \left[1 - \left(G_0 V_{OX}\right)^{-1} I_{BD}\right] I_{BD} V_{OX} \qquad (3)$$

where $V_C$ is the voltage drop inside the breakdown path [8]. Notice that $V_C$ differs from $V_{OX}$ because of the mismatching effects of the electron distribution states at the two ends of the nanocontact. The evolution of $P_C$ is shown in Fig. 5. Initially, Joule heating increases because of the enlargement of the spot area, which in turn lowers the first energy subband level associated with quantum confinement in the transversal direction. As $\widetilde{T}$ approaches unity, the power starts decreasing eventually becoming negligible. Under this circumstance, the power is totally dissipated at the electrodes ($P_E$) and the oxide degradation stops. This approach provides a new explanation for the sigmoidal behavior of the PBD current.
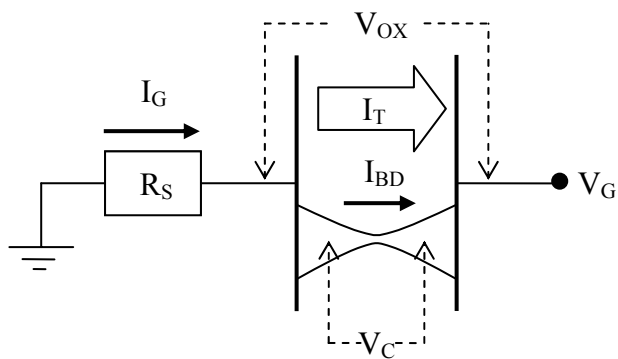
Fig. 1. Equivalent circuit model for the broken down MOS capacitor. The hourglass-like structure represents the breakdown path.
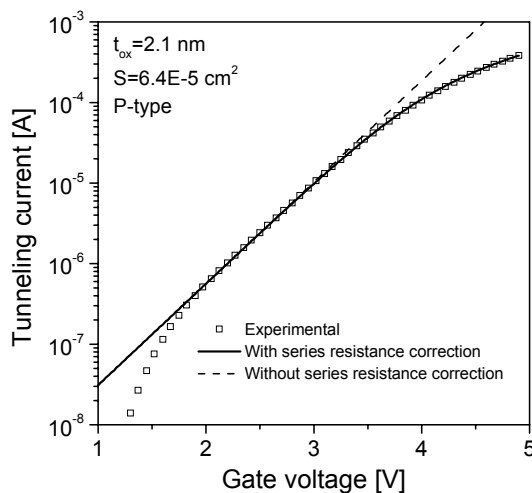


Fig. 2. Tunneling current through the fresh device.
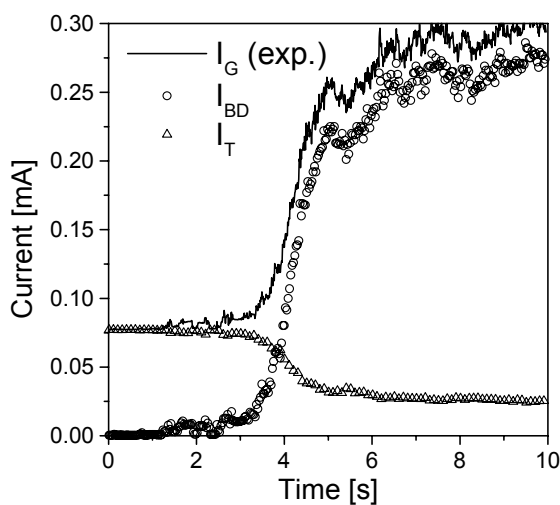


Fig. 3. Progressive breakdown current during a constant voltage stress at -3.75 V.
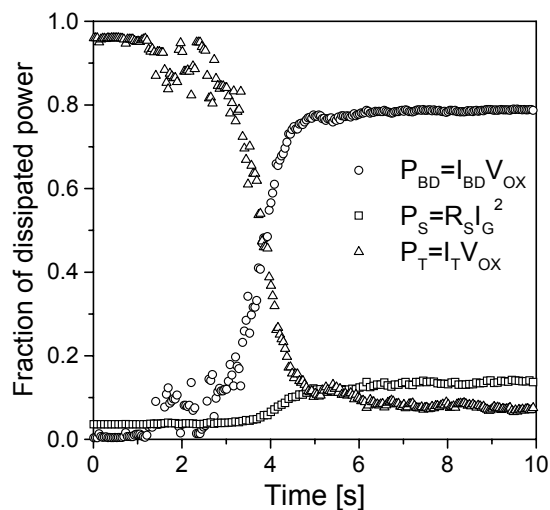


Fig. 4. Fraction of dissipated power as a function of time.
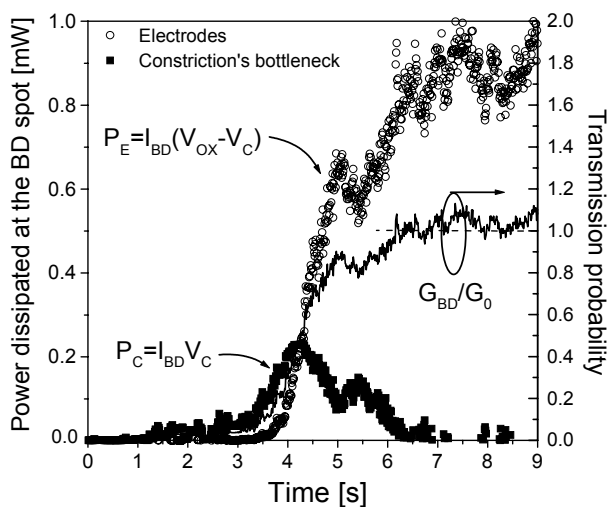


Fig. 5. Power dissipated at the PBD spot as a function of time.

**References**
[1] F. Monsieur *et al, Proc.* IRPS 2002, 45
[2] W. Loh *et al, Proc.* IPFA 2003, 157
[3] E. Miranda *et al*, EDL 24, 604 (2003)
[4] B. Kaczer *et al, Proc.* IEDM 2004, 713
[5] T. Hosoi *et al, Proc.* IEDM 2002, 155
[6] S. Lombardo *et al*, JAP 98, 121301 (2005)
[7] E. Miranda *et al*, MR 44, 1 (2004)
[8] S. Datta, in *Electronic transport in mesoscopic systems*, Cambridge University Press, 1998

# Synthesis and ion beam induced modification of fractal percolating network of Ag nanoparticles in polymer matrix

**Y. K. Mishra[1*], S. Mohapatra[1], D. K. Avasthi[1], D. Kabiraj[1], N. P. Lalla[2], J. C. Pivin[3]**

[1]Inter University Accelerator Centre, Post Box 10502, New Delhi-110067, India

[2]UGC-DAE Consortium for Scientific Research, University Campus, Indore- 452017, India

[3]Centre de Spectrometrie Nucleaire et Spectrometrie de Masse, IN2P3-CNRS, Batiment 108, F-91405, Orsay, France.

**ABSTRACT:** In the present work we report the synthesis of Ag nanoparticles in polyethylene terephthalate (PET) matrix using atom beam co-sputtering [1] of Ag and PET by 1.5 keV argon atoms and their modification by 120 MeV Ni ions. The samples were characterized by UV-visible absorption spectroscopy, Rutherford backscattering spectrometry (RBS) and transmission electron microscopy (TEM). UV-visible spectra revealed a broad surface plasmon resonance (SPR) absorption extending upto 2400 nm and the narrow transmission around ~ 320 nm. The TEM results confirmed the presence of percolating nature of Ag nanoparticles, which increased with the increase in Ag metal fraction in PET. The broad absorption in infrared region can be of technological importance in solar absorbers. [2] Ion irradiation of Ag-PET nanocomposites resulted in decrease (from ~ 30 to ~ 17 nm) in width of the transmission band (~ 320 nm). The narrow transmission of these polymer nanocomposites in UV range could be of use in filter applications.

**[1]** Y. K. Mishra et al., Scripta Materialia **56**, 629 (2007).

**[2]** D. K. Avasthi et al., Nanotechnology **18**, 125604 (2007).

**\*Corresponding Author:**

    Yogendra Kumar Mishra

    Doctoral Student (SRF)

    C/o Dr. D. K. Avasthi (Scientist –H)

    Inter university Accelerator Centre

    Post Box 10502, New Delhi 110067

    India

    Tele-phone: +91-11-26893955

    Telefax: +91-11-26893666

    Email: **ykmnsc@gmail.com**

# Characterization and application of biochemically fabricated inorganic nanoparticle

Atsushi Miura,[1] Yukiharu Uraoka,[1] Ichiro Yamashita,[1,2] Takashi Fuyuki[1]

[1] Nara Institute of Science and Technology, 8916-5 Takayama, Ikoma 630-0192, Japan

[2] Japan Science and Technology Agency, Core Research for Evolutional Science and Technology (CREST), 4-1-8 Honcho, Kawaguchi 332-0012, Japan

E-mail: a-miurat@ms.naist.jp

Biomolecule mediated fabrication of inorganic nanomaterial-biomolecule hybrid system and utilization of resulting hybrid nanocomposite is promising direction for the nano-electronic device fabrication. The functionality of recognizing and solidifying inorganic material is called biomineralization. Some kind of biomolecules such as viruses, proteins, DNAs and certain amino acid sequences have an ability of biominaralization and construct inorganic nanomaterials such as nanoparticles and nanowires. We employed cage-shaped supramolecular protein, apoferritin, to obtain uniform bionanodot (BND) architecture of cobalt oxide nanodot (Co-BND) [1] which used as a charge storage node of FNGM. The restricted protein cage was used as a template for uniform Co-BND synthesis. In order to utilize fabricated BND-ferritin hybrid nanocomposite for device fabrication, it is necessary to understand the precise electronic properties of bio-derived inorganic nanomaterials, such as electronic energy structure and charge retention capability. In this contribution, we demonstrate the characterization of electronic properties of single BND synthesized in the vacant cavity of ferritin by using scanning probe microscopy (SPM), such as Kelvin probe force microscopy (KFM) and scanning tunneling microscopy/spectroscopy (STM/STS). We have examined the charge storage capability of single Co-BND with KFM by monitoring the potential change with varying applied substrate potential for charge injection, and the electronic band structure of the single Co-BND with STS by measuring current-voltage characteristics of single BNDs. We also demonstrated the applicability of ferritin and its bionanodot for electronic devices by fabricating the floating nanodot gate memory with Co-BND as the charge storage node and confirming the memory effect due to the charge confinement to the embedded Co-core.

Figure 1(a) and 1(b) show the STM image of Co-BND deposited on highly oriented pyrolytic graphite (HOPG) and I-V characteristics measured on top of the observed Co-BND, respectively. For STM/STS measurements, Co-BND accommodated ferritins were deposited on HOPG and protein shell of ferritin molecules were eliminated by heat treatment prior to the measurement. Co-BNDs appeared as circular bright dot in STM image and cross-sectional profile indicated that the diameter of the Co-BNDs were approximately 7 nm. It is consistent with the size of reported Co-BND synthesized in ferritin cavity.[2] I-V curve of the Co-BND showed suppressed tunneling current around zero bias voltage. The width of the suppressed region and the current flow at the edge of suppressed region are interpreted as the band gap of Co-BND and resonant tunneling through the edge of valence band and conduction band of the Co-BND, respectively. Calculated tunneling conductance from I-V curves suggests that the band gap of ~2.1 eV and the positions of occupied and unoccupied levels of the Co-BND.

To evaluate charge storage capability, surface potential changes caused by the charge injection to the single Co-BNDs were examined by KFM. Topographic (Fig. 2a) and potential (fig. 2b and 2c) image of Co-BNDs deposited on the $SiO_2$ surface are depicted in Figs.2. Prior to the potential observation, charge injection to the Co-BNDs were carried out by scanning the sample surface with an electrically biased AFM tip under tapping mode. Circular dot structures in topography (Fig. 2a) correspond to the Co-BNDs on the $SiO_2$ surface. Average height of 6.4 nm is consistent with the reported size of Co-BND.[2] The surface potential of Co-BND changed after charge injection depending upon the polarity of applied bias voltage.

Fig. 2(b) shows the potential image obtained after charge injection at $V_{sub}$= -2 V. Co-BND appeared darker relative to the surrounding $SiO_2$ surface. On the other hand, after charge injection at +2 V (Fig. 2c), the Co-BNDs appeared brighter than $SiO_2$ surface. These results indicate that Co-BND can store the charge and can be used as the charge storage node of FNGM.

Fig. 3 shows the drain current-gate voltage ($I_D$-$V_G$) characteristics of Co-BND FNGM. $I_D$-$V_G$ showed clear hysteresis due to the charge confinement in the embedded Co-BND.

**References:**

[1] R. Tsukamoto, K. Iwahori, M. Muraoka, I. Yamashita, Bull. Chem. Soc. J. **78** (2005) 2075.
[2] A. Miura, T. Hikono, T. Matsumura, H. Yano, T. Hatakeyama, Y. Uraoka, T. Fuyuki, S. Yoshii, I. Yamashita, Jpn. J. Appl. Phys. **45** (2006) L1.

**Figures:**
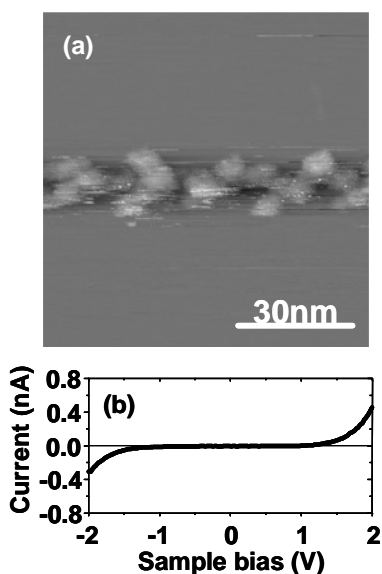


Fig. 1. (a) STM image of Co-BND deposited on HOPG. Observation conditions are: $I_t$=0.15 nA, $V_{sub}$=1.7 V. (b) I-V characteristic obtained from single Co-BND observed in Fig. 1(a). $I_t$=0.15 nA.
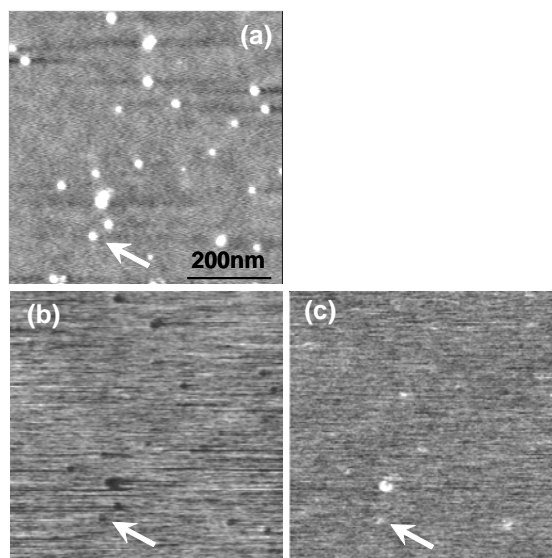


Fig. 2. (a) Topographic and (b), (c) potential image of Co-BND on $SiO_2$ surface. Topography was observed tapping mode AFM. Charge injection was carried out at (b) $V_{sub}$=-2.0 V and (c) $V_{sub}$=+2.0 V, respectively. Corresponding position of BND is indicated by arrow.
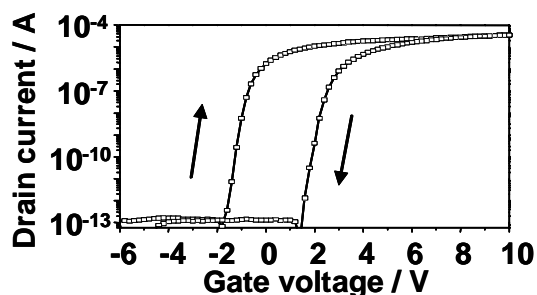


Fig. 3. $I_D$-$V_G$ characteristics of Co-BND embedded MOSFET with a 10-μm gate length and width. The gate voltage is swept from -10 V to +10V and back to -10 V.

# OPTICAL PROPERTIES OF SELF-ORGANIZED GOLD NANOSTRUCTURES IN SILICON OXIDE

*S. Mohapatra[1], Y.K. Mishra[1], J. Ghatak[2], D. Kabiraj[1] and D.K. Avasthi[1]*
*Inter University Accelerator Centre, New Delhi 110067, India*
*Institute of Physics, Bhubaneswar 751005, India*

*smiuac@gmail.com*

Nanocomposite thin films containing self-organized Au nanoparticles embedded in silicon oxide were synthesized by a novel process of atom beam co-sputtering [1-2]. The size distribution of Au nanoparticles was tailored by employing thermal annealing in inert and oxidizing atmospheres. UV-visible absorption measurements revealed the presence of surface plasmon resonant (SPR) absorption at ~ 528 nm which clearly indicates the presence of Au nanoparticles in the as-deposited film. Annealing in oxidizing atmosphere has been found to result in a significant enhancement in the SPR intensity. The SPR peak has been found to red shift to ~ 552 nm for annealing at $600^{o}$C. Interestingly, for annealing in inert atmosphere a drastic reduction in the resonant absorption has been observed with disappearance of SPR peak at temperatures $\geq 500^{o}$C. Transmission electron microscopy (TEM) studies revealed the formation of self-organized Au nanoparticles with a narrow size distribution in the as-deposited films. The presence of core-shell nanostructures with thin shells of Si surrounding Au nanoparticles has also been observed in case of samples annealed in inert atmosphere. The observed reduction in the SPR intensity of Au nanoparticles is possibly due to the formation of silicon nanoshells around them. The mechanisms underlying the self-organized growth of Au nanoparticles and Au-Si core-shell nanostructures in silicon oxide will be discussed. The effect of Au concentration on the optical properties of these nanostructures will be presented.

**References:**

[1] D.K. Avasthi et al., Nanotechnology 18 (2007) 125604.
[2] Y.K. Mishra et al., Scripta Materialia 56 (2007) 629.

# INELASTIC EFFECTS IN ELECTRONIC CURRENTS : A TIME-DEPENDENT APPROACH

Serge Monutret

Laboratoire Collision Agrégats Réactivité

UMR 5589 IRSAMC-UPS-CNRS

Université Paul Sabatier, Toulouse, France

The study of inelastic efects in electronic curents is receiving much attention due to both technological impact (molecular electronics are an emerging field in nanosciences) and the fundamental understanding of physics. From a theoretical point of view, the description of the mutual interaction between atomic vibrations and electrons leads to the development of sophisticated methods that use heavy formalism essentially based on non-equilibrium Green's functions (1). We have developed a method to the treat electron-phonon coupling to all orders in a time-dependent approach. We show that this simple method is a convenient tool to understand electronic transport in the presence of vibrations. Indeed, wave-packet propagation appears to be an intuitive and efficient way of describing phenomena such as inelastic electron tuneling spectroscopy. We will present a one-dimensional tight-binding model, and show how transmission can be calculated with wave-packets. Finally, some results will be discussed in the context of inelastic electron spectroscopy.

We consider a tight-binding one-dimensional chain, described by a tri-diagonal hamiltonian. Each site has equal on-site energy except one or several sites, wich we term « impurity sites ». A wave-packet is generated on the left side of the chain, with an initial kinetic energy. It propagates freely until the impurity sites are reached. There, it is reflected and transmitted, due to elastic scattering. If we switch on the electron-phonon coupling in the impurity sites, inelastic effects can be detected.



Time evolution of a wave packet
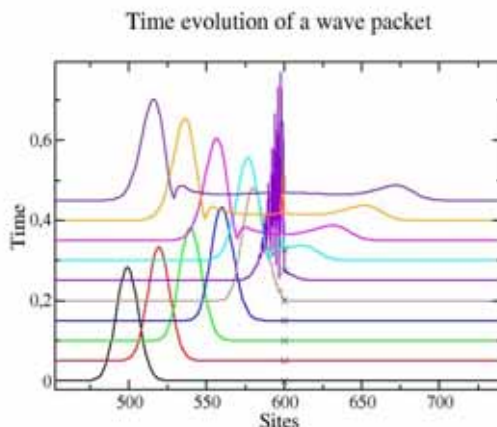
Transmission can be calculated using virtual detectors. The weight of the wave-function is calculated after the impurity sites as a function of time. Using a Fourier transform, we can compute the probability of an electron to be transmitted as a function of its initial energy. The width of the wave-packet is chosen so as to describe the appropriate spectral region where inelastic effects occur. In the presence of vibrations, the shape of the transmission curve is not loretzian anymore. The results show several peaks, spaced by the energy of the phonon, which are termed « phonon sidebands ». They correspond to the opening of  additional channels of conductance.

Transmission
with electron-phonon coupling
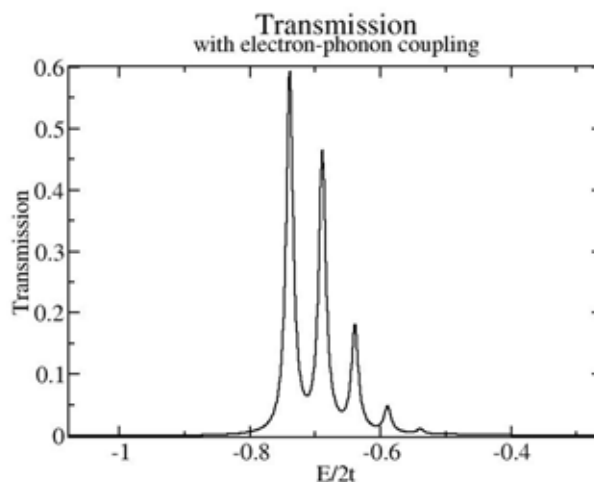
The propagation is performed with the Lanczos algorithm (2), wich allows big time steps, rapid convergence, and flexibility in the implementation of the hamiltonian matrix. This last point is extremely important because, as our method permits us to calculate transmissions with an arbitrary number of phonons, we will need to increase the number of phonons until convergence is reached.

We think that this time dependent approach can provide intuitive explanations of the physics involved in inelastic scattering experiments. Moreover, the efficiency of the calculation shows that for single-electron problems, the physics can be understood with simple approaches like ours, wich are nevertheless capable to show the underlying complexity of the systems where vibrations play an important role in conductance properties (3).

(1) T. Frederiksen, M. Brandbyge, N. Lorente and A.-P. Jauho , Phys. Rev. Letters  93, 256601 (2004).
(2) S; Mahapatra and N. Sathyamurthy, J. Chem. Soc., Faraday Trans., 93, 773 (1997).
(3)  M. Berthe, A. Urbieta, L.M.A. Perdigão, B. Grandidier, D. Deresmes, C. Delerue, D. Stiévenard, R. Rurrali, N. Lorente, L. Magaud, P. Ordejon, Phys. Rev. Lett. 97, 206801 (2006)

# MAGNETIC BEHAVIOUR OF ARRAYS OF NiFe AND CoFe SUB-MICRON ELLIPSES FABRICATED BY INTERFERENCE LITHOGRAPHY

*S. Moralejo[1], C. Redondo[1], F. Castaño[1], C. A. Ross[2] and F. J. Castaño[2]*
*1. Dpto. Química Física, Facultad de Ciencia y Tecnología, UPV, Apart. 644, 48080 Bilbao, Spain*
*2. Depart. of Materials Science and Engineering, Massachusetts Institute of Technology, Cambridge, Massachusetts 02139, USA*
*smoralejo001@ikasle.ehu.es*

Large-area periodic nanomagnet arrays of well-defined sub-micron dimensions have recently attracted remarkable attention because of their applications to patterned recording media, magnetic access random memories (MRAMs) [1] and have also provided model systems to study magnetic interactions and switching behaviour. Most patterned submicron magnetoelectronic devices have been fabricated with e-beam lithography [2,3], a serial process unsuitable for large-area patterning. In recent years interference lithography (IL) has developed as a rapid and economical method to generate large-area ($\sim$ cm$^2$) arrays with periods of a few hundreds nanometers [4-6], using grid templates created by two consecutive IL exposures [7]. The main advantage of the IL as a fabrication tool over classical lithography is its relative simplicity and cleanliness. The precise control of the hole dimensions enables the fabrication of nanomagnets with a variety of sizes suitable to study the correlation between magnetic behaviour and particle geometry.

In this work we report on a simple additive process, using an interference system built around a 325 nm He-Cd TEM$_{00}$ laser, a spatial filter and a Lloyd's-mirror. We have fabricated submicron ellipses arrays of Ni$_{80}$Fe$_{20}$ and Co$_{70}$Fe$_{30}$ with similar aspect ratio (6.4-6.6) and different geometry (hexagonal vs square) over large areas by interference lithography (IL). The method uses a negative-tone-resist (TSMR-iN027)/anti-reflection-coating (WIDE-8B) bylayer and the coating of the templates is made with a non-conformal ion beam sputtering system, followed by a lift-off with 1-methyl-2-pyrrolidinone at 120º C. The samples have been characterized at room temperature by magneto-optical Kerr effect measurements. It has been found that the magnetic properties of the nanomagnets are governed by shape anisotropy, showing these arrays a two-fold and a four-fold anisotropy induced by the pattern architecture.

**References:**

[1] S. A. Wolf, D. D. Awschalom, R. A. Buhrman, J. M. Daughton, S. von Molnar, M. L. Roukes, A. Y. Chtchelkanova, D. M. Treger, Science **294** (2001) 1488.
[2] S. Y.Chou, M. Wei, P. R. Krauss, P. B. Fisher, J. Vac. Sci. Technol. B **12** (1994) 3695.
[3] W. Xu, J. Wong, C. C. Cheng, R. Johnson, A. Scherer, J. Vac. Sci. Technol. B **13** 2372 (1995).
[4] T. A. Savas, M. Farhoud, H. I. Smith, M. Hwang, and C. A. Ross, J. Appl. Phys. **85** (1999) 6160.
[5] A. Fernandez, P. J. Bedrossian, S. L. Baker, S. P. Vernon, D. R. Kania, IEEE Trans. Magn. **32** (1996) 4472.
[6] J. P. Spallas, R. D. Boyd, J. A. Britten, A. Fernandez, A. M. Hawryluk, J. M. Perry, D. R. Kania, J. Vac. Sci. Technol. B **14** (1996) 2005.
[7] B. Vögeli, H. I. Smith, F. J. Castaño, S. Haratani, Y. Hao, C. A. Ross, J. Vac. Sci. & Technol. B **19** (2001) 2753.

**Figures:**
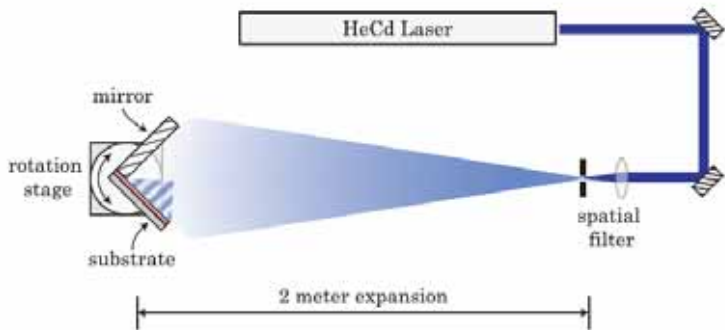


Figure 1. Experimental system.



1 µm
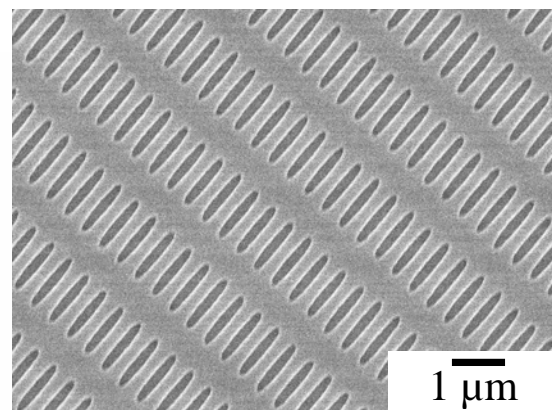
Figure 2. SEM image of the template with hexagonal symmetry.
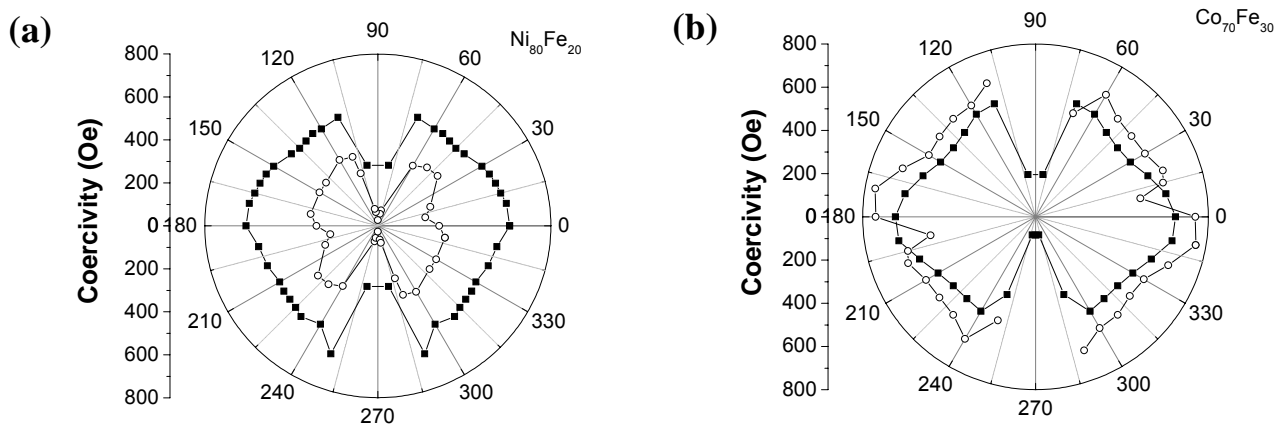


Figure 3. Coercivity angular dependence of $Ni_{80}Fe_{20}$ (a) and $Co_{70}Fe_{30}$ (b). In each sample, the open circles correspond to an square symmetry and the filled squares to an hexagonal symmetry.

# POINT DEFECTS AND THE (√3x√3)⇔(3x3) SURFACE PHASE TRANSITION IN THE Pb/Ge(111) SYSTEM

_M.M. Ugeda_, I. Brihuega[*], A.J. Martínez-Galera and J.M. Gómez-Rodríguez

*Departamento de Física de la Materia Condensada, Universidad Autónoma de Madrid, E-28049, Madrid, Spain*
[*]*Present address: Max-Planck-Institut für Festkörperforschung, Heisenbergstrasse 1, D-70569 Stuttgart, Germany*

miguel.moreno@uam.es

In this work we report on a thorough study of point defects in the 1/3ML-Pb/Ge(111) surface (α phase), performed by means of variable temperature scanning tunneling microscopy (VT-STM) in the 40K-300K temperature range. These point defects, which are mostly substitutional adatoms, are present in the family of systems formed by 1/3 ML Sn or Pb absorbed on Si(111) or Ge(111) surfaces within densities of 2-10%. Their role in temperature-dependent phase transitions that take place for such low dimensional systems have been widely discussed in the last few years[1]. For instance, point defects in the Sn/Ge(111) surface have been considered the driving force for the temperature-mediated (√3x√3)R30º ⇔ (3x3) phase transition taking place at low temperature. For that system, it has been reported that point defects realign during the structural phase transition from a random distribution onto a honeycomb lattice supporting the (3x3) phase [2,3]. However, a different behavior has been found for the apparently similar Pb/Si(111) system where it has been demostrated that substitutional point defects are immobile and they do not play any crucial role in the phase transition [4,5].

Concerning the Pb/Ge(111) system, it is well known that the α-phase exhibits a (√3x√3)R30º symmetry at RT which is lowered to a (3x3) periodicity at 110K [6]. However, the ground state for this system remains a controversial issue since a disordered phase was recently proposed for temperatures below 76K [7, 8]. It has been suggested that these phase transitions are accompanied by a realignment of point defects resulting in non-random distributions at low temperatures. In order to study the point defects mobility in the Pb/Ge(111) system we have recorded STM movies acquired by tracking defective regions while varying continuously the sample temperature from 40K to 300K. These real-time measurements provide an experimental evidence that point defects are not mobile throughout the above mentioned temperature range. Moreover, a statistical analysis has been performed by analyzing the Ge defects distribution from STM images at several temperatures. For the whole range of temperatures studied the point defects have been found to be randomly distributed even well below the transition temperatures. These findings are in clear contrast to previous assumptions for this system.

**References:**

[1] L. Petersen, Ismail, and E. W. Plummer, Prog. Surf. Sci **71**, 1 (2002).

[2] A.V. Melechko, J. Braun, H.H. Weitering, and E.W. Plummer, Phys. Rev. Lett. **83**, 999 (1999).

[3] H.H. Weitering, J.M. Carpinelli, A.V. Melechko, J. Zhang, M. Bartkowiak, and E.W. Plummer, Science **285**, 2107 (1999).

[4] I. Brihuega, O. Custance, R. Pérez, and J.M. Gómez-Rodríguez, Phys. Rev. Lett. **94**, 046101 (2005).

[5] I. Brihuega, O. Custance, M.M. Ugeda, and J.M. Gómez-Rodríguez, Phys. Rev. B **75**, 155411 (2007).

[6] J. M. Carpinelli, H. H. Weitering, E. Ward Plummer, and R. Stumpf, Nature **381**, 398 (1996).

[7] J. Guo, J. Shi, and E.W. Plummer, Phys. Rev. Lett. **94**, 036105 (2005).

[8] I. Brihuega, O. Custance, M. M. Ugeda, N. Oyabu, S. Morita, and J. M. Gómez-Rodríguez, Phys. Rev. Lett. **95**, 206102 (2005).

**Figures:**
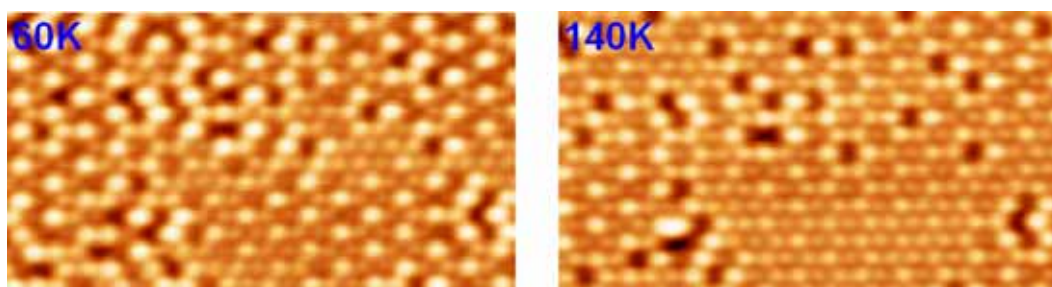


**Figure 1**: STM images of the same region (22x12 nm$^2$) extracted from a movie showing the immobility of defects in the 60K-140K interval of temperatures. Tunneling parameters for both images: Vs = -1.5 V; I = 0.1nA.

# VOLTAGE AND LENGTH-DEPENDENT PHASE DIAGRAM OF THE ELECTRONIC TRANSPORT IN CARBON NANOTUBES

*M. Moreno-Moreno* [a], *C.Gómez-Navarro* [b], *J.S. Bunch* [c], *J.Gómez-Herrero* [a], *Per Sundqvist* [d], *F.J. García-Vidal* [d], *F. Flores* [d]

[a] *Física de la Materia Condensada Dept. Universidad Autónoma de Madrid, 28049- Madrid, Spain*
[b] *Nanoscale Science Dept. Max-Planck-Institute for Solid State Research, D-70569 Stuttgart, Germany*
[c] *Clark Hall Lassp, Cornell University, Ithaca, NY 14853, U.S.A.*
[d] *Física Teórica de la Materia Condensada Dept. Universidad Autónoma de Madrid, 28049-Madrid, Spain*

*miriam.moreno@uam.es*

The electronic transport in carbon nanotubes was the topic of a large number of research works during the last decade. The first studies about the most elemental properties of these fascinating conductors focused on the defect-free nanotubes, however these studies covered only 10% of the measured samples. The reason for that was the not-optimum quality of the nanotubes obtained until then. But, thanks to the development of the CVD (chemical vapour deposition) technique for carbon nanotubes growing on insulator surfaces, it became possible to study defect-free nanotubes.

The electrical resistance of a carbon nanotube, and of any molecular wire, is a consequence of two different contributions:
- the elastic scattering produced by the structural defects/disorder.
- the inelastic scattering produced by the electron-phonon interaction.

In order to address the contribution of the two mechanisms we have done a comparative study of the electronic transport properties of two kind of single wall carbon nanotubes (SWCNTs):
1. the ones grown by arc discharge using HiPco Technique, CVD growth in volume (which contains a certain concentration of defects).
2. the ones grown directly on surface by CVD (with a low concentration of defects).

The electrical characterization of the nanotubes has been done by means of a Conductive Atomic Force Microscope. In this AFM the tip is covered by a metal (AuPd) that is also used as a mobile electrode. This technique allows us to measure the room temperature differential resistance of the nanotubes versus the SWCNT-length (R(L)) [1].

At low bias our data for the first kind of SWCNTs show an exponential dependence of R(L) indicating that the system is in the strong Anderson localization regime (due to the elastic scattering with defects) [2], while for the second kind of SWCNTs, the data reveal a linear dependence of R(L) which corresponds to a quasiballistic regime [3] (due to the low concentration of defects). We can conclude that the electric transport at low bias is governed by the elastic scattering with the structural defects in the nanotube.

As the bias increases the role of the phonons in the electronic transport become more important [4]. At high bias the R(L) for both kind of nanotubes presents a linear behaviour until lengths of 1 μm. Beyond that length, we have no experimental data for HiPco nanotubes (they are too short), but for the CVD-on-surface nanotubes our data show an surprising behaviour: at 1 μm the R(L) first saturates and then even decreases. The acoustic and optical

phonons are responsible for that behaviour. At high bias, at short SWCNT-lengths the SWCNT resistance is controlled by the number of optical phonons excited by one electron, while at long lengths, electron scattering with acoustic phonons controls the resistance.

We also present MonteCarlo numerical simulations for the one-dimensional Boltzmann's equation, describing how the electrons propagate along the tube and how they interact with acoustic and optical phonons. Our theoretical results show a remarkable agreement with the experimental differential resistance allowing us to give a detailed description of the electron distribution function and the chemical potential along the nanotube.

Finally, we present experimental results on the transition from Anderson localization at low bias to high diffusive regime at high bias in defected SWCNTs. This result is combined with those of defect-free SWCNTs to present a general landscape of the electronic transport in carbon nanotubes.

**References:**
[1] P. J. de Pablo, C. Gómez-Navarro, J. Colchero, P. A. Serena, J. Gómez-Herrero, and A. M. Baró, Phys. Rev. Lett. **88** (2002) 36804,
[2] C. Gómez-Navarro, P.J. de Pablo, J. Gómez-Herrero, B. Biel, F.J. García Vidal, A. Rubio and F. Flores. Nature Materials, **4** (2005) 534
[3] Per Sundqvist, Francisco J. Garcia-Vidal, Fernando Flores, Miriam Moreno-Moreno, Cristina Gómez-Navarro, Joseph Scott Bunch and Julio Gómez-Herrero, accepted in Nano Letters (2007)
[4] Ji-Yong Park, Sami Rosenblatt, Yuval Yaish, Vera Sazonova, Hande Üstunel, Stephan Braig, T. A. Arias, Piet W. Brouwer, and Paul L. McEuen, Nano Letters, **4** (2004) 517.

**Figures:**
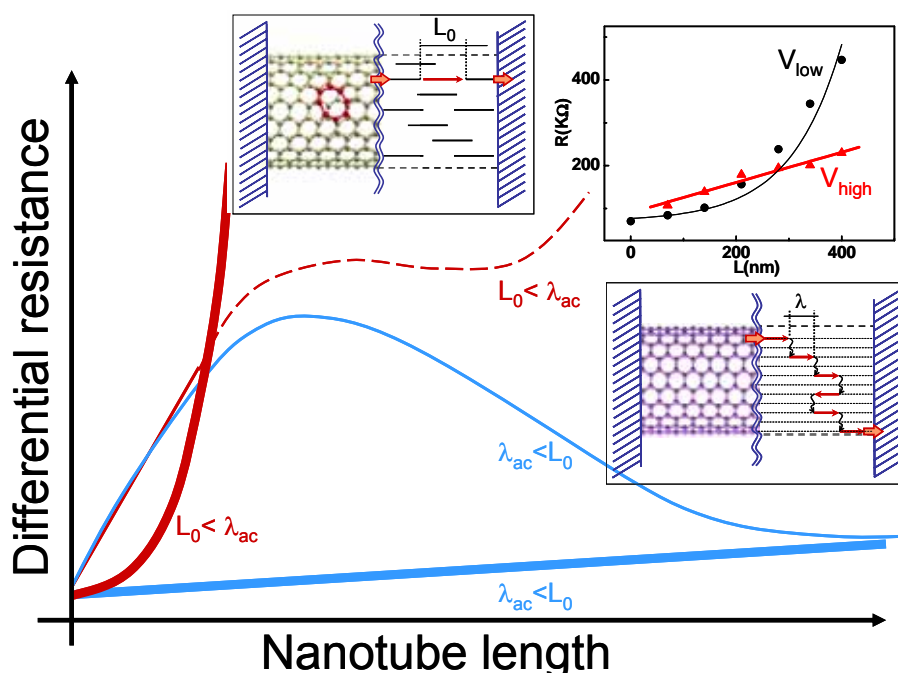


**Figure 1.** This figure summarizes the different electron transport regimes for SWCNTs with and without defects as a function of the bias voltage and length. The thick lines apply to the low bias voltage. The thin lines apply for the high bias voltage. The blue curves are for defect-free SWCNTs (lower inset) and the red ones for defected SWCNTs (upper left inset). The upper right inset shows experimental R(L) at low and high bias voltages for a defected SWCNT.

# Gas sensing with carbon nanotube networks

*Chris Morgan, Mark Baxendale*

*Physics Department, Queen Mary, University of London, Mile End Road, London, E1 4NS*

*c.j.morgan@qmul.ac.uk*

The electronic characteristics of single walled carbon nanotube (SWNT) networks are shown to have a strong dependence on the thickness of deposition. Variable range hopping is identified as the conduction mechanism. The conductometric sensing dynamics at room temperature for molecular oxygen and nitrogen exposure are examined and found to have two distinct time constants $\tau_{fast}$ and $\tau_{slow}$. Deposition of the SWNT network in contact with an oxidised semiconductor substrate forms a Nanotube-Metal on Silicon (NTMOS) capacitor. The total capacitance is determined by the oxide thickness and the thickness of depletion layer, which depends on the carrier concentration in the silicon substrate and the applied DC voltage between the SWNT network and the semiconductor. The presence of gases perturbs the surface potential of the SWNT network thus shifting the flat band potential of the device.

# SUPER ACID-POLYMER NANOCOMPOSITES FOR FUEL CELL APPLICATIONS

[1]*Adina Morozan*, [1]*F. Nastase,* [1]*Anca Dumitru,* [1]*C. Mirea,* [2]*Iuliana Pasuk,* [1]*Adriana Andronie,* [1]*Claudia Nastase,* [1]*S. Vulpe,* [1]*I. Stamatin*

[1]3Nano-SAE Research Centre, University of Bucharest, PO Box MG-38, 077125, Bucharest-Magurele, Romania

[2]National Institute of Materials Physics, PO Box MG-7, 077125, Bucharest-Magurele, Romania

adina.morozan@gmail.com

Since S.M. Haile [1] shown performances reached with solid acids in fuel cells as proton conductor, researchers in field increased continuous. Solid proton conductors are receiving considerable attention, stimulated by the need of fuel cells optimization and pollution control [2, 3]. The key limitation to higher power output is fabrication of fuel cells containing thin electrolyte membranes with minimized ohmic losses [4].

In this work we report the synthesis and the properties of the proton-conducting nanocomposites based on solid acids embedded in a polymer matrix of polyvinylidene fluoride (PVDF). The polymer, with its good mechanical properties, served as a supporting matrix for the high proton conductivity inorganic phase. Emphasis is given to structural composites on the basis of complex solid acids built-up on nanometric oxide (YSZ – yttria-stabilized zirconia) structure with cesium hydrogen sulfate phosphate ($CsHSO_4$-$CsH_2PO_4$) systems. The conductivities of nanocomposite polymer electrolytes with improved transport properties are induced by physical and chemical characteristics at bulk and interface levels.

Structural and morphological characterizations were carried out by X-ray powder diffraction, SEM, FT-IR and Raman spectroscopy. The measurements of electrical conductivity, during heating and cooling with a rate of 2–3$^0$C/min, were evaluated with a Keithley 2400 system. Obtained results provide a valid support for the enhancement of essential properties of solid fuel cell electrolytes.

**References:**

[1] S. M. Haile, D. A. Boysen, C. R. I. Chisholm, R. B. Merle, Nature, **410** (2001) 910-913.
[2] C. R.I. Chisholm, S. M. Haile, Solid State Ionics **136–137** (2000) 229–241.
[3] F. Croce, L. Settimi, B. Scrosati, Electrochemistry Communications **8** (2006) 364–368.
[4] T. Uda, S. M. Haile, Electrochemical and Solid-State Letters, **8(5)** (2005) A245-A246.

# MAGNETIC STUDIES OF FERROFLUID MODIFIED FODDER YEAST CELLS

*Ewa Mosiniewicz-Szablewska[1], Mirka Safarikova[2] and Ivo Safarik[2,3]*
*[1]Institute of Physics, Polish Academy of Sciences, Al. Lotnikow 32/46, 00-132 Warsaw, Poland*
*[2]Departament of Biomagnetic Techniques, Institute of Systems Biology and Ecology, Academy of Science, Na Sadkach 7, 370 05 Ceske Budejovice, Czech Republic*
*[3]Department of General Biology, University of South Bohemia, Branisovska 31, 370 05 Ceske Budejovice, Czech Republic*
*mosin@ifpan.edu.pl*

Magnetically modified biocompatible materials, containing magnetic nanoparticles as labels, have attracted much attention because of their great potential as magnetic affinity adsorbents for various biologically active compounds. They have been successfully applied for the magnetic separation of various proteins (enzymes, antibodies, antigens, receptors), nucleic acids (DNA, RNA, oligonucleotides), drugs and xenobiotics (carcinogens, water-soluble dyes, heavy metal ions, radionuclides) [1, 2].

There are many adsorbents available, but the main attention is focused on cheap and easy to get materials. Among them, living or dead microorganisms (yeast, bacteria, fungi, algae) are intensively studied [3].

Various strains of yeast are among the microorganisms, which can be used to removal and degradation of dyes [4]. In addition, the yeast cells efficiently interact with magnetic nanoparticles stabilized as low-pH ionic magnetic fluid, leading to the formation of magnetically labeled cells, which could be easily separated from the system using an appropriate magnetic separator [5].

This work reports on a new magnetic adsorbent – ferrofluid-modified fodder yeast (*Kluyveromyces fragilis*) cells – containing maghemite nanoparticles as magnetic labels. The prepared material was tested as a possible adsorbent for binding of different substances. It efficiently adsorbed selected water-soluble organic dyes, namely, crystal violet, amido black 10 B, congo red, Saturn blue LBRR 200, acridine orange, Bismarck brown Y and safranin O [6].

Analysis of TEM micrographs showed the presence of both isolated magnetic nanoparticles and their aggregates on the cell surface. The maghemite nanoparticles were roughly spherical in shape and externally attached to the *Kluyveromyces fragilis* cells walls; no particles were found inside the cells.

A possibility of using the magnetically modified fodder yeast cells as the magnetic adsorbent in the magnetic separation procedures was tested by means of magnetization and ESR measurements. The prepared material displayed a superparamagnetic behavior at room temperature, with a transition to a blocked state at $T_B = 180$ K for the applied magnetic field H = 50 Oe.

The room temperature ESR spectrum showed a well-defined single broad signal with the peak-to-peak line width $\Delta H_{pp} = 898$ Oe and an effective g value of about 2.07. The line width of this signal considerably exceeded the magnetocrystalline-anisotropy-determined minimum value, $\Delta H_{pp} = 400$ Oe, for non-interacting single domain maghemite particles. It suggested the existence of non-negligible dipole-dipole interactions between nanoparticles. Upon decreasing the temperature this signal shifted to lower fields and gradually broadened, following closely the predictions for the ESR of superparamagnetic nanoparticles systems.

Ferrofluid-modified fodder yeast cells can thus be a promising magnetic affinity adsorbent which may be used to the removal of dyes by means of magnetic separation techniques.

**References:**

[1] I. Safarik and M. Safarikova, Scientific and Clinical Applications of Magnetic Carriers, ed. U. Hafeli, W. Schutt, J. Teller and M. Zborowski (New York: Plenum Press, 1997) p 323.

[2] I. Safarik and M. Safarikova, Encyclopedia of Separation Science, ed. I. D. Wilson, R. R. Adlard, C. F. Poole and M. R. Cook (London: Academic Press, 2000) p 2163.

[3] I. Safarik and M. Safarikova, Water Res. **36** (2002)196.

[4] M. A. M. Martins, M. H. Cardoso, M. J. Queiroz, M. T. Ramalho and A. M. O. Campos, Chemosphere **38** ( 1999) 2455.

[5] I. Safarik, L. Ptackova and M. Safarikova, Eur. Cells Mater. **3 (Suppl. 2)** (2002) 52.

[6] I. Safarik, L. F. Teixeira Rego, M. Borovska, E. Mosiniewicz-Szablewska, F. Weyda and M. Safarikova, Enzyme Microb. Technol. **40** (2007) 1551.

**Figures:**
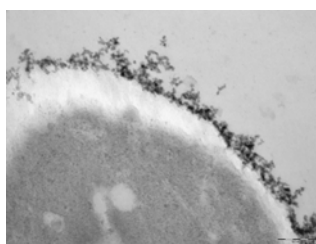


Fig.1. TEM picture of the ferrofluid-modified cell.
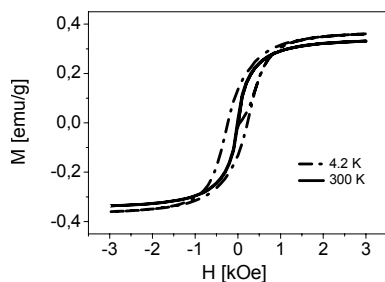


Fig.2. Field dependent hysteresis loops.
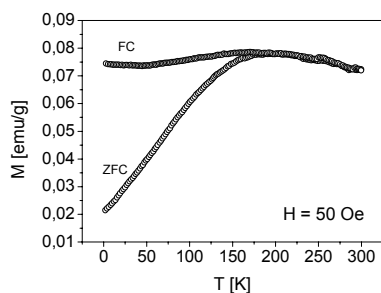


Fig.3. Temperature dependencies of magnetization.
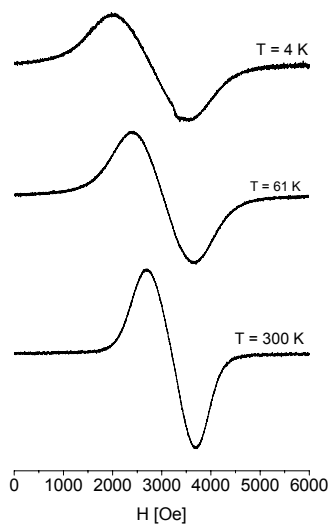


Fig.4. Exemplary ESR spectra.

# Growth of Si and Si/SiGe nanowires for thermoelectricity

*MOUCHET Céline, LATU-ROMAIN Laurence,*
*SIMONATO Jean-Pierre, ROUVIERE Emmanuelle*
*CEA Grenoble DRT/LITEN/DTNM/LCH,*
*17 rue des Martyrs, 38054 GRENOBLE Cedex 9, France*
*celine.mouchet@cea.fr*

The current thermoelectric converters are light, reliable and wireless. So, they are a good alternative to micro-batteries, micro fuel cells and micro-turbines and give the advantage to use a renewable energy. Theoretical [1] and experimental studies [2] evidenced that nanowires and nanostructured materials as superlattices have a high potential in thermoelectricity. The use of those materials increases ZT value, the factor of merit which characterizes a thermoelectric material, and consequently, increases the converter efficiency.

The aim of the study is to synthesize Si and Si/SiGe nanowires [3], to study the growth and the structure and to carry out thermoelectrical measurements in order to obtain a ZT value. On the long range, the goal is to integrate nanowires in thermoelectrical systems to increase the yield. For thermal chemical vapour deposition (CVD), silicon nanowires growth is attributed to the VLS mechanism (Vapour-Liquid-Solid) developed by Wagner in 1964 [4]. Between gaseous phase and solid phase, liquid phase acts as a catalyst for Si nanowires growth. The nanowires grow between the liquid and the solid phase. Today, gold is the more efficient known catalyst for this type of reaction. Silane and germane are injected in a CVD reactor where they undergo a thermal decomposition. N type or p type nanowires are obtained by mixing dopant gas, phosphine or diborane, with precursor gas. In this technique, gold nanoparticle diameters determine nanowire diameters. Two routes have been chosen for nanoparticle preparation. First, a thermal treatment is realized on a gold thin film deposited on the substrate. The average size of gold droplets obtained by this dewetting method is around few tens of nanometer. The advantage of this technique is its simplicity. Then, in order to reach small nanoparticle diameters with narrow dispersion, colloidal solutions have been employed [5] (figure 1). The two routes of gold nanoparticle preparation have led to nanowire growth. A growth parametric study has been performed in order to investigate the influence of each parameter on diameter dimensions and growth rates. A structural study with transmission electron microscope (TEM) has shown nanowire crystallinity and structural defects (figure 2). Moreover, the Si/SiGe heterostructured nanowire synthesis has been evidenced. Nanowire doping and Si/SiGe heterostructured nanowire synthesis are on going. These species will be characterized by electrical and thermoelectrical measurements.

**References:**

[1]: L. D. Hicks and M. S. Dresselhaus, Physical Review B, **47 (24)**, (1993) 16631-16634
[2]: R. Venkatasubramanian, Nature, **413,** (2001) 597-602
[3]: Y. Wu, R. Fan and P. Yang, Nano Letters, **2 (2)**, (2002) 83-86
[4]: R. S. Wagner, Applied Physics Letters, **4 (5)**, (1964) 89-90
[5]: Y. Cui, L. J. Lauhon, M. S. Gudiksen, J. Wang and C. M. Lieber, Applied Physics Letters, **78 (15)**, (2001) 2214-2216

**Figures:**
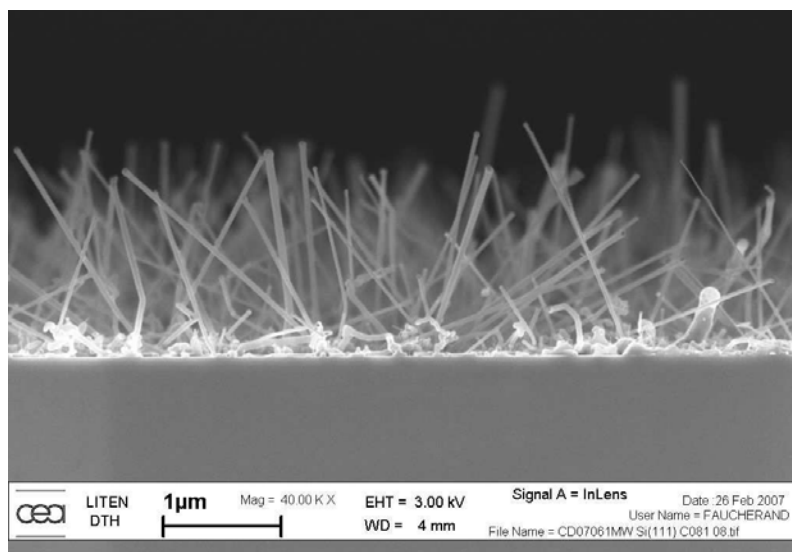


**Figure 1: Silicium nanowires (diameter ~50nm) from gold colloids.**
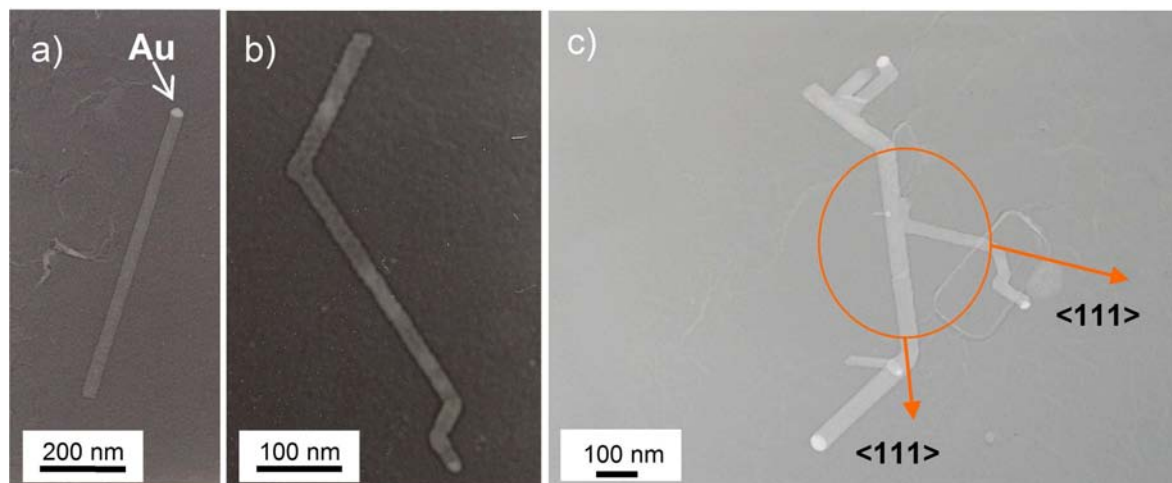


**Figure 2:**     a) **Monocrystalline silicium nanowire observed with TEM.**
                  b) **Polycrystalline silicium nanowire.**
                  c) **Branched silicium nanowire.**

# A COMPACT X-RAY DIFRACTION GENERATOR FOR NANOTECHNOLOGIES

## A. Mozelev

Small Scale Research and Production Company RADICAL
Treuer Str. 92/7/1/4 1200 Wien, Austria

**ABSTRACT**

X-ray portable difractometer for stress and strain measurement (XRD) permits to evaluate stress and strain level in large-size objects aimed at residual resource estimation in order to avoid faults, damages and accidents. The essential part of this arrangement is the source of artificial X-ray radiation. The up-to-date methods of researching radiations effects are usually based on the spectrometry of scattering irradiations exited by different radioisotopic sources. Nowdays, the ecological purity requirement for the geophysical devices with radioisotopes sources stimulates researches of other kinds of sources. In this connection, the sources of X-ray radiation represent an attractive alternative.Electron and ions acquire a high energy and produce X-rays with a relatively high efficiency by interaction with different materials. In this work, a principally new source using a radiation generator is proposed (1,2).

**INTRODUCTION**

Preliminary computation and mathematical simulation have revealed that the X-ray generator has advantages over the traditional radioisotope sources in technical characteristics. The remote handling of physical parameters (intensity, energy of gamma quants, etc.) makes it possible to use a gamma quant generator in different area of science and technique. The designing of the generator was intended for the most difficult application case-a deep borehole with high temperatures and high pressure. It was necessary to minimize dimensions and the power the generator needed and this has resulted in the minimum possible impulse duration. Several variants of vacuum tubes were researched, the results are cited. If we have diameter of vacuum tube D=90 mm., the kinetic energy of electron E=1 Mev.; D=70 mm., E=700 Kev.; D=60 mm., E=500 Kev.; D=45 mm., E=150 Kev. In the course of investigation a model generator was created. Carrying out researches with this model has also shown the expediency of subsequent investigations to confirm theoretical computations. As a result of the researches the following parameters have been received Diameter less than dotfill 70 mm Length less than dotfill 300 mm Weight less than dotfill 2 kg Electron source specification: Kinetic energy dotfill 500 KeV Pulse duration dotfill 10 ns Impulse frequency dotfill 0.5 -- 50 Hz.

**SUBHEADING**

Primary data collecting and processing software together with XRD design features permit to carry out stress and strain express analysis. Numerous stress/strain studies of high-pressure vessels, welded joints, elements of rockets and aircraft engines, parts of structures, mechanisms,

ets. have proved XRD reliability in diagnostics of such objects.The attained high intensity of the irradiation and small pulse duration (10 ns) required the formulation of a new measuring method and special equipment.For this generator need source of supplyers 24 V,50 W. Using a high-speed detector in the couple, X-ray generator can be used for research in hydrology, geophysical assessment of potential sites for the disposal of high-level radioactive wastes investigations and defectoscopy of borehole casing columns, rock density measure, etc. (3)

The essential part of this set up is the source of artificial gamma radiation. A principal advantage of that kind of source for gamma logging is the possibility of remote handling excluding the danger in case of an accident. The souse consequences was designed for the most difficult application case - a deep borehole with a high temperatures and high pressure. Several variants of vacuum tubes were researched, the results are introduced. The up-to-date methods of researching radiations effects are usually based on the spectrometry of scattering irradiations exited by different radioisotopes sources. Now days, the ecological purity requirement for the geophysical devices with radioisotopes sources stimulates researches of other kinds of sources. In this connection, the sources of X-ray radiation represent an attractive alternative. Electron and ions acquire a high energy and produce X-rays with a relatively high efficiency by interaction with different materials. In this work, a principally new source using a radiation generator is proposed [1].



Fig. 1

In this picture Figure1 you can see the X-ray source with natural dimensions compares with telephone.

Preliminary computation and mathematical simulation have revealed that the X-ray generator has advantages over the traditional radioisotope sources in technical characteristics. The remote handling of physical parameters (intensity, energy of gamma quants, etc.) makes it possible to use a gamma quant generator in different area of science and technique. The designing of the generator was intended for the most difficult application case-a deep borehole with high temperatures and high pressure. It was necessary to minimize dimensions and the power the generator needed and this has resulted in the minimum possible impulse duration.
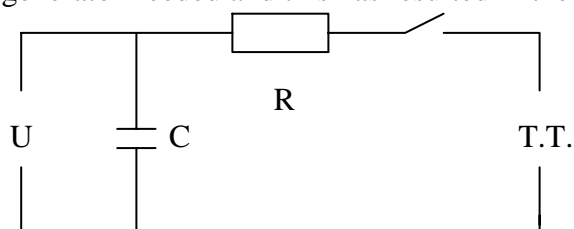


Fig. 2

The principal schema of the inductive accumulator which leading load is shown in Figure2. Preferable, the linear pulse electron accelerator comprises a capacitive energy storage connected to a high voltage charge unit, the output of the energy storage being connected to the primary coil of a Tesla transformer the secondary of which is connected to a cathode[2].The linear pulls electron accelerator preferably comprises a Tesla transformer for generating the high voltage pulses necessary for producing the gamma radiation. The primary coil of the Tesla transformer is connected to a capacitive energy storage and a discharger. The capacitive energy storages preferably connected to a high voltage charging unit. The high voltage output to the Tesla transformer is connected to an anode opposite which aheatable cathode is arranged along the longitudinal axis of the probe. The high voltage charging unit serves to charge the capacitive energy storage to a predetermined state before it is discharged to produce a high dI/dt in the primary coil of the Tesla transformer. The high voltage pulse thus generated by the Tesla transformer and applied between anode and cathode extracts electrons from the cathode and accelerates them to anode where they impact and by their deceleration generate a pulse of gamma radiation. Therefore, it is obvious the need of the minimum value C, which is equal to electronic gun capacitance in our case.

Several variants of vacuum tubes were researched, the results are cited. If we have diameter of vacuum tube D=90 mm., the kinetic energy of electron E=1 Mev.; D=70 mm., E=700 Kev.; D=60 mm., E=500 Kev.; D=45 mm., E=150 Kev. In the course of investigation a model generator was created. Carrying out researches with this model has also shown the expediency of subsequent investigations to confirm theoretical computations. As a result of the researches the following parameters have been received Diameter less than dot fill 90 mm Length less than dot fill 400 mm Weight less than dot fill 3 kg Electron source specification: Kinetic energy dot fill 1000 KeV Pulse duration dot fill 10 ns Impulse frequency dot fill 0.5 -- 50 Hz.

[1] A.Mozelev. Gamma Quant Generator, Int. Symp. On Geologic Disposal of Spent Fuel, High-Level and Alpha-Bearing Waster.  Antwerpen, Belgium, 1992.
[2] Mozelev A. High Voltage Discharge and Vacuum Insulation at the Minimising Volume, Int. Symp. Electrical Discharge and Vacuum Insulation. (ISDEIV1996) Berkeley, California, 1996.
[3] Mozelev A. et al. Probe for Radio logically Determine the Density of  Rock In a Drilled Well, United States Paten Number 5,736,636. Date of Patent: Apr. 7, 1998.

# TESTING THE NANOPARTICLE-SUPPORT ADHESION USING SCANNING FORCE MICROSCOPY

*<u>Martin Munz</u>, David Cox, Peter Cumpson*
*National Physical Laboratory (NPL), Hampton Road, Teddington, UK*
*martin.munz@npl.co.uk*

An increasing number of products involving nanoparticles (NPs) attached to a surface are being developed, such as cosmetic foundation powders containing NPs to fill tiny blemishes or industrial catalysts containing Pt NPs dispersed on porous oxide supports. If the NPs fall off the surface or get washed away after a short period of usage the functionality of the product would be impaired. In addition, safety issues may be raised if the NPs are released to the environment. To ensure the reliability and safety of such products, the strength of the adhesion between the NPs and the support surface needs to be tested. Owing to its high spatial resolution as well as the direct mechanical tip-sample interactions, Scanning Force Microscopy (SFM/AFM) is a promising tool for such nanomechanical testing. Recently, Eppler et al. [1] demonstrated this approach for a model catalyst containing arrays of Pt NPs.

To explore the potential of the approach and to develop a deeper insight into the interactions between SFM-tip and NPs, we investigated arrays of W-NPs deposited on a surface of template-stripped gold. The W-NPs were generated by means of Electron Beam Deposition (EBD) involving $W(CO)_6$ as a precursor gas. The interparticle distance was ~280 nm, and the dwell time of the electron beam was used as a parameter to generate NPs of various sizes. With beam dwell times in the ms range, the height of the NPs was in the range between 2 and 5 nm. One array for each dwell time value was generated, with each array extended over 100x100 microns$^2$.

Using microcantilevers of ~60 pN/nm stiffness, the arrays of NPs were imaged in contact mode. Starting from low values, the normal force was successively increased to find the critical force from which on NPs are detached from the supporting surface. For NPs of a 2 ms beam exposure time, the critical force was found to be ~45 nN. Scanning at this force resulted in complete removal of the NPs (Fig. 1). These results are discussed in terms of the various forces acting at the interfaces tip/NP and NP/surface.

Additional information is available from the lateral force images. In particular, they show tracks that can be attributed to the movement of loose particles as induced by the scanning tip. Such events result in increased lateral forces. The loose NPs tend to pile up along the edges of the scan area. In the course of subsequent scans of expanded scan range some of these loose particles are moved towards the edges of the new scan area.

Also the issue of quantification of lateral forces was addressed. A modification of Varenberg's wedge technique [2] for the determination of the torsional calibration coefficient was studied. Employing Focused Ion Beam (FIB) etching, shallow edges of ~20° slope angle were generated in order to ensure a stable condition of the feedback when scanning across the edges. As compared to the initial slopes, the lateral force profiles show extended plateaus, thus allowing for a more reliable evaluation of the lateral forces measured on the slope.

**References:**

[1] A.S. Eppler, G. Rupprechter, E.A. Anderson, G.A. Somorjai, J. Phys. Chem. B **104** (2000) 7286.
[2] M. Varenberg, I. Etsion, G. Halperin, Rev. Sci. Instr. **74** (2003) 3362.

**Figures:**
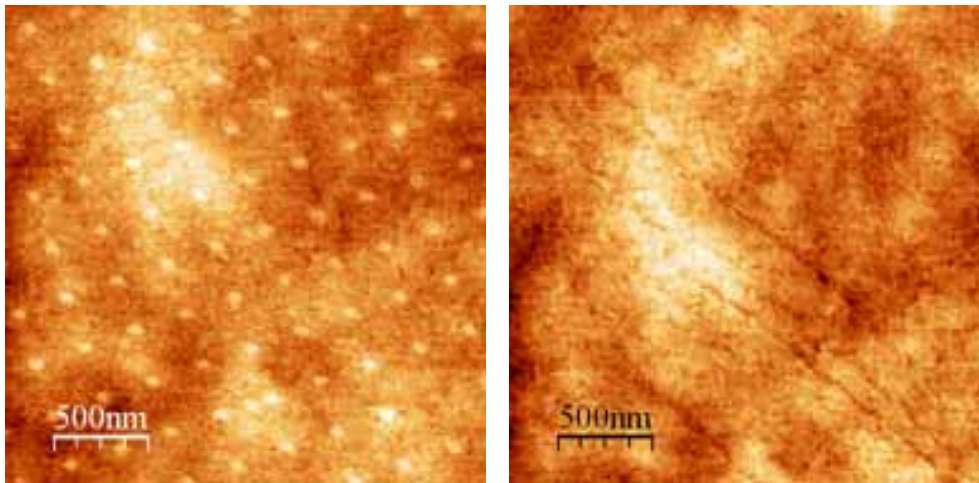


**Fig. 1**: Topography images of an array of W-nanoparticles, measured with normal forces of ~3 nN and ~45 nN, respectively. Total height 5.2 nm and 4.2 nm, respectively. Scan range 2.5 microns.

# Theoretical Modelling of Self-Assembly of Molecular Networks

*Manuela Mura, Natalia Martsinovich,Lev Kantorovich*
*King's College , Strand, London, WC2R 2LS, UK*
*manuela.2.mura@kcl.ac.uk*

The phenomenon of self-assembly of atomic and molecular superstructures on crystal surfaces has attracted an increasing interest in nanotechnology. Self-organised nano-templates where the self-assembled monolayer traps other molecules with selected functional properties, can be used as building blocks for larger nanoscale structures. Self-assembled superstructures can form chiral domains ranging from 1D chains to 2D monolayers.

In particular, there have been many scanning tunneling microscopy (STM) studies of self-assembly of melamine, perylene tetra-carboxylic di-imide (PTCDI) or perylene tetra-carboxylic di-anhydride (PTCDA) molecules on the Au(111) and Ag/Si(111) surfaces [1],[2] [5]. STM images of these networks do not reveal the exact details of the intermolecular bonding and process of network growth. It is therefore the task of theory to determine the exact atomic structure of these networks.

We present a theoretical study of self-assembly of molecular networks based on melamine, PTCDA and PTCDI molecules. We propose a systematic approach to building molecular superstructures based on the notion of binding sites. First, we identify all possible sites for hydrogen bonding between molecules. Then we form molecular pairs and larger structures using all possible combinations of these binding sites. In this way, we construct all possible dimers, chains and 2D monolayers of melamine, PTCDA and PTCDI. Both monomolecular and bimolecular structures are considered. The energies of these structures are calculated using the density-functional theory SIESTA code. The strength of hydrogen bonding in various molecular arrangements is analysed. The theoretically predicted monolayer structures are in very good agreement with the results of STM measurements [4][5].

**References:**

[1]   Pedigão, L.M.A.; Champness, N. R.; Beton, P. H. Chem. commun. 2006, 538-540.

[2]  Staniec, P. A.; Pedigão, L.M.A.;Rogers,B.L.;Champness, N. R.; Beton, P. H. J.Phys.Chem.C 2006,

[3]   Swarbrick,J.C.;Ma,J.;Theobald,J.A.;Oxtoby,N.S.;O'Shea,J.N.;Champness,N.R.; Beton, P. H. J.Phys.Chem.B 2005,109, 12167-12174.

[4] Ma,J.;Rogers,B.L.;Humphry,M.J.;Ring,D.J.;Goretzki,G.; ; Champness, N. R.; Beton, P. H. J.Phys.Chem.B 2006,110,12207-12210.

[5] Pedigão, L.M.A.; Perkins,E.W.; Ma,J.;Staniec, P. A.; Rogers,B.L.; Champness, N. R.; Beton, P. H. J.Phys.Chem.B 2006,110,12539-12542.

# Synthesis, Stability and Electrocatalytic Activity of Polymer Stabilized Monometallic Pd and Pt and Bimetallic Pd@Cu and Pt@Cu Core-shell Nanoparticles

*<u>Dmitri N. Muraviev</u>, Jorge Macanás, Patricia Ruiz and Maria Muñoz.*
*Analytical Chemistry Division, Department of Chemistry, Autonomous University of Barcelona, 08193 Bellaterra, Barcelona, Spain.*
*Contact e-mail: <u>Dimitri.Muraviev@uab.es</u>*

Platinum-group metal (PGM) nanoparticles (MNPs) find wide application in various catalytic and electrocatalytic processes (such as, for example hydrogen and methanol fuel cells, sensors, biosensors, etc.). In many instances application of MNPs is based on the use of their unique properties (electrical, magnetic, optical, ionization potentials, etc.), which are distinct from those of the bulk metal and isolated atoms. On the other hand, they require stabilization to prevent coalescence and aggregation, and hence to save their special size and properties. The development of Polymer-Stabilized MNPs (PSMNPs) is one of the most promising solutions to the MNPs stability problem [1-3]. Another important problem concerning the use of noble metal nanocatalysts is the decrease of PGM loading without dramatic change of their catalytic properties. One of the possible solutions of this problem is the use of core-shell PSMNPs, which are composed of a cheap metal core coated with a thin PGM shell [4].

In this presentation we report the results obtained in a comparative study of electrocatalytic properties of Pt and Pd (monometallic) and Pt@Cu and Pd@Cu (core-shell bimetallic) PSMNPs, which have been synthesized under identical conditions inside the polymeric membranes. The intermatrix synthesis of MNPs included the loading of sulfonated poly(etherether ketone) (SPEEK) with desired metal ions followed by their reduction (intermatrix synthesis stage), what resulted in formation of PSMNPs of required composition and structure. PSMNPs-containing membranes were characterized by different methods (SEM, AFM, TEM and others) to evaluate the structural features of polymer-metal composite membrane and to estimate the MNPs size. Typical TEM images of the Pt- and Pt@Cu-MNPs are shown in Fig. 1. As it is seen, the shape and size of monometallic Pt-MNPs differs dramatically from those of Pt@Cu nanoparticles, although the value of platinum loading in both cases is the same. Pt-MNPs are characterized by a far larger size and absolutely irregular shape. This makes practically impossible to estimate their diameters, while the majority of Pt@Cu-MNPs have almost spherical shape with diameters of 3-6 nm. As the result, the surface area of Pt@Cu-MNPs appears to be far higher than that of Pt-MNPs. In case of Pd- and Pd@Cu-MNPs the difference in particle form and surface area is not so dramatic.

The MNP-loaded membranes dissolved in DMF followed to produce a sort of PSMNP-inks. The inks were used to evaluate the stabilizing efficiency of SPEEK matrix against MNPs aggregation and to study the electrochemical properties of polymer-PSMNP nanocomposites. The results of these experiments are demonstrated in Figs. 2 and 3. Fig. 2 shows the side distribution histograms of Pd@Cu-MNPs when determined for freshly prepared ink and the same ink after 9 months of storage. As it is seen, the distribution of MNP sizes essentially does not change that indicates a very high stabilizing efficiency of SPEEK matrix towards MNPs. Fig. 3 shows the calibration curves of amperometric detection of $H_2O_2$ with Pt- and Pt@Cu-MNP-based sensors. As it is seen, the sensitivity of sensors based on the use of Pt- and Pt@Cu-MNPs with the same platinum loading differs dramatically from each other. A possible reason for this difference is quite different values of surface areas of Pt@Cu- and Pt-MNPs.

**References:**

[1] A.D. Pomogailo, G.I. Dzhardimalieva, A.S. Rozenberg and D.N. Muraviev, J. Nanoparticle Res., **5** (2003) 497.

[2] D.N. Muraviev, Contributions to Science, **3(1)** (2005) 17.

[3] D.N. Muraviev, J.Macanás, M. Farre, M. Muñoz and S. Alegret, Sensors & Actuators B, **118(1-2)** (2006) 408.

[4] S. Zhou, B. Varughese, B. Eichhorn, G. Jackson and K. McIlwrath, Angew. Chem. Int. Ed., **44** (2005) 4539.

**Figures:**
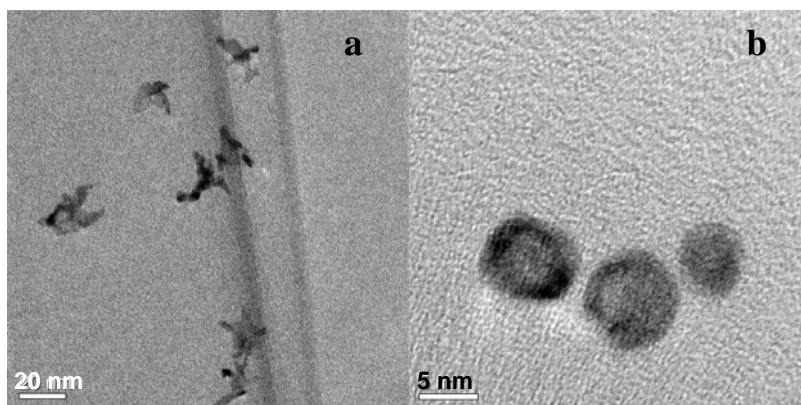


*Figure 1. (a) Typical TEM images of Pt-(a) and Pt@Cu- PSMNPs (b) immobilized in SPEEK matrix.*
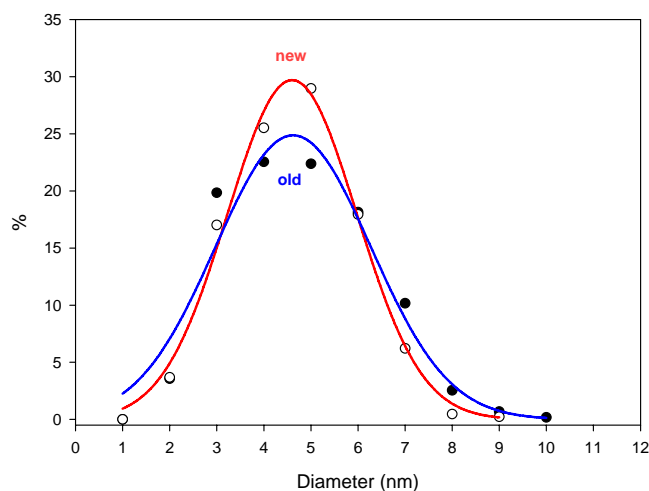


*Figure 2. Typical size distribution histograms of Pd@Cu- PSMNPs in freshly prepared ink (new) and in same ink after 9 months of (old) storage.*
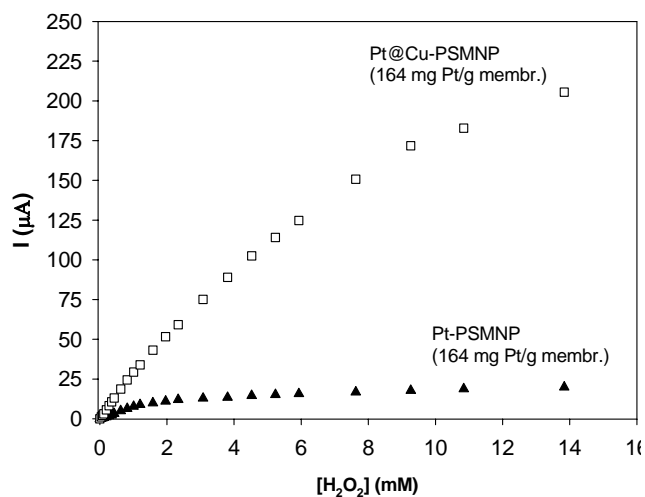


*Figure 3. Calibration curves of amperometric sensors prepared by modification of graphite-epoxy composite electrodes with Pt-(black triangles) and Pt@Cu-PSMNP-SPEEK membranes (white squares) at identical values of platinum loading. Conditions: potential: -250 mV; 0.1 M KCl in 0.1 M acetate buffer, pH = 7.0.*

# SUPPER LATTICE OR ISOLATED NANO CHARACTER ON Gd-Bi IMC

S. Nabavi ,A.Yazdani,i.Karimzadeh

Tarbiat Modares University

Since the heat formation of the binary-IMC of $Gd_xBi_y$ is strongly functional of the percentage of Gd magnetic ion[1,2], the character of nature of conduction electron as well as the band function should be considered.The decreasing of the heat formation by increasing of the magnetic ion is expected to be due to the induced polarization of the conduction band by magnetic ion defined by $J_{ij} \propto F(K_fR_i-R_j)$. Where the heat formation and the magnetic character are considerable through the

1) The energy difference of $\Delta E_{s-d}$ [3]where the character of conduction electron could be s or d-like[4].
2) The population of the fluctuation of the electrons in the valance and conduction band named inter band mixing which can stabilize the structure or a closely related structure.

But the variety of magnetic properties, and its effect on crystal structure, among Gd-Bi (where the Bi is a non metal magnet) seems to be related to electronic structure close to the Fermi level rather than simply the number of conduction electrons which is the basic parameter in the RKKY indirect exchange model.Consequently because of the strenght of exchange interaction, the nature of c.e could be d-like or even of the 5d-state [4]. The 5d-state is believed to be band-like which takes part in chemical bonding and thus could be the main source of ;

a) The excess (or even reduction) of effective magnetic moment in some Gd-compounds .

b) The variety of crystal structure and the heat formation can be study through the energy difference of $\Delta E_{s-dF}$

c)chemical peresure (due to the high density of c.e) is on its critical value Fig.1at which;

 c-i)The reduction structueral correlation lenght by the anneling proces is manifested by the intera cluster exchange (as grain size ) which is shown by the unusaul Ac magnetic suseptibility[2].

c-ii)The cluster size (grain or domain size ) can be formed by short rang exchange (even in a-b plan ) and becomes comparable or even smaller than inter –cluster lenght which is due to the long-range inter-structure –exchange

c-iii)The critical point can be manifested by the stabel AFM above which the sampel behave compeletly P.M;where $\sum \varepsilon_{ij}Jij=0$ (Fig.2a) and the Kondo-like character is manifested on $\rho(T)$(Fig.2.b).

This suggestion can be studied through the temperature dependence of magnetic suseptibility (Fig.2a) and electrical resistivity (Fig.2b) on which:

I)A dramatic change in the electrical resistivity between the $Gd_4Bi_3$ and $Gd_5Bi_3$ happens(Fig1).

Such behavior is presumed to be due to the short-range ordering effect through long-range interaction developed by the above suggestion "conduction electron concentration , c.e.c".

Consequently, if $Gd_5Bi_3$ is close to the critical value, near the double FM, AFM

percolation threshold, it should be a point at which no frustration occurs, and then the system can be stabilized. This point has been found to be at x/y=2 where the system behaves completely para-magnetic as shown in fig. 2(a). So the exchange interaction of magnetic ions at x/y=5/3 are in conflict with each other and do not allow the system to exhibit a long-range order (FM or AFM) but impose a new type of order at x/y=2. This point can be a minimized point in which the system is stabilized "physically" and metallurgical by completing of incomplete metallic bands to chemical covalent bond presented by the Kondo lattice the behavior fig.2 (b) which can be due to the inter-cluster exchange (isolated nano structure) on which $\sum \varepsilon_{ij} J_{ij} = 0$.

PACS: 75.10.Lp; 75.20.Hr

**References:**

[1] J. Szade, M. Drzyzga, J. Al. Comp. **299** (2000) 72-78.
[2] M. N. Abdusalyamova, A. G. Chuiko, E. I. Shishkin et. Al. J. Alloys Comp. **240** (1996) 272.
[3] A. Yazdani, J. ST. Gardner, Phys. Stat. sol. (b) **208** (1998) 465.
[4] Szade J. and Neumann M., J. Phys.: Condens. Matter **11** (1999) 3887.

**Figures:**
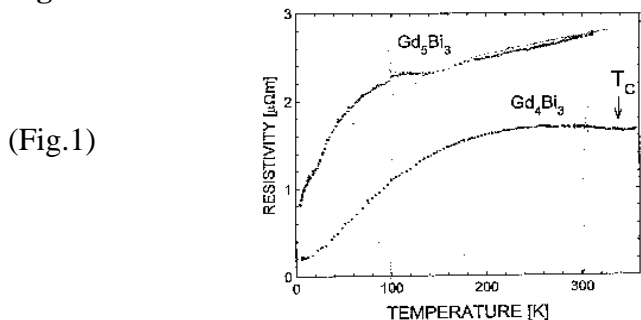
(Fig.1)
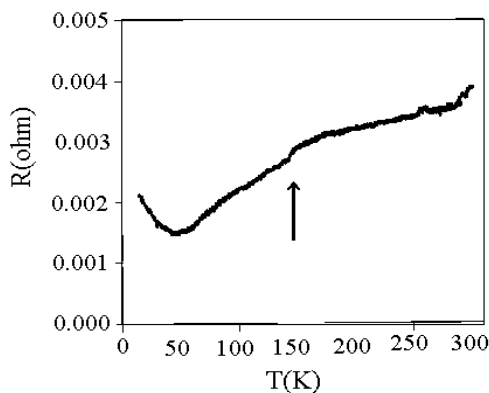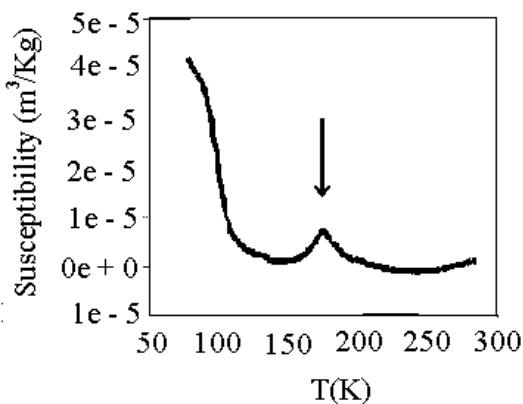




Fig.2 (b)                                                                     Fig.2 (a)

Temperature dependence of the electrical susceptibility (a) and resistivity (b)

# PREPARATION OF GREEN AND BIODEGRADABLE NANOCOMPOSITES BASED ON CHEMICALLY MODIFIED STARCH

## H. Namazi[*] and M. Mosadegh

[*]Lab of Dendrimer and Carbohydrates, Faculty of Chemistry, University of Tabriz, Iran,
namazi@tabrizu.ac.ir

**Abstract**

Nanocomposites of Starch grated polycaprolacton (Starch-g-PCL) were prepared through graft polymerization in situ ring-opening polymerization of ε-caprolacton in the presence of starch and Tin (II) 2-ethyl hexanoate as an initiator/catalyst. A chemically nonmodified $Na^+$-montmorillonite and surface-modified montmorillonite by dimethyl (hydrogenated tallow alkyl) ammonium cation, were used. The nanocomposites were prepared through two methods in solution and in situ, with using different amount loading clay. The effect of swelling time on d-spacing of silicate layers was investigated and nanocomposites were analyzed with X-ray diffraction and morphology of the prepared nanocomposites investigated using SEM (Scanning Electron Microscopic) and thermal degradation behavior of nanocomposites was studied by TGA.

**References**

[1] S. Hizukuri and Y. Takeda, Carbohydr Res., 94, 205-213, 1981.
[2] K. Morikava and K. Nishinari, Carbohydrate polymers, 43, 241-247, 2000.
[3] A. A. Curvelo and A. J. Carvalho, Carbohydrate polymers, 45, 183-188, 2001.
[4] H. Park and X. Li, Macromol.Mater.Eng, 287, 553-558, 2002.
[5] J. K. Pandey and R. P. Singh, Starch/starke, 57, 8-15, 2005

# SYNTHESIS OF ABA TYPE TRIBLOCK NANO COPOLYMERIC DENDRIMERS BASED ON AMINO ACIDS AND PEG

## H. Namazi[*] and H. Abbaspour

[*]Lab of Dendrimer and Carbohydrates, Faculty of Chemistry, University of Tabriz, Tabriz, P. O. Box: 5166616471, Iran; *namazi@tabrizu.ac.ir*

## Abstract

ABA-type triblock nano copolymer (PGL-PEG-PGL) dendrimer was synthesized in a divergent manner using liquid-phase peptide synthesis method. Poly (ethylen glycol) (PEG) 600 diacid was used as the core, and glutamic acid dimethyl esther as the monomeric building block. In this procedure linear-dendritic copolymer were prepared in the presence of DCC and pyridine. Common spectroscopic methods such as ^{1}H and ^{13}C NMR and FT-IR have been used for characterization of the synthesized dendrimers. Thermal behavior of the isolated dendrimers were investigated using DSC and their morphology was examined with Scanning Electron Microscopy. The potential ability of purified dendrimers was examined as the drug nanocarrier systems and the release of some model drug molecules was carried out in different pH's.

## References:

[1]  Namazi, H. and Adeli, M.; Polymer. J., 46, 10788, 2005.
[2] Kricheldorf H. R. and Meier-Haack, J. Makromol Chem. 194, 715, 1993.
[4]. Zhang, L. and Tam, J. P. J. Am. Chem. Soc., 119, 2363, 1997.
[9]. Vinogradov, S., Lo, L. and Wilson, D., Chem Eur. J., 5, 1338, 1999.
[10]  Raganathan, D., Kurur, S., Gilardi, R. and Karle, I., Biopolymer, 54, 289, 2000.

# Stabilization of Copper Oxide Nanoparticles in (w/o) Microemulsions: Experimental and Modeling Results

*Nashaat Nassar, Maen Husein*
*Department of Chemical & Petroleum Engineering, University of Calgary, Calgary, AB, Canada*
*nassar@ucalgary.ca*

## 1. Introduction
Formation of well-dispersed colloidal nanoparticle catalyst is crucial for heterogeneous catalysis in organic media. However, maintaining stable dispersion of the particles is a challenging task since these particles tend to agglomerate with time in order to reduce the high surface energy. One approach of minimizing particle agglomeration is to prepare the fresh catalyst *in-situ*. Very high reaction rates were attained when *in-situ* prepared ultradispersed catalysts were employed for hydrocracking, coprocessing, and coal liquefaction. Water-in-oil (w/o) microemulsions, or reverse micelles, are very good candidates for the *in-situ* catalyst preparation, since they provide control over the particle size, and produce stable ultradispersed nanoparticles. It was found that microemulsion-prepared nanoparticle catalysts exhibited smaller particle size and showed higher catalytic activity compared with the ones prepared by the conventional techniques.

## 2. Objectives
An in-situ approach of copper oxide nanoparticle preparation, in single AOT/water/isooctane microemulsions is demonstrated. The effect of different microemulsion and operating variables, including surfactant concentration, water content and mixing time, on the colloidal concentration (nanoparticle uptake), size and stability of copper oxide nanoparticle in AOT/water/isooctane microemulsions is evaluated. In addition, a mathematical model describing the effect of the aforementioned variables on the nanoparticle uptake and stability is provided.

## 3. Methodology
The colloidal nanoparticles are prepared *in-situ* by exposing AOT/water/isooctane microemulsions to a soluble copper precursor followed by addition of NaOH at a later stage. Upon addition of NaOH, copper oxide nanoparticles stabilized in the water pools form in addition to a bulk precipitate at the bottom. The concentration of the colloidal copper oxide and the particle size are then measured at different times using inductive coupled plasma (ICP), UV-Vis spectroscopy and transmission electron microscope (TEM). Monitoring the concentration of colloidal metal oxide particles and their sizes with respect to time gives indication on their stability.

## 4. Results:
The experimental results have shown that particle size increased with increasing the surfactant concentration, concentration of the precursor salt, and water to surfactant mole ratio. The nanoparticle uptake increased linearly with the surfactant concentration, and displayed an optimum with $R$ and a power function with the concentration of the precursor salt. The model, which was based on water uptake by Winsor type II microemulsion, described well the effect of the variables considered in the study on copper oxide nanoparticle uptake. Below are some samples of our finding. Figures 1 to 3 show a maximum copper oxide nanoparticle uptake coupled with an increase in the particle size, and broader size distribution as the value of $R$ increased. Figure 1 shows that the maximum uptake occurs at $R = 5.0$. The increase and decrease in the nanoparticle uptake reported in Figure 1 is captured by the increase and the decrease in the size of the UV-absorption peaks of Figure 2. The TEM images of Figures 3a,b show an increase in the nanoparticle size and size distribution.

**References:**

[1] Nassar, N., Husein, M., *J. Colloid. Interface Sci.,* 2007 (Submitted)
[2] Nassar, N., Husein, M., *Langmuir*, 2007 (Submitted)
[3] Nassar, N., Husein, M., *Colloids Surf., A.,* 2007 (Submitted)
[4] Nassar, N., Husein, M., *J. Current Nanoscience.,* 2006 (Abstract *accepted*)
[5] Nassar, N., Husein, M., *Phys. Stat. Sol.* (a), 203 (2006) 1324.

**Figures:**
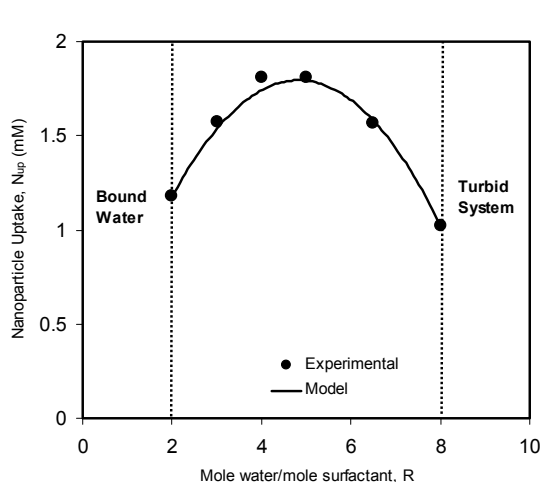


**Figure 1.** Nanoparticle uptake as a function of water to surfactant mole ratio, *R*, obtained when mixing a stoichiometric amount of CuCl$_2$-containing microemulsions {[CuCl$_2$] = 3.0 mM, [AOT] = 200 mM, R = 3.0} with NaOH for 3 h at 300 rpm.
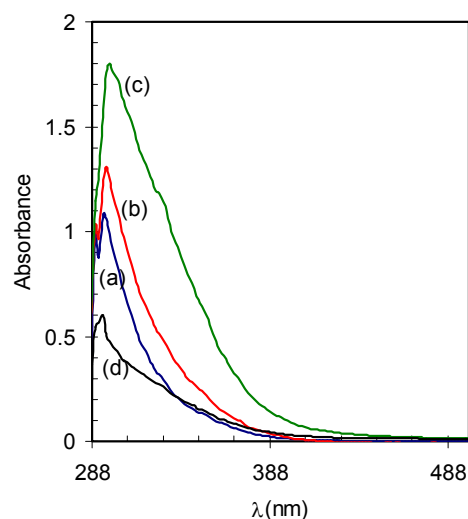


**Figure 2.** UV-absorption spectra of colloidal copper oxide nanoparticles obtained when mixing a stoichiometric amount of CuCl$_2$-containing microemulsions {[CuCl$_2$] = 3.0 mM, [AOT] = 200 mM, (a) *R* = 2.0; (b) *R* = 3.0; (c) *R* = 5.0; (d) *R* = 8.0} with NaOH for 3 h at 300 rpm.
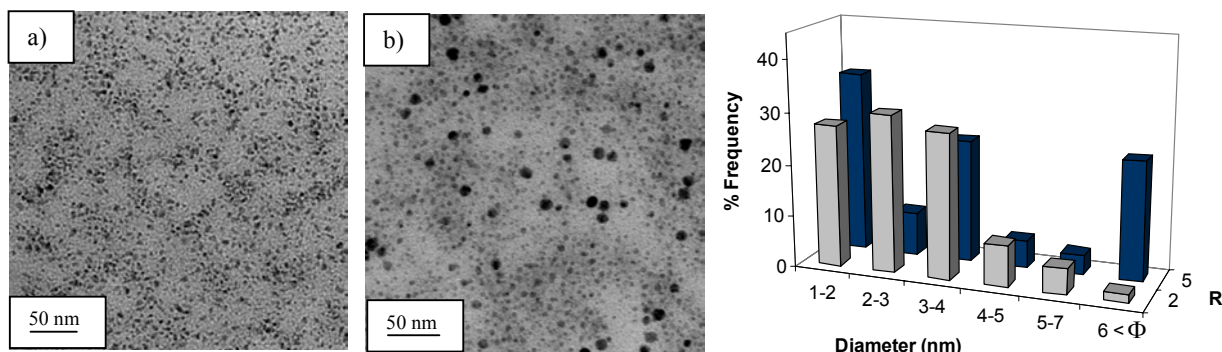


**Figure 3.** TEM photographs and the corresponding particle size distribution histograms obtained when mixing a stoichiometric amount of CuCl$_2$-containing microemulsions {[CuCl$_2$] = 3.0 mM, [AOT] = 200 mM, (a) *R* = 2.0; (b) *R* = 5.0} with NaOH for 3 h at 300 rpm.

# SYNTHESIS OF NANOCOMPOSITE MATERIALS USING PLASMA POLYMERIZATION

*Claudia Nastase*

*3Nano-SAE Research Centre, University of Bucharest,*
*PO Box MG-38, 77125 Magurele, Bucharest - Romania*
*nastasec@3nanosae.unibuc.ro*

The domain of conjugated polymers based nanocomposites materials approach in this paper is actual [1-3] and presents an increased interest in the scientific community due multiple applications of these in organic electronics, sensors, electrodic materials, membrane [4].

In nanocomposites domain was developed different techniques for obtained of polymer nanocomposites by mechanical, chemical, electrochemical process. By combination of classical method of obtained of polymer nanocomposites that implied *in situ* polymerization of monomers of matrix polymer in the presence of nanostructures with plasma polymerization method was developed a interesting technique of processing of nanocomposites. The method involved a single-pass of deposition process, solvent-free and non post deposition treatment. Also synthesis directly on substrate of polymer nanocomposite thin films constituted a huge advantage.

The plasma polymerization method was applied in obtain of multiple polymer nanocomposite thin films: polyaniline- nanocarbon (PAni-NC), polyaniline-carbon nanotubes (PAni-NT), polyaniline-silicon dioxide (PAni-$SiO_2$) and poly thiophene -silicon dioxide (PTh-$SiO_2$).

Complex characterizations by FT-IR and Raman spectroscopic studies, AFM, SEM, TEM, SAED, XRD analyses and electrical characterizations of obtained structures deposited by plasma polymerization method confirm that this technique is a good choice for synthesis of polymer nanocomposite films.

**References:**

[1] Ashis Dey, Sukanta De, Amitabha De and S K De, Nanotechnology **15** (2004) 1277.
[2] P. Parkinson, E. Aharon, M. H. Chang, C. Dosche, G. L. Frey, A. Köhler, and L. M. Herz, Phys. Rev. B **75** (2007)165206.
[3] R Sainz, A M Benito, M TMart´ınez, J FGalindo, J Sotres, AMBar´o, B Corraze, O Chauvet, A B Dalton, RH Baughman andW K Maser, Nanotechnology **16** (2005) S150.
[4] R.A. Vaia, H.D. Wagner, Materials Today, **11** (2004) 32.

# PLASMA POLYMERIZATIONS PROCESS - RECENT ADVANCES IN POLYMER THIN FILMS

*Florin Nastase*
*3Nano-SAE Research Centre, University of Bucharest,*
*PO Box MG-38, 77125 Magurele, Bucharest - Romania*
*nastasef@3nanosae.unibuc.ro*

In literature a vast amount of researches on plasma polymerization can be found. The main reason for applying plasma polymerization is that thin, stable, and pinhole-free films are obtained, which show good adherence to many substrates, but with poor predictability of the chemical structure, high degree of cross-linkage and very high electrical resistivity of the resulting plasma polymerized layer [1-3].

Obtaining of conjugate oligomer/polymer as thin films with low degree of cross-linkage and semiconducting properties deposited by plasma polymerization represents a challenge. I have developed a plasma-polymerization instrument using a direct current (d.c.) glow discharge capable of using liquid monomers and solid-liquid combinations as the starting materials. In this paper several combinations of *p*-xylene monomer with isolated rings (biphenyl - PPD-B and quarterphenyl - PPD-Q) and condensed rings (anthracene - PPD-A and naphthalene - PPD-N) aromatic polycyclic precursors have been plasma polymerized with the objective to obtain polymer films with specific properties related to organic electronic applications.

The characteristics of films prepared by d.c. glow discharge were examined by FT-IR, AFM, SEM, TEM, HRTEM, SAED, XRD. The structures of the deposited plasma polymer films were greatly influenced by the applied d.c. voltages during the discharge. Also, formation process of the plasma thin films depending on the precursor systems. The current–voltage characteristics in asymmetric electrode configuration were studied for determining the conduction mechanism. It was found that the conduction mechanism controlled by SCLC is dominant in plasma polymerized thin films.

**References:**

[1] Martin Y., Boutin D., Vermette P., Thin Solid Films 515 (**17**) (2007), pp. 6844-6852.
[2] Yasuda H.K., Plasma Processes and Polymers 2 (**4**) (2005), pp. 293-304.
[3] Akther H., Bhuiyan A.H., New Journal of Physics **7** (2005).

# Characterization of SiCN Catalytic Chemical Vapor Deposition Film Coatings

*S. Neethirajan[1], T. Ono[2], S. Tanaka[2], M. Esashi[2]\*, D.S. Jayas[1]*

*[1]Department of Biosystems Engineering, University of Manitoba, Winnipeg, MB, Canada R3T 5V6*

*[2]Graduate School of Engineering, Tohoku University, 6-6-01 Aza Aoba, Aramaki, Aoba-ku, Sendai, Japan 980-8579*

*Corresponding author. Tel.: +81 22 7956937; fax: +81 22 7956935. E-mail address: esashi@cc.mech.tohoku.ac.jp (Dr. Esashi).

Polymer derived ceramic materials such as SiCN is gaining momentum because of its excellent thermo-mechanical properties at high temperatures. In addition, the electrical conductivity of SiCN can be tailored and characterized to suit specific application needs. These excellent properties make SiCN a best choice for sensor applications. SiCN has been used for making heat flux sensors (Nagaiah et al., 2006); health monitoring sensors for turbines and power generation systems (Sporian, 2007) and high temperature pressure transducers (Andronenko et al., 2005). For high temperature, corrosive and harsh environment applications in the agricultural and food industry, SiCN based sensors are preferred.

Experimental methods for making thin films of SiCN to facilitate sensor fabrication are being researched worldwide. Radio frequency magnetron sputtering (Xie et al., 2003; Sundaram et al., 2004), pulsed laser deposition (Park et al., 2003), plasma enhanced CVD (Fisher et al., 2007), microwave plasma enhanced CVD and electron cyclotron resonance plasma CVD (Chen et al., 1999) and other methods of depositing SiCN have been explored. Unlike the above high temperature deposition techniques, decrease in the temperature can decrease processing costs, reduce thermally induced stress on the substrate and allow faster heat-up, cool down of the deposition process. Influence of decreased temperature also results in increased resistivity parameter of the material.

In our study, deposition of SiCN film using HMDS by catalytic CVD for low temperature deposition is being explored. Thin films of SiCN were deposited on a silicon substrate using ammonia and hydrogen gas sources. Compositions of SiCN were varied by changing the ammonia gas. Nano-mechanical properties of thin films of SiCN were determined using nano indentation module. Surface morphology of the films was characterized by using Atomic Force Microscope. X-ray Photoelectron Spectroscopy was used to analyse the incorporation of nitrogen in SiC layers grown on the substrate at different gas flow rates. The results showed that composition ratio of SiCN and the dielectric constant can be controlled by varying the flow rate of ammonia. The results of the structural as well as electrical characterization of SiCN under different concentrations of $CO_2$ are also presented in this study.

# References

1) Andronenko, S., Stiharu, I., Packirisamy, M., Moustapha, H., Dionne, P. 2005. The Use of Micro-electro-mechanical Systems for Surge Detection in Gas Turbine Engines Proceedings of the 2005 International Conference on MEMS, NANO and Smart Systems (ICMENS'05) 4 p.

2) Chen, L.C., Chen, K.H., Wei, S.L., Kichambare, P.D., Wu, J.J., Lu, T.R., Kuo, C.T., 1999. Crystalline SiCN: a hard material rivals to cubic BN Thin solid films 355-356(1) 112-116.

3) Fisher, L.M., Wilding, N., Gel, M., Evoy, S., 2007. Low stress silicon carbonitride for the machining of high-frequency nanomechanical resonators. Journal of Vacuum Science and Technology B: Microelectronics and Nanometer Structures 25(1): 33-37.

4) Nagaiah, N.R., Kapat, J.S., An, L., Chow, L., 2006. Novel Polymer Derived Ceramic-High Temperature Heat Flux Sensor for Gas Turbine Environment International MEMS Conference 2006 34: 458-463.

5) Park, N., Kim, S., Sung, G. 2003. Band gap engineering of SiCN film grown by pulsed laser deposition Journal of Applied Physics 94(4): 2725-2728.

6) Sporian, 2007. High Temperature MEMS Sensor Suite for Health Monitoring System of Turbine Engine Components Navy SBIR FY2006.1 www.sporian.com March 31, 2007.

7) Sundaram, K.B., Alizadeha, Z., Todia, R.M., Desaib, V.H. 2004. Investigations on hardness of rf sputter deposited SiCN thin films Materials Science and Engineering A 368(1-2) 103-108.

8) Xie, E., Ma, Z., Lin, H., Zhang, Z., He, D. 2003. Preparation and characterization of SiCN films Optical materials 23(1-2) 151-156.

# One-dimensional growth of PTCDA molecular rows on Sn/Si(111) surfaces

*N. Nicoara*[1, 2]*, Z. Wei*[3]*, C. Polop*[1] *and J.M. Gómez-Rodríguez*[1]

[1]*Dept. Física de la Materia Condensada, Universidad Autónoma de Madrid, 28049-Madrid, Spain*
[2]*Instituto de Ciencias de Materiales de Madrid, 28049-Madrid, Spain*
[3]*Dept. Modern Physics, Univ. of Science and Technology of China, 230026-Hefei, China*
[nicoleta.nicoara@uam.es](mailto:nicoleta.nicoara@uam.es)

The possibility of including organic semiconductors as active components in the inorganic semiconductor-based devices has increased the interest in these materials in the last years. By exploiting this organic-inorganic approach the advantages are two-fold. On the one hand, one can benefit from well-defined surface structure properties and overall quality of the currently used semiconductors such as Si. On the other hand, a wide range of organic molecules along with their tailorable optical and electronic properties may provide new hybrid devices with enhanced capabilities. Nevertheless the controlled deposition of these organic materials to produce epitaxial thin films, required for optimum functional properties of devices, still represents a considerable challenge, due to the increased reactivity of the semiconductor surfaces.

Improved structural order is observed when reactive semiconductors surfaces are passivated e.g. by reaction with hydrogen atoms in the case of Si substrates [1,2], prior to organic film growth. The passivation induces a reduction of the chemically active sites, mainly by saturating the surface dangling bonds.

In the present work a new approach to passivate semiconductor surfaces has been exploited by adsorbing metal atoms, such as Sn on Si(111) substrates. The adsorption and growth of organic PTCDA (3,4,9,10 perylene-tetracarboxylic dianhydride) molecules on the Sn/Si(111) has been investigated at room temperature by means of scanning tunneling microscopy.

For the deposition of PTCDA on Si(111)-$(2\sqrt{3}\times2\sqrt{3})$R30°-Sn surface [3] we have observed the formation of a novel molecular PTCDA structure consisting in quasi 1D molecular rows. The evolution of sample morphology with increasing coverage is showed in Fig. 1. The molecular row formation is observed in the initial stage of deposition i.e. 0.2 ML PTCDA. The length and the density of molecular rows increase for subsequent deposition. At 0.5ML PTCDA molecular rows extend homogeneously over the entire surface, creating a highly ordered overlayer with regularly-spaced rows, in a commensurate $(4\sqrt{3}\times2\sqrt{3})$R30° structure.

The registry of the PTCDA molecule relative to the substrate was determined from high resolution STM images where intramolecular PTCDA features and substrate lattice are resolved simultaneously as shown in Fig. 2. Three symmetry-equivalent PTCDA domains are found. In addition splitting into two domains by a mirror plane exists with the rotation angle R=+/-15° with respect to the three equivalent surface crystal axis of the Sn/Si(111) substrate.

It is proposed that the molecular anchoring process may be the result of a Sn-O bond formation which stabilizes the molecular rows and promotes the commensurate $(4\sqrt{3}\times2\sqrt{3})$R30º. The symmetry and orientation of molecular domains suggest that the molecular arrangement is mainly governed by a molecule-substrate interaction.

The studied system, for which unprecedented 1D PTCDA structure has been obtained, may be used as an organic template to further functionalize silicon-based semiconductor surfaces.

**References:**

[1] J. B. Gustafsson, E. Moons, S. M. Widstrand and L. S. O. Johansson, Surf. Sci. **572**, (2004) 23.
[2] T. Soubiron, F. Vaurette, J. P. Nys, B. Grandidier, X. Wallart and D. Stievenard, Surface Science **581**, (2005) 178.
[3]  T. Ichikawa and K. Cho, Jpn. J. Appl. Phys. **42**, (2003) 5239.

(a) Θ~0.2ML        (b) Θ~0.35ML        (c) Θ~0.5ML
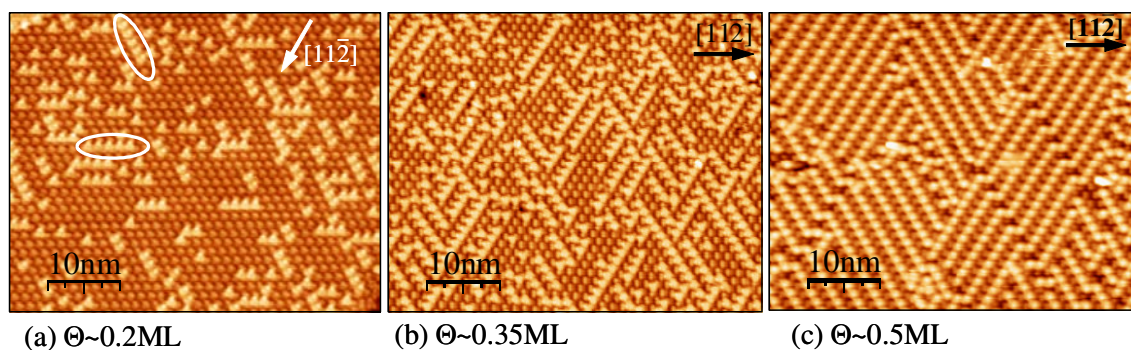
**Figure 1** Representative STM images of the Si(111)-2√3×2√3-Sn surface after the PTCDA deposition, showing the evolution of sample morphology with increasing coverage. (a) The molecule rows formation is observed starting at 0.2ML. (b) With increasing coverage the length and the density of molecular rows increase. (c) At 0.5ML the PTCDA molecular rows extend homogeneously over the entire surface, creating a highly ordered overlayer with regularly-spaced rows, in a commensurate (4√3×2√3)R30° structure. Image sizes: 50nm×40nm, (a),(b) V=+2.2V, I=0.1nA. (c) V=-2.0V, I=0.1nA.



(a)        (b)        (c)
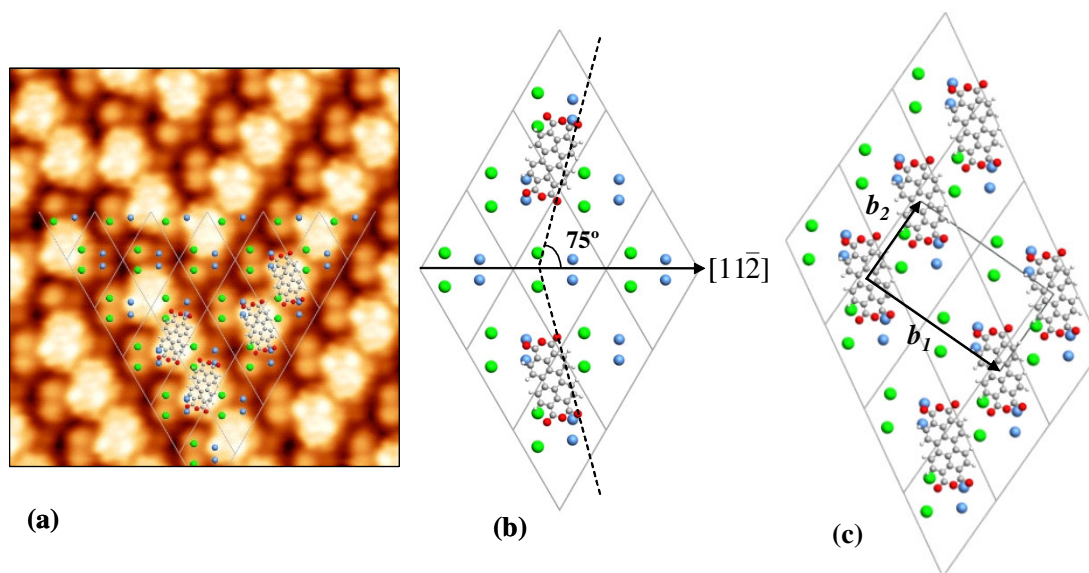
**Figure 2** (a) High resolution STM image shows that within each substrate domain, there are two preferential orientations of the molecule related by mirror symmetry relative to the [11$\bar{2}$] substrate direction   (10nm×10nm, V=+2.0V, I=0.1nA). (b, c) Proposed structural models indicate the molecular adsorption geometry and the PTCDA commensurate (4√3×2√3) R30° structure on the Si(111)-2√3×2√3-Sn surface, respectively.

# PREPARATION AND CHARACTERIZATION OF A NANOSTRUCTURED DENTAL COMPOSITE

*Ecaterina Andronescu, Oana Nicola, Cristina Ghitulica, Mihaela Birsan, Elena Dinu*
*University POLITEHNICA from Bucharest*
*1-7, Gh. Polizu Street, 1-Bucharest, PO – BOX 12-134, Romania*
*Email: cghitulica@yahoo.com; oana_ncl@yahoo.com*

In modern dentistry, the direct techniques of odonto-therapy restorations, based on amelo-dentinal adhesion, have an important place and they represent a large part of the usual medical practice. The requests and the expectations of the patients are aiming to final results with a very good aesthetic aspect, in biomechanical, bio - functional and bio - physiologic optimal conditions, for the hard dental structures and the surrounded tissues. On the other side, the materials and the techniques based on adhesion allowed to realize indeed a therapeutic boarding non-invasive, and this represent the future in dentistry [1, 2].

The current dental composite, including the most modern, are nevertheless operational limited because of the certain characteristics inherent of the structure and the dependent physico-chemical properties of the inorganic part (seeds of filling) and of the organic part (the polymerized resin matrix) [3].

The present paper describes the preparation through sol-gel methods and aims to characterize ceramic nanoparticles used as filling inorganic materials for dental composites of esthetic restorations.

The sol-gel synthesis was carried out using the Stober method [4, 5]. The nanometric powder of silica was obtained starting from TEOS ($Si(OC_2H_5)_4$). That was mixed with the ethanol, the hydrolysis and condensation reactions taking place in the presence of water and ammonia.
Nanometric powder of zirconia/silica composite was also obtained. In this case, the composite was prepared using precursors of the oxide components, as: $ZrCl_4$ and TEOS ($Si(OC_2H_5)_4$). The precursors were mixed in ethanol, the gelation ocuring in the presence of 1,2 – epoxy-propan.

The powder of silica, named "S", was treated at temperatures between 1000 and $1200^0$C for 2 hours, while the composite powder, named "ZS", was treated at temperatures between 700 and $1200^0$C for 2 hours.

The powders "S" and "ZS", were characterized in what it concerns mineralogical composition (using an X-ray difractometer *SCHIMADZU XRD 6000)*, granulometric distribution (using a laser granulometer *FRITSCH PARTICLE SIZER ANALYSETTE 22*) and the microstructure (SEM – using a scanning electronic microscope *EDAX - HITACHI S2600N* and TEM).

X-rays diffraction showed that the crystalline compounds formed are silica in his polymorphic form trydimite (figure 1), for the "S" powder, and tetragonal zirconia, for the "ZS" powder (figure 2).

The granulometric distribution showed that we have obtained powders with the following specific surfaces: for "S" the specific surface is 3,63 $m^2$/cc and for "ZS" the specific surface is 4,08 $m^2$/cc.

The scanning electronic microscopy showed that the powders "S" and "ZS" have a very fine structure, with dimensions of particles smaller than 0,5 micrometers (figure 3).

Electronic transmission microscopy showed that the powder "S" is consisting of particles in spherical form of 200-300nm in diameter, but also of smaller particles, in plate form, with an acicular aspect. The powder "ZS" have the crystals well defined, with spherical form, smooth surfaces and nanometric dimensions that vary between 3 and 5 nm (figure 4).

Taking account the results obtained, we appreciate that powders "S" and "ZS" have a real potential to be used in dental applications, but it is necessary to make more experiments in order to be able to control the dimension of particles and conglomerates.

**References:**
[1]  Blunck U., Marktübersicht Adhesivsysteme. Zahn. Prax., **8, 1 – 2 (Jan.–Feb.)** (2005), 14-37.

[2] Mount G.J., Beyond G.V. Black, J.F., Vanherle G.: Adhesive Technology for Restorative Dentistry. **Quintessence Publishing Co. Ltd., London** (2005) 47-62.

[3] Roberson T.M., Heymann H.O., Ritter A.V., Roberson T.M., Heymann H.O., Swift Jr. E.J.: STURDEVANT'S Art and Science of Operative Dentistry. **4th ed., Mosby Inc., St. Louis** (2002) 473-481.

[4] Moszner M., Klapdohr S., Nanotechnology for dental composite, **Int. J. o Nanotechnology Vol., Nos. 1/2** (2004) 130-156.

[5] Clapsaddle B.J., Sprehn D.W., Gash A.E., Satcher J.H., Simpson R.L., A versatile sol-gel synthesis route to metal-silicon mixed oxide nanocomposites that contain metal oxides as the major phase, **UCRL-JRNL-201444** (2003) 1-27.

**Figures:**
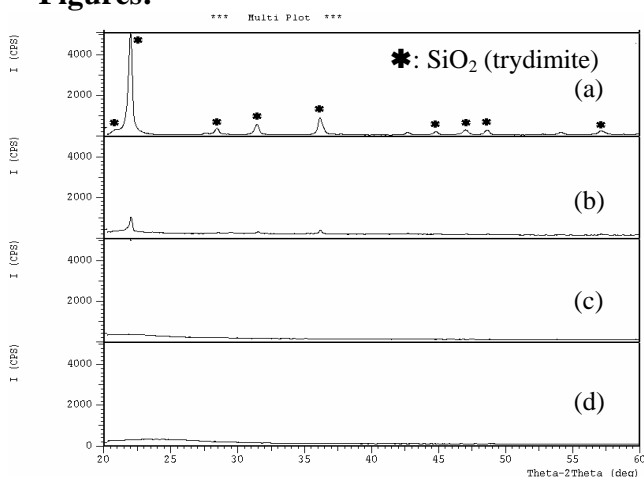


Figure 1. The spectrum of X-ray diffraction obtained on "S" powder, for various thermal treatments
(a) $1200^0$C/2h; (b) $1100^0$C/2h; (c) $1000^0$C/2h; (d) as synthetized
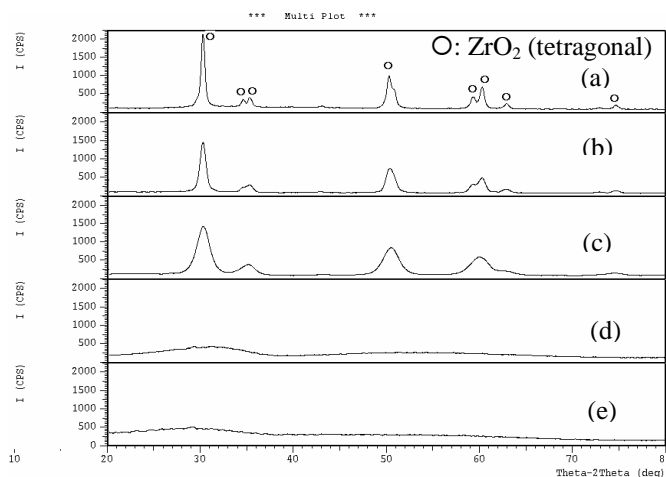


Figure 2. The spectrum of X-ray diffraction obtained on "ZS" powder, for various thermal treatments
(a) $1200^0$C/2h; (b) $1100^0$C/2h; (c) $1000^0$C/2h; (d) $700^0$C/2h; (e) as synthetized
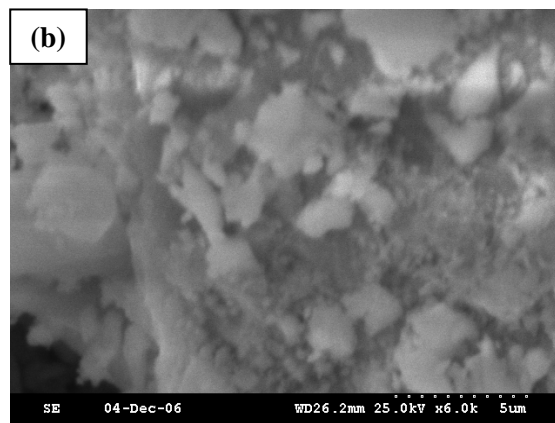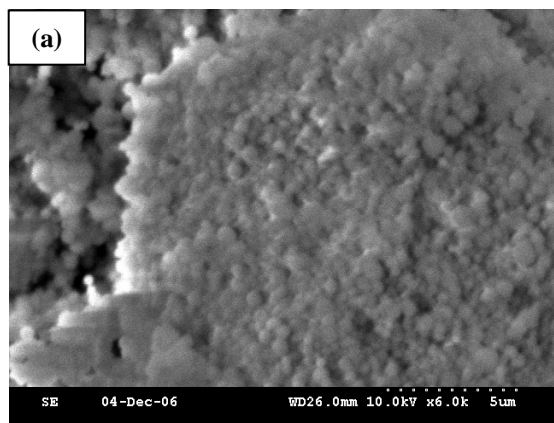


Figure 3. Scanning electron microscopy images of powder "S" (a) and "ZS" (b) thermal treated at $1000^0$C/2h
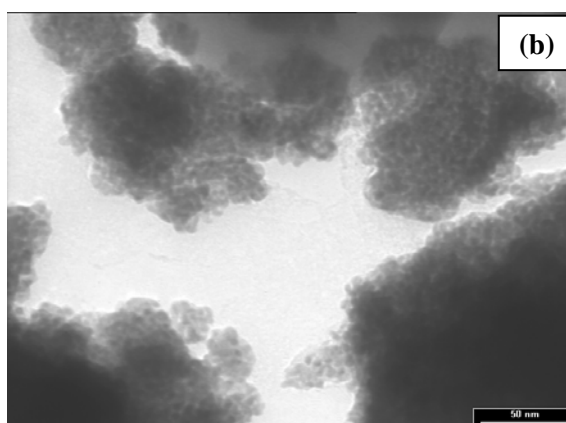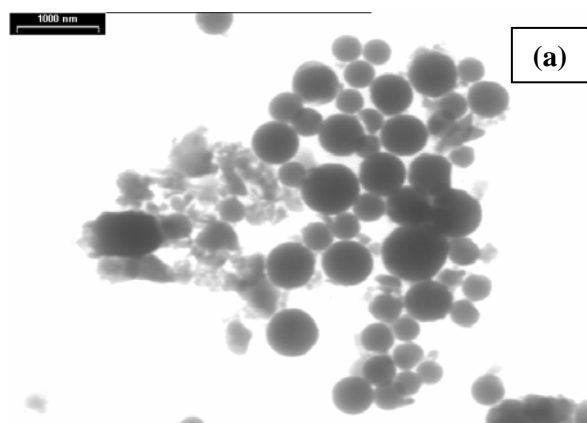


Figure 4. Electronic transmission microscopy of powder "S" (a) and "ZS" (b) thermal treated at $1000^0$C/2h

# SYNTHESIS AND CHIROPTICAL STUDY OF OPTICALLY ACTIVE THIOLATE-CAPPED SILVER NANOCLUSTERS

*Naoki Nishida, Hiroshi Yao, Tomoyasu Ueda, Akito Sasaki, and Keisaku Kimura*
*Graduate School of Material Science, University of Hyogo, 3-2-1 Koto, Kamigori-cho, Ako-gun, Hyogo, 678-1297, Japan,  and X-ray Research Laboratory, Rigaku Corporation, 3-9-12 Matsubara-cho, Akishima, Tokyo 169-8666, Japan*
*nishidann@yahoo.co.jp*

Recently, we have reported the synthesis and chiroptical properties of optically active gold nanoclusters protected by a pair of penicillamine enantiomers [1]. On the basis of kinetic and structural considerations, we have attributed the observed optical activity to a dissymmetric field induced by the chiral penicillamine shell. A recent theoretical study supports the dissymmetric field model [2]; symmetric metal cores can be optically active when perturbed by a dissymmetric field originating from the surface adsorbates. On the other hand, the origin of optical activity of glutathione-protected gold nanoclusters has been discussed in the context of an inherently chiral core model [3,4]. Thus the arguments on the origin of optical activity are still fragmentary due to few examples of well-defined optically active nanoclusters. We report here the synthesis and chiroptical properties of optically active D-/L-penicillamine-capped silver nanoclusters with the core size ranged in 1-3 nm.

Each of three kinds of penicillamines (D/L- or racemate-form) was used as a monolayer protecting agent. Briefly, a freshly prepared aqueous $NaBH_4$ solution was added into mixture of $AgNO_3$ and penicillamine (D/L-pen or rac-pen) in methanol under vigorous stirring, followed by the addition of ethanol into the stored solution, yielding a dark-brown crude precipitate. After completely washing the precipitate, the sample power was obtained by a vacuum-drying procedure. The silver nanocluster sample prepared by using D-pen, L-pen or rac-pen is termed as Ag-D-pen, Ag-L-pen or Ag-rac-pen, respectively. To separate or purify the silver nanoclusters that differ in size and charge, we applied polyacrylamide gel electrophoresis (PAGE) using a slab gel unit that employs a gel of 2-mm thickness. On the basis of electrophoretic mobility of the silver nanocluster compounds, the separated compounds are referred to as **1**, **2**, … (consecutive numbers), with the order of mobility **1** > **2** > …. When distinguishing these compounds in regard to the stereochemistry of the surface ligands, a suffix L, D or rac is added at the end the compound number; for example, $\mathbf{1}_D$, $\mathbf{2}_D$, … for the Ag-D-pen nanocluster sample. Size distributions of silver nanoclusters were determined by a small angle X-ray scattering (SAXS) technique in solution: The SAXS profiles of silver nanoclusters dispersed in solution were first measured, followed by analyzing the profiles based on the assumption that the size distribution of spherical cluster is approximated by the Γ–distribution function.

To obtain information on chiroptical properties of the prepared silver nanoclusters, we measured circular dichroism (CD) spectrum of each numbered compound. CD spectra of the fractioned compounds $\mathbf{1}_D$, $\mathbf{1}_L$ and $\mathbf{1}_{rac}$ are shown in Figure 1. The mean core size of the cluster compound 1 was determined to be 1.05 nm. For homochiral penicillamine-capped silver nanoclusters, ligand chirality had a dramatic effect on the CD spectra of the clusters. Note that optically active penicillamine contributes to the CD signal only in the UV region in the wavelength shorter than ~270 nm. The pair of CD spectra in Figure 1 showed measurable Cotton effects and a mirror-image relationship in metal-based electronic transition resion, suggesting that enantiomeric ligands can produce the corresponding enantiomeric silver nanoclusters.

To sharply elucidate the chiroptical responses of the optically active silver nanoclusters, we calculated the anisotropy factor (or *g*-factor) for the separated compounds $\mathbf{1}_D$ and $\mathbf{1}_L$. The

result is shown in Figure 2. The obtained maximum anisotropy factor is 1.5 x $10^{-3}$. The chiroptical response of the silver nanoclusters is surprisingly several-fold larger than that of the gold nanoclusters having the same ligand in comparable size [1]. In addition, we found that the anisotropy factor was increased with a decreased in the core size of the nanoclusters. In the present silver nanoclusters, the vicinal effect from asymmetric carbons in the ligands should be the universal origin for their optical activity, but its enhancement might be attributed to the additional contributions from a chiral silver core or chiral adsorption pattern. The field of optically active nanoclusters is a very broad one ranging from cluster science to surface science, so that we believe that our findings will give a new development of this fascinating subject in nanoscience.

**References:**

[1] Yao, H.; Miki, K. Nishida, N.; Sasaki, A.; Kimura, K. *J. Am Chem. Soc.*, **127** (2005) 15536.

[2] Goldsmith, M.-R.; George, C. B.; Zuber, G.; Naaman, R.; Waldeck, D. H.; Wipf, P.; Beratan, D. N. *Phys. Chem. Chem. Phys.*, **8** (2006) 63.

[3] Garzón, I. L.; Reyes-Nava, J. A.; Rodríguez-Hernández, J. I.; Sigal, I.; Beltrán, M. R.; Michaelian, K. *Phys. Rev. B*, **66** (2002) 073403.

[4] Schaaff, T. G.; Whetten, R. L. *J.Phys. Chem. B*, **104** (2000) 2630.
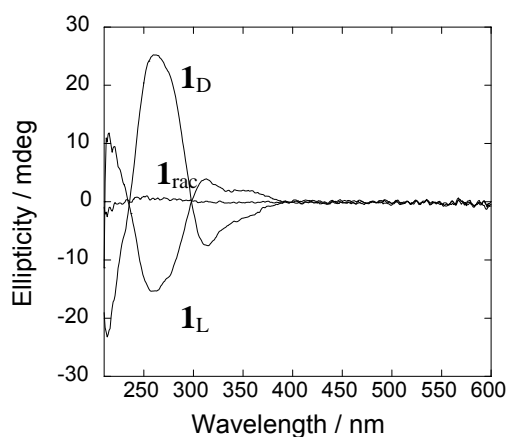
**Figures:**



**Figure 1** CD spectra of compounds **1**.
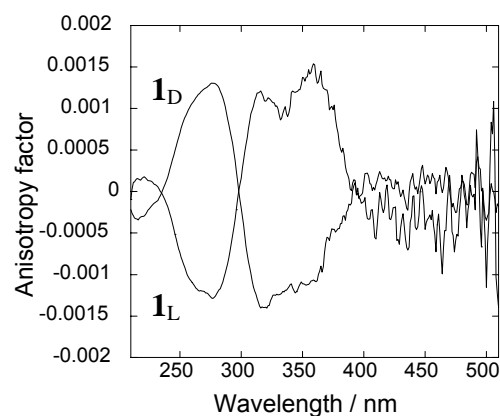


**Figure 2** Anisotropy factor of **1**$_D$/**1**$_L$.

# VERTEX-SHARING POLYICOSAHEDRAL GOLD CLUSTERS: A FIRST STEP TOWARD CLUSTER-ASSEMBLED MATERIALS

*Katsuyuki Nobusada, Takeshi Iwasa*
*Department of Theoretical and Computational Molecular Science,*
*Institute for Molecular Science, Okazaki, 444-8585, Japan*
*nobusada@ims.ac.jp*

Extensive studies of nanometer-sized metal clusters have shown their novel physicochemical properties that are significantly different from those of the corresponding bulk metals. These metal nanoclusters are also expected to have potential for their application to development of new materials functioning as molecular-sized quantum devices. In contrast to the rapidly growing understanding of fundamental properties of each individual metal nanocluster, relatively little is known about whether these clusters are assembled retaining their individual properties while producing new collective features due to the aggregation. The most direct approach to this issue might be to specify a unit cluster that serves as a *building block* of cluster-assembled compounds and then reveal how the assembled compounds are constructed from the units. Very recently, Tsukuda and coworkers made significant progress toward realizing the cluster-assembled compounds in a bottom-up approach [1]. They synthesized a gold cluster compound $[Au_{25}(PPh_3)_{10}(SC_2H_5)_5Cl_2]^{2+}$ (**1**) and characterized its geometric structure through single X-ray crystal analysis. The cluster has a unique structure in the sense that the $Au_{25}$ core is constructed by bridging two icosahedral $Au_{13}$ clusters with thiolates sharing a vertex gold atom and is terminated by two chlorine atoms.

In this study, we theoretically characterize geometric and electronic structures of a dimer cluster $[Au_{25}(PH_3)_{10}(SCH_3)_5Cl_2]^{2+}$ (**2**) mimicking the cluster **1** by carrying out density-functional-theory calculations, and reveal the mechanism of the dimerization [2]. We further discuss polymerization, as an example, the trimerized gold cluster $[Au_{37}(PH_3)_{10}(SCH_3)_{10}Cl_2]^{+}$ (**3**). All the calculations were carried out by utilizing the TURBOMOLE package of ab initio quantum chemistry programs [3]

Fig. 1(a) shows side and top views of the optimized structure of **2** with $C_s$ molecular symmetry. For convenience, we indicate the four layers (I-IV denoted in Fig. 1) of the gold pentagonal rings. It is clearly seen that the two icosahedral $Au_{13}$ clusters are bridged (between II and III layers) by the methanethiolates sharing a vertex gold atom and terminated by the chlorine atoms. In other words, this gold cluster is considered to be a dimer with the biicosahedral structure. This structure reasonably agrees with the experimental X-ray data of **1**. A natural question then arises whether polymerization more than the dimerization is achieved. To answer this question, we have further carried out geometry optimization of a trimer structure within $C_i$ molecular symmetry in the same way as in the dimer one. We succeeded in obtaining the trimer structure of **3** as shown in Fig. 1(b). At the present level of calculation, the 1+ cationic state was preferred. As is similar to the structure of the dimer, the three icosahedral $Au_{13}$ clusters are bridged by the methanethiolates sharing vertex gold atoms at two different sites and terminated by the chlorine atoms. Furthermore, comparison between the absorption spectra of the two structures has revealed that new electronic structures due to the polymerization come into being one after another, whereas the electronic properties of the individual $Au_{13}$ units almost remain unchanged.

It is expected that the scheme of the present polymerization is utilized to achieve cluster-assembled compounds starting from a building block of the icosahedral $Au_{13}$ cluster incorporating with thiolate molecules.

**References:**

[1] Y. Shichibu, Y. Negishi, T. Watanabe, N. K. Chaki, H. Kawaguchi, T. Tsukuda, J. Phys. Chem. C, **111** (2007) 7845.
[2] K. Nobusada, T. Iwasa, submitted to J. Phys. Chem. C.
[3] TURBOMOLE Version 5.7, Quantum Chemistry Group, University of Karlsruhe, Germany.

**Figures:**
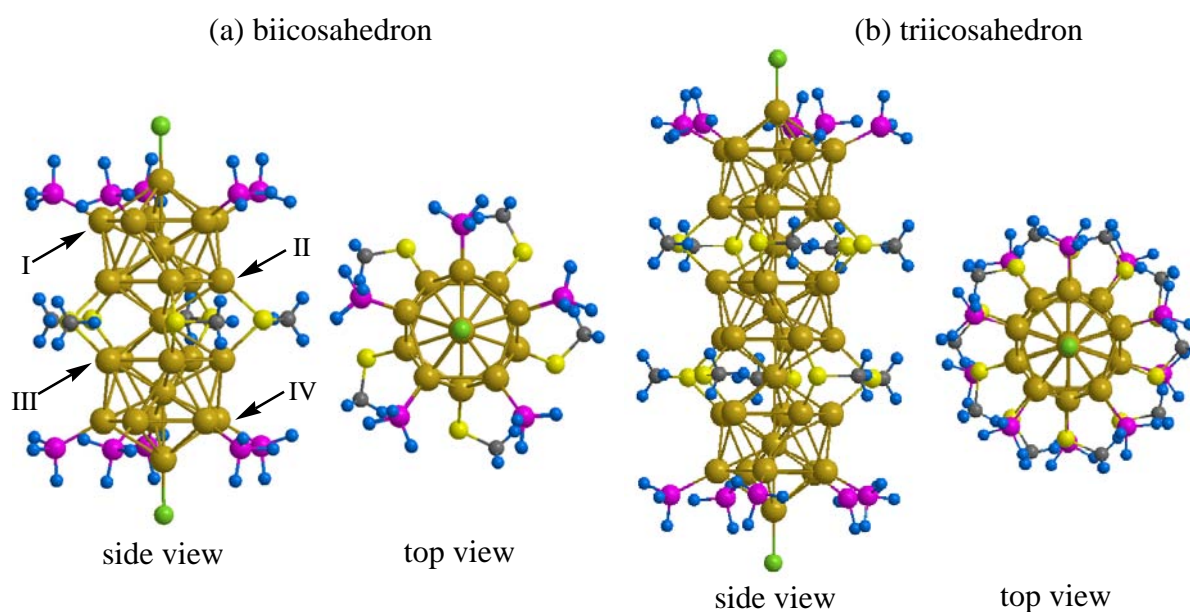


Fig.1 Optimized structures of (a) bi- and (b) triicosahedral gold clusters

# Electronic Properties of Nanomaterials Based on Artificial Atoms

*Javier Nossa, Ángela Camacho*

*Universidad de los Andes, Cra. 1E No. 18ª-10 Edificio H AA. 4976, Bogotá, Colombia*

*ja-nossa@uniandes.edu.co*

Nowadays, the quantum dots (artificial atoms) are considered as tools of interdisciplinary skills, they can be considered around for different purposes [1], in addition these have several applications in different fields as optical and optoelectronic devices, quantum computing, materials for cascade lasers, etc.

In addition to artificial atoms, artificial molecules have been studied coupling two quantum dots. On the other hand the experimental perspectives have lead to the formation of arrays 3D of quantum dots, which are called quantum dots supercrystals. The growth of artificial materials based on quantum dots is imminent. Therefore it is urgent to have theoretical calculations which allow pre-design the optical and electronic properties of these materials.

Following to Tamura et. al.: "*If we consider a quantum dot as a building block and put it on a site of the lattice, we can create an artificial crystal having interesting properties*"[2]. These quantum dots supercrystals are grown as function of both intrinsic geometry of the quantum dot and the geometry of the array of these. Motivated by the experimental perspectives mentioned above we first present the electronic energies and probability distributions of several shapes quantum dots. Second, By means of tight-binding model we show the electronic structure of the simple cubic supercrystal based on several shapes of quantum dots.

**References:**

[1] Steven C. Erwin, Lijun Zu, Michael I. Haftel, Alexander L. Efros, Thomas A. Kennedy, David J. Norris, Nature 436 (2005) 91

[2] Hiroyuki Tamura, Kenji Shiraishi, Takashi Kimura, and Hideaki Takayanagi, Phys. Rev. B 65 (2002) 085324

# TRENDS IN NEW GENERATION OF ELECTROSPUN NANOFIBERS

*M. Nouri, H. Ghanadzadeh, F. Raeesi, V. Mottaghitalab, G.Khiati, A.K. Haghi*[*]
*The University of Guilan, P. O. Box 3756, Rasht, Iran*
[*] Corresponding author E-mail: Haghi@guilan.ac.ir

In the electrospinning process [1-4], polymer nanofibers with submicron-scale diameters are formed when a droplet of viscoelastic polymer solution is subjected to a high voltage electrostatic field. It is the only established method for producing continuous polymeric fibers with diameters in the nanometer range. In this paper we explore some issues related to experimental and structural characterization of new generation of electrospun nanofibers, which interrelates the emerging field of nanofibers with practical case of microelectronics.

It has been more than two decades that conductive polymers are known for their interesting characteristics, having electrical conductivity besides retaining low weight, strength and processability which are the main properties of conventional polymers. Since their discovery in 1977 they have been used in different parts of microelectronics devices, such as FETs, displays, diodes and different kind of sensors. By using nanofiber structure of conducting polymers, due to high porosity and high surface to volume ratio of nanowebs, the performance of conducting polymers can be enhanced.

Among all conducting polymers, polyaniline(PANi) have been of particular interest because of its environmental stability, controllable electrical conductivity and interesting redox properties associated with the chain nitrogen. The excellent processability, together with the presence of a number of intrinsic redox states, has substantially enhanced the potential applications of aniline polymers for use in practical devices [5,6].

In the present work  nanofibers of polyaniline/ polyacrylonitrile blend dissolved in NMP which has utter simplicity and importance. The key process parameters and material properties that control process operation have been identified and operating diagrams proposed to classify regimes of operation(Figures 1-8). The unique characteristic of these polyaniline blend nanofibers is their electroactive nature.

## References:

 [1] A.K.Haghi and M. Akbari, Trends in electrospinning of natural nanofibers, Physica Status Solidi ,  DOI 10.1002/pssa.200675301.

[2] A.K.Haghi,   "On the formation of electrospun nanofibers" Book Chapter, in "Chemistry as music" Edited by LinShu Liu and Gennady E.Zaikov,  Nova Science Publisher, USA, 2007.

[3] A.K. Haghi and M. Akbari "Electrospun nanofibers: a fiber digest for beginners", Book Chapter, in "Some Tasks in Chemistry and Biology; Today, Tomorrow and Perspectives" Edited by Paul Edwin Stott and Gennady Efremovich Zaikov, Nova Science Publishers, New York, 2007.

[4] A.K.Haghi, M. Akbari and V. Mottaghitalab, "Electrospinning of natural fibers", Book Chapter. In "Natural Fiber Reinforced Polymer Composites" Edited by S. Thomas and L.A. Pothan, Old City Publishing, USA, 2007.

[5] E.T. Kang, K.G. Neoha, K.L. Tan. "Polyaniline: A polymer with many interesting intrinsic redox states",  Progressive Polymer Science, Vol. 23, 211-324, 1998.

[6] V. Saxena, B. D. Malhotra, "Prospects of conducting polymers in molecular electronics", Current Applied Physics, 3, 293–305, 2003.
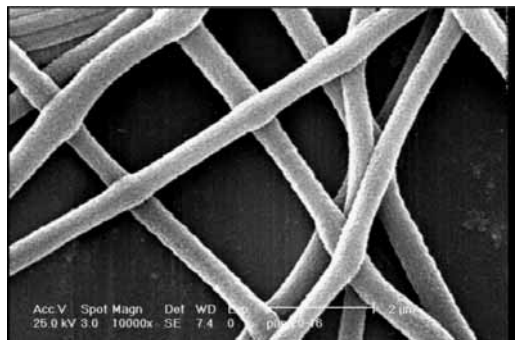
Fig.1. SEM micrograph of 10wt% of PANi (20 Kv)
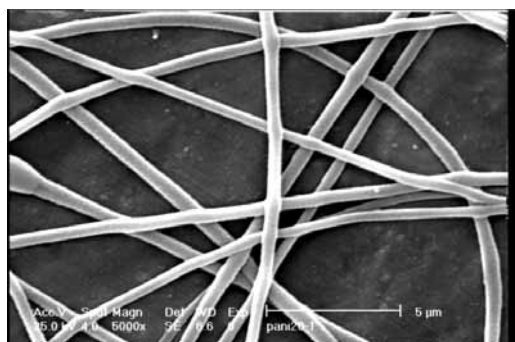


Fig.2. SEM micrograph of 20wt% of PANi (20 Kvs)
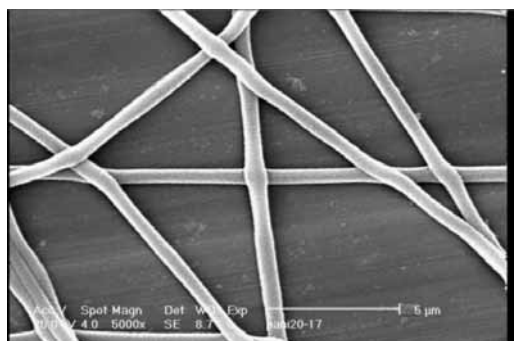


Fig.3.SEM micrograph of 10wt% PANi (25Kvs)
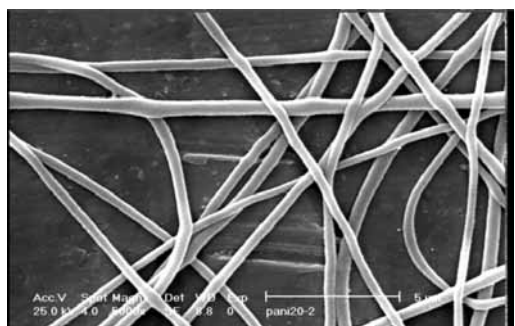


Fig.4.SEM micrograph of 20wt%PANi (25 Kvs)
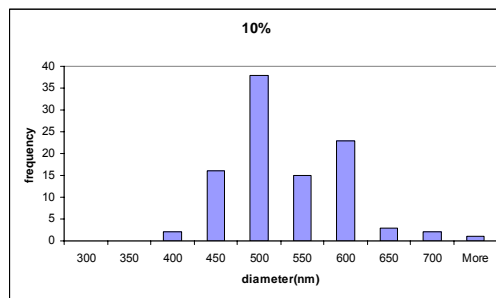


Fig.5. Nanofiber diameter distribution for blend containing 10% PANi
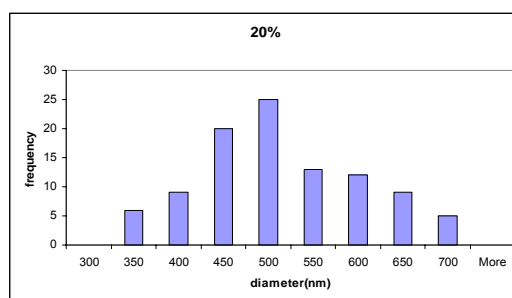


Fig.6. Nanofiber diameter distribution for blend containing 20% PANi
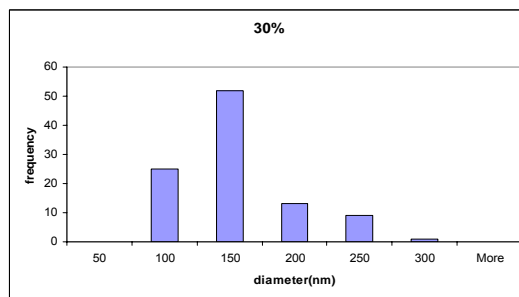


Fig.7. Nanofiber diameter distribution for blend containing 30% PANi
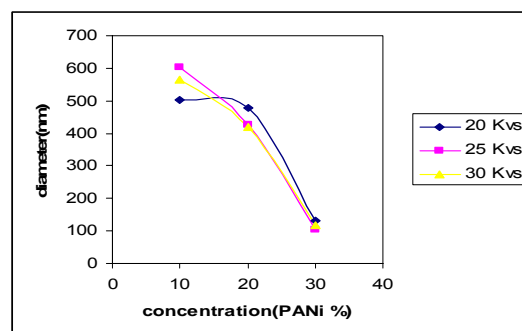


Fig.8. diameter vs. PANi concentration as the voltage increases.

# Inkjet printing of nanomaterials for manufacturing electronic devices

*Arantza Odriozola, José Mº Berrueta, Andreu Cortiella,*
*Iñaki Maiza, Julio Peña, Fernando Varela*

*CEMITEC, Polígono Mocholí, Plaza CEIN, nº4, Noain, Spain*
*aodriozola@cemitec.com*

Inkjet printing process for graphic arts has been known for more than two decades but in recent years is observed as a novel manufacturing process. High accuracy, disposal of toxic waste and no need for additional tools attract electronic industry and turn revolutionary digital printing technology. Several companies are starting to manufacture PCB's, RFID's, OLED's and other electronic devices by inkjet printing and there is a large potential for TFT's, sensors, solar cells, etc…..

Main obstacle up to date is material formulation. It is not easy to find a jettable ink which is also a functional material for manufacturing electronic devices. To be jettable material must fulfil the following specifications:

- Viscosity must be low : 8-20 cps at printing temperature.
- Material surface tension and nozzle wettability must guarantee the correct drop formation.
- Material surface tension must be lower than substrate surface energy to ensure good adhesion properties. Most of substrates are also treated to optimise wettability.
- Particle size of material must be nanometric, otherwise printer nozzle would be clogged.

As expected, design of materials is not an easy task and future of inkjet technology as manufacturing process is linked to development of nanomaterials. It was only recently that these products are available. Silver nanoparticles dispersed in alcoholic vehicles have been already printed to form conductive tracks for PCB's. Great advantage of nanoparticles is their sintering temperature, lower than 200 ºC when diameters are below 50 nm. Conventional silver inks are dispersions of micrometric particles with sintering temperatures above 800 ºC and conductive paths for PCB´s are obtained by screen-printing. However, lots of ink are lost by etching away material and manufacturers are looking for "clean" processes. Inkjet printing avoids the waste of expensive material because is an additive and not sustractive technology and allows to obtain high values of conductivity, similar to those of screen-printed paths.

An industrial inkjet printer was built at CEMITEC with Spectra Nova printheads in order to deliver different functional materials for manufacturing processes. A nanoparticle silver ink was printed on a flexible poliimide, Kapton FPC from Dupont and conductive tracks were obtained once solvent was removed and particles were sintered. It was observed that conductivity values depend on curing temperature and curing time. Formulations of nanoparticle inks are being optimised in order to introduce inkjet technology at industrial scale.

The following pictures show some of the printed conductive devices:
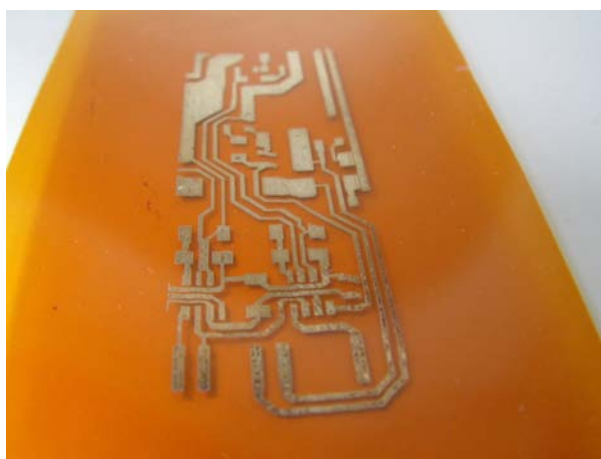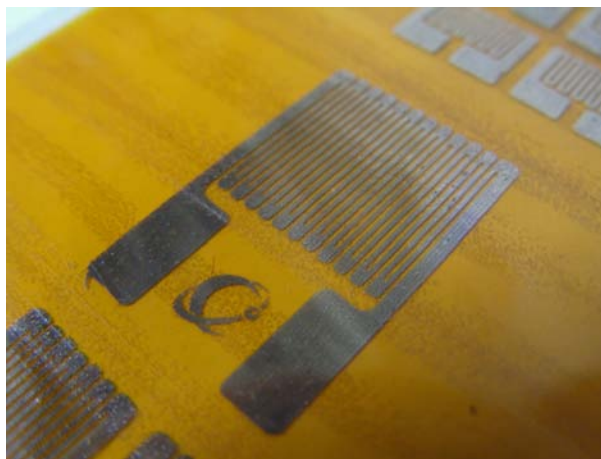
# SINGLE-WALLED CARBON NANOTUBE REINFORCED COPPER MATRIX NANOCOMPOSITES

*Seyoung Oh[1,a], Byeongsoo Lim[2,b], Chulju Kim[2,c], Bumjoon Kim[2,d], Byungho Sung[2,e], Jeehoon Choi[2,f], Untae Shim[2,g], Kijae Hyung[2,h], Seunghyun Baik[1,2,i]*

[1] SKKU Advanced Institute of Nanotechnology, Sungkyunkwan University, Suwon, GyeongGi-Do, 440-746, Korea
[2] School of Mechanical Engineering, Sungkyunkwan University, Suwon, GyeongGi-Do, 440-746, Korea

[a]*osy530@skku.edu*, [b]*bslim@skku.edu*, [c]*cjkim@skku.eud*, [d]*kultra@skku.edu*, [e]*bh03@chol.com*, [f]*choijihoon@skku.edu*, [g]*sut8466@skku.edu*, [h]*mythjh@naver.com*, [i]*sbaik@me.skku.edu*

Carbon nanotubes (CNTs) have excellent properties for improving mechanical, thermal, and electrical characteristics of nanocomposites as reinforcement materials [1]. In order to develop successful CNT-reinforced nanocomposites, it is important to transfer the extraordinary properties of CNTs to the matrix [1]. Two main issues are homogeneous distribution and high interfacial strength[1].

We have studied CNT reinforced copper matrix nanocomposites[2]. In this study, CNT was dispersed by the mechanical mixing process and interfacial strength between the nanotubes and the copper matrix was controlled by coating the nanotubes with nickel. Figure 1 shows nickel-coated nanotubes. The thickness of the nickel layer on nanotubes ranged between 60 and 170 nm. The sintering process was adapted for the fabrication of nanocomposites specimens. The displacement characteristics of nanocomposites at an elevated temperature were investigated by a small punch (SP) creep tester to evaluate the interfacial strength between copper particles and CNTs. Figure 2 shows displacement-time curves of the nanocomposites. Compared with the pure copper specimen or the nanotube reinforced copper matrix composite, the nickel-coated nanotube reinforced copper matrix composite was found to exhibit the significantly improved displacement rate. A pure copper specimen was used as a reference material. For the nanotube reinforced opper matrix composite (0.5 vol %), the displacement rate rapidly increased and the rupture time was shorter than that of the pure copper specimen. This might be due to the poor interfacial strength between carbon and copper [2, 3]. The nickel-coated nanotube reinforced copper matrix composite showed the longest rupture time which is six times longer than that of the pure copper specimen. Probably due to the increased interfacial bonding [2]. The electrical and thermal characteristics of the nanocomposites were also investigated.

**References:**

[1] Taejune Kang, Jang-won Yoon, Dong-iel Kim, Sangseop Kum, Yong-hak Huh, Jun-hee Hahn, sangheup Moon, Ho-young Lee, and Yonghyup Kim, Adv. Mater., 19(2007)
[2] Byengsoo Lim, Chul-ju Kim, Bumjoon Kim, Untae Shim, Seyoung Oh, Byung-ho Sung, Jee-hoon Choi and Seunghyun Baik, nanotechnology, 17( 2006) 5759-5764
[3] S J Sun and M D Zhang, J. Mater. Sci., 26(1991) 5762-5766

**Figures:**
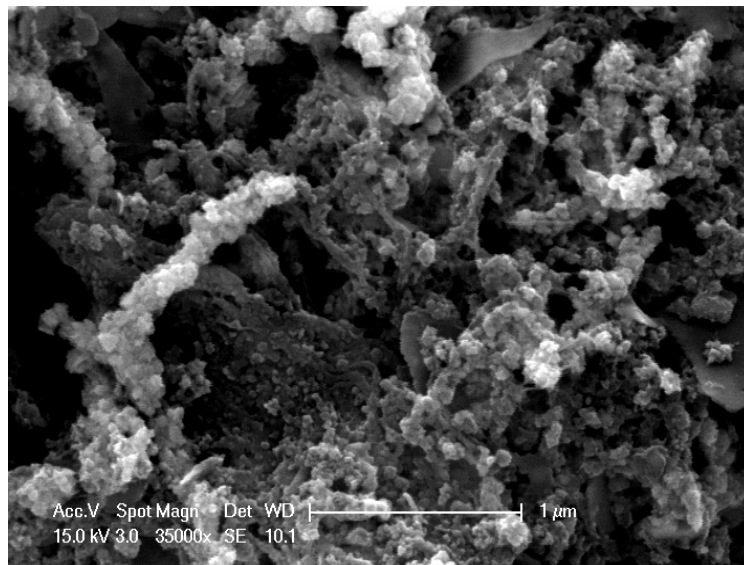


Figure 1. Nickel –coated carbon nanotubes. [2]
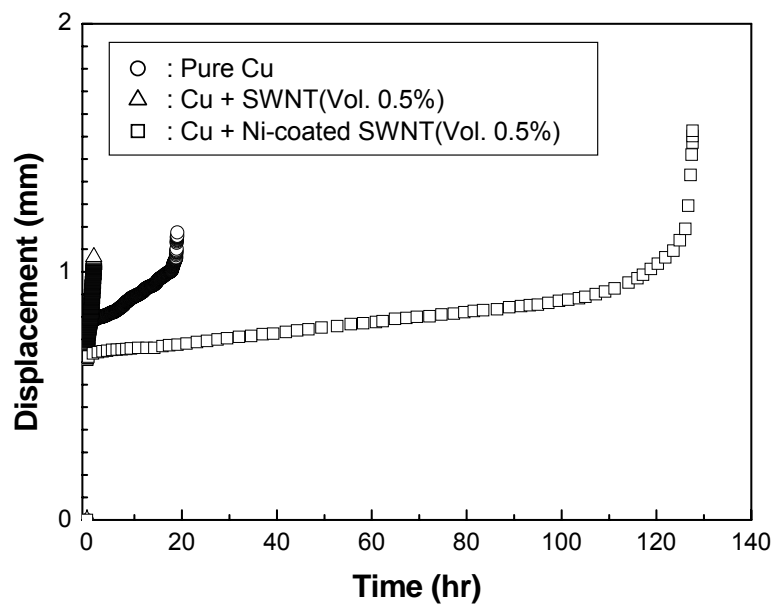


Figure 2. The effects of interfacial strength on displacement rates. [2]

# SINGLE-STEP FABRICATION OF A WAVE PLATE USING INORGANIC-ORGANIC HYBRID GLASS WITH NANOIMPRINT LITHOGRAPHY

*Motoki Okinaka[1], Kenichiro Tanaka[1], Yoshifumi Ichinose[2], Hiroshi Tsushima[2], Toshiyuki Tachibana[2], Kazuhito Tsukagoshi[1], and Yoshinobu Aoyagi[1,3]*

*Nanoscience Research and Development Support Team, RIKEN, 2-1 Hirosawa, Wako-city, Saitama, Japan[1]*
*Nippon Paint Co.,Ltd. 1-15-4, Minami-shinagawa, Shinagawa-ku, Tokyo 140-8675, Japan[2]*
*Interdisciplinary Graduate School of Science and Engineering, Tokyo Institute of Technology, 4259 Nagatsuta, Midori-ku, Yokohama 226-8502, Japan[3],*

[*o-motoki@riken.jp*](mailto:o-motoki@riken.jp) *(Motoki Okinaka)*

Recently, nano-patterning of transparent glassy materials utilizing nanoimprint lithography (NIL) [1] has been conducted intensively for the realization of optical components. This is not only because NIL technique needs only relatively low cost and has high productivity, but also this technique makes it easier to integrate optical components on a chip. For example, achromatic quarter-wave plate utilizing form birefringence [2] or waveguide Bragg grating filter [3, 4] were fabricated using NIL. Up to now, the patterning of glassy materials is processed in the following way: (1) A nano-patterned mold is pressed onto the surface of glassy materials at the temperatures around their glass transition temperatures (typically ~500 °C) and the glassy materials are hardened by cooling [5], or (2) after a nano-patterned mold is transferred into polymers, the glassy materials are dry-etched using the patterned polymers as a shadow mask. However, both methods are not simple enough; the former method needs relatively high temperature, and the latter needs plasma etching after NIL.

In this report, we propose a much easier single-step nano-patterning process using a unique inorganic-organic hybrid glassy material, Glasia®, and report on the fabrication of the wave plate with this material and technique.

Glasia® consists of poly(methylphenylsilane) with 20 % branching degree including of 50 % silicone. As a photosensitizer, a few percent of 3,3',4,4' tetra (*t*-butyl peroxycarbonyl) benzophenone is added to increase the sensitivity for ultraviolet (UV) radiation. In addition, we added 11 vol.% of $ZrO_2$ nanoparticles which are typically 3 nm in diameter, in order to increase the refractive index of Glasia® to make a wave plate with higher retardation. The refractive index of $ZrO_2$-diffused Glasia is 1.6 at 632 nm, which is larger than Glasia itself (1.55 at 632 nm). In this study, we made a line-and-space structure using this material to form a wave plate utilizing form birefringence effect [6].

Figure 1(a)-(f) show our process flow [7, 8]. At first, the $ZrO_2$-dispersed Glasia was spin-coated on $SiO_2$ substrate [Fig. 1(a)]. The film was heated at 80 °C for 5 minutes to remove the residual solvent. Patterned Si mold fabricated with our plasma etching facility was then pressed into the films at lower temperature [Fig. 1(b)]. Subsequently, UV irradiation was applied through the $SiO_2$ substrate [Fig. 1(c)], in which the photo-oxidation started from the substrate side, resulting in the strong adhesion between the film and the $SiO_2$ substrate. After the Si mold was demolded [Fig. 1(d)], the film was irradiated in $O_2$ plasma to harden the surfaces of the replicated structure [Fig. 1(e)]. Then, the Glasia® region was photo-oxidized by the UV irradiation from the patterned surface side [Fig. 1(f)]. Finally, a heat treatment was performed to solidify the material completely [Fig. 1(g)]. The fabricated structure is line-and-space structure, where the width of the line ($d_1$), space ($d_2$), and the height ($h$) are 250 nm, 250 nm, and 900 nm, respectively.

We have measured the retardation of the sample by the conventional Senarmont method. The light source was a output of a $Ti:Al_2O_3$ laser, whose wavelength ($\lambda$) can be changed from 700 nm to 930 nm. The circles in Fig. 2 show the wavelength dependence of the retardation of the obtained wave plate. On the other hand, the triangles in Fig. 2 show the wavelength dependence of the retardation of the wave plate of the same structure made with Glasia® for

comparison. The wave plate made with $ZrO_2$-dispersed Glasia® exhibits larger retardation than that made with Glasia itself because of the larger refractive index of $ZrO_2$-dispersed Glasia®. The observed retardation for $ZrO_2$-dispersed Glasia® was 0.18λ at 700 nm, which is consistent with the theoretical evaluation based on the form birefringence theory [6].

In summary, we have proposed a single-step procedure on a unique inorganic-organic hybrid glassy material, $ZrO_2$-dispersed Glasia®, and have fabricated a form-birefringence wave plate. The obtained wave plate exhibits retardation of 0.18λ at 700 nm, which is consistent with the evaluation from the form birefringence theory. This single-step procedure with newly developed $ZrO_2$-dispersed Glasia® is cost-effective and has higher productivity than conventional nanoimprint lithography, thus it is promising in the mass production of optical components.

**References:**

[1] S.Y. Chou, P.R. Krauss, P.J. Renstrom, Science **272** (1996) 85.

[2] X. Deng, F. Liu, J.J. Wang, P.F. Sciortino, Jr.,L. Chen, and X. Liu, Optics Letters **30** (2005) 2814.

[3] D.-H. Kim, W.-J. Chin, S.-S. Lee, Appl. Phys. Lett. **88** (2006) 071120.

[4] A. Kocalabs and A. Aydinli, Optics Express **14** (2006) 10228.

[5] S.Y. Chou, P.R. Krauss, and P.J. Renstrom, J. Vac. Sci. Technol. **B14** (1996) 4129.

[6] M. Born and E. Wolf, ``Principles of Optics,'' 7th Edition, Section 15.5.2.

[7] M. Okinaka, K. Tsukagoshi, and Y. Aoyagi, J. Vac. Sci. Technol. **B24** (2006) 1402.

[8] M. Okinaka, H. Tsushima, Y. Ichinose, E. Watanabe, K. Yanagisawa, K. Tsukagoshi, and Y. Aoyagi, J. Vac. Sci. Technol **B25** (2007) 1393.

**Figures:**
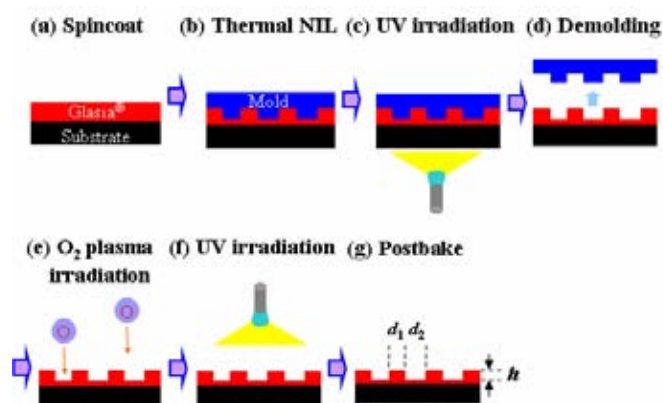


Fig. 1: Our single-step fabrication of a wave plate using inorganic-organic hybrid glass with nanoimprint lithogragphy. (a) spin coating and prebaking, (b) low-temperature nanoimprint, (c) UV irradiation through a $SiO_2$ substrate, (d) Demolding of Si mold, (e) $O_2$ plasma treatment to oxidize and harden the patterned surface, (f) UV irradiation from the patterned surface side, and (f) postbake to further harden the material.
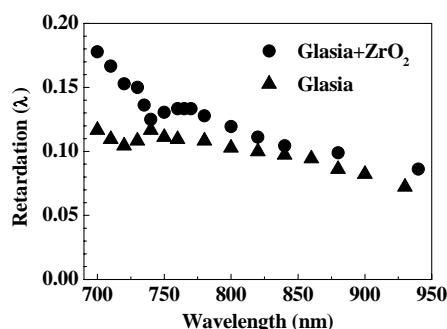


Fig. 2: Wavelength dependence of the retardation of the obtained wave plate made with $ZrO_2$-dispersed Glasia® (circles) and Glasia® (triangles).

# FEW-PARTICLE SYSTEMS IN ASYMMETRIC TRAPS

*Anna Okopińska, Przemysław Kościk*
*Institute of Physics, Świętokrzyska Academy*
*ul. Świętokrzyska 15, 25-406 Kielce, Poland*
*okopin@fuw.edu.pl*

Studies of few-electron systems trapped in confining potentials have attracted considerable attention since their practical realization in the form of quantum dots. The few-boson systems are also interesting and have been experimentally realized in Paul traps. Most frequently, the 2-dimensional systems are investigated with the confinement modeled by an isotropic harmonic potential, however the anisotropic case has been also discussed and the influence of anisotropy on the spectrum has been demonstrated [1,2].

Here we study the system of two charged particles in an anisotropic potential with the harmonic frequencies aspect ratio 2:1, when the problem becomes completely separable. Recently, we have shown that this case is quasi-solvable, i.e. for particular values of confinement frequencies one of the eigenfunctions may be found in a closed analytical form [3]. Here we use these exact solutions to obtain the one-particle density and the correlation function (conditional probability density). It happens that the frequencies at which the exact solution are known correspond to the case of weak confinement when the correlation effects are stronger and manifest by formation of Wigner molecules. We present a detailed analysis of the spectrum of the anisotropic system for both fermionic and bosonic particles, providing a comparison with the isotropic case.

**References:**

[1] A.V.Madhav and T.Chakraborty, Physical Review **B49** (1994) 8163.
[2]  C.Ellenberger, et al., Phys Rev Lett. **96**  (2006) 126806
[3] P.Kościk, A.Okopińska,  J. Phys. A: Math. Theor. **40** (2007) 1045.

**Thermal oxidation of few-layer graphite plates: an SPM study**

*Z. Osváth, P. Nemes-Incze, L. Tapasztó, Z. E. Horváth, and L. P. Biró*

*Research Institute for Technical Physics and Materials Science (MFA), H-1525 Budapest, P.O.Box 49, Hungary*
*osvath@mfa.kfki.hu*

Commercial exfoliated graphite (1 mg material in 20 ml benzene) was treated ultrasonically for 3 hours. Droplets from the suspension were dispersed on Si wafer. Graphite plates of 1-5 μm in diameter were observed by tapping mode atomic force microscopy (AFM) using a Nanoscope IIIa instrument operating in air. After the AFM investigation, the sample was introduced into a quartz reactor of 18 mm inner diameter and oxidized in an electric furnace with an effective heating length of 200 mm [1]. The oxidization was carried out in three steps. In the first step the sample was oxidized at 450 $^o$C for 10 minutes (step I). In the second and the third steps the sample was heated at 550 $^o$C for 10 minutes (step II) and 20 minutes (step III), respectively. AFM measurements were performed after each oxidization step and the effect of oxidization was observed on the same graphite platelet.

To study in more detail the effect of oxidization, we selected an area near the right-hand side edge of the plate in Fig. 1. This portion of the graphite plate is shown in Fig. 2 after the oxidization steps I (Fig. 2a), II (Fig. 2b), and III (Fig. 2c), respectively. The label marks *11'* in Fig. 2a) show a height of 0.7 nm, which corresponds to the thickness of two graphene layers. However, we can easily notice that the plate thickness is not uniform. The marks labeled *22'* show thicker parts with 0.37 nm additional height, which is due to the presence of another incomplete graphene layer. One can observe several pits on the surface in Fig. 2a), at the regions where this top graphene layer is missing. These monolayer deep pits appear due to the oxidization step I. Similar oxidization pits were observed by scanning tunneling microscopy on oxidized highly oriented pyrolitic graphite (HOPG) surfaces [2, 3].

Fig. 2b) shows the graphite plate after oxidization step II (550 $^o$C for 10 minutes). One can observe that in this case the plate edges have also been oxidized and the shape of the analyzed area has changed. The label marks *11'* show a height of 0.39 nm, which means that the thickness of this part has been decreased to one graphene layer. Similarly to Fig. 2a), the plate thickness is not uniform, the label marks *22'* show two-layer thick islands. The effect of the third oxidization step (550 $^o$C for 20 minutes) is illustrated in Fig. 2c. Notice that the thickness of the plate became uniform, the islands of the second layer were removed completely and eventually we obtained a single graphene layer (label marks *11'*). The oxidization decreased also the horizontal diameters of the plate. As a consequence, the analyzed part detached from the body plate and it can be considered a standalone graphene platelet (Fig. 2c). One can observe that the substrate surface (the native SiO$_2$ layer) has also been etched, and approx. 0.4 nm deep trenches have formed along the circumference of the graphene platelet (label marks *22'*).

In this work we have also observed the self-assembly of the few-layer graphite plates into a free-standing film. The unused suspension (few-layer graphite plates dispersed in benzene) was deposited and left untouched. After 2 month, it was observed that the solvent evaporated completely from the bottle and the graphite plates assembled into a continuous and cohesive film. Portions of this free-standing graphite film were investigated by SPM techniques (AFM, STM).

**References:**

[1] L. Tapasztó, K. Kertész, Z. Vértesy, Z. E. Horváth, A. A. Koós, Z. Osváth, Zs. Sárközi, Al. Darabont, L. P. Biró, Carbon **43** (2005) 970
[2] Z. Klusek, Appl. Surf. Sci. **125** (1998) 339
[3] D. Tandon, E. J. Hippo, H. Marsh, E. Sebok, Carbon **35** (1997) 35

**Figures:**
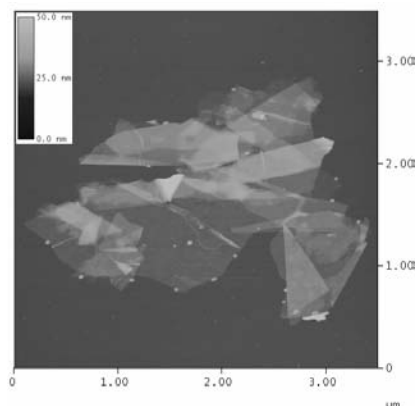


**Fig. 1.** AFM image of a few-layer graphite plate.
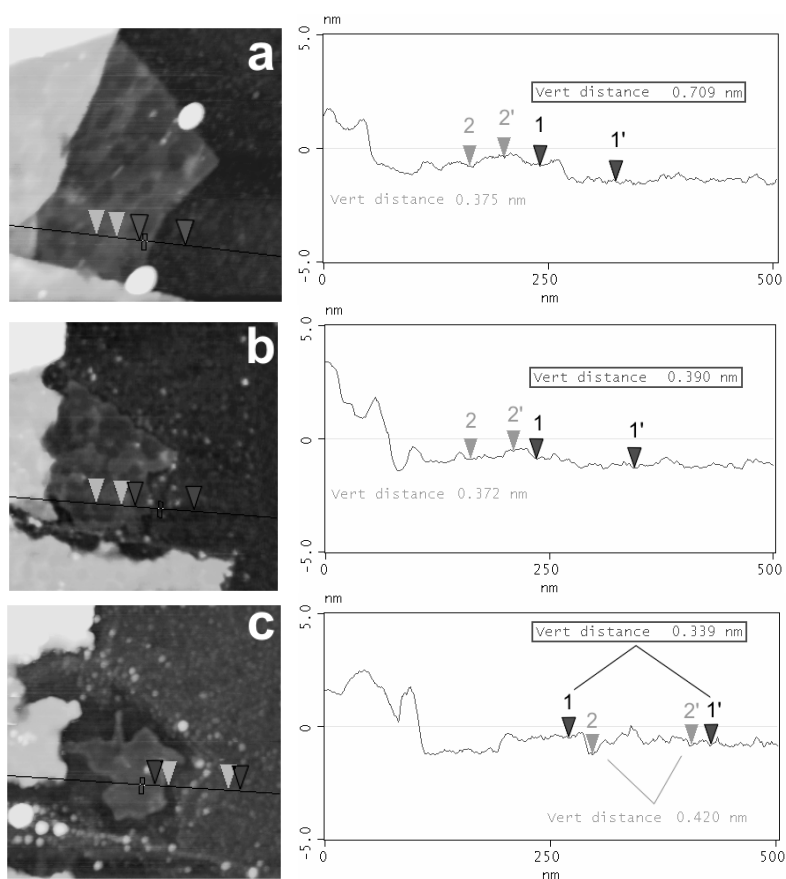


**Fig. 2.** AFM images of the same area of the few-layer graphite plate: (a) – after oxidization step I (450 °C for 10 minutes); (b) – after oxidization step II (550 °C for 10 minutes); (c) – after oxidization step III (550 °C for 20 minutes).

# AN ORGANIC DONOR/ACCEPTOR LATERAL SUPERLATTICE AT THE NANOSCALE: TOWARDS AN OPTIMUM MORPHOLOGY FOR PHOTOVOLTAIC APPLICATIONS

*Roberto Otero[1], David Écija[1], Gustavo Fernández[2], José María Gallego[3], Luis Sánchez[2], Nazario Martín[2] & Rodolfo Miranda[1]*

*Dep. de Física de la Materia Condensada, Universidad Autónoma de Madrid, Campus de Cantoblanco, 28049 Madrid, Spain*
*Instituto de Ciencia de Materiales de Madrid, CSIC, Campus de Cantoblanco, 28049 Madrid, Spain*
*Dep. de Química Orgánica, Universidad Complutense de Madrid, 28040 Madrid, Spain.*
*roberto.otero@uam.es*

Photon absorption by organic molecules with adequate HOMO-LUMO gap excites metastable electron-hole pairs, whose energy can be converted into electrical power by driving the photogenerated electrons and holes to the different electrodes of a solar cell [1]. Facile processing, mechanical flexibility and low cost are some of the advantages of these "plastic" solar cells [2], which have already reached energy conversion efficiencies higher than 5%. Achieving higher efficiencies is however limited by the fact that, instead of free electron-hole pairs, photon absorption usually leads to the formation of tightly bound excitons (bound states of an electron-hole pair) which can diffuse only for a characteristic length of about 10 nm before radiative recombination occurs [3]. The hitherto most successful approach to promote the dissociation of the photogenerated excitons is to use blends of phase-segregated electron-donor/electron-acceptor molecules – the so-called bulk heterojunction concept [1]. At the interface between electron-donor and electron-acceptor areas, the difference in electron affinities drives the exciton dissociation by injecting free electrons (holes) into the electron-acceptor (electron-donor) areas. Provided that continuously connected paths between the interfaces and the electrodes exist, the free electrons and holes will be collected therein. From these considerations a number of morphological criteria can be extracted for optimum solar cell performance: first, the segregated electron-donor and acceptor domains must have a typical sizes of the order of the exciton diffusion length, in order to avoid wasteful radiative recombination events; second, the interface area between donor and acceptor domains, where exciton dissociation takes place, must be maximized; and, finally, donor (acceptor) domains must be continuously connected to the cathode (anode) to favour efficient charge transport. A schematic representation of a morphology that would satisfy these three criteria is shown in panel d) of the Figure: interdigitated donor-acceptor domains and elongated structures (to maximize interface area) with typical diameters of no more than 10-20 nm (to suppress exciton radiative recombination events) connected to the electrodes [4].

In this work we describe variable-temperature Scanning Tunneling Microscopy (STM) experiments that show how monolayer-thick blends of the electron donor molecule 2-[9-(1,3-dithiol-2-ylidene)anthracen-10(9H)-ylidene]-1,3-dithiole (exTTF, see Figure a) [5] with the electron acceptor [6,6]-phenyl $C_{61}$ butyric acid methyl ester (PCBM, see Figure b) [6] on a reconstructed $22 \times \sqrt{3}$ Au(111) surface, segregates laterally into "nanostripes" whose width is of the order of the exciton diffusion length (Figure c); it thus corresponds closely with the morphology for optimum solar cell performance described in Figure d. The reason for such a peculiar nano-scale morphology can be traced back to the different interactions between the two molecular species and the herringbone reconstruction of Au(111). Our results demonstrate the potential of atomistic studies about the growth of organic semiconductors to open new directions for the design and construction of highly-efficient organic electronic devices.

**References:**

[1] G. Yu, J. Gao, J. C. Hummelen, F. Wudl, A. J. Heeger, Science, **270** (1995) 1789.
[2] C. J. Brabec, N. S. Sariciftci, J. C. Hummelen, Adv. Funct. Mat., **11** (2001) 15.
[3] J. Nelson, Curr. Opin. Solid St. M., **6** (2002) 87.
[4] F. Yang, M. Shtein, S. R. Forrest, Nat. Mater., **4** (2005) 37.
[5] N. Martín, L. Sánchez, C. Seoane, E. Orti, P. M. Viruela, R. Viruela, J. Org. Chem., **63** (1998) 1268.
[6] J. C. Hummelen, B. W. Knight, F. LePeq, F. Wudl, J. Yao, C. L. Wilkins, J. Org. Chem., **60** (1995) 532.

**Figures:**
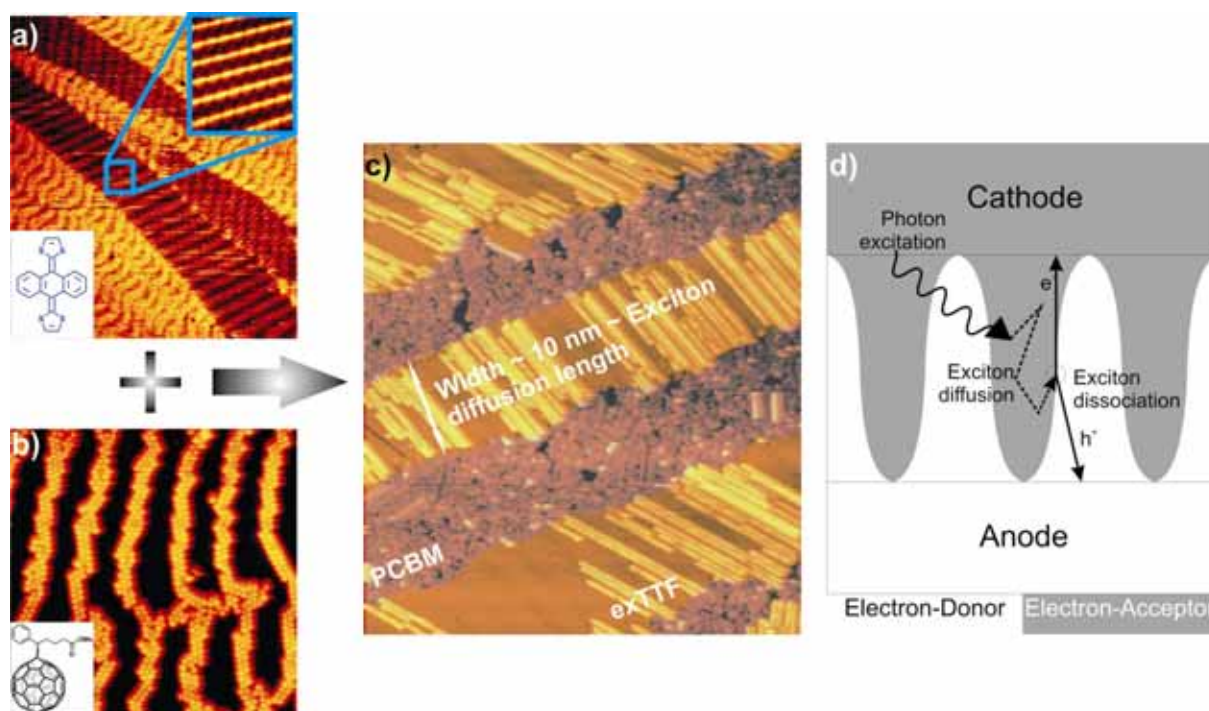


**Figure caption.** a) exTTF striped islands on Au(111) ($176 \times 198$ nm$^2$ STM image). b) PCBM selective growth on FCC areas of the $22 \times \sqrt{3}$ herringbone Au(111) reconstruction ($59 \times 60$ nm$^2$ STM image recorded at 150 K). c) Lateral segregation into nanoscale "fingers" whose width is about 10 nm, which is comparable to the exciton diffusion length ($118 \times 132$ nm$^2$). d) Schematic representation of a hypothetical morphology for optimal solar cell efficiency.

# CONFINEMENT IN SILICON-BASED PHOTONIC CRYSTALS

F. Ouerghi[1], F. AbdelMalek, S. Haxha[2], M. Mejatty[3], and H. Bouchriha[3]

[1] Ecole Supérieure de Technologie d'Informatique, Tunis, Tunisia

National Institute of Applied Sciences and Technology, BP 676 Cedex 1080, Tunisia

[2] Department of Electronics and Photonics, Kent University, UK

[3] Laboratoire de Physique Quantique, Faculté des Sciences de Tunis, Tunis

BP 1060 Cedex Tunis, Tunisie

Emails: Faouzi_Ouerghi@yahoo.fr

Abdelmalek.f@mailcity.com

Since the first proposal in the late 80s by E. Yablonovich and S. John [1, 2] photonic crystals (PCs) have been attracting many people in different areas of physics and engineering. PCs are periodic dielectric structures exhibiting an energy band structure for photons, they are able to control and manipulate the propagation of light in all directions. Most reported studies in this field had focused on two dimension (2D) PCs, however, such consideration can not reflect the complete characteristics of the real structure without incorporating the vertical losses. However, considering 3D PC requires large memory and huge CPU time, to overcome such situation a 2D structure is of importance to be used along with physical understanding. In 2D PCs vertical losses are high and this leads to suppression of PBGs. In order to minimize these losses a distributed Bragg reflector has been considered. In this study, a photonic crystal composed of dielectric cylinders of permittivity 11.56 arranged in hexagonal lattice packed in air is considered. The band structure of the PC embedded between the two Bragg reflectors is calculated by using the developed plane wave method (PWM), the result is reported in Fig.1. It shows that the upper band gap width is increased and shifted towards the higher frequency region and more band gaps appear. It seams that the Bragg reflectors allow additional photonic band gaps, which means that along the vertical direction light is confined and interference phenomenon is taking place. Moreover, the PC structure exhibits four band gaps with widths located at, 0.0045 $\omega a/2\pi c$, 0.036 $\omega a/2\pi c$, 0.018 $\omega a/2\pi c$ and 0.013 $\omega a/2\pi c$, respectively. Also, the transmission spectra in ΓM direction is calculated and given in figure 2. It can seen that the maximum is about 50% in the frequency range varying from 0.5 $\omega a/2\pi c$ and 0.6 $\omega a/2\pi c$ .

Next, the band structure when the number of pairs Bragg layers is increased to eight is presented in figure 3. Figure 3 shows that an additional band gap has been appeared at a higher frequency and a significant increase of the band gap sizes has been achieved. The widths of photonic band gaps are calculated to be; 0.0077 $\omega a/2\pi c$, 0.015 $\omega a/2\pi c$, 0.054 $\omega a/2\pi c$, 0.019 $\omega a/2\pi c$, and 0.015 $\omega a/2\pi c$, respectively. Also, the band gaps have been shifted towards the lower frequencies. The calculation of the transmission coefficient in ΓM direction when the number of the pair Bragg layers is increased to eight is performed and shown in figure 4. It shows that the maximum is about 85%.

Density of state is useful piece of information to locate the band gaps, so that we calculate the density when the number of Bragg layers is kept equal to eight. In figure 5 we report the variation of the density of state as a function of the frequency, it can be seen that this structure posses forbidden states. It means that there is no allowed state for the photons to propagate in all these gap regions, which confirms the calculation of the band structure.

Based on our simulation results it is shown that the Bragg reflectors affect the band structure by opening up more band gaps in higher frequency region. Also, it is demonstrated that an increase in the number of Bragg layer pairs can lead to significant reduction of the vertical losses. The developed plane wave method is used to optimise the photonic crystal, it is shown that 2D PC structure can be considered and used when the vertical confinement is involved in the calculations.

**References**

[1] E. Yablonovitch, "Inhibited Spontaneous Emission in Solid-State Physics and Electronics," *Phys. Rev. Lett*. vol. 58, pp. 2059-2062, 1987.

[2] S. John, "Strong localization of photons in certain disordered dielectric superlattices," *Phys. Rev. Lett*. vol. 58, pp. 2486-2489, 1987.
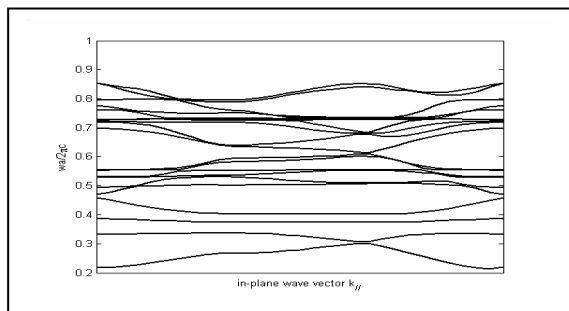


Figure 1. Band structure of the PC with 4 Si/SiO$_2$
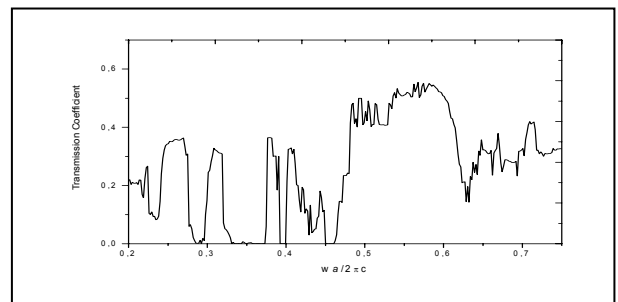


Figure 2 Transmission of the PC with 4 Si/SiO$_2$
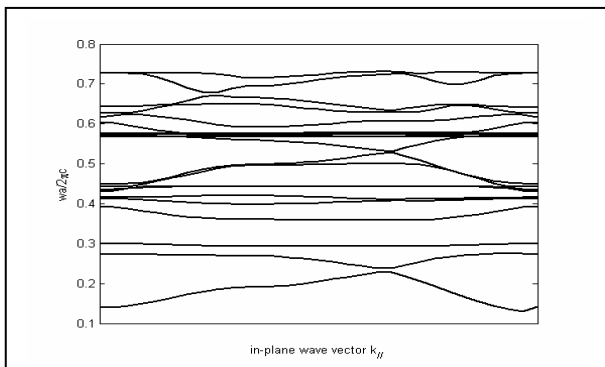


Figure 3. Band structure of the PC with 8 Si/SiO$_2$
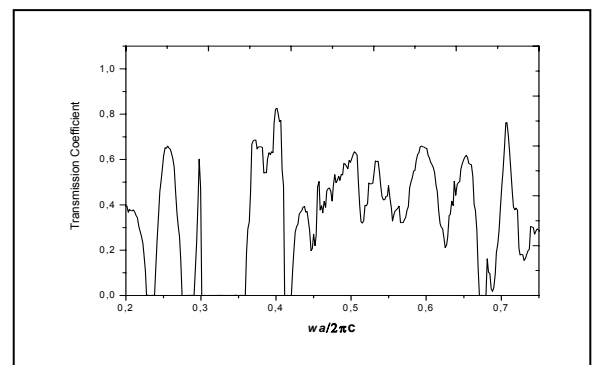


Figure 4 Transmission of the PC with 8 pair Si/SiO$_2$
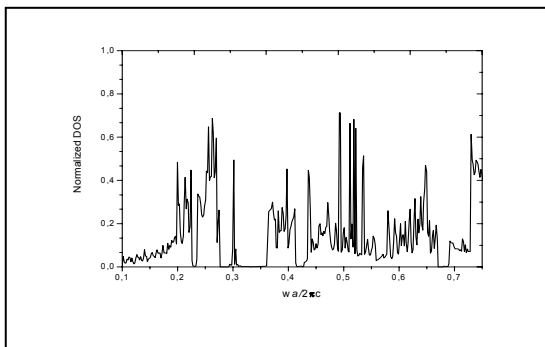


Figure 5 Density of state of the PC with 8 Si/SiO$_2$

# GRAFTING ORGANIC POLYMER FILMS ON SURFACES FROM AQUEOUS SOLUTIONS

*L. Azoulay, L. Bougerolles, G. Deniau, V. Mevellec, S. Roussel, S. Palacin*
*CEA-Chemistry of Surfaces and Interfaces, CEA Saclay 91191 Gif sur Yvette, France*
*serge.palacin@cea.fr*

Electrografting of vinylic polymers onto conducting surfaces has historically been achieved via a direct electron transfer from the cathode to the electro-active monomers in solution. The resulting radical-anion, together with the anions that allow the propagation of the growing grafted polymer chains, are highly sensitive to proton sources. The "classical" cathodic electrografting process thus requires strictly anhydrous conditions.

Radical polymerization does not suffer the same drawback and are easily performed in aqueous conditions. We thus demonstrated that cathodic electrografting on conducting surfaces can be achieved in protic conditions, provided the polymerization is radically initiated by an electro-active moiety. The best initiators are actually diazonium salts.

Indeed, as shown by Pinson, diazonium salts can be easily electro-grafted on conducting substrates by cathodic reduction to phenyl radical species in mild conditions. However, when the applied potential is higher than the reduction potential of the diazonium salt, a significant part of the resulting phenyl radicals are diverted to the solution and may act as initiators of radical processes.

We demonstrated that this initiation is efficient and delivers polymer chains from vinylic monomers solubilized within the electrolyte (either directly or in micellar conditions). The resulting polymer chains normally grow in solution or within the micelles, and are eventually terminated by any radical or radical scavenger present in the medium. Among the termination processes, the most interesting is the reaction of the growing polymer chains with the already grafted aromatic rings coming from the direct electrografting of the diazonium initiator. Hence, the diazonium salts act both as an initiator for the radical polymerization in solution, and as a primer for the chemical grafting of the resulting polymer chains on the surface of the electrode.

Angle-resolved XPS analysis confirmed that the polyphenylene grafted films arising from the direct electrografting of the diazonium moieties are actually located below the vinylic chains, in direct contact with the electrode.

That new grafting process we called SEEP (Surface Electroinitiated Emulsion Polymerization) allows the formation of truly grafted polymer films from aqueous media, provided suitable surfactants are used to solubilize the polymer precursors. From the mechanistic point of view, SEEP combines the 'grafting to' and 'grafting from' methods in one fast electrochemical step at room temperature.(1-3)

More recently, we demonstrated that similar results can be obtained via a purely chemical initiation of the formation of phenyl radicals from diazonium salts. This latter process allows the true chemical grafting of various polymer on any surface, conducting or not, including for example the surface of nano-objects like carbon nanotubes.

**REFERENCES**

[1]. *G. Deniau,* Patent FR06 08945, 12/10/2006.

[2]. *G. Deniau et al.,* Patent FR06 01804, 28/02/2006.

[3]. *G. Deniau et al.*, Chem. Mater. **18** (2006) 5421-5428.

**Figures:**
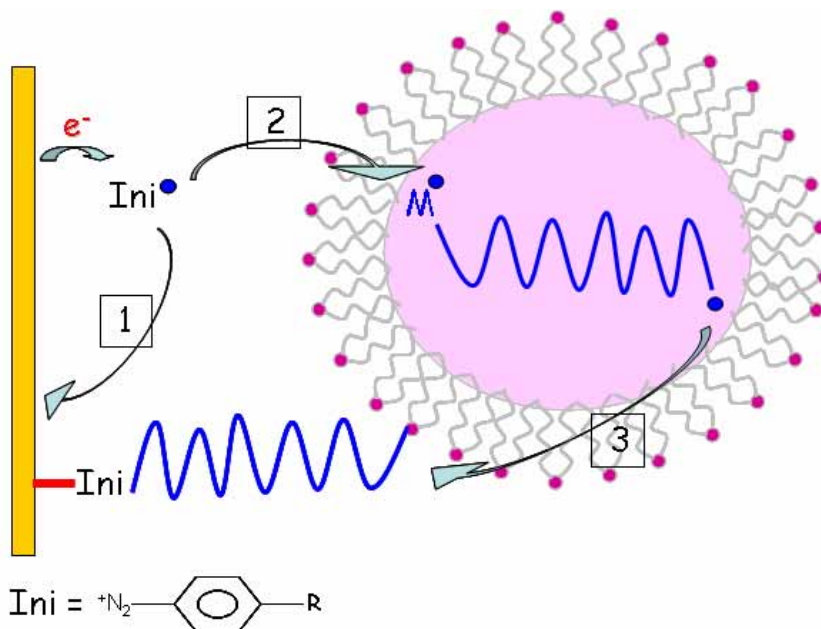


*Figure 1: Proposed mechanism for the SEEP process. The 3 steps are highlighted: 1 is the direct electrografting of the diazonium initiator; 2 is the initiation of the radical polymerization of the monomer M; 3 is the termination reaction that grafts the growing chain to the polyphenylene grafted film.*
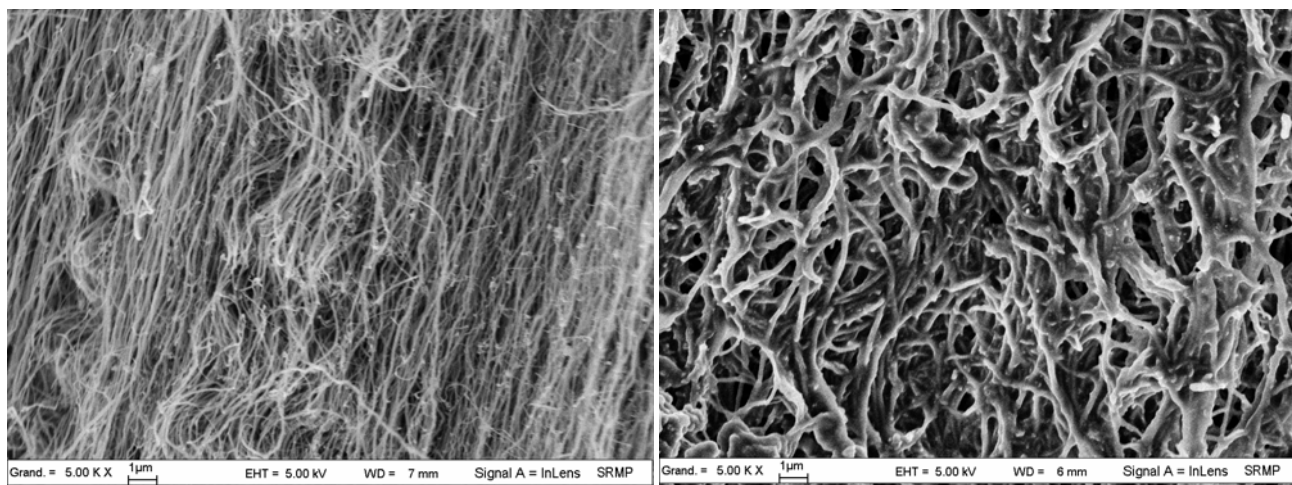


*Figure 2: Multiwall carbon nanotubes as obtained by CVD growth from aerosols (left) and after chemical grafting of poly(hydroxyethylmethacrylate).*

# STRUCTURAL AND SURFACE ELECTRONIC PROPERTIES OF ZnO THIN FILMS GROWN ALONG THE NON POLAR [11 2̄ 0] DIRECTION

*E. Palacios-Lidón[1], B. Pérez-García[1], J. Colchero[1], V. Muñoz-Sanjosé[2],*
*P. Venegues[3], J. Zúñiga-Pérez[2,3]*

[1] *Dep. Fisica, Facultad de Quimica (Campus Espinardo), Universidad de Murcia, E-30100 Murcia, Spain*
[2] *Dpto. Física Aplicada y Electromagnetismo, Universidad de Valencia, C/ Dr. Moliner 50, 46100 Burjassot, Spain*
[3] *Centre de Recherche sur l'Hétéro-Epitaxie et ses Applications (CRHEA), Centre National de la Recherche Scientifique (CNRS), Rue Bernard Grégory, Parc de Sophia Antipolis, 06560 Valbonne, France*

*elisapl@um.es*

ZnO has aroused an enormous interest in recent years due to its wide bandgap (3.3 eV) and large exciton binding energy (60 meV), which have stimulated its use in optoelectronic devices working in the blue and ultraviolet wavelength regions.[1] ZnO crystallizes in the wurtzite structure and, thus, does not possess inversion symmetry. This lack of inversion center leads to a charge asymmetry along the polar [0001] direction that generates a net dipole moment parallel to [0001].[2] Besides the spontaneous polarization, a piezoelectric component due to stressed films can also appear.[3] To overcome the detrimental effects of these electrostatic fields the growth along nonpolar directions has been proposed,[4] with recent studies showing that further requirements must still be fulfilled.[5,6]

In this communication, the morphological and surface electrical properties of ZnO thin films grown along the nonpolar [11 2̄ 0] direction have been studied with scanning force microscopy (SFM) related techniques, including SFM-Nanogoniometry[7] and Kelvin probe microscopy (KPM). The morphological study shows that the ZnO sample surface is completely covered by rhombohedral pyramids whose sidewalls belong to the $\pm\{10\bar{1}1\}$ crystallographic family (Fig. 1(a)). The corresponding KPM images show that two different surface contact potential domains coexist within the ZnO surface, alternating along the [0001] axis (bright and dark regions in Fig. 1 (b)). This alternation points towards a polarity effect arising from the polar nature of the exposed facets. To gain further insight into the mechanism leading to this surface contact potential distribution the samples have been chemically etched by immersion in a diluted hydrogen chloride solution. The SFM study shows that a preferential etching takes place: facets presenting a higher work function (darker contrast on the KPM images are highly damaged and tend to disappear as etching time increases, while the lower work function (bright contact potential) facets remain mainly unaltered (Fig. 1(c),(d) and (e)). Finally the sample has been studied by means of transmission electron microscopy (TEM) and convergent beam electron diffraction (CBED) (Fig. 1(f) and (g) respectively). By combining TEM images on the etched pyramids, recorded with the electron beam perpendicular to the ZnO polar <0001> axis, and CBED measurements, it has been possible to assess the absolute polarity of the pyramids. This has enabled us to establish a complete picture of the structural and surface electronic properties leading to the detected surface contact potential distribution.[8]

**References:**

[1] Ü. Özgür. Ya. I. Alivov, C. Liu, A. Teke, M. A. Resschikov, S. Dogan, V. Avrutin, S. J. Cho, and H. Morkoç, *J. Appl. Phys*. 98, **2005,** 041301.

[2] C. Noguera, *J. Phys. Condens. Matter* 12, **2000,** R367.

[3] T. Makino, Y. Segawa, M. Kawasaki, and H. Koinuma, *Semicond. Sci. Technol*. 20, **2005,** S78.

[4] P. Waltereit, O. Brandt, A. Trampert, H. T. Grahn, J. Menniger, M. Ramsteiner, M. Reiche, and K. H. Ploog, *Nature*, 406, **2002**, 865.

[5] J. Zúñiga-Pérez, V. Muñoz-Sanjosé, E. Palacios-Lidón, and J. Colchero, *Phys. Rev. Lett*. 95, **2005**, 226105.

[6] J. Zuniga-Perez , V. Munoz-Sanjose V, E. Palacios-Lidon, J. Colchero, *Appl. Phys.Lett*. 88, **2006**, 261912.

[7] E. Palacios-Lidon, L. Guanter, J. Zuniga-Perez ,V. Munoz-Sanjose, and J. Colchero, *Small* 3, **2007**, 474

[8] E. Palacios-Lidón, B. Perez-Garcia, J. Colchero, V. Munoz-Sanjose, P. Vennegues and J. Zuniga-Perez, *to be published*.

**Figures:**
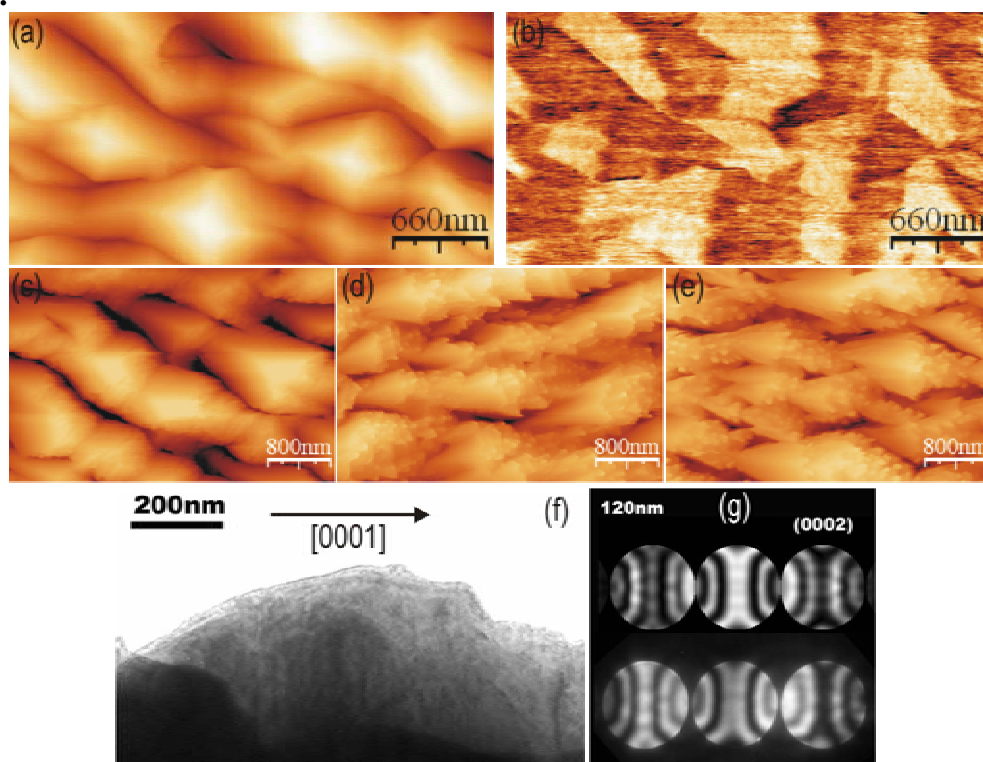


**Fig 1:** (a) SFM topography and (b) KPM images of a ZnO thin film sample grown along the [11$\bar{2}$0] direction. Topography images of the same sample etched (c) 30s in a 0.01M, (d) 5s in a 0.1M and (e) 10s in a 0.1M HCl solution. (f) TEM image of an etched pyramid and (g) CBED patterns (simulated and experimental) establishing the absolute polarity of the pyramid.

# SURFACE POTENTIAL MEASUREMENT OF PHOTOVOLTAIC MATERIALS AT THE NANOSCALE: IMAGING OF CHARGE TRANSFER IN NANOCRYSTALS, POLYMERS AND MULTI-CHROMOPHORIC ARRAYS.

Vincenzo Palermo,[a] Andrea Liscio,[a] Giovanna De Luca,[a] Matthijs B.J. Otten,[c] Alan E. Rowan,[c] Roeland J.M. Nolte,[c] Klaus Müllen,[d] Paolo Samorì [a,b]

[a] Istituto per la Sintesi Organica e la Fotoreattività - Consiglio Nazionale delle Ricerche Via Gobetti 101, 40129 Bologna, Italy.
[b] Nanochemistry Laboratory, Institut de Science et d'Ingénierie Supramoléculaires (ISIS), Université Louis Pasteur, 8, allée Gaspard Monge, F-67083 Strasbourg (France)
[c] Institute for Molecules and Materials Radboud University Nijmegen, Toernooiveld 1, 6525 ED, Nijmegen (The Netherlands)
[d] Max-Planck Institute for Polymer Research, Ackermannweg 10, D-55124 Mainz (Germany)

In this work, we describe the electrical characterization of nanocrystals, nanofibers and thin layers of polymeric and small self-assembling molecules (polythiophene, perylene, hexabenzocoronene) used in photovoltaic blends.

We characterized these materials with Kelvin Probe Force Microscopy (KPFM)[1], a powerful technique to map simultaneously in real-space and real-time the structure and electrical potential of a surface, as proven by detailed characterization of organic[2] and inorganic[3] materials. Maps of the electric potential of the photovoltaic blends were acquired with a lateral resolution <50 nm and a potential resolution <10 mV.

In particular, as electron acceptor (EA) in the photovoltaic blend we used multi-chromophoric wires composed by ultra-stiff isocyanodipeptides polymers (PIC) exposing semiconducting perylenes in the side chains (fig. 1). These materials can be mixed with an electron donor (ED) such as polythiophene to be used in solar cells.

Scanning Force Microscopy revealed that the two polymers form interpenetrated bundles, having a high density of contact points between the two different types of molecules. KPFM measurements on monolayer thick films showed the different electric potential between EA and ED molecules.

Upon illumination, excitons were generated and split at the interface: EA polymers got negatively charged while ED became positively charged, thus the voltage difference between the two materials increased, as monitored in real time with a true nanometric resolution (fig. 2). The results obtained were compared with measurements performed on 100 nm thick solar cells fabricated with the same materials, as well as with KPFM measurements performed on blends of monomeric perylene and polythiophene.

The correlation between charge generation and diffusion in thick and thin layers was discussed, allowing a greater understanding on the processes involved in organic photovoltaic devices on the nanoscale.

**References:**
[1]    V. Palermo, M. Palma, P. Samori, Advanced Materials, **18** (2006) 145.
[2]    V. Palermo, G. Ridolfi, A. M. Talarico, L. Favaretto, G. Barbarella, N. Camaioni, P. Samori, Advanced Functional Materials, **17** (2007) 472. M. Chiesa, L. Bürgi, J.-S. Kim, R. Shikler, R. H. Friend, H. Sirringhaus, Nano Lett., **5** (2005) 559.
[3]    S. Sadewasser, T. Glatzel, S. Schuler, S. Nishiwaki, R. Kaigawa, M. C. Lux-Steiner, Thin Solid Films, **431** (2003) 257.

**Figures:**
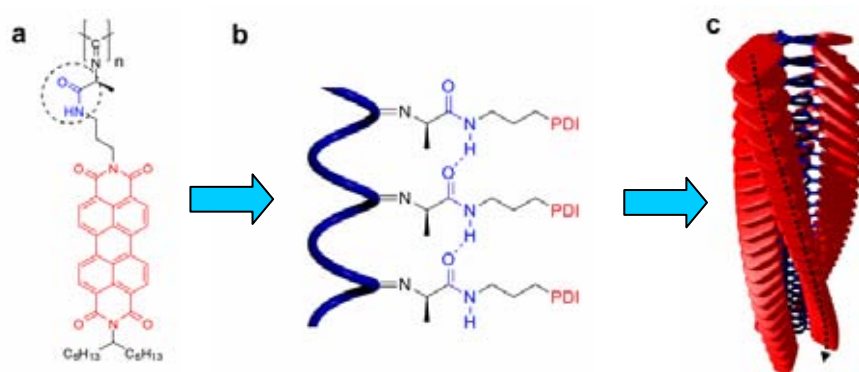


Fig.1 a) Chemical structure of a multi-chromophoric array based on poly(isocyanide) units functionalized with perylene (P-PDI); The amide unit responsible for the hydrogen bonding that stabilizes the helical structure is encircled. b) due to hydrogen bonding, the polymeric chain adopts a coiled structure. c) Cartoon showing the complete helical structure of the P-PDI. The dashed arrow indicates one of the four stacks of PDI units present along the central polyisocyanide backbone.
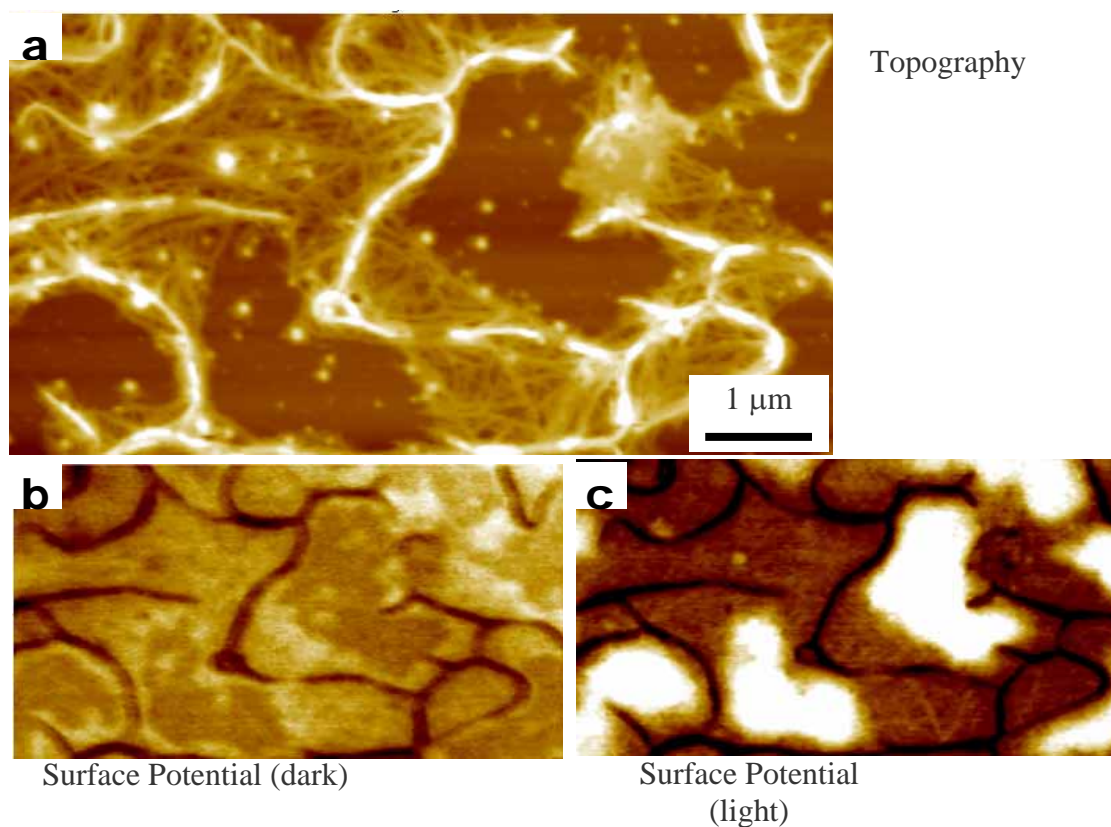


**Fig. 2** a) SFM topography image of an ultra-thin blend of P-PDI and polythiophene deposited on silicon. b) Surface potential image of the same area as in a), with no illumination and c) under white light (~60 mW cm$^{-2}$) illumination. Z range: a) 32 nm, b) 120 mV and c) 120 mV.

# Spin transport and structural characterization of carbon nanotubes

*[1]E. Pallecchi, [1]D. Preusche, [1]S. Schmidmeier, [2]H. van der Zant amd [1]Ch. Strunk.*
*[1]Institut fuer Experimentelle und Angewandte Physik, Universitaet Regensburg, Germany*
*[2]Kavli Institute, TU Delft, Netherlands*

*emiliano.pallecchi@physik.uni-r.de*

In spintronics devices, the electron spin is manipulated to produce the desired electrical response. This devices can be used to investigate new physical phenomena and are promising for applications. Carbon nanotubes are an ideal system to study spin transport and a good candidate for novel devices: depending on their chirality they can be metallic or semiconducting, they can show ballistic transport and sustain a very high current density. To be able to detect spin dependent transport in carbon nanotubes it is necessary to produce contacts which have both good electrical and magnetic properties.

We developed a scheme by using Palladium and Iron which ensures a uniform magnetization and transparent contacts. Contacts with different shapes will have different coercive fields allowing a crossover between the parallel and antiparallel configuration. The relative orientation of two contacts can be controlled by an external magnetic field applied parallel to the contacts.
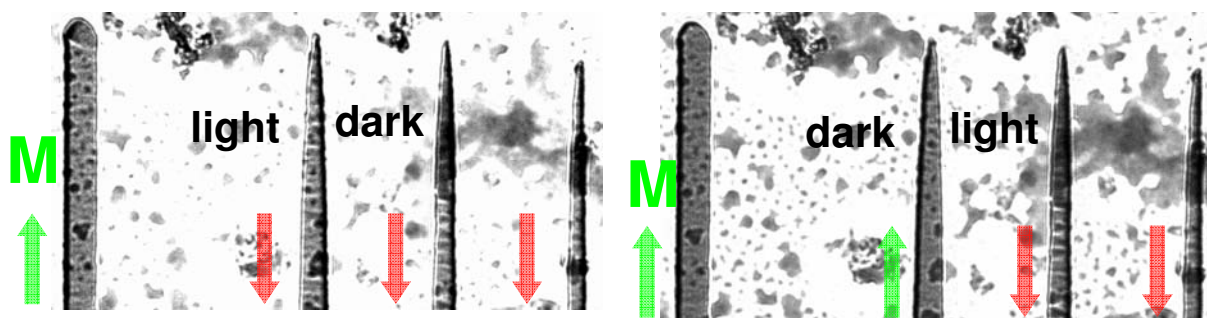


*Figure 1: When sweeping the external magnetic field to 7.3 mT, the broadest (rightmost) contact switches magnetisation M.*

*Figure 2: At 14.6 mT, the second (to the left) contact switches. This can be seen from the magnetic contrast changing from dark to light et vice versa.*

Lorentz microscopy is a powerful tool which allows to investigate the micromagnetic properties of the contact: in particular it is possible to study the dynamics of domain walls. We used this technique to characterize several contacts and we found a single domain switching behavior. Moreover we tuned the contact shape in order to maximize the difference in the switching fields.

We used selected area electron diffraction (SAED) on CVD-grown carbon nanotubes on a membrane: by comparing the measured data with a simulation we can distinguish between single wall, double wall and small bundles. For single and double wall carbon nanotubes we can also identify the chiral indices (n,m).

For this purpose, we succeeded to grow carbon nanotube partially laying on a membrane where slits where patterned: on these samples, we will combine magnetic characterization of the contacts, transport measurements and structural characterization of the nanotubes. This information will allow direct comparison theoretical predictions with measured data.

**R [h/e$^2$]**
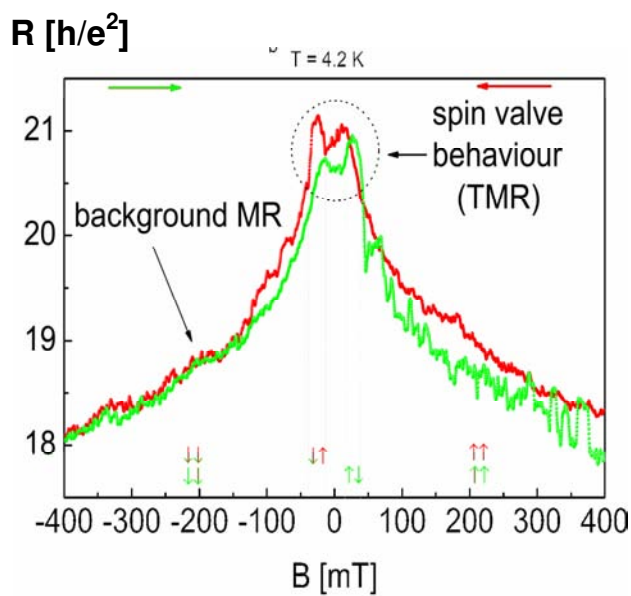


*Figure 3: TMR effect in a SWCNT sample with ferromagnetic contacts. The pairs of arrows indicate the two contacts' relative magnetization at the given external magnetic field.*
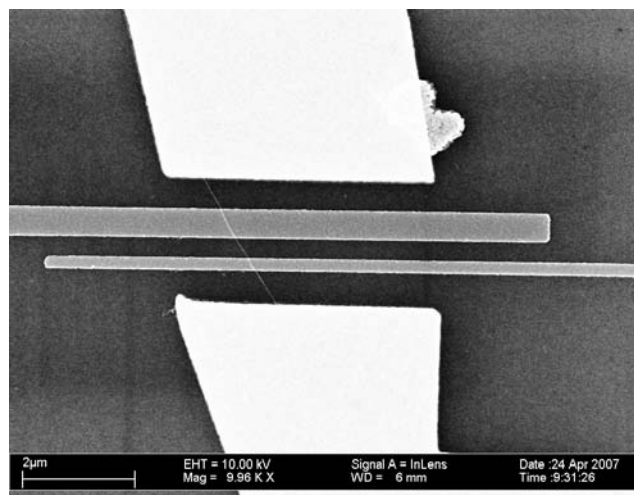


*Figure 4: SEM picture of a typical sample. The two inner contacts on the CNT are made of PdFe and the outer ones of Au.*

We performed low temperature measurements on both single and multiwall carbon nanotube samples with aluminium and silicon oxide backgate. The magnetoconductance shows hysteretic switching that we attribute to spin transport. We observed a gate-dependent spin valve effect of up to five percent.

Control experiments with one ferromagnetic and one gold contact has been carried out in order to rule out other effects.

# Ni NANOCONTACTS RUPTURES: DEPENDENCE ON STRETCHING DIRECTIONS

<u>*R. Paredes*</u> [a,b], *P. García-Mochales* [c], *P.A. Serena* [a], *S. Peláez* [a]

[a] *Instituto de Ciencia de Materiales de Madrid (ICMM), Consejo Superior de Investigaciones Científicas (CSIC), Cantoblanco, 28049 Madrid , Spain*

[b] *Centro de Física, Instituto Venezolano de Investigaciones Científicas (IVIC), Apartado  21827, Caracas 1020A, Venezuela*

[c] *Dpto Física de la Materia Condensada, Facultad de Ciencias C-III, Universidad Autónoma de Madrid (UAM), Cantoblanco, 28049 Madrid, Spain*

*Contact: rparedes@icmm.csic.es*

The comparison of experimental conductance histograms and results from computational simulations has allowed establishing a relation between the electronic and structural properties of Au and Al nanocontacts [1-3]. In the Ni case, there is in the literature a great variety of experimental results showing a noticeable diversity of behaviours of the conductance histogram H(G). Furthermore, theoretical approaches to the study of the breaking mechanism of Ni nanowires do not shed light on the problem since different results appear in the literature [4,5]. With the aim of helping to the interpretation of the experimental results as well as previous computational studies, we have performed simulations of rupture of nickel nanocontacts along different directions to analyse their structural evolution as well as the minimum cross section histograms.

Nanowires are simulated using Molecular Dynamics (MD) where the interatomic interactions are described within the framework of the embedded atom method (EAM). In our simulations we use state of the art EAM inter-atomic potentials able to fit bulk and surface properties [6]. We start with a parallelepiped ordered according to a fcc structure. After a relaxation process, two bilayers slabs at the top and bottom of the parallelepiped are frozen and separated at constant velocity of 2 m/s till the nanocontact breaks. The full determination of the atomic positions in the simulation allows us to study the evolution of the nanocontact geometry during its breakage and to determine the existence of preferred atomic configurations (as in previous Au and Al works [1-3]). The exact knowledge of the set of atomic coordinates also allows monitoring the evolution of the minimum cross-section $S_m$ of the nanocontact.

Minimum cross-section histograms $H(S_m)$ have been built accumulating $S_m$ traces during 300 ruptures. We analysed the histograms dependence on the stretching directions, temperature and original size of the samples. Six of these histograms are shown in Figure 1. All the histograms show marked peaks indicating the presence of favourable configurations during the last stages of the breaking process. However, the relative height of these peaks differs, indicating that preferred structures where atoms accommodate are different. The main conclusion of our study is that the expected conductance histogram strongly depends on the nanocontact stretching direction.

Additionally we performed a statistical analysis of the presence of monomers and dimmers during last steps of the rupture. When the stretching direction is the [111] the system mainly evolves trough a sequence monomer-dimmer towards the rupture. On the other hand, for the [100] and [110] stretching directions, the system directly evolves from more complex structures, than monomers and dimmers, to the final rupture. Finally, we found that for all the stretching directions and temperatures the peaks around $S_m = 0.5$, 1.0 and 1.5 are mainly originated from dimmers, monomers + dimmers and complex structures respectively (See Figure 2.). Some anomalies are observed for the [100] stretching direction at 4K.

**References.**
[1] E. Medina *et al.*, Phys. Rev. Lett. **91,** 026802 (2003).

[2] A. Hasmy. E. Medina, and P. Serena, Phys. Rev. Lett. **86,** 5574 (2001).

[3] A. Hasmy et al., Phys. Rev. B **72**, 245405 (2005).

[4] P. García-Mochales et al., Appl. Phys. A **81**, 1545 (2005).

[5] F. Pauly et al., Phys. Rev. B **74**, 235106 (2006).

[6] Y. Mishin *et al*. Phys. Rev. B **59**, 3393 (1999).
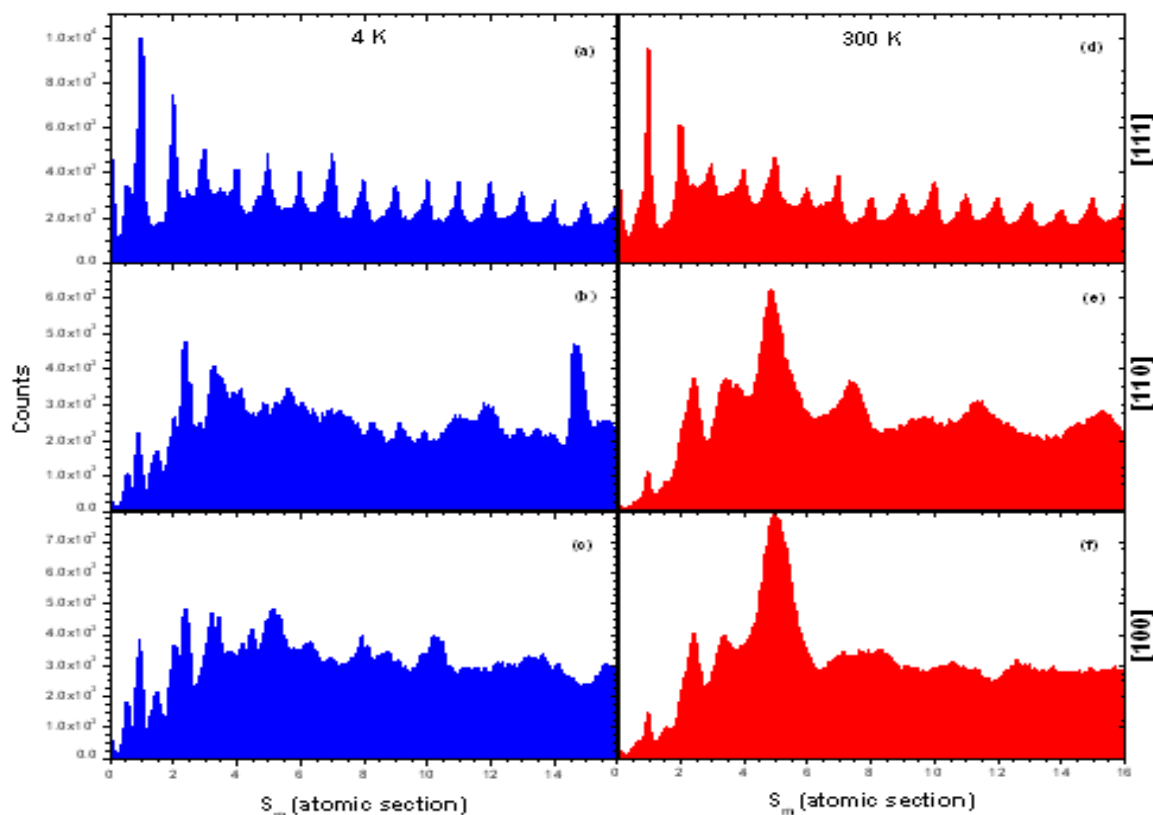
**Figure 1**: Minimum cross-section $S_m$ histograms of Ni nanocontacts at T=4 K (a,b,c) and 300K (d,e,f) evolving under stretching along the [111] (a,d), [110] (b,e), and [111] (c,f) orientations. Histograms have been built with 300 independent ruptures from the initial released parallelepiped of 390 (a,d), 420 (b,e) and 375 atoms (c,f).
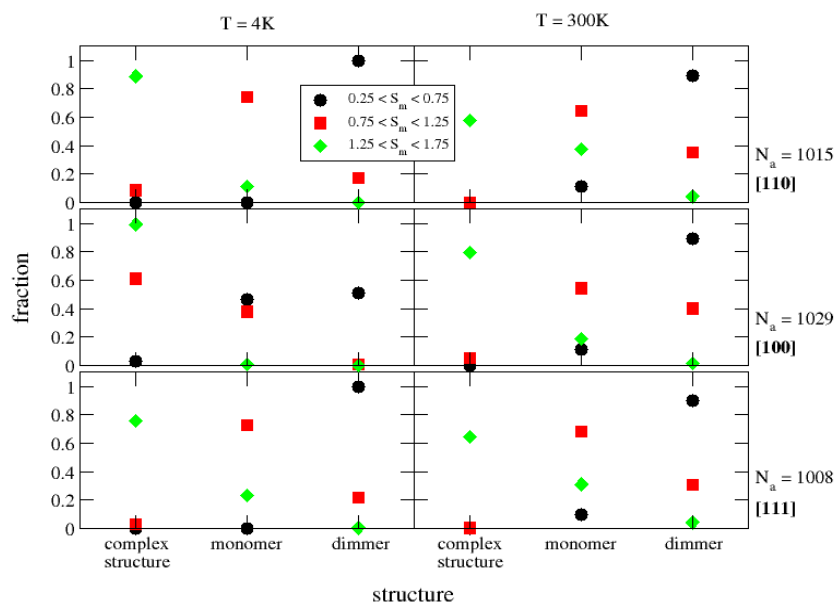


**Figure 2:** Fraction of monomers, dimmers and other complex structures for each one of the histograms peaks in the interval $0.25 < S_m < 1.75$ for different temperatures and stretching directions.

# FORMATION OF SiOX NANOWIRE BUNCHES ON Si WAFER BY USING SiNX DIFFUSION BARRIER LAYER

Nae-Man Park, Chel-Jong Choi, and Tae-Youb Kim
*IT Convergence & Components Laboratory, Electronics and telecommunications Research Institute, Daejeon 305-700, Korea*
*nmpark@etri.re.kr*

$SiO_x$ has been extensively studied because it may act as a waveguide and highly sensitive sensor [1]. It also show a stable visible light emission [2], which might have potential applications in, for example, integrated optical devices and high-resolution optical heads for scanning near-field optical microscopes [3]. Therefore, $SiO_x$ nanowire (NW) growth represents a topic of considerable interest. Sun et al. obtained a cherrylike $SiO_x$ NW structure [4] and Pan et al. reported on five different $SiO_x$ NW structures [5]. Other morphological features such as nanosprings, treelike, or tadpolelike NWs have also been reported [6-8]. These interesting structures demonstrate the complexity of $SiO_x$ growth. One wire may split up while many NWs may branch together forming several NW bundles. These features are unique to $SiO_x$, and are seldom observed in the growth of other nanomaterials. Therefore, it is of great fundamental interest and relevance to applications to examine the structure of $SiO_x$ NWs grown under various conditions. Until now, some groups have used a Co or Ni metal in order to grow $SiO_x$ NW bunch [1], and other groups controlled the atomic ratio of Si to O [7]. In this work, we report on the fabrication of $SiO_x$ NW bunch using an Au coated $SiN_x$ film grown on a Si substrate to control the initial growth step of $SiO_x$ NW. $SiO_x$ NW bunches were fabricated on a 50-nm $SiN_x$ film with Au catalytic metal in the presence of Ar flow of 50 sccm at 1150 . The resulting samples were characterized by field-emission scanning electron microscopy, transmission electron microscopy, and energy dispersive x-ray spectroscopy. Figure 1 shows typical morphologies of the SiOx NW bunches on the SiNx film, showing flowerlike (a), featherlike (b), and jellylike (c) NW bunches. The structures are randomly aligned and distributed on the same film. The cross-sectional TEM was examined and the results are presented in Figure 2. As shown in Figure 2(a), there is no Au metal between the SiNx film and the Si substrate. Figure 2(b) clearly shows that a NW is amorphous.

A $SiN_x$ film serves as a barrier to the diffusion of Si atoms from the Si substrate to the catalytic metal and a Si substrate itself only as a Si source material. Using this process, we could temporally control the initial growth step of $SiO_x$ NWs and easily observe the morphology of NW bunches.

Until now, the desirable morphology of SiOx NW bunch has been out of control. However, this work suggests a possible method for controlling the morphology of NW by employing a catalytic metal and a SiNx film as a barrier to the diffusion of the Si atom from Si substrate and temporally adjusting the initial growth step of SiOx NW.

**References:**

[1] X. Cai, A. Djurisic, and H. Xie, J. Appl. Phys. 98 (2005) 74313.

[2] D. Yu, Q. Hang, Y. Ding, H. Zhang, Z. Bai, J. Wang, Y. Zou, W. Qian, G. Xiong, and S. Feng, Appl. Phys. Lett. 73 (1998) 3076.

[3] J. Wang, C. Zhan, and F. Li, Solid State Commun. 125 (2003) 629.

[4] S. Sun, G. Meng, M. Zhang, Y. Tian, T. Xie, and L. Zhang, Solid State Commun. 128 (2003) 287.

[5] Z. Pan, Z. Dai, C. Ma, and Z. Wang, J. Am. Chem. Soc. 124 (2002) 1817.

[6] Y. Zhu, W. Hsu, M. Terrones, N. Grobert, W. Hu, J. Hare, H. Kroto, and D. Walton, Chem. Mater. 11 (1999) 2709.

[7] H. Zhang, C. Wang, E. Buck, and L. Wang, Nano Lett. 3 (2003) 577.

[8] Y. Chen, J. Li, Y. Han, and J. Dai, J. Mater. Sci. Lett. 21 (2002) 175.

**Figures:**
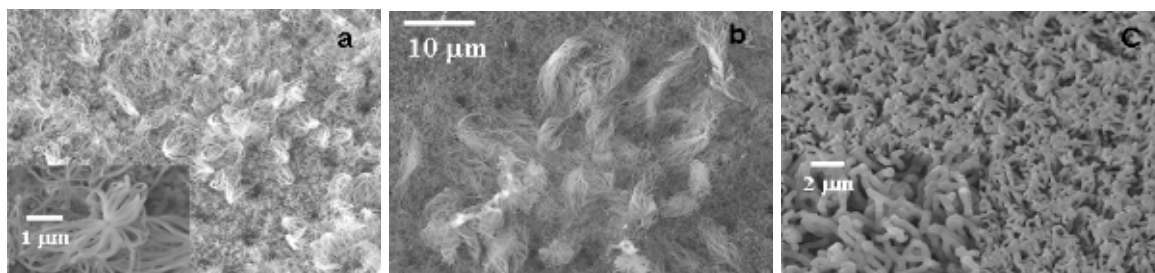


Fig. 1. SEM images of various morphologies of $SiO_x$ NW bunches; (a) flowerlike, (b) featherlike, and (c) jellylike bunch.
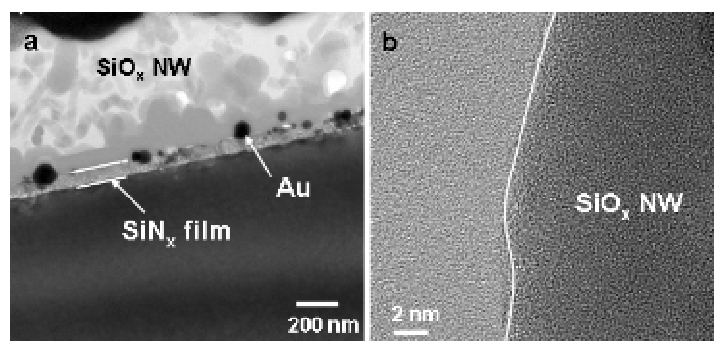


Fig. 2. TEM images of (a) cross section of the sample and (b) high-resolution of a single $SiO_x$ NW.

# FABRICATION OF Al/AlO OPTICALLY ABSORBING FILMS USING A FILTERED CATHODIC VACUUM ARC.

*N. Abaffy, J. G. Partridge and D. G. McCulloch*
*Applied Physics, RMIT University, 124 LaTrobe Street, Melbourne, Australia*
*jim.partridge@rmit.edu.au*

A Filtered Cathodic Vacuum Arc (FCVA) deposition system [1] has been used to produce multilayer thin-films of aluminium and aluminium oxide for use as optically absorbing coatings (also known as 'black mirrors') [2]. Characterisation of these layers has been performed using ellipsometry, X-ray Photoelectron Spectroscopy (XPS), Atomic Force Microscopy (AFM) and electrical conductivity measurements.

For the intended application, a single aluminium layer of 6-8 nm thickness (accounting for 3-4 nm surface oxide thickness) was required to be sandwiched between aluminium oxide layers of ~120 nm and ~70 nm thickness. These multi-layers are supported on silicon substrates. The surface roughness and continuity of the aluminium and aluminium oxide films are critical parameters in the design of the coatings and the focus of our study was to minimise roughness in these films and in particular, to minimise island type growth in the thin aluminium films.

The FCVA system used for these experiments was supplied by Nanofilm Technologies International Pte. Ltd. The system is equipped with a double-bend filter which prevents deposition of macro-particles and a substrate holder which was connected to an electrical feed-through for application of substrate bias. The effect of the substrate bias, process gas mix and ultimate film thickness on the RMS roughness of the aluminium and aluminium oxide films was investigated using AFM. It was found that with an applied pulsed substrate bias of -500V, aluminium films of 6-8 nm were produced with an average RMS roughness of less than 0.2 nm (see Figure 1).

Ellipsometry and XPS were used to verify the optical constants of our AlO films and these measurements allowed us to select Ar/O gas flow-rates which produced stoichiometric $Al_2O_3$.

Electrical conductivity measurements showed that Al films of 6-8 nm could be produced with resistivities approximately one order of magnitude larger than the bulk. The oxidation of these films self-limits (with a final thickness at room temp of ~3 nm) and therefore FCVA deposition of aluminium/aluminium oxide stacked layers with prescribed thicknesses is possible. Several aluminium/aluminium oxide multilayers have been produced with various layer thicknesses and their simulated and experimental absorption characteristics have been compared. In Figure 2, simulated and experimentally obtained optical responses of $Al_2O_3$-Al-$Al_2O_3$ trilayer black mirrors are shown. (The optical CAD package Filmstar supplied by FTG software was used for the simulations).

**References:**

[1] J. Mouchart, Applied Optics, **16** (1977) 3237.
[2] I.I. Aksenov, V.A. Belous, V.G. Padalka and V.M. Khoroshikh, Fiz. Plazmy, **4** (1978) 758.

**Figures:**
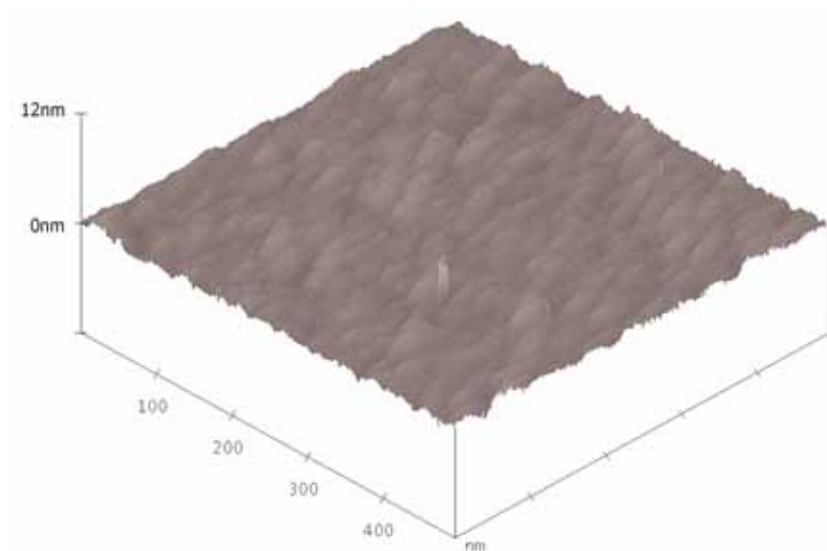


**Figure 1.** An AFM image of a FCVA deposited 7.0nm thick Al film supported on a Si substrate and with RMS roughness 0.35nm.
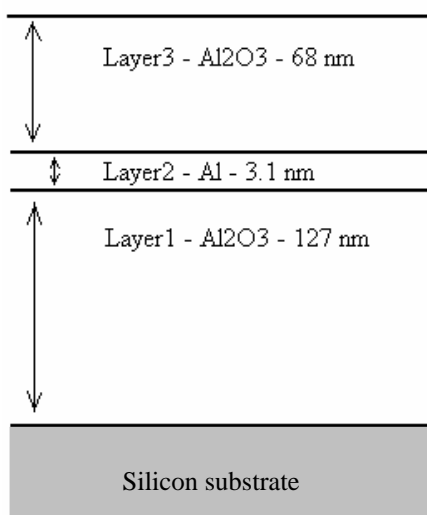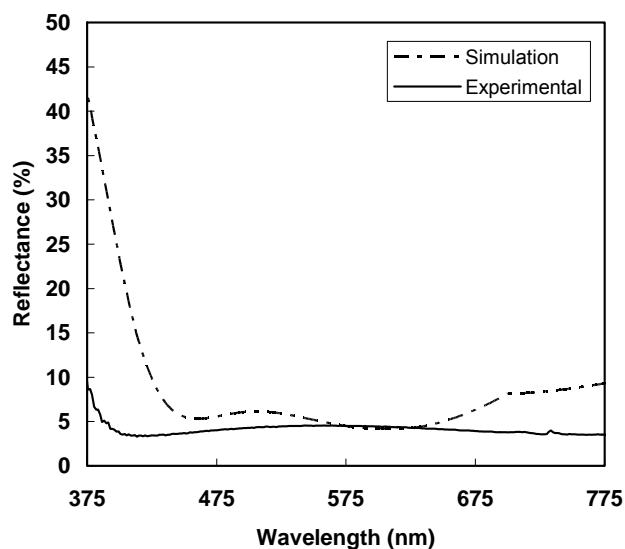


| (a) | (b) |

**Figure 1.** (a) Schematic showing an $Al_2O_3$-Al-$Al_2O_3$ black mirror formed on silicon and (b) its simulated and experimentally obtained reflection characteristics.

# A QUANTUM-THEORETICAL STUDY OF CONFORMATIONAL BASIS FOR SINGLE-MOLECULE SWITCHING PHENOMENA: THE DYNAMICS OF CENTRAL PHENYLENE RING TORSIONAL MOTION IN PHENYLENE ETHYNYLENE OLIGOMERS.

*Ljupco Pejov[a], Manuela La Rosa[b], Ljupco Kocarev[c]*
*[a]Institute of Chemistry, Faculty of Natural Sciences and Mathematics,*
*Sts. Cyril and Methodius University, POB 162, 1000 Skopje, Macedonia*
*[b]PST Group - M6, STMicroelectronics, Stradale Primosole 50, 95121 Catania, Italy*
*[c]Macedonian Academy of Sciences and Arts, bul. Krste Misirkov 2, P.O.Box 428*
*1000 Skopje , Republic of Macedonia*
*ljupcop@iunona.pmf.ukim.edu.mk*

The dynamics of intramolecular torsional motion of central phenylene ring in a series of phenylene ethynylene oligomer derivatives (Fig. 1) was investigated. On the basis of calculated hindered rotational potentials corresponding to this motion, the torsional energy levels were obtained by solving the torsional Schrödinger equation (Fig. 2).

Subsequently, the torsional correlation time and transition probability was computed within the Bloembergen-Purcell-Pound (BPP) formalism, considering both the classical and quantum mechanical tunneling contributions to the intramolecular rotation. The results were interpreted in the context of molecular conductivity switching behavior of the considered series of compounds.

Also some other parameters relevant to molecular admittance were calculated, such as the HOMO-LUMO energy difference (HLG) and the spatial extent of the frontier molecular orbitals. Classical electrostatic arguments were applied to understand the physical basis of the conformational stability differences in the studied compounds.

It was found that although halogenation of the central phenylene ring may be basically used for fine-tuning of molecular conduction behavior, the time scale of the "on"-"off" states conformational switching is not substantially changed. The tunneling contributions to the torsional correlation time were found to be of minor importance in this context, and this quantity may be quite correctly estimated with the classical BPP approach. The perhalogenation of the central phenylene ring does not affect the conductive ("on") and non-conductive ("off") states of the molecular wires in a qualitative sense, *i.e.* the planar conformations correspond to the conductive, while perpendicular ones to non-conductive status. HLG values as well as the spatial extents of the frontier molecular orbitals are affected by the halogenation of the central phenylene ring, and it is thus possible to fine-tune the single-molecule admittance properties in the phenylene-ethynylene oligomer derivatives. The central phenylene ring torsional barrier heights are modulated by the halogenation – the computed trends may be rationalized by classical electrostatic arguments. Besides the possibilities for fine-tuning of the molecular admittance properties by halogenation of the central phenylene ring, the torsional correlation time and the corresponding transition probability computed by the classical or quantum BBP approach changes by not more than an order of magnitude. The quantum tunneling contributions to the transition probability account for about 2 % of the classical values. Thus, it is the incoherent classical jump-over-the-barrier motion that governs the torsional dynamics in the studied systems.

**References:**

[1] Lj. Pejov, M. La Rosa, Lj. Kocarev, Chem. Phys., in press.

**Figures:**
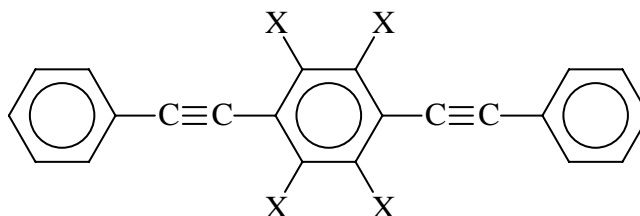


Fig. 1. A schematic presentation of the basic phenylene ethynylene oligomer and its substituted derivatives considered in the present study; X ∈ {H, F, Cl, Br, I}.
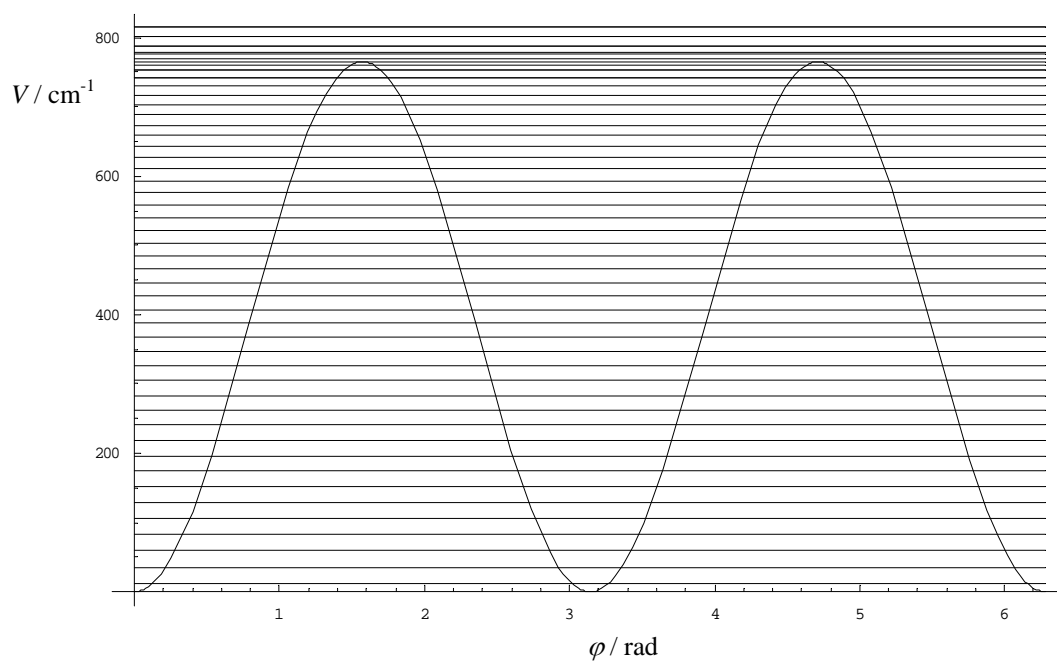


Fig. 2. The energy levels of the intramolecular rotator for the nonsubstituted basic compound obtained by the FGH method.

# PHOTOELECTRICAL PROPERTIES OF THIN FILMS COMPOSED BY 3D ASSEMBLIES OF TIN(II) SELENIDE QUANTUM DOTS

*Biljana Pejova[a], Atanas Tanuševski[b], Ivan Grozdanov[a]*
*[a]Institute of Chemistry, Faculty of Natural Sciences and Mathematics,*
*[b]Institute of Physics, Faculty of Natural Sciences and Mathematics,*
*Sts. Cyril and Methodius University, POB 162, 1000 Skopje, Macedonia*
*biljana@iunona.pmf.ukim.edu.mk*

Three-dimensional arrays of close packed tin(II) selenide quantum dots (QDs) were synthesized in thin film form by the chemical deposition method which has recently been developed by our group [1]. The average crystal radius in the chemically synthesized SnSe QD thin films, calculated on the basis of Debye-Scherrer approach, was 14.8 nm and 23.3 nm in the case of unannealed and annealed nanostructured films correspondingly. Residual lattice strain was found to be negligible in both cases.

The charge-carrier transport properties of 3D QD array thin films were studied both in the dark and under conditions when internal photoelectric effect is manifested in the nanostructured material. To characterize the photophysics of quantum-confined nanocrystals synthesized in thin film form, stationary and time-resolved experimental studies were performed.

On the basis of thermoelectrical measurements, the charge-carrier transport through the films was found to occur predominantly by the thermionic emission mechanism in the temperature range from 300 to 585 K. The corresponding crystal boundary barrier height in the case of as-deposited films calculated on the basis of extended model of Seto [2,3] was found to be 107.5 meV, with the trap states causing a partial charge-carrier depletion of the nanocrystals being situated below the Fermi level. By combined reasoning based on Seto's-type model equations and the X-ray diffraction data it was concluded that the barrier height decreased by 50 meV upon post-deposition thermal annealing treatment. Thermal band gap energy calculated on the basis of temperature dependence of dark conductivity in the region where intrinsic conduction mechanism is activated was found to be 0.90 eV. This value is somewhat lower than the one calculated from optical spectroscopic data (1.10 eV [1]). A physical basis for these differences was proposed.

The spectral dependence of stationary photoconductivity of the nanostructured films (*i.e.* the photoconductivity spectral response curve) was measured by the constant field method. By a careful analysis of this dependence, it was concluded that both the internal photoelectric effect and the crystal boundary barrier height modulation upon illumination contribute to the photoresponse. Surface and bulk charge-carrier recombination velocities were found to be comparable. Accounting for the direct proportionality between absorption coefficient and the non-equilibrium conductivity in the low absorption regime, on the basis of Fermi's golden rule for interband electronic transitions within the parabolic approximation for the dispersion relation, the indirect and direct band gap energy values of 1.23 and 1.54 eV were calculated (Fig. 1). Both values are in excellent agreement with those derived from the optical absorption spectroscopy data [1].

Time-resolved experiments were performed to study the transient photoconductivity in the nanocrystalline films. It was found that the non-equlilibrium conductivity relaxes exponentially (*i.e.* follows a linear kinetics mechanism), with a time constant of 1.78 ms. Assuming the predominance of the Schockley-Reed-Hall mechanism for charge-carrier

recombination via trap states in the case of the studied indirect band gap material, the measured time constant corresponds to average lifetime of minority charge carriers (electrons in this case).

Lux-ampere characteristics of the films further support the linear photoconductivity relaxation mechanism, contrary to what has usually been found in the case of amorphous materials.

**References:**

[1] B. Pejova, I. Grozdanov, Thin Solid Films, **?????** (2007) page???.
[2] J. Y. W. Seto, J. Appl. Phys., **46** (1975) 5247.
[3] D. S. Ginger, N. C. Greenham, J. Appl. Phys., **87** (2000) 1361.

**Figures:**



a)                                                            b)
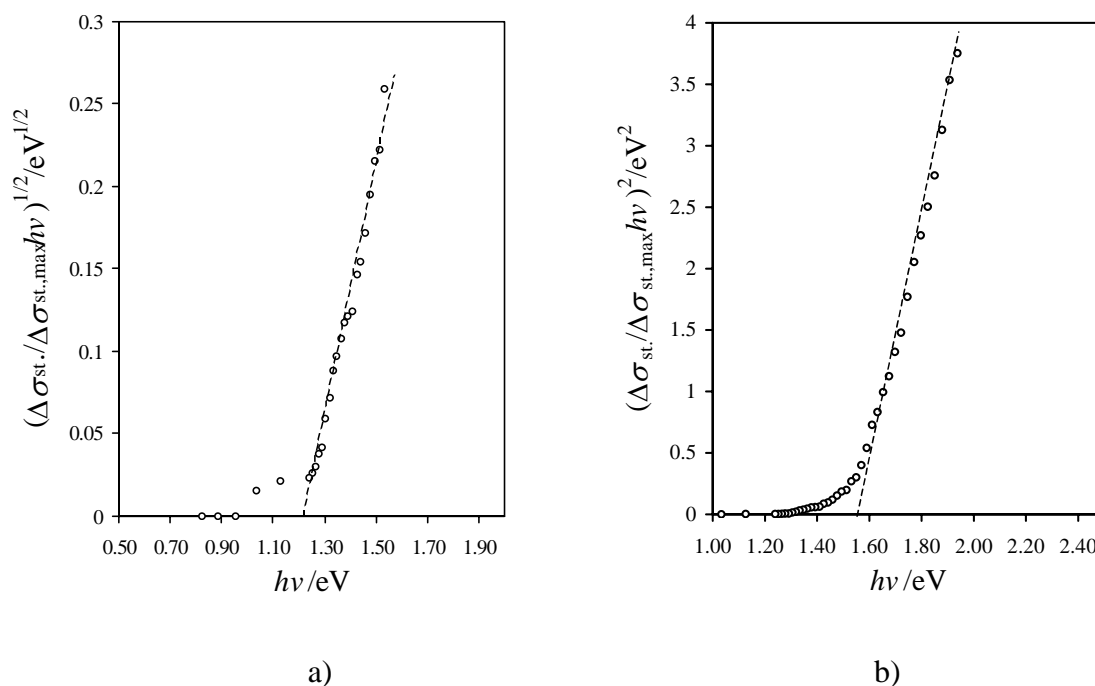
Fig. 1. Determination of the indirect (a) and direct (b) band gap energies for a nanocrystalline tin(II) selenide film sample on the basis of its photoconductivity spectrum using the parabolic approximation for the dispersion relation.

# ROUGNESS AND FRACTAL DIMENSION MEASUREMENTS IN THE NANOSCALE BY SFM.

*Beatriz Pérez-García, Jaime Colchero*

*Departamento de Física, Edificio CIOyN, Campus de Espinardo30100, Murcia, España*

*beatrizp@um.es*

SFM allows an simultaneously measure of the most important tribological properties: topography, normal force and lateral force. Related to the precise description of topography, the surface roughness is a fundamental quantity that determines the tribological behavior [1,2] of surfaces, even though the precise way in which this occurs is still under discussion. An important issue in this context from the experimental as well as from the theoretical point of view is the question: down to which scale is surface roughness important, and which scale is the most relevant one for tribology. In this work, we study how surface roughness can be correctly measured from the several micrometer scale down to the nanometer scale with Scanning Force Microscopy (SFM) techniques.

SFM is used to characterize the roughness at different length scales with a simple model for the surface roughness of a statistically rough surface by means of the analisis of power spectral density curves obtained from SFM topographical images. This issue has been addressed previosly in the literature[3,4], but we believe that but some important aspects have not yet been discussed [5]. Since data analysis is based on the evaluation of log-log plots it is important to acquired a large number of image points in order to be able to cover several length scales. We believe that at least 3 order of magnitudes should be covered which implies a at least one million data points for an image. A sufficiently high number of image points not only allows to cover a larger length scale of measured surface roughness, in addition the statistical significance of the measured surface roughness increases.

A fundamental issue is related to the perfect acquisition of topographic data. Roughness analysis requires very high quality topographic data. In this context it is fundamental to note that successful data processing and data interpretation may be severely limited by a series of technical issues. Since each data point should be "correct" scanning speed and settling time have to be selected so that the feedback loop is capable of adjusting the correct topographic height at each image point. A fundamental first step for roughness analysis is the acquisition of a topography image free of any noise. In particular, spikes due to lack of response of the feedback loop or oscillation of the feedback system, often present in SFM images, will severely degrade the quality of SFM data. Optimization of feedback parameters (fast enough but no oscillation) and scanning speed was crucial. In addition, thermal drift and instrumental noise will additionally degrade data analyis.

In this work we will present and discuss nanoscale surface roughness of differents samples hard samples (steel, sapphire and hard metal balls) as well as soft samples like polymers (P3OT poly-3-octylthiphene).

**References:**

[1]Persson BNJ, Albohr O,Tartaglino U,Volokitin AI and Tosatti E; Journal of Physics-Condensed Matter 17 (1) 2005.

[2] Zappone B, Rosenberg KJ, Israelachvili J; Tribology Letters 26 (3), 2007

[3] Gomez-Rodríguez JM, Naro AM, Vazquez L, Salvarezza RC, Vara JM, Arvia AJ, Journal of Physical Chemistry 96 (1) 1992.

[4] Duparré A, Ferre-Borull J, Gliech S, Notni G, Steinert J and Benett JM, Applied Optics 41 (1) 2002.

[5] Perez García B and Colchero J, to be published.

**Figures:**
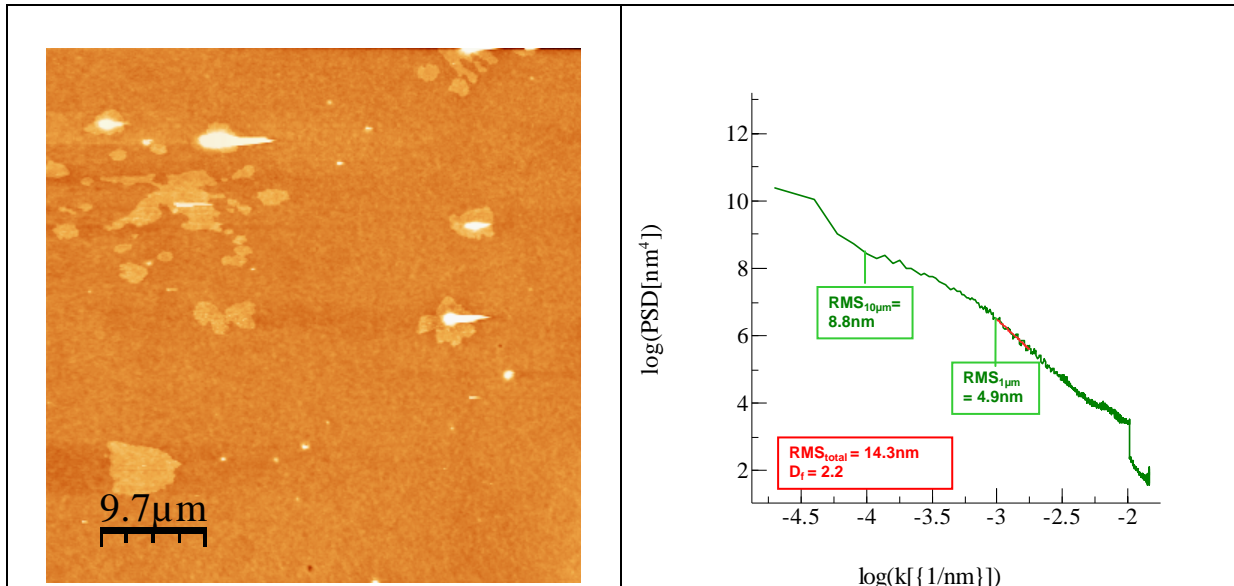


Fig 1. Topography image of P3OT (left) and its power spectral density curve(right). RMS at different scales and fractal dimension ($D_f$) are shown.
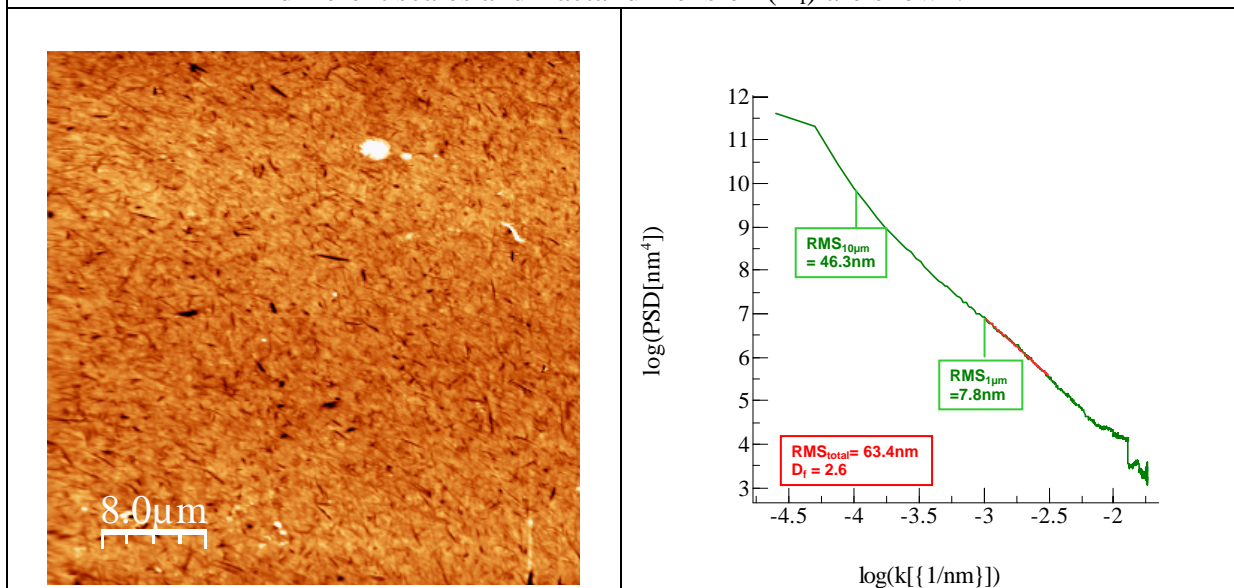


Fig 2. Topography image of Saphire ball surface (left) and its power spectral density curve (right). RMS at different scales and fractal dimension ($D_f$) are shown.

# OPTIMIZATION OF THE PROCESS TEMPERATURE FOR THE FABRICATION OF SELF-ASSEMBLED COLLOIDAL CRYSTALS

N. Pérez, M. Ellman, A. Rodriguez, S.M. Olaizola

CEIT and Tecnun (University of Navarra) Manuel de Lardizábal 15, 20018 San Sebastián, Spain

*nperez@ceit.es*

The catalytic, magnetic, mechanic, thermal and optical properties of some materials can be tailored by nanostructuring them. State-of-the-art nanostructuring techniques include micromachining [1] and nanolithography [2], which are either slow or expensive. For this reason, a lot of effort is being devoted to the research in low cost and long scale fabrication methods as self-assembly [3] and laser interference lithography [4].

In this work, the self-assembly of polystyrene spheres to be used as templates for the nanostructuring of materials is studied. In particular, a study of the influence of the process temperature on the final structure of the colloidal crystal is carried out. Optical reflectance measurements in addition to SEM and FEG-SEM micrographs are used in order to characterize the quality of the fabricated structures.

EXPERIMENTAL

Polystyrene samples with different process temperatures (between 30 ºC and 60 ºC) have been fabricated. A monodisperse solution of 419 nm colloidal polystyrene beads with a concentration of 1% is used for the deposition. The chosen method is the vertical deposition technique [5] with a substrate inclination of 10 º.

RESULTS AND DISCUSSION

An inspection of the surface of the samples shows that the superficial quality of the structure is enhanced by increasing the process temperature up to 50 ºC, being the characteristics of the 50 ºC and 60 ºC fabricated samples very similar. The surface roughness is minimal for the samples fabricated at 50 ºC. The presence of bcc areas and amorphous zones in the samples is also improved with increasing process temperature, up to 50 ºC. Although none of the conditions tested in this work gives rise to defectless surfaces, FEG-SEM micrographs of the cracks in the 50 ºC fabricated samples show that the order is conserved in subsequent layers, as shown in Figure 1. For this reason, reflectance measurements are performed in order to check the three-dimensional order of the samples.

The effective refractive index of the structure, $n_{eff}$, is defined as $n_{eff}^2 = \varepsilon_a \cdot f + \varepsilon_b \cdot (1 - f)$, where $\varepsilon_a$ and $\varepsilon_b$ are the dielectric constants of the material (polystyrene) and the voids, respectively, and f is the filling factor of the crystal. This parameter provides information about the quality of the structure, taking into account that if the fabricated crystals were perfectly packaged in an fcc structure, their $n_{eff}$ would be approximately 1.41 ( $f = 0.74$ ). Using the Bragg-Snell law [6], which relates the position of the reflectance peaks to the effective refractive index and the angle of incidence of the light on the sample, $\theta$,:

$$\lambda = 2D\sqrt{n_{eff}^2 - \sin^2 \theta} \tag{1}$$

where $D = d\sqrt{\dfrac{2}{3}}$, and d is the diameter of the spheres, the $n_{eff}$ of the fabricated samples can be calculated using reflectance measurements.

Calculating the $n_{eff}$ with the theoretical values of the reflectance peaks obtained from simulation of the structure [7], a small dependence on the angle of incidence is observed. The most approximate value to the theoretical is obtained with an angle of incidence of 45º.

In Figure 2, the average values for the $n_{eff}$ are shown, in comparison with the theoretical value calculated from the simulations. As can be seen, this parameter becomes closer to its theoretical value with increasing temperature, which implies the improvement of the fabricated structures, in agreement with the surface analysis previously carried out.

CONCLUSION

In this work, the dependence of the process temperature on the quality of self-assembled colloidal structures has been studied. In addition, it has been shown that the surface roughness of the structures, which is minimal at 50 ºC, has a direct dependence on the effective refractive index. This result provides a way of structurally characterize the quality of the colloidal crystals via reflectance measurements.

REFERENCES

[1] J. G. Fleming and S. -Y. Lin, Opt. Lett. 24 (1999) 49

[2] T. W. Odom, V. R. Thalladi, J. C. Love, and G. M. Whitesides, J. Am. Chem. Soc. 124 (2002) 12112

[3] P. N. Barlett, P. R. Birkin and M. A. Ghanem, Chem. Commun. (2000) 1671

[4] S. Shojia, R. P. Zaccaria, H.-B. Suna and S. Kawata, Optics Express 14 (2006) 2309

[5] P. Jiang, J. F. Bertone, K. S. Hwang, and V. L. Colvin, Chem. Mater. 11 (1999) 2132

[6] H. Míguez, A. Blanco, F. Meseguer, C. López, H.M. Yates, M.E. Pemble, V. Fornés and A. Mifsud, Phys. Rev. B 59 (1999) 1563

[7] N. Pérez, A. Hüls, D. Puente, W. González-Viñas, E. Castaño and S.M. Olaizola, Accepted 4 December 2006 for Sensors and Actuators B: Chemical. (doi:10.1016/j.snb.2006.10.057)

FIGURES
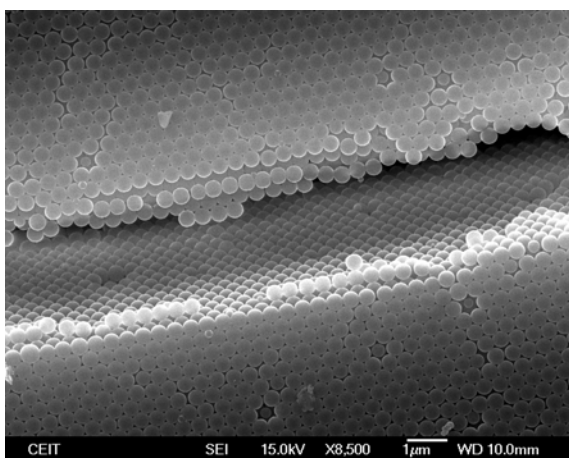


Figure 1. FEG-SEM micrograph of the insight of a crack in a 50 ºC fabricated sample
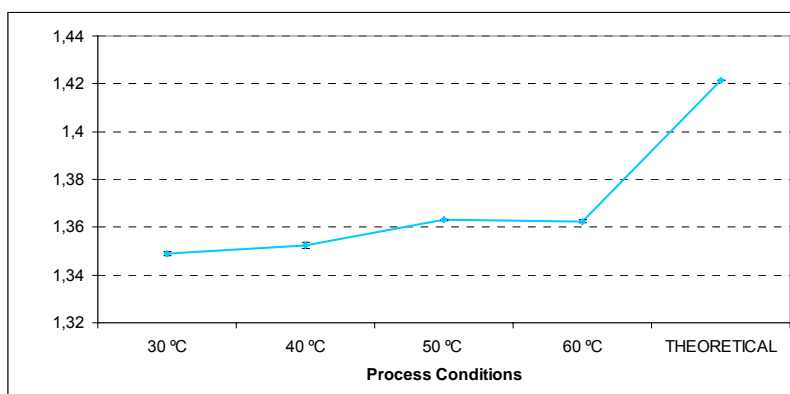


Figure 2. Effective refractive index with respect to the process temperature

# CATHODOLUMINESCENCE EMISSION FROM CARBON NANOTUBES AND ITS SENSITIVITY WITH CONTAMINANT CONCENTRATION

V. Pingitore[*], M. Barberio; P. Barone; A. Bonanno; M. Camarca; A. Oliva; F. Xu.

Laboratorio IIS, Università della Calabria and INFN – gruppo collegato di Cosenza –
87036 Arcavacata di Rende, Cosenza, Italy

Carbon nanotubes (CNTs) have attracted many attentions for their electrical and optical properties. There are two kinds of carbon nanotubes single walled carbon nanotubes (SWNT) and multi walled carbon nanotubes (MWCNT). Multiwalled nanotubes (MWNT) are more complex systems composed of several (typically 10 to 20) concentric graphite shells[1-2]. In principle the shell of a MWNT can have different chiralities[3]. A major obstacle to study the CNTs has been the diversity of tube diameters, chiral angles, and aggregation states in nanotubes sample obtained from the various preparation methods. Theory predicts, to first order, that two-thirds of SWNTs on a mat are semiconductors. Semiconducting nanotubes have a band gap in momentum space with a diameter/chirality dependent energy. In a direct band gap semiconductor the probability of light emission from electron-hole recombination is high. But it was only recently that SWNTs were found to emit light from interband recombination of electron-hole pair[4-5]. O' Connell et al. in 2002[4] find that photoluminescence intensity is reduced by aggregation of the isolated nanotubes, they presume that the presence of metallic nanotubes within a bundle quenches electronic excitation on an adjacent semiconducting tube, preventing its luminescence.

Upon illumination, infrared photoluminescence (PL) was detected from the ensemble of isolated nanotubes in solution[6-7] and ensembles of bare SWNTs suspended in air also emit band gap PL[6-7]. The PL spectrum of an individual SWNT in air at room temperature has a single asymmetric peak while ensemble measurements are a superposition of many PL peaks from many different specie.

Theory predicts that the electronic structure of a SWNT depends on the diameter and on the chiral angle describing its construction from a graphene sheet[8]. Quasi one-dimensionality causes the electronic density of state to have a series of sharp van Hove maxima at energies depending mainly on tube diameter. For the semiconducting tubes

---

[*] Corresponding author: pingitore@fis.unical.it (V. Pingitore)

the DOS is therefore sharply peaked at the band gap. Theoretically, nanotubes should show strong band gap photoluminescence.

Spectrofluorimetric measurements[4] on SWNTs have revealed distinct electronic and emission transitions for different semiconducting nanotube species. By combining these results with resonance Raman data, each optical transition has been mapped to a specific (n, m) nanotube structure. Optical spectroscopy can be used to determine the detailed composition of bulk CNT samples.

Luminescence emission induced both by heating (TL) and by ion bombardment (IL) has demonstrated that MWNT carbon nanotubes exhibit an appreciable luminescence signal and, moreover, that the presence of several peaks are common in spectra obtained by different techniques. Such peaks are originated by intrinsic defects in the crystal lattice[9].

In this work luminescence emission induced by electron bombardment (Cathodoluminescence, CL) has been performed on bundles of single walled (SWCNT) and multi walled (MWCNT) carbon nanotube. We compare the CL spectra with the spectra obtained by ion (IL) and thermo-luminescence (TL) on multiwalled carbon nanotube bundles and our conclusions are supported by TEM and SEM analysis of our samples. We observe that several peaks are common to SWNT and MWNT and that all the peaks are removed by heating the samples at temperature of 600-700 K. We assign each peak to an external impurities as confirmed in the TEM and SEM result analysis. Moreover the impurity concentration can be obtained from the study of peak temporal decay under electron bombardment. From our study this technique is revealed to be a suitable tool to control the cleanliness of carbon nanotube samples.

1. C. Journet et al. *Nature 388* (1997)
2. J. E. fisher et al *PRB 55 R4921* (1997)
3. K. Liu et al, *PRB 63, 161404(R)*, (2001)
4. M. J. O'Connel, S. M. Bachilo, C. B. Huffman, V. Moore, M. S. Strano, E. Haroz, K. Rialon, P. J. Boul, W. H. Noon, C. Kittrell, J. Ma, R. H. Hauge, R. B. Weisman, R. E. Smalley, *Science 297, 593* (2002)
5. S. M. Bachilo, M. S. Strano, C. Kittrell, R. H. Hauge, R. E. Smalley, R. B. Weisman, *Science 298, 2361* (2002)
6. J. Lefebvre, J. M. Fraser, P. Finnie, Y. Homma, *Physical Review B 69, 075403* (2004)
7. J. Lefebvre, Y. Homma, P. Finnie, *Phys. Rev. Lett. 90, 217401* (2003)
8. V. Berl, I. Huc, J. M. Lehn, A DeCian, J. Fisher *Eur. J. Inorg. Chem. 3089* (1999)
9. M. Barberio, P. Barone, A. Bonanno, M. Camarca, A. Oliva, F. Xu, *Radiation Physics and Chemistry* 76, 492-492 (2007)

# NEW SOLIDS BASED ON $B_{12}N_{12}$ FULLERENES

*J.M. Matxain, J.M. Mercero, X. Lopez, M. Piris, J.M. Ugalde*

*Kimika Fakultatea, Euskal Herriko Unibertsitatea, P.K. 1072, 20018
Donostia, Euskadi (Spain) and Donostia International Physics Center,
20080 Donostia, Euskadi (Spain).*

*L.A. Eriksson*
*Department of Natural Sciences and Örebro Life Sciences Center, Örebro
University, 70182 Örebro, Sweden.*
*J. Poater*
*Afdeling Theoretische Chemie, Scheikundig der Vrije Universiteit,
De Boelelaan 1083, NL-1081 HV Amsterdam, The Netherlands.*
*E. Matito*
*Institut de Quimica Computacional, Departament de Quimica, Universitat
de Girona, 17071 Girona, Catalonia, Spain.*
*M. Sola*
*Institut de Quimica Computacional, Departament de Quimica, Universitat
de Girona, 17071 Girona, Catalonia, Spain.*

In recent years BN fullerenes have been synthesized experimentally. As their carbon counterparts, these BN fullerenes could be assembled in molecular solids, but this possibility has been shortly studied in the literature. In this work we focus on the smallest synthesized BN fullerene, B12N12, which is built by squares and hexagons.

First, the interaction between two of these fullerenes has been analyzed, using the hybrids B3LYP and MPW1PW91 density functional methods. Two different interactions have been studied in the dimer, a square facing a square (s-s), and a hexagon facing a hexagon (h-h). In both cases a B is facing a N. The most stable dimer was found to be (s-s) facing, with covalent interactions between the monomers, but other dimers with weak interactions have been found as well, which opens possibilities of new systems, as in the case of fullerene dimers and solids. The solids resulting from the infinite repetition fo the characterized dimers were optimized, finding two different solids, with covalent and weak interactions between monomers, respectively. The solid with covalent interactions is a nanoporous material that is more stable by around 12 eV. Due to the nanoporous character of this solid it could be used for heterogeneous catalysis, molecular transport, etc. The SIESTA code with the GGA-PBE density functional method has been used for the solid state calculations.

# Adsorption of ice on top of Pd⟨111⟩ surfaces: Neural Network mapping of the ab-initio Potential Energy Surface

Adrien Poissier,[1, *] Berend Smit,[1] and Marivi Fernández-Serra[1]

[1] *CECAM ENS Lyon, 46 allee d'Italie, 69007 Lyon, France*

(Dated: May 29, 2007)

## I.  ABSTRACT

The understanding of the origin of the interactions between water and metal surfaces at the nanoscale is essential to characterize chemical processes where the metal/water interface is a key component such as corrosion, catalysis and electrochemical reactions[1–4]. While many classical force-fields exist for both water and metals, the treating of the two systems together requires the use of first-principle approaches, because the nature of the binding and interactions between both components is not well defined and both electronic and electrostatic interactions need to be described by a self-consistent ab-inito approach. This however imposes a limitation to the size of the systems studied, due to the very large computational loads (both in memory and time) involved in this calculations. We use Density Functional Theory calculations[7, 8] (DFT), including ab-initio molecular dynamics to study the adsorption of a monolayer of ice on top of a Pd⟨111⟩ surface. We are interested in the comparison between different Exchange and Correlation functionals [11–14] given that the description of the localized states of water together with the extended metallic states is a very delicate issue, at the limit of the approximations involved in DFT. According to ice rule and considering the smallest cell $(1 \times 1)$ (2 water molecules), there are only two different possible configurations for one layer of ice on top of our Pd⟨111⟩ surface. Clearly, as the cell increases, the number of possible configurations satisfying the ice rule increases dramatically. We counted for example that there are 2400 different configurations for a $2 \times 2$ unit cell (8 water molecules), (see fig : 1). It is impossible to calculate every configurations of these kind of systems using DFT. An idea to solve this problem is to use Neural Networks [5, 6] (NN). Based on the DFT energies of a few studied configurations, we then extrapolate the results to all the unknown wanted configurations. We show how this procedure is very powerful and present preliminary results for the NN extrapolated potential energy surface of all possible ice-1h monolayers grown on top of a

---

*Electronic address: `adrien.poissier@cecam.org`

Pd⟨111⟩ surface compatible with the periodic boundary conditions.
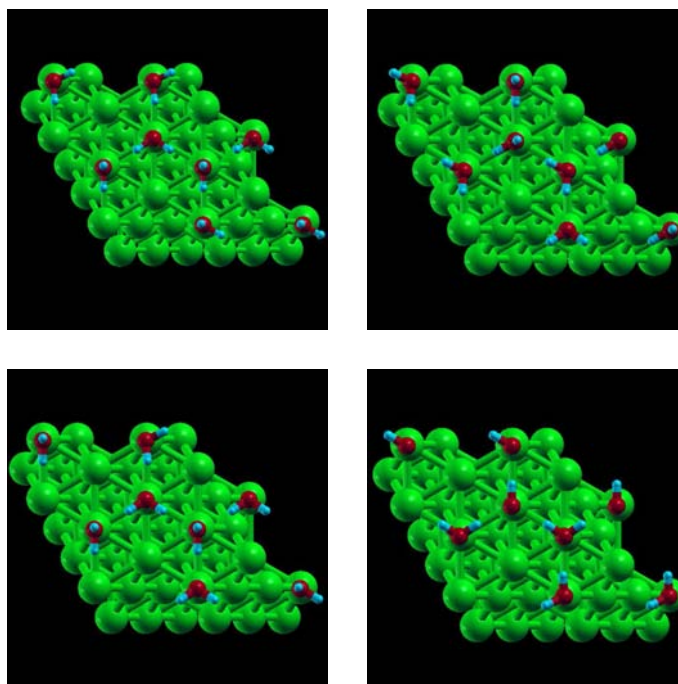


FIG. 1: *Here are represented 4 different possible configurations of one layer of ice on top of a Pd surface. For this unit cell size (8 water molecules), we counted 2400 different possible configurations saisfying the ice rule.*

All the DFT calculations are performed with the code SIESTA [9, 10]. The use of a Neural Network permits us to reduce by a factor of 15 the total number of DFT calculations, with an average 1% error on the rms of the energies.

[1] A. Michaelides, V.A. Ranea, P.L. de Andres and D.A. King, Phys. Rev. Lett. **90**, 216102, (2003)

[2] A. Michaelides and al. Phys. Rev. Lett. **93**, 116101, (2004)

[3] H. Ogasawara and al. Phys. Rev. Lett. **89**, 276102, (2002)

[4] Y. Cao and Z.X. Chen, Surface Science **600**, 4572, (2006)

[5] T.B. Blank, S.D. Brown, A.W. Calhoun and D.J. Doren, J. Chem. Phys. **103**, 4129, (1995)

[6] S. Lorenz, A. Groß and M. Scheffer, J. Chem. Phys. **395**, 210, (2004)

[7] P. Hohenberg and W. Kohn, Phys. Rev. **136**, 864, (1964).

[8] W. Kohn and L. J. Sham, Phys. Rev. **140**, 1133, (1965)

[9] P. Ordejón, E. Artacho and J. M. Soler, Phys. Rev. B **53**, R10441, (1996).

[10] J. M. Soler, E. Artacho, J. D. Gale, A. García, J. Junquera, P. Ordejón and D. Sánchez-Portal, J. Phys.: Condens. Matter, **14**, 2745 (2002); see also http://www.uam.es/siesta/
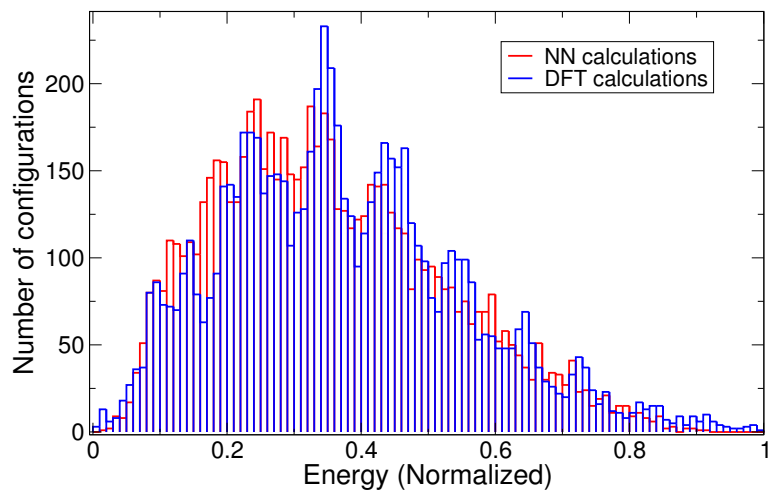
FIG. 2:   *These plots are energy histograms of DFT (blue) and Neural Network calculations (red). Learning 500 patterns, the NN is able to give a good estimation of the 7200 other configurations.*

[11]  J. P. Perdew, K. Burke and M. Ernzerhof, Phys. Rev. Lett. **77**, 3865 (1996).

[12]  B. Hammer, L. B. Hansen and J. K. Norskov Phys. Rev. B. **59**, 7413 (1999).

[13]  Y. Zhang and W. Yang Phys. Rev. Lett. **80**, 890 (1998).

[14]  Z. Wu and R. E. Cohen Phys. Rev. B. **73**, 235116 (2006).

# Alloy nano-cluster surface phenomena modeled using DFT-based coordination-dependent bond-energy variations

*Micha Polak and Leonid Rubinovich*
*Department of Chemistry, Ben-Gurion University, Beer-Sheva 84105, Israel*
*mpolak@bgu.ac.il*

In model computations of site-specific compositions and thermodynamic properties of Pt-Pd and Rh-Pd cuboctahedron nanoclusters, we use a new procedure for deriving the underlying interatomic energetics, based on a search for a functional dependence of surface-induced bond energy variations on the corresponding pair coordinations. In particular, polynomial functions were fitted to DFT data reported recently for energies of six surfaces, (111), (100), (110), (311), (331) and (210) [1], and of small pure Pt, Pd and Rh clusters. The elemental energy variations were incorporated in the statistical-mechanical "free-energy concentration expansion method" (FCEM [2]), employed before using semi-empirical energetics [3].

While all alloy clusters exhibit Pd segregation to specific surface sites, certain segregation profiles for Pt-Pd and Rh-Pd differ considerably (Fig.1). For example, Pt-Pd and Rh-Pd exhibit maximal Pd enrichment and depletion, respectively, in the 2-nd layer. These unique profiles originate from particular variations in elemental bonding between the 1-st and 2-nd layers.

Further computations reveal for Rh-Pd intra-cluster (surface/core) and inter-cluster separation involving "magic number" Pd segregated structures exhibiting various types of "demixed" order. At higher temperatures atomic exchange among surface sites as well as surface-core desegregation processes are reflected in distinct configurational heat capacity peaks of the Schottky type, at temperatures and magnitudes depending on the cluster overall-composition, shape and size (Fig. 2). In case of the Pt-Pd clusters, the predicted structures do not exhibit distinct surface/core separation, primarily due to the interplay between surface-modified bond strengths of the two constituents and their mixing tendency. Using the highly efficient FCEM enables to explore also compositional structures and properties of Rh-Pt-Pd ternary nano-clusters.

**References:**

[1] I. Galanakis et al., Surf. Sci. **511** (2002) 1.
[2] M. Polak and L. Rubinovich, Surf. Sci. Rep. **38** (2000) 127.
[3] M. Polak and L. Rubinovich, Phys. Rev. B **71** (2005) 125426; L. Rubinovich at al., Phys. Rev. B **74** (2006) 035405.
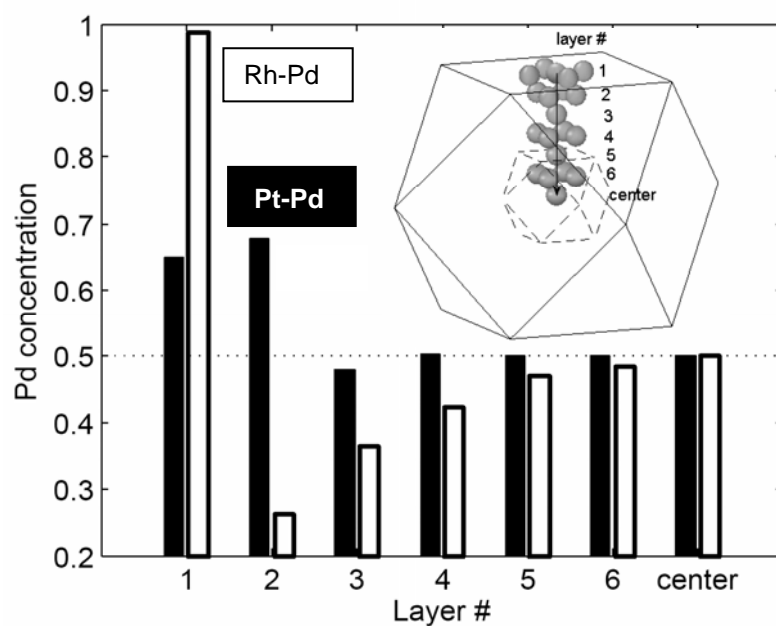
Fig.1. Pd segregation profiles computed for the (100) face of the 923-atom alloy cuboctahedron clusters (1500 K). Inset: schematics showing the pertinent profile layers.
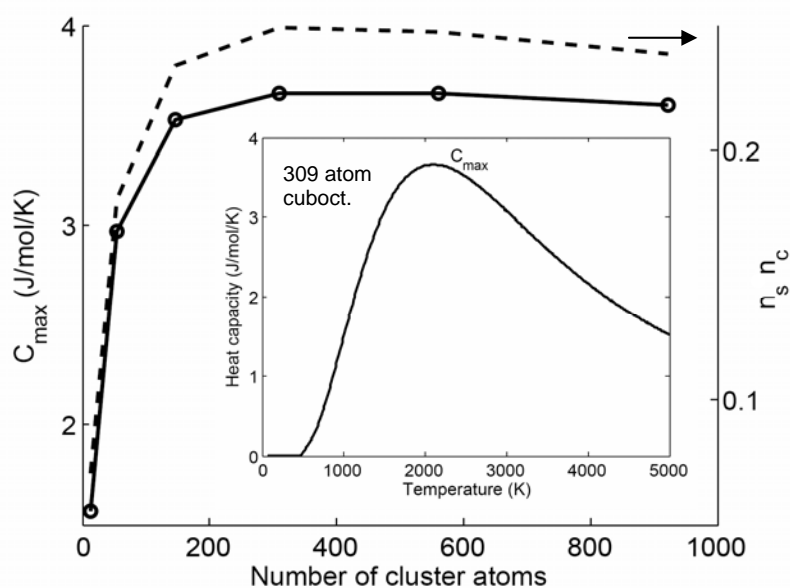


Fig.2. Nanocluster size effects: the heat capacity maximal value computed for 13 to 923-atom cuboctahedron Rh-Pd clusters having pure Pd surface and Rh core at low temperatures. Dashed line: the product of surface and core site fractions, representing the number of surface-core desegregation excitations. Inset: characteristic Schottky-type desegregation contribution to the cluster heat capacity.

# FABRICATION OF TWO DIMENSIONAL PHOTONIC CRYSTAL MICRO AND NANOCAVITIES: FROM ULTRA LOW THRESHOLD LASERS TO SOLID STATE BASED OPTICAL QUANTUM LOGIC

**Pablo Aitor Postigo**

*Instituto de Microelectrónica de Madrid (CNM, CSIC), Isaac Newton 8,
E-28760, Tres Cantos Madrid, Spain*

*aitor@imm.cnm.csic.es*

Two-dimensional photonic crystal lasers have been fabricated on III-V semiconductor slabs. Tuning of the spontaneous emission in micro and nanocavities has been achieved by accurate control of the slab thickness [1]. Different structures based in the coupling of light between nanocavities have been fabricated, like the Suzuki-phase [2], the hybrid lattice [3] or coupled-cavity ring-like resonators [4]. Laser emission has been obtained by pulsed optical pumping with very low power density. The capability of confining light in very small dimensions allows to obtain enhanced effects on cavity-QED. Photonic crystal cavities fabricated on self-assembled quantum dot active material (like quantum rings and quantum wires) have been fabricated for the first time with special attention to the control of the Purcell factor and the emission wavelength. These structures open new ways for single emission of photons, enhanced emission of entangled photon pairs and optical quantum gates.

**References:**

[1] A.R. Alija, L.J. Martínez, A. García-Martín, M.L. Dotor, D. Golmayo and P. A. Postigo, "Tuning of spontaneous emission of two-dimensional photonic crystal microcavities by accurate control of slab thickness", Applied Physics Letters 86 (14) 1101-1103 (2005)

[2] A. R. Alija, L. J. Martínez, J. Sánchez-Dehesa, P. A. Postigo, M. Galli, A. Politi, M. Patrini, L. C. Andreani, C. Seassal, and P. Viktorovitch, "Theoretical and experimental study of te Suzuki-phase photonic crystal lattice by angle-resolved photoluminescence spectroscopy" Optics Express 15 (2) 704-713 (2007)

[3] L.J. Martínez, A. García-Martín, and P. A. Postigo "Photonic band gaps in a two-dimensional hybrid triangular-graphite lattice" Optics Express, 12 (23) 5684-5689 (2004)

[4] A. R. Alija, L. J. Martínez, P. A. Postigo, C. Seassal, and P. Viktorovitch ,"Coupled-cavity two-dimensional photonic crystal waveguide ring laser" Applied Physics Letters, 89,101102- 01105 (2006)

# FUNCTIONALISED CARBON NANOTUBES FOR INTEGRATED NANO-ELECTRONIC SENSORS

*Yann Pouillon, Angel Rubio*

*Universidad del País Vasco UPV/EHU*

*&*

*European Theoretical Spectroscopy Facility (ETSF)*

*Donostia-San Sebastián, Spain*

Despite an exponentially increasing interest for using carbon nanotubes (CNTs) as sensors in industrial or medical environments, most of the efforts carried out so far still have to address the issue of recording and analysing a signal coming from a very small number of sensing elements. The unreliable contact interfaces between the CNTs and the rest of the electrical circuit are also greatly hindering progresses in this field. Moreover a better theoretical understanding of the transport phenomena responsible for signal generation and transduction inside the CNTs is clearly needed.

The SANES (Self-Adjusting Nano-Electronic Sensors) project aims at designing, building, and characterising multifunctional nanotube-based sensor micromodules, which will have to monitor simultaneously several factors, e.g. temperature, pressure, gas concentration, in various conditions. These modules will be integrated into a matchbox-sized electronic device which will hopefully be produced industrially afterwards. Potential applications range from security to medicine, covering communication and environmental issues as well.

In this project, the sensing unit is made of functionalised CNTs. Our objective is to provide the experimentalists with a valuable insight into the electronic properties of these CNTs, and to speed-up the process of selection of the functional molecules. Our calculations thus focus on the transport properties of single functionalised metallic and semi-conducting CNTs. In a first series we study the contact between a CNT and different metallic pads. In a second series we compare the influence of a large number of potentially interesting functional groups when the system is exposed to various gases. We investigate the effects of the presence of water as well.

# FABRICATION AND CHARACTERIZATION OF PHOTONIC CRYSTALS INFILTRATED WITH SINGLE WALL CARBON NANOTUBES FOR NEW OPTOELECTRONIC DEVICES

I. Prieto[a], L.J. Martinez[a], B. Alén[a], M.A. Correa-Duarte[b], L. Liz-Marzán[b] and P. A. Postigo[a]

*a) Instituto de Microelectrónica de Madrid (CNM, CSIC), Isaac Newton 8, E-28760, Tres Cantos Madrid, Spain*

*b) Departamento de Química Física, Universidade de Vigo, 36310 Vigo, Spain*

*ivanpg@imm.cnm.csic.es*

Single wall carbon nanotubes (SWCNTs) are promising nanostructures for optoelectronic applications, due to their semiconducting behaviour that shows a electronic bandgap around 0.8 eV (1.5 µm)[1]. High purity SWCNTs (~66%) have been encapsulated using an specific procedure developed at the Universidad de Vigo and based on the works of O'Connell and Smalley[1]. The absorption spectrum of the SWCNTS diluted in deuterium oxide $D_2O$ has been measured (Fig.1a) showing very similar features than what shown in Ref. 1. Optical emission of the SWCNTs has been performed by photoluminescence spectroscopy at room temperature of the diluted SWCNTs for volumes ~1 ml and smaller (Fig. 1b). The spectra show different maxima in the range 800-1700 nm that correspond to the different families of SWCNTs that differ in size and quirality. Two dimensional photonic crystals based on a triangular lattice of holes in dielectric have been infiltrated with the solutions of $D_2O$-SWCNTs and their optical emission has been measured, showing enhancement of the luminescence for specific wavelengths, which can allow the control of optical properties of SWCNTs and pave the way to their use in new optoelectronic devices.

---

[1] Michael J. O'Connell et al., "Band Gap Fluorescence from Individual Single-Walled Carbon Nanotubes" Science 297, (2002)
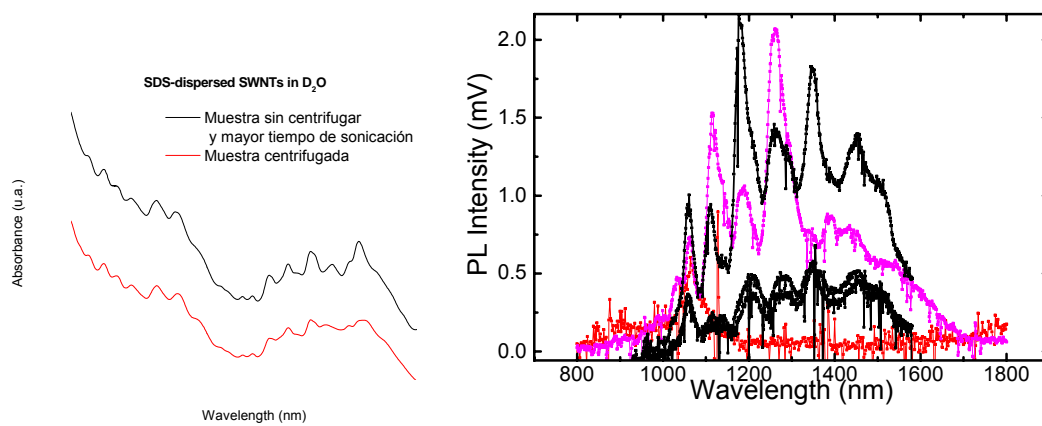
Fig.1. Left: Spectra of the absorption of the SWCNTs diluted in $D_2O$ for different sonication times. Right: Room temperature photoluminescence spectra showing the emission of the SWCNTS in $D_2O$.

# DEGREE OF SUPERSATURATION: AN EFFICIENT TOOL TO CONTROL SIZE DISTRIBUTION AND LUMINESCENCE IN COLLOIDAL SEMICONDUCTOR NANOCRYSTALS

*Amiya Priyam[a], Srabanti Ghosh[a], Subhash C. Bhattacharya[b] and Abhijit Saha*[a]*
*[a]UGC-DAE Consortium For Scientific Research, Kolkata Centre,*
*III/LB-8, Bidhannagar, Kolkata -700098, India*
[b]Department of Chemistry, Jadavpur University,
Jadavpur, Kolkata-700 032, India
*abhijit@alpha.iuc.res.in*

Over the past several years, numerous synthetic routes have been reported for preparation of II-VI and III-V colloidal quantum dots [1]. Some of these nanocrystals, specifically, II-VI semiconductor NCs (CdTe, CdSe, HgTe etc.) exhibit stable and high luminescence and have found tremendous applications in photovoltaic cells, photonic switches and optoelectronic devices. In recent times, novel bio-medical applications of these fluorescent NCs, i.e., biosensing, biolabeling and drug delivery [2-4] have also come up. A pre-requisite for such high-end applications is the obtainment of high quality nanocrystals. 'Quality', in this context, refers to the high fluorescence, photochemical stability, narrow size distribution and desired surface functionality of the nanocrystals. Out of these, controlling the size distribution of nanocrystals is one of the most nagging problems faced by the nanotechnologists around the globe. Although, several mechanisms have been developed to control the size and surface of nanocrystals [5], there are hardly any reported methods to control the particle size distribution in an ensemble. One such method, 'Size selective precipitation' [6] can narrow down the size distribution by gradual addition of a non-solvent to the solution of nanocrystals after the synthesis.

Here, we had a fresh look into the various aspects of synthesis and taken a different approach to address the problem. Evolution of the colloidal nanocrystals essentially involves three steps: supersaturation, nucleation and growth. If a proper control is developed at the very first step, it could have far reaching repercussions on the subsequent stages leading to attainment of particles with improved properties. For the first time, we show that a remarkable focusing of size distribution can be achieved just by increasing the degree of supersaturation of the initial synthetic mixture. This obviates the need for a post-preparative treatment like size selective precipitation and provides a handle to control the particle size distribution during the synthesis itself. Additionally, it also augments the fluorescence quantum yield of the nanocrystals.

In this work, CdS and CdTe nanocrystals with surface capping of cysteine were synthesized following the method reported earlier [7,8]. Briefly, an appropriate amount of $Na_2S$ or NaHTe solution was added to an $N_2$-purged solution of $Cd^{2+}$-cysteine solution in order to achieve a final molar ratio of 1: 2.5:0.5 for $Cd^{2+}$:Cysteine: $S^{2-}/Te^{2-}$. All the solutions so obtained were refluxed for 10 minutes. In order to change the degree of supersaturation, absolute concentrations of the reagents was varied to obtain supersaturation of 0.5 S, S, 2S, 3S and 4S while keeping their molar ratio same in the final mixture. Here, S denotes the supersaturation corresponding to the $Cd^{2+}$ concentration of $2.34 \times 10^{-2}$ M in the reaction mixture. For this particular set, degree of supersaturation S was found to be $4.17 \times 10^{11}$ assuming the solubility of bulk CdS to be $2.8 \times 10^{-14}$ M. (Degree of supersaturation = [CdS monomer concentration]/ [solubility of bulk CdS])

As shown in Figure 1, the absorption spectra of CdS NCs display a broad shoulder at lowest degree of supersaturation, 0.5 S, indicating a broad size distribution. As the degree of supersaturation is doubled, absorption profile shows an improvement with appearance of the peak and it gets further sharpened with increasing degree of supersaturation indicating narrowing of the size distribution. In order to gauge the extent of focusing, $\Delta\lambda_{abs}(\lambda_{peak}-\lambda_{onset})$ has been plotted against the degree of supersaturation in Figure 2. In an ensemble of particles,

larger nanocrystals are expected to absorb in longer wavelength region due to their smaller bandgap and smaller ones in shorter wavelength region. So, larger difference in absorption onset and peak indicates larger size distribution and *vice-versa* [9]. It can be easily noticed that size distribution gets narrowed down by $\approx$52% on moving from 0.5S to 4S and the variation appears to follow a linear trend. The luminescence spectra of CdS also follow a similar reduction in FWHM with increasing degree of supersaturation. In case of CdTe NCs, focusing effect was observed only for the supersaturation of 0.5S to 2S (data not shown). Beyond that no further change in $\Delta\lambda_{abs}$ was observed.

One of the most striking aspects of the present study is the enhancement in photoluminescence quantum efficiency (PLQE) of the nanocrystals with increasing degree of supersaturation at the time of synthesis. The CdTe NCs synthesized at supersaturation of 0.5 S exhibited a PLQE of 5%, which shoots up to 20% for the supersaturation value of 2S. It is quite intriguing to see how the high degree of supersaturation manifests itself into production of nanocrystals with remarkably higher value of PLQE. Further investigation to unravel the mechanism for the supersaturation dependent narrowing of size distribution and enhancement of PL efficiencies is in progress.

**References:**
[1] D. Crouch, S. Norager, P.O'Brien, J. H. Park, N. Pickett, Phil. Trans. R. Soc. A **361** (2003) 297.
[2] A. Priyam, A. Chatterjee, S. K. Das and A. Saha , Chem.Commun., **32** (2005) 4122.
[3] M. Ozkan, Drug Discovery Today, **9**(2004) 1065.
[4] X. Michalet, F. Pinaud, T. D. Lacoste, M. Dahan, M. P. Bruchez, A. P. Alivisatos, S. Weiss, Single  Mol. **2** (2001) 261.
[5] N. Gaponik, D. V. Talapin, A. L. Rogach, K. Hoppe, E.V. Shevchenko, A.  Kornowski, A. Eychmuller, H. Weller, J. Phys. Chem. B **106** (2002) 7177.
[6] C.B.Murray, D.J.Norris, M.G.Bawendi, J.Am.Chem.Soc. **115** (1993) 8706.
[7] A. Priyam, A. Chatterjee, S. K. Das and A. Saha , Res. Chem. Intermed. **31** (2005) 691
[8] A. Priyam, A. Chatterjee, S.C. Bhattacharya and A. Saha, J.Cryst. Growth, 2007, doi:10.1016/j.jcrysgro.2007.02.026
[9] S. Modes, P. Lianos,  J. Phys. Chem. 93 (1989) 5854.

**Figures:**
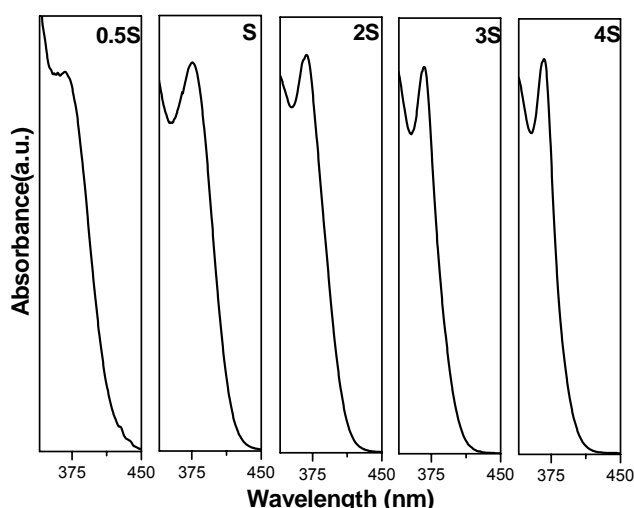


**Figure 1.** Absorption spectra of CdS NCs prepared at different degree of supersaturation
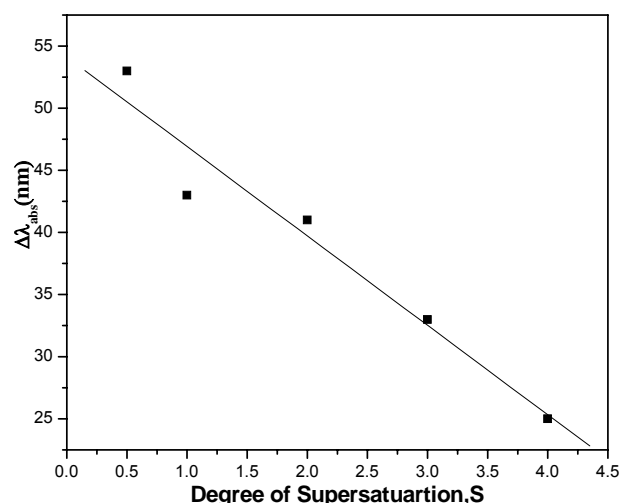
**Figure 2.** A plot of $\Delta\lambda_{abs}$ against degree of supersaturation for CdS NCs. (where $\Delta\lambda_{abs}=\lambda_{peak}-\lambda_{onset}$)

# Controlling entanglement in a double quantum dot

*Antonio Puente, Miquel Pons and Montserrat Casas*
*Departament de Física, Universitat de les Illes Balears, 07122 Palma de Mallorca, Spain*
*Toni.Puente@uib.es*

The production of entanglement, obtained by unitary transformations (quantum gates), is a basic prerequisite for any quantum computer. Due to the comparatively long spin coherence time and the feasibility of coherent manipulation of entangled pairs [1], semiconductor nanostructures are one of the best candidates to obtain an adequate set of quantum gates, through which individual electron spins (representing the basic qubits) can be manipulated. As an example, the possibility of controlling the wave function of two electrons in quasi-one-dimensional nanorods has been explored recently [2].

In this work, we analyze the physical realization of different quantum gates through two interacting electrons confined in a quasi-1D double quantum dot. Starting from different initial states (device initialization) several basic operations, such as SWAP or entanglement creation are performed by tuning the time evolution with a variable electric field.

In our model, the electrons are strongly confined in both the vertical and one lateral direction, giving rise to an effective quasi-1D system with a corresponding effective coulomb interaction. The potential in the remaining dimension is modulated with external gates to create a finite double well profile with a controllable interdot barrier height. The spin independent Hamiltonian, in effective atomic units (a.u.) corresponding to typical GaAs-AlGaAs parameter heterostructures, is given by

$$\mathcal{H} = -\frac{1}{2}\left(\frac{\partial^2}{\partial x_1^2} + \frac{\partial^2}{\partial x_2^2}\right) + V(x_1) + V(x_2) + \mathcal{V}_c\left(\left|x_1 - x_2\right|\right),$$

where $V(x)$ represents the confining (including time dependent barrier) potential and $\mathcal{V}_c\left(\left|x_1 - x_2\right|\right)$ is the effective interaction responsible for non-trivial correlations and hence for the entanglement of the two qubit system. Both for the SWAP and entanglement creation operations the system is initialized with a definite electron spin in each potential well ($L_\downarrow R_\uparrow$), representing a non-entangled mixture of the lowest energy singlet and triplet states. The appropriate quantum gate is then obtained by a suitable modulation of the interdot barrier height leading at the end of the time evolution to the desired final state.

The evolution is computed by numerically integrating the time dependent Scrhödinger equation with a unitary implicit finite difference scheme in space and time coordinates. The amount of entanglement as well as several spin-localization measures are followed through the evolution and serve as signals of the success and quality of the gate operation. Our results, which are exact for the model hamiltonian, are compared with the predictions of a two-level Landau-Zener model [3].

## References:

[1] J. R. Petta, A. C. Johnson, J. M. Taylor, E. A. Laird, A. Yacoby, M. D. Lukin, C. M. Marcus, M. P. Hanson, A. C. Gossard, Science, **309** (2005) 2180.
[2] G. E. Murgida, D. A. Wisniacki, P. I. Tamborenea, Phys. Rev. Lett., **99** (2007) 036806.
[3] L. D. Landau, Phys. Z. Sowjetunion, **2** (1932) 46.; C. Zener, Proc. R. Soc. London, **A 137** (1932) 696.

# PREPARATION AND CHARACTERIZATION OF DUAL-MODE NANOCOMPOSITES FOR IN VITRO CELL IMAGING AND SORTING

*Alessandra Quarta*, *R. Di Corato, R. Buonsanti, P. D. Cozzoli, G Barbarella., L. Manna and T. Pellegrino*
*National Nanotechnology Laboratory of CNR-INFM, Lecce, Italy*
alessandra.quarta@unile.it

Several efforts have been focused recently on the development of nanocomposites which display at the same time fluorescence and magnetic properties. Such nanostructures can be exploited for biomedical applications as dual modality imaging probes based on optical and magnetic resonance imaging (MRI) and for bio-separation and bio-sensing. One example of potential application of these nanocomposites is the simultaneous magnetic separation and multiplexing optical detection of different tumour cell populations. Oligothiophenes represent a novel class of fluorescent organic compounds characterized by a good photochemical stability. The main advantage of employing oligothiophenes as compared to the standard organic dyes (more commonly used in detection) is that oligothiophenes have broad optical absorption spectra. Therefore, different types of oligotiophene molecules, emitting at different colours, can be excited with a single excitation source, allowing for easy multiplexing analysis. This feature, along with their robustness to photodegradation, makes oligothiophenes comparable to colloidal semiconductor nanocrystals (such as CdSe), with the advantage that these molecules are much less toxic than semiconductor nanocrystals.

Here we report the preparation of hybrid bifunctional nanostructures made of colloidal iron oxide nanoparticles conjugated to oligothiophene molecules. The resulting nanostructures are water-soluble and preserve both magnetic and fluorescent properties. To assess their potential use as optical and magnetic probes in vitro, the hybrid nanocomposites have been incubated with human tumour cells. We shown that the oligothiophene-magnetic nanoparticles are uptaken by the cells and they accumulate into the cytoplasm. Furthermore, under the application of an external magnetic field, the cells which internalized the hybrid nanostructures are attracted to the region where the magnet is located. To asses the citotoxicity of these nanostructures a viability test has been carried out.

**References:**

1) Pellegrino, T., Manna, L., Kudera, S., Liedl, T., Koktysh, D., Rogach, A. L., Keller, S., Radler, J., Natile, G., and Parak, W. J. *Nano Letters 4*, (2004) 703-707.

2) Sperling, R. A., Pellegrino, T., Li, J. K., Chang, W. H., and Parak, W. J. *Advanced Functional Materials 16*, (2006) 943-948.

3) Pellegrino T., Kudera S., Liedl T., Javier A.M., Manna L., Parak W.J. *Small 1 (1),* (2005) 48-63

4) Barbarella G., Zambianchi M., Ventola A., Fabiano E., Della Sala F., Gigli G., Anni M., Bolognesi A., Polito L., Naldi M., Capobianco M. *Bioconjugate Chem 17*, (2006) 58-67

# ENERGY LOSS OF CHARGED PROJECTILES INTERACTING WITH METALLIC NANOPARTICLES

M. Quijada[1,2], A.G. Borisov[2,3], R.Díez Muiño[2,4], and P.M. Echenique[1,2,4]

[1] *Departamento de Física de Materiales, Facultad de Químicas UPV/EHU, Apartado 1072, 20080 San Sebastián, Spain*
[2] *Donostia International Physics Center DIPC, P. Manuel de Lardizabal 4, 20018 San Sebastián, Spain*
[3] *Laboratoire des Collisions Atomiques et Moléculaires (CNRS UMR 8625), Bâtiment 351, Université Paris-Sud, 91405 Orsay Cedex, France*
[4] *Unidad de Física de Materiales, Centro Mixto CSIC-UPV/EHU, P. Manuel de Lardizabal 3, 20018 San Sebastián, Spain*
*marinaquijada@ehu.es*

We present a theoretical study on the interaction of moving charged particles with metal clusters and nanoshells. First, we make use of time-dependent density functional theory (TDDFT) to calculate the energy lost by antiprotons colliding through the center of spherical jellium clusters of different size and electronic density parameter, $r_s$. The results allow us to define an effective stopping power S as the energy loss per unit path length inside the cluster. Analysing the dependence of S on the projectile velocity, we obtain results which are unexpectedly close to the ones corresponding to the free electron gas, even for very small clusters (e.g. clusters with as few as 18 electrons, corresponding to a radius of ~5 atomic units for $r_s = 2$) and low velocities (down to ~0.1a.u.). We thus conclude that the collision process is quite local, and that the discreteness of electronic states in the cluster does not play an important role in the screening process. Moreover, the stopping powers obtained from our calculations using nanostructures of a few nanometeres in size are comparable to experimental values for macroscopic materials, both for protons and antiprotons [1]. This reassures us that the dynamic screening within the cluster is essentially that of a homogeneous system in the velocity range considered. For completion of the study, we also show the velocity dependence of the S in collision processes with off-center projectile trajectories, as well as the case of the interaction of antiprotons with nanoshells of different electronic density parameters and size.

**References:**

[1] M.Quijada, A.G. Borisov, I. Nagy, R. Díez Muiño, and P.M. Echenique, Phys. Rev. A **75**, 042902 (2007).

# DENSITY FUNCTIONAL STUDY OF OXYGEN ADSORPTION ON ARMCHAIR SINGLE WALL CARBON NANOTUBE

**A. A. Rafati[a], S. M. Hashemianzadeh[b], Z. B. Nojini[a]**

*[a]Department of Chemistry, faculty of Science, Bu-Ali Sina University, Hamadan, Iran*

*[b]College of Chemistry, Iran University of Science and Technology, Tehran, Iran*

*Contact@E-mail*

## Abstract

Density Functional calculation were employed to study the adsorption of O atom and $O_2$ molecule on the armchair (n= 4-10) nanotubes. Calculations have been performed at the B3LYP/3-21G** density functional level of theory. Several possible adsorption sites, T (top of the carbon atom), B (top of the C-C bond) and interstitial site in the tube have been considered. Also when $O_2$ molecule has angles 90 and 135 with tube axis have been studied. Results show that when $O_2$ adsorb in the T site has minimum adsorption energy and minimum distance between C atom and O atom. An O atom is found to bind to the outside surfaces of the nanotube to give stable structures. We found that the interaction between atomic oxygen and single wall carbon nanotube is stronger than the $O_2$ molecule. Also the equilibrium position, binding energy, charge transfer and the energies of the HOMO and LUMO for components and complexes have been calculated for different nanotubes. For all calculations a-one dimensional periodic boundary condition is applied along tube axis.

**References:**

[1] J. Zhao, A. Buldum, J. Han, J. P. Lu, *Nanotechnology 13(2002)195-200*

[2] A. Ricca, C. W. Bauschlicher, *Physical Review B 68 (2003) 035433*

[3] H. Rafii- Tabar, *Physics Reports 390 (2004) 235-425*

[4] A. Mavrandonakis, S. C. Farantos, G. E. Froudakis, *J. Phys. Chem. B 110 (2006) 6048-6050*

**Figures:**
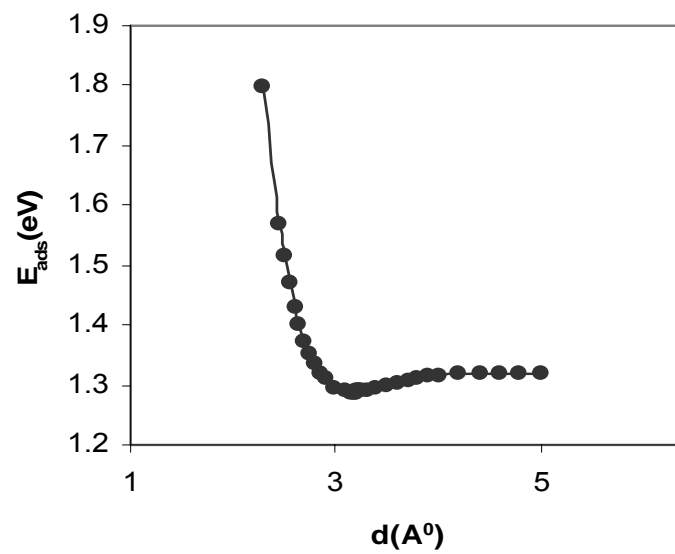


Figure **1**: Typical adsorption energy (eV) as a function of tube molecule distance (Å) for $O_2$ molecule on (5, 5) carbon nanotube.
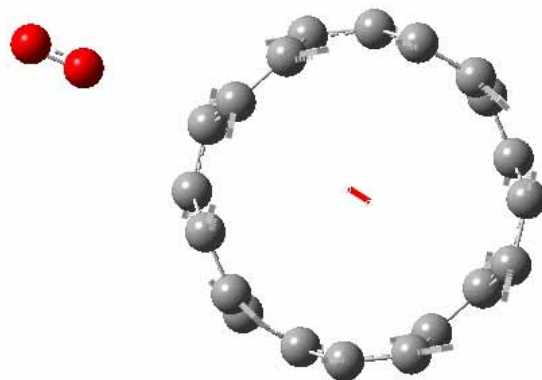


Figure **2**: Geometric structure of $O_2$ attached to an individual (5, 5) carbon nanotube.

# NOVEL ROUTE FOR PREPARATION OF MICRO- AND NANO-SCALE TUBULAR OXIDE STRUCTURES

[1,2] **Valter Reedo,** [1]**Martin Järvekülg,** [2]**Uno Mäeorg**
[1]Institute of Physics, University of Tartu, Riia 142, 51014 Tartu, Estonia
[2]Institute of Organic and Bioorganic Chemistry, University of Tartu, Jakobi 2, 51014 Tartu, Estonia
E-mail: valterre@fi.tartu.ee

Nano- and microscale tubular structures have exceptional properties and have great potential as the building blocks of nano- and microdevices systems of high efficiency. This kind of structures have been for that the subject of intensive research. Since the discovery of carbon nanotubes [1] there has been active interest in exploring other layered and nonlayered materials that form tubular structures. Many different methods of obtaining various materials in nanotube form have been reported and summarized in revews [2].

$TiO_2$, $ZrO_2$ and $HfO_2$ are wide band gap materials of great interest since they can be used in sensorics [3], photocatalysis, electronics and solar cells. Metal oxide nanotubes have been obtained through various sol-gel related methods and the suggested formation models are often complemented or corrected afterwards [4]. Obviously, exploring different possibilities for obtaining tubular nano- and micro-sized materials and explaining their formation is of great importance in order to establish correct theorys and be able to synthesise materials with desired properties.

In present work we report a novel phenomenon and mechanism of low-dimensional tubular oxide structure formation. Microtubes of hafnium, zirconium (figure 1, 2) and titanium oxide were obtained by deposition of solvent free metal butoxide polymer layer on glass substrate and exposing it with controlled amount of humid atmosphere. Dissolving formed layered system in hexane led to the formation of microtubular oxide structures.

Current work include:

- Characterisation of formed tubular structures by AFM and SEM visualization.
- Observation effect of moisture content and temperature for the dimensions of formed particles.
- Observation the rate of polymerization of Ti, Zr and Hf alkoxides for the dimensions of forming tubular structures.
- Some possible mechanisms are also proposed to explain the formation of observed novel structures.

**References:**

[1] Iijima, S. Helical microtubules of graphitic carbon. *Nature*, 1991, **354**, 56.

[2] Remškar, M., *Adv. Mater.* 2004, **16**, 1497.

[3] V. Reedo, S. Lange, V. Kiisk, T. Tätte, A. Lukner and I. Sildos, SPIE Proceedings, **5946** (2005) 5946 OD1-5.

[4] Kukovecz, A., Hodos, M., Horvath, E., Radnoczi, G., Konya, Z., Kiricsi, I. Oriented Crystal Growth Model Explains the Formation of Titania Nanotubes. *J. Phys. Chem. B,* 2005, **109**, 17781-17783.

**Figures:**

Figure 2. Typical SEM image of tubular zirconium oxide structure.
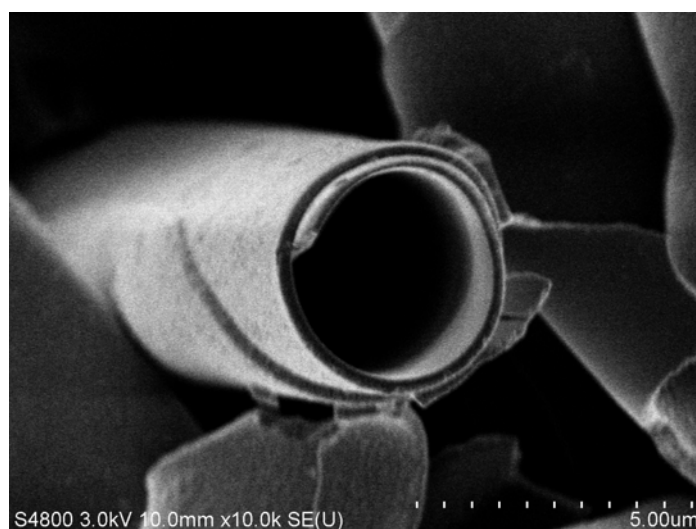


Figure 2. SEM image of tubular $ZrO_2$ structures.
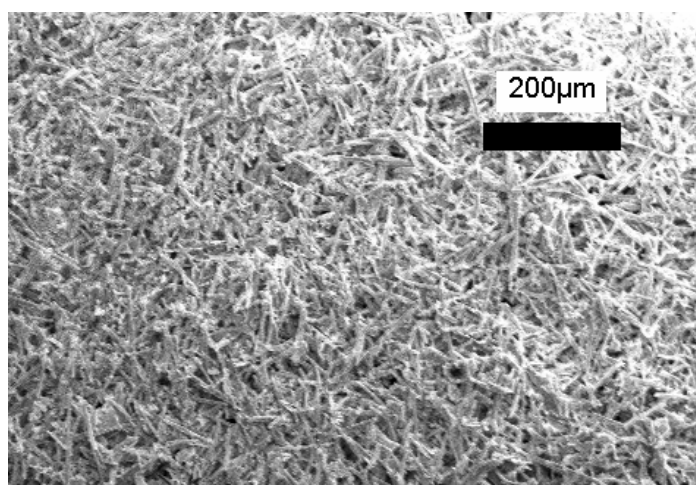
# SELF-ASSEMBLED FLUOROCARBON-SILICA NANOCOMPOSITES: STRUCTURE AND PROPERTIES

*Carlos Rodríguez-Abreu,[a)]*, Pablo M. Botta,[b)] José Rivas [b] , Kenji Aramaki [c] , Manuel Arturo López Quintela[d)]

a)Institut d`Investigacions Químiques i Ambientals de Barcelona. Consejo Superior de Investigaciones Científicas (IIQAB/CSIC), Jordi Girona, 18-26, 08034 Barcelona, Spain.
b) Departamento de Física Aplicada, Facultad de Física, Universidad de Santiago de Compostela, E-15782, Santiago de Compostela, Spain
c) Graduate School of Environment and Information Sciences, Yokohama National University, Tokiwadai 79-7, Hodogaya-ku, Yokohama 240-8501, Japan
d) Departamento de Química Física, Facultad de Química, Universidad de Santiago de Compostela, E-15782, Santiago de Compostela, Spain
*craqci@iiqab.csic.es*

Self-assembly is a "bottom-up", low energy method used to prepare nanomaterials, usually assisted by amphiphilic compounds [1]. Among such compounds, fluorocarbon surfactants show special features which make them much more efficient than hydrocarbon surfactants in many applications. The functionalization of silica with fluorocarbon chains offers possibilities for applications such as protective coatings [2] and low dielectric constant materials for semiconductors [3]. We report on the properties of hybrid fluorocarbon-silica materials formed by the self-assembly of a fluorocarbon surfactant and aminoalkoxysilane coupling agents. The characterization was carried out by X-ray diffraction, Small angle X-ray scattering, Thermal Analysis, and NMR spectroscopy. The obtained materials have a structure consisting of alternated fluorinated and condensed silica nanosheets in a non-crystalline state. Time-resolved X-ray scattering measurements indicate that during the synthesis, the system undergoes a morphological transition from disordered aggregates (where the aminosilane acts as a reactive counterion) to the mentioned lamellar structure; this transition seems to be driven by a decrease in interfacial curvature induced by the hydrolysis and condensation of the aminosilane. The hybrid materials are hydrophobic and show a low dielectric constant ($\approx 2.8$), which is almost independent on frequency, as predicted by the Maxwell-Wagner model

**References:**

[1] M. Lazzari, C. Rodríguez, J. Rivas, M. A. López-Quintela, J. Nanosci. Nanotechno., **4** (2006) 892.
[2]. A. F. Thünemann, Langmuir, **2** (2000)824.
[3] G. J. A. A. Soler-Illia, P. Innocenzi, Chem. Eur. J., **17** (2006) 4478.
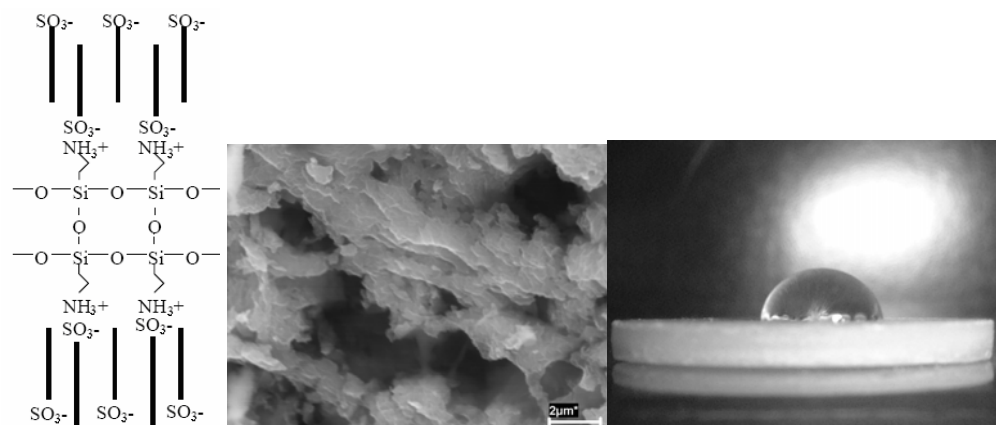
Fig. 1: Scheme of possible lamellar nanostructure in the hybrid material (left); SEM image showing a lamellar morphology (center); and photograph of a water droplet on a pellet of the material depicting the hydrophobicity of the surface(right).

# ELECTRO-OXIDATION OF CARBON MONOXIDE AND METHANOL ON CARBON-SUPPORTED $Ni_{59}Nb_{40}Pt_{(1-X)}Y_X$ (Y =Sn, Ru; X =0, 0.4% AT.) NANOPARTICLES AS ANODIC IN A DMFC.

**A. R. Pierna**\*, **J. Barranco, F. F. Marzo, A. Lorenzo, B. Cartón, M. M. Antxustegi,  and F.Lopez.**

*Dpto de Ingeniería Química y Del Medio Ambiente. Universidad del País Vasco. Plaza de Europa 1. 20018 San Sebastián. Spain*
*\*e-mail: iapropia@sp.ehu.es      web: http://scsx01.sc.ehu.es/iaweb/*

## ABSTRACT

The electrochemical oxidation of methanol and related small molecules has been of special interest in relation to fuel cell research (1,2). This work will focus on the investigation of the electro-oxidation of carbon monoxide and methanol on carbon-supported $Ni_{59}Nb_{40}Pt_{(1-x)}Y_x$ (Y =Sn, Ru; x =0, 0.4% at.) nanoparticles as anode, that are considered as catalysts, in acid solutions.

The amorphous structure of the nanoparticles, leads to considerable enhancement of the oxidative currents, which is more than the double of that of the platinum polycrystalline electrodes.

Moreover, there is a slight shift to more negative potentials of the "onset" potential as a function of the alloy composition, as well as, the activation time of the alloy. These new alloys show a very interesting behavior, taking into account their high tolerance to CO molecules, which are the main cause of poisoning of the anodes materials in fuel cells.

It was observed that both $Ni_{59}Nb_{40}Pt_{0.6}Ru_{0.4}$ and $Ni_{59}Nb_{40}Pt_{0.6}Sn_{0.4}$ containing MCPEs, shift the onset potential for CO (ca. 0.23 V) to lower potentials compared to $Ni_{59}Nb_{40}Pt_1$ electrodes. While ruthenium promoted the catalytic activity for methanol and CO electrooxidation, tin showed the same enhancing behaviour for a shorter period of time, probably due to the facile dissolution of tin from the surface[1].

Concerning the reactivity of methanol, the current density is drastically decreased with the presence of tin, susceptible to the potential range, followed by the $Ni_{59}Nb_{40}Pt_1$ and $Ni_{59}Nb_{40}Pt_{0.6}Ru_{0.4}$ alloys. However, these new electrodes show a very interesting behaviour, taking into account their high tolerance to CO molecules, and the decrease of the onset potential for methanol electrooxidation, which are the main causes of poisoning  of  anode materials in fuel cells.

## Acknowledgements

## References

1.- J. Barranco  and  A. R. Pierna, J. of Non Crystalline Solids, 353/ 8-9, (2007) 851.
2.- J. Barranco  and  A. R. Pierna. J. of Power  Sources, 166/1, (2007) 157.

# BIOSENSORS BASED ON BIO-NANOSTRUCTURES IMMOBILIZED ON SILICON CHIPS.

C. Rogero,[a,b] E. Mateo-Marti,[a] B.R. Horrocks,[b] A. Houlton,[b] A. Gutierrez,[c] C. Briones,[a] J. A. Martin-Gago.[a]

[a]*Centro de Astrobiología (CSIC-INTA)Carretera de Ajalvir, Km. 4. 28850 Torrejón de Ardoz. Madrid. Spain.*
[b]*Chemical Nanoscience Laboratories, School of Natural Sciences, University of Newcastle upon Tyne, Newcastle upon Tyne, NE1 7RU, U.K.*
[c]*Departamento de Física Aplicada, Universidad Autónoma de Madrid, Ctra. Colmenar Viejo, Km. 15. 28049 Cantoblanco, Madrid, Spain.*
*rogerobc@inta.es*

Biochips, devices with biological macromolecules located in spatially-defined areas, play an increasingly important role in the molecular and medical biosciences. Fluorescence is the dominant method for array interrogation but requires a label to be added to one of the components, bulky and expensive instrumentation and sophisticated software for data interpretation. Recently attention has been focused on electronic and electrochemical sensors based on self-assembled molecules on surfaces, because they present the sensitivity of fluorescence-based systems but being cheaper, more compact and potentially allowing near instant diagnostics at the point of use [1]. One of the most studied systems as biosensor is the self-assembled functionalized monolayer of alkanethiols on gold [2]. It is clear, however, that deserve importance to construct ordered molecular layers on semiconductor surfaces, mainly on Si, because the wide range of possible applications in conjunction with the advanced silicon technology.

In this context, we have been working in an easy and widely applicable method for the attachment of different nano-objects [3] (nucleic-acids, enzymes, proteins, nanoparticles…) to semiconducting silicon wafers. The chemistry involves the reaction of Si-H layer with a bifunctional hydrocarbon containing different alkene chains (alkylation reaction). Since the reaction is irreversible, via the stable Si-C bond [4], and it is not influenced by the functional groups at the other end of the molecule, the resulting monolayer presents an uniform composition where both components are well mixed, despite being of different chain length and tail-group. Moreover the results reveal that the resulting molecular films present a composition that is representative of the composition of the solution. Therefore, by a simple dilution method it is possible to control the mean spacing between reactive groups on the surface and this is an useful method for nanoscale surface design [5].

When alkene and aldehyde terminated chains are mixed, it is possible to specifically localise proteins or nucleic acids, such as the PNA (Peptide Nucleic Acid), to defined surface positions, with little non-specific adsorption at non-reactive sites. Proteins or the peptidic bonds in the PNA structure are immobilized by reaction of surface lysine residues (common to almost every protein) with the aldehyde terminated group of the monolayer, but not on the methyl terminated group.

This protocol opens the way for using semiconducting silicon surfaces for the production of protein or PNA biochips, since all the proteins and the peptide nucleic acids immobilised appear to remain in their functional state. Therefore, it is possible to detect protein-protein interactions, protein-small molecule or PNA_DNA interactions on the surface electronically. This feature is critical in allowing electrochemical/electronic methods to be exploited in

protein or nucleic acids analysis [6]. Such chips would be expected to be of tremendous utility for comparative proteomics and in molecular medicine, drug discovery and diagnostics or even for the detection of mutations of DNA.

**References:**

[1] Drummond, T. G.; Hill, M. G.; Barton, J. K. *Nature Biotechnology* 21 (2003), 1192.

[2] Briones C, Mateo-Marti E, Gomez-Navarro C, Parro V, Roman E, Martin-Gago JA *Phys. Rev. Lett.* 93 (2004), 208103.

[3] Patole SN, Pike AR, Connolly BA, Horrocks BR, Houlton A. Langmuir 19 (2003), 5457.

[4] M. R. Linford and C. E. D. Chidsey, *J. Am. Chem. Soc* 115 (1993) 12631. M. R. Linford, P. Fenter, P. M. Eisenberger, C. E. D. Chidsey, *J. Am. Chem. Soc*. 117 (1995) 3145.

[5] Q. Hong, S. Carlsson, B.A. Connolly, J.H. Lakey, A. Gutierrez, E. Mateo-Marti, C. Briones, J. A. Martin-Gago, B.R. Horrocks, A. Houlton and C. Rogero. Submitted to J. Chem. Phys.

[6] Qi Hong, Celia Rogero, Jeremy H. Lakey, Benjamin R. Horrocks, Andrew Houlton and Bernard A. Connolly. Submitted to *J. Am. Chem. Soc*.
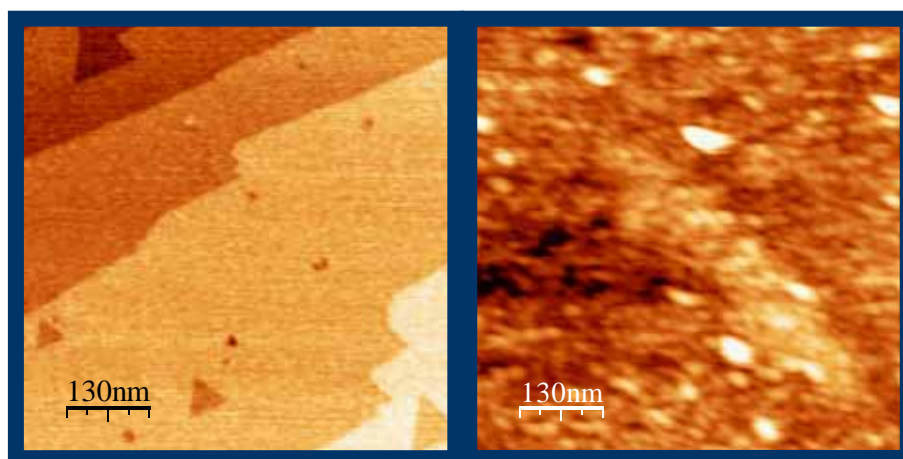
**Figure 1: A)** AFM images in air of a mixed monolayers 1:1 $C_{11}/C_{10}CHO$, on Si(111). B) Same surface after the immobilization of PNA molecules.

# PROTECTIVE NANOLAYERS ON METAL SURFACES FABRICATED BY LANGMUIR-BLODGETT AND SELF-ASSEMBLY TECHNIQUES

*Loránd Románszki, Judit Telegdi, Erika Kálmán*
*Chemical Research Center of the Hungarian Academy of Sciences, Pusztaszeri út 59-67,*
*1025 Budapest, Hungary*
*L.Romanszki@chemres.hu*

Microbiological corrosion (MC) is a corrosion process which undergoes in the presence of microorganisms, which, by their chemically aggressive metabolites and sticky biofilm contribute to the deterioration of metals. If one manages to impede the adhesion of the cells and the biofilm-formation, then the MC can be eliminated. Our studies [1-5] concern the inhibition of corrosion of and bacterial cells' adhesion on copper surfaces via protective molecular films of organic compounds, prepared by the Langmuir-Blodgett technique (LB) and self-assembly.

Both LB and self-assembly require amphiphile molecules. Such molecules contain hydrophilic functional groups and hydrophobic chains (see left figure). In our experiments we tried thirteen different amphiphiles, saturated and unsaturated carboxylic and hydroxamic acids. First Langmuir monomolecular films at the air/water interphase have been prepared by spreading the film-forming compounds' solutions in chloroform onto water subphases. The surface pressure vs. area per molecule isotherms have been recorded in each case. Upon analysing these isotherms, the best conditions (i.e. constant pressure, temperature, speed) of film transfer have been defined.

Using these parameters, the Langmuir-films have been transferred onto solid substrates such as mica, glass and copper, as mono- and multimolecular LB-films, as well. The molecular ordering of these LB films has been studied by second harmonic generation spectroscopy (SFS). The spectra revealed high molecular order in the films of the studied saturated compounds, while low ordering degree in the films of the unsaturated amphiphiles. In parallel to the LB-films, films of the amphiphiles have been prepared on polished copper substrates by self-assembly technique too.

Coated copper samples have been immersed for 15 hours in 0.5 M NaCl solution. The corroded surfaces then were investigated by atomic force microscope (AFM). Mean roughness and bearing factors were used to numerically evaluate the deterioration of the surfaces and hence to draw conclusions about the corrosion inhibitive effect of these molecular layers. Results showed the efficiency of the saturated hydroxamic acids.

To investigate the bacterial adhesion inhibitive efficiency of these coatings, treated copper samples were immersed for 48 hours in industrial cooling water containing mixed population of microorganisms. Then the samples were stained with acridine orange and visualized under fluorescence microscope and AFM (see middle and right figures). The two parallel techniques proved the inhibition effect not on the cell adhesion itself, but on the biofilm formation. The number of adhered microorganisms was roughly the same in each case, and seemed to not depend on the applied protective coating. However, a sticky biofilm was detected with the AFM cantilever in the case of unprotected samples, which was absent on the nanofilm-coated surfaces.

**References:**

[1]    J. Telegdi, T. Rigó, E. Kálmán, Corr. Eng. Sci. Technol. **39** (2004) 65.
[2]    J. Telegdi, T. Rigó, J. Beczner, E. Kálmán, Surface Eng. **21** (2005) 107.
[3]    T. Rigó, A. Mikó, J. Telegdi, M. Lakatos-Varsányi, A. Shaban, E. Kálmán,
       Electrochem. Solid St. **8** (2005) B51.
[4]    J. Telegdi, T. Rigó, E. Kálmán, J. Electroanal. Chem. **582** (2005) 191.
[5]    J. Telegdi, H. Otmačić-Ćurković, K. Marušić, F. Al-Taher, E. Stupnišec-Lisac, E.
       Kálmán, Chem. Biochem. Eng. Q. **21** (2007) 77.
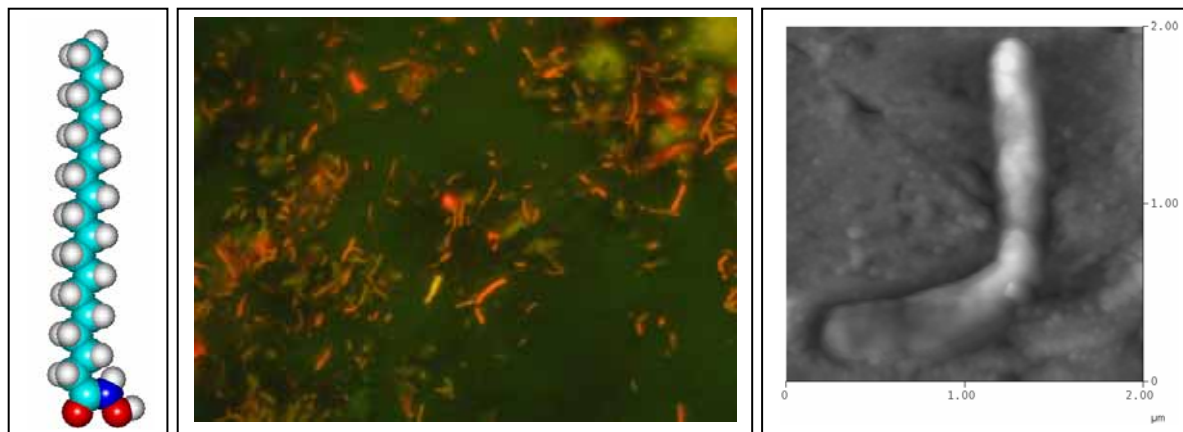


**Figures. Left: Molecule model of the stearoyl hydroxamic acid, one of the nanofilm-forming compounds. Middle: Rod-like bacilli on a copper surface imaged under fluorescence microscope after 48 h immersion of the substrate. Right: A dividing bacillus on copper surface (scan area: 2×2 µm², z-range: 200 nm)**

# FORMATION OF NANOSPHERES FROM SELF-ASSEMBLED OLIGOSQUARAMIDES

*Carmen Rotger, Antoni Costa, Manuel Vega*
*Departament de Química, Universitat de les Illes Balears*
*Carretera de Valldemossa, Km 7,5; 07122 Palma de Mallorca, España*
*carmen.rotger@uib.es*

Oligosquaeramides are a new family of unnatural oligomers based in squaramide units and aliphatic linkages, represented by the general structure shown in figure 1a. Squaramides, considered as vinylogous amides, are versatile molecules with considerable hydrogen bonding capabilities, as well as favorable dynamic properties to adopt secondary structures. These oligomers are palindromically constituted and fold in a hair-pin like structure driven by an array of hydrogen bonds, analogously to proteins. The oligosquaramides folded structures are stable even in highly competitive media as methanol and ethanol solutions.[1] Some short peptides self-organize and form vesicular assemblies that can aggregate though different mechanism[2]. These processes can drive to highly ordered nanoarchitectures.

In this study, we present the formation and characterization of globular nanostructures from oligosquaramide n=5.

Preliminary AFM and TEM studies show the formation of nanospheres in a range of size of ~20-200 nm (figure 1b) from methanolic solutions. These structures are concentration dependent and the presence of non-specific aggregates and layers are observed upon different conditions.

These nanostructures constitute a new class of preorganized material with potential applications.

**References:**

[1] Rotger, C., Piña, M. N., Vega, M., Ballester, P., Deyà, P. M., Costa, A. *Angew. Chem. Int. Ed*., **45** (2006) 6844.
[2] a) Vauthey, S., Santoso, S., Gong, H., Watson, N. Zhang, S. *Proc. Natl. Acad. Sci. USA,* **99** (2002) 5355; b) Reches, M., Gazit, E. *Nano Lett*., **4** (2004) 581.
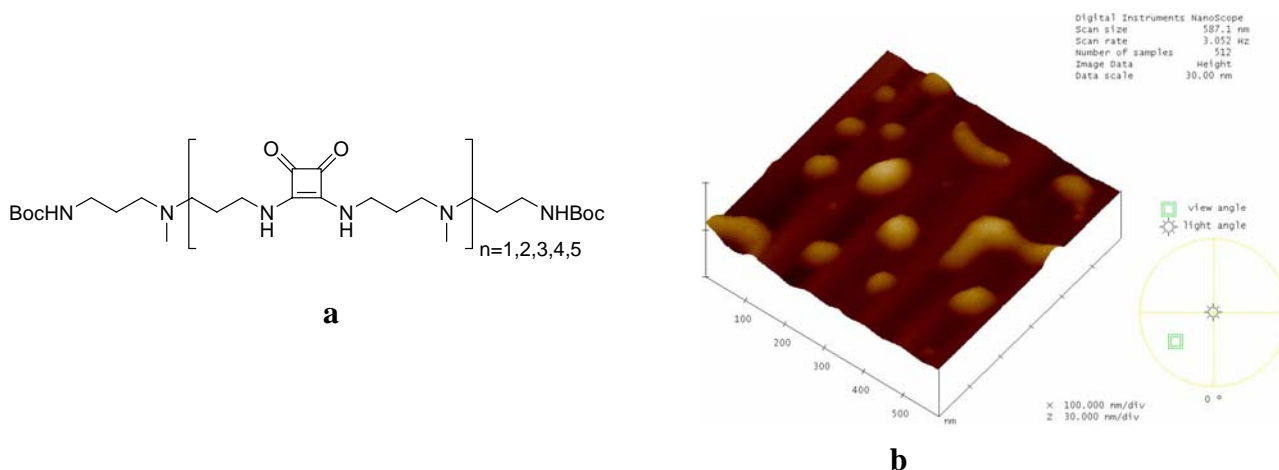
**Figure 1. a) general structure of oligosquaramides. b) AFM image of globular nanostructures of oligosquaramide n=5**

# FERMI EDGE SINGULARITY IN XRAY STUDIES OF GRAPHENE.

*A. Sindona, <u>S. Rudi</u>, A. Cupolillo, G. Falcone and L. PapagnoDipartimento di Fisica,*
*Universita` della Calabria, Via P. Bucci 31C, 87036 Rende (CS), INFN, Gruppo collegato di*
*Cosenza, Italy*
*[Sindona@fis.unical.it](mailto:Sindona@fis.unical.it)*

We present a model to describe shake up effects in X-ray photoemission spectra from a monolayer of Graphene absorbed on a substrate of Ni(111).

Using the tight binding method, we determine the effect of the suddenly created core hole, in the 1s-state of a carbon atom, on the many electron states of $\pi$ and $\pi^*$ bands.

We compare our results with the asymmetric lineshapes measured from bundles of clean single-walled carbon nanotubes, specifically examining the energy distributions of many body excitations created at the expense of the photoelectron in (10, 10) and (16, 0) tubes.

We discuss the variation of the core hole progator either in graphene or in nanotubes of different chirality. We show a good a agreement of the theory and the experiments.

**References:**

References
[1] A. Sindona, R. A. Baragiola, G. Falcone, A. Oliva, and P. Riccardi, Phys. Rev. A 71, 052903 (2005)
[2] A. Sindona, S.A. Rudi, S. Maletta, R.A. Baragiola, G. Falcone and P. Riccardi, Surf. Sci. 601, 1205 (2007)
[3] A. Sindona, F. Plastina, A. Cupolillo, C. Giallombardo, G. Falcone and L. Papagno, Surf. Sci., in press (Available online 22 December 2006)

# DIRECT ELECTROCHEMISTRY OF *DESULFOVIBRIO GIGAS* [NiFe]-HYDROGENASE COVALENTLY BOUND AND ORIENTED ON CARBON NANOTUBE ELECTRODES.

<u>Olaf Rüdiger</u>[a], Asunción Alonso-Lomillo[a], Marisela Velez[b] Immaculada Rodríguez-Ramos[a],

Francisco Muñoz-Pascual[c], V.M. Fernandez[a] and Antonio L. De Lacey[a]

a) Instituto de Catalisis, CSIC, c/Marie Curie 2, Cantoblanco, 28049 Madrid, Spain; b)

Facultad de Ciencias, Universidad Autónoma, 28049 Madrid, Spain c) Centro Nacional de

Microelectónica, CSIC, Campus de Bellaterra, 08193 Barcelona, Spain; e-mail:

olaf@icp.csic.es

The use of hydrogen technology for energetic purposes, as an alternative to fossil fuels, is one of the solutions to obtain a clean energy free of $CO_2$ emmisions. In nature the oxidation or evolution of $H_2$ is catalyzed by hydrogenases. The stable immobilization of such enzymes on electrodes is an interesting target for their application on biological fuel cells. In order to study the mechanism of catalytic hydrogen evolution or consumption by *Desulfovibrio Gigas* [NiFe]-Hydrogenase, through direct electrochemistry, several methods of covalent oriented immobilization were studied.

In the *Desulfovibrio Gigas* [NiFe]-Hydrogenase the distal 4Fe4S cluster is used by the protein to exchange electrons with his redox partner, the Cytochrome c3. The coupling between both proteins has a strong electrostatic component[1,2]. The target of this work was to emulate this interaction and force the enzyme to face the electrode with the aim of having direct electrochemistry. Near the distal cluster, the [NiFe]*Deslifovibrio Gigas* hydrogenase has several glutamate residues resposable of a negative potential, compared to the other side of the protein. This phenomenon, used to orientate the protein on an electrode, was studied by modifying the pH of incubation and the ionic strength[4]. The MWCNT were grown on the electrodes by chemical vapor deposition (CVD) of acetylene with a floating iron catalyst[5]. These deposited carbonaceous materials were analyzed by scanning electron microscopy (SEM, Hitachi S-3000N) and transmission electron microscopy (TEM, JEOL JEM 2000FX) measurements. The supporting carbon nanotube electrode was modified with a 4-aminophenyl monolayer and the hydrogenase was covalently bound to the amine groups through the glutamic residues. The electrode showed a very stable non-mediated catalytic $H_2$ oxidation current[3]. The catalytic current was also munch higher than the one measured on polished HOPG carbon electrodes "edge" modified in the same way[4]. The increase of the catalytic current was also in good agreement with the electroactive area of the electrodes measured by chronocoulommetry. This result confirms that only the electroactive surface sites of the MWCNT electrode are modified by the 4-aminophenyl rings. The hydrogenase-modified

MWCNT were imaged with an atomic force microscope (Nanotec Electronica, Madrid, Spain). The height and roughness difference shown in Figure 1 can be attributed to the presence of a 5 nm thick protein layer covering the modified nanotube, which is in agreement with the three dimensional structure of *D. gigas* hydrogenase[6]. All those results have been just published on Nano Letters.

**References:**

[1]  I.A.C. Pereira, C.V. Romao, A.V. Xavier, J. LeGall, A.Teixeira, *J. Biol. Inorg. Chem.* **1998**, *3*, 494-498.

[2]  Yahata, N.; Saitoh, T.; Takayama, Y.; Ozawa, K.; Ogata, H.; Higuchi, Y.; Akutsu, H., *Biochemistry* **2006**, 45, 1653-1662.

[3]  **Hydrogenase-Coated Carbon Nanotubes for Efficient H2 Oxidation**
Alonso-Lomillo, M.A., Rudiger, O., Maroto-Valiente, A., Velez, M., Rodriguez-Ramos, I., Munoz, F.J., Fernandez, V.M., and DeLacey, A.L. *Nano Lett.*, 2007,  10.1021/nl070519u  (ASAP)

[4]  Rudiger, O.; Abad, J. M.; Hatchikian, E. C.; Fernandez, V. M.; De Lacey, A. L. *Journal of the American Chemical Society* **2005**, *127*, 16008-16009.

[5]  Sampedro-Tejedor,P.; Maroto-Valiente, A.; Nevskaia, D.M.; Muñoz, V.; Rodríguez-Ramos, I.; Guerrero-Ruíz, A. *Diamond & Related Mater.*, in press.

[6]  Volbeda, A.; Charon, M. H.; Piras, C.; Hatchikian, E. C.; Frey, M.; Fontecilla-Camps, J. C. *Nature* **1995**, *373*, 580.

**Figures:**
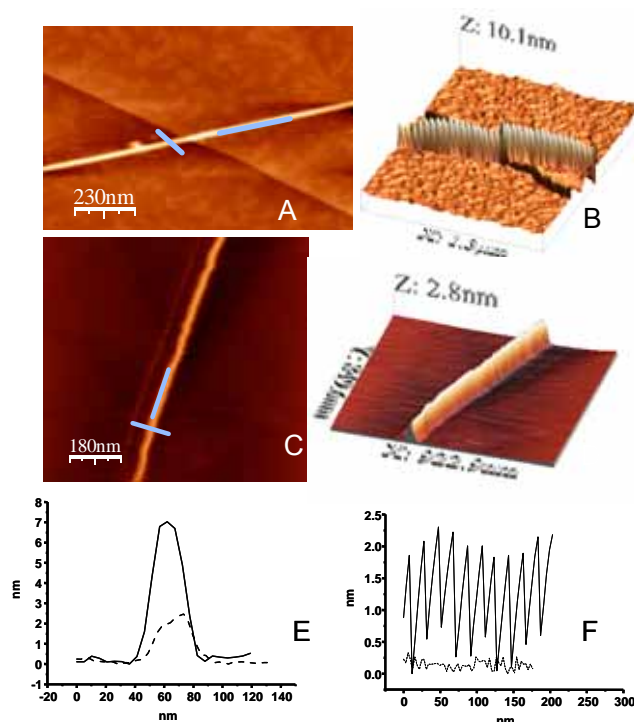


**Figure 2.** AFM characterization of the height and roughness of control MWCNT (panels C, D, and dashed line in panels E and F) and hydrogenase-coated MWCNT (panels A, B and solid line in panels E and F) deposited on highly oriented pyrolytic graphite.

# Polymer-Stabilized Monometallic Pd and Pd@Cu Core-Shell Nanoparticles: Preparation, Characterization and Electroanalytical Applications

*P. Ruiz,  J. Macanás, M. Muñoz and D.N. Muraviev*
*Analytical Chemistry Division, Department of Chemistry, Autonomous University of Barcelona, 08193 Bellaterra, Barcelona, Spain.*

*Patricia.Ruiz.Nicolas@uab.cat*

Metal nanoparticles (MNP) attract great interest of scientists and technologists due to their unique physical and chemical properties, which are distinct from both those of the bulk metal and those of isolated metal atoms. A high trend for aggregation is considered to be the main drawback of MNP, which substantially limits their practical application, as due to MNP coalesce, they lose their special shape and properties. The development of Polymer-Stabilized MNP (PSMNP) is considered to be one of the most promising solutions to the MNP stability problem [1, 2]. In many instances the electrochemical applications of MNP are based on the use of noble metals due to their unique electrocatalytic properties. One of the most important problems in this case is the decrease of the noble metal loading without dramatic change of the performance of sensing element. A possible solution of this problem is the use of core-shell PSMNP, which are composed of a cheap metal core coated with a thin noble metal shell [3, 4].

In this presentation we report the results obtained by the comparative studying electrocatalytic properties of bimetallic (core shell) Pd@Cu -MNPs with their monometallic analogs (Pd-MNPs), which have been synthesized under identical conditions by using the polymeric membranes as a nanoreactor. The intermatrix synthesis of MNPs was carried out by sequential loading of the functional groups of sulfonated poly(etherether ketone) (SPEEK) with desired metal ions followed by their reduction inside the membrane, what resulted in formation of PSMNPs of required composition and structure. Metal nanoparticles were characterized by TEM, XRD and EDS techniques to evaluate the MNPs structure and composition and to estimate their size. Typical TEM images of the Pd- and Pd@Cu-MNPs are shown in Fig. 1. As it is seen, the size of monometallic Pd-MNPs is higher than that of Pd@Cu nanoparticles, although the value of palladium loading in both cases is the same. This also clearly follows from the respective MNP size distribution histograms shown in Fig. 2. Comparison of histogram of the initial core Cu-MNPs (also shown in Fig. 2) with that of Pd@Cu-MNPs indicates that an average size of core-shell MNPs is lower than that of the core nanoparticles.

PSMNP-inks (prepared by dissolution of MNP-containing membranes in organic solvent) were deposited on the surface of graphite-epoxy composite electrodes to study the electrochemical properties of polymer-PSMNP nanocomposites and to evaluate their electrocatalytic activity. The results of these experiments are shown in Fig. 3, where the calibration curves of amperometric detection of $H_2O_2$ are presented. As it is seen, the sensitivity of sensors based on the use of Pd- and Pd@Cu-MNPs synthesized by using the same value of palladium loading differs from each other. Indeed, the amperometric response of the later is higher than that of the former at the same concentration of hydrogen peroxide. One of the possible reasons for this difference is different values of surface areas of Pd@Cu- and Pd-MNPs. Another reason can be the influence of the core-metal on the catalytic activity of the shell. However, this point requires additional clarification and we continue our research in this direction.

**References:**

[1] A.D. Pomogailo, G.I. Dzhardimalieva, A.S. Rozenberg, D.N. Muraviev, J. Nanoparticle Res., **5** (2003) 497-519.

[2]. D.N. Muraviev, Contributions to Science, 3(1) (2005) 17-30.

[3] D.N. Muraviev, J. Macanás, M. Farre, M. Muñoz, S. Alegret, Sensors & Actuators, **118(1-2)** (2006) 408-417.

[4] J. Macanas, M. Farre, M. Muñoz, S. Alegret, D. N. Muraviev, Phys. Stat. Sol. (a), 203, **6**, (2006) 1194-1200.

**Figures:**
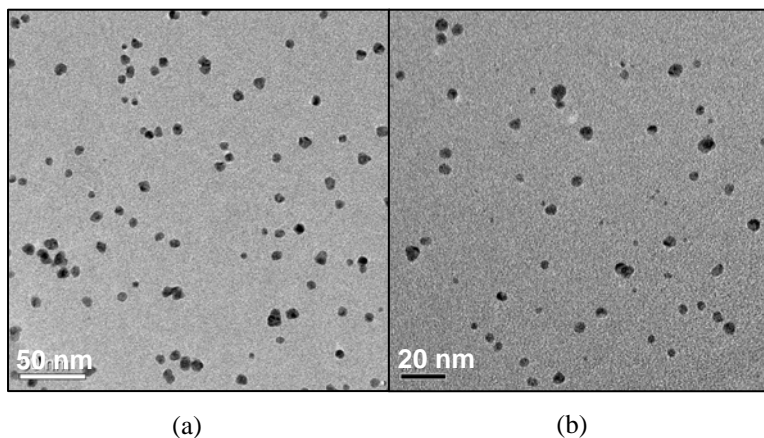


***Fig. 1:*** *Typical TEM image of Pd- (a) and Pd@Cu-PSMNPs (b) prepared by intermatrix synthesis technique.*

(a)                    (b)

***Fig. 2:*** *Typical size distribution histograms of monometallic Pd-, Cu- and bimetallic core-shell Pd@Cu-PSMNPs.*
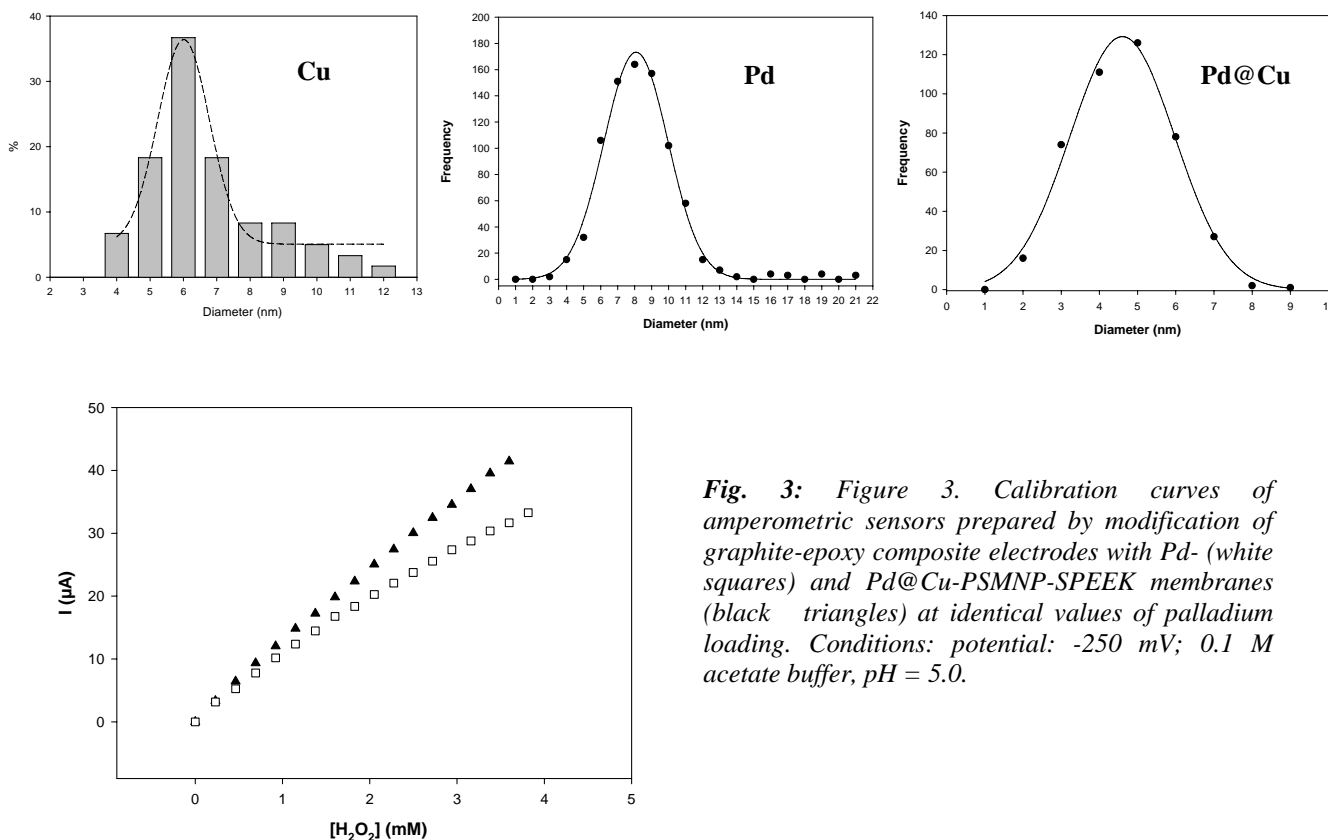




***Fig. 3:*** *Figure 3. Calibration curves of amperometric sensors prepared by modification of graphite-epoxy composite electrodes with Pd- (white squares) and Pd@Cu-PSMNP-SPEEK membranes (black triangles) at identical values of palladium loading. Conditions: potential: -250 mV; 0.1 M acetate buffer, pH = 5.0.*

# Optical fiber pH sensor formed by Neutral Red and Poly(acrylic acid) nanostructurated films.

*C. R. Zamarreño, J. Goicoechea, I. R. Matias, F. J. Arregui*
*Sensor Research Laboratory, Electrical and Electronic Engineering Department, Universidad Pública de Navarra (UPNA), Campus de Arrosadía, Edif. los Tejos, Pamplona, SPAIN.*
*carlos.ruiz@unavarra.es*

In this article we propose a new approach to the construction of a fiber optic pH sensor based on the absorbance changes of the well known Neutral Red (NR) colorimetric pH indicator [1] attached via the Layer-by-Layer (LbL) method to the polymer poly(acrylic acid) (PAA), see Figure 1. Several methods have been studied in literature to add this pH sensitive molecule (NR) to the substrate [2-3]. Here we propose the utilization of Layer-by-Layer (LbL) deposition technique, a widely studied method by our group and already used in some of our previous works [3-4]. The LbL method has attracted a great interest in the past few years and it is very suitable for our purpose due to the advantages associated with the construction of nanosized and well organized multilayer films [5]

The structure of this device is formed by the co-deposition of NR as the cationic monolayer and PAA as the anionic monolayer deposited along a bare optical fiber core section as is represented in the sensor detail of Figure 2. This bilayer structure is grown onto the optical fiber core using the LbL technique up to 15 bilayers. The construction process is monitored using the setup showed in Figure 2 by measuring the absorbance changes of the reflected optical power arrived to the spectrometer after the double transmission path across the sensitive section of the fiber. The excitation used in all measurements is a broad band white light source from 400 to 800 nm. The curves in Figure 3 represent the absorbance changes per bilayer of the $[NR/PAA]_{15}$ structure build up process. The absorbance increases almost linearly with the number of bilayers deposited as is shown in Figure 3. The growth in absorbance also occurs in the region associated to the absorbance spectrum of the NR molecule which also indicates the correct deposition of the NR small molecule. This new approach, the construction of a structure formed by a small molecule (NR) and a large chain polymer (PAA) by the LbL method, is very promising because it opens a new path to be investigated with the LbL technique and instead of using polycationic and polyanionic species (big molecules) that form a polymeric matrix which embeds the sensing indicator (small molecules) it is also possible to use a wide variety of these small molecules as monolayers of the LbL process, therefore eliminating the polymeric matrix [6].

Additionally, Figure 4 shows the changes in absorbance of the probe at 520 nm when the probe was immersed in pH 3.0 and pH 7.0 solutions alternatively. The response of the NR/PAA coatings was very fast (around a few seconds) when pH was increased from 3.0 to 7.0 while the response was slower (about 30 seconds) when the pH was decreased from 7.0 to 3.0. In addition it has been probed that this structure is suitable to be used for measuring pH in the neutral range with high precision, fast response times and repetitive signals.

**References:**

[1] M. K. Singh, H. Pal, A. C. Bhasikuttan and A. V. Sapre, Photochemistry and Photobiology, 1999, Vol. 69, No. 5, pp. 529–535.

[2] P. Hashemi, R. A. Zarjani, M. M. Abolghasemi and Å. Olin, Sensors and Actuators B, 2007, 121, pp. 396-400.

[3] F. J. Arregui, I. Latasa, I. R. Matias and R.O. Claus, Proceedings of the IEEE Sensors, 2003, Vol. 1, pp. 107-110.

[4] J. Goicoechea, C. R. Zamarreño, I. R. Matias and F. J. Arregui, E-RMS, 2006

[5] G. Decher, J. D. Hong, Phys. Chem, 1991, 210/211, pp. 831-835

[6] Y. Egawa, R. Hayashida and J. Anzai, Analytical Sciences, 2006, Vol 22, pp. 1117-1119.

**Figures:**
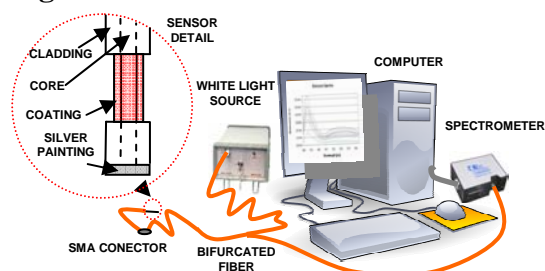


Figure 1. Experimental setup for absorbance measurement.
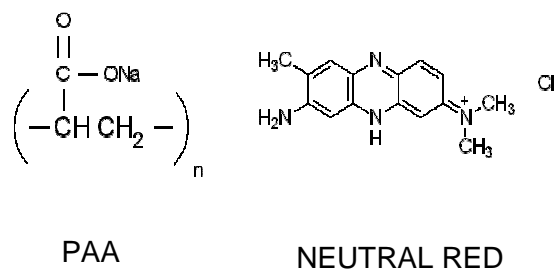


Figure 2. Molecular structure of the chemicals used in this work.
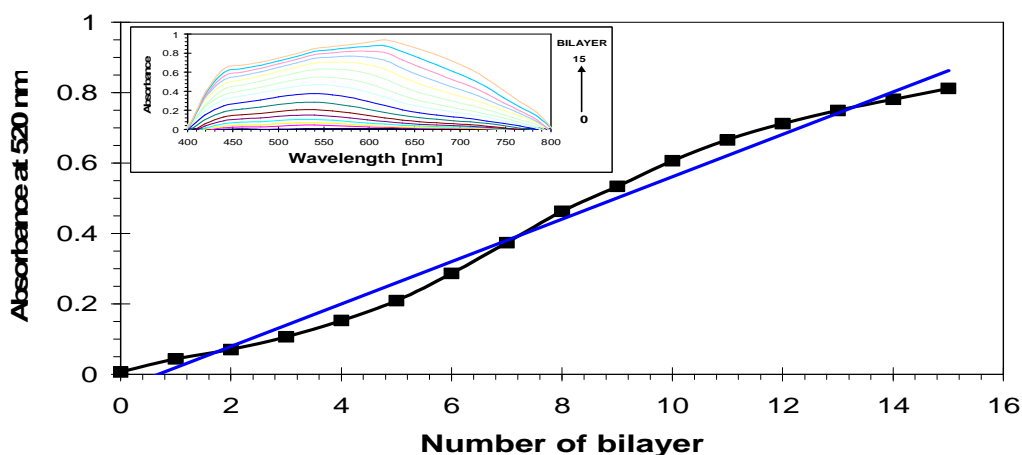


Figure 3. Absorbance at 520nm against the number of NR/PAA bilayers. Inset: Absorption spectra when the number of NR/PAA bilayers is increased.
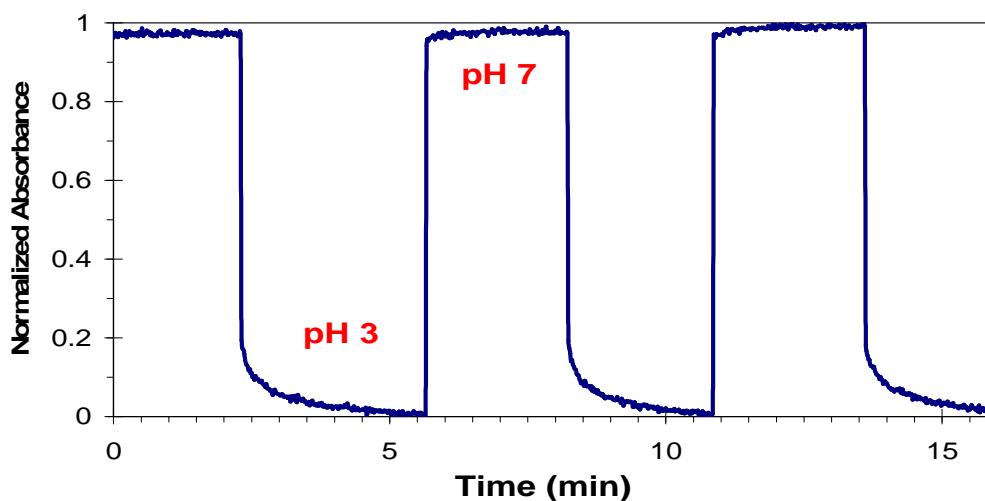


Figure 4. Normalized absorbance when the coating was alternately immersed in pH 7.0 and pH 3.0 solutions.

# SELF-ASSEMBLY OF BINARY SUPRAMOLECULAR NETWORKS ON AU(111): GEOMETRY AND ELECTRONIC STATES

*Miguel Ruiz-Osés[1], T. Kampen[2], N. González-Lakunza[3], I. Silanes[4], P. M. Schmidt[2], A. Gourdon[5], A. Arnau[3,4,6], K. Horn[2], J. E. Ortega[1,4,6].*

*[1]Departamento Física Aplicada I, Universidad del País Vasco, Plaza de Oñate 2, E-20018 Donostia-San Sebastián, Spain*
*[2]Fritz-Haber-Institut der Max Planck-Gesellschaft, Faradayweg 4-6, 14195 Berlin, Germany*
*[3]Departamento de Física de Materiales UPV/EHU, Facultad de Química, Apartado 1072, San Sebastián E-20080, Spain.*
*[4]DIPC, Manuel Lardizabal 4, E-20018 San Sebastián, Spain.*
*[5]Groupe NanoScinces, CEMES-CNRS (UPR 8011), BP 94347, 29 Rue J. Marving, 31055 Tolouse Cedex 4, France.*
*[6]Unidad de Física de Materiales, Centro Mixto CSIC-UPV/EHU, Manuel Lardizabal 3, E-20018 San Sebastian, Spain.*

*e-mail address:* [miguelruiz@ehu.es](miguelruiz@ehu.es)

One-dimensional supramolecular structures with strong heterogeneous amine/imide H bonding are self-assembled on Au(111). The 1:1 mixture of linearly shaped naphthalene tetracarboxylic diimide (NTCDI) and 1, 4-di ( 4, 6-diamino-1, 3, 5-triazin-2-yl) benzene (BDG) gives rise to two-dimensional stacks of binary chains, which can be aligned along monoatomic steps using vicinal surfaces [1]. Here we will present a broad analysis of the different structures by means of STM, photoemission, X-ray absorption, and density-functional theory, thereby providing the atomic scale characterization of the geometries and the electronic states.

**References:**

[1] M. Ruiz-Osés, N. González-Lakunza, I. Silanes, A. Gourdon, A. Arnau, J. E. Ortega, J. Phys. Chem. B 110, 25573 (2006).

# CATALYST SIZE AND CARBON FEED-RATE CONSTRAINTS FOR CARBON NANOTUBE SYNTHESIS

*M. H. Rümmeli[1], F. Schäffel[1], M. Löffler[1], C. Kramberger[1], T. Gemming[1], P. Ayala[2], A. Grüneis[1], E. Mohn[1], B. Rellinghaus[1], R. Kaltofen[1], B. Büchner[1], T. Pichler[1]*

*1. IFW Dresden, P.O. Box 270016, D-01171 Dresden, Germany.*
*2. Departamento de Fisica, PUC-Rio, CP38071, 22452-970 Rio de Janeiro, Brazil.*

*m.ruemmeli@ifw-dresden.de*

Systematic spectroscopic and microscopic studies on single-walled carbon nanotubes synthesized via laser evaporation and laser assisted chemical vapor deposition (LA-CVD) were conducted. Our findings show upper and lower diameter limits that represent a nanotube nucleation window, which can be attributed to catalyst particle volume to surface area constraints. However, the precipitating carbon saturated cluster size distribution depends solely on thermal aspects. SWCNT are only obtained when both the nucleation window and the catalyst size distribution crossover. The degree to which these two windows overlap establishes the diameter distribution of the obtained SWCNT[1]. Figure 1 illustrates the proposed model.
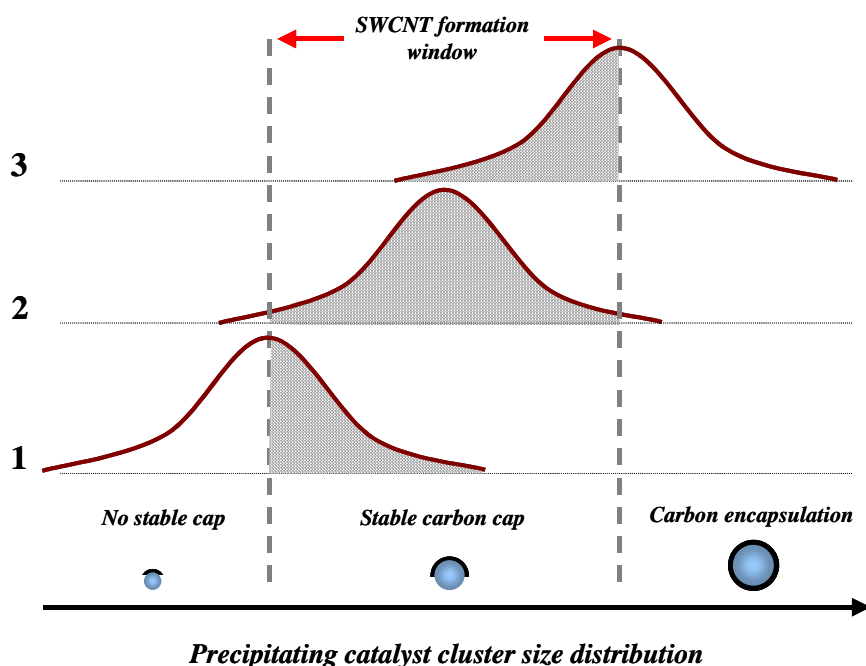


**Figure 1.** Proposed nucleation mechanism. The schematic shows the precipitating particle diameter distributions at three snapshots in time for 3 increased oven temperatures (1 to 3). Within the SWCNT formation window stable nucleation caps allow SWCNT growth. SWCNT are only formed in the overlap (shaded region) between the precipitating catalyst (size) distribution and SWCNT growth window. The degree of the overlap determines the SWCNT diameter distribution and mean diameter. Particles that are too large are encapsulated by graphite and particles that are too small are unlikely to form a stable cap.

Further the developed model points not only to catalyst geometrical constraints but also to the carbon feed rate determining if a nanotube can nucleate or not. LA-CVD pressure and feedstock flow rate experiments highlight the carbon feed-rate constraints.[2]

The same principles behind the proposed model can be applied to supported catalysts in CVD. Studies of ours in which we were able to deposit catalyst particles, as obtained from inert gas condensation, onto substrates in a controlled manner (size and density) enabled us to directly examine the catalyst particles prior to CVD synthesis and compare them with the resultant CNT in terms of their diameter and number of walls. The studies show that both the diameter and number of walls of the resultant CNT increase proportionally to the size of the catalyst particle. Figure 2 shows typical TEM images for catalyst (Fe) particles with different size distributions and their resultant CNT after CVD synthesis.[3] This behavior is fully consistent with catalyst volume to surface area constraints.
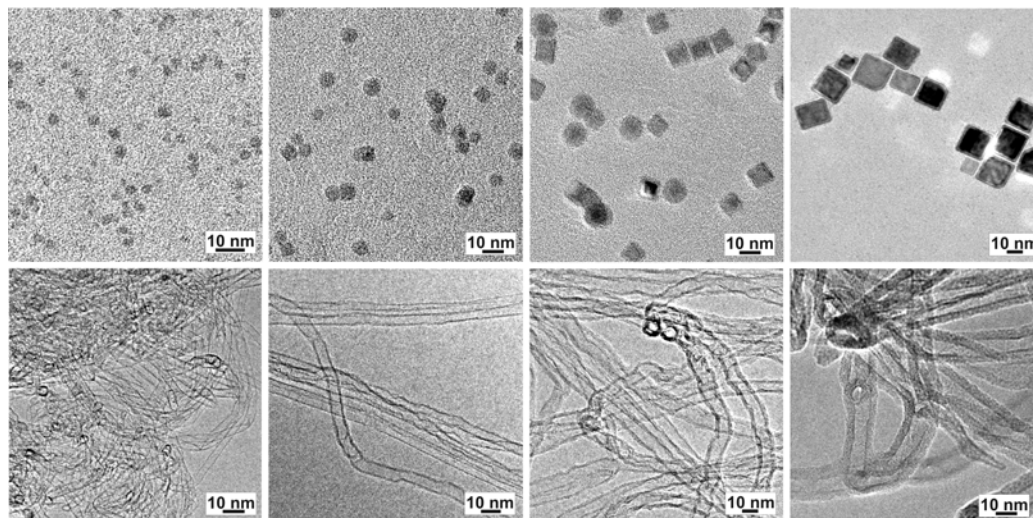


*Figure 2.* Upper panels: TEM images of the starting Fe catalyst particles. Increasing size from left to right. Lower panels, resultant CNT after CVD synthesis on $Si/SiO_2/Al_2O_3$.

In addition, our studies suggest that the root of a growing nanotube stems from the oxide support. Previous studies have shown that oxides typically used as supports in CVD can graphitize carbon in CVD synthesis conditions.[4]

**References:**

[1] Rümmeli M. H. et al., *J. Phys. Chem. B*, 111, (2007) 8243
[2] Löffler M. et al., Chem. Mat, submitted (2007)
[3] Schäffel F. et al., *phys. stat. sol. (a)*, 204 (2007) 1786
[4] Rümmeli M. H. et al., Chem. Mat., DOI 10.1021/cm0712220 (2007)

# FERROMAGNETIC NANOPARTICLES EMBEDDED IN SELF-ARRANGED MATRICES

*<u>K. Rumpf</u>[a], P. Granitzer [a], P. Pölt [b], A. Reichmann [b], H. Krenn [a]*
*[a] Institue of Physics, Karl Franzens University Graz, Universitaetsplatz 5, A-8010 Graz, Austria*
*[b] Institute for Electron Microscopy, University of Technology Graz, Steyrergasse 17, A-8010 Graz, Austria*
*klemens.rumpf@uni-graz.at*

The investigated nanoscopic system, consisting of a non magnetic host material and precipitated ferromagnetic nanostructures shows a magnetic behavior due to spin magnetism at low magnetic fields and an enhanced magnetism in the high field region. The nanostructures are deposited electrochemically into an etched silicon wafer which offers an array of channels of a few ten nanometers in diameter and a length up to 50 μm. The self-assembled grown templates offer the opportunity of tuning the magnetic properties by varying the geometrical characteristics of the membrane which is loaded with different metals like Ni, Co and NiCo alloy. The deposited metal-structures occur with different shapes between spheres and wires which determine the magnetic behavior too. At low magnetic fields the magnetization can be explained by magnetization reversal of the incorporated metal-particles. They are single domain and the reversal process occurs either by curling or homogeneous rotation depending on the size of the particles [1]. The obtained hysteresis curves are a combination of these processes because of the diversity of the deposited nanostructures. Due to the orientation of the channels perpendicular to the surface the precipitated metal offers shape anisotropy. The tunable coercivity ranges between 200 Oe and 1000 Oe for easy axis magnetization whereas hard axis magnetization exhibits half of these values. At high magnetic fields far above the saturation magnetization of the deposited metals the samples are still not saturated and show a paramagnetic-like enhancement of the magnetization curve. This supplementary magnetic term, additional to the spin magnetism at low fields, seems to be due to an enhanced orbital magnetism [2], generated by the spin polarized electrons of the transition metals which has been reported in literature [3] and is currently under investigation. This ferromagnetic nanocomposite system is not only of interest for basic research but also gives rise to applications in magneto-optics, spintronic and sensor technology.

**References:**

[1] M. Vazquez, K. Pirota, J. Torrejon, D. Navas, M. Hernandez-Velez, JMMM **294** (2005) 174.
[2] A. Hernando, P. Crespo, M. A. Garcia, Phys. Rev. Lett. **96** (2006) 57206.
[3] A. B. Klautau, S. Frota-Pessoa, Surface Science **579** (2005) 27.

**Figures:**
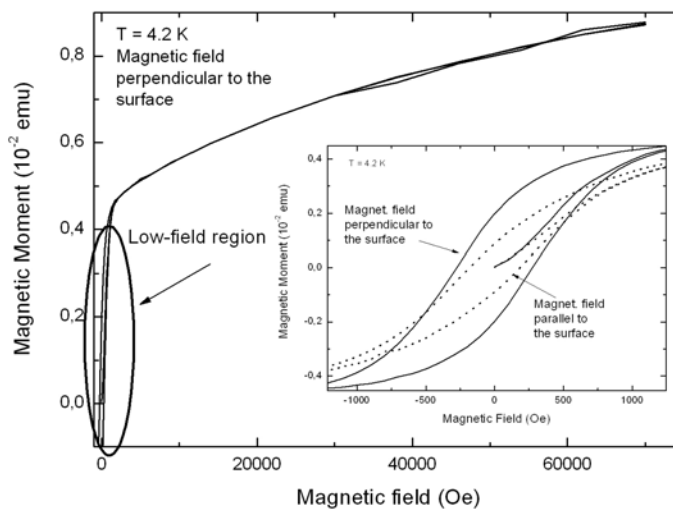


Magnetization curves of a Ni-filled sample exhibiting a non-saturating magnetic behavior at high magnetic fields far above the saturation magnetization of Ni (0.62 T). In the inset the hystereis loops for easy axis and hard axis magnetization at low magnetic fields are shown.

# ORDERED ARRAYS OF QUANTUM WIRES THROUGH HOLE PATTERNING: *AB INITIO* AND EMPIRICAL ELECTRONIC STRUCTURE CALCULATIONS

*Riccardo Rurali, Jordi Suñé, and Xavier Cartoixà*
*Departament d'Enginyeria Electrònica, Universitat Autònoma de Barcelona,*
*Campus de la UAB, Bellaterra 08193, Spain*
*Riccardo.Rurali@uab.cat*

We propose a novel method for the engineering of one-dimensional nanostructure fabrication with no need of catalyst agents. The method is based on a lithography design of a pattern of channels onto a conveniently cleaved semiconductor surface. We believe that this method opens a range of possibilities for optoelectronic nanodevices with improved efficiencies. We demonstrate by means of electronic structure calculations that when the channel diameter is sufficiently larger than the interstitial space, the resulting pillars constitute an ordered array of electronically independent, though mechanically interconnected nanowires. We also show that a controlled coupling of the nanowires can be achieved, as long as one is capable to tune, at fabrication time, the thickness of the interconnections, which are ultimately responsible of the efficiency of the quantum confinement. This method, being based on a top-down approach, would yield an ensemble of identical nanowires, grown along the same crystallographic orientation and with similar properties concerning the length and the diameter. We study different templates, where the channels are distributed according to a square or a hexagonal network, discussing the case of Si and GaAs [1]. The hexagonal distribution of channels proved to offer the best confining properties. Calculations have been performed with the Siesta *ab initio* package [2]. For a Si substrate and holes in a square disposition, we observe that states remain in the wire section. However, after widening the interconnect, laterally propagating states appear. The dispersive behaviour is conclusively determined from the observation of the band width for the bands of interest. We also present results for GaAs structures with less demanding (i.e. larger) feature sizes obtained with the Effective Bond Orbital Model. Structures with the same hole pitch can present both isolated nanowire and 2D superlattice behaviour depending on the channel diameter. The use of such structures could be easily extended to quantum well or superlattice substrates, e.g. GaAs/InGaAs or GaAs/GaAsP, leading to the fabrication of 1D heterostructures or quantum dots with potential applications as light emitting devices.

**References:**

[1] R. Rurali, J.Suñé, and X. Cartoixà, Appl. Phys. Lett. **90** (2007) 083118.
[2] J. M. Soler, E. Artacho, J. D. Gale, A. García, J. Junquera, P. Ordejón and D. Sánchez-Portal, J. Phys.: Condens. Matter **14** (2002) 2745.

**Figures:**
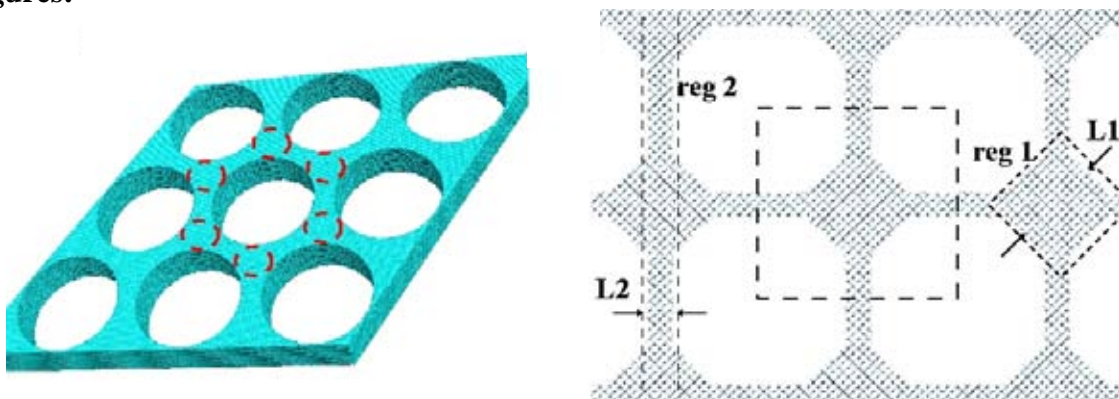


**Figure 1**: Schematic of the approach.
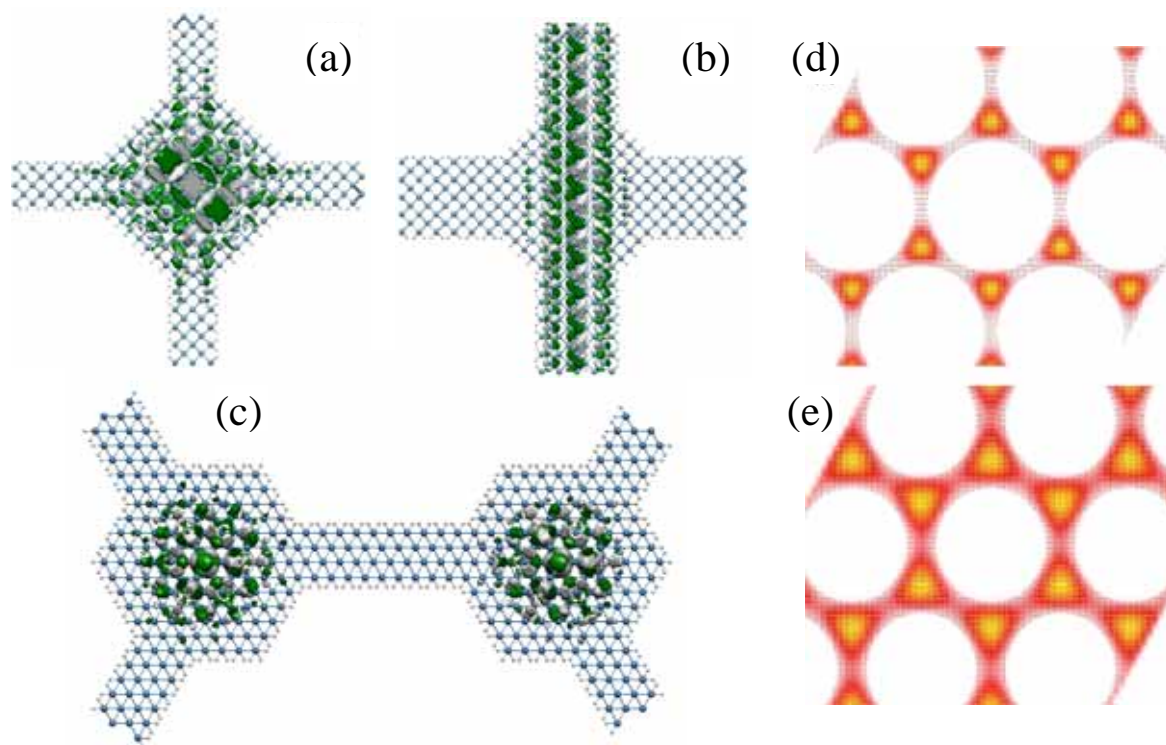


**Figure 2**: Wave-function of the lower state of the conduction band in the case of square and hexagonal arrays of channels in silicon (a,b,c) and GaAs (d,e); showing nanowire (a,c,d) and 2D (b,e) superlattice regimes.

# EFFECTS OF NANO-SIO$_2$ ON PHYSICAL PROPERTIES OF GREEN COMPOSITE

A. Sadrmomtazi,  I.Sadrinejad, H. Ghanadzadeh and A. K. Haghi[*]

The University of Guilan, P. O. Box 3756, Rasht, Iran

(*) Corresponding author, E-Mail: Haghi@Guilan.ac.ir

Recently, nano technology has attracted considerable scientific interest due to the new potential uses of particles in nanometer  scale. The nano scale-size of particles can result in dramatically improved properties from conventional grain-size materials of the same chemical composition. Thus, industries may be able to re-engineer many existing products and to design new and novel products that function at unprecedented levels. Nano-materials show unique physical and chemical properties that can lead to the development of more effective materials than ones which are currently available [1]. The extremely fine size of nano-particles yields favorable characteristics. For instance, carbon-based materials such as carbon nanotubes are becoming significant in the field of electronics because of their high surface area and excellent electrical conductivity [2]. The use of nano-particles can improve the function and properties of many types of materials. Reinforced plastics, fire-retardant materials, protective films or cloths, and high-quality coatings are among the many diverse applications of nanocomposites [3].

Application of nano-materials into the production of cement and concrete can lead to improvements in civil infrastructure because the mechanical strength and life of concrete structures are determined by the micro-structure and by the mass transfer in nano-scale [4]. In past years, superfine industrial by-products with pozzolanic and cementious properties such as fly ash, slags, and silica fume have been ingredients for high-strength cement [5, 6]. Some research suggests that silica fume is valuable for enhancing such things as mechanical properties, abrasion resistance, bond strength with steel bars, and corrosion resistance of steel bars [6]. Additional studies have also concluded that nano-SiO2 added to high-volume fly ash high strength concrete (HFAC) could improve short and long term strengths [7].

Nano-particles are unique because their size affects the behavior of cement. M.P. Ginebara et al. reported that particle size can greatly affect the kinetics of cement [8]. Their findings indicate that a reduction in particle size can lead to a more rapid setting and hardening of cement due to stronger electrostatic attractive forces and a greater specific surface [8]. Other studies have shown that the compressive and flexural strengths of cement mortars enhanced with SiO2 and Fe2O3 nano-particles or organo-modified montmorillonites (OMMT) were higher than those of plain cement mortar [1, 9]. Researchers found that nano-particles uniformly dispersed in a cement paste willaccelerate cement hydration due to their high activity [1]. Additionally, the nano-particles will fill pores to increase strength and these characteristics will improve the microstructure of cement and the interface between the cement paste and aggregates in concrete [1].

Recent studies have shown that nano-particles used as an additive to cement mortar can improve its mechanical properties; however, the behavior of cements composed exclusively of nano-particles has not yet been reported. This experiment focused on synthesizing the major components of Portland cement Type I with nano sio$_2$ (Figure 1).

Nano-sio$_2$ behaves not only as a filler to improve microstructure but also as an activator to promote pozzolanic reaction. This paper presents a research study on the properties of cement mortars mixed with nano-sio$_2$ and silica fume. The physical properties of nano-sio$_2$ cement, silica fume cement and silica fume - nano-sio$_2$ cement mortars were studied. Three different kinds of composite mortars based on substitution of cement by silica fume, nano-sio$_2$ and silica fume - nano- sio$_2$ were made and tested. The results were compared with those of control Portland cement mortars.

**References:**

[1] Hui Li, Hui-gang Xiao, Jie Yuan, Jinping Ou. Microstructure of cement mortar with nano-particles. Composites: Part B 2004;35:185-189.
[2] Vinay Gupta, Norio Miura. Influence of the microstructure on the supercapacitive behavior of polyaniline/single-wall carbon nanotube composites. Journal of Power Sources 2006;157:616-620.
[3] Y.C. Ke, P. Stroeve. Polymer-Layered Silicate and Silica Nanocomposites. Amsterdam: Elsevier B.V.; 2005. p. 52-55, 330-341.
[4] S. Hanehara, M. Ichikawa. Nanotechnology of cement and concrete. Journal of the Taiheiyo Cement Corporation 2001;141:47-58.
[5] V.G. Papadakis, E.J. Pedersen. An AFM-SEM investigation of the effect of silica fume and fly ash on cement paste microstructure. Journal of Material Science 1999;34:683-690.
[6] Zhenhua Li, Huafeng Wang, Shan He, Yang Lu, Miao Wang. Investigations on the preparation and mechanical properties of the nano-alumina reinforced cement composite. Materials Letters 2006;60:356-359.
[7] Gengying Li. Properties of high-volume fly ash concrete incorporating nano-SiO$_2$. Cement and Concrete Research 2004;34:1043-1049.
[8] M.P. Ginebra, F.C.M Driessens, J.A. Planell. Effect of the particle size on the micro and nanostructural featuresa calcium phosphate cement: a kinetic analysis. Biomaterials 2004;25:3453-3462.
[9] Wen-Yih Kuo, Jong-Shin Huang, Chi-Hsien Lin. Effects of organo-modified montmorillonite on strengths and permeability of cement mortars. Cement and Concrete Research 2006;36:886-895.

Figure 1 Nano-cement samples

# A Tuning-fork low-temperature nanotribometer

*G. Sáenz-Arce* and *C. Untiedt*

*LT-NanoLab, Departamento de Física Aplicada. Facultad de Ciencias (Fase II), Universidad de Alicante, Campus de S. Vicente del Raspeig, E-03690 Alicante, Spain.*

*giovanni.saenz@ua.es*

Quartz Tuning Fork (TF) has been in recent years successfully implemented in force detection schemes for scanning probe microscopy applications [1, 2]. Here we report its use as a nanotribometer for exploring shear and friction force in atomic size areas. The idea behind such a non contact shear and friction forces detector, is to take advantage of the mechanical resonance of a TF which has a large q-factor ($q_{air}$~6000, $q_{vac}$~40000 at room temperature) which is a function of the tip-sample dissipative forces.

We describe two models to understand the behaviour of the TF and its calibration. First, a mechanical model (fig 1, left) similar to mechanical pendulum or spring base [3]. Second, an electrical model or the Butterworth-Van Dyke circuit (fig 1, right) [4].

We used a phase locked loop (PLL) from NanoMagnetics Instruments Ltd. to measure the q-factor and the resonance frequency for various TFs. We measure the reactive forces that are associated with the combined local elastic properties of the sample and the tip, and calculated the damping rate associated with changes of the tip-sample distance.

Finally, we show some of the results using the TF-nanotribometer in Au and Pb, measuring at different temperatures from 4.2 K to room temperature in high vacuum.

## References:

[1] Khaled Karrai and Robert d. Grober, Appl. Phys., **66** (1995) 1842-1844.

[2] Khaled Karrai and Ingo Tiemann. Phys. Rev. B, **62** (2000) 13174-13181.

[3] J.M. Friedt and É. Carry. Am. J. Phys. **75** (2007) 415-422.

[4] J. Rychen, T. Ihn, P. Studerus, A. Herrmann, K. Ensslin, H. Hug, P. J. A. van Schendel, and H. J. Güntherodt. Rev. Sci. Instr. **71** (2000) 1695-1697.

## Figures:
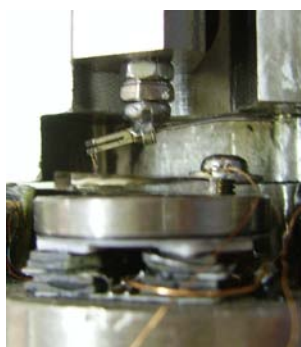


**Fig 1.** Tuning-fork low-temperature nanotribometer.
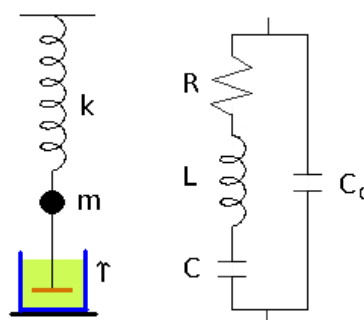


**Fig 2.** (Left) Mechanical model, m is effective mass of the fork's arms, k is static spring constant and g is the damping rate term. (Right) Electrical model.  Butterworth-Van Dyke circuit.

# Thermodynamic Based Theory for Extreme Activity of Metallic Nano-Particles

Maziar S Yaghmaee[1-2,*], Babak Shokri[1,3] and Mohammad R Rahimipour[2]

*Abstract*- **In order to understand the physics behind the extreme behavior of materials in nano-scale, one of the most important factors is to know the activity of nano-scale materials in different environments. This information comes directly from the surface cohesion binding energy of materials. We first review a simple thermodynamic-based theory for size dependence feature of surface binding energy of metallic nano-particles. Then a hypothesis for activity of metallic nano-particles through the modified classical physico chemical formalism of activity in a reactive medium will be presented. Qualitative computations for Al, Ag, Ga and W metallic nano-particles in a reactive solution shows that by decreasing the size of particles less than 100 nm, the reaction equilibrium constant and consequently the activity of particles increases.**

## THE STATE OF ART

In nano-application areas the charge, activity and stability of surface of nano-materials are the most important characteristics, for which there is still no exact formulation in literature, and our knowledge is yet based on experimental observations. The term activity in classical thermodynamic represents the active portion of concentration. Experimental observations show that respect to micro- or macro-scale, the activity of nano-materials increases [1]-[2] and this tendency increases by decreasing the size. In addition, some metallic nano-particles such as Ag show antibacterial effect [2], but others shows toxic feature [3]. These unpredicted features of nano-particles can be interrelated to their instable surface structures and extreme activity.

## MODEL OF SURFACE INSTABILITY ENERGY

Cohesion energy represents how strongly atoms or molecules stick together to hold the structure [4] and at nano-scale by decreasing the size of particle, the bulk and surface cohesion energy decrease [5]. Binding energy of atoms at surface determines the ability of surface for reaction, thus, the decrease of surface cohesion energy represents the surface instability

[1] Plasma Physics and Engineering Group, Laser and Plasma Research Institute, Shahid Beheshti University, Tehran, Iran.

[2] Materials and Energy Research Center, Tehran, Iran.

[3] Institute for Studies in Theoretical Physics and Mathematics, School of Physics, Tehran, Iran.

[*] Contacting Author: Maziar S Yaghmaee is with Plasma Physics and Engineering Group, Shahid Beheshti University, Tehran, Iran.
(phone: 0098-21-22431773; fax: 0098-21-22431775;
email: fkmsahba@uni-miskolc.hu and yaghmaee@sbu.ac.ir).

feature or in other words the reaction tendency. Figure. 1 shows the mono-layer surface model and different energy terms considered in our hypothesis. Regarding the authors' previous theory [5], a new formulation for inner and surface instability of metallic nano-particles will be presented respectively by Eq. (1) and Eq. (2), as:

$$G_p^{coh} = G_b^{coh}\left(1 - \frac{d_a}{f_v D_p}\right), \qquad (1)$$

where $G_p^{coh}$ is cohesion energy in kJ with subscript $p, b$ respectively standing for particle and bulk value, $d_a$ is diameter of atom in neutral state in nm, $D_p$ is diameter of the particle in nm, $f_v$ is the volume packing factor, and

$$G_s^{coh} = G_b^{coh}\left(\frac{7}{6} - \frac{d_a}{f_v D_p} + \frac{d_a D_p^{\ 2}}{f_s(10xD_p^2 - 12x^2 D_p + 8x^3)}\right), \qquad (2)$$

where here $s$ stands for surface value, $f_s$ is the surface packing factor, and $x$ is the actual atomic thickness of mono surface layer in nm as illustrated in Fig. 1.

## EFFECT OF SIZE ON ACTIVITY OF NANO-PARTICLES

In nano-scales by reducing the size of particles, the reaction rate and the reaction efficiently increase [6]. Here we reformulate the classical kinetics of reaction considering the size dependency of activity of metallic nano-particles in a reactive medium. Regarding Eqs. (1-2), previous results [5] and Fig. 1, in nano-scales by neglecting the entropy change, it is believed that the Gibbs free energy change is due to enthalpy (cohesion) differences [4]. This difference can be written as:

$$-H^* = \Delta_f H_B^{macro} - \Delta_f H_B^{NP} \approx G_B^{coh} - G_{B,NP}^{coh} : F(D_p) \le 0, \qquad (3)$$

where $\Delta_f H_B^{NP}, \Delta_f H_B^{macro}$ are respectively the enthalpy formation of $B$ type particle in nano- and macro-scale in kJ/mol, $H^*$ is the enthalpy difference value between the nano- and macro-scale and $F(D_p)$ represents the size dependency function.

The reaction of a metallic nano-particle with atoms/molecules of a medium leads the formation of either a surface layer or

release of ions/atoms from particle. Thus, the extended classical physics of reactions, considering the increase of equilibrium constant due to surface instability and higher activity of particle in nano-scale respect to macro-scale, can be formulated as:

$$as\ K = \exp\left(\frac{-\Delta_r G}{R \cdot T}\right) \Rightarrow K^{NP} = K \cdot \exp\left(\frac{b \cdot H^*}{R \cdot T}\right), \qquad (4)$$

where $K, K^{NP}$ are the reaction constant for macro- and nano-scale respectively; $\Delta_r G$ is the change of Gibbs free energy change of reaction in kJ/mol, $R$ is the universal gas constant, $T$ is the temperature in absolute scale, and $b$ is stoichiometric number related to nano-particle of $B$ type in our reaction.

Using the results of Eq. (3), we rewrite the Eq. (4), as:

$$\frac{K^{NP}}{K} = \exp\left(\frac{b \cdot H^*}{R \cdot T}\right) \approx \exp\left(\frac{b \cdot (G_{NP}^{coh} - G^{coh})}{R \cdot T}\right) \geq 1. \qquad (4)$$

Figure. 2 shows computation simulation for Al, Ag, Ga and W metallic nano-particles for $b = 1$. One can see that for example at 50 nm Al, Ag, Ga and W metallic nano-particles respectively the

rate of increase of $K$ (represented by $K / K^{NP}$) is 1.280, 1.279, 1.424 and 1.295 respect to macro-scale. It should be noticed that this value increases by decreasing the nano-particle size due to activity increase, which conforms experiential observations.

## REFERENCES

[1] G. M. Whitesides, "The 'right' size in nanobiotechnology," *Nature Biotechnology*, No. 10, Vol. 21, pp. 1161-1165, Oct. 2003
[2] S. Y. Yeo and S. H. Jeong, "Preparation and characterization of polypropylene/silver nanocomposite fibers," *Polymer International*, 52, pp. 1053-1057, 2003
[3] P. HM Hoet, I. Brüske-Hohlfeld and O. V. Salata, "Nanoparticles – known and unknown health risks," *J. Nanobiotechnology*, 2:12, pp. 1-15, 2004
[4] G. Kaptay, G. Csicsovszki and M. S. Yaghmaee, "An absolute scale for the cohesion energy of pure metals," *Mater.Sci. Forum*, Vols. 414-415, pp. 235-240, 2003
[5] M. S. Yaghmaee and B. Shokri, "Effect of size on bulk and surface cohesion energy of metallic nano-particles," *Smart Mater. Struct.* 16, pp. 349-354, 2007
[6] A. Zaluska, L. Zaluski and J. O. Ström-Olsen, "Structure, catalysis and atomic reactions on the nano-scale: a systematic approach to metal hydrides for hydrogen storage," *Applied Physics*, A 72, pp. 157-165, 2001
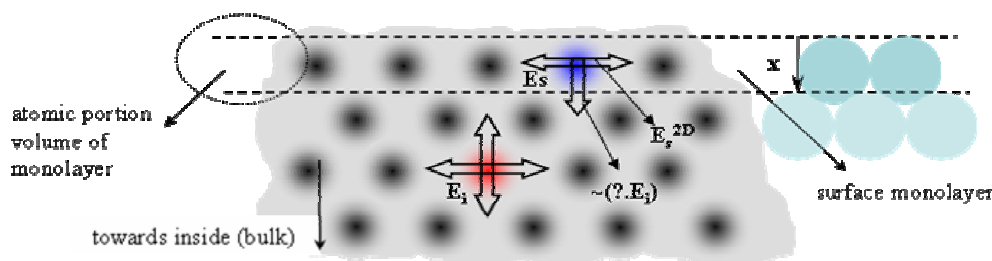
Fig. 1 Schematic representation of bulk and surface of metallic nano-particles considering different binding energies.
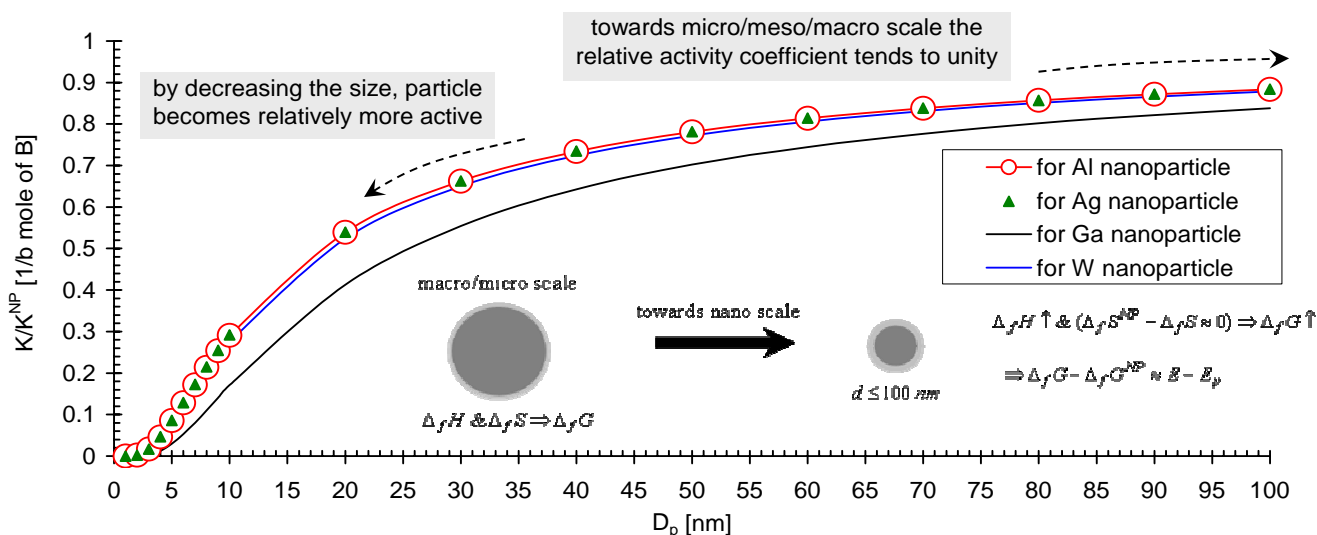


Fig. 2 Relative representations of size dependency effect on activity of Al, Ag, Ga and W nano-particles in a reactive medium.

# PIXE and RBS Investigation of Growth Mechanism of Nanocrystalline Chemical Bath Deposited ZnS Thin Films

*R. Sahraei[1,3], G. Motedayen Aval[1], A. Baghizadeh[2], M. Lamehi-Rachti[2], and A.Goudarzi[1]*

[1]*Physical Chemistry Department, Faculty of Chemistry, Tarbiat Moallem University, 49 Mofatteh Avenue, Tehran, Iran*
[2]*Van de Graaff Laboratory, Nuclear research center, AEOI, P. O. Box 14155-1339, Tehran, Iran*
3*Chemistry Department, Faculty of Science, Ilam University, Pajhohesh Avenue, Ilam, Iran*

r_sahraei@tmu.ac.ir

**Abstract:** In recent years, nanocrystalline ZnS thin films have received much attention because of their very important role in the photovoltaic technology and optoelectronic devices [1]. They are presently used as buffer layers in several types of thin film solar cells, such as $Cu(In,Ga)Se_2$ (CIGS) and $Cu(In,Ga)(SeS)_2$ (CIGSS) [2]. Chemical bath deposition is a suitable method for the deposition of some metal chalcogenide thin films [3-5]. In this work nanocrystalline ZnS thin films, with thicknesses typically 10-100 nm, have been chemically deposited on glass and silicon substrates using an ammonia free reaction solution, where ethylenediamine acts as a complexing agent for zinc ions and thioacetamide acts as a source of sulfide ions. Film elemental composition, thickness and homogeneity have been examined using particle-induced X-ray emission in conjunction with a two dimensional micro-beam probe and Rutherford backscattering. Compositional analysis indicates that the pH of deposition solution plays a critical role in ZnS thin film growth. Films deposited in the acidic solution (4<pH<7) show a consistent 1:1 Zn:S atomic ratio of the film, and have good substrate adhesion. Those deposited in a basic solution (7<pH<10) show a consistent 1.3:1 Zn:S ratio and have weak adhesion to the substrate. A mechanism is proposed to explain this difference in film composition and properties. The results obtained from the 2D micro-probe scan images approves that finding too. Furthermore, morphological characteristics and surface roughness of thin films have been investigated by atomic force microscopy.

**References:**
[1] T. Nakada, M. Mizutani, Y. Hgiwara, A. Kunioka, Solar Energy Materials & Solar Cells **67** (2001) 255.
[2] A. Ennaoui, W. Eisele, M. Lux-Steiner, T. P. Niesen, F. Karg, Thin Solid Films **431- 432** (2003) 335.
[3] A. M. Chaparro, C. Maffiotte, M. T. Gutierrez, J. Herrero, Thin Solid Films **358** (2000) 22.
[4] R. S. Mane, C. D. lokhande, Mater. Chem. Phys. **65** (2000) 1.
[5] K. Yamaguchi, T. Yoshida, D. Lincot, H. Minoura, J. Phys. Chem. **B 107** (2003) 387.

# SYNTHESIS CONTROL AND MAGNETIC PROPERTIES OF CORE-SHELL Fe$_3$O$_4$@Au NANOPARTICLES.

*J. Salado, M. Insausti, I. Gil de Muro, L. Lezama and T. Rojo*
*Dpto. Química Inorgánica, U.P.V.-E.H.U., Apdo. 644, 48080, Bilbao, Spain*
*bcbsarij@ehu.es*

The preparation of size controlled metal-coated magnetic nanoparticles is increasingly important for exploring technological applications in different areas. Iron oxide nanoparticles have been studied as magnetic resonance contrast agents, in high-density magnetic recording or controlled drug delivery [1]. Gold coated magnetic nanoparticles enhance chemical stability and exhibit good biocompatibility [2]. Along the same line, we present controlled sized iron oxide nanoparticles coated with a gold shell and stabilized with oleic acid and oleylamine.

The preparation of Fe$_3$O$_4$@Au nanoparticles involved the previous synthesis of Fe$_3$O$_4$ from Fe(acac)$_3$ in the presence of 1,2-hexadecanodiol, oleic acid and oleylamine [3]. The reduction of Au(OOCCH$_3$)$_3$ in the presence of as-synthesized iron oxide seeds, with sizes of 5.7(3) and 3.6(2) nm, yield gold coated nanoparticles in the 5–7 nm range, surrounded by organic ligands. The synthesis method, iron and gold concentration and the nature of the solvents used for separation have been changed in order to optimize the preparation method. The characterization of the samples was performed by means of X-ray diffraction (XRD), transmission electron microscopy (TEM) and thermogravimetric analysis (TGA). Magnetic properties have been investigated using electron paramagnetic spectroscopy (EPR) and SQUID magnetometer.

The presence of Fe$_3$O$_4$ and gold was confirmed by XRD and the concentrations of the metals by energy-dispersive X-ray analysis. Transmission microscopy has shown particle sizes below 7 nm (Fig. 1), as well as a narrow size distribution. The nanoparticles contain between 10 -15% of capped ligands, as was observed in the TG-DTA curves of the samples recorded in air atmosphere.
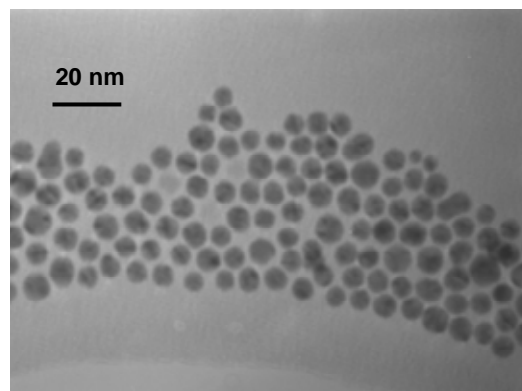


Fig. 1. TEM picture of Fe$_3$O$_4$@Au NPs.

Magnetic measurements show a different behavior depending on the nanoparticle size. For samples of 7.5 nm a ferromagnetic behavior is observed at room temperature. EPR measurements of these particles show a broad signal, which show an orientational dependence of the ferromagnetic resonance. An exhaustive study with temperature and orientation has been performed. Nanoparticles with lower size present susceptibility plots which exhibit a cusp in the ZFC curve, which corresponds to the blocking temperature, T$_B$. Above T$_B$, in the superparamagnetic regime no hysteresis loop is observed.

**References:**

[1] S. Mornet, S. Vasseur, F. Grasset, E. Duguet, J. Mater. Chem. **14** (2004) 2161.
[2] J.M. de la Fuente, D. Alcántara, P. Eaton, P. Crespo, T.C. Rojas, A. Fernández, A. Hernando, S. Penadés J. Phys. Chem. B **110** (2006) 13021.
[3] L. Wang, J. Luo, Q. Fan, M. Suzuki, I.S. Suzuki, M.H. Engelhard, Y. Lin, N. Kim, J.Q. Wang, C-J. Zhong, J. Phys. Chem. B **109** (2005) 21593.

# NANOLAYERS FOR OPTOELECTRONIC DEVICES BASED ON PEDOT FORMULATIONS IN ORGANIC MEDIUM

[1]Salsamendi, M.;[1] Pozo-Gonzalo, C.[*]; [1]Pomposo, J.; [1]Marcilla, R.; [1]Mecerreyes, D.; [1] Rodriguez, J.; [2]Bolink, H.

*[1]CIDETEC, Paseo Miramón, 196, San Sebastián, Spain*

*[2] Instituto de Ciencia Molecular (ICMoI), Universidad de Valencia, P.O. Box 22085, 46071 Valencia ,Spain.*

cpozo@cidetec.es

Polymer electronics has attracted a lot of attention in the past decade due to potential applications in novel optoelectronic devices such as organic light emitting diodes (OLEDs), photovoltaic (FV) and electrochromic (EC) devices.[1] The main reason for using conducting polymers in polymer electronics is related to light weight, high flexibility and the possibility of manufacturing all-plastic devices.[2] Intrinsically conducting polymers (ICPs) have received a great deal of investigation due to the important properties such as high conductivity, low cost and weight, and mechanical durability.[3] From all conducting polymers, polythiophenes are one prominent class of ICPs present in the market due to the high stability to moisture in both doped and undoped state. Specially, a derivative from polythiophene, poly(3,4-ethylenedioxythiophene) (PEDOT), has emerged as a promising material for optoelectronic devices due to many advantageous properties such as high transparency in the visible range, excellent thermal stability, electric conductivity and optoelectronic performances.[4,5,6] Current issues under investigation are the improvement in processability, for instance attaining conducting polymers soluble in organic solvents (formulations), enhancement of the electrical conductivity of the films, as well as the tuning of the hydrophobic/hydrophilic properties.

In this communication, we report some of our work related to the synthesis of novel PEDOT formulations for different optoelectronic applications[7] such as transparent electrodes, organic light emitting diodes and electrochromic devices (Figure 1).

a)                                    b)                                    c)
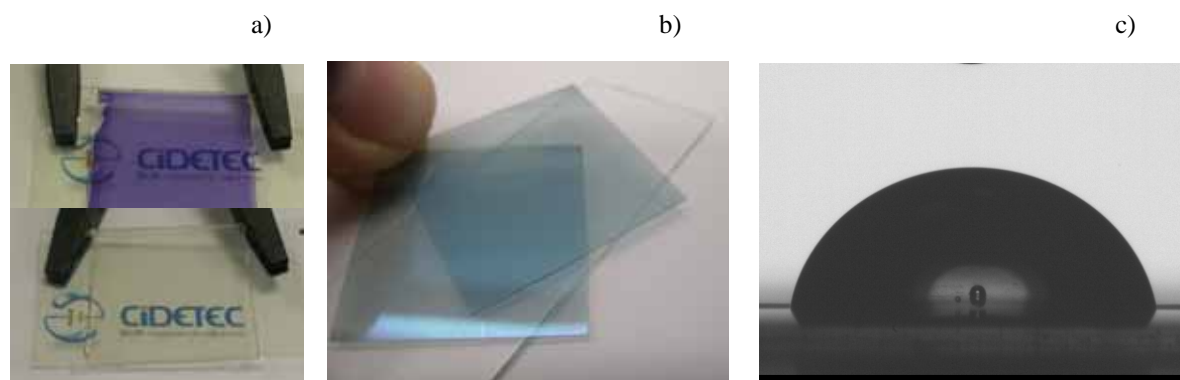


**Figure 1** Nanolayers for optoelectronic devices prepared at CIDETEC. a) Electrochromic device prepared on plastic substrate, b) transparent and conductive layer based on PEDOT on plastic substrate, c) hydrophobic character of PEDOT formulations on plastic substrate.

Hence, commercial PEDOT:PSS formulations in water have been modified using water soluble ionic liquids as secondary dopants to enhance the conductivity in order to replace traditional ITO as transparent electrode.[8] Nanolayers of pure PEDOT:PSS (Baytron P HC V4) prepared by spin coating showed an average conductivity of 14.5 S/cm, which upon addition

of a minor percentage of ionic liquid based on imidazolium cation was significatively enhanced to give a final value of 136 S/cm. Furthermore, PEDOT formulations in organic solvents such as acetonitrile and dimethylformamide have been prepared using stabilizers based on poly (1-vinyl imidazolium) (typical particle size < 50 nm). Several formulations have been developed depending on the final properties desired. These organic formulations have been electrochemically characterised and successfully tested in both OLEDs[9] and electrochromic devices[10] with promising results. The most relevant ones include optical contrast as high as 44% in the visible region with switching time in the order of seconds for electrochromic devices, conductivity in the range of $10\text{-}10^{-3}$ S/cm and increased hydrophobic character of the optoelectronic nanolayers.

## References

[1] a) Scharber, M.C.; Wuhlbacher, D.; Koppe, M.; Denk, P.; Waldauf, C.; , Heeger, A.J.; Brabec, C.L.; Adv. Mater. **18** (2006) 789; b) Granstrom, M.; Petritsch, K.; Arias, A.C.; Lux, A.; Andersson, M.R.; Friend, R.H. Nature. **395** (1998) 257; c) Coakley, K. M.; McGehee, M. D. Chem. Mater. **16** (2004) 4533.

[2] Ouyang, J.; Chu, C-W.; Chen, F-G.; Xu, Q.; Yang, Y., Adv. Funct. Mater.; **12** (2005) 203.

[3] Wnek, G.E. In handbook of conducting polymers; Skotheim, T.J., Ed.:New York, 1986, 205.

[4] Kirchmeyer, S.; Reuter, K.*;* J. Mater. Chem.; **15** (2005**)** 2077.

[5] Kim, TY.; Kim, JE.; Suh; KS.; Polym. Int.; **55** (2006**)** 80.

[6] Heywang, G.; Jonas, F.; Adv. Mater., **4** (1992) 117.

[7] Marcilla, R.; Ochoteco, E.; Pozo-Gonzalo, C.; Grande, H.; Pomposo, J. A.; Mecerreyes, D.; Macromolecular Rapid Communications, **26** (2005)1122.

[8] Döbbelin, M.; Marcilla, R.; Salsamendi, M.; Pozo-Gonzalo, C.; Pomposo, J. A.; Mecerreyes, D.; Chemistry of Materials **19**(2007) 2147.

[9] Pozo-Gonzalo, C.; Marcilla, R.; Salsamendi, M.; Mecerreyes, D.; Pomposo, J. A.; Rodriguez, J.; Bolink; HJ.; Macromolecules, en preparación

[10] Pozo-Gonzalo, C.; Mecerreyes, D.; Pomposo, J.A.; Salsamendi, M.; Marcilla, R.; Grande, H; Vergaz, R.; Barrios, D.; Sánchez-Pena, J, Solar energy Materials and Solar Cells, 2007, ASAP.

# PULSE-INDUCED SPIKING IN ARTIFICIAL NERVE NANOFIBRES

*A.S. Samardak[1], S. Taylor[1], A. Nogaret[1], G. Hollier[2], J. Austin[2], D.A. Ritchie[3]*

*[1]Department of Physics, University of Bath, BA2 7AY, UK*

*[2]Department of Computer Science, University of York, YO10 5DD, UK*

*[3]Cavendish Laboratory, University of Cambridge, CB3 0HE, UK*

*asamardak@gmail.com*

Biological neurons encode information in both the firing rate and the timing of electrical impulses[1] (spikes). An input stimulus has the effect of triggering spiking patterns whose rate increases with the stimulus intensity. As a result, the firing rate may be said to encode the amplitude of the stimulus. Within a spike train the timing of spikes usually fluctuates by a few milliseconds. Since, neurons are sensitive to the precise timing of spikes, it has been suggested[2] that neurons separately encode information in the phase of spikes. Neurons control the phase difference between spikes by using nerve fibres, i.e. dendrites and axons, as transmission delay lines.

Here we propose a spatially structured artificial neuron that is similarly able to compute the phase difference introduced by its dendrites. The timing of spikes and the firing rate are believed to channel information independently, yet the former offers subtler and more interesting coding possibilities. Spike timing is currently stimulating mathematicians to develop general purpose programming languages for parallel neural calculators[4].

From a technological standpoint, our artificial neuron is the first active device specifically designed for parallel spike computation[5-7]. It solves the key issues of signal transmission, neuronal coding and synaptic plasticity that allow one to build pulse-timing networks.

It has been shown[8] that semiconductor *pn* nanowires are a remarkable novel medium for propagating action potentials in the solid state. The diffusion equation continuously integrates voltage transients in time and space, hence artificial neurons can be built that perform calculations in real time using the laws of Physics.

We have fabricated neurons based on two GaAs *pn* junctions grown by molecular beam epitaxy. The donor and acceptor doping concentrations were $N_A=N_D=5\cdot10^{22}\text{m}^{-3}$ (low doped) and $N_A=N_D=5\cdot10^{23}\text{m}^{-3}$ (high doped). The *n*- and *p*-type electrodes formed thin metallic strips on both sides of the depletion layer. Lithography, etching and deposition techniques were then implemented to fabricate a neuron with the freestanding nanowire shown in Fig.1. The nanowire has *n*- and *p*-type Ohmic contacts at regular intervals along its length. Individual layers were contacted by etching mesas to appropriate depth and by depositing cold-annealed Pd(60nm)/Ge(120nm)/Au (*n*-type) and Ti(33nm)/Pd(30nm)/Ti(33nm)/Au (*p*-type) Ohmic contacts. The *pn* junction was found to rectify with knee voltage of ~1V. The wire was undercut by milling lateral trenches with reactive ion etching. A citric acid solution $C_6H_8O_7(4) : H_2O_2(1)$ was then applied to selectively etch the GaAs substrate underneath the stop etch layer.

We obtained the spike amplitude decays exponentially (Fig.2) from the input on a length scale of 2-4 mm which corresponds to the diffusion length as predicted from theory. We found pulse velocities of 5-20 km/s in the range 100 kHz - 10 MHz. We have applied digital pulse trains at opposite ends of the neuron to measure their interferences at intermediate points of the composite structure, Fig.3. Spike trains arriving in phase at a given node interfered with the resulting amplitude equaling the sum of the two individual pulses measured separately at the respective node, Fig.3a. By contrast, the positive and negative spike trains in phase interfered with the resulting amplitude being close to zero, Fig.3b.

In summary, *pn* nanowires were shown to act as transmission delay lines and to perform the spatio-temporal integration of multiple spike trains. The trends in our results are qualitatively

described by the properties of the diffusion equation where ideal *pn* junction behavior is assumed. These results make possible spike timing artificial neurons for parallel computation based on spike trains.

**References:**
[1] W.Gerstner, W.M.Kistler, Spiking Neuron Models, CUP (2002)
[2] W.Softky and C.Koch, J.Neurosci. **13**, 334 (1993)
[3] M.Konishi, Sci.Am. **268**, 66 (1993)
[4] A.Carnell and D.Richardson, preprint May 2005, see www.bath.ac.uk/~masdr/par_1.pdf
[5] A.F.Murray, IEEE Micro **9**, 64 (1989)
[6] D.D.Coon and A.G.U.Perrera, Neur.Net. **2**, 143 (1989)
[7] S.C.Liu, J.Kramer, G.Indiveri, T.Delbrück, T.Burg, R.Douglas, Neur.Net. **14**, 629 (2001)
[8] A.Nogaret, N.J.Lambert, S.J.Bending, J.Austin, Europhys.Lett. **68**, 874 (2004)

**Figures:**
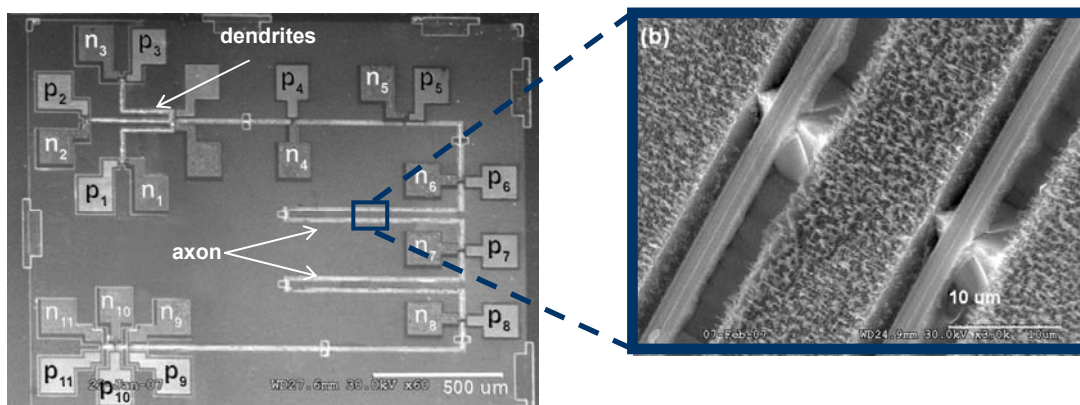


Fig.1. (a) – STM image of the GaAs-based neuron comprises of three dendrites, an axon and eleven pairs of Ohmic contacts ($n_i$, $p_i$). (b) – The inset shows the fragment of the free-standing nanowire based on supporting bridges. The nanowire length is 6 mm, the width is 2 μm and the thickness is 320 nm and 140 nm for low and high doped neurons respectively.
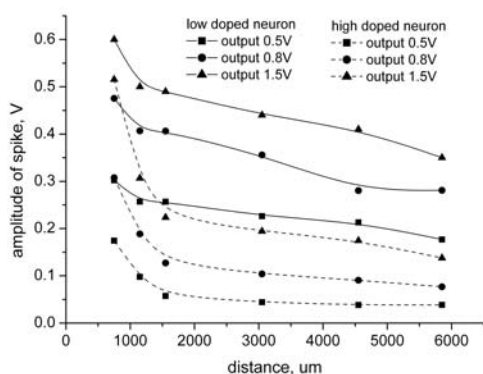


Fig.2. The attenuation of spike amplitude with wire distance dependent on output voltage. Diffusion lengths are 2 and 4 mm for low and high doped neurons respectively.
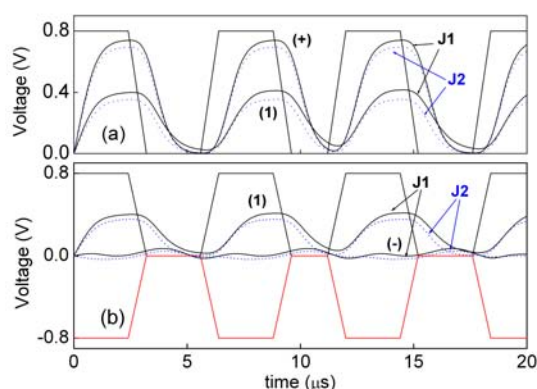


Fig.3 (a) – The result of spike interference when two square pulse trains in phase were applied to the neuron at n6-p6 and $n_8$-$p_8$ contacts. Curves (1) indicate the individual spike trains for low doped (J1) and high doped (J2) neurons. Curves (+) indicate the amplitude of a spike train from the summation of two individual spike trains. The resulting amplitude was measured at the mid-point ($n_7$-$p_7$) between the input contacts. (b) – The result of spike annihilation when positive and negative square pulses were applied to the input contacts (n6-p6 and $n_8$-$p_8$). Curves (-) indicate the amplitude of spike train from the summation of two individual spike trains.

# MOLECULAR DYNAMIC STUDY OF THE N-A-S-H GEL IN ALKALI-ACTIVATED FLY-ASHES CEMENTS.

*J. S. Dolado* [1,2], *H. Manzano*[1], *J. Hamaekers* [3], *M. Griebel* [3], *A.Palomo*[4,2].
*[1] LABEIN-Tecnalia, Parque Tecnológico de Bizkaia, Derio, Spain.*
*[2] Nanostructured and Eco-efficient Materials for Construction Unit, Associated Unit LABEIN-Tecnalia/CSIC, Derio, Spain.*
*[3] Institut for Numerical Simulation, University of Bonn, Wegelerstraße 6, D-53115 Bonn, Germany*
*[4]Eduardo Torroja Institute (CSIC), 28080 Madrid, Spain.*
*jsanchez@labein.es*

Ordinary Portland Cement (OPC) is one the most employed materials in construction and its importance is beyond any doubt. The main component of the cement paste is the Calcium Silicate Hydrated (C-S-H) gel, which is the principal responsible for the cohesion and hardness of the final cementitious material. This C-S-H gel is an amorphous product, with variable composition, although it has some order at the nanoescale [1, 2]. This variable and amorphous nature implies difficulties in the characterization, and many aspects of the atomic- and nano-structure of the C-S-H gel remain unclear. Fortunately recent atomistic simulations have provided crucial information such as the number of Si-OH and Ca-OH bonds, the length of silicate chains, or degree of polymerization for different Ca/Si ratios [3], and present themselves as a promising tool to shed light on the nanostructure of CSH gels.

Parallel to the OPC, the interest in new types of cement is increasing. The durability, mechanical properties, design and even esthetical requirements for cementitious materaials are increasing continuously. Other important aspects are the sustainability of the manufacture process and wastes recycling. One of the most promising alternatives are the alkali-activated fly-ashes cements. Analogous to the C-S-H gel in OPC, an amorphous reaction product is obtained in the curing process of alkali-activated fly-ashes cements, the N-A-S-H gel. It has a disorder network structure related to that of zeolites, based in silicon-aluminium-sodium and water. The N-A-S-H gel has a similar function to the C-S-H gel, being the main responsible of the properties of the material [4, 5]

The nanostructure of the C-S-H gel has been recently studied by Molecular Dynamics simulations providing useful information. Some important parameters as the number of Si-OH and Ca-OH bonds, length of silicate chains, or degree of polymerization were studied for different Ca/Si ratios [3] finding a reasonable agreement with the experimental evidence. In this work we apply the same scheme to study the nanostructure of N-A-S-H gel. For this purpose, three different samples with different Si/Al ratios (1.5, 1.75 and 2) will be studied by means of Molecular Dynamics simulations, with the Tremolo code [6]. To this end, both important chemical parameters such as the as the number of Si-OH, Al-OH and Na-OH bonds and the connectivity of the (alumino)silicate structures will be analysed.

**References:**

[1] H. F. W. Taylor, Cement Chemistry, 2nd ed., Thomas Telford, London, (1997)

[2] I. G. Richardson, "Tobermorite / jennite and tobermorite / calcium hydroxide-based models for the structure of C-S-H: Applicability to hardened pastes of tricalcium silicate, b-dicalcium silicate,Portland cement, and blends of Portland cement with blast-furnace, metakaolin, or silica fume," Cement and Concrete Research, **34** (2004)1733-1777.

[3] A. Palomo, M. W. Gurutzeck, M. T. Blanco, Alkali-activated fly ashes. A cement for the future. Cement and Concrete Research, **29** (1999) 1323-1329.

[4] A.Fernández-Jimenez, A.Palomo, Mid-infrared spectroscopic studies of alkali-activated fly ash structure. Microporous and Mesoporous Materials, **86** (2005) 207-214.

[5] J. S. Dolado, J. Hamaekers, M. Griebel. A molecular dynamics study of cementitious silicate hydrate (C-S-H) gels. Journal of the American Ceramic Society. (2007). Accepted. Also available as INS preprint No. 0701.

[6] M. Griebel, S. Knapek, G. Zumbusch, and A. Caglar, "Numerische Simulation in der Moleküldynamik; Numerik, Algorithmen, Parallelisierung, Anwendungen"; Springer, Berlin,Heidelberg, 2003.

# WATER ADSORPTION ON O(2X2)/Ru(0001)

*Pepa Cabrera-Sanfelix[1], Daniel Sánchez-Portal[2], Aitor Mugarza[3,4], Tomoko K. Shimizu[3,5], Miquel Salmeron,[3,5] and Andrés Arnau[2,6]*

[1] *Donostia International Physics Center (DIPC), Manuel de Lardizabal 4, San Sebastian, Spain.*
[2] *Unidad de Física de Materiales, Centro Mixto CSIC-UPV, Manuel de Lardizabal 4, San Sebastian 20018, Spain*
[3] *Materials Sciences Division, Lawrence Berkeley National Laboratory, University of California, Berkeley CA 94720/ USA*
[4] *Institut de Ciencia de Materials de Barcelona, CSIC, Bellaterra, Spain 08193*
[5] *Department of Materials Science and Engineering, University of California Berkeley, CA94709. USA*
[6] *Departamento de Física de Materiales UPV/EHU, Facultad de Química, Apartado 1072, San Sebastián 20080, Spain*
*sqbsapod@sc.ehu.es*

We present a combined theoretical and experimental study of water adsorption on Ru(0001) pre-covered with 0.25 monolayers (ML) of oxygen forming a (2x2) structure. Several structures were obtained by means of Density Functional Theory calculations for which STM simulations were performed and compared with experimental data.[1] Up to 0.25 monolayers the molecules bind to the exposed Ru atoms of the 2x2 unit cell via the lone pair orbitals. The molecular plane is almost parallel to the surface with its H atoms pointing towards the O atoms of the 2x2 unit cell with which they form H-bonds. The adsorption energy of this configuration is approximately 616 meV, which is 220 meV more stable than on the clean surface in a similar configuration.[2,3] This is due to the additional H-bonds with the O atoms of the unit cell. The energy shows only a weak dependence on water coverage, with a shallow minimum for a row structure at 0.125 ML. This is consistent with the STM experiments that show a tendency of the molecules to form rows at intermediate coverage. Our calculations also suggest the possible formation of water dimers near 0.25 ML.

**References:**

[1] Cabrera-Sanfelix, P.; Sanchez-Portal, D.; Mugarza, A.; Shimizu, T. K.; Salmeron, M.; Arnau, A. *Physical Review B. submitted* 2007.
[2] Michaelides, A.; Alavi, A.; King, D. A. *Journal of the American Chemical Society* 2003, **125**, 2746-2755.
[3] Feibelman, P. J. *Science* 2002, **295**, 99-102.

# INFLUENCE OF PHASE SEPARATION ON THE ROOM TEMPERATURE MECHANICAL PROPERTIES OF PM 2000 ODS ALLOY

*C. Capdevila[1], M. K. Miller[2], J. Aldazabal[3], I. San Sebastián[3], J. Chao[1], J.L. González-Carrasco[1]*

[1] *Centro Nacional de Investigaciones Metalúrgicas (CENIM-CSIC), Avda. Gregorio del Amo, 8; Madrid, E-28040, Spain*
[2] *Materials Science and Technology Division, Oak Ridge National Laboratory, PO Box 2008, Oak Ridge, TN 37831-6136, USA*
[3] *CEIT and Tecnun (University of Navarra), Paseo Manuel de Lardizábal 15, 20018 San Sebastián, Spain*

In the last few years, PM 2000(trademark of Plansee GmbH) alloy has been shown to be an advanced material where high temperature applications are paramount. PM 2000is an Fe-based, oxide dispersion strengthened (ODS) alloy, which can be considered as a composite material consisting of a metallic matrix (Fe-20 at.% Cr-11 at% Al) strengthened with a homogeneous dispersion of nanometer-size oxide particles. This oxide dispersion, in combination with a recrystallized coarse grained microstructure, gives PM 2000high hot strength and creep strength up to 1350°C. Due to its high aluminium and chromium content, PM 2000 forms a dense, adherent $Al_2O_3$ scale when used at high temperatures under oxidizing atmospheres. In addition to the high temperature applications, PM 2000 has been shown to be a biomaterial for its outstanding combination of mechanical properties and corrosion resistance at room temperature.

In this work, the effects of an additional nanometer-scale, phase-separation-producing Fe-rich ($\alpha$) and Cr-rich ($\alpha'$) phases during low temperature annealing on the room temperature mechanical properties are described. The three-dimensional microstructure, as determined from atom probe tomography, resulting from phase separation during aging for 2040 h at 748 K is shown in Fig. 1. At this aging temperature, and due to the relatively low chromium content of the alloy, the Cr-rich $\alpha'$ phase is in the form of isolated particles rather than the interconnected network structure observed previously in higher chromium (30-45% Cr) alloys [1]. The kinetics of phase separation were quantitatively determined by analyzing the evolution of the geometrical domain size ($\lambda$) and the composition amplitude ($\Delta C$). The composition amplitude was determined from the composition frequency distribution with the Langer-Bar-on-Miller (LBM) method [2], and the scale from the 3D autocorrelation function [2]. The evolution of $\lambda$ and $\Delta C$ with aging time, $t$, at 748 K, shown in Fig. 2, varies as $\sim t^{1/3}$ and is consistent with the Lifshitz-Slyozov-Wagner (LSW) theory [3-4]. It has been shown that annealing at 748 K is responsible for an increase in the yield and ultimate tensile strength with a resulting decrease in ductility. However, despite some loss of ductility, the material exhibited ductile behavior as observed by the necked zone in tensile specimens. This behavior contrasts the so-called "475 ℃ embrittlement" observed in other ferritic alloys. Moreover, material aged at 475 ℃ exhibits a higher fatigue limit than unaged material (Fig. 3).

**References:**
[1]    M.K. Miller, et al., *Acta Metall. Mater.* 43 (1995) 3385.

[2]     M. K. Miller, *Atom Probe Tomography*, Kluwer Academic / Plenum Press, New York, 2000, pp.177 and
        185.
[3]     I. M. Lifshitz and V. V. Slyozov, *J. Phys. Chem. Solids* 19 (1961) 35.
[4]     C. Wagner, *Z. Elektrochem.* 65 (1961) 581.

**Figures**
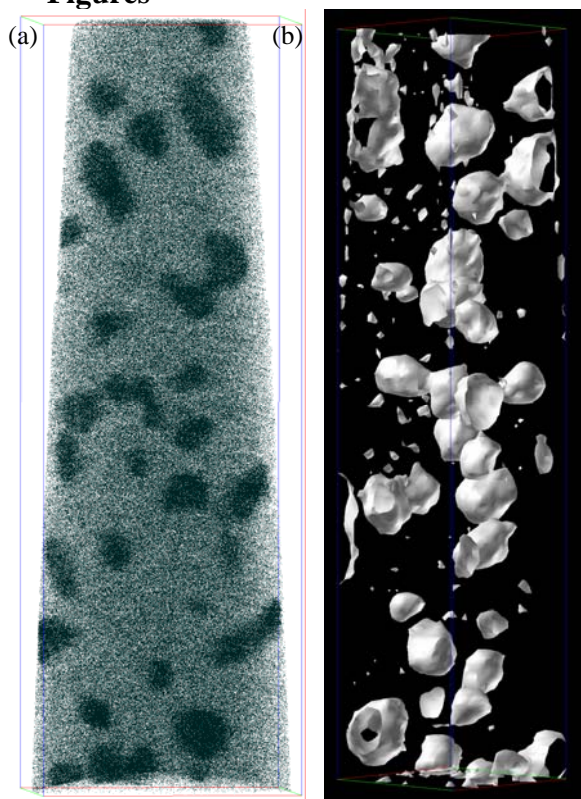


**Figure 1:** (a) Cr atom map and (b) 20% isoconcentration surface after 2040 h aging at 748 K. At this late stage, the Cr-enriched α′ particles are isolated (volume=30x30x127 nm).
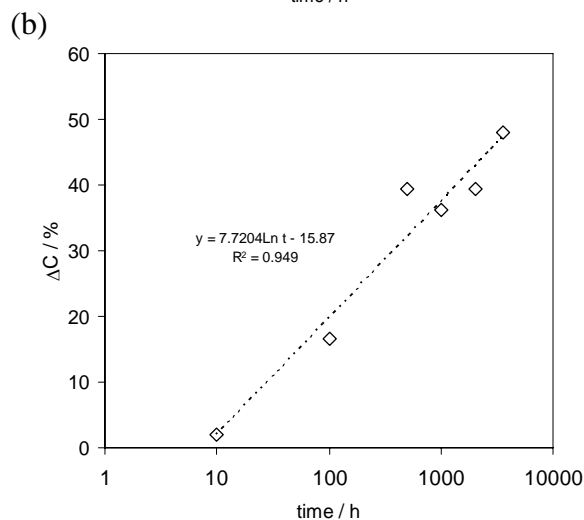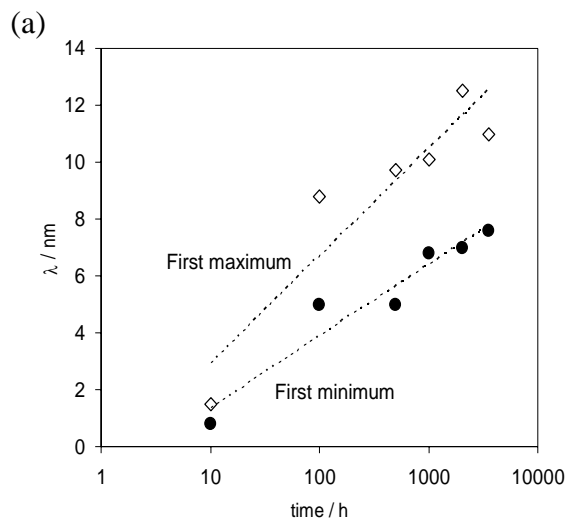


**Figure 2**: Evolution of (a) $\Delta C$ and (b) $\lambda$ with time
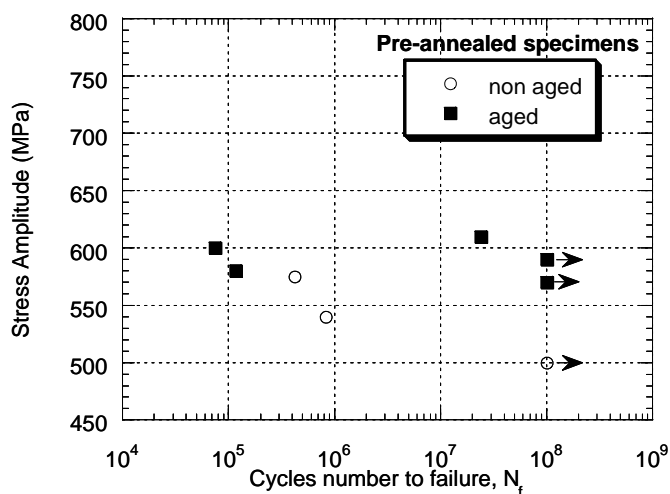


**Figure 3:** S-N diagram for pre-annealed specimens with and without ageing at 475ºC. The arrows indicate that test was interrupted without failure of the specimen.

# Characterization of Plasma-Functionalized Buckypapers

*G. Santoro[1], E. Muñoz[2], I. Jiménez[3], G. Ellis[1], P. Jiménez[2], A. Fernández[2], A.M. Benito[2],*
*M.T. Martínez[2], W.K. Maser[2*], M.A. Gómez[1*]*
*[1]Instituto de Ciencia y Tecnología de Polímeros (CSIC-ICTP), c/ Juan de la Cierva 3,*
*E-28006 Madrid (Spain)*
*[2]Instituto de Carboquímica (CSIC-ICB), c/ Miguel Luesma Castán 4,*
*E-50018 Zaragoza (Spain)*
*[3]Instituto de Ciencia de Materiales de Madrid (CSIC-ICMM), c/ Sor Juana Inés de la Cruz 3,*
*E-28049 Madrid (Spain)*
*wmaser@icb.csic.es* and *mgomez@ictp.csic.es*

Applications based on the properties of individual carbon nanotubes (CNT), such as electronic devices, involve highly demanding separation and assembly processing [1-3]. Nevertheless, for many other less challenging applications, overall statistical properties of nanotube assemblies provide interesting alternatives and may lead to materials of superior performance, especially in the field of electrochemically based applications, energy storage, and sensor devices [4-6]. "Buckypapers" [7,8] are a special form of CNT assemblies, comprising of statistical networks of carbon nanotubes in sheet-like form, typically some tens of microns in thickness, made by filtration of CNT dispersions. Post-processing, functionalization, and integration into different kind of devices is relatively easy.

In this communication we present details of the preparation of buckypapers from single-walled HiPco CNTs, and their subsequent surface treatment using a proprietary nitrogen and oxygen cold-plasma process. We report on the characterization of the obtained and treated buckypapers using scanning electron microscopy (SEM), micro-Raman spectroscopy at three different excitation wavelengths (514.5, 532 and 785 nm), and Fourier-transform Raman spectroscopy at 1064 nm. Additionally, surface four-probe conductivity measurements were carried out.

The entangled network structure of the as-prepared buckypapers can be easily observed by SEM. However, the plasma treated side of the buckypapers shows significant modifications of the surface, *Figure 1*, with the generation of an apparently bead-like morphology. Initial conductivity values of about 50 S cm$^{-1}$ measured for the as-produced buckypapers were found to decrease only slightly in the plasma treated buckypapers. Raman spectroscopy reveals good sample homogeneity for the buckypapers analysed. In the plasma treated buckypapers an enhanced D-band (disorded carbon) intensity and a lower G/D-band ratio is observed. Furthermore, the plasma-treated buckypapers show interesting variations in the low frequency radial breathing modes (RBM) as well as a systematically lower Raman response, *Figure 2*.

The observations will be discussed in terms of the modification of the resonance conditions in the plasma-modified samples, as a function of the different laser wavelengths, and its relation with type and degree of aggregation of the CNTs at the Buckypaper surface, and the nature of the oxygen or nitrogen functionalization induced by the plasma.

**References**:
[1]   P. Avouris, MRS BULLETIN **29** (2004) 403 – 410
[2]   A. Star, J.C.P. Gabriel, K. Bradley et al., Nano Lett. **3** (2003) 459 – 463
[3]   G.S. Duesberg, A.P. Graham, M. Liebau et al., Nano Lett. **3** (2003) 257 – 259
[4]   R. H. Bauhgman, A.A. Zakhidov, and W.A. de Heer., Science **297** (2002) 787 – 792
[5]   F. Picó, J.M. Rojo, M.L. Sanjuán et al., J. Electrochem. Soc. **151** (2004) A831 – A837
[6]   I. Sayago, E. Terrado, E. Lafuente et al., Synth. Met. **148** (2005) 15 – 19
[7]   J. Lui, A.G. Rinzler, H. Dai et al., Science **280** (1998) 1253 – 1256
[8]   L. Berhan, Y.B. Li, A.M. Sastry, E. Muñoz, M. Selvidge, R. Baughman, J. Appl. Phys. **95** (2004) 4335 – 4345

**Figures**:

*Figure 1:* SEM of buckypapers (scale bar = 500 µm)
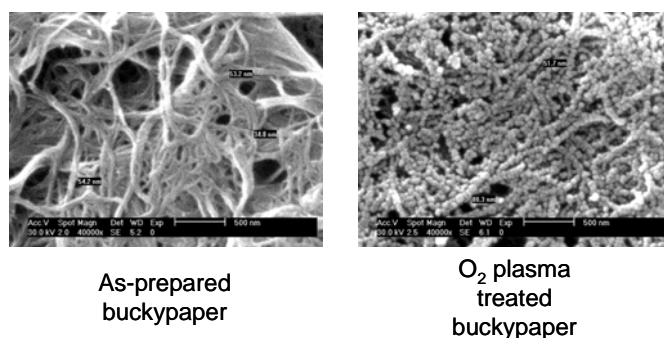


*Figure 2:* Raman spectra ($\lambda_{ex}$ = 514.5 nm) of buckypapers
(inset = expanded RBM region)
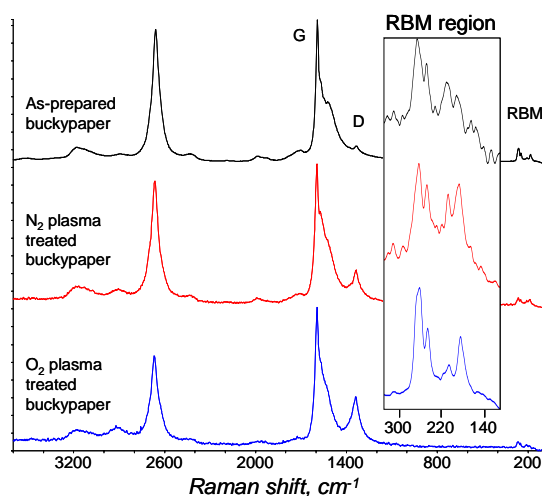
# Surface relief nano-micro structures from Rayleight's instabilities in block copolymers

*E. Sarantopoulou*[1], *J. Kovač*[2], *S. Kobe*[3], *S. Pispas*[1], *Z. Kollia*[1],  *A. C. Cefalas*[1]

[1]*National Hellenic Research Foundation, TPCI,48 Vas. Constantinou Aven.  Athens 11635 Greece*

[2] *Department of Surface Engineering and Optoelectronics -F4, Jožef Stefan Institute, Teslova 30, 1000 Ljubljana, Slovenia*

[3] *Jožef Stefan Institute, Department of Nanostructured Materials, Jamova 39, SI-1000 Ljubljana, Slovenia*

email: esarant@eie.gr

Hierarchical surface relief nano-micro structures on thin films of block copolymers/ of Fe and Sm-Fe hybrid materials were induced either by wet chemistry or laser vacuum ultraviolet (VUV) light at 157 nm. Poly(styrene-b-2-vinylpyridine) polymers were synthesized by anionic polymerization high vacuum techniques using the sequential monomer addition technique. Micelle preparation has taken place in toluene solutions. The loading of the micelle cores was accomplished by addition of varying amounts of salt precursors $FeCl_3$ or $SmCl_3$ and $FeCl_3$ [1]. Reduction was achieved either by wet chemistry or by vacuum ultraviolet (VUV) laser   irradiation of the film. Furthermore, a variety of self-assembled and surface relieved structures in the nano/ micro scale were obtained and analyzed by imaging and other analytical techniques, including SEM and AFM, Fig.1. The structures have their origin at the thermal instabilities, which were developed in the polymer films due to the temperature gradient induced between the film and the substrate either by fast film evaporation following chemical reduction or the VUV light. The laser light disturbs the thermodynamic equilibrium of the diblock polymer/intermetallic hybrid surface and the average surface roughness was progressively increasing with prolonged irradiation. At the onset of instability the layer of the fluid on the substrate resolves itself into a number of cells, which form regular patterns with characteristic spacing depending on the film thickness. The obtained results confirm the surface modification changes of diblock copolymer/hybrid materials after the disturbance of the thermodynamic equilibrium by VUV light.

## References

 [1]  E. Sarantopoulou, K. Gatsouli, Z. Kollia, S. Pispas, S. Kobe, and J. Kovač,   phys. stat. sol. (a), 1– 8 (2007)

**Figures:**
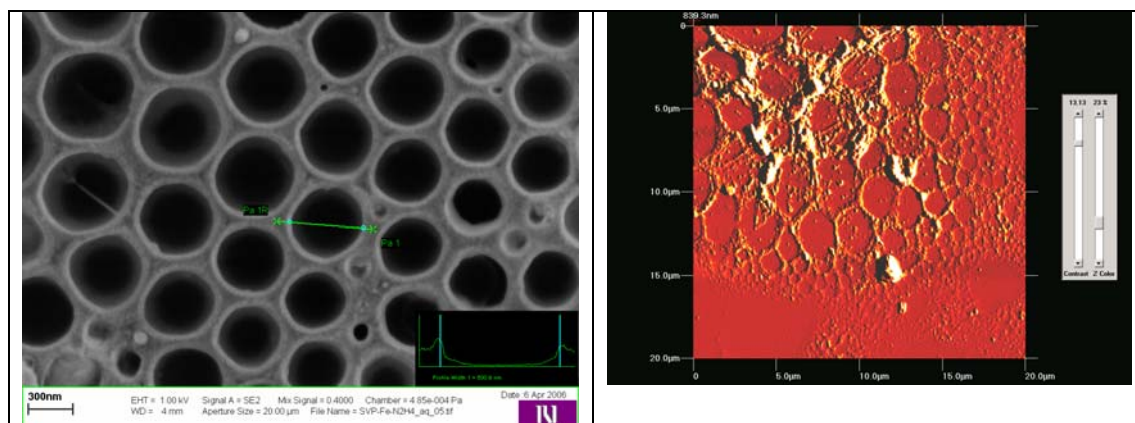


**Fig. 1** Cylindrical (SEM) and hexagonal (AFM) surface relieved gratings at Fe block copolymers

# MESOSCALE ELASTIC THEORY IN GRAPHITE

*G. Savini*[1, 2]*, J. M. Campanera*[1] *and M. I. Heggie*[1]
[1]*Dept of Chemistry, University of Sussex, Falmer, Brighton, BN1 9QJ, United Kingdom*
[2]*Dept of Physics, University of Bologna, Bologna, 40126, Italy*
*g.savini@sussex.ac.uk*

First principles density functional calculations within the Local Density Approximation (LDA) have provided highly plausible [1-3] results but the folklore of interlayer interactions is that LDA does not include an important part of the physical interaction between layers (dispersion forces *i.e.* van der Waals force) and therefore should not be relied upon.

The main disagreement between theory and experiment is the value of the elastic constant $C_{13}$ (positive for experimental studies [4, 5] and negative for theoretical studies [6]). The sign of this elastic constant is crucial for the elastic properties of the material; a positive (negative) value of $C_{13}$ means that under compression of the in-plane lattice constant, the out-plane lattice constants tend to expand (contract), respectively. Therefore theory and experiment describe graphite as a material with an opposite elastic behavior.

In this work we have demonstrated that LDA performs excellently for graphite and reproduces with precision all the elastic properties. We have shown that, under compression, graphite tends to bend with amplitude directly proportional to the applied strain. These bending modes introduce a new kind of elastic constants called *mesoscale elastic constants*.

We have developed a elastic theory beyond the harmonic approximation that describes the behaviour of graphite/graphene under any applied strains $\varepsilon$. Within this theory the elastic formation energy $E(\varepsilon)$ describing the behaviour of a graphite layer under any applied strain $\varepsilon$ can be written as [7]:

$$E(\varepsilon) = \left\{ K \cdot \frac{-\varepsilon + \varepsilon_{critical}}{L(1+\varepsilon)^2} + C \cdot \varepsilon_{critical}^2 \right\} \cdot \vartheta\left(-\varepsilon + \varepsilon_{critical}\right) + C \cdot \varepsilon^2 \cdot \vartheta\left(+\varepsilon - \varepsilon_{critical}\right)$$

where $K$ is the bending constant of graphene, $C$ is the elastic constants along the bending direction, $\theta$ is the Heaviside step function, $L$ is the length of the plane along the bending direction and $\varepsilon_{critical}$ is the critical strain.

Therefore a graphite layers can be flat or bent depending on the value of the applied strain $\varepsilon$. The critical strain separates homogeneous in-plane compression (at low compression) from the bent plane behaviour (at high compression). Under small deformation the critical strain $\varepsilon_{critical}$ can be written as:

$$\varepsilon_{critical} : -\frac{K}{2 \cdot L \cdot C}$$

This theory predict that under the critical strain the elastic behaviour is due to the classical elastic constants while above the critical strain the elastic behaviour is dominated by the mesoscale elastic constants. The corresponding $C_{13}$ classical and mesoscale elastic constants are -2.3 GPa and +6.2 GPa, respectively both in agreement the previous theoretical calculations ($C_{13}$ = -2.8 GPa, [6]) and experiments ($C_{13}$ = 7.9±3.5 GPa, [4, 5]).

Therefore the elastic constants measured by experimental studies are the mesoscale elastic constants (the elastic constants that really describes the elastic behaviour of HOPG graphite samples) while the elastic constants determined by *ab-initio* studies are the common elastic constants.

We observe that, different quality of graphite samples could favourite the rising of one elastic behaviour over the other. For instance, polycrystalline graphite samples should favourite the mesoscale elastic behaviour while single crystal graphite (Kish graphite) should favourite the classical elasticity. Furthermore different experimental measures could be able to detect the mesoscale or classic elasticity depending on the type of the techniques (x-ray, ultrasonic, sonic resonance or static test methods).
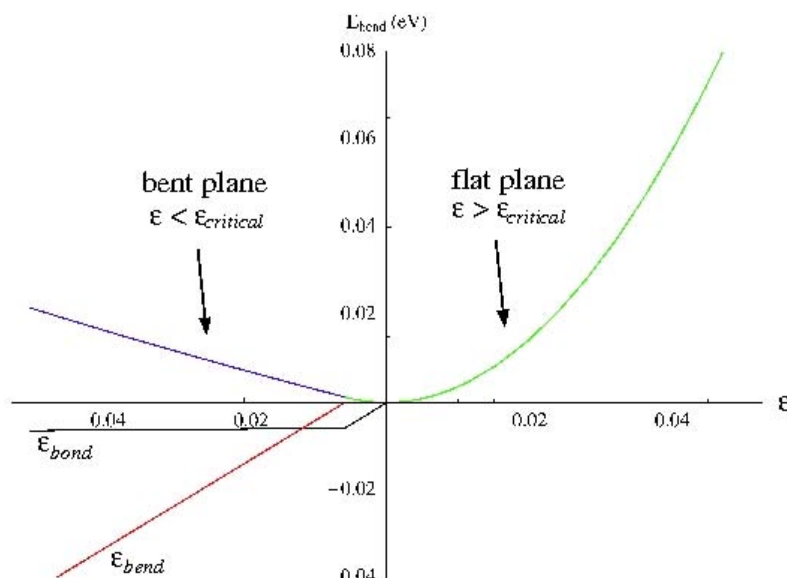
**Figures:** The formation energy of a graphite plane when compressed ($\varepsilon < 0$) or expanded ($\varepsilon > 0$). The green and blue curves represent the formation energies when the strain $\varepsilon$ is above or under the critical strain $\varepsilon_{critical}$, respectively. The red line represents the strain component due to the bending, while the black line represents the strain component in-plane compression.

We must observe that the only theoretical value that is not completely in agreement with respect to the experimental data is the mesoscale elastic constant $C_{13}^{M} = 31.8$ GPa (the respective experimental value is $36.5 \pm 1$ [4.5]). Nevertheless, the temperature effects [6] and/or crystal defects [2] can explain this relatively small difference (10.4 %) between theory and experiment.

Finally using the same background theory but applied for the graphene case, we have demonstrated:

1. The bending modes possess always sinusoidal solutions;
2. The 1-dimensional bending is always more favourable than a 2-dimensional one;

The latter results give new insight into the structural atomic properties of 2-dimensional materials with strong implications for the new field of graphene science. We observe that the mesoscale elastic theory should extend to all the other important layered materials like BN, clays and $MgB_2$.

**References:**

[1] I. Suarez-Martinez, A. A. El-Barbary, G. Savini, M. I. Heggie, Phys. Rev. Lett. **98** (2007) 015501.
[2] A. A. El-Barbary, M. I. Heggie, R. H. Telling, I. Suarez-Martinez, G. Savini, Phys. Rev. Lett. Submitted.
[3] J. M. Campanera, G. Savini, I. Suarez-Martinez, M. I. Heggie, Phys. Rev. B. In press.
[4] O. L. Blakslee, C. G. Proctor, E. J. Seldin, G. B. Spence, T. Weng, J. Appl. Phys. **41** (1970) 3373.
[5] C. S. G. Cousin, M. I. Heggie, Phys. Rev. B. **7** (2003) 024109.
[6] N. Mounet, N. Marzari, Phys. Rev. B **55** (1996) 11202.
[7] G. Savini, J. M. Campanera, M. I. Heggie To be submitted

# TAILORING THE DIAMETER, DENSITY AND NUMBER OF WALLS OF CARBON NANOTUBES THROUGH PREDEFINED CATALYST PARTICLES

*Franziska Schäffel, Christian Kramberger, Mark H. Rümmeli, Daniel Grimm, Thomas Gemming, Thomas Pichler, Bernd Büchner, Bernd Rellinghaus, and Ludwig Schultz*
*IFW Dresden, P.O. Box 270116, D-01171 Dresden, Germany*
*f.schaeffel@ifw-dresden.de*

Owing to their excellent mechanical and electronic properties, carbon nanotubes (CNTs) are promising candidates for the integration into nanoelectromechanical systems such as nanorelays and actuators or transistors. Effective control of the CNT growth, orientation and positioning is still considered to be a mayor challenge within the scientific community. Progress has been made by using catalyst thin films prepared and patterned by lithography [1] or shadow masking [2]. Yet, such thin film techniques do not offer concurrent control of the catalyst size with a narrow size distribution and the areal density of the catalyst particles. Novel routes that allow for an independent control of both the diameter and the density of catalyst nanoparticles are beginning to emerge. These approaches demonstrate that the preparation of the catalyst material is a crucial step in carbon nanotube synthesis. A notable work is for example the use of block-copolymer micellar thin films [3]. An alternative and advantageous method is to prepare individual nanoparticles in the gas phase that then act as nucleation sites for CNTs [4]. Gas phase preparation techniques allow for the production of nanoparticles with a higher degree of purity as compared to processes where the preparation of catalyst particles requires a series of chemical procedures (see, e.g. [3]).

In this contribution, we show that gas phase prepared catalyst particles for CNT growth allow for independent and simultaneous control over the CNT diameter and the CNT density on substrates. While the size of the catalyst particles can be adjusted by varying the sputtering power, the gas pressure, and/or the gas mixture, their density is conveniently controlled by the deposition time. Thus the whole ranges from thick multi-wall to narrow single-wall CNTs and from individual CNTs to dense mats of CNTs become accessible. Figures 1 a-c show TEM micrographs of (oxidized) iron particles with different mean diameters of 3 nm, 10 nm, and 18 nm as deposited on TEM "witness" grids. The corresponding TEM micrographs of CNTs grown from these particles are shown in Figures 1 f-d. The mean outer CNT diameters have been found to be 4 nm, 9 nm, and 17 nm, respectively. This indicates that the diameter of the catalyst particles determines that of the resultant CNTs which is in agreement with other studies on single wall CNTs [5]. Further, an intimate correlation between the catalyst particle size and the number of walls in the obtained CNTs is observed. This confirms other studies [6] where a correlation between different catalyst film thicknesses and both the obtained diameter and number of walls of the CNT was shown; the authors had attributed this finding to changes in the catalyst particle size. The separate preparation of the catalyst particles and the use of TEM "witness" grids in our approach enables us to reveal a clear link between the catalyst size on the one side and the CNT diameter as well as the number of walls on the other side.

**References:**

[1] J. Kong, H. T. Soh, A. M. Cassell, C. F. Quate, H. Dai, Nature **395** (1998) 878; A. J. Hart, A. H. Slocum, J. Phys. Chem. B **110** (2006) 8250; M. S. Kabir, R. E. Morjan, O. A. Nerushev, P. Lundgren, S. Bengtsson, P. Enoksson, E. E. B. Campbell, Nanotechnology **17** (2006) 790.

[2] L. Delzeit, C. V. Nguyen, B. Chen, R. Stevens, A. Cassell, J. Han, M. Meyyappan, J. Phys. Chem. B **106** (2002) 5629.

[3] R. D. Bennett, A. J. Hart, R. E. Cohen**,** Adv. Mater. **18** (2006) 2274.

[4] F. Schäffel, C. Kramberger, M. H. Rümmeli, R. Kaltofen, D. Grimm, A. Grüneis, E. Mohn, T. Gemming, T. Pichler, B. Büchner, B. Rellinghaus, L. Schultz, phys. stat. sol. (a) (2007), DOI 10.1002/pssa.200675339; F. Schäffel, C. Kramberger, M. H. Rümmeli, D. Grimm, E. Mohn, T. Gemming, T. Pichler, B. Rellinghaus, B. Büchner, L. Schultz, submitted to Chem. Mater. (2007).

[5] Y. Li, W. Kim, Y. Zhang, M. Rolandi, D. Wang, H. Dai, J. Phys. Chem. B **105** (2001) 11424.

[6] T. Yamada, T. Namai, K. Hata, D. N. Futaba, K. Mizuno, J. Fan, M. Yudasaka, M. Yumura, S. Iijima, Nature Nanotechnology **1** (2006) 131.

**Figures:**
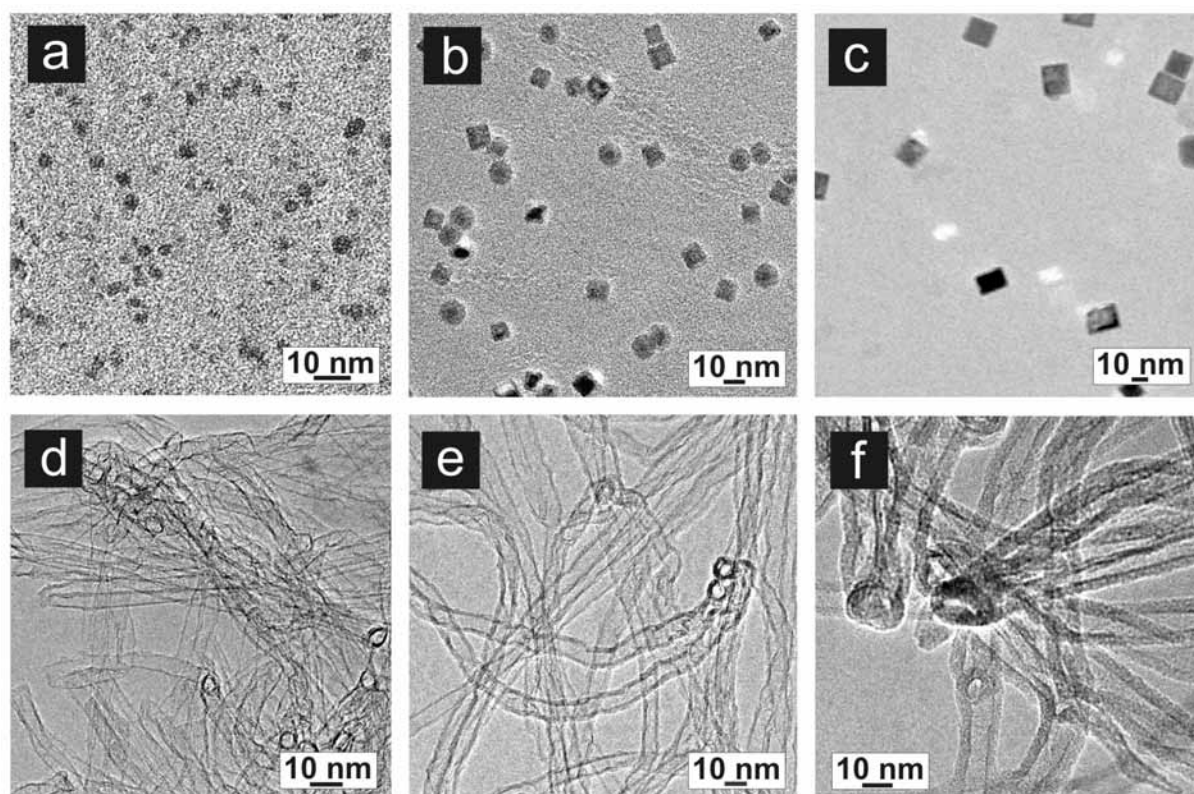


Figure 1: a-c) TEM micrographs of (oxidized) Fe nanoparticles deposited on TEM "witness" grids. d-f) Corresponding TEM micrographs of CNTs grown from these particles.

# Self-assembly of methionine on noble metal surfaces: steering biomolecular nanostructures by substrate reactivity and thermal activation

*Agustin Schiffrin[1], Joachim Reichert[1], Andreas Riemann[2], Yan Pennec[1], Willhem Auwaerter[3], Alexander Weber-Bargioni[1], Dean Cvetko[4], Albano Cossaro[4], Alberto Morgante[4], and Johannes V. Barth[1, 3]*

[1]University of British Columbia, 2329 West Mall, Vancouver, Canada
[2]Western Washington University, Bellingham, Washington, USA
[3]Technische Universitaet Muenchen, Garching, Germany
[4]Laboratorio Istituto Nazionale per la Fisica della Material (INFM/TASC), 34012 Trieste, Italy
*aeschiff@chem.ubc.ca*

Molecular self-assembly on surfaces yields promising pathways for the design of functional architectures at the nanoscale [1]. Notably the use of biologically relevant species, such as amino acids or nucleic acids with their inherent qualities as building blocks for the conception of nanostructures, led to fundamental discoveries in the domain of molecular recognition and organization [2, 3, 4]. In general, the state of stable configurations at thermodynamic equilibrium is not only defined by intermolecular interactions, but also by the influence of the underlying support.

Here we report a low-temperature scanning tunneling microscopy (STM) study on the self-assembly of the amino acid methionine under ultra-high vacuum conditions. Methionine provides functionalities which are both relevant for zwitterionic self-assembly and for metal binding sites in peptide chains. We employed two different close-packed metal substrates Ag(111) and Cu(111) with chemical nature. On Ag(111) the molecules dimerize and self-assemble in extended one-dimensional nanostructures running parallel to the closed-packed crystallographic orientations of the underlying atomic lattice (fig. 1) [5]. These commensurate chains arrange mesoscopically into regular biomolecular gratings whose mesoscopic ordering can be tuned by the molecular coverage, as confirmed by STM and complementary helium atomic scattering (HAS) observations. The combined STM and X-ray photoemission spectroscopy (XPS) analysis demonstrates zwitterionic self-assembly over a wide temperature range. By contrast, on Cu(111) the molecular ordering is strongly influenced by the reactivity of the substrate. At low temperatures (243 K) disordered molecular clusters evolve for submonolayer coverages, whereas the saturated monolayer exhibits partial ordering arising from the influence of the substrate, with linear structures growing with a -10° shift with respect to the <110> crystalline orientations (fig. 2a). On the other hand, following deposition on the substrate held at 303K, a regular one-dimensional phase arises with a +10° shift with respect to the <110> orientations (fig. 2b) coexisting with patches of the disordered phase. Molecular resolution measurements of the ordered 1D arrangements indicate dimerization and a second-order commensurability with the atomic lattice of the substrate along the chain direction. These results are comfirmed by HAS observations. The combined STM/XPS data show that the disordered phase comprises the molecules in their anionic state, with a deprotonated carboxylic group and a neutral amino group, whereas the ordered phase reflects zwitterionic self-assembly.

Finally, the regularity and tunability of the methionine nanogratings on Ag(111) was used for the confinement of the surface state electrons [6], and to steer the positioning of single Fe and Co adatoms in molecular trenches at low temperatures (fig. 3). STM data sequences were obtained to monitor the restricted thermal motions of the confined transition metal atoms that experience a complex lateral energy landscape.

**References:**

[1] Barth JV, Costantini G, Kern K, Nature, **437** (2005) 671; Barth JV, Annu. Rev. Phys. Chem., **58** (2007) 375.

[2] Kuehnle A, Linderoth TR, Hammer B, and Besenbacher F, Nature, **415** (2002) 891.

[3] Barlow SM, Raval R, Surf. Sci. Rep., **50** (2003) 201.

[4] Chen Q, Richardson NV, Nature Materials, **2** (2004) 324.

[5] Schiffrin A, Riemann A, Auwaerter W, Pennec Y, Weber-Bargioni A, Cvetko D, Cossaro A, Morgante A, and Barth JV, PNAS, **104** (2007) 5281.

[6] Pennec Y, Auwaerter W, Schiffrin A, Weber-Bargioni A, Riemann A, and Barth JV, Nature Nanotechnology, **2** (2007) 99.

## Figures:
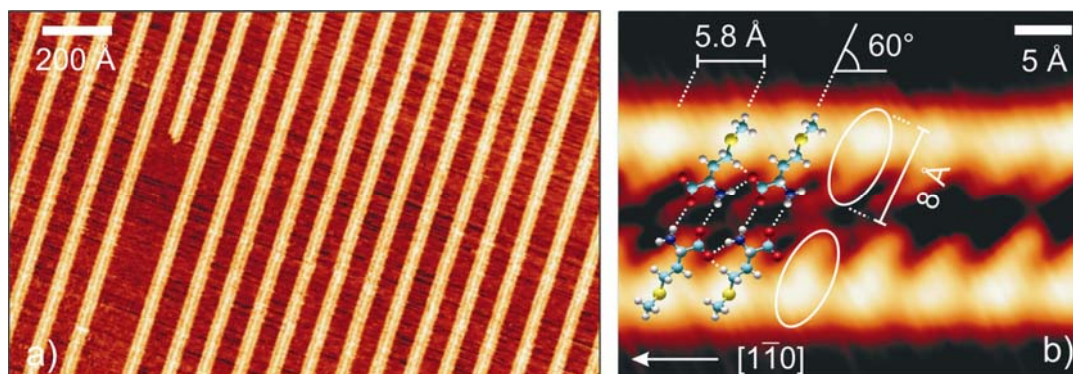


Figure 1 – STM images of the self-assembly of the *L*-methionine amino acid on Ag(111). (a) Regular and tunable 1D biomolecular nanogratings with a periodicity of 94Å ($I$ = 0.1 nA, $U$ = -500 mV, $\theta$ = 0.38 ML). (b) Molecular resolution imaging shows molecular dimerization and commensurate growth along the closed-packed crystalline orientations ($I$ = 0.9 nA, $U$ = -80 mV).
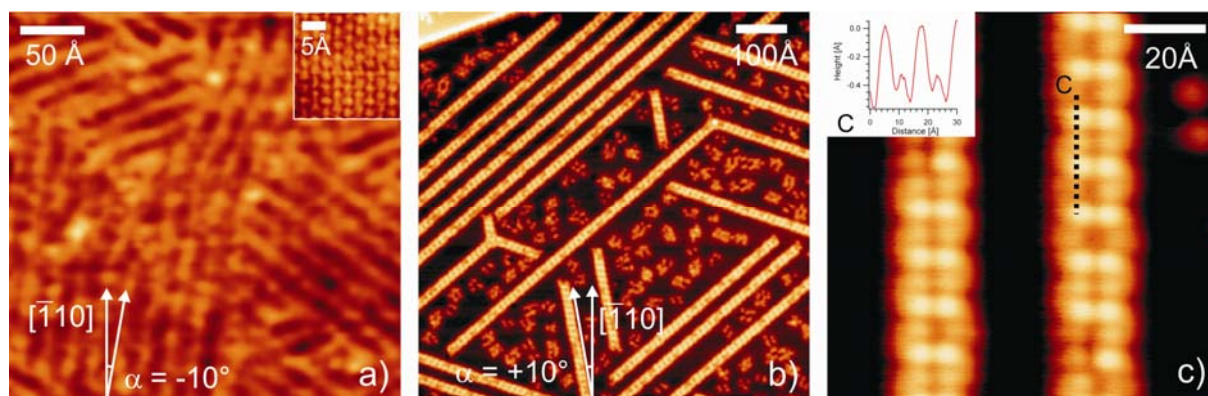


Figure 2 – *L*-Methionine on Cu(111). (a) Saturated monolayer deposited with the substrate held at 243K: molecular structures grow with a -10° with respect to the <110> crystalline orientations. Inset shows atomic resolution of the Cu(111) substrate ($I$ = 0.05 nA, $U$ = -100 mV). (b) Deposition at 303K shows commensurate 1D ordering with a +10° shift with respect to the <110> crystalline orientations. The disorderd phase is still present ($I$ = 0.1 nA, $U$ = -500 mV). (c) Molecular resolution of the ordered phase shows 2x2 Moiré pattern due to the structure commensurability along the growth direction. Inset: height profile along line C ($I$ = 0.1 nA, $U$ = -600 mV).
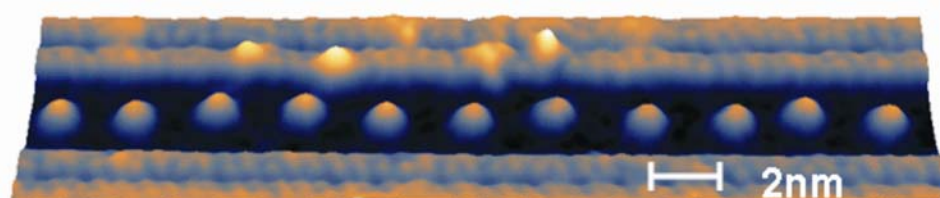


Figure 3: Self-alignment of Fe adatoms between *L*-methionine rows on Ag(111) at 18K.

# ELECTRONIC STRUCTURE OF HIGHLY ORDERED C$_{60}$ CLUSTERS ON Au(887)

F. Schiller, M. Ruiz-Osés, and J. E. Ortega

*Donostia International Physics Center, Paseo Manuel Lardizabal 4, E-20018 Donostia-San Sebastián, Spain; Departamento de Física Aplicada I, Universidad del País Vasco, Plaza de Oñate 2, E-20018 Donostia-San Sebastián, Spain; and Centro Mixto CSIC/UPV, Paseo Manuel Lardizabal 4, E-20018 Donostia-San Sebastián, Spain*

P. Segovia and J. Martínez-Blanco

*Departamento de Física de la Materia Condensada, Universidad Autónoma de Madrid, E-28049 Madrid, Spain and Instituto Universitario de Ciencia de Materiales "Nicolás Cabrera," Universidad Autónoma de Madrid, E-28049 Madrid, Spain*

B. P. Doyle

*Laboratorio Nazionale TASC, INFM-CNR, ss. 14, km 163.5, Area Science Park, I-34012 Basovizza, Trieste, Italy*

V. Pérez-Dieste and J. Lobo

*Swiss Light Source, Paul Scherrer Institut, CH-5232 Villigen, Switzerland*

N. Néel, R. Berndt, and J. Kröger

*Institut für Experimentelle und Angewandte Physik, Christian-Albrechts-Universität, D-24098 Kiel, Germany*

We present an analysis of the electronic structure of C$_{60}$ adsorbed on a vicinal Au(111) surface at different fullerene coverage using photoemission, x-ray absorption, and scanning tunneling microcopy/spectroscopy (STS). STS provides a straightforward determination of the highest occupied molecular orbital (HOMO) and the lowest unoccupied molecular orbital (LUMO) levels with respect to the Fermi energy. At C$_{60}$ coverage of 0.5 and 1 ML a 2.7 eV wide HOMO-LUMO gap is found. The near-edge x-ray absorption fine structure (NEXAFS) spectrum for the 0.5 ML C$_{60}$ nanomesh structure displays a significant intensity at the low energy side of the LUMO exciton peak, which is explained as due to absorption into HOMO-LUMO gap states localized at individual C$_{60}$ cluster edges. From 0.5 to 1 ML we observe a rigid shift of the HOMO-LUMO peaks in the STS spectra and an almost complete quenching of the gap states feature in NEXAFS.

# MOLECULAR RECOGNITION BY CALIX[4]ARENE-MODIFIED GOLD NANOPARTICLES IN AQUEOUS SOLUTION

*Robert Tshikhudo,[a] Domenico Demuru,[b] Zhenxin Wang,[a] Mathias Brust,[a] Arturo Arduini,[b] Andrea Pochini,[b] and Andrea Secchi[b]*

*[a]Centre for Nanoscale Science, Department of Chemistry, University of Liverpool, Liverpool, UK; [b]Dipartimento di Chimica Organica ed Industriale dell'Università, Parco Area delle Scienze 17/a, 43100 Parma, Italy.*

*andrea.secchi@unipr.it*

The concept of exploiting metal clusters for nanotechnology applications dates back to the development of the original $Au_{55}$ cluster by Schmid et al. in 1981.[1] Over the past decade, so-called monolayer protected clusters (MPCs) of gold and, to a lesser extent, silver have been studied extensively owing to their extreme stability and the plethora of tunable properties that are controlled by the particle size and by the ligand chemistry.[2] The stability is usually achieved by the use of thiolate ligands, which form a protective shell around the particles to which they are attached by the strong Au−S interaction. In view of future bioanalytical applications it is desirable to develop new MPC systems that are not only stable and soluble in water, but also capable of molecular recognition in aqueous systems. Very stable, yet chemically versatile watersoluble MPCs are obtained when a sulfanylalkyl oligo(ethyleneglycol) is used as a stabilizing ligand. Herein we report the preparation and chemical properties of 14-nm gold MPCs, which are stabilized in this way and, in addition, carry in their ligand shell calix[4]arene moieties, which confer their specific molecular recognition properties to the particles. The sulfanylalkyl oligo(ethyleneglycol) ligands in the system described herein act therefore not only as stabilizers for the MPCs but also as solubilizers for the attached calix[4]arene units. The particles prepared have been characterized by transmission electron microscopy (TEM) and by UV/Vis, and NMR spectroscopy. Specific recognition of immobilized cationic pyridinium moieties by the calixarene-modified MPCs in aqueous solution has been demonstrated by atomic force microscopy (AFM).

**References:**

[1] G. Schmid, R. Pfeil, R. Boese, F. Bandermann, S. Meyers, G. H. M. Calis, W. A. Vandervelden, Chem. Ber., **114** (1981), 3634. [2] R. L. Whetten, M. N. Shafigullin, J. T. Khoury, T. G. Schaaff, I. Vezmar, M. M. Alvarez, A. Wilkinson, Acc. Chem. Res., **32** (1999), 397.

**Figures:**
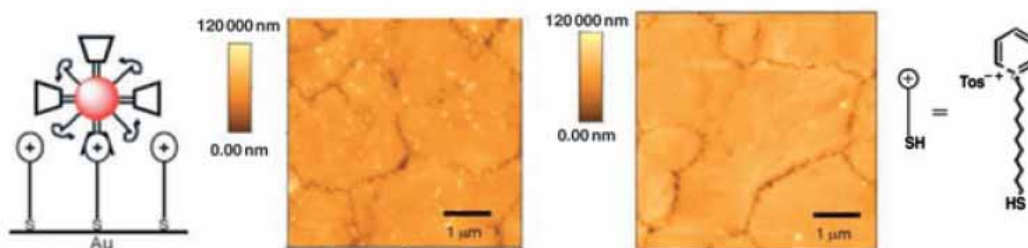


Specific binding of the calixarene-modified gold nanoparticles, from aqueous solution to a self-assembled monolayer (SAM) of the pyridinium salt on a gold surface shown by AFM (left). The control experiments (right) show the nonspecific attachment of only very few particles to the SAMs.

# Impregnation synthesis of gold nanoparticles – carbon nanotubes hybrids

*Rodrigo Segura del Río, Alejandra Tello and Patricio Häberle*
*Departamento de Física, Universidad Técnica Federico Santa María, Valparaíso,  Chile*
*rodrigo.segura@usm.cl*

The hybrid nanostructures, formed by combining two kinds of materials, such as nanotubes and nanoparticles, might improve the performances or extend the applications of these new materials. Their technological perspectives in fields as catalysis, gas and electrochemical sensing, solar energy conversion or optoelectronics has attracted the imagination of many researchers in the last few years. In this work we present the synthesis of hybrid nanostructures composed of gold nanoparticles and carbon nanotubes (AuNPs@CNTs)

The AuNPs@CNTs nanohybrids were prepared by the impregnation of chloroauric acid, $HAuCl_4$, and subsequent calcination in oxygen and reduction in hydrogen atmosphere. This methodology is very common to prepare supported noble metal nanoparticles on alumina or silica supports, but we have not found reports in the use of this procedure to prepare nanoparticle-nanotube hybrids. Preliminary results seem to be interesting since nanoparticles, as compared with other methods, were formed in the inner cavity of MWCNTs (See figure 1).
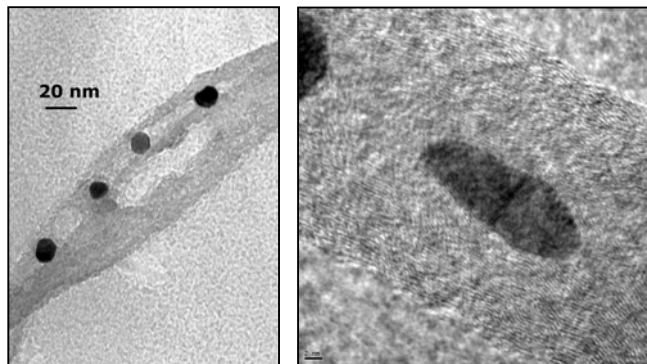
**Figure 1.** TEM and HRTEM images of AuNPs@MWCNTs hybrids obtained by the impregnation method.

# MAGNETIC FIELD-DEPENDENCE STUDY OF THE MAGNETOCALORIC PROPERTIES OF A SUPERPARAMAGNETIC NANOPARTICLE SYSTEM: A MONTE CARLO SIMULATION

*D. Serantes,[1,2] D. Baldomir,[1,2] M. Pereiro,[1,2] J. Rivas,[2]*
*C. Vázquez-Vázquez,[3] M. C. Buján-Núñez,[3] J. E. Arias[1]*

[1] *Instituto de Investigacións Tecnolóxicas, Universidade de Santiago de Compostela; 15782 Santiago de Compostela, Galicia (Spain)*

[2] *Facultade de Física, Departamento de Física Aplicada, Universidade de Santiago de Compostela; 15782 Santiago de Compostela, Galicia (Spain)*

[3] *Facultade de Química, Departamento de Química Física, Universidade de Santiago de Compostela; 15782 Santiago de Compostela , Galicia (Spain)*
*davidsa@usc.es*

The influence of the applied magnetic field on the magnetocaloric properties of a fine magnetic particle system has been studied using a Monte Carlo technique. By simulating the entropy variation of the anisotropy for different applied magnetic fields, we have observed that exists a particular field able to produce a larger entropy change. It is also observed that the blocking temperature diminishes with increasing field, as it is expected.

# Controlling the size of Cdse-nano particles by simultaneous application of high Ar/He gas pressure and fast evacuation

Z. Shadrokh, A. Yazdani, F. Karami

Tarbiat Modares University, P.O.Box: 14155-175, Tehran, Iran

negin_kamali6184@yahoo.com

It is suggested that, when the grain and domain size becomes comparable to or smaller than the characteristic length scale of interaction process, the shape and surface effect (which are the main controlling parameters of biomedical applications) play an important role [1, 2]. But, the relation of the grain boundaries and domain walls as well as the cluster size to the characteristic length scale of interaction processes, which can be due to the exchange correlation energy, are still a key issue of fundamental researches for understanding the dimensions of nanoparticle scales [3, 4].

Although it is well understood that the grain size or domain walls are dependent to the imperfections of crystalline materials which could be also resulted from the method of preparation, "fast" or "slow", as well as the homogeneity of preparation process which are controlled by the ligand field as well as the band strength, ("length" and "bond angle") of the contributing elements (the primary purity of elements). Hence based on "the evaporation in vacuum by rotor system" method we have simultaneously applied (a) high Ar/He gas pressure flow, (b) fast evacuated evaporation and (c) evaporation by heating the liquid surface in vacuum.

Therefore the effect of the following competing parameters which could be important factors, define by prevention of aggregation (agglomeration) of nanoparticles biological compatibility, are considered;

1) Increasing the energy gap of the inter particle correlation which is related to the decreasing of nanoparticle size, named the geometrical constraints of quantum – size effect, could be a useful parameter which prevents the aggregation of nanoparticles[5] .

2 ) Because of the atomic-electronic structure of zinc blend, as bond length and bond angle, the formation of structure could have some imperfections with vacancies at certain sites which leads to distortion of atoms in vicinity of the vacancies .

3) A shift in electronic transitions to higher energies which can cause dangling bond and

4) Increasing of the oscillator strength with decrease in particle size.

It should be mentioned that in each case the induced polarized force as well as magnetic susceptibility which is due to the antisymetry of spectral wave function must be regarded [6].

However in order to investigate the effect of suggested character by applying "the evaporation in vacuum by rotor system" preparation method the X-ray pattern and photoluminescence IR and FTIR are studied for the prepared CdSe.

**References:**

[1] K.F.Berggren and I.I.Yakimenko, Phys.Rev.B **66**, 085323 (2002)
[2] N.Sanz, P.L.Baldeck, and A.ibanez, Synth. Met. **115**,229 (2000)
[3] M. Rutnakornpituk, et. Al. Polimer **43**, ( 2002), 2337
[4] A. Jordan, et. Al. J. Magn. Magn. Mater. **194**, (1999) 185
[5] Victor I.Klimov ,Los Alaqmos Science ,**Num 28**(2003)
[6] S. Neeleshwar, et. Al, Physical Review B. 71, (2005) 201307(R)

# THERMAL STABILITY OF POLYSTYRENE-CLAY NANOCOMPOSITE

S. Shaghaghi [*, a]

a. Iran Polymer and Petrochemical Institute, P. O. Box 14965/115, Tehran, Iran,
*S.Shaghaghi@ippi.ac.ir*

**Abstract**: In this research, polyvinyl alcohol was grafted on the copolymer of styrene- maleic anhydride (PVA- g-S/MA), in order to make styrene to be more compatible with nano clay which has hydrophilic nature. FT-IR spectroscopy indicates that grafting was done successfully. Ultrasound technique was used to disperse nano clay in to the terpolymer (PVA- g- S/MA). The intercalated PVA-g-S/MA-clay nanocomposite exhibited thermal stability better than pure PVA-g-S/MA.

**Key Words: Poly styrene (PS), Styrene (S), Maleic Anhydride (MA), Polyvinyl Alcohol (PVA), Nano Clay, Ultrasound technique.**

## Introduction

Several attempts to prepare polystyrene-clay composite have been reported(1-5). A common technique involves impregnating clay in styrene monomer followed by polymerization. The hydrophilic nature of untreated clay impeded its homogeneous dispersion in polymer matrix. Friedlander and Grink (5) repoted a slight expansion of the 001 spacing of clay galleries and concluded that polystyrene was intercalated in clay galleries; but Blumstein (6) questioned intercalation by polystyrene because no increase in the basal spacing could be detected. In this research, in order to overcome the differences in nature of polymer and nano clay, polyvinyl alcohol (PVA) which is a hydrophilic material was grafted on copolymer of styrene-maleic anhydride copolymer (PVA-g-S/MA), in order to increase hydrophiles of polystyrene. Also ultrasound which is a powerful instrument was employed to disperse inorganic nano clay in to the terpolymer (PVA-g-S/MA).

## Experimental
### Reaction 1:
### Copolymerization of styrene(S) and maleic anhydride (MA).

The copolymerization reaction was carried out a four-necked flask equipped with a stirrer, thermometer, condenser, and nitrogen inlet. The general experimental procedures were as follows: 1 mole of S and 1 mole of MA were dissolved in 400 mL toluene after being stirred in an atmosphere of nitrogen. The reaction temperature was adjusted at 100.degree. C., and 1 g benzoyl peroxide was added as an initiator. The reaction was allowed to proceed for 5 h. The products were precipitant in toluene which were separated by filteration.

### Reaction 2:
### Coupling Reaction between S-co-MA and polyvinyl alcohol (PVA).

Ten gram of copolymer of styrene and maleic anhydride

(S-co-MA) which prepared as described above was dissolved in 50 mL of dimethyl sulfoxide (DMSO), and after complete dissolution, PVA (10 g) was added. The

reaction was allowed to react at 100.degree. C. for 24 h with mechanical stirring under nitrogen. The products were precipitated in water. The products precipitated from water in Reaction 2 were a mixture of grafted terpolymer PVA-g-S/MA, unreacted PVA, and unreacted S-co-MA. They were separated and purified. After the separation, all materials must be dried in a vacuum below 30.degree. C. Data of grafting terpolymerization were calculated.

### Reaction 3:
### Preparation of nano composite of PVA-g-S/MA with nano caly

Ultrasonic irradiation was carried out with the probe of the ultrasonic horn immersed directly in the mixture of 10 g of PVA-g-S/MA, 3 g nano clay and 30 mL DMSO, for 30 minutes. The products which is nano composite of PVA-g-S/MA with nano caly was separated from other side products.

### Result

The main product of the reaction 2, copolymer of styrene-maleic anhydride which is grafted on polyvinyl alcohol (PVA-g-S/MA), was characterized by FT-IR spectrum (Fig 1). As it can be seen in figure 1, grafting was successfully done. FT- IR spectrum of the copolymer shows three characteristic regions leading us to the primary identification. A broad peak in 3000-3800 $cm^{-1}$ region shows the presence of -OH functional group of the polyvinyl alcohol. Symmetrical and asymmetrical stretching of C=O bond in maleic anhydride have been appeared at 1854 and 1730 $cm^{-1}$. The peak at 700 $cm^{-1}$ reveals the presence of benzene ring of the polystyrene The STA analysis shows (figure 2) that the intercalated PVA-g-S/MA-clay nanocomposite exhibited thermal stability better than pure PVA-g-S/MA, The pure PVA-g-S/MA lost 45% of its weight at $300\,^{\circ}$C while nanocomposite lost only 30%.
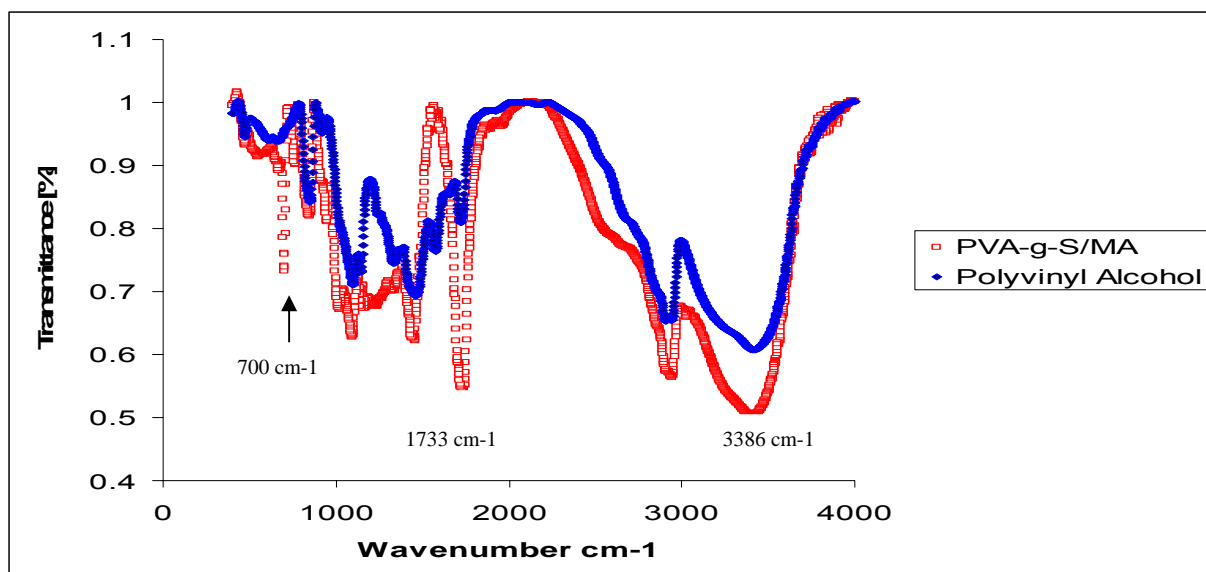
Figure 1. FT-IR spectroscopy of copolymer of styrene - maleic anhydride which is grafted on polyvinyl alcohol (PVA-g-S/MA) & pure polyvinyl alcohol (PVA).
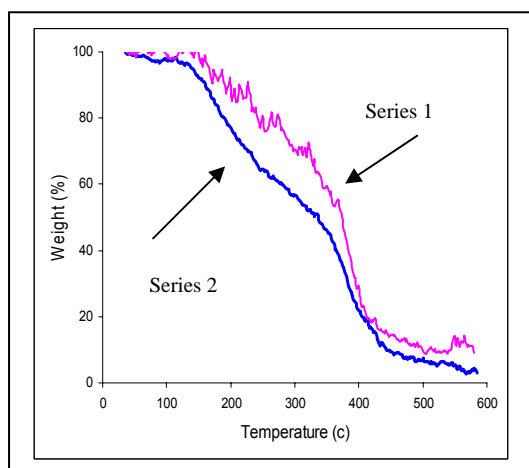


Figure 2. STA experiments of nanocomposite (series 1). & PVA-g-S/MA (series 2).

**Conclusion**

Nano composite of clay and PVA-g-S/MA has exfoliated structure.

**References**

[1] Doh, J. G; Cho, I. *Polymer Bulletin*., 1998, 41, 511.

[2] Vaia, R.; Ishii, H.; Giannelis, *E. Chem. Mater.,* 1993, 5, 1694.

[3] Giannelis, E. P.; *Adv. Mater.*, 1996, 8, 29.

[4] Akelah, A.; Moet, a. *J. Mater. Sci.*, 1996, 31, 3189.

[5] Friedlander. H. Z; Grink, C. R. *J. Polym. Sci.*, *Polym. Lett.,* 1964, 2, 475.

[6] Blumstein, A. *J. Polym. Sci.*, *Part A*. 1965, 3, 2653.

# ELECTRIC TRANSPORT PROPERTIES OF THE p53 GENE AND THE EFFECTS OF POINT MUTATIONS

*C. T. Shih[1], S. Roche[2]*

*[1]Department of Physics, Tunghai University, 181 Taichungkang Road Sec.3, 40704 Taichung, Taiwan*
*[2]CEA/DSM/DRFMC/SPSMS, 17 avenue des Martyrs, 38054 Grenoble, France*

*ctshih@thu.edu.twl*

The transport properties of the p53 gene are studied by the transfer matrix method on a tight-binding model. The position-dependent transmission coefficient and the effects of point mutations on the transmission are evaluated for p53 sequence. The different behaviours of the cancerous and non-cancerous mutations provide a possible explanation why the cancerous mutations can get rid of the DNA-repairing mechanism and cause cancers.

# EFFECTS IN NANOSTRUCTURE

*G.Sh. Shmavonyan*

*State Engineering University of Armenia, 9a/4 Parpetsi street, Yerevan, 375002, Armenia,*
*gshmavon@yahoo.com*

Broadband characteristics are attractive for optical fiber communication. Recent technology has made optical fiber exhibits very broad bandwidths, almost covering the range from 1.2 μm to 1.6 μm with a loss of less than 1 dB/km. Superluminescent diodes (SLDs) are good candidates of light sources for optical fiber communication, because they are of compact size, can be directly integrated with electronic components. However, to cover the entire usable bandwidth of an optical fiber, many conventional SLDs having different spectral range are required, because each conventional SLD usually has a bandwidth of less than 50nm. Therefore, if the bandwidth of SLDs could be broadened, they will be even more attractive. Multiple quantum well (MQW) engineering is a convenient way that has been widely used to broaden the bandwidth of SLDs. However, the design is not straightforward because the carrier distribution within the MQW is not uniform. By considering the uniform carrier distribution within MQWs, we demonstrate that the spectral bandwidth of SLDs can be significantly broadened by using properly designed non-identical MQWs grown on InP substrate.

To achieve the broadband characteristics, a sequence of non-identical MQWs were designed. Typical processing techniques were used to fabricate bent-waveguide SLDs. When designing a broadband SLD using a non-identical MQW structure, factors such as QW transition energy, number and sequence of different QWs, the thickness of the separate confinement heterostructure (SCH) layer, the selection of the dominant carrier, the ability of the QW to trap the 2D carrier, the uniformity of the 2D carrier within the QWs, etc. must be taken into account. Using a properly designed non-identical MQW structure, the fabrication of even more broadband SLDs should be possible. For SLDs fabricated on the substrate with five 6 nm InGaAsP quantum wells and two 150 nm InGaAsP quantum wells, a very broad emission spectrum is obtained. The spectral width is ~ 400 nm, covering range from 1250 to 1650 nm.

The broadest bandwidth for SLD (400 nm) allows us to achieve the broadest tunability for semiconductor laser for optical communication (100 nm) and to observe three novel effects:
1. Novel bi-directional guided effect of lasing mode is observed in a bending waveguide of SLD.
2. An optical switching effect in one SLD is observed. Switching from one of the most usable wavelength (1540 - 1445 nm) to another (1378 - 1348 nm) in optical communication band using only one SLD is experimentally explored.
3. The SCH layer thickness effect is observed in SLD.

# Investigation of Kinetics of Surface Processes and CH$_4$-H$_2$-Ar Plasma Gas Reactions in Diamond Thin Film Deposition

Babak Shokri[1-2,*] Maziar S Yaghmaee[1-3] and Abdollah Sarani[1]

*Abstract*- **Reaction rate constant is a quantity, which describes the kinetics of physico-chemical behaviors of reactions. In this report, in a plasma medium the reactions kinetics of gas-phase and surface deposition of diamond film will be investigated. In case of gas-phase, a kinetic model is presented in a non-thermal plasma environment. The calculations have been made through Maxwellian EEDF assumption and considering different electron cross sections. The computational algorithm and results will be presented briefly on the example of CH$_4$-H$_2$-Ar ternary system. In addition, to analysis the diamond deposition process, we use the reaction probability algorithm for different surface phenomenon. Then, using the Motz and Wise modified relation, the reaction probability was transformed to the mass action kinetic rate constant. Our results lead to calculation of rate coefficients for surface processes take place during the diamond deposition from plasma medium.**

## INTRODUCTION

Due to extreme hardness, high thermal conductivity and extensive electric properties of diamond-like carbon and polycrystalline diamond thin films, they are an important material choice for advanced nano-technologies.

Among usual methods like CVD "chemical vapor deposition", PE-CVD "plasma enhanced-CVD" due to its better operations conditions for diamond thin film growth is getting more interest to use [1]. The physico-chemical processes involved in PE-CVD processes can be categorized into the gas-phase reactions and the processes taking place on the surface [1]. However, PE-CVD is not fully understood due to its more complicated plasma-chemistry processes and its complex physics behind the gas-phase reactions and surface processes. In this work for plasma gas-phase phenomenon, the rate coefficients for electron impact reactions includes electronic and vibrational excitation, ionization, dissociation and attachment processes have been calculated. Then, regarding the diamond deposition in plasma medium, the rate coefficients of surface reactions, which convert activated gas-phase species to diamond structure have been calculated.

[1] Plasma Physics and Engineering Group, Laser and Plasma Research Institute, Shahid Beheshti University, Tehran, Iran.
[2] Institute for Studies in Theoretical Physics and Mathematics, School of Physics, Tehran, Iran.
[3] Materials and Energy Research Center, Tehran, Iran.
[*] Contacting Author: Babak Shokri is with Plasma Physics and Engineering Group, Shahid Beheshti University, Tehran, Iran.
(phone: 0098-21-22431775; fax: 0098-21-22431773; email: b-shokri@sbu.ac.ir).

## MODEL DESCRIPTION FOR GAS-PHASE PLASMA

Here the modified Arrhenius algorithm [1]-[2] has been used to describe the temperature dependency of rate coefficients chemical reactions, which occur between the species in plasma, as:

$$k_f = AT^\beta \exp\left(\frac{-E_a}{RT}\right), \qquad (1)$$

where $k_f$ is the forward reaction rate constant in mol.cm$^3$/s, $A$ is the pre-exponential factor in cm$^3$.mol.K/s, $T$ is the temperature in absolute scale, $\beta$ is constant, $E_a$ is the activation energy in kJ/mol, $R$ is the universal gas constant in kJ/mol.K.

In case of electron-impact reactions, the estimation of activation energy and pre-exponential factor is difficult. Therefore, through determination of the electron energy distribution function (EEDF) and electron-impact cross-sections [2]-[3], the rate coefficient of electron-impact reactions can be, as:

$$k(T) = \langle \sigma(v)v \rangle_v, \qquad (2)$$

where $\sigma(v)$ is the electron impact cross-section in cm$^2$, and $v$ is the velocity of electrons in cm/s.

In Eq. (2) considering the EEDF, we assumed the Maxwellian distribution [3]-[4] as follows:

$$k = \left(\frac{8}{\pi m_e}\right)^{1/2}\left(\frac{1}{k_B T_e}\right)^{3/2}\int_0^\infty \varepsilon\sigma(\varepsilon)e^{\frac{-\varepsilon}{k_B T_e}}d\varepsilon, \qquad (3)$$

where $m_e$ is the electron mass in gr, $k_B$ is the Boltzmann constant in J/K, $T_e$ is the mean electron temperature in absolute scale and $\varepsilon$ is the electron energy in ev.

Cross-section data for electron collisions with methane have been obtained from the experimental observations in [5]-[6]. For some elementary reactions, during the diamond deposition like ionization and dissociation of the methane, the electron energy dependency of electron impact cross-section (that is $\sigma(\varepsilon)$ in Eq. (3)) has been approximated via Lorentz function. Figure. 1 and 2

show the cross-section data for ionization and dissociation of methane as function of electron energy fitted to experiments. Finally, we calculated the reaction rate coefficient for these elementary reactions which presented in Table. 1.

## MODEL DESCRIPTION FOR SURFACE REACTIONS

Reaction (4) was considered for surface reactions between a gas-phase specie and surface:

$$A(g) + B(S) \leftrightarrow products \qquad (4)$$
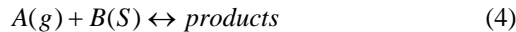
where $A$ stands for gas-phase specie as neutral, radical or ion, and $B$ stands for surface

Here we assume an Arrhenius form for the temperature dependency of the forward reaction rate constant in reaction (4). Moreover, we used the reaction probability algorithm for processes that take place on the surface [1]. Using the Motz and Wise modified relation [7], the reaction probability algorithm has been transformed to mass action kinetic rate constant, as:

$$\gamma_i = a_i e^{-b_i/RT} \implies k_{f_i} = \left(\frac{\gamma_i}{1 - \gamma_i/2}\right) \frac{1}{\Gamma^m}\left(\frac{RT}{2\pi W}\right) \qquad (5)$$

where $\gamma_i$ is the probability of reaction (4), $a_i$ is dimensionless factor, $b_i$ is an energy barrier in kJ/mol, $W$ is molecular weight of the gas-phase species, $\Gamma$ is the total surface site concentration of $B$ type atom, and $m$ is the sum of surface reactant's stoichiometric coefficients.

Table 2. represents the dominate reactions in diamond depositions in plasma medium. By considering $\Gamma = 5.22 \times 10^{-9}$ mol/cm$^2$ [1] as the total surface site concentration, the reaction rate constants of diamond surface processes has been calculated and its results can be seen in Table. 2.

Here a methodology is presented for estimation of different reactions rate constant in gas phase state of plasma medium and surface processes. This model can be used to determine the rate coefficient of different kind of reactions in other nano-materials' processes in a non-thermal plasma medium.

## REFERENCES

[1] M. E. Coltrin and D. S. Dandy, "Analysis of diamond growth in subatmospheric dc plasma-gun reactors," *J. App. Phys.* 74 , pp. 5803-5820, 1993
[2] Y. Yang, "Direct Non-oxidative Methane conversion by non-thermal plasma: modeling study," *Plasma Chem. Plasma Process* 23, pp. 327-346, 2003
[3] M. A. Lieberman and A. J. Lichtenberg, *Principles of Plasma Discharges and Materials Processing*, Wiley, New York, 1994
[4] E. Meeks and P. Ho, "Modeling plasma chemistry for microelectronics manufacturing," *Thin Solid Films* 365, pp. 334-347, 2000
[5] W. L. Morgan, "A critical evaluation of low energy electron impact cross section for plasma processing modeling IICF4,SiH4 and CH4," *Plasma Chem. Plasma Process* 12, pp. 477-493, 1992
[6] D. K. Davies, L. E. Kline and W. E. Bies, "Measurement of swarm parameters and derived of electron collision cross section in methane," *J. Appl. Phys.* 65, pp. 3311-3323, 1989
[7] H. Motz and H. Wise, "Diffusion and heterogeneous reaction III atom recombination at a catalytic boundary," *J. Chem. Phys.*31, pp. 1893, 1960
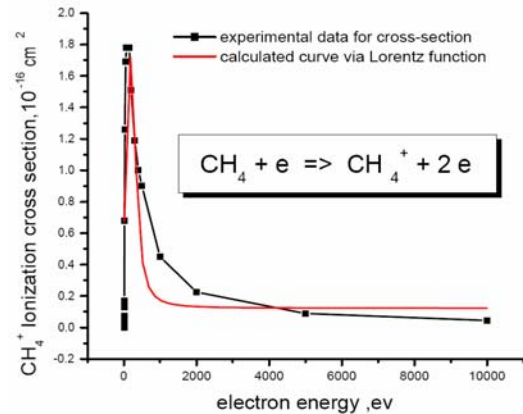
Fig. 1 Data for methane ionization reaction.
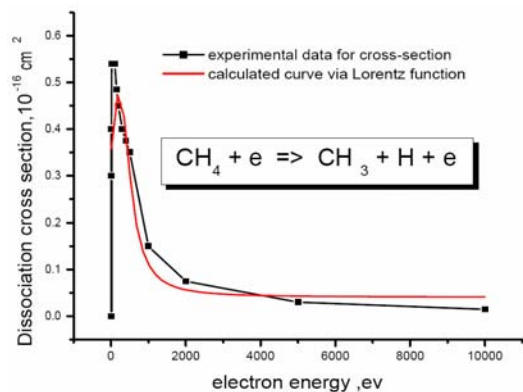


Fig. 2 Data for methane dissociation reaction.

Table. 1
CALCULATED REACTION RATE COEFFICIENT FOR SOME ELEMENTARY REACTIONS IN GAS-PHASE

| reaction | rate constant | remark |
|---|---|---|
| e + CH$_4$ → CH$_4^+$ + 2 e | 1.5285 e$^{+15}$ | CH$_4$ ionization |
| e + CH$_4$ → CH$_3^+$ + H + 2 e | 1.8987 e$^{+15}$ | CH$_3^+$ ionization |
| e + CH$_4$ → CH$_3$ + H + e | 5.9802 e$^{+14}$ | dissociation |
| e + CH$_4$ → CH$_2$ + H$_2$ + e | 5.9842 e$^{+14}$ | dissociation |
| e + CH$_4$ → CH + H$_2$ + H + e | 8.4977 e$^{+14}$ | dissociation |
| e + CH$_4$ → C + H$_2$ + H$_2$ + e | 8.6205 e$^{+14}$ | dissociation |
| e + CH$_4$ → CH$_2$ + CH$_2^-$ | 3.12 e$^{+12}$ | CH$_2^-$ attachment |

Table. 2.
CALCULATED RATE CONSTANTS FOR DOMINATE REACTIONS IN DIAMOND DEPOSITION PROCESS

| reaction | rate constant | remark |
|---|---|---|
| CH $_{(S)}$ + H → C $_{(S,R)}$+ H$_2$ | 7.16 e$^{+10}$ | initiation |
| C $_{(S,R)}$ + C → D + C $_{(S,R)}$ | 3.1 e$^{+9}$ | C atom addition |
| C $_{(S,R)}$ + HCCH → D + HCCH $_{(S,R)}$ | 7.9 e$^{+10}$ | HCCH addition |
| C $_{(S,R)}$ + CH$_3^+$ → D + CH$_3^+$ $_{(S,R)}$ | 5.07 e$^{+9}$ | CH$_3^+$ addition |

# POLY(STYRENE-CO-VINYLBENZYLCHLORIDE-CO-DIVINYLBENZENE) COATED IRON OXIDE:  SYNTHESIS AND EFFECTS ON SIZE AND MORPHOLOGY

*M. D. Shultz[1], J.R. Marin[2], S. H. Naik[1], J. Wilkins[1] J.M. Laza[2], J.L.Vilas[2], L.M. Leon[2], E. E. Carpenter[1]*
*[1]Virginia Commonwealth University, Richmond, VA, USA*
*[2]Basque Country University, Bº Sarriena s/n, Leioa, Spain*
*shultzmd@vcu.edu*

Funtionalization of magnetic nanoparticles is a key step for their integration into mainstream applications.  This has been accomplished by several different methods ranging from simple chelating ligands to large polymer shells.[1-4]  Polymer shells have a greater effect on particle size, but can offer more stability when compared to some chelating agents.[5]  In this work, iron oxide nanoparticles are coated with poly(styrene-co-vinylbenzylchloride-co-divinylbenzene) that is formed by precipitation polymerization.  The synthesis was carried out by similar methods used to produce poly(styrene-co-divinylbenzene) microspheres,[6] with the addition of iron oxide nanoparticles (0 – 5% by mass) to the monomer solution and the replacement of some styrene with vinylbenzylchloride.  The addition of the chlorine to the polymer coating should increase hydrophilicity of the resultant particles and also open the possibility of further functionalization reactions.  The iron oxide nanoparticles were synthesized by a polyol technique.[7-8] Powder x-ray diffraction confirmed the spinel structure for the iron oxide.  Vibrating sample magnetometry yielded a saturation magnetization of 60 emu/g, thus suggesting maghemite ($\gamma$-Fe$_2$O$_3$).

As seen in Fig. 1, the resultant polymer microspheres without nanoparticles are fairly monodispersed with a diameter of 4 µm.  The addition of nanoparticles appears to decrease the size of the microspheres as well as increase the polydispersity as seen in Fig. 2. This trend is also seen to continue as you add more nanoparticles to the system going from 4 µm with 0 % nanoparticles, down to below 1 µm for 5 % nanoparticles.  This indicates that the particles are not just incorporated into the polymer matrix, but act as nucleation sites to begin the polymerization process.  The polymerization process was found to have no effect on the nanoparticles themselves as the magnetic characterization showed only a mass dilution in saturation when corrected by thermal gravimetric analysis.

**References:**
(1)      Burke, N. A. D.; Stover, H. D. H.; Dawson, F. P. *Chemistry of Materials* **2002**, *14*, 4752-4761.
(2)      Jeong, J. R.; Lee, S. J.; Kim, J. D.; Shin, S. C. *Ieee Transactions on Magnetics* **2004**, *40*, 3015-3017.
(3)      Pyun, J. *Polymer Reviews* **2007**, *47*, 231-263.
(4)      Shultz, M. D.; Calvin, S.; Fatouros, P. P.; Morrison, S. A.; Carpenter, E. E. *Journal of Magnetism and Magnetic Materials* **2007**, *311*, 464-468.

(5)      Shultz, M. D.; Reveles, J. U.; Khanna, S. N.; Carpenter, E. E. *Journal of the American Chemical Society* **2007**, *129*, 2482-2487.

(6)      Shim, S. E.; Yang, S. H.; Choi, H. H.; Choe, S. *Journal of Polymer Science Part a-Polymer Chemistry* **2004**, *42*, 835-845.

(7)      Ammar, S.; Jouini, N.; Fievet, F.; Stephan, O.; Marhic, C.; Richard, M.; Villain, F.; Moulin, C. C. D.; Brice, S.; Sainctavit, P. *Journal of Non-Crystalline Solids* **2004**, *345-46*, 658-662.

(8)      Fievet, F.; Lagier, J. P.; Blin, B.; Beaudoin, B.; Figlarz, M. *Solid State Ionics* **1989**, *32-3*, 198-205.

**Figures:**
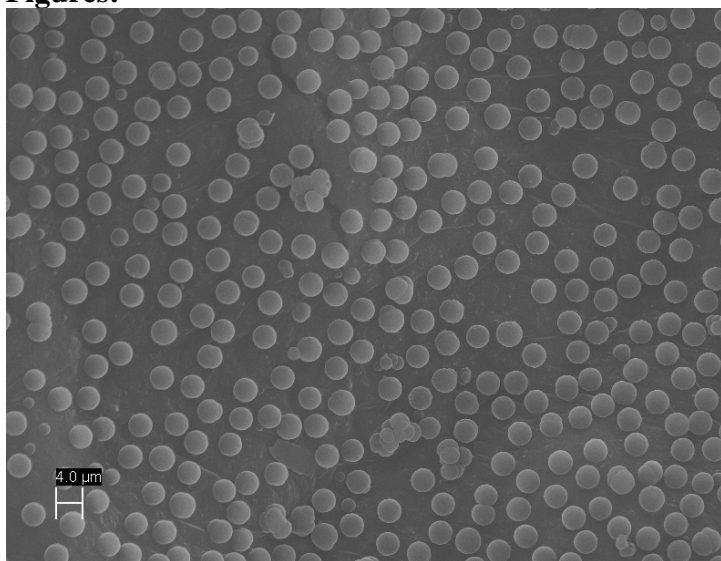


Fig. 1.  Scanning electron microscopy image of PS-VBC-DVB microspheres without nanoparticle loading.
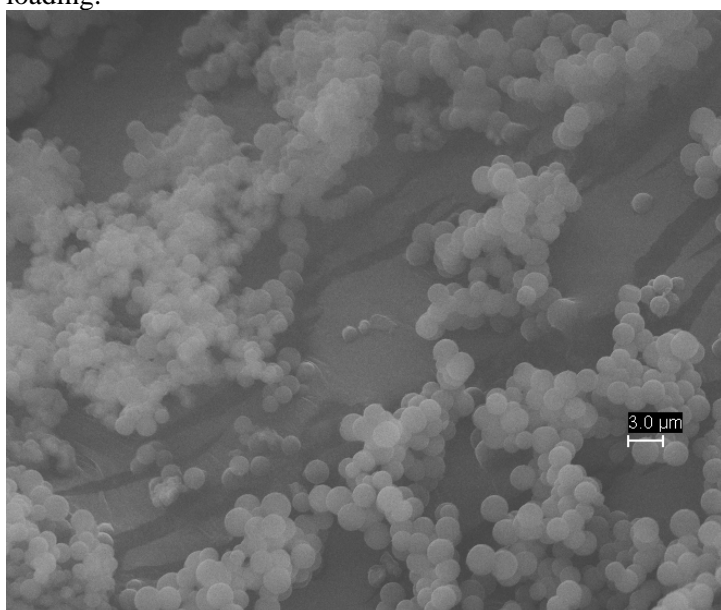


Fig. 2.  Scanning electron microscopy image of PS-VBC-DVB with nanoparticles loaded at 1% by mass to the amount of monomer.

# Self-assembly of NC-PH$_3$-CN molecules on Ag(111): Formation of 2D hydrogen-bonded and organometallic networks

**I. Silanes**[1,*], U. Schlickum[2], R. Decker[2], F. Klappenberger[2,3], G. Zoppellaro[4],
S. Klyatskaya[4], M. Ruben[4], K. Kern[2,5], H Brune[2], J.V. Barth[2,3,6] and A. Arnau[1,7,8]

[1] *Donostia International Physics Center (DIPC), Manuel Lardizabal 4, 20018 San Sebastián, Spain*
[2] *Institut de Physique des Nanostructures, Ecole Polytechnique Fédérale de Lausanne, CH-1015 Lausanne, Switzerland*
[3] *Physik Department E20, Technische Universität München, D-85748 Garching, Germany*
[4] *Institut für Nanotechnologie, Froschungszentrum Karlsruhe, D-76021 Karlsruhe, Germany*
[5] *Max-Plank-Institut für Festkörperforschung, D-70569 Stuttgart, Germany*
[6] *PHAS-AMPEL, 2355 East Mall, University of British Columbia, Vancouver V6T 1Z4, Canada*
[7] *Departamento de Física de Materiales UPV/EHU, Facultad de Química, Apartado 1072, San Sebastián 20080, Spain*
[8] *Unidad de Física de Materiales, Centro Mixto CSIC-UPV/EHU, Manuel Lardizabal 3, 20018 San Sebastián, Spain*

*\* e-mail: inaki\_silanes@ehu.es*

## Abstract

Ditopic linear cyano-organic molecules are of great interest for the generation of bidimensional networks on metallic surfaces, because of their ability to form self-assembled hydrogen-bonded all-organic monolayers, as well as shape-resistant organometallic networks upon addition of transition metal atoms, to which cyano groups are known to bind strongly.

In this poster we show a study for the case of the NC-Ph$_3$-CN molecule on a Ag(111) surface, before and after addition of cobalt atoms. In the case of the all-organic monolayer, different structures are proposed (see Figure 1), and their relative stability is discussed. We also discuss the effect of the surface upon the intrinsic binding scheme of the cyanophenyls, modelled by a planarization of the structures. For the Co-coordinated networks, an energetic explanation is found for the experimental 3-fold coordination of the cobalt centers, comparing it with an alternate 4-fold coordination (see Figure 2).

Chevron        Rectangular        Rhombic
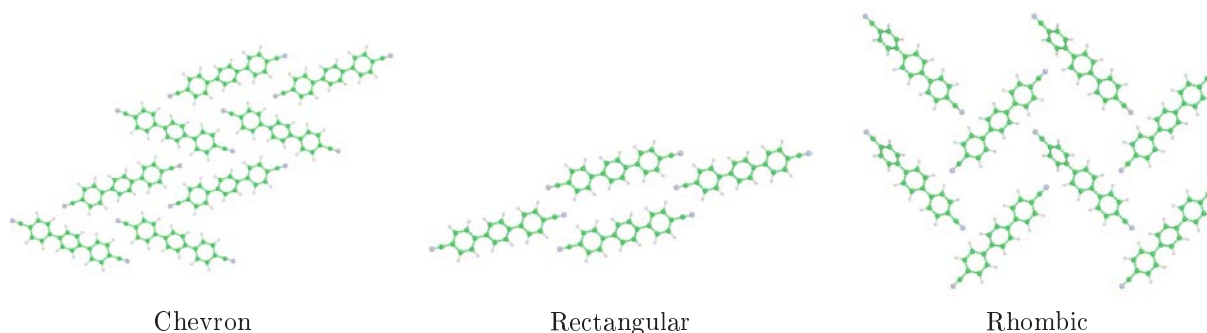
Figure 1: Three different patterns proposed for NC-Ph$_3$-CN self assembly.

3-fold coordination        4-fold coordination        Honeycomb periodic structure

Figure 2: Induced charge density plots around the cobalt atom for 3-fold and 4-fold coordination. The corresponding honeycomb lattice for the 3-fold coordination is also shown.

# SINGLE-WALLED CARBON NANOTUBES (SWCNTs): DIELECTRIC FUNCTION AND EXCITON SPECTRA

*Oleksii A. Smyrnov*
*Department of Theoretical Physics, Odessa I. I. Mechnikov National University,*
*2 Dvoryanskaya St., Odessa 65026, Ukraine*
*smyrnov@onu.edu.ua*

A lot of experimental papers on optical absorption in SWCNTs describe obtained results in terms of band-to-band direct transitions between single particle states, though it is clear that the inherent to 1D systems strong interparticle interaction cannot be neglected. It seems obvious that the strong electron-hole attraction should bind electron-hole pairs in SWCNTs into Wannier-Mott like excitons. Furthermore, the exciton contributions were already revealed experimentally in optical absorbtion spectra [1], [2], and in spectra of fluorescence [3], [4] of individual SWCNTs. There are also some works devoted to theoretical study of excitons in CNTs [5]-[8]. However, as it follows from results of the latter a simple translation of basic hydrogen-like models of 3D large radius excitons fails to function in one dimension without a certain specification.

Here we propose the following 1D large radius exciton model for semiconducting SWCNTs in vacuum.

- We study the spectrum of large radius excitons in semiconducting nanotubes and corresponding wave functions within the framework of elementary potential model, in which exciton is modeled as bound state of two oppositely charged quasi-particles confined on the nanotube surface and interacting through the attractive Coulomb potential. Due to the parity of the potential, exciton states split into the odd and even series.

- Early such models, for example [9], [10], worked with some sequences of the 1D exciton Hamiltonians with regularized at the origin Coulomb potentials. The limit negative spectra for these Hamiltonians reduced to the Balmer series, each eigenvalue of which was doubly degenerate (the odd and even states eigenvalues coincided) except of the eigenvalue of (even) ground state, which was assumed tending to infinity.

- We show that foregoing models are not the only possible and by selection of a suitable boundary condition for even exciton wave functions $\psi(z)$ at the origin any finite negative value lesser than the minimal eigenvalue of the odd series may be given to the ground state eigenvalue.

- We take the following boundary condition

$$\lim_{z \to 0} \frac{d}{dz}\left[\left(1 + 2A|z|\ln\left(2A|z|\right)\right)\psi(z)\right] = 0,$$

   where $A = \mu e^2 / \eta^2$ as the nearest analog of the boundary condition $\psi'(0) = 0$ for the even series in the case of potentials without Coulomb singularity. Using the von Neumann formulae [11] we show that the 1D exciton Schrodinger differential operator defined by this boundary condition is self-adjoint. We obtain the corresponding spectrum, which appeared to be close to that for the two-dimensional hydrogen atom [12] for the states with zero angular momentum.

- This fact is not yet a valid reason to consider the proposed Hamiltonian as an appropriate one for the large radius exciton in nanotubes. However, the modified electron-hole (e-h) interaction potential, that accounts, that these particles actually are not pointwise and their charges are smeared along infinitesimal narrow bands on the nanotube surface, appeared to be locally quadratically integrable (unlike the 1D bare Coulomb potential). And in the case of nanotubes of small radii the Hamiltonian with this quadratically integrable potential gives the energies of ground and first excited states of the standardly defined (with boundary condition: $\psi'(0) = 0$) even exciton series, which differ slightly from those for the proposed Hamiltonian.

- It turned out that the ground state energy of even excitons, calculated for individual semiconducting carbon nanotubes in vacuum for both of the Hamiltonians and without account of the effect of the e-h interaction potential screening by nanotube electrons, well exceeds the energy gap.
- To make clear whether the screening of e-h interaction by the nanotube electrons could result in the shift of exciton levels into the gap we consider different forms of screening of the interaction potential of non-pointwise electron and hole.
- We obtain the nanotube dielectric function within the framework of the Lindhard method (the so-called RPA) then in the limiting case of small wavenumber values we get the Thomas-Fermi screening theory for charged particles in semiconducting SWCNTs and also the contribution to the screening of free charges at high temperatures.
- Using the values of effective masses and energy gaps obtained in [13] within the framework of the null-range potential method [14] we have calculated unscreened and screened e-h interaction potentials and corresponding exciton binding energies of the ground and excited states, which either explicitly or implicitly depend on parameters of concrete semiconducting SWCNT (chirality, radius, reduced effective mass, band gap magnitude) and the temperature of medium.
- In the all cases the binding energies of SWCNTs even excitons in the ground states nevertheless appeared to be larger than corresponding band gaps. The same results have been obtained in [15]. It is asserted in [15], that the exciton binding energy cannot be larger than the energy gap because of the singularity of the frequency-dependent dielectric function $\varepsilon(\omega)$ at $\omega = E_g / \eta$. But the frequency dependence has to be taken into account only if the retardation effect becomes important which is not the case for SWCNTs.

  We conclude that single-electron states in SWCNTs in vacuum are most likely unstable at least in the vicinity of the energy gap as regards to formation of excitons.

**References:**

[1] Ichida M., Mizuno S., Tani Y., Saito Y., Nakamura A., J. Phys. Soc. Japan **68** (1999) 3131-33.

[2] Ichida M., Mizuno S., Saito Y., Kataura H., Achiba Y., Nakamura A., Phys. Rev. B **65** (2002) 241407(R).

[3] O'Connell M. J. *et al.*, Science **297** (2002) 593-6.

[4] Bachilo S. M., Strano M. S., Kittrell C., Hauge R. H., Smalley R. E., Weisman R. B., Science **298** (2002) 2361-66.

[5] Ando T., J. Phys. Soc. Japan **66** (1997) 1066-73.

[6] Ando T., J. Phys. Soc. Japan **73** (2004) 3351-63.

[7] Spataru C. D., Ismail-Beigi S., Benedict L. X., Louie S. G., Phys. Rev. Lett. **92** (2004) 077402.

[8] Chang E., Bussi G., Ruini A., Molinari E., Phys. Rev. Lett. **92** (2004) 196401.

[9] Loudon R., Am. J. Phys. **27** (1959) 649-55.

[10] Cornean H. D., Duclos P., Pedersen T. G., Few-Body Systems **34** (2004) 155-161.

[11] Akhiezer N. I., Glazman I. M., Theory of Linear Operators in Hilbert Space vol. 2 (Monographs and Studies in Mathematics vol. 10) ed. E. R. Dawson, W. N. Everitt (Boston: Pitman (Advanced Publishing Program)) (1981).

[12] Yang X. L., Guo S. H., Chan F. T., Wong K. W., Ching W. Y., Phys. Rev. A **43** (1991) 1186-96.

[13] Tishchenko S. V., Low Temp. Phys. **32** (2006) 1256-61.

[14] Albeverio S., Gesztesy F., Hoegh-Krohn R., Holden H., Solvable Models in Quantum Mechanics. Texts and Monographs in Physics (New York: Springer) (1988).

[15] Bulashevich K. A., Rotkin S. V., Suris R. A., Excitons in single-wall carbon nanotubes, 11th. Int. Symp. "Nanostructures: Physics and Technology" (June 23-28, St Petersburg, Russian Federation) (2003).

# Improvement of Porous-Structure Controllability for Fabrication of Sintered Porous Aluminum Materials by Coating Al Powder with Tin

*Tsutomu Sonoda, Kiyotaka Katou*
*National Institute of Advanced Industrial Science and Technology (AIST),*
*2266-98 Anagahora,  Moriyama-ku, 463-8560, Nagoya, Japan*
*tsutomu.sonoda@aist.go.jp*

The deposition of pure tin onto pure aluminum powder in its self-convective motion by magnetron DC sputtering was examined in order to prepare Al-Sn composite powder and thereby to improve the sintering of the aluminum particles, aiming at the development of highly structure-controlled porous aluminum materials by space-holder method in powder metallurgy processing. The effects of the sputter-deposition of tin on porous structure and mechanical properties of the sintered compact were investigated.

Figure 1 shows typical SEM images of the surface of the aluminum particles before the sputter-deposition and those obtained after the sputter-deposition. The surface of the obtained particles appeared to be covered with deposited tin fine particles without any peelings of the deposits of tin observed. Thus it seemed that the sputtered tin could be adherently deposited onto the surface of the aluminum particles.



|  (a) Before the sputter-deposition | (b) After the sputter-deposition |
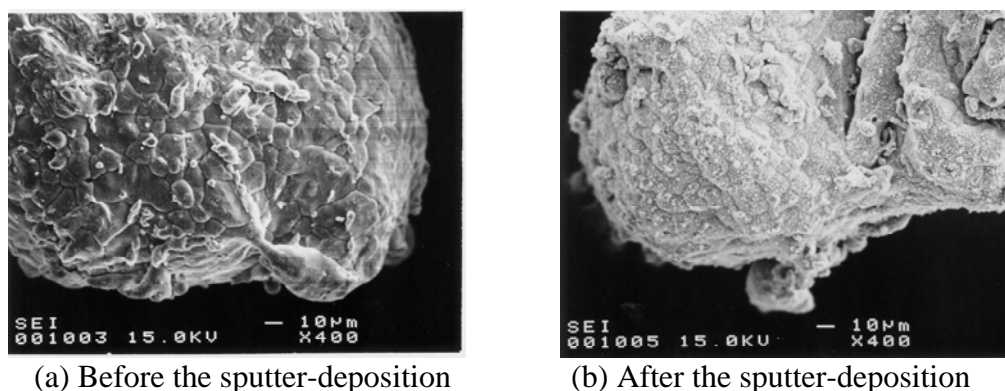
**Fig. 1.** SEM image of the surface of the aluminum particles before the sputter-deposition(a) and that obtained after the sputter-deposition(b).

Figure 2 shows the result of EPMA analysis on the surface of the particles obtained after the sputter-deposition in this study. According to EPMA analysis, K$\alpha$  X-ray peaks of Sn were definitely detected on the surface of the particles. Thus it was confirmed that the obtained particles were coated with the tin deposits. According to DSC analysis, it was found that the obtained particles were coated with  pure tin deposits because endothermic peak was detected at the temperature of the melting point of pure Sn, which was lower than around 250℃. Furthermore, according to its quantitative analysis of the tin film, the average thickness of the tin film could be estimated to be around 1 nm from its  endothermic calorie.

Next the preparation of porous aluminum materials was carried out using the Al-Sn composite powder obtained above by space-holder method in ordinary powder metallurgy processing. It was found that the mechanical durability of the pre-sintered compacts obtained after heating up to the removing temperature (400℃) for the sublimation of resinous spacer materials was improved by the sputter-deposition. It was also found that the sintering of the aluminum particles was highly enhanced at the temperature of 650℃ by the sputter-deposition and thereby that mechanical properties of the sintered compacts was considerably improved.
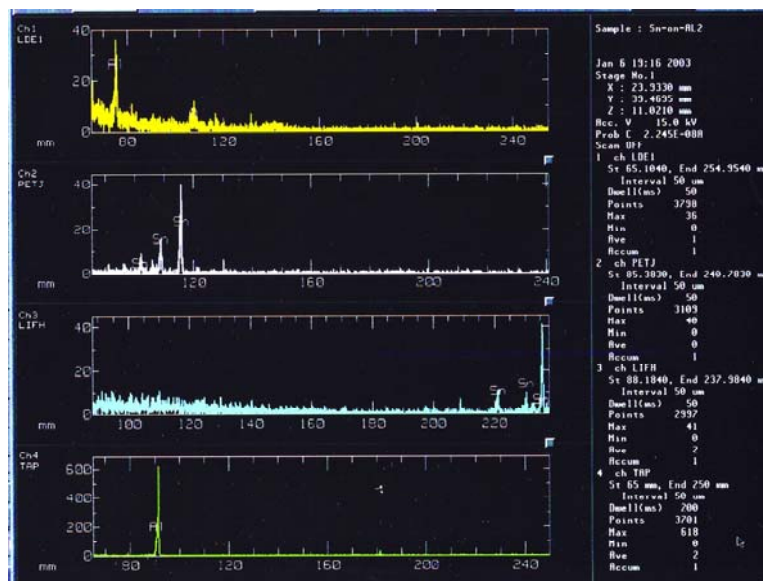
**Fig. 2.** Result of EPMA analysis on the surface of the particles
obtained after the sputter-deposition in this study.

Figure 3 shows the X-ray C.T. images for porous structures of the sintered porous compacts with the porosity 80% obtained from aluminum powder without the tin sputter-deposition and with the tin sputter-deposition. According the C.T. images, it was found that the porous structure of the sintered porous materials with the porosity 80% was better regulated by the sputter-deposition, compared to that without the deposition. Furthermore, regarding to their compressive properties, it was found that the plateau stress of the sintered porous materials reached by the sputter-deposition twice as high as than that without the deposition.



(a) Without sputter-deposition of Sn        (b) With Sn sputter-deposition of Sn
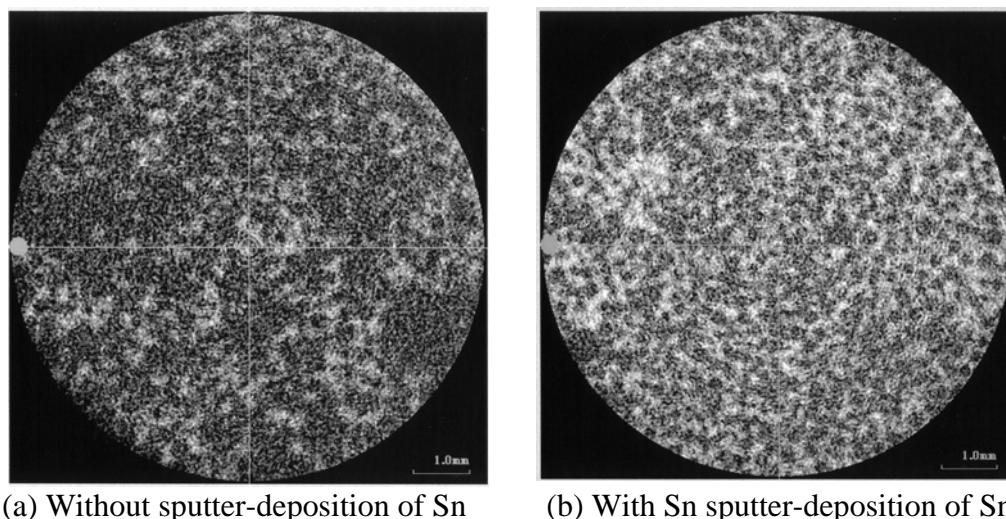
**Fig. 3.** X-ray C.T. images for porous structures of the sintered porous compacts
with the porosity 80% obtained from aluminum powder without the tin
sputter-deposition(a), and with the tin sputter-deposition(b).

Therefore it was concluded that the coating of aluminum powder with nano-order thick tin deposits enables the porous-structure to be controlled more effectively in fabricating sintered highly porous aluminum materials, as well as improves their mechanical property.

# ELECTRONIC STRUCTURE AND SELF-ASSEMBLY OF SEMICONDUCTOR NANOCRYSTALS ARRAYS

*Dov Steiner*, *Doron Azulay, Assaf Aharoni, Assaf Salant, Oded Millo and Uri Banin*

*Departments of Physics and Physical Chemistry and the Center for Nanoscience and Nanotechnology, the Hebrew University of Jerusalem, Jerusalem 91904, Israel.*

The electronic level structure of colloidal InAs quantum dots (QDs) in two-dimensional arrays, forming a QD-solid system, was probed using scanning tunneling spectroscopy. The band gap is found to reduce compared to that of the corresponding isolated QDs. Typically, the electron ('conduction-band') ground state red shifts more than the hole ('valence-band') ground state. This is assigned to the much smaller effective mass of the electrons, resulting in stronger electron delocalization and larger coupling between electron states of neighboring QDs compared to the holes. This is corroborated by comparing these results with those for InAs and CdSe nanorod assemblies, manifesting the effects of the electron effective mass and arrangement of nearest neighbors on the band gap reduction. In addition, in InAs QD arrays, the levels are broadened, and in some cases their discrete level structure was nearly washed out completely and the tunneling spectra exhibited a signature of two-dimensional density of states.

In an attempt to achieve long-range order and alignment in CdSe nanorod arrays, various techniques were used. Arrays of close-packed standing rods were formed by applying electric field of $\sim 10^{6}$V/m perpendicular to the substrate during solution evaporation. For the alignment of laying rods, very slow evaporation of nanorods solution ($\sim 20$ nm/sec) perpendicular to the substrate was found most effective for achieving long-range ordered 2D arrays.

# STRUCTURE AND MECHANICAL PROPERTIES OF NANOCOMPOSITES BASED ON POLYPROPILENE

**_M.Strat_**[2], *Georgeta Strat*[1], *Irinel Grecu1, S. Gurlui*[2], *V. Grecu*[1], *I. Lihtetchi*[3],
*S. Stratulat*[4]
[1]*"Gh.Asachi "Technical University of Iasi, Romania*
[2]*"Al.I.Cuza" University of Iasi, Romania*
[3]*Transilvania University of Brasov,Romania*
[4]*UMF GR T Popa ,Iasi, Romania*
mstrat@uaic.ro

Polymer clay nanocomposites are a new class of materials which show improved properties at very low loading levels of nanofiller comparing to conventional particulate composites of thermoplastic material[1]. Polymer nanocomposites exhibit superior mechanical properties, reduced gas permeability, improved solvent resistance and enhanced conductivity over polymers. The effect of clay treatment on physical and structural properties of polypropylene (PP J600) nanocomposite has been studied. The analysis of polypropylene nanocomposites was made by means of XRD, FT-IR, and AFM methods.

Although the terms *nanomaterial* and *nanocomposite* represent an early new and exiting field in materials science, such materials have already existed for a long time in the polymer industry and have always existed in nature. A nanocomposite is defined as a composite material with at least one of the dimensions of one of the constituents on the nanometer scale. Despite such complicated structures the smallest building blocks in these materials are generally on the nanometer scale. The manufacturing of polymer nanocomposites usually consists of two stages: the compounding of a nanocomposite and the subsequent melt-forming process such as injection-molding. A primary concern is the achievement of a polymer nanocomposite containing homogeneously distributed and well-dispersed nanoparticles. The dispersion of nanoparticles especially depends on a magnitude of processing parameters, e.g. shear rate and processing temperature, as well as on the selection of appropriate materials. The major reason is that, as it has been demonstrated, introducing clay into polymers at the nanoscale level one can obtain improved mechanical, thermal, flammability and other properties at low clay contents (1-10wt.%). Polymer layered silicates have been prepared in different ways: intercalation in solution [2], in situ polymerization and direct melt intercalation [3]. Since natural clay, as all natural products, suffers a lack of reliability, and therefore exhibits an experimental irreproducibility we choose to use in our research work with the nanoblend MB 1201 (40% nanoclay and 60% PP J600). This material was imported from PolyOne Company, USA.

Three main types of composites (phase separated, intercalated and exfoliated or delaminate structure) may be obtained when layered clay is associated, for example, with polypropylene matrix. These primarily depend on the method of preparation and the nature of components used (layered silicates, organic cations and polymer matrix).

This fact allows in the greater degree to realize their useful qualities and to carry out the directed influence on processes of structure formation and improvement of the operational characteristics of polymeric composites

The experiments carried out were focused on obtaining the polypropylene nanocomposite samples. In all the experiments the polypropylene (PP J600) with flow rate in melt of 9.21g/10min and nanoblend MB 1201 (40% nanoclay and 60% PP J600) were used. The dimensions of nanoblend MB 1201 nanoclay usually range between 1- 100 nm. It can be completely dispersed, the average size of the dispersed layers being around 25 nm, while the

L/D ratio ranges between 100 and 1000. Nanoblend MB 1201 was chosen for the experiments, with the following characteristics: interlayer distance (d-001) 3.5 nm, color-white, organic compound of smectite. The technological processes have different stages for the obtaining of the samples. We have used the segments of experiments which were repeated for different percentage mixtures of concentrate and polypropylene necessary to obtain the samples with final nanoclay contents of 4% (NPP4) and 6% (NPP6), respectively.

The concentrate was obtained on a laboratory extruder with two co-rotating helical conveyers type APV Baker, England, working at temperatures between 200- 220$^o$C on the heating zones. Fig. 1, shows the XRD spectra of the nanoblend MB 1201, PP J600 and the various PP nanocomposites compounded in a single-screw extruder configured with different temperature arrangements. The organosilicate, nanoblend MB 1201, exhibited three distinct peaks characterising its interlayer basal spacing, at 1.63, 3.82 and 8.26 ° 2θ angles. The nanocomposites spectra showed evidence of intercalation and exfoliation, indicated by the smoothening, the shifting of the second and thread, order organosilicate reflections. In addition, intercalation of the organosilicate galleries by polymer matrix can be witnessed by the shift to lower 2θ angles of the second and third order organosilicate peaks.

The organo- nanocomposites show improved mechanical properties: both tensile strength and, surprisingly, charpy impact were higher than the ones of the pure polymer.

References.

[1]. Bousmina M., Proceeding of PPS-21, (2005) 16-19 June, Leipzig, Germany

[2]. Ogata N., Jimenez G., Kawai H., Ogihara T., J. Polym. Sci. Polym. Phys.,(1997), **35**, p.389

[3]. Fornes, T. D.; Yoon, P. J.; Keskkula, H.; Paul, D. R., Nylon 6 Nanocomposites: The Effect of Matrix Molecular Weight, Polym., (2001), **42**, p. 9929

Figure.
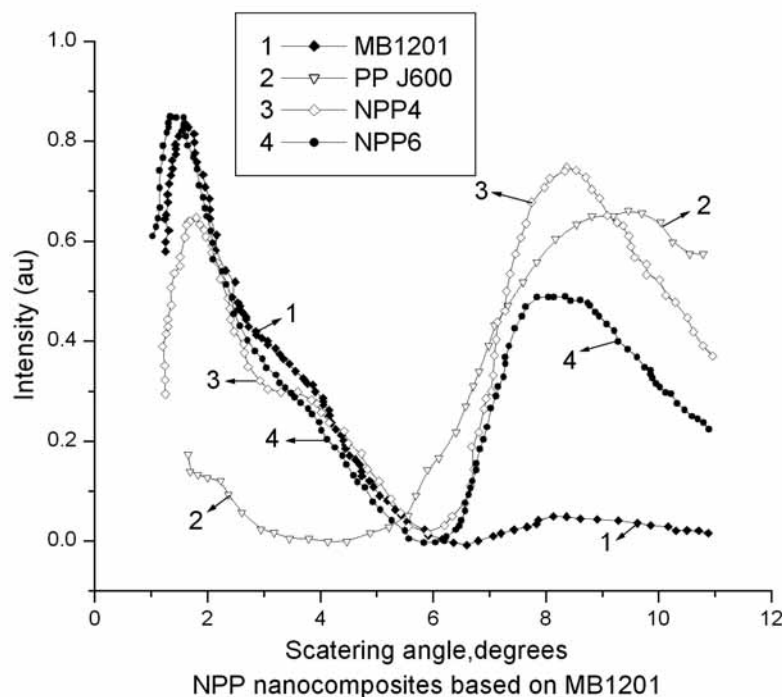


Fig.1 XRD pattern for NPP nanocomposites (1-10 degree)

# ION BEAM DEPOSITION OF NANOSCALED TITANIUM NITRIDE AND OXYNITRIDE FILMS ON SILICON

*A. Styervoyedov [1, 2], V. Farenik [1, 2]*
*[1] Scientific Centre of Physical Technologies of MES and NAS of Ukraine, Svobody sq.6, 61022 Kharkiv, Ukraine*
*[2] V.N. Karazin Kharkiv National University, Svobody sq. 4, 61077 Kharkiv, Ukraine*
*standrey@yahoo.com*

Nanoscaled films of metal nitrides and oxynitrides due to their remarkable physical and chemical properties are intensively studied and applied in technology both as wear and corrosion resistant coatings and as functional films for novel electronic devices fabrication in semiconductor industry. Titanium compounds are intensively studied as, for example, optical coatings [1], buffer layers in multilayer structures [2, 3] and high-temperature contacts [4]. One of the perspective methods of nanoscaled functional films formation is sputtering of materials by ion beam and its deposition on the prepared substrate [5]. During ion sputtering particles emitted by target have energies from several to hundred eV. Affecting on condensation surface they are strongly influence on nucleation, growth and final film characteristics. The important advantage of ion-beam sputter deposition is also the possibility of using of only one source for substrate surface cleaning, sputtering of several targets with different composition and also for ion assistance of film growth [6].

X-ray photoelectron spectroscopy (XPS) is one of the few instruments for chemical state analysis of surface due to its perfect elemental sensitivity. High surface sensitivity makes XPS more and more popular because of great interest to investigations of ultra-thin films for nanotechnology and nanoelectronics applications. When the film thickness doesn't exceed several monolayers, XPS also allows to investigate film / substrate interface and reactions, which occur there as the result of thermal annealing or ion bombardment. Such investigations are very interesting, for example, in nanoelectronics where the formation of different oxides or silicates (in the case of Si or SiC) on the interface strongly influences on electric characteristics of obtained structures.

The current work presents both theoretical and experimental study of low-current ion beam sputter deposition of nanoscaled titanium nitride and oxynitride films on silicon. Elemental composition and chemical state of obtained films were investigated by X-ray photoelectron spectroscopy with using of Mg-K$\alpha$ X-ray radiation (photon energy 1253.6 eV).

Ultra thin (~5 nm) TiN, Ti/TiN and $TiN_xO_y$ films were formed on silicon by ion beam sputtering of titanium target of 99.99% purity in nitrogen atmosphere using cold cathode ion gun. Ion gun was installed with the possibility of ion beam direction changing during the experiment, as shown on Fig.1. Such installation allows us to clean both the target and substrate with ions from natural oxides and contaminations before deposition. Titanium was sputtered by argon ions with the 5 keV energy and 15 $\mu$A/cm$^2$ ion current density. Vacuum before switching on the ion source was $4 \cdot 10^{-8}$ mbar. During switching on the ion source, Ar gas was introduced into discharge chamber of ion source up to the vacuum chamber pressure of $5 \cdot 10^{-6}$ mbar. After deposition samples were transported from the preparation chamber to the analytical chamber without breaking vacuum for investigation by XPS. X-ray characterization was performed at the pressure of $5 \cdot 10^{-10}$ mbar. After the primary analysis samples were annealed for 5 minutes at the temperatures of 650°C and 750°C by electric current going directly through the sample. After each stage of annealing samples were investigated by XPS (Fig.2). The influence of thermal and vacuum conditions during sputtering and post deposition annealing on characteristics of obtained films were studied and will be presented.

**References:**

[1] J.E. Klemberg-Sapieha et al., Applied Optics, Vol. **43**, No.13 (2004) 2670.
[2] P. Tiwari et al. Appl. Phys. Lett., **65** (21) (1994) 2693.
[3] H. Wang, Ashutosh Tiwari, A. Kvit, X. Zhang, and J. Narayanet, Appl. Phys. Lett., **80** (2002) 2323.
[4] J.R. Waldrop, Appl. Phys. Lett., **43** (1983) 87.
[5] A.Styervoyedov, V.Farenik, Surface Science **600** (2006) 3766.
[6] N. Popovic et al., Thin Solid Films, **459** (2004) 286.

**Figures:**
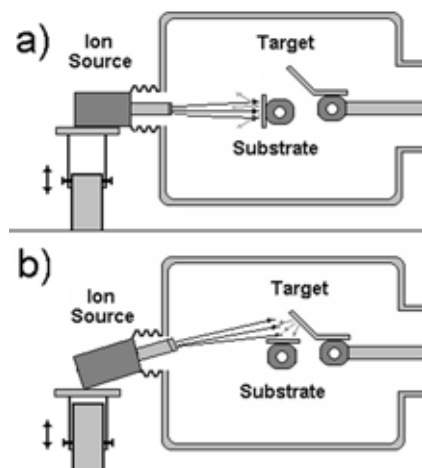


Fig.1. Schematic sketch of ion gun installation: a) substrate cleaning; b) ion beam sputter deposition.
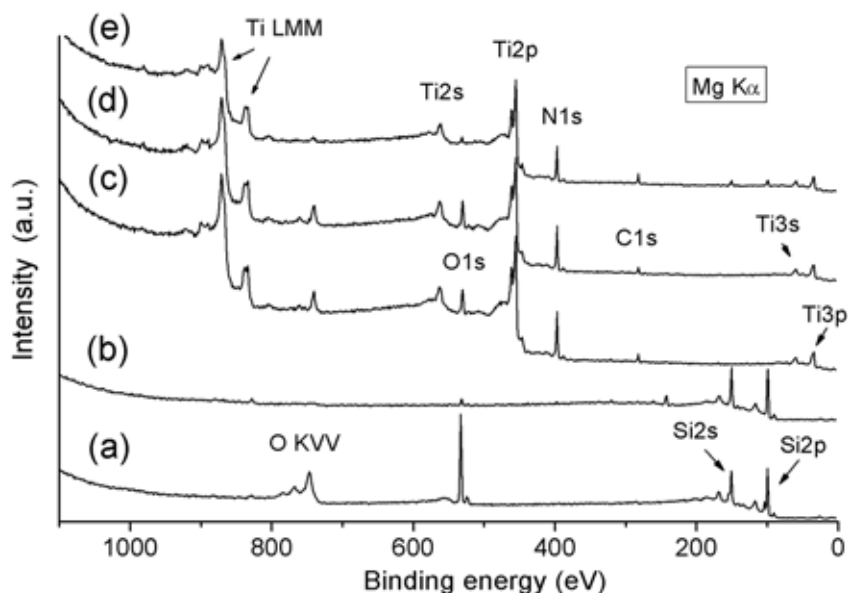


Fig.2. Wide scan XPS spectra of sample surface: (a) substrate before cleaning by ion beam; (b) after cleaning; (c) after titanium sputtering in nitrogen atmosphere; (d) after temperature annealing at 650°C 5 min; (e) after annealing at 750°C 5 min.

# ELECTRIC FIELD MODULATION OPTICAL SPECTROSCOPY USING FIELD ENHANCEMENT NEAR OPTICAL ANTENNAS

*Kenichiro Tanaka* and *Yoshinobu Aoyagi*

*Nanoscience Research and Development Support Team, RIKEN, 2-1 Hirosawa, Wako-city, Saitama, Japan*

*kenichiro@riken.jp* (Kenichiro Tanaka)

Electromodulation spectroscopy is one of powerful tools to investigate electronic properties of a material. For instance, the excitonic and electronic structures of a unique quantum-well material $(C_6H_{13}NH_3)_2PbI_4$ were well clarified by electroabsorption spectroscopy. The crystal $(C_6H_{13}NH_3)_2PbI_4$, whose crystal structure is shown in the inset in Fig. (b), is a self-organized crystal, in which the excitons are tightly confined in the inorganic monomolecular layer of $[PbI_6]$ octahedra (~6.37 Å) sandwiched between organic barrier layers consisting alkyl-ammonium chains $[C_6H_{13}NH_3]$ (~ 9.97 Å). In this crystal, the bandgap of the barrier layer is at least 3 eV larger than that of the well layer, and the interfaces between the well and the barrier layer are intrinsically flat; thus the excitons in this crystal behave as an ideal two-dimensional (2D) excitons system. In addition, since the dielectric constant of the barrier layers is much smaller than that of the well layers, the effective Coulomb interaction between electron and hole in the well layer is substantially enhanced, resulting in the enhanced excitons binding energies (image charge effect). Because of this image charge effect and 2D spatial confinement effect, the excitons in this crystal have extremely large binding energy (361 meV), have large oscillator strength (~0.7), and exhibits many fascinating properties. In our previous research, the electroabsorption technique was quite effective to clarify its electronic and excitonic properties, where we observed anomalous blue shifts of the 1s excitons under the applied electric fields perpendicular to the quantum well layers, for which we demonstrated that the image charge effect plays an important role [1].

On the other hand, it was reported recently that the optical field is greatly enhanced at the gap between gold triangles in a bowtie antenna, and the Raman spectra of *p*-mercaptoaniline molecules attached with gold bowtie were observed. In this paper, we report on the electromodulation spectroscopy on the PL of $(C_6H_{13}NH_3)_2PbI_4$ thin film spin-coated on the bowtie antenna, and show that electromodulation spectroscopy can be performed on the enhanced PL at the gap between triangles in bowtie antenna [2].

Gold bowtie antennas were fabricated with electron beam lithography and evaporation technique on a glass substrate. Each bowties are composed of 2 nm Ti adhesion layer and 20 nm gold layers. The obtained sample consisted of multiple bowtie arrays, with 0.5 μm spacing between bowties. The gap lengths between the tips of the triangle in the antennas were varied from 10 nm to 30 nm. A $(C_6H_{13}NH_3)_2PbI_4$ polycrystalline film was then spin-coated onto the substrate. The excitation light source was a cw semiconductor diode laser with photon energy of 2.62 eV. A half-mirror was used to reflect excitation light to the sample through microscope objective (×100). The polarization of the excitation light (*E*) was parallel to the long axis (*x*) or short axis (*y*) with a polarizer. There were about 300 bowties in the spot of the excited light. The same objective collected the PL, which passed through a Raman notch filter to reduce the excitation light, dispersed with a 30-cm monochromator, and detected with a photomultiplier tube. The PL intensities at each wavelength were measured by sweeping the monochromator.

Electromodulation spectroscopy on the PL of $(C_6H_{13}NH_3)_2PbI_4$ were performed, where the electric fields were applied parallel to the quantum well layers and perpendicular to the long axis of the bowtie antennas. Ac electric fields with no dc bias were applied with a frequency of 1 kHz. The PL has dc component *P* and ac component $\Delta P$; *P* was measured with a digital multimeter, and the modulated $\Delta P$ were decomposed with a lock-in amplifier synchronized at twice the field modulation frequency.

Figure (a) shows the PL spectra of $(C_6H_{13}NH_3)_2PbI_4$ polycrystalline thin film (~5 nm) near the bowtie antennas at room temperature. The excitation intensity is ~0.5 kW/cm$^2$. We found clear PL spectra with the peak energies of 2.41 eV for all samples. Though the PL intensity with a gap length of 20 nm is almost same as that with a gap of 30 nm, PL with a gap below 20 nm is substantially enhanced as the gap length is decreased. In addition, the PL intensity of 10 nm gap with the excitation light polarized parallel to the short axis of antennas is much smaller than that with the excitation light polarized to the long axis of antennas, and nearly equal to that of 30 nm gap. These results suggest that the PL intensity is increased due to the optical field enhancement at the gap of optical antennas with the gap length below 20 nm.

The electromodulation PL spectra for the sample with the average gap of 10 nm under several electric fields are shown in Fig. (b). The incident light's polarization (*E*) was parallel to long axis of the bowtie gap (*x*) and perpendicular to the applied electric fields (*y*). The shape of the modulated PL spectrum can be reproduced by linear combination of the first and second derivatives of the PL spectrum with respect to the photon energy, indicating that this electromodulation PL spectrum is originated from both the Stark shift and broadening of the 1s excitons. The obtained result indicates that the phonon-assisted ionization of the 1s excitons occur at room temperature.

In summary, we have performed electro-modulation photoluminescence spectroscopy on an inorganic-organic perovskite-type material $(C_6H_{13}NH_3)_2PbI_4$ thin film at the gap between the gold bowties. This result indicates that electromodulation spectroscopy can be performed on the enhanced PL at the gap between triangles in bowtie antennas.

**Acknowledgements:**

**References:**

[1] Kenichiro Tanaka *et al.*,  Phys. Rev. B **71** (2005) 045312, and references therein.
[2] D.P. Fromm *et al.*,  J. Chem. Phys. **124** (2006) 061101.

**Figures:**
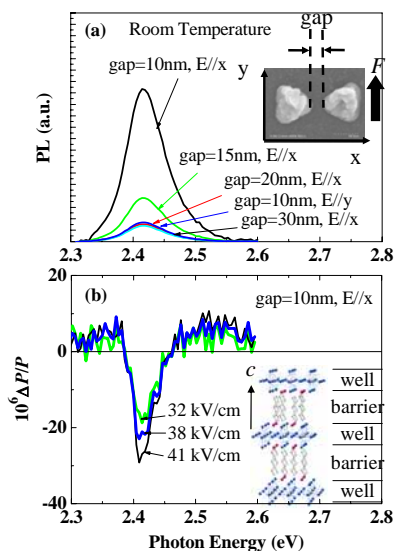


Figure:   (a) Photoluminescence spectra of $(C_6H_{13}NH_3)_2PbI_4$ polycrystalline thin film (~5 nm) near the ~300 bowtie antennas with an average gap lengths from 10 nm to 30 nm at room temperature. The excitation intensity is about 0.5 kW/cm$^2$, and the polarization of the excitation laser (*E*) is parallel to the bowtie antenna's long axis (*x*) or short axis (*y*). The inset shows the scanning electron microscope (SEM) image of a bowtie antenna composed of two-opposing 80 nm-long gold triangles, with a gap length of 10 nm, and the direction of the applied electric field (*F*). (b) Electromodulation photoluminescence spectra of $(C_6H_{13}NH_3)_2PbI_4$ under several electric fields parallel to the quantum well layers near the ~300 bowtie antennas with an average gap length of 10 nm. The inset shows the crystal structure of $(C_6H_{13}NH_3)_2PbI_4$ with the crystal axis *c*.

# IMMOBILIZED TiO$_2$ AND ZnO NANOPARTICLES FOR HIGHLY EFFICIENT PHOTOCATALYSIS

*Sumeyra Tek[a,c] and Hilmi Volkan Demir[a,b,c]*
*[a]Department of Physics, [b]Department of Electrical and Electronics Engineering,*
*[c]Nanotechnology Research Center, Bilkent University, Ankara, 06800, Turkey*
*Dilek Yucel and Gulsen Celiker*
*DYO, Yasar Group, A. O. S. B., 10003 Sk. No:2, Cigli, Izmir 35620 Turkey*
*volkan@bilkent.edu.tr*

Nanostructured metal-oxide semiconductors have drawn great attention with their photocatalytic properties for chemical and biological decontamination of surfaces, air, and water polluted with undesired or hazardous organic and inorganic materials. In photocatalytic processes, semiconductors such as TiO$_2$, ZnO, Fe$_2$O$_3$, CdS, and ZnS are optically activated to act as sensitizers for light-induced redox-processes [1-5]. Among these various semiconductors, TiO$_2$ and ZnO are the most common photocatalysts especially employed for the degradation of several environmental contaminants because of their high photosensitivity, stability, and large band gaps [5]. To date most of the applications reported in the literature are conducted in aqueous media. This, however, gives rise to technical difficulties associated with the removal of photocatalyst from the medium and use in wide-scale industrial applications. To circumvent these issues, one remedy is to immobilize the photocatalyst in thin films on a suitable substrate. But the immobilization then leads to the reduction in the active surface area (and thus in the photocatalytic activity) [2]. To compensate for this reduction in the photocatalytic efficiency, though, metal-oxide nanoparticles can be utilized to effectively increase the active surface area provided that these nanoparticles are integrated into the thin film properly and well dispersed. In this work to this end, we developed photocatalytic nanocomposites that incorporate immobilized TiO$_2$ and ZnO nanoparticles well dispersed in a three-dimensional solgel matrix through a novel approach of full chemical integration for highly efficient environmental decontamination. Here we experimentally investigated their spectral photocatalytic efficiencies from 270 to 370 nm in the UV and demonstrated very high photocatalytic efficiencies up to 93%.

TiO$_2$ is a large band gap semiconductor, with its conduction and valence bands composed of pure 3d orbital of titanium and 2p orbitals of oxygen hybridized with Ti 3d states, respectively. Electrons in TiO$_2$ valence band are conveniently excited to its conduction band when exposed to UV light. The dissimilar parity of the respective bands desirably reduces the electron-hole recombination rate to allow the e$^-$-h$^+$ pair to diffuse to the surface and initiate a chain of chemical reactions for decontamination. Similarly, ZnO is a member of the 3d metal-oxide series. As in TiO$_2$, the photoexcited e$^-$-h$^+$ pair of ZnO has also dissimilar parity, making ZnO a good candidate for photocatalyst. ZnO and TiO$_2$ are the only two among the 3d transition metal-oxide semiconductors that remain stable upon photoexcitation. Comparing ZnO and TiO$_2$, it is reported that ZnO powder has significantly larger quantum efficiency than that of TiO$_2$ powder [3]. Also for comparative work, many research studies in aqua have been conducted, but there is little research available in the literature for immobilized nanoparticles, although immobilized form is by far more versatile for applications. This motivates us to focus on the photocatalytic efficiency characteristics of both ZnO and TiO$_2$ in thin films.

In this work, we chemically embedded our metal oxide nanoparticles into the 3D solgel resin via covalent bonding. As a result of the chemical integration, we obtained nanocomposite materials with their nanoparticles dispersed more uniformly than mere blending. Here we used TiO$_2$ nanoparticles of 6 nm in size and ZnO nanoparticles of 150 nm in size, with the mass ratio of the incorporated nanoparticles to the host solgel of 6.0% for TiO$_2$ and of 9.5% for ZnO in thin films of about 10 μm in thickness. Figure 1 shows the spectral photocatalytic efficiencies of the resulting ZnO and TiO$_2$ nanocomposite films parameterized with respect to the excitation wavelengths (from 270 to 370 nm) as a function of the incident total optical energy per unit area (i.e., incident optical intensity $x$ time) (increased from 18000 Joules/m$^2$ to

73000 Joules/m$^2$). These photocatalytic efficiency curves were experimentally measured using transmission spectroscopy in the visible spectral range with intervals of UV exposure at select wavelengths for the decontamination of the nanocomposite films.

In Fig. 1, we observe a general trend of higher photocatalytic activity for the smaller-size TiO$_2$ nanoparticles (despite their lower concentration in this work) than the larger-size ZnO nanoparticles, although ZnO has higher quantum efficiency. Thus, for immobilized metal oxides, we show that the size effect (surface-to-volume ratio) and the total active surface area (morphology of the thin film) are evidently very effective in photocatalytic process, in addition to the metal oxide type. We also find out that there is an optimal activation wavelength to spectrally maximize the photocatalytic activity due to the optical absorption properties of the nanoparticles and the host. Here we achieve the highest optical efficiency of 93% with TiO$_2$ at 310 nm and of 55% with ZnO at 290 nm. Using the slopes of the linear fits to these efficiency curves in Fig. 1, we obtain the differential efficiencies at different activation wavelengths as a figure-of-merit to represent the incremental photocatalytic efficiency per unit optical energy/area (optical intensity $x$ time). Table 1 shows the differential efficiencies both for TiO$_2$ and ZnO films, with TiO$_2$ having higher differential efficiencies. Here we observe good correlation between the photocatalytic efficiency and the differential efficiency in general since the photocatalytic efficiency curves require larger slopes to reach high levels within a finite period of optical activation at a certain optical intensity. We expectedly achieve the highest differential efficiencies for both nanoparticles at the same activation wavelengths where the highest photocatalytic efficiencies are obtained.

In conclusion, we developed and investigated photocatalytic TiO$_2$ and ZnO nanocomposite films for environmental decontamination and demonstrated very high optical efficiencies up to 93%. We presented their photocatalytic efficiency curves and reported their differential efficiencies at excitation wavelengths from 270 nm to 370 nm for a comparative study of TiO$_2$ and ZnO nanoparticles immobilized in thin films.

**References**

[1] S. Banerjee, J. Gopal, P. Muraleedharan, A. K. Tyagi, B. Raj, Current Science, **90** (2006) 1378.
[2] G. Mascolo, R. Comparelli, M. L. Curri, G. Lovecchio, A. Lopez, A. Agostiano, Journal of Hazardous Materials, **142** (2007) 130.
[3] S. Chakrabarti, B. K. Dutta, Journal of Hazardous Materials, **112** (2004) 269.
[4] S. Kundu, S. K. Ghosh, M. Mandal, T. Pal, A. Pal, Talanta, **58** (2002) 935.
[5] S. Sakthivel, B. Neppolian, M. V. Shankar, B. Arabindoo, M. Palanichamy, V. Murugesan, Solar Energy Materials &Cells, **77** (2003) 65.
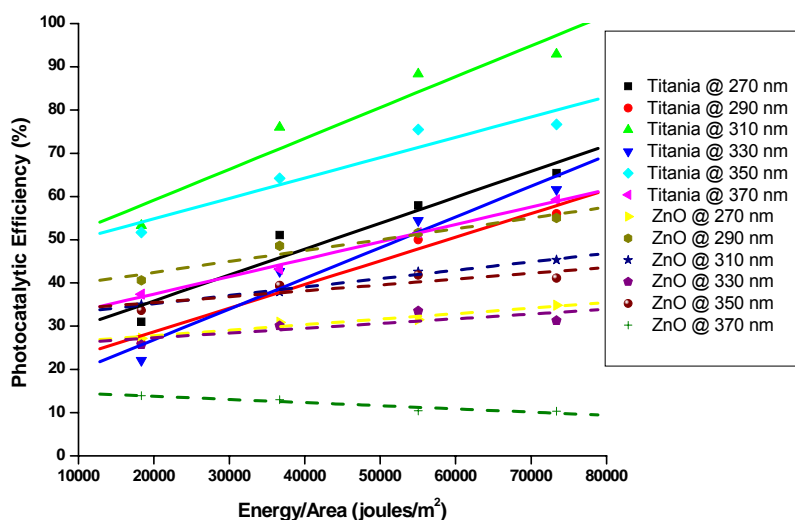
**Fig. 1.** Spectral photocatalyic efficiency of TiO$_2$ and ZnO nanocomposite films at activation wavelengths (270-370 nm) as a function of incident total optical energy per unit area (incident optical intensity $x$ time).

**Table 1.** Differential efficiencies of TiO$_2$ and ZnO nanocomposite films (1/Joules/m$^2$).

| Wavelength | 270 nm | 290 nm | 310 nm | 330 nm | 350 nm | 370 nm |
|---|---|---|---|---|---|---|
| TiO$_2$ | 6.00 x 10$^{-4}$ | 5.47 x 10$^{-4}$ | 7.15 x 10$^{-4}$ | 7.10 x 10$^{-4}$ | 4.70 x 10$^{-4}$ | 4.02 x 10$^{-4}$ |
| ZnO | 1.28 x 10$^{-4}$ | 2.52 x 10$^{-4}$ | 1.94 x 10$^{-4}$ | 1.10 x 10$^{-4}$ | 1.36 x 10$^{-4}$ | -0.73 x10$^{-4}$ |

# THE EFFECT OF THE BILAYER BENDING MODULUS ON THE EXTENT OF DEFORMATION OF SURFACE ADSORBED VESICLES.

*Edurne Tellechea Malda and Ilya Reviakine*
*CIC Biomagune*
*Paseo Miramón 182*
*Parque Tecnológico de San Sebastian*
*20009 San Sebastián – Donosita*
*Guipúzcoa, Spain*
*etellechea@cicbiomagune.es*

Supported lipid bilayers are used as a model system for studying cell membranes and as a platform in various biotechnological applications. [1,2] Their formation begins with the adsorption of intact vesicles to the surface. The behaviour of the surface-adsorbed vesicles (e.g., the extent of vesicle deformation) is governed by the competition between two contributions: lipid-surface interaction strength on one hand, and the bilayer bending modulus on the other. [3] Vesicle-surface interactions remain poorly understood despite the abundance of studies where various contributions to the interaction potential were varied (such as the nature of the lipid headgroup, surface, pH, and ionic strength). On the other hand, the effect of the bending modulus has not been investigated, despite the fact that this property of lipid bilayers is well-characterised. [4,5] Therefore, in this study, we investigate the effect of the bilayer bending modulus on the deformation of the phosphatidyl choline vesicles adsorbing on the titania surface. Establishing a definitive relationship between the extent of vesicle deformation and bilayer bending modulus is expected to help us understand the nature of the vesicle-surface interactions.

**References:**

[1]  Sackmann, E. *Science* **1996**, *271*, 43-48.

[2]  Edwasd T. Castellana, Paul S. Cremer   Benkoski, J. J.; Höök, F. *Surface Science Reports* **2006**, 61, 429-444.

[3]  Seifert, U. *Advances in Physics* **1997**, *46*, 13-137.

[4] NIGGEMANN, G.; Kummrow, M.; Helfrich, W.  *Journal de Physique Ii* **1995**, *5*, 413-425.

[5]  Rawicz, W.; Olbrich, K. C.; McIntosh, T.; Needham, D.; Evans, E. *Biophysical Journal* **2000**, *79*, 328-339.

# NANOSCALE SUPERCONDUCTING ELECTRONICS

_G.C. Tettamanzi[1]_ , A. Potenza[2], S.K.H. Lam[3], C.H. Marrows[2], S. Prawer[1],

D.N. Jamieson[1], C.I. Pakes[4].

[1]_Centre for Quantum Computer Technology, University of Melbourne, Victoria 3010, Australia._

[2]_School of Physics and Astronomy, University of Leeds, Leeds LS2 9JT, United Kingdom._

[3]_CSIRO Industrial Physics, PO Box 218, Lindfield, NSW 2070, Australia._

[4]_Department of Physics, La Trobe University, Victoria 3086, Australia._

* _gct@physics.unimelb.edu.au_

Miniaturization had become an impellent necessity in electronics. This is not only because of the need to have a much higher density of devices in each chip, or a much smaller energy consumption, but also because miniaturization is a driving force for the appearance of new quantum phenomena and device functionality. In the case of superconductivity, the development and the miniaturization of single Josephson junctions (JJ) and of wires has led to important advancement in fields like metrology and quantum computation[1], while pairs of junctions incorporated into a Superconducting Quantum Interference Device (SQUID) architecture could eventually lead to magnetic detection with quantum-limited sensitivity[2].

The size of the loop incorporated in a dc SQUID is a critical characteristic of the device. It has been anticipated[2] that the spin-noise sensitivity of the SQUID is directly proportional to the diameter of this loop, and we are interested in exploring the regime of loop size, some tens of nm, for which a single-spin flip within the SQUID loop may be detectable. In its original conception the SQUID was based on Josephson tunnel junctions, but devices with sub-100 nm necessitate the development of so-called "weak link" junctions, which exhibit Josephson behaviour[3]. This approach is based on the realization of very short and small superconducting wires (length and diameter ~ some ten of nm) that connects two regions of bulk superconducting film. Weak links have very good noise properties, due to a low intrinsic capacitance[3], and recently there have been new interesting approaches for realizing small weak links, using electron beam[4], and atomic force[5], lithography. Limits to, respectively, minimum feature size and reproducibility have eased the initial promise of utilising these technologies. We have taken an alternative fabrication approach, employing focused ion beam (FIB) technology to create weak link junctions and SQUIDs on Nb thin films in a rather straightforward fabrication protocol where a 35 keV Ga ion beam is utilised to mill Nb material. We have carried out accurate studies of the scaling of electronic properties for a number of devices (wires, single JJ and SQUIDs) as a function of device dimensions.

For single weak-link devices we have examined the evolution of device characteristics with variation in the physical length and width of the junction, focusing on achieving reproducible control of device properties and on demonstration of phase behaviour. Short, wide junctions exhibit typical Josephson properties, with a critical current that depends of the device dimensions as expected. In narrow junctions, typically with sub-200 nm width, measurements reveal voltage steps, characteristic of dynamic phase-slip centres. For our narrowest microbridge, of sub-100nm width, transport measurements reveal a suppression of superconductivity below $T_c$ and the data is well described by theoretical predictions for thermally activated phase-slip behaviour, with a evolution to quantum phase-slip below about

$6K^6$. Quantum phase slip behaviour is anticipated in Nb filaments with dimensions below the superconducting coherence length, $\xi \sim 10$ nm. For FIB-fabricated junctions we are able to enter this regime by exploiting Ga poisoning in the periphery of the weak-link, the effective size of the superconducting junction, of order of a nanometre, being significantly smaller than the physical dimensions of the device.

We have explored the scaling of SQUID spin sensitivity with loop size, and compared the scaling characteristics for weak-link based SQUIDs with those of tunnel-junction devices[7], for a range of loop dimensions from 10 μm to 50 nm. Furthermore, we have fabricated and characterized a dc SQUID with a loop diameter of about 50 nm (Fig. 1). For this SQUID, a flux noise of approximately $10^{-6}$ $\Phi_0/Hz^{1/2}$ at 6K has been achieved, from which a calculated spin sensitivity of $\sim 30$ spin/$Hz^{1/2}$ is predicted. Methods to improve this noise figure by utilising a SQUID-based amplification stage, will be discussed.

**References:**

[1] J. Mooij and Yu. Nazarov, Nature Phys., **2** (2006), 169
[2] M.B. Ketchen, et al, IEEE Trans. Magn., **25** (1989) 1212
[3] K.K. Likharev, Rev. of Mod. Physics **51** (1979) , 101
[4] S. Lam and D. Tilbrook, Appl. Phys. Lett., **82** (2003), 1078
[5] V. Bouchiat et al, Appl. Phys. Lett., **79** (2001), 123
[6] G.C. Tettamanzi, A. Potenza, C.H. Marrows, S. Prawer, D.N. Jamieson, and C.I. Pakes, in preparation for Appl. Phys. Lett.
[7] C.I. Pakes, et al, IEEE Inst. Meas., 50 (2001), 310.

**(a)**                                                    **(b)**
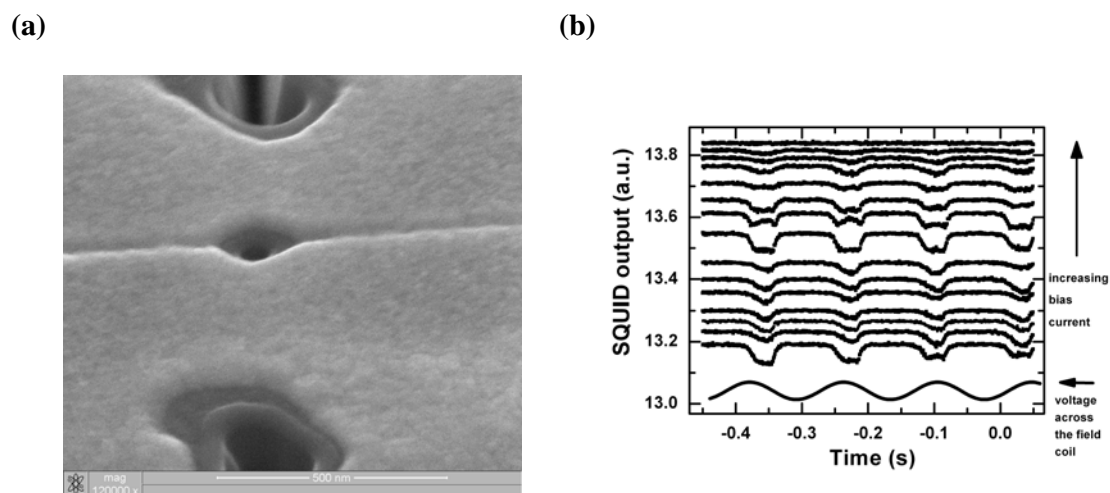


**Figure 1:** (a) Scanning electron micrograph of an Au-shunted Nb dc SQUID (scale bar: 500 nm) with an estimated loop diameter of about 50 nm.  (b) Output of this device at different bias currents in response to an ac-modulated magnetic field applied perpendicular to the plane of the SQUID. The lowest trace is the ac modulation voltage, corresponding to a peak-to-peak field of 100 μT.

# INTER-SHELL INTERACTIONS OF SPHEROIDAL CARBON ONIONS AND GIGAHERTZ OSCILLATORS

*Ngamta Thamwattana, James M. Hill*
*Nanomechanics Group, School of Mathematics and Applied Statistics, University of Wollongong, Wollongong, NSW 2522 Australia*
*ngamta@uow.edu.au*

The manipulation at the nanoscale has led to the creation of many interesting nanostructures, one of which is the nested fullerenes, which are also known as carbon onions. Experimentally, a number of different shapes are obtained, including both spherical and spheroidal carbon onions. A spheroid is an ellipsoid with two major axes equal. Assuming the onion structures are either concentric spherical or spheroidal fullerenes comprising $n$ layers, we determine the interaction energy between adjacent shells for both spherical and spheroidal carbon onions. The continuum approximation together with the Lennard-Jones potential is utilized to obtain analytical expressions for the potential energy and the equilibrium spacing between adjacent shells. Our results show that for spheroidal carbon onions, the equilibrium spacing between shells decreases for shells further out from the inner core. This is due to the decreasing curvature of the outer shells for a concentric structure.

Further, high frequency nanoscale oscillators or "gigahertz oscillators" created from fullerenes and both single- and multi-walled carbon nanotubes have attracted much attention due to the large number of proposed applications. For example, these include ultra-fast optical filters and ultra-sensitive nano-antennae. Here we explore some of the issues relating to the oscillation of a carbon onion inside a single-walled carbon nanotube. We address issues such as the acceptance condition for nested fullerenes into carbon nanotubes, the total force and energy of the nested fullerenes, and the velocity and gigahertz frequency of the oscillatory molecule. In particular, optimum nanotube radii are determined for which nested fullerenes oscillate at a maximum velocity and frequency. The results obtained will be of considerable benefit for the design of future nano-oscillating devices.

# BIOLOGICAL APPLICATION OF ATOMIC FORCE MICROSCOPY USE ON CANCER CELL LINE

**Tomankova K, Kolarova H, Bajgar R**

Department of Medical Biophysics, Faculty of Medicine, Palacky University in Olomouc, Hnevotinska 3, 775 15 Olomouc, Czech Republic
tomanko@tunw.upol.cz

Atomic Force Microscopy (AFM) has been used to image the morphology of developing tumor cells and their processes. However, it is frequently reported that prior fixation is required for reliable imaging of cells with lower adhesive properties. We used Dry Scanner in Non-contact mode used in biological application of AFM. We imaged the cancer cells before and after photodynamic effect (PDE) and sonodynamic effect (SDE) of photosensitizer $ClAlPcS_2$. PDE was induced by efficient LED source with total light dose of 15 $Jcm^{-2}$.

We obtained two types of pictures: topography and phase image. In some cases we could observe signs of apoptosis. We also sonicated the cell samples by ultrasonic therapeutic device to improve the effectiveness of PDE. Other results show time-course of ROS production within cells during combination PDE and SDE and their subsequent morphological features and changes investigated by AFM.

The utility of AFM strongly varies depending on the cell type, its membrane structure [1] and adhesion properties [2]. The minimal forces between tip and surface of the sample avoid damage of the biological preparation [3]. Interactions between the cantilever tip and the cell surface are so complex, there is no simple way to control tip-cell interactions and to eliminate the disruptive effect of the scanning cantilever [4]. We used a Dry Scanner and cells were scanned in the Non-contact or the Tapping mode [5]. NC-AFM mode was developed for improving imaging of soft samples by AFM. Difficulties in the proper adjustment of the scanning parameters are often encountered when using tapping–mode atomic force microscopy (TM-AFM) for imaging thick and soft materials, and particularly living cells in aqueous buffer. To increase quality of our images, we scanned cells in non-contact mode (NC-AFM) [6]. Recognition of the cells and control of their surrounding during imaging have already been accepted as essential conditions for cell biological application of AFM [7].

Photodynamic therapy (PDT), originally developed and used mainly as a minimally invasive tumour therapy, has been known for over a hundred years [8]. In clinical PDT, dyes such as porphyries or phthalocyanines are administered to a patient along with irradiation. PDT is predominantly used in anticancer treatment approaches that depend on the retention of photosensitizes in tumour cells and their activation within the tumour through irradiation with light of the appropriate wavelength [9].

The aim of the presented study is to picture tumor-cell surface in air by AFM. We focused to obtain topography pictures and pictures involving elastic properties of cell surface. We examined the cell line G361 before and after induction of PDE. Differences in altitude over surface of cells gave us information about cell damage and about different component parts of the cell wall.

The treatment of the cells with the photosensitizer leads the loss of surface rigidity and eventually to dramatic changes of the cell shape. Individual cells before PDE were characterized by smooth surface without protrusion on the whole surface

**References**

[1] Méndez-Vilas A., Corbacho I., González-Martín M. L., Nuevo M. J.: Direct surface probing of cell wall-defective mutants of Saccharomyces cerevisiae by atomic force microscopy. Appl. Surf. Sci. **238**, 2004, 51 - 63

[2] Kim H., Arakawa H., Osada T., Ikai A.: Quantification of cell adhesion force with AFM: distribution of vitronectin receptors on a living MC3T3-E1 cell. Ultramicroscopy **97**, 2003, 359 – 363

[3] Dufrêne Y. F., Boonaert Ch. J. P., van der Mei H. C., Busscher H. J., Rouxhet P. G.: Probing molecular interactions and mechanical properties of microbial cell surfaces by atomic force microscopy. Ultramicroscopy **86**, 2001, 113 - 120

[4] You H. X., Lau J. M., Zhang S., Yu L.: Atomic force microscopy imaging of living cells: a preliminary study of the disruptive effect of the cantilever tip on cell morphology. Ultramicroscopy **82**, 2000, 297 - 305

[5] Lehenkari P. P., Charras G. T., Nykänen A., Horton M. A.: Adapting atomic force microscopy for cell biology. Ultramicroscopy **82**, 2000, 289 - 295

[6] Vié V., Giocondi M. C., Lesniewska E., Finot E., Goudonnet J. P., Le Grimellec C.: Tapping-mode atomic force microscopy on intact cells: optimal adjustment of tapping conditions by using the deflection signal. Ultramicroscopy **82,** 2000, 279-288.

[7] Bolshakova A. V., Kiselyova O. I., Filonov A. S., Yu O., Lyubchenko Y. L., Yaminsky I. V.: Comparative studies of bacteria with an atomic force microscopy operating in different modes. Ultramicroscopy **86**, 2001, 121 – 128

[8] Kaestner L.: Evaluation of human erythrocytes as model cells in photodynamic therapy. Gen. Physiol. Biophys. **22**, 2003, 455 - 465

[9] Dougherty T. J.: Photodynamic therapy. J.Photochem. Photobiol. **58**, 1993, 895 - 900

**Figure1:** One non-irradiated cell of A549 cell line before PDE and SDE. The image was obtained in non-contact topography mode (size 52.33 × 52.33 µm, resolution 300 × 300 pixels, scan rate 50 µms⁻¹). The height of the cell is expressed in colour scale 0 (dark fields) – 2.06 µm (light fields).

# SCATTERING MATRIX APPROACH FOR THE ANALYSIS OF MAGNETO-PLASMONIC PERIODIC LATTICES

*J. B. González-Díaz, <u>J.F. Torrado</u>, A. Garcia-Martin and G. Armelles*
*Instituto de Microelectrónica de Madrid, Consejo Superior de Investigaciones Científicas,*
*C\Isaac Newton 8 (PTM) 28760 Tres Cantos, Spain*
*jftorrado@imm.cnm.csic.es*

Localized surface plasmons are under intensive study since long ago because they play a very important role in the optical properties of metallic systems. In particular, they become especially relevant in the optical properties of nanostructures, such as tiny particles embedded in dielectric matrices or nanoperforated membranes. The intensity as well as the spectral position of these resonances strongly depends on a variety of parameters such as the size, the shape, or the concentration of the metallic particles/holes or the refractive index of the matrix.[1] The vast majority of the studies have been so far devoted to study noble metal particles/holes since their free electron contribution to the optical properties in the infrared and visible spectral range is predominant, exhibiting also a low damping constant. In other metals such as palladium, platinum, cobalt, nickel or iron, the free electron contribution to the optical properties is smaller, and have a higher damping constant, therefore their surface plasmon resonances appear broader and less defined.[2] On the other hand, ferromagnetic metals posses spontaneous magnetization which enables them to present magneto-optical properties, which are absent in noble metals. This characteristic can be used to design new kind of plasmonic structures. Moreover, different theoretical works have suggested that surface plasmon resonance of magnetic metallic nanoparticles/holes could enhance the magneto-optical activity with respect to that of a continuous medium.[3] However, the size of the nanoparticles/holes under consideration is always much smaller than the wavelength of light and the interaction between the particles/holes was rarely not considered. But the particle/hole size[1] and the radiative coupling between them strongly modify the optical properties of the system[4] and, therefore, it may also modify its magneto-optical response. This is precisely the scope of this work, where we theoretically analyze the dependence of the magneto-optical properties on the size of a system consisting on periodically arranged Ni nanowires embedded in a dielectric environment and on the *negative* of this structure, i.e. metallic Ni membranes with nanometer scale periodic perforations. Such systems have already shown to exhibit interesting effects, such as an enhancement of the magneto-optical Kerr rotation and faraday[5]. We will show that the enhancement is due to a surface plasmon resonance of the Ni nanowires/pores, its spectral position depending on the wire diameter.

In the figure we show the magneto-optical part of the reflectivity ($r_{ps}$) as a function of the energy of the incoming wave (normal incidence) normalized to that of the Ni bulk. The left panel corresponds to the Ni nanowires array in two different environments, and shows a peak in each one revealing the position of the plasmonic structure. The right one corresponds to the Ni perforated membrane, where the pores have the same geometrical parameters as the nanowires in its "positive" counterpart. The peak in each curve appears at the very same position, meaning that the plasmonic structure is one that travels along the wire/pore and will depend on its geometrical parameters.

On a different framework, the impact of the dielectric environment holding (filling) the nanoparticles (nanoholes) on the magneto-optical properties of such kind of systems is also of great interest. A previous study has been focused on how the magneto-optical response is affected when the whole surrounding environment changes.[6] However, in many cases the environment shows a characteristic non isotropic profile. For example, the growth of nickel nanowires in an alumina matrix membrane obtained by anodization processes. A recent

work[7] presents a clear difference between the optical properties of the alumina close to the wires and that related to the bulk alumina matrix. We will address the magneto-optical response dependence of periodic Ni nanowires arrays (and its *negative* structure perforated Ni membranes) on localized dielectric changes consisting on a shell surrounding (filling) the wires (pores), whose refractive index different to that of the whole dielectric medium.

**References:**

[1] K.Lanve Kelly, E. Coronado,L.L. Zhao and G. C. Schatz, *J. Phys. Chem B* **2003**,107, 668

[2] S. Coyle, M. C. Netti, J. J. Baumberg, M. A. Ghanem, P. R. Birkin, P. N. Bartlett, and D. M. Whittaker, *Phys. Rev. Lett.* **2001**, 87, 176801

[3] P.M. Hui and D. Stroud, *Appl. Phys. Lett. 1987*, 50, 950

[4] M. Meier, A. Wokaun, and P.F. Liao, *J. Opt. Soc. Am. B 1985*, 2, 931; E. M. Hicks, S. Zou, G. C. Schatz, K. G. Spears, R. P. Van Duyne, L. Gunnarsson, T. Rindzevicius, B. Kasemo, and M. Käll, *Nano Lett. 2005*, 5 1065

[5] S. Melle, J. L. Menéndez, G. Armelles, D. Navas, M. Vázquez, K. Nielsch, R.B. Wehrspohn, and U. Gösele, *Appl.Phys. Lett. 2003*, 83, 4547; A. García-Martín, G. Armelles, S. Pereira, *Phys. Rev. B* **2005**,71, 205116

[6] J.B. González Díaz, A. García-Martín, G. Armelles, *Adv. Mat.* (submitted)

[7] J. Choi, Y. Luo, R. B. Wehrspohn, R. Hillebrand, J. Schilling, and Ulrich Gösele *J. App. Phys.* **2003**,94,4757

**Figures:**
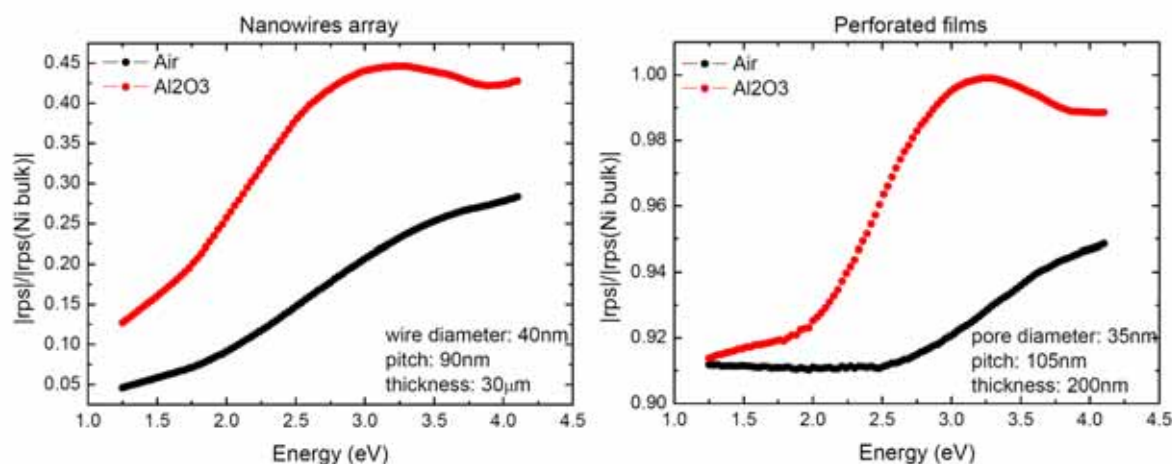
# THEORETICAL TREATMENT OF THE TMOKE IN MAGNETO-PLASMONIC PATTERNED NANOSTRUCTRURES: A SCATTERING MATRIX APPROACH

*J.F. Torrado, J. B. González-Díaz, G. Armelles and A. García-Martín*
*Instituto de Microelectrónica de Madrid, Consejo Superior de Investigaciones Científicas,*
*Isaac Newton 8 (PTM) 28760 Tres Cantos, Spain*
*jftorrado@imm.cnm.csic.es*

The study of the Magneto-Optical (MO) properties of ferromagnetic metals is a topic under study since long ago. Nowadays, the study of the properties of nanostructures with magneto-optical activity is increasing due to the progress in miniaturization of optical devices. In this progress towards miniaturization of optical devices surface plasmons are playing an outstanding role [1]. These are excitations existing in the interface of a metallic medium and a dielectric one, whose associated electromagnetic field is spatially confined to that interface. Also, localized plasmon resonances in small particles are important since their spectral position strongly depends on a variety of parameters such as the size, the shape, the concentration of the metallic particles holding them. The vast majority of the studies have been so far devoted to study noble metal particles since their free electron contribution to the optical properties in the infrared and visible spectral range is predominant, exhibiting also a low damping constant. In ferromagnetic metals, relevant from the point of view of their MO activity, the free electron contribution to the optical properties is smaller, and has a higher damping constant; therefore their surface plasmon resonances appear broader and less defined [2]. Different works suggest that the proper combination of noble and ferromagnetic metals could lead to enhanced magneto-optical activity [3]. These kinds of structures are being currently studied on the basis of a scattering matrix (SM) approach in the so-called polar configuration [4] (magnetic field applied perpendicular to the sample plane and parallel to the polarization plane of the incoming light).

On another context, plasmon excitations are the basis of high sensitive biosensor devices. These devices are based on the dependence of the modification of the spectral location of the resonance with the refractive index of the dielectric side (Surface Plasmon Resonance -SPR- sensors). An evolution of the SPR lies in the introduction of MO elements. In this case the magnetic field must be applied lying in the sample plane and perpendicular to the incident light (Transverse configuration) [5]. The measured quantity is then the so-called Transverse Magneto-Optical Kerr Effect (TMOKE). To analyze this signal when nanostructuration of any of the components is present only approximate effective medium theories can be employed. Thus, an exact SM treatment is desirable. This is, however, not a trivial generalization of the polar case. In fact, in this work we show that SM treatment of the TMOKE for nanopatterned structures is only achievable if the magnetic component is homogeneous, remaining the rest free to be nanostructured on demand. We will present the theoretical method to tackle the aforementioned situation in detail and will apply it to a real system consisting on a homogeneous magneto-plasmonic trilayer (Au/Co/Au) coupled to a periodically patterned metallic layer (square array of Au discs) as it is shown in the figure.

**References:**

[1] L. Novotny and B. Hetch in "*Principles of Nano-Optics*", Cambridge University Press (2006).
[2] S. Coyle, M. C. Netti, J. J. Baumberg, M. A. Ghanem, P. R. Birkin, P. N. Bartlett, and D. M. Whittaker, *Phys. Rev. Lett. 2001,* 87, 176801
[3] C. Herman et al., Phys. Rev. B **64**, 235422(2001), N. Richard et al., Phys. Rev. B **59**, 5936(1999)
[4] A. García-Martín, G. Armelles, S. Pereira, *Phys. Rev. B* **2005**,71, 205116
[5] B. Sepúlveda, A. Calle, L. M. Lechuga, and G. Armellas, Opt. Lett. **31**, 1085 (2006)

**Figures:**
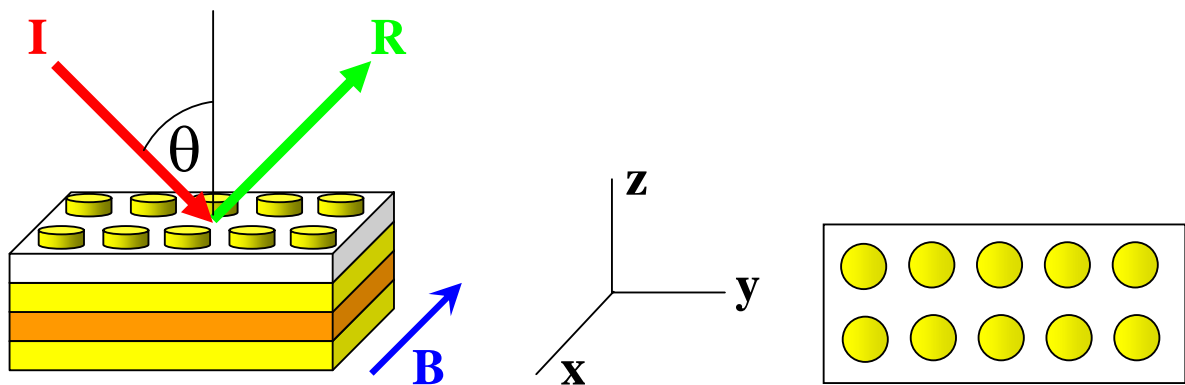


**Figure:** Schematical view of the system under consideration.

# ASYMPTOTIC ANALYSIS OF COAGULATION–FRAGMENTATION EQUATIONS OF NANOTUBE CLUSTERS

*Francisco Torrens, Gloria Castellano*
*Institut Universitari de Ciència Molecular, Universitat de València, Edifici d'Instituts de Paterna, P. O. Box 22085, 46071, and Instituto Universitario de Medio Ambiente y Ciencias Marinas, Universidad Católica de Valencia San Vicente Mártir, Guillem de Castro-94, 46003, València, Spain*
*francisco.torrens@uv.es*

Finding a manageable approximation to the behaviour of the coagulation–fragmentation equations is an interesting and challenging task [1]. The approximation is presented by means of an asymptotic analysis, in a case that is simple enough to be studied, but still realistic enough to be a good candidate as a model for physical processes [2]. Results will be checked against numerical solutions to the equations [3]. It deals with the Becker–Döring equations when the binding energy depends linearly on the cluster size; *i.e.*, $\varepsilon_k = (k-1)\alpha kT$, where $\alpha kT$ is the monomer–monomer binding energy ($k$ is Boltzmann's constant, and $T$, the temperature, Fig. 1) [4]. It is taken into account reactions only between monomers and other clusters (Fig. 2). This expression for the binding energy is suitable for aggregates of certain kinds of lipids, when these form rodlike clusters. The molecules of these lipids typically have a hydrophilic head and a hydrophobic tail so, in aqueous solution, they spontaneously arrange themselves so that tails are away from the surrounding water, and heads are in contact with it. They can form spherical aggregates with tails pointing inwards and heads pointing outwards, or form lipid bilayers such as those found in cell membranes, where lipid molecules form a double layer with heads on the external surface and tails on the inside. Clusters formed by lipids in aqueous solution are called *micelles*, and the process by which they form is called *micellization.* Conclusions. Based on a simple kinetic model and starting from the initial state of pure monomers, it is shown that the process of micellization of rodlike aggregates at high critical micelle concentration occurs in three separated stages or eras. In the first era, many clusters of small size are produced, while the number of monomers decreases sharply. During the second era, aggregates are increasing steadily in size, and their distribution approaches a self-similar solution of the diffusion equation. Before the continuum limit can be realized, the average size of the nuclei becomes comparable to its equilibrium value, and a simple mean-field Fokker–Planck equation describes the final era until the equilibrium distribution is reached. Provisional conclusions follow. (1) Fullerene–SWNT cluster formation suggests that the cluster *sheath* is filled with pores. The *membranous character* of growth process in clusters explains experimental data dispersion. The model yields an activation barrier and predicts that pores with a radius below a certain critical value are unstable, while those above this radius will grow indefinitely until the membrane ruptures. During the latter stage of fusion the site expansion velocity slowed down by two orders of magnitude. Dynamics were governed by the displacement of the volume of liquid around the fusion site. The model predicts that pores with a radius below a certain critical value are unstable, while those above this radius will grow indefinitely until membrane ruptures. (2) Based on a simple kinetic model, *micellization* of rod-like aggregates occurs in three separated stages: (a) many small clusters are produced and the number of monomers decreases; (b) aggregates increase in size; (c) a mean-field Fokker–Planck equation describes the third era.

**References:**

[1] F. Torrens and G. Castellano, Comput. Lett., **1** (2005) 331.
[2] F. Torrens and G. Castellano, J. Comput. Theor. Nanosci., **4** (2007) 588.
[3] F. Torrens and G. Castellano, Microelectron. J., in press.
[4] F. Torrens and G. Castellano, Nanoscale Res. Lett., in press.

**Figures:**
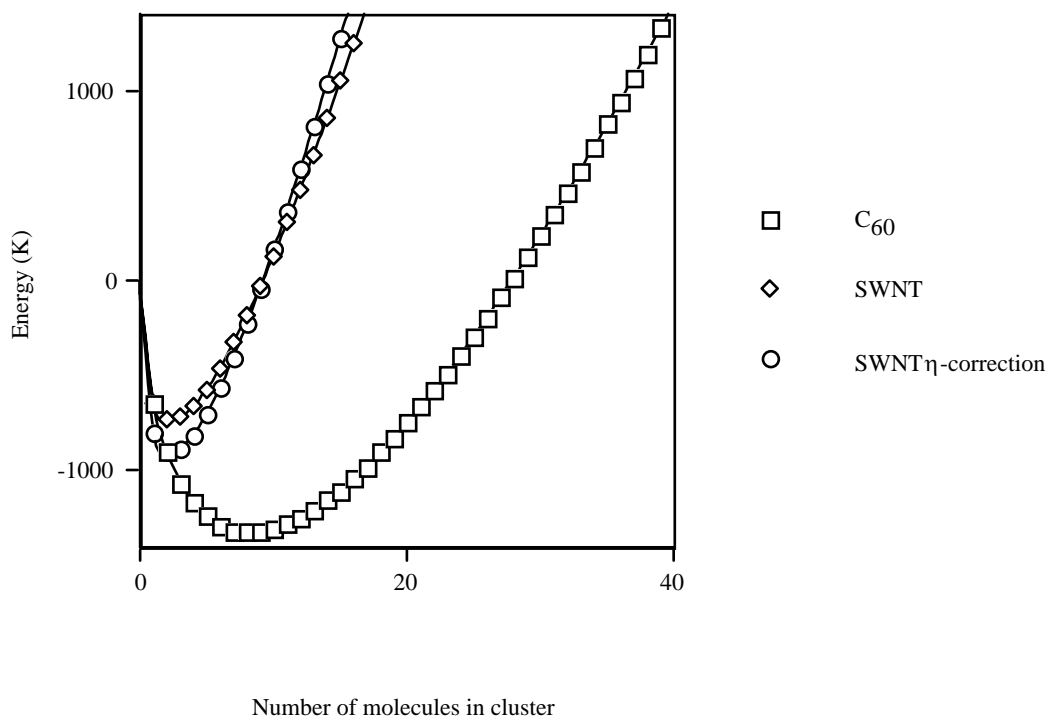


Fig. 1. Energy of interaction of an SWNT with its surroundings in the cluster volume/surface.
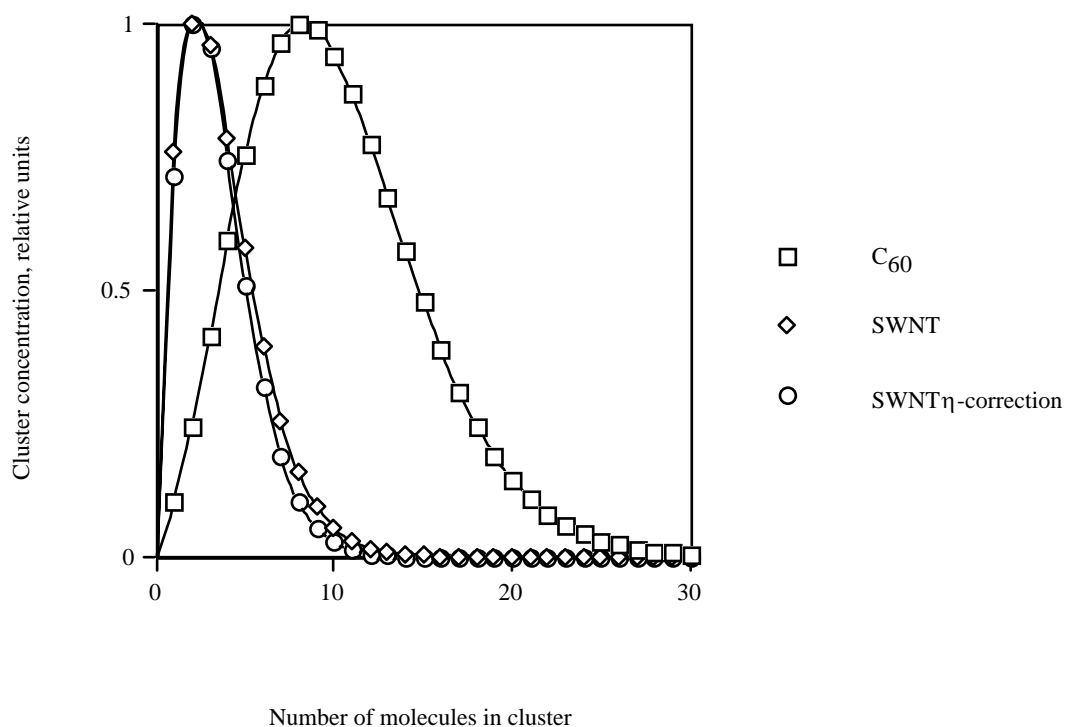


Fig. 2. Cluster distribution by size saturated in $CS_2$ at $T = 298.15K$ of $C_{60}$ and SWNT.

# CHARACTERIZATION OF MODIFIED SOLID ELECTRODES WITH ORGANIZED THIN FILMS OF A ZINC PHTHALOCYANINE

*J. Torrent-Burgués, E. Guaus*
*Departament d'Enginyeria Química, Universitat Politècnica de Catalunya,*
*C/ Colom 1, 08222-Terrassa Spain. E-mail: juan.torrent@upc.edu*

Phthalocyanines (Pc) and metallo-phthalocyanines (MPc) have been used for many years as blue and green dyes, but recently they have also been investigated for their applications as catalyst and chemical sensors, and in electronic and photonic technologies [1]. These applications usually require a thin film deposited on a solid substrate. Several studies have investigated these systems, and some of them have studied the characteristics of organized Langmuir and Langmuir-Blodgett (LB) films. The redox behaviour of these compounds has been mainly studied in solution, but modified Pc and MPc solid electrodes have deserved much more attention in recent years. Solid electrodes can be modified by using several techniques, such as casting, adsorption or LB film formation, and different film characteristics should be expected from each technique, and consequently different electrochemical responses.

In particular, zinc phthalocyanines (ZnPc) have received less attention [2-4]. In this work the electrochemical response of modified carbon solid electrodes with ZnPc thin films will be reported and discussed in relation to the ZnPc deposition techniques. Topographic characterization was made using Atomic Force Microscopy. The voltammograms of these modified electrodes show differences in respect to those obtained from solutions in organic solvents, but still showing some oxidation ($I_o$) and reduction ($I_r$) peaks. Films obtained by immersion and LB techniques present more similar behaviour than those obtained by drop casting, and this behaviour can be correlated with the differences in structure shown by the films. For the LB films, an influence of the extraction pressure and of the number of layers has been observed. Drop casting films show a more pronounced response to the exposure to air oxygen, a fact that could be used for oxygen sensing applications. Figure 1a shows the voltammogram of the response of a LB film of a tetra-tert-butyl substituted ZnPc deposited on a glassy carbon electrode (GCE), and Figure 1b shows the corresponding AFM image.

## References
[1] S.M. O'Flaherty et al., Langmuir, **21** (2000) 11161.
[2] B. Schöllhorn et al., Thin Solid Films, **326** (1998) 245.
[3] K. I. Ozoemena and T. Nyokong, Microchem. J., **75** (2003) 241.
[4] S. Yoshimoto et al., Chem. Phys., **319** (2005) 147.



a)                                                         b)
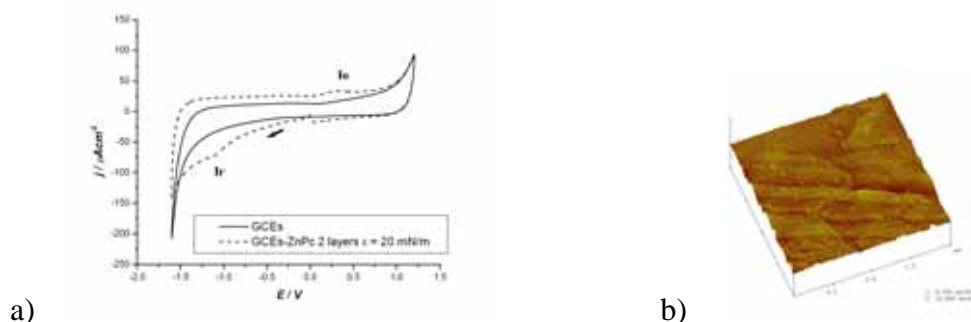
Figure 1. a) Voltammogram, and b) AFM image, of a ZnPc LB film at Π=20 mN/m.

# DISPERSION OF INORGANIC WS₂ FULLERENE-LIKE PARTICLES AND ITS INCORPORATION INTO CARBON CVD FILMS FOR PRODUCTION OF NANOCOMPOSITE COATINGS

R. Torres, J. Buijntsters, R. Escobar, C. Gómez-Aleixandre, J. M. Albella and I. Jiménez.
Instituto de Ciencia de Materiales de Madrid, CSIC, C/ Sor Juana Inés de la Cruz 3, Campus de Cantoblanco, 28049 Madrid (Spain).

Ricardotg@icmm.csic.es

A new trend in the area of protecting coatings for mechanical applications is the incorporation of lubricant nanoparticles into hard matrixes to combine lubricantion and wear resistance in the same composite coating. However, the dispersion and incorporation of the nanoparticles in a coating remains a scientific and technological challenge. In particular, achieving a good disperion of nanoparticles is a major problem because they tend to agglomerate, both in air, in vacuum and in most solvents.

In this work we are considering $WS_2$ inorganic fullerene-like materials (IFLM) as the nanoparticles with extreme lubricating properties. $WS_2$-IFLM consists in onion-like arrangements of curved basal planes of the chalcogenide $WS_2$ with an average particle diameter of ~80 nm. As the hard matrix, we used carbon films partially hydrogenated, deposited by Electron Cyclotron Resonance Chemical Vapor Deposition (ECR-CVD) with a hardness of ~20 GPa. To obtain a nanocomposite coating, we are using a two step process: first, we cover the substrate surface with isolated and well dispersed $WS_2$-IFLM particles, and second we deposit a by ECR-CVD a carbon layer thicker than the particle diameter.

To obtain a homogeneous coverage of the sample surface with well dispersed particle, we have studied first the dispersion of the $WS_2$-IFLM nanoparticles in liquids, by testing the effect of sonication (with ultrasounds) in solutions of various concetrations of IFLM partciles in different alcohols of increasing aliphatic chain length. Afterwards, these solutions were used to deposit the IFLM's on Si (100) substrates by dip coating. Two effects could be observed: firstly, the linear dependence in a log-log scale of the surface coverage with the solution concentration and, secondly, the decrease of the IFLM agglomerate size on the Si surface with the average solvent polarity, i.e. with increasing alcohol chain length. The best agglomerate mean diameter was 450 nm in case of pentanol (C5 alcohol), despite being still far away from the single particle mean diameter of 80 nm.

On these pre-treated substrates some carbon coatings have been deposited by Electron Cyclotron Resonance – Chemical Vapour Deposition (ECR-CVD). SEM observations as well as profile analysis and composition depth profiling by Glow Discharge Optical Emission Spectroscopy (GDOES) confirm that the IFLM's remain buried under the coating. Finally, tribological measurements by pin-on-disk tests indicate that incorporation of 8% of IFLM in the surface coverage allows a reduction of 15% in the friction coefficient from a value of 0.10 in the reference carbon coating to 0.085.

# Biotemplated Co-Pt nanowire synthesis in TMV

*Rikako Tsukamoto,† Masahiro Muraoka,† Munetoshi Seki,‡ Hitoshi Tabata,§*
*Ichiro Yamashita †,//,#*

*† CREST, Japan Science and Technology Agency, Honcho, Kawaguchi, Saitama 332-0012, Japan*

*‡ Institute of Scientific and Industrial Research, Osaka University, 8-1 Mihogaoka, Ibaraki 567-0047, Japan*

*§ Department of Bioengineering, The University of Tokyo, 7-3-1 Hongo, Bunkyo-ku, Tokyo 113-8656, Japan*

*// Graduate School of Materials Science, Nara Institute of Science and Technology, Takayama, Ikoma, Nara 630-0192, Japan*

*# Advanced Technology Research Laboratories, Matsushita Electric Industrial Co., Ltd., Seika, Kyoto 619-0237, Japan*

*ichiro@ms.naist.jp*

The semiconductor field using photochemical processes has been fast approaching its theoretical limit. Therefore, some breakthrough has been needed to make smaller devices. Recently, bottom-up processing such as building up atoms or molecules into functional structures has been studying actively. We are proposing "Bio Nano Process" of the bottom up technique to make inorganic nano-structure which uses protein's abilities, self-assembly, mineralization, and atomically same sizes. We have succeeded in fabricating the floating gate memory using cage shaped protein, ferritin[1]. We further has been trying to make nanowires to construct more functional nano-structures in future. We employed the inside cavity of Tobacco Mosaic Virus (TMV) to make nano-wires.

TMV is a tube-shaped protein, 300 nm in length with an outer diameter of 18 nm. It is composed of 2130 identical coat protein molecules, which are self-assembled in helical manner together with the TMV RNA and it has hollow central channel with a 4 nm diameter. Until now, monometallic nanowire have been synthesized inside TMV[2], no bimetallic alloy nanowire have been reported yet. We devised a simple and novel technique to synthesize bimetallic Co-Pt and Fe-Pt alloy nanowires in the central channel of the TMV.

The Sample was prepared an aqueous solution of 0.3 mg/ml TMV in 150 mM NaCl in a microtube. $(NH_4)_2Co(SO_4)_2$ and $K_2PtCl_4$ were added twice, first to a final concentration of 0.5 mM and 5 minutes later, to 1.0 mM. After 5 minutes, $NaBH_4$ was added twice at 5 minute intervals to a final concentration of 1.0 mM. This procedure was repeated three times, i.e., the final concentration of $(NH_4)_2Co(SO_4)_2$, $K_2PtCl_4$ and $NaBH_4$ was 3 mM each. Throughout the procedure, the reaction solution was exposed to ultrasonication with the bottom half of the microtube immersed in an ice-water bath. The sample was sonicated for 1 second at intervals of 5 seconds by direct immersion of the tapered microtip into the microtube. (20 kHz, ~20 W, Digital Sonifier Model 450, BRANSON, USA) To make Fe-Pt nanowires, $(NH_4)_2Fe(SO_4)_2$ was used instead of $(NH_4)_2Co(SO_4)_2$. The sample solution was observed by TEM after staining with aurothioglucose (Figure 1), we confirmed the formation of a wire in about 30 % TMV. Furthermore, we investigated existence ratio of Pt and Co by EDS which indicated that the obtained nanowires were CoPt(111) or $CoPt_3$(111). The high resolution TEM (HR-TEM)

image showed clear lattice fringe of nanowire, its distance were from 0.21 to 0.22 nm, which is consistent with CoPt(111),CoPt$_3$(111).(Figure 2) We measured magnetometry using a superconducting quantum interference device (SQUID), the M-H curve showed a hysteresis loop.(Figure 3) It indicates that the fabricated nanowire is ferromagnetic.

**References:**

[1] A. Miura, T. Hikono, T. Matsumura, H. Yano, T. Hatayama, Y. Uraoka, T. Fuyuki, S. Yoshii, I. Yamashita, *Jpn. J. Appl .Phys*. **2006**, 45**,** (1), L1-L3.

[2] Knez, M.; Bittner, A. M.; Boes, F.; Wege, C.; Jeske, H.; Mai, E.; Kern, K. *Nano Lett.* **2003**, 3, 1079.

**Figures:**
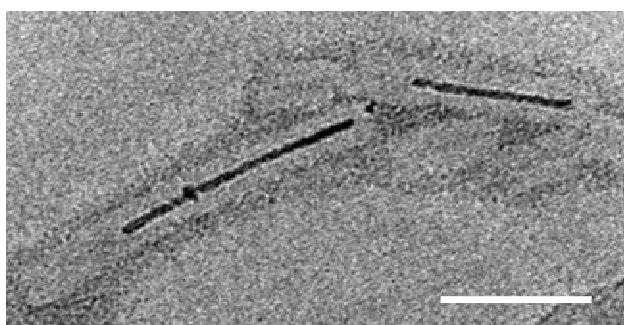


Figure 1: TEM micrograph of TMV-nanowire composites after biomineralization of Co-Pt alloy in the hollow central channel of TMV (stained by aurothioglucose). Scale bar is 50 nm.
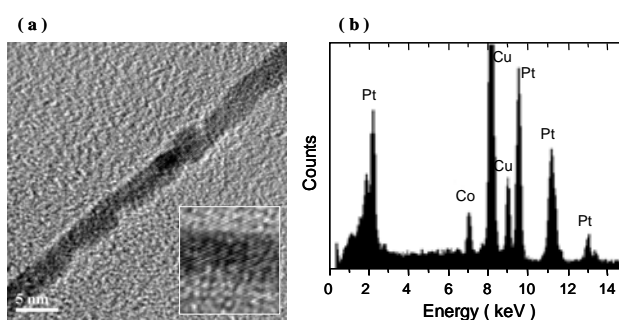


Figure 2: (a) HR-TEM micrograph of CoPt nanowire produced in the TMV central channel(no staining).Scale bar is 5 nm. The inset shows a lattice image of the nanowire.
(b) EDX spectrum of the nanowire showing the presence of Co and Pt.
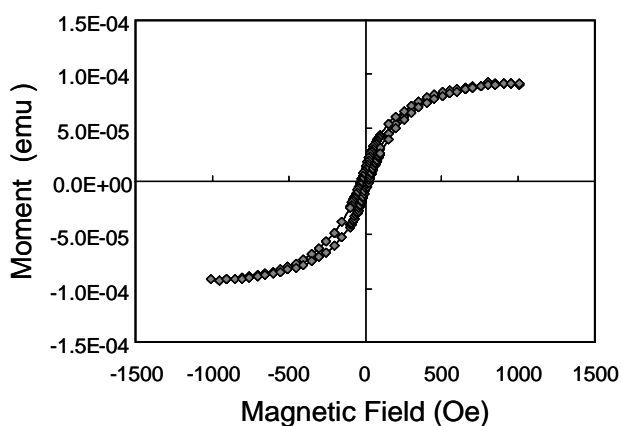


Figure 3: Magnetometry measurement of the nanowires produced in TMV central channel.

# INFLUENCE OF TECHNOLOGICAL FACTORS ON PROCESSES OF STRUCTURIZATION OF CARBON NANOPARTICLES IN OLIGOMER MEDIUM

I. Valtsifer, V. Strelnikov, V. Valtsifer

Institute of Technical Chemistry, 3, ak. Koroleva, Perm, 614013, RU

Techem@permonline.ru

Recent ways of regulation of electric and heat conductivity of olygomer materials are based on introduction of nanodispersed fillers into the composition. In particular, structure formation and generation of continuous clusters penetrating into the bulk takes place due to introduction of 1-10% (mass) carbon nanoparticles into the olygomer binding agent at given processing conditions. Electric and heat conductivity increases along with substantial increase of viscous properties of the composition. In spite of the lower electric conductivity of the carbon materials compared to metals, they have a pronounced structuring ability. This allows to obtain compositions with an electric conductivity comparable to that of metal-filled materials at relatively low filling degrees.

Main processing factors, influencing on the formation of continuous arrangement of carbon nanoparticles in the polymer matrix, have been studied in the context of this work. Temperature, volume filling, shear rate, time of structure formation, binding agent viscosity are among these factors. Experimental studies of structure formation were carried out using rotary viscometer Rheotest RN4.1 and retrofitted rheoconductometric installation based on viscosimeter Reotest 2.1 for determination of electric conductivity of the composition.

Electric conductivity of the composition was shown to be the main parameter used for determination of initiation of the nanocarbon continuous structures. Existence of the electric current, passing through the composition, indicates the structure of carbon in the composition to be continuous and the structure elements to be commensurable to the distance between electrodes and cylinders of the viscosimeter. It was determined, that the current increases proportionally with the increase of the number of carbon nanoparticle chains per volume unit. Formation of the claster structures in the polymer nanomaterials was confirmed by the visual image obtained using optical microscope Olimpus BX 51. The results obtained make possible creation of the materials with electric conductivity level lying in the range of $(1 \div 20) \times 10^{-6}$ cm/m.

# SILANES AND SURFACE ACTIVATION WITH ACTIVE –NH$_2$ GROUPS FOR APPLICATIONS IN BIOSCIENCES

*Marion van de Waterbeemd, T. Sen, S.C.G. Biagini, I.J. Bruce*
*University of Kent, Department of Biosciences, School of Physical Sciences, Canterbury, Kent CT2 7NJ, UK*
*mv33@kent.ac.uk*

In the last decade, there has been increasing interest in describing and understanding the exact mechanism(s) involved in surface silanisation, i.e. surface activation on flat [1] and particulate surfaces [2]. Organosilanes are based on the chemical structure $X-(CH_2)_m-SiR_n(OR')_{3-n}$ which can function as coupling agents and are widely used to mediate the introduction of a functional group to an inorganic or organic surface.

Organosilanes react with surface –OH groups (silanol: in the case of silica surfaces) under appropriate conditions (i.e. solvent, reaction time and temperature) to leave the surface covered with a layer of functional groups which can then be used in grafting ligands.

Research to date, has involved establishing the methods and approaches necessary to produce amine functionalised surfaces using silica-magnetite nanoparticles as substrates. Commercially available organosilanes particularly aminopropyl triethoxysilane (APTS), aminopropyl diethoxymethylsilane (APDS) and aminopropyl monoethoxydimethylsilane (APMS) have been used in these experiments. A colorimetric assay has been used and standardized for surface -NH$_2$ density measurement as well as CHN combustion analysis. Initial results indicate that APDS works best in generating -NH$_2$ activated surfaces (up to 8.5 amine molecules/nm$^2$) whilst APMS was poorest in this respect (0.1 amine molecules/nm$^2$). Amine modified silica-magnetite nanoparticles were further used for surface functionalisation to aldehyde for subsequent surface oligonucleotide grafting and hybrid capture of its complimentary fluorescently labelled sequence.

**References:**

[1] J. H. Moon, J. W. Shin, S. Y. Kim and J. W. Park, Langmuir **12** (1996), 4621-4624
[2] I. J. Bruce, J. Taylor, M. Todd, M. J. Davies, E. Borioni, C. Sangregorio and T. Sen, Journal of Magnetism and Magnetic Materials **284** (2004), 145-160.

**Figures:**
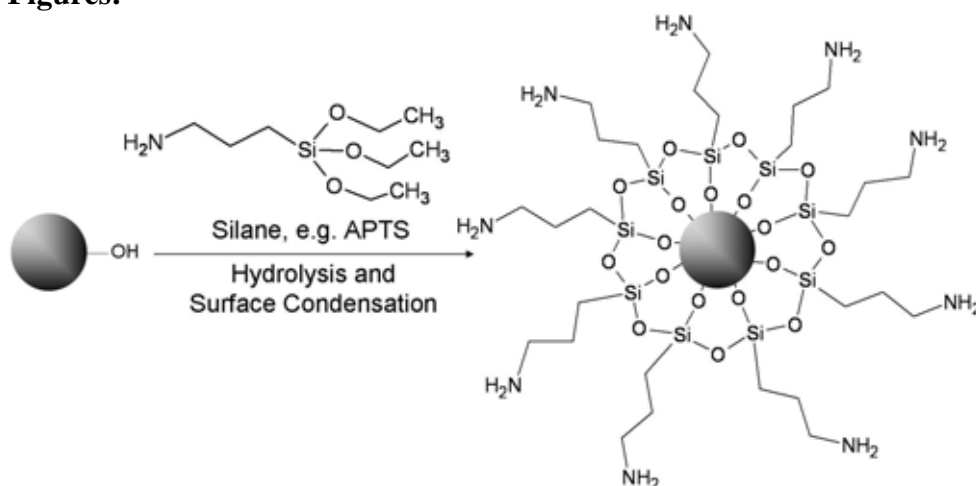


**Figure 1:** Silanisation of silica-magnetite nanoparticles.

**Figure 2:** Surface amine to aldehyde conversion with glutaraldehyde, oligonucleotide grafting and hybrid capture of a complimentary fluorescently labelled oligonucleotide.

# Energy-level Alignment of Chemisorbed Monolayers on Metal Surfaces: Implications for Molecular Electronic Junctions

*Roger D. van Zee*
*National Institute of Standards & Technology*
*Gaithersburg, Maryland USA 20899-8362*
roger.vanzee@nist.gov

Charge-transport through the interface is a key part of the behavior of any electronic junction. One specific interface property important to molecular-electronic junctions is the energetic alignment of the frontier molecular orbitals relative to the Fermi level of the contact material.

This poster will discuss the energy-level alignment of "molecular wires" chemisorbed on metal surfaces. One-photon, two-photon, and inverse photoemission spectra have been used to determine the energy-level alignment for well-characterized self-assembled monolayers of *para*(phenylene-ethynylene) oligomers chemisorbed on metal surfaces.[1-2]

The valence electronic structure of the chemisorbed monolayer is established by comparing the monolayer spectra to those of the isolated molecule.[3] The effects of molecular length, linker group (thiol and isocyanide), and substrate (copper, silver, gold, platinum) on the energy-level alignment will be presented.[4-6] The observed alignment and its trends can be qualitatively understood in terms of the material properties and a localized interface dipole.

The implications of these results for the design of molecular-electronic devices will be considered.
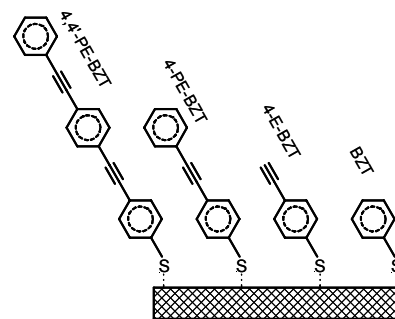


Self-assembled monolayers studied in this investigation: 4,4'-bis-(phenylethynyl)benzenethiol (4,4'-PE-BZT), 4-(phenylethynyl) benzenethiol (4-PE-BZT), 4-ethynylbenzenethiol (4-E-BZT), and benzenethiol (BZT).

**References:**
[1] C. A. Hacker, J. D. Batteas, J. C. Garno, M. Marquez, C. A. Richter, L. J Richter. R. D. van Zee, and C. D. Zangmeister, *Langmuir,* **20** (2004) 6195.
[2] L. J. Richter, C. S.-C. Yang, P. T. Wilson, C. A. Hacker, R. D. van Zee, J. J. Stapleton, D. L. Allara, X. Yao, and J. M. Tour, *J. Phys. Chem. B,* **108** (2004) 12547.
[3] C. D. Zangmeister, S. W. Robey, R. D. van Zee, Y. Yao, and J. M. Tour, *J. Am. Chem. Soc.,* **126** (2004) 3420.
[4] C. D. Zangmeister, S. W. Robey, R. D. van Zee, X. Yao, and J. M. Tour, *J. Phys. Chem. B,* **108** (2004) 16187.
[5] C. D. Zangmeister, S. W. Robey, R. D. van Zee, J. G. Kushmerick, J. Naciri, Y. Yao, J. M. Tour, B. Varughese, B. Xu, and J. E. Reutt-Robey, *J. Phys. Chem. B,* **110** (2006) 17138.
[6] C. D. Zangmeister, L. B. Picraux, R. D. van Zee, Y. Yao, and J. M. Tour, *Chem. Phys. Lett.,* **442** (2007) 390.

# PLASMON DISPERSION IN QUANTUM WIRES AT FINITE-TEMPERATURE

T. Vazifehshenas

Department of Physics, Shahid Beheshti University, Evin 1983963113, Tehran, Iran

t-vazifeh@cc.sbu.ac.ir

**Abstract**. We have investigated the effect of temperature on plasmon dispersion in a GaAs – based quasi one-dimensional electron gas (Q1DEG) by finding the roots of the temperature dependent dielectric function of the system in which the local field correction has been included through a one-dimensional generalized or temperature dependent Hubbard approximation (T-HA). We have compared T-HA plasmon frequencies with zero-temperature Hubbard approximation (HA) results and obtained the increase in plasmon energy with increasing temperature. We have also recalculated the plasmon frequencies of a single quantum wire in random phase approximation (RPA) at both zero- and finite-temperatures. Our results show lower energy for HA plasmons in comparison with those in RPA not only at zero-temperature but also at finite-temperature.

# Spin configuration in a frustrated ferromagnetic/antiferromagnetic thin film system

*A.L. Vázquez de Parga[1] , T.K. Yamada[2], E. Martinez[3], A. Vega[3], R. Robles[4], D. Stoeffler[5], T. Mizoguchi[2], H. van Kempen[6]*

*[1]Dep. Física de la Materia Condensada,Universidad Autónoma de Madrid, Spain*
*[2]Faculty of Science, Gakushuin University, 171-8588 Mejiro, Tokyo, Japan*
*[3]Dep. De Física Teórica, Atómica y Optica, Universidad de Valladolid, 47011, Spain*
*[4]Department of Physics, Uppsala University, SE-75121, Sweden*
*[5]Institut de Physique et Chimie des Matèriaux de Strasbourg, France*
*[6]Institute for Molecules and Materials, Radboud University, Nijmegen, The Netherlands*
*al.vazquezdeparga@uam.es*

The interface of ferromagnetic and antiferromagnetic material is important from a scientific point of view because the competing ferromagnetic and antiferromagnetic interactions may lead to complex solutions particularly when there is frustration in the system. Especially when an antiferromagnetic layer is deposited on a ferromagnetic substrate with an atomic step ("hidden atomic step") the magnetic frustration around this extended defect can give rise to interesting magnetic structures. Due to the localized nature of the frustrations, it has not been possible to resolve the spin configurations until the introduction of the Spin-Polarized Scanning Tunneling Microscopy/Spectroscopy (SP-STM/STS).

This problem is also important from the technological point of view because exchange bias is essential in many practical applications. In the world of magnetic devices, the goal is to get smaller. The smaller space one bit of information can occupy, the more data you can get into a device. Between two magnetic domains with opposite magnetization directions always exists a domain wall. Therefore a deep understanding of the parameters that control the domain wall width are crucial in order to achieve higher density for data storage.

Mn is exactly in the middle of the 3$d$ transition metal series, just between Fe, which is a natural ferromagnet in the bulk, and Cr, which is an antiferromagnet. Therefore, Mn stands as one of the more complex 3$d$ transition metals from the point of view of the magnetic coupling, and it is a clear candidate to exhibit a great variety of magnetic structures. Mn systems have been experimentally investigated by spin-polarized electron energy loss spectroscopy, scanning electron microscopy with polarization analysis and SP-STM/STS. A layered antiferromagnetic arrangement (LAF) was found in the Mn film. Recently, part of the authors have studied the same system using the *ab-initio* tight-binding linear muffin-tin orbitals method, assuming the experimental interlayer distances and a p(1×1) magnetic arrangement at the surface as experimentally observed. Different magnetic solutions with energy differences of few meV were obtained, with the LAF configuration the less energetic state, in good agreement with the experiments. The LAF as well as the closest metastable solutions had some common features: i) parallel coupling at the interface between Mn and Fe, ii) antiparallel coupling between the Mn-surface and subsurface layers and iii) antiparallel coupling between the two Mn layers closest to the interface. This set of solutions only differ in the couplings at the central Mn layers, that were parallel or antiparallel depending on the Mn thickness, which make these systems clear candidates to exhibit noncollinear magnetic arrangements under structural defects like monoatomic steps.

By means of SP-STM/STS, we measure in real space and with high spatial resolution the magnetic structure of the films around steps on the Fe(001) substrate. The experimental results are interpreted with the help of *ab-initio*-parametrized self-consistent real-space tight binding calculations in which the spin quantization axis is independent for each site thus allowing noncollinear magnetism. Throughout the paper, comparisons are made with the

Cr/Fe(001) system to get a deeper understanding of which material parameters are crucial to determine the resulting magnetic structure.

**Figure:**
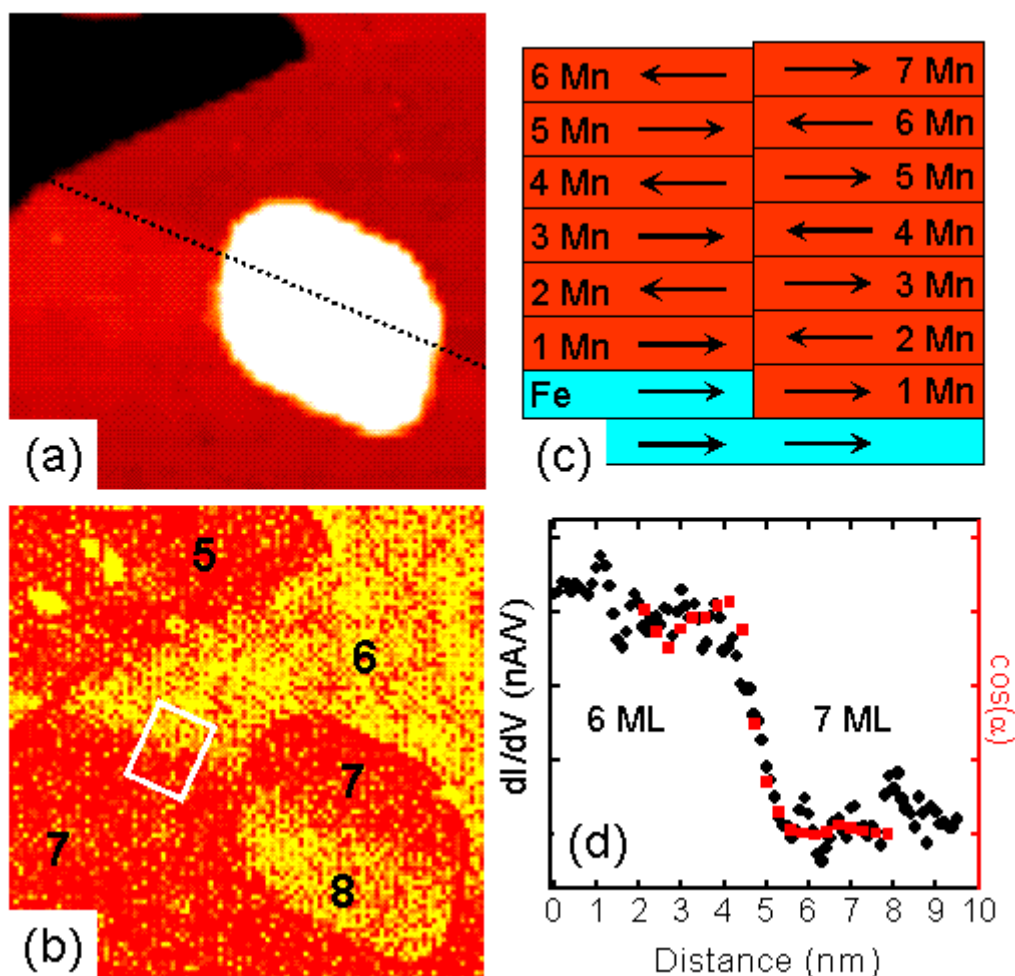


(a) STM image after deposition of 5 Mn ML's ($70\times70nm^2$). The dotted line marks the position of the hidden step. (b) *dI/dV* map taken at +0.2 V. The numbers indicate the Mn local thickness. (c) Model of the Mn structure around the hidden step. (d) (black dots) Average experimental profile across the hidden step measured inside the white box shown in (b). (red squares) Cosine of the angle of the magnetic surface moments with respect to the bulk obtained in the theoretical calculation for 6-7 ML.

# MAGNETOCALORIC EFFECT AND SIZE-DEPENDENT STUDY OF THE MAGNETIC PROPERTIES OF COBALT FERRITE NANOPARTICLES PREPARED BY SOLVOTHERMAL SYNTHESIS

*Carlos Vázquez Vázquez,*[1] *Marcos Lovelle Gómez,*[1] *Cintia Mateo Mateo,*[1]
*María del Carmen Buján Núñez,*[1] *M. Arturo López Quintela,*[1]
*David Serantes Abalo,*[2] *Daniel Baldomir Fernández,*[2] *José Rivas*[2]
[1] *Facultade de Química, Departamento de Química Física, Universidade de Santiago de Compostela, Avenida das Ciencias, s/n; 15782 Santiago de Compostela (Spain)*
[2] *Facultade de Física, Departamento de Física Aplicada, Universidade de Santiago de Compostela, Campus Sur, s/n; 15782 Santiago de Compostela (Spain)*
*qfmatcvv@usc.es*

Cobalt ferrite ($CoFe_2O_4$) nanoparticles from 2 to 15 nm were synthesized using a solvothermal procedure. In this non-aqueous method, acetophenone was used as solvent and the particle size was controlled by changing the reaction temperature from 120 to 200 ºC. Nanoparticles show good crystallinity and uniformity, as determined by x-ray diffraction and transmission electron microscopy.

Magnetic measurements indicate superparamagnetic behaviour. Zero-field-cooling (ZFC) dc-magnetization experiments at 100 Oe show blocking temperatures ranging from 215 K to more than 325 K. Increasing the applied magnetic field has only a small effect on the blocking temperature and a slight shift was observed to lower temperatures.

Saturation magnetization increases with particle size and a small decrease is observed when increasing the temperature. The Verwey transition is observed at 150K.

The magnetocaloric effect shown by these cobalt ferrite nanoparticles is reasonably high for nanomaterials.

# THE INVESTIGATION OF THE INTERMEDIATE PHASE OBSERVED DURING MAGHEMITE FORMATION USING FTIR SPECTROMETER

*Mürvet Volkan,*[1]*Bilsen Tural*[1,2]*, Arife Gençer İmer*[3] *, Raşit Turan*[3]*, *[*]

[1]Middle east Technical University, *Faculty of Arts and Sciences, Department of Chemistry, 06531 Ankara, Turkey*
[2]*Dicle University, Department of Chemistry, 21280, Diyarbakır, Turkey*
[3]Middle east Technical University*, Faculty of Arts and Sciences, Department of Physic, 06531 Ankara, Turkey*

murvet@metu.edu.tr

Maghemite ($\gamma$-$Fe_2O_3$) is one of the phases of iron oxide that finds numerous applications such as magnetic storage media [1], printing inks [2], magnetic resonance imaging [3], drug delivery [4], biomedicine [5], biosensors [6], and magnetic refrigeration [7] due to its extraordinary magnetic and optical properties. The physical and chemical properties of magnetic nanoparticles strongly depend on their size. Most of the technological and diagnostic applications require magnetic particles of size smaller than 20 nm and a narrow size distribution. Hence the shape- and size-controlled synthesis of magnetic oxide nanoparticles is of great technological and scientific importance.

The stabilization of nanometric $\gamma$-$Fe_2O_3$ is usually achieved by dispersing maghemite in a polymeric, glassy or ceramic matrix. Matrix support, which in principle, modifies the properties of nanomaterials, thus opening new possibilities to the control of their performance [8].

Isolated nanometric particles of $\gamma$-$Fe_2O_3$ in a silica matrix have been prepared by the hydrolysis of $Fe(NO_3)_3.9H_2O$ and tetraethylorthosilicate (TEOS) and heating at high temperatures. The hydrolysis reaction was promoted only by the hydration water of the salt. Small superparamagnetic nuclei are formed during the hydrolysis and condensation of the gel and the $\gamma$-$Fe_2O_3$ nanoparticle formation takes place through a reduction-oxidation reactions which occur during the subsequent calcination step[9].

The aim of this work was to identify the intermediate phase observed during thermal studies of maghemite nanoparticles prepared in alcohol rich type sol-gel matrix using Fourier transform infrared spectrometer (FTIR). The

FTIR measurements were done for pure sol gel at room temperature and the fresh monolithic gels containing $Fe_2O_3$ nanoparticles calcined at 90, 120, 145, 160, 200, 400 $^{o}C$ in static air for 4 h. Potassium bromide pellets were prepared in a diameter of 12 mm and the thickness 0.4 - 0.6 mm. FTIR measurements were done with unpolarized light in absorbance mode in the wavenumber range of 400-4000 $cm^{-1}$ with a resolution of 4 $cm^{-1}$ at a normal incidence using pure KBr pellet as reference.

The vibrational modes of OH groups are mainly located at 2500 to 3800 $cm^{-1}$ region. Silica and iron oxyhydroxides have strongly overlapping absorptions in this region. Goethite *(α-FeO(OH))*, Akagenite *(β-FeO(OH))* and lepidocrocite *(γ -FeO(OH))* are some of the oxyhydroxides of iron that absorb in the given region. The deconvolution procedure was applied to FTIR spectrum ın the region of 2500 to 3800 $cm^{-1}$ to obtain information about the changes in the silanol structure and the possibility of the presence of *γ* iron oxide hydroxides. Phase transformation studies for each calcination temperature were also supported by X-ray diffraction (XRD) analysis.

**References**

[1] J. F. Bobo, L. Gabillet and M. Bibes, J. Phys.: Condens. Matter, 16, (2004) S471

[2] W. Voit, W. Zapka, L. Belova and K.V. Rao, Sci. Meas. Technol., Vol. 150, No. 5 (2003)

[3] C. Billotey, C. Wilhelm, M. Devaud, J.C. Bacri, J. Bittoun and F. Gazeau, Magnetic Resonance in Medicine , 49, (2003) 646–654

[4] C. Gruettner , J. Teller , F. Westphal, R. Ivkov, (Germany). U.S. Pat. Appl. Publ. (2005) 24 pp., Cont.-in-part of U.S. Ser. No. 360, 561.

[5] Q. A. Pankhurst, J. Connolly, S. K. Jones and J. Dobson, J. Phys. D: Appl. Phys. , 36, (2003) R167–R181

[6] C. Jianrong , M. Yuqing , H. Nongyue , W. Xiaohua , L. Sijiao , Biotech. Adv. ,22, (2004) 505–518

[7] R. Skomski,J. Phys: Condens. Matter , 15 **,** (2003) R841

[8] R. F. Ziolo, E. P. Giannelis, B. A. Weinstein, M. P. O'Horo, B. N. Ganguly, V. Mehrotra, M. W. Russel and D. R. Huffman, Science**,** 257, (1992) 219

[9] C. Cannas, D. Gatteschi, A. Musinu, G. Piccaluga, and C. Sangregorio , J. Phys. Chem. B**,** 102, (1998) 7721-7726

# FABRICATION AND FOUR PROBE ELECTRICAL CHARACTERIZATION OF NANOWIRES

*Alex Walton, Stephen Evans*
*School of Physics and Astronomy, University of Leeds, Leeds, UK*
*phyaw@leeds.ac.uk*

Nanowires were fabricated by templated electrochemical deposition. This is a versatile technique that allows the deposition of both metallic and semiconducting nanowires. It also allows for a variety of complex morphologies such as multi-component wires and hollow nanotubes.

We present the fabrication of nanowires composed both metallic and semiconducting transition metal oxides. Compositional and morphological analysis was performed by TEM (including EDX, EELS and Selected Area Electron Diffraction) and UV- vis spectrometry.

Electrical transport measurements were taken using an Omicron nanoprobe. This devices comprises a high resolution SEM and four independent STMs. The SEM allows the STM tips to be brought into contact with a single nanowire and a rigorous electrical characterization can be performed. This includes:

1. four point probe measurements at varying separations on the same nanowire
2. Using a tip as a gate electrode and testing response to electric fields.
3. Four probe measurements as a function of temperature

**References:**

[1]  Walton et al. Nanotechnology **18** (2007) 065204

**Figures:**
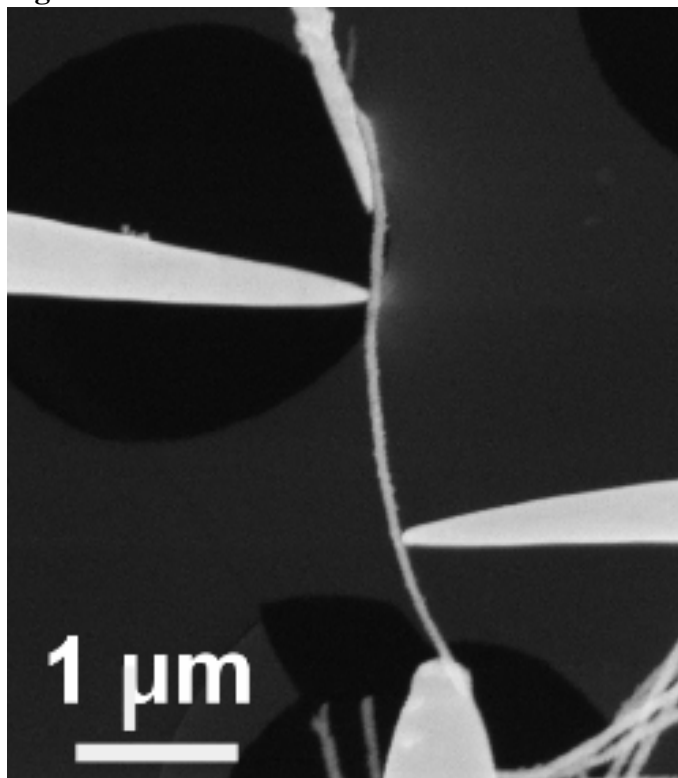


*SEM image of a 4 – probe measurement on a copper (I) oxide nanowire*

# DIRECT EVIDENCE OF NANOWIRES FORMATION FROM A Cu(II) COORDINATION POLYMER

*Lorena Welte [a], Eva Mateo-Martí [b], Pilar Amo-Ochoa [a], Pablo J. Sanz Miguel [a], Julio Gómez-Herrero [c], José A. Martín-Gago [b,d], Félix Zamora [a.]*

*a Departamento de Química Inorgánica, Universidad Autónoma de Madrid, Madrid, Spain*
*b Centro de Astrobiología (CSIC-INTA), Madrid, Spain*
*c Departamento de Física de la Materia Condensada, Universidad Autónoma de Madrid, Madrid, Spain.*
*d Instituto de Ciencia de Materiales de Madrid (CSIC), Madrid, Spain.*
lorena.welte@uam.es

Coordination polymers, also named metal-organic frameworks (MOF), are formed by self-assembly of selected metal or metal complex and bridging ligands. They have been studied in recent years since they show relevant structural features and potential applications in many fields[1,2]. Our current research is focused on the isolation and morphological characterization of well-ordered individual 1D-MOF chains on surfaces aiming the investigation of their potential application as molecular wires. In first state, this has required the development of new adsorption methods to organized individual chains of MOF on surfaces[3]. Once the polymer is adsorbed on a surface, Atomic Force Microscopy (AFM) allows its morphological and physical characterization among others, conductivity and magnetism. However, just from AFM data it is not possible to elucidate the structure of the MOF and its interaction with the surface. For that reason, we have selected a particularly interesting 1D-MOF Cu(II) polymer with isonicotinic acid as terminal ligand, to study the composition of the coordination polymer on a surface (Figure 1a). Its selection has been done based on its structure (suitable for a supramolecular interaction via H-bonds of the carboxylic groups) and physical properties (semiconductor behaviour).

To adsorb $[CuBr(IN)]_n$ on different surfaces two methods has been used: (i) casting deposition of sonicated suspensions and (ii) solubilization of the compound by deprotonation of the carboxylic groups. The deposition methods employed so far to adsorb $[CuBr(IN)]_n$ lead to 1D-fibres formation on different surfaces (HOPG, mica and gold) (Figure 1b-d). Novel spectroscopic characterization, Polarization Modulated Reflection Adsorption Infrared Spectroscopy (PM-RAIRS) and X-ray Photoelectron Spectroscopy (XPS), of these fibers let us to establish their structure once adsorbed on gold. In situ PM-RAIRS characterization of the polymer immobilized on gold surfaces confirms the already known structure of the compound as determined by X-ray crystallography (Figure 2a). In addition, the vibrations found in the PM-RAIRS indicate that the $COO^-$ groups are acting as linkers with the gold surface. On the other hand, XPS studies provides information about the metallic part of the compound, identifying the chemical state and composition of the polymer once is adsorbed on the gold surface (Figure 2b).

In summary, we present direct evidence of the subnanometer structure of the $[CuBr(IN)]_n$ on surface.

**References:**

[1] S. Kitagawa and S. Noro, In Comprehensive Coordination Chemistry II, T.J McCleverty, Eselvier, 2004.

[2] C. Janiak, Dalton Trans., 2003, **14**, 2781

[3] D. Olea, S.S Alexandre, P. Amo-Ochoa, A. Guijarro, F. de Jesus , J. M. Soler, P. J. de Pablo, F. Zamora, J. Gomez-Herrero, Adv. Mat, 2005, **17**, 1761

**Figures:**
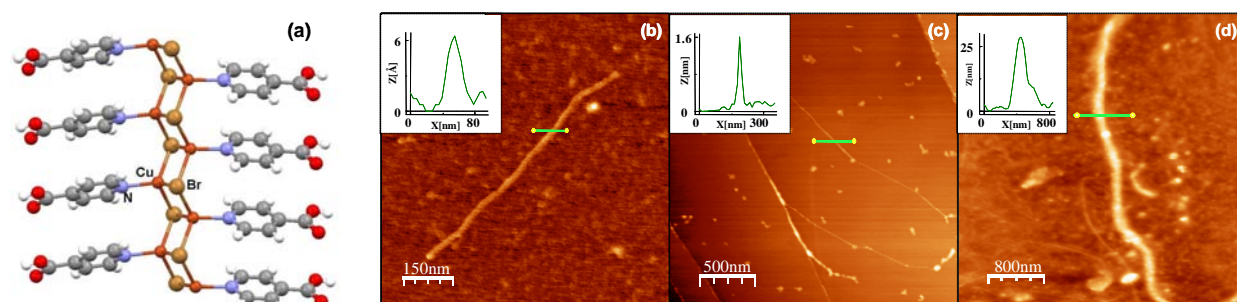


**Figure 1.** (a) Schematic representation of a $[CuBr(IN)]_n$ polymer chain. (b) AFM topography image of $[CuBr(IN)]_n$ deposited on mica treated with polylisine (b) HOPG (c) and gold (d) surfaces.
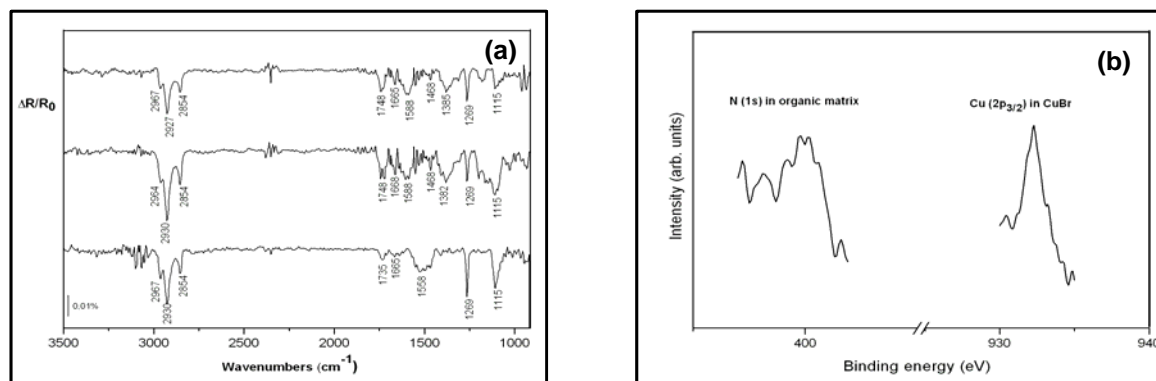


**Figure 2.** (a) PM-RAIR spectra after adsorption of $[CuBr(IN)]_n$ on gold from different adsorption methods. (b) XPS spectra after adsorption of $[CuBr(IN)_n]$ on gold surface.

# STM study of azobenzene self-organized on the Ag/Ge(111)-($\sqrt{3} \times \sqrt{3}$)R30° surface

*H.-C. Wu[1,2], C.-S. Tsai[1], and J.-C. Lin[1,2]*

[1]*Institute of Atomic and Molecular Sciences, Academia Sinica, P. O. Box 23-166*
[2]*Department of Chemistry, National Taiwan Normal University, Taipei, 106, Taiwan*
hcwu@pub.iams.sinica.edu.tw

The interfacial structures of organic molecule, azobenzene, on Ag/Ge(111)-($\sqrt{3} \times \sqrt{3}$)R30° (replaced as Ag/Ge(111)-$\sqrt{3}$) under ultrahigh vacuum conditions were studied by low-temperature scanning tunneling microscopy (LT-STM). Azobenzene is an important molecule because it undergoes a reversible, photoactive *trans-cis* isomerization that may allow it to serve as an optically active device. The STM images of azobenzene adsorbed on Ag/Ge(111)-$\sqrt{3}$ were properly resolved. The overlayer of azobenzene was found to form a (2×1) structure as shown in Figure 1.

Due to the excellent matching the molecular lengths of azobenzene with the lattice constant of Ag/Ge(111)-$\sqrt{3}$, the molecular films deposited onto Ag/Ge(111)-$\sqrt{3}$ form three equivalent domains which were rotated by 120°. High resolution images allowed the identification of individual molecules and the image of azobenzene appeared as a dumbbell sharp, similar to the related stilbene molecule that has been observed in films on the Ag/Ge(111)-$\sqrt{3}$ surface[1]. The azobenzene molecule consists of two phenyl rings connected by a pair of doublebonded nitrogen atoms. The hydrogen bonds may be formed, as shown in the cycle in Figure2 (a). Figure 2(b) is our proposed model.

**References**

[1] C.-S. Tsai, C. Su, J.-K. Wang, J.-C. Lin, *Langmuir,* **19** (2003), 822-829

**Figures:**
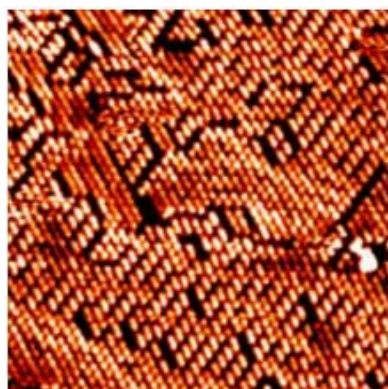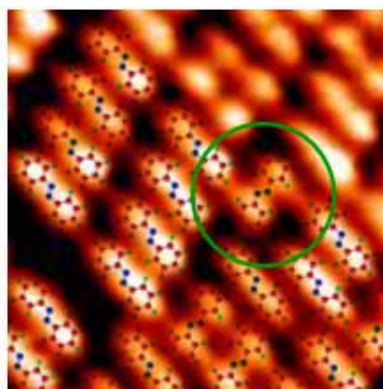
Figure 1                   Figure 2(a)                   Figure 2(b)
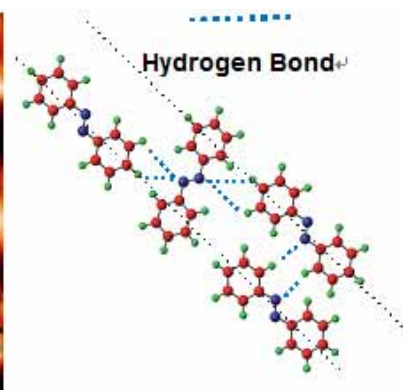
# Spin-transfer torque switching in exchanged-biased spin valve nano-pillar fabricated by 3-D focused-ion beam lithography

*<u>M. C. Wu</u>[1], A. Aziz[1], M. Ali[2], M. G. Blamire[1]*

*1. Department of Materials Science and Metallurgy, University of Cambridge, Pembroke Street, Cambridge, CB2 3QZ, United Kingdom*
*2. School of Physics and Astronomy, University of Leeds, Leeds, LS2 9JT, United Kingdom*
*Contact email: <u>mcw42@cam.ac.uk</u>*

In 1996, Slonczewski and Berger predicted that a spin-polarized current, which is caused to flow between one relatively thick, and fixed, ferromagnetic layer through a non-magnetic layer to another free nanomagnetic layer could transfer spin momentum from the current to the free layer[1,2]. Depending on the direction of the spin current flow, the spin transfer effect can either force the free layer into parallel or antiparallel alignment comparing with the fixed layer when the spin transfer force is strong enough to overcome the coercive field of the free nanomagnet. The experimental evidence was proved by Myers[3] and Katine[4]. Since the spin transfer effect depends on the local spin current density, the effect dominates the self magnetic field generated by the current when the current perpendicular to the plane (CPP) device diameter is small enough. Furthermore, when a strong external pinning field is applied to such a nanoscale CPP structure, the effect of spin transfer can be the excitation of strong and uniform spin wave precessional modes in nanomagnet[5,6]. The nanomagnet precession could be a source of microwave radiation and possibly a source of a precessional spin current. Some experimental works have demonstrated the spin transfer torque switching and spin wave excitation effects[7,8]. The spin transfer phenomena open up the possibility of new types of nanoscale magnetic devices for memory such as MRAM and other spin electronics applications.

The spin transfer phenomenon has been observed in a number of device geometries, which include mechanical point contacts, lithographically-defined point contacts, and lithographically-defined nanopillars. These devices all share two characteristics, megnetoresistive readout of the magnetic state and small cross-sectional area. Most of the nanopillars were fabricated by e-beam lithography. Here, we report a novel 3-D focused ion beam lithography for the study of the spin transfer torque switching. This technology provides an efficient route to fabricate reliable CPP magnetic spin valve devices.

Our devices were fabricated using the following steps. First, a multilayer of Ta(5)/Cu(200)/CoFe(3)/Cu(6)/CoFe(6)/IrMn(10)/Cu(200)/Ta(5) (thickness in nanometers) were deposited onto a thermally oxidized Si substrate in an ultrahigh vacuum sputtering system with the base pressure below ~5x10$^{-8}$ Torr. An external magnetic field of ~200 Oe was applied during the sputtering in order to induce an in-plane magnetic easy axis. Second, the multilayered thin film was patterned by optical lithography and then was etched by Ar ion milling through the film to the substrate. 4um wide tracks with 4um wide voltage leads are produced by those steps. Third, a course etching (width down to 300nm) is performed using 150pA Ga ion beam current. Then, a fine etching (width down to 150nm) and side wall cleaning process is performed using 11pA beam current. Side etching by 11pA beam current with a custom-built 45$^{o}$ wedge holder is performed. The geometry of the nanopillar is shown as Fig. 1. Transport measurements were conducted in a four-point contact geometry. An ac lock-in technique was used to measure the dynamic resistance (dV/dI) of the spin valves in an in-plane magnetic field applied along the geometric easy axis (long axis of the rectangle), with an ac current excitation of 200uA rms at 77Hz. A dc bias current was simultaneously applied during the dV/dI measurement, with the positive direction corresponding to electron flowing from fixed to the free layer. The dynamic resistance was measured as a function of

magnetic field and dc bias current. The Fig.2 shows a megnetoresistance (MR) loop at 300K and zero bias current for a CPP exchanged-biased spin valve with a size of 150nm by 200nm. The external field aligns the moment of free layer and fixed layer to be either parallel (P) or antiparallel (AP), resulting in an MR value of ~0.5%, which is defined as MR=$(R_{AP}-R_P)$/Rp, where $R_{AP}$(Rp) is the resistance of the AP(P) state. The current induced magnetization switching (CIMS) can be clearly observed in zero external magnetic fields, as shown in Fig.3. The resistance switches to the Parallel (P) state at $I_{AP \to P}$= 10.1mA while it flips back to antiparallel parallel state at $I_{P \to AP}$= -1.2mA. The corresponding change in the resistance at zero bias dc current in Fig.3 is as the same as the change in the resistance at zero external applied fields in Fig.2, confirming that the magnetization is fully reversed by the spin-polarized current injection. The critical current density is estimated to be 3.4 x $10^7$A/cm$^2$ (for $I_{AP \to P}$) and -4x $10^6$A/cm$^2$ (for $I_{P \to AP}$). These agree well with the value estimated from Slonczewski's spin transfer model.

In summary, we have successfully fabricated an exchanged-biased spin valve nanopillar by 3D focused ion beam lithography for the study of spin transfer torque switching. We have observed the CIMS in the CPP nanopillar. The technique provides the fabrication of nanopillar for fast exploration of spin transfer torque effect in magnetic thin film.

**References:**

[1] J. C. Slonczewski, Journal Of Magnetism And Magnetic Materials 159 (1-2), L1-L7(1996)
[2] L. Berger, Physical Review B 54 (13), 9353-9358 (1996)
[3] E. B. Myers, et al., Science 285 (5429), 867-870 (1999)
[4] J. A. Katine, et al., Physical Review Letters 84 (14), 3149-3152 (2000)
[5] M. Tsoi, et al., Physical Review Letters 80 (19), 4281-4284 (1998)
[6] S. M. Rezende, et al., Physical Review Letters 84 (18), 4212-4215 (2000)
[7] F. J. Albert, et al., Applied Physics Letters 77 (23), 3809-3811 (2000)
[8] S. Urazhdin, et al., Physical Review Letters 91 (14), 146803 (2003)

**Figures:**
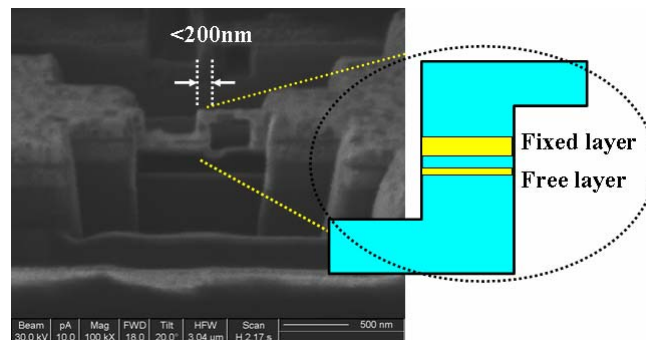


Fig.1 The geometry of the nanopillar fabricated by 3D focused ion beam lithography.
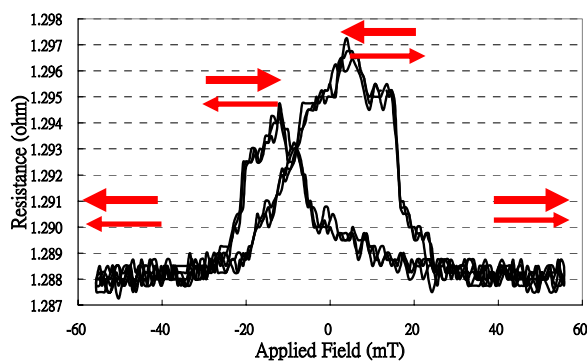


Fig.2 MR curve of the nanopillar
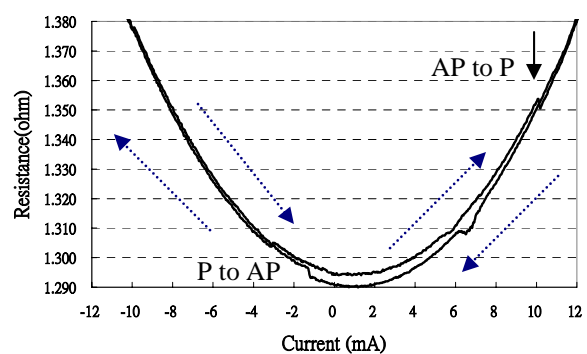


Fig.3 CIMS curve of the nanopillar

# THREE-DIMENSIONAL SUPERLATTICES OF *N*-ACETYLGLUTATHIONE-PROTECTED GOLD NANOPARTICLES: EMERGENCE OF FIVEFOLD SYMMETRY

*<u>Hiroshi Yao</u>, Takayuki Minami, Keisaku Kimura*
*Graduate School of Material Science, University of Hyogo, 3-2-1 Koto, Kamigori-cho, Ako-gun, Hyogo, 678-1297, Japan*
*<u>yao@sci.u-hyogo.ac.jp</u>*

Construction of ordered assemblies or superlattices on nanoscale dimensions is of key interest not only in electronics applications but also in fundamental nanoscience [1]. Metal nanoparticles, which can be considered as "artificial atoms", are ideal building blocks for two- (2D) and three-dimensional (3D) superlattice structures. The organic surface protection of nanoparticles enables to control their chemical functionality and allows the collective properties of the nanoparticle superlattices to be engineered. Unlike the most successful approaches that utilize hydrophobic alkanethiols as a surface ligand [1], we have developed the syntheses of carboxylate-protected water-soluble gold nanoparticles [2]. Application of such hydrophilic nanoparticles is one of the new fields for the construction of superlattices not by weak van der Waals interaction but by strong hydrogen-bonding and/or electrostatic interactions [3]. In the present study, we report the fabrication of 3D superlattices consisting of *N*-acetylglutathione (NAG)-protected gold nanoparticles. The strategy is using hydrogen-bonding networks among the surface carboxylic acids to form nanoparticle superlattices. During the syntheses, we found that fivefold symmetric (decahedral or icosahedral) superstructures could be built from the nanoparticles.

NAG-protected gold nanoparticles self-assembled into ordered arrays or superlattices at an air/aqueous solution interface by adding a concentrated hydrochloric acid of 0.05–0.1 M [3]. Their morphology and packing structure were characterized by X-ray diffraction (XRD) and scanning electron microscopy (SEM) observations. The small-angle XRD profile shows several peaks (Figure 1), suggesting nanometer-scale periodicity caused by the formation of ordered arrays of NAG-protected gold nanoparticles. The constituent nanoparticles were stacked in a pattern of fcc (face-centered cubic) rather than hcp (hexagonal close-packing) with the lattice constant of 11.1 nm. The mean gold core diameter of the constituent gold nanoparticles was ~6.8 nm.

SEM observations have elucidated a variety of shapes in the 3D nanoparticle superlattices, where many of them had plate-like or complicated morphologies. In addition, some characteristic geometries of superlattices were observed; tetrahedron, decahedron, and icosahedron as shown in Figures 2a–2c, respectively. The strong emphasis is placed on the first observation of fivefold symmetry in the nanoparticle superlattices (Figures 2b and 2c). These shapes in fivefold symmetry would come from multiple twinning.

It is known that the two most typical fivefold twinning are decahedron and icosahedron. A decahedron is assembled from five tetrahedral subunits sharing an edge. An icosahedron is assembled using twenty tetrahedral subunits via sharing an apex [4]. Intrinsically, tetrahedral subunits in fcc cannot form a complete space-filling structure, so that there remains angular misfit yielding internal strain. The strain is relaxed by a reduction of surface energy up to a certain size above which transformation to single crystalline particles is expected. Hence a fivefold twined particle is commonly bounded by the lowest-energy triangular facets. In regular decahedra, they have a large surface/volume ratio, which can be lowered by truncating the edges around the common basis. One of better structures is the Marks decahedra, obtained by introducing re-entrances that separate the {100}-like facets [5a]. In Figure 2b, the observed re-entrant corners are well characterized by a typical Marks decahedron.

On the other hand, an icosahedral particle normally contains a larger strain inside due to the distortion of the intershell and intrashell distances, so that this form could be present only at small sizes in metal nanoparticles. For example, the size limit of 27.35 nm has been obtained in single icosahedral silver nanoparticles (4–5 x $10^5$ atoms included). Surprisingly, in Figure 2c, 1–2 x $10^8$ nanoparticles would be included in the superlattice assuming that they are made of spheres of 7.9 nm in diameter (= center-to-center distance between adjacent nanoparticles), which correspond to 300–400 shells [5b]. This is probably due to the fact that a large relaxation of the internal strain caused by the size non-uniformity and/or surface flexibility) of the constituent nanoparticles makes the icosahedral structure much stable. The field of fivefold twinned structures is a very broad and complicated one ranging from cluster science to surface science, so that we believe that our findings will give a new development of this fascinating subject in nanoscience [6].

**References:**

[1] (a) Brust, M.; Kiely, C. *J. Colloids Surf. A*, **202** (2002) 175. (b) Sampaio, J. F.; Beverly, K. C.; Heath, J. R. *J. Phys. Chem. B*, **105** (2001) 8797. (c) Storhoff, J. J.; Mirkin, C. A. *Chem. Rev.*, **99** (1999) 1849. (d) Burghard, M.; Philipp, G.; Roth, S.; von Klitzing, S. K.; Pugin, R.; Schmid, G. *Adv. Mater.*, **10** (1998) 842.

[2] (a) Chen, S.; Kimura, K. *Langmuir*, **15** (1999) 1075. (b) Yao, H.; Momozawa, O.; Hamatani, T.; Kimura, K. *Chem. Mater.*, **13** (2001) 4692.

[3] Yao, H.; Kojima, H.; Sato, S.; Kimura, K. *Langmuir*, **20** (2004) 10317.

[4] Hofmeister, H. *Fivefold Twinned Nanoparticles*; in Encyclopedia of Nanoscience and Nanotechnology, Vol. 3, ed. Nalwa, H. S.; American Scientific, Stevenson Ranch, 2004, 431.

[5] (a) Marks, L. D. *Philos. Mag. A*, **49** (1984) 81. (b) Baletto, F.; Ferrando, R. *Rev. Mod. Phys.*, **77** (2005) 371.

[6] Yao, H.; Minami, T.; Hori, A.; Koma, M.; Kimura, K. *J. Phys. Chem. B*, **110** (2006) 14040.

**Figures:**
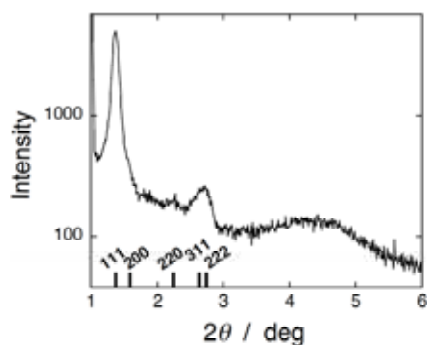


**Figure 1.** Small-angle XRD profile of the superlattice sample, suggesting a nanoscale periodicity caused by the formation of ordered arrays of NAG-Protected gold nanoparticles.
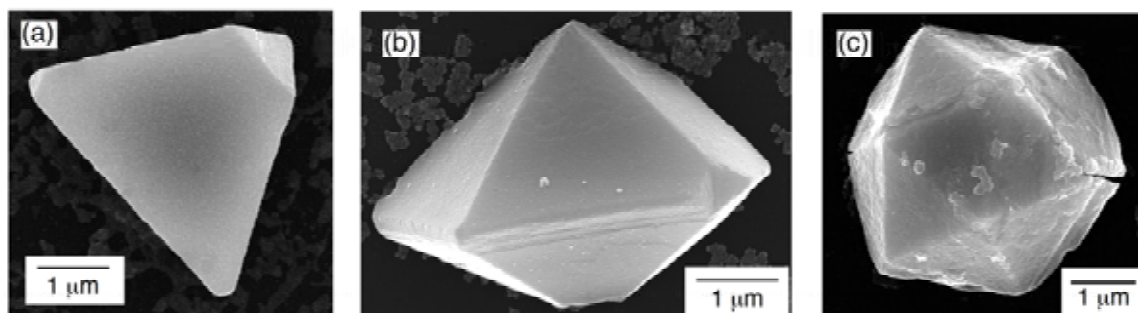


**Figure 2**. Nanoparticle superlattices of (a) tetrahedral, (b) decahedral, and (d) icosahedral shapes.

# HOW SMALL HOW LARGE THE MAGNETIC PARTICLE SHOULD BE IN THE FIXED DRUG DOSAGE

*A. Yazdani, Z. Shadrokh, F. Karami*

*Dep. Physics, Tarbiat Modares University, P.O. Box: 14115-175, Tehran,Iran*
*yazdania@modares.ac.ir*

Even though the small magnetic particles offer a proportionally larger surface area for absorption and therefore reducing the amount of magnetic carriers which are required to delivering fixed drug dosage, but increasing of the particle size would undoubtedly affect;
1) The external magnetic field, as it should be convenient for the high magnetic moment per unit volume and hence the higher magnetic saturation [1].
2) The larger particles are also more likely to be repelled from body very quickly [2,3].

However, while the fixed drug dosage for delivery should be exactly defined, the effect of size, chemical stability of structure and the number of particles in each convenient volume should be considered carefully by minimizing of the following internal materials' energy (potential) by three important controlling parameters of $\theta_i$, $R_c=2k_f r_{ij}$ and $\sigma_e$. Where $\theta_i$ is the angle between the direction of the magnetic particle's moment and the line which joins the magnetic centers. $R_c$ to be the effective correlation length between particles which are related to interatomic distance and the distance of the orbital and spin of electric charge and $\sigma_e$ demonstrates the elastic shear constant which describes the effect of long range ion-ion oscillatory interaction which is proportional to $[\cos(2k_f r_{ij}+\varphi)]/(2k_f r_{ij})^3$.
As first the sharp and high magnetic moment in low external magnetic fields are functions of $\theta$ and $R_c$, as Crystal Field Effect, CFE, secondly the defined superparamagnetic structure where caused by the lack of anisotropy and thirdly controlling the chemical stability of nanoparticles distribution size as well as their hardness and softness, therefore for minimizing the following internal energies they play an important role;
1) the magnetic potential energy of a magnetic moment "$\mu_A$" and its length "l" in the field of a similar magnet can be determined by:

$$U_p = -\frac{2\mu_A{}^2}{r_{ij}{}^3}\left[1.202 P_2(\theta) + 1.038 P_4(\theta)\left(\frac{l}{r}\right)^2 + ...\right]$$

Where $P_n(\theta)$s are Legendre functions.
2) the behavior of the linear moment when subjected to an external magnetic field "H" which can be defined by;
$$U_H = -H\mu_A \cos(\theta_0 - \theta)$$
3) the exchange interaction of the mean field approximation is given by:

$$\langle s_i \rangle = \frac{J\beta s_i \cdot H_i}{k_B T} \text{ where } H_i = \frac{2}{g\beta}\sum J_{ij} J_J \text{ results to}$$

$$U_{exchange} = \sum \frac{J(0)}{r_{ij}{}^3}\cos(\theta)\frac{J_{0j}}{J_{0i}}$$

Where $J_{0i}$ and $J_{0j}$ are the total quantum angular momentum and $J(0)$ is the exchange interaction.
Consequently minimizing of the energy could be manifested by;

$$\frac{d}{d\theta}\big[U_P + U_H + U_{exchange}\big] = 0$$

$$\frac{d}{dR_c}\big[U_P + U_H + U_{exchange}\big] = 0$$

$$\frac{d}{d\sigma}\big[U_P + U_H + U_{exchange}\big] = 0$$

The minimizing energy equations have been applied to the size distribution of magnetic particles [4] experimentally which as shown in the fig. 1 satisfies the super paramagnetic conditions.

**References:**

[1] Wanquan Jiang, et. Al. Journal of magnetism and magnetic materials 283 (2004) 210-214
[2] Mornet, S., et. Al. J. Mater. Chem. 14 (2004) 2161
[3] Paula Gould, nanotoday, Vol. 1, Number 4 (2006) 34
[4] S.I. Denisov, et. Al. Physical Rev. Lett. 97 (2006) 227202

**Figures:**
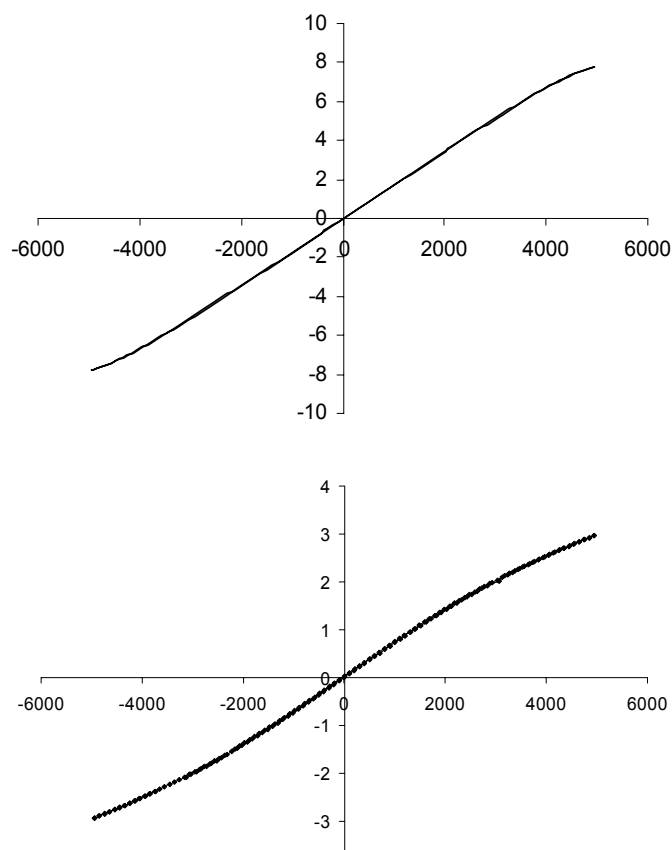


Fig. 1: Magnetization curve versus magnetic field strength for two different nanoparticle sizes

# Tuning the redox potential in molecular monolayers covalently bound to H-Si(100) electrodes via distinct C-C tethering arms

*<u>R. Zanoni</u>[a], M. Cossi[b], M. F. Iozzi[b], F. Cattaruzza[a], E. A. Dalchiele[c], F. Decker[a], A. G. Marrani[a]*

*[a]Dipartimento di Chimica, Università degli Studi di Roma "La Sapienza", p.le Aldo Moro 5, 00185 Rome, Italy; [b]Dipartimento di Scienze dell'Ambiente e della Vita, Università del Piemonte Orientale, via V. Bellini 25/G, 15100 Alessandria; [c]Instituto de Fisica, Facultad de Ingenieria, Herrera y Reissig 565, C.C. 30, 11000 Montevideo, Uruguay*

*robertino.zanoni@uniroma1.it*

Redox-active organic monolayers on Si electrodes constitute a promising step toward molecule-based hybrid devices compatible with the crystalline silicon platforms. Due to the attractive electrochemical properties of ferrocenes (fast e-transfer rates and favorable redox potentials), their introduction in organic monolayers bound to gold has been widely described in the literature.

We report here a combined experimental/theoretical approach on ferrocene (Fc)-silicon hybrids redox potential.[1,2] The systems were modeled with a slab of H-terminated Si(100) 1x1 and 2x1 surfaces: geometries were optimized using the ONIOM method, and solute-solvent interactions were included through the polarizable continuum model (PCM) method.

Two new routes for Si functionalization with ethyl- (EtFC) and ethynyl-Fc (EFC) differing only for the unsaturation degree of the anchoring arm have been successfully explored, and the redox potential of the resulting hybrids has been measured by cyclic voltammetry: 0.675 and 0.851 V vs. NHE for the EtFC and EFC derivatives, respectively. These values, along with the previously measured potential (0.700 V) for the mono-unsaturated derivative, vinyl-Fc (VFC), allow to study the relation between the unsaturation degree and the adduct redox potential.

The comparison among the measured and computed potentials allows to discriminate between different adduct isomers for the saturated species, and more importantly provides strong indications that the carbon-carbon unsaturation initially present in the molecular arm used for anchoring to the surface is preserved upon addition, in contrast with the commonly accepted reaction mechanism. A full characterization is reported by AFM and XPS of the resulting hybrids.

## Acknowledgements

## References

[1] Decker, F.; Cattaruzza, F.; Coluzza, C.; Flamini, A.; Marrani, A.G.; Zanoni, R.; Dalchiele, E.A. J. Phys. Chem. B, 2006, 110, 7374-7379.

[2] Cossi, M.; Iozzi, M. F.; Marrani, A. G.; Lavecchia, T.; Galloni, P.; Zanoni, R.; Decker, F. J. Phys. Chem. B, 2006, 110, 22961-22965.
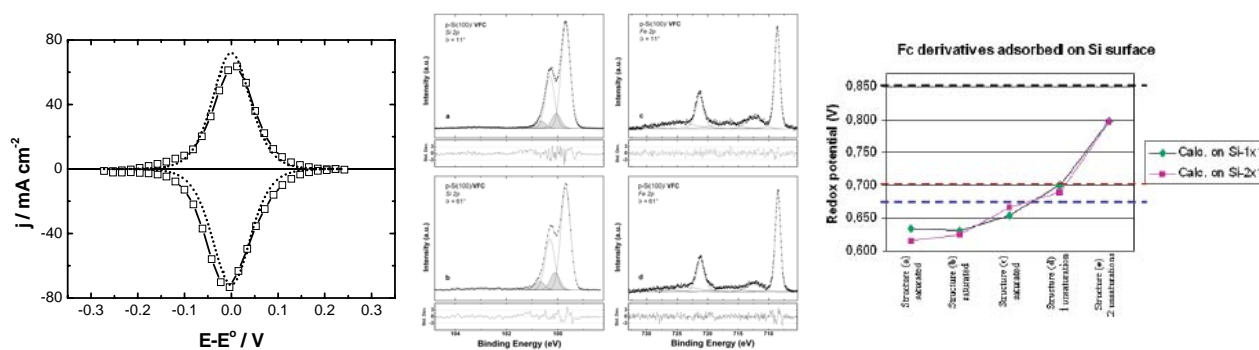


Figure 1. (Left) Experimental CV of a VFC/p-Si(100) electrode in 0.1 M TEAP/CH₃CN compared with the theoretical calculated response for an ideal Nernstian curve. $E^o$ is the formal potential (73 mV). Scan rate: 1 Vs$^{-1}$; (Middle) XPS spectra from the same system, taken on Si2p and Fe2p ionization regions at 11° (top) and 61° (bottom) photoemission directions from the surface normal. (Right) Computed redox potential (volts, referred to NHE) for different Fc derivative adducts on mono- and di-hydrogenated silicon surfaces. The experimental values for the adducts obtained with EfFC (top dashed line), VFC (middle), and EFC (bottom) are also reported for comparison.

# SYNTHESIS OF UNIFORM AND MONODISPERSED NaYF₄ NANOCRYSTALS WITH NIR-TO-VISIBLE UPCONVERSION FLUORESCENCE

*Yong Zhang,*[1] *Zhengquan Li*[2]

[1] *Division of Bioengineering, National University of Singapore, 7 Engineering Drive 1, Singapore 117574;* [2] *Singapore-MIT Alliance, National University of Singapore, Singapore 117576*

*biezy@nus.edu.sg*

Monodispersed NIR-to-visible upconversion nanocrystals have been developed in our lab, which have a wide range of biological and clinical applications. Optical window for *in vivo* imaging of cells and tissues are in the wavelength range of 700–1100 nm. The upconversion fluorescent nanocrystals are excited using a near infrared (NIR) laser at a wavelength of 980nm which falls in the optical window. Compared to conventional down-conversion fluorescent materials such as organic dyes and quantum dots, the upconversion nanocrystals have the following advantages: high light penetration depth in tissues, no photodamage to living organisms, weak autofluorescence from cells or tissues, low background light and high sensitivity for detection. To date, NaYF₄:Yb, Er/Tm nanocrystals have demonstrated to be the best NIR-to-visible upconversion materials and hexagonal-phase nanocrystals have higher upconversion efficiency than cubic phase nanocrystals. It is important to develop efficient and convenient methods for synthesizing high-quality and monodispersed hexagonal-phase NaYF₄:Yb,Er/Tm nanocrystals for various biomedical applications. Some efforts have been made to the synthesis of hexagonal-phase NaYF₄ nanocrystals in recent years, but there are still some problems yet to be solved. For examples, hexagonal-phase NaYF₄ nanocrystals can be obtained via annealing cubic-phase nanocrystals or long-time hydrothermal treatment, but more often the nanocrystals with mixed crystal phases, big size and non-uniformity are produced. There are no functional chemical groups on the surface, so biomolecules can not be attached to the nanocrystals. An efficient and user-friendly method has been developed for synthesis of uniform hexagonal-phase NaYF₄ nanocrystals with strong upconversion fluorescence, by consuming fluorine reagents completely before the growth and ripening of the nanocrystals. The nanocrystals are chemically and photochemically stable (not photo-bleaching), and biocompatible (much less toxic than quantum dots). They are also well dispersed in some common organic solvents, and more importantly, in water.

**References:**

[1] Z. Q. Li, Y. Zhang, Angew. Chem. Int. Ed. Engl., **45** (2006) 7732.
[2] F. Wang, D. Chatterjee, et. al. Nanotechnology, **17** (2006) 5786.
[3] J. C. Boyer, F. Vetrone, et. al J. Am. Chem. Soc., **128** (2006) 7444.

**Figures:**
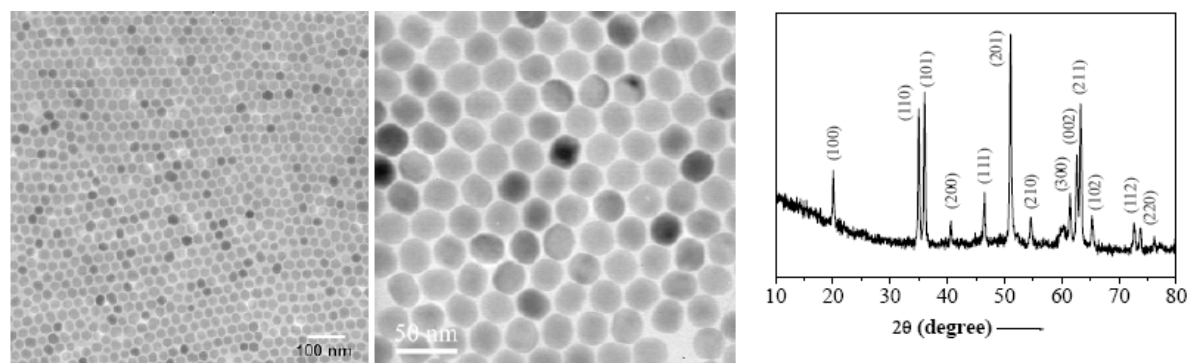


Figure 1 TEM images and XRD pattern of hexagonal-phase NaYF$_4$: Yb, Er/Tm nanocrystals
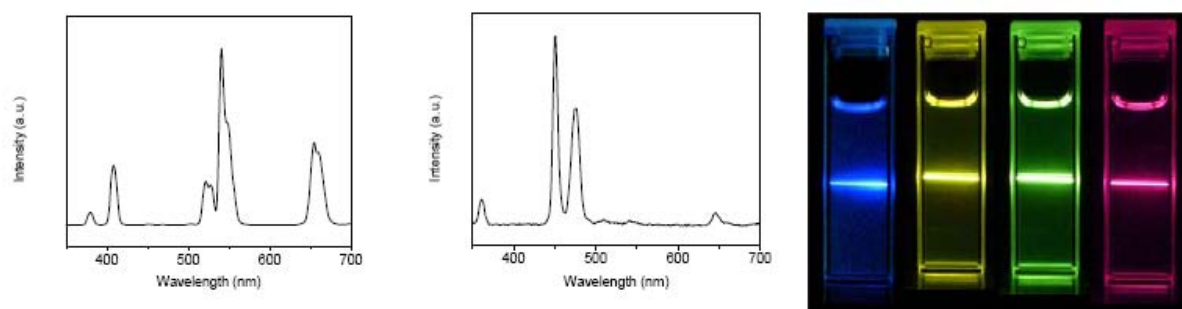


Figure 2 Fluorescence spectra of hexagonal-phase NaYF$_4$: Yb, Er/Tm nanocrystals (left, middle) and photographs showing the upconversion fluorescence from the nanocrystals when irradiated by a 980nm laser (right).

# New non-volatile Logic based on Spin-MTJ

*Weisheng Zhao[1,2], Eric Belhaire[2,1], Claude Chappert[2,1], François Jacquet[3], Pascale Mazoyer[3]*

1. *IEF, Univ Paris-Sud, UMR 8622, Orsay, 91405, France*
2. *CNRS, Orsay,91405, France*
3. *STMicroelectronics, 850, Rue Jean Monnet Crolles, 38026, France*

*zhao@ief.u-psud.fr*

Spin Transfer Torque (STT) writing approach based Magnetic Tunnel Junction (Spin-MTJ) (Fig.1) is excellent candidate to be used as Spintronics device in Magnetic RAM (MRAM) [1] and Magnetic Logic [2]. This effect was predicted by Slonczewski and Berger [3] in 1996, which shows that the spin magnetization in the storage layer of MTJ could be changed by flowing through a spin polarized current and the critical switching mechanism depends on the current density value. This critical current density has been found lately as low as $8*10^5$ A/cm$^2$ [4] in Co40Fe40B20/ MgO /Co40Fe40B20 stack structure; and as the dimension of Spin-MTJ is very small (e.g.113nm×75nm), the critical current could be thereby less than 150uA and easily generated by a small CMOS current source.

We have investigated two non-volatile logic circuits based on Spin-MTJ for Field Programmable Gate Array (FPGA) and System on Chip (SOC). The first one is a Spin-MTJ based non-volatile Look Up Table (Spin-LUT) (Fig.2). Working as a programmable and reconfigurable logic function generator, it memorizes all the configuration data in the MTJ arrays; and thus allows the FPGA logic circuit to reduce significantly its start-up latency from some microseconds down to some nanoseconds. It also allows realizing a sub-ns dynamical reconfiguration of the LUT during the signal processing. Spin-LUT non-volatile logic circuit has great potential in the field of complex logic digital system such as high performance game console and radar signal processing. The second one is Spin-MTJ based non-volatile Flip-Flop (Spin-FF) (Fig.3), data register and synchronizer, it stores permanently all the intermediate data processed in the FPGA or SOC circuit, thereby improves the data security and enable the complex logic system to restart immediately. Spin-FF could be advantageously used in the field of aviation and space where the security of data is one of the most important considerations. The lower critical current of STT writing approach makes these logic circuits work in less power and occupy smaller chip surface than with other writing techniques. Therefore the reduction of critical current has a strong impact on the performance of these Spin-MTJ based non-volatile logic circuits.

Another advantage of Spin-MTJ technology is that the storage element does not take much die area, because it is processed over the chip surface (see Fig.4). By using STMicroelectronics 90nm CMOS technology and a behavior Spin-MTJ simulation Model [5], Spin-LUT and Spin-FF have been demonstrated that they could work with high speed performance and small layout surface (Fig.5).

## References:

[1] M.Hosomi et al, "A novel nonvolatile memory with spin torque transfer magnetization switching: Spin-RAM" IEEE International Electron Device Meeting, USA, pp.473-476, 2005.

[2] W.Zhao et al, "Integration of Spin-RAM technology in FPGA circuits" 8th International Conference on Solid-State and Integrated Circuit Technology, China, pp.799-802, 2006.

[3] J.C.Slonczewski et al, "Current-driven excitation of magnetic multi-layers", Journal of Magnetism and Magnetic Materials, Vol159, pp.1-7, 1996.

[4] J.Hayakawa et al, "Current-driven magnetization switching in CoFeB/MgO/CoFeB magnetic tunnel junctions", Japanese Journal of Applied Physics, 2005, Vol44, pp. 267-1270.

[5] W.Zhao et al, "Macro-model of spin-transfer torque based Magnetic Tunnel Junction device for hybrid Magnetic-CMOS design", IEEE International Behavioral Modeling and Simulation Workshop, USA, pp. 40-43, 2006.

**Figures:**
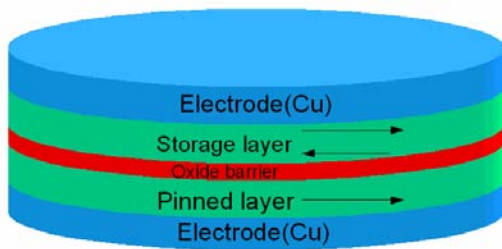




*Fig.1 Magnetic Tunnel Junction is composed of three principle layers: an oxidation barrier, such as MgO and AlxOy; a Pinned layer and a storage layer, which are ferromagnetic Materiaux (e.g.CoFe). The spin direction in pinned layer is fixed, but can be changed in the storage layer, there are so that two states of MTJ: parallel and anti-parallel when the spin magnetization in pinned layer and storage layer is in the same direction or the opposite direction. For Spin Transfer Torque (STT) switching approach, the two MTJ states are decided by the critical current density Ic.*
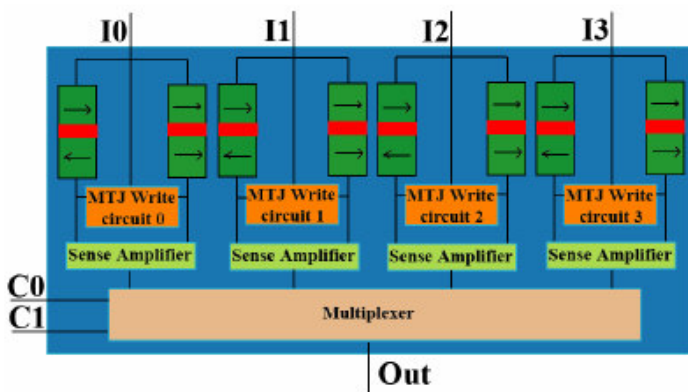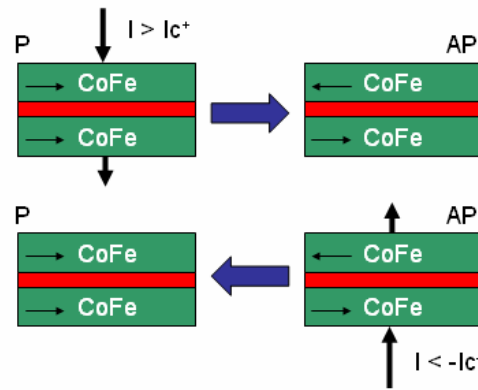


*Fig.2 2-input Spin-LUT architecture*
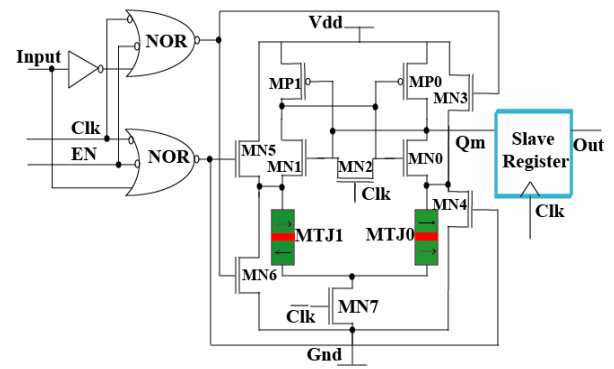


*Fig.3 the full schematic of Spin-MTJ based Non-Volatile Flip-Flop (Spin-FF)*



A: (10.0916n 50.4493m)    delta: (305.289p 34.9083m)
B: (10.3969n 85.3575m)    slope: 114.345M
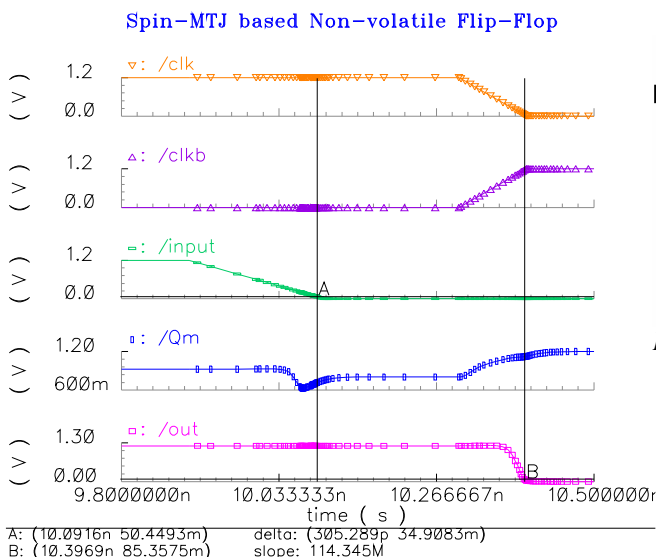
*Fig.5.1 Simulation of Spin-FF, the points show that the propagation delay is abut 300 ps*
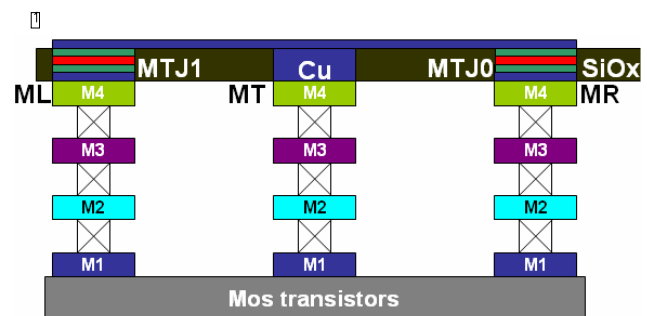


*Fig.4 MTJ memory cells are implemented above the CMOS circuits*
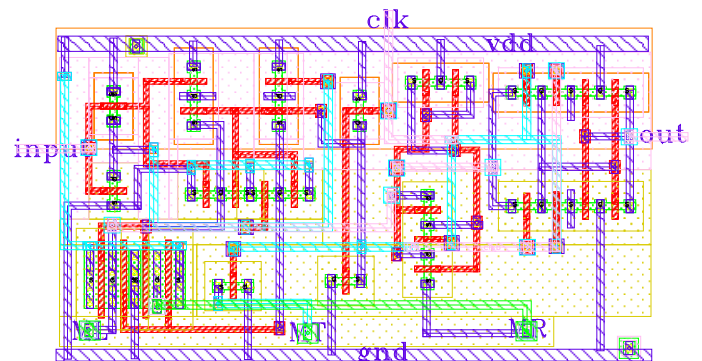


*Fig.5.2 Full layout (5.65um×10.15um) of Spin-FF, MTJs are placed above the two points ML and MR, see also Fig.4*

# DEVELOPMENT OF ULTRA-THIN GLASS-COATED AMORPHOUS MICROWIRES FOR HF MAGNETIC SENSORS APPLICATIONS

*A. Zhukov[1], M. Ipatov[1], V. Zhukova[2], J. [Gonzale1z], J.M. Blanco[2],*
*Dpto. de Física de Materiales, Fac. Químicas, Universidad del Pais Vasco, 20009, San Sebastián, Spain*
*Dpto. de Física Aplicada, EUPDS, Universidad del Pais Vasco, 20018, San Sebastián, Spain*
*E-mail: wupzhuka@sp.ehu.es*

The recent tendency in miniaturization of the magnetic sensors requires the development of extremely thin magnetic wires with enhanced magnetic softness. The solution of this problem can be the composite wires produced by the Taylor-Ulitovsky method (1 - 30 μm in diameter) consisting of metallic nucleus coated by glass [1]. Recent significant progress in tailoring of magnetically soft Co-rich glass coated microwires with metallic nucleus diameter of about 20 μm fabricated by this method enabled to enhance significantly the GMI ratio (up to about 600%) [2]. Such thin microwires are very useful for designing of the microsensors. Particularly it is an important task to develop thin wires, because of the effect of the demagnetizing factor on GMI effect. It is demonstrated that if the microwire diameter is about 15 μm the demagnetizing factor can affect their remagnetization process for the samples length below 2 mm [3]. Therefore if sensor size is about 1 mm, the microwires with the diameter below 10 μm are very useful.

In this paper we report novel results on magnetic properties and GMI effect at frequencies between 10 MHz and 500 MHz in ultra-thin Co-Fe-rich amorphous glass-coated microwires with nearly-zero magnetostriction constant with metallic nucleus diameter ranging between 5 and 22 μm. $Co_{67.05}Fe_{3,84}Ni_{1,44}Si_{14,47}B_{11,51}Mo_{1,69}$ glass-coated amorphous microwires with the metallic nucleus diameter ranging between 5 and 22 μm and total diameter between 10 and 23 μm with vanishing magnetostriction constant of the order of $-(1-3) \cdot 10^{-7}$) fabricated by the Taylor-Ulitovsky method have been studied. Most of studies samples exhibiting excellent soft magnetic behavior and high GMI effect. Off –diagonal components, real and imaginary part of the GMI have been analyzed.

Even in the thicker sample (metallic nucleus 22 μm) the penetration skin depth calculated from the GMI curves at 30 MHz is about 1 μm. Therefore the surface magnetization process and surface defects are of special importance to achieve good HF properties in this wires.

## References:

[1] A. Zhukov and J. Gonzalez, "Amorphous and Nanocrystalline Soft Magnetic Materials", in *Advanced Magnetic Materials, book 3 "**Processing of advanced magnetic materials.**"* Edited by Y. Liu, D.J. Sellmyer and D. Shindo, (Kluwer Academic Publishers, Norwell, MA, USA, 2004) **Vol.3,** Chaper 5, p. 115-181.
[2] V. Zhukova, A. Chizhik, A. Zhukov, A. Torcunov, V. Larin and J. Gonzalez, IEEE Trans. Magn. 38, 5, part I, (2002) 3090.
[3]. A. P. Zhukov, M. Vázquez, J. Velázquez, H. Chiriac and V. Larin, J. Magn and Magn, Mater, 151, (1995) 132.

# FIRST-PRINCIPLE GW+SO APPROACH TO THE STUDY OF SPIN RELAXATION TIMES OF EXCITED ELECTRONS IN METALS

*Vladlen P. Zhukov*, *E.V. Chulkov*, *P.M. Echenique*

*Donostia International Physics Center*
*paseo Manuel de Lardizabal 4, 20018,*
*San Sebastian, Spain*

*waxvlvlj@ehu.es*

Spin dynamics of itinerant electrons in metals and semiconductors is one of the paramount issues of modern spin electronics [1]. The first- principle evaluations of spin relaxation path and similar temporal characteristics of spin dynamics are important for the theoretical analysis and invention of new spintronic devices. We have developed an *ab initio* method of calculating the inelastic spin relaxation time of excited electrons in metals basing on the GW approach of many-body theory that incorporates spin-orbit coupling. We have studied the spin relaxation times and path's in Al, Cu, Au, Nb and Ta. The concept of spin-flip phase space has been introduced, and it has been shown that the trend in the values of spin-flip time, with respect to lifetime, is well described basing on this concept. The spin-relaxation time and path in Nb and in particular in Ta appear to be much less than that in Al, Cu, Au. Comparing our results and previous data associated with impurity-induced and phonon-induced spin relaxation times and path's, we find that at the energy about 0.9 eV, which is a typical energy of electrons in spin-valve and magnetic-tunnel transistors, the inelastic electron-electron scattering mediated by the spin-orbit coupling is the dominating mechanism of spin relaxation.

References:

[1] I. Zutic, J. Fabian, S. Das Sarma, Rev. Mod. Physics, **76**, (2004) 323.

# MAGNETIC MULTILAYERS AND SPIN-TRANSFER IN MAGNETIC NANOSTRUCTURES

## A. *Zolanvari and H. Sadeghi*

*Department of Physics, University of Arak, P.O. Box: 38156-879, Arak, Iran.*

Magnetic multilayers for current flowing perpendicular to the interfaces can also exhibit an effect called spin transfer. Description of the spin transfer and their consequences depends on a hierarchy of models. Quantum mechanical calculations describe the behavior of spins when they scatter from interfaces. In these approaches, the spin-dependent reflection amplitudes to compute the behavior of electrons that have spins that are not collinear with the magnetization of the ferro magnet are used. When electrons in a non-magnet scatter from an interface with a ferro magnet, the two spinor components of the electron's spin along the magnetization separate spatially because the reflection amplitudes are different for the majority and minority electrons. In the process, angular momentum is effectively transferred from the electron spin to the ferromagnetic magnetization. This transfer of angular momentum can be described as a torque from the electron spin on the magnetization.

In this work we applied a effective theory for theoretical description of interactions and behavior of spins when they scatter from interfaces. The result of the quantum mechanical calculations, that the transverse spin current is absorbed by the ferromagnetic magnetization at the interface, enters into transport calculations as a boundary condition. We have used the effective theory for obtaining amplitude and the diffusion equation to compute the torque for various system geometries and magnetic configurations. This calculation reveals the importance of spin flip scattering in determining the polarization of the currents for magnetic multilayers and spin-transfer in magnetic nanostructures.

# NANOCOMPOSITES BASED ON POLY (P-DIOXANONE) AND ORGANICALLY MODIFIED CLAYS

M. Zubitur*, A. Fernandez, A. Mugica, M. Cortázar

Departamento de Ciencia y Tecnología de Polímeros. Facultad de Química de San Sebastián. Apartado 1072. 20080 Donostia-San Sebastián
**\*Departamento de Ingeniería Química y del Medio Ambiente. Escuela Universitaria Politécnica, 20018 Donostia-San Sebastián

**manuela.zubitur@ehu.es**

Poly(p-dioxanone)[1] (PDS) is an aliphatic poly (ether ester) with numerous medical applications as it can be metabolized or bioabsorbed by the human body. Moreover, the PDS is a crystallisable polymer suitable for melt extrusion which confers it great potential for general applications other than biomedical uses. In order to prepare materials with tailor made mechanical properties the addition of nanometric dimension fillers[2] to the polymeric matrix can be interesting, as a way to improve the polymer matrix properties with low filler content.

Clays are suitable material for preparation of polymer nanocomposites[3] due to their ability to be exfoliated by polymer molecules originating a material with excellent properties, as consequence of the high polymer/ filler surface area.

In this study the ability of cationic (1:2 phyllosilicates) and anionic (hydrotalcite) clays to obtain exfoliated nanocomposites using poly(p-dioxanone) as matrix polymer has been analyzed. Fluorohectorite (FH) and vermiculite (VMT) were employed as 1:2 phyllosilicate type clays and hydrotalcite (HT) as layered double hydroxide (LDH) type clay.

In order to obtain nanometer size dispersions, the hydrophilic clays have been organically modified (OM) to improve the compatibility with the more hydrophobic PDS. In this way, the interlayer ion of the cationic clays has been replaced by oleyl bis(2-hydroxyethyl) methyl ammonium chloride (Ethoquad). In the case of the anionic clays the organic modification involved sodium 4-hydroxy benzene sulphonate and sodium 12-hydroxy dodecanoate.

Nanocomposites of PDS and organically modified clays (5 wt%) were melt-mixed using a Mini-Max molder at 160º C. The intercalation of the organic modifier in the clays and the dispersion degree of the organically modified clays in the PDS composites have been analyzed by wide-angle X-ray scattering (WAXS) and Atomic Force Microscopy (AFM) in a complementary manner.

WAXS patterns of unmodified and modified clays were interpreted taking into account the position of the basal peak which depends on the distance between two adjacent clay layers. In Fig. 1 (a) WAXS patterns of the organically modified clays show that the position of the (001) peak shift to lower 2θ value for phyllosilicates treated with Ethoquad, resulting in an enlargement of interlayer distance from 1.43 to 2.88 nm for fluorohectorite (OMFH) and from 1.39 to 4.17 nm for vermiculite (OMVMT). Therefore, the observed d-spacing suggests a parallel monolayer of the organic modifier in case of fluorohectorite and a perpendicular monolayer structure in case of vermiculite.

Refering to hidrotalcite (Figure 1 (b)), the position of the (003) diffraction peak also shift to a lower 2θ value when it was treated with sodium 4-hydroxy benzene sulphonate (OMHTA), resulting in an increase of basal space of 0.74 nm that corresponds to a horizontal orientation of interlayer organic anion. In the case of hydrotalcite modified

with sodium 12-hydroxy dodecanoate (OMHTB) the interlayer dodecanoate anions are vertically arranged leading to an expansion of the basal spacing of 1.54 nm.

PDS nanocomposites of organomodified hydrotalcites (PDS-OMHTA and PDS-OMHTB) did not show the characteristic peak of basal spacing (Fig. 1 (c)) indicating that the clay layers could be completely exfoliated and dispersed in the PDS matrix, being nanometer-scale composites. Contrarily, for the composites based on fluorohectorite and vermiculite modified with Ethoquad (PDS-OMFH and PDS-OMVMT, respectively) the peaks of modified clay are shown clearly, giving evidence that the exfoliation of these clays had not taken place.

AFM was used to investigate the dispersion of the clay in the PDS matrix. In PDS-OMFH sample AFM image reveals tactoids and sometimes agglomerates of organo-fluorohectorite, suggesting that a good dispersion has not been achieved. However, in nanocomposites of PDS and organo-LDHs (PDS-OMHTA and PDS-OMHTB) AFM reveals that the clay is well dispersed throughout the polymer with no significant aggregation consequence of a completely mixed nanocomposite systems. These results can be explained on the basis of the different lengths and flexibility of the clay platelets. HT clay platelets, being smaller in size (70-100 nm) and more flexible than FH (500-600 nm) and VMT (200-300 nm), are easily distorted and dispersed by means of mechanical forces allowing the penetration of the polymer.

In summary, novel composites based on poly(p-dioxanone) and organically modified cationic and anionic clays have been prepared using the environmentally benign technique of melt-extrusion. The dispersion morphologies were observed by X-ray diffraction and AFM, indicating that exfoliation has been achieved for nanocomposites of organically modified anionic clays.

**Refences:**
[1] K. Yang, X. Wang, Y. Wang, J. Macromol. Sci. Polymer Reviews, **C42** (2002) 373.
[2] G.H. Michler and F.J. Baltá-Calleja, Mechanical Properties of Polymers Based on Nanostructure and Morphology, Taylor and Francis Group, Boca Raton, 2005.
[3] T.J. Pinnavaia and G.W. Beall, Polymer Clay Nanocomposites, Wiley, Chichester 2000.

**Figures:**
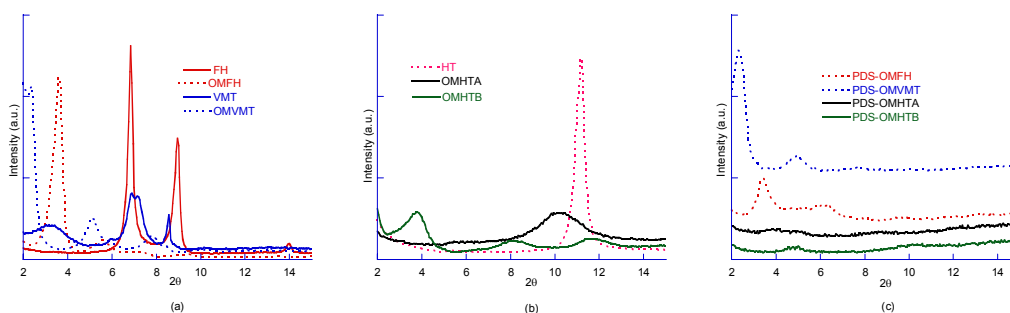


**Figure 1.** XRD profiles of: (a) cationic clays and its organic modifications, (b) anionic clays its organic modifications (c) nanocomposites of PDS with anionic and cationic clays.

# EFFECT OF TIP SHAPE ON ELECTROSTATIC FORCE MICROSCOPY

Fredy Zypman, Eli Lansey, Ben Kandel

Yeshiva University, Department of Physics, New York, NY 10033, USA

zypman@yu.edu

Electrostatic Force Microscopy (EFM) is a probe microscopy technique derived from Scanning Force Microscopy (SFM). Like in SFM, a tip senses proximity interactions forces of a sample surface. In EFM, the forces are of electrostatic nature and typically generated by an applied electric field. It has been extensively used to study liquid and solid surfaces, as well as polarization of small atomic chains [1].

It has been established [2] that the size and shape of the tip are relevant parameters in the electrostatic field and consequently, in the EFM interactions. In the same reference, the authors explain the problems with finite-element and similar numerical calculations –due mostly to the dissimilar spatial extend of the micrometer cantilever-tip system, and the nanometer tip-sample system.

To contribute to overcome the above described scale problem, we present here a semi-analytical algorithm to calculate EFM forces of realistically shapes tips (figure 1).
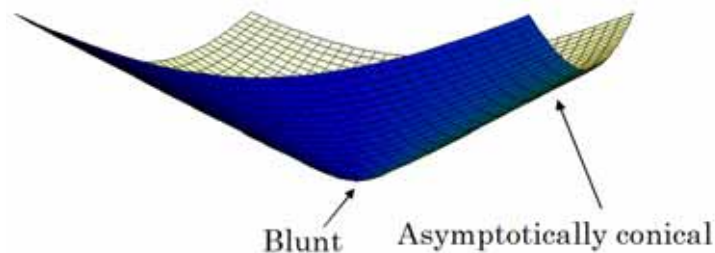


Figure 1. A real tip looks like a cone at large scales, but like a sphere at small scales.

The model consists of two main ingredients figure 2). First, the shape of the tip is considered to be a blunt-terminated cone. That is, at its apex the tip has a radius of curvature Ro. Far from the apex, the tip becomes asymptotically a circular cross section cone. The parameter Ro is allowed to vary to obtain tips ranging from very blunt to very sharp. Second, The surface of the tip is considered as a collection of charged rings. Each of these charged rings generate an electric field which in turn can be computed with the fast algorithm developed previously [3].
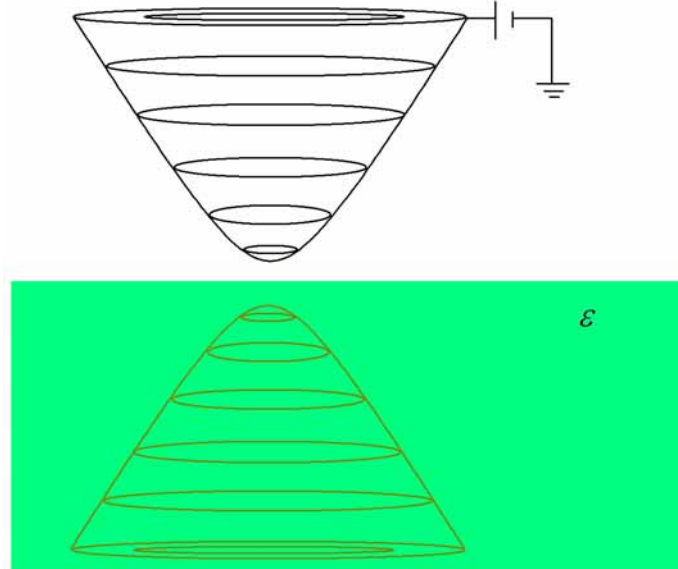
Figure 2. Schematic diagram of the tip made up of charged rings. In the presence of a dielectric material, an image set of charged rings is considered.

When the tip is close to a dielectric material, the whole electric field is the sum of those produced by the real rings and those produced by the image charge rings.

Thus posed, the problem becomes a linear inversion for the unknown charges on the rings. They are found by imposing the equipotential condition on the surface of the tip.

We emphasize that all this program is doable for real dimension tips due to the use of analytically simple expressions for the electric fields produced by rings of charges as demonstrated in reference [3].

[1] P Girard , "Electrostatic force microscopy: principles and some applications to semiconductors", Nanotechnology **12** (2001) 485-490
[2] GM Sacha, E Sahagún, JJ Sáenz, A method for calculating capacitances and electrostatic forces in atomic force microscopy", J Appl Phys **101** (2007) 024310
[3] FR Zypman, "Off-axis electric field of a ring of charge", Am J Phys **74** (2006) 295